UNCLASSIFIED

AD 276 205

*Reproduced*
*by the*

ARMED SERVICES TECHNICAL INFORMATION AGENCY
ARLINGTON HALL STATION
ARLINGTON 12, VIRGINIA



UNCLASSIFIED

NOTICE: When government or other drawings, specifications or other data are used for any purpose other than in connection with a definitely related government procurement operation, the U. S. Government thereby incurs no responsibility, nor any obligation whatsoever; and the fact that the Government may have formulated, furnished, or in any way supplied the said drawings, specifications, or other data is not to be regarded by implication or otherwise as in any manner licensing the holder or any other person or corporation, or conveying any rights or permission to manufacture, use or sell any patented invention that may in any way be related thereto.

276 205

PROCEEDINGS

# 7TH CONFERENCE ON RADIO INTERFERENCE REDUCTION AND ELECTRONIC COMPATIBILITY

*sponsored jointly by*
*U. S. Army, U. S. Navy*
*and U. S. Air Force*

*conducted by*
*Armour Research Foundation*
*of Illinois Institute of Technology*

*in cooperation with the*
*Professional Group on Radio Frequency Interference*
*of the Institute of Radio Engineers*

**NOVEMBER, 1961**

# PROCEEDINGS

# OF THE SEVENTH CONFERENCE ON

# RADIO INTERFERENCE REDUCTION

# AND ELECTRONIC COMPATIBILITY

Held at
Grover M. Hermann Hall
Illinois Institute of Technology
Chicago, Illinois
November 7, 8, and 9, 1961

Sponsored Jointly by
U. S. Army
U. S. Navy
U. S. Air Force

Conducted by
Armour Research Foundation
of Illinois Institute of Technology
Chicago, Illinois

In Cooperation with
The Professional Group on Radio
Frequency Interference of the
Institute of Radio Engineers

CONTENTS


Foreword . . . . . vii

Welcome . . . . . H. M. Sachs ix

Keynote Address . . . . . Brig. Gen. J. A. [illegible] David xi

SESSION I - DOD COMPATIBILITY PROGRAM

The Mission and Operating Philosophy of the Analysis Center . . . . . Col. C. C. Woolwine 1

The Technical Program of the Analysis Center . . . S. [illegible] Cohn 7

SESSION II A - COMPATIBILITY ANALYSIS

A Digital Computer Program for Reduction and Presentation of Electromagnetic Interference Data . . . . . C. B. Pearlston 16

Preparation of Statistical Input Functions for Interference Prediction . . . . . K. G. Heisler, Jr. 29

Radio Interference Reduction and Spectrum Utilization in Field Army Radio Relay Systems . . . . . R. M. Cowgill 55

A Comparison of Two Methods of Determining System Compatibility . . . . . E. D. Knowles 66

SESSION II B - INSTRUMENTATION I

Spectral Measurements of Radio Interference with a Coherent Memory Filter . . . . . J. Capon 75

A MIL-I-006051B Audio Transient Generator . . . . R. C. Dyer 84

A High-Power, Wide-Range, Ultra-Stable, Microwave Signal Source - D. E. Farmer, W. J. Messmer and L. R. Moses 95

Existing Current Probes and Development of New Probes to 1 KMC . . . . . J. F. Fischer, Jr. and H. K. Mertel 111

SESSION III A - SPECTRAL SIGNATURE MEASUREMENT TECHNIQUE

A Comparison of the Spectrum Signatures of AM, FM, and SSB Communications Equipments . . . J. G. Holey and E. W. Wood 140

Spectrum Compatibility Measurement Capability - J. E. Browne T. R. Gardner, R. Vonallmen, J. E. Parham, H. M. Reid and K. H. Gerred . . . . . 173

A Discussion of Test Procedures for Obtaining Spectrum Signatures of Pulse Communications Equipment . . . . . R. N. Bailey and P. Johnson, Jr. 180

A Pulse Technique for Measuring Susceptibility at Audio and RF Frequencies - J. H. Schukantz, G. C. Cooper and P. W. Broome 207

SESSION III B - ANTENNA SYSTEM ANALYSIS

Three Dimensional Quantized Antenna Pattern Model . . . . . L. E. Silverman, J. J. Krstansky and H. M. Sachs 284

Fresnel Region and Far Field Patterns of a Horn Antenna at Fundamental and Harmonic Frequencies - O. Salati and D. Lewis 315

Prediction of the Far Field of Parabolic Reflectors Excited with Plane Apertures of Arbitrary Field Distribution . . H. Zucker 337

Estimates of the Radiation in the Shadow Region of Aperture Antennas . . . . . H. N. Kritikos 359

SESSION IV A - MEASUREMENT TECHNIQUES AND ANALYSIS

Wide Band Noise Interference in the HF Spectrum - W. Gossard 386

New Methods of Insertion Loss Measurement of RF Filters Under Rated Load Conditions, Between 14 KC to 1000 MC and Higher . . . . . J. C. Klouda 409

Spurious Frequency Measurements in Transmission Lines - A Comparative Review of Available Techniques . . . . . W. A. Edson and V. G. Price 419

SESSION IV B - SHIELDING AND FILTERING TECHNIQUES

An Integrated Approach to Bonding, Grounding, and Cable Selection . . . . . I. M. Newman and A. L. Albin 434

Requirements of Measurements of Shielded Installations . . . . . R. G. Klouda 460

A Polarized Dissipative RFI Suppression Filter . F. N. Hansen 473

Shielding Efficiency Calculation Methods For Screening, Wave Guide Ventilation Panels, and Other Perforated Electromagnetic Shields . . . . . W. Jarva 478

SESSION V A - SPURIOUS EMISSION AND SUSCEPTIBILITY

Radio Interference and Susceptibility Study of High Power Transmitter Jammers . . . T. B. Brown and W. S. Schwagart 499

Receiver Susceptibility Under Multi-Mode Conditions . . . . . P. C. Yuen and J. J. Krstansky 509

A Survey of FM Receiver Techniques for Reducing Co-Channel and Adjacent-Channel Interference . . . . . E. J. Baghdady, H. G. Fritz, A. F. Ghais, and J. M. Gutwein 532

Capture Effects of Diode Envelope Detectors - A Determinant of Receiver Selectivity . . . . . J. E. Bridges 533

SESSION V B - INSTRUMENTATION II

A 1 to 10 KMC Panoramic Receiving System for R. F. I. Monitoring . . . R. H. Sugarman, K. E. Walker and R. Powers 555

New Instrumentation for Accurate Measurement of Broadband Interference in the 1 to 10 KMC Frequency Range . . . . . G. Lopez and M. Engelson 569

A Sensitive Recording System for Harmonic Pattern Measurements at Microwave Frequencies . . . . R. J. Doviak and D. J. Lewis 584

The Voice Interference Analysis Set, and Instrument for Evaluating the Performance of a Communication Channel . W. M. Grim, Jr. 597

## SESSION VI A - INTERFERENCE IN SOLID STATE SYSTEMS


Electromagnetic Compatibility in Microminiaturization . . . . . J. W. Hohmann and J. D. Meindl 609

Interference Effects in Parametric Amplifiers . . M. L. Wright 623

Interference in Masers . . . . . J. F. Lyons 643


## SESSION VI B - RADIATION EFFECTS


Field Evaluation of the NCEL Interference Attenuating Power Conductor . . . . . D. B. Clark and J. L. Brooks 662

Skin Current Probes . . . . . J. F. Fisher, Jr. 709

The Interference Problem Associated with Power Systems and Communication Lines . . . . . R. F. Ficcki 736


## SESSION VII - THE ELECTROMAGNETIC ENVIRONMENTAL TEST FACILITY


A Digital Representation of Interference Within a Communication Receiver Including the Demodulation Process . . . . . N. Wilde, A. J. Hoehn, and L. A. Follett 758

Engineering Aspects of the EMETF Interference-Prediction Model . . . . . A. J. Hoehn 771

A Facility for the Investigation of Radio-Interference Problems . . . . . L. F. Babcock 811

The Computer Approach to the Interference-Prediction Model of the Electromagnetic Environmental Test Facility . . J. B. Scott 833

Recently Issued Reports . . . . . 847

## FOREWORD

The Seventh Conference on Radio Interference Reduction and Electronic Compatibility has been evidence of the increasing awareness of the need for increased exchange of information in the area of electromagnetic interference analysis and control. More than 550 attendees were evidence to this fact. The widespread interest was attested to by the joint sponsorship of the three services, the U. S. Army, U. S. Navy, and the U. S. Air Force.

A total of forty-four technical papers were presented during the three days of the conference, together with an informal luncheon address, and forty-three of these papers are included in this volume.

The conference committee would like to extend its thanks to the authors and speakers, to the various session chairmen, and also to those who attended the technical sessions for their part in making this conference the most successful yet.

Conference Committee:

S. I. Cohn, Armour Research Foundation
Commander B. D. Inman, U. S. Navy,
Bureau of Ships
B. Lindeman, RADC
W. J. Magee, Armour Research Foundation
H. M. Sachs, Armour Research Foundation
H. G. Tobin, Armour Research Foundation
S. Weitz, USASRDL

WELCOME

H. M. Sachs
Armour Research Foundation
Annapolis, Maryland

As chairman of the Seventh Conference on Radio Interference Reduction and Electronic Compatibility, I would like to take this opportunity to again welcome you to Chicago, and to the campus of the Illinois Institute of Technology.

The implementation of this conference has again been brought about through the interest and generous support of the Army, Navy, and Air Force, and with the cooperation of the Professional Group on Radio Frequency Interference of the Institute of Radio Engineers. This year's program again reflects the increasing concern of military, government and industrial agencies over problems arising out of complex electronic equipment operation in denser and denser environments.

During the thirteen months since our last conference, the complexion of existing and potential additions to the electromagnetic spectrum has changed markedly. Spread-spectrum techniques in both the radar and communication fields are available. Man has orbited the earth, and with this fete has emphasized space communication requirements. Effective noise temperatures of receiving equipment continue to drop. Advancements in multi-megawatt power generation has continued. Project "Needles" and other space experiments are opening up new concepts for spectral usage.

Many more such advancements could be listed. From the viewpoint of the radio frequency interference engineer, most of them point up potentially serious compatibility problems. The constraint of having to live, from practical consideration within a finite frequency spectrum, means that against the advantages to be gained by any new system or concept must be weighed the disadvantages accrued with regard

to the degradation of other system performance.

Major strides have been made during the past year to analyze, measure, predict, and reduce the effects of this incompatibility monster. Notable action has been spearheaded by the Department of Defense's RF Compatibility Program. Many of the technical papers to be presented during the next three days represent some of the outputs of the program--the progress of the Analysis Center established in Annapolis, the status of programs to obtain spectrum signature data, the results of support programs to improve interference measurement techniques, develop specialized instrumentation, and the like.

Other efforts will also be highlighted during the conference. The first detailed presentation of the Electromagnetic Environment Test Facility at Ft. Huachuca, Arizona, will be given. Government and commercial investigations in such areas as antenna analysis, cable coupling, shielding evaluation, advanced system performance prediction, etc., will be presented. I believe you will find the overall conference program very comprehensive and informative, and keyed to the problems facing most of us today.

The campus facilities we have available with regard to the conference technical sessions and luncheons have likewise been chosen with the expanding conference interest in mind.

I sincerely hope that on Thursday afternoon you will agree with me that the Seventh RI Conference was a very valuable means of exchanging technical information dealing with electromagnetic compatibility.

KEYNOTE ADDRESS

# BY-PRODUCT OF THE ELECTRONIC REVOLUTION

Brigadier General John A. McDavid
Director, Communications-Electronics
Joint Chiefs of Staff

It is a personal pleasure to appear before this group as it prepares to continue its attack on one of the most insidious by-products of what can properly be called the "Electronic Revolution" -- radio frequency interference. I hope to give you some thoughts to tickle your gray matter at the inception of your conference.

I refer to the "by-product" as insidious because of the deceptive way in which it has come to plague our progress toward fulfillment of the promise of electronic technology. Since Marconi first spanned the English Channel, this by-product -- RFI -- has been spinning its web in near secrecy while we have concentrated our attention on building more and better electronic mousetraps; in other words, we have been preoccupied with the premium that has been placed on the extension of the state of the electronics art and its adaptation of our most vital resources -- the radio frequency spectrum -- rather than toward efficiency and conservation.

Since the end of World War II, pressure on the spectrum has increased at a rate many times that realized in expanding the efficiency of its use. In fact, during the same period which has witnessed a mushrooming growth in demands on the spectrum there has been an incredible lack of reduction in the

waste of this vital resource. True, the capability to use higher frequencies has greatly increased and the 1959 International Radio Conference extended allocation control to 40,000 Mc. But you know as well as I do that usage above 10,000 Mc is still extremely limited.

Meanwhile, reliance on propagated radio energy has grown by leaps and bounds. Think of the tremendous growth in public and private microwave since the installation of the first commercial system in 1948. Think of the expansion of the land mobile radio service -- originally exclusive to police operations, it now includes just about every service activity, public and private, that you can name, from public utilities to diaper pick up. Today there are close to one million transmitters in the United States in this service alone. It is estimated that the figure will triple in ten years. Consider the growth in aircraft radio requirements, almost all of which has occurred since World War II. These are just a few examples and I haven't even mentioned the phenomenal growth of military dependence on radio.

In contrast with this growth in demand, the efficiency with which we use the spectrum has advanced quite slowly. We still use channel widths many times as wide as the intelligence we transmit; we still use antennas that spray energy all over the landscape across wide frequency ranges; we still depend on tubes and components such as the magnetron, which wander aimlessly through large chunks of the spectrum.

I do not imply that we have made no progress in the matter of better use of the spectrum. There have been numerous advances such as the development

of Single Sideband, more efficient antenna systems -- in terms of directivity and the suppression of spurious and harmonic emissions -- greater frequency stability in many applications, and significant compression of the intelligence to bandwidth ratio in some instances. It's not that there hasn't been improvement, it's just that demands are growing so much faster than improvements.

However, emphasis on this aspect of electronics is growing rapidly. A serious awareness of its importance has developed, some of which has assumed spectacular proportions as, for example, the Congressional concern and intense national interest in the frequency aspects of the VHF/UHF television problem and space communications. There is a growing and healthy realization that we are faced with a degree of necessity that will no longer be denied.

You are all aware to one degree or another, of the phenomenal growth in military dependence on electronics. After all, most of the enterprises which you represent have been directly involved in that expansion. In modern warfare, the compression of time and distance has become the common denominator of operation. Greater dependence on electronics is the inevitable result. The small geographical area occupied by a field army on today's battlefield contains some 60,000 emitters of radio energy, compared with the approximately 15,000 present in World War II. A guided missile cruiser carries nearly 1200 pieces of electronic equipment, compared to less than 300 on a World War II ship of the same size. A modern interceptor requires 7,000 electron tubes and transistors, compared to less that 200 in a World War II interceptor. The need for maintaining operational control of high-speed aircraft, the advent of guided missiles as a primary means

of armament, prospects for the use of satellites, the unprecedented demand for responsiveness from early warning systems, and many other similar facts and circumstances make realistic and determined attention to the problem of radio frequency compatibility among all these uses an urgent necessity for national defense.

I believe it is safe to conclude that the lack of motivation in this area is a thing of the past. A positive effort to enhance compatibility is now a reality.

I refer specifically to what has been named the Department of Defense Electromagnetic Compatibility Program. The name isn't important, of course. It could have been called the Program for the Reduction of Radio Interference or some other. It is its objective that counts.

That objective is straightforward and deceptively simple: to ensure, to the maximum practicable extent, that military electronic systems will not suffer operational degradation due to the absence of appropriate means for rejecting interference.

The first step in implementing an objective is to understand it, and, as obvious as that step is, I can assure you that a common understanding isn't easy to reach. With that in mind I will endeavor to elaborate the objective of this program as we see it.

The key element in understanding the objective and approaching it with realism, is an understanding of the term "degradation." Degradation is relative

and cannot be defined in simple "one-two-three" terms. [illegible]
multitude of variants that the primary factor becomes judgment. In the sense intended in the objective of the Defense Compatibility Program, "degradation" means that a transmission fails to serve its purpose.

Marginal circuits are not at all uncommon among military operation, particularly in the field, where tolerable levels of interference are considerably different from those acceptable in commercial practice. But a large amount of intelligence can be the victim of the narrow margins existing. It is our purpose to minimize that loss. Furthermore, the steady growth in the automation of electronic systems is constantly lowering the threshold of operational degradation.

This does not mean, however, that we expect to achieve perfection in military electronic systems, with respect to either the interference or the degradation that results therefrom.

We do expect the maximum practicable improvement. That is the practical objective of the Defense Radio Frequency Compatibility Program.

The effort necessary to accomplish this objective embaces a tremendous range of activity, much more than described by Richard Haitch in his recent fine article in the Saturday Evening Post. Mr. Haitch referred to the program as ".....an enormously ambitious attempt to 'fingerprint' every type of electronic equipment owned by the military.....and to analyze these (fingerprints) for potential interference with other equipment."

Our intentions are even more ambitious. Increased compatibility, or reduced interference, among existing equipments is our immediate objective but the longer range objective is built-in compatibility for equipment which hasn't yet reached the drawing board. We must build maximum practicable compatibility into every component, every black box and every system we engineer. We must ensure that these equipments and systems are accomodated within the radio frequency spectrum -- that they have their respective places in the sun -- in terms of the operational electromagnetic environment they will encounter. Only by the accomplishment of this entire spectrum of purposes can we put in the hands of military commanders the equipment and systems which will fulfill their intended operational purposes.

The program to attain this goal obviously embraces both research and development and operational areas of activity. It provides for the development of improved measurement techniques and test procedures and better test equipment to enable the collection of a complete and accurate picture of transmitter radiation and receiver susceptibility. It provides for research leading to improved performance by tubes and components -- greater stability, reduced power variation and tunability. Antennas and their associated circuitry, oscillators, filters, multipliers, non-linear devices and power amplifiers are all included.

Attention to tubes and components is only part of the task, however. The equipments which use them have specific characteristics which contribute or react adversely on the electromagnetic environment. A specific, positive effort to minimize that contribution or reaction must be prosecuted.

Aside from the dollars required to underwrite the program, the key to success lies in the availability of complete and reliable data and the capability to analyze it. This thought brings us to the data collection and analysis parts of the program.

The data required is of two fundamental types -- spectrum signatures and a picture of the operational environment.

The term "Spectrum signature" is the popular name for the package of data which describes the radiating or receiving characteristics of equipment. The procedures, methodology and equipment involved in collecting this package could probably be best described as embryonic. The exact data required for reliable prediction and control of interference are not known completely. But good progress has been made toward defining the information needed.

Immediately after the program was approved, a joint effort was undertaken by the Army, Navy, and Air Force to prepare plans for the collection of spectrum signatures and environmental data. It was recognized that whatever plans were produced would require early revision but it was also appreciated that we had to start filling the void in this area if the program was ever to be effective. The first tangible result of this effort was the approval and issuance of the "Military Spectrum Signature Collection Plan," more than 500 copies of which were widely distributed in government and industrial circles. The drafting and publication of such a comprehensive document only three months after the program was approved attests to the enthusiasm and determination of those responsible. There was never any doubt that it represented a first cut, that it

would require substantial revision. It has now undergone its first collection test, been reviewed by government and contractor representatives, and revised in collaboration with the analysis facility contractor. The revised collection plan was promulgated on 1 September and has been distributed even more widely than the first version. It can be anticipated that it, perhaps with additional revisions as a result of experiences with it, will become a standard for more effective control of the design and production of electronic equipment.

While the term "spectrum signature" denotes the data with which designers and manufacturers will be in closest association, the operational environment data is equally vital to the success of the DOD program. Without knowledge of the operational configuration and physical environment in which equipments and systems will operate and the manner in which they will be used, their spectrum signatures will be of limited use.

Picture if you will the enormity of the problem of establishing and analyzing the operational complex of 60,000 emitters in a field army, all either mobile or transportable, their positions changing in conformance with tactical requirements. Large naval and air formations confront us with the same problem and when you think in terms of a large joint amphibious assault your head really begins to ring.

Development of the capability to cope with such situations is obviously a tough nut. However, as in the case of signature collection, an early first cut has been taken and is currently under revision on the basis of experience and increasing understanding within the Department of Defense.

This revision takes into account the results of pilot projects directed for the purpose of confirming or refuting the course we were on. These projects -- in the San Diego, California and Montgomery, Alabama areas -- are serving as valuable proving grounds for the signature and environmental data collection plans. You will hear more about them later this morning and about the closely related tests to validate the mathematical models that hold the key to rapid, reliable analysis of the signature and environmental data and the consequent prediction of interference.

Gathering this data is a costly operation and there are severe handicaps to be overcome. In the field of measurement, techniques and equipment require major improvement. The search for solutions to these problems is underway and, as the history of military electronics progress relates, private enterprise -- the electronics industry of the United States -- will play an important role in this search.

Accurate and reliable data is of extreme importance but of itself it will accomplish very little. It must be analyzed in such a way that reliable conclusions can be drawn -- conclusions that lead to positive action to bring RFI under control and increase the efficiency with which we use vital frequency resources.

Toward the fulfillment of this requirement the DOD Program provides for a joint analysis facility under the direction of the Director for Communications-Electronics for the Joint Chiefs of Staff and the Director of Electronics for the Research and Engineering. The Department of the Air Force has been

assigned the mission of establishing the Electromagnetic Compatibility Analysis Center at Ananpolis, Maryland under coordinated policy direction from those two offices. Permanent housing facilities are scheduled for occupancy in February; staffing is approximately 60% complete. Colonel Charles C. Woolwine, the Director of the Center, will give you more details on its status and prospects.

The technical program of the Center which Mr. Stan Cohn, the Director of Technical Operations at the Center, will cover in some detail, is well under way. On the basis of the data being collected and furnished by the Military Departments under the data collection program I have described, the data base is being established in a form suitable for computerized analysis. The development and validation of mathematical models, the installation of the computer and the establishment of the technical reference library are all being actively prosecuted.

The first output of operational significance is expected from the Center in December. From that time the quantity and quality of output will increase as rapidly as data can be collected and larger models validated. Close control will be exercised as Colonel Woolwine will explain.

It's fairly obvious that the Analysis Center is the heart of the program but care has been taken to avoid encumbering the analysis mission, for which the Center was established, with other aspects of the program. The research and development and data collection programs which I have described have been made the responsibilities of the Military Departments, directed and coordinated by Jim Bridges, the Director of Electronics, Director of Defense Research and

Engineering and, myself, the Director for Communications-Electronics, Joint Chiefs of Staff.

Still in the study stage is the use of simulation techniques to enhance the versatility of the analysis capability and to facilitate the prediction and control of RFI at the earliest possible time in the engineering and development of equipment and systems. When I refer to a study, I do not mean, however, that we are just thinking about it. A contract for a feasibility study has been let.

No one dares to predict at this time what ultimate level of achievement will be reached in this program, though a high degree of effectiveness is certainly anticipated. Unquestionably we won't move as fast as we would if there were no constraints. Technological progress is not going to be suspended while we catch up in the control of interference. Nor can we scrap everything, or even the worst culprits, and start from scratch. Even if we could we would be constrained by the fact that the frequency spectrum is a public domain. We can't use it arbitrarily but must conform with national and international plans, regulations and treaties.

As I have suggested, the earliest payoff from this extensive undertaking will be in the area of alleviating existing problems. Solutions may take the form of equipment and system modifications or revisions of operational plans.

Frequency planning techniques will be reviewed and revised to take advantage of the greater know-how that will develop and the computerized electronic data processing capability which will be available.

Emphasis will gradually shift to the design and engineering phase of equipment development as improvements in tubes and components permit greater efficiency in the use of the spectrum and as the capability for earlier identification and control grows.

The frequency allocation process, by means of which control is exercised over the use of the spectrum by military equipments, will be improved. As the preciseness and accuracy of frequency allocation decisions increases, the control exercised can be tightened. Conflicts can be largely eliminated before they occur.

The end result of these payoffs will be minimum degradation of electronics operations, the main objective of the Department of Defense Electromagnetic Compatibility Program.

Ambitious? Sure, it's ambitious. And there are a lot of problems that have to be solved. But the hazards of radio frequency interference must be reduced drastically and this program is a major step in that direction -- positive, determined action instead of talk.

Success in this undertaking is one of the most important tasks facing the communications-electronics community. The increasing frequency of meetings such as this, the growing interest and concern throughout the industry and the dedication of you and others like you make it a foregone conclusion that we will realize success.

We don't expect a spectacular effect overnight; we do anticipate radical results in time, with a consequent better capability to meet the constantly growing challenge which military operations present to the communications-electronics community. The Defense Electromagnetic Program provides a realistic vehicle for an all-out attack on the gremlin of all gremlins -- at least to the communicators -- the by-product of the electronics revolution -- radio frequency interference.

# THE MISSION AND OPERATING PHILOSOPHY OF THE ANALYSIS CENTER

Colonel C. C. Woolwine
Electromagnetic Compatibility Analysis Center
Annapolis, Maryland

Abstract. - This paper discusses four areas involving the Electromagnetic Compatibility Analysis Center, which has recently been established by the Department of Defense in Annapolis, Maryland. These areas are:

1) BACKGROUND
2) MISSION
3) ORGANIZATION
4) OPERATING PHILOSOPHY

The paper traces the steps which took place to establish the Analysis Center, some of the tasks which have been assigned to it, and the methods which have been used in an attempt to insure the success of its operation.

## BACKGROUND

On 19 July 1960, Mr. James H. Douglas, Acting Secretary of Defense, sent a memorandum to the Secretary of the Army, the Secretary of the Navy, and the Secretary of the Air Force, in which he defined the policy and identified the action that was to be taken by the Department of Defense in order to cope with the interference problem.

Subsequent to Mr. Douglas' memorandum, Mr. Roswell S. Gilpatric, Deputy Secretary of Defense issued a memorandum of 25 September 1961, to the Director of Defense Research and Engineering, and the Chairman, Joint Chiefs of Staff in which it was recommended that each designate a representative to take action jointly in carrying out the Electromagnetic Compatibility Program as set forth in Mr. Douglas' memorandum.

It is stated that the ECAC, as part of the Compatibility program shall be a joint activity of the three Military Departments, subject to the authority direction and control of the Secretary of Defense.

In addition, Mr. Gilpatric's memorandum designated the Department of the Air Force as the responsible agency for establishing the ECAC and developing its capabilities in accordance with the policy guidance probided by the designee of the DDR and E in coordination with the designee of the JCS.

It is within the scope of these documents that the ECAC was founded and will initially operate.

## MISSION

The mission of the Electromagnetic Compatibility Analysis Center is to provide to the Department of Defense the analytical capability to determine whether electronic systems will suffer operational degradation due to the absence of appropriate means for rejecting interference. Also to provide a means whereby recommendations may be made which will insure, insofar a practicable, the capability of electronic systems and equipments to operate in the intended environment at designed levels of efficiency without degradation due to unintentional interference.

One of the major tasks that has been handed the Center is to establish a "Data Base" adequate to satisfy the Center's three broad mission objectives. These objectives are (1) to predict interference potentialities among military electronic equipment under operational environment conditions, (2) provide means whereby improved radio frequency management may be exercised within the Military Services, and (3) provide consultant service to the three services research and development programs in the electromagnetic compatibility area. All work performed by the Center, all data furnished by the Center to other agencies, and all support and consultant services performed by the Center will result from and directly depend upon the data base. The tools are now being developed to establish this data base. The paper by Mr. Cohn discusses this in more detail.

## ORGANIZATION (Figure 1)

The organization is that which will produce the team which is best suited to fulfill the first years requirements and does not reflect the manning which will be required to support the future program.

The box that contains the Director and Technical Director will manage and guide the overall activities of the Center. In order that this group might better fulfill its responsibilities, a Scientific Advisor will assist the Director in arriving at sound technical decisions as they affect the Center.

The boxes labeled DEP/DIR, ARMY, DEP/DIR, NAVY and DEP/DIR Air Force will assist the Director of the Center to more appropriately carry out his Joint-Service responsibilities. This will keep the Director apprised of the interest of each service and also provide the channel for each service's inputs to the Center.

The operating management function is centered in the contractor, Armour Research Foundation, the box labeled Technical Operations, whose primary responsibility is the detailed technical accomplishment of directed programs and projects.

## OPERATING PHILOSOPHY

The organizational structure, although straightforward, is unique in that it is designed to accomplish two separate objectives. The first of which is to provide a common ground upon which the three military Departments can meet and present their individual and common problems in the electromagnetic compatibility area and seek solutions to same. In addition, that of providing a base for cross coordination of required research and development effort in this area in the respective services programmed effort for same. The second is that of assigning programs and projects to the Center contractor and providing the mechanism whereby the resultant knowledge which will be accumulated can be made available to the services and industry.

Management of this effort is accomplished by adherence to the fundamental and well-established principle of the vertical classification of management function, corresponding to top management, staff and operating management.

This alignment of management functions is reflected in the organization of the Electromagnetic Compatibility Analysis Center whereby the Director, Technical Director, and Deputies represent top management and are responsible for the policies, procedures and organizational facilities necessary to accomplish the assigned mission.

The staff function is obtained through a logical grouping of closely related work problems into areas corresponding to the mission role or intended application of the work. These specialized work areas are supervised by Chiefs who are responsible to the Director for appropriate actions related to the orderly and timely accomplishment of the imposed workloads.

The operating management function is centered in the contractor (Armour Research Foundation) whose primary responsibility is the detailed technical accomplishment of directed programs and projects.

The programs and projects usually have their origin outside the Center and flow to the Center through the Deputy Directors. The Deputies perform an initial evaluation of the program or project to determine the validity and then pass it on to a Board; chaired by the Technical Director, and consisting of the Scientific Advisor, Deputies, Chief of Plans and Programs, and Director of Technical Operations where it is explored with regard to feasibility within present state-of-the-art, available resources, and priority with respects to other programs and projects. The output of the Board will be a programs and project schedule which will flow to the Center Director for his consideration and coordination and hence to the Plans and Programs Office for incorporation into the Center's program schedule. In all cases where there are unresolved factors such as priority, etc., the proposed program and projects schedule will flow from the Center Director to the DOD/JCS Board of Governors for resolution and hence back to the Center as program directives.

Implementation of a program or project, as based on an approved plan, means that a program or project has been launched with definite predetermined objectives in mind and contemplates certain output delivery schedules. Immediately, however, there are two major problems of control, one of which is to keep the program in consonance with the original plan and objective except for necessary deviation in the technical areas, the other is the problem of extraneous influences tending to reorient or realign the program or project in some major way. These two problems are in fact the basis for an operating procedure that is designed especially to cope with these distinct categories of control.

Referring to the organization chart, the Chief of Plans and Programs will be the medium through which top management, is kept appraised that established programs are kept on schedule and headed toward their predetermined objectives. He will have no direct responsibility for the activities that involve major program changes and, therefore, is mainly concerned with the control of programs or projects as directed at any particular time.

In the other category, i. e., the control of factors tending to realign the objectives or schedules of established programs, the Director and his immediate staff will normally conduct the investigations and make the contacts for establishing a Center position.

These two areas of control or separation of functions do not relieve the Director from full accountability for the Center's activities and actions. Coordination is the answer to any procedure that involves a Joint Service effort and it is intended that close coordination will be effected on all important actions, either current or contemplated.

In closing, I want to state that the success of this program depends on two major elements. One, the Data that we consider as the Life Blood of the Center, without which it cannot live. Two, the Research and Development that we consider as the red marrow or origin of new Blood. Without this new Blood the Center cannot grow and flourish but only stagnate and ide. I want to quote from a speech given by Mr. Bridges, Director, Office of Electronics ODDR and E to the FCWG/AFTRCC. "I want to state that the success of this program depends very critically upon the cooperative efforts of R and D and operational management people in DOD and the understanding and assistance of the industry that develops and produces the kind of weapons and equipments involved." We at the Center see the overall DOD program as portrayed in Figure 2.

For the Center to successfully accomplish its mission and in order for the overall DOD program to succeed it is essential that all areas be given wholehearted support.

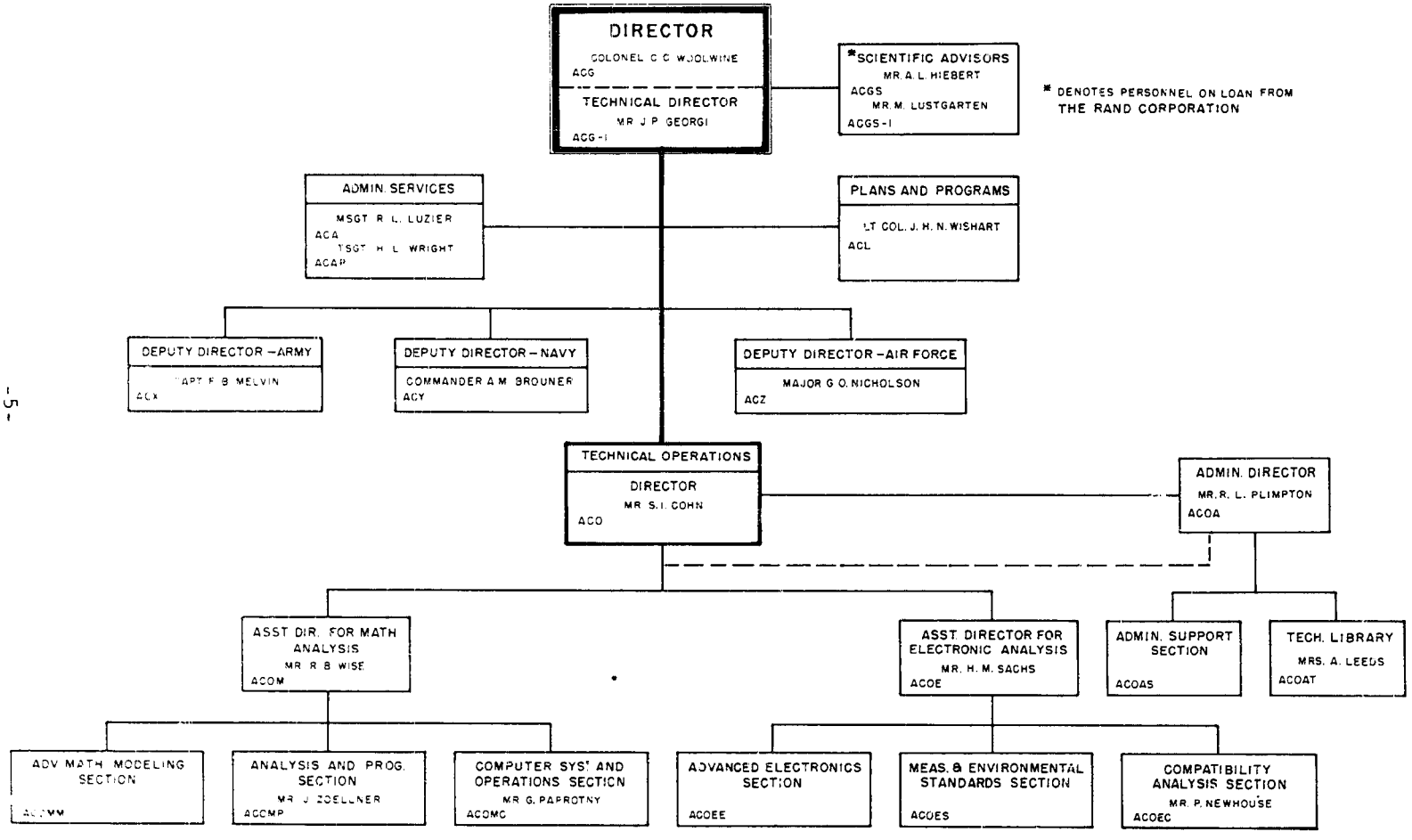



FIG. 1 ORGANIZATION OF ELECTROMAGNETIC COMPATIBILITY ANALYSIS CENTER

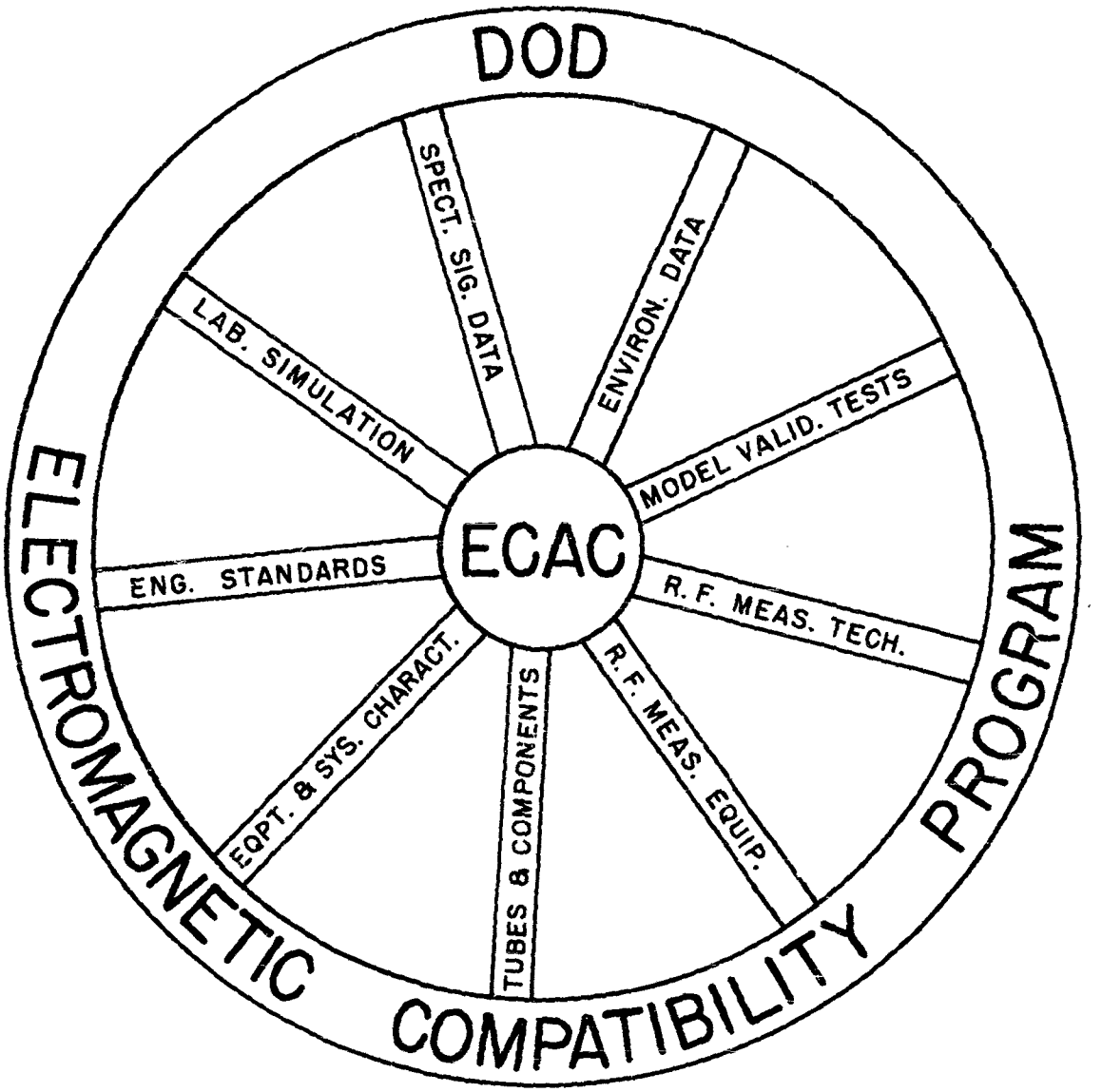



FIG. 2 OVERALL DOD ELECTROMAGNETIC COMPATIBILITY PROGRAM

# THE TECHNICAL PROGRAM OF THE ANALYSIS CENTER

S. I. Cohn
Electromagnetic Compatibility Analysis Center
Armour Research Foundation
Annapolis, Maryland

Abstract. - The technical program of the Electromagnetic Compatibility Analysis Center is composed of four broad categories of effort. These are (1) the acquisition of the data base (2) the formulation and adoption of validation tests (3) establishment of permanent facilities and activities, and (4) operational problem analysis.

This paper covers the progress which has been made on this technical program. In addition, a discussion of the plans for effort in the immediate future is also given.

## I. INTRODUCTION

To understand the various functions that must be performed at the Electromagnetic Compatibility Analysis Center, it is best to consider first the given input and output information required. Input information consists basically of military situations and equipment deployment (environmental data) as well as the data regarding the characteristics of electronic equipment (spectrum signatures). The required outputs are descriptions of environmental interaction, frequency allocation data, operational procedures needed to increase compatibility, and possible interference and susceptibility reduction measures for offending equipment. From these results better utilization of the radio frequency spectrum, both in the frequency allocation and equipment characteristics areas, should be obtained. Although initial emphasis will be placed on radar, the Analysis Center will eventually attack problems in the communication area.

Since the spectrum signatures of equipment are rather complex and hand calculations of the interaction of equipment are quite lengthy, it is obvious that automatic processing must be used to evaluate compatibility in any realistic military situation. This requires that spectrum signatures and environmental data must be maintained in a central library in a form that is suitable for a computer. In order to process these data one must use a mathematical model which is a computer representation of the situation and physical phenomena to be analyzed.

Data processing techniques for analysis of compatibility are relatively new, and effort must be directed toward refining these and

developing more sophisticated computer programs for analysis. In addition, techniques of operations research must be developed and applied to determine optimum frequency allocations and operational procedures that will enhance compatibility. Methods of handling the immensely complex results of the analysis must also receive consideration. This requires research in the application of data read-out systems, map printing, and environmental display techniques to facilitate comprehension of staggering quantities of interrelated data.

Another factor that will be considered is the validity of the data to be used. As experience is gained in compatibility analysis, the accuracy and types of data required will change in order to obtain more meaningful results. The Analysis Center staff must respond to these changes by aiding in revisions of data collection standards, both in the spectrum signature and environmental data areas. Measurement techniques must be reviewed and revised periodically, taking into account resulting data accuracy, ease of measurement, and instrumentation requirements.

It is anticipated that the analytical results will point up problems in equipment characteristics. Possible corrective measures for reducing interference susceptibility and undesired radiation must be proposed. These may take the form of equipment circuit modifications or addition of selective filters. In certain cases, it may be wise to replace certain types of equipment because of poor compatibility characteristics.

In the case of equipment under development, compatibility analysis can be a design aid by pointing out which equipment characteristics need improvement. Along these lines technical personnel must not only be familiar with the state of the art in interference reduction but must also be aware of new equipment developments. New techniques in the rapidly changing electronics art must be examined for possible interference problems so that electromagnetic compatibility will be considered by the designers of future complicated equipment. This is of paramount importance since equipment designed for compatibility will cost far less than equipment that has to be modified to reduce interference.

The knowledge that the Electromagnetic Compatibility Analysis Center will accumulate must be made available to others concerned with various facets of the overall compatibility program if the maximum benefit is to be obtained. To this end the Analysis Center must aid the military services by providing required consultant services and by preparing information to be included in manuals and specifications.

Anticipated areas of consultation include equipment standards, measurement techniques, instrumentation, data collection methods, interference reporting techniques, field test, susceptibility and inter-reduction techniques and devices, transmitting and receiving equipment, future equipment requirements, simulation methods, and design procedures for equipment.

The technical program of the Analysis Center is composed of four broad categories of effort. These are (1) the acquisition of the data base, (2) the formulation and adoption of validation tests, (3) the establishment of permanent facilities and activities, and (4) operational problem analysis.

## II. DATA BASE

One of the most important functions of the Analysis Center is the establishment of the data base. All work performed by the Center, all data furnished by the Center to other agencies, and all support and consultant services performed by the Center will result from and directly depend upon the data base. The tools are now being developed to establish this data base. It will be only through analysis, review, and model validation, and through continued analysis of predicted results in operational problems that the Center will develop the necessary sophistication and refinements of this data base. The data will consist of:

a. Spectrum signatures of all military electronic equipment designed to emit or receive. A spectrum signature is a complete characteristic description of the significant outputs of an emitter throughout the frequency spectrum and a similar description of the response characteristics of a receiver.

b. A complete description of the operational or proposed useage and location. The environmental file will contain the geographical location of the emitters and receivers, hours of operation, authorized frequency, bandiwdth, height of antenna, etc.

In addition to these data supplied to the Center, the following information is being obtained for supplementary data:

a. Technical literature (T.O.'s, T.M.'s, schematic diagrams, etc., on all military emitters and receivers).

b. Current and future R and D programs of the military services concerning development of electronic-electromagnetic equipment, measuring equipment, testing procedures and system compatibility testing.

c. Engineering standards, and

d. Interference reports.

From this data base, the ECAC will develop a comprehensive electromagnetic compatibility analysis program analyzing present and projected electromagnetic operational environments by (1) developing mathematical computer models of the operational equipment and environment, (2) predicting the degree of degradation (present and projected), (3) providing recommendations leading to improved electromagnetic compatibility in future designs and to modifications to present equipment, (4) providing information to facilitate planning of frequency allocations and assignments, (5) providing

information to facilitate the operation of an electromagnetic compatibility simulation facility and (6) furnishing assistance or consultant services to the military departments as requested in the areas covered by the data base and in the education area.

1. Spectrum Signatures

The Spectrum Signature Collection Plan has been revised with the aid of a joint committee in early May. The plan has been approved by DOD and the three military departments and was published on 1 September 1961. Further revisions to the plan are being considered which will involve guided missile systems, tracking radars, homing systems, non-conventional radar and communication systems, and 3-D antenna patterns.

The Center recognizes the fact that obtaining this data is very costly. Plans are being formulated and some work has started in synthesis of spectrum signatures. It is, however, too early to predict how much of this data can be synthesized and how much must be measured.

A number of research and development contracts are also underway in the measurement area. It is believed that the resulting techniques and equipment will play a significant role in simplifying spectrum signature measurement.

2. Environmental Data

The environmental data sheets for the San Diego area have been reviewed by Center personnel. This review brought up a number of possible misinterpretations of some of the questions on the form. Together with a joint committee the form was revised to reflect these changes and has been tested in a limited number of cases. A few further revisions to the form were necessitated by these tests. It is believed that the form is now adequate for collecting environmental data.

In order to process the forms in a most expeditious manner, it was decided that an automatic process to transfer the written information to magnetic tape would be desirable. Discussions with the Bureau of Census revealed that these forms could be designed in a manner which would allow processing on a mark sensing device (FOSDIC). Arrangements have been made with the Bureau of Census for aid in printing the forms and processing the completed forms to an output tape.

## III. MODEL VALIDATION

Since one of the primary tasks of the Analysis Center is the computation of signal density and prediction of interference by analytical means, it is essential that valid and appropriate mathematical models be formulated. Mathematical models are computer representations of the physical phenomena

and operational conditions. Since the reliability of analytical results will be no better than the reliabilities of the model and the input data, it is necessary that supporting information be supplied to determine the relative accuracy and possible limitations of any mathematical model that is employed.

A number of mathematical models for interference prediction have been described in the literature. Many portions of these models may be useful to the Analysis Center in conjunction with models developed at the Center. The validity of these models has not, however, been verified completely by experiment. To establish model validity on a full scale operational problem would require resources greatly in excess of those available. In addition, the amount of control that the Center would have in changing parameters or other measures required for validation in an actual operational situation would be quite limited. The resulting confidence in the evaluation of a particular model would therefore be low.

In order to obtain confidence in the analytical models to be used three model validation tests are being conducted. Each of these tests is designed to verify certain portions of the models and will be used to determine the usefulness of various approaches. The results of this procedure for model validation will result in a set of models which can be used in large-scale environments with a high degree of confidence.

The first model validation test is being held at NANEP at Patuxent River, Maryland. It is designed to provide two types of information. The first is a check on the Spectrum Signature Collection Plan at the equipment level. It is intended that revisions to the Collection Plan will be aided by these tests. The second portion of the test is a validation of a one-to-one radar prediction model between the AN/TPS-1D and AN/SPS-6C L-band surveillance radars. The test plan has been evolved and the spectrum signatures for the equipments are currently being obtained. The rest of the test will be completed and evaluated early next year.

The second model validation test is being conducted at the Verona Test Site of RADC. The purpose of this test is to establish the validity of the propagation models to be used and terrain reflection effects upon the one-to-one radar model. This test involves two L-band surveillance radars, the AN/FPS-20 and AN/TPS-1D. The measurements have started and they will be completed in early 1962.

The third model validation test to be held at Fort Huachuca, Arizona, will be a larger scale environment. A preliminary test plan on the test has been submitted and a more detailed test plan has been completed. Six or more M-33 S-band surveillance radars will be used. It is anticipated that these tests will be completed by and evaluated by mid 1962.

This process of designing and validating first a one-to-one model and then a more complex model allows for a logical buildup to a large scale model. Since each portion of the model has been verified experimentally the application of statistical data is the main requirement for a more complex case. Although the Center believes that this is the most logical way to obtain a solution to a large scale problem, this does not mean that all work on larger scale models must wait until the model validation tests are complete. Quite the contrary is true. As will be mentioned later, a great deal of work is going on on large scale models and the results of the various portions of the model validation process will be used as they become available. It is anticipated that no time delay will result in operational problem analysis from this process.

## IV. PERMANENT FACILITIES AND ACTIVITIES

Another major task of the Analysis Center is the establishment of a set of permanent facilities and activities. The permanent facilities will consist of a computer facility, Technical Library, Spectrum Signature File, Environmental Data File, and Interference Reporting File. The permanent activities include research in advanced models, analysis techniques, computation methods, visual display techniques and measurement techniques and equipment. Some of the salient efforts in this area are given below:

### 1. Computer Selection Study

The functions of ECAC will necessitate that the processing of a large volume of data as well as many scientific computations. A study of the various large scale digital computers which could be used by the Center has been made.

A comparison of these systems was made based on the Center's expected work load, the processing time of the computer, and various other features. The preliminary study completed by the Center has been forwarded to ESD for further evaluation.

### 2. Computer Input and Output Devices

A number of computer-associated devices will be required to process effectively data at the Center. Considering the requirements of the Center, a two-part study has been initiated, (1) to consider devices and methods for visual presentation of the computer output, such as scope displays and plotters, and (2) to study existing and projected spectrum signature measuring systems and techniques so that compatible data read-in devices may be acquired. These devices, which may be connected on-line or off-line to the computer, will be ordered early in 1962.

### 3. Computer Programming Activities

A continuing effort is being expended in the development of computer programs in support of the Center's activities. These include, for the Foundation's

UNIVAC 1105, partial support in major development efforts such as an ALGOL 60 translator and a general purpose statistical package as well as specific programs such as Fouier transform routines, etc. Following completion of staff training activities in October, concentrated efforts will be initiated for the development of service and utility programs for the Center's new computing facility.

4. Mathematical Models

Various computer models for the three levels of modeling anticipated; namely equipment models (receiver, transmitter, antenna, and propagation conditions), system models (a number of equipments plus deployment and operational conditions), and optimization models (changes in deployment, operational conditions, and equipment characteristics to improve compatibility) are being developed. In this process a review of currently used models is also being conducted.

At the equipment level the antenna, receiver, transmitter, and propagation models are being established in a building block fashion so that various degrees of complexity can be incorporated or removed in a relatively simple manner.

A number of problems in the prediction of antenna pattern characteristics are being studied. These include near field effects, effects of terrain on the antenna pattern, instrumentation for antenna pattern measurements, and statistical and quantized antenna patterns. The results of these studies will be used for the antenna portion of the equipment models.

In the area of system models, the literature has been reviewed and several existing models are being programmed for the 1105 computer in Chicago. The one-to-one system model is being developed and will be validated by the Verona and Patuxent tests described previously.

The literature is currently being reviewed for optimization models and their applicability to the frequency allocation and equipment modification area will be established.

5. Study of Frequency Allocation and Assignments Procedures

Since the Center will devote a major portion of its efforts to problems involving frequency allocation and assignment, it is essential that it be aware of current procedures and policies in these areas. When sufficient knowledge and pertinent data have been amassed, the Center is expected to be in a position to advise on and perform studies in these areas. In order to acquaint Center personnel with procedures used for allocation and assignment of frequencies for the military, a study is being conducted on this topic with the aid of the Joint Frequency Panel.

6. Interference Fixes Survey

The Center will conduct a continuing effort in the field of interference fixes. When experience is gained typical problems that arise will have known preferred remedies. In the event that extended analysis is not indicated, the Center may be in a position to recommend a preferred fix, or alternate fixes for many relatively simple interference problems. The knowledge in this area will also be applicable to large scale problems, requiring intensive analysis. The survey will include the nature or method of operation of the fixes and the expected interference reduction which would result from its use. Ultimately, each major item will be fully evaluated to determine its capabilities and limitations, including such items as cost and availability.

## V. OPERATIONAL PROBLEM ANALYSIS

One of the major outputs of the Center will be the analysis of specified operational problems. These tasks may include consideration of a single equipment in a relatively restricted environment or examination of a large number of systems. The results will be recommendations of various types, including; suggested changes of frequency allocation or assignment, time sharing arrangements, or technical fixes such as filters, signal discrimination devices, or recommendations for future specifications or design changes.

Two problems, the San Diego and MOADS problems, have been assigned to the Center. In a sense these problems are designed to permit the Center to develop its analytical capability on real, rather than a hypothetical problem although it is anticipated that useful outputs will be produced. It is contemplated that other problems in the ZI will be assigned to the Center in the near future.

1. San Diego

The San Diego L-band radar problem has been started. The environmental data which has been obtained is being put on tape for computer processing. Certain voids have been found and when the data has been completely analyzed, requests will be made for additional data. Definition of the specific problems and establishment of a model for this problem will be completed shortly. Results of analysis of this problem will depend on the availability of the spectrum signatures of equipments involved. These data are being obtained and when they are received at the Center, prediction of the interference conditions existing in this area can be made.

2. MOADS

The environmental data on MOADS (225-400 Mc) has been received. It will shortly be put on tape for computer processing and the data voids determined. When this is accomplished requests for additional data will be

made. An interim problem is being worked on in the MOADS area. This is a co-site problem involving a frequency diversity radar and a time-division data-link equipment. Spectrum signatures are not as yet available for this equipment and in the interim they are being synthesized from the equipment characteristics.

3. Zone of the Interior

Environmental data has been requested by the Center for radar and communication equipments within the Zone of the Interior. Specific problems in the ZI must be formulated before analysis can begin.

In addition to the above-mentioned problems, a survey is underway within ECAC on future problems which may be undertaken. Future allocation and utilization of the Center's resources will be based on this survey.

## VI. ACKNOWLEDGEMENT

The work described above is sponsored by the three Military Departments and is being conducted under Contract Number AF 19(604)-8440 with the Electronic Systems Division, Air Force Systems Command.

# A DIGITAL COMPUTER PROGRAM FOR REDUCTION AND PRESENTATION OF ELECTROMAGNETIC INTERFERENCE DATA

C. B. Pearlston, Jr.
Nortronics, a Division of
Northrop Corporation
Hawthorne, California

Abstract. - Many interference specifications for airborne electronic equipment require measurements to be made from 30 cps to 10 Gc, both for generated interference and susceptibility to interference. A minimum of three measurements are required in each frequency octave; measurements must be made on all power leads and interconnecting cables, and the equipment must be operated in each of its possible operational modes. The resultant of these measurements can total several thousand data-pieces for each equipment tested. These data-pieces must be adjusted by various correction factors, compared with the specification limits, and used to prepare data report sheets and graphs of the measured levels.

This paper will present a program, currently in use, which utilizes a digital computer for performing all the functions of data reduction and data report preparation. This program not only relieves the interference test engineer from the manual performance of this task, but has the advantages of eliminating human error and standardizing report format.

## I. INTRODUCTION

The amount of time required to perform interference and susceptibility measurements in accordance with the latest military interference specifications has increased considerably in recent years due to the extended frequency range over which measurements are required. For example, GM-07-59-2617A, among others, has extended the range downward to 30 cps, while MIL-I-11748B has extended the range upward to 36,000 mc. The range has approached the proverbial "dc to daylight". When it is considered that a minimum of three measurements of interference and a possibly greater number of susceptibility measurements are required for each octave of the frequency range, and that these measurements must be repeated on each power line and cable, for each mode of equipment operation, the number of information pieces needed and the corresponding time required approach considerable magnitudes. For example, the interference specification on a current Nortronics program requires 39 octaves of conducted interference measurements and 39 octaves of radiated interference measurements, in addition to a corresponding number of octaves for conducted and radiated susceptibility measurements. The resultant number of data-pieces approaches 10,000 for one typical, multimode, complex, airborne module.

Time and trained technical manpower are two of our most critical resources. To conserve these resources, our engineering manpower must be used in as efficient a manner as possible. One method of increasing this efficiency is by reducing the number of men and the time required to perform interference and susceptibility measurements. This approach leads to the development of automatic interfcrence and susceptibility measurement equipment. Many organizations, including Nortronics, are investigating this approach.

Another method of increasing engineering efficiency is by minimizing the engineering time required for the reduction and presentation of the interference and susceptibility data gathered. This approach has been adopted at Nortronics by utilizing a digital computer facility to process all interference and susceptibility data. The processed data is presented in a suitable standardized format which meets all the test report requirements of the military interference specifications. In addition, graphical presentation of the data is mechanized and automated.

The advantages inherent in this program over conventional manual interference data reduction techniques are of three types: 1) manpower is conserved by eliminating manual preparation of tabular data sheets and graphs, 2) human error is minimized by recording and reducing data in standardized, mechanized steps, and 3) report format is standardized for all interference and susceptibility measurements.

## II. INTERFERENCE DATA BOOK

The heart of the interference data reduction program is the interference test Data Book. This book is a numbered and bound volume of 50 pages, with each page numbered, and duplicate vellum tear-out sheets for each page. Figure 1 shows a sample data page. Space is available for recording 22 individual measurements of any specific interference or susceptibility type over certain defined frequency ranges. For example, measurements of conducted interference with a current probe over the frequency range of 30 cps - 15 kc would be on one data sheet; the same type of measurements from 15 kc to 150 kc would necessitate a separate data sheet, as would measurements with an LSN. The format of the program is arranged so that only those frequencies covered by one interference meter , or a tuning head of that meter, will be on one data page. All descriptions of test setup, test equipment, and other pertinent test details are contained in a separate Engineering Log Book, which is referenced on the page of the Data Book. As is seen from Figure 1, space is available on the data sheet for recording the date of test, the test sample serial number, the date of interference meter calibration, and the serial number of the interference meter used.

For each line of data, space is available for recording the band of the interference meter used and whether the meter is directly calibrated or if a substitution technique has been used. The frequency of measurement is recorded directly as would be indicated on the interference meter used, i.e., cps, kc, mc, or kMc. The meter-indicated interference voltage (in db relative to 1 uv or 1 uv/mc) is recorded, as well as the radiated ambient or internal meter noise level, depending on whether radiated or conducted measurements are being performed. Other spaces are available for recording the type of signal, CW or broadband, gain and bandwidth correction factors, and various mismatch, antenna, and transfer impedance factors. While determination of the calculated level is usually left for computer reduction, space is available on the data sheet to record it, if desired.

Naturally, when recording susceptibility data, several of the columns are not applicable and are left blank; only the frequency, measured susceptibility, and antenna factors for radiated susceptibility tests are entered. These empirically determined antenna factors serve to enable calculation of an approximate field strength or field intensity which simulates a given rf environment.

## III. CALCULATION CODE

The key to the data reduction program under discussion is the calculation code; this is a four-digit number with sign ($\pm$xxxx), which appears at the top of each data sheet. This number codes the information concerning type of measurement, frequency range of measurement, type of interference meter, type of pickup or susceptibility injection device, and the type of phenomena under measurement, as well as the instructions to the computer for the reduction and printout of the data. Figure 2 shows the inside front cover of a Data Book, wherein the calculation code is posted for convenient reference. As can be seen, any type of interference or susceptibility measurement in current usage from 30 cps - 10 kMc can be expressed by proper combination of the four digits and sign.

The sign, + or -, indicates whether a radiated or conducted measurement is being performed, and hence, whether the ambient reading recorded is that of the area or of the internal instrument noise level. The first digit of the calculation code specifies whether interference or susceptibility measurements are being recorded, and if interference measurements, which manufacturer type of interference meter is used. The second digit of the code defines the frequency range and, if appropriate, the specific interference meter used. The pickup or susceptibility injection device is indicated by the third digit of the code, and the fourth digit both indicates the type of measurement and controls the computation and printout format.

## IV. COMPUTER PROGRAM

After the data sheets have been filled out, the duplicate vellum tear-out sheets are forwarded to the computer data reduction facility where the information on the sheets is used to prepare punched cards. One master card, containing the information at the top of the data sheet (see Figure 1) and including the calculation code, is needed for each data sheet. Each line of data on the sheet requires an additional punched card, so that a maximum of 23 cards could be required for any one data sheet. After the master card and data cards are prepared for each data sheet, the computer utilizes a program as shown in Figure 3 to process and printout the data.

After reading the master card, the computer prints the title, reference data, date, and test sample serial number. The computer then compares the calculation code with the stored program and decides whether interference or susceptibility test data is being processed. In accordance with this decision, the computer prints the frequency range or interference meter used and the appropriate column headings. An auxiliary program, not yet in use, enables the notes on the data sheet to be included in the computer printout. The computer then prints the data contained on the punched card in the appropriate columns of the tab sheet. Figure 4 shows a sample printout for interference measurements. As this figure illustrates, the last three columns of the printout contain the significant test information, i.e., the corrected ambient level, the corrected true signal level, and the specification limit at that frequency. The true signal level used is the square root of the difference between the squares of the measured signal level voltage and the measured ambient voltage $(\sqrt{S^2-a^2})$. Since all measurements are recorded in db relative to one microvolt or one microvolt/mc, it is necessary for the computer to find the antilog of the recorded measured signal/10 and of the recorded ambient/10. These are subtracted, the log is found, multiplied by ten, and then the various correction factors are applied to give the corrected true signal level in db. Similarly, the specification limit at any frequency is found by calculating the logarithm of the frequency at which the measurement is made, multiplying it by a constant and then adding another constant to it. Each of the specification limit curves is thus broken into the form of $k(\log f) + c$, where k and c are constants and f is the frequency expressed in cps, kc, or mc.

Figures 5 and 6 are further illustrations of sample computer printouts for various interference measurements.

When processing susceptibility data, the information printed is the actual level of threshold susceptibility of the test sample, measured either in volts at the sample input, gauss, or volts at a radiating antenna. For radiated susceptibility measurements, an empirical antenna factor is applied which permits the calculation of an

approximate field strength or field intensity to which the equipment is being subjected. This level serves to give rough correlation with the expected environment to which the equipment will be exposed. Figures 7 and 8 show sample susceptibility printouts.

## V. GRAPHICAL PLOTTING

The time required to plot a graph of interference or susceptibility levels represents yet another costly use of engineering manpower. An automated approach can save much time in this area and has the further benefit of standardizing all graphical plotting. The simplest approach to mechanization consists of using an X-Y plotter (Mosley Autograf) with a digital keyboard (model 40c), in conjunction with a logarithmic converter (model 60B) for the X axis so that frequency may be displayed on a logarithmic scale. A character printer (model D-1A) is used on the plotter so that the ambient level and interference level for different modes of equipment operation can each be plotted with a different symbol. In this method of operation, the data is entered manually on the digital keyboard from the tabulated data sheets.

To fully automate graphical plotting of interference data, the computer which processes the data also generates punched cards (or tape) showing the calculated interference and ambient levels at each frequency of measurement. The cards (or tape) are then fed to an IBM 523 Summary Card Reader which is connected to a Digital Data Translator (Dymec DY-2742). This feeds the data through the logarithmic converter to the X-Y plotter at the rate of 50 points per minute. One plotting run is required for the ambient level and one for the signal level. Special graph sheets having the interference and susceptibility limits already printed thereon are used, and the only task required of the human operator is to insert these sheets into the plotter and to ensure its proper calibration.

## VI. CONCLUSION

The data program which has been discussed herein trades interference engineering manpower for computer time. The data reduction task of the interference engineer ceases upon filling out the data book page; the computer facility returns to him tabulated data sheets and complete graphs. Whether this choice is practical for all companies depends, of course, on the amount of interference data to be processed and the availability of computing and plotting equipment. For those companies having large amounts of interference work and the availability of computer data reduction facilities, the use of an automated data reduction and presentation program seems logical. Equally logical is the next step in the semi-automation of interference testing, wherein the data and all correction factors will be recorded directly on punched

cards by the interference meter operator, thus eliminating the need for manual recording of data. This finally leads to the completely automated operation of interference testing, wherein the interference meter has internal storage of all correction factors, and itself generates the punched cards, thus displacing the human operator. By feeding the punched cards directly to the X-Y plotter system, the interference meter will produce a rapid, graphical plot of all data. Thus, at some future point in time, the main task of the interference test engineer will be the evaluation of the test data, and a computer program can no doubt also be devised for that task. However, non-automated homo sapiens will continue to make fixes as required.

ACKNOWLEDGEMENT

**Appreciation** is extended to Mr. R. Thornton, formerly of Nortronics, who first formulated the data reduction program, and to Mr. J. Weiss of Nortronics, who prepared the complete programming for the IBM 1620.

## ELECTROMAGNETIC INTERFERENCE MEASUREMENTS

NORTRONICS FORM 287 (8-61)

NORTRONICS

A Division of Northrop Corporation

**MASTER CARD:**

| NO. LINES OF DATA | CALCULATION CODE | LOG BOOK NUMBER | PAGE NUMBER | DATE TEST PERFORMED | SERIAL NUMBER OF TEST SAMPLE | DATA BOOK NUMBER | PAGE NUMBER |
|---|---|---|---|---|---|---|---|
| 1 2 3 | 4 5 6 7 8 9 | 10 11 12 13 14 | 15 16 17 | 18 19 20 21 22 23 24 25 26 | 27 28 29 30 31 32 | 33 34 35 36 37 | 38 39 40 |
| | | | | | | A - 5 | 1 |

| DATE DETECTOR CALIBRATED | SERIAL NUMBER OF METER USED |
|---|---|
| 41 42 43 44 45 46 47 48 49 | 50 51 52 53 54 55 |
| | |

TEST ENGINEER

**DATA CARD:**

| CARD | SUBSTITUTION OR DIRECT READING TECHNIQUE | DETECTOR CENTER FREQUENCY (CPS < 15000, MC < 1000, KC < 150, KMC > 1.0) | MEASURED INTERFERENCE VOLTAGE: FI-CW, PEAK-BB (IN DB); OR MEAS. SUSCEPTIBILITY (IN VOLTS OR GAUSS) | AMBIENT OR DETECTOR NOISE (PEAK FOR BB, FI FOR CW) (DB) | TYPE SIGNAL (CW OR BB) | DETECTOR GAIN & BANDWIDTH CORRECTION FACTOR (IN DB) | LOSS, MISMATCH, ANTENNA, OR TRANSFER IMPEDANCE FACTOR (IN DB) | CALCULATED LEVEL (IN DB) |
|---|---|---|---|---|---|---|---|---|
| 1 | | | | | | | | |
| 2 | | | | | | | | |
| 3 | | | | | | | | |
| 4 | | | | | | | | |
| 5 | | | | | | | | |
| 6 | | | | | | | | |
| 7 | | | | | | | | |
| 8 | | | | | | | | |
| 9 | | | | | | | | |
| 10 | | | | | | | | |
| 11 | | | | | | | | |
| 12 | | | | | | | | |
| 13 | | | | | | | | |
| 14 | | | | | | | | |
| 15 | | | | | | | | |
| 16 | | | | | | | | |
| 17 | | | | | | | | |
| 18 | | | | | | | | |
| 19 | | | | | | | | |
| 20 | | | | | | | | |
| 21 | | | | | | | | |
| 22 | | | | | | | | |
| | 1 2 3 4 | 5 6 7 8 9 10 11 12 | 13 14 15 16 17 18 | 19 20 21 23 | 25 24 25 | 26 27 28 29 30 | 31 32 33 34 35 | 36 37 38 39 40 |

| INDICATED F.I. (DB) | INDICATED Q.P. (DB) |
|---|---|
| | |
| | |
| | |
| | |
| | |
| | |
| | |
| | |
| | |
| | |
| | |
| | |
| | |
| | |
| | |
| | |
| | |
| | |
| | |
| | |
| | |

| NOTES: | TYPE OF MEASUREMENT: | TEST SAMPLE: |
|---|---|---|
| | | |

Figure 1

## CACULATION CODE
### (a four digit number with sign: ± XXXX)

SIGN:

+ is for "area ambient" measurement

− is for "instrument ambient" measurement

FIRST DIGIT:

0000 Stoddart or Polarad FIM measurement device

1000 Empire Devices NF–105 or NF – 112 instrument

2000 indicates a susceptibility device

SECOND DIGIT (instrument and corresponding frequency range):

| | | | |
|---|---|---|---|
| 0100 | NM–40 | | ( 30 cps – 15 kc ) |
| 0200 | NM–10 | 1200 NF–105, TX–105 | ( 15 kc – 150 kc ) |
| 0300 | NM–20 | 1300 NF–105, TA–105 | (150 kc – 25 mc ) |
| 0400 | NM–30 | 1400 NF–105, T1–105 | ( 25 mc – 200 mc ) |
| 0500 | NM–30 | 1500 NF–105, T2–105 | (200 mc – 400 mc ) |
| 0600 | NM–50 | 1600 NF–105, T3–105 | (400 mc – 1000 mc ) |
| 0700 | URM–42 | 1700 NF–112 | ( 1 kmc – 10 kmc) |
| 0800 | FIM | | ( 1 kmc – 10 kmc) |

THIRD DIGIT (pickup or susceptibility device):

0010 Rod Antenna

0020 Current Probe

0030 Loop Antenna

0040 Horn Antenna

0050 Dipole Antenna

0060 Line Impedance Stabilization Network

0070 Broadband Antenna

0080 Isolation Transformer

0090 Capacitance Network

FOURTH DIGIT (type of measurement and computation scheme):

0001 RF Voltage

0002 Conducted Current

0003 Antenna Induced Voltage

0004 Electric Field Strength

0005 Field Intensity

0006 Magnetic Field Strength

0007 Audio Voltage

Figure 2

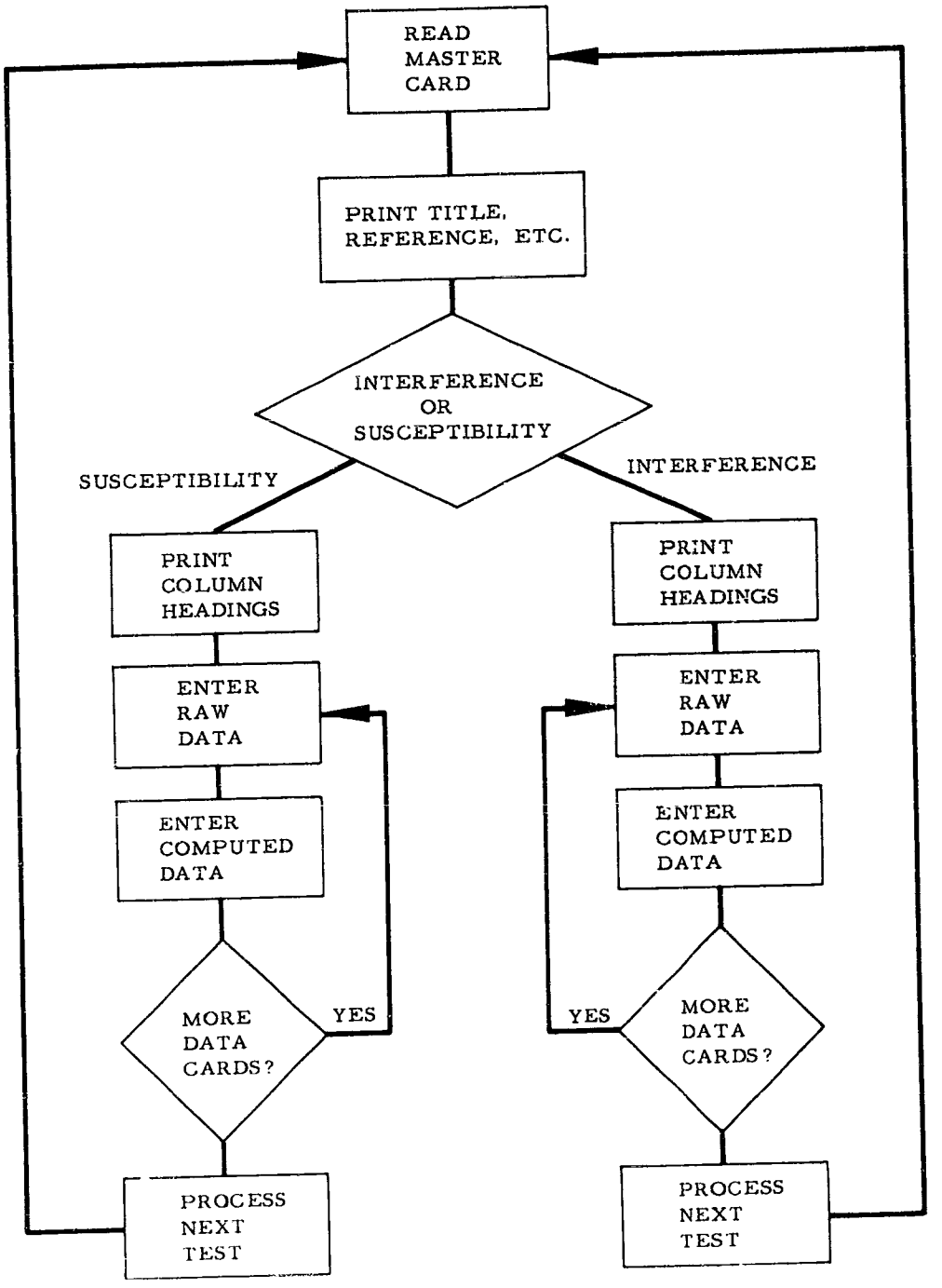

READ MASTER CARD
PRINT TITLE, REFERENCE, ETC.
INTERFERENCE OR SUSCEPTIBILITY
SUSCEPTIBILITY
INTERFERENCE
PRINT COLUMN HEADINGS
ENTER RAW DATA
ENTER COMPUTED DATA
MORE DATA CARDS?
YES
PROCESS NEXT TEST
PRINT COLUMN HEADINGS
ENTER RAW DATA
ENTER COMPUTED DATA
YES
MORE DATA CARDS?
PROCESS NEXT TEST

Figure 3

ELECTROMAGNETIC INTERFERENCE DATA

REFERENCE= LOG BOOK A-714 PAGE 22, DATA BOOK A- 2 PAGE 39, AUG 15 1961
TEST SAMPLE(462-3)
LINE MEASURED
EQUIPMENT= NF-105, TA-105 SERIAL NO. 1517 CALIBRATED JUN 14 1961

***RF VOLTAGE MEASUREMENTS(IMPEDANCE STABILIZATION NETWORK)***

| BAND | METHOD | DETECTOR CENTER FREQUENCY (MC) | MEASURED VOLTAGE PK(BB)-FI(CW) SIGNAL MET AMB | TYPE | DETECTOR GAIN AND BANDWIDTH FACTOR (DB) | SIGNAL LOSS CORR (DB) | CALCULATED LEVELS (DB*UV) OR (DB*UV/MC) FIFTY-OHM IMPEDANCE AMBIENT (DB) | SIGNAL (DB) | SPEC (DB) |
|---|---|---|---|---|---|---|---|---|---|
| 1 | S | 0.150 | 68.0 | 4.0 CW | 0.0 | 0.0 | 4.00 | 67.99 | 62.50 |
| 1 | S | 0.270 | 67.0 | 7.0 CW | 0.0 | 0.0 | 7.00 | 66.99 | 57.73 |
| 1 | S | 0.310 | 65.0 | 4.0 CW | 0.0 | 0.0 | 4.00 | 64.99 | 56.61 |
| 2 | S | 0.535 | 76.0 | 6.0 CW | 0.0 | 0.0 | 6.00 | 75.99 | 52.17 |
| 2 | S | 0.625 | 66.0 | 5.0 CW | 0.0 | 0.0 | 5.00 | 65.99 | 50.91 |
| 2 | S | 0.700 | 64.0 | 6.0 CW | 0.0 | 0.0 | 6.00 | 63.99 | 49.99 |
| 2 | S | 0.820 | 57.0 | 6.0 CW | 0.0 | 0.0 | 6.00 | 56.99 | 48.71 |
| 3 | S | 1.08 | 72.0 | 7.0 CW | 0.0 | 0.0 | 7.00 | 71.99 | 46.47 |
| 3 | S | 1.47 | 65.0 | 13.0 BB | 0.0 | 0.0 | 13.00 | 64.99 | 85.04 |
| 3 | S | 1.62 | 64.0 | 6.0 CW | 0.0 | 0.0 | 6.00 | 63.99 | 43.18 |
| 4 | S | 2.16 | 88.0 | 4.0 CW | 0.0 | 0.0 | 4.00 | 87.99 | 40.84 |
| 4 | S | 2.70 | 83.0 | 5.0 CW | 0.0 | 0.0 | 5.00 | 82.99 | 39.03 |
| 4 | S | 3.25 | 85.0 | 6.0 CW | 0.0 | 0.0 | 6.00 | 84.99 | 37.52 |
| 4 | S | 3.80 | 66.0 | 3.0 CW | 0.0 | 0.0 | 3.00 | 65.99 | 36.25 |
| 4 | S | 4.60 | 55.0 | 2.0 CW | 0.0 | 0.0 | 2.00 | 54.99 | 34.70 |
| 5 | S | 6.50 | 59.0 | 4.0 CW | 0.0 | 0.0 | 4.00 | 58.99 | 34.00 |
| 5 | S | 8.60 | 55.0 | 3.0 CW | 0.0 | 0.0 | 3.00 | 54.99 | 34.00 |
| 5 | S | 10.2 | 43.0 | 5.0 CW | 0.0 | 0.0 | 5.00 | 42.99 | 34.00 |
| 6 | S | 13.0 | 43.0 | 4.0 CW | 0.0 | 0.0 | 4.00 | 42.99 | 34.00 |
| 6 | S | 16.0 | 52.0 | 6.0 CW | 0.0 | 0.0 | 6.00 | 51.99 | 34.00 |
| 6 | S | 18.5 | 54.0 | 8.0 CW | 0.0 | 0.0 | 8.00 | 53.99 | 34.00 |
| 6 | S | 24.0 | 57.0 | 15.0 CW | 0.0 | 0.0 | 15.00 | 56.99 | 34.00 |

ELECTROMAGNETIC INTERFERENCE DATA

REFERENCE= LOG BOOK A-812 PAGE 24, DATA BOOK A- 2 PAGE 40, AUG 16 1961
TEST SAMPLE(143-2)
ANTENNA LOCATION
EQUIPMENT= NF-105, T1-105 SERIAL NO. 1517 CALIBRATED SEP 16 1961

***ANTENNA INDUCED VOLTAGE MEASUREMENTS(DIPOLE ANTENNA)***

| BAND | METHOD | DETECTOR CENTER FREQUENCY (MC) | MEASURED VOLTAGE PK(BB)-FI(CW) SIGNAL (DB) | RN AMB | TYPE | DETECTOR GAIN AND BANDWIDTH FACTOR (DB) | ANTENNA INDUCED VOLTAGE CORR (DB) | CALCULATED LEVELS (DB*UV) OR (DB*UV/MC) ANTENNA INDUCED AMBIENT (DB) | SIGNAL (DB) | SPEC (DB) |
|---|---|---|---|---|---|---|---|---|---|---|
| 1 | S | 25.0 | 48.0 | 0.0 BB | | 0.0 | + 8.2 | 8.20 | 56.19 | 43.81 |
| 1 | S | 26.0 | 52.0 | 0.0 BB | | 0.0 | + 8.2 | 8.20 | 60.19 | 44.51 |
| 1 | S | 28.0 | 53.0 | 0.0 BB | | 0.0 | + 8.3 | 8.30 | 61.29 | 45.83 |
| 1 | S | 31.0 | 51.0 | 0.0 BB | | 0.0 | + 8.3 | 8.30 | 59.29 | 47.64 |
| 1 | S | 35.0 | 50.0 | 0.0 BB | | 0.0 | + 8.4 | 8.40 | 58.39 | 50.04 |
| 1 | S | 40.0 | 46.0 | 0.0 BB | | 0.0 | + 8.6 | 8.60 | 54.59 | 50.46 |
| 1 | S | 50.0 | 54.0 | 0.0 BB | | 0.0 | + 8.7 | 8.70 | 62.69 | 51.16 |
| 1 | S | 60.0 | 57.0 | 0.0 BB | | 0.0 | + 8.7 | 8.70 | 65.69 | 51.73 |
| 2 | S | 70.0 | 54.0 | 0.0 BB | | 0.0 | + 8.8 | 8.80 | 62.79 | 52.22 |
| 2 | S | 80.0 | 53.0 | 0.0 BB | | 0.0 | + 8.9 | 8.90 | 61.89 | 52.64 |
| 2 | S | 90.0 | 55.0 | 0.0 BB | | 0.0 | + 9.0 | 9.00 | 63.99 | 53.00 |
| 2 | S | 100.0 | 57.0 | 0.0 BB | | 0.0 | + 9.1 | 9.10 | 66.09 | 53.34 |
| 2 | S | 110.0 | 55.0 | 0.0 BB | | 0.0 | + 9.1 | 9.10 | 64.09 | 53.63 |
| 2 | S | 120.0 | 57.0 | 0.0 BB | | 0.0 | + 9.2 | 9.20 | 66.09 | 53.91 |
| 2 | S | 130.0 | 54.0 | 0.0 BB | | 0.0 | + 9.2 | 9.20 | 63.19 | 54.16 |
| 2 | S | 140.0 | 56.0 | 0.0 BB | | 0.0 | + 9.3 | 9.30 | 65.29 | 54.39 |
| 2 | S | 150.0 | 44.0 | 0.0 BB | | 0.0 | + 9.4 | 9.40 | 53.39 | 54.61 |
| 2 | S | 160.0 | 48.0 | 0.0 BB | | 0.0 | + 9.5 | 9.50 | 57.49 | 54.81 |
| 2 | S | 170.0 | 56.0 | 0.0 BB | | 0.0 | + 9.5 | 9.50 | 65.49 | 55.00 |
| 2 | S | 180.0 | 48.0 | 0.0 BB | | 0.0 | + 9.6 | 9.60 | 57.59 | 55.18 |
| 2 | S | 190.0 | 44.0 | 0.0 BB | | 0.0 | + 9.6 | 9.60 | 53.59 | 55.35 |
| 2 | S | 200.0 | 42.0 | 0.0 BB | | 0.0 | + 9.7 | 9.70 | 51.69 | 55.51 |

ELECTROMAGNETIC INTERFERENCE DATA

REFERENCE= LOG BOOK A-546 PAGE 32, DATA BOOK A- 2 PAGE 41, AUG 16 1961
TEST SAMPLE( 892)
LINE MEASURED
RANGE= 30 CPS - 15 KC

***AUDIO VOLTAGE SUSCEPTIBILITY MEASUREMENTS(ISOLATION TRANSFORMER)***

| SUSCEPT FREQ (CPS) | THRESHOLD SUSCEPTIBILITY (VOLTS) | SPEC LIMIT (VOLTS) |
|---|---|---|
| 33. | 1.21 | 3.0 |
| 45. | 1.82 | 3.0 |
| 50. | 1.96 | 3.0 |
| 60. | 2.03 | 3.0 |
| 100. | 2.14 | 3.0 |
| 200. | 2.21 | 3.0 |
| 300. | 2.39 | 3.0 |
| 1000. | 2.66 | 3.0 |
| 1500. | 2.58 | 3.0 |
| 2000. | 2.92 | 3.0 |
| 3000. | 2.83 | 3.0 |
| 3500. | 2.64 | 3.0 |
| 4500. | 1.82 | 3.0 |
| 6000. | 1.81 | 3.0 |
| 8000. | 2.01 | 3.0 |
| 10000. | 2.00 | 3.0 |
| 10500. | 2.02 | 3.0 |
| 11000. | 2.21 | 3.0 |
| 12000. | 2.31 | 3.0 |
| 13000. | 2.42 | 3.0 |
| 14000. | 2.82 | 3.0 |
| 15000. | 2.99 | 3.0 |

ELECTROMAGNETIC INTERFERENCE DATA

REFERENCE= LOG BOOK A-546 PAGE 34, DATA BOOK A- 2 PAGE 42, AUG 18 1961
TEST SAMPLE( 892)
ANTENNA LOCATION
RANGE= 200 MC - 400 MC

***FIELD INTENSITY SUSCEPTIBILITY MEASUREMENTS(DIPOLE ANTENNA)***

| SUSCEPT FREQ (MC) | THRESHOLD SUSCEPTIBILITY (VOLTS) | SPEC LIMIT (VOLTS) | ANTENNA FACTOR (DB) | CALCULATED FIELD INTENSITY (DB*V/M) | (V/M) |
|---|---|---|---|---|---|
| 204.0 | 9.84 | 0.1 | - 8.0 | 11.85 | 3.917 |
| 210.0 | 9.42 | 0.1 | - 7.0 | 12.48 | 4.207 |
| 234.0 | 9.32 | 0.1 | - 5.0 | 14.38 | 5.241 |
| 250.0 | 9.21 | 0.1 | - 3.0 | 16.28 | 6.520 |
| 282.0 | 9.24 | 0.1 | - 2.0 | 17.31 | 7.339 |
| 298.0 | 9.28 | 0.1 | - 1.0 | 18.35 | 8.270 |
| 306.0 | 9.31 | 0.1 | - 1.0 | 18.37 | 8.297 |
| 310.0 | 9.12 | 0.1 | 0.0 | 19.19 | 9.119 |
| 312.0 | 9.04 | 0.1 | 0.0 | 19.12 | 9.039 |
| 325.0 | 8.94 | 0.1 | 0.5 | 19.52 | 9.469 |
| 328.0 | 8.92 | 0.1 | 0.5 | 19.50 | 9.448 |
| 330.0 | 8.43 | 0.1 | 0.5 | 19.01 | 8.929 |
| 335.0 | 7.92 | 0.1 | 0.5 | 18.47 | 8.389 |
| 338.0 | 7.93 | 0.1 | 1.0 | 18.98 | 8.897 |
| 350.0 | 7.95 | 0.1 | 1.0 | 19.00 | 8.920 |
| 355.0 | 8.00 | 0.1 | 1.0 | 19.06 | 8.976 |
| 360.0 | 8.05 | 0.1 | 1.5 | 19.61 | 9.567 |
| 370.0 | 8.10 | 0.1 | 1.5 | 19.66 | 9.626 |
| 380.0 | 8.21 | 0.1 | 2.0 | 20.28 | 10.335 |
| 385.0 | 8.32 | 0.1 | 2.0 | 20.40 | 10.474 |
| 390.0 | 8.42 | 0.1 | 2.0 | 20.50 | 10.600 |
| 400.0 | 8.53 | 0.1 | 2.5 | 21.11 | 11.374 |

# PREPARATION OF STATISTICAL INPUT FUNCTIONS FOR INTERFERENCE PREDICTION

K. G. Heisler, Jr.
Jansky & Bailey
A Division of Atlantic Research Corporation
Alexandria, Va.

Abstract. Interference prediction is, to a great extent, a statistical problem. Most cases of practical importance fall in the region of uncertainty lying between those systems confidently compatible within their environments and those systems completely incompatible within their environments.

Since the inputs for interference analysis have by nature significant random components, determining the characteristics of the random variations is a prime part of preparing input functions.

This paper explores examples of statistical methods that may be used and discusses some tentative conclusions. The more important conclusions are:

1. The average harmonic output from transmitters decreases with increasing harmonic number and follows a straight line with the logarithm of harmonic number.

2. A number of random variables introduce a random deviation from the average harmonic output from transmitters, which is distributed normally at each harmonic and has a standard deviation that is independent of harmonic number.

3. Most spurious response frequencies for superheterodyne receivers are predictable from the equation

$$f = \frac{pf_o \pm f_{if}}{q}$$

where

$f$ = the spurious response frequency
$f_o$ = the local oscillator frequency of the receiver
$f_{if}$ = the IF frequency of the receiver
$p$ = harmonic number associated with $f_o$
$q$ = harmonic number associated with $f$

It has been tentatibely concluded that the average power required to interfere with the receiver decreases with increasing p and follows a different straight line with the logarithm of p for each q.

4. A number of random variables introduce a random deviation from the average power required to interfere with the receiver which is distributed normally at each p and has a standard deviation that is independent of p.

A number of tentative conclusions are drawn concerning the nature of the antenna pattern distribution function.

The type of interference prediction answers these forms of input functions will provide is briefly discussed.

## I. INTRODUCTION

In the affairs of man, nothing is either all good or all bad. So it is with interference. As Fig. 1 portrays, there is a middle ground between an assured knowledge of interference and an assured knowledge of no interference in which the interference situation is at best uncertain, even when the problem is subjected to the most rigorous forms of attack.

To accomplish interference analysis, the first temptation is to consider worst-possible situations, thereby transferring this middle region of uncertain interference into the completely useless range of certain interference. The worst-possible situation type of approach is all right if the middle region is small. Unfortunately, however, the region of uncertain interference must be used if the existing electromagnetic requirements are to be even approximately fulfilled. In fact, most of the important equipments today are already operating in this middle region between no interference and certain interference.

Thus, we must be able to predict interference when we can be certain it occurs and to analyze the causes of interference. We must be able to predict the absence of interference when we can be sure it is truly absent. Finally, and most important of all, we must be able to predict the possibility (probability) of interference when the situation is uncertain. Only in this way can we provide system planners with the information they need to properly consider all of the odds and decide upon the most expedient system among the many trade-offs that may be made.

In order to predict and analyze interference in the large region of uncertainty, it is important that we gain an insight into the detailed statistical characteristics of the random variables that give rise to the uncertainty.

Recently an intensive study of the available measured data for the input functions to interference analysis was carried out. This study has led to some important conclusions concerning the spectral output power of transmitters and the response spectra of receivers. The following discussion will present these conclusions

* This work was supported in part by Rome Air Development Center under Contract AF 30(602)-1934.

along with some general discussion of the methods that have been used to arrive at the conclusions.

## II. TRANSMITTER SPECTRA

Fig. 2 is a typical measured spectrum from an existing classified radar transmitter. It has been generally concluded in the past that little information is represented by this single spectrum since the spectrum is a function of a number of random variables which have a significant effect on the power output at each harmonic. Actually, with a proper understanding of the detailed statistical characteristics of transmitter spectra, one can deduce a great deal more information from a single spectrum than appears on the surface.

Before discussing in any detail the amount of information that may be extracted from a single spectrum, it will be necessary to discuss the statistical characteristics of transmitter spectra in general. To carry out the discussion, a sample analysis will be presented based on 33 different spectra from the transmitter that was used to generate the spectrum shown in Fig. 2. The 33 samples produce a data spread that is typical of many equipments observed to date. Fig. 3 portrays the data spread for this illustrative case and as is expected the spread is large. Based on an examination of a number of plots of the type shown in Fig. 3, it is immediately suspected that two phenomena are taking place.

(1) In general the power output is decreasing with increasing harmonic number.
(2) There are other variables involved which are introducing a large variability in the data at each harmonic.

The questions to be answered are: What is the functional relationship between harmonic number and power output? What is the nature of variability at each harmonic? Is the variability dependent upon harmonic number? What other variables might the variability be dependent upon? Is the variability random? If so, what are the statistical characteristics of the variability?

The following paragraphs will be directed toward the development of a satisfactory approximation to the functional relationship between harmonic number and transmitter power output. Evidence will be presented in favor of the theory that the variability at each harmonic may be considered as random and statistics will be presented which adequately describe the variability.

The median value of harmonic power output is shown by the horizontal bars on Fig. 3. The median value at each harmonic tends to decrease with increasing harmonic number. Thus, the lowest values in the range of observed values also decrease as the harmonic number increases. We see on Fig. 3 that at the 5th harmonic the range of observed values has decreased to a point that has forced several of the values that should have been observed below the noise level.

Although it is known that these values exist, they cannot be measured and therefore cannot be used in any but the more complex types of statistical inquiries. The fact that some of the values have dropped below the noise level is shown on Fig. 3 by the missing lower portions of each data range. As long as the median value is above the noise level at a particular harmonic some information can be extracted at that harmonic without undue complications. However in the present case, above the 7th harmonic, the median value falls below the noise level and the few data points which were available have been discarded as practically useless.

The first question to be answered is: What is the functional relationship between transmitter power output and harmonic number? In order to find the functional relationship, some curve fitting will be attempted. The first and most desirable possibility that comes to mind is a straight line. Figure 4 shows the results of fitting a straight line to the median values of the sample shown in Fig. 3. The sum of the squared deviations from this curve is significantly high, being 45. More important, however, is that the median values denoted by the plotted points on Fig. 4 have an obvious systematic deviation from the solid straight line which was fit to them. The deviation shown by the dotted line is suggestive of a logarithmic curve. Obviously, the next step is to fit a logarithmic curve and see if it does represent the desired functional relationship more adequately. To fit a logarithmic curve, it is only necessary to change the independent variable from harmonic number to the logarithmic number by replotting the data on semilog paper and then fitting a new straight line to the replotted data. The new straight line will represent the best logarithmic function which could be fit to the data. The result of the above steps is shown in Fig. 5. The sum of the squared deviations of the data points from the line shown in Fig. 5 has dropped to 14 which is much more satisfactory. Of much greater importance is the fact that the data points have no significant systematic departure from the logarithmic fit represented by Fig. 5. Thus it appears that a satisfactory fit has been found to the points and it may be said that the median power output, P in db down from the fundamental power output for transmitters may be expressed as

$$P = A \log n + B$$

where n is the harmonic number ( $n \geq 2$) and A and B are constants which must be evaluated for each equipment. For the equipment used in the present example, A = 43 and B = 36.

The evidence that the functional relationship between power output and harmonic number from transmitters is logarithmic is so strong, upon examination of a number of different equipment, that the result will be stated formally as Hypothesis I.

Hypothesis I. The median harmonic output from a transmitter decreases with increasing harmonic number and follows a straight line with the logarithm of harmonic number.

The next step is to inquire into the nature of the variability of the data at each harmonic. The task of using the data would be greatly simplified if it were true that the data are normally distributed, since the normal distribution is one of the most common and easily handled types of statistical distributions. An adequate method for determining the normality of the data is to assume that it is normal, estimate its standard deviation and mean value, and then use one of the several statistical methods which are available to test the credulity of the normality assumption.

As an example, the 2nd, 3rd and 4th harmonics from the sample transmitter will be tested for normality by means of the commonly used chi-squared test[1]. The 5th, 6th and 7th harmonics were not tested since some of the sample values for these higher harmonics were lost in the noise and a sufficient number of samples did not remain.

At the 2nd harmonic, 33 values were measured. The hypothesis that we would like to test is that these 33 values were drawn at random from an infinite set of values (commonly known as a population) that are normally distributed. From our sample of 33 values we can estimate the characteristics of the parent population. We can then compute the deviation of our 33 sample values from the ideal normal distribution which has been hypothesized. Now it is important to note that even if the parent population is normally distributed, we would expect our 33 samples to display some deviation from normality. Indeed, statistical theory tells us just how likely each possible deviation is. If we observe a deviation that is too unlikely, we can conclude that the parent population from which we drew our samples was not normal. However, if the observed deviation from normality is fairly likely, then we can conclude that there is no evidence in the observed data to rule against normality, which when repeatedly observed becomes strong evidence in favor of the theory that the parent population is indeed normally distributed.

The curve of Fig. 6 is the distribution of the possible deviations from normality that would be observed if we estimated the normal characteristics from 33 samples that were drawn from a much larger normal population. The vertical axis is a measure of the observed deviation from the normal. The horizontal axis is the probability that we would not observe a deviation this great if all our normality assumptions are correct. Thus, the horizontal axis of Fig. 6 becomes a measure of the significance of the observed deviation. If the significance of the observed deviation is greater than 95, we will in general rule that the parent population was not normally distributed. If the significance of the observed deviation is less than 95, we will conclude that the normality assumption con-

cerning the parent population was correct at least as far as the particular set of samples is concerned.

The deviation from normality of our 33 samples taken at the 2nd harmonic of the radar transmitter is 1.8 as shown in Fig. 6. A deviation of 1.8 has a significance of only 38, certainly not ruling against normality at the 2nd harmonic. Figure 6 also shows that the level of significance at the 3rd harmonic is only 52 and at the 4th harmonic only 40, all well below the rejection level of 95.

Repeated observations of this type give strong indications that at each harmonic from a transmitter the variations due to different serial numbers, tuned frequencies, output tubes and the like are normally distributed.

We now know the type of statistical distribution, and from Hypothesis I we know how to find and represent the median value of this distribution. The standard deviation of the distribution is the one remaining bit of data that is needed to completely specify the harmonic output levels.

Our set of 33 samples at each harmonic provided an estimate of the standard deviation. Since the estimate is based on a relatively small sample there is to be expected a great deal of deviation from the true standard deviations. We do expect, however, to see a noticeable upward or downward trend in the standard deviation as harmonic number increases. In fact, intuitively it would seem that the standard deviation (which is a direct measure of the variability or data spread) should increase with increasing harmonic number. To our surprise, statistically, we were unable to find any trend in the standard deviation with increasing harmonic number. Thus, the possibility that the standard deviation at each harmonic is independent of harmonic number is to be theorized. If true, this means that all measured harmonic levels are drawn from the same normally distributed population regardless of the harmonic at which they were drawn. The only difference between harmonics is that each value is biased by some amount that depends solely on harmonic number.

Thus, we form still another hypothesis to be tested, which states that the standard deviations of our normal distributions at each harmonic are independent of harmonic number. This hypothesis has been tested in exactly the same way that the normality hypothses was tested at each harmonic. We assume that all samples for all seven harmonics shown on Fig. 3 were drawn from the same normal distribution but that their values were biased at each harmonic by a value predicted by the solid line of Fig. 5. It will be recalled that Fig. 5 shows the functional relationship between the median value of harmonic output and the harmonics number.

Figure 6 shows that the deviation from normality which was observed, under the assumption that the standard deviation at each harmonic is independent of harmonic number, has a significance

of only 72, again well below our rejection level of 95.

The results so far can be summed up in the two following hypotheses:

Hypothesis I. The average harmonic output from transmitters decreases with increasing harmonic number and follows a straight line with the logarithm of harmonic number.

Hypothesis II. A number of random variables introduce a random deviation from the average harmonic output from the transmitter, which is distributed normally at each harmonic and has a standard deviation that is independent of harmonic number.

There exists strong evidence in favor of these two hypotheses and if they are correct our confidence in them will grow as more data are collected.

It is of interest to give one more example of the testing of these two hypotheses against measured data. In this case, we will use a communications transmitter. Figure 7 shows that the significance of the observed deviation from normality for the 2nd through 24th harmonic of a typical HF transmitter is 88 which is safely below the rejection level of 95.

If Hypotheses I and II hold, then we see that Fig. 2 no longer represents one sample from each of seven different statistical distributions, but rather seven samples from the same distribution. Thus, it turns out that a single spectrum can provide a significant amount of information. A least squares fit to the spectrum will provide an estimate of the median value at each harmonic and the deviation of the spectral values from this straight line will provide an estimate of the standard deviation which under Hypothesis II is the same at each harmonic. Of course, the more values that are used, the more accurate the estimates will be. However, it is important to note that once the distributions are known, statistical theory will tell the error involved by estimating with any given sample size.

For example, let us try to estimate the statistical characteristics of our radar transmitter from only a single spectrum. An LSF was made to each of the 33 measured spectra for the radar transmitter that had all seven harmonic values above the noise. Each of the least squares fits are estimates of the nearly true functional relationship shown in Fig. 5.

To demonstrate the error that would have been involved in the functional relationship between median harmonic output level and harmonic number, the individual least squares fits have been plotted on Fig. 8. Of course, the difference between each individual

line is great, but we must remember that seven samples went into determining each line. Statistical theory predicts exactly the deviations we note on Fig. 8, when seven samples are used. As the number of samples (i.e., the number of harmonics in a spectrum and/or the number of available spectra) increases, the deviation, and hence the accuracy of any single line, increases rapidly.

A single spectrum will also give some information concerning the standard deviation ($\sigma$). Fig. 9 shows a comparison of the standard deviation as predicted from all samples (totaling 200) and from a single spectrum (seven samples) chosen at random from the 33 spectra available.

Hypotheses I and II tell us that to obtain adequate transmitter information it is only necessary to measure the statistical detail at two harmonics or equivalently it is only necessary to make a few measurements at each harmonic. Statistical theory may be used to tell us exactly how many samples must be taken to estimate the statistical parameters to any given degree of accuracy.

## III. RECEIVER RESPONSE SPECTRA

It has been found that Hypotheses I and II may be extended to handle the receiver response spectra as well as the transmitter harmonic output spectra. Almost all of the spurious response frequencies for superheterodyne receivers may be predicted from the equation

$$f = \frac{Pf_{LO} \pm f_{IF}}{q} \qquad (1)$$

where

$f$ = the response frequency

$f_{LO}$ = the first local oscillator frequency of the receiver

$f_{IF}$ = the first intermediate frequency of the receiver

$p$ = a positive integer

$q$ = a positive integer.

Eq. 1 shows that there is a response frequency for each possible p and q. Those responses for which q = 1 are in general the most serious. As the example of Fig. 10 shows, the responses for which q = 1 are paired, one of the pair generated by the plus sign of Eq. 1 and the other generated by the minus sign. Successive pairs are separated by a distance equal to $f_{LO}$ and each member of any particular pair is separated from the other by $2f_{IF}$. The q = 2 responses are distributed in frequency in just the same way,

but are generally lower in amplitude and are always twice as dense in frequency as shown by Fig. 10. The q = 3 responses are generally lower in amplitude than either the q = 1 or q = 2 responses and are three times as dense as the q = 1 responses.

A logical subdivision of the receiver responses is therefore made by q. Fixed p becomes analogous to harmonic number for any fixed q if $f_{IF}$ is small compared to $f_{LO}$, which is almost always the case. Further if $f_{IF}$ is small as compared to $f_{LO}$ the difference in frequency between those responses generated by Eq. 1 with a plus sign and those responses generated by Eq. 1 with a minus sign is small.

Thus, if we divide the possible receiver responses into separate groups by q and allow p to be identified with harmonic number, we may investigate the validity of the following two hypotheses concerning receiver spurious responses:

Hypothesis III. The average power required to interfere with the receiver increases with increasing p and follows a different straight line with the logarithm of p for each q.

Hypothesis IV. A number of random variables introduce a random deviation from the average power required to interfere with the receiver which is distributed normally at each p and has a standard deviation that is independent of p.

As an example of the strong evidence in favor of these two hypotheses, a series of measurements made on a classified radar receiver will be considered. First, the deviation from normality for the measured values is computed at each p for q = 1. The computation is carried out in exactly the same manner as the normality computations at each harmonic for the transmitter example previously discussed. As shown in Fig. 11, the significance of the observed deviation from normality at p = 3 was 82; at p = 4, 60; at p = 5, 38; all of which are well below the rejection level of 95. Again, just as in the transmitter case, we assume that all observed values were drawn from the same normal distribution, but that the values were biased by some fixed amount which depends upon p. Under these assumptions, the deviation from normality for the combined responses between p = 1 and p = 5 was only significant at a level of 46, which is another bit of evidence in favor of Hypotheses III and IV.

An interesting example of an extension of Hypotheses III and IV that was necessary for certain types of receivers is shown in the next illustrative example. Let us consider a receiver which tunes in the 0.5 - 30 Mc range, and has a series of three intermediate frequency stages. If we test Hypotheses III and IV for a receiver of this type by assuming that all measurements at q = 1 are drawn from the same normal distribution, but biased by some amount which is a

function of p, the significance of the observed deviation falls well into the rejection region. We immediately become curious as to what happened. The estimated median values were plotted as a function of p as shown on Fig. 12. Figure 13 shows clearly that there are three separate phenomena taking place, one from p = 1 to p = 4, another from p = 4 to p = 10 and the third from p = 8 to p = 30. Surprisingly enough, each of the three phenomena seems to follow our familiar straight line.

Applying our tests to each region separately, we find that they are all above the rejection level, although the region p = 1 to p = 4 falls dangerously close to the rejection level.

To summarize, four important hypotheses have been suggested that could have far-reaching importance in the fields of interference measurement and interference prediction and analysis. The four hypotheses which have strong evidence to support them are restated as follows:

Hypothesis I. The median harmonic output from a transmitter decreases with increasing harmonic number and follows a straight line with the logarithm of harmonic number.

Hypothesis II. A number of random variables introduce a random deviation from the average harmonic output from a transmitter, which is distributed normally at each harmonic and has a standard deviation that is independent of harmonic number.

Hypothesis III. The average power required to interfere with the receiver increases with increasing p and follows a different straight line with the logarithm of p for each q.

Hypothesis IV. A number of random variables introduce a random deviation from the average power required to interfere with the receiver which is distributed normally at each p and has a standard deviation that is independent of p.

## IV. APPLICATION TO INTERFERENCE ANALYSIS

As an example of the usefulness of the four hypotheses just presented, a brief look will be taken at the results obtained by applying these hypotheses to a general interference prediction procedure which has recently been developed and used. A detailed knowledge of the prediction input statistics allows the probability

of interference to be accurately computed. A knowledge of the probability of interference allows a system planner to properly appraise the chances he is taking with any particular system configuration. Otherwise, he must either disregard a large area that in all probability is usable or plunge in "by-the-seat-of-the-pants" and hope that the law of averages is in his favor.

Several types of interference answers are available if the statistical characteristics of the input function are used in interference prediction. Figure 14 is one example, which shows each possible emission from a particular transmitter that could cause interference to a particular receiver and the probability that it does indeed cause interference. From Fig. 14 one can compute the total probability of interference between the particular transmitter and receiver. The total probability of interference for the case shown in Fig. 14 is shown in the upper right hand corner of Fig. 14. The spectral type of interference prediction answer, illustrated by Fig. 14 allows an appraisal of the total probability of interference and a detailed look at the most likely source or sources of interference.

Figure 15 shows another type of interference answer that is available. Here seven receivers and twelve transmitters are present in a given complex. The table entries show the probability of interference between each transmitter and each receiver. If a statistical sum is taken down any column, the total probability of interference to any receiver from all sources may be obtained.

ACKNOWLEDGEMENT

The author wishes to acknowledge the technical assistance of Delmer C. Ports.

REFERENCES

1. For a discussion of the chi-squared test, see any standard text on statistical theory; for example, Chapter X of Introduction to Mathematical Statistics by Paul G. Hoel.

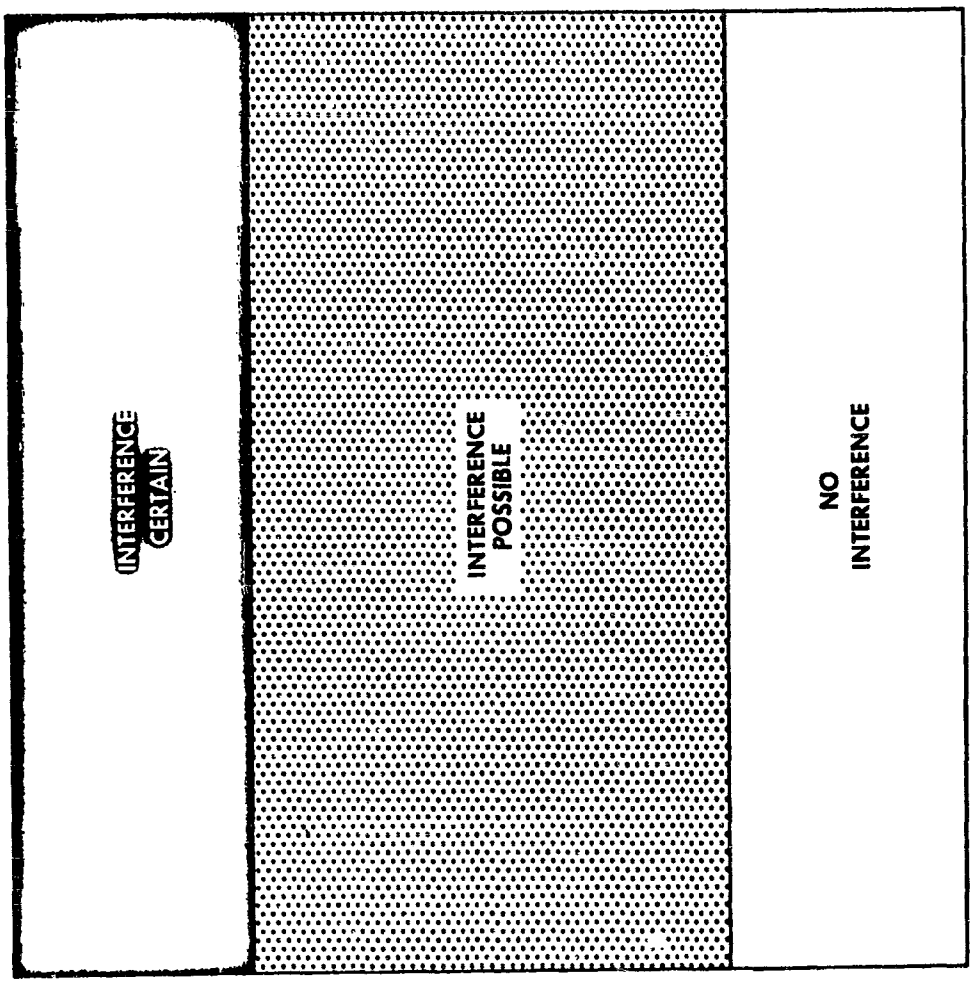



Fig. 1. INTERFERENCE PREDICTION

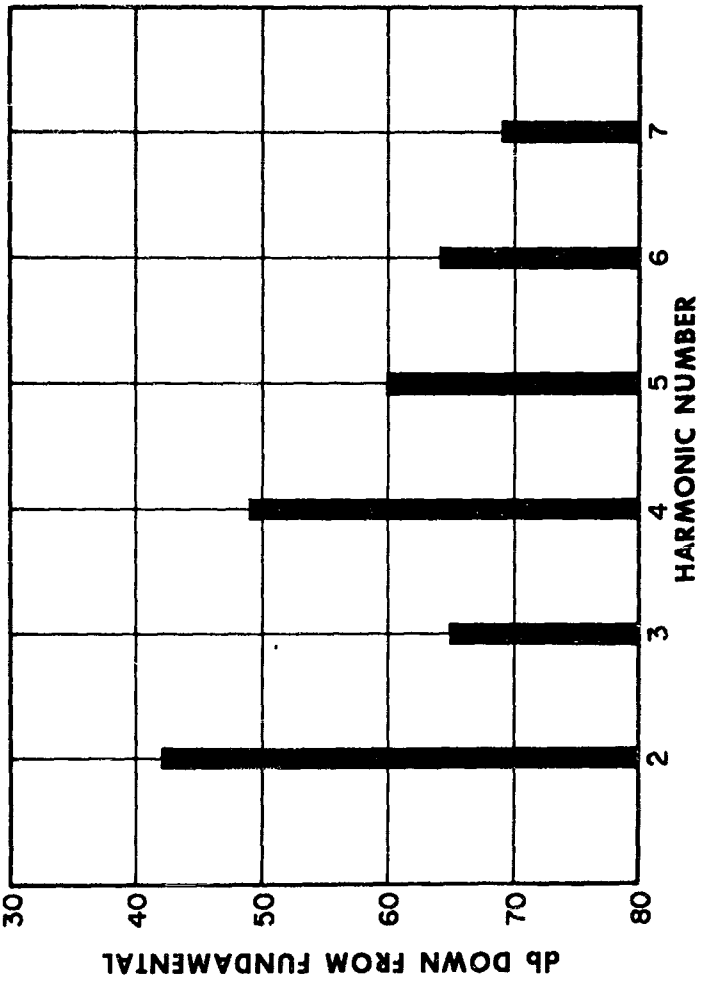



Fig. 2. TYPICAL RADAR OUTPUT SPECTRUM

Fig. 3. RANGE OF 33 MEASUREMENTS AT EACH HARMONIC FOR THE SAME TRANSMITTER NOMENCLATURE

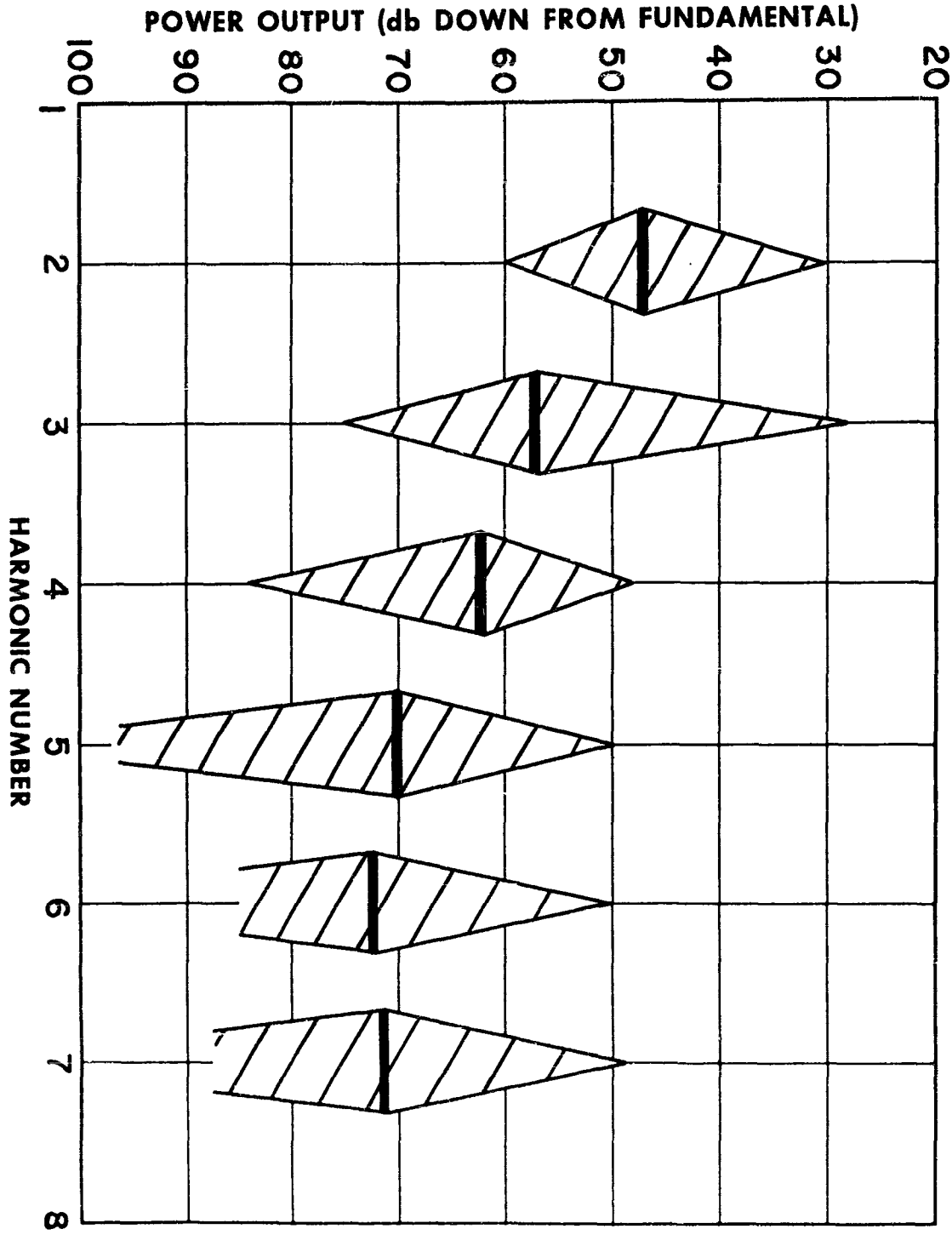


Fig. 4. TRANSMITTER POWER OUTPUT AS A FUNCTION OF HARMONIC NUMBER

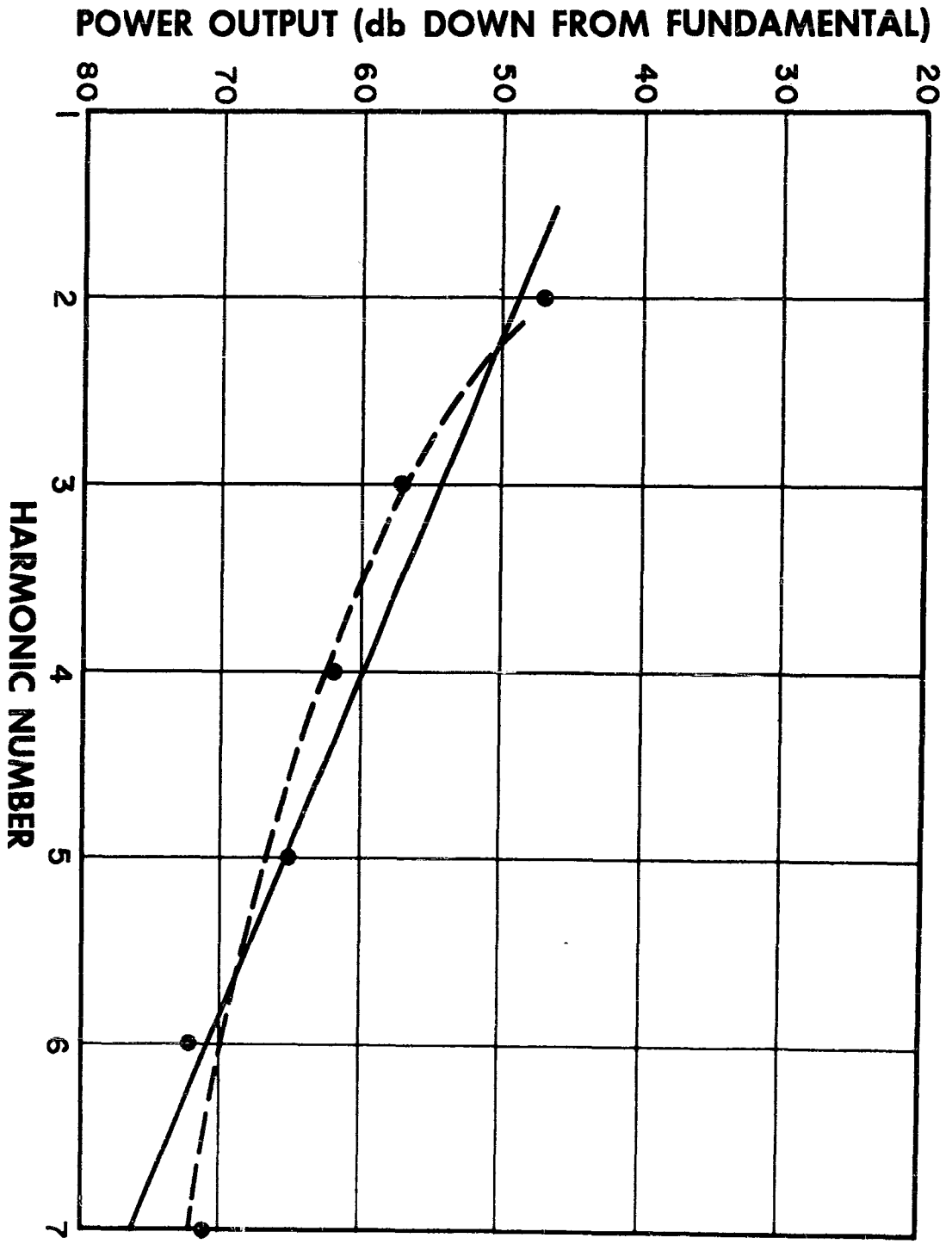
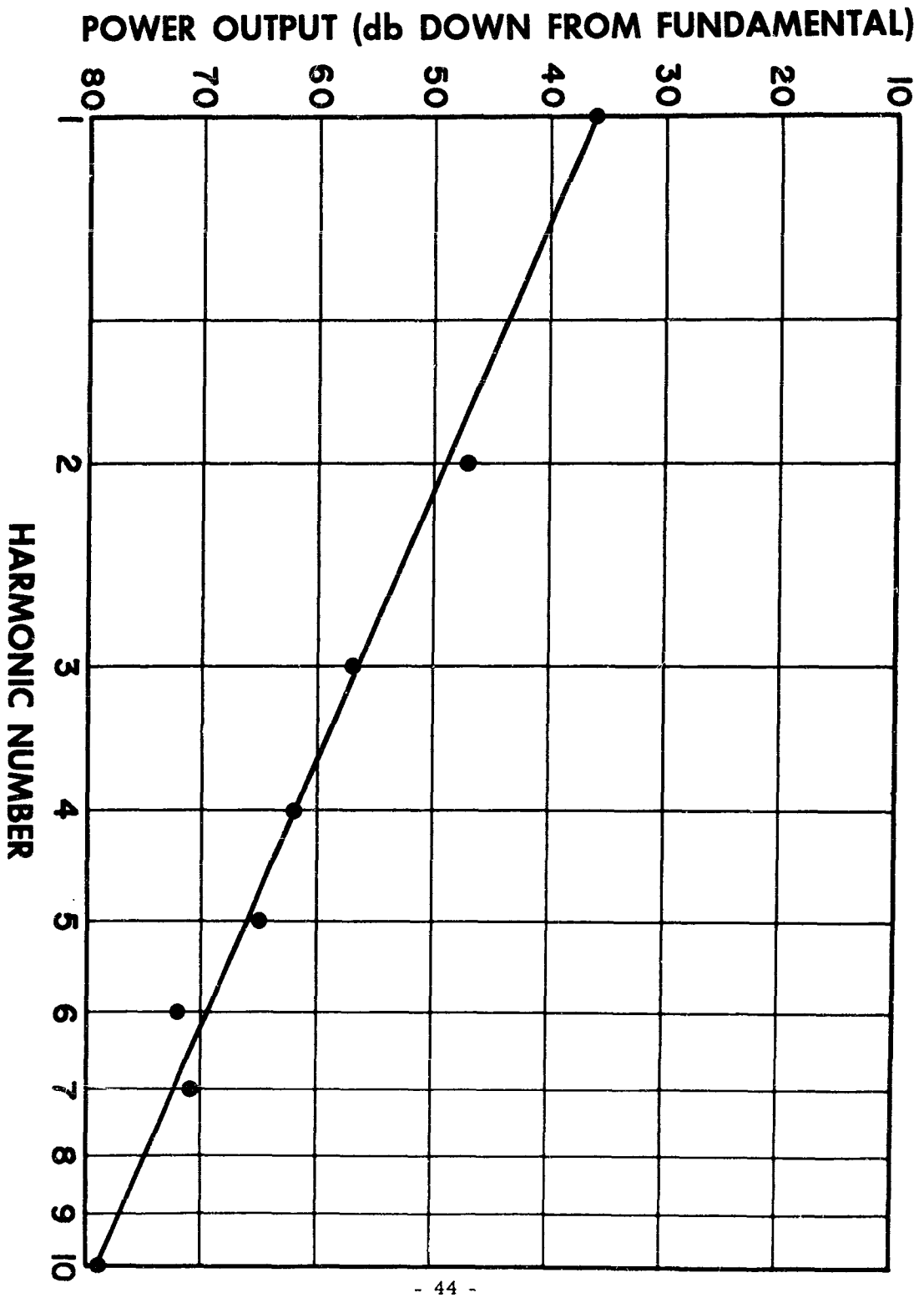


Fig. 5. TRANSMITTER POWER OUTPUT AS A FUNCTION OF THE LOGARITHM OF HARMONIC NUMBER



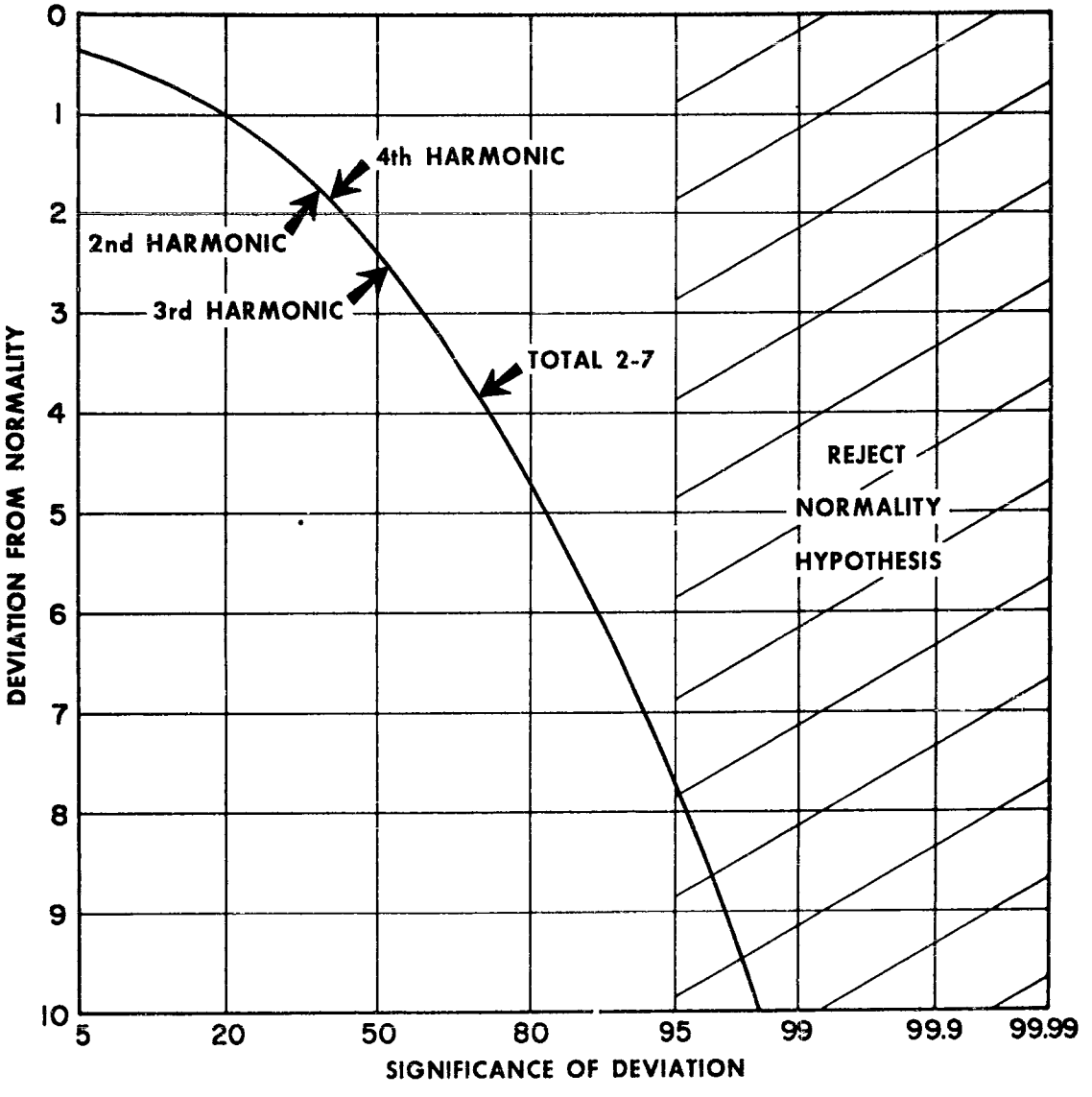



Fig. 6. HYPOTHESIS TESTING FOR A RADAR TRANSMITTER

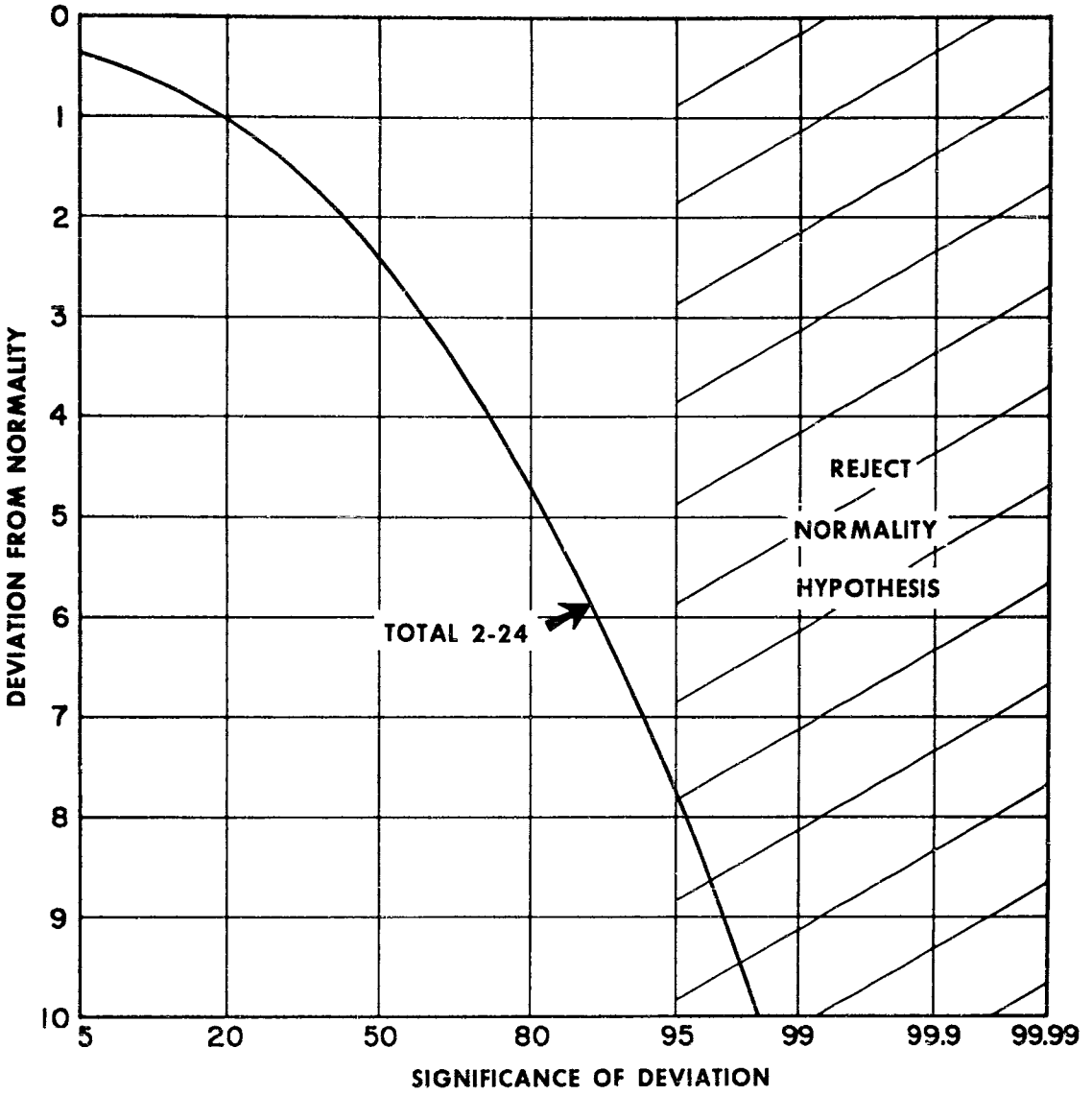



Fig. 7. HYPOTHESIS TESTING FOR A COMMUNICATIONS TRANSMITTER

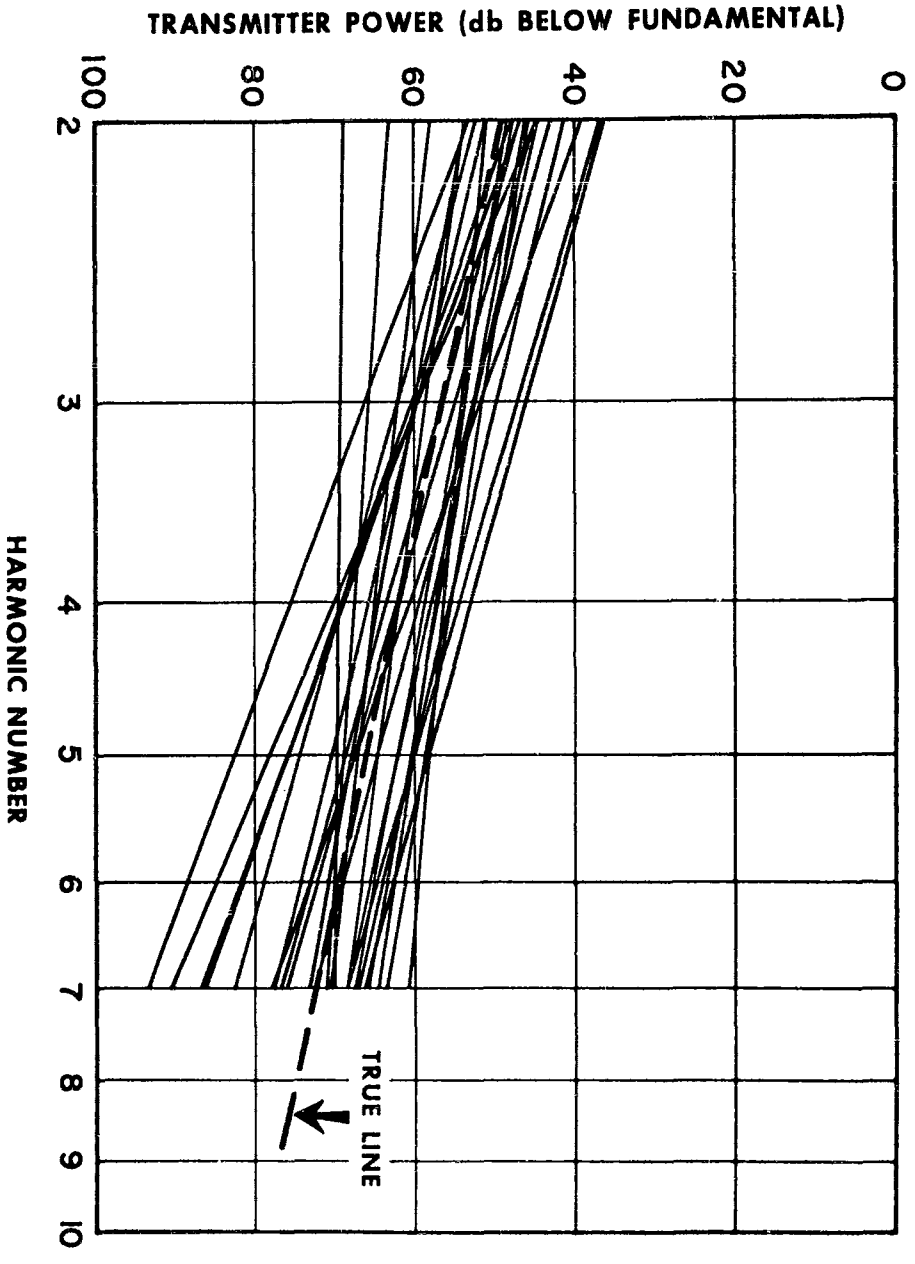



Fig. 8. COMPARISON OF COMPUTED MEAN VALUE FUNCTIONS BASED ON SINGLE SPECTRUM FOR THE SAME TRANSMITTER

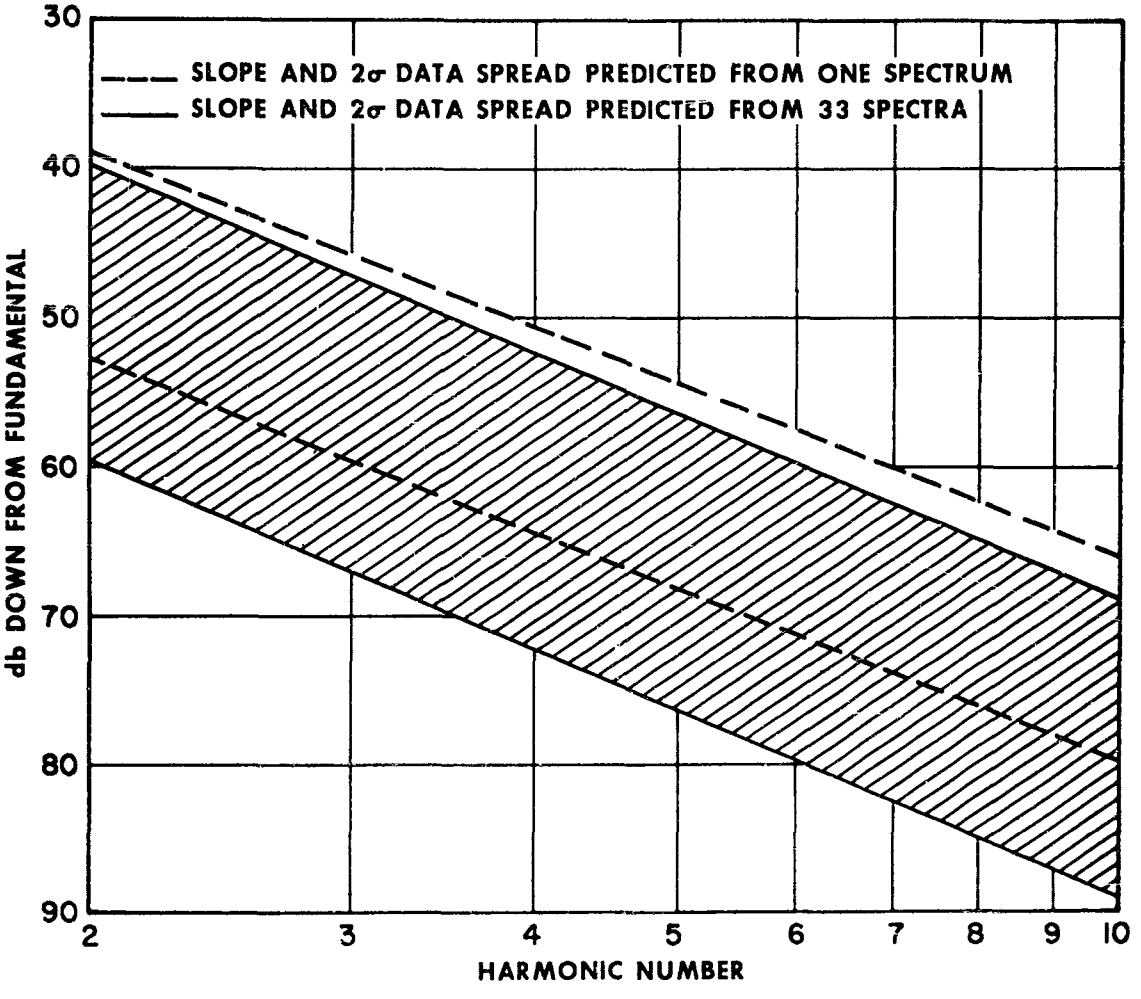



Fig. 9. COMPARISON BETWEEN COMPUTED DEVIATIONS BASED ON ONE SPECTRUM AND MANY SPECTRA

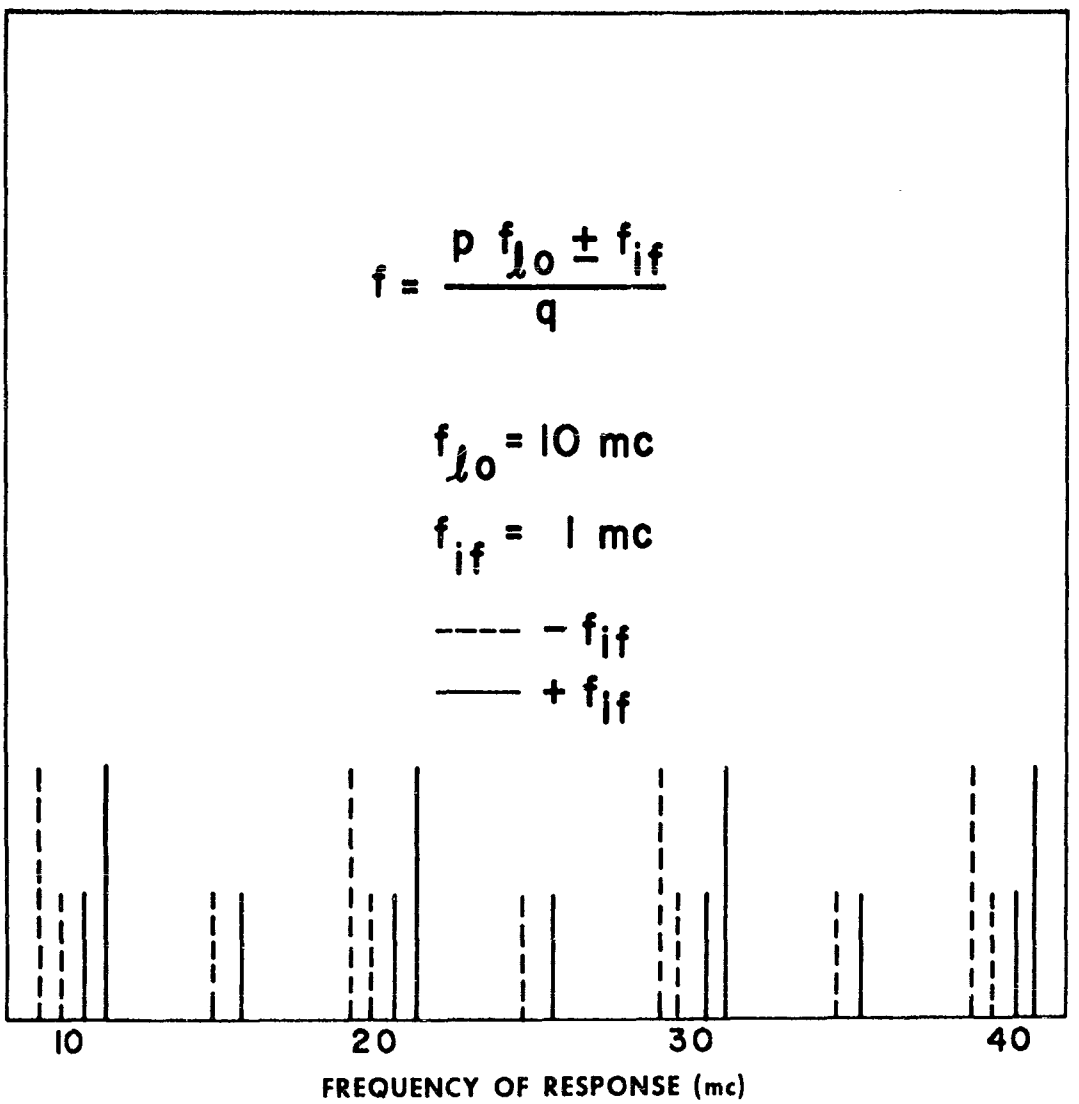



Fig. 10. P-Q EQUATION

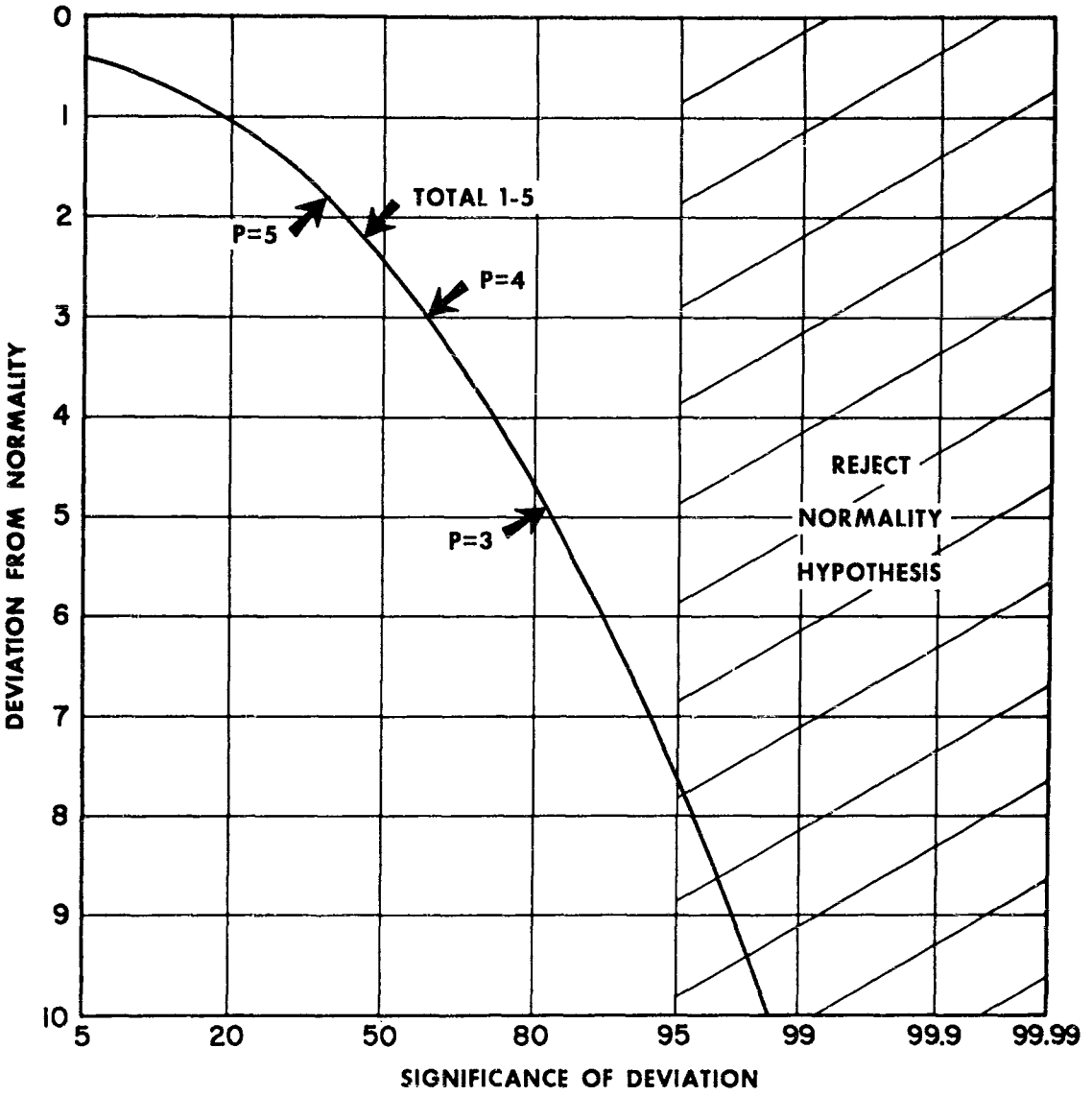



Fig. 11. HYPOTHESIS TESTING FOR A RADAR RECEIVER

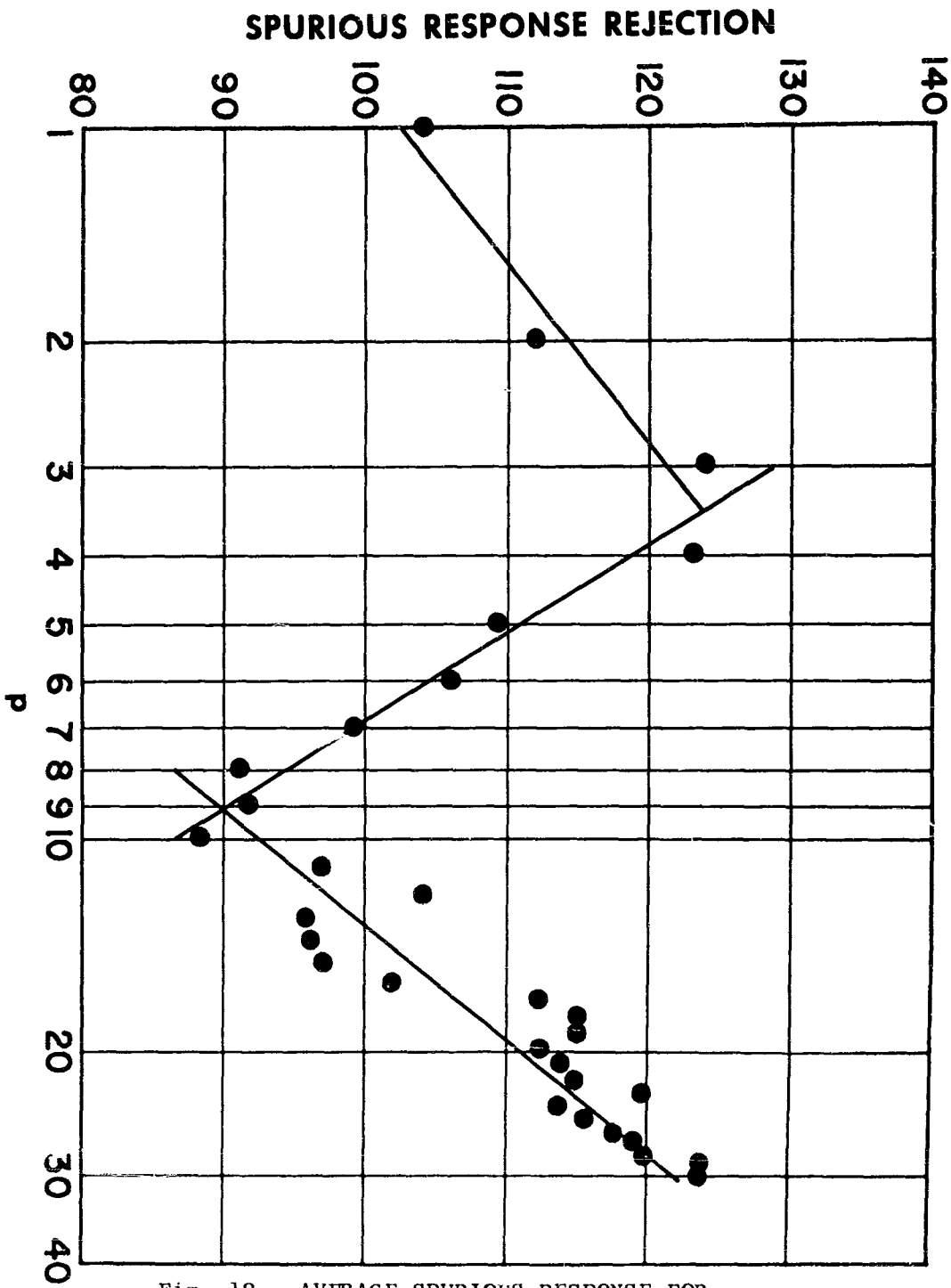



Fig. 12. AVERAGE SPURIOUS RESPONSE FOR A COMMUNICATIONS RECEIVER

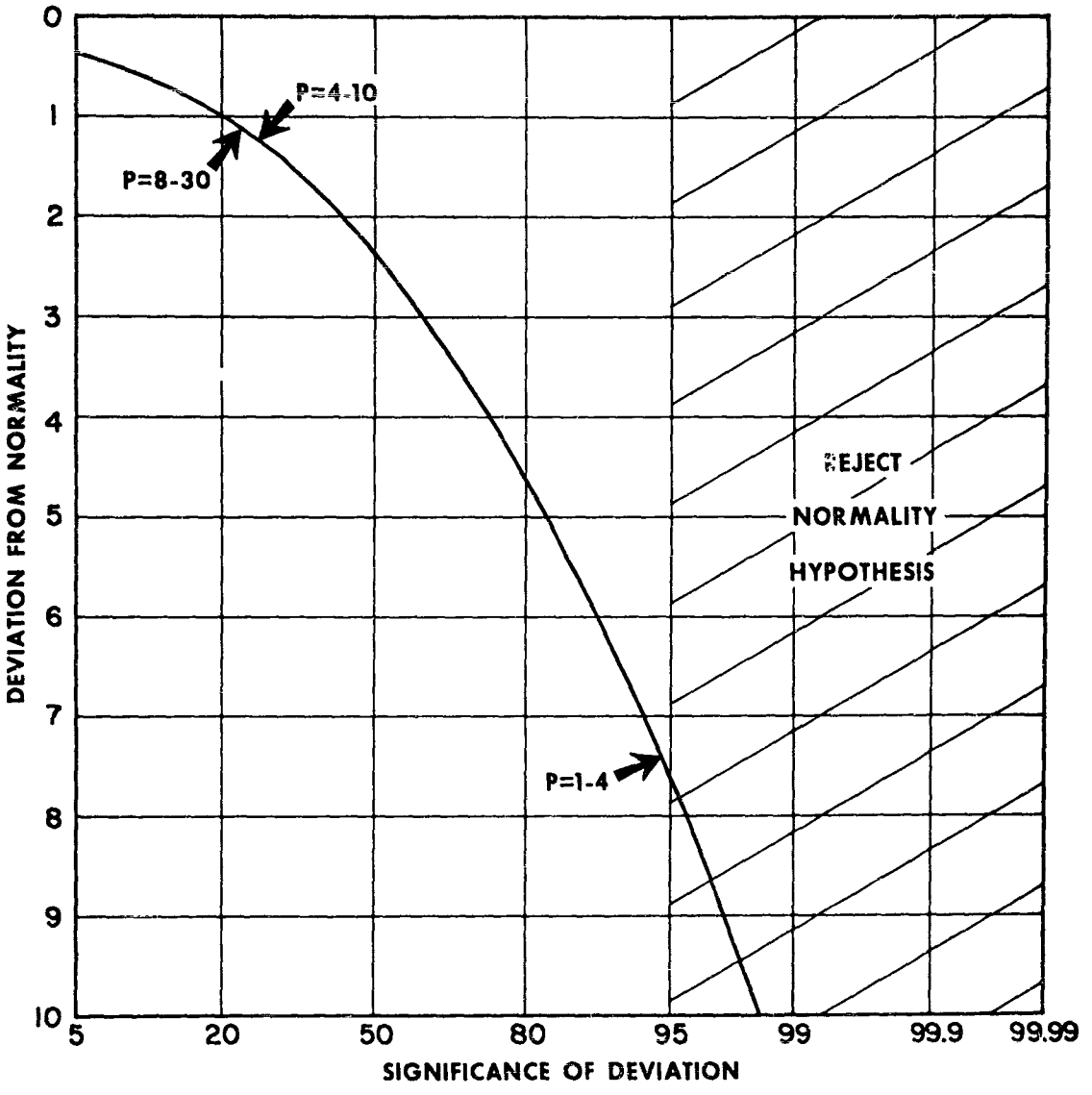



Fig. 13. HYPOTHESIS TESTING FOR A COMMUNICATIONS RECEIVER

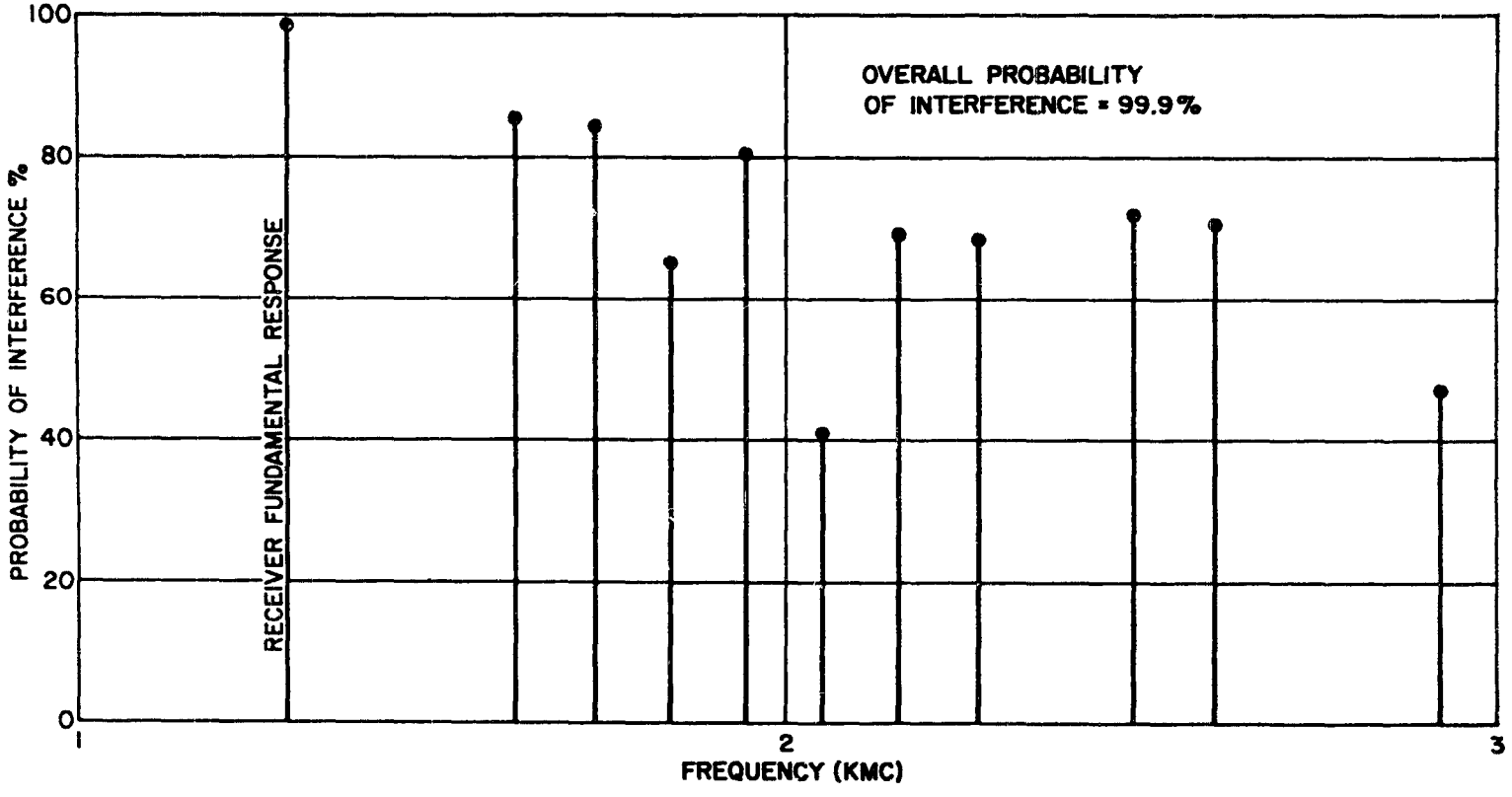



Fig. 14. PROBABILITY OF INTERFERENCE

| | $R_1$ | $R_2$ | $R_{3-1}$ | $R_{3-2}$ | $R_4$ | $R_{5-1}$ | $R_{5-2}$ |
|---|---|---|---|---|---|---|---|
| $T_{1-1}$ | 30 | 34 | | | | | |
| $T_{1-2}$ | | 99.9 | | | | | |
| $T_2$ | 99.9 | 99.9 | | | 3 | 89 | 52 |
| $T_3$ | | 99.6 | | | | | |
| $T_4$ | 99.9 | 44 | 99.8 | 78 | 29 | 96 | 6 |
| $T_5$ | | 99.3 | | | 98 | 11 | |
| $T_6$ | | | | | 0.3 | 68 | 30 |
| $T_{7-1}$ | 99.9 | 86 | | | 98 | 99.9 | 99.1 |
| $T_{7-2}$ | 99.6 | 13 | | | 62 | 99.9 | 97 |
| $T_8$ | | | | | | | |
| $T_{9-1}$ | 5 | | 5 | | | | |
| $T_{9-2}$ | | | | | | | |

Fig. 15. TOTAL PROBABILITY OF INTERFERENCE

# RADIO INTERFERENCE REDUCTION AND SPECTRUM UTILIZATION IN FIELD ARMY RADIO RELAY SYSTEMS

R. M. Cowgill
Raytheon Company

Abstract. - A great deal of study has been devoted - and effectively - to the reduction of interference in what might be considered the "on-site" or "colocated" environment. This emphasis has resulted, in part, from the fact that this type of interference was the earliest type which presented a real problem which was amenable to definition, laboratory simulation and study, and therefore to relatively easy and permanent solutions. These have made it practical to use numerous equipments on one site and established the rules for making frequency assignments under such conditions.

The army, of atomic necessity, has become very dispersed and mobile while its communications requirements have gone up as a result of the fast reaction times required by the modern weapons systems and tactics. This has meant that radio relay must be used in many places where wire or net type radio were used before. As a result, the density of radio relay type radiators has gone up. As a result of this and the progress made in "on-site" interference control, cochannel and adjacent channel interference have become the dominant contributors to interference. These are both "off-site" type factors which are much more difficult to deal with on a sound engineering basis.

This article will deal with the factors which affect the choice of equipments and systems configurations for implementation of a Field Army radio relay system. One of the overriding objectives of any such consideration must be the efficient use of the spectrum in order to assure a minimum of radio frequency interference.

## I. BACKGROUND

A great deal of study has been devoted to the reduction of interference in what might be considered the "on-site" or "colocated" environment. This emphasis has resulted, in part, from the fact that this interference was the earliest type presenting a real problem which was amenable to laboratory simulation and study and therefore to relatively easy and permanent solutions. These solutions have made it practical to operate a reasonably high number of electromagnetic radiators from the same site. Therefore, on-site interference reduction will not be covered in this paper. However, as engineers were arriving at these solutions, the requirements of the Field Army were changing and new and more difficult problems were presenting themselves. The army, of atomic necessity, has become more mobile and dispersed. In addition, the army in its quest for new ways to replace manpower with machines has embraced automatic data processing. As a result of these two factors and the need for spectrum economy, radio relay has replaced wire and, in some cases, net radio. Its use has thus been extended to ever lower echelons of command.

This more dense use of radio relay has aggravated the "off-site" mutual interference problem until it has become the major one. In addition, this problem is much more difficult to attack by reason of the large numbers of equipments and personnel and the large area of terrain required to simulate battlefield conditions. Should the equipments, personnel and area be available for such simulation, the range of conditions which might be anticipated, both in spacing and propagation, varies much more radically. This then becomes a statistical problem with a very broad deviation. It is very likely that no absolute answer is possible. Therefore, all possible means must be used to reduce interference. Since for the purpose of this paper it has been assumed that the on-site problem has been solved, we are concerned here primarily with cochannel and adjacent channel far field interference. This is not to say that we need not observe the frequency assignment rules dictated by the on-site interference problem; it is just assumed that we know what these rules are and the extent to which they restrict our overall network configuration and frequency assignment.

## II. PROBLEMS IN SYSTEMS DESIGN

The conditions under which the Field Army might have to operate vary so widely that it may be difficult to provide a communications system which is general enough in its application to meet all requirements and yet well enough defined so that advanced planning can assure efficient equipment and spectrum usage. The communications requirements basically follow well defined channels, but from a system's standpoint, they may be best served by a common user type communications system. An acceptable system must provide a degree of alternate routing in order to make it less vulnerable to disruption as a result of physical or electronic neutralization of any site. At the same time, it must do so without introducing restrictive complications of equipment usage and frequency assignment. The frequency assignment must be flexible enough not to restrict the movement of the units and yet efficient enough to be able to provide the necessary communications with an acceptable level of interference within the spectrum. It follows that a system's approach should be used to arrive at a standardized network configuration - using the characteristics of existing equipments in order to be able to arrive at firm and currently useful conclusions. The process of engineering such a system efficiently should provide some guidelines for the design of new equipments for a better future system. The system must take into account the terrain on which it might be called upon to operate and yet these terrain factors must not be allowed to restrict the usefulness of the system. The same equipments must be applicable under all these conditions in order not to load down the budget and the soldier with extra equipment. This is quite an order and requires an orderly approach.

## III. SYSTEMS REQUIREMENTS

It is desirable in the design of a trunk communications system serving an area such as that occupied by a Field Army to use an irregular cellular type of radio relay interconnection with major communications centers at the intersections. This provides the high degree of alternate routing needed for reliability and common user trunks for efficiency of

trunk usage. However, it seems inevitable that the full system will build up by degrees rather than appear all at once. The axis of required command communications will be installed first. As these axes build up, cross connections will be installed as time permits, remembering that there are heavy pressures dictating this stiffening of the system in order to make it less susceptible to destruction or electronic countermeasures. The system which results is a command oriented area system.

The network described so far provides only the interconnections between major communications centers. These sites, however, in addition to being the nodal points for the links interconnecting the centers, will undoubtedly be the gathering points for connections to multi-voice-channels customers as well (Figure 1). The coarseness of the network will, therefore, be a function of both these requirements. Under some conditions, however, the density of customers may be so great that with a reasonable separation of communications sites from the standpoint of the interconnecting links, the density of terminating links required at any one center may be so high as to be impractical from the standpoint of frequency assignment and other on-site complications. Under these conditions, it may be advisable to install consolidation facilities - radio relay sites which do nothing more than make connections to several customers and then relay them through one link to the communications center. The resulting density of communications centers will mean that radio relay can easily interconnect them on a one hop basis. Any relay point which might be required to tie centers together would probably itself evolve into a communications center in order to reduce the concentration of customer connections to any one center. The length of the radio relay links tying this system together would probably average somewhere between 10 and 20 miles in length, depending upon the terrain. Both ends of such links could be favorably located since they need not coincide exactly with any one tactical unit nor move with every move of a headquarters. The configuration only warps and changes when the changing situation can no longer be served from the existing communications complex.

There are several choices open to the systems designer in deciding how to tie the customers into the centers. The most obvious answer may be low capacity radio relay. However, this results in quite a forest of antennas at each site. This complex may be difficult to install and, at VHF, may present frequency assignment problems since the rather broad beam patterns of these mobile antennas will make them a potential interference source over rather large areas.

Another possible solution may be found in the so-called radio relay central (Figure 2). In this concept, one or more transmitters are fed into one omni-directional antenna to provide the outgoing legs to some larger number of multi-voice-channel customers. Each customer demultiplexes only those channels assigned to him. He receives using a directional antenna and transmits the return half of the duplex link through a directional antenna. This requires a separate rf frequency assignment for each of these return links. However, the central may receive all of these, with one omni-directional antenna, using preselectors to separate the rf channels and thereby reduce the danger of cross product modulations in the receivers.

Both radio relay and radio relay central will undoubtedly find their place in future army communications networks. The radio relay central will probably find its place in VHF. Antennas of reasonably mobile size at these frequencies are only moderately directional. Interference is only slightly increased when omni-directional antennas are resorted to. The major advantage of the central is that the central terminals for several multi-channel customers can be moved into place intact, complete with all necessary multiplexing and other auxiliary equipment. This makes the central system more mobile and standardized. Since the equipments are in a fixed physical relationship to each other, the mutual interference matrix may be worked out ahead of time and posted within the shelter, so that intra-central restrictions to the frequency assignment are known quantities. In addition, the central conserves frequencies. For example, a central designed to serve six customers all from one multiplexed transmitter using one frequency, will need 6 additional frequencies to provide the other half of the six multiple-voice channel duplex connections, making a total of 7 frequencies. Use of straight radio relay would require use of 12 frequencies.

At UHF frequencies, straight radio relay may gain an advantage over the central concept as a result of the more directional antennas which become practical at these frequencies. The advantage gained by a reduction in the number of frequencies required by the radio relay central may well be counter-balanced by the increased directivity of the antennas. In general, highly directional antennas are necessary in order to obtain the desired ranges at these frequencies. In addition, it is not necessary for all of the antennas to be in one place on the top of the hill. They can be dispersed around the top and below the crest of the hill making them less vulnerable to detection and destruction. There are also less restrictions to the on-site frequency assignment as a result of the separation and possible shielding. However, there is a high price in capability attached to the use of these UHF frequencies. Some diffraction can be expected at VHF frequencies so that paths, especially short ones, which are not entirely line-of-sight are usable. At UHF frequencies this is much less likely to be true. As a result, more stringent propagation path restrictions are imposed upon UHF users than upon VHF users. This is to some small extent counter-balanced by less severe requirements concerning Fresnel zone clearance in the site foreground at the higher frequencies. The VHF portion of the spectrum has become so crowded, however, that the use of UHF frequencies becomes inevitable to satisfy at least a part of these requirements.

A picture of the army trunk communications system begins to emerge. However, nothing has been said about the voice channel capacity of the interconnecting radio relay links. Experience in laying out radio relay systems has shown that the capacity of the radio relay link is less significant than the number of such links, especially when UHF radio relay equipments are used. The rf channels at these frequencies are inherently wide and can accept modulation which provides numerous voice channels without a commensurate penalty in spectrum usage. Apparently then, voice channels become less expensive in terms of spectrum usage and equipment as we go up in frequency. At some point additional channels become cheaper than the switching required to provide efficient use of the chan-

nels in any trunk group. This means that we may have less switching and more patching with the result that the higher capacity equipments are used. It appears to be chiefly a matter of the proper choice of available equipments at this point.

The number of multichannel terminations provided army wide is the prime controlling factor in the mutual interference problem. The tendency should be toward fewer terminals of higher capacity. Active alternate connections to these customers must, in most cases, be foregone. The requirements for alternate communications can undoubtedly be satisfied by the capability to reorient antennas or install links to additional centers if and when it becomes necessary. Net radio furnishes a limited alternate communications means which may prove adequate in emergencies. The number of multichannel terminations at any one site is a major factor restricting the frequency assignment scheme. It has already been suggested that consolidation relay facilities might be used to contain this problem.

## IV. SPECTRUM USAGE

As radio relay voice channel capacity goes up in new equipments, the operating frequencies go up. Possibly this should be stated in reverse, as the operating frequencies of radio relay equipment go up, so does the voice channel capacity. In any event, both seem to be going up together. This trend has opened up new areas of the spectrum and these additional rf channels constitute one means of providing for increasing numbers of radio relay terminations without necessarily increasing the interference level. This gross approach has its limitations, however, and it becomes apparent that every means available must still be used in order to assure an acceptable level of interference. One problem lies in the fact that commercial users and other military users also invade any new bit of spectrum opened up by advances in the state of the art and many of these services will still be needed even in time of war. As a result, only a fraction of the tuning range of these equipments may be available for the use of army radio relay. What means are available to assure efficient spectrum usage and still provide the flexibility required by modern mobile and dispersed concepts? One such means lies in proper frequency assignment.

With the introduction of computers into the field army, it might be considered practical to make a centralized and efficient assignment of frequencies using the computer. However, considerable communications are required just to keep the computer informed of the location of each unit and then to disseminate the assignments as they are made. Continual revisions of the frequency assignment would be required as units move if efficiency of spectrum usage is to be maintained. This places a need for good communications upon a system whose quality is dependent upon the adequacy of the frequency assignment which is in turn dependent on good communications. Such a system might be very difficult to administer.

The preceding paragraph indicates that what really limits the field army's ability to efficiently use the spectrum is constant movement. Frequency assignments must include this provision for movement without imposing restrictions. The units should not be dependent upon communi-

cations for their assignments and they should not be required to know where all other units are with respect to themselves. Certain units will have to move through others. It might be very wasteful to provide a permanent set of frequencies compatible with all others regardless of changes in deployment. The answer appears to lie in a predetermined frequency assignment based upon terrain separation. Mr. Roger A. Burt of C-E-I-R, Inc., Arlington, Virginia, has done preliminary work on this approach under contract with the U. S. Army Signal Research and Development Laboratory, Fort Monmouth, New Jersey, which seems to indicate this could be a powerful tool not only for frequency assignment, but for the design and evaluation of communications systems. The frequency assignment for a given radio relay equipment throughout the field army could consist of a map overlay and/or table dividing the terrain into areas with associated frequency assignments. For equipments with narrow beam widths, these assignments might be tied to the direction of the link. Figure 3 shows one possible map overlay chart and indicates its application.

The method used to develop the frequency assignment pattern is based on the use of the statistical irregular terrain propagation model developed by John Egli.[1] The pattern is designed to allow a given maximum probability of mutual interference. Under this concept, all a unit needs to know is its own location and direction of desired transmission in order to determine its own compatible frequency assignments. The pattern of assignment is repetitive and can be used over large areas.

The predetermined frequency assignment approach can be used in systems evaluation or design in several ways. Given the coarseness of the communications system structure, the type and maximum number of interconnections required and the level of permissible interference, analysis on the basis of predetermined area frequency assignments can indicate how many rf channels are required to provide the required service, or given the number of rf channels available to do the job, the limitations which this factor imposes upon the number of connections, coarseness of structure or level of interference can be studied.

It might be argued that this system of frequency assignment is wasteful of frequencies since at no one time will all of the possible connections be installed, resulting in unused frequencies. However, this is true of all systems of frequency assignment to some extent since a certain pattern of assignment is required to minimize interference and this pattern is related to the deployment of the units. This results in the availability of a certain number of channels in any one area though not all may be required. The condition is very similar to the predetermined assignment case with the advantage of unrestricted mobility accrueing to the latter case, though the pattern may impose some maximum rf channel restrictions.

There are many advantages in the predetermined frequency assignment pattern besides mobility. The frequency assignments can be made beforehand with the aid of a computer if deemed advisable, yet no communications are required other than the distribution of the map overlays and/or code books. Frequency assignments may be changed by a simple substitution of code books or by a shift of the map overlay with respect to the terrain map. An infinite extension of the pattern already established can be made without additional effort because of the repetitive nature of the pattern. The frequency assignment patterns provide fundamental building blocks which are useful in gaining an understanding of the field army's communications capabilities.

Although the initial effort has been based on a general terrain statistics model, it could be adjusted to any statistical model which might be developed for specific types of terrain which are encountered. Any improvement of the propagation model used would also improve the frequency assignment.

In general, each of the army's radio relay equipment types occupies a separate portion of the spectrum. Each has different characteristics. As a result, separate predetermined assignments would be required for each equipment type. Each equipment could serve a different purpose within the army communications systems. The high voice channel capacity equipment could serve to provide heavy long distance links along the main axes of communication. Medium capacity equipments might provide the lateral connections necessary to reinforce the system and provide connections to centers not along the main axes of communications. A low capacity equipment or a radio relay central might be used to provide the customer links to the system. Should an additional equipment type be available, it could be used to provide the consolidation relay facilities in areas of high density. These requirements all overlap on the terrain and the provision of separate equipments using separate sections of the spectrum for each job greatly reduces the interference problem.

## V. FUTURE OF RADIO RELAY

Radio relay will undoubtedly continue to provide the backbone of the field army communications system for quite some time to come. The trend toward use of higher frequencies in order to open up new areas in the spectrum and to facilitate providing higher channel capacities and narrower beams will continue. However, sooner or later all of these bands will also be occupied by other numerous users and there will still be a need to further develop spectrum conserving techniques. The system of predetermining frequency assignments suggested by Mr. Burt appears to be a most promising scheme for providing a means of applying the systems engineering approach to field army communications. By such application, we may in the future be able to say of the off-site as of on-site compatibility that we understand the problem and know how to go about solving it. Further refinements are still required in our understanding of the statistical nature of the attenuation of radio waves propagated over irregular terrain.

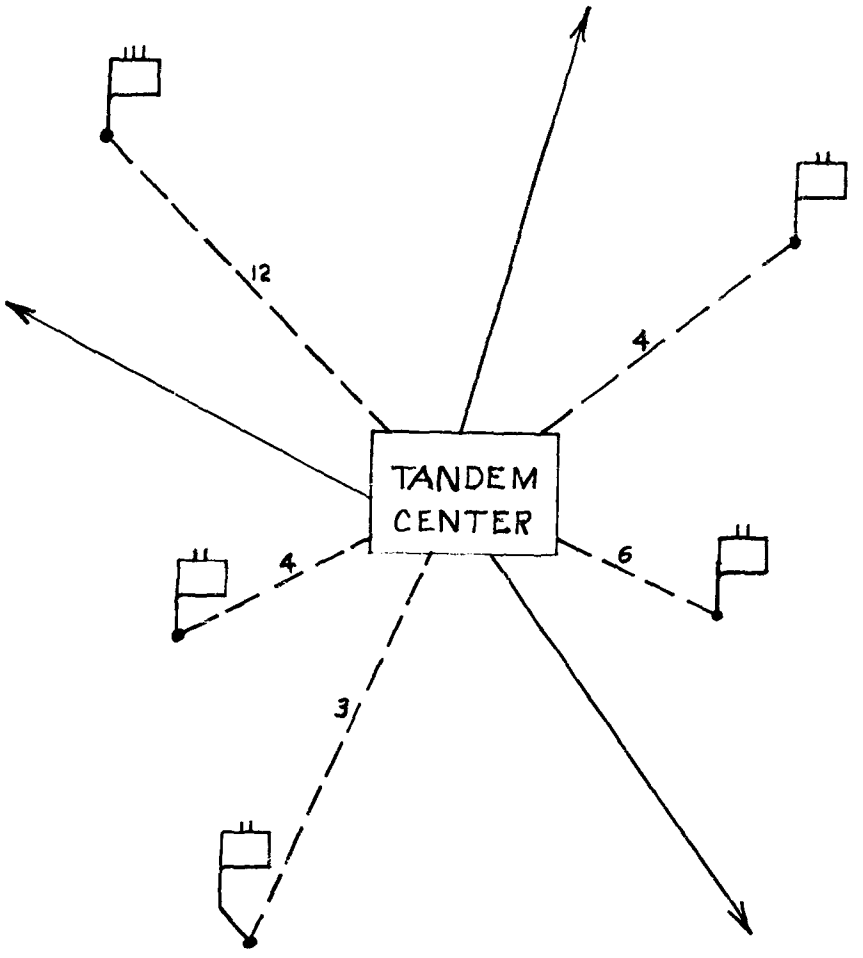
Our present system of radio relay for field army use is inefficient in that it is of necessity a duplex system. Any one communications link direction is in use considerably less than half the time, particularly when voice communications are involved. This results from the fact that in any two party connection only one party can talk at one time and from the pauses inherent in any conversation. One possible answer may lie in providing each information bit with a discrete address with numerous conversations sharing the same transmission medium on a random time basis. A simpler solution which might prove more practical and just as effective would involve push-to-talk operation though still provide full duplex operation. Activation of the push-to-talk button would send out a string of

stored address pulses which would make up the connection anew for each transmission. A light or absence of a beep would indicate when the connection had been completed. Such a system should allow any given multi-voice-channel link to carry approximately twice as many conversations. Overloading of the link would result in slowing down all traffic rather than stopping some. Of course, patched through channels could be provided where no delay can be tolerated -- as is the case with present systems.

Miniaturization of radio relay equipment is necessary and progress will be made in that direction for this and other field army equipments. However, the real promise for the increased usefulness of radio relay in the future mobile and dispersed army lies in preplanning and standardizing systems plans and frequency assignments.

## REFERENCES

1. J. J. Egli, "Radio Propagation Above 40 MC Over Irregular Terrain," Technical Memorandum 1818, USASRDL, Fort Monmouth, N. J., 6 August 1956.




LEGEND

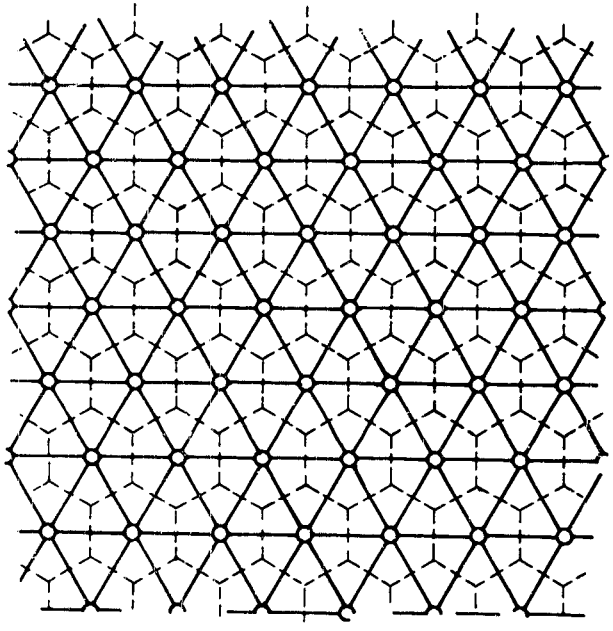
——Links to other centers

——Customer terminal links with voice channel capacity.

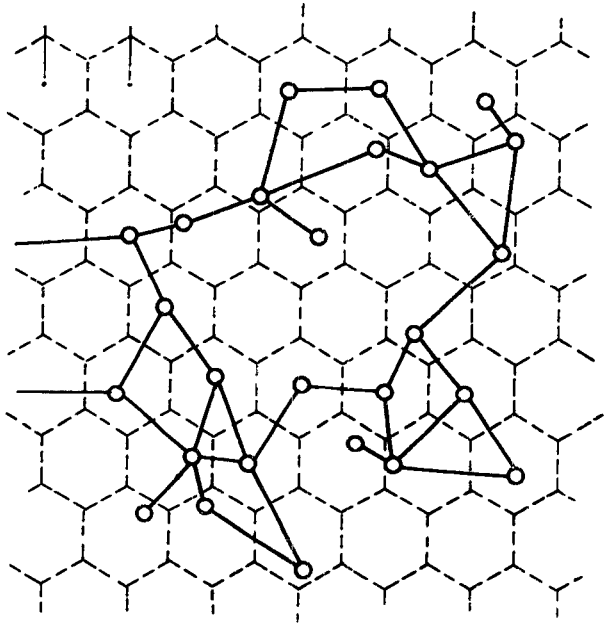
FIG. 1. TYPICAL COMMUNICATIONS CENTER



FIGURE 2



IDEALIZED MAXIMUM
DENSITY SYSTEM



TYPICAL FIELD
SYSTEM

FIGURE 3
SIMPLE TRIANGLE RADIO RELAY NETWORK

# A COMPARISON OF TWO METHODS OF DETERMINING SYSTEM COMPATIBILITY

E. D. Knowles
The Boeing Company
Seattle, Washington

Abstract. - This paper discusses two testing methods used to determine system compatibility and to satisfy requirements of MIL-E-6051. Method A and Method B are described separately and the advantages and disadvantages of each one discussed. The measurement and susceptibility tests are accomplished in parallel when Method A is used and in series when Method B is used. Method A requires more equipment and personnel but conserves time. Method B takes longer but is more realistic and provides better assurance of compatibility.

## I. INTRODUCTION

The basic philosophy of testing a system for interference compatibility is to assure that all subsystems do, in fact, operate together in the system with an adequate margin of safety in regard to interference. This paper discusses two approaches to system interference compatibility testing and compares the two methods. Both methods have the common objective of verifying by test that, as a result of interference control, the system meets the requirements of MIL-E-6051.

### Introduction to Methods

The primary reason for considering two methods of accomplishing a system test is time. Frequently, hardware delivery schedules require system interference tests to be accomplished in the least time with cost a secondary consideration. Most often however, cost is the controlling factor. The interference engineer must consider these two factors, as well as the technical aspects, when planning a system test. The two methods discussed consider these factors.

Both methods require prior analysis of the system to determine major problem areas before the test begins. Both methods require measurement of interference voltages within the system, analysis of the interference data, and determination of the effect of increased interference voltages upon the subsystems and upon the system.

The differences between the methods occur from the manner in which the increased interference is introduced and in the resulting time required to complete the entire system test. Figure 1 shows the basic time comparison of the two methods.

Method A is essentially a parallel operation even though the subsystem susceptibility, or interference insertion, portion of the test lags slightly the measurement portion of the test. Method B is a serial operation, since it is necessary to complete the measurement portion of the test before embarking on the susceptibility portion.

## II. METHOD A

Method A requires that an initial measurement be made of all the interference voltages within the system. The measurement portion of the system test is a data-gathering expedition divided into two parts: (1) measurement of radiated interference appearing on receiver inputs and (2) measurement of interference conducted on power lines. As these data become available, they are analyzed and organized for insertion into the subsystems. The inserted interference, measured interference increased by 6 db, is applied to each subsystem while the output of the subsystem is monitored to determine if the interference results in a malfunction.

During the data analysis and susceptibility portions of the test, more data are obtained from other parts of the system. The overall result is a steady flow of data; from the initial system analysis through to the final monitoring of the subsystems involved.

### Radiated Interference Measurement

Each antenna of the system is monitored in turn by disconnecting the associated receiver and connecting a field-intensity receiver to that antenna. While the other subsystems are energized in a normal sequence, the field-intensity receiver is tuned over the frequency band of the system receiver and the transient interference level recorded. During this portion of the test, time is saved by using multiple, field-intensity receivers connected to recording oscillographs.

The measurement process is repeated until the transient interference at each system antenna has been measured over the allocated frequency band, the image frequencies, and any other frequencies of interest. As measurements for each antenna are completed, the data are analyzed for the susceptibility test.

After the measurement of transient interference, normal interference on antennas is measured. Particular attention is given to system fundamental and harmonic frequencies and to possible combinations that could result in spurious receiver response.

The data from measurements on each antenna are analyzed and prepared for insertion in the receiving subsystems that use the antenna.

### Conducted-Interference Measurements

Besides the measurements on antennas, interference data must be obtained from power lines. Transient interference, as well as normal operating interference must be measured.

Power-line transient interference is measured while each electrically operated unit in the system is energized. After the measurement of transient interference, normal interference (exclusive of transients) on power lines is measured. Particular attention is given to system operating frequencies. In both cases, the data are recorded for subsequent analysis.

Data Analysis

All data from the measurement phase are analyzed for applicability to each subsystem. Amplitude, frequency, time sequence, and character of interference are considered in this analysis.

The set of data for each subsystem is tabulated for the power lines used by that subsystem. Where the subsystem is a radio-frequency receiver, the data obtained from its antenna are also tabulated. The data, with the amplitude increased by 6 db, are tabulated as to frequency, modulation characteristics, and antenna or power lead on which measurements were made. As the system measurement test progresses, more data becomes available and the analyzed data are supplied continuously for the subsystem tests.

Susceptibility Test

Concurrent with the start of the system measurement tests, the subsystems are set up in the laboratories for susceptibility tests.

The laboratory subsystems are adjusted for the most sensitive operating conditions. The operating signal inputs to receivers are adjusted approximately 3 db above minimum operating level. Power inputs are set to normal values. The interference data supplied by the analysis is inserted in power lines and receiver inputs. This interference is simulated with standard signal generators, impulse generators, and special transient generators. The signals are monitored by field-intensity receivers.

During these susceptibility tests, each subsystem is monitored for proper operation and evidence of malfunction caused by interference. When the analyzed data have been applied to all subsystems without malfunction resulting, the system has satisfied the requirements of MIL-E-6051, and compatibility has been verified.

Advantages

The primary advantage of Method A is the saving of calendar time. The subsystem tests follow soon after the measurement tests and when the subsystem tests are completed, the overall system test is finished. This time saving is achieved by using more test personnel, equipment and laboratory facilities.

Subsystems are operated for a short time during Method A tests, since each subsystem is energized only for the time required to conduct the test.

With Method A interference insertion problems are few. The accessibility of test monitor points, power line inputs, and receiver inputs allows easy insertion. Receivers can be tuned easily for the worst condition of interference.

Disadvantages

However there are some disadvantages to Method A, and one of these is the use of many subsystems. Since each sensitive sub-unit in the system is required to have its laboratory counterpart, at least two of these units are removed from production delivery channels for the duration of the test. Very often, because of unique modulation characteristics, a third subsystem must be used as an interference source. This requirement for a relatively large number of units during early production can be undesirable.

Manning the laboratory test requires personnel other than those engaged in the measurement and analysis. Each subsystem must be manned individually when the interference data for common power lines is inserted. Use of a single test team would increase the time to complete the tests.

When several subsystems and test teams are operating at one time, the requirements for interference simulation signal generators can become acute. Testing several subsystems simultaneously requires considerable laboratory space and facilities. It may be necessary to rent equipment and space for the duration of the susceptibility tests. It may even be necessary to pre-empt laboratory space of other departments, thus affecting their work schedule.

An important technical disadvantage of Method A is the inability to duplicate system conditions exactly. Power-line impedance in an aircraft system can vary from one ohm to over 700 ohms in the test frequency range. It is not possible to duplicate these system impedance conditions exactly in the laboratory. The Line Stabilization Network of MIL-I-6181 is useful, but this device can be used only in a narrow frequency range and it does not duplicate system conditions.

Also, the problem of interference standing waves on the system power lines must be considered. In small systems where power-line length is short, the problem is of concern only at the higher frequencies. In large systems, such as Saturn and Dyna-Soar, the electrical power lines can be very long and the standing wave problem must be considered even in the broadcast frequencies.

## III. METHOD B

Method B uses the same basic approach of system interference measurement, data analysis, and data insertion as Method A. The objective, determining system compatibility, is the same for each. Measurement data is obtained in a similar manner but there are differences due to Method B insertion techniques. The data from the measurement operation are analyzed for effect on the subsystem operating in the system. Analyzed data must be completed before the system susceptibility test can begin. In Method B, completion of each operation is dependent upon completion of the preceding one.

Radiated Interference Measurements

As in Method A, radiated measurements are conducted first. Monitoring the system antennas for interference signals, using Method B, is different from Method A because of the difference in the susceptibility test techniques. For Method A, the antenna interference is inserted in the subsystem

alone. For Method B, it is inserted in receiver subsystems operating within the system. The system antennas remain connected during the antenna measurement period for Method B.

The system is operated in the normal manner and interference voltages on the antenna are measured. The procedure for measuring transient as well as normal operating radiated interference is the same for both methods.

The data from the antenna portion of the system test are analyzed and stored while the next part of the measurement test is performed.

Conducted-Interference Measurements

Following the antenna tests, conducted interference measurement data for Method B are obtained exactly as in Method A. Power-line transient interference and normal operating interference are measured in the system. The resulting data are analyzed for the system susceptibility test.

Data Analysis

Analysis of data from the measurement tests begin as each segment of the test is completed. The measured interference data are analyzed with regard to the effect on the subsystems when they are operated in the system. Interference amplitude, frequency and time sequence are related to each subsystem that could exhibit malfunction in the system. The measured interference data, increased by 6 db, are tabulated and organized on the basis of the antenna or power-line on which it was measured. A set of data is prepared for each system network. The subsystems that should be monitored during the susceptibility test on that network are noted.

Data from early part of the system test have been prepared and are ready for the susceptibility test when the measurement test is completed. Analysis continues until all data are prepared for this susceptibility test.

Susceptibility Tests

Upon completion of the system interference measurements, insertion of the analyzed data begins. The same test engineers who obtained the system measurement data also are responsible for susceptibility tests.

Subsystems are tested as units of the system during these susceptibility tests. Data prepared by the analysis engineers are inserted on each system power line and antenna, in turn. The interference susceptibility level is monitored in the same manner it was measured for the original data, using the same instruments connected to the same test points. The increased interference level in each receiver input can be simulated by system transmitters, connected in place of the antenna.

The mechanics of injecting interference in power lines is often difficult since system power lines usually carry large currents. Inserting interference in these lines, without appreciably disturbing the system, requires

specially designed current transformers and high-power interference generators. This problem is not evident in Method A, since the power lines to individual subsystems usually conduct small currents and the susceptibility test methods of MIL-I-6181 are usually sufficient.

During these system tests, the critical outputs of all subsystems are monitored for evidence of malfunction. If no malfunction occurs which is attributable to interference, the subsystems are compatible within the system and the requirements of MIL-E-6051 have been satisfied.

Advantages

An important advantage of Method B is the need for fewer test personnel than Method A. A separate crew for subsystem tests is not required since all testing is done in the system.

Less laboratory space, test equipment, and other facilities are required by Method B. This requirement is especially important when these facilities are limited and is one of the main reasons Method A is more costly. Method B provides more realistic system testing by approximating the usual operating interference conditions more closely. Since all subsystems are operating, each is affected by the total system interference environment. As each part of the system is subjected to an additional amount of interference, the total interference environment is increased. The result is that each unit of the system is tested not only by the normal environment but by interference to which it may be particularly susceptible. Therefore, determination of system compatibility is achieved more realistically.

System conditions are duplicated in another way. The increased interference is introduced into the same power lines on which the original data were measured. The effect of the power line impedance at the monitoring test point is therefore minimized.

Verification of the 6 db safety margin is easier and more valid with Method B than with Method A. The same monitor receivers are still connected to the same system test points as were used for measurement, and all subsystems are tested at once. When the interference is inserted, the increase of 6 db can be readily measured with the receiver.

Disadvantages

The main disadvantage of Method B is that more test time is required on the complete test vehicle or system. In Method B, the system is operated during the entire time measurement data is obtained, as well as during the time required to conduct the susceptibility tests. The test time on a system used with Method B is therefore greater than Method A since the latter only requires the entire system while measurements are obtained.

The length of system operating time for Method B also presents subsystem logistic problems. The subsystems are operated almost continuously during the entire test. The test time often will be greater than the designed life of the equipment. Provision must be made to continually monitor the subsystems for operating malfunctions and replace them at the proper time.

Method B presents more interference insertion problems than Method A because of the low impedance of system power lines. Special high-power transient generators, current transformers, and other devices are necessary to reproduce and insert power-line interference at the required level.

The advantages and disadvantages of both methods are summarized and compared in Figure 2.

## IV. CONCLUSIONS

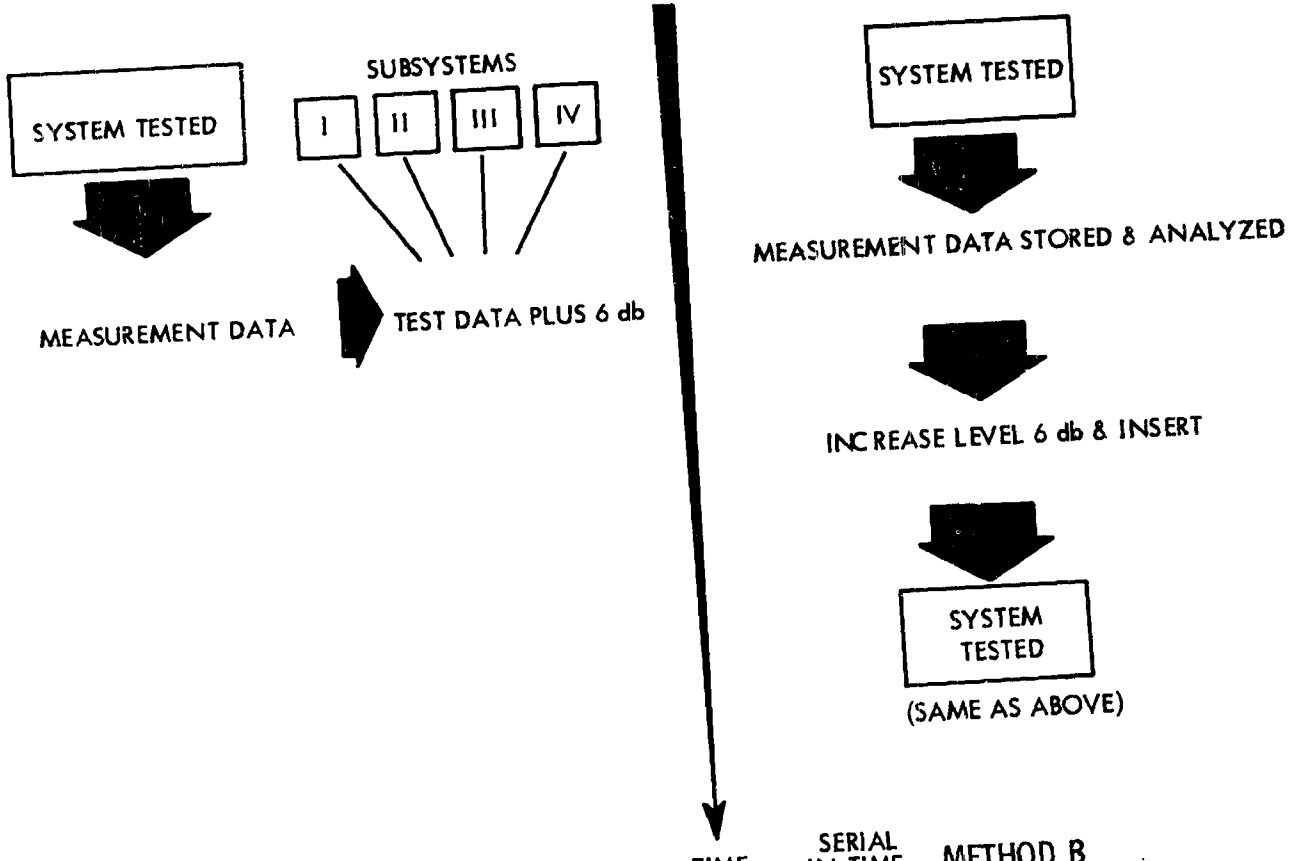
Method B is preferred, since it tests each subsystem in the presence of the actual system interference environment, eliminates the anomaly of power-line impedance, and requires fewer personnel and fewer laboratory facilities than Method A. Therefore, the cost of Method B is less as compared to the cost of Method A.

The great advantage of Method A is the considerable saving in over-all test time. However, the decreased test time is purchased with increased expenditure for laboratory facilities and personnel.

Circumstances may dictate a judicious combination of the two methods to obtain a reasonable balance of cost and time.

## ACKNOWLEDGEMENTS

The author wishes to acknowledge the helpful contributions of Messrs. J. J. Dicomes, A. E. Dorband, H. H. Judson, Jr., J. E. Maynard, Lee Trippett and H. C. Todd who reviewed the paper.




TIME COMPARISON

FIGURE 1

METHOD "A"

ADVANTAGES

- LESS CALENDAR TIME
- LESS SUBSYSTEM OPERATING TIME
- FEWER INTERFERENCE INSERTION PROBLEMS
- EASIER RECEIVER TUNING

DISADVANTAGES

- MANY SUBSYSTEMS
- MORE TEST PERSONNEL
- DUPLICATE TEST EQUIPMENT
- SYSTEM CONDITIONS NOT EXACTLY DUPLICATED

METHOD "B"

ADVANTAGES

- FEWER TEST PERSONNEL
- LESS LAB EQUIPMENT & FACILITIES
- MORE REALISTIC SYSTEM TESTING
- SYSTEM CONDITIONS DUPLICATED
- EASIER VERIFICATION OF 6 db SAFETY MARGIN

DISADVANTAGES

- MORE TIME ON TEST VEHICLE
- SUBSYSTEM LOGISTIC PROBLEMS
- MORE INTERFERENCE INSERTION PROBLEMS

COMPARISON OF METHODS

FIGURE 2

# SPECTRAL MEASUREMENTS OF RADIO INTERFERENCE WITH A COHERENT MEMORY FILTER

J. Capon
Federal Scientific Corporation
615 West 131st Street
New York 27, New York

Abstract. It is often desirable to know the spectrum of a signal. This measurement has been performed by devices which could be divided, with few exceptions, into two groups: the heterodyne type, and the bank-of-filters type. The heterodyne type of spectrum analyzer utilizes a fixed narrow-band intermediate-frequency filter and a tunable local oscillator. This device does not analyze the spectrum in real time; i.e., it is not possible to measure the entire spectrum without recording the signal and playing it back many times.

The second type of spectrum analyzer employs a bank of filters. The measurement of the spectrum with this device can take place in real time, so that this type of analyzer possesses an advantage over the previous one, in this respect. However, it is cumbersome to implement a bank of filters, and, in addition, it yields only a gross approximation of the signal spectrum.

A different approach to the spectrum analysis problem has been proposed. This approach utilizes a recirculating delay-line-heterodyne feedback loop to obtain an excellent approximation of the signal spectrum in real time. This device is known as the coherent memory filter, and it has the advantages, with respect to the bank of filters, of being capable of observing rapid changes in the input spectrum that occur from one processing period to the next, and of providing continuous spectral coverage. In addition, the processing period, or integration time, of the coherent memory filter is easily adjustable, so that variable-resolution analysis of nonstationary spectra is possible. This is the equivalent of continually changing the number of filters, and their bandwidths, in a filter bank consisting of hundreds of filters.

Experimental results obtained in the analysis of radio interference signals are presented. It is found experimentally that a processing time of about 20 msec is desirable for the measurement of the spectra of these signals. The frequency coverage of the spectral analysis was 0 to 8kc, and triangular-weighting was employed, so that an effective resolution of 73 cps was obtained. Thus, roughly speaking, the equivalent of a filter bank with approximately 100 filters, each with an effective bandwidth of 73 cps, was synthesized.

## I. INTRODUCTION

There are many types of radio interference signals which are of a random nature. In many instances, these signals can be characterized by their spectra. In the present work, experimental results concerning the spectra of two kinds of radio interference will be presented, namely, atmospheric whistlers and ignition noise.

These spectral measurements have been made previously by analyzers which could be divided, with few exceptions, into two groups: the heterodyne type, and the bank-of-filters type. The heterodyne type of spectrum analyzer utilizes a fixed narrow-band intermediate-frequency filter and a tunable local oscillator. This device cannot analyze the spectrum in real time; i.e., the information concerning the spectrum of the signal cannot be read out in a time which is short, or comparable, to the processing, or integration, time of the analyzer.

The second type of spectrum analyzer employs a bank of filters. The measurement of the spectrum with this device can take place in real time, so that this type of analyzer possesses an advantage over the previous one, in this respect. However, it is cumbersome to implement a bank of filters, and, in addition, only a gross approximation of the signal spectrum is yielded (as with the previous analyzer).

The coherent memory filter[1] represents a relatively new approach to the spectrum analysis problem. This approach utilizes a recirculating delay-line-heterodyne feedback loop to obtain an excellent approximation of the signal spectrum in real time. This analyzer also has the advantages, with respect to the bank-of-filters type, of being capable of observing rapid changes in the input spectrum that occur from one processing period to the next, and of providing continuous spectral coverage. The purpose of the present work is to illustrate the accuracy with which the spectra of radio interference signals can be measured, and to point out the high speed with which these results can be obtained. In fact, the coherent memory filter operates at a speed which is very close to the theoretically maximum information extraction rate.

## II. EXPERIMENTAL RESULTS

The experimental results obtained with the coherent memory filter concerning atmospheric whistlers are shown in Figs. 1 to 4, and those on ignition noise are shown in Figs. 5 and 6. It was found experimentally that a processing time of about 20 msec is desirable for the measurement of the spectra of atmospheric whistlers and ignition noise. The spectra are read out in a time of about 0.1 msec, which is quite small compared to the processing time. Successive frames in Figs. 1, 3, and 5 are sequential in time and are read from top to bottom and then from left to right.

The frequency coverage of the spectrum analysis is 0 to 8 kc, and the horizontal axis in each frame is calibrated linearly in frequency between 0 and 8 kc. At the bottom of each column of frames in Figs. 1, 3, and 5, there is a frame containing frequency markers that are spaced 400 cps apart, from 0 to 8 kc.

A triangular-weighting function was employed to time-weight the input signal of the coherent memory filter, so that an effective resolution of 73 cps was obtained. Thus, roughly speaking, the equivalent of a filter bank extending from 0 to 8 kc, with approximately 110 filters, each having an effective bandwidth of 73 cps, was synthesized.

The fine detail which can be obtained in the spectrum analysis is pointed out in Figs. 2, 4, and 6. In these figures, a single frame is shown, and this frame represents an enlargement of a particular frame, in the preceding figure, which has an arrow pointing to it.

The manner in which the frequency content of the atmospheric whistler varies with time is shown quite vividly in Figs. 1 and 3. It is seen that the energy of the signal is concentrated at about 6 kc at the beginning of the whistler and shifts to about 1 kc at the end of the whistler. The results on the ignition noise in Figs. 5 and 6 illustrate clearly the random nature of this type of radio interference.

## III. CONCLUSIONS

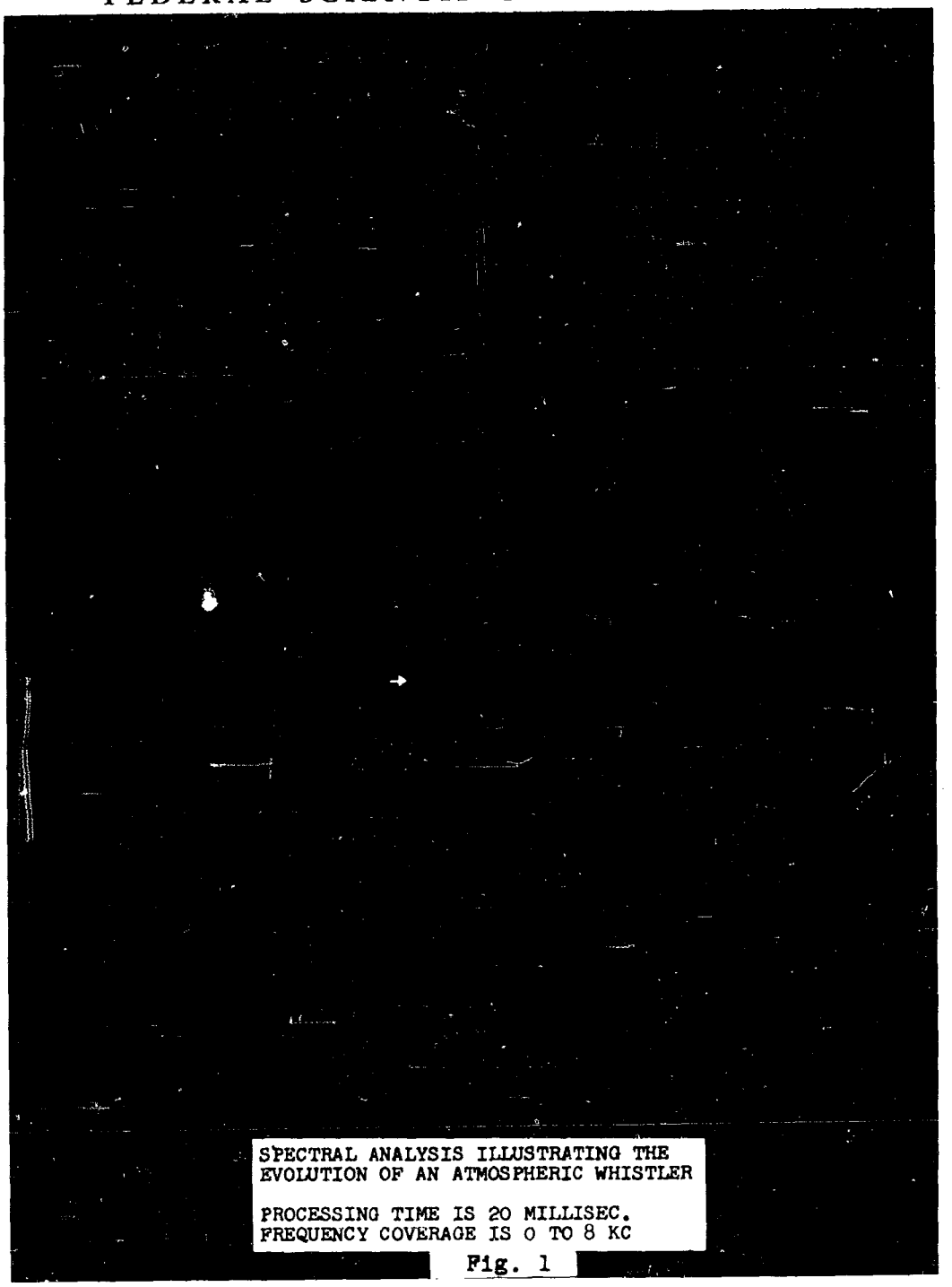
The precision and speed with which spectral measurements of radio interference signals can be made with a coherent memory filter have been illustrated for atmospheric whistlers and ignition noise. The output of the coherent memory filter can be put in digital form so that the spectral information can be processed in a digital computer, in real time. Thus, vast amounts of spectral data can be processed automatically by a digital computer, in real time. This has important implications in any research program dealing with a determination of the salient characteristics of radio frequency interference signals.

## ACKNOWLEDGEMENT

The radio interference signals were supplied on a tape recording through the kindness of Prof. R. A. Helliwell of Standford University.

## REFERENCE

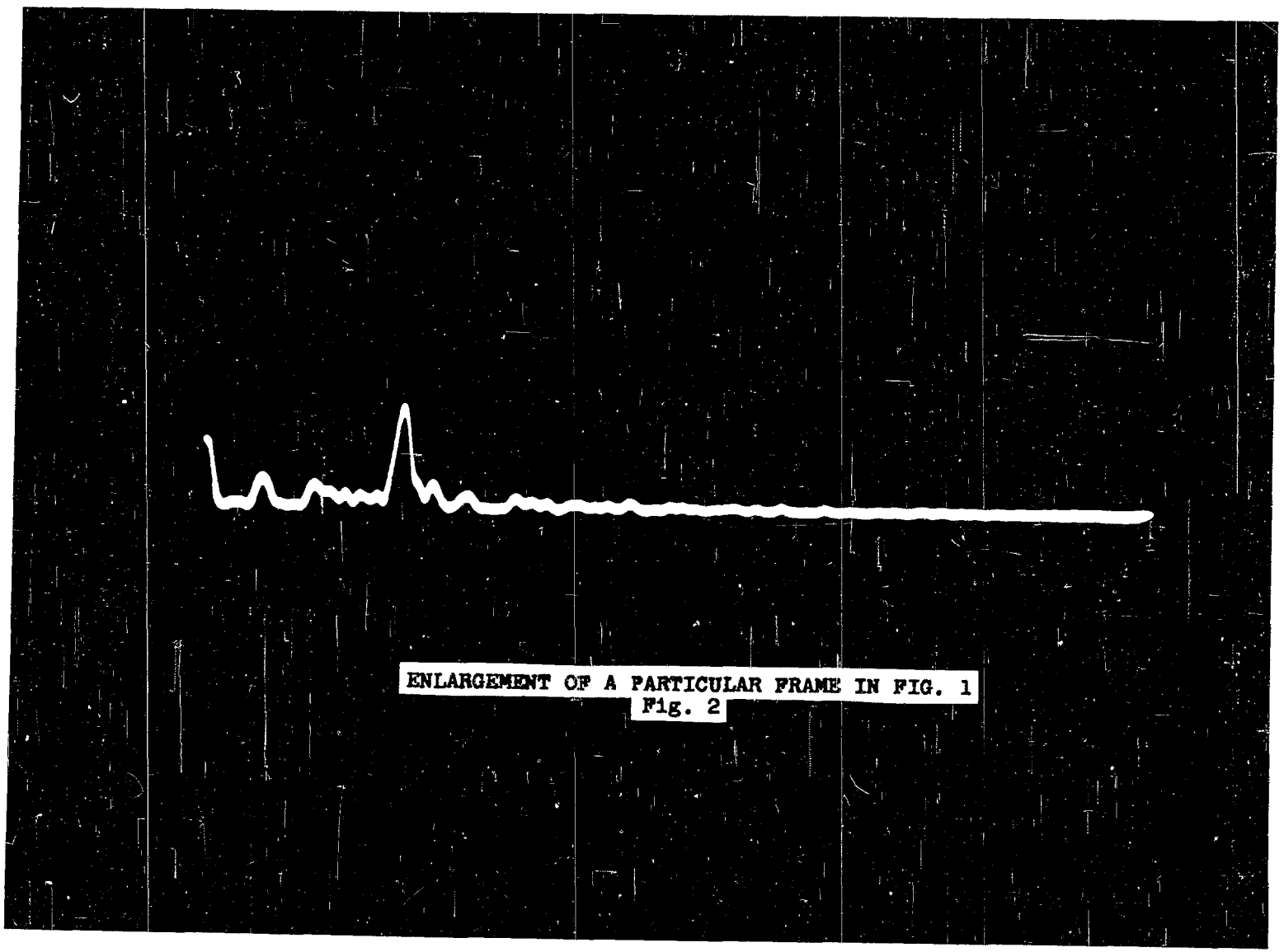
1. J. Capon, "High-Speed Fourier Analysis with Recirculating Delay-Line-Heterodyne Feedback Loops", IRE Transactions on Instrumentation, Vol. I-10, pp. 32-37; June 1961.



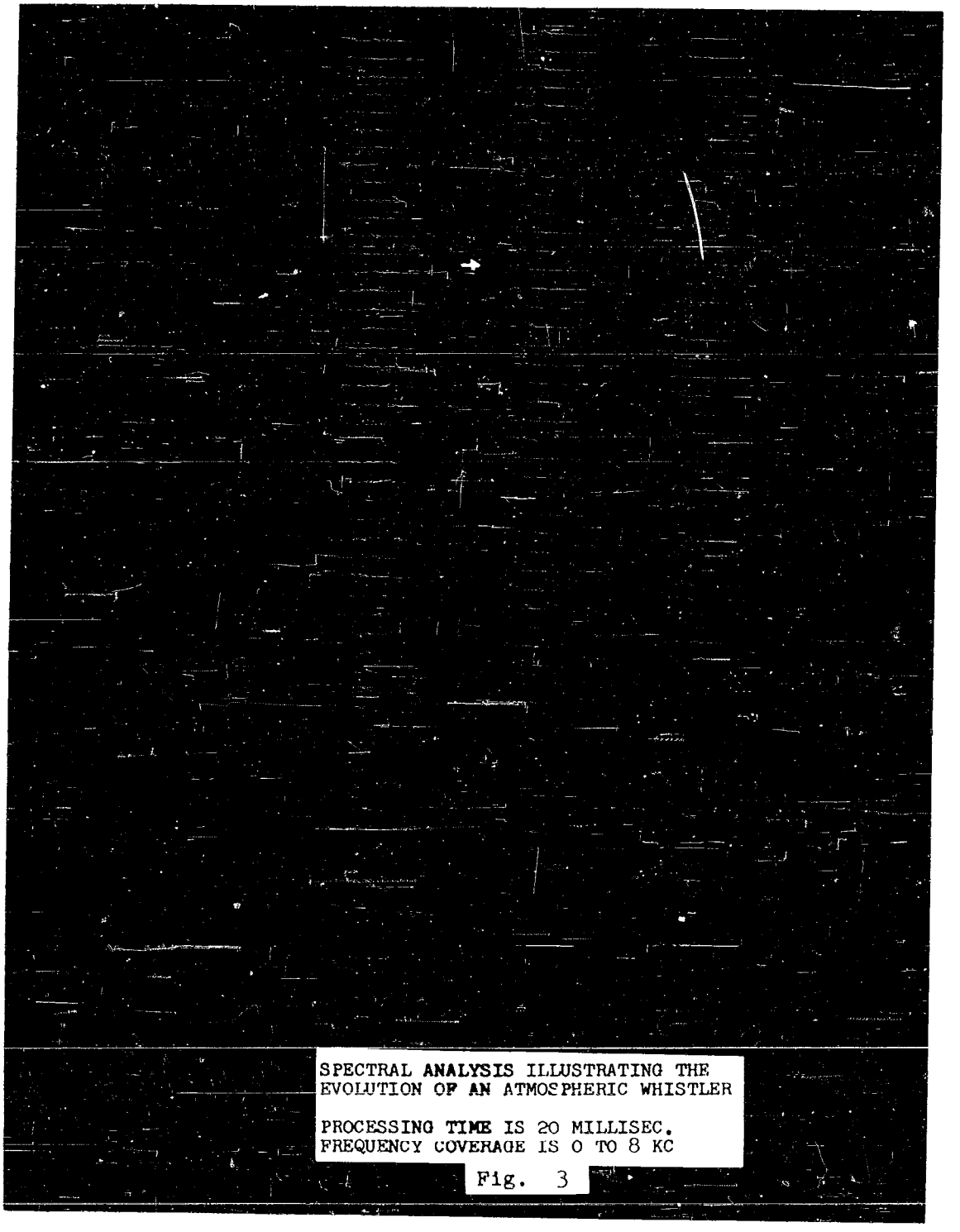
SPECTRAL ANALYSIS ILLUSTRATING THE EVOLUTION OF AN ATMOSPHERIC WHISTLER

PROCESSING TIME IS 20 MILLISEC.
FREQUENCY COVERAGE IS 0 TO 8 KC

Fig. 1



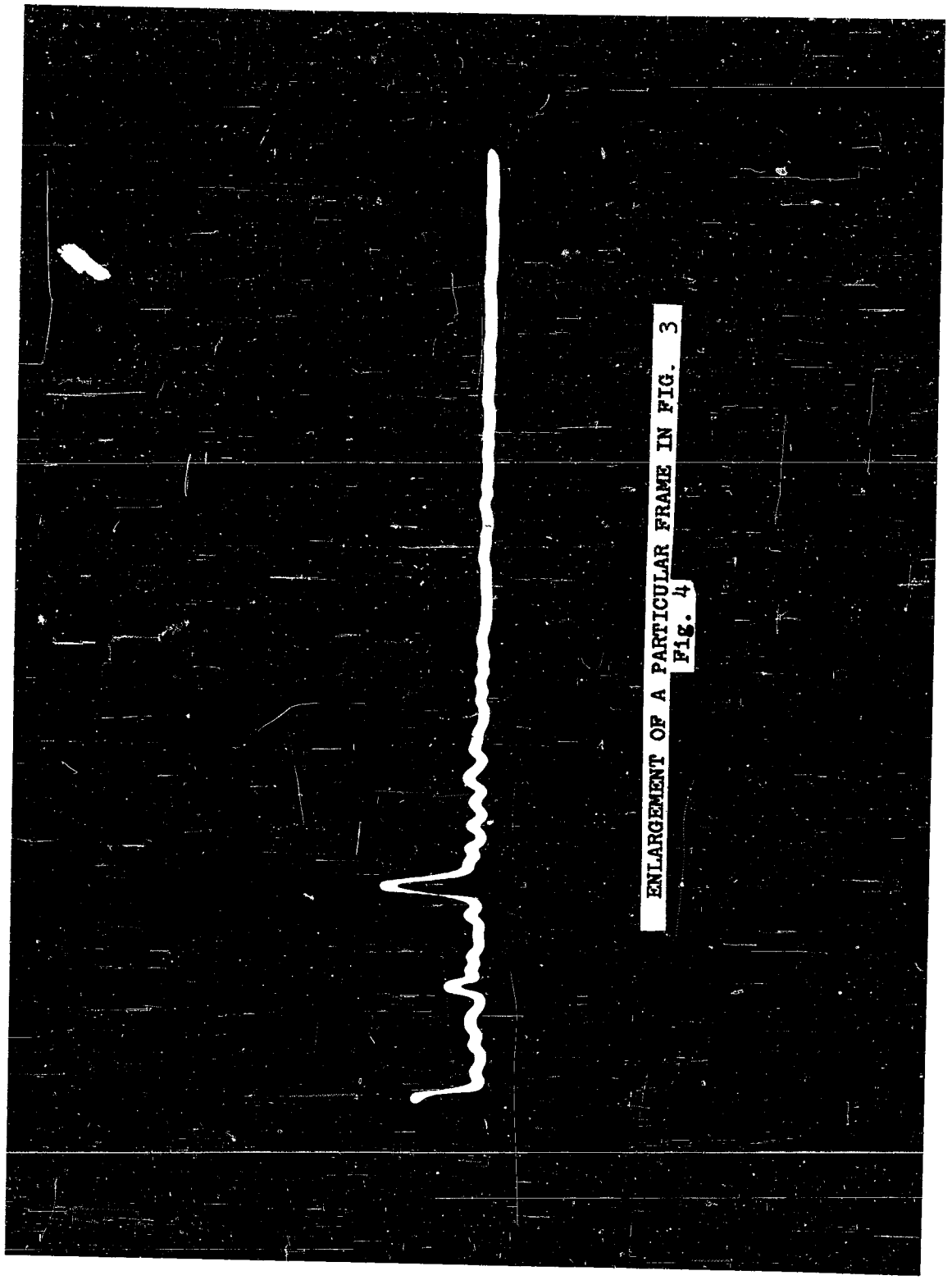
ENLARGEMENT OF A PARTICULAR FRAME IN FIG. 1
Fig. 2



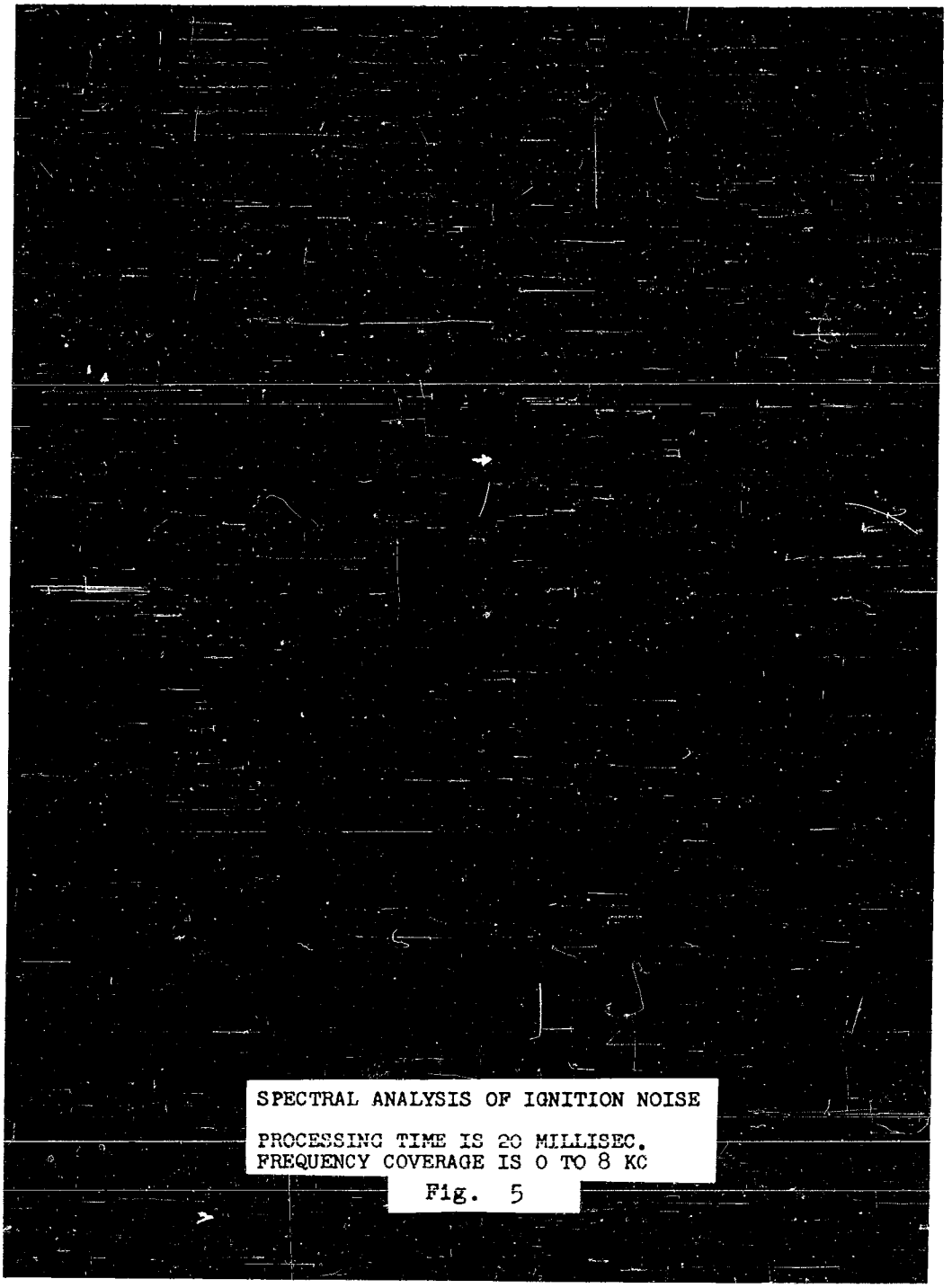
SPECTRAL ANALYSIS ILLUSTRATING THE EVOLUTION OF AN ATMOSPHERIC WHISTLER

PROCESSING TIME IS 20 MILLISEC.
FREQUENCY COVERAGE IS 0 TO 8 KC

Fig. 3



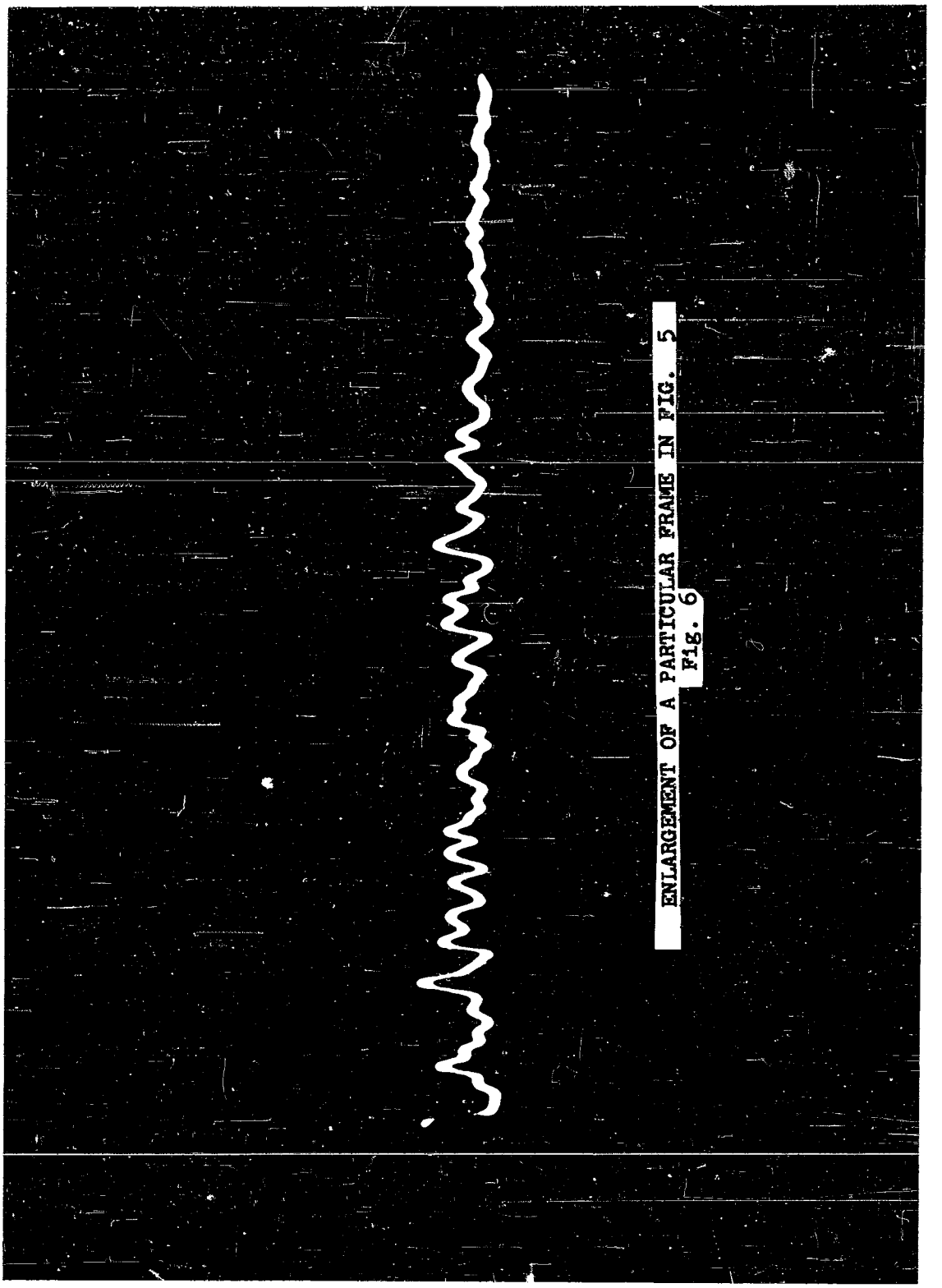
ENLARGEMENT OF A PARTICULAR FRAME IN FIG. 3
Fig. 4



SPECTRAL ANALYSIS OF IGNITION NOISE

PROCESSING TIME IS 20 MILLISEC.
FREQUENCY COVERAGE IS 0 TO 8 KC

Fig. 5



ENLARGEMENT OF A PARTICULAR FRAME IN FIG. 5
Fig. 6

# MIL-I-006051B AUDIO-TRANSIENT GENERATOR

R. C. Dyer
The Boeing Company
Seattle, Washington

Abstract. - Interference susceptibility testing per MIL-I-006051B requires that the interference present in aeronautical weapon systems be no greater than one-half the amplitude required to cause malfunction. One method of testing weapon systems to this criteria is to double the magnitude of the interference present and determine if malfunction occurs.

This paper describes an audio-frequency transient generator built to generate interference external to the system at twice the measured amplitude and to inject this interference back into the weapon system. The generator acts as the operating power source as well as the transient source for the equipment under test. Both a-c and d-c power sources are available for the equipment under test, with or without transients on these power sources. Shaping of transients and injecting them on the power lines are discussed. Operation of the generator has proven highly successful.

## I. INTRODUCTION

The Boeing Company has constructed an audio-transient generator used in testing aeronautical weapon systems (missiles, aircraft, etc.) to the requirements of MIL-I-006051B.

MIL-I-006051B is the military specification that defines the limit of allowable radio self interference in aeronautical weapon systems.

The primary requirement of MIL-I-006051B is that all normally present interference shall be no greater than one-half the level necessary to cause malfunction. The method used to prove compliance with this requirement is to measure the existing, internal interference of the missile or system, simulate a similar interference pattern external to the missile; and insert the simulated interference back into the missile at twice the original measured value. If no missile malfunction occurs, the requirement of MIL-I-006051B is met.

The philosophy behind this method of testing is that all areas of the system under test are completely infiltrated by the test transient, eliminating the necessity of analyzing the system for the most susceptible points and monitoring only these. The possibility of overlooking some critical point is eliminated and internal modification of the equipment under test is not necessary. Assembly of special monitoring equipment is obviated as normal operation is the only quality monitored.

This test system involves two major problems. The first is the external generation of audio-frequency transients of the same shape as those observed in the missile. The second is the generation of the transients with sufficient power to inject the transient onto the missile power lines.

The audio-transient generator was built to perform both functions. The transient shape is adjustable over a wide range and a transient power output of 400 watts is available. Assembling general purpose test equipment to do this job is difficult and time consuming.

## II. TRANSIENT SHAPE GENERATION

### Required Transients

The shapes of the required a-c and d-c transients were determined by observation of the transients existing in various systems. All of the d-c transients observed were of one basic shape (Figure 1) or deviations thereof. The most common deviation was a "carrier" amplitude modulated by the pulse of Figure 1 (Figure 2).

All the a-c transients were basically the quiescent a-c line voltage amplitude modulated by the transients of Figure 2 (Figure 3).

All of the transients observed, first in experimentation and later in actual missile testing, were variations of the above three patterns. The observed transients varied in time duration but the proportionate shape was consistent.

These shapes are to be expected when consideration is given to the missile circuitry involved. The pulse of Figure 1 is comparable to the output of a low-pass circuit with a square-wave input, Figure 4. The missile wiring offers high-capacitance paths to ground for any high-frequency transient components; that is, it acts as a natural, low-pass filter.

The pulse of Figure 2 is essentially a ringing pulse caused by exciting an inductance-capacitance circuit with a step function. Both the inductance and capacitance are easily provided by the missile wiring and circuitry.

### Shape Generation

Since the basic transient shapes were consistent, the problem was to generate these families of shapes over an adjustable range of pulse length. The shaping process was started with the pulse of Figure 1.

This shaping was accomplished by integrating, clipping, and differentiating a rectangular wave.

The rectangular wave is integrated (Figure 5).

The pulse of Figure 5 is then differentiated and the trailing edge clipped (Figure 6).

The resultant pulse is the desired shape due to the imperfect differentiation of the leading edge of the pulse of Figure 5. The duration and proportion of this pulse are varied by changing the initial rectangular pulse length and by changing the time constants of the integrating and differentiating circuits. Pulse lengths from 0.01 seconds to 10 seconds are obtainable from the transient generator.

The shape of Figure 2 can be made by amplitude modulating a "carrier" with the pulse of Figure 6.

The "carrier" is obtained from a gated, free-running multivibrator. Three carrier shapes are available; rectangular, triangular, and sinusoidal. The rectangular wave is the multivibrator output, the triangular wave is obtained by integrating the multivibrator output, and the sine wave is approximated by putting the triangular wave through a sine-wave synthesizer. The synthesizer is a resistor-diode network that converts the triangular wave to an approximate sine wave by changing the slope of various sections of the triangular wave. The synthesizer output is shown in Figure 7.

The final, desired transient shape is obtained by amplitude modulating the carrier with the pulse. The amplitude modulation is accomplished by phase splitting the carrier, modulating, and subtracting the undesired frequency components. Figure 2 is a typical transient. If desired, the pulse alone may be used as the transient shape without any modulation, giving an output similar to Figure 1. Typical d-c transients are shown in Figure 8.

Transients on a-c voltages (Figure 3) are produced by amplitude modulation of the a-c voltage with the pulses of Figures 1 and 2.

## III. APPLYING TRANSIENTS TO POWER LEADS

### Comparison of Methods

The second major problem in building the transient generator was devising a method for putting large transients onto missile a-c and d-c power lines without lowering normal operating voltages and without damaging the transient or missile power sources.

If the transient supply is simply connected across a missile power line (Figure 9-a) the transient supply is operating into the parallel combination of the missile load and the output impedance of the missile power supply.

The low, output impedance of the missile power supply will make it difficult to vary the missile line voltage without causing large currents in the missile supply, with the attendant danger of burning out the missile supply.

If the transient source were placed in series with the missile supply (Figure 9-b), the output impedance of the transient source must be kept low to maintain normal operating voltage on the missile load and to prevent the transient source from absorbing power from the missile supply.

If the turns ratio of the coupling transformer is such as to keep the output impedance low, the transient output voltage will also be low, and the magnitude of the transient that can be applied will be limited accordingly.

Transients on D-C Power

The system of transient application used on d-c power lines (Figure 9-c), is in essence one of supplying power to the missile loads from an external power source through a controlled series resistance. Varying the series resistor according to the transient shape causes the voltage across the missile load to vary in inverse fashion. In terms of actual hardware, the series resistor is a series voltage regulator. The regulator supplies both normal operating voltage and transient voltages to the missile. In the quiescent state, the regulator supplies a constant regulated voltage. When a transient is desired, the transient shape is used to modulate the regulator reference voltage and the regulator output follows accordingly, applying the transient to the missile power line.

The series regulators are conventional circuits employing differential amplifiers operating over a wide dynamic range, allowing the regulator output voltage to follow changes in the reference voltage.

Output impedance of the regulators is less than 1 ohm. D-C power to operate both the regulators and their missile loads is furnished by conventional d-c power supplies.

Transients on A-C Power

The method for applying transients to a-c power lines differs from that used on d-c lines. In the a-c case, an a-c amplifier is used to operate the equipment under test, with an a-c modulator supplying the low-level a-c input to the amplifier. When transient shapes are put into the a-c modulator, transient modulation of the low-level a-c signal occurs. The transient-modulated signal then goes to the a-c amplifier where it is amplified and applied as primary a-c power to the item being tested. Typical a-c transients are shown in Figure 3.

Special A-C Method

Some loads draw more a-c power than can be supplied by readily available a-c amplifiers. A different method of generating a-c transients is used in these cases.

This method consists of operating the missile a-c load from two transformer secondaries connected in series. When a transient is desired, one of the secondaries is shorted, giving an instantaneous reduction in missile a-c voltage. The second transformer, actually a variable-power transformer, is then activated by a mechanical system to return the missile voltage to the normal operating value. A fuse must be replaced and the device set through a reset cycle each time a transient is thus generated. The type of transient generated is shown in Figure 10. Figure 11 is a schematic of the system and Figure 12 is a photograph of a preliminary hardware configuration.

## IV. GENERAL

Figure 9 is a block diagram of the complete transient generator. The signal generator and the d-c regulator-modulator are the transient shaping and voltage-regulator circuits described above. The sync unit is a reference-time generator that triggers the signal generator.

To test the susceptibility of equipment to transients, the item to be tested is connected to the d-c regulator-modulator. When the sync unit triggers the signal generator, the desired transient shape is produced by the generator. The transient then is fed to the d-c regulator-modulator as a reference voltage, and appears at the output of the d-c regulator-modulator as a transient applied to the primary d-c power source of the equipment under test.

When a-c lines are being tested the transient shape from the signal generator is fed to the a-c modulator-oscillator where the oscillator signal is modulated by the transient shape at a low signal level. The modulated a-c signal is then amplified by the a-c amplifier and used to drive the load under test.

Figure 14 is a photograph of the generator. The rack as pictured contains 6 signal generators, 7 d-c regulator-modulators, 3 a-c amplifiers, a sync unit and all supporting functions. This hardware configuration allows the simultaneous generation of 6 independent transients and the operation of at least as many separate power lines.

The transient generator can supply the following operating voltages with or without audio-frequency transients.

| Voltage | Maximum Current |
|---|---|
| + 400 vdc | 2.0 amps |
| + 300 vdc | 2.0 amps |
| + 250 vdc | 2.0 amps |
| + 150 vdc | 2.0 amps |
| + 28 vdc | 5.0 amps |
| - 28 vdc | 0.5 amps |
| - 150 vdc | 0.5 amps |
| - 250 vdc | 0.5 amps |
| - 300 vdc | 0.5 amps |
| 40 vac, 900 cps | 60 watts |
| 10 vac, 900 cps | 60 watts |
| 6 vac, 900 cps | 60 watts |

The maximum transient power that can be applied to the d-c voltages is limited by the maximum regulator current which in turn is limited by the current capacity of the series regulating tubes. When the impedance of the load is so large that current is not the limiting factor, the maximum transient power available is plus or minus 75 volts from the regulator operating voltage.

## V. CONCLUSION

The transient generator provides a satisfactory and very flexible means of testing the susceptibility of electronics systems to audio-frequency transients.

By injecting the transients on equipment power lines all maximum susceptibility points are checked without the necessity of analyzing the design and estimating the location of these points. Use of the generator requires no modification and little detail knowledge of the internal operation of the equipment being tested.

A wide variety of readily adjustable transient shapes expedites equipment testing and precludes the necessity of off-hand fabrication of each transient shape. Four hundred watts of conveniently usable transient power are available.



FIGURE 1 TYPICAL TRANSIENT

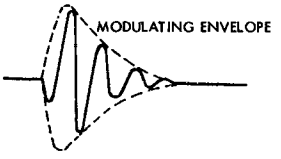



FIGURE 2 TYPICAL TRANSIENT




FIGURE 5 INTEGRATED SQUARE WAVE WITH TRAILING EDGE CLIPPED

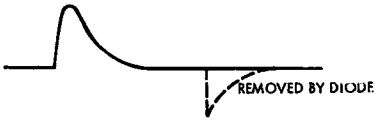
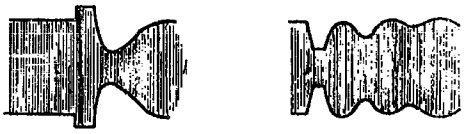



FIGURE 6 PULSE OF FIGURE 4 DIFFERENTIATED AND TRAILING EDGE CLIPPED



(a) VERTICAL 20V/CM HORIZONTAL 10MS/CM

(b) VERTICAL 20V/CM HORIZONTAL 20MS/CM

FIGURE 3 TYPICAL GENERATED A-C TRANSIENT

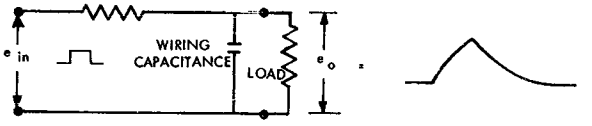



FIGURE 4 LOW PASS NETWORK CREATED BY WIRING CAPACITANCE

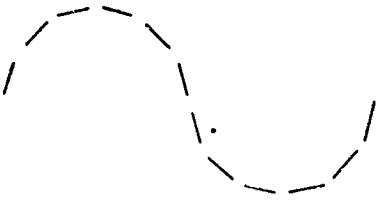


FIGURE 7 SYNTHESIZER OUTPUT

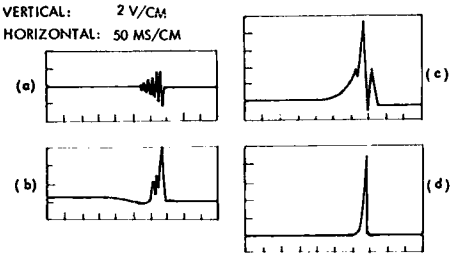



FIGURE 8 TYPICAL GENERATED D-C TRANSIENT

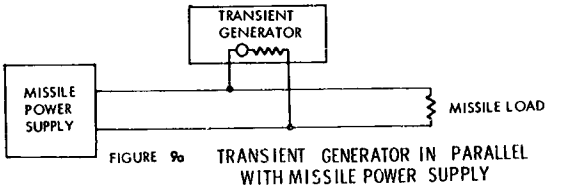



FIGURE 9a TRANSIENT GENERATOR IN PARALLEL WITH MISSILE POWER SUPPLY

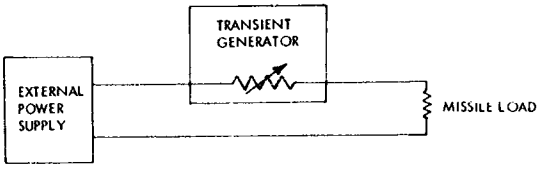



FIGURE 9c TRANSIENT GENERATOR AS PASSIVE DEVICE IN SERIES WITH MISSILE LOAD

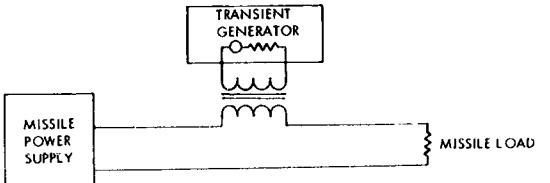



FIGURE 9b TRANSIENT GENERATOR IN SERIES WITH MISSILE POWER SUPPLY

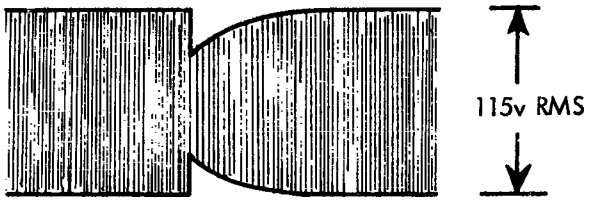



FIGURE 10 A-C TRANSIENT GENERATED BY TRANSFORMER CIRCUIT OF FIGURE 12.

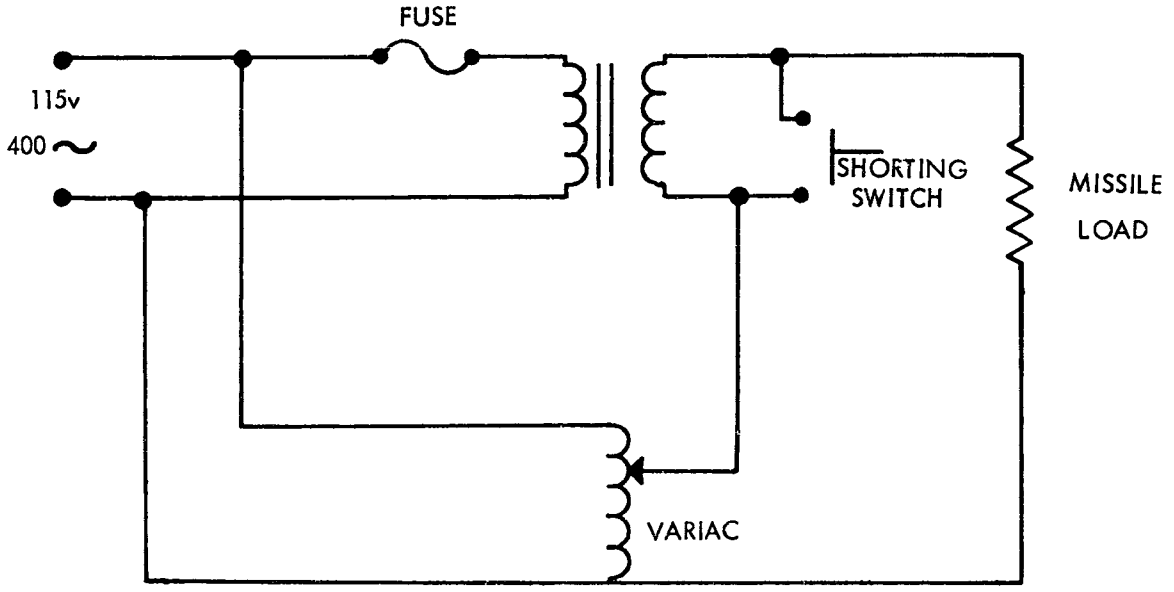
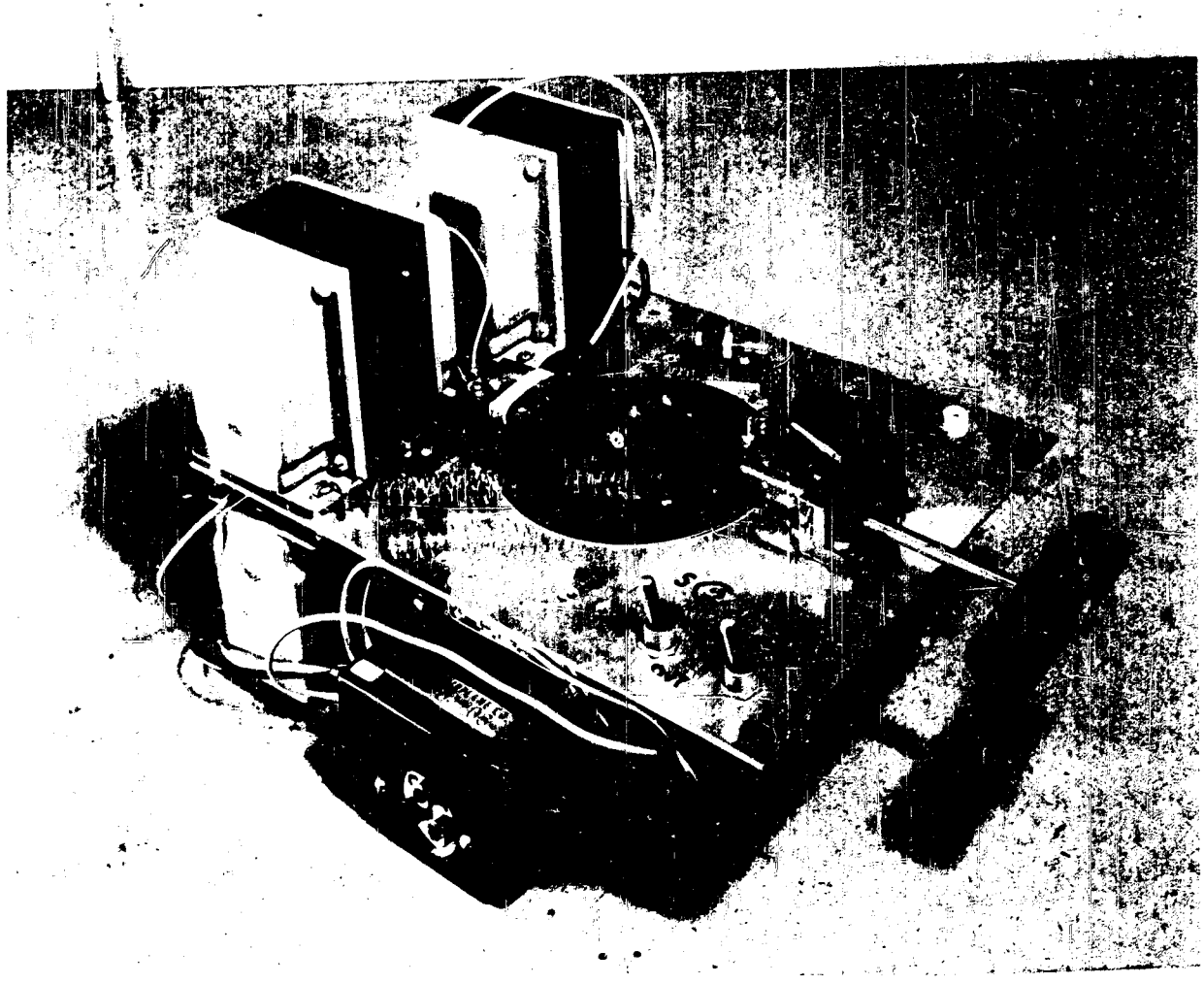



FIGURE 11 CIRCUIT USED TO PUT TRANSIENTS ON 115v, 400 CPS POWER LINE



SPECIAL A-C TRANSIENT GENERATOR

FIGURE 12

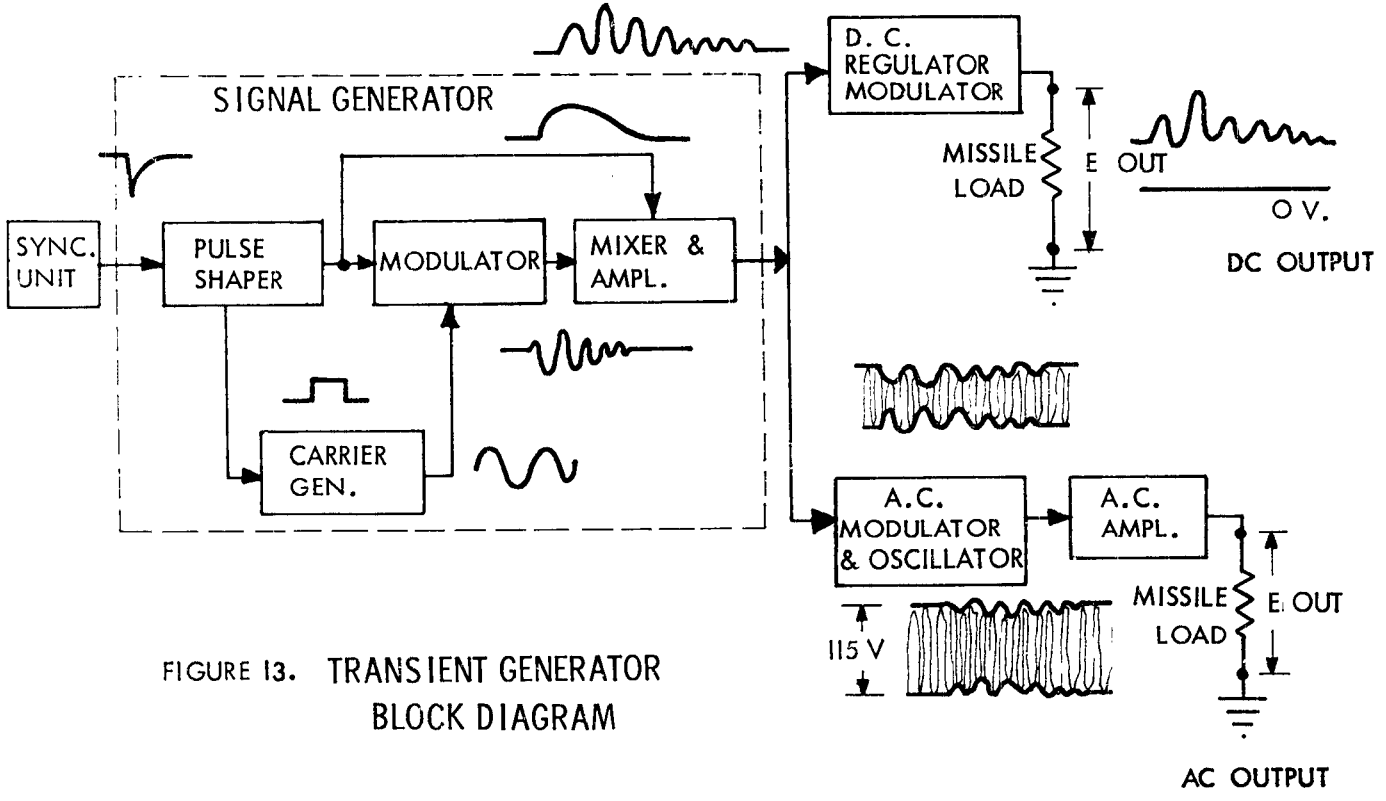
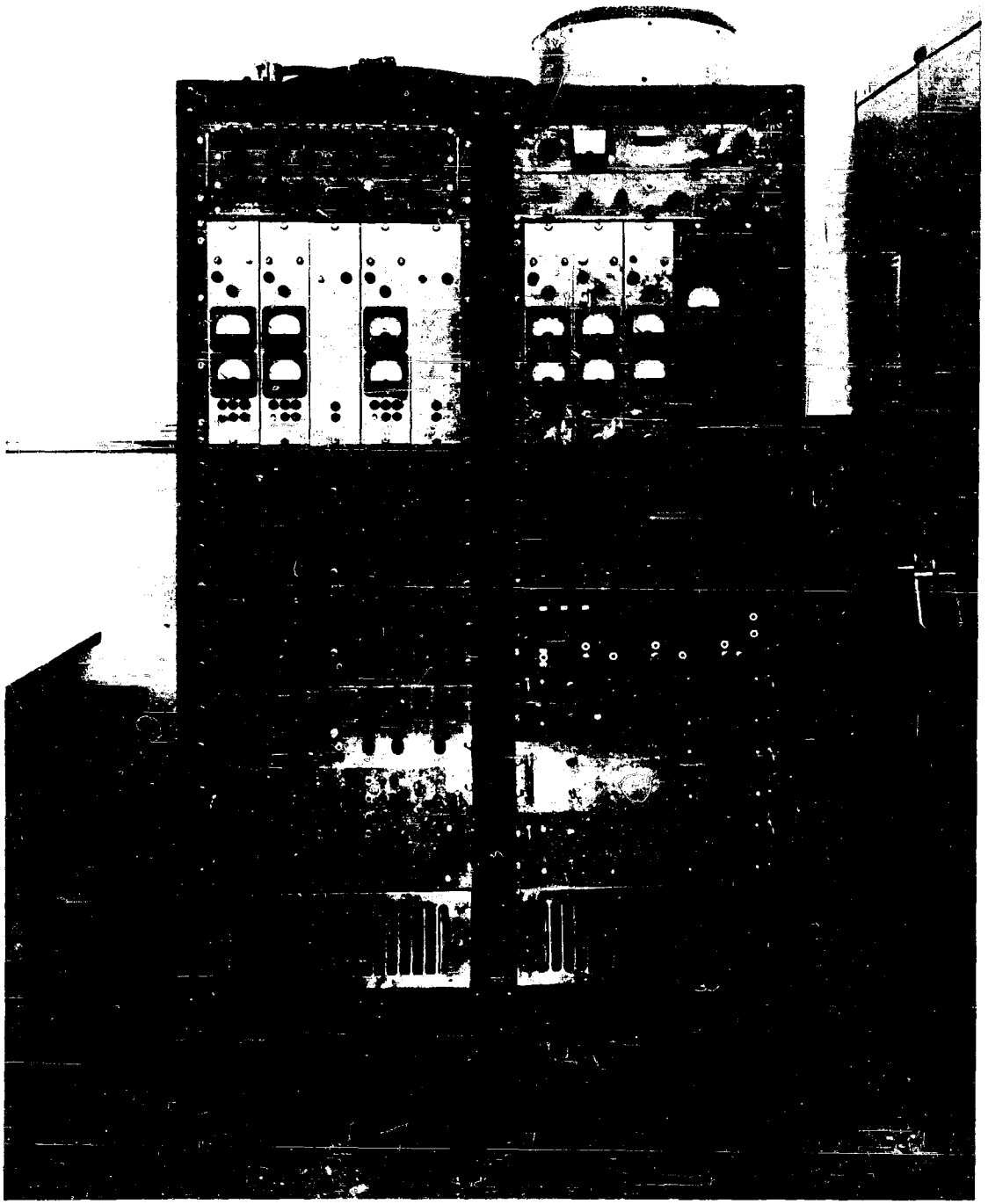



FIGURE 13. TRANSIENT GENERATOR BLOCK DIAGRAM



TRANSIENT GENERATOR

FIGURE 14

# A HIGH-POWER, WIDE-RANGE, ULTRA-STABLE MICROWAVE SIGNAL SOURCE

L. R. Moses
Electromagnetic Vulnerability Lab., RADC
Rome, N. Y.

D. E. Farmer and W. J. Messmer
American Electronic Laboratories, Inc.
Philadelphia, Pa.

Abstract. - This paper discusses the design and performance of a high-Power RF Signal Source developed by American Electronic Laboratories, Inc. for Rome Air Development Center. The Signal Source covers the frequency range of 40 mc to 40 kmc. The RF power output can exceed 100 watts at frequencies below 4 kmc. Above 4 kmc the power output falls off. Frequency stability of the order of one part in one hundred million is achieved by locking the system to an ultrastable standard. Pulse, sine, and square-wave amplitude modulation, and sawtooth frequency modulation are provided.

## I. INTRODUCTION

The intensive efforts now in progress to study and reduce the effects of radio frequency interference will require innumerable RF signal generators possessing a wide variety of properties. To the extent that versatility can be designed into a signal generator, the number of special-purpose instruments needed can be reduced. In that direction, the Electromagnetic Vulnerability Laboratory of the Rome Air Development Center has consolidated many of its instrumentation requirements in its specifications for a "High-Power, Wide-Range, Ultra-Stable, Microwave Signal Source." The purpose of this paper is to describe the equipment which has been developed by AEL to fulfill RADC's needs. Although most of the desirable properties of a versatile RF source are obvious, reviewing them briefly will provide a background to the description of the instrument:

### High Power Output

The maximum RF test power establishes, with other factors, the lower limit of sensitivity at which measurements can be made. Measurements of highly attenuated antenna lobes, skirt characteristics of filters, RF fields inside well-shielded enclosures and attenuator characteristics are among the

applications where high relative power is useful. High absolute RF power is needed to reproduce the field strengths generated by transmitters in order to study their influence on nearby equipment.

### Wide Frequency Range

Many RFI tests will require exploring large portions of the spectrum to ascertain the effects of interference on equipment. It is advantageous to have wide frequency coverage in a single instrument, not only to reduce set-up time, but also to minimize the problem of determining and controlling the relative performance of separate narrow-range generators.

### Frequency Stability and Accuracy

Repeatability of tests on frequency-sensitive equipments and components, measurement of fine grain frequency-response structure, and RFI susceptibility measurements on narrow-band systems require test signals at stable and accurately known RF frequencies.

### Signal Purity

Easy interpretation of susceptibility test data calls for RF test signals of high purity. Spurious and harmonic signal content must be at a minimum. Amplitude modulation should produce no frequency modulation and frequency modulation should not be accompanied by incidental amplitude modulation. Signal-to-noise ratio should be as high as possible.

## II. DESIGN AND PERFORMANCE SUMMARY

### Performance

The High-Power Signal Source is continuously tunable over the frequency range 40 mc to 40 kmc. The RF power output is 100 watts CW from 40 mc to 4 kmc. From 4 kmc to 18 kmc the power output exceeds one watt. Above 18 kmc the output falls to the order of one milliwatt at 40 kmc. The power output is adjustable over a 100 db range. The set power is maintained constant automatically as the frequency is tuned through each band. Two modes of stable operation are provided. In one mode, a stability of one part in $10^8$ is available. A second mode allows a simplified operating procedure at a stability of five parts in $10^5$. Pulse, sine, and square-wave amplitude modulation over a frequency range of 10 cps to 20,000 cps is available in the system. The shortest pulse width attainable is 30 nanoseconds. Sawtooth frequency modulation is also included in the Signal Source. The FM rate is adjustable between 10 cps and 10,000 cps. The maximum attainable FM deviation is dependent on the RF frequency. At 40 kmc a deviation of 65 mc can be obtained. Both FM and AM can be applied simultaneously. Signal

purity is maintained by applying amplitude modulation at a frequency-insensitive point and frequency modulation at an amplitude-insensitive point in the system. Spurious and harmonic signals are minimized by the use of fixed and tunable filters.

Design Principles

The design of the Signal Source is an expansion of the Master Oscillator - Power Amplifier technique. An elementary form of the system is shown in Figure 1. A tunable oscillator provides an RF signal between 500 mc and 1,000 mc. This signal is amplified to produce a high-power output in the same band. Any signal between 1 kmc and 40 kmc is produced by successive steps of harmonic generation and amplification. Filters are used to select the desired harmonic and reject all unwanted signals. In order to produce a signal between 40 mc and 500 mc, the output of the variable 500 mc to 1,000 mc oscillator is heterodyned with the output of a second oscillator operating at a fixed frequency of 1,000 mc. The desired signal is selected by filters. Both fixed and variable oscillators are stabilized by referencing their output to a crystal-controlled oscillator.

The RF output of the system is amintained constant by amplifying a rectified sample of the output and applying the result to reduce the gain of an amplifier in the signal chain. The ratio of the leveling sample to the RF output is manually adjusted to control the power output of the Signal Source.

Both with respect to power output and RF frequency only those portions of the amplifying chain are energized which are required to give the desired output. This extends component life, conserves power and reduces output noise.

The frequency-modulating signal is applied to an electrically variable reactance in the frequency-determining element of the 500 mc to 1,000 mc oscillator. Pulse amplitude modulation is applied to crystal switches in the 500 mc to 1,000 mc line common to the entire RF subsystem. Audio AM is introduced at a gain-controlling element in the 500 mc to 1,000 mc amplifier common to all RF signal paths.

All components are designed for rack installation. The cabinets housing the components include forced-air cooling. Controls, indicators, and output connectors are mounted on the front panels of the units. Interconnections are made at the rear.

## III. RF DESIGN DETAILS

### The RF Subsystem

Figure 2 is a block diagram of the RF Subsystem. The signal originates in the 500 mc to 1,000 mc tunable oscillator for all frequencies above 500 mc. This signal is amplified in a medium-power travelling-wave-tube amplifier which drives a high-power TWT amplifier to yield 100 watts CW in the 500 to 1,000 mc band. Alternatively, the medium-power TWT can be adjusted to yield sufficient second harmonic to drive a high-power TWT in the 1 kmc to 2 kmc band. The change in operating mode is controlled by the manual band switch, which also actuates coaxial relays to change the signal path and introduce a 1 kmc to 2 kmc tunable filter into the line. In turn, the second harmonic of the 1 to 2 kmc signal is generated in a TWT amplifier to drive a 2 to 4 kmc high-power TWT amplifier. The medium-power amplifier is operated also under a different set of conditions to generate harmonics to produce signals for the 4 kmc to 8 kmc band. A third medium-power TWT serves as an output amplifier between 4 and 8 kmc and a harmonic generator from 8 kmc to 18 kmc. Its harmonics in turn are used to drive a medium power TWT in the 12 kmc to 18 kmc band. A crystal doubler, driven by signals in the two lower bands provides an output between 18 and 26 kmc. A second crystal doubler yields a 26 to 40 kmc signal, when energized from one or the other of the two lower bands.

In order to generate signals between 40 mc and 500 mc, the output of a 1,000 mc oscillator is added to the output of the 500 to 1,000 mc tunable oscillator. The summed signals are fed to the 500 to 1,000 mc TWT amplifier, which is readjusted to function as a mixer. The difference signal is fed through switches and low-pass filters which subdivide the 40 to 250 mc range into less-than-octave bands for harmonic elimination. The signal is then amplified in five wide-band distributed amplifiers cascaded to provide 100 watts RF output between 40 mc and 250 mc. Between 250 mc and 500 mc sufficient beat signal is obtained to drive a high-power TWT amplifier directly.

Nineteen bands are required to cover the 40 mc to 40 kmc range. They are not all shown in Figure 2, in the interest of pictorial clarity. Octave bands were feasible where tunable filters could be used for signal sorting. Where fixed filters were used the bands were subdivided to insure rejection of all unwanted harmonic or beat signals. Many of the bands are switched to common output terminations so that the total number of outputs is reduced. This permits the use of power sampling, leveling, and measuring components common to many bands.

### RF Power Control

The profile of RF power vs. frequency is shown in Figure 3. The upper line indicates the maximum power output of the system. This has been

intentionally limited to 100 watts in order to provide a margin for leveling, a reserve for handling higher maximum load VSWR, and protection for connected components. The basic power capability reaches 350 watts in some bands. Space, power supply, control, metering, and cooling provisions have been made for high-power TWT's for operation between 4 and 12 kmc. These tubes can be added when they become available. The lower line on the power profile represents the maximum RF power obtained when the signal is extracted in some bands.

A typical RF power leveling loop is shown is Figure 4. The RF output is sampled with a directional coupler. The sample is fed to a crystal detector through a manually variable attenuator. The output of the detector is then amplified in a high-gain, stabilized amplifier and the output signal applied to the gain-control grid of a medium-power TWT. Adjustment of the variable attenuator sets the power which will be maintained by the leveling loop. A separate RF power meter is provided for monitoring the power output.

### Frequency Stabilization

The 500 mc to 1,000 mc oscillator is actually a triode oscillator and triode amplifier in coupled cavities which are tuned by ganged, adjustable coaxial lines connected to a manual control and frequency dial. The dial has a frequency scale for each of the 19 bands. Stability of this arrangement is five parts in $10^5$. Alternatively, the tunable oscillator can be phase-locked to the harmonics of crystal-controlled 20 mc to 40 mc oscillator to achieve an accuracy and stability of one part in $10^8$. The 1,000 mc beat oscillator is stabilized to one part in $10^6$ by a similar technique.

### Band Switching

A single manual band switch controls all relays, switches, meters and amplifier operating conditions required for proper operation in each band.

## IV. MODULATION DESIGN DETAILS

### Frequency Modulation

A variable-frequency sawtooth signal is produced in a sawtooth generator. This signal is applied to a crystal diode and resistor connected across the adjustable coaxial line controlling the frequency of the 500 mc to 1,000 mc oscillator, as shown in Figure 5. The variation in reactance of the diode-resistor combination introduces frequency modulation into the system. The diode and resistor are also used in the frequency stabilization network previously described.

### Sine and Square-Wave AM

Variable-frequency sine or square-wave signals originate in the Waveform Generator. As shown in Figure 6, these are applied to a reference input point in the RF leveler amplifier; the resulting audio signals modulate a carrier oscillator which is transformer coupled to a rectifier in the control grid circuit of the 500 mc to 1,000 mc TWT amplifier, common to all RF signal paths. The TWT gain variations thus produced, amplitude modulate the RF carrier.

### Pulse AM

A Pulse Generator produces pulses variable in width and repetition rate. The pulses are applied to wide-band crystal swtiches inserted in the common 500 mc to 1,000 mc RF line. The switches are of the type, as shown in Figure 7. For "pulsed-on" operation each switch is biased so that the series diodes are non-conducting and the shunt diode is conducting application of the pulse reverses this condition, thus turning the switch ON. By exchanging the roles of pulse and bias "pulsed-off" operation is obtained. Two switches are connected in series to achieve 110 db isolation and 3 db insertion loss. The switching time of these switches is one or two nanoseconds.

## V. AUXILIARY SUBSYSTEMS DESIGN

### Input Power

The Signal Source requires about 15 kw of power from a three-phase, four-wire, 60-cycle service. The input voltage is regulated within 1% by a servo-controlled, motor-driven, ganged-variac arrangement.

### 28-Volt DC Service

All remote control circuits are energized from a 28-volt DC supply. A portion of the 28-volt output is made available for external use.

### Medium-Power TWT Beam Supplies

A separate beam supply is provided for each medium-power TWT. These are alike in that three-phase bridge rectifiers are used to reduce ripple, and series vacuum-tube regulators are used in the high-voltage output circuit. The output voltage of each is programmed from the band switch so as to establish correct TWT operation for the band in use. These power supplies also furnish DC for the TWT heaters to prevent hum modulation of the RF signal.

## High-Power TWT Beam Supply

Two six-phase half-wave rectifiers are connected in parallel or in series to provide the beam voltage for the high-power TWT amplifier in use. Ripple before filtering is about 1-1/2% at 720 cps. The beam voltage is regulated and programmed from the band switch by means of servo-driven, ganged variacs in the primary circuit of the supples. "Crow-bar" arc-over protection is included. This supply can energize high-power TWT's added to the "Signal Source."

## High-Power TWT Solenoid Supply

A three-phase bridge rectifier supples the current for the TWT solenoid in use. This is current regulated, and programmed from the band switch, by means of a current-sensing servo driving a ganged variac assembly in the AC input to the supply. This supply can furnish solenoid current for TWT's that may be added to the "Signal Source."

## Controls and Indicators

Operating controls and indicators are grouped within the reach and vision of an operator standing at a fixed position in front of the Signal Source. Infrequently used controls and indicators are mounted on the units to which they relate circuit-wise.

## Cooling

Each vertical stack of units is forced-air cooled. Air is inducted through a dust filter at rear, bottom and exhausted at rear, top. The air outlets are aligned for eash ducting outdoors. Individual components are spot cooled with small blowers, as required.

The solenoids and some of the high-power TWT's require water cooling. A pump-circulated closed water system is included for this purpose. A fan-cooled, water-air heat exchanger removes the heat.

## Protective Circuits

The high-power TWT's are protected against loss of cooling, beam over-current, helix over-current, heater under-current, excessive RF power out, excessive reflected RF power, and arc-over. Controls and relays are interlocked to prevent tube damage due to failure of programming circuit components. Medium-power TWT's are similarly protected. Fuses or circuit breakers are used to protect all other units of the "Signal Source." Doors and drawers are interlocked, and dangerous circuits covered and marked for personnel safety.

## Packaging

Figure 8 is a photograph of the "High-Power Signal Source," taken during assembly. Six stacks of rack-width units are mounted in three dual cabinets. Almost all units are slide-mounted for withdrawal to the front. Rear access dorrs are also furnished. Units producing RF fields are fully shielded. A steel base is provided to distribute the weight and maintain alighment of the cabinets. The weight of the Signal Source is approximately 4,800 lbs.

## VI. CONCLUSIONS

The "High-Power Signal Source" is a versatile instrument producing relatively ideal RF test signals over a large portion of the spectrum. The extended power range and the high power output make the instrument useful in RFI tests requiring either large or small RF signals.

The High-Power Signal Source is expandable with respect to frequency coverage. Only switches and filters need be added to make 100 watts output available down to 100 kc. The frequency may be extended above 40 kmc by the addition of passive doublers or amplifiers, for which the energizing power and control circuits are already incorporated in the equipment.

Power output may be raised in the C, X and K Bands by the addition of TWT amplifiers when they become available. Power supply and control provisions had been included for this expansion.

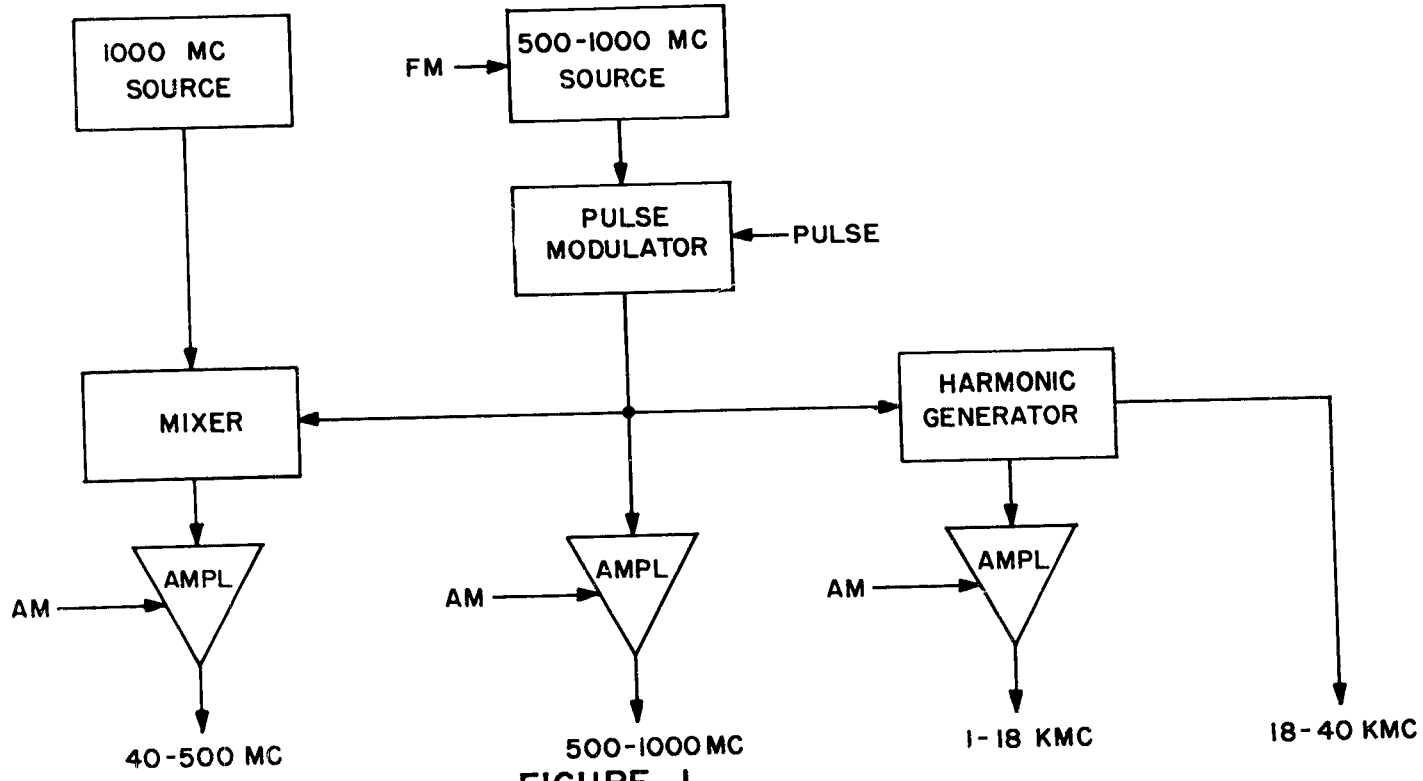



FIGURE 1

SIMPLIFIED BLOCK DIAGRAM

CALIBRATED HIGH POWER RF SIGNAL SOURCE

RADC CONTRACT NO. AF30(602)-2219 AEL, INC PROJECT NO. 60016

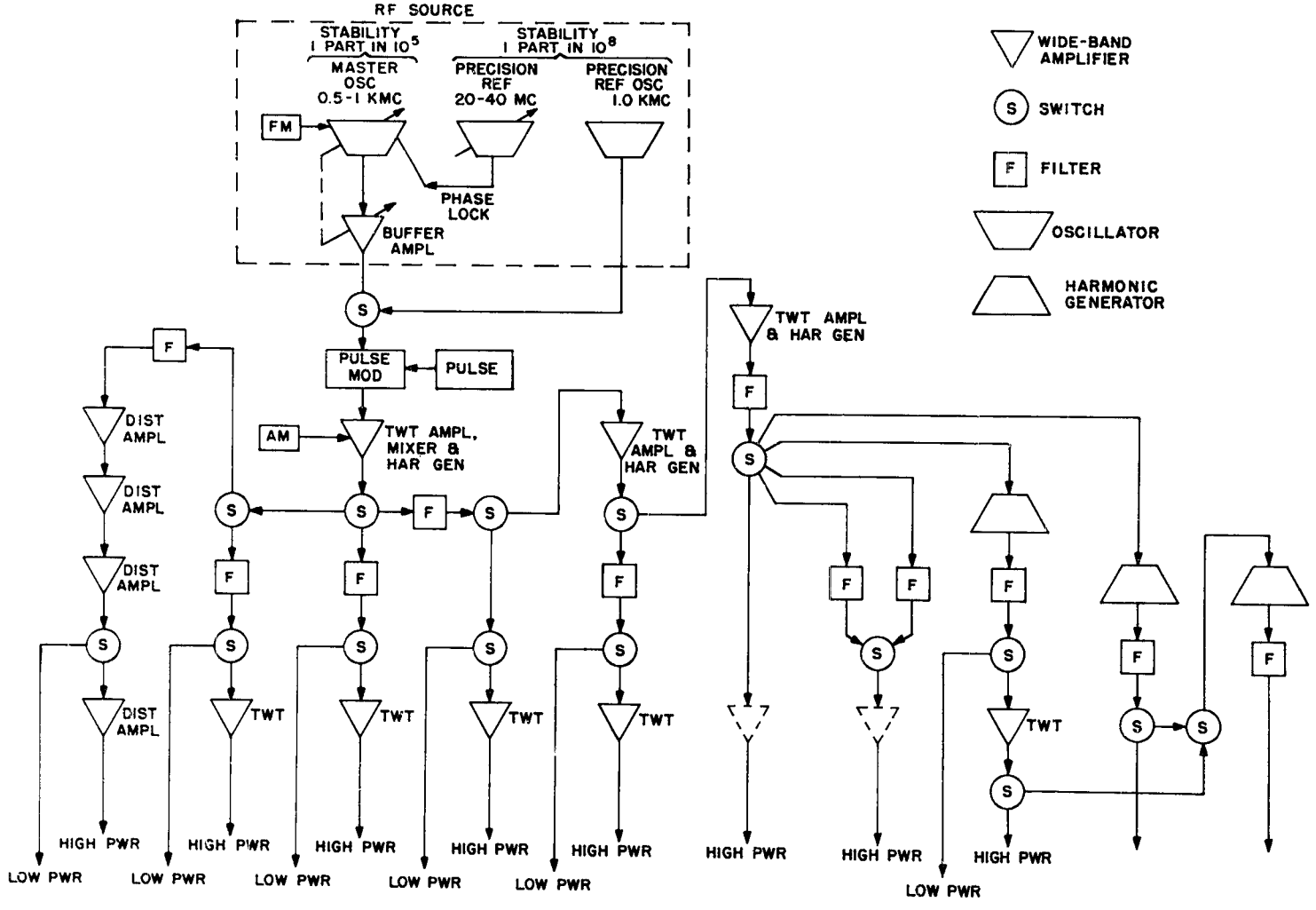



FIGURE 2
DETAILED BLOCK DIAGRAM
CALIBRATED HIGH POWER RF SIGNAL SOURCE
RADC CONTRACT NO. AF30(602)-2219 AEL, INC PROJECT NO. 60016

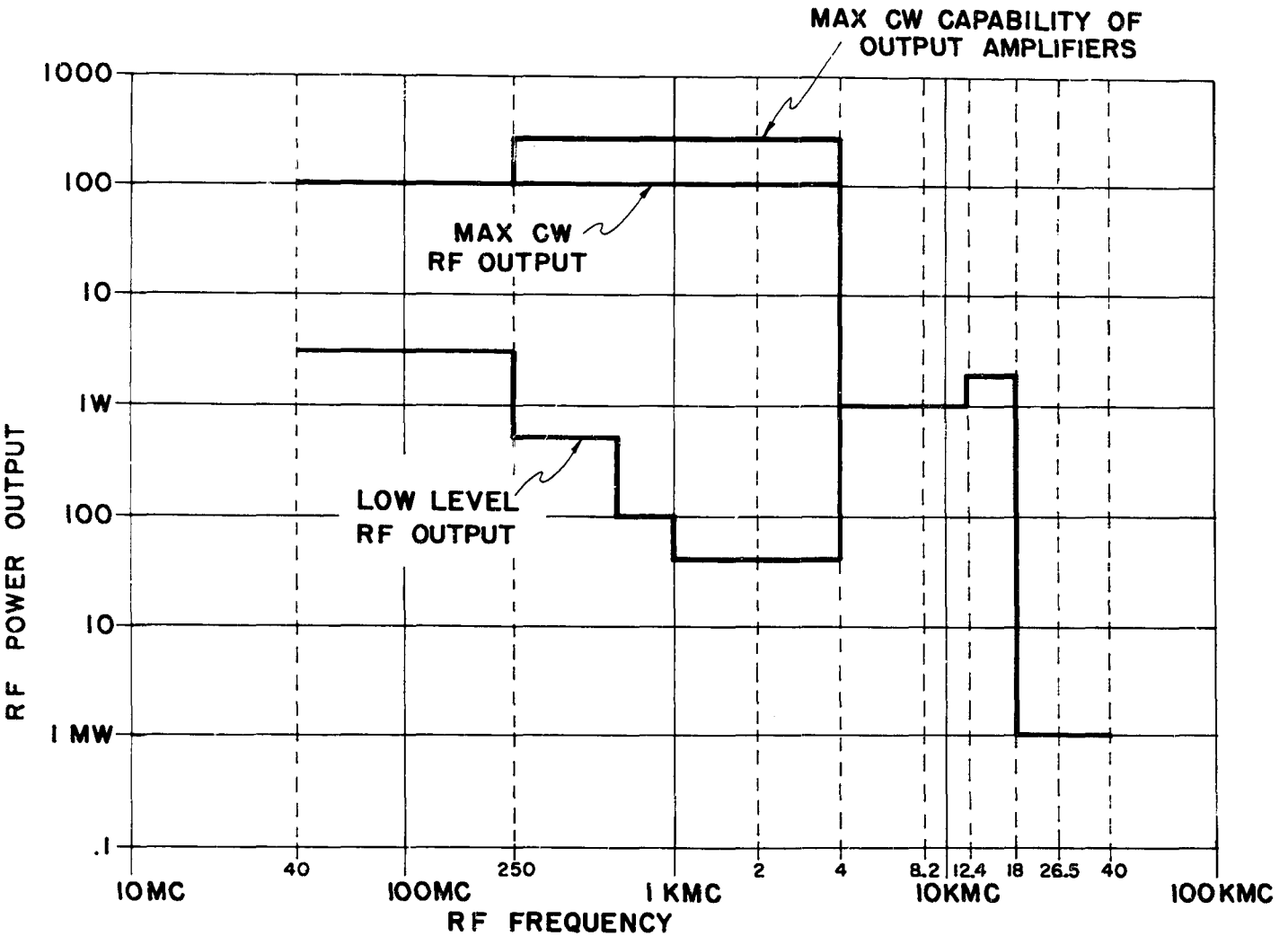



FIGURE 3 RF POWER OUTPUT PROFILE

RADC CONTRACT NO. AF30(602)-2219 AEL, INC PROJECT NO. 60016

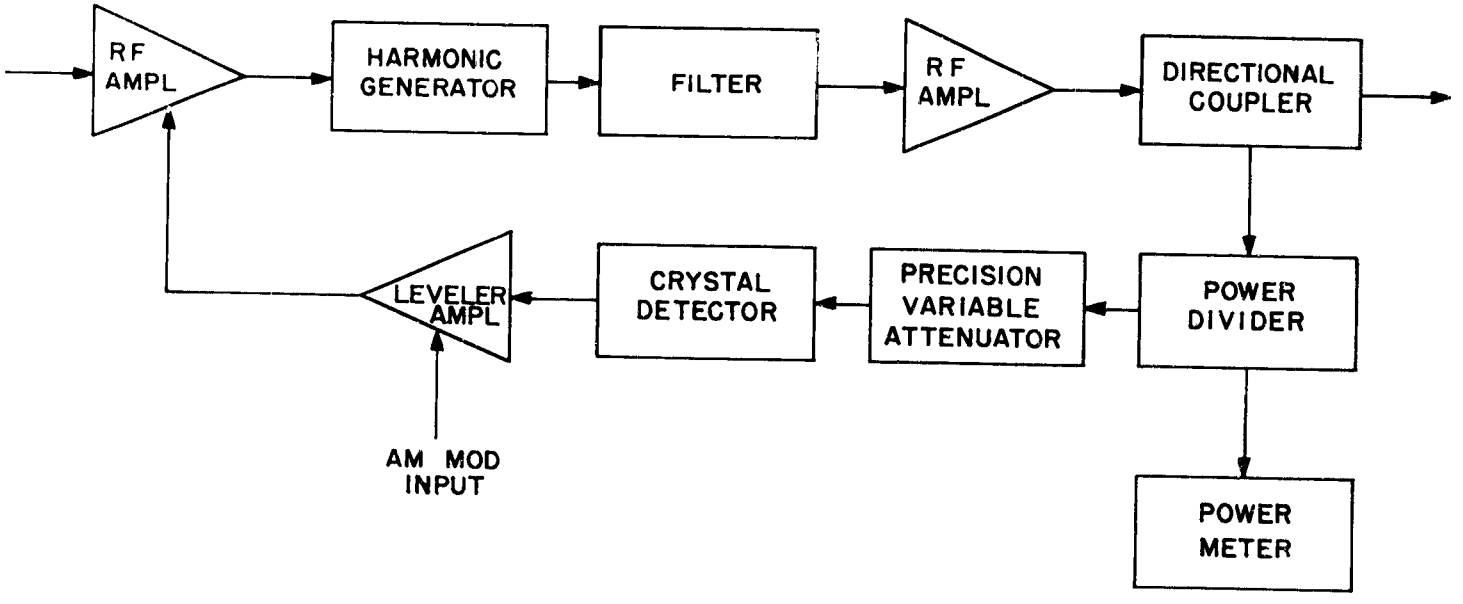



FIGURE 4

SIMPLIFIED BLOCK DIAGRAM
TYPICAL RF POWER LEVELING LOOP

RADC CONTRACT NO. AF30(602)-2219 AEL, INC PROJECT NO. 60016

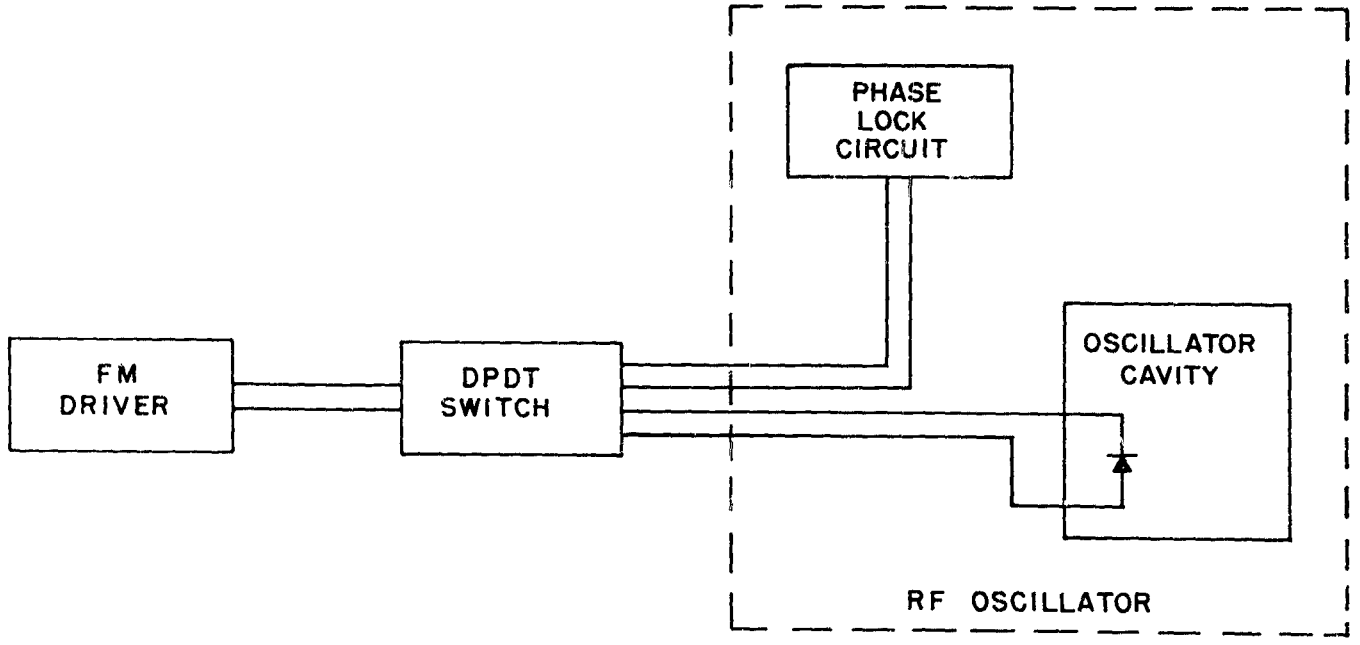





FIGURE 5
SIMPLIFIED BLOCK DIAGRAM
FM SUBSYSTEM

RADC CONTRACT NO. AF30(602)-2219 AEL, INC PROJECT NO. 60016

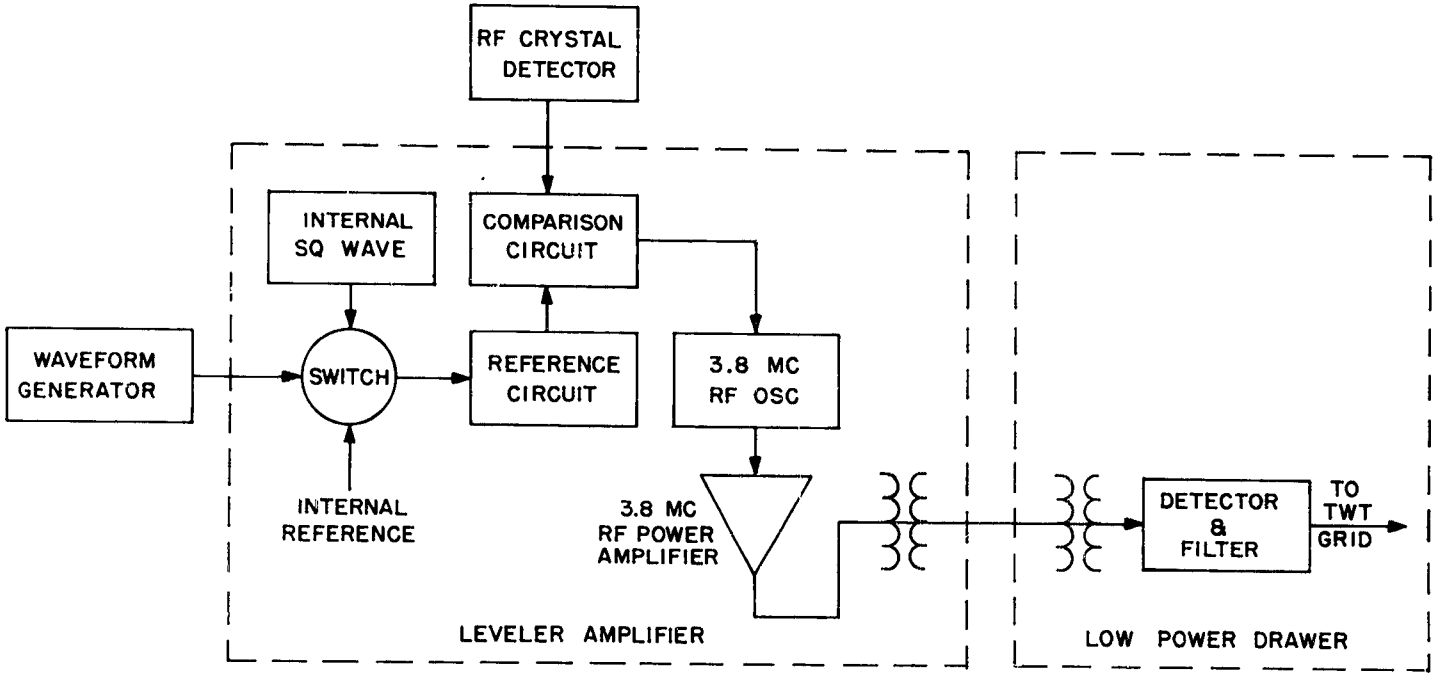
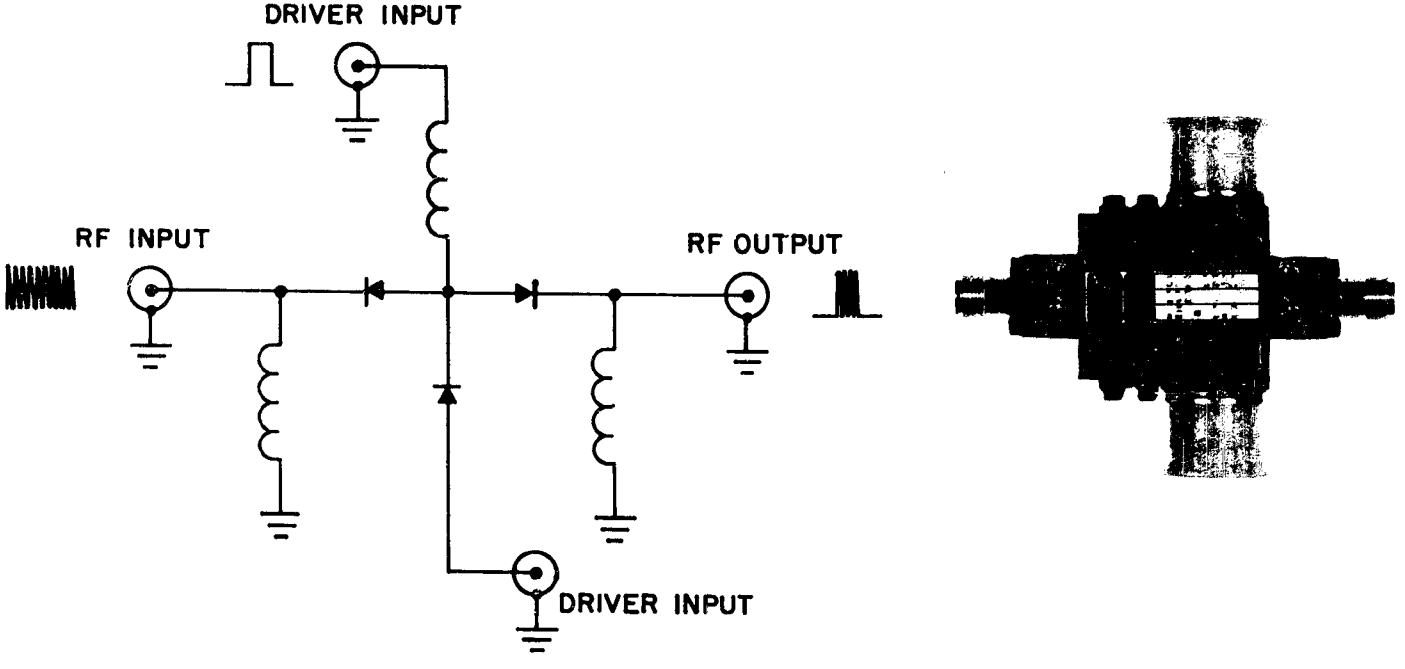



FIGURE 6

SIMPLIFIED BLOCK DIAGRAM

AMPLITUDE MODULATION & LEVELING CIRCUIT

RADC CONTRACT NO. AF30(602)-2219 AEL, INC PROJECT NO.60016




SIMPLIFIED SCHEMATIC

FIGURE 7
PULSE MODULATOR SWITCH

RADC CONTRACT NO. AF 30(602)-2219 AEL, INC PROJECT NO. 60016

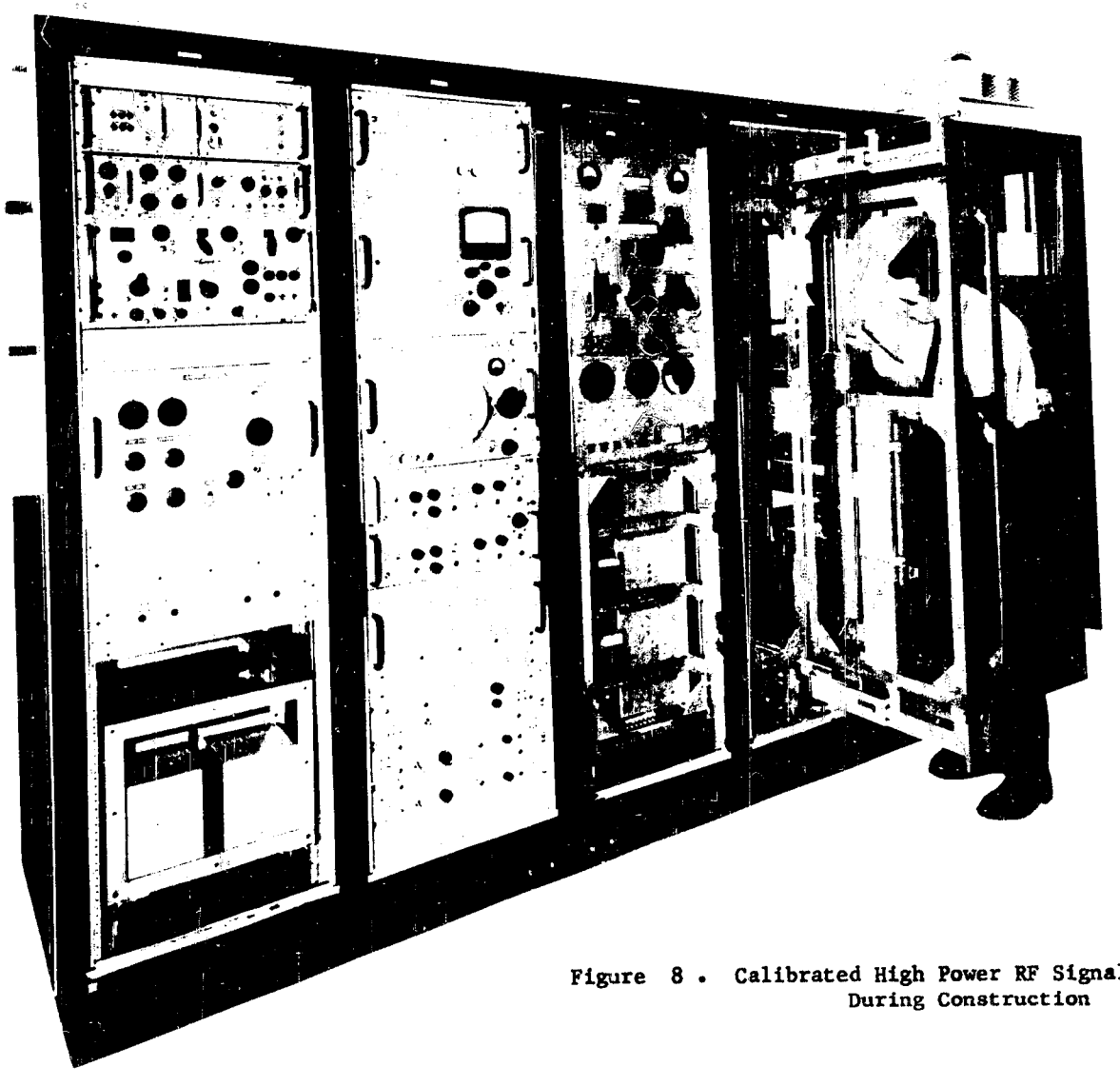


Figure 8 . Calibrated High Power RF Signal Source During Construction

# EXISTING CURRENT PROBES AND DEVELOPMENT OF NEW PROBES TO 1 KMC

H. K. Mertel*
United Control Corporation
Seattle, Washington

J. F. Fischer*
Genistron Incorporated
Los Angeles, California

**Abstract.** - This paper presents the development and the evaluation of current probes to measure conducted interference in the frequency range of 30 cps to 1000MC. Four commercially available current probes for the 30 cps to 1000MC frequency range were evaluated. Two current probes were developed for the 20MC to 1000MC frequency region. One current probe was developed to measure interference currents in large diameter cables. The sensitivity of these current probes is sufficient to detect interference currents below most existing specification limits.

Several methods are given to calibrate the current probes. In the 300MC to 1000MC frequency range, the current probes were calibrated by an antenna method.

## I. INTRODUCTION

The measurement of conducted electro-interference may be accomplished with several different pick-up devices. The level of electro-interference on a conductor may be measured in units of voltage or current. Conducted interference voltage measurements require some method of coupling an interference source conductor directly to the measurement meter input. One accepted standard method of establishing this physical contact is the insertion of a Line Impedance Stabilization Network into each lead to be tested. Conducted interference current can be measured, without making direct contact with the source conductor and without modification of either the conductor or its circuit, by use of specially developed clamp-on current transformers. The utility of the latter method is self-evident: the interference in complex wiring systems, electronic circuits, etc. may be measured without interruption of the normal operation or configuration.

*Authors formerly with General Dynamics/Astronautics, San Diego, California.

The current transformer, otherwise known as the current probe, is constructed so that it may conveniently be clamped around the conductor to be measured. The conductor represents a one-turn primary winding. The secondary winding is contained within the current probe. One specific current probe has proved extremely useful for interference measurement in the frequency range of 150 kc to 25 Mc for some time. In an effort to further extend the utility of current probe measurements, several current probes were developed and/or evaluated for effectiveness in the frequency range of 30 cps to 1000 Mc.

## II. THEORETICAL AND PHYSICAL CONSIDERATIONS FOR CURRENT PROBES

### Physical and Electrical Considerations for Current Probes

The physical size of the current probe is a function of the maximum cable size to be monitored, the maximum power current flowing in the cable, and the range of signal frequencies to be measured. The current probe is usually of toroidal shape with the conductor to be measured placed within the center opening of the toroid. Existing requirements and manufacturer's specifications for probes show that the center opening may vary from 1/16 in. to 8 in. diameter. The secondary winding is placed on the toroid in such a manner as to facilitate the clamp-on function of the probe. The toroidal core and winding is enclosed with a shield to prevent electrostatic pick-up. The shield is gapped to prevent it from being a shorted turn on the transformer.

### Current Probe Sensitivity and Transfer Impedance

Development and/or evaluation of current probes for 30 cps to 1000 Mc usage required that levels of minimum sensitivity be determined outside the 150 kc to 25 Mc range of conducted interference defined in MIL-I-26600. In the region from 30 cps to 150 kc, the specification GM 07-59-2617A was used as a reference. Space Technology Laboratories is the source of this specification, and its limits are pertinent as an indication of trends in present day weapon systems thinking. No endorsement of these limits is intended by its reference. From 25 Mc to 1000 Mc, existing specification limits consider only radiated interference. In this frequency range the limit was empirically determined (by a simulated radiated interference measurement) to be equivalent to one micro-ampere.[1,2] The composite specification limit from 30 cps to 1000 Mc is shown in Figure 1 for CW interference. The broadband specification limit would be correspondingly higher.

The current probe must have sufficient sensitivity to detect interference currents below the levels of the referenced specification limits. The sensitivity of the current probe may be conveniently expressed in terms of transfer impedance. Transfer impedance is defined as the ratio of secondary voltage (across a 50 ohm resistive load) to the primary current ($Z_T = E_s/I_p$). Overall sensitivity of the current probe and RFI receiver is also a function of the receiver sensitivity. Minimum detectable interference current in a conductor is the ratio of receiver sensitivity (volts) to current probe transfer impedance (ohms). For instance, if a one microvolt receiver and a current probe with a transfer impedance of 10 ohms are used, then the minimum measurable interference current is 0.1 micro-ampere. However, if a 10 microvolt receiver and a 1 ohm current probe are used, then the minimum measurable current is 10 micro-amperes. To obtain maximum sensitivity, the transfer impedance should be as high as possible.

The transfer impedance is often expressed in terms of db above one ohm. This is a convenient unit in reference to the more general RFI units of db above one microvolt or micro-ampere. ($Z_T$ in terms of db above one ohm = 20 Log $Z_T$.)

Equivalent Electrical Circuit of Current Probe

The current probe may be represented by an exact equivalent circuit from general transformer theory. It is not necessary to repeat the circuit here since it is shown in many standard textbooks[3] and special reports.[4] After considerable simplification of the exact circuit and derived equations, the following equations for the transfer impedance result:

High frequency case: $$Z_T = \frac{\omega M}{\left[\left(\frac{\omega L}{R_L}\right)^2 + \left(\omega^2 LC - 1\right)^2\right]^{\frac{1}{2}}}$$

Mid frequency case: (when $\omega^2 LC = 1$) $$Z_T = \frac{MR_L}{L}$$

Low frequency case: $Z_T = \dfrac{\omega M}{\left[\left(\dfrac{\omega L}{R_L}\right)^2 + 1\right]^{\frac{1}{2}}}$

where:
$Z_T$ = Transfer impedance
$M$ = Mutual inductance between primary and secondary
$L$ = Inductance of secondary winding
$R_L$ = Load impedance of secondary (usually 50 ohms)
$C$ = Distributed capacitance of secondary
$\omega$ = Frequency in radian/second

The following conclusions may be drawn from these equations:

1. The maximum transfer impedance at mid-frequency, for a constant load impedance, is directly proportional to the ratio of mutual inductance to secondary inductance.

2. The low frequency half power point occurs when the reactance of the secondary winding is equal to the load resistance.

3. The high frequency half power point occurs when the reactance of the secondary distributed capacitance is equal to the load resistance.

The design parameters for a current probe in the frequency range of 150 kc to 25 Mc were previously evaluated.[4] The highest linear transfer impedance was obtained with two secondary windings of 8 turns connected in parallel.

Deleterious Effects of Current Probe Measurements

The current probe is essentially a transformer and therefore reflects the secondary impedance into the primary. The reflected impedance is a function of the secondary winding only, since both the primary windings and the load resistance are constant. For an 8-turn secondary winding, the reflected impedance is approximately one ohm. So long as the combination of source and load impedance of the circuit to be measured is greater than one ohm, the application of the current probe will not greatly alter the primary current flow. However, if the sum of the circuit source and load impedance is less than the reflected impedance, the application of the current probe may alter the primary current flow considerably.

One intended current probe application is the measurement of interference current on primary power lines which may carry up to 300 amperes of dc or 50 amperes of ac. The current probe may also be used in the vicinity of devices which generate strong external magnetic fields. The current probe transfer impedance must not be altered by these power currents or flux densities. Therefore, the magnetic circuit must be designed so that it will not saturate. Since the ac power current may be in the frequency range of 20 to 15,000 cps; it is possible that the current probe output at these power frequencies may damage the input resistor of the associated receiver. A possible solution is the insertion of power frequency rejection filters between the current probe and the receiver.

## III. AVAILABLE COMMERCIAL CURRENT PROBES

### Stoddart 91550-1 Current Probe

The Stoddart current probe was specifcally designed for interference current measurements and has been in use for several years. The transfer impedance for this probe is sufficiently high to detect interference current below the specification limits with a one microvolt receiver for the 30 cps to 100 Mc frequency range. Table 1 is a comparison of physical and electrical data for several current probes. Figure 2 shows the transfer impedance for the Stoddart current probe.

### Empire Devices C P-105 Current Probe

The Empire Devices current probe is similar to the Stoddart current probe. The size of the probe aperture, winding configuration, and number of turns are the same for both probes. The transfer impedance is one ohm over the frequency range of 150 kc to 30 Mc. The output voltage, as measured by the interference receiver, has a 1:1 relationship to the primary current. The readings obtained on the NF-105, or equivalent receiver, in db above one microvolt become db above one micro-ampere without the need for additional correction factors. The specifications for this probe are also shown in Table 1. Figure 3 shows the transfer impedance.

### Tektronix Type P 6016 Current Probe

The Tektronix current probe is primarily designed for current measurement with an oscilloscope or high impedance VTVM. The probe is of relatively new design and may be of particular value in RFI trouble shooting of wiring harnesses or electronic assemblies. It is a clamp-on type with an aperture diameter of 1/8 in. The overall size of 3/4 in. x 3/4 in. x 7 in. is comparatively small and suited for measurements in areas of moderately restrictive space. The transfer impedance is shown in Figure 4. From 1 kc to 15 Mc, the transfer impedance is - 8 db above one ohm. If a one micro-

volt receiver is used, the minimum sensitivity is 8 db above one micro-ampere. Since this level is above the CW specification limits from 1 Mc to 25 Mc, the probe is not suitable for qualification testing in this frequency range. However, it is usable in this range as a trouble-shooting device after excessive interference is detected by some other device.

The effect of dc on the probe output was also evaluated in the same manner as determined for the other current probes. Since the Tektronix probe opening will accept wires up to No. 12 AWG, the maximum test current was 10 amperes. From 20 kc to 100 Mc the effects are negligible as shown in Figure 4. The probe is not usable for accurate signal current measurement below 20 kc unless the dc is small or the probe output is corrected for each specific dc value. The effects of the dc are linear up to 10 amperes of dc. For example, a current of 5 amperes produces one-half the decrease in output as a current of 10 amperes.

Hewlett Packard Type AC-21F Current Probe

The Hewlett Packard probe is similar to the Tektronix probe. The evaluation carried out was the same as for the Tektronix probe. The transfer impedance is constant at a value of -6 db above one ohm in the frequency region of 4 kc to 15 Mc as shown in Figure 5. Here again, if a one microvolt receiver is used, the minimum probe sensitivity is 6 db above one micro-ampere. This level is above the CW limits of the referenced specifications from 1 Mc to 25 Mc; thus, the probe is not suitable for qualification testing in this frequency range. However, it is usable as an RFI trouble shooting device over this frequency range. The same general remarks as given for the Tektronix probe are also applicable to the Hewlett Packard probe concerning sensitivity when 10 amperes dc are applied. The results are also shown in Figure 5.

## IV. INSTRUMENTATION FOR TRANSFER IMPEDANCE EVALUATION

Transfer Impedance Evaluation for the 20 cps to 100 Mc Frequency Range

The current probe transfer impedance, which is a convenient parameter of expressing the sensitivity of a current probe, is defined as the ratio of secondary voltage across a 50 ohm load to the primary current ($Z_T = E_s/I_p$). To evaluate a current probe, the secondary voltage may be accurately (± 2 db) measured with the calibrated interference receiver, but the primary current must also be accurately determined. One method of determining the primary current is to insert a known resistance in series with the primary current wire and to measure the voltage drop across the resistor.

The test procedure for evaluating the transfer impedance is as follows:

1. Set up the signal generator, current probe, and receiver for the specific frequency. Terminate the signal generator with a short length of wire and a 50 ohm non-inductive resistor.

2. Clamp the current probe around the wire between the signal generator and the 50 ohm load. Terminate the current probe with a 50 ohm RF load.

3. With the current probe and its load clamped around the wire, increase the signal generator output and measure the voltage across the 50 ohm signal generator load with a high impedance frequency selective VTVM. The primary current can now be calculated.

4. Measure the voltage across the 50 ohm current probe load with a high impedance VTVM.

5. The transfer impedance is defined as $Z_T = E_s/I_p$ and may be calculated from steps 3 and 4.

6. Repeat steps 3, 4, and 5 for the frequencies of interest.

NOTE: For the 50 ohm load and VTVM of steps 3 and 4, the RFI receiver with its 50 ohm load may be conveniently used. Use the shortest possible length of coaxial cable between the open wire and the receiver.

Transfer Impedance Evaluation for the 100 Mc to 400 Mc Frequency Range

For frequencies below 100 Mc, the previously mentioned transfer impedance evaluation method is valid. This method is accurate since the same receiver may be used to measure the current probe output ($E_s$) and the current in the primary wire ($I_P = E_P/R_D$). The position of the current probe and the position of the dropping resistor are not the same since the receiver is connected to the primary wire with a coaxial cable. However, by keeping the electrical length of the coaxial cable short, the current at the 50 ohm load and at the position of the current probe are practically the same.

Above 100 Mc, the lead length between the signal generator and the load may become an appreciable portion of a wavelength. The lead length is necessary for application of the current probe. The characteristic impedance of an open wire line is normally different from the signal generator source impedance or the load impedance; therefore, a current standing wave results. The current amplitude at any point along the line varies as a function of the impedance mismatch and the frequency. (The use of a slotted line

was considered for measuring the current standing waves. However, slotted line measurements are difficult to apply to current probe instrumentation since the probe evaluation requires an open wire line, but available slotted lines require matched coaxial lines.) So long as the voltage dropping resistor is positioned electrically close to the position of the current probe, there is reasonable assurance that the current being measured by the probe is of the same magnitude as that current which develops a specific voltage drop across the resistor. As the frequency increases, the position of the current probe relative to the dropping resistor becomes quite critical, and the dropping resistor must be purely resistive.

Because of the above considerations, a special test jig for primary current measurement was designed as shown in Figure 6. The determination of the transfer impedance was carried out by placing a high-frequency and high-impedance VTVM (Boonton Electronics 91 CA VTVM with 91 - 3 H probe) and the load at a distance electrically close to the current probe. The non-inductive coaxial resistor (40 ohms) is shunted only by the input capacitance of the high-impedance voltage probe. The input capacitance of this probe is 2.5 pf. Assuming an additional distributed capacitance of 2.5 pf, the capacitance which shunts the resistor is approximately 5 pf. At 800 Mc, this shunting capacitive reactance is 40 ohms. Based on these considerations, this test jig will determine the primary current with accuracy to at least 400 Mc.

Transfer Impedance Evaluation for the 200 Mc to 1000 Mc Frequency Range

For the upper frequency range of current probe development, the previously described conventional methods of measuring current presented a number of difficult problems. These problems were avoided by using a new approach. The new approach utilized a quarter-wave monopole antenna for the necessary calibrated current source.

The antenna method of accurately determining UHF currents consists of measuring the impedance at the base of a monopole antenna which is mounted on a ground plane. After the antenna impedance is measured, a known power is applied to the antenna terminals. The current flow at the base of the monopole antenna can then be easily calculated if the antenna impedance is resistive. If the antenna is kept approximately a quarter wavelength long, the antenna current distribution is sinusoidal with a maximum at the base. An adjustable antenna must be used so that it can be made longer or shorter than a quarter wavelength. The length of the antenna is adjusted until resonance occurs and the antenna impedance is entirely resistive. Thus the power delivered to the antenna terminals will always be real. Since the antenna will be approximately a quarter wavelength long, its resistive impedance will be such that a VSWR of not more than 2 to 1, in a 50 ohm characteristic impedance system, is anticipated. With a 2 to 1 VSWR, only

0.5 db of the incident power will be reflected and not utilized. This eliminates the need for correction factors to determine the actual power delivered. However, in the event that the antenna impedance is of such a value to cause a substantial VSWR, the power reflected can be calculated and the true transmitted power may be determined.

The antenna impedance is determined by utilizing a bridge and a variable length of transmission line, which is necessary to adjust the length of the coaxial line between the bridge and the antenna exactly to one half wavelength at the frequency of measurement. If this is accomplished, the impedance measured by the bridge is the impedance of the antenna.

The current measuring procedure is as follows:

1. Disconnect the antenna from the coaxial cable and short circuit the end of the coaxial cable at the ground plane with a coaxial short.

2. Adjust the General Radio type 874-LT constant impedance trombone line so that the Hewlett Packard Model 803A bridge balances at zero ohms and zero phase angle.

3. Remove the short circuit from the end of the cable and replace with antenna.

4. Clamp the current probe, terminated with a 50 ohm receiver, around the base of the antenna.

5. Adjust the length of the antenna until the bridge balance is resistive. Record the value of antenna resistance.

6. Disconnect the trombone line from the bridge terminal and attach trombone line directly to the signal generator output terminals.

7. Adjust the signal generator so that a known power level is delivered to the base of the antenna.

8. Calculate the current at the base of the antenna using the following formula:

$$I_P = \sqrt{\frac{P}{R}}$$

$I_p$ = Current at the base of the antenna

P = Power delivered to the antenna terminals

R = Antenna resistance measured in Step 5.

9. Measure the output voltage of the current probe with an NF-105 (or equivalent) receiver.

10. Calculate the transfer impedance of the current probe using the following formula:

$$Z_T = \frac{E_s}{I_p}$$

where $E_s$ = output voltage of the current probe

$I_p$ = current at the base of the antenna

The Hewlett Packard Type 803A bridge has an upper frequency limit of 500 Mc. A satisfactory replacement for the Hp 803A is the HP 805A slotted line for frequencies above 500 Mc. The procedure remains essentially the same. The antenna impedance is found by standard VSWR measurements and the use of the Smith Chart.

This antenna method of measuring primary current was compared with the voltmeter method shown in Figure 6. The transfer impedance of the CVA-1 current probe was evaluated using both methods. The agreement between the two methods was very good.

## IV. DEVELOPMENT OF CURRENT PROBES FROM 25 MC TO 1000 MC

### Shielding Effectiveness

The Stoddart current probe was evaluated for frequencies above 100 Mc. Theoretically, the current probe output should decrease, but a series of peaks, varying between approximately ± 10 db, appeared from 100 Mc to 1000 Mc. The output above 100 Mc was primarily attributed to capacitive coupling and secondary resonances. The capacitive coupling was attributed to direct voltage pick-up between the interference carrying wire and the toroidal winding. The shield of the Stoddart current probe has an air gap to prevent the shield from shorting the toroidal transformer as shown in Figure 7. Since this shield gap is on the inside of the aperture and therefore closest to the signal wire, it was assumed that placing this gap on the outside periphery of the shield might overcome the electrostatic coupling to a certain extent. At the same time it was realized that any break of metallic continuity will decrease the shielding effectiveness for the VHF and UHF range.

A shield was designed with the gap placed on the outer periphery of the cylindrical shielding case. The shielding effectiveness was then evaluated. The data showed that the shielding effectiveness was less than for the Stoddart shield. This unexpected characteristic was explained in the following way: (1) The Stoddart shield has its coaxial connector symmetrically placed

with respect to the shield gap; therefore, the ground path from connector to gap has the same length for both sides. For the other shield the coaxial connector had no symmetry; therefore, two different lengths of ground path existed. The crossections of the two shields are shown in Figure 8. A voltage gradient may be induced because the ground paths from connector to shield gap lips are of two different lengths. This assumption was later confirmed. (2) The gap on the outer periphery has a greater surface area and greater leakage can occur. For a detailed analysis consult Reference 2.

From the high frequency shield evaluation the following conclusions were drawn: (1) The current probe shield must have RF-connector to shield symmetry. (2) The two facing shield gap lips should be held to a minimum surface area.

Current Probe for the 25 Mc to 300 Mc Range

The development of high frequency current probes began with the evaluation of air core transformers. The transfer impedance for various secondary winding configurations was in the vicinity of one ohm. To increase the transfer impedance, a probe was developed which used a General Ceramics CF 116 Q-3 ferrite core. This core was considered to be the best high frequency core and was the physically largest core available commercially. The shield dimensions were selected to render a usable current probe. The best compromise between practicability and electric characteristic for the CF 116 core was a cylindrical shield of the following dimensions:

OD. = 2.375 in., I.D. = 1.0 in., Height = .75 in. This current probe was designated as CVA-1.

The transfer impedance was evaluated with the high frequency method shown in Figure 6. A sketch of the current probe is shown in Figure 9. The transfer impedance is shown in Figure 10.

The sharp decrease in current probe output at about 350 Mc was attributed to the shield resonating. The shield surrounding the toroidal secondary coil may be represented by a one-turn tertiary winding terminated with a capacitor. The shield has a specific inductance which will series resonate with the capacitance. The facing shield gap lips determine the capacitance. The sharp, resonant decrease in output was noted also with all the evaluated air core probes.

The deleterious effects were also evaluated for this probe. These characteristics are shown in Table 1 in the CVA-1 current probe column.

Current Probe for the 200 Mc to 1000 Mc Range

The secondary windings of the previously developed current probes exhibited excessive electrostatic coupling and capacitance from winding to shield. These two effects had to be minimized before accurate current measurement to 1000 Mc could be achieved. A balanced winding with respect to ground was considered since the winding to shield capacitance for this winding is evenly distributed over the entire winding. The electrostatic pick-up is minimized since each termination of the winding will develop the same potential with respect to the grounded shield and not a potential difference as with the unbalanced winding. With a balanced winding, the output of the probe results principally from the magnetic field of the primary conductor under test.

Initial balanced probes were not successful since a balun was required to make the transformation from the balanced winding to the unbalanced input of the receiver. The baluns are normally narrow band devices; consequently a narrow band current probe response resulted.

Further experimentation utilized an untuned wideband transformer manufactured by the TRAK ELECTRONICS CO. The transformer is a Type BPC 200/50 providing a linear 200 ohms balanced to 50 ohms unbalanced impedance transformation from 1 Mc to 1000 Mc. The unbalanced output was connected to the receiver while the balanced input terminals were connected to an air core toroidal winding. The winding is not grounded at any point. The outside case of the BPC 200/50 was extended to shield the toroid. To accommodate the primary conductor under test, tubing of one inch diameter was placed through the extended case. As in the other shield designs, the tubing was cut to give the necessary air gap for prevention of a shorted turn. The shield gap is 0.025 in. wide. The air core toroid has a cross-sectional diameter of 1/4 in. The wire size is No. 26 AWG. Figure 13 shows the probe partly disassembled. This current probe was designated as CVA-3.

The transfer impedance of the probe and BPC 200/50 combination was measured with windings that were varied from 9 to 25 turns. The results indicated that the larger the number of turns the better the low frequency response. For the 200 Mc to 1000 Mc range, an 11 turn winding gave the best transfer impedance as shown in Figure 14. The remaining electrical characteristics are shown in Table 1 in the CVA-3 current probe column.

Although the current probe does not utilize magnetically saturable devices, the construction materials for the BPC 200/50 wideband transformer indicated a ferrite material. Therefore, the possible change in characteristics caused by large magnetic fields was evaluated. The transfer impedance

was not changed by large magnetic fields as shown in Table 1. The current probe should have sufficient sensitivity to detect one microampere of RF current from 25 to 1000 Mc. The transfer impedance is approximately 1.5 ohms at 1000 Mc. If a 1 microvolt receiver is used with the probe, a primary current of 0.7 micro-ampere can be detected.

Current Probe for Large Diameter Cables

The requirement existed to measure the net magnetic field emanating from a large cable with diameter up to eight inches. To facilitate such a measurement, a current probe with 8 in. diameter aperture was developed. The toroidally shaped core of the probe consisted of 4 mil, grain oriented silicon steel tape. The crossection of the core was 1/2 in. by 1 in. Insulation consisting of one layer each of spun glass tape, teflon tape, and mylar tape was wrapped around the core. The windings were evenly distributed over the insulation and the composite toroid was placed in a laminated nonconductive case. The case was spray coated with zinc and copper to provide electrostatic shielding. An air gap of 0.02 in. was placed on the inner periphery of the shield to prevent the shield from shorting the toroid. Figure 11 shows the probe partly disassembled. The probe is not a clamp-on type; however, it was later modified to be a clamp-on device. This current probe was designated as CVA-2.

The transfer impedance was evaluated with the number of secondary turns being varied from 8 to 100. The highest and flattest response was obtained with 18 turns of 1 mil by 1/2 in. wide copper tape. The transfer impedance for this probe is shown in Figure 12. The notch in the transfer impedance curve occurred in all the evaluated probes at 250 Mc. It was caused by the shield resonating and shorting the toroid. The other electrical characteristics are shown in the CVA-2 current probe columm of table 3.

The transfer impedance was evaluated with a 1/4 in. diameter conductor at the center of the probe aperture. This conductor was moved to the edge of the aperture to determine a possible change in probe output. For frequencies below 40 Mc, there was no change in probe output. For frequencies above 40 Mc, the output changed from zero to + 5 db at 100 Mc. This increase was caused by electrostatic coupling through the shield gap. The change in output could be reduced by using small diameter wire instead of the 1/2 in. wide copper winding. Since this change also reduced the overall probe response, it was not employed.

## VI. SUMMARY

As the electromagnetic spectrum becomes even more congested, extremely restrictive interference control requirements must be enforced; consequently, the number of required interference tests will increase. The employment of current probes for these tests will help to reduce the test time. It has been shown that current probes can detect interference currents below the existing and the assumed specification limits in the frequency range of 30 cps to 1000 Mc. The design of the newly developed current probes is not yet optimized and further work is being carried out.

This paper stresses mainly the advantages and feasibility of conducted interference measurements with current probes. The limitations and disadvantages of current probes, the development of ac and dc skin current probes, and other phases of probe measurements were not mentioned because of limited space. This information will be published at a later date. Detailed information on these subjects may be obtained from reference 2.

## VII. ACKNOWLEDGEMENTS

The work described above was carried out at General Dynamics/Astronautics as a portion of U. S. Air Force Contract AF 33 (616)-7393 (Development of Improved Techniques for Current Probes) which was under the cognizance of Communications Laboratory, Wright Air Development Division (now Aeronautical Systems Division).

Acknowledgment is gratefully made to Mssrs. L. G. Chase, E. Beaver, D. Grisel, and S. Babcock for their assistance; and to Messrs. C. Hatchett and L. G. Clough for continuing the development of current probes.

## VIII. REFERENCES

1. F. S. Scarborough and F. E. Garlington, "An Approach to Designing Interference-Free Electronic Systems", Sprague Technical Paper No. 56-1, May 1956, Figure 4.

2. "First, Second, Third, and Fourth Quarterly Progress Reports for Development of Improved Techniques of Current Probes", U. S. Air Force Contract No. AF 33(616)-7393 (WADD Aeronautical Systems Division), General Dynamics/Astronautics, June 1960 - June 1961.

3. MIT Staff, "Magnetic Circuits and Transformers", John Wiley & Sons Inc., New York, 1947.

4. "Final Development Report for Current Probe, U. S. Air Force Contract No. AF 23 (600)-23620, E. O. No. R-591-75 SR-1e, to Wright Patterson Air Force Base, from Stoddart Aircraft Radio Co., Oct. 1954.

| Current Probe | Frequency Range Of Use | 3 db Passband | Passband Transfer Impedance db above one ohm | Probe Aperture inches | Maximum tolerable dc conductor-current in amperes | Maximum tolerable ac conductor-current in amperes | Maximum tolerable magnetic fields Gauss |
|---|---|---|---|---|---|---|---|
| Stoddart 91550-1 | 30 cps to 100 Mc | 0.5 Mc to 40 Mc | 14 | 1.25 | >300 | >50 | 1000 |
| Empire Devices CP-105 | 30 cps to 100 Mc | 0.1 Mc to 50 Mc | 0 | 1.25 | >300 | >50 | 1000 |
| Tektronix P6016 | 30 cps to 15 Mc | 1 Kc to 15 Mc | -8 | 0.125 | 10 | ? | ? |
| Hewlett Packard AC-21F | 30 cps to 15 Mc | 2 Kc to 15 Mc | -6 | 0.125 | 10 | ? | ? |
| CVA-1 | 20 Mc to 300 Mc | 12 Mc to 320 Mc | 14 | 1.0 | 300 | >50 | 500 |
| CVA-2 | 20 cps to 100 Mc | 0.1 Mc to 100 Mc | 5 | 8.0 | >300 | >50 | ? |
| CVA-3 | 20 Mc to 1000 Mc | 170 Mc to 1000 Mc | 5 | 1.0 | > 300 | >50 | 1000 |

Table 1. Comparison of Current Probes

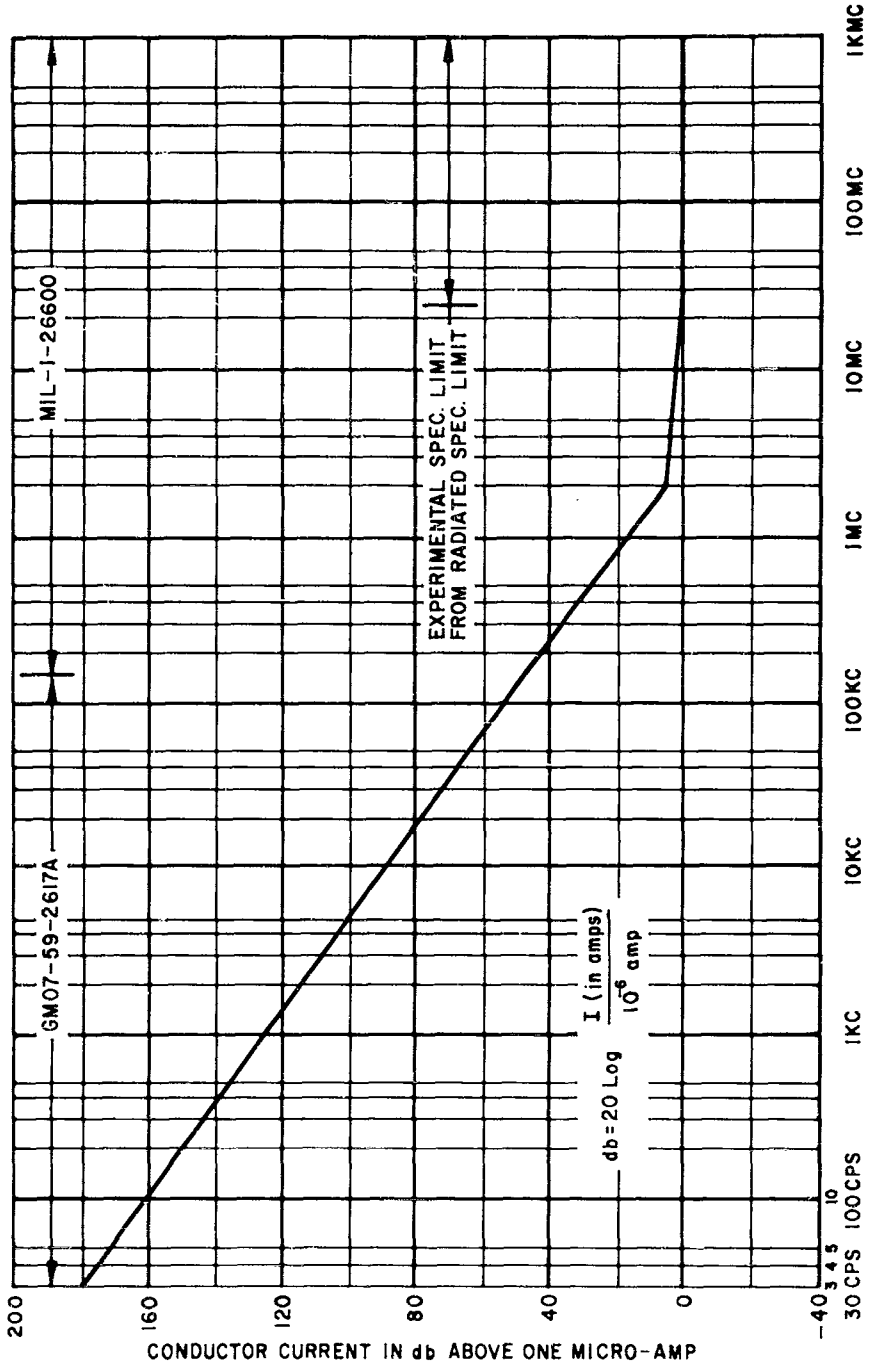



**Figure 1. Specification Limit for C-W Interference**

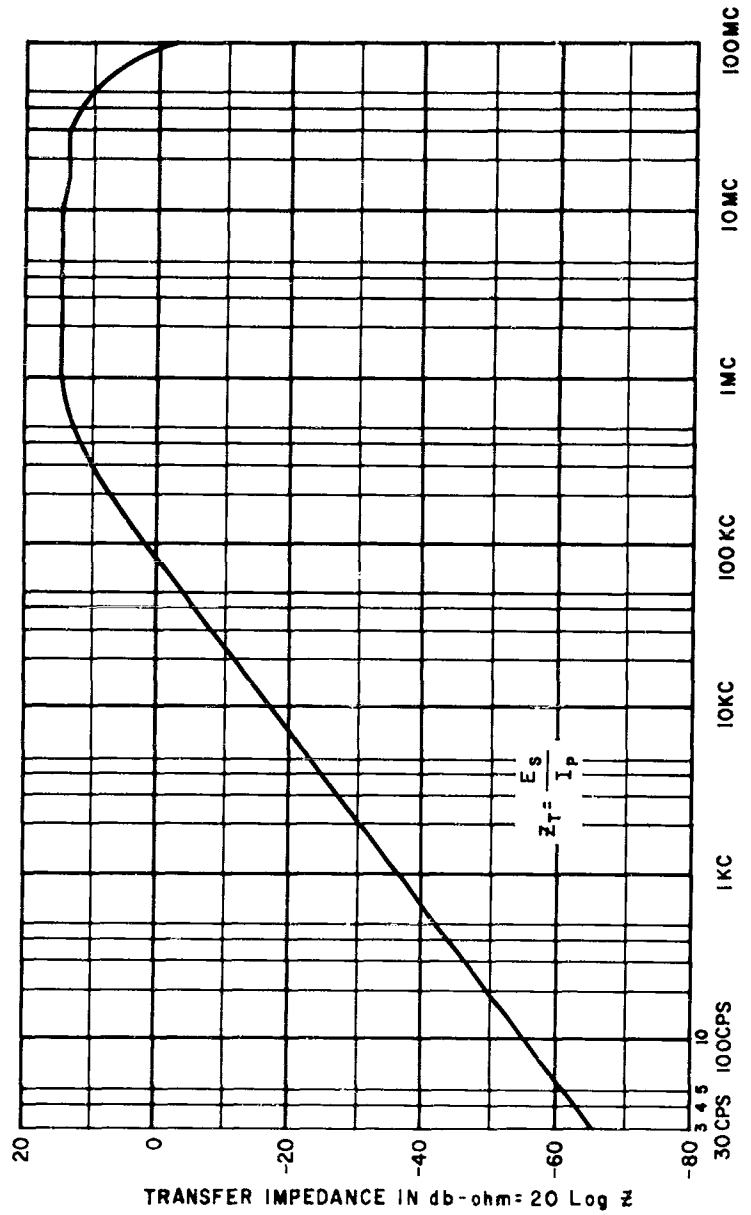



**Figure 2. Transfer Impedance of Stoddart 91550-1 Current Probe**

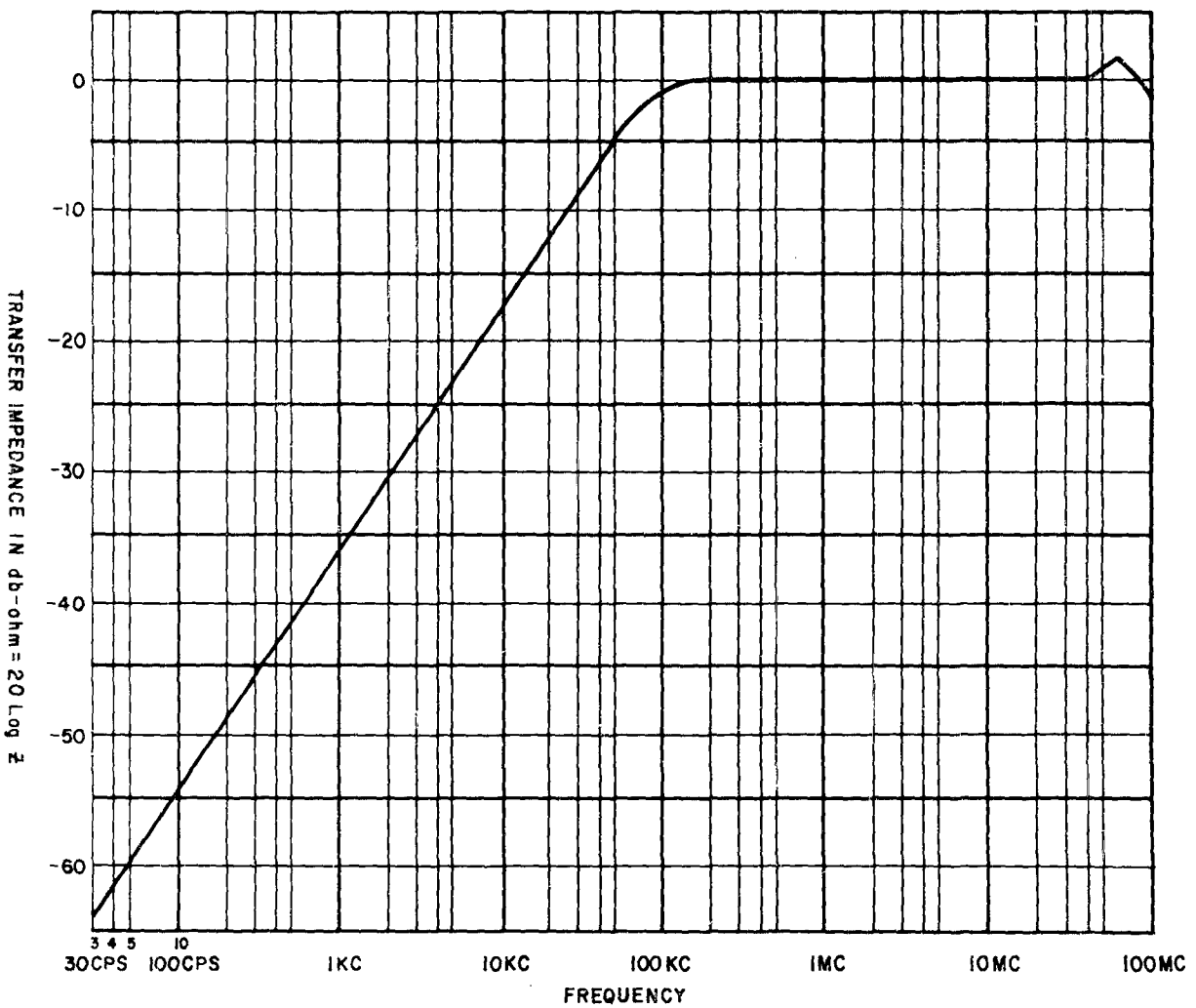



**Figure 3. Transfer Impedance for Empire Devices CP-105 Current Probe**

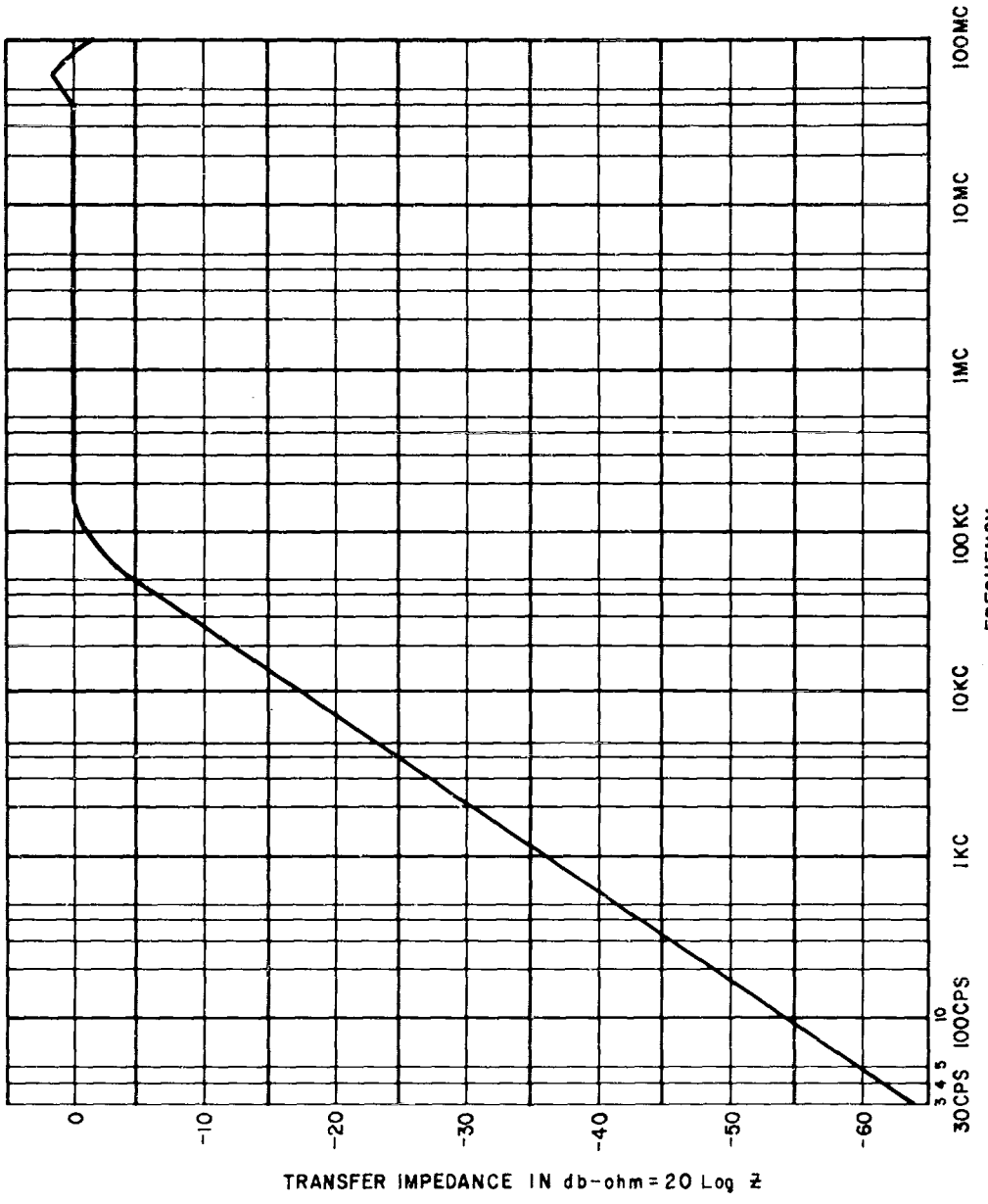



**Figure 3. Transfer Impedance for Empire Devices CP-105 Current Probe**

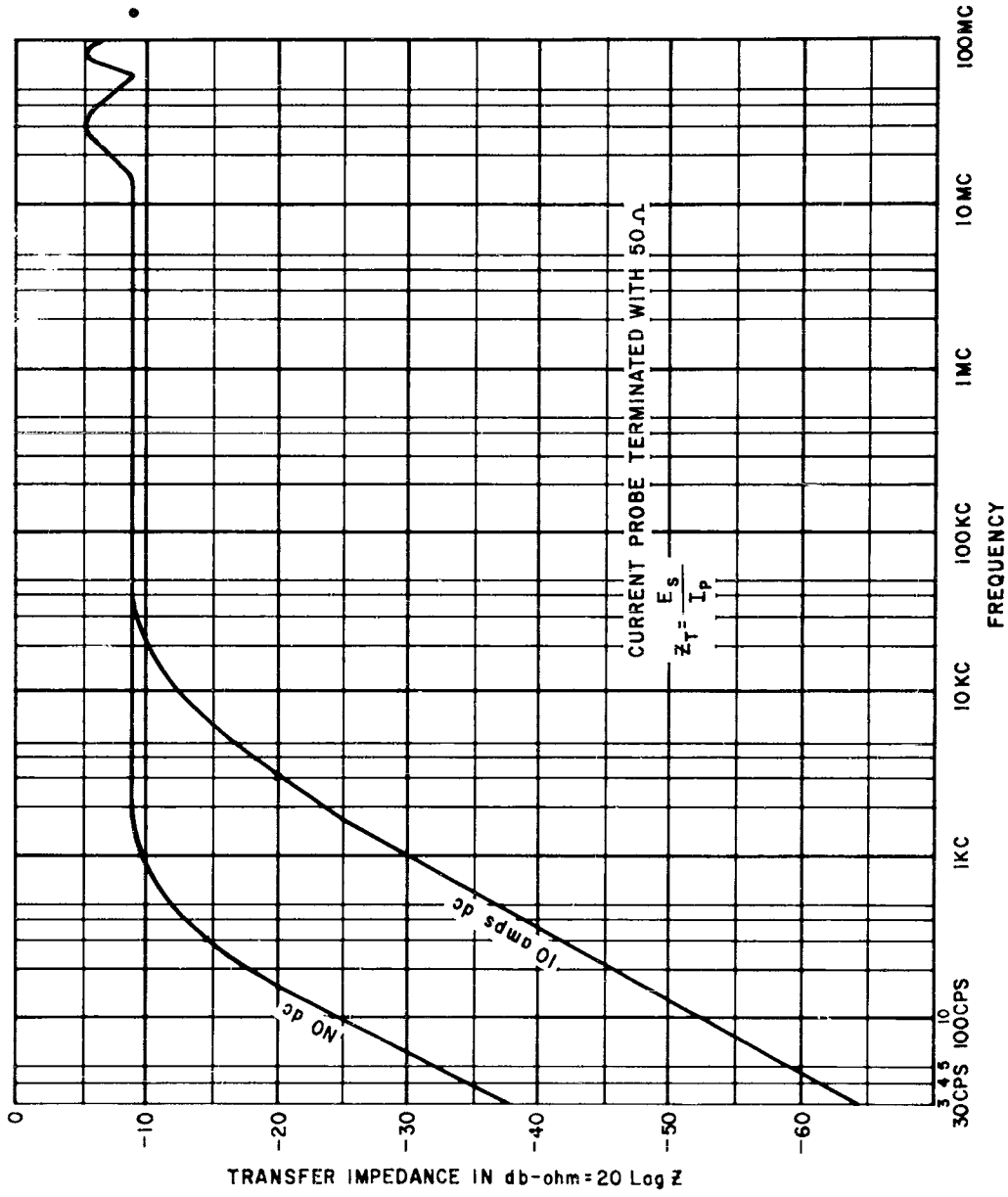



**Figure 4. Transfer Impedance for Tektronix P6016 Current Probe**

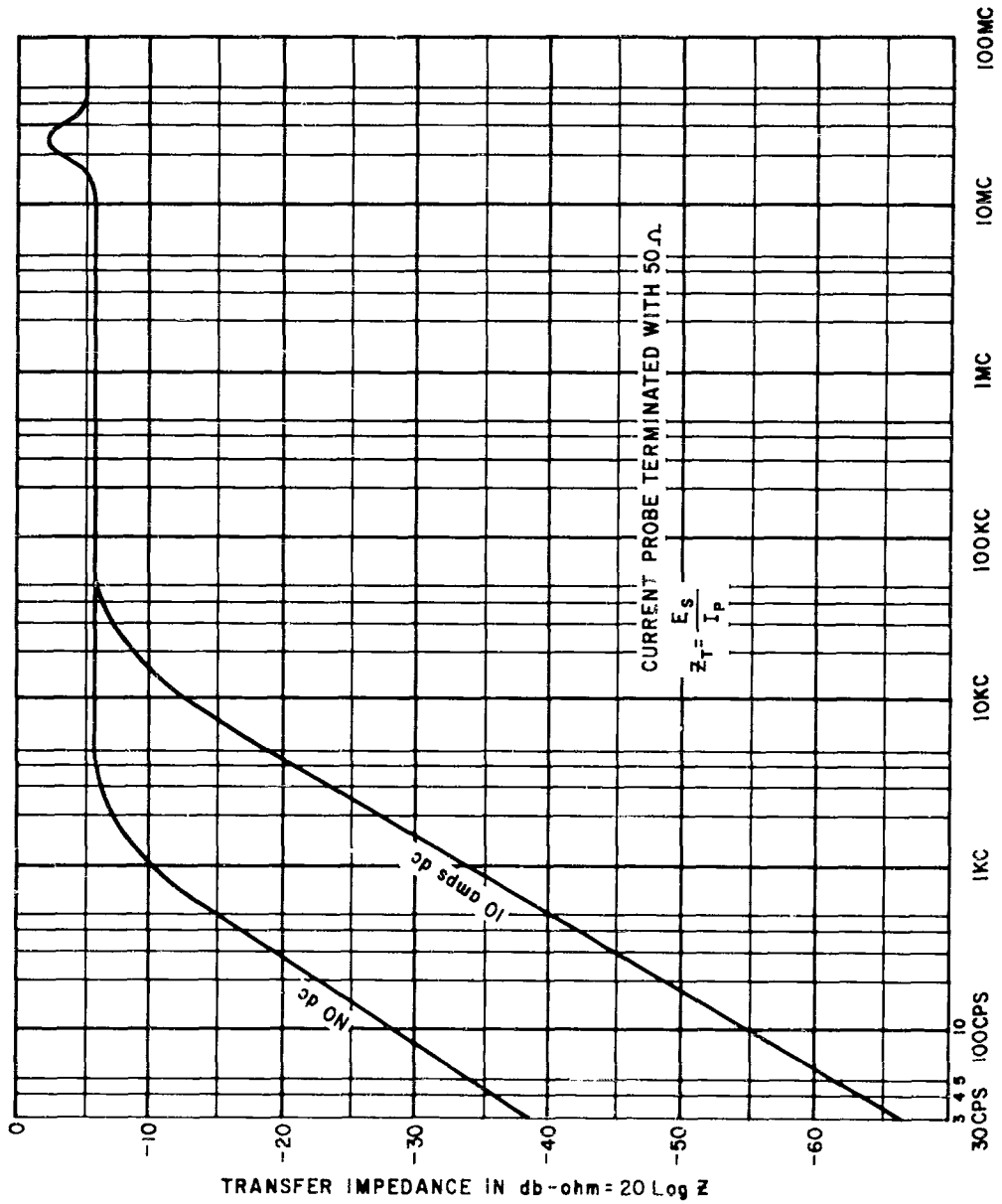



**Figure 5. Transfer Impedance for Hewlett-Packard AC-21F Current Probe**

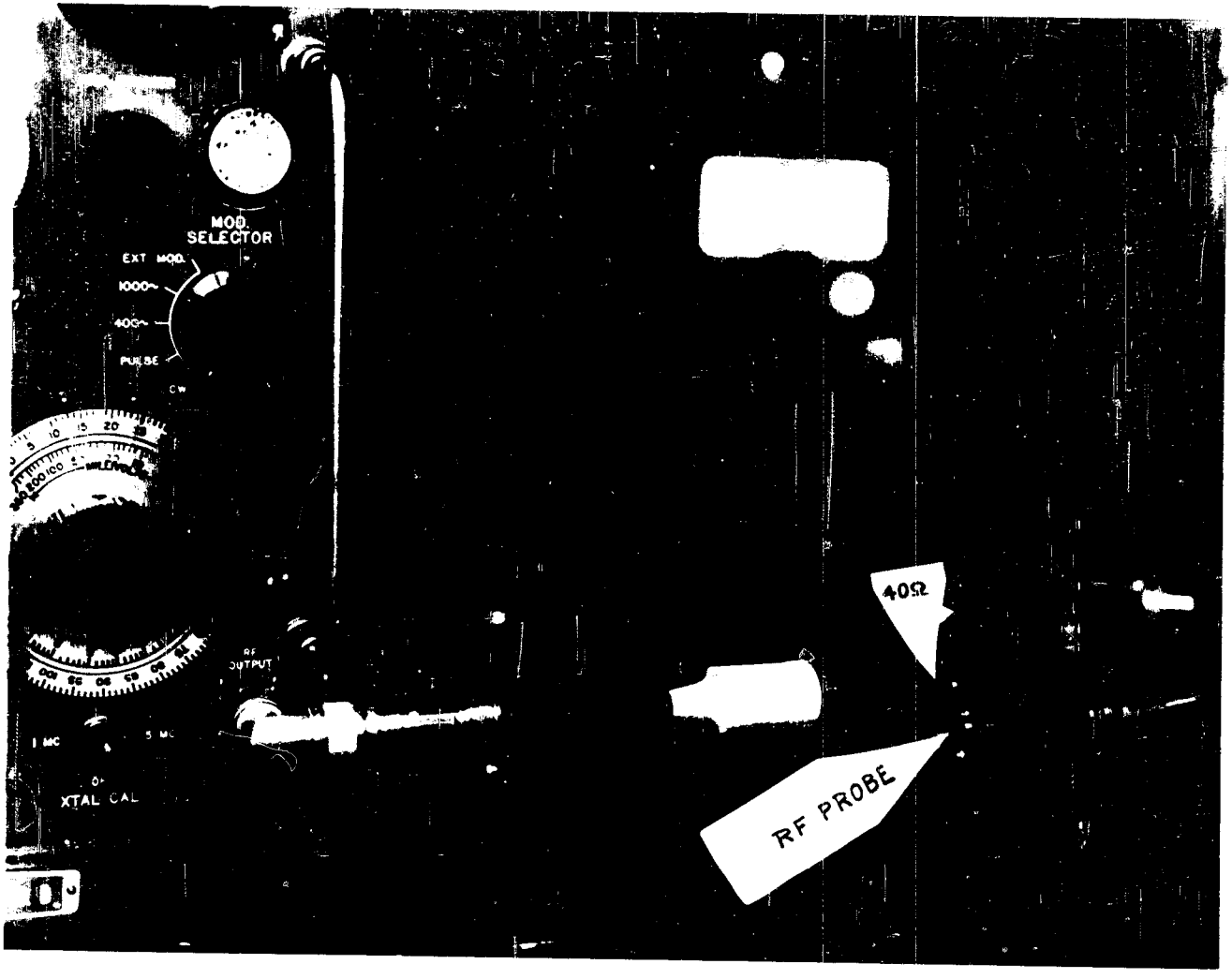



**Figure 6. Set-up for UHF Current Measurement**

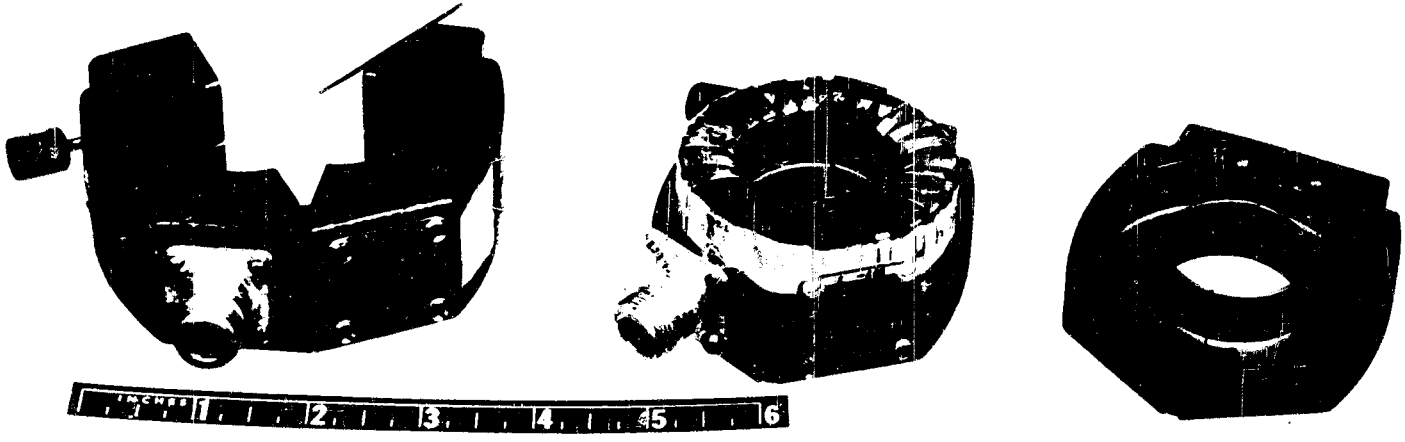
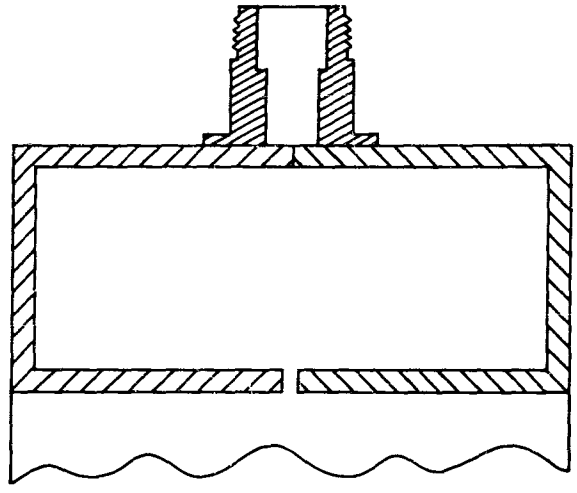
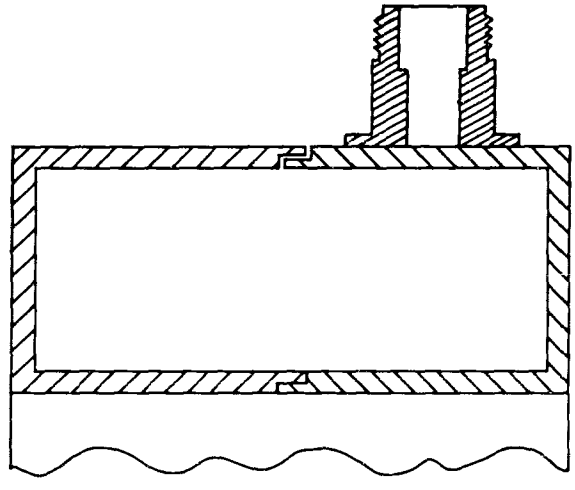



**Figure 7. Stoddart 91550-1 Current Probe**



STODDART PROBE
CONNECTOR-TO-GAP SYMMETRY



MODIFIED SHIELD
NO CONNECTOR-TO-GAP SYMMETRY

**Figure 8. Cross-section of Shields**

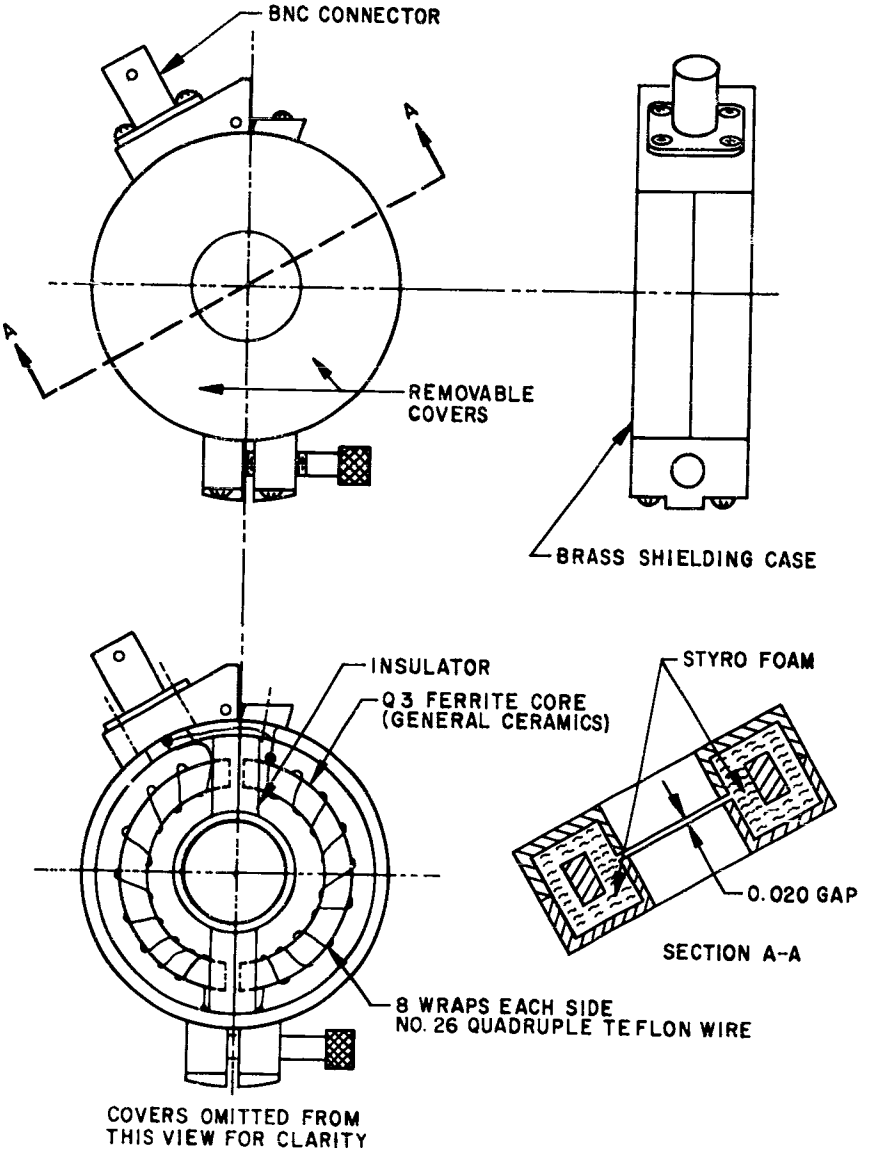



Figure 9. CVA-1 Current Probe

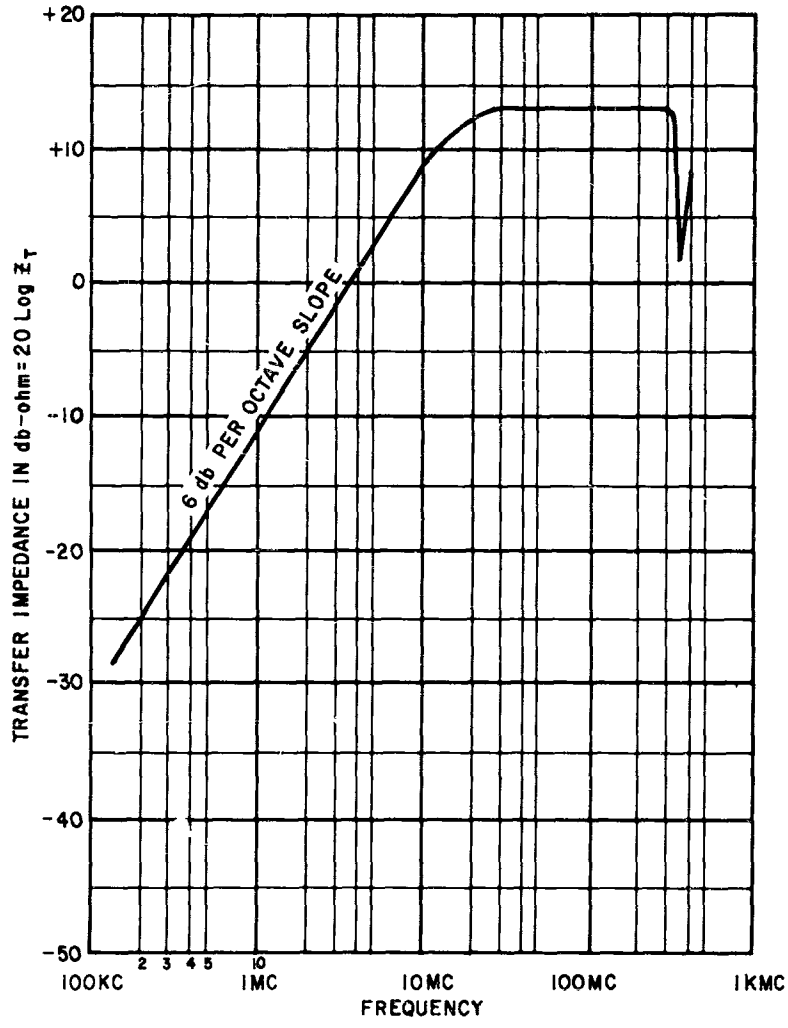



Figure 10. Transfer Impedance of CVA-1 Current Probe

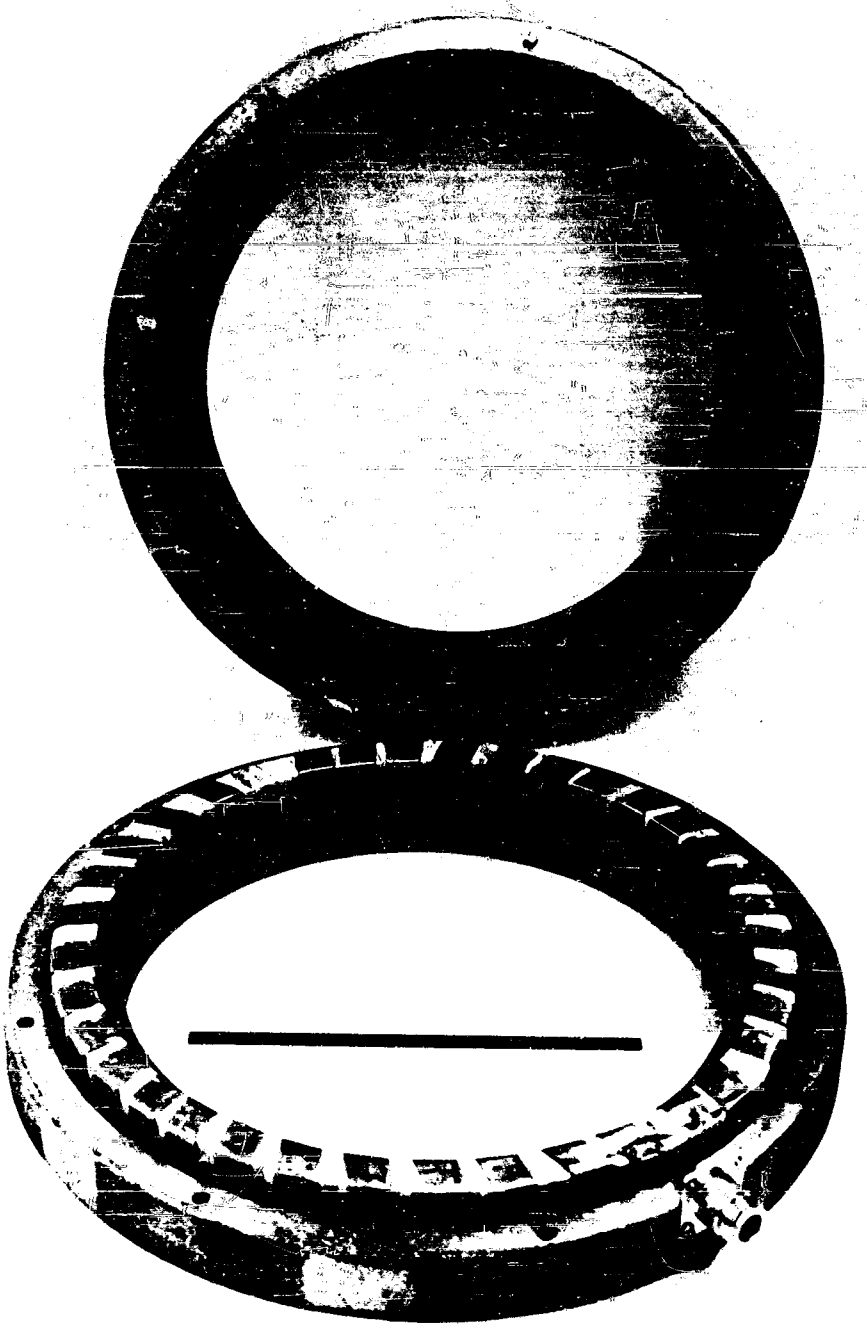


Figure 11. CVA-2 Current Probe

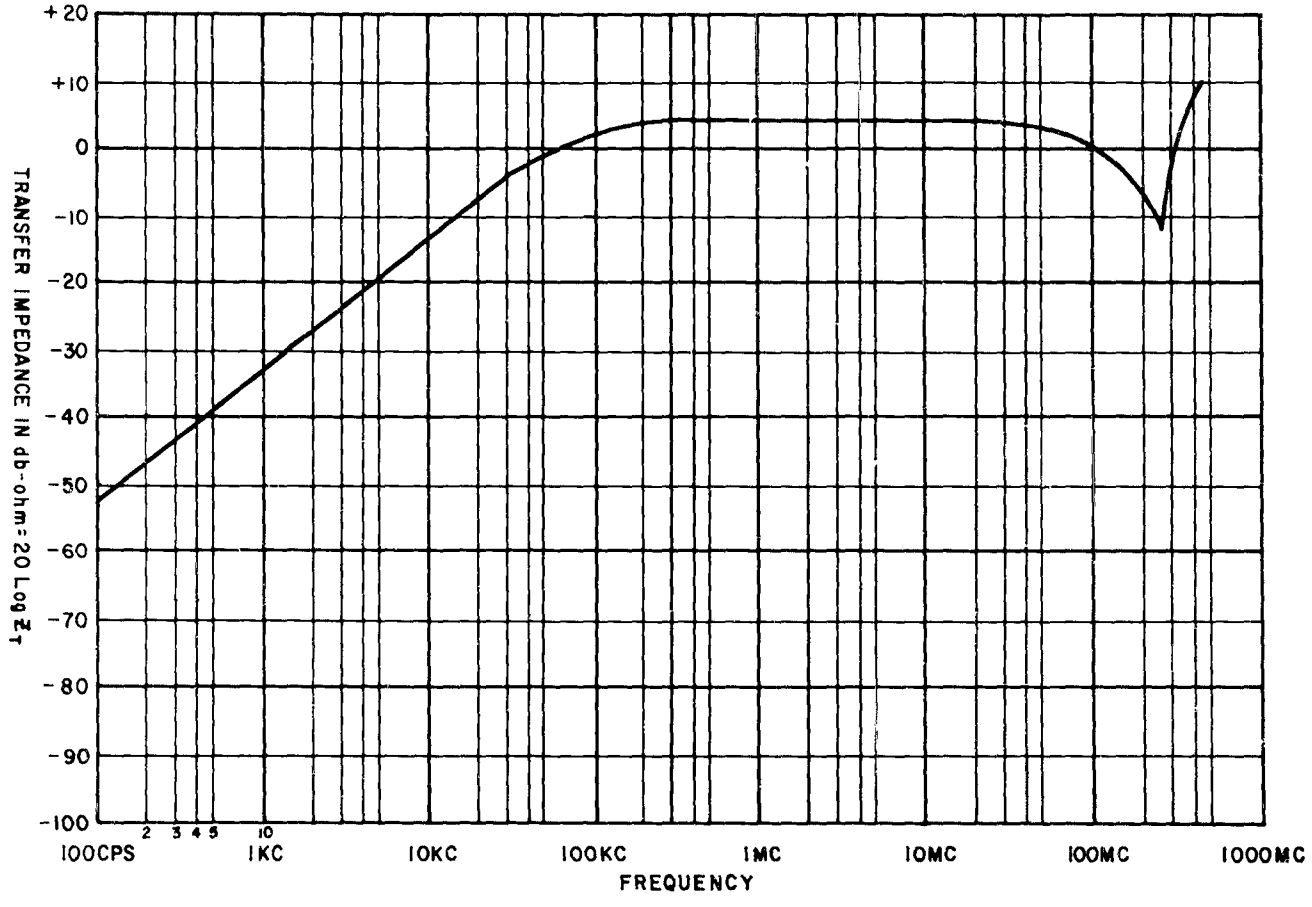



**Figure 12. Transfer Impedance for CVA-2 Current Probe**

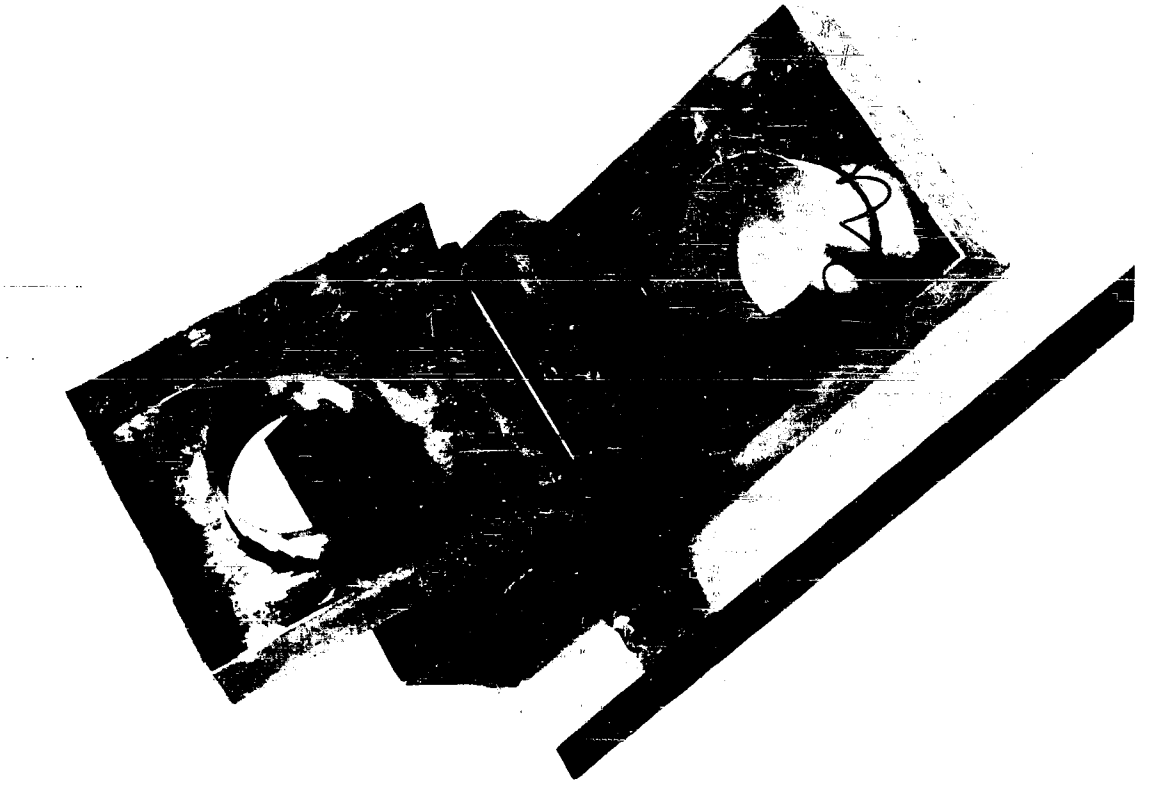


Figure 13. CVA-3 Current Probe

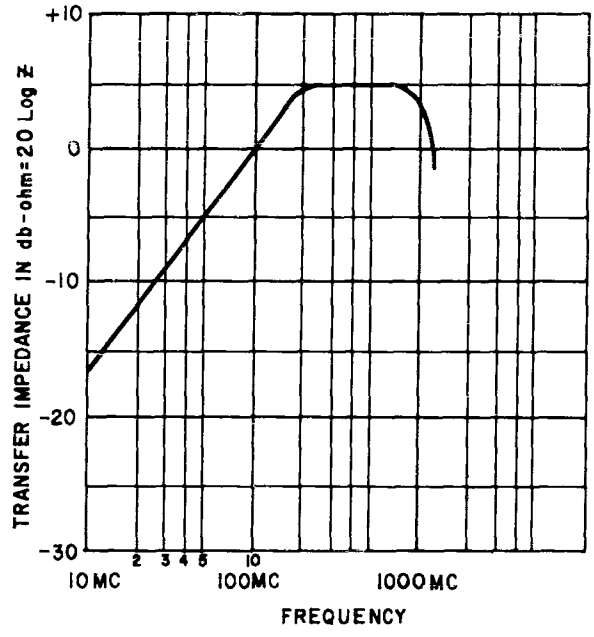



**Figure 14. Transfer Impedance for CVA-3 Current Probe**

# A COMPARISON OF THE SPECTRUM SIGNATURES OF AM, FM, AND SSB COMMUNICATIONS EQUIPMENTS

J. G. Holey and E. W. Wood
Georgia Institute of Technology
Engineering Experiment Station
Atlanta, Georgia

(Work Done Under Contract With The U. S. Army Signal Corps)

Abstract. - The spectrum signature of a device is sometimes defined merely as the frequency spectrum of the energy that may be radiated from the device, or the spectrum of frequencies to which the device will respond. In the field of communications the devices usually of interest are receivers and transmitters, and the spectrum signatures are defined in a manner such that both desirable and undesirable characteristics of receivers and transmitters are determined. Both types of information are necessary for radio frequency interference prediction.

The theory for comparison of AM, FM and SSB equipments has been established in recent years, and this paper offers results of measurements which supplement the theory. This discussion is based on actual laboratory measurements made on more than 48 transmitters representing 24 different types and 52 receivers of 23 types.

Co-channel interference for AM receivers is not severe if the interfering signal is over 40 decibels below the desired signal, but becomes increasingly severe for decreasing signal differential. An interfering signal does not "capture" an FM signal until the interfering signal is within 8-12 db of the desired signal. Results of spurious responses, two-signal selectivity and RF intermodulation tests are also discussed.

The SSB transmitter harmonic rejection appears to be the best above the first few harmonics, FM the best for the second harmonic, and AM the worst in all cases. SSB RF intermodulation characteristics are slightly better than FM, and extremely good bandpass filters are available which improve RF intermodulation over 11 db at 0.6% spacing in the VHF/UHF region. Transmitter modulation characteristics, system linearity, audio intermodulation, splatter, and carrier noise are also considered.

## I. INTRODUCTION

One of the most important and rapidly expanding problems in the communications field today is that of compatible operation of several communications equipments located at a particular geographical location. Until the last decade, the size of a communications complex was such that the interference problem could usually be resolved locally. However, with the communications requirement of both the military and civilian user increasing at the present rate, frequency assignment for interference-free communication has become a critical obstacle.

It would be assumed by the layman that frequency selection is a relatively simple problem with the primary factor being the choice of transmitting frequencies such that they do not coincide with any receiving frequencies. However, it is fairly well known that receivers may respond to hundreds of frequencies if the input level is sufficiently strong; these spurious frequencies at which the receiver responds are known as spurious responses. Also, the vast majority of transmitters in operation at the present time produce outputs in addition to the carrier frequency; these are referred to as spurious and harmonic emissions.

To further complicate the problem, two signals of sufficient amplitude may combine in either a receiver or a transmitter to produce new frequencies, or RF intermodulation products. This type of interference is of particular concern to shipboard communications complexes, due to the restricted area. In addition, common practice in radio-relay installations is to place all antennas, both receiving and transmitting, on a single structure such as a water tower or forestry fire tower. The frequencies of intermodulation products are predictable according to the equation

$$f_{IM} = m f_A \pm n f_B$$

where m and n are non-zero integers.

It has been the purpose of the Georgia Tech Interference Group for the past several years to: 1) study the various types of mutual interference, 2) evolve frequency selection schemes for interference-free operation,[1,2] and 3) catalog the interference characteristics of U. S. Army communications equipments operating in the frequency range from 150 kilocycles to 1000 megacycles. Tests have been completed thus far on some 48 transmitters representing 24 different equipments, and 52 receivers representing 23 equipments.[4] The test methods have been in accordance with the Spectrum Signature Collection Plan of the Electromagnetic Compatibility Analysis Center, with minor variations.

It is the purpose of this paper to discuss some of the important interference characteristics which have been measured in the laboratory, and in particular to compare the characteristics of AM, FM, and SSB equipments. They include the following:

| Receivers | Transmitters |
|---|---|
| Co-Channel Interference | Harmonic Emissions |
| Spurious Responses | RF Intermodulation |
| RF Intermodulation | Modulation Characteristics |
| Two-Signal Selectivity | AF Intermodulation |
| | Carrier Noise |

While some of the above characteristics do not usually differ with different types of receivers and transmitters, others are determined by stages such as the receiver detector and transmitter modulator sections. Case Radiation, Case

Susceptibility, Power Line Radiation, and Power Line Susceptibility are a few remaining characteristics which are not considered.

## II. RECEIVERS

In examining spectrum signatures of the various types of receiver systems, susceptibility to several types of interference should be examined. The most obvious, of course, would be co-channel interference. For a more complete analysis, spurious responses, RF intermodulation and two-signal selectivity should also be considered.

### Co-Channel Interference

Data taken from co-channel interference tests on six types of AM receivers, six types of FM receivers, and one SSB receiver are shown in Figures 1 through 3. Considering first the AM receiver data in Figure 1, the curves are found to follow their maximum until the interfering signal is some 40 to 45 decibels below the desired signal, where they begin a gradual decrease. As the signal differential becomes less than 40 decibels the interference becomes increasingly severe until a slope of one is reached.

As expected, the SSB characteristic was somewhat similar except that a higher initial S/N ratio was obtainable. This is attributed to not only noise bandwidth improvement but also lack of modulation on the desired signal source. For this test the desired signal was merely displaced in frequency by the desired audio frequency and thus was devoid of audio distortion as contrasted with AM and FM signal generators. Since the interfering signal for each receiver type was unmodulated, the receiver output distortion and noise increased directly with the interfering signal level, and this resulted in the curve shown in Figure 2.

The characteristics of the six FM receivers are shown in Figure 3. Here the well-known "capture" effect of wideband FM is graphically illustrated. Each receiver, with the exception of the narrowband receiver whose characteristics deviate markedly, holds its maximum ratio in the presence of a co-channel signal until the interfering signal is within 8-12 db of the desired signal. At this point the discriminator rapidly becomes "captured" by the interfering signal.

The mean curve of each receiver type is shown superimposed in Figure 4. The distinct noise and interference advantage of wideband FM is seen, which of course is at the expense of increased bandwidth.

The test setup for the co-channel test is illustrated in Figure 5.

As mentioned previously the co-channel interference characteristics, or the knowledge of the degradation effects of an interfering signal whose frequency coincides with the frequency of the desired signal are particularly important because RF intermodulation and spurious response interference both result in interfering or spurious signals appearing at a particular amplitude within the IF passband of the receiver. Therefore, the equivalent level of a

co-channel signal which would produce the same IF signal amplitude as the spurious product can be determined fairly easily and the co-channel interference characteristics curves used to estimate the actual degradation of the desired signal at the audio output of the receivers. This method is used in cases where the RF intermodulation and spurious response tests are conducted with no desired signal present, as shown in Figures 6 and 7. In these tests, the interfering signal (or signals) are adjusted in amplitude and frequency until a product, which causes some specified audio output indication, is obtained within the IF passband. With FM receivers, 6 decibels quieting is the usual measure, and with AM and SSB receivers a modulated signal is used with 6 decibels audio output signal-to-noise as the quantity. Hence the equivalent signal of the receiver tuned frequency will be of the same amplitude as the predetermined sensitivity level of the receiver, which is that desired signal level which produces the same output indication as above.

Spurious Responses

To extend the analysis to stronger interfering signals the particular stage of the receiver which causes the spurious IF product must be considered along with amplitudes of all involved signals. For instance, consider the spurious response interference. The process here consists of the interfering signal (or harmonics thereof) combining with the receiver local oscillator (or harmonics thereof) in the receiver mixer stage to produce a signal at the IF frequency, according to the equation

$$f_{SR} = \left| \frac{pf_{LO} \pm f_{IF}}{q} \right|$$

where p is any positive integer and q is any nonzero positive integer. For example, insertion of a value of 1 for both p and q results in two solutions of the equation, one being the frequency to which the receiver is tuned and the other the image frequency. Assuming linear RF amplifiers, a harmonic-free local oscillator, and a mixer stage whose transfer characteristics contain curvature to and including third order, the following analysis illustrates the manner in which the amplitude of the IF signal produced by the spurious input signal varies with the input signal level.

Let $e_i = A \cos \omega_1 t$

$e_{LO} = B \cos \omega_2 t$

mixer response $y = a_o + a_1 x + a_2 x^2 + a_3 x^3$

where $x = (A \cos \omega_1 t + B \cos \omega_2 t)$

$$x^2 = A^2 \cos^2 \omega_1 t + B^2 \cos^2 \omega_2 t + 2AB (\cos \omega_1 t \cos \omega_2 t) = \frac{A^2}{2} (1 + \cos 2\omega_1 t) +$$

$$\frac{B^2}{2} (1 + \cos 2\omega_2 t) + \frac{2AB}{2} [\cos (\omega_1+\omega_2)t + \cos (\omega_1-\omega_2)t] ;$$

$$x^3 = \frac{A^3}{2} (\cos \omega_1 t) (1 + \cos 2\omega_1 t) + \frac{A^2B}{2} (\cos \omega_2 t) (1 + \cos 2\omega_1 t) +$$

$$\frac{AB^2}{2} (\cos \omega_1 t) (1 + \cos 2\omega_2 t) + \frac{B^3}{2} (\cos \omega_2 t) (1 + \cos \omega_2 t) + A^2B (\cos \omega_1 t) \cos(\omega_1+\omega_2)t +$$

$$AB^2 (\cos \omega_2 t) \cos (\omega_1-\omega_2)t = \frac{A^3}{2} \cos \omega_1 t + \frac{A^3}{4}[\cos 3\omega_1 t + \cos \omega_1 t] +$$

$$\frac{A^2B}{2} \cos \omega_2 t + \frac{A^2B}{4} [\cos (\omega_2+2\omega_1)t + \cos (\omega_2-2\omega_1)t] + \frac{AB^2}{4}[\cos (\omega_1+2\omega_2)t +$$

$$\cos (\omega_1-2\omega_2)t] + \frac{AB^2}{2}\cos \omega_1 t + \frac{B^3}{3}\cos \omega_2 t + \frac{B^3}{4}[\cos 3\omega_2 t + \cos \omega_2 t] ;$$

assuming $f_{IF} = f_i - f_{LO}$, $e_{IF} = AB \cos (\omega_1-\omega_2)t$,

$n\omega_1 \neq \omega_{IF}$, $n\omega_2 \neq \omega_{IF}$, $n = 1,2,3,\ldots$, then $\frac{A^2B}{4}[\cos (\omega_2+2\omega_1)t +$

$\cos (\omega_2-2\omega_1)t]$ and $\frac{AB^2}{4} [\cos (\omega_1+2\omega_2)t + \cos (\omega_1-2\omega_2)t]$ are the only terms from the cubic expansion which may result in signals appearing at the IF frequency. Thus the output of the mixer stage which is of interest is

$a_2AB [\cos (\omega_1+\omega_2)t + \cos (\omega_1-\omega_2)t] + \frac{a_3A^2B}{4} [\cos (\omega_2+2\omega_1) + \cos (\omega_2-2\omega_1)t] +$

$\frac{a_3AB^2}{4} [\cos (\omega_1+2\omega_2)t + \cos (\omega_1-2\omega_2)t]$ .

If $a_2AB \cos (\omega_1-\omega_2)t$ represents the desired product, then $a_2AB \cos(\omega_2+\omega_1)t$, $\frac{a_3}{4} A^2B \cos (\omega_2-2\omega_1)$, $a_3 A B^2 \cos (\omega_1+2\omega_2)$, and $\frac{a_3}{4} A B^2 \cos (\omega_1-2\omega_2)$ represent spurious responses if any argument becomes equal to the IF frequency. As an example, assume $\omega_1$ to be the local oscillator frequency and $\omega_2$ to be the input frequency, and further assume the local oscillator frequency to be greater than the IF frequency.

Spurious responses will then occur for three values of $\omega_2$:

$$\omega'_2 = 2\omega_1 + 2\pi f_{IF},$$

$$\omega''_2 = \frac{\omega_1}{2} \pi f_{IF},$$

and

$$\omega'''_2 = \omega_1 + 2\pi f_{IF} \text{ (image)}.$$

Considering only $\omega'_2$ for the present, the envelope of the IF product is seen to be $\frac{3}{4}A^2B$ where a is a mixer constant, B is the amplitude of the local oscillator and A is the amplitude of the input signal. This IF product is identified by the spurious response equation where p is equal to one (the coefficient of $\omega_2$) and q is equal to two (the coefficient of $\omega_1$).

This analysis can be extended to show that the amplitude of the IF product is proportional to the (n - 1) power of the input level, where n is the power of the series term producing the product.

Spurious response rejection varies widely even between receivers of the same type, and is usually affected in a predictable manner only by such devices as high-Q filters or by using frequency-translation schemes other than the local-oscillator-mixer method.

Intermodulation

The intermodulation characteristics of a receiver are of importance because they give an indication of the interference possibilities when the receiver is used in the presence of two off-channel signals. This test is conducted as shown in Figure 6. Assuming that these signals have not been mixed before arriving at the receiver, some mixing may be expected in the RF amplifier tubes and/or the first mixer. If one of the extraneous signals generated in this manner happens to fall at the tuned frequency and is of sufficient amplitude, interference of a co-channel nature is the result.

Usually it is assumed that the third order mix is potentially the most serious type of intermodulation because both signals may be within the passband of the input circuits. The frequency relationships for this type of mix are given by

$$f_o = 2f_a - f_b$$

where $f_o$ is the receiver tuned frequency and $f_a$ and $f_b$ are the interfering signal frequencies.

It is also possible that higher order intermodulation products caused by two interfering signals near the tuned frequency could produce interference. An example of a higher order mix is the fifth order, defined by

$$f_o = 3f_a - 2f_b.$$

These high order mixes, however, are not usually sufficiently strong to cause appreciable interference.

The second order, or primary, mix cannot be neglected as a possible cause of interference. This mix is defined by

$$f_o = f_b - f_a.$$

Although one or both interfering signals must be far removed from the passband, they may still develop enough voltage at the grid of the first tube to produce strong interference. The above analysis also applies for determining effects of input amplitude variations.

Since the three types of receivers all contain similar conversion processes in general, neither of the above two forms of interference is very dependent on the modulation system. However, a comparison of intermodulation tests results as shown in Figures 8 and 9 shows that AM interference is somewhat more predictable; the AM rejection ratio curves are characterized by a 3 db/octave slope at extremely small $\frac{\Delta f}{f_o}$ ratios, where $\Delta f$ is the frequency separation of the nearest interfering signal and the tuned frequency of the receiver. The slope increases to 9-12 db octave at some ratio between .003 and .01; data for rejection ratios greater than 90 db are subject to error due to signal generator imperfections and other factors. FM intermodulation rejection curves vary more erratically since the RF amplifier bandpass characteristics are dependent on the modulation index or $\beta$ for the receiver. Since only one type of SSB receiver was tested, no conclusion may be drawn empirically, regarding intermodulation. However, it is expected that SSB exhibits characteristics similar to AM.

Two-Signal Selectivity

The selectivity of a receiver to an interfering signal near in frequency, with a desired signal present, is referred to as the two-signal or "true" selectivity. The two-signal test is conducted by inserting two RF signals into the receiver under test, as shown in Figure 5. One signal is tuned to the frequency of the receiver and represents a desired signal. The second is tuned to some near frequency and represents an interfering signal. As this interference is brought nearer the tuned frequency of the receiver, the desired signal level is reduced in the audio output of the receiver. This is usually caused by AVC action in the receiver, or by overloading of the first RF stage by the interfering signal. Either results in a reduction of the audio output ratio of the receiver.

Results were examined for various receivers tested, but no conclusions could be drawn. In general, FM will have less selectivity (require greater bandwidth) except in the case of narrowband FM. The one SSB receiver tested showed the highest selectivity, a result of the sideband filters used in the IF strip of the SSB converter. The selectivity, in fact, of this receiver was such that noise on the carrier of the signal generator providing the interfering signal caused difficulty in measurements.

## III. TRANSMITTERS

The transmitters which were tested to obtain spectrum signature data and interference characteristics include portable, fixed, mobile, aircraft and relay equipments. Table 1 shows the number and types of transmitters and Table 2 outlines the frequency range according to the type of modulation systems. The power outputs for the different systems are presented in Table 3.

All of the transmitters were tested in accordance with the procedures outlined in the reference[3] and were tuned as specified in the technical manual provided with the equipment.

### Harmonic Emissions

The majority of emissions from a transmitter are related to the fundamental and/or harmonics of the master oscillator, multipliers, driver, and power amplifier frequencies. Other frequencies which are not harmonically related to the master oscillator may be present due to mixing of the various frequencies present in a transmitter. A linear amplifier is expected to have a smaller harmonic content than a non-linear amplifier; therefore, SSB transmitters are expected to produce weaker harmonics than AM or FM transmitters. The harmonic emissions from AM, FM and SSB transmitters will now be considered.

The limit set by Military Specifications MIL-I-11748B (SigC) for any harmonic emission is 60 db below the carrier. The first 10 harmonics of each type of transmitter have been categorized and analyzed, and about 68% of the transmitters were found to exceed this limit for the second harmonics and 45% exceeded the limit for the third harmonics. Table 4 shows the percentage of each type of transmitter exceeding the 60 db limit for the first 10 harmonics. The FM transmitters were better with respect to second harmonic emissions than the AM or SSB transmitters. The SSB transmitters, however, had greatly improved third and higher harmonic rejections.

More than 35 AM, 62 FM and 32 SSB test frequencies were investigated, and their mean harmonic outputs tabulated in db below the carrier are presented in Table 5. These data support the results in Table 4. The FM second harmonic rejection was about 17 db more than AM and 14 db better than SSB. The SSB fourth and higher harmonic rejections were better than either AM or FM. In general, the SSB harmonic rejection appears to be the best above the first few harmonics, FM the best for the second harmonic, and AM the worst in all cases.

It is necessary to point out some reasons for the above results. The SSB transmitters contained Class B push-pull final amplifiers with little non-linear curvature and therefore the harmonic emissions were at a lower level than the emissions from the AM Class C final amplifiers. The FM transmitters had low power output and operated in the VHF and UHF regions. It is usually easier to produce and use VHF and UHF filters to reduce spurious and harmonic emissions than it is to use HF filters because of size consideration. An FM transmitter was tested with and without the bandpass filters provided with the installation, and it was found that the bandpass filters produced more than 50 db of rejection for the second and third harmonics, which represents a considerable improvement. However, the cost of producing HF filters for high powered transmitters must be weighed with the improvement obtained and other considerations in determining the feasibility of their use.

Two 50 watt, AM VHF/UHF transmitters were tested and their harmonic rejections were similar to those of FM VHF/UHF transmitters. Thus it appears that the overall transmitter linearity, circuitry, frequency range, and power range usually determines the nature of the harmonic content, and not the type of modulation that the system is capable of handling. The same is true for other spurious emissions from the transmitter as well.

Actual radiated output level should be analyzed also, because a transmitter which radiates +71 dbm and has a second harmonic rejection of only 44 db is capable of a second harmonic output of 1/2 watt.

RF Intermodulation

RF intermodulation is the mixing of two or more carrier frequencies in a non-linear manner to produce other frequencies which are in turn radiated. Only the third order intermodulation will be dealt with here since it is the most serious type of interference. An example of third order intermodulation is produced in a transmitter when the second harmonic of the fundamental frequency, $f_o$, is mixed with an incoming interfering signal, $f_i$, to produce signals $|f_o - f_i|$ away from $f_o$ and $f_i$. The test setup for measuring RF intermodulation is shown in block diagram form in Figure 10. Table 6 shows normalized values for third order RF intermodulation data for AM, FM, and SSB transmitters for 5% and 10% spacings and -20, -40, and -60 db couplings. The coupling values represent the difference in levels of the two signals at the desired transmitter, and 5% spacing means that the interfering signal is 5% of the desired signal frequency away from the desired signal.

It is seen that the SSB intermodulation was less than AM or FM intermodulation for all values of couplings for 5% spacing. Data were not available for SSB intermodulation at 10% spacing. The mean levels of third order IM products on the desired signal side relative to the desired carrier were -57 db for SSB, -53 db for FM, and -45 db for AM at coupling of -20 db, and the third order IM products on the interfering signal side were about 20 db less. Figure 11 shows a plot of the mean normalized third order IM at 5% spacing,

and the SSB IM rejection is seen to be slightly better than the FM and considerably better than the AM IM rejection. For every db decrease of interfering signal, the third order IM product on the desired signal side decreased by about 1 db and the third order product on the interfering side decreased about 2 db.[4] This means that the products on the interfering side fall off twice as fast as the ones on the desired signal side for decreasing interfering signal.

An increase of spacing from 5% to 10% produced further rejection from 5 to 10 db for both the AM and FM systems. The FM intermodulation was about 10 db better than the AM intermodulation for all values of spacings and couplings. Again circuit design, because of frequency and power considerations, is responsible for the outcome of the RF intermodulation study. Linear operation in the SSB system causes far less mixing than in non-linear output stages. A VHF/UHF FM transmitter was tested which employed bandpass filters capable of 8 db rejection at a spacing of 1% from the desired frequency, 37 db at 5% and 49 db at 10%; the desired signal was decreased only 1 db. This system can be tuned to contain hardly any RF intermodulation at 10% frequency spacing. It was found in an actual test that the minimum intermodulation improvement with bandpass filters was 11 db for the 3rd order low product with spacing of 0.6%, and with greater spacings the 3rd order products were attenuated 25 decibels or more by the filters alone. The size and cost of such a filter for the HF region would probably be greater than these VHF/UHF filters.

Modulation Characteristics

The modulation characteristics show the modulator capabilities of the transmitter. If the modulator input voltage versus percentage modulation or percentage of rated deviation is not linear the output of the transmitter will be degraded. The desired modulation will be distorted and unwanted adjacent channel emission will likely occur.

The modulation characteristics for 4 AM transmitters are presented in Figure 12. The percentage modulation is plotted against audio input in dbm. A large audio input signal is necessary to modulate transmitter 4 above 80% modulation, and considerable distortion is generated within the modulator section. Curve 2, however, represents the typical AM transmitter modulation characteristic curve.

The percentage of rated deviation versus audio input in dbm is plotted in Figure 13 for 5 FM transmitters. Curves 1 and 2 show the result of limited deviation in an FM transmitter and curves 3, 4 and 5 show unlimited modulation up to 150% of rated deviation Above 80% of rated deviation the information present in transmitters 1 and 2 becomes distorted, and transmitters 3, 4 and 5 transmit the information with little distortion However, it is possible to modulate transmitters 3, 4 and 5 well above 100% and cause excessive sideband splatter without the limited deviation provisions.

SSB modulation characteristics are somewhat different from AM or FM characteristics because of the different way in which modulation is expressed.

Figure 14 shows the percentage of rated power output (PEP) versus audio input in dbm for 4 SSB transmitters. Rated power was obtained for a two-tone audio input when the distortion products were 25 db below the two tones. Curves 1 and 2 are very non-linear and curve 4 is most linear, even up to 150% of rated power. Curve 3 represents a typical curve for Class B operation. Transmitters 1 and 2 are considered poor SSB transmitters since audio intermodulation products are extremely high when they are operated near rated power output because of the non-linearities present in the system.

Audio Intermodulation

The audio intermodulation produces new frequencies similar to RF intermodulation. If two audio tones, $f_1$ and $f_2$, are mixed in a non-linear manner, new signals will be produced at $2f_1 - f_2$ and $2f_2 - f_1$ which are called third order AF intermodulation products; $3f_1 - 2f_2$ and $3f_2 - 2f_1$, 5th order; $4f_1 - 3f_2$ and $4f_2 - 3f_1$, 7th order; etc. The mixing may occur in the RF section as well as in the modulator and audio sections. The intermodulation products are illustrated in Figure 15a, which is a spectrum photograph of the SSB transmitter modulated with two equal tones of 400 cps and 2500 cps. It is observed that the 3rd, 5th, 7th, 9th, 11th, and 13th audio intermodulation products are present. The unused sideband contains distortion components almost as strong as the distortion components in the desired sideband. This indicates that the audio intermodulation occurs after the sideband filter circuit which is near the balanced modulator section and where the single sideband signal is produced. The non-linearities of the system cause the presence of these unwanted products in the desired and unused sidebands and limit the usefulness of the unused sideband for further information transmission.

Figure 15b is a photograph of the spectrum output for an FM transmitter whose rated deviation is 15 kc/sec. Sideband splatter extends 23 kc/sec from the carrier at 60 db below the unmodulated carrier. Figure 15b illustrates AF intermodulation for an AM transmitter.

Noise-loaded modulation is shown in Figure 16 for SSB, FM, HF AM, and VHF AM. The effect of single sideband modulation is fully realized in Figure 15a. The roundness of the FM output is seen in Figure 16b, and splatter effect of AM is observed in Figures 16c and 16d.

Carrier Noise

Carrier Noise is defined as that modulation of the carrier which is produced by noise generated in the oscillator, multiplier, modulator and power amplifier stages, plus hum components emanating from the power supplies. Figure 17a shows components at ±120 cps from the carrier, and 32 db below the carrier level for an SSB carrier output. This is caused by the second harmonic of the power line frequency. Figure 17b is an FM carrier output and components are present which are caused by noise generated in the modulation section and/or power line noise. The rated deviation for this FM transmitter is 15 kc/sec. Figure 17c

is an AM output carrier which has a noise component similar to the SSB output, but not as large in magnitude. Proper power supply filters usually eliminate these carrier noise components.

## IV. CONCLUSIONS

The important differences found in the data for various interference characteristics of the three types of receivers have been primarily in the co-channel interference test, as expected. These co-channel characteristics do not, in themselves, specify the spurious response and intermodulation susceptibility as measured using present methods, but do determine the interference to a desired signal when present if the equivalent IF interfering signal and desired signal amplitudes are determined. It should be mentioned that most receivers tested, regardless of type, showed at least 80 db rejection to most of the spurious response signals and therefore may not be affected by this type of interference if a sufficiently strong desired signal level is maintained.

The majority of transmitters which were tested did not conform to the military specifications for second harmonic output. FM and SSB transmitters were better than the AM transmitters with respect to harmonic output and RF intermodulation output because of circuit design and more linear operation, respectively. Bandpass filters are available which provide as much as 49 db of attenuation at a frequency spacing of 10% from the desired signal and offer considerable reduction in harmonic output and RF intermodulation in the VHF/UHF region. The AF intermodulation products in the unused channel of an SSB signal were about equal in amplitude to those in the desired sideband. FM deviation limiting produces a great deal of distortion near the rated deviation of the transmitters tested; however, unlimited deviation is capable of causing excessive sideband splatter.

ACKNOWLEDGEMENTS

The authors wish to express thanks to R. N. Bailey and W. B. Wrigley for their assistance in making this paper possible. The contents of this paper are a result of Contract DA-36-039-sc-87183 placed with the Engineering Experiment Station of the Georgia Institute of Technology by the U. S. Army Signal Research and Development Laboratories, Fort Monmouth, New Jersey.

REFERENCES

1. T. T. Spengler, and I. E. Perlin, "Construction of Mutual Interference Matrices," Proc. of 6th Conf. on Radio Interference Reduction and Electronic Compatibility, October 1960.

2. I. E. Perlin, "Possessing Non-Symmetrical Mutual Interference Matrices," Proc. of 6th Conf. on Radio Interference Reduction and Electronic Compatibility, October 1960.

3. C. E. Blakely, R. N. Bailey, J. G. Holey, and E. W. Wood, "Electronic Equipments Interference Characteristics - Communication Type," Manuscript of Catalogue, Volume 1A, Test and Test Procedures.

4. C. E. Blakely and R. N. Bailey, "Making Transmitters RFI Free," Electronic Industries, Vol. 19, No. 3, March 1960.

TABLE 1
TYPES OF TRANSMITTERS TESTED

| TYPE OF TRANSMITTER | NUMBER |
|---|---|
| AM | 16 |
| FM | 26 |
| SSB | 6 |

TABLE 2
FREQUENCY RANGE FOR THE DIFFERENT TYPES OF TRANSMITTERS TESTED

| Frequency Range | Number of Transmitters in Frequency Range | | |
|---|---|---|---|
| | AM | FM | SSB |
| LF/MF | 2 | 0 | 0 |
| HF | 12 | 2 | 6 |
| HF/VHF | 0 | 14 | 0 |
| VHF/UHF | 2 | 10 | 0 |

TABLE 3
OUTPUT POWER RANGE FOR THE DIFFERENT TYPES OF TRANSMITTERS TESTED

| Output Power (Watts) | Number of Transmitters in Output Power Range | | |
|---|---|---|---|
| | AM | FM | SSB |
| 100 or less | 6 | 22 | 2 |
| 101 to 1000 | 8 | 4 | 0 |
| 1001 or more | 2 | 0 | 4 |

TABLE 4
PERCENTAGE OF TRANSMITTERS WHOSE HARMONIC OUTPUT EXCEED THE MILITARY SPECIFICATION LIMIT OF 60 db BELOW THE CARRIER FOR THE DIFFERENT TYPES OF TRANSMITTERS

| Harmonic | Percentage of Transmitters Exceeding Limit | | |
|---|---|---|---|
| | AM | FM | SSB |
| 2 | 81 | 62 | 100 |
| 3 | 56 | 46 | 25 |
| 4 | 31 | 14 | 0 |
| 5 | 31 | 19 | 0 |
| 6 | 31 | 12 | 0 |
| 7 | 31 | 4 | 0 |
| 8 | 31 | 4 | 0 |
| 9 | 25 | 4 | 0 |
| 10 | 25 | 0 | 0 |

TABLE 5
MEAN HARMONIC OUTPUT FOR THE DIFFERENT TYPES OF TRANSMITTERS THROUGH THE 10th HARMONIC

| Harmonic | Harmonic Output (db below the carrier) | | |
|---|---|---|---|
| | AM | FM | SSB |
| 2 | 51 | 67 | 56 |
| 3 | 65 | 77 | 81 |
| 4 | 76 | >76* | >87* |
| 5 | 80 | >79* | >93* |
| 6 | 82 | >78* | >88* |
| 7 | 82 | >82* | >90* |
| 8 | 83 | >81* | >88* |
| 9 | 87 | >85* | >90* |
| 10 | 85 | >84* | >90* |

*No data available for 1/3 to 1/2 of the harmonics because of weak harmonic output. The estimated figure is probably more than 10 db greater than the value shown.

TABLE 6

MEAN NORMALIZED 3rd ORDER RF INTERMODULATION
FOR AM, FM, AND SSB TRANSMITTERS

| Frequency | db relative to desired signal carrier | | | Coupling (db) | Spacing (%) |
|---|---|---|---|---|---|
| | AM | FM | SSB | | |
| $2f_o - f_i$ | -45 | -53 | -57 | -20 | 5 |
| $f_o$ | 0 | 0 | 0 | | |
| $f_i$ | -20 | -20 | -20 | | |
| $2f_i - f_o$ | -65 | -71 | -78 | | |
| $2f_o - f_i$ | -63 | -75 | -77 | -40 | 5 |
| $f_o$ | 0 | 0 | 0 | | |
| $f_i$ | -40 | -40 | -40 | | |
| $2f_i - f_o$ | -107 | -113 | <-115 | | |
| $2f_o - f_i$ | -90 | -101 | -103 | -60 | 5 |
| $f_o$ | 0 | 0 | 0 | | |
| $f_i$ | -60 | -60 | -60 | | |
| $2f_i - f_o$ | <-110 | <-115 | <-115 | | |
| $2f_o - f_i$ | -52 | -58 | - | -20 | 10 |
| $f_o$ | 0 | 0 | - | | |
| $f_i$ | -20 | -20 | - | | |
| $2f_i - f_o$ | -70 | -77 | - | | |
| $2f_o - f_i$ | -69 | -82 | - | -40 | 10 |
| $f_o$ | 0 | 0 | - | | |
| $f_i$ | -40 | -40 | - | | |
| $2f_i - f_o$ | -110 | <-110 | - | | |

(Continued)

TABLE 6 (Continued)

MEAN NORMALIZED 3rd ORDER RF INTERMODULATION
FOR AM, FM, AND SSB TRANSMITTERS

| Frequency | db relative to desired signal carrier | | | Coupling (db) | Spacing (%) |
|---|---|---|---|---|---|
| | AM | FM | SSB | | |
| $2f_o - f_i$ | -102 | -110 | - | -60 | 10 |
| $f_c$ | 0 | 0 | - | | |
| $f_i$ | -60 | -60 | - | | |
| $2f_i - f_o$ | <-110 | <-110 | - | | |

Identification

$2f_o - f_i$ = 3rd Order Low IM Product
$f_o$ = Desired Signal
$f_i$ = Interfering Signal
$2f_i - f_o$ = 3rd Order High IM Product

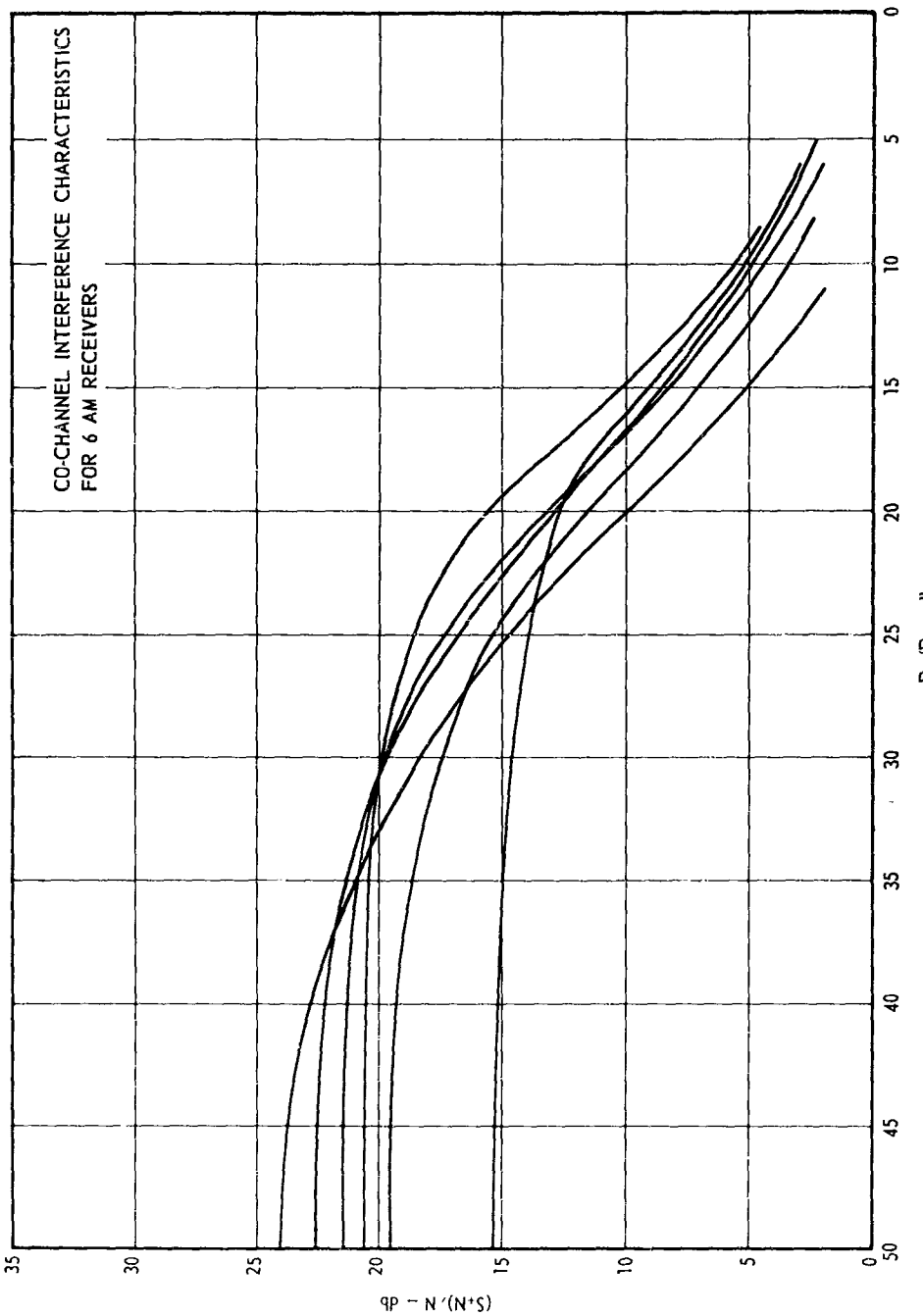

CO-CHANNEL INTERFERENCE CHARACTERISTICS
FOR 6 AM RECEIVERS
35
30
25
20
15
10
5
0
50
45
40
35
30
25
20
15
10
5
0
(S+N)/N - db
Pd/Pi - db

Figure 1.

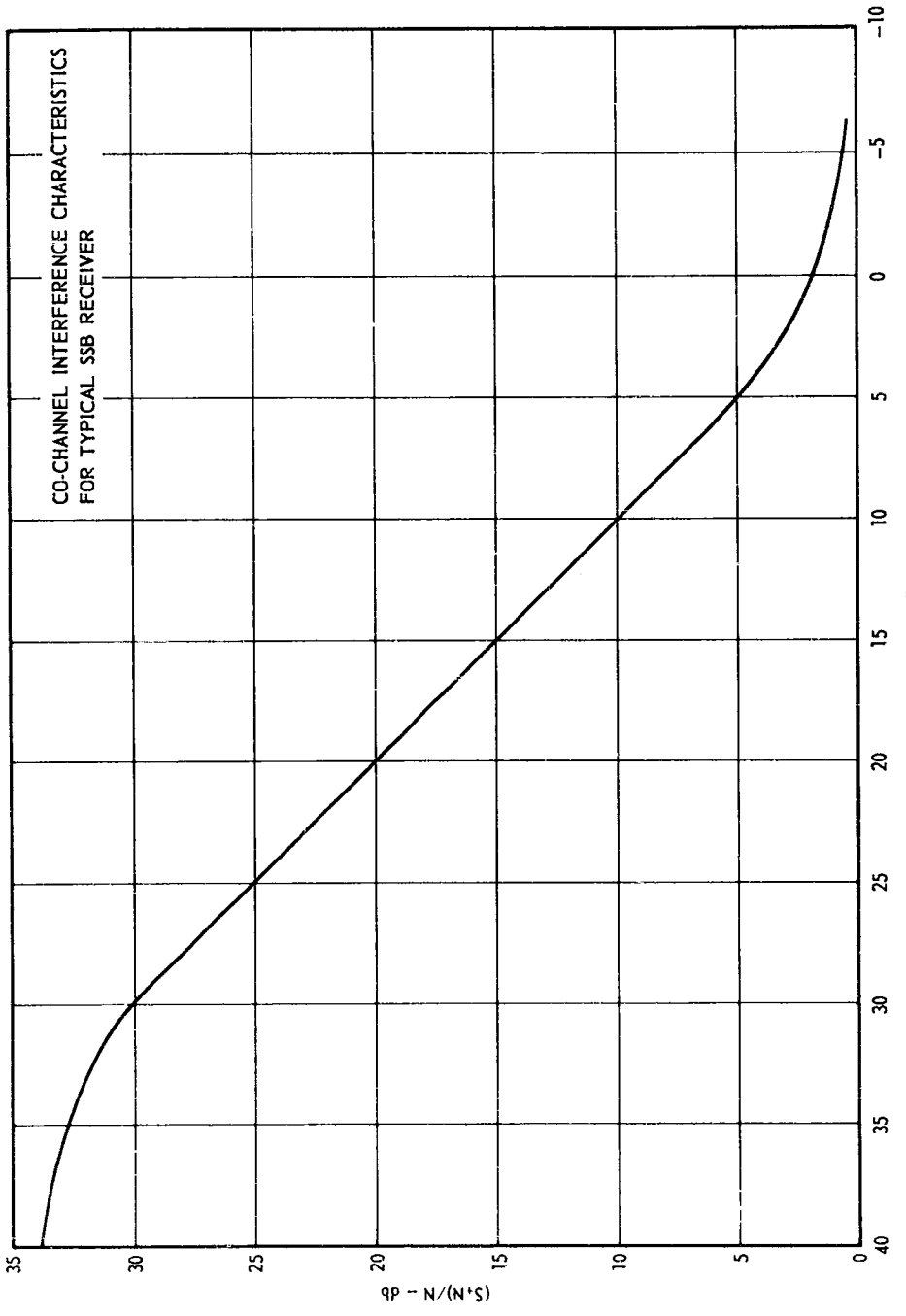

CO-CHANNEL INTERFERENCE CHARACTERISTICS
FOR TYPICAL SSB RECEIVER
(S+N)/N – db
35
30
25
20
15
10
5
0
40
35
30
25
20
15
10
5
0
5
10
–5
–10
$P_d/P_i$ – db

Figure 2.

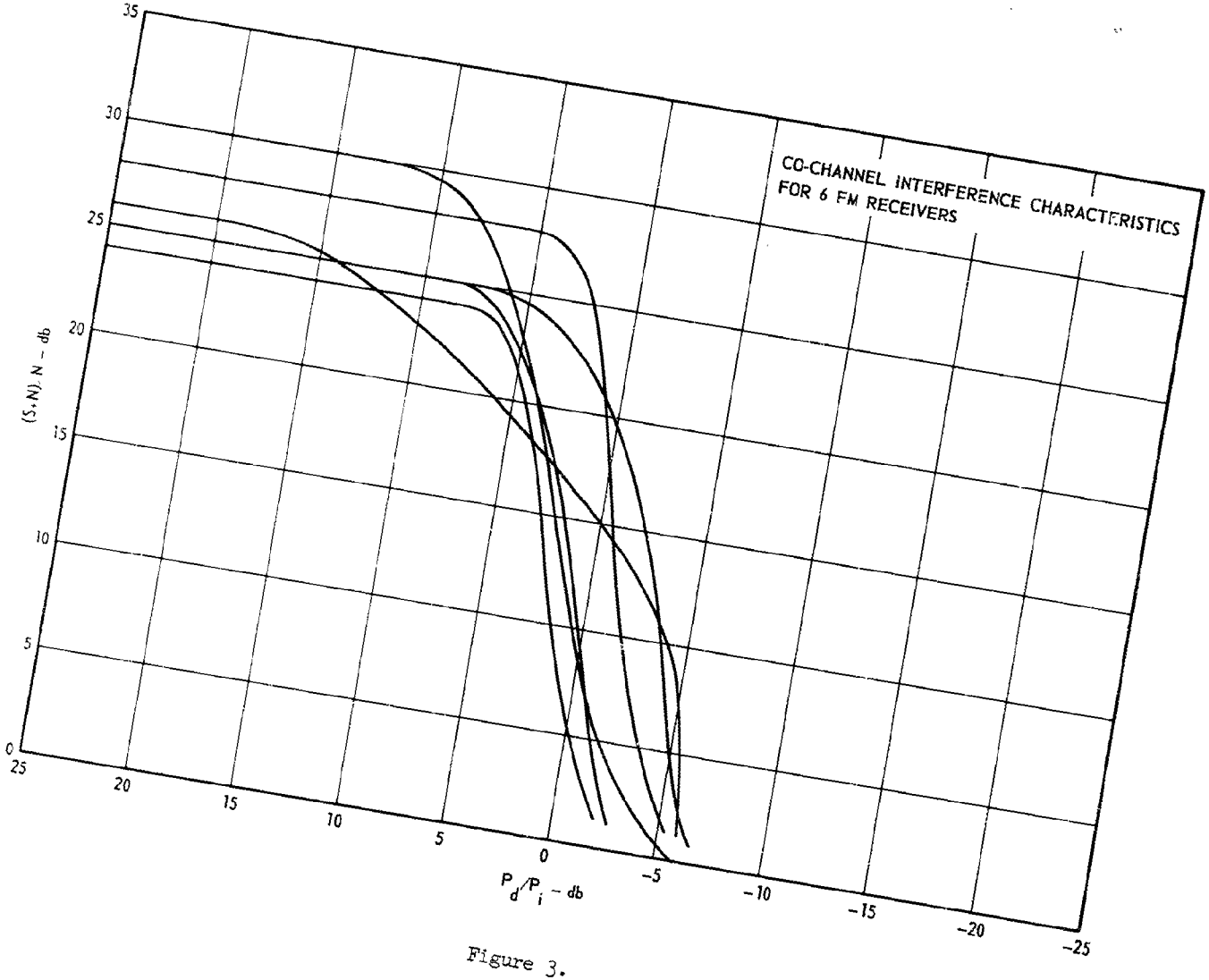

CO-CHANNEL INTERFERENCE CHARACTERISTICS
FOR 6 FM RECEIVERS
(S+N)/N - db
35
30
25
20
15
10
5
0
25
20
15
10
5
0
-5
-10
-15
-20
-25
Pd/Pi - db

Figure 3.

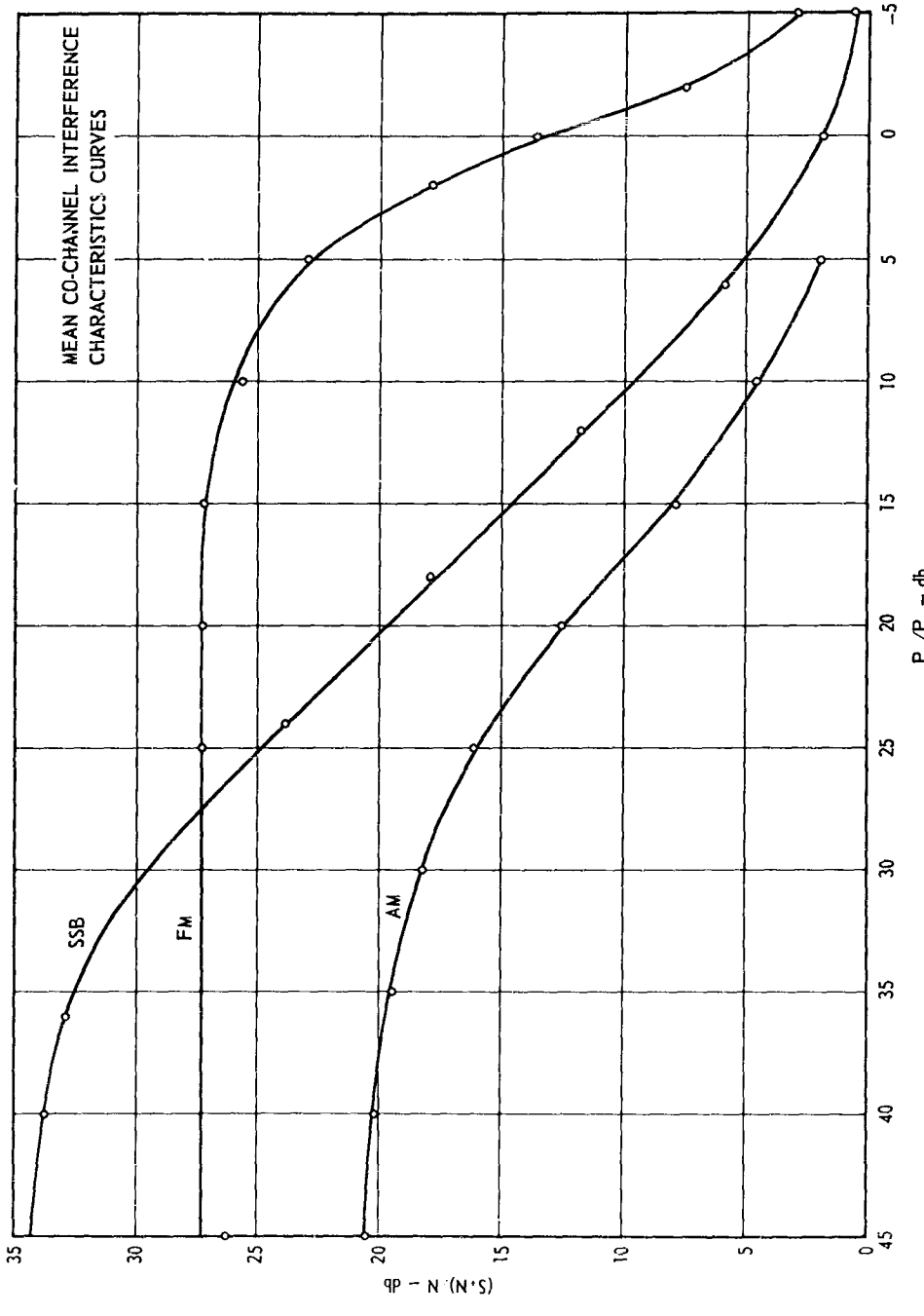
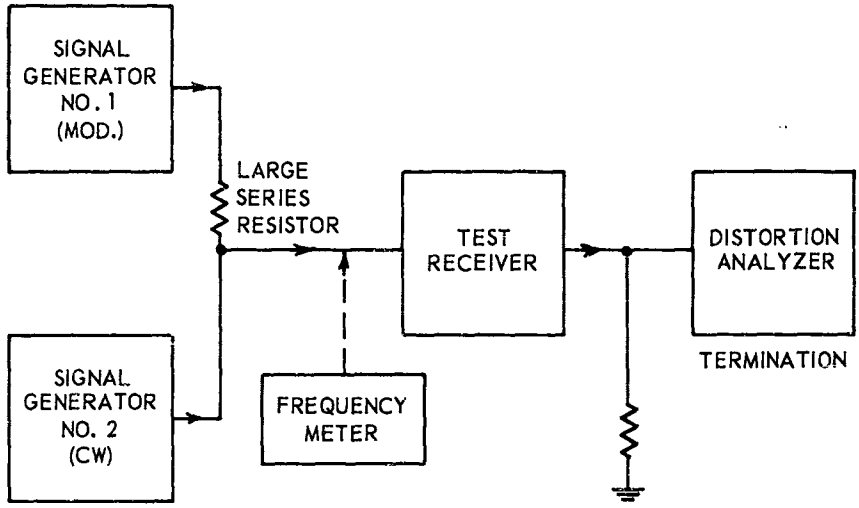
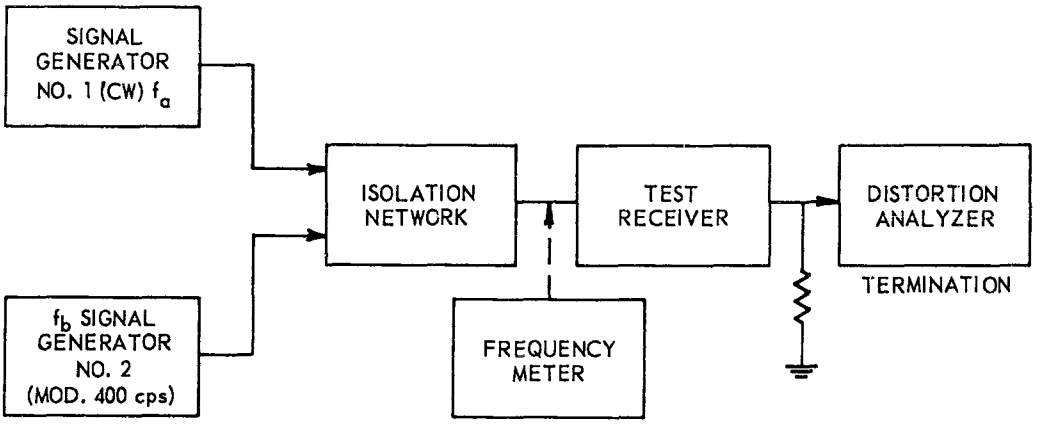

MEAN CO-CHANNEL INTERFERENCE
CHARACTERISTICS CURVES
SSB
FM
AM
(S+N)/N - db
35
30
25
20
15
10
5
0
45
40
35
30
25
20
15
10
5
0
-5
$P_d/P_i$ - db

Figure 4.



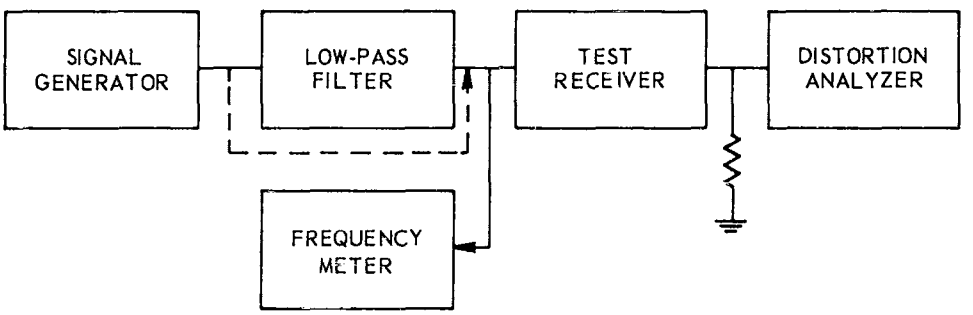

BLOCK DIAGRAM OF TWO-SIGNAL SELECTIVITY AND CO-CHANNEL TESTS

Figure 5.




BLOCK DIAGRAM OF INTERMODULATION TEST SETUP

Figure 6.




BLOCK DIAGRAM OF SPURIOUS RESPONSE TEST SETUP

Figure 7.

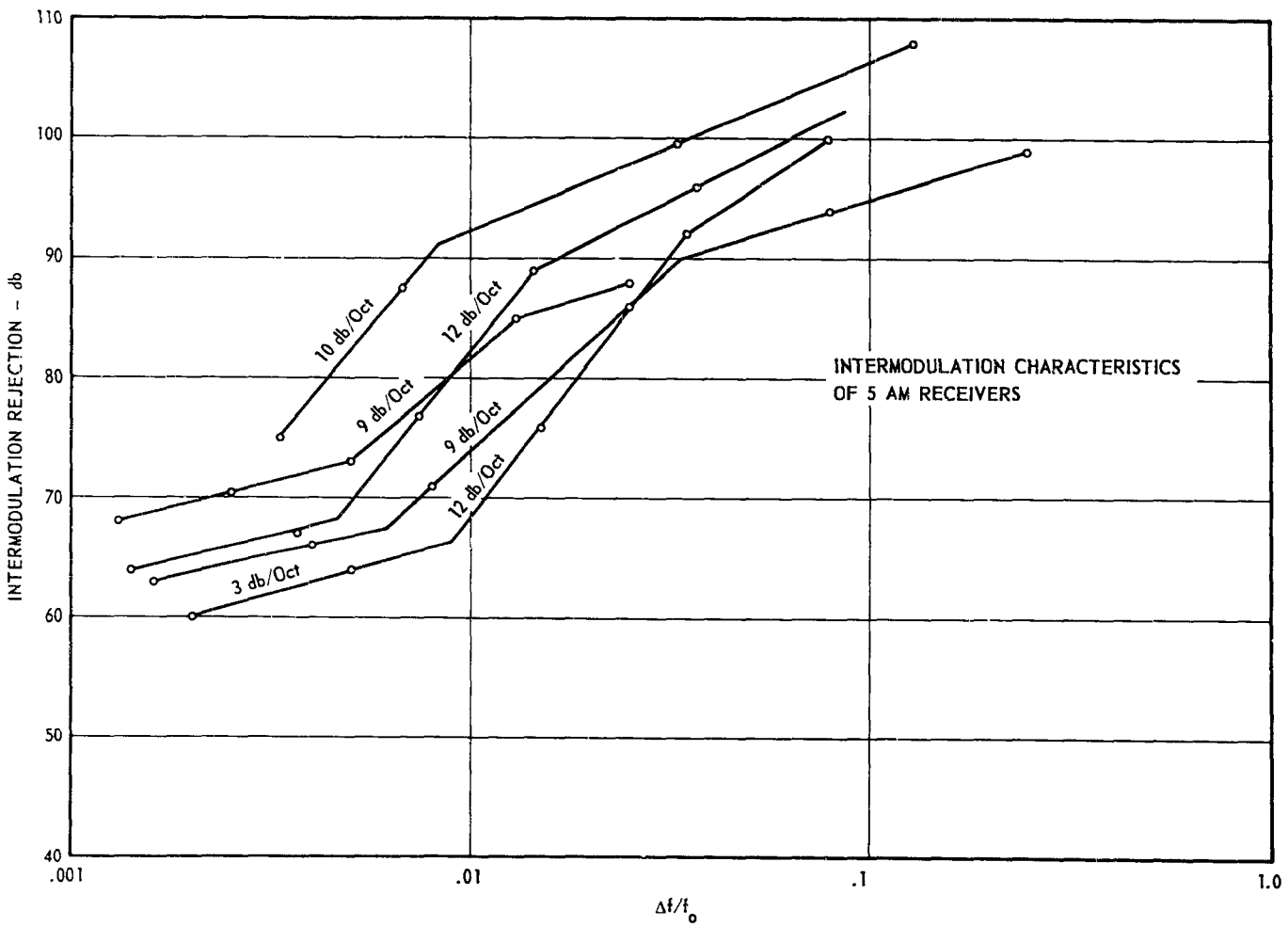

110
100
90
80
70
60
50
40
INTERMODULATION REJECTION - db
.001
.01
.1
1.0
Δf/f_o
10 db/Oct
12 db/Oct
9 db/Oct
9 db/Oct
12 db/Oct
3 db/Oct
INTERMODULATION CHARACTERISTICS
OF 5 AM RECEIVERS

Figure 8.

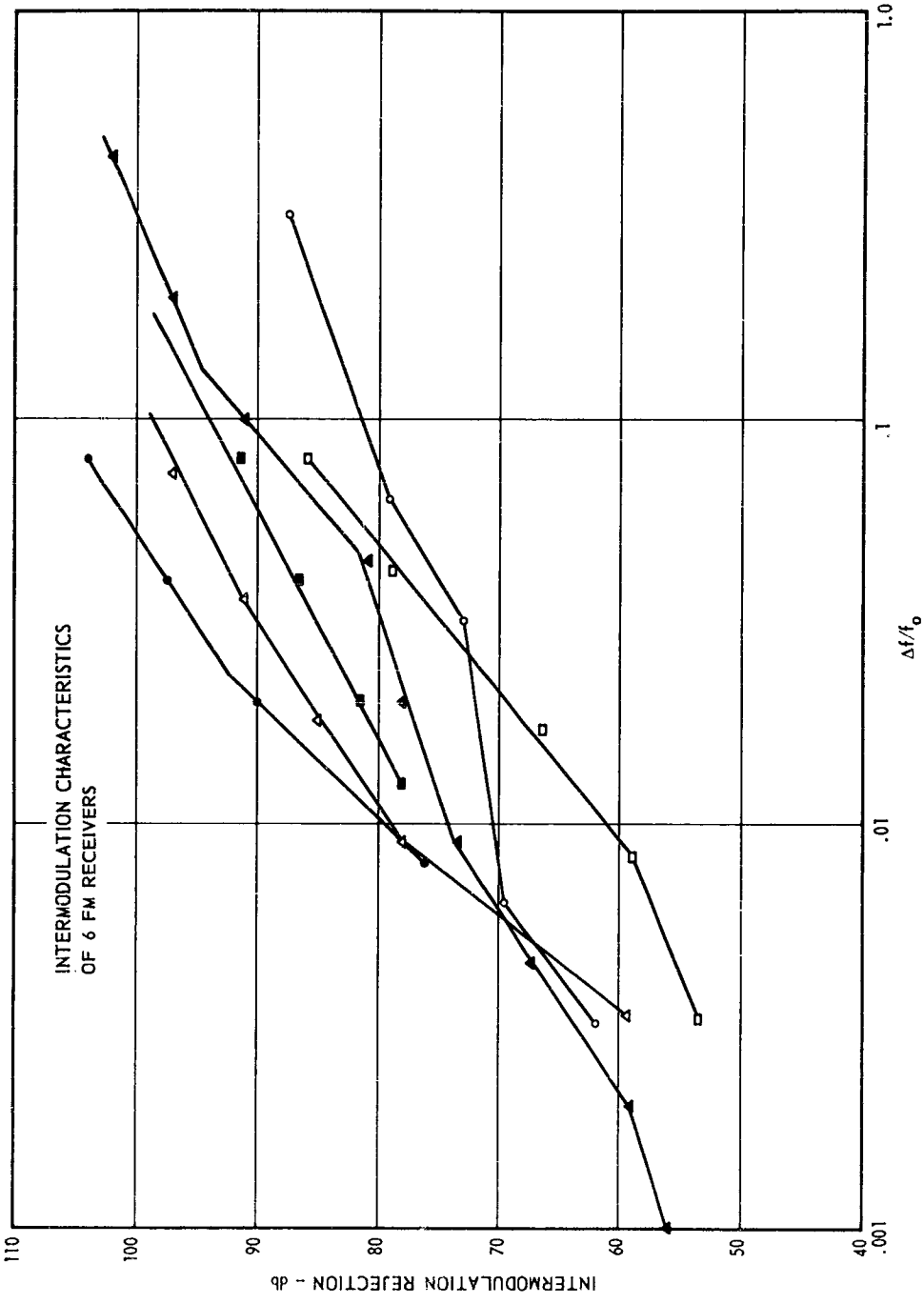
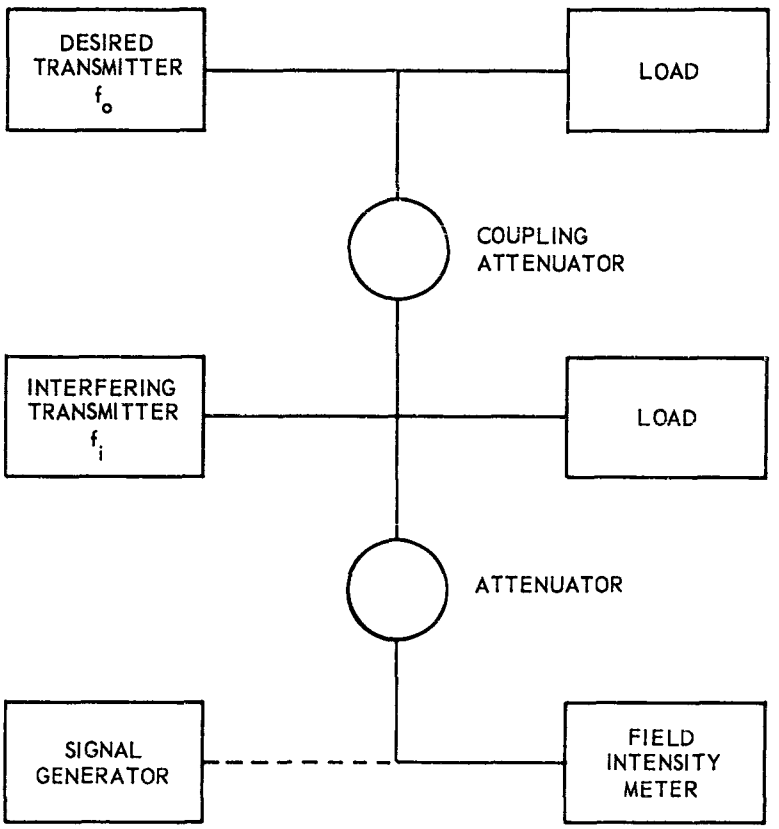

INTERMODULATION CHARACTERISTICS
OF 6 FM RECEIVERS
INTERMODULATION REJECTION - db
110
100
90
80
70
60
50
40
.001
.01
.1
1.0
Δf/f₀

Figure 9.




BLOCK DIAGRAM OF INTERMODULATION TEST SETUP

Figure 10.

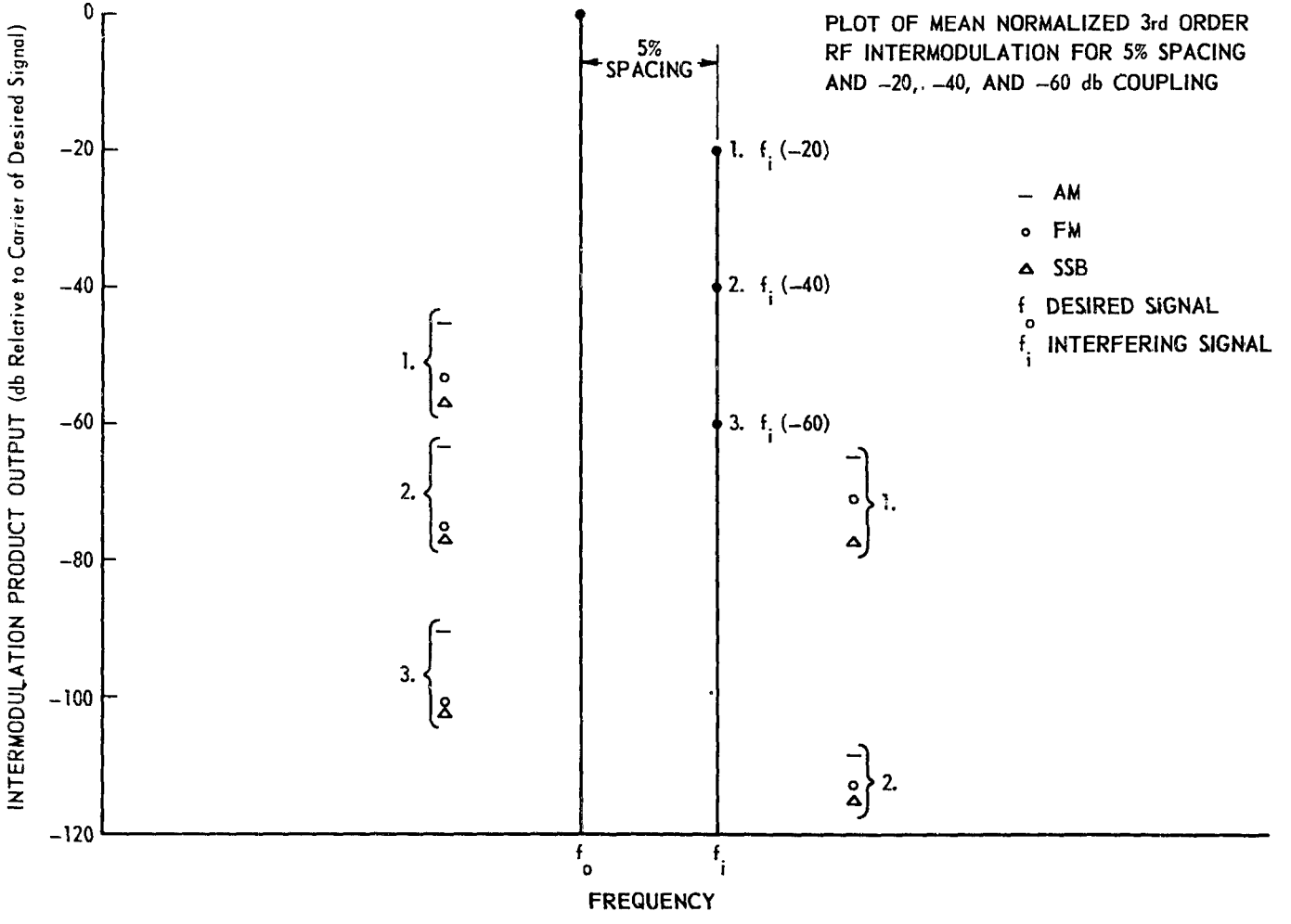

PLOT OF MEAN NORMALIZED 3rd ORDER
RF INTERMODULATION FOR 5% SPACING
AND –20, –40, AND –60 db COUPLING
INTERMODULATION PRODUCT OUTPUT (db Relative to Carrier of Desired Signal)
0
–20
–40
–60
–80
–100
–120
5%
SPACING
1. $f_i$ (–20)
2. $f_i$ (–40)
3. $f_i$ (–60)
– AM
o FM
Δ SSB
$f_o$ DESIRED SIGNAL
$f_i$ INTERFERING SIGNAL
1.
2.
3.
1.
2.
$f_o$
$f_i$
FREQUENCY

Figure 11.

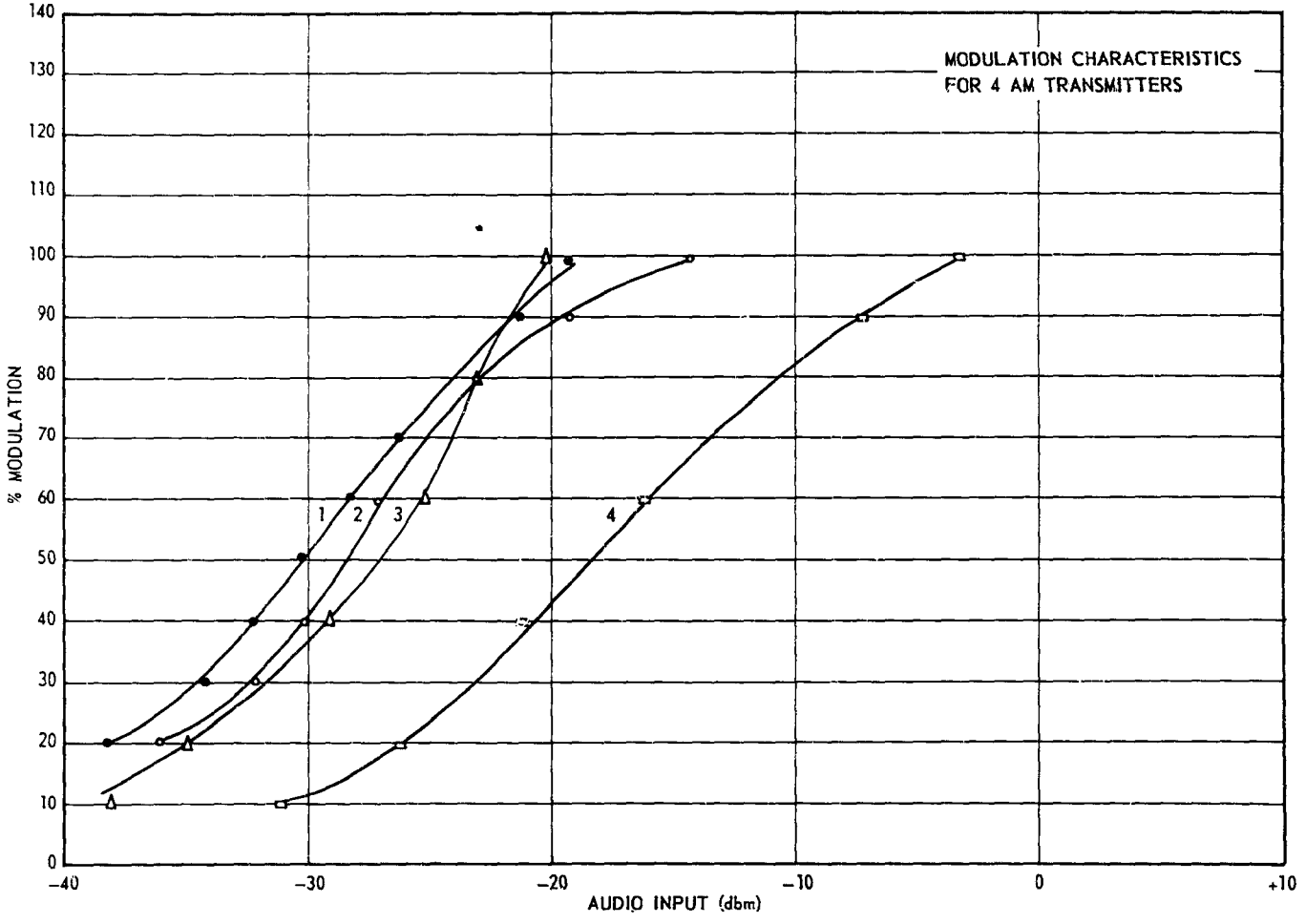

MODULATION CHARACTERISTICS
FOR 4 AM TRANSMITTERS
% MODULATION
140
130
120
110
100
90
80
70
60
50
40
30
20
10
0
-40
-30
-20
-10
0
+10
AUDIO INPUT (dbm)
1
2
3
4

Figure 12.

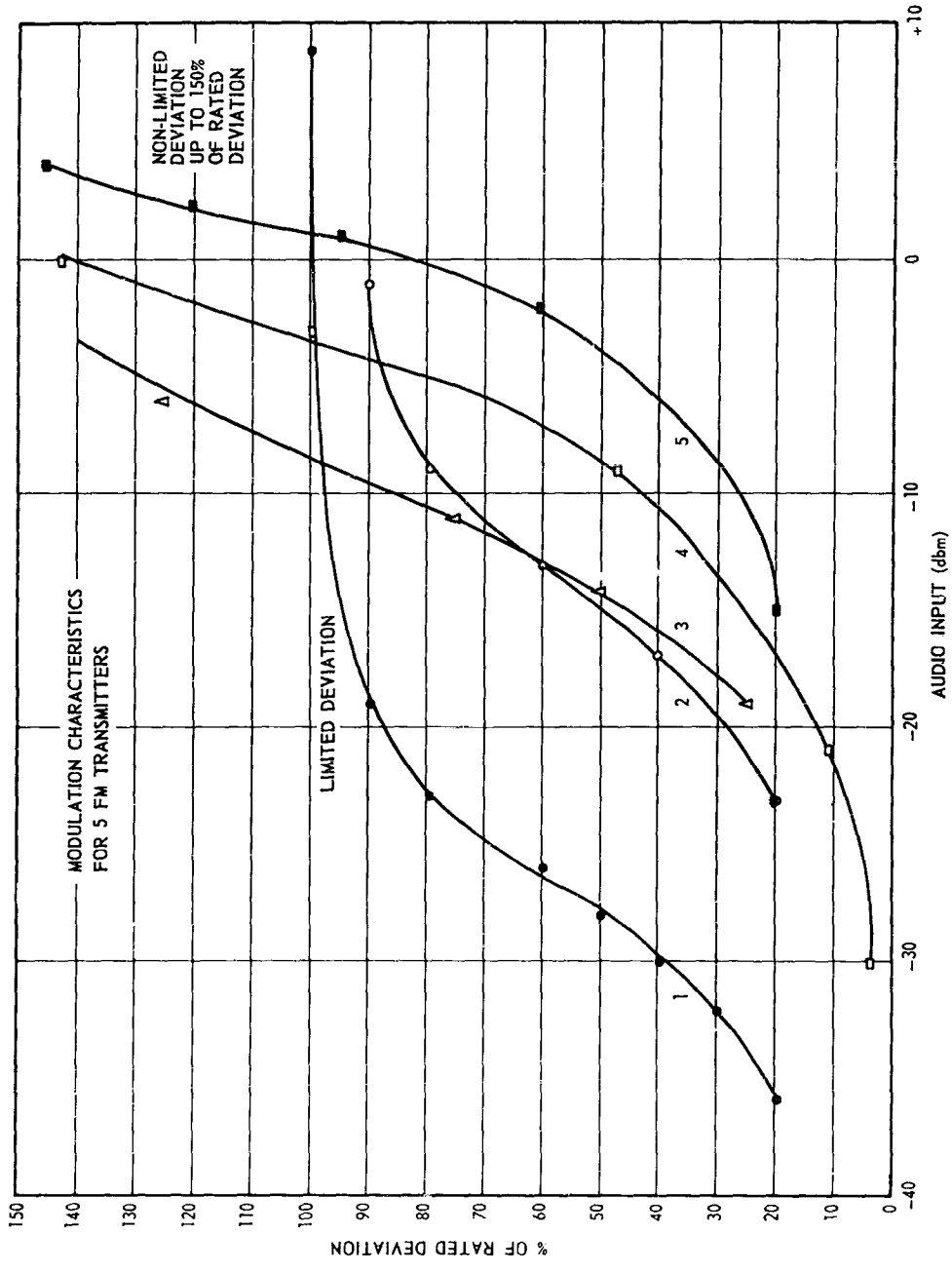

MODULATION CHARACTERISTICS
FOR 5 FM TRANSMITTERS
NON-LIMITED
DEVIATION
UP TO 150%
OF RATED
DEVIATION
LIMITED DEVIATION
1
2
3
4
5
% OF RATED DEVIATION
150
140
130
120
110
100
90
80
70
60
50
40
30
20
10
0
-40
-30
-20
-10
0
+10
AUDIO INPUT (dbm)

Figure 13.

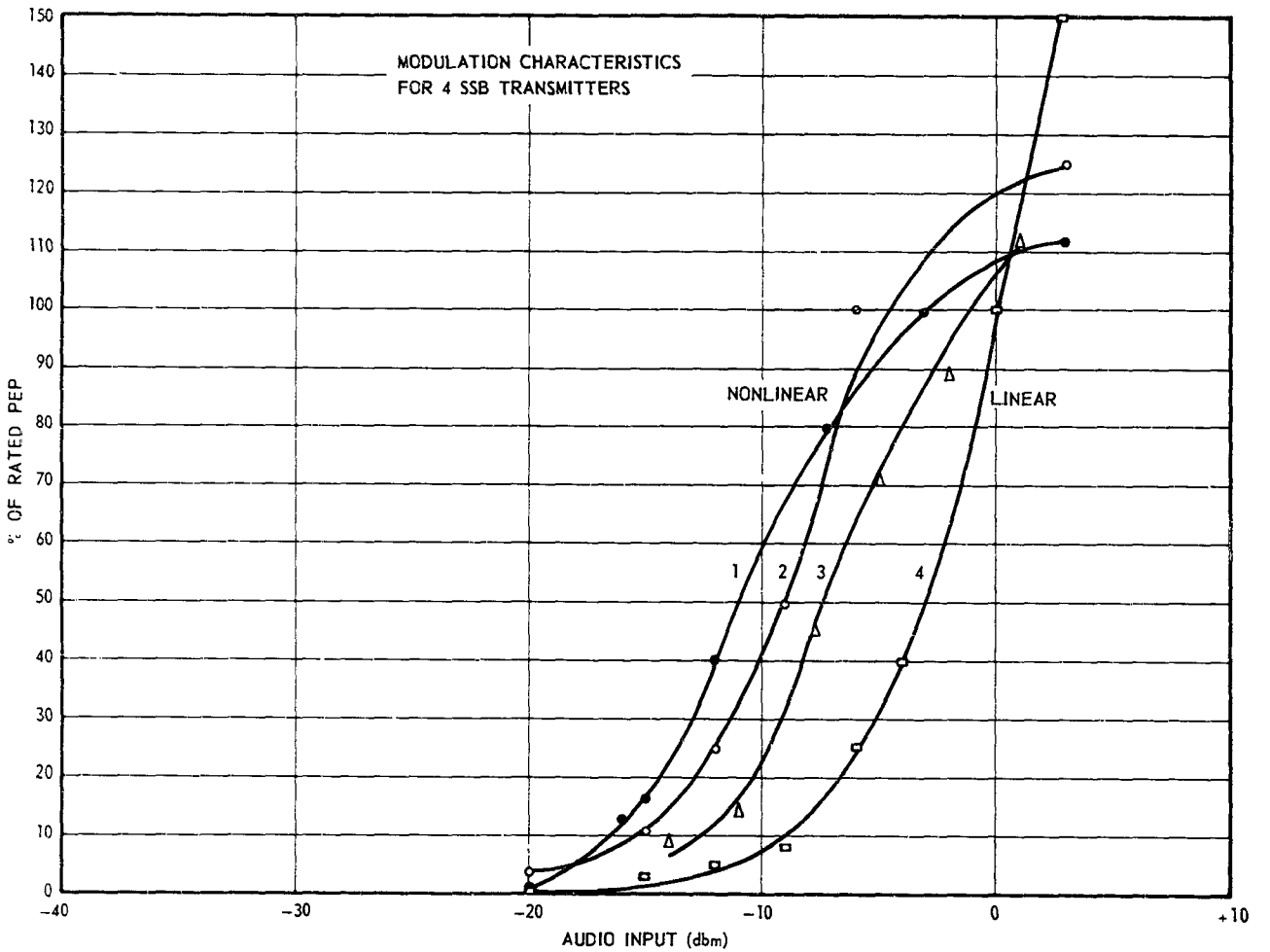
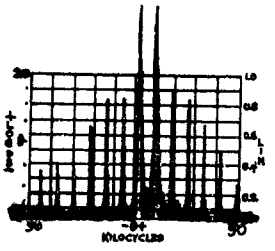
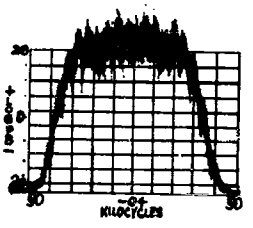

MODULATION CHARACTERISTICS
FOR 4 SSB TRANSMITTERS
NONLINEAR
LINEAR
1
2
3
4
% OF RATED PEP
AUDIO INPUT (dbm)
150
140
130
120
110
100
90
80
70
60
50
40
30
20
10
0
-40
-30
-20
-10
0
+10

Figure 14.

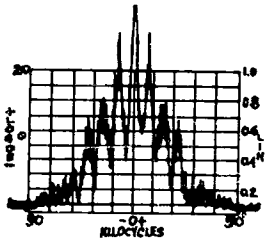
TWO-TONE AUDIO INTERMODULATION




(a) SSB
Scale 60 db Below Tones
25 kc/sec Sweep Width
Rated Power



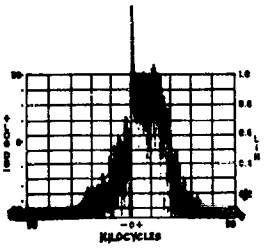

(b) FM
Scale 60 db Below Carrier
50 kc/sec Sweep Width
90% Rated Deviation



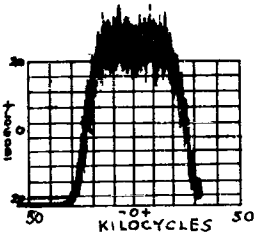

(c) AM
Scale 60 db Below Carrier
30 kc/sec Sweep Width
90% Modulation

Figure 15.

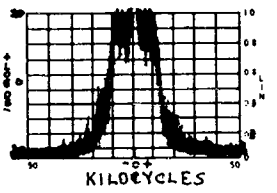
NOISE-LOADED MODULATION



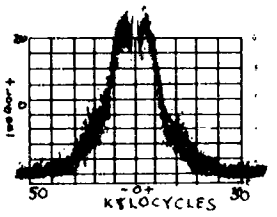

(a) SSB
Scale 60 db Below Carrier
25 kc/sec Sweep Width
Rated Power




(b) FM
Scale 60 db Below Carrier
100 kc/sec Sweep Width
90% Rated Deviation
Rated Deviation is 15 kc/sec

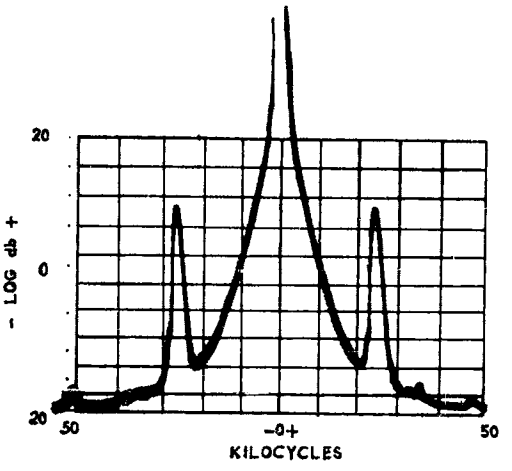



(c) AM (VHF)
Scale 60 db Below Carrier
30 kc/sec Sweep Width
90% Modulation

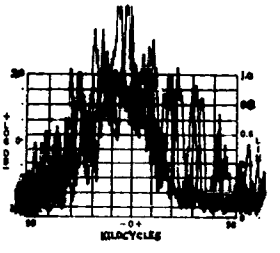



(d) AM (HF)
Scale 60 db Below Carrier
30 kc/sec Sweep Width
90% Modulation

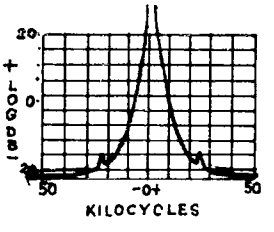
Figure 16.




(a) SSB
Scale 60 db Below Carrier
0.5 kc/sec Sweep Width



(b) FM
Scale 60 db Below Carrier
2 kc/sec Sweep Width




(c) AM
Scale 60 db Below Carrier
0.5 kc/sec Sweep Width

Figure 17.

# SPECTRUM COMPATIBILITY MEASUREMENT CAPABILITY

J. E. Browne
Navy Air Navigation Electronics Project
Weapons Systems Test Division
NATC, Patuxent River, Maryland

Abstract. - The Navy Air Navigation Electronics Project's (NANEP) chief role as lead laboratory for the Navy in the field of RF Spectrum Compatibility is the measurement of spectrum signatures, development of measurement techniques, and the evaluation of related test equipment. Application of instrumentation and facilities to the measurement of L-band radar spectrum signatures is discussed. Also discussed are measurement techniques and special problems involved in the measurements of the two L-band spectrum signatures currently in progress at NANEP.

## I. INTRODUCTION

The Navy Air Navigation Electronics Project is an activity under the technical control of the Bureau of Ships and the administrative control of the Bureau of Naval Weapons. NANEP is engaged in test and evaluation of the ground or shipboard air navigation equipment, evaluation of electronic equipments procured for the Marine Corps, and spectrum compatibility measurements. NANEP is presently designated lead laboratory for the Navy in the Spectrum Compatibility field.

## II. MEASUREMENT CAPABILITY

A spectrum compatibility measurement capability consists generally of spectrum signature measurement and the necessary support facilities. A considerable quantity of instrumentation, coupled with appropriate measurement techniques, is required for spectrum signature measurement. Among the facilities necessary to support a spectrum signature program are such things as an antenna pattern range, maintenance equipment, and screened enclosures, both fixed and mobile. Two requirements the antenna pattern range must meet are the ability to operate over a wide frequency range, at least up to 12 Gc, and the necessary flexibility to accommodate $D^2/\lambda$ for the large variety of antennas encountered. A wooden tower at one end of NANEP's 1100-foot pattern range holds the antenna positioner and the remote tuned signal sources. These sources are located in the enclosure just below the positioner, as shown in Figure 1. Figure 2 shows the recorder console which is housed in a semi-trailer van. The receiving antenna tower is mounted on the van, thus allowing easy change in antenna separation.

Maintenance equipment is that equipment needed to maintain the integrity of the basic test instrumentation. An example is sweep signal generators covering a wide frequency range (100 kcs to 18 Gc). These are used to check receiver band-pass alignments, which must necessarily be maintained to a good accuracy to check on the quality of detector frequency characteristics, to maintain the integrity of filters, and numerous other uses. NANEP has found precision attenuation measuring equipment to be quite useful, not only in maintaining test equipment such as attenuators, filters, etc., but as a secondary standard, and not infrequently, as basic test instrumentation for evaluation of operational equipment. Figure 3 shows the precision attenuation measuring equipment, arranged in the "dual channel insertion loss" configuration, being used to measure insertion loss (in the order of 0.1 to 0.5 db) of an operational 5-band filter.

In addition to our support facilities, NANEP has a program of basic test equipment evaluation. Evaluations are made on production models of commercial equipment, as well as engineering and prototype models, to determine the best available equipment for the Navy. An example of work done in NANEP's instrumentation evaluation program is the recently completed evaluation of a field intensity meter covering the frequency range of 1 to 10 Gc developed by Stoddart Aircraft Corporation under Navy contract. Following this, we are engaged in a similar evaluation of a commercially available 1 to 10 Gc field intensity meter built by Empire Devices Products Corporation. Figure 4 shows some of the instrumentation used in one of the evaluation tests. Equipments of other manufacturers are scheduled for future evaluation.

## III. PROBLEMS AND MEASUREMENT TECHNIQUES IN RADAR SPECTRUM SIGNATURES

Extensive instrumentation has been found, by those recently embarking on a spectrum signature measurement program, to be a necessity rather than a luxury. A fair amount of adequate instrumentation is currently produced. However, further developments on portions of the current instrumentation, as well as a number of new developments, are badly needed. Measurement techniques are constantly being improved and new developments are being made as instrumentation permits. A number of spectrum signatures are being collected at the present time on radars. NANEP is currently conducting spectrum signatures on two L-band radars and has developed several measurement techniques while conducting these measurements.

As an example, a rather unique combination of test equipments has been developed for use in measuring side lobe detail of the spectral shape of a radar output pulse close to the main lobe of energy. This consists of the IF section of a spectrum analyzer coupled to the IF output of an AN/APR-9 Tuning Head. The triple tuned cavity of the RF tuning head provides in the order of 80 db rejection for the fundamental lobe of energy, and the IF section of the spectrum analyzer, which has a narrow bandwidth, provides the resolution necessary to obtain side lobe detail. This technique, developed with currently available instrumentation while meeting requirements, indicates a need for new instrumentation. Analyzers or spectrascopes with multiple cavity tuning for greater selectivity are being considered for development by several manufacturers. Band reject filters, to reject the fundamental lobe of energy, could be used with current spectrum analyzers if they were available. Some band reject filters are made for VHF and UHF, but apparently none in the microwave region. These filters will need to have a wide tuning range and variable bandwidths, together with a high cutoff ratio.

A handy addition to the necessary mobile shielded enclosure facility, for making transmitter measurements in the field, is a mobile telescoping antenna tower shown in Figure 5. It is mounted on a trailer having leveling jacks at each corner, and the tower can be elevated from 5 to 70 feet. Since the maximum vertical lobe of power, with respect to the receiving antenna, varies in elevation with frequency, this tower affords a convenient method of maintaining proper receiving antenna orientation when measuring transmitter spurious and harmonic radiations. This tower also incorporates an electric rotor with dynamic braking, which greatly facilitates the azimuthal orientation of antennas.

Multiple moding and impedance change with frequency are problems in receiver measurement which have had considerable study. These problems occur when power from a calibrated signal source is coupled into receiver input terminals at other than the designed frequency range. Not only is the output from the calibrated signal sources in error, due to mismatch, but it can also be in error due to power lost in higher order modes. In order to obtain an accurate measure of the receiver's susceptibility to energy at spurious frequencies, the antenna, transmission line, and receiver are treated as a single entity. This is the "Overall Susceptibility" test in the Military Collection Plan and is applicable to receivers, such as radar receivers, which operate with one, or possibly two antennas. Energy is radiated into the system antenna from its far field ($D^2/\lambda$), and the assumption is made that attenuation due to mismatch or

loss due to multiple moding in either the antenna, transmission line, or receiver, will be the same for an interfering signal as for the test signal. The chief drawback to this test is that a considerable amount of power is required in the far field to obtain spurious responses in the receiver. There is, at the moment, a pressing need for high powered calibrated signal sources in the 10 watt and up class. NANEP has approached the problem from two directions and, with present instrumentation, can deliver over a milliwatt to microwave radar receivers from the far field. TWT amplifiers are used to boost the output power of standard signal generators to a watt (peak power), and large aperture high gain antennas are used as transmitting antennas. These range in size from an 8-foot parabolic dish, with a log periodic feed covering 0.9 to 7.0 Gc, shown in Figure 6, through a 4-foot parabolic dish, with appropriate feed horns covering 7.0 to 15 Gc, to a 1-foot parabolic dish, with appropriate feed horns covering 15 to 26.5 Gc.

Another measurement technique NANEP has developed with currently existing instrumentation provides for good isolation between two signal sources when their signals are coupled together into a receiver, without appreciable loss of power. Several receiver tests in the Military Collection Plan - among them, intermodulation - utilize this dual source configuration. The output of each signal source is coupled through a ferrite isolator into an input terminal of a coaxial hybrid, and the receiver under test is coupled to one of the output terminals. When the remaining output terminal is properly terminated, the hybrid provides 20 db of isolation between the inputs. Using 20 db isolators, a total nominal isolation of 40 db is obtained between signal sources with only about a 4 db loss.

A number of measurement techniques have been developed already in the course of spectrum signature collection, and a good many more should be forthcoming as the spectrum signature measurement program increases in magnitude and scope. It is earnestly hoped that test instrument manufacturers in particular, and the electronics industry in general, will heed the hue and cry from the spectrum compatibility field, and not let development and production lag too far behind our needs.

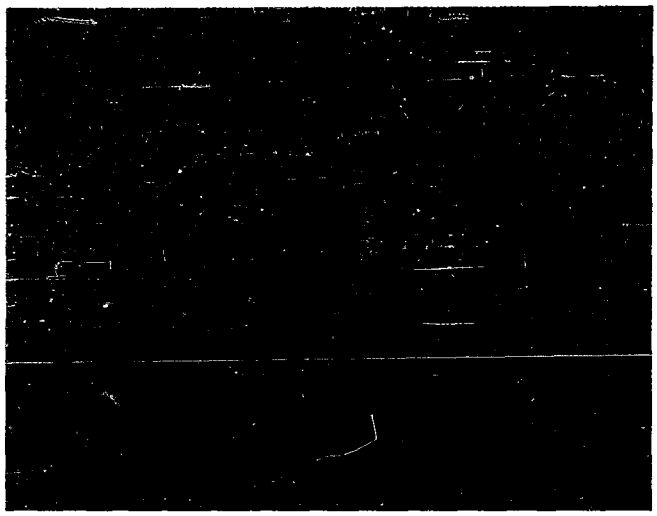


Fig. I

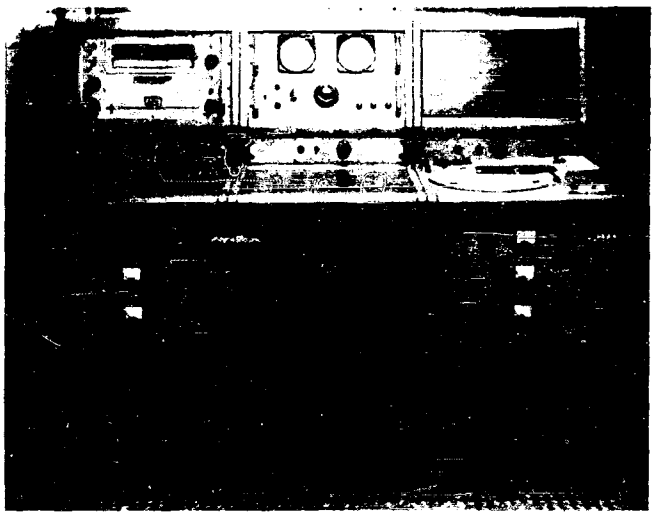


Fig. 2

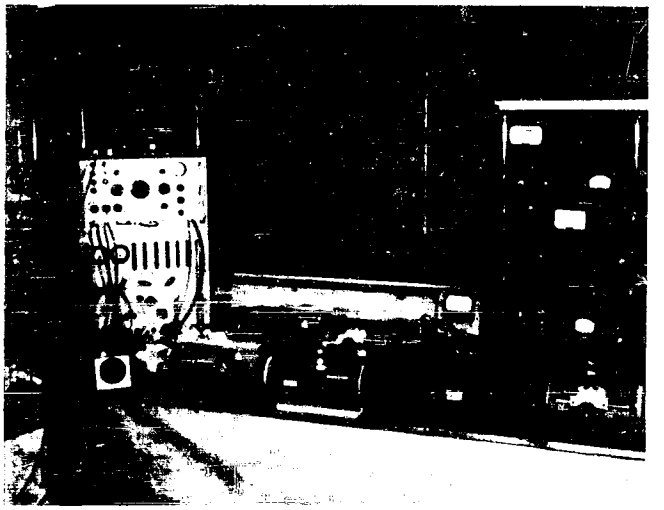


Fig. 3

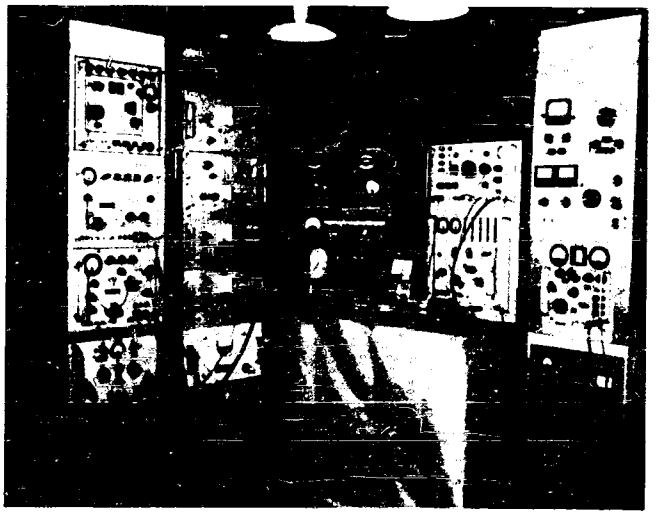


Fig. 4



Fig. 5

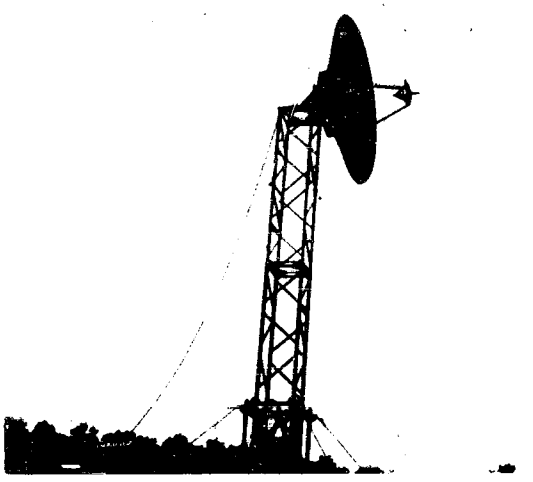


Fig. 6

# A DISCUSSION OF TEST PROCEDURES FOR OBTAINING SPECTRUM SIGNATURES OF PULSE COMMUNICATIONS EQUIPMENT

R. N. Bailey and P. Johnson, Jr.
Georgia Institute of Technology
Engineering Experiment Station
Atlanta, Georgia

**(Work Done Under Contract With The U. S. Army Signal Corps)**

Abstract. - Evaluation of the interference characteristics (spectrum signature) of pulse or pulse-modulated microwave communications equipments requires slightly different test procedures from those used with AM, FM, and SSB systems; although some of the techniques are very similar, since many pulse-modulated communications systems utilize AM or FM carrier systems.

As in AM and FM systems, spurious and harmonic emissions, intermodulation, sideband splatter, and the desirable characteristics should be evaluated for transmitters; spurious responses, intermodulation, and the characteristics with respect to various types of interference, should be evaluated for receivers. In addition, error rate and cross talk should be evaluated for transmitters and receivers.

Transmitter and receiver test procedures, and the advantages and limitations of these methods, which are used to evaluate the interference and desirable characteristics of pulse communications equipments are illustrated and discussed.

## I. INTRODUCTION

Test Procedures for measurement of interference characteristics for AM, FM, Navigational, and SSB communications type receivers and transmitters have been developed for the Signal Corps, U. S. Army. Test Procedures for pulse modulated radio communications receivers and transmitters have been developed and are being verified.

At the present time the Signal Corps uses primarily the PPM-FM and PCM-FM "double modulation" systems.[1,3] However, in addition a modified commercial PDM (pulsed carrier) and a PPM (pulsed carrier) "single modulation" system are used. Radio links operating at microwave frequencies commonly employ FM, because at these frequencies it is difficult to obtain amplitude modulators and amplifiers that have sufficient amplitude linearity. The advantage of a multiplex system is that a single carrier can be used to transmit many channels of information. Of course, the information rate, or capacity, and bandwidth are related. Therefore, for a large capacity communications system it is necessary to have a large bandwidth. Because of the wide bandwidth required for the reliable transmission of video pulses, a microwave carrier is normally used. Most of the Signal Corps pulse communications equipments operate in the 1700-7400 Mc and 4400-5000 Mc bands.[2,3]

One of the simplest schemes of time-division multiplexing employs a pulse train, in which, each channel is represented by a single pulse in the pulse train.

A marker pulse is placed between each sequence of channel pulses. Each information channel is periodically sampled at the same rate. This sampling rate corresponds to the time separation between the center position of two successive pulses in any one information channel. The sample obtained for each channel is used to pulse modulate (modulate one or more characteristics of a pulse) the corresponding pulse in the pulse train. This pulse train must be impressed upon an RF carrier for transmission by radio means, which is commonly accomplished by: (1) A "single modulation" system in which the RF carrier is keyed "on" for the duration of each pulse only; also referred to as "pulsed carrier" or (2) a "double modulation" system in which the pulse train is treated as any video signal and modulates the carrier by AM, FM, SSB or other conventional modulation schemes. The first method, because of its on-off character should be less susceptible to co-channel or close-channel interference. RF modulation and demodulation techniques place a limitation on the number of possible channels used in this method. The continuous carrier used in the second method permits the use of continuous order-wire and monitor circuits. The fidelity of reproduction permits a greater number of communications channels; however, the necessary relay equipment is more complex. It is possible to adapt the relay equipment used with method (2) to a wide variety of terminal equipment since it is possible to transmit and receive any video signal within the required bandwidth of the pulse train. This includes frequency multiplexing terminal equipment.

Superheterodyne receivers are commonly employed in microwave systems. The input usually contains a frequency selective circuit followed by a mixer. In the mixer, the incoming signal is heterodyned against a signal generated by a local oscillator to obtain the difference frequency. This difference frequency is usually amplified in one or more tuned stages of intermediate frequency amplification after which it is detected and amplified in an audio-or video-frequency amplifier.

Difficulty is often encountered in maintaining a high degree of frequency stability of the transmitter oscillator or the receiver oscillator at microwave frequencies. An AFC system is normally used to stabilize the frequency. Another problem exists in receivers due to the large bandwidths in microwave systems, and the large bandwidths required in the IF amplifiers. Consequently a large amount of noise is admitted into the receiver. This results in a low signal-to-noise ratio and reduced overall sensitivity. The noise effect is compounded because some microwave oscillators exhibit high noise output. Due to these latter factors, microwave systems favor modulation techniques which allow the intelligible signal to be separated from the noise, such as frequency modulation or pulse modulation.

A majority of the interference effects in pulse modulation systems should be independent of the modulation method except for noise effects, and are therefore independent of the multiplexer unit. However, the system is not complete without the multiplexer; therefore, the multiplexer should be used in the system evaluation, particularly in the modulation and demodulation and cross talk tests since these characteristics are a function of the multiplexer equipments.

## II. TRANSMITTER TEST PROCEDURES

### General

As in AM and FM systems, spurious and harmonic emissions, intermodulation, sideband splatter and the desirable characteristics of pulse modulated transmitters should be evaluated. In addition, the system error rate and cross talk should be determined. The following sections give methods for determining these characteristics.

### Power Output Test

The power output of a transmitter is a good indication of its overall condition and operation. It should be determined with a high degree of accuracy since the amplitudes of interfering signals as related to the carrier will give an indication of the severity of the interference. The effects of all unstable conditions such as "Mode jumping" or frequency variation should be minimized prior to measurement of the power output.

The power output of a pulsed carrier system will normally have to be converted from the average power as measured with a power meter to peak power unless measured with a peak power meter.

It is necessary to assure that the power measured is the fundamental power only, unless the spurious and harmonic radiation is less than about 5%, in which case, the error would be one-half decibel or less. This amount of error can be tolerated since, in general, measurement accuracy is usually no better than ±0.5 decibel. Generally speaking, the second harmonic of the fundamental frequency should be at least 30 decibels below the fundamental.

The method of measurement of microwave energy normally consists of sampling the signal with an appropriate attenuator or coupler which has a known value of attenuation, and measuring the power with a power meter. There are a number of different types of power meters which may be used; but the thermistor bolometer type offers certain advantages over the other types. For example, it has a longer time constant and is therefore more suitable for average power measurements; in addition, it is less sensitive to overloads than the barreter type. A disadvantage is that it can only be used for relatively low power levels.

Figure 1 shows block diagrams of test setups used for measurements of the power output of microwave transmitters having a power output up to 1 kilowatt.

### Spurious and Harmonic Emissions

Spurious and harmonic emissions are measured in the same manner as those of any AM or FM transmitter. As shown in Figure 2 a spectrum analyzer is used and a signal is substituted from a signal generator at each detected emission. Since a spectrum analyzer is used, it is necessary to use a high pass filter of known characteristics at the input. First the level of the fundamental frequency is measured without the filter in the circuit. The filter is then placed in the circuit which reduces the level of the fundamental. The levels of all detected

emissions are then measured and referenced to the fundamental since the power output and therefore the level of the fundamental is known.

The spectrum analyzer has the advantage that many spurious responses can be easily detected by the direction of movement on the analyzer screen. It has the disadvantage that there is no preselection before the diode. Because of the lack of preselection a filter must be used when measuring harmonic emissions. Other instruments, such as a noise and field intensity meter, offer a dynamic range of about 80-100 db but spurious responses are numerous and difficult to identify; however, the advantages of the added preselection may outweigh the limitations.

Intermodulation

There are a number of pitfalls which must be avoided in the measurement of intermodulation characteristics. Desensitization must be prevented, and intermodulation within the measuring device must be eliminated. To avoid either requires an extremely selective circuit, or a rejection network to eliminate the strong carrier signals. Usually the selectivity is not adequate to eliminate all desensitization or intermodulation effects so it is necessary in many cases to utilize bridged "T" rejection networks. Unfortunately it is not always easy to obtain such networks for some frequencies.

The method of measurement shown in the block diagram of Figure 3 is the same as the method used in lower frequency intermodulation measurements.

Sideband Splatter

Sideband splatter can be defined in a number of ways. To be meaningful, however, it is necessary to know to what degree the splatter will cause interference. In general, any signal or noise which extends into the adjacent channel may cause interference; therefore, the spectral distribution of the transmitted signal is of interest. Undesirable sideband splatter may be caused by audio intermodulation due to tube nonlinearities, and a nonlinear modulation characteristic, and may also result from excessive bandwidth in the modulator. Generally, adequate filtering reduces the undesired sidebands due to the above causes to a tolerable level. Other effects which may result in undesired sidebands are incidental AM and FM effects.

The method of determining the splatter is to modulate the transmitter at 90% of its rated modulation and observe the signal on a spectrum analyzer. The information is normally recorded on photographs.

Modulation Characteristics

Since amplitude modulation monitors and deviation detectors are not usually available for microwave frequencies, modulation characteristics must be measured in a different manner from the conventional procedures. For AM and FM transmitters it is necessary to measure the amplitude modulation and deviation, respectively, as a function of the input. Pulse type transmitters have complex

modulation characteristics which are difficult to analyze; however, this type of transmission system is normally not used for communications but may be found in systems such as telemetering, radar, IFF, etc.

## Zero-counting Method of Measuring Deviation[4]

### Discussion

For wideband FM transmitters in the microwave range it is usually necessary to use the zero-counting method for measuring deviation. This method is based on the fact that a frequency-modulated wave may be resolved into carrier and sideband frequencies in a similar manner to an amplitude-modulated wave. The required mathematics and the results are much more complex in the case of a frequency-modulated wave. The strength of the carrier and side frequencies vary as Bessel functions of the modulation index.

Modulation index is defined as follows:

$$B = \text{Modulation index}$$

$$B = \frac{\Delta f}{f}$$

$$= \frac{\text{peak deviation from mean frequency}}{\text{modulating frequency}} .$$

The amplitude of the carrier varies as a Bessel function of the first kind and of zero order whose argument is the modulation index. There are a number of values of modulation index which make this function zero and consequently all of the energy is converted to the sidebands and no energy exists at the carrier frequency.

If the modulating frequency is properly chosen, one of the carrier null points can be made to correspond to the desired deviation. This point may be detected by observing the spectrum on a spectrum analyzer or by heterodyning the carrier against a stable frequency source such as a Frequency Meter.

The carrier and the beat note as shown in Figure 4 will disappear at the desired deviation. If it is necessary to use a null other than the first one, the nulls must be counted as the deviation is gradually increased in order to identify the correct null. The procedure is outlined in the following steps.

### Measurement Procedure

Select the proper modulating frequency. This should be the highest frequency within the audio passband of the transmitter which causes a carrier null at the desired deviation. This frequency is given by the formula

$$f = \frac{\Delta f}{B}$$

or

$$\text{modulating frequency} = \frac{\text{deviation}}{\text{modulation index}}$$

where B has one of the values which gives a carrier null.

Table I gives values of B which result in carrier nulls. The first null should be used if the required modulating frequency is within the audio passband of the transmitter.

TABLE I

THEORETICAL VALUES OF MODULATION INDEX TO REDUCE THE AMPLITUDE OF THE CARRIER TO ZERO

| Null Number | Modulation Index: B |
|---|---|
| 1 | 2.4048 |
| 2 | 5.5201 |
| 3 | 8.6537 |
| 4 | 11.7915 |
| 5 | 14.9309 |
| 6 | 18.0711 |
| 7 | 21.2116 |
| 8 | 24.3525 |
| 9 | 27.4935 |
| 10 | 30.6346 |
| 11 | 33.7758 |
| 12 | 36.9171 |
| 13 | 40.0584 |
| 14 | 43.1998 |
| 15 | 46.3412 |
| 16 | 49.4826 |
| 17 | 52.6421 |
| 18 | 55.7655 |
| 19 | 58.9070 |
| 20 | 62.0485 |

Spectrum Analyzer Method of Measuring AM

Discussion

Spectrum analyzers are commonly used to view the sideband spectrum of [illegible] as well as [illegible] transmitters. The requirements of the analyzer are [illegible] linearity, [illegible] range, and low noise.

Low-noise crystal-controlled local oscillators are required for translating the transmitter fundamental to the center of the analyzer sweep (center frequency). The local oscillator signal must have considerably less noise than the transmitter under test, which usually requires that the oscillator be operated by batteries. Extremely good stability is also necessary if a narrow sweepwidth is to be used.

A spectrum analyzer may be used, if necessary, for measurement of amplitude modulation. This method is based on the following.

The power in an AM wave due to the carrier, upper and lower sidebands is:

$$P = \frac{\dot{I}^2 R}{2} + \frac{m_a^2 \dot{I}^2 R}{8} + \frac{m_a^2 \dot{I}^2 R}{8}$$

or

$$P = \frac{\bar{V}^2}{2R} + \frac{m_a^2 \bar{V}^2}{8R} + \frac{m_a^2 \bar{V}^2}{8R} .$$

The ratio of the power in one sideband (for a single tone input) to that in the carrier is

$$\frac{m_a^2}{4},$$

where $m_a$ is the modulation index. Since it is convenient to operate the spectrum analyzer in the log mode, Table II gives the percentage modulations in terms of one sideband level in db below the carrier.

TABLE II

SIDEBAND LEVEL IN DB BELOW THE CARRIER
FOR SINGLE-TONE AND TWO-TONE MODULATION

| Single-Tone Level (db) | Two-Tone Level (db) | Modulation (percent) |
|---|---|---|
| 6.0 | 9.0 | 100 |
| 6.9 | 9.9 | 90 |
| 8.0 | 11.0 | 80 |
| 9.1 | 12.1 | 70 |
| 10.5 | 13.5 | 60 |
| 12.0 | 15.0 | 50 |
| 14.0 | 17 | 40 |
| 16.5 | 19.5 | 30 |
| 20 | 23 | 20 |
| 26 | 29 | 10 |

Measurement Procedure

Select an attenuator to provide sufficient voltage to operate the spectrum analyzer.

Select a crystal local oscillator which when mixed with the carrier signal in the analyzer will position the carrier at the center of the sweep.

Determine from Table II the sideband level required for the desired percent modulation.

Adjust the transmitter audio drive to obtain the desired level as indicated on the spectrum analyzer as shown in Figure 5.

## III. RECEIVER TEST PROCEDURES

### General

Present test procedures for FM receivers not using pulse modulation include the following: sensitivity, weak-signal selectivity, noise figure, S-N characteristics, deviation sensitivity, electric fidelity, co-channel, close-channel, two-signal selectivity, spurious response, intermodulation and spurious emissions tests. The use of pulse modulation in addition to FM necessitates modification of the above tests and the addition of an error rate and an inter-channel cross talk test.

### Sensitivity

Sensitivity has been defined in a number of ways. The tangential sensitivity as shown in Figure 6 is defined as the signal power which is equal to the noise power and is usually expressed as that signal which causes a 3-db rise above the noise level reading on the receiver output meter. For observation on a cathode ray tube it is necessary that the signal be pulsed. A commonly used definition of sensitivity, illustrated by Figure 7, is the signal level required to produce a 6 decibel signal-plus-noise to noise ratio. This signal for determining the sensitivity of an AM receiver is modulated at 30% and the signal for FM receiver evaluation is modulated at the rated deviation.

The minimum discernable signal, which is a measure of sensitivity often used for radar receivers, is extremely subjective and may vary from observer to observer by as much as several decibels.

The conventional FM receiver sensitivity test used is based on the radio frequency input in dbm required at the antenna input terminals to give a 6 db audio output ratio (S+N)/N or 6 db of quieting. No modification is required for this test; however, the transmitter will be required as the signal source if a 6 db (S+N)/N ratio is used since there are no known PTM-FM modulated signal generators commercially available. The transmitter will have to be sufficiently [illegible] from the receiver to avoid appreciable error due to

extraneous RF radiation from the transmitter. Grounding the transmitter chassis may reduce extraneous radiation sufficiently. A good way to check for sufficient isolation is to measure the RF input required to give a certain quieting ratio, then turn the transmitter off and replace it with a signal generator. The signal generator output is then adjusted to give the same quieting ratio. When the required signal generator output is nearly equal to or less than the transmitter power required to give the same quieting ratio, the isolation is sufficient.

Because of the varied definitions and the degree of subjectivity of some of the observations, a more useful measure of the sensitivity of AM microwave receivers is the noise figure.

Noise Figure

The noise figure is defined as the ratio of the available signal-to-noise ratio at the input terminals to the signal-to-noise ratio at the output terminals, assuming matched impedances at both the input and output terminals.

Since the internal noise generated in a receiver is the fundamental limitation on the receiver sensitivity the noise figure gives a repeatable quantity for determination of receiver operation and optimum design.

The noise generated within an amplifier or receiver is primarily due to the "front end" for two reasons. The "front end" usually consists of high-gain stages, and the noise in the front end is amplified through several succeeding stages. The noise present at the output of a receiver is proportional to the effective noise bandwidth of the tuned circuits. Since the IF strip usually contains the most selective circuits it effectively determines the noise bandwidth.

The noise figure will always be greater than unity since the output signal to noise power is always less than the input signal to noise power. A noise figure of one corresponds to an ideal receiver, i e. the receiver introduces no additional noise.

In the design of receivers it is necessary to reduce the noise figure to a minimum since the output signal to noise ratio varies inversely as the noise figure. A reduction in receiver noises, thereby decreasing the noise figure, is just as beneficial as a proportionate increase in the transmitter power output.

There are several pitfalls which must be avoided in the measurement of noise figure Some of these are quoted from a paper by A J. Hendler.[5]

> "First and foremost, the effect of the signal source of the actual noise figure must be considered The noise figure of microwave mixers, grounded-grid amplifiers, and low-noise intermediate-frequency amplifiers are all a function of the source impedance. Frequently, in the design of IF amplifiers, the input cable is part of the input network. Alteration of this cable length or of the source impedance (both resistive and reactive) can make serious changes in the actual noise-figure value

In the grounded-grid amplifiers, a change of the signal source impedance changes the available gain of the stage. As the resistance increases, the gain decreases and the effect of second-stage noise becomes more pronounced. To determine the optimum source resistance for a particular amplifier usually involves a series of noise-figure measurements as a function of this resistance. The available gain variation may introduce serious errors.

Another problem that is encountered almost daily is the proper measurement of receivers that have spurious responses. Using a signal generator that provides signals only within the useful channel, no spurious response data are required for the measurement. Use of a wide-band noise source, however, makes it mandatory that all spurious passbands be known. Effectively, each additional response allows the noise source to introduce more noise power into the system. Failure to include one reasonably large spurious response makes the receiver appear to have a better noise figure than it actually has.

Now that the significance of spurious responses is appreciated, what happens when a traveling-wave (TWT) is measured? If a high-gain wide-band TWT is followed by a single-response receiver or by a multiple-response receiver (all responses lying within the acceptance band of the TWT), the same noise figure will be measured and no correction will need to be applied. Consideration of the basic noise figure definition shows that the signal-to-noise ratio at the output of the TWT is uniquely determined by the noise figure and the input signal-to-noise ratio. Since the circuits that follow do not usually contribute appreciable noise, and both the signal and noise are noise, the ratio is independent of the bandwidth of the measuring equipment. For engineers who are accustomed to correcting for image responses in microwave mixers, it is sometimes difficult to remember not to correct when making TWT measurements.

Receiver dynamic range has also been a constant source of trouble. Dynamic range is usually determined by plotting the input-output characteristic of the receiver. When a signal generator is used to obtain this characteristic, a greater dynamic range is obtained than if a noise generator is used. For a c-w signal, the peaks are always 40 percent greater than the rms value. The peaks of the noise, on the other hand, can be much greater than the rms values. Noise spikes, therefore, will cause overload much sooner than c-w peaks, and the dynamic range will be suppressed. For noise-figure measurements, the levels used should be at least 10 db below the saturation level as determined with a signal generator.

One last pitfall is the failure to account for the temperature of the noise generator. The definition of noise figure requires the measurement at a room temperature of 290° K. The measurement setup, if [illegible] is made at this temperature. Specifically, in a well-designed

noise-diode generator, the terminating resistor is close to the tube and, therefore, becomes hotter than room temperature. For high noise figures, the correction is small and is usually neglected. With low noise figures, on the other hand, the correction is significant. A plot of the temperature correction is shown in Figure 2.

Headaches that have been occasionally encountered include relaxation oscillation in the gas tubes, failure to terminate the receiver when the noise source is off, and having the noise source behave like an efficient antenna when fired. These pitfalls are less common, and they should only be checked when all other precautions have been taken."

There are a number of different methods for measurement of noise figure. The first method involves the use of a CW signal generator and the other methods utilize a noise source.

CW Generator Technique[6]

The c-w "noise" generator is a well-shielded signal generator with a calibrated output of a 0.1 microvolt or less. If the receiver input requires a coaxial cable, the signal generator is connected via a matching cable. On the other hand, if the receiver input requires a waveguide, it is necessary to couple into the receiver with a similar waveguide from the c-w generator. In this case, a klystron oscillator, with suitable means of determining frequency and amplitude feeds into a calibrated attenuator and thence into a waveguide probe. The klystron must operate, of course, at the desired radio frequency of the receiver.

The procedures for making noise figure measurements using a "c-w" noise generator is as follows:

1. Assemble the test setup as shown in Figure 8.
2. Set the attenuator of the generator for maximum attenuation. This insures a good match.
3. With the output of the generator turned off - but with the noise generator connected in position - note the output noise power level.
4. Turn on the generator output. Set the frequency of the noise generator to the center frequency of the receiver response curve.
5. Increase the output of the noise generator until the power output level indicated by the output measuring device is twice that of step 3. The noise figure is now calculated from

$$F = \frac{250\ E_{in}^2}{R_o BW}$$

where

$E_{in}$ is the signal generator output, of step 5, in microvolts

$R_o$ is the signal generator output characteristic impedance, in ohms

BW is the effective IF bandwidth of the receiver, in megacycles.

When the signal generator output is zero (Step 3 of procedure), the output-measuring device receives a random noise signal. With the signal generator turned on, the signal becomes noise plus c-w. The output measuring device must respond to noise plus c-w in the same manner as it responds to noise alone, or an error is introduced.

This method has the disadvantage that the IF bandwidth (between the 70.7 percent amplitude points) must be known in advance. Errors in measurement of this bandwidth will contribute to the error in the noise figure determination.

Manual-Noise Generator Technique[7]

Another method which may be used for noise figure measurement uses a gas tube noise generator. A gas tube noise generator consists mainly of a gas filled tube, similar to an ordinary flourescent tube, which is mounted in a waveguide. When direct current (of the order of 225 ma) is passed through the gas tube, noise power which is uniform over the frequency range of the waveguide is emitted.

Since it is not possible to control the amount of noise power by variations of the gas tube current, a calibrated attenuator must be used. The procedure is as follows:

1. Assemble the circuit illustrated by Figure 9 using the gas tube noise generator in place of the klystron oscillator.
2. With the gas tube operating normally set the attenuator at maximum attenuation. (Note that in this method the output of the noise generator is not set first to zero. If the gas tube current were set to zero it would not be a good match for the waveguide section leading to the receiver. Instead, the gas tube is allowed to operate normally and the attenuator used to isolate the receiver.)
3. Observe the noise power level in the output measuring device.
4. Reduce the attenuation until the value of noise power in the output measuring device is twice that of step 3.
5. Read the noise figure from the calibration chart which gives noise figure versus attenuator setting. This chart is prepared by calibrating the gas tube-attenuator combination by the c-w generator method.

Automatic Noise Figure Measurement[8]

As defined previously, the noise figure of a network (with a generator connected to its input terminal) is the ratio of the available signal-to-noise power ratio at the signal generator terminals to the available signal-to-noise

power ratio at the output.[9] For noise-figure measurement purposes it is convenient to define a Y-factor, which is the ratio of the available receiver output power (with the noise source on) to the available receiver output power with the receiver input connected to a termination whose temperature is 290°K. From Mumford[10] and assuming a single-response, receiver, noise figure as a power ratio is determined from

$$F = \frac{\frac{T_2}{290} - 1}{Y - 1}$$

where

$T_2$ = the effective temperature of the noise source in degrees Kelvin

Y = as defined above, and

F = the noise figure in power ratio.

In these instruments, gaseous noise sources of either coaxial or waveguide construction are used. These noise sources are transmission devices whose terminations are at 290°K. With the noise source on, the effective temperature is $T_2$; with the noise source off, the temperature is that of the termination. Since the effective temperature of the noise source is a constant determined by the diameter, gas pressure, and gas content of the discharge tube, it is only necessary to measure Y − 1 to determine the noise figure.

The Y ratio can be written as

$$Y - 1 = \frac{P_{on}}{P_{off}} - 1$$

Rewriting,

$$\frac{P_{on}}{P_{off}} - 1 = \frac{P_{on} - P_{off}}{P_{off}}$$

it can be seen if the gain of the receiver is controlled to maintain either $P_{on}$, $P_{off}$, or their average constant, a differential power meter that measures $P_{on} - P_{off}$ would indicate Y − 1 and may be calibrated directly in noise figure.

Figure 10 is a block diagram of an Automatic Noise-Figure Indicator. The noise source is squarewave modulated at about a 300-cps rate. The modulated noise signal is fed to the receiver under test, where it is converted to the intermediate frequency. It then enters the indicator IF amplifier, where it is amplified and detected. The voltmeter then measures the square of the voltage which proportional to the noise power.

Weak Signal Selectivity

The selectivity as measured by this test gives an indication of overall gain and sensitivity at the center-tuned frequency. Furthermore, the test shows

the response at frequencies slightly removed from the tuned frequency.

As with the sensitivity test, the weak signal selectivity test is based on a 6 db audio output ratio. To obtain such a ratio a PTM-FM signal generator or transmitter is required; therefore, 6 db of quieting will be used as the output parameter.

*S-N Characteristics

This test is intended to show three things: (1) the limiter action, or how the noise and signal levels change with input signal levels; (2) the relative freedom of the receiver from noise during pauses in modulation; and, (3) the internal gain of the receiver. Poor noise quieting indicates insufficient IF gain.

The unmodulated signal for this test is adjusted for standard levels of quieting and a ratio obtained with respect to no signal. Then the same signal is modulated and the increase in output level measured.

Deviation Sensitivity

This test serves to determine the variation in audio output ratio as the frequency deviation is changed. If a curve of frequency deviation versus audio output ratio does not peak at approximately the rated frequency deviation of the receiver and drop rapidly above this value, the receiver has excessive bandwidth. The deviation sensitivity can be measured in the conventional manner if some method of measuring deviation is available.

Electric Fidelity

The electric fidelity test shows the manner in which the electric output of a radio receiver depends upon the modulating frequency of the signal. It takes into account all characteristics of the receiver except those of the loudspeaker or headphones, although these are of importance. The standard signal source level used for this is -60 dbm. The audio output ratio at this signal level is recorded. The modulating frequency is then varied over the audio bandwidth and the relative audio output ratio is recorded. This same test can be applied to PTM-FM equipment when the transmitter with its multiplexer is used as the signal source

Co-Channel

This test is intended to show the effect of an interfering signal at the same frequency as the desired signal, and includes the inherent effect of the discriminator limiter and AVC. The masking effect of an interfering signal

---

*Corresponds to quieting-signal sensitivity except that the input signal level is varied from a minimum value to the overload condition.

is obtained with the desired signal modulated and with standard input levels of the desired signal, the audio output ratio being noted as the level of the interfering signal is increased from zero.

A convenient method uses two signal generators. The desired signal is modulated and the interfering signal is unmodulated for the conventional FM receiver test. The interfering signal is unmodulated because the depression or capture effect in FM, due to an interfering co-channel signal, is a function of the relative ratio of the interfering signal level to the desired signal level. The shape of this function is independent of the modulation on the interfering carrier.

This same test can be applied to PTM-FM equipment using the transmitter with its multiplexer as the desired signal source and a signal generator as the interfering signal source.

Close-Channel

This test is intended to show the effect of an interfering signal whose frequency is inside the RF passband but is outside the IF passband. It is also a measure of true receiver selectivity since it shows the inherent effect of the selective circuits, limiter, AVC and the discriminator in the presence of interference. The test is performed at various interfering and desired signal levels in order to show the selectivity at several different interfering signal level to desired signal level ratios.

As with the co-channel test, this test can be applied to PTM-FM equipment using the transmitter with its multiplexer as the desired signal source and a signal generator as the interfering signal source.

Two-Signal Selectivity

The two-signal selectivity is a measure of the receiver response to weak and strong desired signals in the presence of weak and strong undesired signals. In FM receivers, interference to the desired signal is caused by increases in noise, desensitization and capture. A two-signal test is the only test that will correctly show the selectivity curve, at reduced sensitivity, of an FM receiver having automatic gain control.

This test is performed by tuning the interfering signal off channel and increasing the desired signal for a 6 db audio output ratio. The desired signal level is then increased by 10 db and the interfering signal is moved towards the desired signal at various standard interfering signal levels, until the 6 db audio output ratio is restored. As with the co-channel and close-channel test, this test can be applied to PTM-FM systems by using the transmitter with its multiplexer as the desired signal source and a signal generator as the interfering signal source.

Adjacent and Alternate Channel Rejection

The adjacent and alternate channel rejection is obtained by adjusting the desired signal for a 12 db audio output ratio with the interfering signal generator on the adjacent or alternate channel adjusted for a minimum possible output. The incremental increase in the interfering signal level required to reduce the audio output ratio to 6 db is the rejection ratio.

This same test can be applied to PTM-FM equipment using the transmitter with its multiplexer as the desired signal source and a signal generator as the interfering signal source.

Spurious Responses

With the receiver tuned to one of the standard test frequencies, the signal generator should be tuned over a wide range of frequencies to discover receiver output responses at frequencies other than the one to which it is tuned. These other frequencies are called spurious responses. Each spurious response frequency is measured and the interfering signal level is adjusted to give 6 db of quieting or 6 db S+N/N ratio. The value of desired signal at the tuned frequency which produces 6 db of quieting or audio output ratio is subtracted from the interfering signal obtained above to give the spurious response rejection ratio.

This test can be applied to the receiver of a PTM-FM system without any variation since a signal generator can supply the unmodulated signal.

Intermodulation

The intermodulation characteristics of a receiver are of primary importance because they give an indication of the interference possibilities when the receiver is used in the presence of two off-channel signals. Assuming that these signals have not been mixed before arriving at the receiver, some mixing may be expected in the RF amplifier tubes and/or the first mixer. If one of the extraneous signals generated in this manner happens to fall at the tuned frequency and is of sufficient amplitude, interference of a co-channel nature is the result.

The types of mix that are considered are the following: $f_o = 2f_a - f_b$, $f_o = f_a - f_b$ and $f_o = f_a + f_b$ where $f_o$ is the receiver tuned frequency and $f_a$ and $f_b$ are the interfering signal frequencies.

Care must be taken in conducting this test to insure that intermodulation does not occur within the signal generators themselves. If the signal generators are of a type such that generator intermodulation is appreciable, it is essential that a device (such as a bandpass filter at $f_o$) be used to couple the generator outputs to the receiver

This test requires two unmodulated microwave signal sources to test the receiver of a PTM-FM system. Transmitters may be used to advantage in these tests since the output is usually such a high level that the necessary attenuation between the transmitters and the receiver normally reduces the transmitter intermodulation to negligible proportions. This method is preferable since transmitters normally have better intermodulation characteristics than signal generators; however, it has the disadvantage that most microwave transmitters are not easily retuned for another frequency.

Interchannel Crosstalk

Interchannel crosstalk in a multichannel system results from the transfer of modulation from one channel to another. The transfer may result from heterodyning or over-modulation. The test for interchannel cross talk interference is conducted with the transmitter modulated by 400 cycles at 100%. The input level to the receiver is adjusted for the standard desired signal level. The transfer of modulation, or increase in noise in the adjacent channels is measured to determine the degree of crosstalk. Figures 11 and 12 illustrate some results from performance of cross talk tests. It will be noted that there is no apparent spill-over into adjacent channels. This was expected since adequate time spacing was allowed between channels.

Error Rate

The error rate test is designed to show the effects of co-channel and close-channel interference on PPM-FM when used with FSK teletype and on PCM-FM.

An "exclusive or" circuit is used with the equipment arranged as in Figure 13 to check for errors. The digital counter is used to produce a cumulative count of errors. A phase shift network is required to adjust the two inputs to the "exclusive or" circuit for coincidence on an oscilloscope. It is desirable to use a teletype printer as a check for adjusting the input levels to the "exclusive or" circuit.

The test should be conducted with the desired signal at optimum (S+N)/N ratio. The interfering signal is then increased in increments and the effects on error rate is observed.

Possibly these tests can be conducted in somewhat the same manner as the regular co-channel, close-channel and two-signal selectivity tests except that error rate rather than audio output ratio will be measured. The interfering signal can be PPM-FM, PCM-FM or unmodulated. It is hoped that a simple relationship can be found between the audio output ratio and error rate so that only one of these tests is necessary.

The tests for the PPM and PWM (pulsed carried) can be conducted in the same manner as the tests for the PPM-FM and PCM-FM except that the deviation sensitivity test would be excluded and the weak-signal selectivity test could be taken at the IF frequency. It is possible to use a signal generator to simulate the transmitter for pulsed carrier equipments.

ACKNOWLEDGEMENTS

The helpful suggestions of W. B. Wrigley, J. H. Holey and E. W. Wood are gratefully acknowledged.

The work described in this paper was performed under Signal Corps contract DA-36-039-sc-87183.

REFERENCES

1. "Principle Technical Characteristics of Communication Equipment," U. S. Army Signal Engineering Laboratories, Fort Monmouth, New Jersey, June 1957.

2. Ibid.

3. Fobes, Lawrence G., "Multichannel Radio Communications Within the Army," IRE Transactions on Military Electronics, October 1960.

4. Robert Rorden, "Application of the Gertsch Frequency Meters for Deviation Measurements," Bulleting Gertsch Products, Inc.

5. Hendler, A. J., "Noise Figure Measurements - Definitions, Techniques and Pitfalls," Airborne Instruments Laboratory, Inc., Mineola, N. Y.

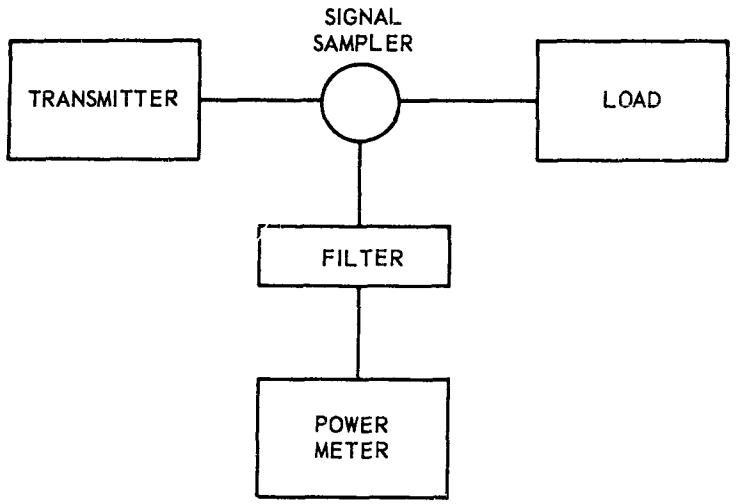
6. "Handbook of Microwave Measurements," Volumes I and II, Polytechnic Institute of Brooklyn, 1955.

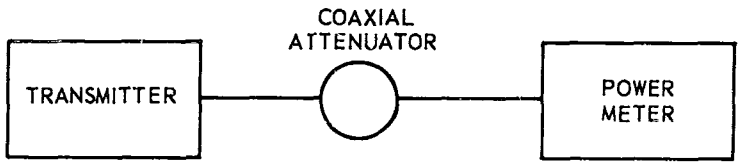
7. Ibid.

8. Haneman, F. G. and Hendler, A. J., "Automatic Indication of Receiver Noise Figure," Airborne Instruments Laboratory, Inc., Mineola, N. Y.

9. Mumford, W. W., "A Broadband Microwave Noise Source," BSTJ, Vol. 28, P608-618, October 1949.

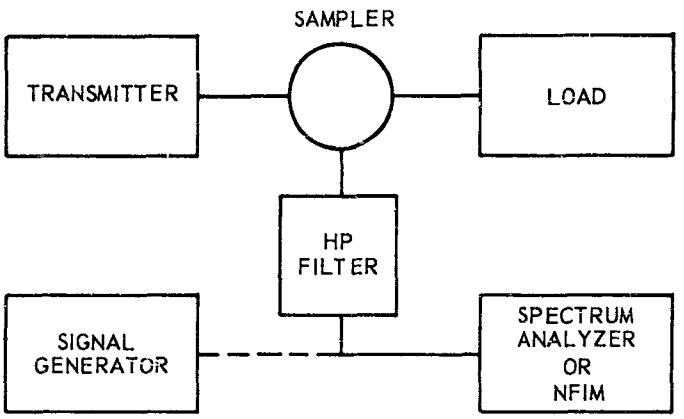
10. Ibid.



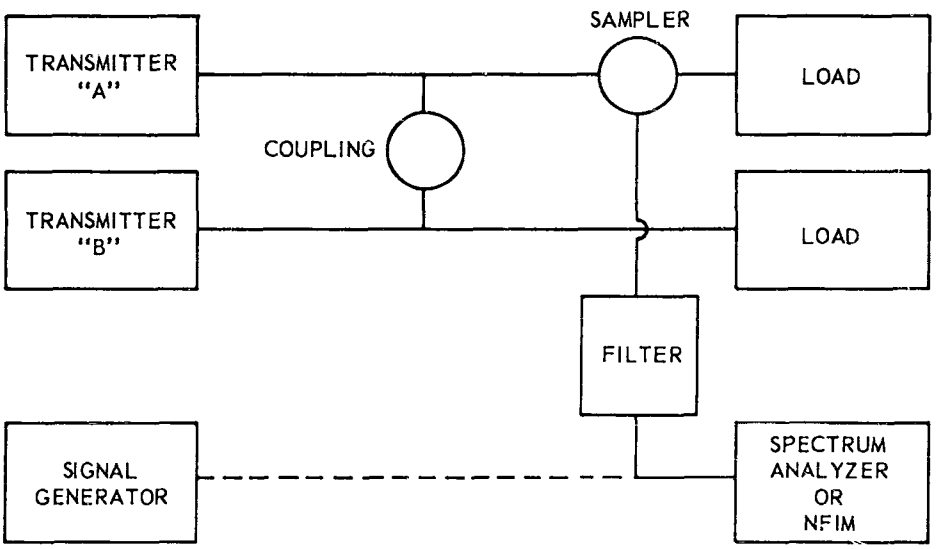

TEST SETUPS FOR MEASUREMENT OF POWER OUTPUT

Figure 1.



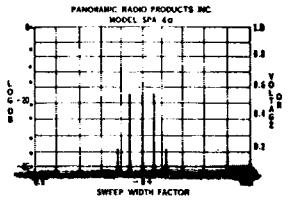

TEST SETUP FOR MEASUREMENT OF SPURIOUS AND HARMONIC EMISSIONS

Figure 2.



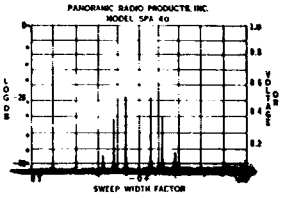

TEST SETUP FOR MEASUREMENT OF INTERMODULATION

Figure 3.




25 mc/sec Sweep Width
Linear Scale
1.5 mc/sec Modulation

B = 1.44
2.16 mc/sec Deviation (60%)

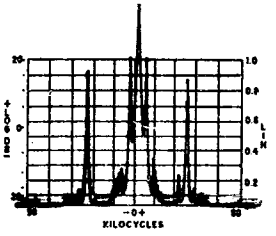



25 mc/sec Sweep Width
Linear Scale
1.5 mc/sec Modulation
B = 2.4
3.6 mc/sec Deviation (100%)

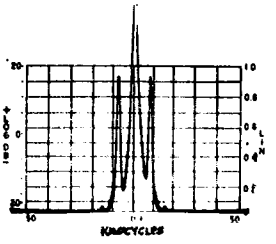
ILLUSTRATION OF ZERO COUNT METHOD
OF MEASURING DEVIATION

Figure 4.

ILLUSTRATION OF SPECTRUM ANALYZER METHOD FOR MEASURING AMPLITUDE MODULATION




10 kc/sec Sweep Width
30% Two-Tone Modulation
Scale 60 db Below Carrier




10 kc/sec Sweep Width
15% Single-Tone Modulation
Scale 60 db Below Carrier

Figure 5.



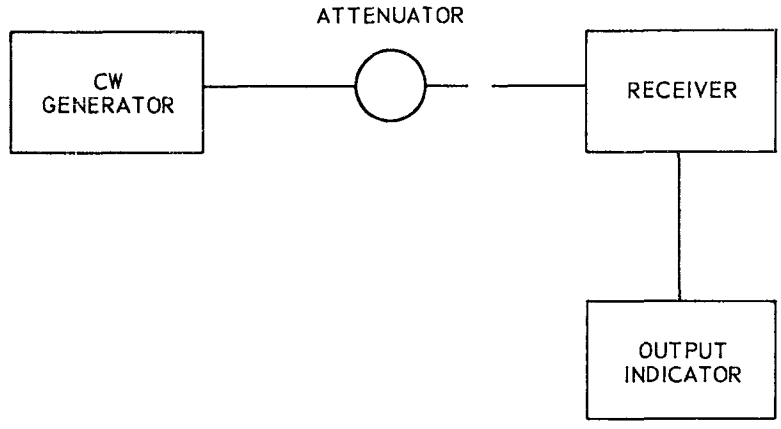

TANGENTIAL SENSITIVITY

Figure 6.



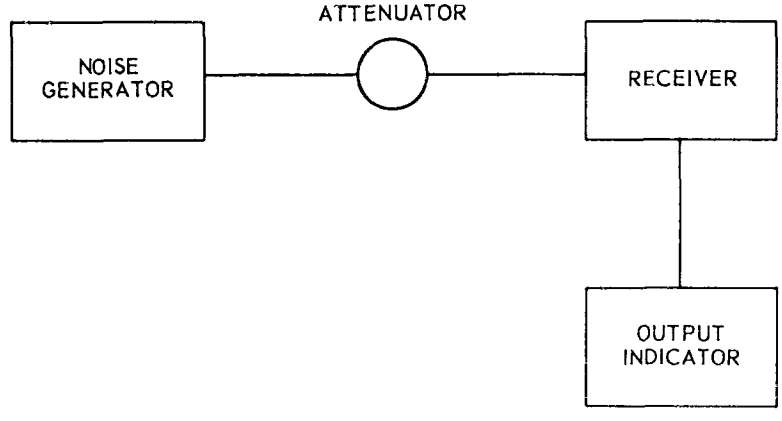

STANDARD SENSITIVITY (S+N = 2N)

Figure 7.



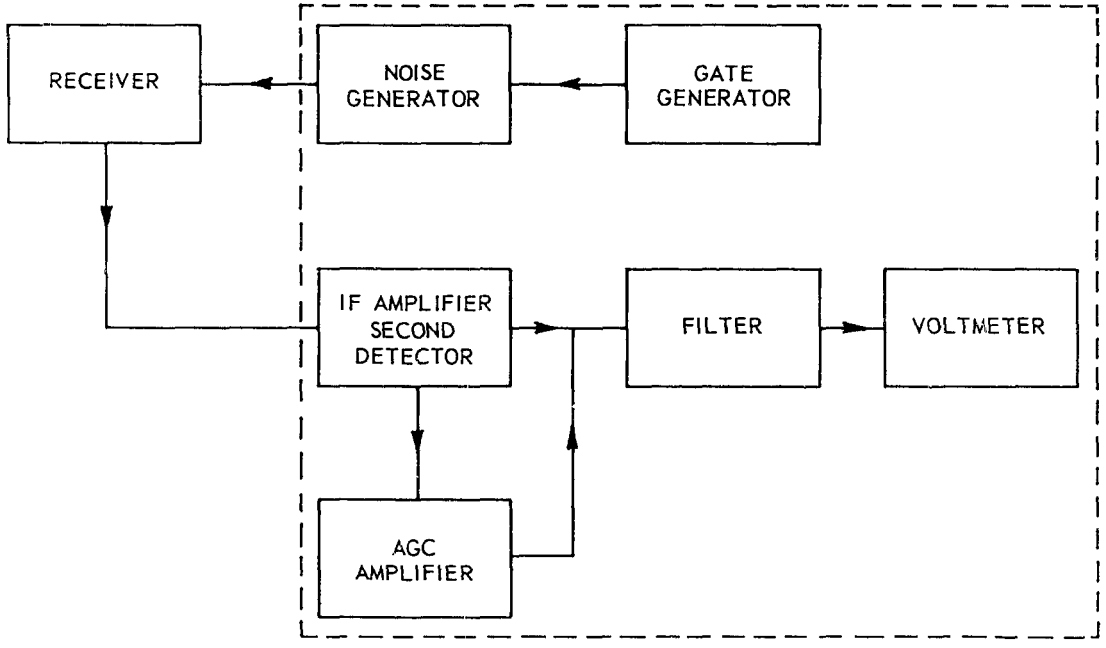

"CW" METHOD OF NOISE FIGURE MEASUREMENT

Figure 8.



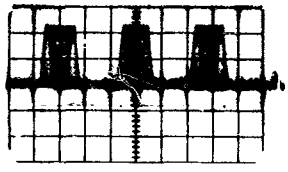

MANUAL-NOISE GENERATOR TECHNIQUE FOR MEASUREMENT OF NOISE FIGURE

Figure 9.




BLOCK DIAGRAM OF AN AUTOMATIC NOISE FIGURE INDICATOR

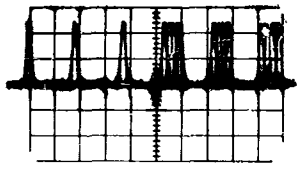
Figure 10.



Multiplexer Output Spectrum
Channels 1, 2 and 3
Pulse Position Modulation

RESULTS OF MULTIPLEXER CROSSTALK TESTS - 6 CHANNELS

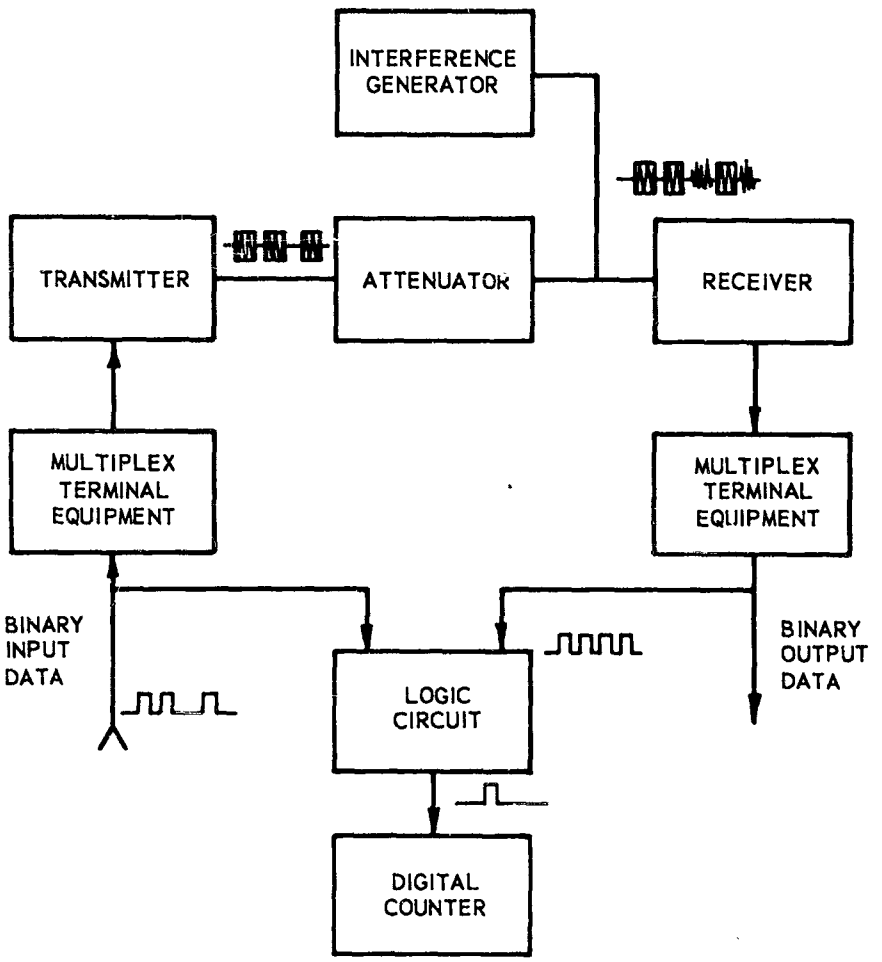
Figure 11.



Multiplexer Output Spectrum
Channels 1-6
Channels 1, 2 and 3 Modulated

RESULTS OF MULTIPLEXER CROSSTALK TESTS - 6 CHANNELS

Figure 12.




BLOCK DIAGRAM OF ARRANGEMENT FOR MEASUREMENT OF ERROR RATE

Figure 13.

# A PULSE TECHNIQUE FOR MEASURING SUSCEPTIBILITY AT AUDIO AND RF FREQUENCIES

J. H. Schukantz, G. C. Cooper and P. W. Broome
General Dynamics/Astronautics
San Diego, California

Abstract. A technique for measuring the susceptibility of any four terminal linear network using transient energy as a test function instead of sine wave energy was developed as part of a study contract titled, "Development and Evaluation of Improved Techniques for Measuring Susceptibility" Air Force Contract Number AF33(616)-7436. The technique involves the use of a transient or a pulse with a known frequency spectrum as a signal generator and an analog computer as an analysis tool. The main frequency range of interest was the audio frequency spectrum from 3 cycles to 15 kcps, but the natural progression of the study allowed the use of this method to measure both conducted audio and RF susceptibility with the upper frequency limit as yet not determined and limited only by coupling techniques and pulse generators available to perform the task.

The method consists of coupling a transient with a known frequency spectrum to any two terminals (including power input terminals presently covered by audio susceptibility tests) and noting the response to the transient at any other two terminals of interest. A Fourier integral analysis of the input transient and response transient is rapidly performed on an analog computer which allows a comparison of the input frequency vs amplitude spectrum to the response frequency vs amplitude spectrum and a measure of the insertion loss or transfer characteristics between any two pairs of terminals obtained. With this information, any peak or rms sine wave amplitude at any frequency in the spectrum covered by the test function transient can be assigned to the input transient and the response of the network at this frequency can be obtained by noting the response of the network to the transient energy. This type of analysis makes use of the concept that the susceptibility of a test sample is contained in its frequency response characteristics.

The computer analysis technique consists of performing a Fourier integral analysis of the input and response transients using an automated analog computer and a choice of function generators. The frequency vs amplitude spectrums are rapidly plotted on an xy plotter which provides a permanent record of the tests performed. It is believed that extensions of this type of analysis would provide a valuable tool in the field of measurement techniques and storage of interference characteristics of pieces of equipment tested.

This paper will be presented in two parts. Part I will deal with the mechanics of performing the tests and Part II will deal with the computer technique used in analyzing test results.

## I. FOURIER INTEGRAL ANALYSIS

It has been known for a long time that given a time-amplitude wave shape, by applying the Fourier transform, the time-amplitude wave shape can be examined in the frequency domain. This fact immediately points to the Fourier integral analysis as a tool for evaluating transients by considering the frequency components in that transient. Figure I shows some time amplitude plots and the frequency spectrum associated with them. Although these time amplitude plots are of a well known variety there is no reason why the Fourier integral analysis cannot be applied to irregular wave shapes such as those that might be encountered in examining responses of networks to well defined wave shapes. The only limitation in using this type of an analysis lies in the fact that long hand methods of mathematical analysis would be time consuming and more tedious than using RFI meters such as an NF105 to examine the spectrum of a pulse. The use of an analog computer however, presents a method of rapid analysis which can be applied to this problem.

## II. THE USE OF A PULSE OR TRANSIENT AS A SUSCEPTIBILITY MEASUREMENTS TOOL

One of the first pre-requisites in the use of a pulse as a susceptibility test function is the acceptance of the fact that the susceptibility of any linear network is contained within its frequency response characteristics. This statement can be explained by considering what happens if a malfunction occurs in a package under test due to sine wave energy at a given frequency placed on the power input lines to that package. In order for the malfunction to occur, energy at the frequency induced has to be passed from the power lines to some output terminals on the package under test which may actuate or cause operation of some output device which is outside of the realm of normal operation. At some other frequency, energy may still be passed to these same two terminals but a malfunction may not occur. This may or may not represent a dangerous condition presently ignored in susceptibility measurements procedures and serious consideration of this problem should be made on the design level.

In view of the fact that susceptibility test is in reality a form of response test it was thought to be convenient if sweeping a spectrum of interest one frequency at a time could be replaced by a pulse technique which would present the same spectrum of interest to the terminals under test. Figure 2 shows a comparison of the sine wave technique vs the pulse technique. If audio susceptibility is the test being performed the package under test, Figure 2a will be subjected to voltages in the frequency range from 50 cps to 15 kcps one frequency at a time and the output device may or may not operate in response to this energy. If a pulse is used of the form shown in Figure 2b, the same response characteristics of the package under test can be obtained by applying a pulse which contains the frequencies from 50 cps to 15 kcps. The only difference in these two tests is that in the sine wave test malfunction or operation of the output device in response to the sine wave energy is the criterion for failure, while in the case of the

pulse technique, input and output spectrums are evaluated to obtain a measure of the response characteristics of the package under test. These response characteristics are obtained by analyzing the Fourier components of the input and output pulses and obtaining the frequency vs amplitude plots shown in Figure 2b. Once these characteristics are known it would become the job of the designer to determine whether or not the attenuation characteristics of the network between the injection point and the output device are sufficient to prevent actuation of the output device.

It should also be noted that once these response characteristics are obtained it becomes possible to assign any value of amplitude to the input pulse spectrum to obtain the actual value of amplitude at terminals of the output device at a given frequency. For example, if three volts rms of sine wave energy is to be applied to any frequency from 50 cps to 15 kcps at the input of the package under test, the exact value of rms voltage at the output device can be obtained by comparing amplitudes of the input and output pulse spectrums.

Once a procedure or technique is developed for subjecting a package under test to pulse type energy and evaluating the results, another desirable condition can be achieved. This would be to use a pulse which would have a flat spectrum in the frequency range of interest, for instance DC to 15 KC. With this type of an arrangement it would only be necessary to examine output response pulses compared to a standard input pulse which would be flat over the frequency range specified and would thus cut the analysis time down to one half of the time necessary to conduct frequency analysis of both input and output pulses.

## III. TOOLS NECESSARY TO PERFORM SUSCEPTIBILITY MEASUREMENTS USING THE PULSE TECHNIQUE

Pulse Generator - The first tool necessary to conduct susceptibility measurements using transient or pulsed energy is the pulse generator. This item can take any form from designed pulse generators for testing in a limited frequency range, to off-the-shelf pulse generators which have the feasibility of carrying frequency components as high as 1 KMC.

For limited conducted susceptibility testing in the audio and low RF frequency ranges several designs of pulse generators were considered to meet the basic requirements. The designs used will be covered later in the section under types of tests performed. Some of the basic requirements, however, should be made clear at the outset. The first of these being that the pulse generator to be used should have as low as possible output impedance. This requirement stems from the fact that when low frequencies are considered the impedance of circuits into which the injection of a pulse test function is desired could feasibly have impedances as low as one ohm or less. This would be the case of a 28V DC power line feeding a package under test. Although the package under test may have a high input power line impedance it is ultimately in parallel with a battery through a limited cable length which would represent a low impedance. At higher frequencies it becomes feasible to use standard pulse generators such as

the HP 202A with a 50 ohm output impedance. The use of this generator allows the generation of frequency components as high as 30 mc.

Another consideration is the means of coupling to the circuit under test and after examining several approaches to this problem the most desirable means of accomplishing this type of coupling was through a pulse transformer with a 1:1 or low turns ratio. This also provided isolation between the generator and the circuit under test and also allowed generation of a controllable exponential pulse.

Oscilloscope and Polaroid Camera - The scope used to detect input and response transients should have a high frequency response equivalent to the highest detected frequencies desired. The Tektronix 545 series with the 30 mc pre-amp was found to be suitable for usage in the pulse testing covered thus far. The ultimate use of the oscilloscope in this type of testing is to provide information upon which the analog computer can work, therefore a permanent record of the transients detected is obtained using the scope in conjunction with a Polaroid Land camera. The photographs of the transients allows the production of photo former plates which can take the form of the original photograph or reproduced transparencies. These plates become the inputs to the analog computer.

Analog Computer - Although the computer used in the tests performed can accomplish many tasks, the only task performed in susceptibility testing using the pulse techniques was to obtain the Fourier analysis of the test functions used and obtained. The analog computer is therefore the analysis tool in this type of testing and can be thought of as equivalent to other detectors such as RFI meters presently used to detect transients.

Figure 3a shows a block diagram of the components necessary to perform the susceptibility test using pulsed energy. Tracing the steps of the analysis can be done by referring to this figure. The test function is injected into the network under test and a photograph of the input and output transients is obtained. These photographs are modified by cutting out the pictures taken with the polaroid camera to fit the photoformer function generator. The analog computer then performs the Fourier analysis of the input and output transients and a direct comparison can be made of the frequency spectrums of these transients by examining the XY plotter outputs. This comparison describes the response characteristics of the network under test.

An alternate scheme for performing this same analysis is seen in Figure 3b. The function generator in this scheme becomes a HP 160 scope which has incorporated in it a display scanner which applies a time scaling factor to the transient analyzed slowing it down to computer time. In this analysis the process of producing a photoformer plate is eliminated by using this scope since the analog computer works directly on the output of the display scanner. This analysis requires, however, that a rep rate be associated with the test function pulse used to examine the response of the network under test.

Linearity Tester - The pulse technique of susceptibility testing requires that the network under test is linear in nature within the frequency range of usage. It is therefore implied that there has to exist some technique by which the linearity of the network in question can be checked prior to performing the test and subsequent analysis. This linearity test takes the simple form of using an oscilloscope and the amplitude control of the pulse generator as tools for determining linearity. Figure 4 shows how the linearity test would be performed. The pulse generator amplitude would be placed at some value K necessary to obtain a response pulse amplitude A at the output of the network under test. Polaroid pictures could be taken for comparison purposes or visual observations could be used. Having obtained the response of the network to amplitude K of the pulse generator, the amplitude of the pulse generator can be reduced to $\frac{K}{2}$ or increased to 2K and the scope gain can be increased to 2C or decreased to $\frac{C}{2}$ in the order shown in Figure 4b. If the amplitude K of the response and the shape of waveform B does not change with respect to these amplitude changes, the network under test can be considered linear for the amplitude ranges of the test. It is assumed, of course, that the network under test is loaded at its input and output as it would be in normal usage.

## IV. TESTS PERFORMED TO SHOW EQUIVALENT BROADBAND SUSCEPTIBILITY TESTING TO SINE WAVES AND THE ACCEPTABILITY OF THE COMPUTER TECHNIQUE OF ANALYSIS

During the first step of investigations designed to investigate the validity of the computer analysis approach, several tests were made to show that the analog computer Fourier analyses of a waveform agreed with other methods available to perform the same task. Other tests were performed on idealized low pass filters to prove that the pass characteristics of any linear network does not differ whether sine wave or a pulse is used as a test function assuming of course, that the pulse has energy content in the frequency range of interest.

The first method used to check the computer method of Fourier integral analysis of a broadband waveform was to check a known waveform distribution against readings obtained for that same waveform using an RFI meter. The pulse to be evaluated was repeated for each tuned frequency of the RFI meter and readings were checked against a known distribution.

The circuit shown in Figure 5 was used to generate pulses which could be varied in shape or size by varying the circuit parameters, C, R and the L associated with the transformer used. The silicon control rectifier was used to discharge the capacity C because of its acceptably short time rise. Using this circuit, several pulses were generated with rise times ranging from 0.05 u sec. to 0.25 u sec. These pulses were analyzed for frequency content using analog computer techniques, and one of the waveforms generated closely approximated a cosine squared pulse which has a known frequency vs. amplitude function. This pulse was analyzed using this known function. The waveform analyzed is shown in Figure 6 and is compared with the standard

cosine squared pulse. Figure 7 shows the frequency vs. amplitude function given by the Fourier integral which applied to the cosine squared pulse and a comparison is made within the frequency vs. amplitude function of the analyzed transient.

Since the first computer analysis used to obtain frequency vs. amplitude information of any transient gave only relative amplitudes of frequencies contained in a transient, it was necessary that measurements be taken at a few frequencies in the spectrum of interest in order to establish the frequency vs. absolute amplitude function in terms of the amount of broadband energy present at any frequency contained in the transient. In this case the NF105 (frequency range, 0.15 to 25 mc) Empire Devices interference receiver was used to measure peak amplitudes of the frequencies present in the analyzed transient in terms of microvolts per megacycle. The values obtained are shown in Table 1.

The frequency vs. amplitude curve for the analyzed transient in Figure 7 was plotted from the values shown in Table 1 and normalized to fit the theoretical curve. As can be seen from the curves, the theoretical frequency function of the cosine squared pulse and the analyzed transient compare very closely (within 3 db) below 3.75 mc. The deviations at the high frequency end of the spectrum were attributed to the steeper slope of the analyzed transient and some of the variations at the low end of the spectrum were attributed to the fact that the analyzed transient did have some high amplitude low-frequency components which can be seen by comparing the plots of Figure 6.

In investigating the use of pulse type susceptibility testing, several problems were encountered concerning the ideal pulse shape, frequency content of the pulse, the amplitudes of the frequencies contained in the pulse and the total amplitude of the pulse to be used. It should be noted that the pulse to be used will have to be developed across a low-impedance generator in order to be useful in applications requiring testing of power circuits which are inherently of a low-impedance nature.

TABLE I. Measured spectral distribution of the cosine squared pulse

| Frequency | DB ABOVE 1 uV | MV/MC | VOLTS/MC ACROSS $R_1$ |
|---|---|---|---|
| 150 kc | 93 | 44700 | 1.97 |
| 300 kc | 93 | 44700 | 1.97 |
| 400 kc | 93 | 44700 | 1.97 |
| 500 kc | 93 | 44700 | 1.97 |
| 750 kc | 93 | 44700 | 1.97 |
| 850 kc | 92 | 39800 | 1.75 |
| 1 mc | 91 | 35500 | 1.56 |
| 1.5 mc | 90 | 31600 | 1.38 |
| 2.0 mc | 88 | 25100 | 1.10 |
| 2.5 mc | 87 | 22400 | 1.00 |
| 3.0 mc | 86 | 22400 | 1.00 |
| 3.75 mc | 85 | 17800 | 0.80 |
| 5 mc | 82 | 12600 | 0.07 |
| 6 mc | 75 | 5620 | 0.025 |
| 6.5 mc | 74 | 5010 | 0.022 |
| 7mc | 74 | 5010 | 0.022 |
| 7.5 mc | 70 | 3160 | 0.014 |

Search for a pulse shape which would be both easily generated and easily analyzed from the standpoint of frequency amplitude content indicate the exponential pulse shown in Figure 14 along with its frequency transform would lend itself to experimental investigation.

As can be seen in Figure 8, the frequency content of this exponential pulse can be regulated by changing the rise time of the pulse. Since the range of frequencies of interest in the primary investigation was between 15 cps and 200 kc, primarily to ensure fairly flat amplitude in the audio range of the frequency spectrum, the rise time of the pulse was kept to values of about 1 u sec. which was still easy to achieve by changing the value of the resistance $R_L$ in Figure 5. Referring to Figure 8, it can be seen that an exponential pulse with a rise time of 1 u sec. would contain frequencies of considerable amplitudes out to 1 mc and would have frequency components down 6 db from maximum amplitude at about 190 kc.

Referring again to Figure 5, it can be seen that the point of generation of the pulse considered for susceptibility studies would be across $R_L$ in the secondary of the pulse transformer. This resistance would ultimately have to be a very low value of pulse-type testing to be considered for low-impedance power circuits. The lowest value of $R_L$ that was tested was 1 ohm.

It was possible to generate the 1 u sec. pulse mentioned above with amplitudes between 90 and 110v across an $R_L$ of 1 ohm with a primary supply of 250 v and a pulse transformer that was not matched. It was believed that this can be improved upon by using silicon controlled rectifiers with higher breakover potentials and a matched pulse transformer. Further investigations lead to the development of a different pulse generation which could be used to place transients on both 28V DC lines and 115V 400 or 60 cps lines. This generation will be covered later. Studies covered in this section used the pulse generator shown in Figure 5.

The waveform shown in Figure 8 was used to examine the response of several different passive circuits comparing the transient response characteristics to the steady state response characteristics but only one such case will be included here for the purpose of illustration, i.e., the case of a low pass filter.

The filter designed is shown in Figure 9. This filter was a low pass constant K T-section with a cutoff frequency of 1.5 kc and a characteristic impedance of 10 K ohms terminated in 10 K ohms. The steady state response characteristics of this filter are shown as the solid curve of Figure 9. No attempt was made to match the filter at the input due to the fact that a low impedance pulse generator and audio oscillator was used at the input. The transient shown in Figure 10a was used as the test function against which the steady state response was to be checked. The frequency amplitude distribution of this transient is also shown in Figure 10b along with an indication of where $f_c$ of the filter was located in that distribution.

The resultant waveform at the output of the filter for the input transient of Figure 10A is shown in Figure 11A. This waveform was analyzed for frequency amplitude characteristics using analog computer techniques and found to have the spectral distribution of Figure 11B. This spectral distribution checked with the frequency characteristic of the filter, i.e., the frequencies in the pass band of the filter contained in the transient shown in Figure 10A were passed by the filter giving the waveform in Figure 11A. The amplitude of the waveform in Figure 11A was down 40 db from the input transient amplitudes but it should be noted that this is only due to the fact that the filter is passing only a small portion of the total available spectrum in the original transient.

The spectral distribution of the transient is flat in the region of the filter pass band and the computer analysis of the waveform in Figure 11A is produced with reasonable accuracy the characteristics of the filter. This comparison is shown in Figure 9.

The above results demonstrate the feasibility of using a transient type test to determine the frequency characteristics of a susceptibility test sample by merely noting the effect of a test sample on a transient with a known frequency amplitude characteristic. It should be noted also that the steady-state frequency characteristics of the test sample should agree with the transient analysis based on the frequency amplitude model of the transient used and the frequency amplitude model of the response transient at the output of the network tested.

At this point it can be seen that although present techniques used in audio susceptibility dictate the use of sine wave energy on power lines to produce malfunctions, the pulse technique could become a simple test to predetermine whether or not the power lines in any particular test sample could conduct energy to any other two terminals of interest in the audio frequency range. In fact, the present gap in frequency coverage in MIL-I-26600 from 15 KC to 150 KC could be covered in the same simple test by modifying the rise time of the test function in Figure 10A so that an essentially flat spectrum from DC to 150 KC could be presented to the power terminals of a package under test.

Optimization of the transient test function toward increasing the spectrum of investigation was also considered. It was found that the generating techniques shown in Figure 5 and a subsequent model of the same circuit was limited to a spectrum coverage from DC to approximately 1 or 2 MC. This limitation was due to the inherent rise time capability of several switches investigated including the SCR presently used in designed pulse generators. Devices capable of switching high currents necessary to develop an appreciably high voltage across low impedances were limited to SCR's, push buttons, switches, and mercury switches. Of the above three, the SCR's proved to be the easiest to work with even though their impedance at breakdown was higher than that of a mercury switch.

The best possible rise time attainable with an SCR firing into a 1 ohm load was about 0.4 u sec. Figure 12b shows that with this test function, shown in figure 12a, the -12 db point in the frequency amplitude distribution was at approximately 0.9 mc. It is therefore assumed that the analysis could be carried out successfully out to 1 mc and possibly farther without any difficulties. The generating circuitry for this test function will be shown in the section under test techniques. The pulse transformer used to couple this test function was flat out to 1 mc with a secondary current carrying capacity of 5 amps. Thus for test samples requiring more than 5 amps (ac or dc) another transformer would have to be designed.

It was desired to investigate means of extending the usage of a transient test function in susceptibility studies to 25 mc. Since it was previously determined that the generation of a test function to include this frequency range would require rise times in the millimicrosecond range ($10^{-9}$ sec.), studies were made of devices which could accomplish the generation of such pulses. It was also necessary to study the means of coupling such a test function to the ac or dc power lines under susceptibility tests and still maintain the quality of having a low impedance generator.

A method which proved to be quite satisfactory involved the use of the HP 212A Pulse Generator and a Stoddart Current Probe (Model 91550-1) as a pulse transformer. The signal generator was capable of generating rise times in the 0.01 to 0.02 u sec. range. The current probe was found to have a fairly flat frequency amplitude characteristics from 1 to 25 mc and an 8:1 turns ratio. If negligible losses are assumed in the probe, the voltage in the generator circuit would be stepped down by a factor of 8 and the impedance (assuming a 50 ohm generator) would be stepped down to 50/64 ohms. This generating circuit still maintains the low impedance generating source at the sacrifice of the test function amplitude.

The actual circuit used is shown in Figure 13 with a schematic representation in Figure 13a. The metallic tube inserted in the probe was used to minimize leakage reactance. A 50 ohm Bird load was used to load the secondary circuit and the injected transient was monitored at the input to the probe (E in Figure 13a and across the 50 ohm Bird load (E/8 in Figure 13a). The input transient and output transient and their characteristics can be seen in Figure 14a and Figure 14b respectively. The frequency amplitude distribution of the input and output transient can be seen in Figure 15. The output transient is down in amplitude by a factor which would be considered due to the 8:1 turns ratio and the losses due to the distributed parameters of the current probe. What should be noted from the curves of Figure 15 is the fact that the current probe follows closely the response of the transient and could therefore be used as a flat coupling device from 1 to 25 mc if the test function contained these frequencies. Although the analysis in Figure 40 is only carried out over a 13 db range data has shown that this analysis could be carried out to 15 mc with the test function described in Figure 14a. The actual amplitude of the transient across the 50 ohm load in the secondary of the current probe could be made as high as 17v peak. This is presently considered

adequate to carry out transients analysis over the above mentioned frequency range. It was also found that since the current probe represented a low reflected impedance in the circuit under test (i.e., a low impedance generator) this analysis could be carried out for a range of loads (test samples) from 4 ohms to an open circuit over a frequency range from 1 mc to 25 mc maintaining the transient amplitude (peak) of approximately 17v.

The results thus far obtained show the feasibility of using a transient test function as far as 25 mc in the frequency spectrum. Any further advance in the high end of the spectrum will depend on limitations of pulse generators which may be considered as off the shelf items.

## V. TEST TECHNIQUES USING TRANSIENTS AND EXAMPLES OF EQUIPMENTS TESTED

### Transient on D-C Power Lines

A d-c powered transducer power supply, Figure 16, was known to exhibit audio susceptibility based on tests conducted in accordance with MIL-I-26600. Two outputs of this transducer power supply were examined to prove correlation between the transient and sine wave tests. Because one output had been previously shown to exhibit susceptibility in the audio range, this output was examined in the audio range using a 15 kc low-pass filter. Another output was examined without the filter using the entire spectrum of the transient which was flat within 3 db out at 100 kc since this output had previously exhibited no susceptibility in the audio frequency range. With the transient technique it was found that the latter ouput exhibited susceptibility above the audio range. This test also showed the feasibility of extending the range of the transient test method to 150 kc without any change in method or equipment.

The test setup used in the transient tests is shown in Figure 17. The test procedure using the set up is as follows:

A. $S_1$ open (no pulse applied).

B. $S_2$ in the 1 position.

C. Apply 28v d-c to operate package under test.

D. $S_1$ closed (pulse applied).

E. Take picture of pulse through filter at input of package under test.

F. $S_1$ open.

G. $S_2$ in 2 position.

H. $S_1$ closed (pulse applied).

I. Take picture of pulse through filter at output of package under test.

If the photos in steps E and I compare exactly, then at least all the frequencies in the pass band of the filter are present and indicate that the package under test could be susceptible in this region. If the waveform do not compare, an analog computer analysis of the output waveform will show the frequencies present or absent in the output of the package under test and their relative amplitudes. It should be emphasized that a computer analysis might not be required if a set of filters covering different bands of frequencies were used in that these filters would outline bands of susceptibility.

The two outputs of the package in Figure 16 that were investigated were pins 4-10 and pins 13-10. Audio susceptibility tests in accordance with MIL-I-26600 were performed on the package in July 1960 and showed that pins 4-10 exhibited susceptibility in the audio spectrum and that pins 13-10 did not exhibit susceptibility in this range of frequencies. The transient test was used to check these results.

The output waveform obtained from pins 4-10, or the response of the package under test to the input transient through the 15 kc filter is shown in Figure 18a. The waveform had superimposed on it the ripple frequency or chopper frequency normally present at the output. It was found that the waveform could be approximated by taking the average of the ripple level because the ripple would add only frequency components at the ripple frequency. The waveform analyzed for frequency amplituue content is shown in Figure 18b. The frequency amplituue characteristics of this waveform is shown in Figure 19 by curve $E_{ot}$. The data obtained from the sine wave susceptibility test and contained in the report previously mentioned is shown in Figure 19 by the curve $E_{os} + E_{r}$. As can be seen the sine wave results show a leveling out above 4 kc. This was found to be due to the fact that the sine wave output plus the ripple was measured. Above 4 kc, the only voltage measured was the normal ripple voltage. A re-run of the sine wave test was performed using the test setup shown in Figure 20. In this test only the sine wave response of pins 4-10 was measured for a constant amplitude sine wave input. The results of this test are shown plotted by curve $E_{os}$ in Figure 19. As can be seen the sine wave response and transient response compare closely. It should be noted here that all responses were plotted with respect to the peak response of the network in db and all the plots of Figure 19 are therefore in relative amplitudes at the frequencies shown.

Since pins 13-10 show no susceptibility in the audio frequency range it was decided to try the whole spectrum of the transient, the filter was therefore removed from the test setup of Figure 17. The transient used is shown in Figure 21a. Its frequency amplitude transform is shown in Figure 21b. The response of the package under test to this transient at terminal 13-10 is shown in Figure 21c. The waveform in Figure 21c was analyzed to obtain the frequency amplitude characteristics and was found to have the spectral distribution shown in curve $E_{ot}$ of Figure 22. This curve was checked using the sine wave test for a constant amplitude input as shown by curve $E_{os}$ of Figure 22, and as can be seen the sine wave test compares closely to the transient results. In this particular test the results were not carried

beyond 150 kc because the spectral distribution of the transient used in the test falls off exponentially after 150 kc. The sine wave test was not carried out any farther because of the limitations of the instrumentation being used.

The results obtained above indicate that susceptibility testing could be carried out to 150 kc using the transient type test within the limitations of the spectral distribution of the transient being used in the test. It should also be noted that this test would not require any added instrumentation or time since the response waveform of the package under test would yield all of the information shown in Figure 22.

The results thus far obtained using transient techniques for susceptibility studies demonstrate a definite merit in that they can be verified with steady state techniques. Also shown is the capability of susceptibility measurements over an extended frequency range without any additional instrumentation. In general this type of susceptibility testing would only require knowledge of the spectrum being generated by the pulse and an accurate knowledge of the response waveform of the network under test. This waveform could then be analyzed to see which frequencies contained in the pulse were passed by the network and in this way frequency bands of susceptibility would be known. It should be noted that both the steady state analysis and the transient analysis of susceptibility tests are accurate only if the system under test is linear.

Transients on A-C Power Lines

The feasibility of injecting transients on 115v a-c power lines for the purpose of susceptibility testing was investigated. Two of the first considerations in this investigation were at what point in the power frequency cycle to inject the transient and if it were possible to inject a transient what would be sufficient amplitude to yield the same results (response of black box) as would be yielded in a sine wave test. The same transient used to demonstrate feasibility on d-c power lines can be injected to a-c power lines, anywhere in the power frequency cycle without changing the response of the black box under test. Since the transient used on d-c power lines was approximately five microseconds in total duration, this transient would occupy a small time interval on the power frequency cycle of 400 cps line and the slope of the power frequency cycle would have a negligible effect on the frequency amplitude distribution of the transient. It was decided to place the injected susceptibility transient on the crest of each positive swing of the power frequency to both further minimize any slope effects of the power frequency cycle and to be able to examine the effects of maximum allowable amplitude of the transient. Placing the transient at the crest of each positive swing would then include the study of any possible adverse effects in the operation of circuits which may be sensitive to voltage changes on 115v a-c lines within the range of maximum allowable rms power line ripple. Due to the short time duration of the transient, the allowable rms power line ripple would never be exceeded and maximum transient amplitude would then be a prime consideration. The concept for placing the transient

at the crest of each positive swing of the power frequency cycle can be seen in Figure 23 along with the method for viewing this transient.

Figure 24 shows that test circuit designed to inject transients on 115 v a-c lines. The circuit function is similar to the one designed to inject transients on d-c power lines and mentioned previously with the exception that an a-c charging source voltage is used. Also, the triggering circuit for the SCR is replaced by 115v a-c of the same phase as that used to supply power to the load in the circuit under test. The package under test was simulated with a variable resistance for the first investigations. The operation steps of the test circuit are briefly explained below.

If 400 cps is used the triggering and charging voltages ($V_c$ and $V_g$) must be of the same phase as the voltage supplied to the load.

A. Set load $R_{load}$ to nominal value such that no more than 5 amp is drawn through the pulse transformer (limitation due to particular pulse transformer used).

B. Adjust $V_3$ to 115v rms and monitor at VTVM No. 3.

C. Adjust charging voltage Vcrms to nominal value below 50v rms.

D. View $V_t$ with CRO.

E. Adjust $V_1$ to rms value necessary to gate SCR.

F. Adjust $R_t$ for minimum gate voltage necessary to insure 100% gating of SCR.

G. View output transient $V_t$ and re-adjust Verms to attain desired amplitude of transient.

The function of $D_1$ is to supply only positive a-c voltages to the gate circuit so that the transient will be injected only on the positive crests of the 115v a-c, 400 cps swings and to insure that no appreciable negative voltage will appear on the gate of the SCR. The purpose of $D_2$ is to supply only a positive charging voltage and to shut off the SCR for each half-cycle. $R_3$ is included in the primary of the pulse transformer to insure a low impedance generating source. If $R_3$ were not included on each cycle when the SCR would be shut off the reflected impedance from primary to secondary would be high, causing the power voltage to be dropped across the secondary of the pulse transformer causing possible damage. The various waveforms seen at points circled in Figure 24 are shown in Figure 25.

With the test setup of Figure 24 it was found that the predicted transient was generated as shown in Figure 23, and the location of this transient on the power frequency cycle could be varied on the positive slope from approximately 80° to 90°. It should be noted that with a repetition rate of 60 or 400 cps the Fourier Integral analysis

of this transient still held because the repetition rate of the transient is slow compared to the duration of the transient. It was also noted that load currents from 0 to 5 amp. through the secondary of the pulse transformer did not affect the size or shape of the injected transient to any noticeable degree.

With the instrumentation available to perform sine wave and transient tests on 115v a-c lines it was desirable to note the results of these tests on a package under test. For the purpose of this investigation a typical broadband amplifier, McIntosh Model MC-60, was chosen as a test sample.

The test setup for the transient susceptibility test is shown in Figure 26. The procedure as outlined above was used to inject the transient into the a-c power line to the amplifier. The input transient measured across the pulse transformer is shown in Figure 27a, and its frequency amplitude distribution is shown in Figure 27b. The transient as it appeared at the power input of the amplifier is shown in Figure 27c on top of the 60 cps power frequency with $A_t$ equal to 10v. The response transient measured across the 4 ohm output of the amplifier is shown in Figure 27d. This response transient was analyzed using an analog computer and was found to have the frequency amplitude distributed shown by the dotted curve in Figure 28. Since the input transient has a fairly flat frequency amplitude distribution ($\pm$ 1 db) from 15 cps to 150 kc, the analysis was carried out over this range of frequencies. The analysis shows that frequencies in the audio range are 12 db below higher frequencies so the analysis was discontinued below 1 kc.

With the transient analysis on the amplifier available, it was attempted to verify the transient derived output response using a sine wave test on the 115v 60 cps power input of the amplifier and at the same time evaluate the sine wave susceptibility test on the 115v a-c line with a test sample on the line. Figure 26 shows the test setup for the sine wave analysis. The injected susceptibility sine wave sine wave as seen through the 60 cps notch filter was kept at a constant amplitude of 10v peak-to-peak. The gain of the amplifier was kept at a nominal setting (the same as that used in the transient test) and the audio oscillator feeding the amplifier under test was used as an input load with a zero output setting. The response sine wave was read at the 4 ohm output tap of the amplifier using an oscilloscope. Since the sine wave injected at the power input of the amplifier experienced an overall attenuation of 60 db or greater at the output of the amplifier, it was difficult to read through the nominal noise appearing at the output of the amplifier. The transient analysis in this case was easier to perform because the transient appeared at the beginning of the oscilloscope trace (the trace was triggered by the transient) and contained in it were all the frequencies describing the response of the amplifier to the energy in the susceptibility transient on the 115v a-c power line.

The curve obtained from the sine wave data is seen in Figure 28 (solid line). As can be seen, the transient and sine wave data agree closely. Some discrepancies were noted on the low frequency end of the band but these are attributed to the difficulties in reading out the sine wave data. If the susceptibility sine wave voltage at the power input was increased above 10v peak-to-peak, distortion of the input sine wave was encountered. In this particular case, the low-frequency end of the spectrum could not be exactly determined by the sine wave test. Since the values at the low end of the band in Figure 28 are 13 to 19 db below the 150 kc values, the discrepancy in this portion of the spectrum was not considered too serious.

## VI. PULSE TECHNIQUE VS STEADY STATE ANALYSIS

Present techniques used in audio susceptibility testing in accordance with MIL-I-26600 use the 3V rms open circuit secondary transformer voltage as a test function and malfunction of the equipment in response to this 3V rms as a failure criterion. Although arguments for and against this type of test have been going on for some time no one can actually argue its validity as a test but in the strict sense of the word "susceptibility" it is a brute force technique. The malfunction which would define failure can occur for several reasons such as, how long an operator dwells on any one frequency, the extraneous voltage drops within the injection circuit, how much of the open circuit voltage that actually appears across the test sample terminals and the type of equipment under test. Therefore, in the strict sense, the test should be termed the Audio Malfunction test since the susceptibility of the network under test is never really defined by the test results and since in most cases the malfunction is due to a power transfer.

The pulse technique, however, offers a means of rapid evaluation of any network under test and defines the transfer characteristics of that network. In defining the transfer characteristics from any power terminal to any other two terminals in the package under test, the susceptibility of the network is defined in that the presence of frequencies injected at the power terminals is seen at some end device. This then defines the susceptibility of the end device due to frequencies injected at the power terminals and whether or not the device responds to the frequencies passed should be examined by the designer of the equipment. If the end device was a dc high current relay, high frequency susceptibility of course would not be a consideration, however, other circuits sensitive to high audio frequencies could be of some concern.

The pulse technique of evaluation could easily be placed in the hands of the designer as an additional tool to be used to evaluate his design. The attainability of the susceptibility characteristics of his design would then involve the simple process of taking oscilloscope pictures which could either be evaluated by the designer himself or could be given to an interference control group for evaluation. Because of the inherent simplicity of the test and equipments used in obtaining data this technique could easily encourage the consideration of susceptibility in the breadboard stage of a design instead of considering susceptibility of an end item which if uncovered can result in cumbersome supression requirements.

The pulse technique also offers an attractive advantage once a first test sample of a series has been evaluated in that subsequent units manufactured to the same design can be rapidly evaluated by comparing the transients response pictures without actually performing the end analysis on an analog computer.

Another more apparent advantage is the fact that the pulse technique of evaluation can easily cover a frequency range from DC to

upper frequencies limited by availability of pulse generators and coupling techniques. The present gap from 15 kc to 150 kc in MIL-I-26600 can be covered in this type of investigation without the cumbersome addition of specially designed transformers and high power audio amplifiers.

Other advantages that can be mentioned come under the headings of time savings and low skill level requirements. In most cases the test could be performed by taking a few polaroid pictures from oscilloscopes. The analysis portion on an analog computer to the present date would take only a few minutes on an automated set up. The present analysis technique at GD/A would allow an evaluation of the Fourier components of a response transient up to 15 or 25 mc in about 5 minutes or less, depending on the resolution requirements of any test.

## VII. FUTURE APPLICATIONS OF PULSE TECHNIQUES AND ANALOG COMPUTER ANALYSIS

The pulse technique as applied to conducted susceptibility measurements in this study could also be extended for usage in radiated susceptibility measurements. It would however, become very difficult to determine what the limits of the generated broadband field should be in fact if limits to be used in all types of susceptibility testing continue to be non-existant or arbitrary perhaps the solution lies in using the allowed specification limits for both measured conducted and radiated interference as the amount of conducted energy or radiated field any package should be subjected to. If limits were defined in this way it would not be difficult to generate shaped pulses with shaped spectrums which would create the broadband specification limit whether conducted or radiated and subject the package under test to only this amount of energy. Steps have already been taken during the course of this study to produce measured specification limits and results show that there is feasibility in this approach.

Inherent in this pulse technique is the advantage of being able to store information in the form of photographs and xy plots which cover the whole spectrum of interest. It is also possible to conduct the same type of computer analysis of received information by recovering data from magnetic tapes which forms another method of information storage. Although these methods have not yet been studied extensively new vistas in the use of the analog computer as an interference measurement and storage tool could be opened by investigation of the newer developments in the fields of magnetic tape and core memory storage.

Some steps were made to apply the transient analysis techniques using analog computers to the field of interference measurement during the course of this study. Of particular interest was the applicability of this type of measuring and analysis technique to the problematic and time consuming task of measuring the broadband interference emanating from transients generated by slow

cycling equipment such as battery heater thermostats although the technique applied in general to all measurements made of generated transients by such devices as solenoids and switches. The results of these investigations showed that a very noted time savings could be achieved by taking oscilloscope pictures of these occurrences and using the analog computer technique to perform a rapid evaluation of the spectrum generated. For example a battery heater thermostat tested cycled at the rate of once every 10 minutes. The measurements of the conducted interference to MIL-I-26600 specifications using a current probe and an NF105 took on the average four to eight hours. Taking a picture of the transient and performing the computer analysis with other proven curve smoothing techniques took approximately 15 to 30 minutes.

It was also found during the course of these investigations that an operator could train himself in the technique of categorizing characteristics of transients in such a way that by viewing certain transient for the first time he could determine if the viewed transient represented an out of specification condition for conducted broadband interference. Using this as a basis for a new technique, nomagraphs are presently being investigated which would allow an untrained observer to determine an in or out of specification condition by merely noting characteristics of the transient such as rise time, duration, amplitude and area.

## VIII. SUMMARY

The results of this investigation have shown that a pulse with a known spectrum can be used as a tool to measure the conducted susceptibility of any linear network. The use of this tool allows the injection of all the frequencies of interest at one set of terminals (28V DC power input or 115V AC power input if using MIL-I-26600) of a package under test simultaneously and the examining any other two sets of terminals for the response characteristics. The versatility of this test technique does not limit its usage to only the audio spectrum. It has been shown that techniques could be applied in two steps to cover the complete frequency range from DC to 25 MC thus representing a considerable time savings over present methods used.

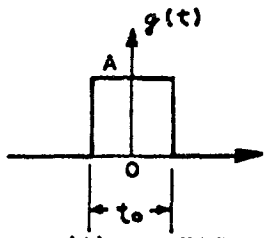
If malfunction remains, the criterion for specification limits the pulse test technique could be used as a one shot test to determine in what portions of the spectrum an audio or RF susceptibility would exist and could then be followed up with tests using present techniques.

It should also be noted that the transient or pulse type test would more nearly represent the true situation encountered in integrated weapon systems. Experience in examining power lines (28V DC and 115V AC/400) in weapon systems integrated at General Dynamics/ Astronautics as common couplers of interference has shown that at no time are pure sine waves encountered on these lines and in almost all cases erratic waveforms and transients are encountered. It is

therefore believed that more thought should be given to present versions of susceptibility tests performed on DC and AC lines of components of any integrated system since their ultimate environment will surely be of a broadband nature.

FIGURE 1

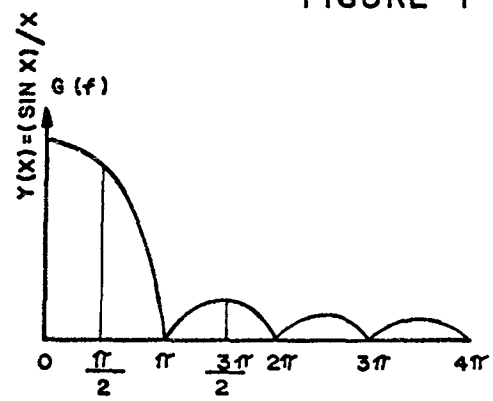
RECTANGULAR PULSE




$g(t) = A$ FOR $-\frac{t_o}{2} < t < \frac{t_o}{2}$

$= 0$ OTHERWISE

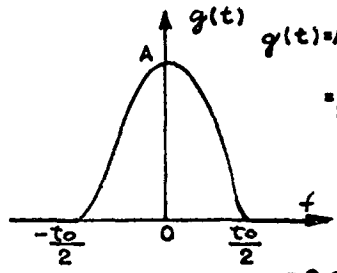
AREA $A = A t_o$




X IN RADIANS $\quad G(f) = A(\text{SIN}\alpha)\alpha$

WHERE $\alpha = \pi t_o f$

COSINE-SQUARED PULSE



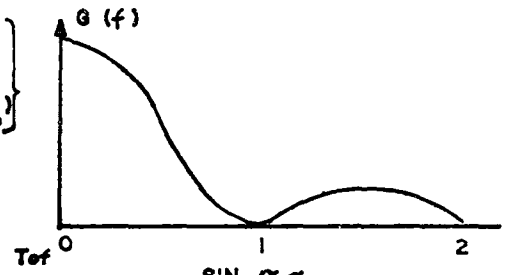

$g(t) = A\cos^2 \pi \frac{t}{t_o}$

$= \frac{1}{2} A\left(1 + \cos 2\frac{t}{t_o}\right)$

$-\frac{t_o}{2} < t < \frac{t_o}{2}$

$= 0$, OTHERWISE

AREA $A = \frac{1}{2} A t_o$

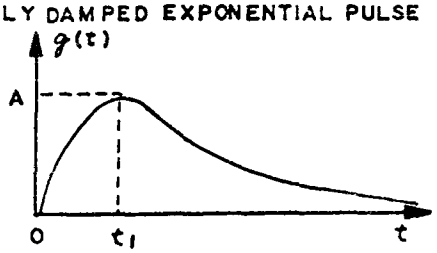



$G(f) = \frac{\text{SIN } \pi\alpha}{(1-\alpha^2)}$

WHERE $\alpha = t_o f$

FOR $\alpha = 1$, $\quad = G(f)\frac{1}{2} A$

CRITICALLY DAMPED EXPONENTIAL PULSE

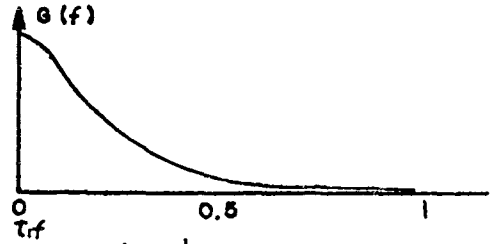



$g(t) = A e \frac{t}{t_1} \text{EXP}\left(-\frac{t}{t_1}\right), t > 0$

$= 0, t < 0$

$= 2.71828$

AREA $A = A e t_1$




$G(f) = A\frac{1}{(1+j\alpha)^2}$

WHERE $\alpha = 2\pi\tau_1 f$

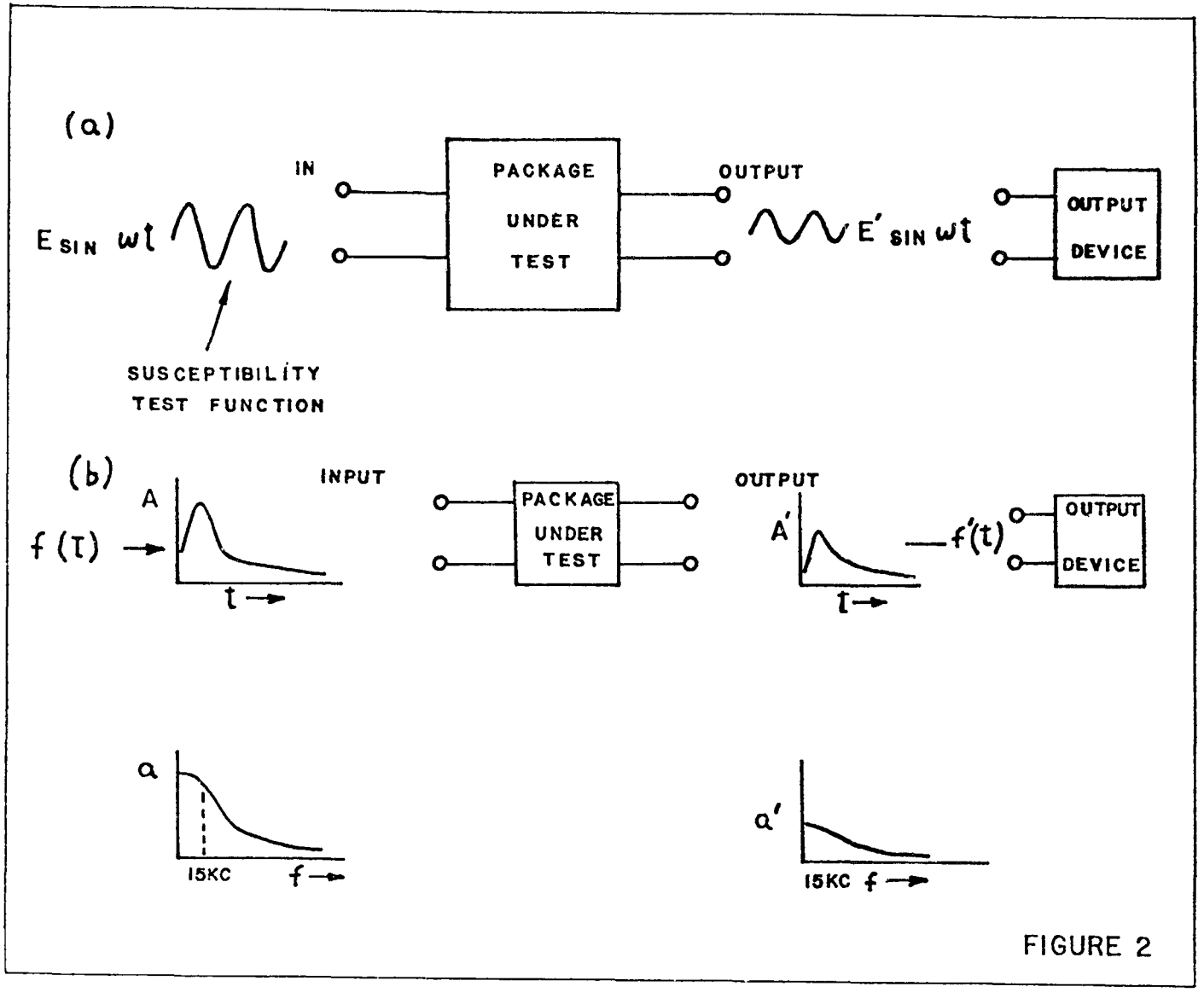

(a)
IN
E SIN ωt
PACKAGE UNDER TEST
OUTPUT
E' SIN ωt
OUTPUT DEVICE
SUSCEPTIBILITY TEST FUNCTION
(b)
INPUT
A
f (T)
t
PACKAGE UNDER TEST
OUTPUT
A'
f'(t)
OUTPUT DEVICE
t
a
15KC
f
a'
15KC f

FIGURE 2

FIGURE 3

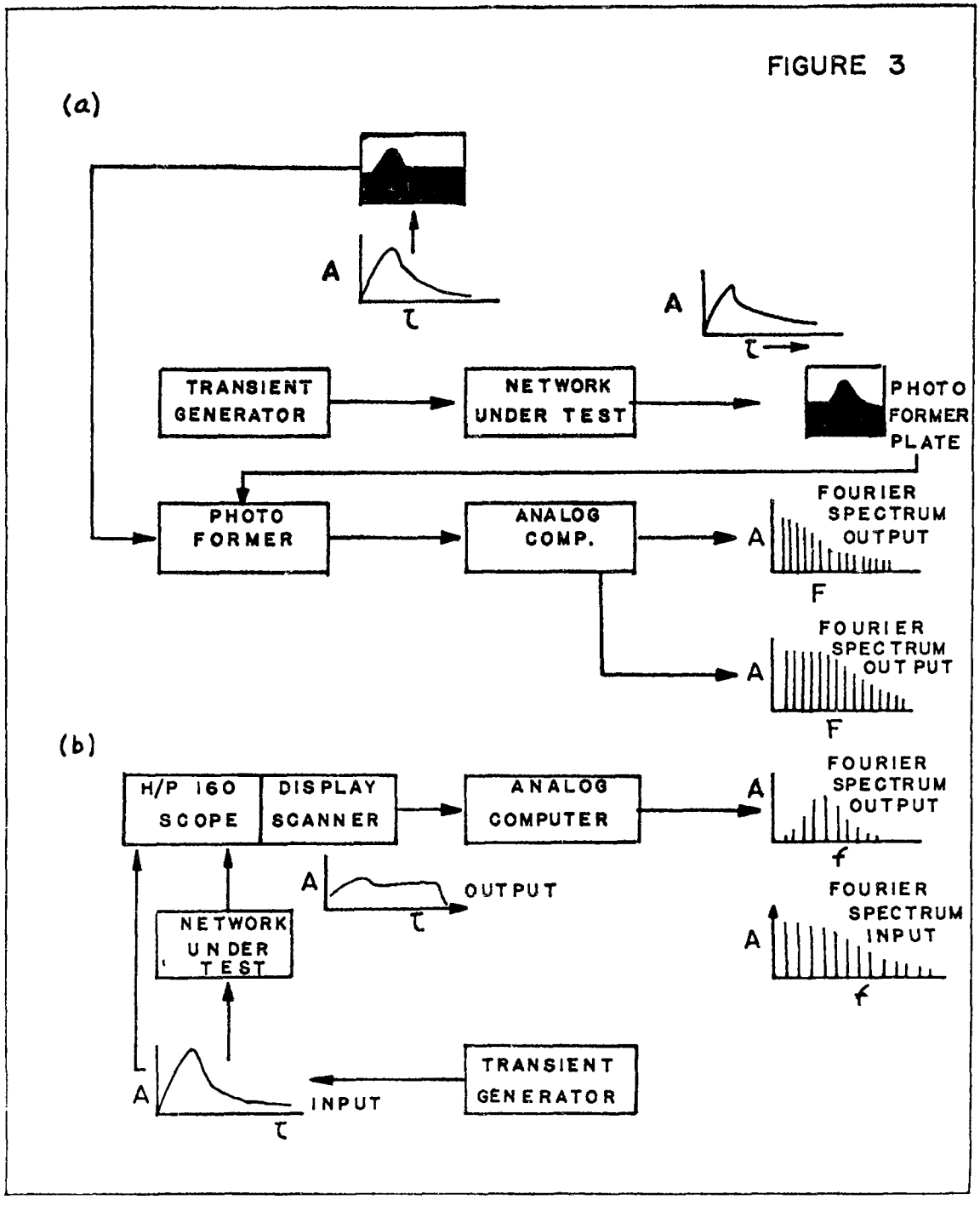
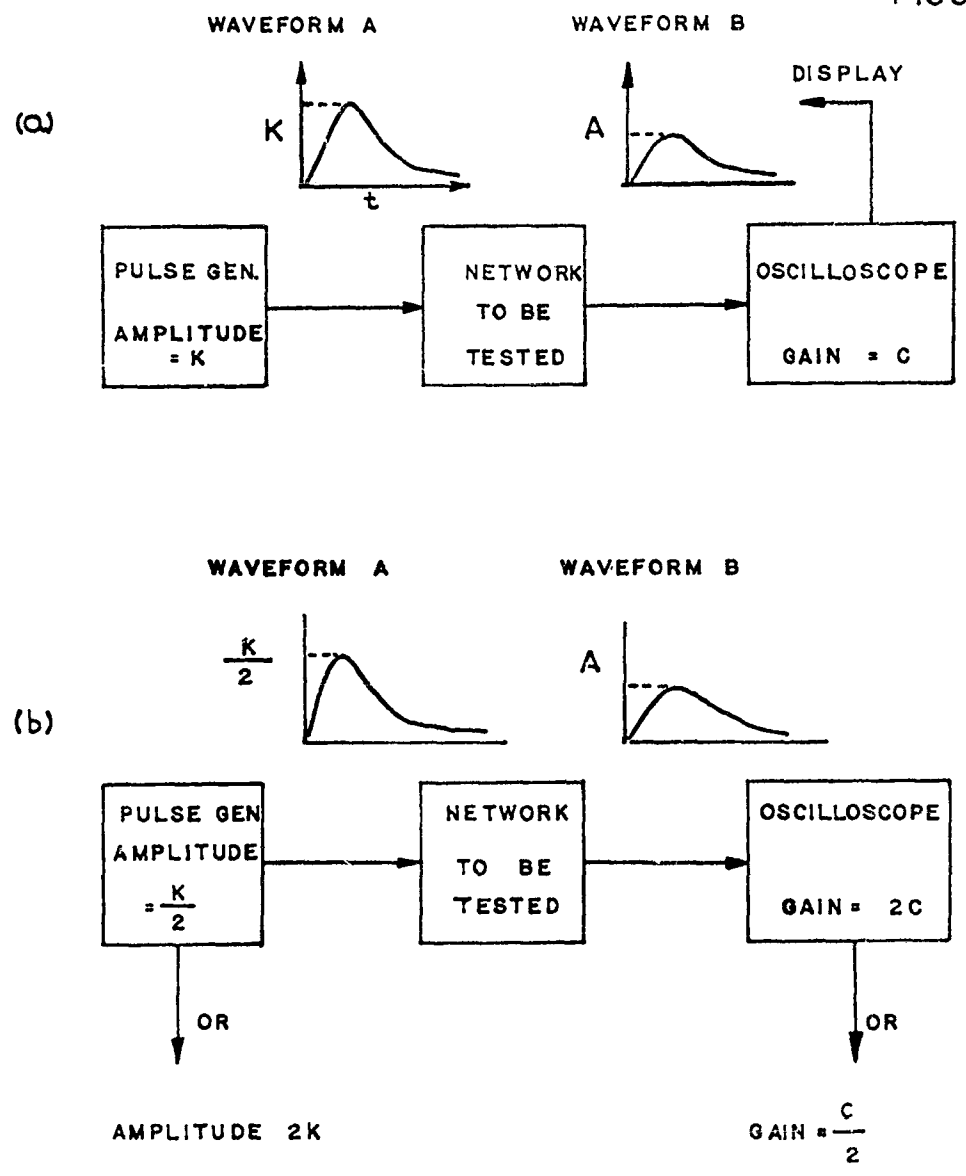
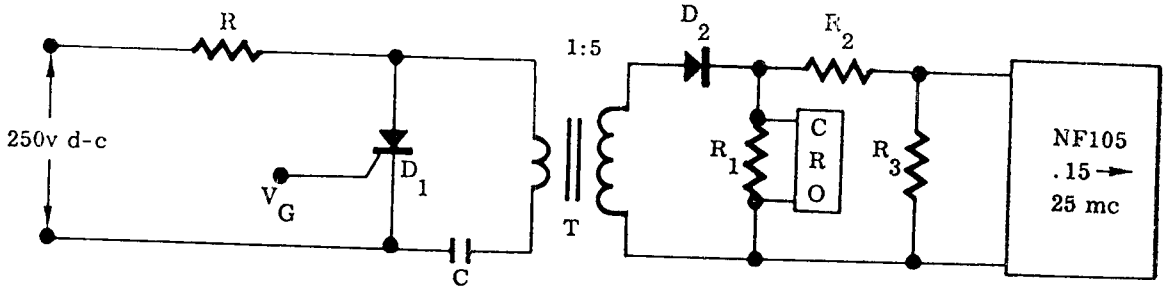

(a)
A
τ
A
τ
TRANSIENT GENERATOR
NETWORK UNDER TEST
PHOTO FORMER PLATE
PHOTO FORMER
ANALOG COMP.
A
FOURIER SPECTRUM OUTPUT
F
A
FOURIER SPECTRUM OUT PUT
F
(b)
H/P 160 SCOPE
DISPLAY SCANNER
ANALOG COMPUTER
A
FOURIER SPECTRUM OUTPUT
f
A
OUTPUT
τ
NETWORK UNDER TEST
A
FOURIER SPECTRUM INPUT
f
TRANSIENT GENERATOR
A
INPUT
τ

FIGURE 4


(a)
WAVEFORM A
WAVEFORM B
DISPLAY
K
t
A
PULSE GEN.
AMPLITUDE
= K
NETWORK
TO BE
TESTED
OSCILLOSCOPE
GAIN = C
(b)
WAVEFORM A
WAVEFORM B
K/2
A
PULSE GEN
AMPLITUDE
= K/2
NETWORK
TO BE
TESTED
OSCILLOSCOPE
GAIN = 2C
OR
OR
AMPLITUDE 2K
GAIN = C/2




R 1000 Ω Current Limiting Resistance.

$D_1$ C35B Silicon Controlled Rectifier.

C .0022μf Capacitor.

T 1/5 Step Up Transformer Loosely Coupled.

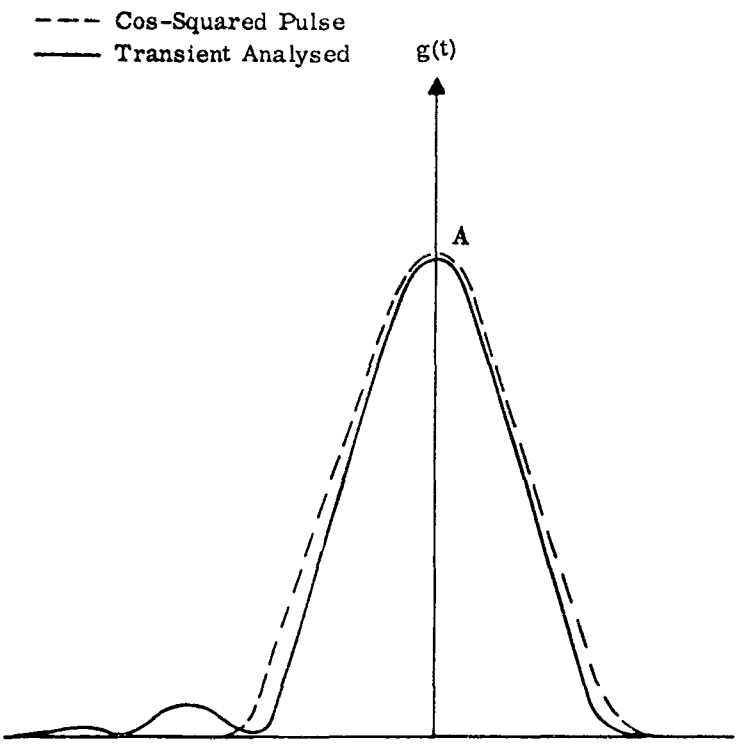
$D_2$ IN307 Diode Rectifier.

$R_1$ 100 Ω Load Resistor.

$R_2$ 212K Ω
$R_3$ 50Ω
} Voltage Divider Network.

CRO Tektronics 545 Oscilloscope.

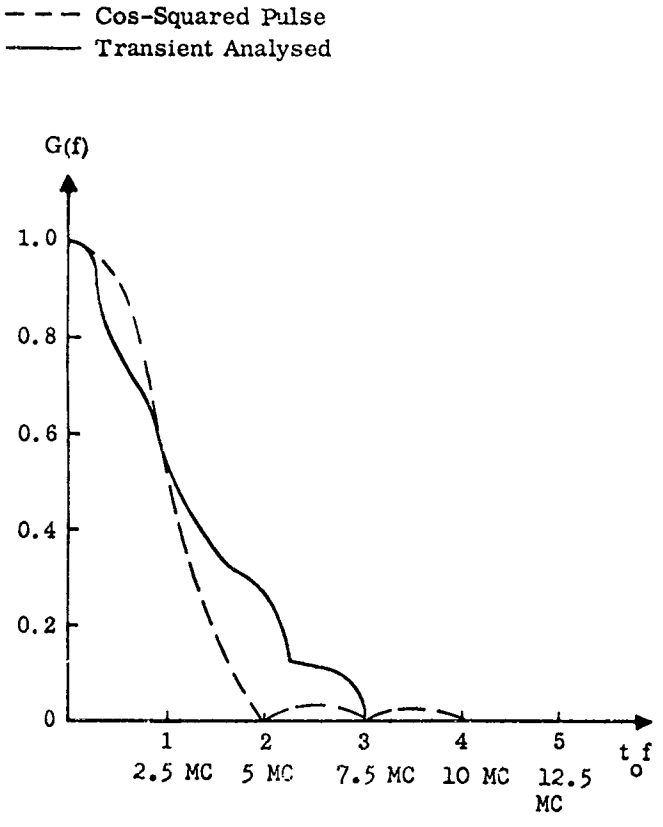
Fig. 5. Pulse generating circuit




$$g(t) = A \cos^2 \pi \frac{t}{t_o} = \frac{1}{2} A \left(1 + \cos 2\pi \frac{t}{t_o}\right) \quad \Bigg\} \; -\frac{t_o}{2} < t < \frac{t_o}{Z}$$

$$\text{area } A = \frac{1}{2} A t_o$$

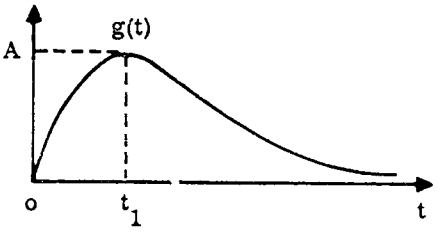
Fig. 6. Time function.




$$G(f) = A \frac{\sin \pi \alpha}{\pi \alpha (1-\alpha^2)}$$

$$\alpha = t_o f$$

Fig. 7. Frequency function.

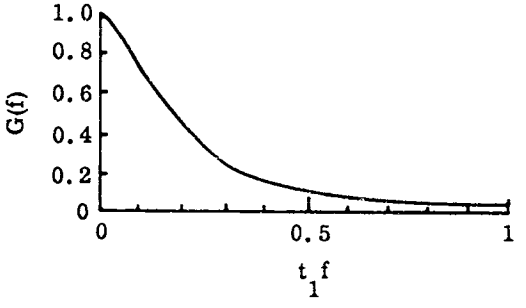



$$g(t) = Ae \frac{t}{t_1} \exp\left(-\frac{t}{t_1}\right) \quad t > 0$$

$$= 0, \quad t < 0$$

$$e = 2.71828$$

$$\text{Area } A = Aet_1$$




$$G(f) = A \frac{1}{(1 + j\alpha)^2}$$

Where $\alpha = 2\pi t_1 f$

Fig. 8. Exponential pulse and its frequency transform.

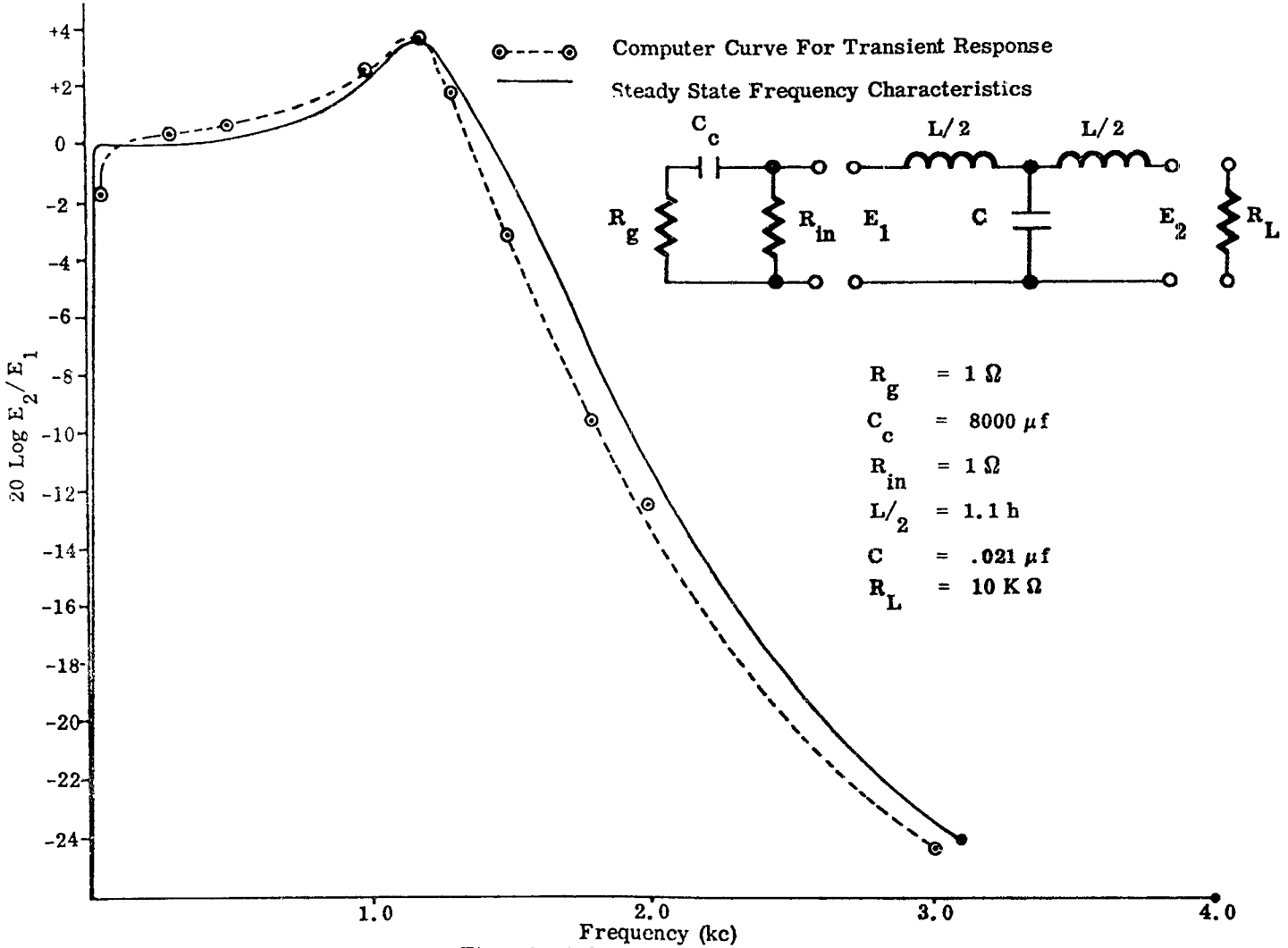



Fig. 9. Filter characteristic curves.

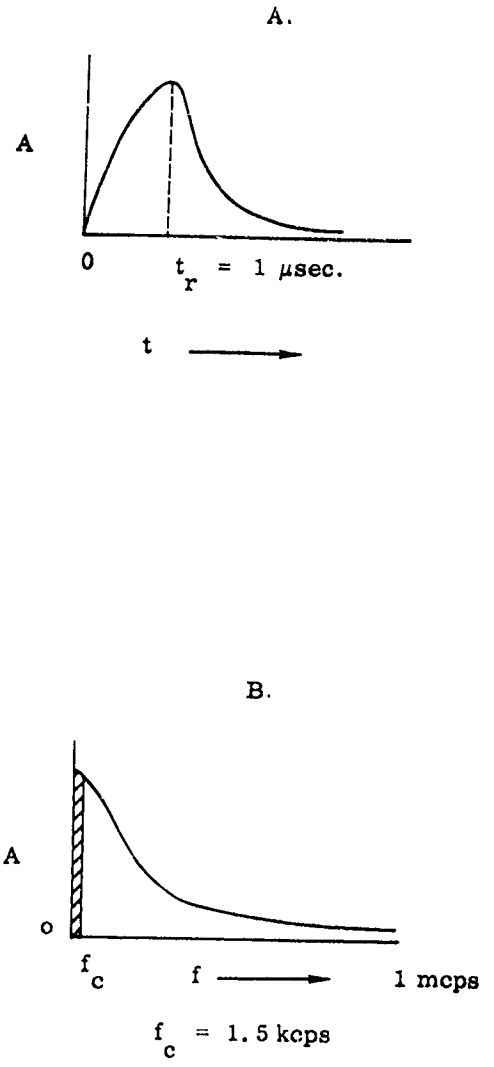
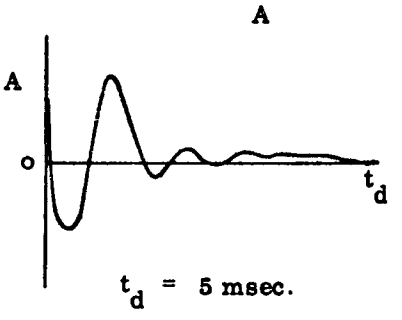



Fig. 10. Transient filter test function.



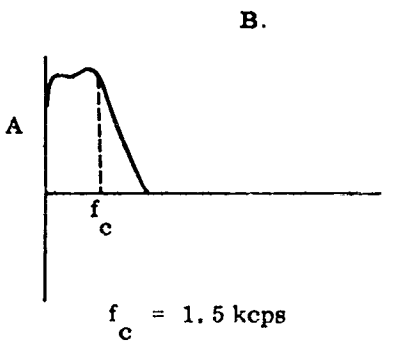




Fig. 11. Transient and spectral distribution.

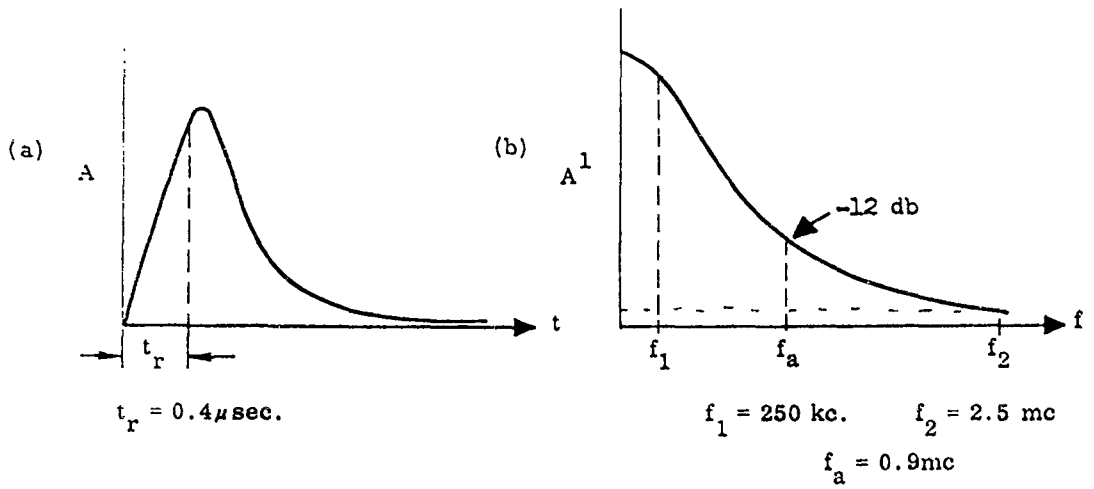



Fig. 12. Transient used for d-c to 1 mcps analysis

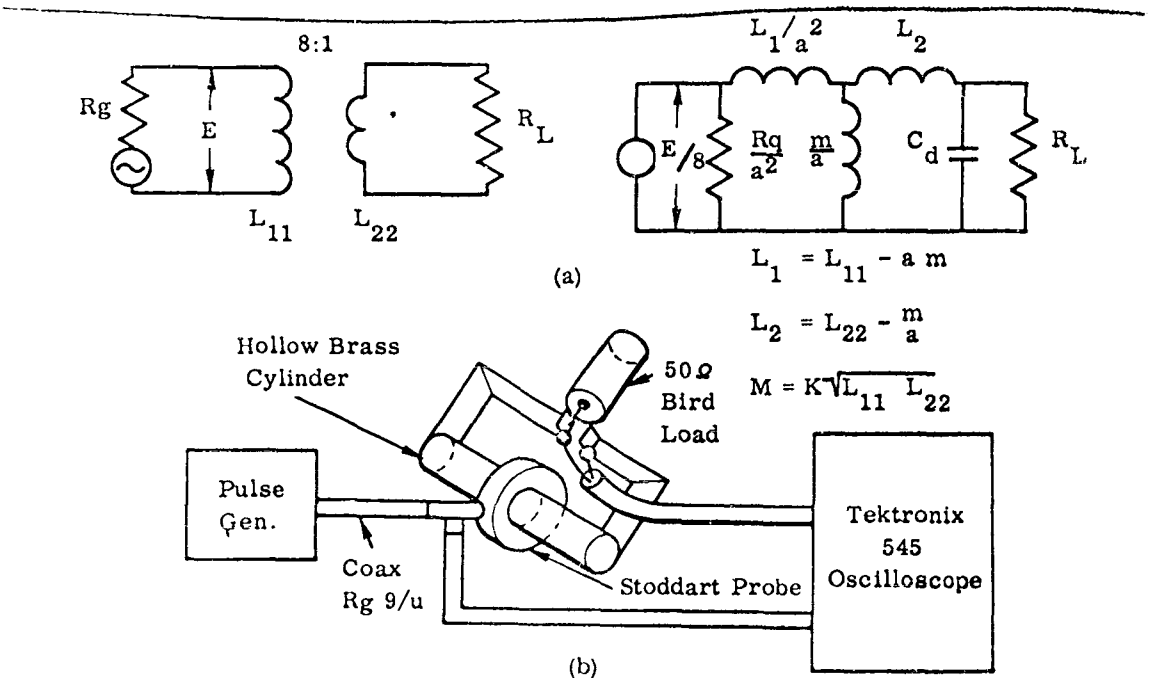
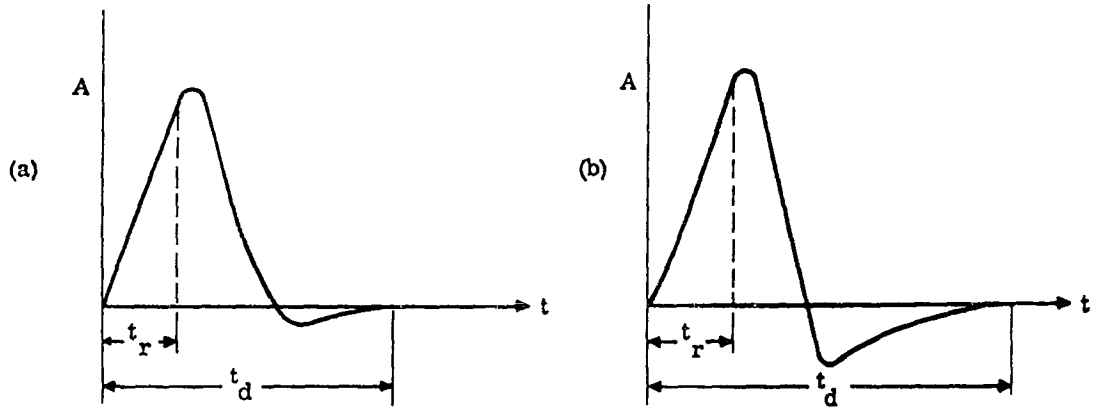



Fig. 13. Test setup for evaluating current probe as a coupling device for transients from 1 mcps to 25 mcps.




$t_d = 0.9\ \mu$ sec.
$t_r = .02\ \mu$ sec.

$t_d = 1\ \mu$ sec.
$t_r = .02\ \mu$ sec.

Fig. 14. Input and output transient used in evaluating current probe.

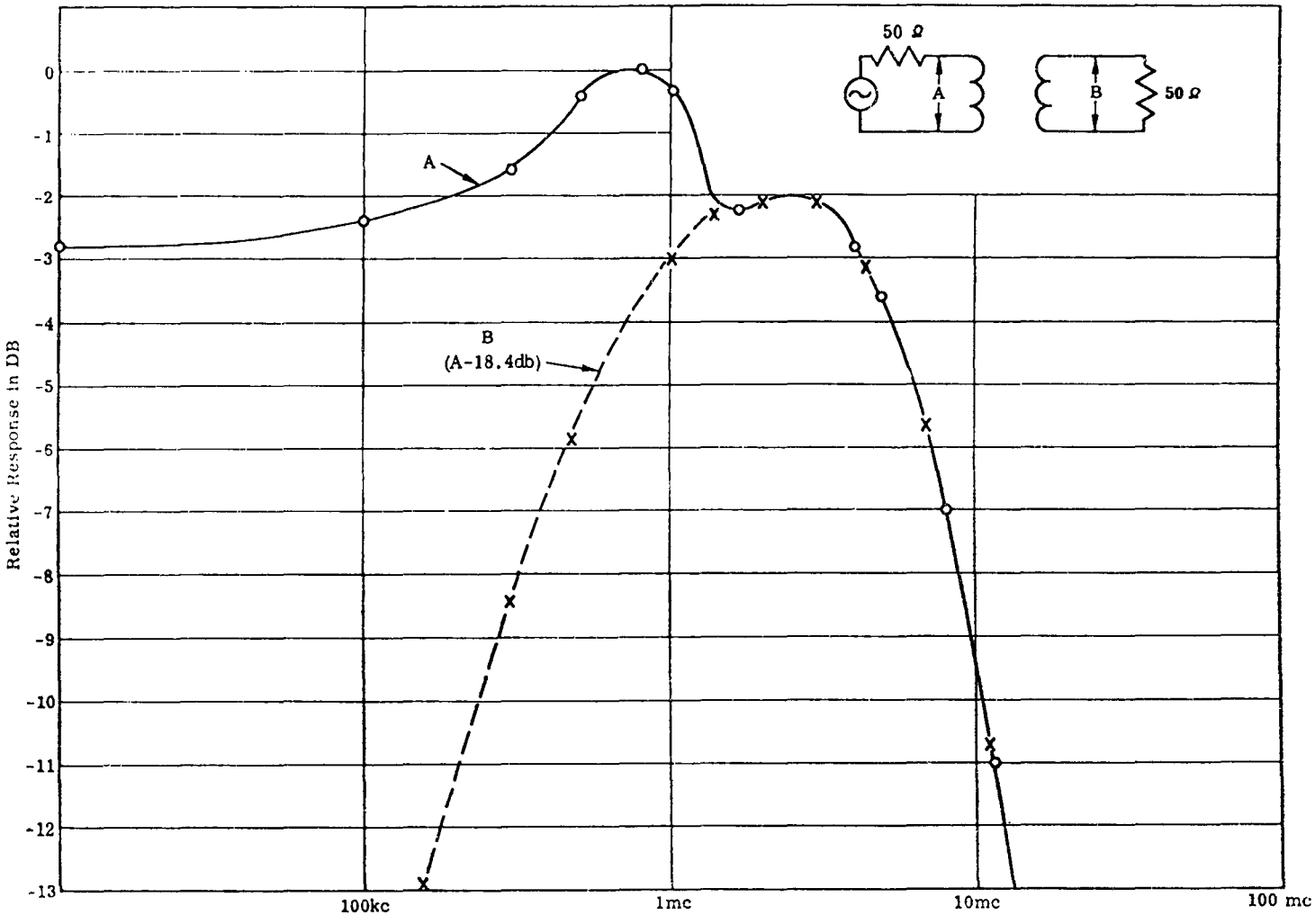



Fig. 15. Frequency versus Amplitude Response of Transients in Figure 39.

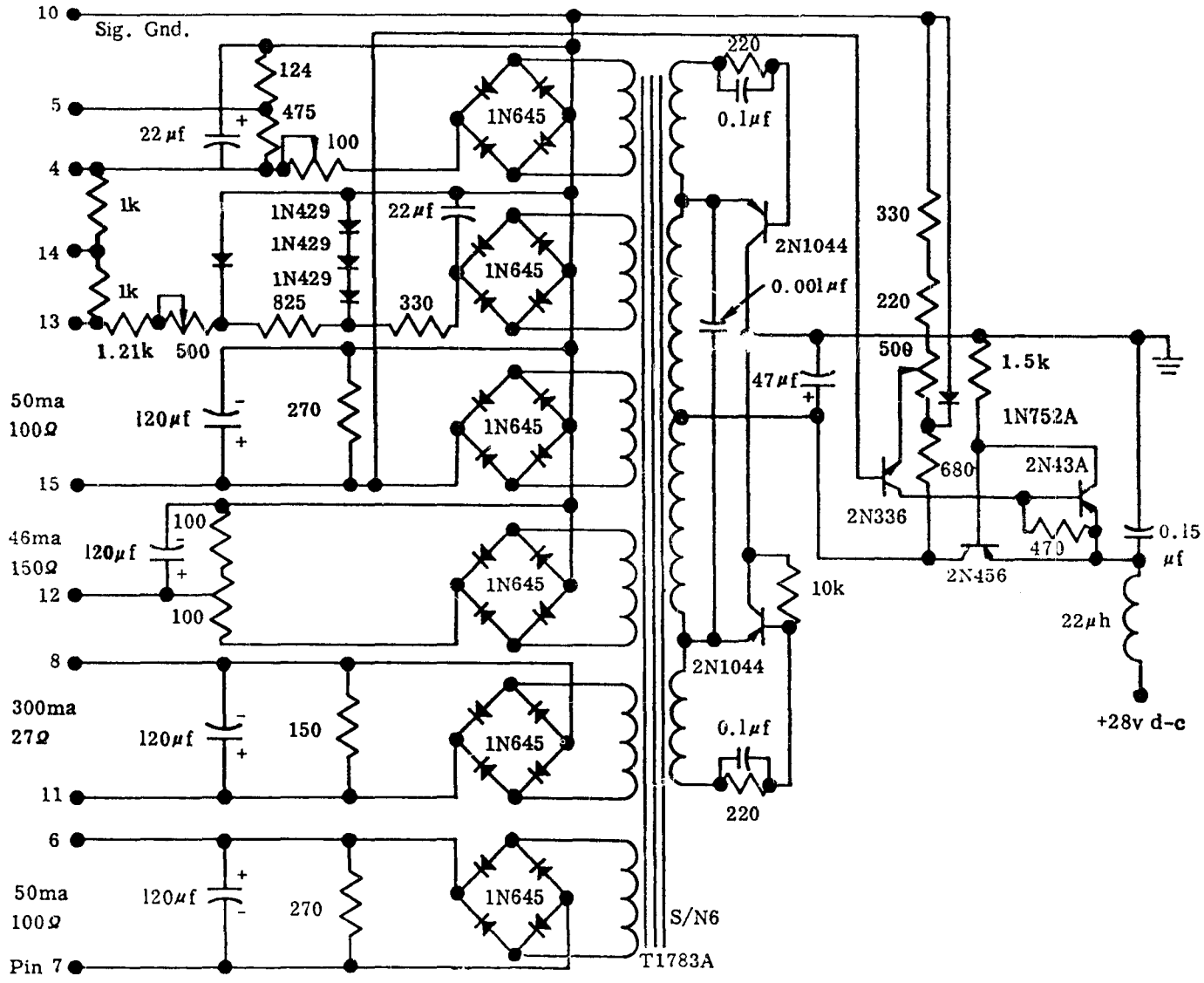



Fig. 16. Transducer power supply Model 55-57

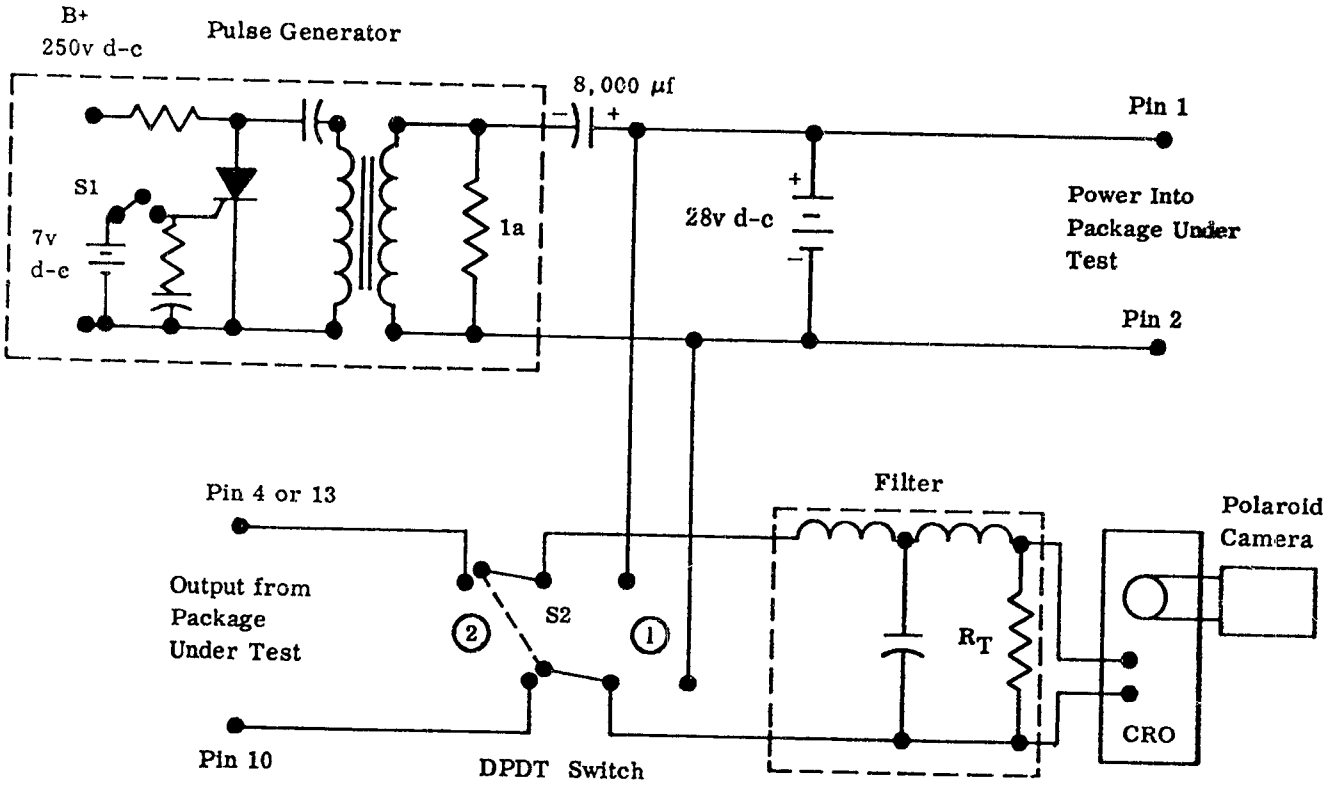
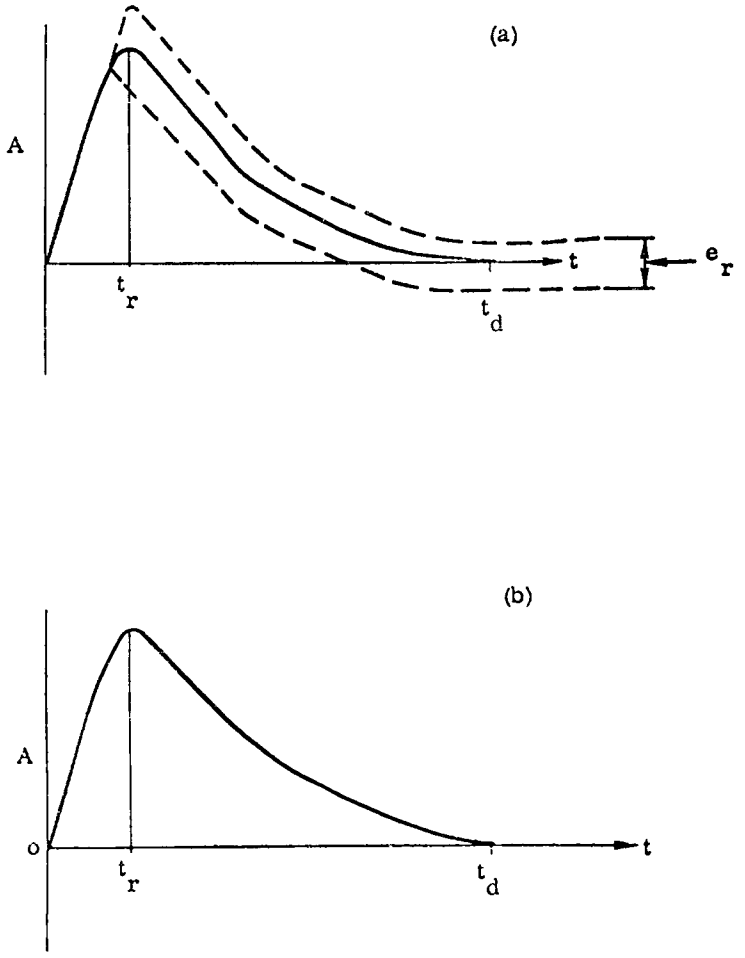



Fig. 17. Transient susceptibility test setup.




$t_r$ = 200 $\mu$ sec.

$t_d$ = 1 m sec.

$e_r$ = Ripple Voltage

Fig. 18. Response wave form measured at terminals 4-10.

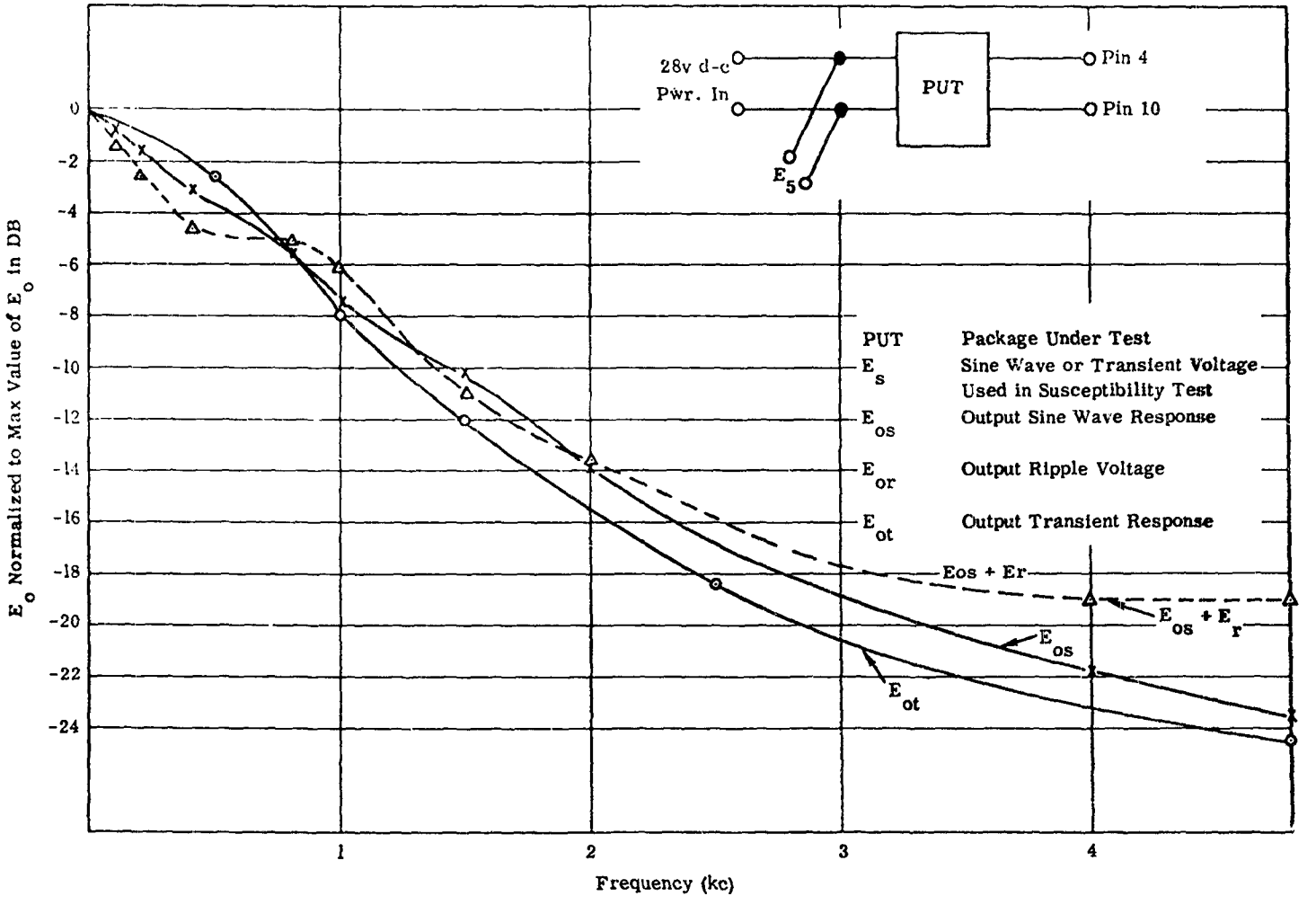



Fig. 19. Sine wave and transient response comparison

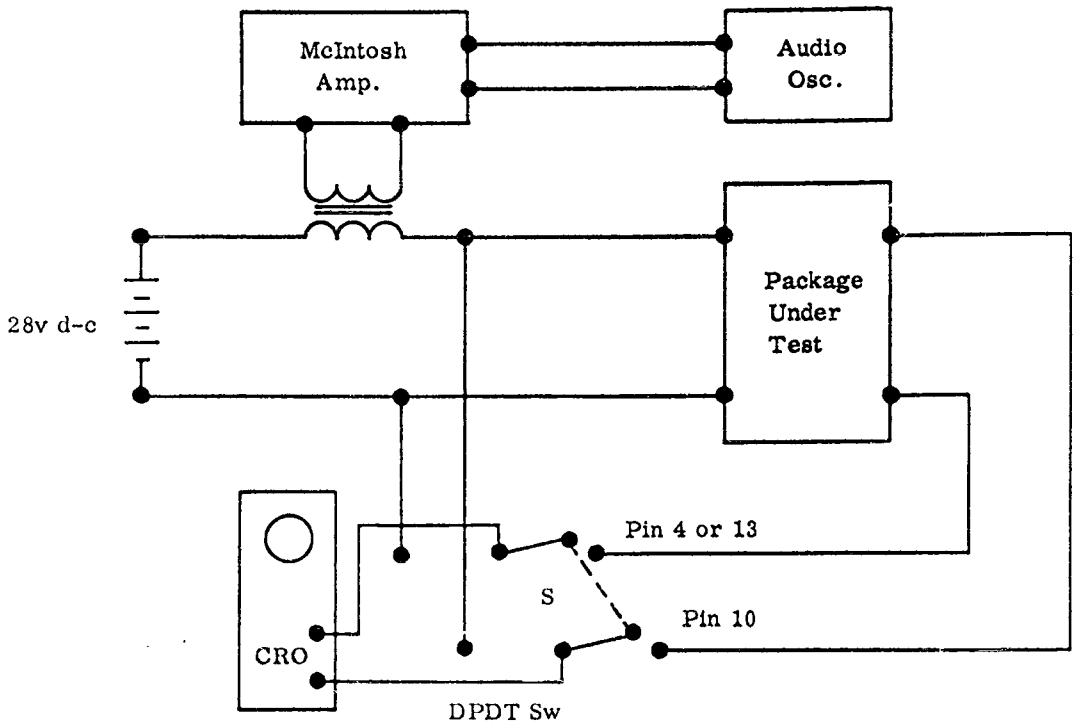
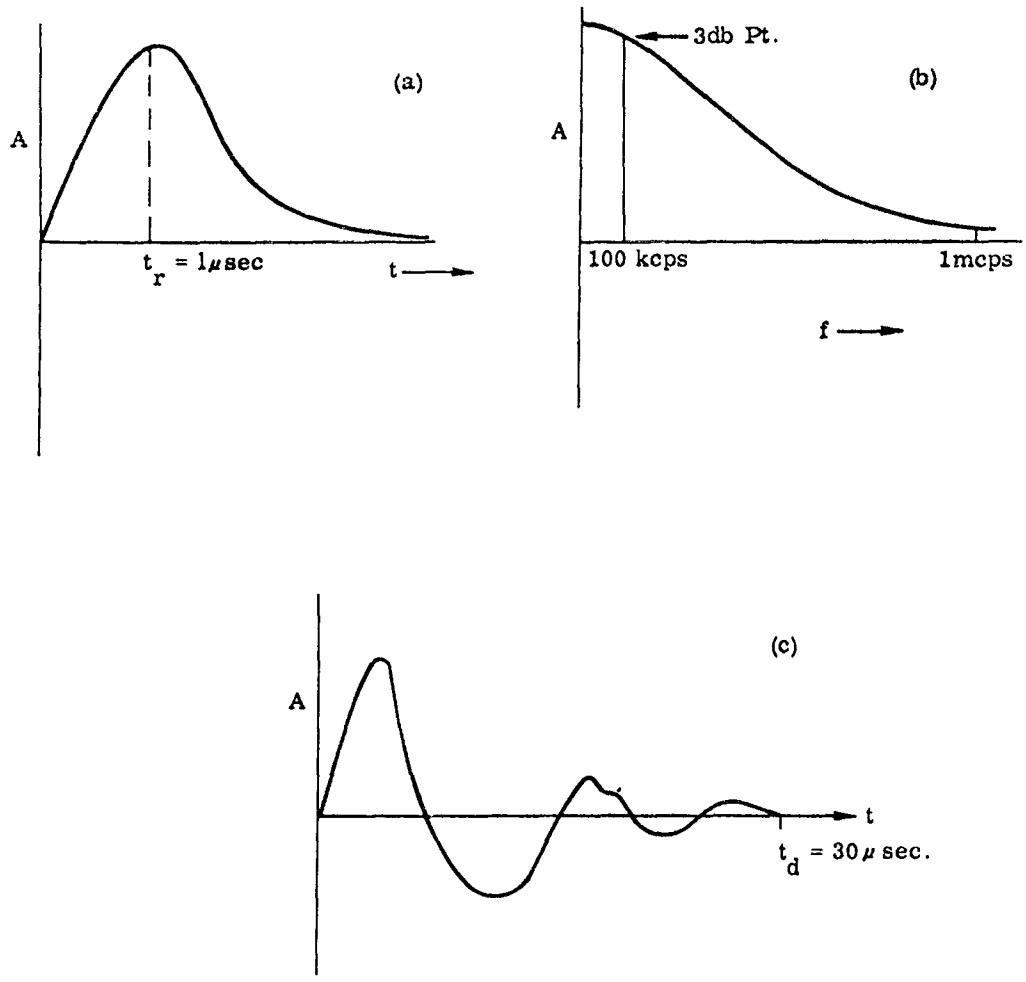



Fig. 20. Sine wave audio susceptibility test setup.




(a) Amplitude vs. Time Plot of Transient Used in Test

(b) Frequency vs. Amplitude Plot of (a)

(c) Response Waveform to (a) at Pins 13-10

Fig. 21, Frequency amplitude characteristics.

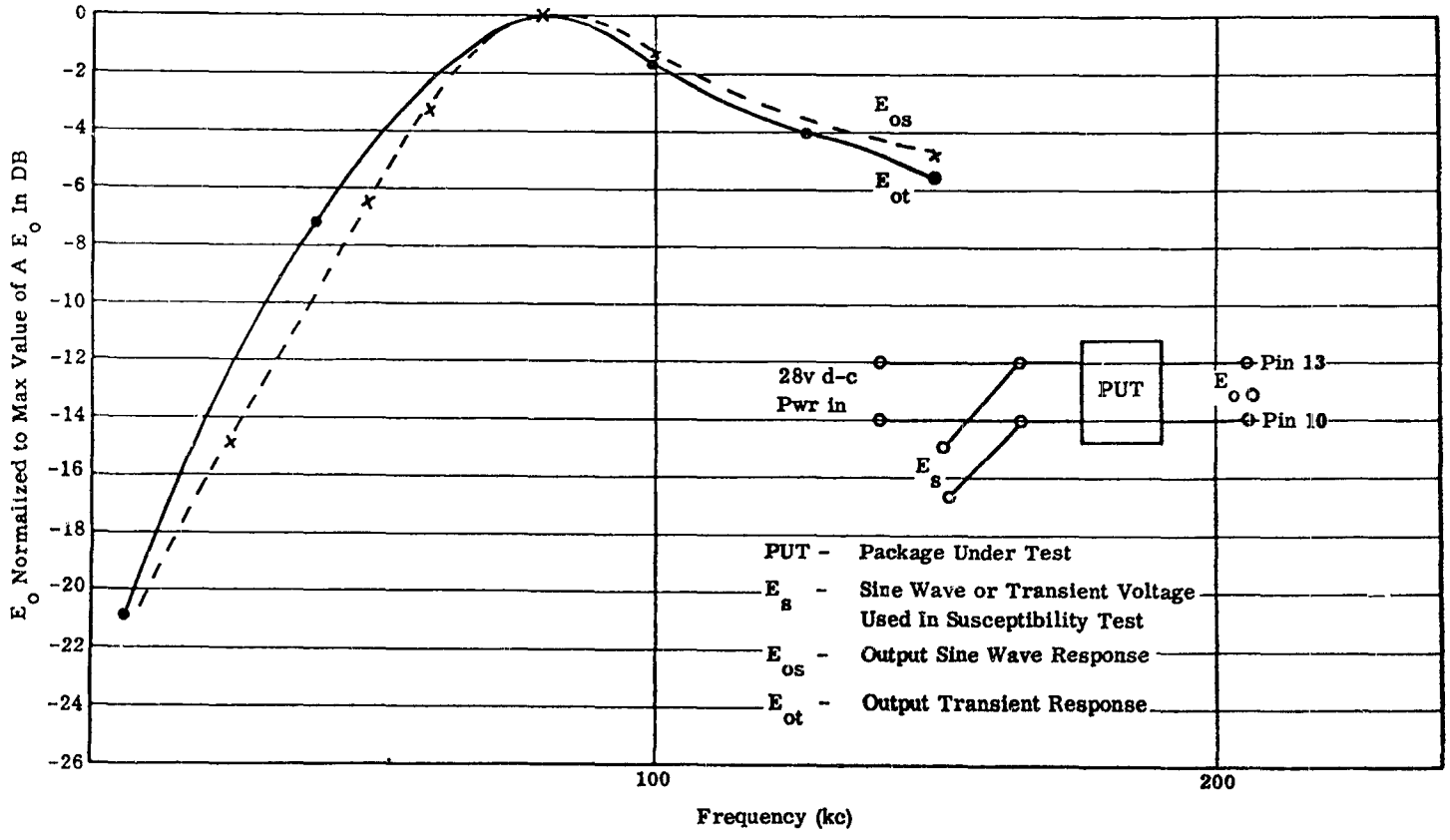
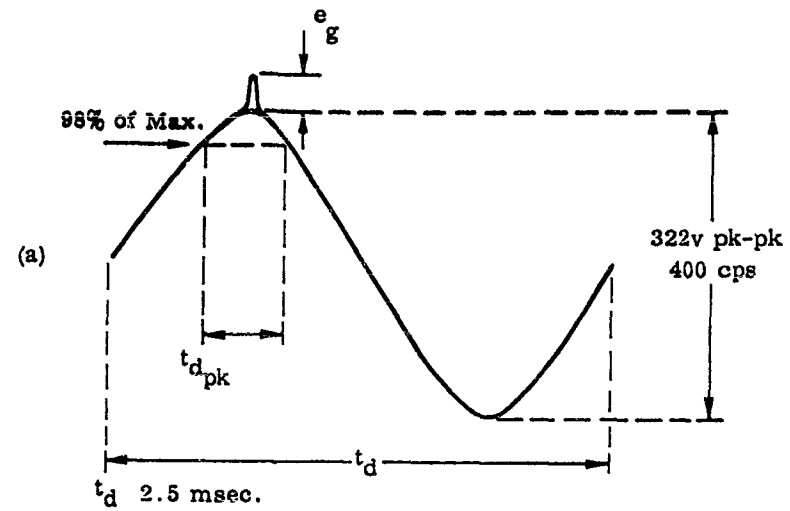



Fig. 22. Sine wave and transient response comparison




Since the peak positive swing reaches 98% of it's peak value in 80° the max. time available to inject the pulse at the peak of the swing is:

$$t_{d_{pk}} \cong \frac{20°}{360°} \times 2.5 \text{ msec.} = 140 \text{ usec.}$$

Viewing the transient on top of the 400 cps then consists of using an oscilloscope sweep rate of 10 usec./cm which makes the transient appear to be impressed on an approximately horizontal axis as axis as pictured below.

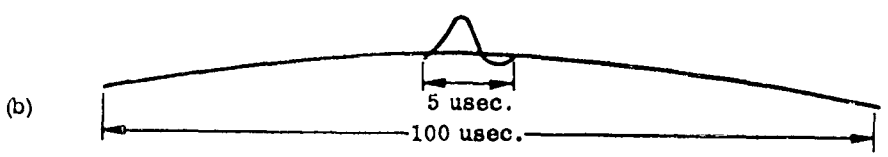



Fig. 23. Transient at crest of positive swing.

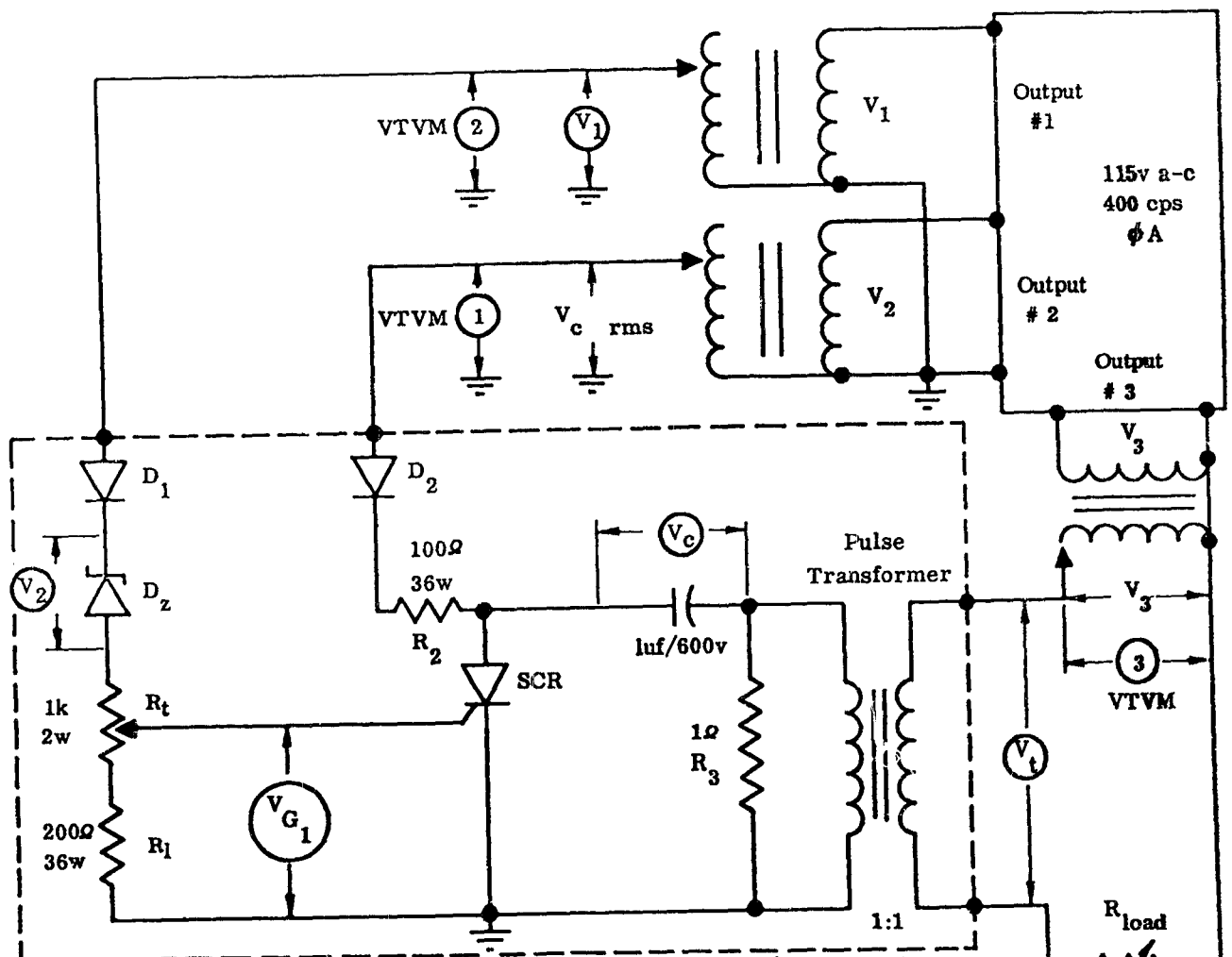



Fig. 24. Pulse injection circuit for 115v power lines.

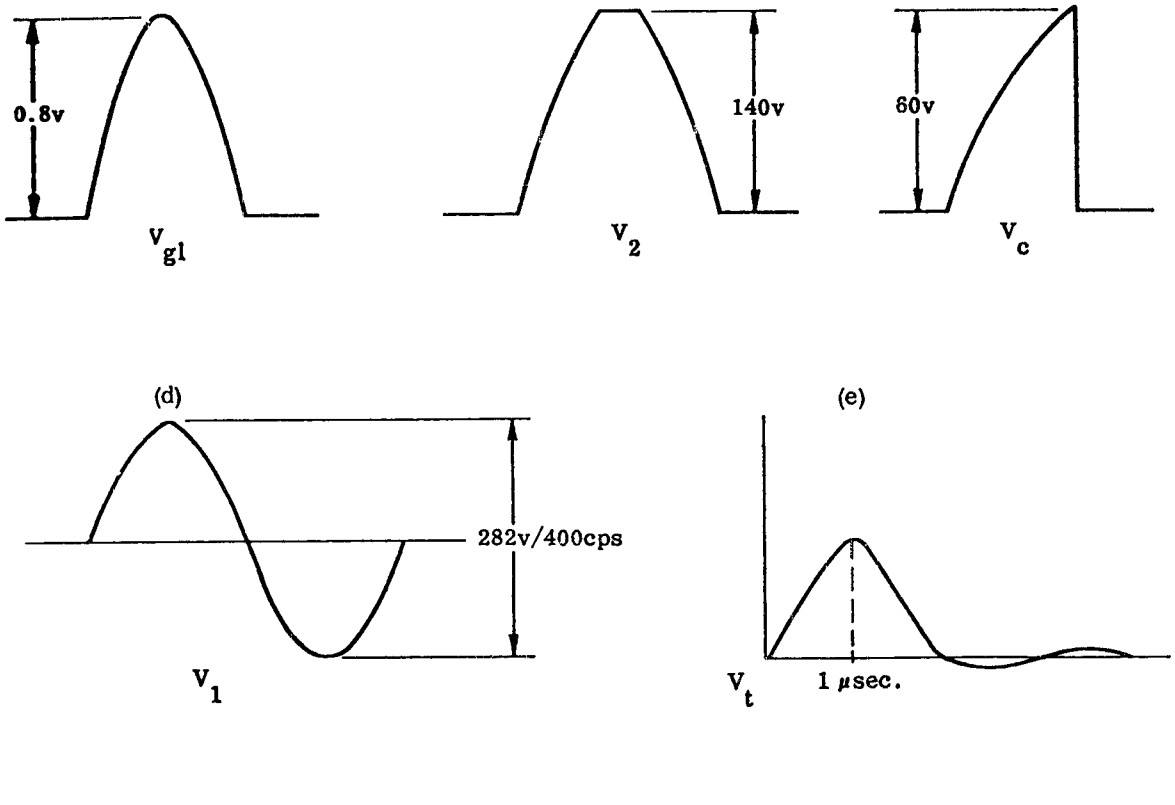



Fig. 25. Waveforms at threshold of transient triggering.

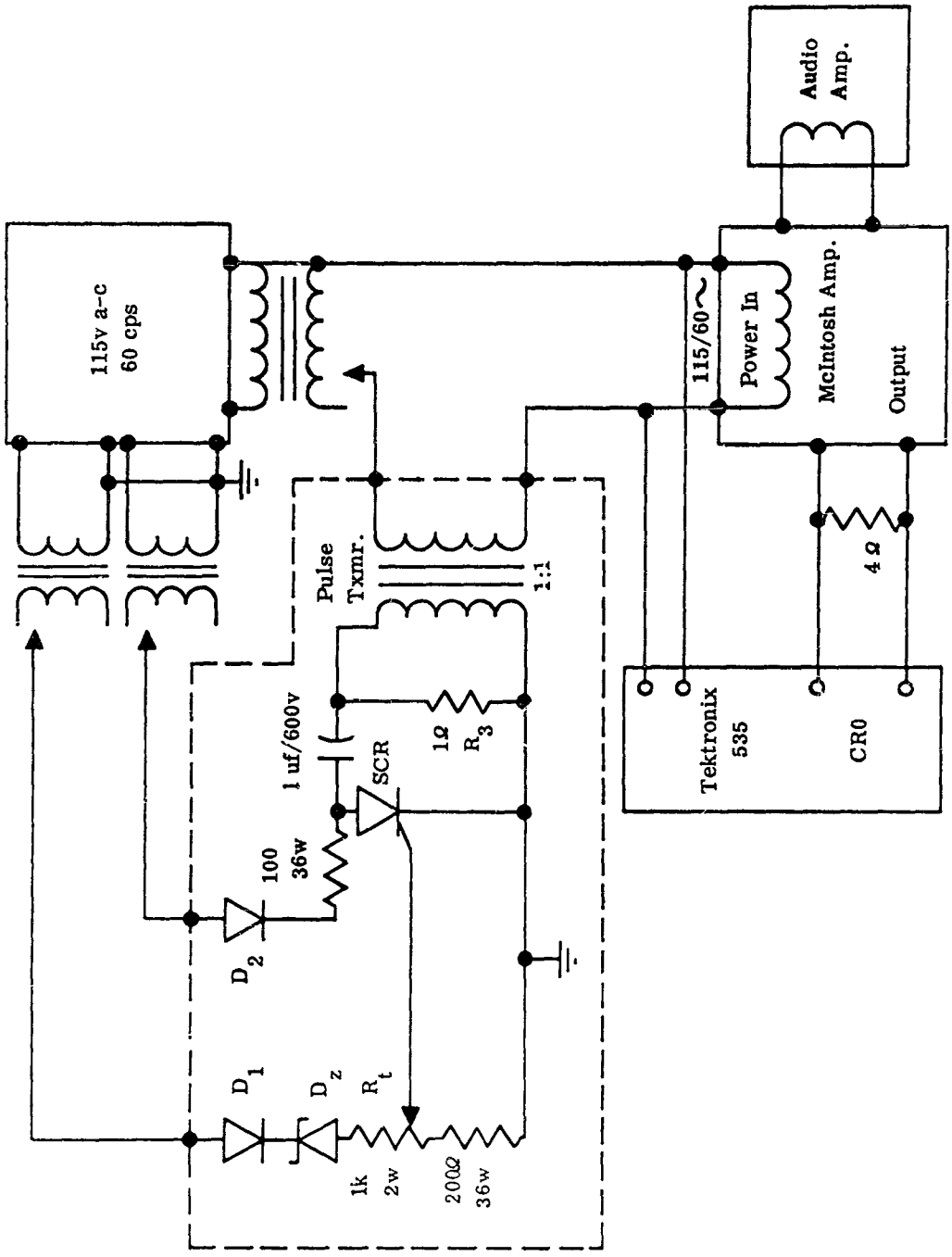



Fig. 26. Transient test on audio amplifier.

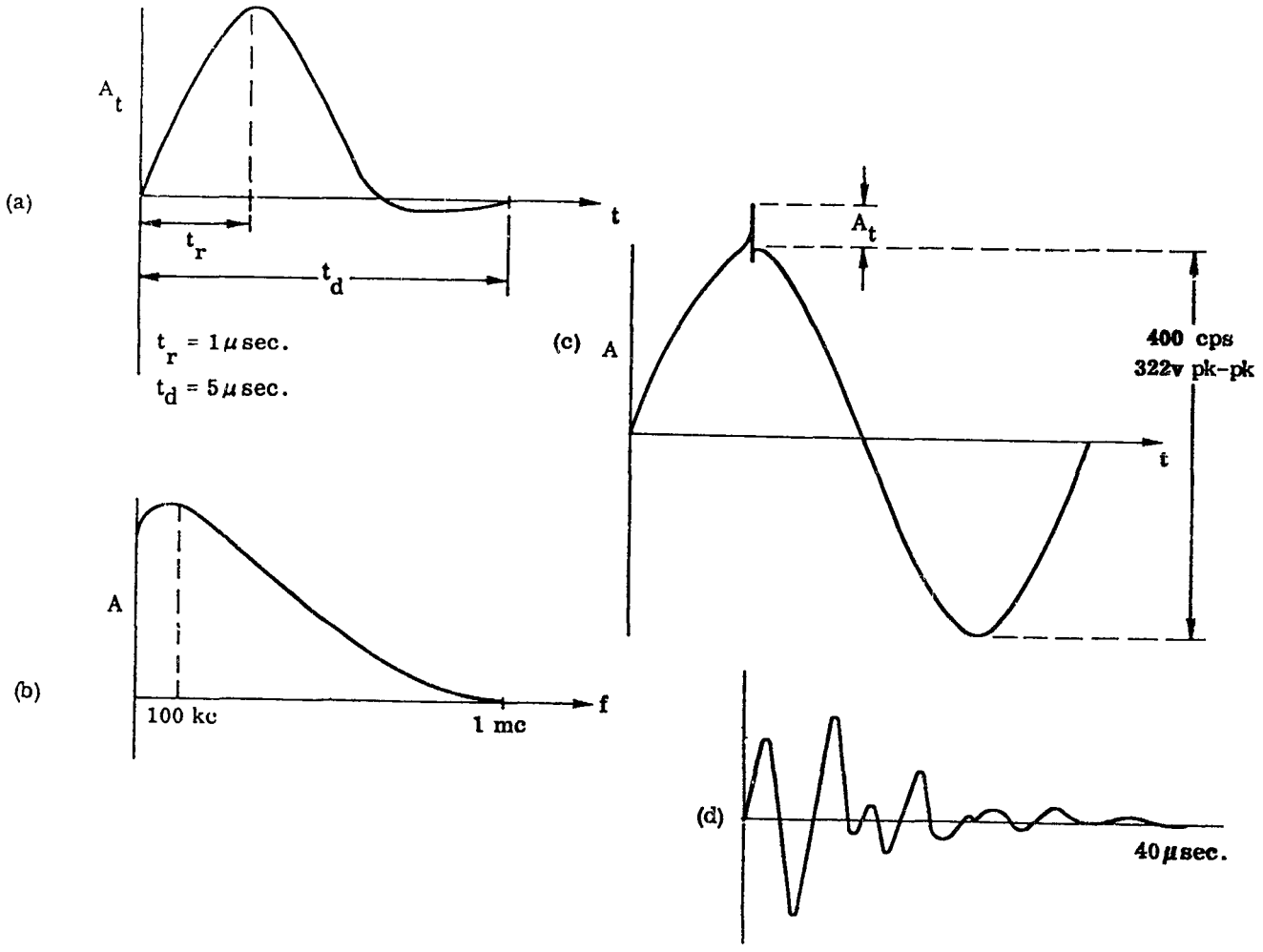



Fig. 27. Transient susceptibility test wave forms.

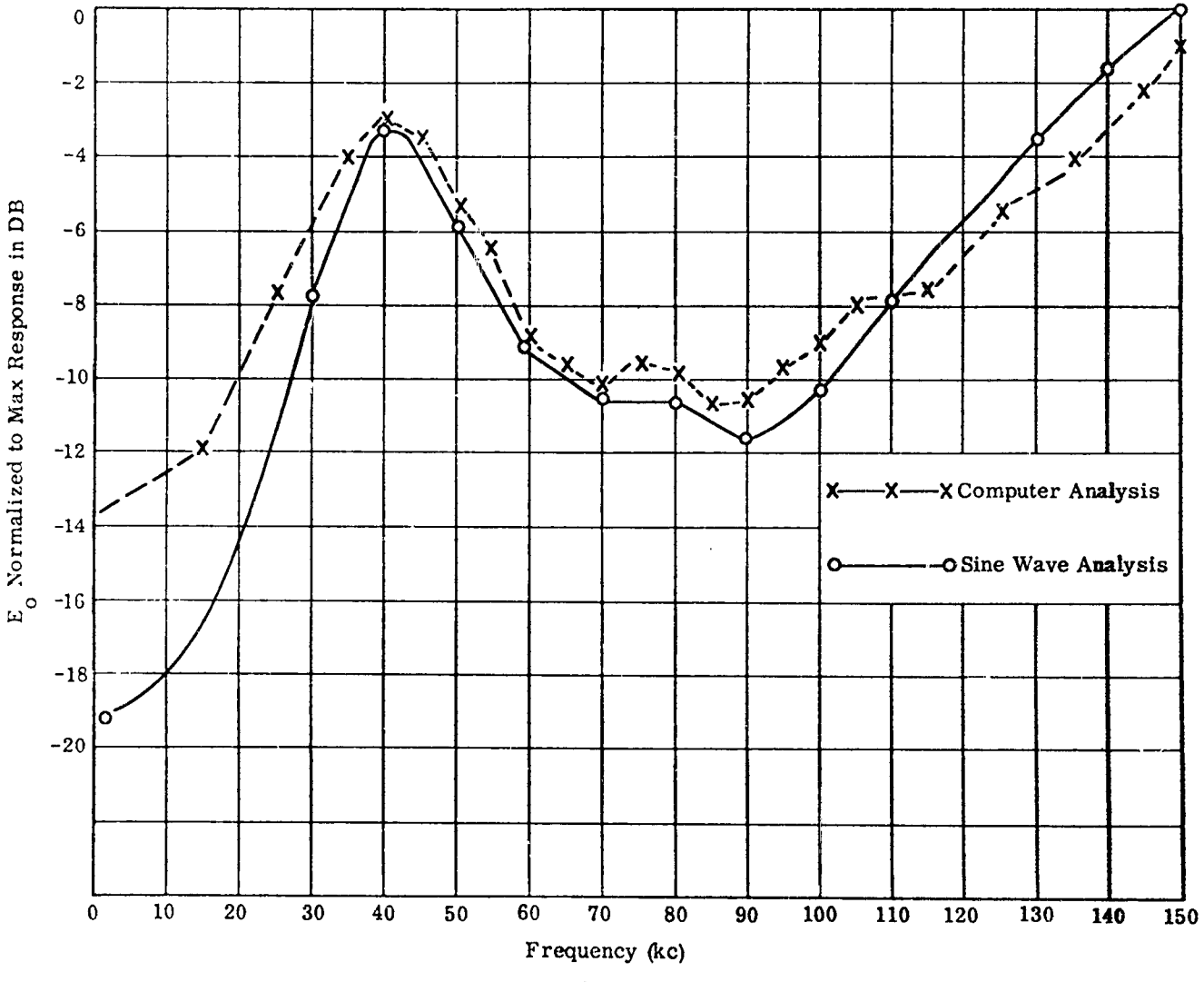



Fig. 28. Frequency response characteristic of McIntosh Model MC-60 power amplifier to sinusoidal and transient susceptibility test functions on the a-c power line.

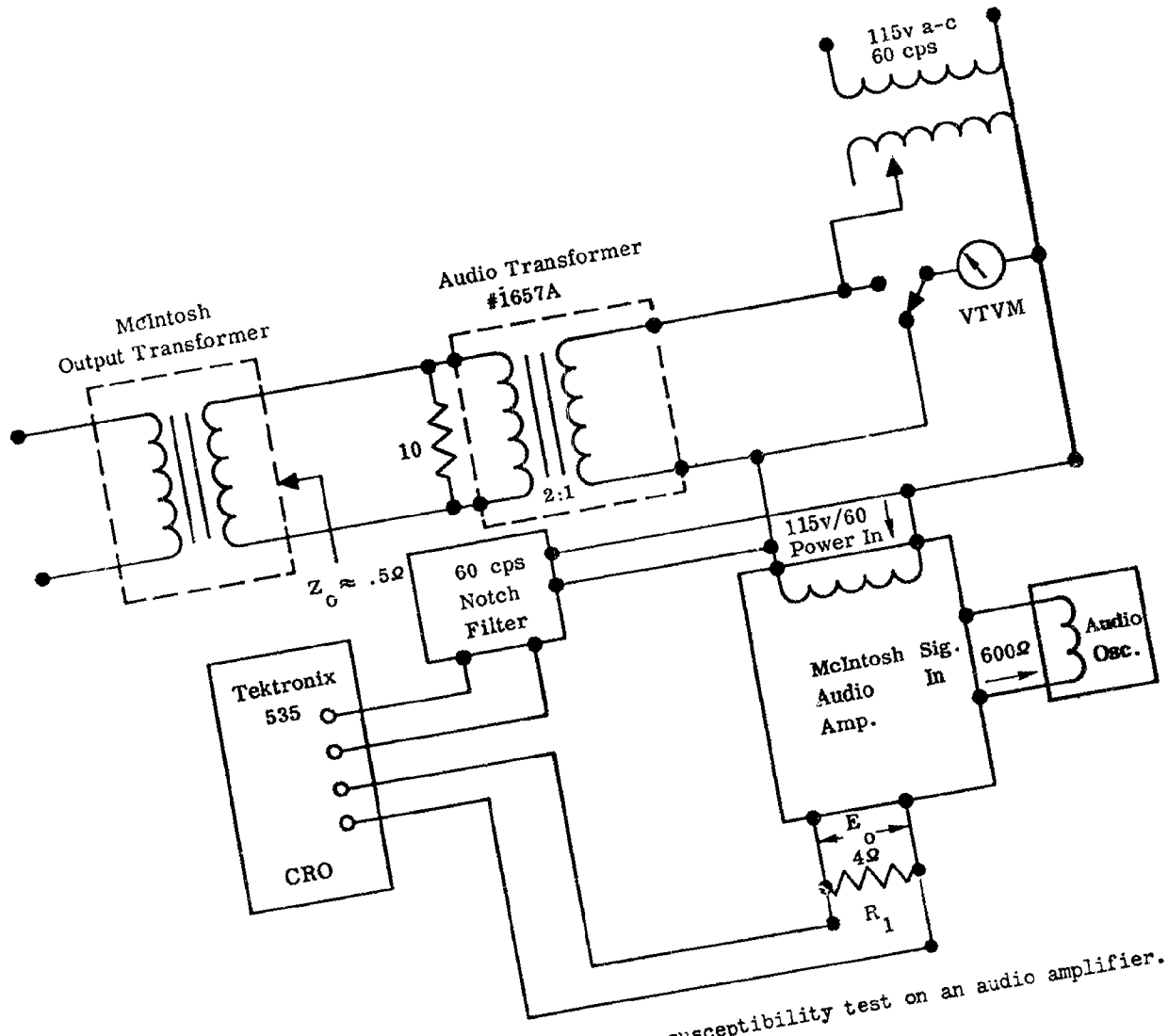



Fig. 29. Test setup for sine wave susceptibility test on an audio amplifier.

# I. INTRODUCTION

Analog methods of reducing a function of time into its sinusoidal components have been used for some time at our installation. During the last year, however, the number of persons who have shown interest in this problem has been on the increase. This, we feel is due in part to our knowledge of the subject, but mostly to the fact that more people are feeling the need for computer methods to do spectrum analysis.

The purpose of this paper will be two-pronged. First, an attempt will be made to show where these problems arise and, second, a description of some of our instrumentation will be given. Our instrumentation of the transform equations using the Convolution theorem is one point that will be covered in detail.

To begin we will define the Fourier Spectrum and explain its meaning in a way which we have found convenient although heuristic.

The Fourier Spectrum of a periodic function (defined as one which has been in existence forever and which will continue to be present forever) is generally described by a single cycle of the wave. An infinite amount of source energy is implied and the representation also contains infinite energy if any energy is used during a single cycle.

The method is as follows: a periodic function, i.e.,

$$f(t) = f(t + n\tau), \quad -\infty < n < \infty \tag{1}$$

where n is an integer may be decomposed into an infinite sum of sinusoids

$$f(t) = C_o + \sum_{k=1}^{\infty} a_K \sin \frac{2\pi k}{\tau} t + \sum_{k=1}^{\infty} b_K \cos \frac{2\pi k}{\tau} t \tag{2}$$

by application of the formulas.

$$C_o = \frac{1}{\tau} \int_o^{\tau} f(t)\, dt \tag{3}$$

$$a_K = \frac{1}{\pi} \int_o^{\tau} f(t) \sin \frac{2\pi k}{\tau} t\, dt \tag{4}$$

and

$$b_K = \frac{1}{\pi} \int_o^{\tau} f(t) \cos \frac{2\pi k}{\tau} t\, dt \tag{5}$$

This expansion is possible since the integral

$$\int_{\tau_o}^{2\pi + \tau_o} \left[\frac{1}{\sqrt{\pi}} \sin n t\right] \left[\frac{1}{\sqrt{\pi}} \sin m t\right] dt + \delta_{nm}, \qquad (6)$$

where n and m are integers. In other words, by assuming that f(t) is periodic and given by the sum (2), it is possible to use (6) to obtain equations (4) and (5) for the coefficients $a_K$ and $b_K$. An artifice is used to obtain the offset, $C_o$,

$$\int_{\tau_o}^{2\pi + \tau_o} \sin nt \, dt = \int_{\tau_o}^{2\pi + \tau_o} \cos nt \, dt = 0; \; n \neq 0 \qquad (7)$$

Another way of stating Equation 6 is to say that the set, sin n t , is orthogonal over any range $[\tau_o \; 2\pi + \tau_o$. $1/\sqrt{\pi}$ is a normalizing constant to make the set orthonormal.

f(t) according to Equation 3 consists of a d.c. component plus sinusoidal components at discrete frequencies $\omega = \frac{2\pi k}{\tau}$. A plot of the magnitude of the sinusoids is often plotted as a function of frequency and is called a spectrum plot. The magnitude at frequency $\frac{2\pi k}{\tau}$ is

$$A\left(\frac{2\pi k}{\tau}\right) = \sqrt{a_K^2 + b_K^2}, \qquad (8)$$

A plot of phase angle vs frequency is also sometimes made. The phase angle is

$$\phi\left(\frac{2\pi k}{\tau}\right) = \tan^{-1} \frac{a_K}{b_K} \qquad (9)$$

A spectrum of the square wave in Figure 1a is shown in Figure 1b.

The Fourier series is not applicable to non-periodic functions. It is modified by a limiting process to the form:

$$F(\omega) = \int_{-\infty}^{+\infty} f(t) \, e^{-j\omega t} \, dt \qquad (10)$$

so that the spectrum is now a continuous function of frequency, $\omega$. This is in contrast to the periodic functions discrete spectrum.

$F(\omega)$ is a complex variable representing the amplitude

and phase of sinusoids at the frequencies $\omega$. If

$$\int_{-\infty}^{\infty} f(t)^2 dt \tag{11}$$

is finite, in other words if f(t) were the voltage across a resistance, the power dissipated in that resistance would be finite, then each sinusoidal component in $F(\omega)$ must have zero amplitude.

This means that the infinite spectrum of a finite energy transient consists of an infinite number of sinusoids packed with infinite density along the axis with each sinusoid having zero amplitude but having different magnitudes relative to one another.

The energy of the approximation must be the same. If f(t) is considered to be the voltage across a 1-ohm resistor, the squared spectrum, $|F(j\omega)|^2$ vs $\omega$, is the energy density spectrum, a direct indication of the energy dissipated in the one ohm resistor as a function of frequency.

The area under the curve between $\omega_1$ and $\omega_2$ is proportional to the total energy of all frequencies within these limits. The total energy is proportional to the total area under this curve:

$$\mathcal{E} = \int_{-\infty}^{+\infty} f(t)^2 dt = \frac{1}{2\pi} \int_{-\infty}^{\infty} |F(j\omega)|^2 \, d\omega \tag{12}$$

For example: the transient defined as

$$f(t) = \begin{cases} 0 & t < 0 \\ e^{-at} & t > 0 \end{cases} \tag{13}$$

has a spectrum

$$F(j\omega) = \frac{1}{a + j\omega}$$

$$|F(j\omega)|^2 = \frac{1}{a^2 + \omega^2} \tag{14}$$

then

$$\mathcal{E} = \int_{0}^{\infty} e^{-2at} \, dt = \frac{1}{2\pi} \int_{-\infty}^{\infty} \frac{1}{a^2 + \omega^2} \, d\omega = \frac{1}{2a} \tag{15}$$

The spectrum of the square pulse of Figure 2a is shown in Figure 2b.

## II. TRANSIENT ANALYSIS

Transients can arise both naturally and by being forced in all physical systems. Their form may be energy, potential, displacement, velocity, thermal, electrical, mechanical, etc. They may be functions of time or even of a time independent variable although time dependency is the most common.

The reasons for decomposing transients into a sum of known functions are varied. Ones which have come into our laboratory in the last few months have been

1) Determination of the energy spectrum of a transient received on an antenna and recorded on an oscillograph recording so that an optimum (signal/noise) filter can be designed.

2) Determination of the spectrum of a magnetic transient resulting from a physical experiment where it was expected that currents taking circular paths were causing the magnetic transient. The spectra then tells how much current was flowing at each radius.

3) Determination of the input voltage spectra and output voltage spectra of linear networks to determine interference susceptability of the networks. This appears to be a problem in a production area. It will be discussed in greater detail for this reason later in the paper.

4) Determination of the amount of fundamental which is present at the output of a non-linear filter.

5) Determination of the frequency characteristics of various linear transducers as prerequisite to building inverse filters. This will also be discussed in greater detail.

6) Determination of the input and output spectrum of a very low frequency filter to determine the filter characteristics. Steady state methods were impractical because of time required - frequencies were .001 to 1 cps and measurement time was two hours per filter.

All of the transients were supplied to us as curves or as actual transient voltage vs time. In all cases we converted the data to voltage vs time information. If an analog solution is performed, this data is used directly. If a digital computer solution is required, analog to digital converters are used and the point data

is stored in digital memory.

The above list of six items is only a sampling of the ways in which the problem arises. Other situations are listed in the literature: for which: see the accompanying bibliography.

At this point we will discuss problem types 3 and 5 which involve finding the frequency characteristics of a linear system between two input terminals and two output terminals.

Figure 3 gives some idea of the types of systems which generate this problem. Note that energy form transformations may take place inside the system.

The systems of Figure 3 have one thing in common. They distort the source data. Sometimes this distortion is desirable - improving signal to noise ratio. Sometimes it is undesirable - the thermal inertia of a thermocouple metering a high speed temperature change.

These distortions can be of two types: linear and non-linear. Simply put, the difference between a linear and a non-linear distortion is this: the output level, of a linear system is linearly proportional to the input level (even though they don't look the same) whereas the output level of a non-linear system is not linearly proportional to the input. A large number of systems are linear or at least are nearly linear over some range of input levels. Linearity of a system can be checked empirically by increasing the drive and seeing if the form of the output remains the same and proportional to the input level.

The effects of linear distortion can be removed by placing an inverse filter in the instrumentation chain. The inverse filter has the exact opposite frequency effects of the system. That is, ideally it should have the opposite effect. Certain limitations enter, usually either reliability criteria or noise problems. Figure 4 shows the effect of a sluggish system on data. This problem is amenable to solution by Fourier Spectrum analysis.

The effect of a pure non-linear distortion can be removed by building a non-linear black box which again does the opposite thing from the system. For example, if the system squares the source values, the black box square-roots the system output and this output is then a faithful representation of the input. This is shown in Figure 5. This will not be covered further.

The analysis and synthesis of black boxes which produce both linear and non-linear distortions is beyond the scope and purpose of this paper. A method is mentioned by: Norbert Wiener, Nonlinear Problems in Random Theory, The Technology Press of MIT and John Wiley and Sons, Inc., N. Y., pgs. 97-100.

The first problem in describing the frequency characteristics of a system is generally the instrumentation of a physical

test of the system. Some systems can be solved theoretically. These will not concern us especially since the number that cannot be solved is by far the majority.

If the source can be made to present a sinusoidal drive to the system then the frequency effect of the system is the amplitude and phase shift between input and output. The system gain then has two values:

$$A(\omega_o) = \text{amplitude gain} = \frac{\text{output sinusoid magnitude}}{\text{input sinusoid magnitude}} \tag{16}$$

$\phi(\omega_o)$ phase shift = shift (output-input) in degrees.

of, in complex variable terms, the complex gain is

$$G(\omega) = \frac{A_o e^{i\phi_o} e^{i\omega t}}{A_1 e^{i\phi_i} e^{i\omega t}} = \frac{A_o}{A_i} e^{i(\phi_o - \phi_i)} \tag{17}$$

where $A_1$ and $A_o$ are the input and output levels respectively and $\phi_1$ and $\phi_o$ are their phase angle. $e^{i\omega t}$ is the unit sinusoid which cancels in the equation.

$G(\omega)$ is then plotted as a function of $\omega$, and is the frequency response of the system.

The steady state method is often impractical because mechanical or thermal sinusoids are not always readily available.

Transients are generally available. These are used in the second method to obtain the curve $G(\omega)$ vs $\omega$. The philosophy here is as follows: a transient is composed of an entire spectra of sinusoids. If the amplitude and phase of these sinusoids are known for both the input and the output transient then in the same sense as the steady state case, the system frequency response is known. Thus, if an input transient has a spectrum $I(\omega)$ and the output spectrum is $\phi(\omega)$, then the system gain is:

$$G(\omega) = \frac{\phi(\omega)}{F(\omega)} \tag{18}$$

The single transients contain all the frequency data, both amplitude and phase, for all frequencies present in the input, transient. Zero content of a set of frequencies at the input leads to an indeterminate gain value at those frequencies.

The transient method is instrumented as follows:

1) The input of the system is forced with a transient which is know or which can be recorded faithfully.*

*Faithfully can be taken to mean that the recorder may cause linear distortion but that this distortion is known and can and will be removed by inverse filtering.

2) The output of the system, a transient is recorded faithfully.*

3) These transients are then resolved into their spectral components by computer methods.

4) The complex gain of the system is the quotient of the output spectra divided by the input spectra. In other words, the spectra are divided at each frequency.

## III. COMPUTER METHODS OF FINDING THE FOURIER SPECTRUM

The frequency domain representation of a transient f(t) is given by Equation 10. The alternate form is

$$F(\omega) = \int_{-00}^{00} f(t) \cos \omega t \, dt - i \int_{-00}^{00} f(t) \sin \omega t \, dt \quad (19)$$

This is a form amenable to solution on either analog or digital computers when is treated as a constant. If f(t) is a simple enough transient it can be expressed mathematically and an analytic solution is possible. We haven't found enough of these to recommend trying to find an expression for f(t), although the method is valid and can be used for approximating.

The phase response of this transient is

$$\phi(\omega) = \tan^{-1} \frac{\int_{-00}^{-00} f(t) \sin \omega t \, dt}{\int_{-00}^{00} f(t) \cos \omega t \, dt} \quad (20)$$

and the amplitude response is

$$A(\omega) = \left[ \left( \int_{-00}^{00} f(t) \cos \omega t \, dt \right)^2 + \left( \int_{-00}^{00} f(t) \sin \omega t \, dt \right)^2 \right]^{1/2} \quad (21)$$

These are computed for values of in an range specified by the requirements of the analyses.

Both trapezoidal rule and Weddle's rule integration have been used to evaluate $\Theta(\omega)$ and $A(\omega)$ on the digital computer

*Faithfully can be taken to mean that the recorder may cause linear distortion but that this distortion is known and can and will be removed by inverse filtering.

after digitalizing f(t). This resulted in good accuracy for band limited transients where the sampling rate is at least twenty times the maximum frequency using the trapezoidal rule or ten times when using Weddle's rule.

Analog methods using active computer elements have been found to be sufficient or more than sufficient for most of the transient computations which we have had. The analog solutions have been comparable with digital solutions when using transients recorded by oscilloscopic photographs. They have been more than comparable when using perfect data when the digital sampling rate was too low, i.e., non-band limited or just plain not enough samples.

A variety of digital integration schemes are available in books on numerical analysis. J. M. Salzer [2] described a method by which these schemes can be analyzed in the frequency domain so that an intelligent choice of sampling rate may be made.

A brute force and a filter scheme have been used to reduce transients on the analog computer. In the brute force method, shown in Figure 6, equation 19 is solved by integrating the product f(t) sin $\omega$ t and f(t) cos $\omega$ t over the interval in which f(t) is non-zero and resolving the vector relation into terms of A and $\theta$ with a servo resolver.

Frequency limitations and other errors in forming the f(t) sin $\omega$ t and f(t) cos $\omega$ t product somewhat limited the accuracy.

The filter method is a by product of the filter convolution theorem (appendix A) which states that the output of a filter which has an impulse response of h(t) to an input f(t) is

$$O(t) = \int_{-\infty}^{t} f(\tau)\ h(t-\tau)\ d\tau\ , \qquad (22)$$

or at zero time is

$$O(o) = \int_{-\infty}^{o} f(\tau)\ h(-\tau)\, d\tau\ . \qquad (23)$$

This is identical to equation 19 if h($-\tau$) is made to be sin $\omega$ t (cos $\omega$ t) and if f(t) is zero for all positive time.

Now the requirement of f(t) being zero for all positive time seems like an unrealistic type of restriction since most transients don't begin until zero reference time. It isn't a strict requirement though. Most transients can be shifted, f(t + a) or mirrored about the t = 0 axis, f(-t), so that they have zero value for all positive time.

A shift, as shown in Figure 7, causes the phase angle of the spectrum to vary proportionally to frequency and has no effect on the spectrum amplitude.

A mirroring about the t = 0 axis changes the spectrum to its conjugate. The amplitude response is not changed but the phase angle now has a negative sign in front. See Figure 7.

Figures 8 and 9 show the ways in which a transient can be reduced to its spectrum using analog components. Circuits 8 and 9 can be used interchangeably when the phase angle is not of importance.

For computation, the transient may be generated by either an analog function generator, or if the time relations are acceptable, the data from the source is wired into the machine. An automated set-up which plots $A(\omega)$ vs $\omega$ by incrementing $\omega$ was used to plot Figure 10, the response of a unit height rectangle of 1 second duration. Figure 12 shows the schematic of the automated system.

Several pulse forms have useful properties. For example, the spectrum of a short pulse of unit area approaches a constant value for all frequencies. A pulse of width b has a spectrum $\sin \frac{\omega b}{2}$ which is constant to within 2% up to a frequency $\frac{2}{\omega}$ of $\frac{2\pi}{10\ b}$ cps. This is useful because it eliminates the division operation of Equation 18. The output spectrum is the spectrum response of the system if the input spectrum can be called flat over the range of interest.

Of course, many other short pulses can be used in the same way.

The step function has a spectrum given as $\frac{1}{j\omega} \cdot 1$ Division of the output spectrum by the input spectrum is simply done. Also, this function is probably the easiest of all to generate.

## IV. SIMULATION

In order to take advantage of the theoretical concepts previously stated an automated computer program was prepared and patched. Different computers may require different sequencing or special external sequencing may be more practical.

First a block diagram in Figure 11 will be explained, then an explanation will be made of Figure 12 which is a detailed analog computer diagram.

There are several ways that a real time function may be recorded in real time and then played back in computer time. The ratio of the recording time to the play back time is called a scaling

factor. One method requires the use of a scope camera (preferably a polaroid). The sweep rate of the oscilloscope becomes the recording time. After developing the picture the area above the scope trace is cut out and the photo is used in a photoformer function generator. The time base t drives the photoformer whose output f(t) is in computer time. Other function generators can be used. The important thing is that the function f(t) is synchronized in some sense with the time base t. Examples other than the photoformer are: DIODE function generator, tape recorders, and oscilloscopes equipped with display scanners. If an oscilloscope that is equipped with a display scanner is used the time base t drives the horizontal sample rate. Oscilloscopes so equipped are generally used for recording the functions appearing on the cathode ray tube's face on a x-y recorder. The y output of the display scanner is the time scaled function. Therefore, the sweep rate is the real time and the time base t is computer time.

The time base t also determines when the coefficient computing box labeled $\int_{-\infty}^{0} f(t)\, e^{-j\omega t}\, dt$ begins to integrate and when it terminates. The time base also determines the time at which to plot the computed coefficients.

The $\omega$ base determines the coefficient, $\omega$ , of transformation $\int_{-\infty}^{0} f(t)\, e^{-j\omega t}\, dt$. If a function whose Fourier coefficients decays at a rate of $\frac{1}{f}$ then $\omega$ may be used as a multiplier of the function, i.e. compute $\int_{-\infty}^{0} f(t)\, e^{-j\omega t}\, dt$ in order that any deviation may be detected from the $\frac{1}{f}$ spectrum. The $\omega$ base also controls the x position of the recorder so that a $F(\omega)$'s $\omega$ readout is plotted.

The right triangle symbolizes a resolver used for translating from rectangular coordinates to polar coordinates. The purpose of this was explained earlier in the test where

$$\sqrt{a_K^2 + b_K^2} = A\left(\frac{2\pi k}{\tau}\right)$$

and

$$\phi\left(\frac{2\pi k}{\tau}\right) = \tan^{-1} \frac{a_K}{b_K} .$$

Since this resolver solution is essentially a static measurement maximum accuracy may be expected. One or two recorders have been used depending on whether both phase and magnitude were desired; one recorder if just magnitude is required. The base controls the x axis and the resolver output controls the y axis while the time base t controls the pin in its up or down write mode.

Figure 12 and the following explanation of the sequencing logic demonstrates an approach rather than an optimized circuit. An enumeration of the sequencing is as follows:

1. Integrator number one generates the time base. The Potentiometer numbered 42 is an initial condion for the function generators.

2. Comparator amplifier number 21 drops the recorder pin, energizes the hold buss, and provides voltage for the sequence timer.

3. Integrator number two is connected so that its normal switching functions are independent of the control busses.

4. Comparator-amplifier number 22 prevents the outputs from integrators 11 and 12 from driving the servo resolver before the solution of the Fourier coefficient is found. This saves wear and tear on the resolver and the x-y recorder.

5. After comparator 22 allows the Fourier coefficient to be plotted comparator 23 lifts the recorder pin and takes over the task of a voltage to integrator 2.

6. Comparator 24 provides integrator three with an exponential pulse. The output of integrator three is the frequency base . While the value of is being changed comparator 24 is also supplying a voltage to the control buss which causes all integrators connected to the conventional control buss to change from hold to reset mode.

7. Comparator amplifier number 25 lets the computer change from the reset to the hold condition long enough for switching transients to decay.

8. Comparator amplifier number 26 allows the computer to start the next computation cycle as well as resetting integrator #2 to its initial condition.

9. Comparator amplifier number 27 is an automatic shutoff so that the computer will remain in the reset condition after the last value of has been computed.

10. Comparator amplifier 28 is used to generate a test function that has a known Fourier spectrum.

## V. DISCUSSION

This paper has been tutorial in nature and references

were not included in the text. The number which could have been cited at many points were very large as much of this material has appeared in text books for many years. The "bibliography" included at the end, although short, should be of interest to those wishing to read further. References 6 and 7 are especially useful as they provide additional examples in a method similar to that presented in this paper.

## APPENDIX A

## USE OF THE SUPERPOSITION THEOREM FOR EVALUATING THE FOURIER SPECTRUM

1. The infinite Fourier spectrum of a function f(t) is defined

$$F(\omega) = \int_{-\infty}^{\infty} f(t)\, e^{-j\omega t}\, dt$$

or alternately

$$F(\omega) = \int_{-\infty}^{\infty} f(t)\, \cos\omega t\, dt \; -i \int_{-\infty}^{\infty} f(t)\, \sin\omega t\, dt$$

This may be evaluated directly using either analog or digital methods by integrating the products f(t) cosωt and f(t) sinωt over the range in which f(t) has a non zero value.

A simpler analog method exists, however, which eliminates multiplication and integration in favor of filtering.

2. First, consider the effects of modifying the function f(t) by shifting it to be f(t + a) or inverting it so that it mirrors itself about the t = 0 point i.e., f(-t). The reason for this is that the transient needed for the analysis must be zero for all positive time.

Consider a shift first: By definition,

$$F(\omega) = \int_{-\infty}^{\infty} f(t)\, e^{-j\omega t}\, dt$$

For the shifted function,

$$F_s(\omega) = \int_{-\infty}^{\infty} f(t + a)\, e^{-j\omega t}\, dt$$

$$= e^{j\omega a} \int_{-\infty}^{\infty} f(u) e^{-j\omega u}\, du$$

This equals $e^{j\omega a}\, F(\omega)$

Thus, a shift in the origin of f(t) results in a phase shift in its spectrum which is linearly proportional to frequency. If phase relations are not of interest, the shifted spectrum amplitude is identical to the original. In any case, nothing is lost and corrections for shift are simple to make.

Next, consider a reversal in direction; by definition,

$$F_R(\omega) = \int_{-\infty}^{\infty} f(-t)e^{-j\omega t}\, dt$$

$$= \int_{-\infty}^{\infty} f(u)e^{j\omega u}\, du$$

or if $F(\omega) = A + i\,B$ ,

then $F_R(\omega) = A - i\,B = \overline{F(\omega)}$

The amplitudes are the same at all frequencies but the phase is inverted.

In general, transients may be shifted or reversed so that they have zero value for either all negative time or all positive time. The Fourier spectrum then can be one-sided, i.e.,

$$F(\omega) = \int_{-0}^{\infty} f(t)e^{-j\omega t}\, dt$$

See Figure 1.

The Superposition Theorem which relates the output of a filter to its input is derived from the impulse response of the filter. The input to the filter is assumed to be broken into a succession of elementary rectangular pulses applied at intervals of $\Delta\tau$ along the time axis. Each of these pulses when applied to the system produces an elementary response, the sum of these responses being the output. As the interval length, is made to approach zero, the response produced approximates the impulse response of the filter to a greater and greater degree.

If the impulse response of a filter is g(t) when the impulse is applied at zero time, it is $g(t-n\Delta\tau)$ if the impulse is applied at a time equal to $n\Delta\tau$. The height and width of the nth pulse are $f(n\Delta\tau)$ and $\Delta\tau$ respectively where f(t) is the input function. Thus,

the elementary response caused by the rectangle at time $n\Delta\tau$ is $f(n\Delta\tau)\Delta\tau \quad g(t-n\Delta\tau)$.

The response at any time, t, is considered to be the limit of the sum of all the elementary rectangles applied between -oo and t as $\Delta\tau \to 0$, i.e., the output, h(t), is:

$$h(t) = \lim \sum_{\tau=n \quad \Delta\tau=-oo}^{t} f(\tau)\Delta\tau\, g(t-n\Delta\tau)$$

where $n\Delta\tau$ is adjusted so that as $\Delta\tau$ decreases, the value of n increases so that the product remains at a fixed time, $\tau$ .

The limit is;

$$h(t) = \int_{-oo}^{t} f(\tau) \quad g \quad (t-\tau) \quad d\tau .$$

For the purpose of obtaining the Fourier spectrum, we will evaluate the integral at t = 0, i.e., zero time,

$$h(0) = \int_{-oo}^{o} f(\tau) \quad g \quad (-\tau) \quad d\tau .$$

With the forcing function reversed from its normal direction in time this becomes

$$h(0) = \int_{-oo}^{oo} f_R(\tau) \quad g(-\tau) \quad d\tau .$$

or;

$$h(0) = \int_{o}^{oo} f_R(\tau) \quad g(\tau) \quad d\tau .$$

The weighting function or impulse response of the filter, $g(\tau)$, is made to be $\cos\omega t$ in one case and $-i\sin\omega t$ in the other so that the output is given as

$$h(0) = \int_{o}^{oo} f_R(\tau)\cos\omega\tau d\tau - i \int_{o}^{oo} f_R(\tau)\sin\omega\tau d\tau .$$

Thus, to summarize:

1. The output of a $\cos\omega t$ filter driven by a function which is zero for all positive time and evaluated at zero time is the same as the real coefficient of the Fourier spectrum of the same function reflected about the zero time axis.

2. The real part of the spectrum of the reflected function. Thus, reflecting or not reflecting the function is not important to a cosine filter.

3. The output of a $-\sin\omega t$ filter driven by a function which is zero for all positive time and evaluated at zero is the same as the imaginary coefficient of the Fourier spectrum of the same function reflected about the zero axis.

4. The imaginary part of the spectrum of a function is the negative of the imaginary part of the spectrum of the reflected function. Thus, reflecting the function merely changes the sign of the imaginary part.

5. Use of a $\sin\omega t$ filter instead of a $-\sin\omega t$ filter and not reflecting the spectrum are compensating operations.

4. Analog Instrumentation of the $\sin\omega t$ and $\cos\omega t$ filter is straight forward. Figures 6, 8 and 9 show three methods of reducing a transient which is defined as;

$$F(t) = \begin{cases} 0 & t < 0 \\ 40 - 20t & 0 \leq t \leq 2 \\ 0 & t > 2 \end{cases}$$

The first method, Figure 8, is the brute force method. The transient is simply multiplied by $\sin\omega t$ and $\cos\omega t$, the product is integrated, and a resolver is used to determine the magnitude and angle of $F(\omega)$.

The second method, Figure 8, is to reverse the direction of f(t), play it into the $\sin\omega t$ and $\cos\omega t$ filters and throw the computer into hold at the zero time of the transient. The resolver is used as in the first method. The revised transient is defined as;

$$f(-t) = \begin{cases} 0 & t > 0 \\ 40 + 20t & -2 \leq t \leq 0 \\ 0 & t < -2. \end{cases}$$

The third method, Figure 9, is to shift f(t) by two seconds so that it is zero for all positive time. Filter two would not find the spectrum of the shifted function but rather would find the spectrum of a transient which was the mirror of the shifted function about the zero time axis. That is, it would find the spectrum of a function defined as;

$$f(t) = \begin{cases} 0 & t < 0 \\ 20t & 0 \leq t < 2 \\ 0 & t > 0 \end{cases}$$

This transient contains both a shift and a reversal and would thus be modified as:

$$F_{SR}(\omega) = e^{2j\omega} \overline{F(\omega)}$$

The conjugate is removed by using a weighing function of + $\sin\omega t$ instead of -$\sin\omega t$. This is the only difference between filter three and filter two. The angle 2 is subtracted by the resolver as shown in Figure 3.

Note that the spectrum magnitude function is not a function of the direction or time of occurance of the transient. The phase is affected but can be corrected so that the read-out value is for a transient going in the desired direction and originating at a given time.

The advantages of methods 2 and 3 over the conventional method 1 are:

1. Multiplier limitations do not enter the problem.
2. The amount of equipment is decreased by about 50%.
3. More accurate results are obtained.

## BIBLIOGRAPHY


1. Electronics Training Staff of the Cruft Laboratory, Harvard University. "Electronic Circuits and Tubes", Chapter IX p. p. 236-259, Chapter XVIII p. 579-611, McGraw-Hill, 1947.

2. I. S. Sokolnikoff, R. M. Redheffer, "Mathematics of Physics and Modern Engineering", p. 171-211, McGraw-Hill, 1958.

3. C. R. Wylie, Jr., "Advanced Engineering Mathematics", Chapter 5, p. 113-149, McGraw-Hill, 1951.

4. International Telephone and Telegraph Co., "Reference Data for Radio Engineers", Fourth Edition, Chapter 35, p. 1002-1024.

5. H. A. Samulon, "Spectrum Analysis of Transient Response Curves", Proceedings of the IRE, Vol. 39, No. 2, p. 175-186, February, 1951.

*6. F. C. Harbert, "The Generation of Fourier Transforms and Coefficients on an Analog Computer", Electronics Engineering, p. 496-498, Vol. 32, No. 390, August, 1960.

*7. Stanley Fifer, "Analog Computation", Chapter 25, p. 966-991, McGraw-Hill, 1961.

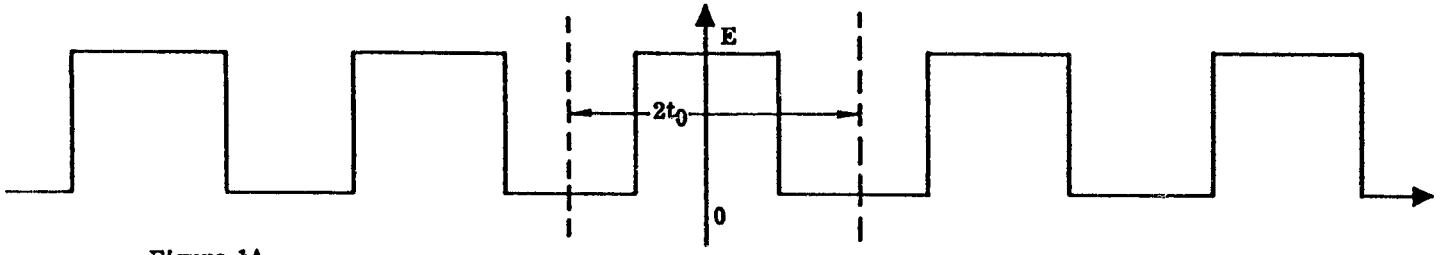



Figure 1A

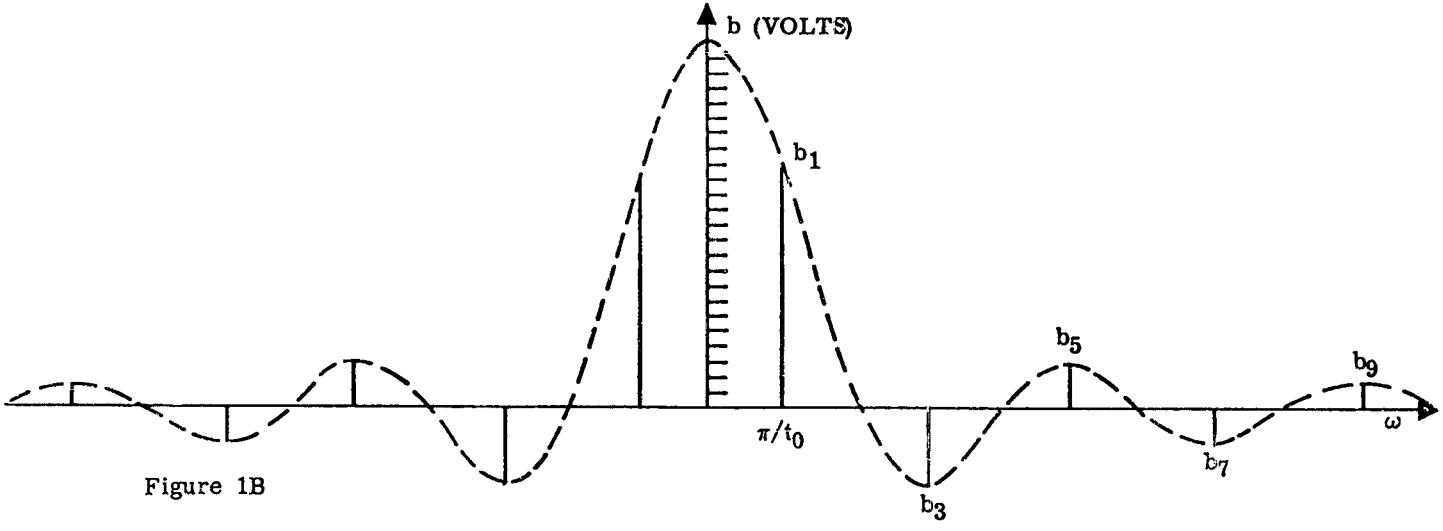



Figure 1B

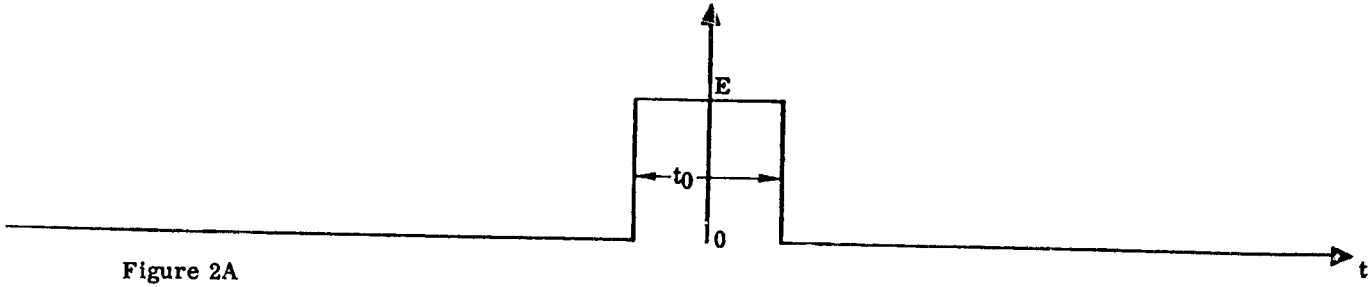



Figure 2A



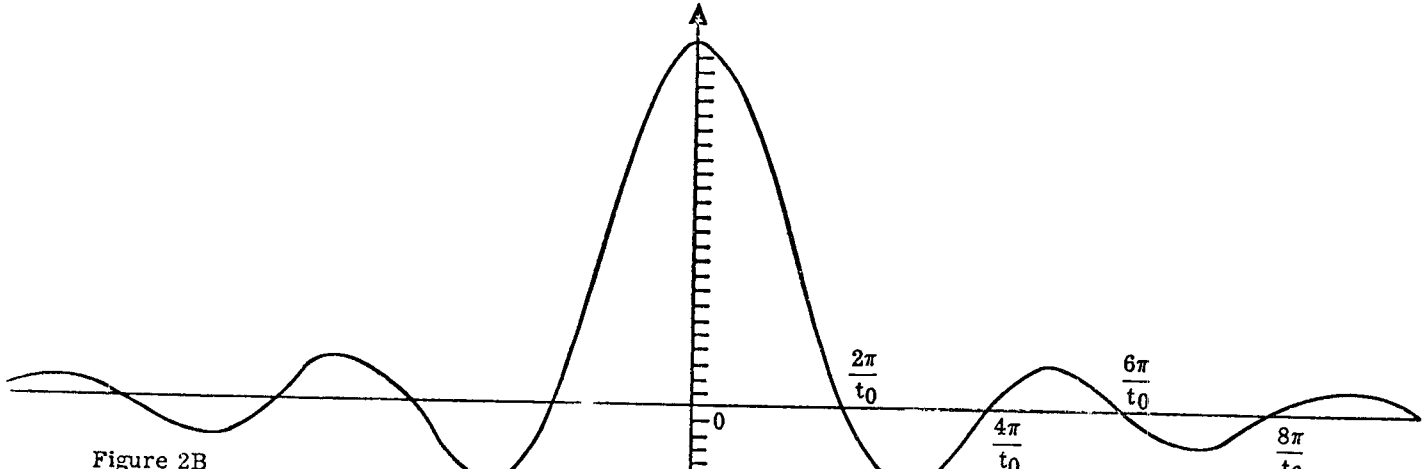



Figure 2B

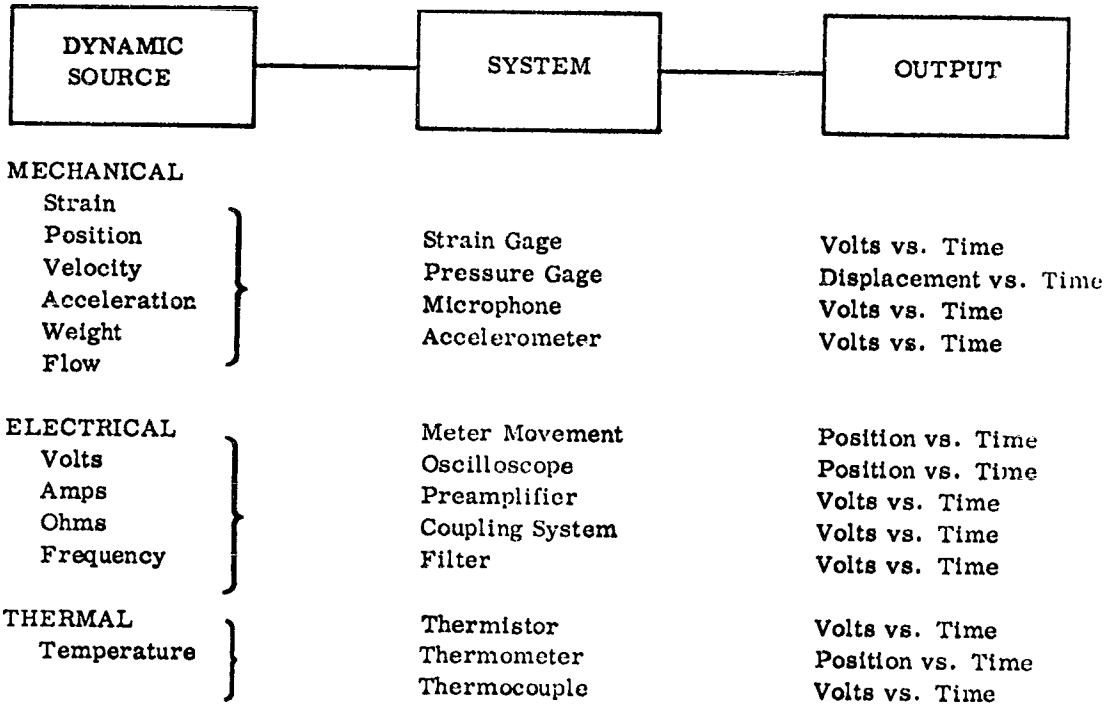



**Figure 3.** Types of Systems

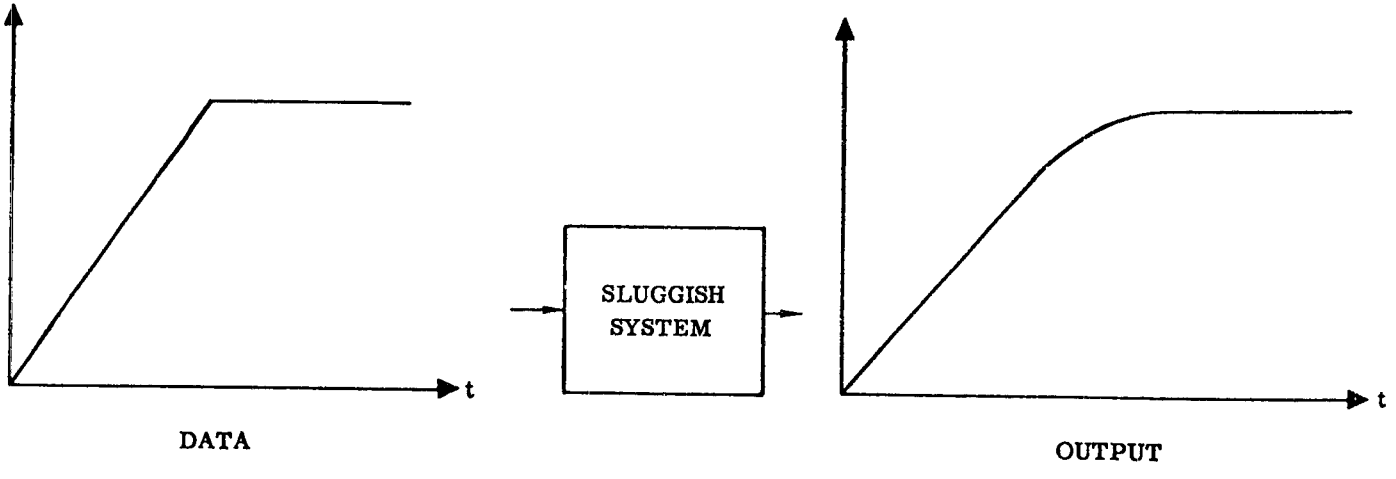



Figure 4

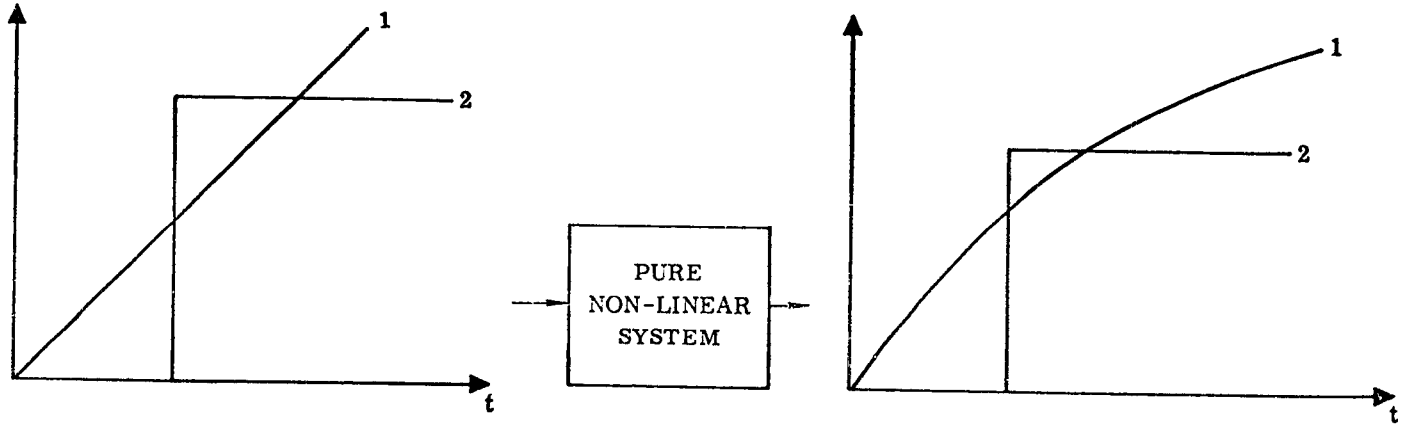



Figure 5

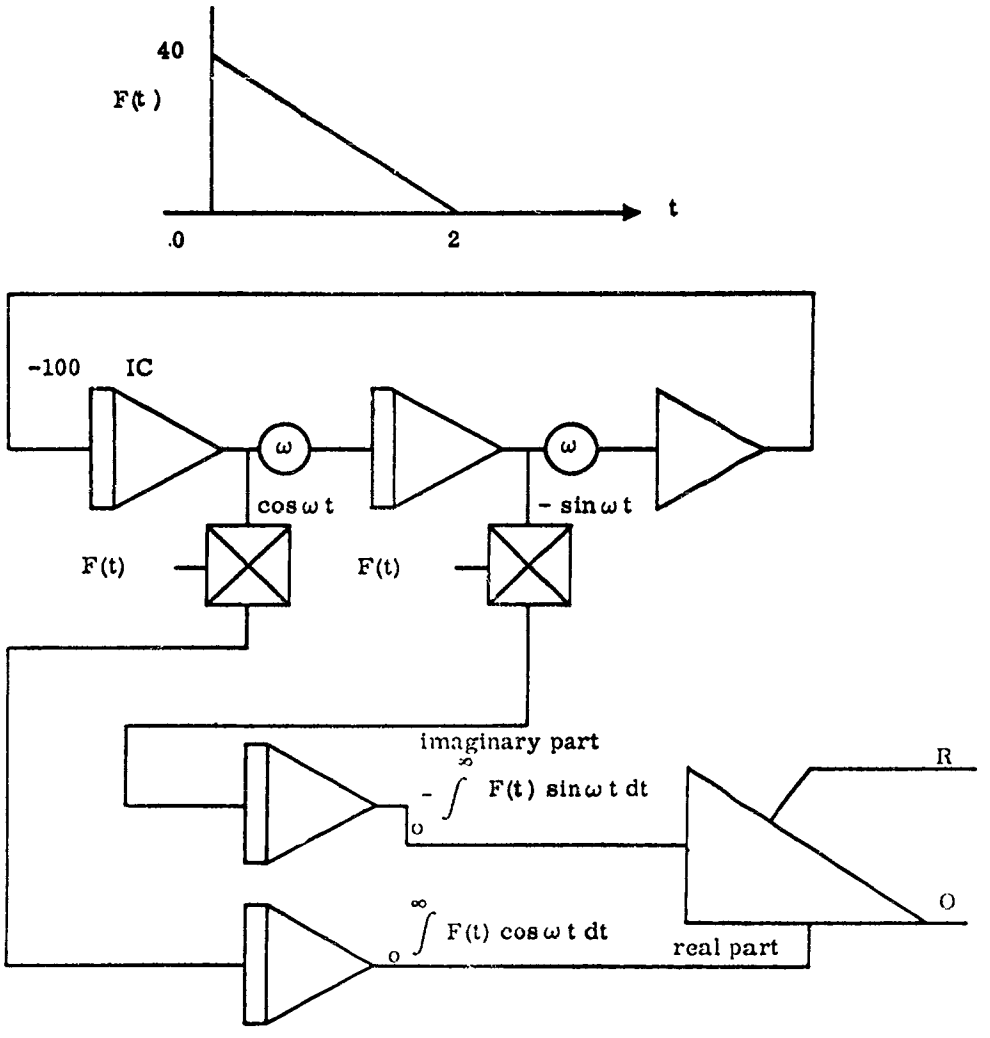
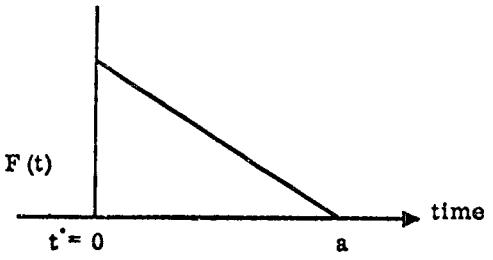
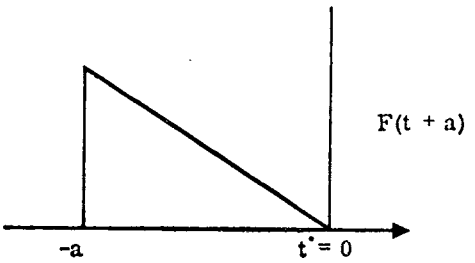

40
F(t)
t
.0
2
-100
IC
ω
ω
cos ω t
- sin ω t
F(t)
F(t)
imaginary part
$-\int_0^\infty F(t) \sin \omega t \, dt$
R
O
$\int_0^\infty F(t) \cos \omega t \, dt$
real part

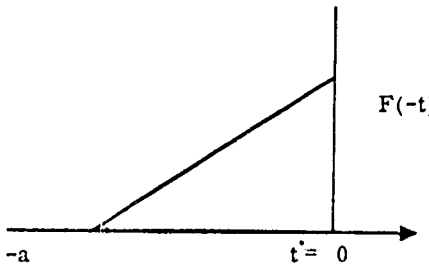
Figure 6.




Spectrum $G(\omega)$

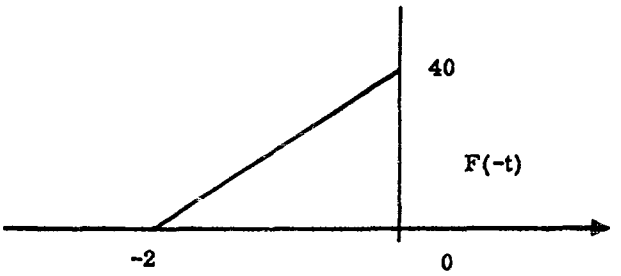



Spectrum $e^{-ja}\, G(\omega)$




Spectrum $\overline{G(\omega)}$

Figure 7.


40
F(-t)
-2
0

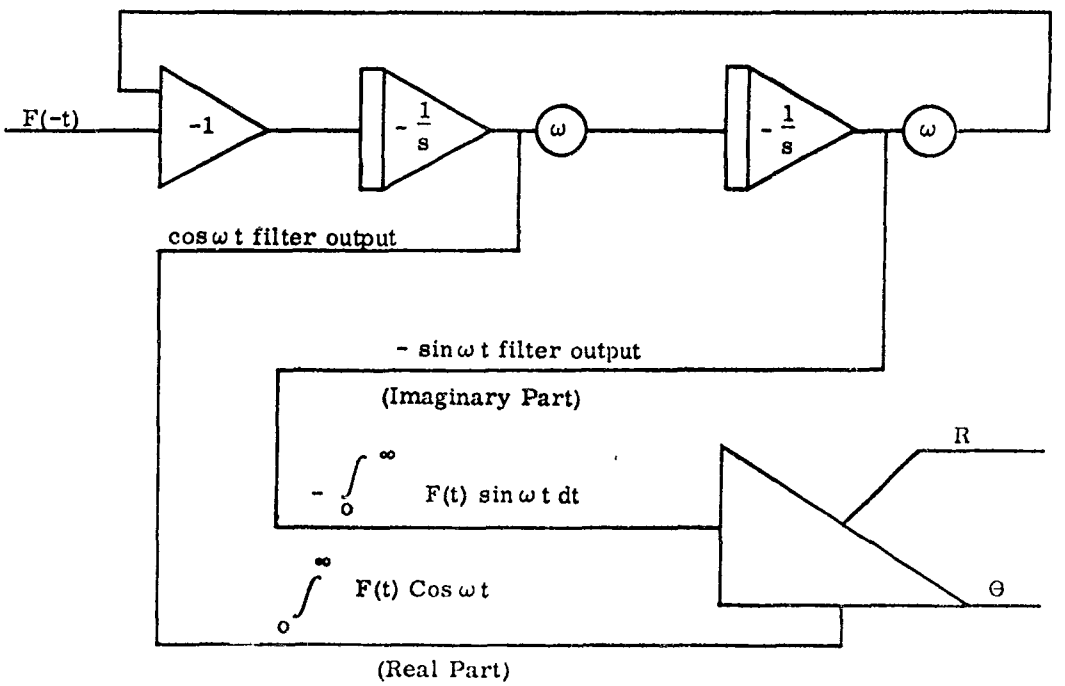

F(-t)
-1
- 1/s
ω
- 1/s
ω
cos ω t filter output
- sin ω t filter output
(Imaginary Part)
R
- ∫ from 0 to ∞ F(t) sin ω t dt
∫ from 0 to ∞ F(t) Cos ω t
Θ
(Real Part)

Figure 8.

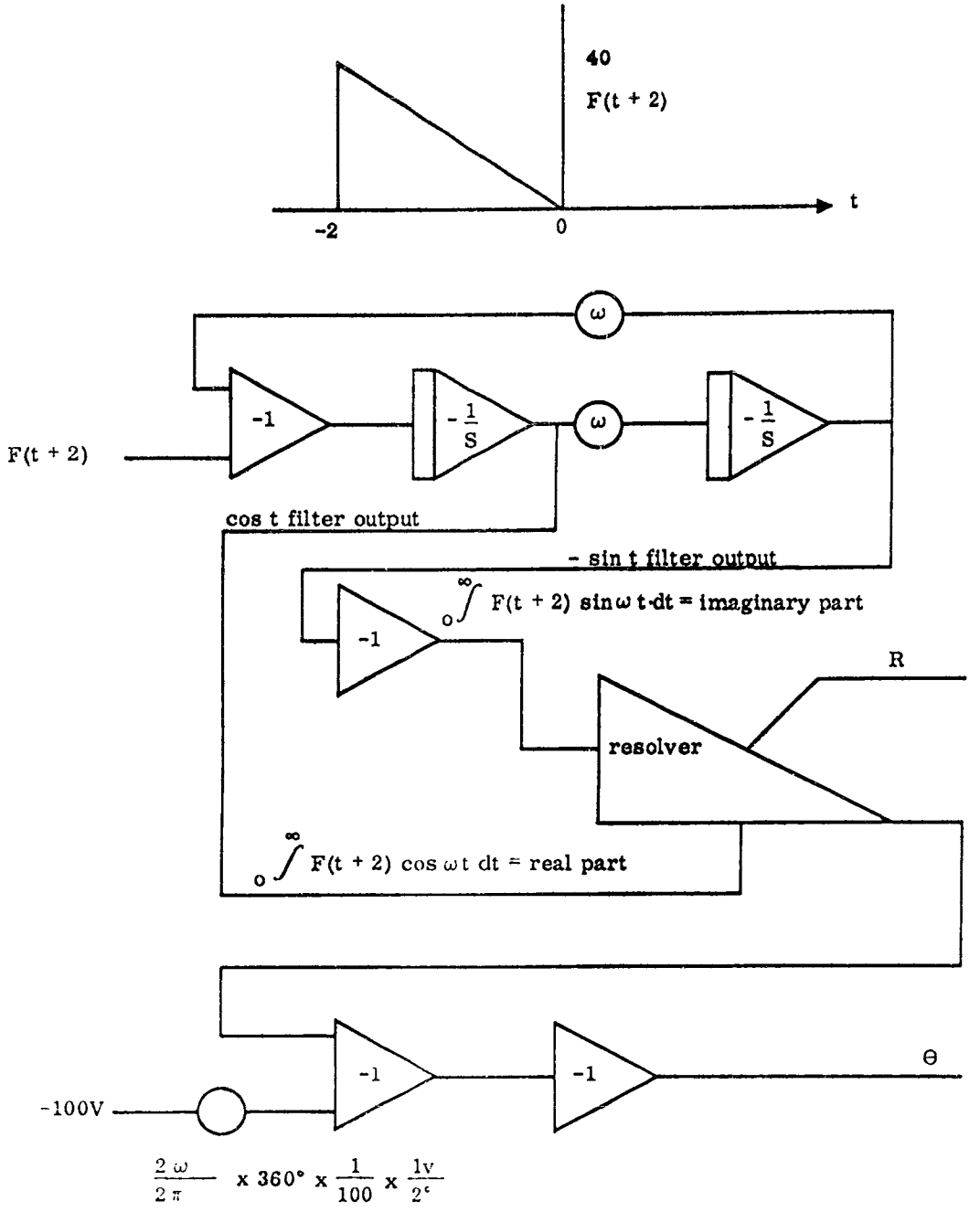

40
F(t + 2)
t
-2
0
ω
-1
$-\frac{1}{S}$
ω
$-\frac{1}{S}$
F(t + 2)
cos t filter output
- sin t filter output
$\int_0^\infty$ F(t + 2) sin ω t·dt = imaginary part
-1
R
resolver
$\int_0^\infty$ F(t + 2) cos ω t dt = real part
-1
-1
Θ
-100V
$\frac{2\omega}{2\pi}$ x 360° x $\frac{1}{100}$ x $\frac{1v}{2^c}$

Figure 9.

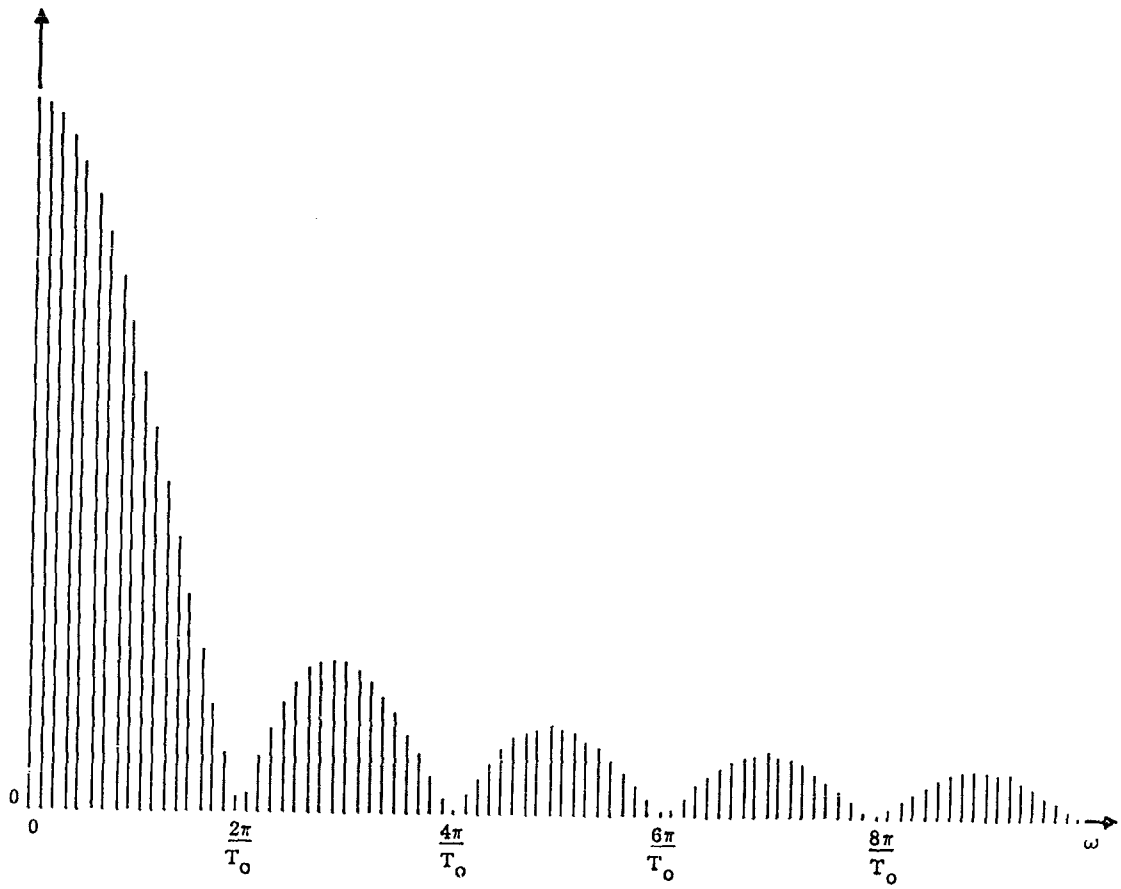



Figure 10. Computer Data - Rectangular Pulse Spectra

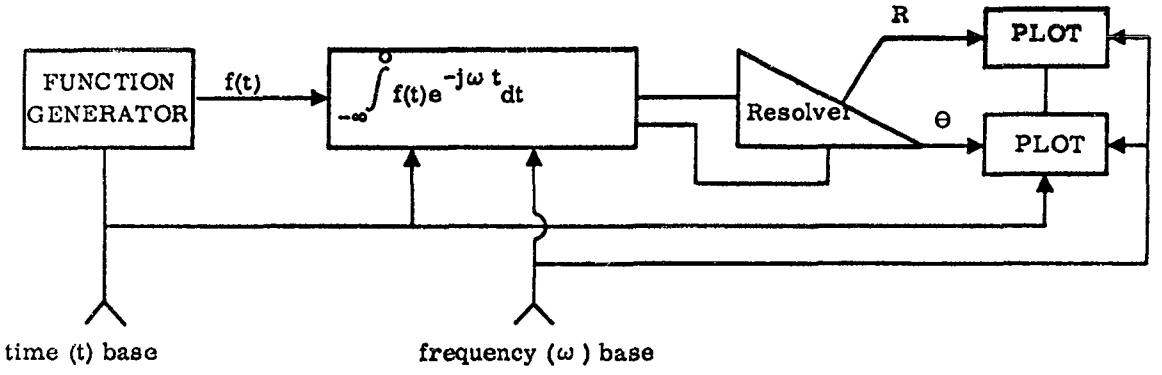

FUNCTION GENERATOR
f(t)
$\int_{-\infty}^{\infty} f(t)e^{-j\omega t}dt$
Resolver
R
θ
PLOT
PLOT
time (t) base
frequency (ω) base

Figure 11.

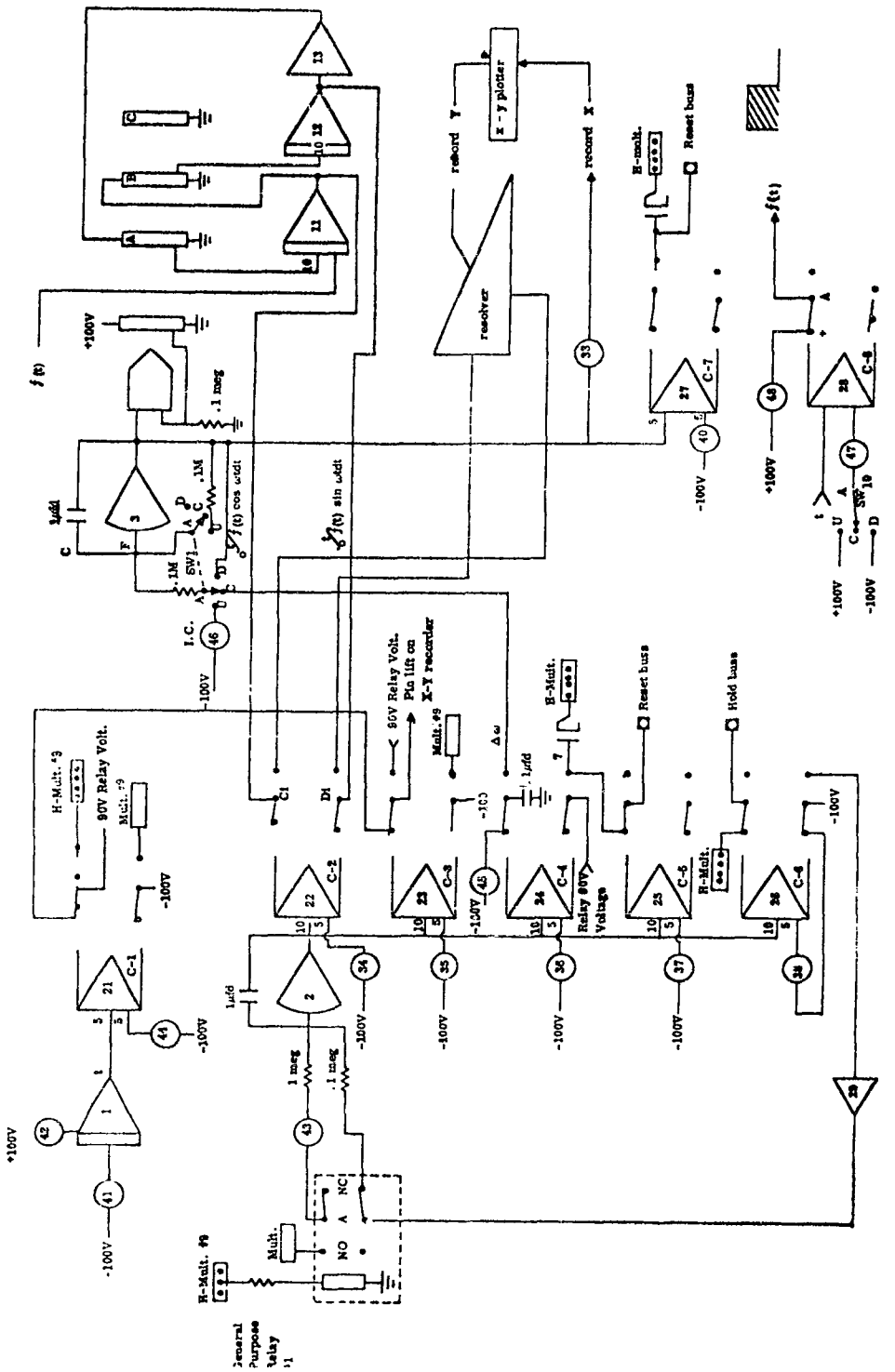

x - y plotter
record Y
record X
resolver
E-mult.
Reset buss
f(t)
+100V
-100V
1 meg
.1 meg
1 μfd
.1M
f(t) cos ωdt
f(t) sin ωdt
I.C.
60V Relay Volt.
Pin lift on
X-Y recorder
Mult. #9
Δω
Hold buss
Relay 60V
Voltage
R-Mult.
Mult.
NC
NO
A
General
Purpose
Relay

Figure 12.

# THREE DIMENSIONAL QUANTIZED ANTENNA PATTERN MODEL

L. E. Silverman, J. J. Krstansky and H. M. Sachs
Armour Research Foundation
Chicago, Illinois

Abstract. - This paper discusses the construction of a three dimensional quantized model for antenna radiation patterns for the purpose of analysis and prediction of interference. Construction of the model depends upon the observation that while antenna patterns exhibit a high degree of irregularity, these irregularities appear as oscillations about several power levels. The amin beam is treated separately. The model is a quantized version of the true pattern and is represented as a unit radius sphere with the direction of the radius vector being the direction of power flow from the antenna. Antenna statistics are obtained from the model of a symmetrical antenna using several methods. Relative accuracy of the model statistics on an arbitrary selection of quantized levels is determined. The study indicates that the statistical representation is relatively insensitive to the method used to quantize the analog pattern. Arbitrarily quantized patterns yield useable results for interference prediction purposes.

A three dimensional quantized model based on the asymmetric cosecant squared antenna patterns is also described and evaluated by comparison with experimental data.

## I. INTRODUCTION

Any practical interference prediction technique must include the storage of antenna pattern characteristics in sufficient detail to satisfy the analysis requirements. If several antennas are involved this may result in a prohibitive or impractical quantity of data. Either the exact or a simplified description of a given cut through the pattern could be used in the prediction process, or the gain statistics (the likelihood or probability of the power density being at a particular value) as represented by the cut might be used. Many cuts could be taken through the three dimensional antenna pattern in an attempt to gain an insight into the nature of the pattern.

Ordinarily, a considerable amount of data collection is necessary to describe the three-dimensional antenna characteristics. In addition, a problem often arises as to how the collected data should be stored and processed to provide meaningful information relative to interference analysis. Another problem is concerned with the number of patterns needed to

adequately describe the three dimensional radiation characteristics of a typical antenna. Since the three dimensional patterns need to be repeated for a number of frequencies including harmonic and spurious, it seemed desirable to investigate techniques of reducing the amount of analog information to be obtained or required to be stored.

The technique to be described indicates a method to obtain three dimensional statistical information of antenna patterns. It is based on the collection of a minimum amount of analog antenna pattern data, reducing the analog information to digital information and the processing of this digital information onto a three dimensional model from which the statistical results may be abstracted. The model is concisely described in digital form.

## II. STATISTICAL TREATMENT OF INDIVIDUAL PATTERNS

Evaluation of a generalized three dimensional antenna pattern model was performed using data that was available from measurements on a cosecant-squared dish antenna (reflector-feed horn type). The coordinate system used in this discussion is shown in Figure 1. The X-axis corresponds to the axis of the dish and passes through the main beam. The X-Y plane corresponds to the plane of zero elevation antenna pattern. To correlate the model predictions with the actual experimental data spherical coordinates were used but with different designations. The azimuth angle taken from the main beam is denoted by $\alpha$ the elevation angle at zero azimuth is called $\xi$ , and the co-latitude will always be denoted by $\theta$.

Measurements of the cosecant-squared antenna were taken with the antenna at various aspects to the receiver. For the purpose of construction of the model, only two aspects of the dish were of interest, as measured by $E_\theta$. The vertical, or elevation pattern corresponds to $E_\theta$, $\theta = 0°$; and $E_\theta$, $\theta = 90°$ corresponds to a horizontal, or azimuth pattern. These patterns were analyzed and quantized using the following method.

Analog patterns were reduced to digital data by determining relative amplitude of the pattern at two degree intervals. All readings were corrected for any difference between zero db reference on the recording paper and the actual recorded peak. Thus all digital data were in db relative to zero db peak amplitude (main beam). Since the patterns were recorded in two steps in order to have a dynamic range of approximately 60 db, the overlap of the second (lower) pattern with the top part of the first was determined and the digital data from the second pattern was corrected to db relative to zero db peak. The corrected digital data was used to make a scaled plot of the antenna patterns.

Figure 2 is a scaled plot of the zero elevation pattern for the cosecant-squared antenna ($\phi = 0$). It is reasonably symmetrical about the main beam. The first method used to quantize the pattern was the 10-db quantization technique. One determined the portion (in degrees) of the pattern which exceeds specified levels. The levels were arbitrarily chosen as 10 db steps. One finds the angular amount of time that each 10 db level was exceeded, and quantizes that amount at the five db level above the one from which the information was obtained. Thus the main beam will be quantized at 5 db and levels will progressively decrease in 10 db intervals. By this quantizing procedure, if a low relative power density occurs close in to the main beam, the 10 db quantized levels will not show this lower level where it actually occurs but will have it show up in some angular region farther away from the amin beam. Since only the probability statistics are concerned, this should not cause an appreciable error for the particular pattern analyzed, but as discussed later, an error in the three dimensional pattern model will be incurred with this particular method of quantization. Figure 3 shows the 10-db quantized azimuth pattern. The quantized levels were balanced to present a symmetrical quantization.

Figure 4 is a plot of the azimuth antenna pattern given in Figure 2, but both sides of the pattern in Figure 2 have been averaged to give one pattern which can be analyzed. The second method of quantization is to determine angular regions where oscillations tend to take place and then roughly estimate by eye the level of oscillation, taking into account any large positive or negative fluctuations. The main beam was considered as extending to that angle where power was 3 db down from the main lobe peak; hence, the main beam is quantized at 3 db. This method of quantization causes ambiguity between different observers doing the quantizing since one can choose different angular bounds and different power density levels than another observer. Although this is true, it has been found that slight differences in range and amplitude of quantization yield similar results when compared to experimentally obtained statistics. When a more exact method of averaging the power levels is used to determine the amplitude at which to quantize, it is found that the more tedious, time consuming exact method yields results which differ from the more arbitrary coarse-grain quantization by at most 4-5 db in the worst cases encountered. In many prediction techniques, this degree of accuracy may easily be tolerated. This method of quantization does have an advantage over the 10 db quantization method in that lower levels of oscillation appearing close to the main beam are accounted for in the position where they actually occur by the very technique used to quantize the pattern.

Figure 5 shows the derived quantized pattern obtained by the arbitrary quantizing technique described above. Note the difference in this quantized pattern from that shwon in Figure 3 in that the levels do not progressively decrease but tend to follow the true pattern more closely, though with far fewer power levels used to describe the pattern characteristics.

Figure 6 shows the asymmetrical elevation pattern for zero azimuth ($\alpha = 0$). The 10 db method of quantization of this asymmetrical pattern proceeds in the same straightforward manner as for the symmetrical patterns previously described. The 10 db quantized version of this pattern is shown in Figure 7. For the second method of quantization, arbitrarily by eye, the asymmetrical pattern cannot be averaged on both sides of the main beam. The quantization into arbitrary levels about oscillation levels is done using the entire pattern and angular bounds are determined on each side of the main beam. Figure 8 shows the quantized pattern determined by arbitrary decision on the asymmetrical elevation pattern. In Figure 7 the relative power level successively decreases as one proceeds away from the main beam. In Figure 8 the same is true for one side of the pattern but the other side has a dip near the main beam which is similar to that encountered in the true pattern shown in Figure 6.

Follwoing the quantization of the analog antenna patterns, the gain statistics or the cumulative probability density function is derived. The cumulative probability density function, that is, the probability that a relative power density is less than or equal to some value of relative power density versus that value of relative power density, was plotted for both methods of quantization and compared with data obtained from the original patterns. The angular amount of time the pattern is less than or equal to a certain power level is plotted versus that relative power level. A step function curve is obtained where straight line segments connecting midpoints is used to approximate the step curve, and hence the actual statistics.

Figures 9 and 10 show the gain statistics derived from the quantized patterns using both techniques of quantization for the azimuth and elevation patterns, respectively. The crosses are the values measured from the actual antenna pattern. It is seen that the maximum error is about four db at the worst point in the azimuth pattern. The straight line segments deviate from the measured values due to sharp changes in slope occurring in the pattern quantization. Figure 10 for the elevation pattern has more steps quantized and thus the measured data come extremely close to the derived gain statistics. It is obvious that in the limit the more quantized levels one has, the more the pattern which is quantized approaches the actual measured pattern and the derived gain statistics will approach the actual measured gain statistics.

## III. CONSTRUCTION OF THE THREE DIMENSIONAL ANTENNA MODEL

The three dimensional quantized antenna pattern model is represented as a unit radius sphere with the direction of the radius vector being the direction of power flow from the antenna. Various regions of the sphere are assigned a single power density level corresponding to the levels about which pattern oscillations occur. At the main beam peak,

at unit radius, the power level will be designated as zero db, and all other levels are relative power density levels, relative to zero db.

Polar Coordinates Representation of Model

Two methods of representing the antenna model sphere were used. The first method investigated was to plot the quantized patterns for the two orthogonal cuts on polar coordinates (both patterns in the same plane). For the model under discussion, this is illustrated in Figure 11. The azimuthal pattern is represented by the negative sloped plot and the elevation pattern is illustrated by the positive sloped plot. To form a mental image of the three dimensional quantized model, one must mentally rotate the elevation cut 90° to a position orthogonal to the azimuth cut. A plane view of the model is shown in Figure 12.

Having established the quantized antenna pattern model in this fashion, one can then obtain the quantized great circle cuts at any elevation angle $\pm$ 90°. For example, on the elevation cut, assume that the quantized great circle cut for an elevation angle of 20° is desired (antenna main beam pointing 20° above 0° elevation). From Figure 11, the 20° elevation angle line (dotted) is seen to intersect the quantized elevation pattern at the 25 db level. For a 20° great circle cut, therefore, the azimuth pattern would be quantized from the 25 db level as indicated in Figure 13 as dotted lines. The straight line antenna statistics approximation is then drawn from the 20 db level through the midpoints of the quantized pattern. A similar procedure is followed for the 40° and 60° elevation angle cuts except that since the elevation pattern is first intersected at the 35 db level, the azimuth pattern is quantized from 35 db as shown by the solid heavy line in Figure 13. Again, the straight line approximation is shown as a heavy solid line through the midpoints of the quantized pattern. A similar procedure was used to establish the 0° elevation quantized pattern and approximation shown as a light solid line in Figure 13.

Measured gain statistics were obtained from the experimental data by determining the percentage of time (in degrees) that a gain level was exceeded directly from the analog patterns. This data was obtained in one db increments of gain. The straight line approximations shown in Figure 13 were than compared to the fine grain antenna gain statistics obtained from the measured analog patterns for these same elevation cuts. The results of this comparison are shown in Figure 14. The data in this figure are plotted as cumulative probability distribution functions. The 0° elevation cut statistics and the straight line approximation are shown as extending from 0 db relative gain level. The maximum error, occurring at the sharp break in statistics between -20 and -30 db, appears to be on the order of 4 db, while the average error for the remainder of the curve is about 1 db. The 20° elevation angle cut starts at approximately -20 db and the order of magnitude of the errors is about the same as for the zero

elevation pattern statistics. The 40° and 60° elevation cuts begin at about -30db and be about 2 1/2 db, primarily because no sharp breaks occur in the actual statistical curve.

These results look promising, especially since they were obtained by a rather crude approximate model constructed in an arbitrary fashion. The statistics obtained from the straight line approximations fit reasonably well over considerable portions of the curve. The maximum and average errors involved seem quite compatible with most anticipated interference prediction technique accuracies.

Certain aspects of the application and utility of a model such as has been described should be kept in mind. Because of the fact that exact azimuthal or elevation gain levels and their precise location have been lost in this 10-db quantized model, the application of this model is restricted to antennas rotating at a reasonably constant speed. In addition, the manner in which the antenna patterns were quantized limits the application of the model primarily to azimuthal great circle cuts at arbitrary elevation angles. This is true because azimuthal gain vs. azimuthal angle information has not been retained in the model. This can be verified by noting that the side lobes near the main beam are of lower gain than some of the lobes in the spillover region in the actual patterns while the quantized patterns do not indicate this particular feature of the patterns. Although this does not affect azimuthal great circle cut statistics, it would have a bearing on statistics of elevation great circle cuts. It is obvious that more complex antenna models can be constructed to retain the azimuthal location vs. gain feature to overcome this limitation. In fact, a more generalized model was investigated which shows promise of providing considerable more flexibility regarding the manner in which it is employed to obtain gain statistics of arbitrary receptor positions relative to the model center.

Rectangular Grid Representation of Model

In order to provide a more general model, the second method was to lay out the quantized levels of the azimuth and elevation patterns on a rectangular plane view. It should be kept in mind that the plane view is simply a convenient method of showing power levels and is not a mapping of a sphere onto a plane technique. The quantized azimuthal levels were laid out along the abscissa with X = 0 = main beam, and the quantized elevation levels were laid out along the ordinate with Y = 0 = main beam. The original lay-out was made utilizing full 360° data ($\pm$ 180° from 0°) for both elevation and azimuth patterns. The boundaries of each gain level were projected vertically for azimuth gain levels and horizontally for elevation gain levels to the point where similar gain boundary levels intersect, forming a rectangle for each particular quantized gain level. In the case where patterns were quantized in 10 db levels the intersections are unizue; however, when arbitrarily quantized

levels were used, the intersections must be formed by boundaries of gain levels which were similar and the gain level assigned to the rectangle would be the average of the two gain levels. The range of values in azimuth and elevation gain levels should be approximately the same average db level. The ranges may extend between different angular bounds on the azimuth and elevation patterns. It is not necessary for all regions to include both azimuth and elevation points. Thus, if the azimuth pattern exhibits a level unrelated to an elevation pattern level, the region can be defined for the azimuth pattern with no corresponding region for the elevation pattern.

An example of a typical plane view of gain levels is shown in Figure 15 for 10 db quantization. This model is based on the patterns of Figure 2 (azimuth) and Figure 6 (elevation) which were quantized in 10 db steps as shown in Figures 3 and 7, for the cosecant-squared antenna. In the form shown in Figure 15 the model displayed redundant and/or overlapping information and was not in a form needed, that is, in a spherical coordinate system. In order to process the model shown in Figure 15 into the required form, the following steps were taken:

1. The angles shown on the ordinate were limited to -90° and +90° so that the horizontal line at the top of the model represents the upper pole of the model sphere and the lower horizontal line represents the lower pole of the model sphere.

2. The gain levels in the region between $\pm$ 90° and $\pm$ 180° elevation and 0° to $\pm$ 90° in azimuth were analyzed to determine which portions of the data in the 90° to 180° azimuth were overlap sections and the necessary gain level corrections were determined. For example, in Figure 15, the gain level for -90° to -98° elevation over the 0° to $\pm$ 90° azimuth is -35 db; therefore, this level occurs in the back portion of the sphere (from + 90° to 180° to -90° azimuth) over an elevation angle from -90° to -82°.

The application of these two steps to the configuration of Figure 15 results in the final model configuration for the 10-db quantization method which is shown in Figure 16. In the final model, which represents a spherical coordinate system, the various gain levels were laid out in plane view as shown. In this model an elevation cut at a given angle is represented by the horizontal line at the angle and the quantized levels can be determined directly. The antenna gain statistics can be determined from the quantized pattern by the straight line approximation technique discussed earlier.

Similarly, a great circle cut in elevation at a given azimuth angle, that is, a meridian great circle, is represented by two vertical lines, one at the azimuth angle ($\alpha$) of the intersection of the great circle with the 0° azimuth line within the 90° -0° -90° sector. For example, a great

circle in elevation at $\alpha = 60°$ would be a vertical line at $\alpha = 60°$ and one at $\alpha = 120°$. The intersections of these two lines determine the quantized levels for this particular cut and, again, gain statistics can be approximated.

A similar technique was used to model the arbitrary quantization of the same patterns, Figures 2 and 6, quantized versions Figures 5 and 8. The model, in this case, became slightly more complicated as shown in Figure 17 which is the 360° x 360° plane view of the preliminary model. Note that the gain levels are more variate and the gain level rectangles are not necessarily concentric as in the 10 db quantized level case. Essentially the same procedure of determining gain level overlap was used to construct the final model of the arbitrarily quantized gain levels as shown in Figure 18. It should be noted that this model may be somewhat more realistic in that gain level versus azimuth angle has been more faithfully retained in this model than in the model of Figure 16. This model may be treated in a similar manner to that described previously to obtain various pattern statistics.

Non-Meridian Great Circle Representation

Any other great circle cut, other than a meridian great circle cut, can be described in terms of spherical coordinates, similar to the description of great circle sailing around the Earth. The information needed is the elevation of the great circle at the prime meridian, or vertical elevation at 0° azimuth angle ( $\alpha = 0$), and the angle along the great circle. Any non-meridian great circle intersects the prime meridian at a right angle; thus use can be made of Napier's rules for the solution of right spherical triangles.

Figure 19 shows the geometry of the problem. Given an elevation angle $\xi$ at the prime meridian and an angle $\phi$, along the great circle starting at zero for zero azimuth and elevation $\xi$. In the figure, a great circle is drawn through the pole P which is perpendicular to the arc RN. Let these arcs meet at point R. In the right spherical triangle NPR,

$$PR = \text{col-}\xi = 90° - \xi = \theta$$

(where col- signifies colatitude). Knowing the angles $\xi$, col- $\xi$, $\phi$, and $\measuredangle R = 90°$, then angle P = longitude and r = colatitude of the point of interest need to be determined. From relations for right spherical triangles:

$$\sin (\text{col-}\xi) = \tan \overline{P} \tan \phi$$

where $\overline{P}$ = complement of $P = 90° - P$

$$\sin \theta = \sin (\text{col-}\xi) = \text{ctn } P \tan \phi$$

Thus

$$\text{ctn } P = \frac{\sin(\text{col-}\ \xi\ )}{\tan \phi} = \frac{\cos \xi}{\tan \phi} = \frac{\sin \theta}{\tan \phi}$$

$$\measuredangle P = \text{ctn}^{-1}\left(\frac{\cos \xi}{\tan \phi}\right)$$

Thus,

$$\alpha = P = \text{ctn}^{-1}(\cos \xi \ \text{ctn}\ \phi) = \text{azimuthal angle of point of interest.} \quad (1)$$

Also, from spherical trigonometry

$$\sin \overline{r} = \cos \phi \cos \theta = \cos \phi \cos\ (\text{col-}\ \xi\ )$$

Therefore,

$$\cos r = \cos \phi \cos \theta = \cos \phi \cos\ (\text{col-}\ \xi\ )$$

$$\cos r = \cos \phi \sin \xi$$

$$r = \cos^{-1}(\cos \phi \sin \xi\ ) \quad (2)$$

$$\psi = 90° - r = 90° - \cos^{-1}(\cos \phi \sin \xi\ ) = \text{elevation angle at a point of interest.} \quad (3)$$

This procedure defines the azimuth angle $\alpha$, Eq. (1), and the elevation angle $\psi$, Eq. (3), of any point along the great circle of interest in terms of known quantities, the elevation at the prime meridian and the angle along the great circle. Thus the great circle cut may be projected on the plane view and the quantized levels may be determined accordingly. As an example, a great circle cut for $\xi = + 60°$ was calculated to find the azimuth and elevation points of intersection of the + 60° great circle with the power density sphere both the 10 db quantized model and the arbitrarily quantized model. These patterns are shown in Figures 20 and 21, respectively. The approximated cumulative probability distribution for these patterns based on straight line approximations is shown in Figure 22. The x marks in this figure are actual data points obtained from the analog pattern for this cut. The straight line approximation based on the 10 db quantized patterns shows a maximum error of about 2.5 db from the actual data points. The arbitrary approximation shows slightly greater error, on the order of 5 db. In both cases, it appears that the magnitude of error may be compatible with expected prediction accuracies. Also, it is interesting to note that the more general approach of 10 db quantizing, at least in this case, led to more accurate approximations.

## IV. CONCLUSIONS

The investigation of antenna models indicates that, based on two orthogonal major cuts through the main beam of an antenna, one in azimuth and the other in elevation, a relatively simple three dimensional model can be constructed from which useful statistical gain information can be obtained for prediction purposes. Accuracy obtained from the model is within five db of actual measured data. This appears to be quite compatible with most anticipated interference prediction technique accuracies. A refinement of this technique to increase its accuracy, and incidently its complexity, might be to have the plane view consist of gain level regions other than rectangles, such as circles or ellipses, which are probably somewhat more representative of the true radiation pattern than rectangles.

## ACKNOWLEDGEMENTS

The experimental work used in these investigations was performed by Messrs. Marvel W. Scheldorf and Robert D. Standley, of Armour Research Foundation of Illinois Institute of Technology.

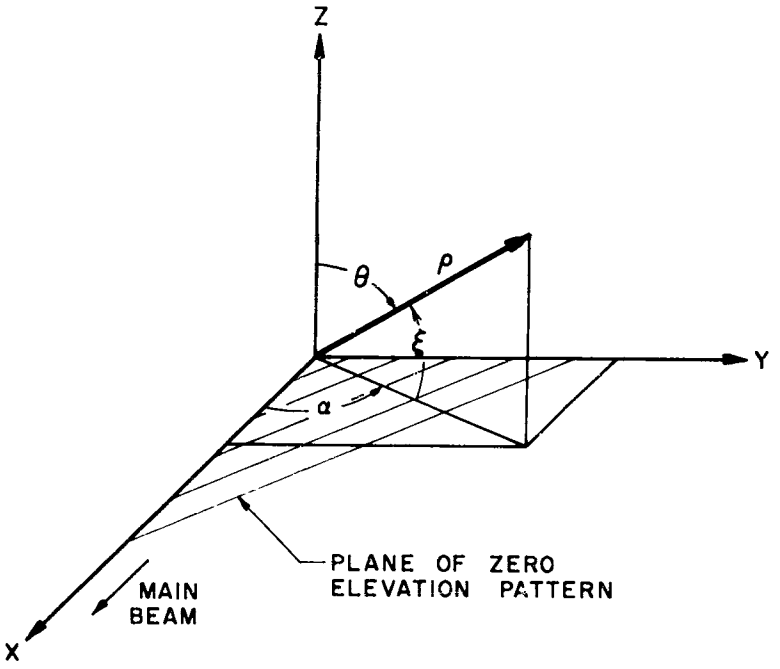



Fig. 1 CO-ORDINATE SYSTEM

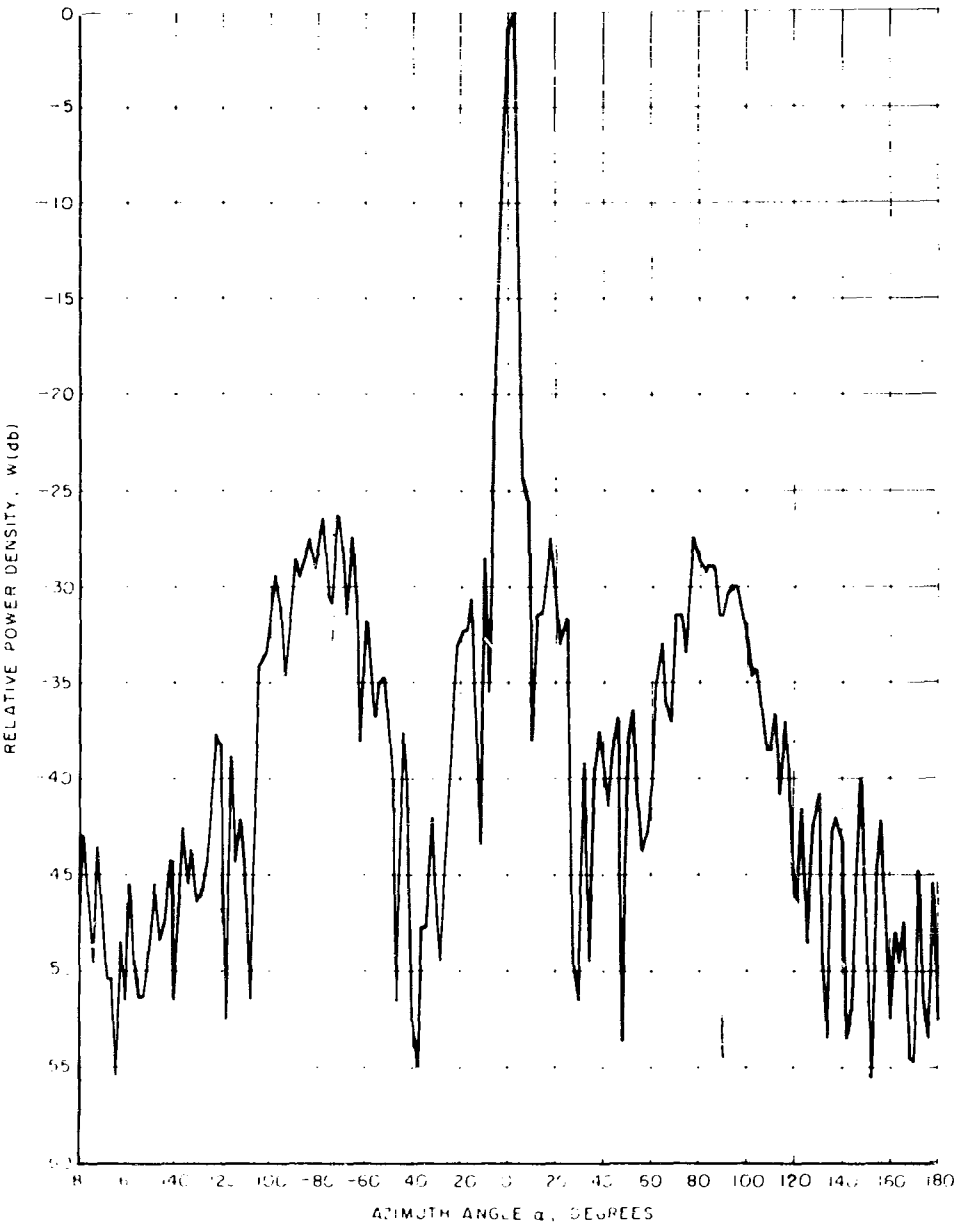



Fig. 2 MEASURED ANTENNA PATTERN — $\xi = 0°$

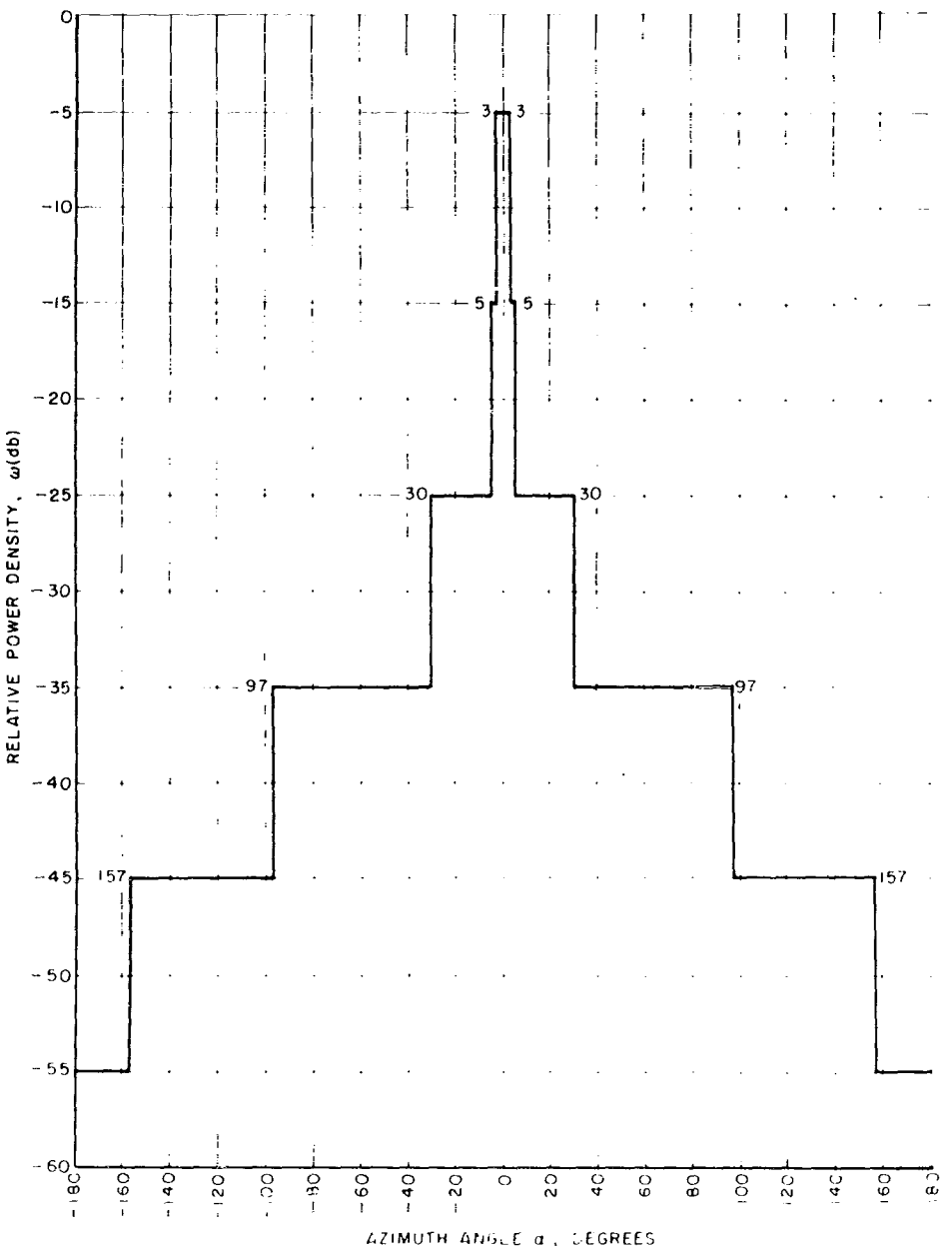



Fig. 3 10 db QUANTIZED AZIMUTH PATTERN — $\xi = 0°$

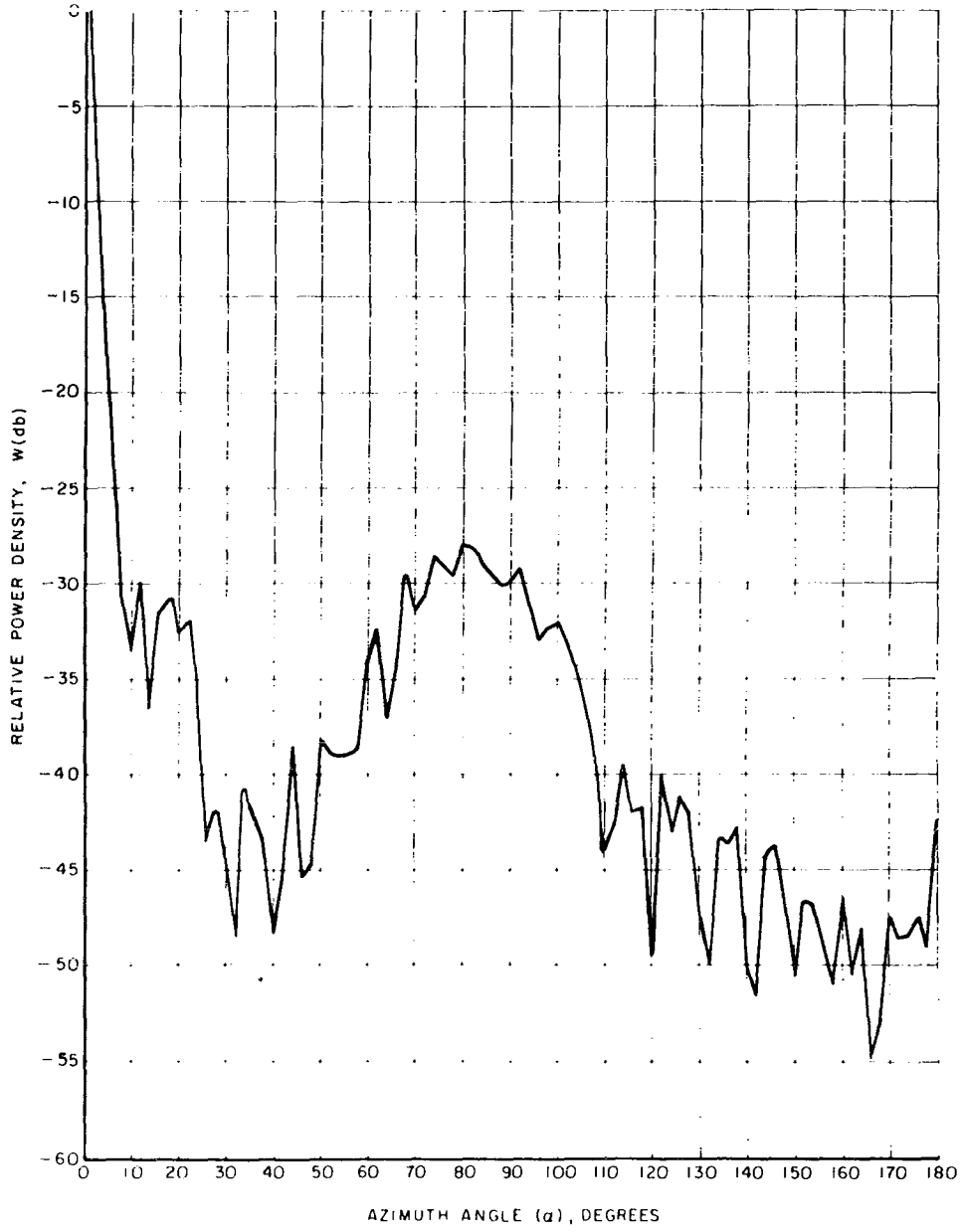



Fig. 4 AVERAGED AZIMUTH ANTENNA PATTERN —$\xi = 0°$

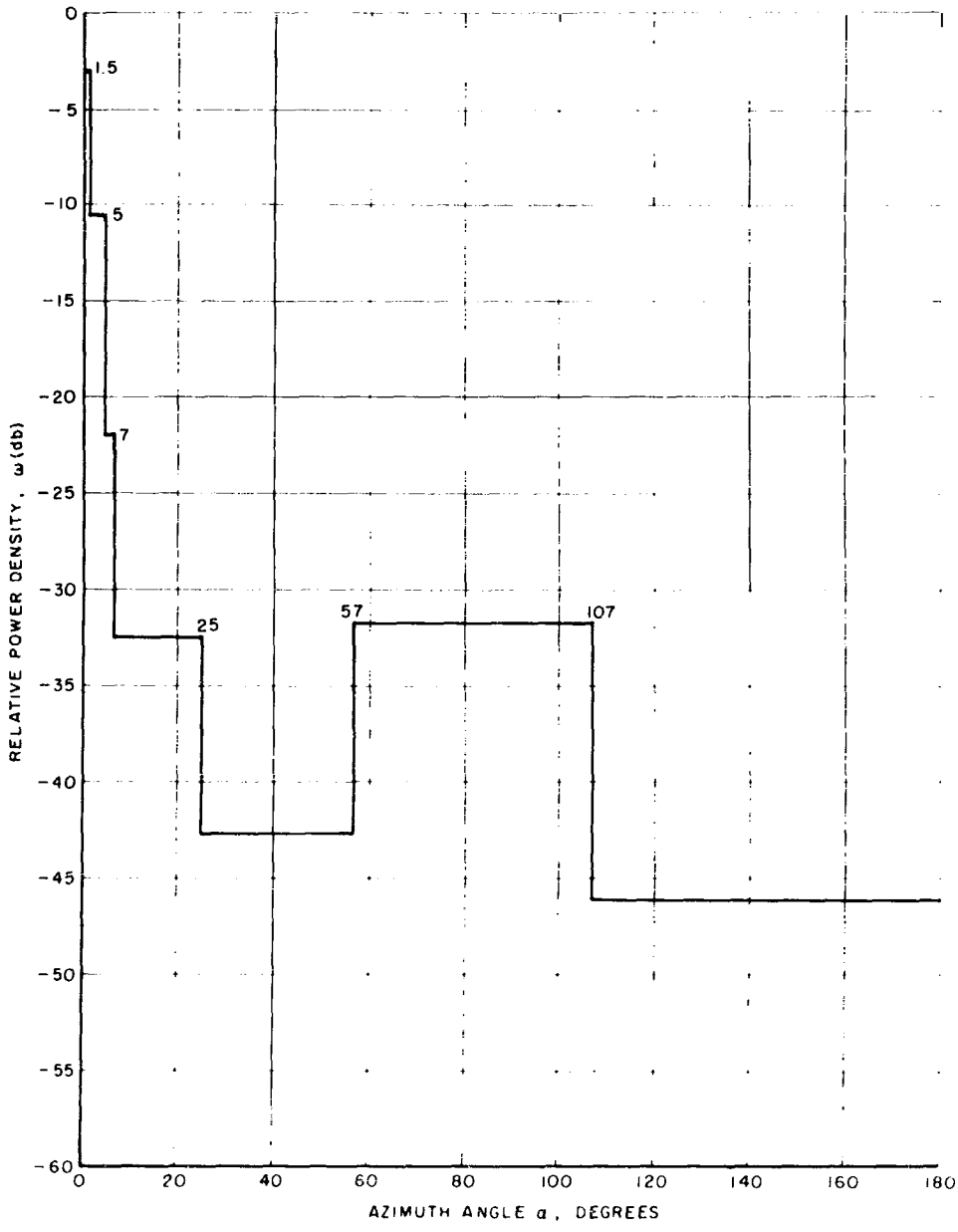



Fig. 5 ARBITRARY QUANTIZED AZIMUTH PATTERN — $\xi = 0°$

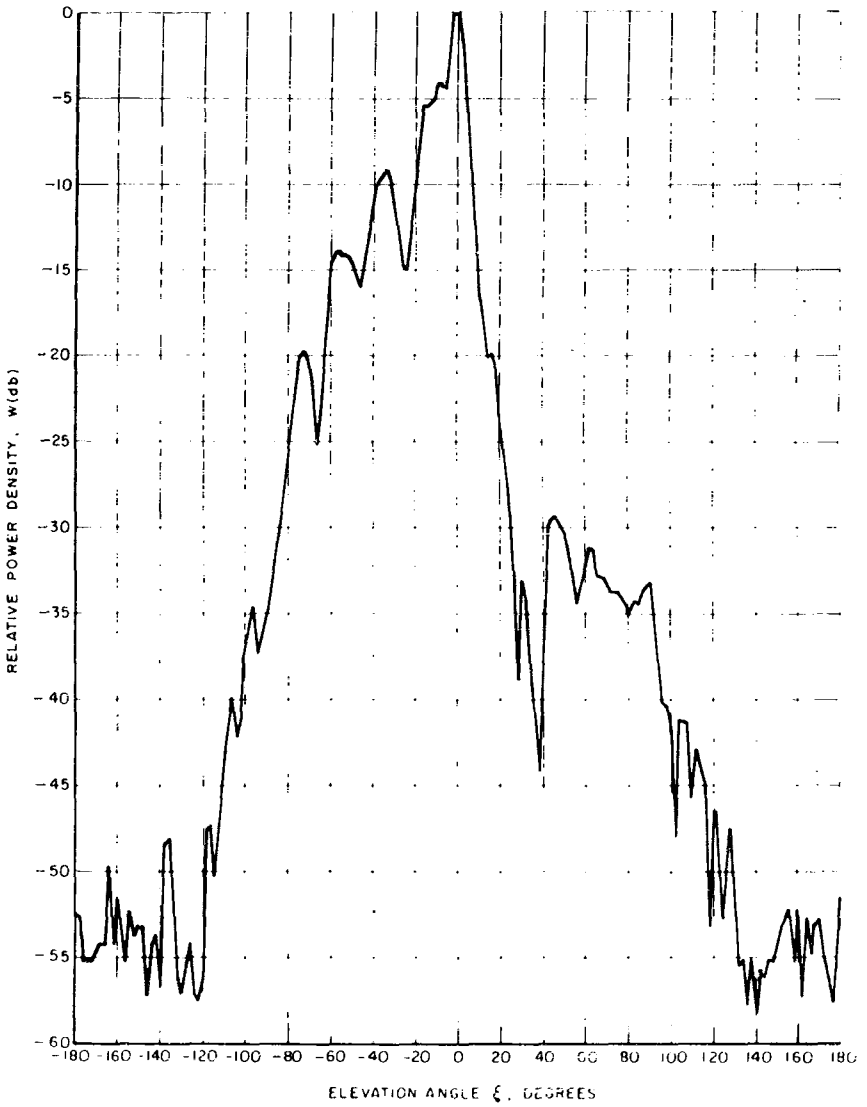



Fig. 6 MEASURED ANTENNA PATTERN — $\alpha = 0°$

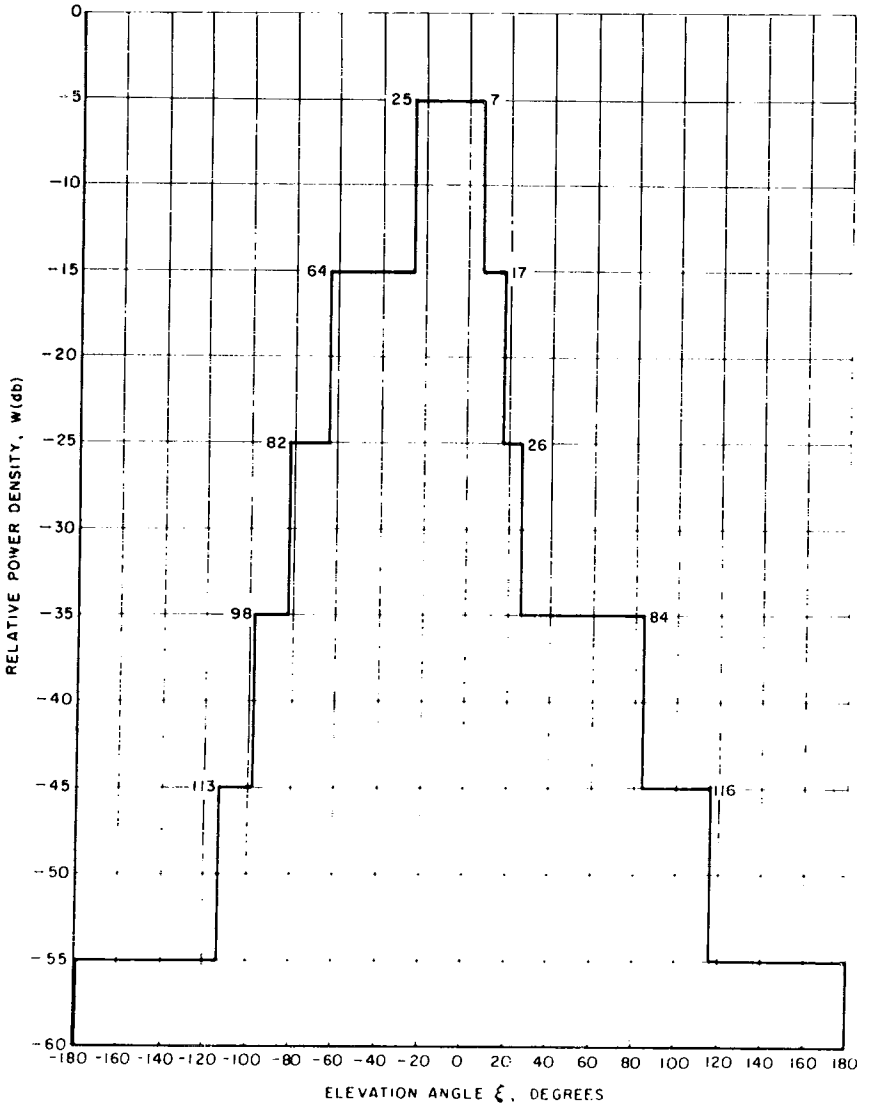



Fig. 7 10 db QUANTIZED ELEVATION PATTERN — $a = 0°$

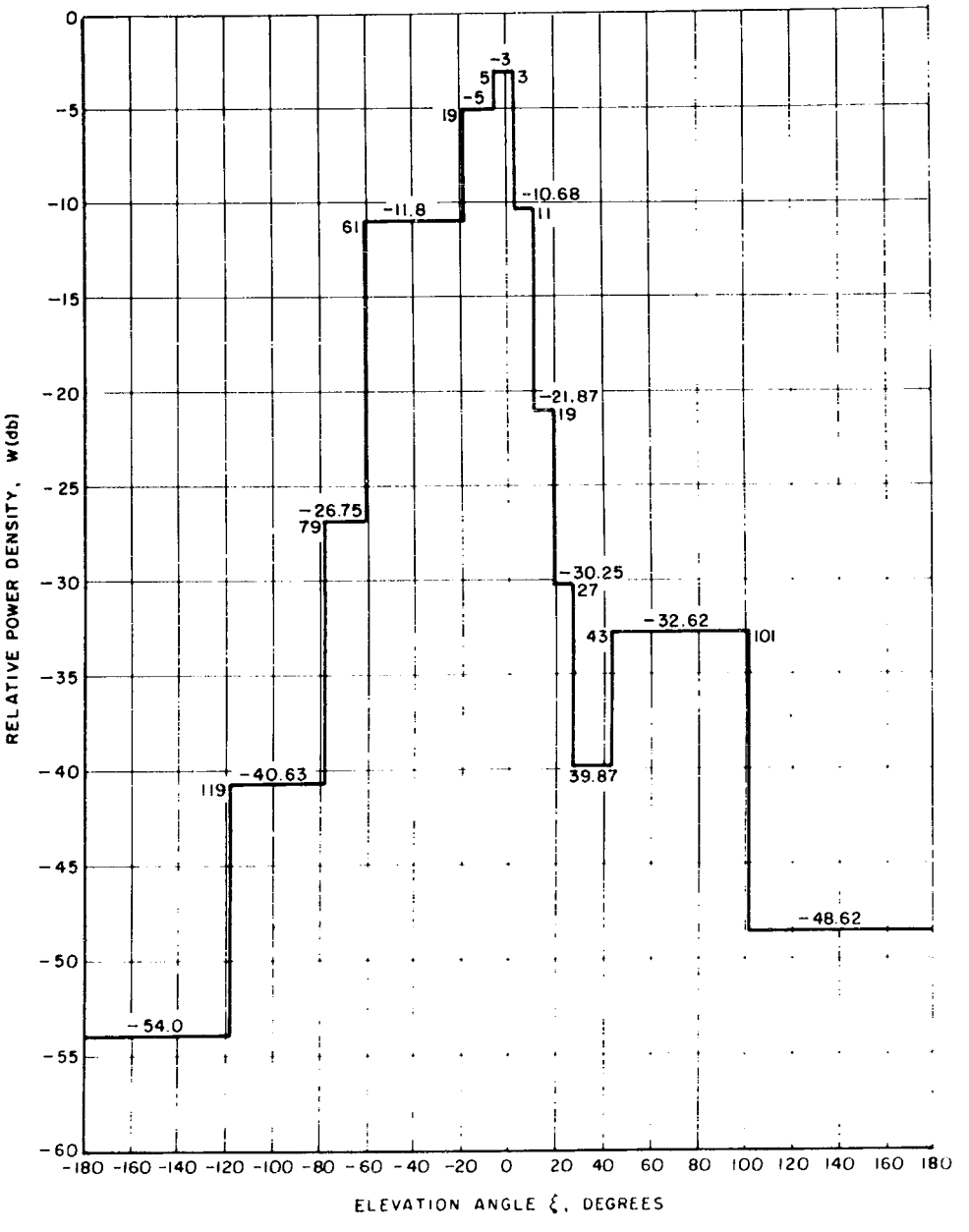



Fig. 8 ARBITRARY QUANTIZED ELEVATION PATTERN — $\alpha = 0°$

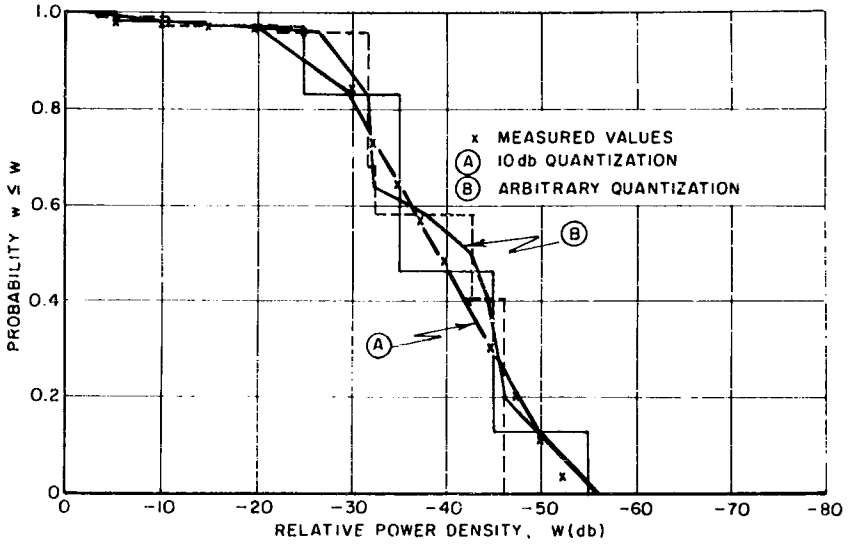



Fig. 9 CUMULATIVE PROBABILITY DISTRIBUTION FOR AZIMUTH CUT

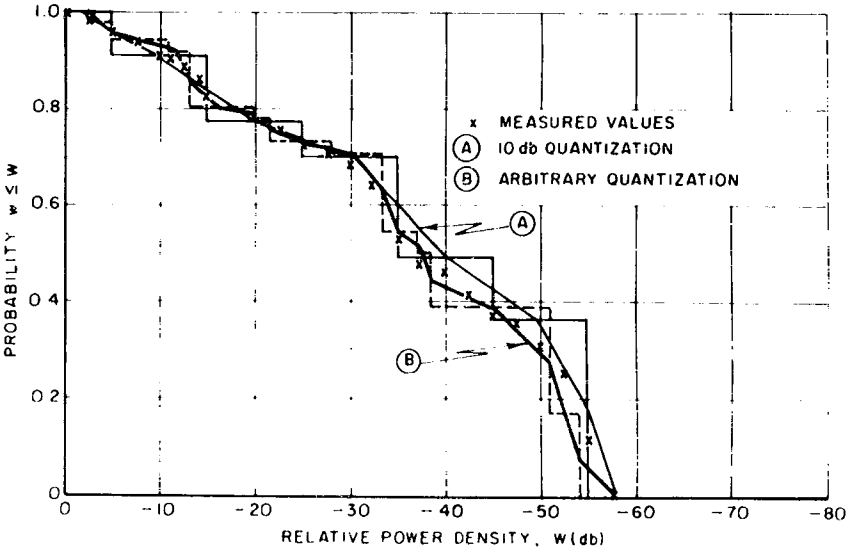



Fig. 10 CUMULATIVE PROBABILITY DISTRIBUTION FOR ELEVATION CUT
ASYMMETRIC PATTERN

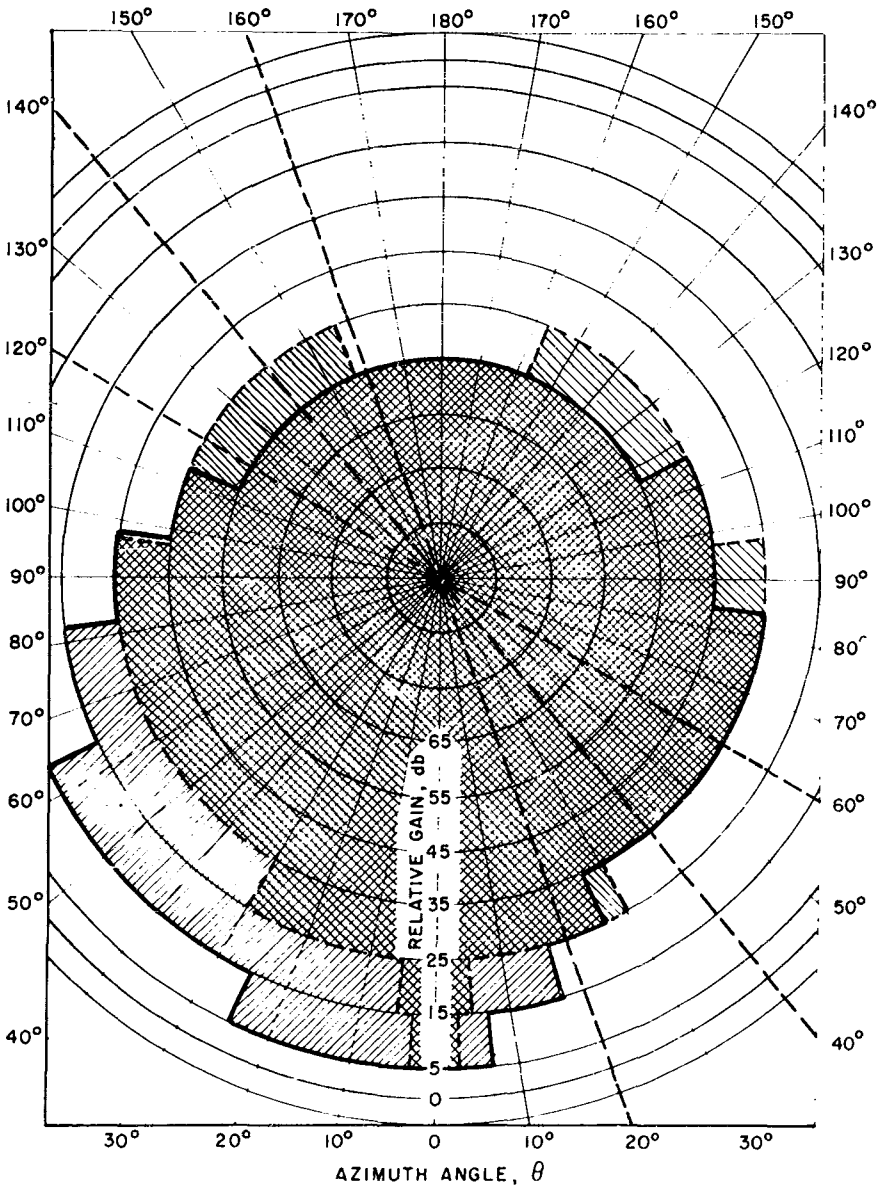



Fig. 11 COSECANT SQUARED QUANTIZED ANTENNA PATTERN

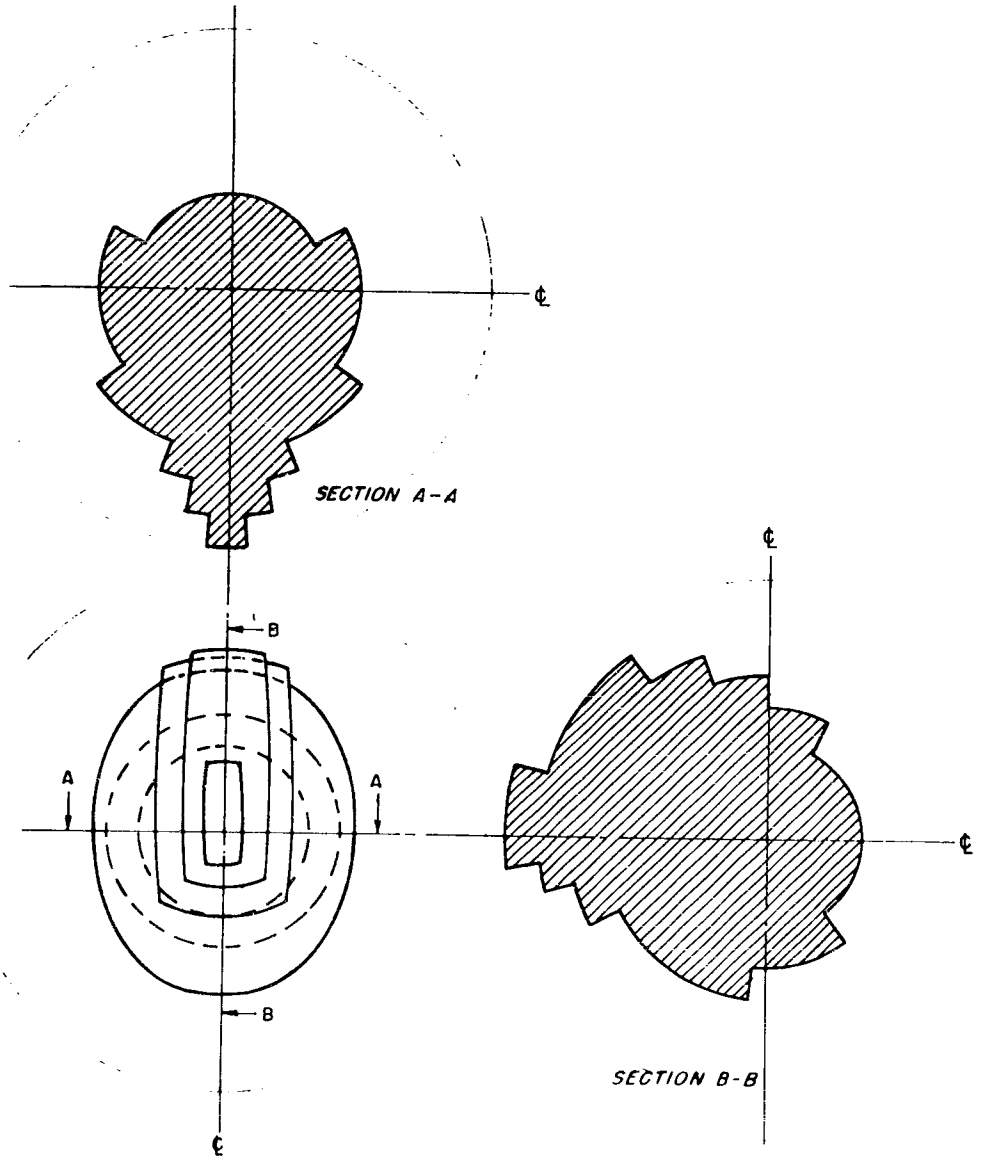



Fig. 12 COSECANT SQUARED ANTENNA MODEL

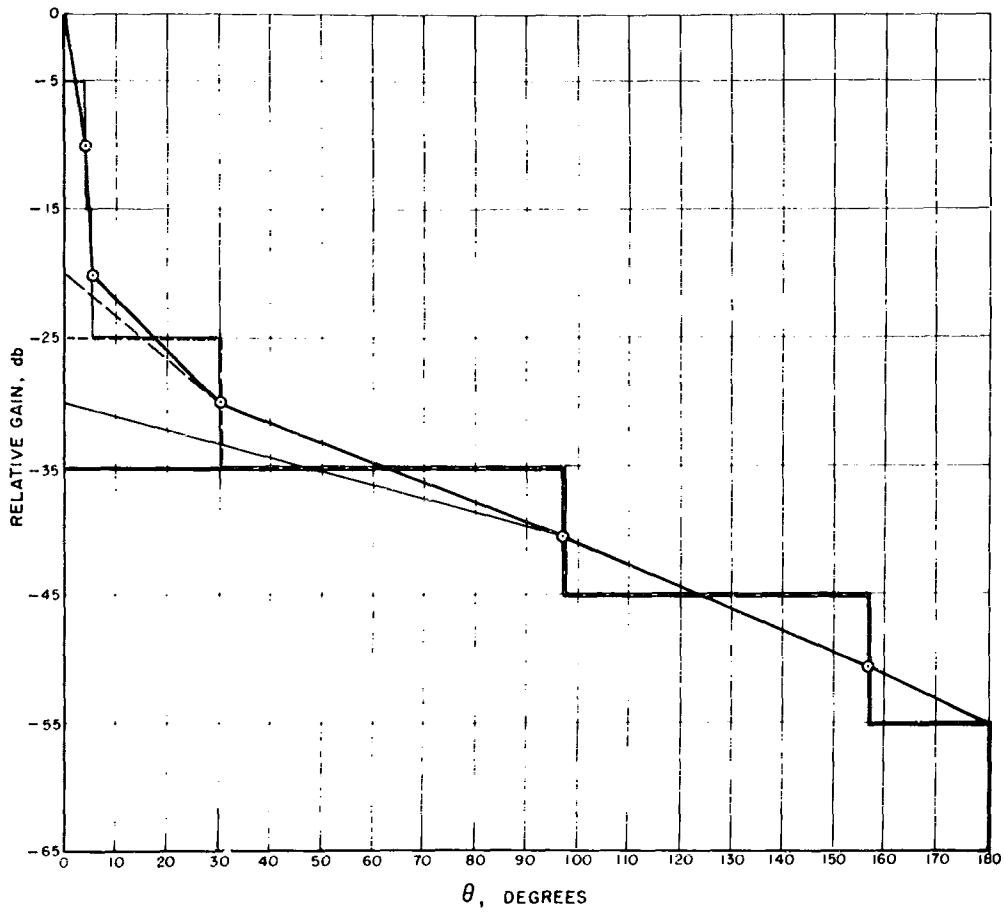



Fig. 13 QUANTIZED ANTENNA PATTERN

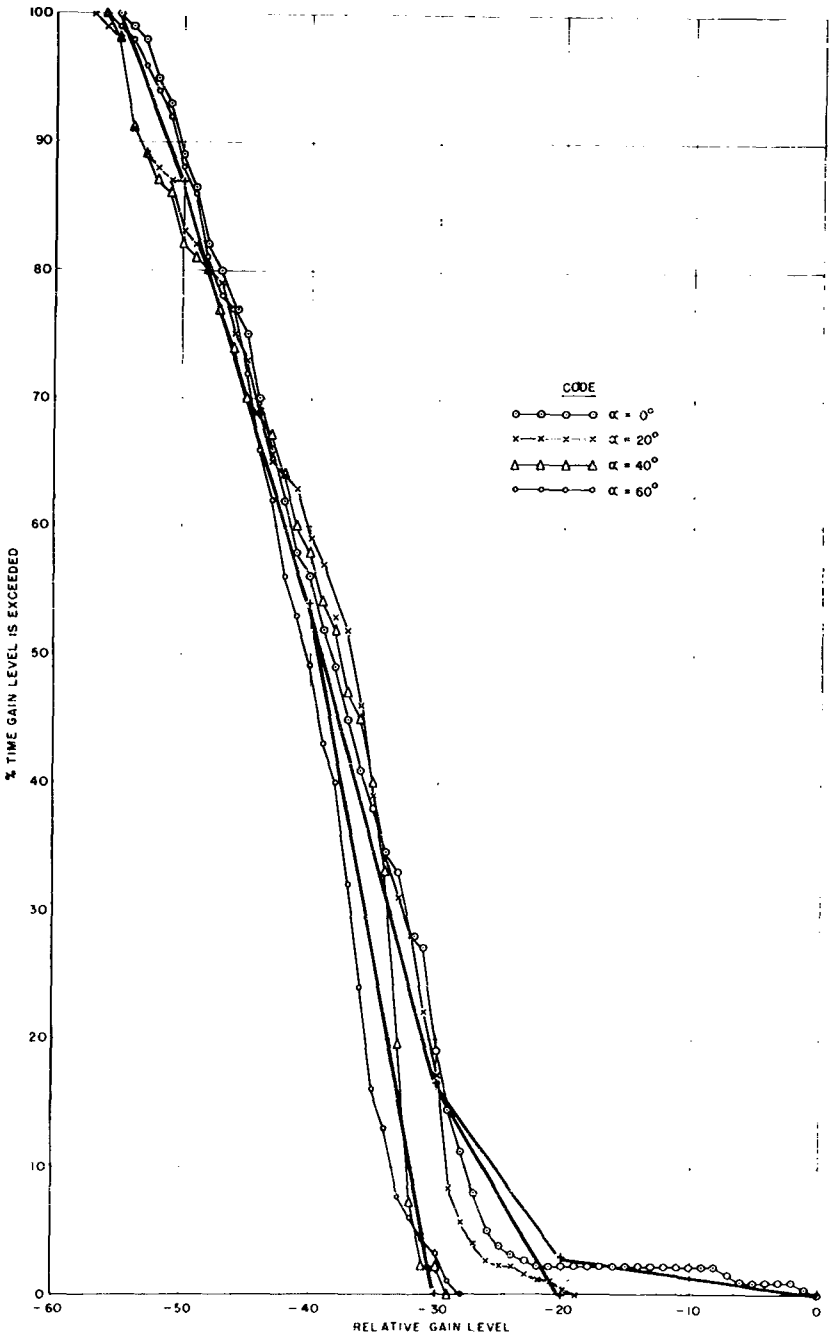



Fig. 14 COSECANT SQUARED ANTENNA STATISTICS

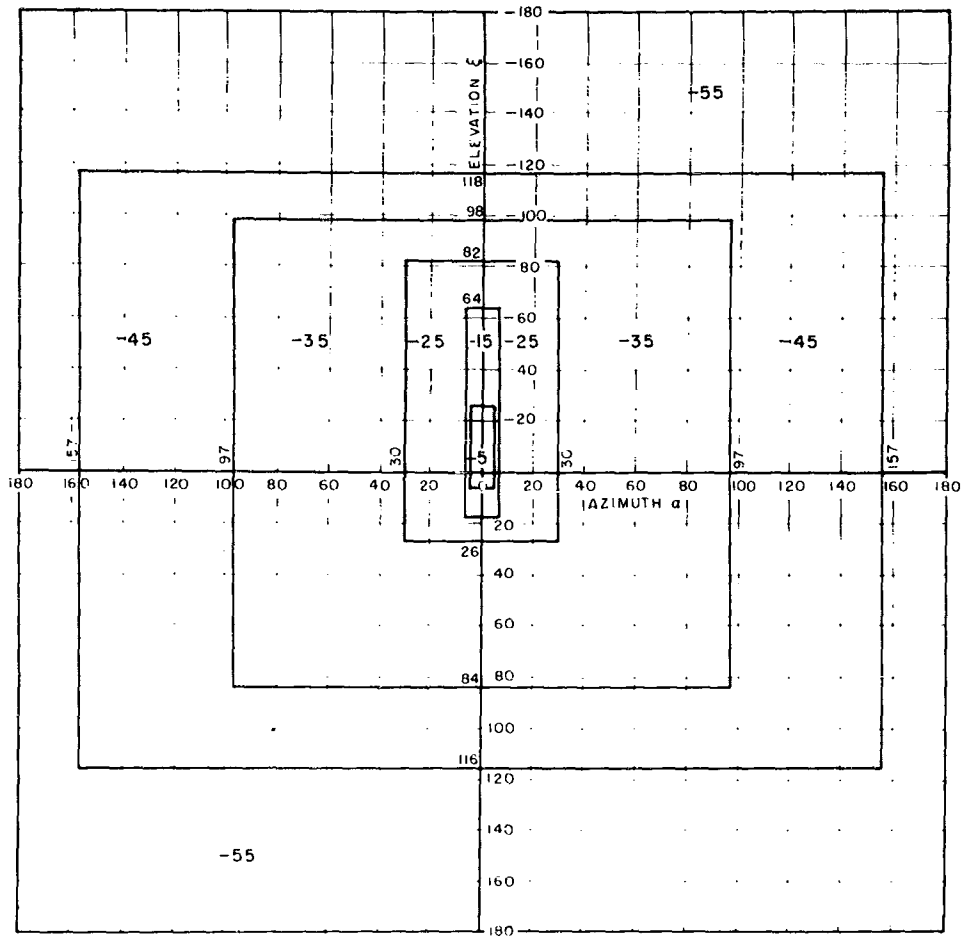



**Fig. 15** MODEL FOR QUANTIZED ANTENNA PATTERNS
(10 db STEPS)

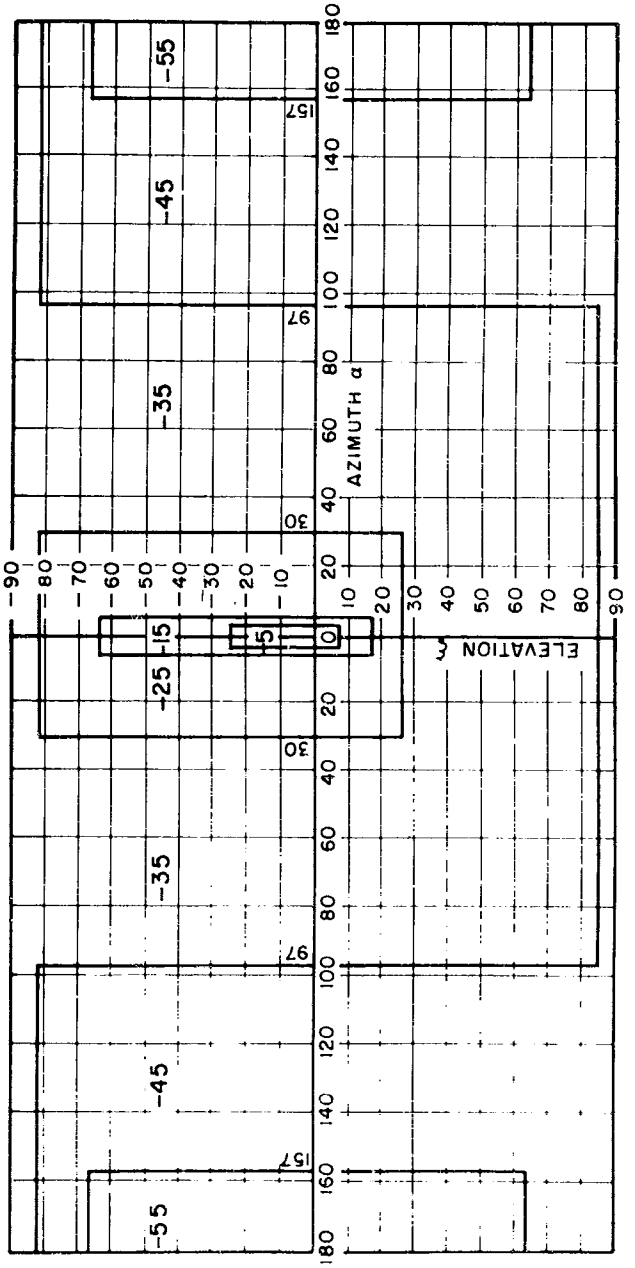



Fig. 16 FINAL MODEL FOR QUANTIZED ANTENNA PATTERNS
(10 db STEPS)

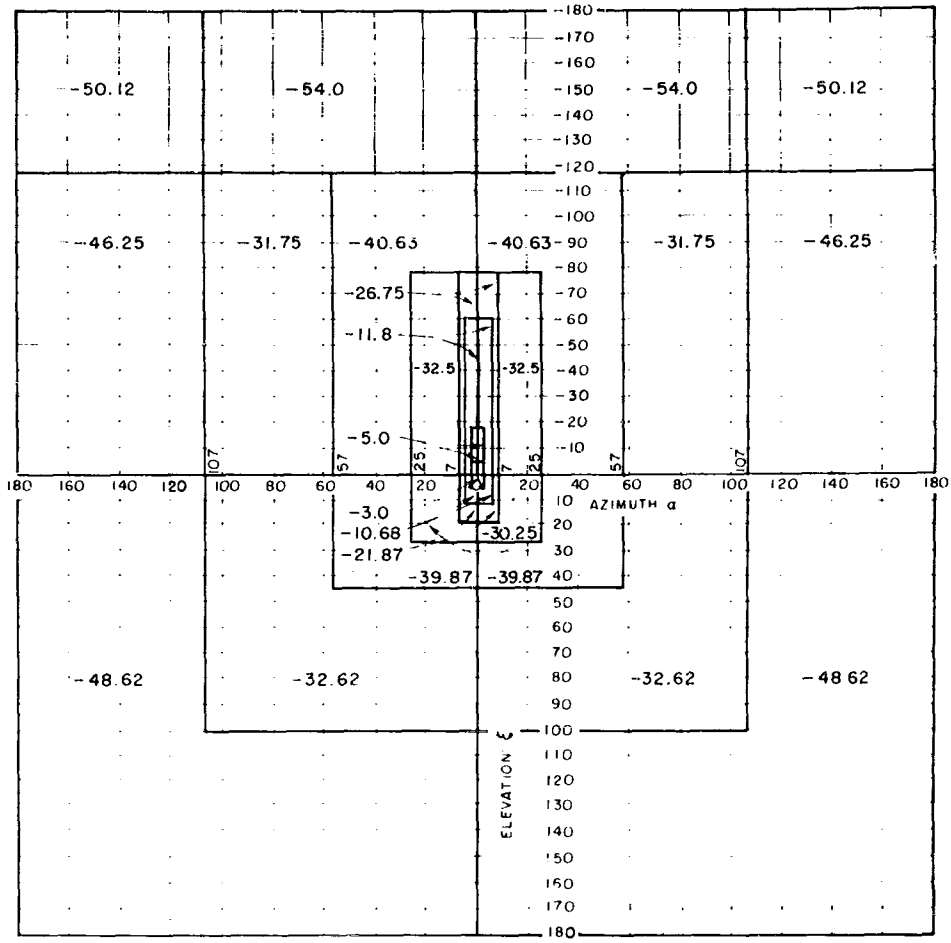



Fig. 17 MODEL FOR QUANTIZED ANTENNA PATTERNS
(ARBITRARY QUANTIZATION)

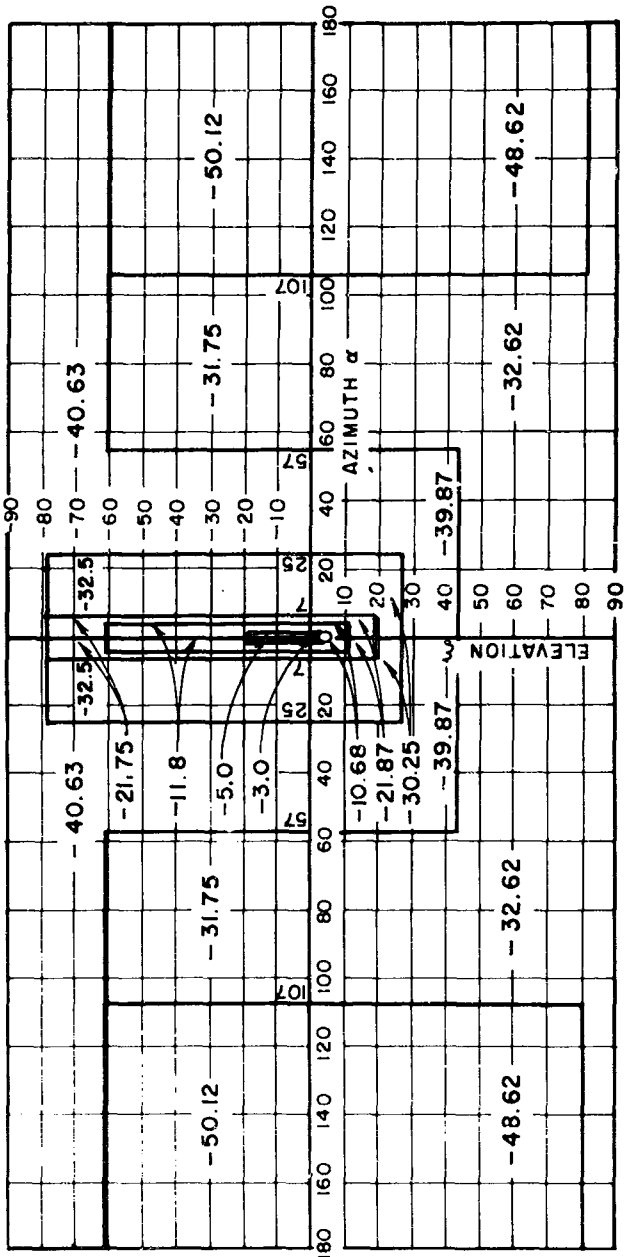



Fig. 18 FINAL MODEL FOR QUANTIZED ANTENNA PATTERNS (ARBITRARY QUANTIZATION)

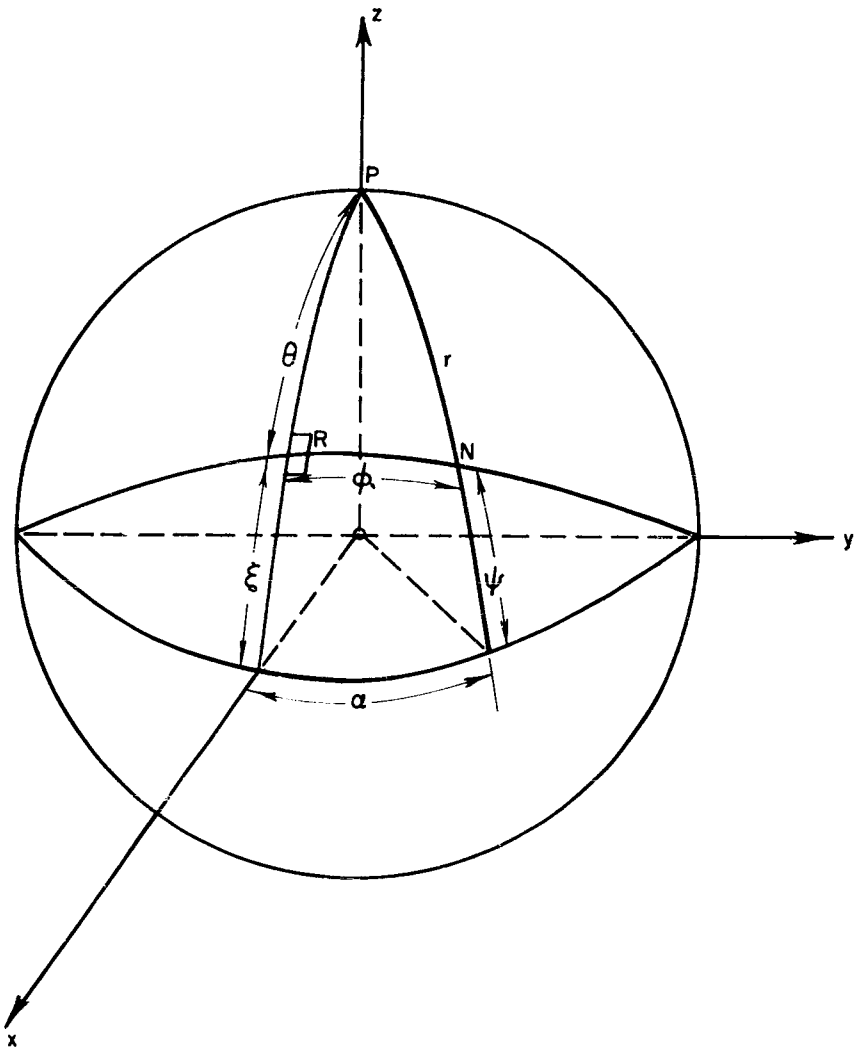



Fig. 19 COORDINATE SYSTEM TO DETERMINE SPHERICAL ANGULAR COORDINATES WHEN ANGLE ALONG A GREAT CIRCLE IS GIVEN

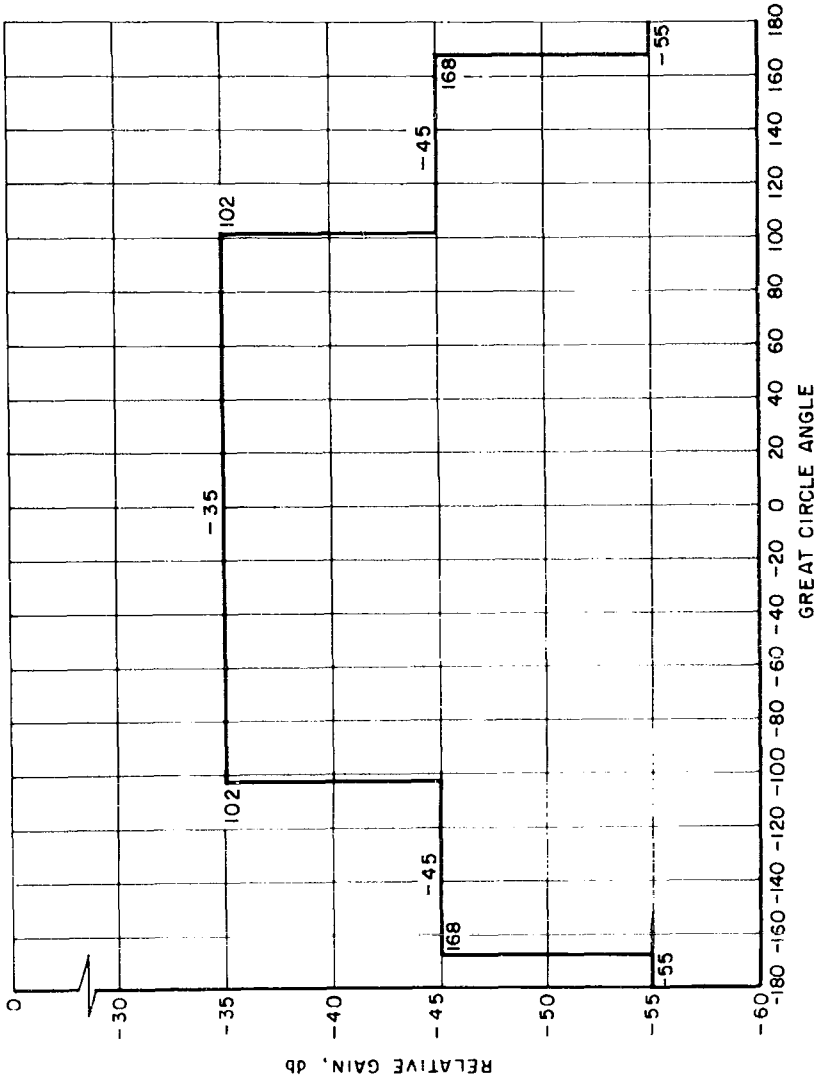



Fig. 20 DERIVED 10 db QUANTIZED PATTERN FOR $\xi = +60°$ GREAT CIRCLE CUT

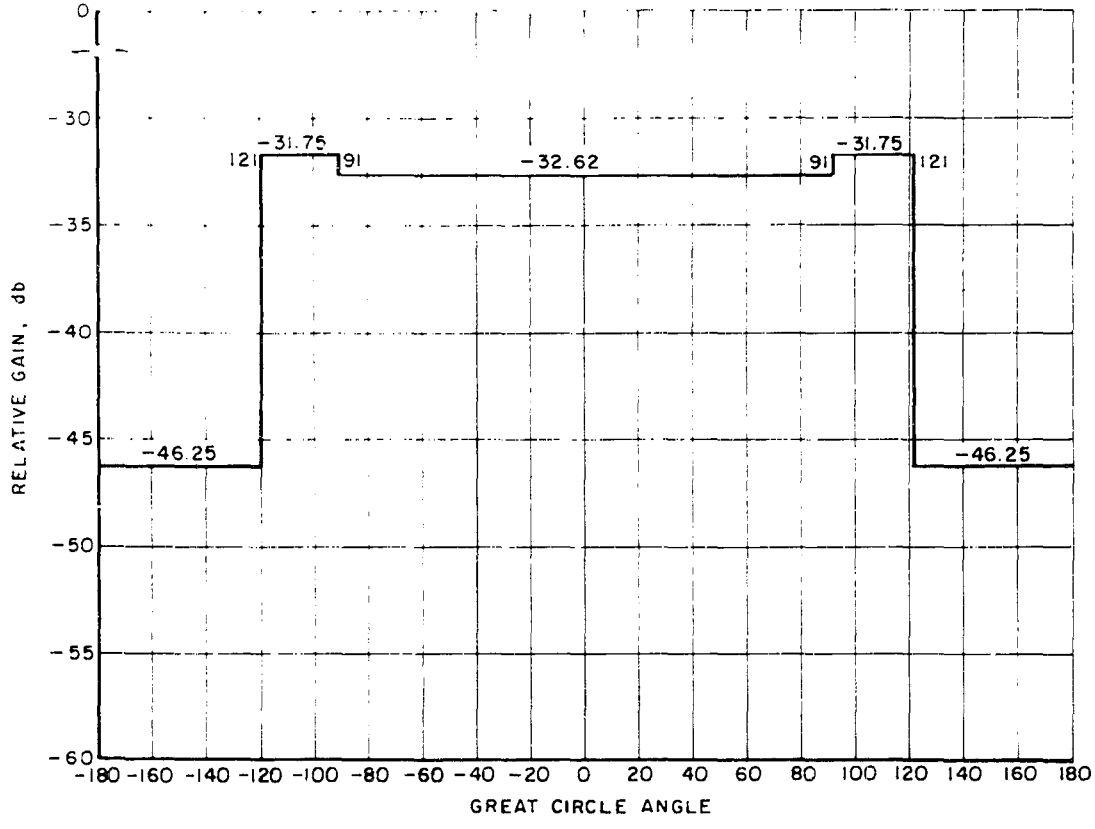



Fig. 21 DERIVED ARBITRARY QUANTIZED PATTERN FOR $\xi = +60^{\circ}$ GREAT CIRCLE CUT

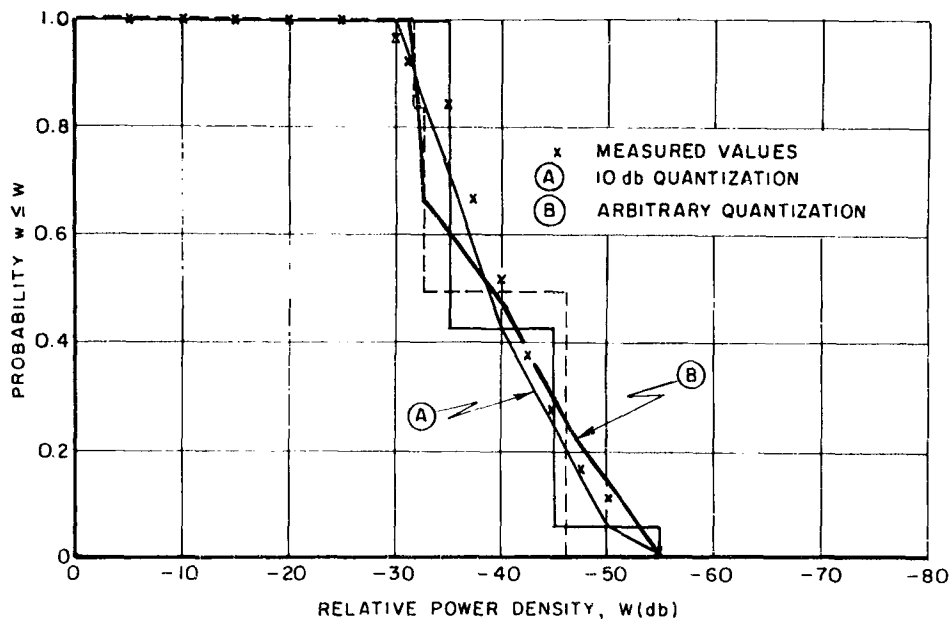



Fig. 22 CUMULATIVE PROBABILITY DISTRIBUTION FOR $\varepsilon = +60°$
GREAT CIRCLE CUT

# FRESNEL REGION AND FAR FIELD PATTERNS OF A HORN ANTENNA AT FUNDAMENTAL AND HARMONIC FREQUENCIES

O. M. Salati and D. J. Lewis
The Moore School of Electrical Engineering
University of Pennsylvania
Philadelphia 4, Pennsylvania

Abstract. - A description is given of a test facility for measuring the patterns of microwave antennas at fundamental and harmonic frequencies in both the Fresnel region and the far field region. The facility was calibrated by using standard gain horn antennas and dipole antennas. The effects of nearby objects are essentially negligible.

The patterns and impedance of an "L" band horn antenna, AT-316, excited by a, UG-953/U, waveguide to coax transducer were then measured as a function of distance from the antenna from well into the Fresnel region to the far field region. The measurements were made at three frequencies in the design band and at harmonics up to the tenth for both horizontal and vertical polarization.

The antenna patterns at second harmonic frequencies and higher showed a break-up phenomena which one would expect theoretically because of the presence of many modes of propagation in the transmission system and the exciting transducer. Nulls as deep as 70 db below main lobe gain were found.

## I. INTRODUCTION

Historically, the communications industry has been satisfied with antenna performance at one or more frequencies in the design band of the equipment. The usual data requirements consisted of beam width and patterns in the azimuth and elevation planes for design polarization, gain and antenna impedance. Occasionally data on cross polarization gain was available. The above data all in the antenna far field not only exists (even though it may be difficult to examine) but is frequently required by well written procurement specifications.

Before the advent of high equipment densities, high site densities, higher powers, more sensitive receivers, larger antennas and the recognition of sophisticated propagation paths, interference was not an apparent or real problem and the above mentioned antenna data were adequate. Theoretical antenna performance was available, for a few types of aperture illumination and for very simple aperture shapes, in the forward hemisphere of the antenna, in the far field and only in the design band.[1] Of course, when required, experimental data could have been obtained (but usually wasn't) for any situation if the cost of acquisition could be justified.

As the insidious nature of interference was recognized and its potential magnitude predicted, it was apparent that insufficient data were available on antenna performance in the near field and at other than design frequency and design polarization. Over the past five years some of these problems have been examined and solutions are currently available. For instance, for simple aperture shapes and illumination, Fresnel region gain[2,3] and power transfer data

between antennas[4] are now available. Antenna patterns or estimates of patterns can now be calculated, in the design band and with reasonable accuracy, over the complete sphere surrounding the antenna.[5]

The calculation of antenna patterns at other than design frequency has, however, remained a very difficult task. Experimental data on simple dipoles, dipole arrays, and Disc-cone antennas are currently available[6,7]. This paper describes the results of experimental work carried out on a waveguide horn antenna. Its impedance and its patterns over a ten to one frequency range for both azimuth and elevation cuts and vertical and horizontal planes have been measured as a function of separation distance from the antenna. Typical patterns are shown and graphs of antenna gain as a function of frequency presented. In addition, a brief description is given of the antenna pattern range. It must be emphasized that the work reported here is of a preliminary nature.

## II. GENERAL

Theoretically, given an antenna and the distribution of energy, in magnitude and phase, over its aperture, one can calculate the near field and far field patterns. In principal, however, this has been done only for simple apertures and aperture distributions in the design frequency band of the antenna. At frequencies outside the normal band of interest, the antenna and its transmission line system may support higher order modes.

The presence of these higher order modes in the feed system of the antenna will affect the aperture distribution and thus the radiation pattern[8] and impedance. Since the principle of superposition holds, one could calculate the pattern resulting from each mode by itself, if proper boundary conditions can be physically determined, and then combine the individual results to get a net pattern. The above can easily be done experimentally but only with great difficulty theoretically. If one knew what modes were present, the amount of labor could be reduced considerably.

The cutoff frequencies for all of the modes which can propagate in the WR-650 waveguide line, feeding the horn used in this investigation, are shown in Table I. It has also been recognized that there may be mode generation and conversion within the horn itself but no attempt has been made to analyze this effect at this time. Only a few of the modes shown in the table will be found because of mode selectivity in the transition between the tube generating the power and the transmission line[9] and thus the number of measurements required can be materially reduced. In addition, in the experimental work, the frequencies at which the patterns have been recorded were chosen so as to avoid coincidence with the cutoff frequency of any mode.

## III. IMPEDANCE MEASUREMENTS

An "L" band exponential horn having an aperture of 41 by 54 centimeters and a taper length of 93 centimeters, Figure 1, was set up in an outdoor area free of reflections. Standing wave measurements were made at the input to the horn (WR-650 waveguide) using a coaxial slotted line with a UG-953/U waveguide to coaxial adapter and also by using a standard "L" band waveguide slotted line. The results obtained are shown in Table II.

It can be seen from the table that the performance is satisfactory within the operating band for both waveguide and coax-waveguide feed. Waveguide measurements were not made at 1000 mc/s when using waveguide feed since a stretching section was not available. Above 2000 mc/s, waveguide VSWR measurements were not made because of the presence of higher order modes in the slotted section. By using a coaxial slotted section, it was possible to measure VSWR up to 4000 mc/s before higher order modes were present in the slotted line.

These measurements illustrate that impedance measurements are necessary if one wishes to understand the behavior of antenna gain as a function of frequency.

## IV. PATTERN MEASUREMENTS

The above mentioned waveguide horn including its waveguide to coaxial adapter was used in all of the pattern measurements. Since all measurements were made with the adapter in place, the results apply only to this particular horn-adapter combination. The introduction of a small length of waveguide, for instance, between the horn and the adapter would change the relative phase of the various propagating modes and thus give different results for the patterns.

The equipment set-up used for the pattern measurements is illustrated in Figure 2. The "L" band horn, which is used as the transmitting antenna, was mounted on a radar antenna rotator on a moving tower. The center of rotation of the antenna was located 75 centimeters behind the plane of the aperture while the height of the antenna axis was 2.78 meters above the roof.

The movable tower is mounted on a track so that the distance between the transmitting and receiving antennas can be varied up to 15 meters. The movable tower with the antenna, rotator and signal generator is shown in Figure 3. The pattern site with its track, movable tower and equipment shelter is shown in Figure 4. While a few obstacles are visible, none of them are closer than four meters to the antenna under test and except for the equipment shelter, all of them are at least one meter below the antenna axis. To check for the possibility of reflections, antenna patterns were recorded both with and without absorbing material on the obstacles. Very little change could be detected.

The receiving antennas used to probe and record the radiation field produced by the transmitting antenna were a series of standard gain exponential horns. These antennas were available in pairs and their gains were accurately standardized before tests were made. The appropriate receiving antenna for each test frequency was mounted on a stationary wooden tower. To check for the presence of ground reflections, the movable tower was moved along the track while the field strength variation at the receiving antenna was recorded. No serious reflections were found except at the extreme end of the range (15 meters). In the future this will be corrected by raising the tower height.

A series of patterns were recorded at each of the following frequencies: 1200 mc, 1600 mc, 2600 mc, 3200 mc, 4200 mc, 5000 mc, 6000 mc, 7200 mc, 8000 mc, 8900 mc, and 9900 mc. At each frequency a pattern was recorded for each component of the field in both the vertical and horizontal planes. The entire set of near field measurements were of primary interest, some measurements were made into the far field at every frequency.

The gain of the antenna was compared to the gain of the standard gain horn in each frequency range. This was done by replacing the "L" band horn once during each series of measurements with a duplicate of the standard gain horn being used as a field probe. The reference level thus obtained was used as a basis for comparing the maximum forward gain of the "L" band horn to the gain of the corresponding standard gain horn. This gave a reference level for the entire set of patterns recorded at each frequency, since the gain of the recording system was maintained at a constant level during any one set of measurements.

## V. RESULTS OF PATTERN MEASUREMENTS

The patterns which were obtained at the higher frequencies were, as might be expected, quite complex. In general it was found that the forward beam had broken up into a number of smaller beams and a considerable amount of cross polarization was evident. In order to discuss these results it is necessary to arbitrarily establish certain terms and definitions. These are given below and also illustrated in Figure 5.

Major Lobe — Any lobe within 20 db of the strongest portion of the pattern, and separated from the rest of the pattern by at least a 3 db minimum.

Beamwidth — The angular distance measured in degrees between the most extreme parts of the pattern which are above a specified level. The beam defined in this manner may contain a number of major lobes.

Gain — The gain is measured relative to the pattern produced by a standard gain horn. It is defined as the ratio of the field of an isotropic radiator to the maximum field strength produced by the horn (with its' associated adaptor) in a given plane and for a given polarization.

### Polarization

The polarization of the receiving antenna was used to define the field component being received. Thus if the receiving antenna was orientated to sense the vertical component of the electric field, the pattern was so labeled regardless of the orientation of the "L" band horn. Since the horn being measured was rotated 90 degrees to measure the vertical radiation pattern this means that the vertical component of the vertical pattern, for example, will actually become a horizontal field component when the horn is in its normal position.

### Gain

The gain of the "L" band horn as a function of frequency is plotted for both vertical and horizontal field components for both vertical and horizontal patterns in Figures 6 and 7. The data contained in these plots were taken from the patterns recorded at a distance of one meter, a distance within the near field in every case. It is interesting to observe that the gain remains surprisingly constant over the entire frequency range. This is in contradiction to what one might expect and what has been assumed in the past.[10]

Theoretically, the gain for the vertical component of the horizontal

pattern should be exactly equal to the horizontal component of the vertical pattern. The differences in the two curves in Figures 6 and 7 indicate either a lack of symmetry in the horn itself, uneveness in the track, or an error introduced by incorrect positioning of the horn when the planes of polarization were shifted.

Beamwidth

Both the 3 db and 20 db beamwidths for all field components in both patterns have been plotted in Figures 8 through 11. As for the gain curve, perhaps the most significant point about these curves is the remarkable constancy of the beamwidths over the wide frequency range explored. It is true, however, that it would be dangerous to assume that points do not exist where both the beamwidth and gain changes drastically.

Patterns

A typical set of patterns is shown in Figures 12 and 13 as an illustration of the behavior that may exist outside the normal operating range of the antenna. The breakup of the main beam into a number of narrower lobes is almost certainly the result of the multimode excitation of the aperture. A logical follow up of this type of result might be a mode by mode study of the antenna at a given frequency. This could be done on both an experimental and theoretical basis. In either case the techniques to be used seem rather obvious.

A particularly interesting set of patterns were obtained at a frequency of 8 kmc. It was found that at this frequency, the pattern structure of the vertical component in the near field was drastically different from the far field pattern. Specifically it can be seen from Figure 12 that there is a change from a two lobe pattern to a three lobe pattern as the separation increases. No explanation has been offered for this effect.

In most cases very little change in the pattern was observed as the antenna separation was increased beyond two or three meters. This suggests that far field conditions may be obtained at relatively close range. To support this idea, plots of field intensity in db as a function of antenna separation were made for different field components and patterns as shown in Figures 14 and 15. These data were taken from the patterns recorded and show the maximum field strength for each separation. The field strength at one meter has been used as a reference level. Nearly all of the curves approach a slope of 10 db per decade within a distance of about three meters. This would seem to suggest that the far field of the horn is within this range.

## VI. ACCURACY

In a companion paper "the instrumentation of the set-up used in the measurements has been described in detail." It is shown that a dynamic range of 100 db was achieved and the accuracy of measurement was at least as good as the standard attenuator used, that is, better than $\pm$ 1 db.

## VII. CONCLUSIONS

The results of this preliminary experimental investigation of the pat-

terns, gain, and impedance of an exponential horn antenna suggest the following:

1. The gain is approximately constant up to the 7th or 8th harmonic and then increases.

2. In the vicinity of the 7th harmonic, the cross polarization gain becomes comparable with the gain for design polarization.

3. The antenna beamwidth is approximately constant up to about the 7th harmonic.

4. The number of major lobes in the pattern changes as the distance from the antenna is increased.

5. The usual near field-far field criterion, that is distance $> D^2/\lambda$, does not apply when other modes exist.

The above observed phenomena, as previously mentioned are preliminary. It is now necessary to measure a few more horns to observe the statistics of gain, pattern, and polarization. Future plans include other antenna types and other feed arrangements.

## ACKNOWLEDGEMENT

This work was supported by the Rome Air Development Center on contract AF 30(602)1785.

## REFERENCES

1. Silver, S., "Microwave Antenna Theory and Design," vol. 12, Radiation Laboratory Series, McGraw-Hill, New York, N. Y., 1949.

2. Polk, C., "Systems Interference Evaluation," vol. 2, June 1956, University of Pennsylvania, Report 56-39, Astia AD-97882.

3. Hansen, R. C., Bailin, L. L., "Near Field Analysis of Circular Aperture Antennas," Contract AF 19(604)3508, August 1959, Astia AD-228 778.

4. Jacobs, E., "Maximum Power Transfer Between Large Aperture Antennas In The Fresnel Region," University of Pennsylvania, Report IS-60 UR-6, September 1960, Astia AD-248 663.

5. Kritikos, H. N., "Estimates of the Shadow Region Radiation of Aperture Antennas," University of Pennsylvania, Proc. 7th Conference on Radio Interference Reduction, Armour Research Foundation, 8 November 1961.

6. Polk, C., "Systems Interference Evaluation," 4th QTPR., University of Pennsylvania, July 1954, Report No. 54-49.

7. Terman, F. E., "Radio Engineers Handbook," McGraw-Hill, New York, New York.

8. Anne, A., "Study of The Fresnel-Zone Field of A Horn Antenna," Masters Thesis, University of Pennsylvania, 1960.

9. Salati, O. M., Lewis, D. J., "Interference Studies," University of Pennsylvania, Report IS-61 UR-1, Jan. 1961, AD-259 533.

10. Salati, O. M., Jacobs, E., "The Gain of Aperture Antennas at Spurious Frequencies," University of Pennsylvania, Contract AF 30(602)1785, Proc. 5th Armour Conference, 6, 7, 8 October 1959.

11. Doviak, R. J., Lewis, D. J., "A Sensitive Recording System For Harmonic Pattern Measurements at Microwave Frequencies," University of Pennsylvania, Contract AF 30(602)1785, Proc. 7th Armour Conference, 9 November 1961.

| m \ n | 0 | 1 | 2 | 3 | 4 | 5 | 6 |
|---|---|---|---|---|---|---|---|
| 0 | - | 1.82 | 3.63 | 5.45 | 7.26 | 9.08 | 10.9 |
| 1 | .908 | 2.03 | 3.74 | 5.52 | 7.74 | 9.12 | |
| 2 | 1.82 | 2.57 | 4.06 | 5.75 | 7.90 | 9.25 | |
| 3 | 2.72 | 3.27 | 4.56 | 6.08 | 8.17 | 9.46 | |
| 4 | 3.27 | 4.06 | 5.13 | 6.53 | 8.50 | 9.76 | |
| 5 | 4.56 | 4.87 | 5.81 | 7.08 | 8.93 | 10.13 | |
| 6 | 5.45 | 5.75 | 6.53 | 7.68 | 9.43 | | |
| 7 | 6.35 | 6.60 | 7.30 | 8.35 | 9.62 | | |
| 8 | 7.26 | 7.47 | 7.58 | 9.08 | | | |
| 9 | 8.17 | 8.35 | 8.93 | 9.81 | | | |
| 10 | 9.08 | 9.25 | 9.76 | | | | |
| 11 | 10 | | | | | | |

Table I. Table of cutoff frequencies for $TE_{mn}$ and $TM_{mn}$ modes. (Note that for TM modes neither m or n can be zero.)

| Freq. mc/s | VSWR Waveguide Directly | VSWR Coax-Waveguide Transition |
|---|---|---|
| 1000 | ___ (Line stretching section needed) | 1.7 |
| 1200 | 1.1 | 1.1 |
| 1300 | 1.07 | 1.1 |
| 1500 | | 1.12 |
| 1900 | 1.05 | 1.1 |
| 2000 | 1.1 | 2.1 |
| 2200 | ↑ | 2.6 |
| 2500 | Mode Conversion | 1.8 |
| 2800 | Present | 6.3 |
| 3000 | ↓ | 3.3 |
| 3100 | | 2.7 |
| 3300 | | 8.9 |
| 3900 | | 3.8 |
| 4000 | | 4.4 |

Table II. Impedance Measurements On "L" Band Exponential Horn

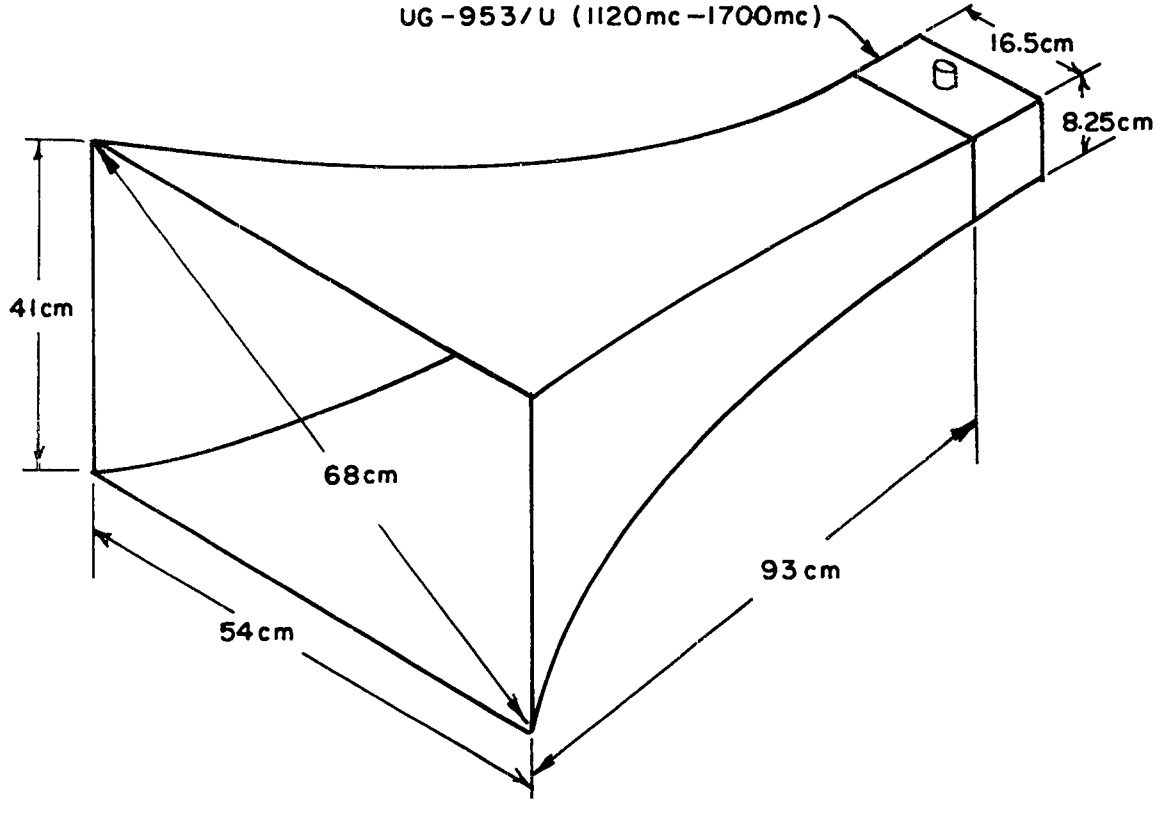



FIG. 1 L BAND HORN ANTENNA UNDER STUDY. 37046 - 9 - 1

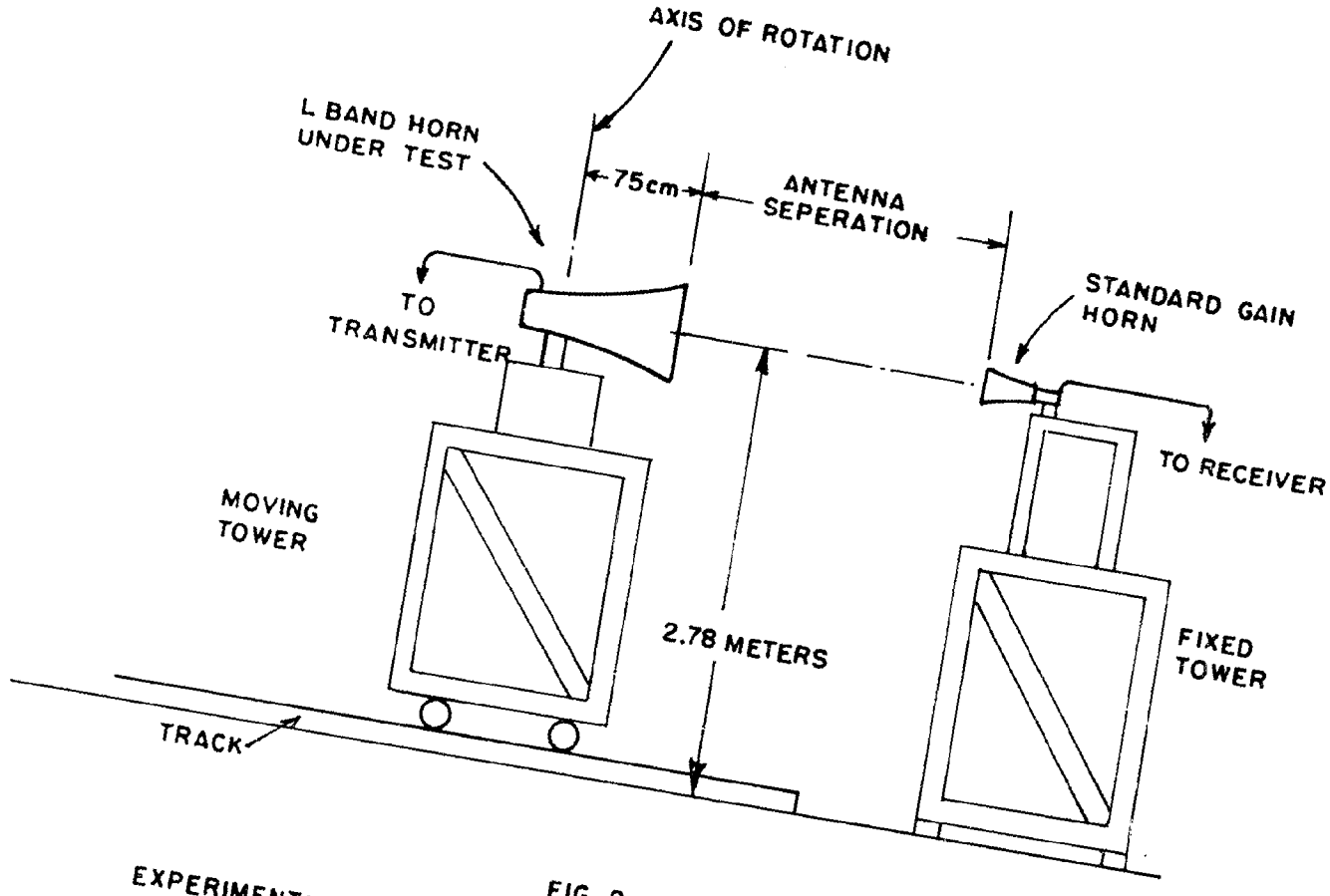



FIG. 2

EXPERIMENTAL SETUP USED TO OBTAIN PATTERN MEASUREMENTS

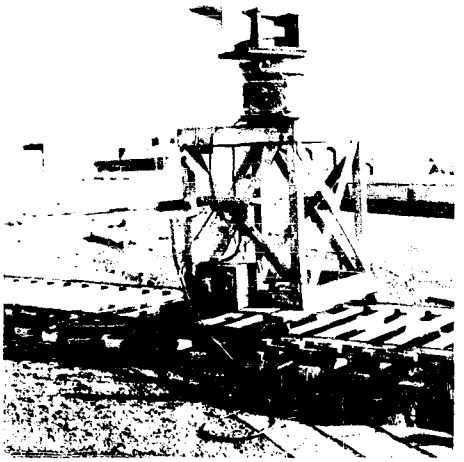


Fig. 3

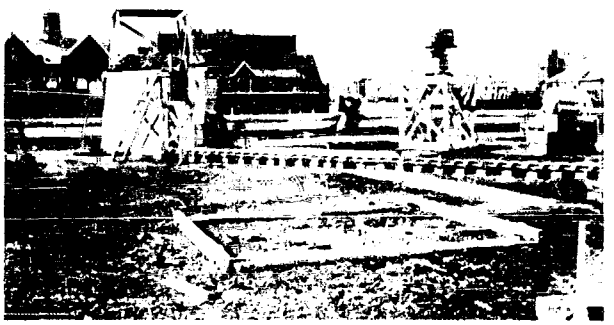


Fig. 4

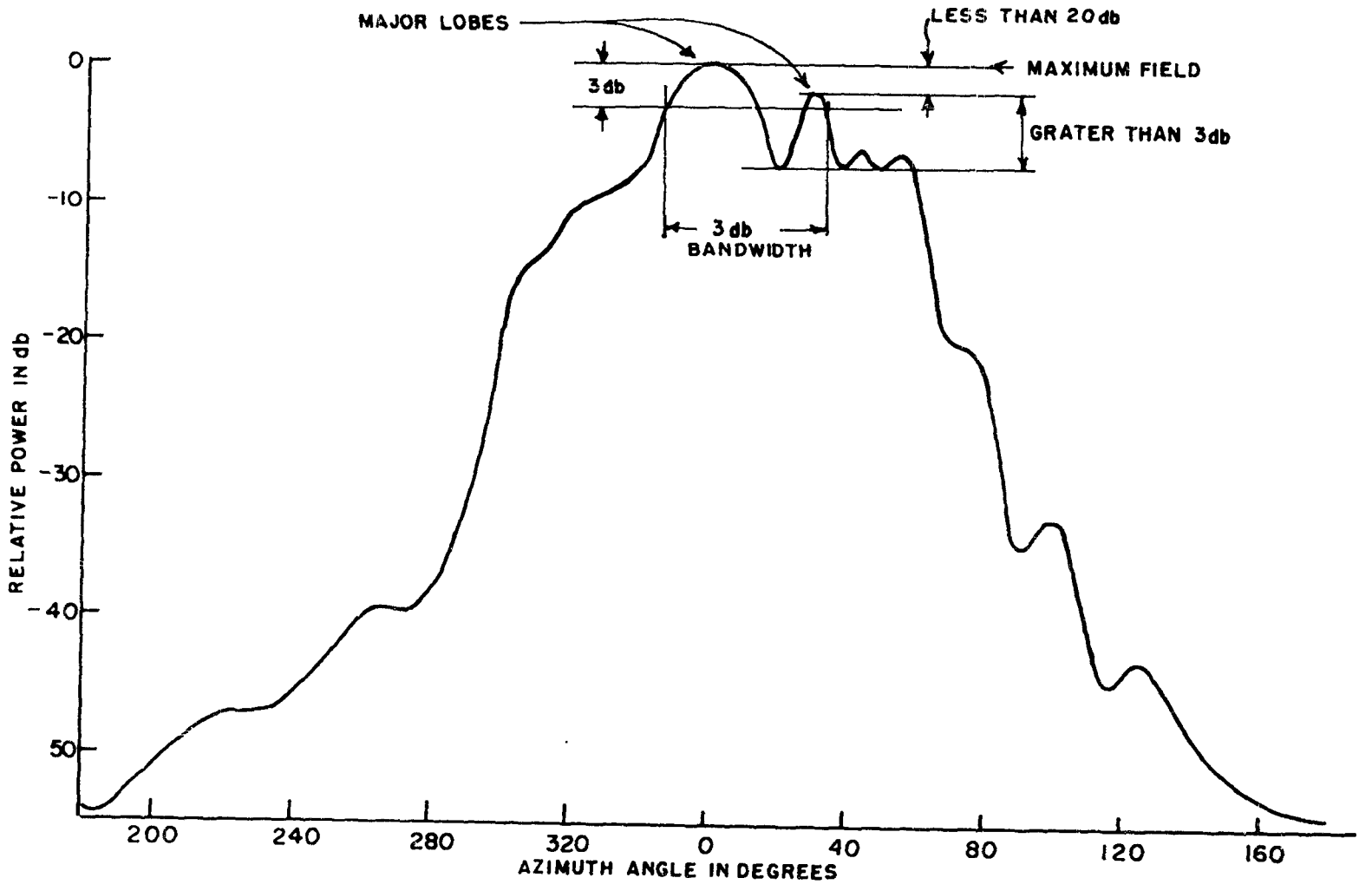



FIG. 5 DEFINITIONS USED IN DESCRIBING PATTERNS 37046 - 9 - 5

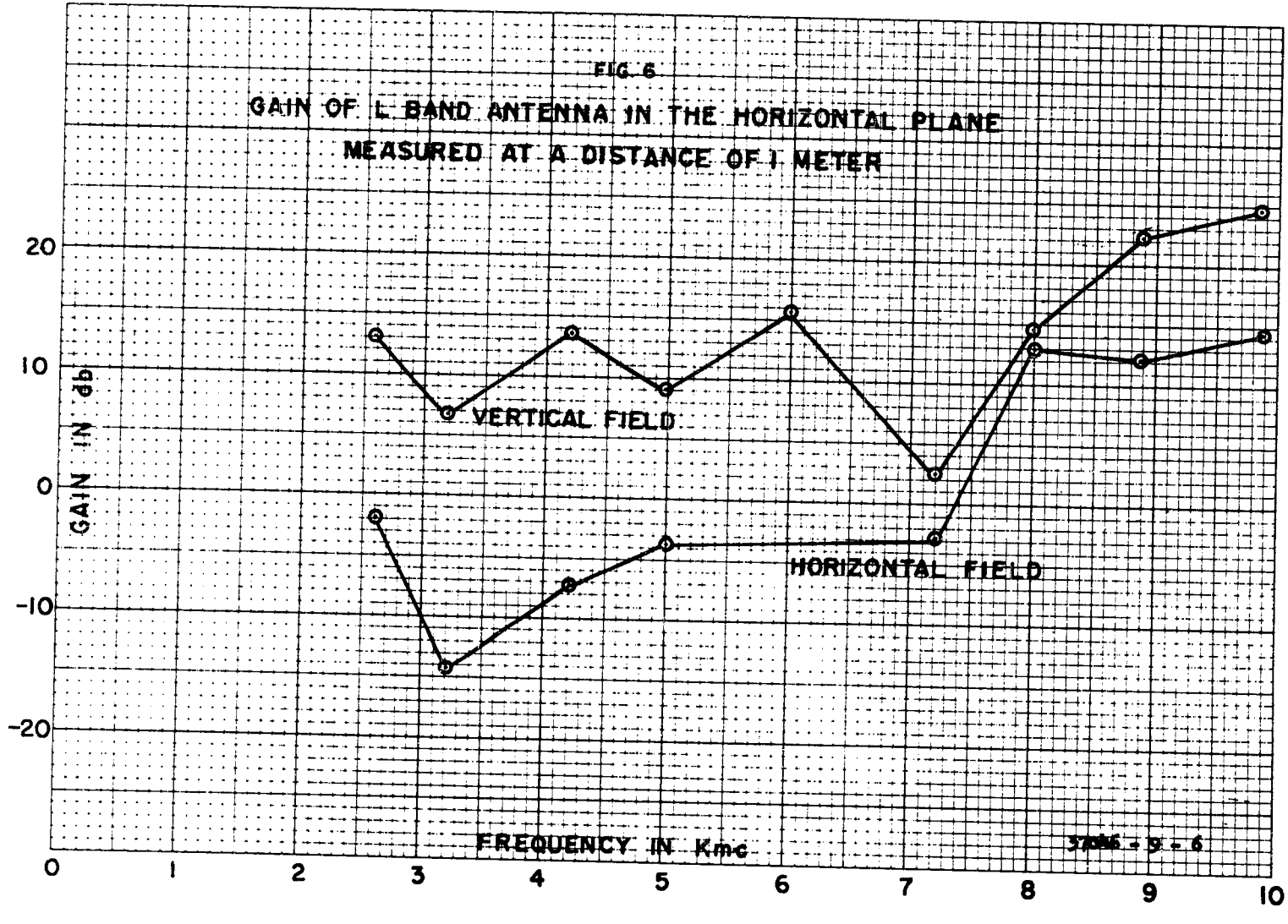
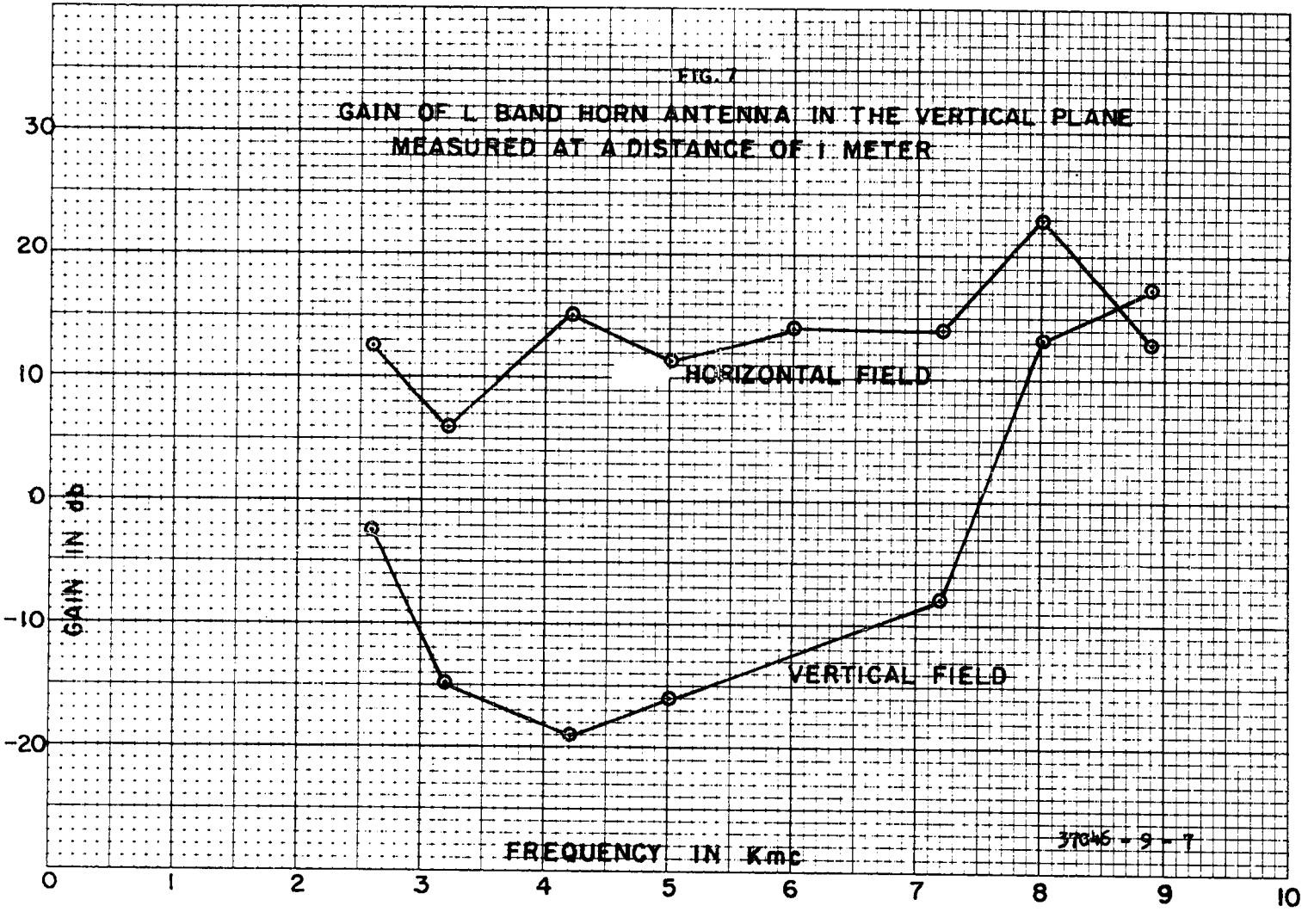
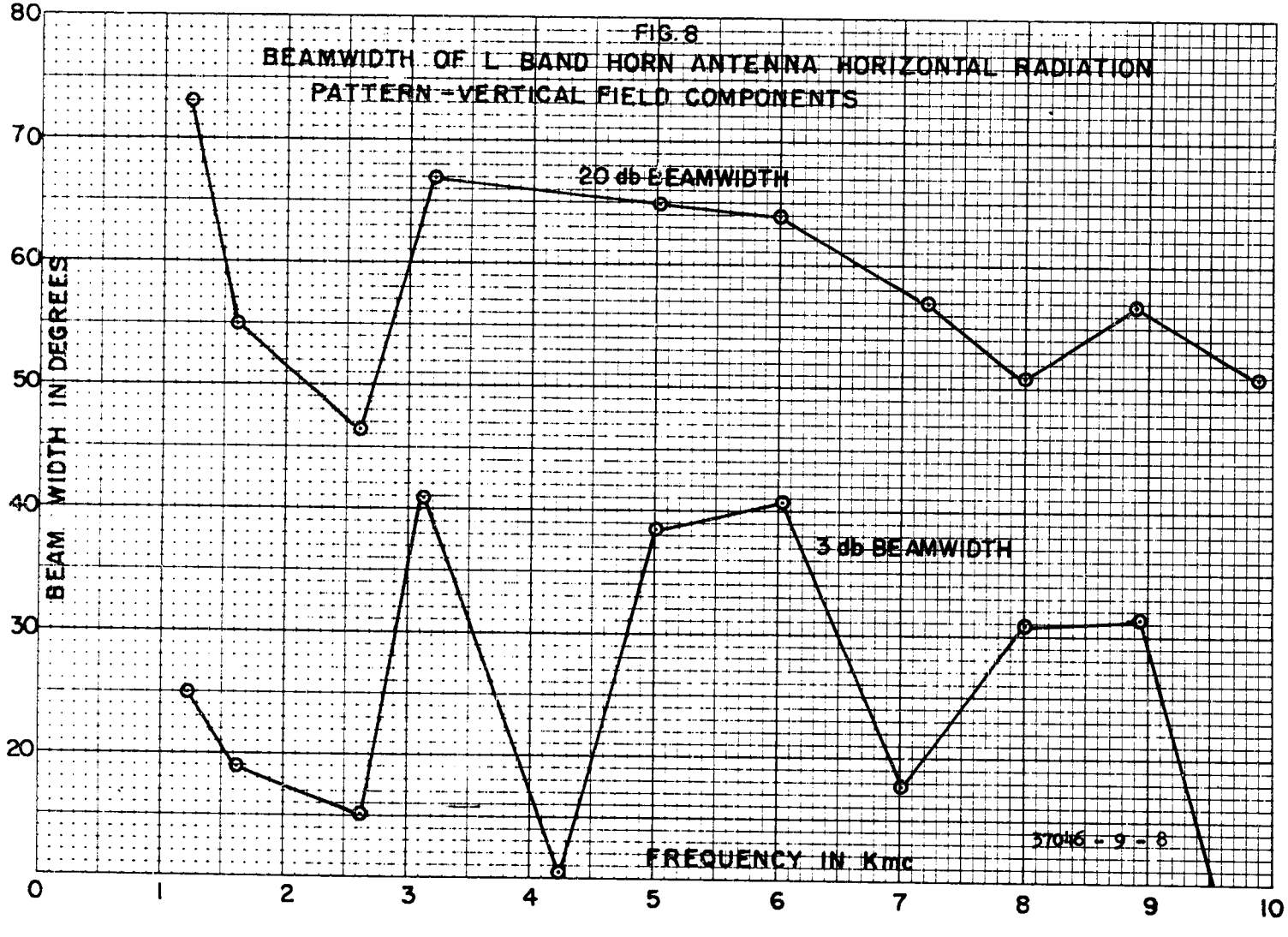
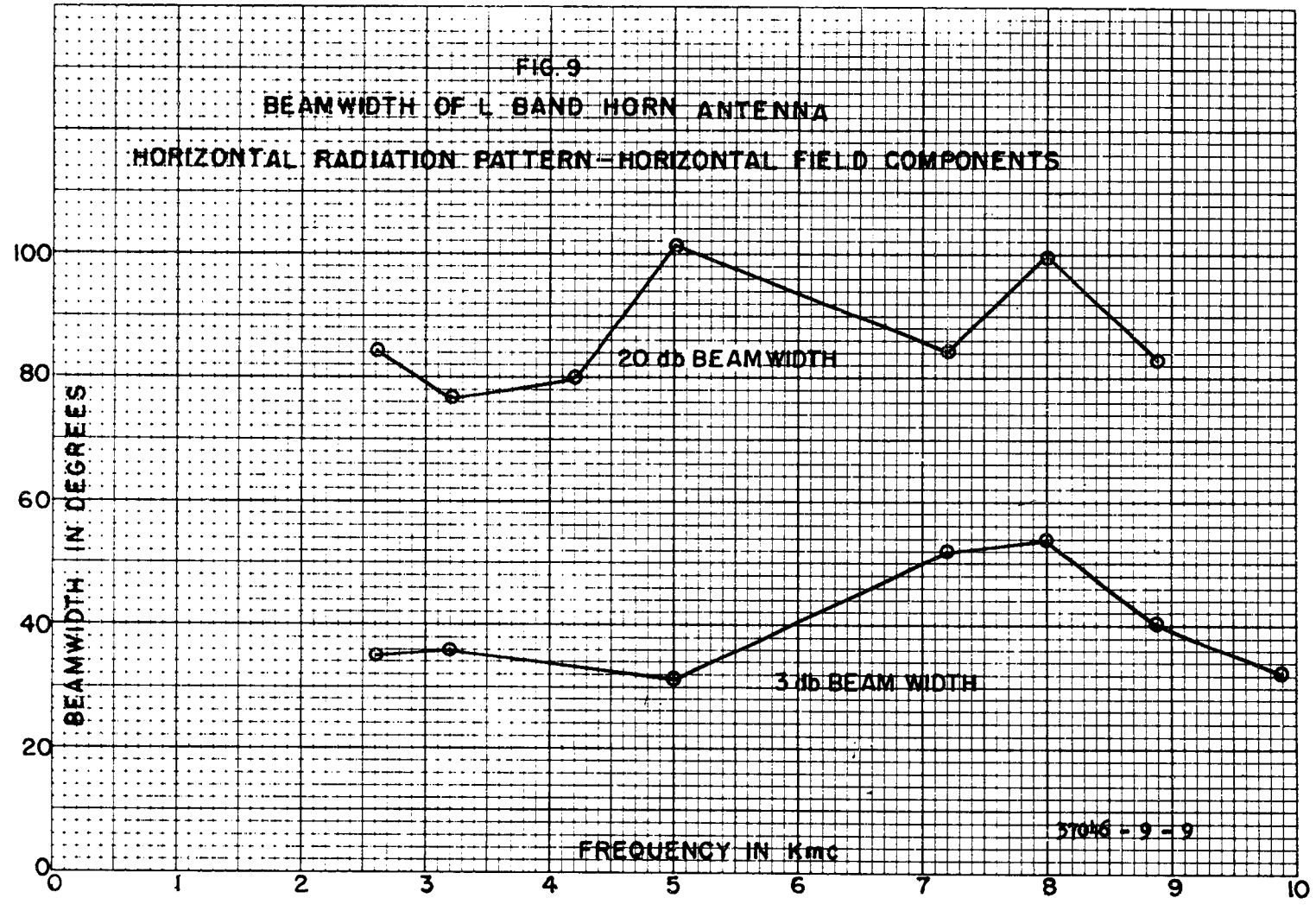
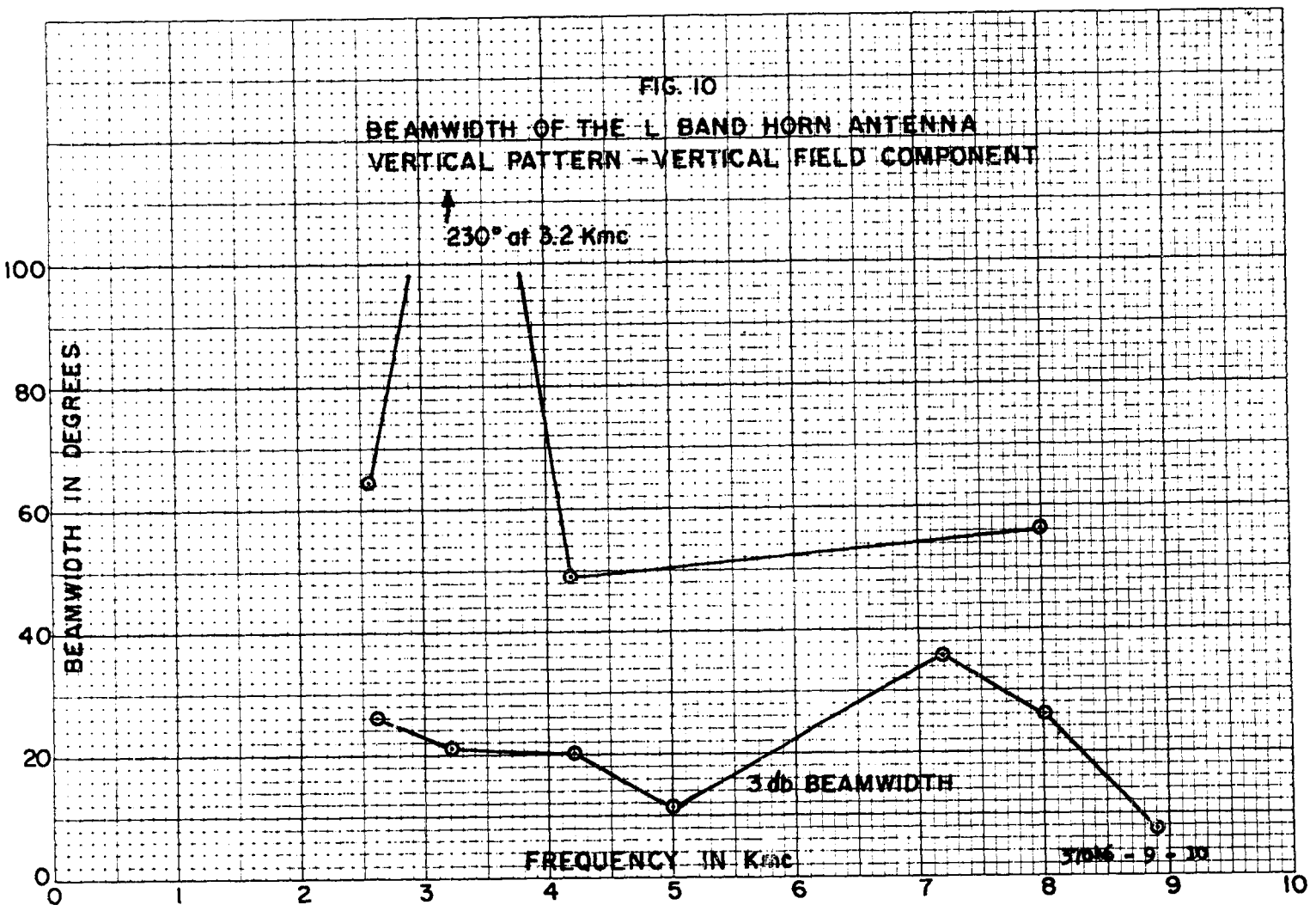

FIG 6
GAIN OF L BAND ANTENNA IN THE HORIZONTAL PLANE
MEASURED AT A DISTANCE OF 1 METER
GAIN IN db
20
10
0
-10
-20
VERTICAL FIELD
HORIZONTAL FIELD
FREQUENCY IN Kmc
0
1
2
3
4
5
6
7
8
9
10

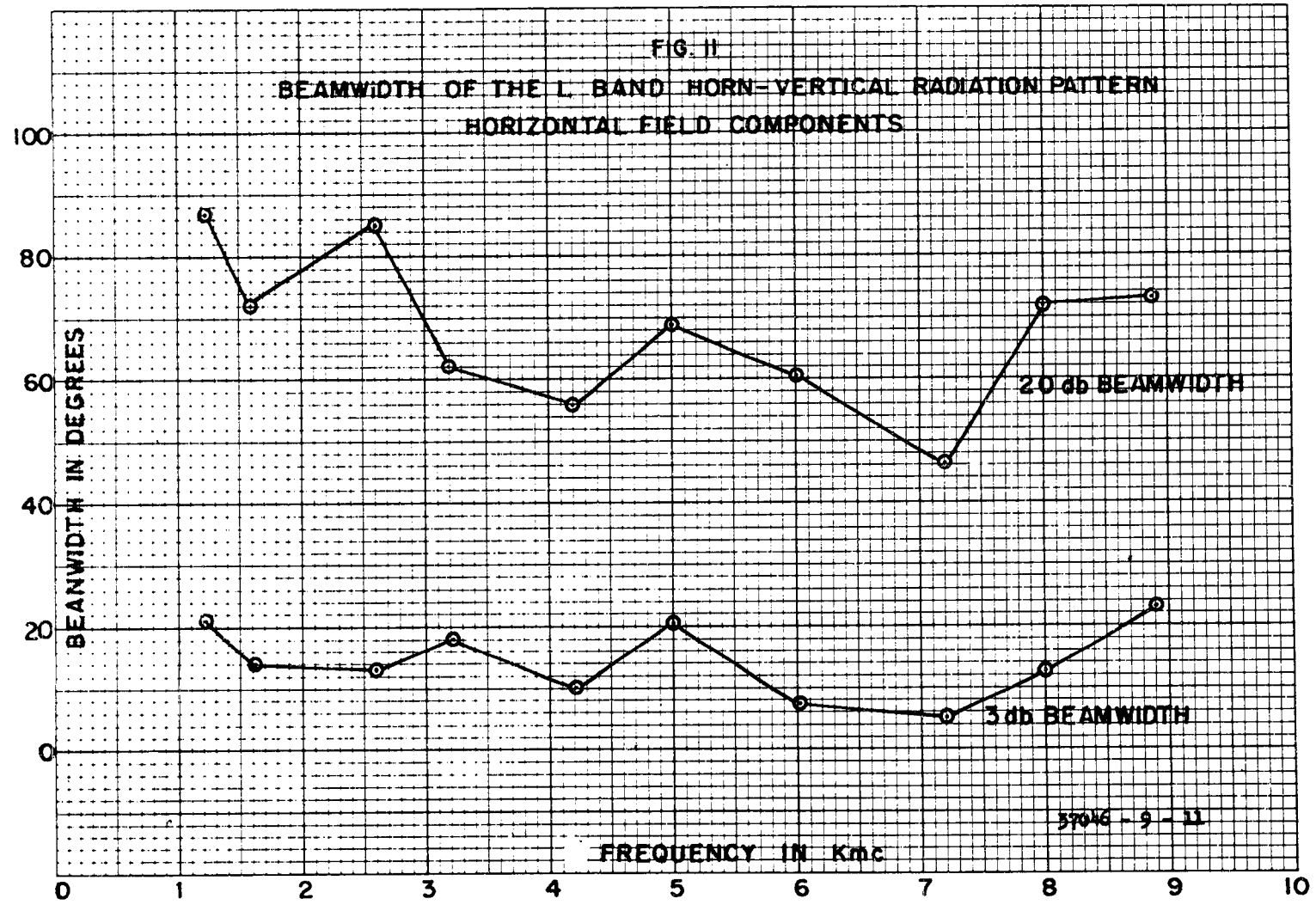
FIG. 7


GAIN OF L BAND HORN ANTENNA IN THE VERTICAL PLANE
MEASURED AT A DISTANCE OF 1 METER
HORIZONTAL FIELD
VERTICAL FIELD
GAIN IN db
FREQUENCY IN Kmc
37046-9-7
30
20
10
0
-10
-20
0
1
2
3
4
5
6
7
8
9
10


FIG. 8
BEAMWIDTH OF L BAND HORN ANTENNA HORIZONTAL RADIATION PATTERN - VERTICAL FIELD COMPONENTS
20 db BEAMWIDTH
3 db BEAMWIDTH
BEAM WIDTH IN DEGREES
FREQUENCY IN Kmc
37046 - 9 - 8
80
70
60
50
40
30
20
0
1
2
3
4
5
6
7
8
9
10


FIG. 9
BEAMWIDTH OF L BAND HORN ANTENNA
HORIZONTAL RADIATION PATTERN - HORIZONTAL FIELD COMPONENTS
BEAMWIDTH IN DEGREES
FREQUENCY IN Kmc
20 db BEAMWIDTH
3 db BEAM WIDTH
57046 - 9 - 9
0
20
40
60
80
100
0
1
2
3
4
5
6
7
8
9
10


FIG. 10
BEAMWIDTH OF THE L BAND HORN ANTENNA
VERTICAL PATTERN – VERTICAL FIELD COMPONENT
230° at 3.2 Kmc
BEAMWIDTH IN DEGREES
FREQUENCY IN Kmc
3 db BEAMWIDTH
0
20
40
60
80
100
0
1
2
3
4
5
6
7
8
9
10


FIG. 11
BEAMWIDTH OF THE L BAND HORN-VERTICAL RADIATION PATTERN
HORIZONTAL FIELD COMPONENTS
BEAMWIDTH IN DEGREES
100
80
60
40
20
0
20 db BEAMWIDTH
3 db BEAMWIDTH
57046 - 9 - 11
FREQUENCY IN Kmc
0
1
2
3
4
5
6
7
8
9
10

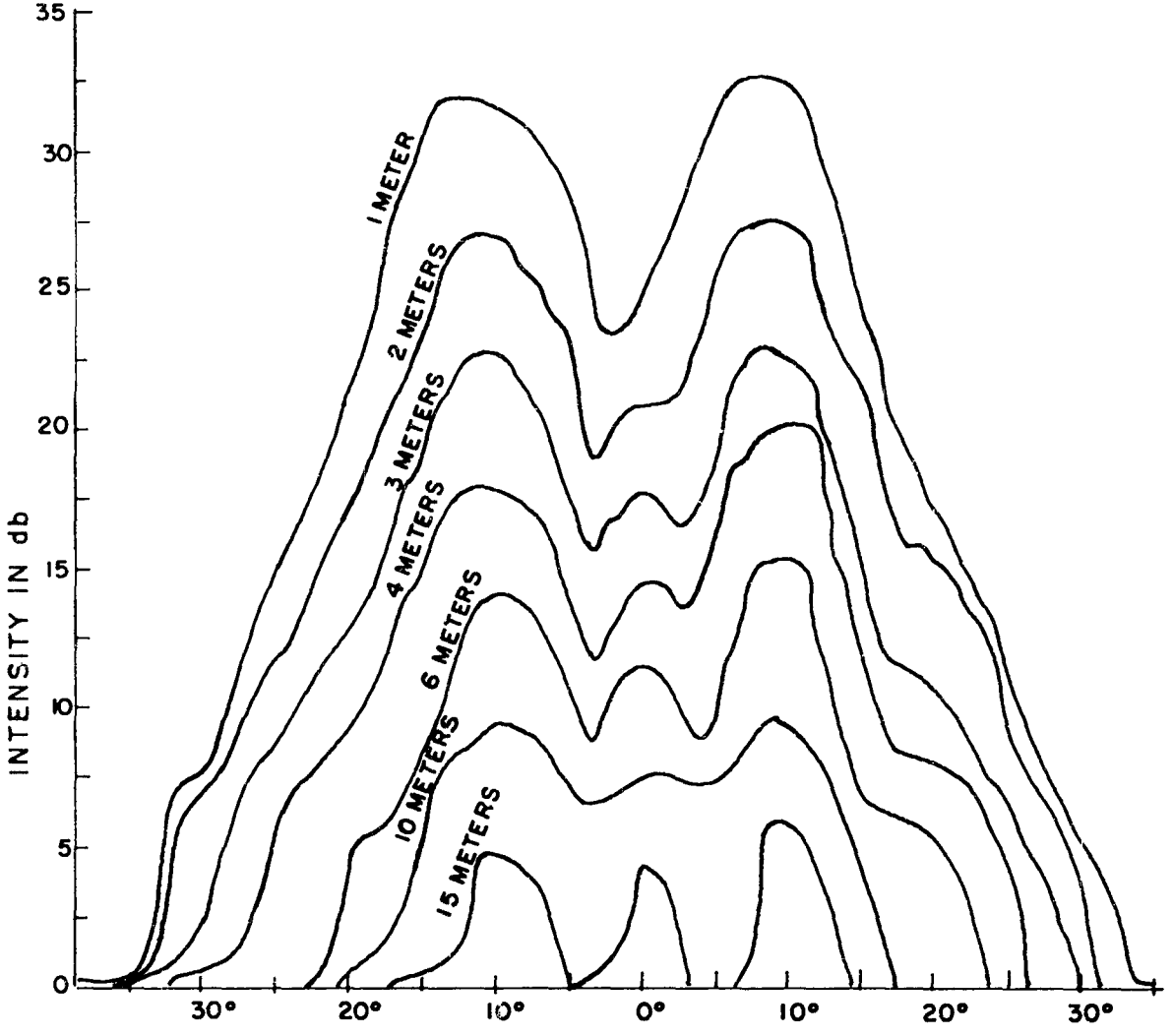



FIG. 12 VERTICAL FIELD COMPONENT OF THE HORIZONTAL RADIATION PATTERN AT 8 Kmc.

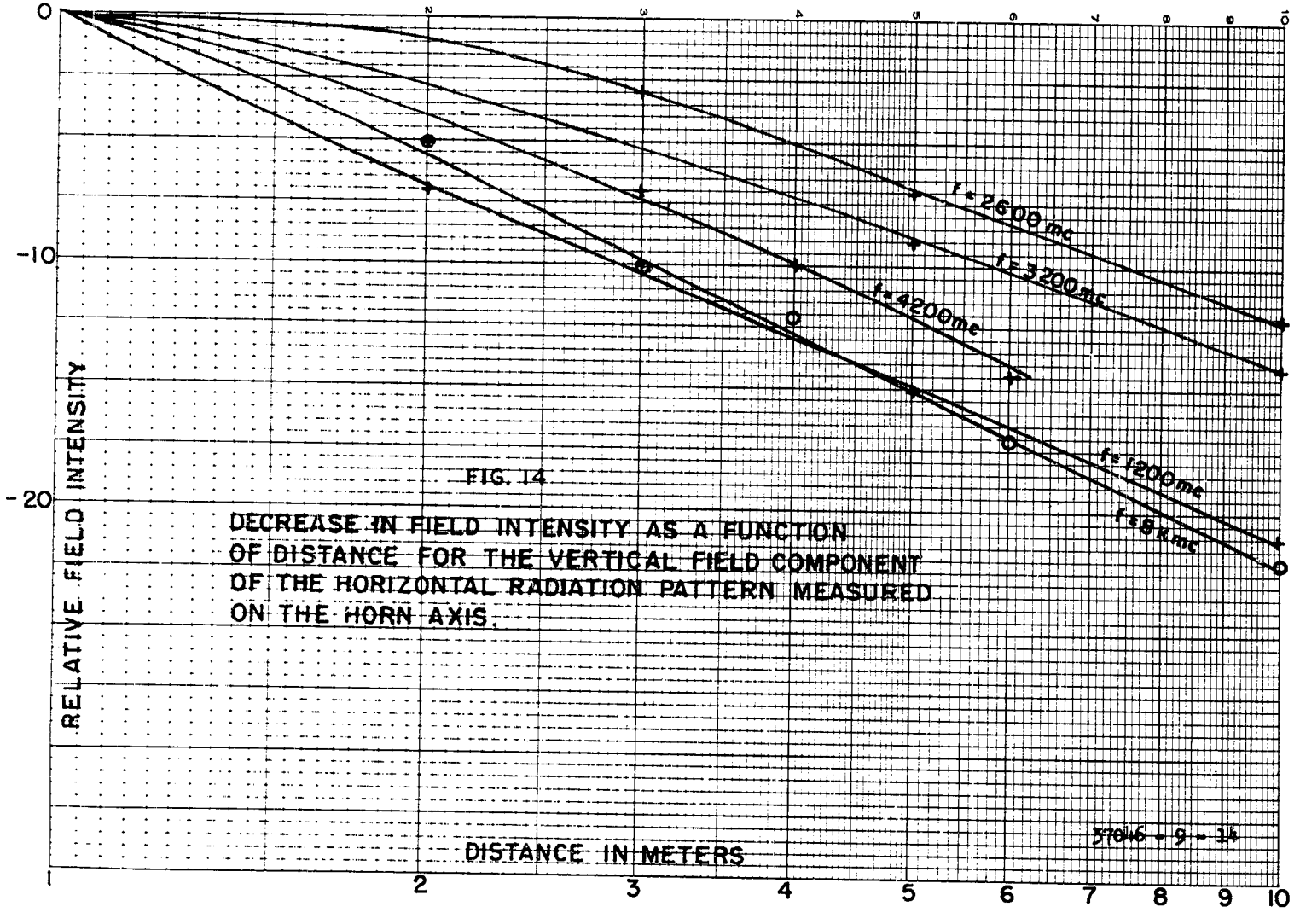



FIG. 14

DECREASE IN FIELD INTENSITY AS A FUNCTION OF DISTANCE FOR THE VERTICAL FIELD COMPONENT OF THE HORIZONTAL RADIATION PATTERN MEASURED ON THE HORN AXIS.

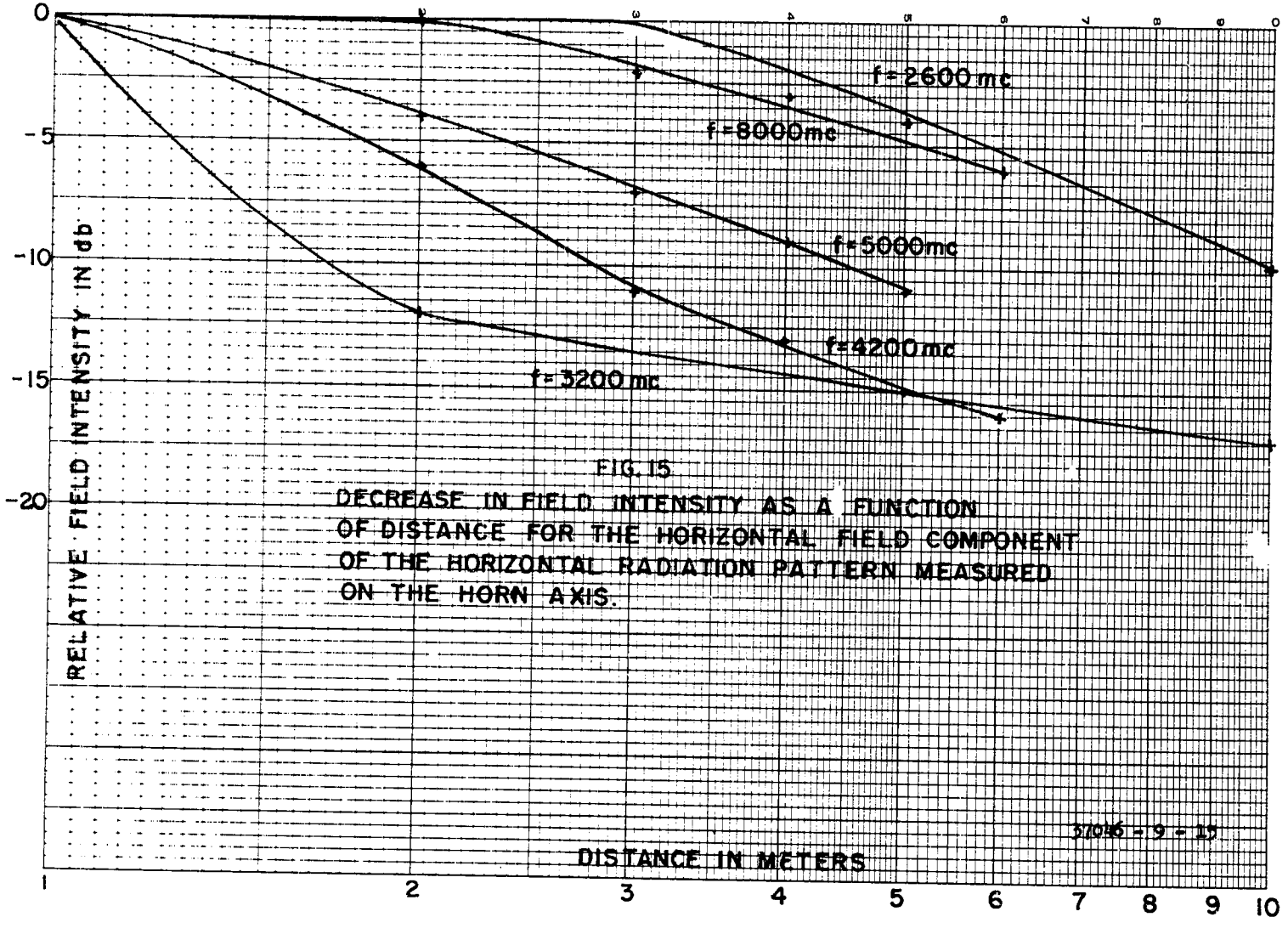
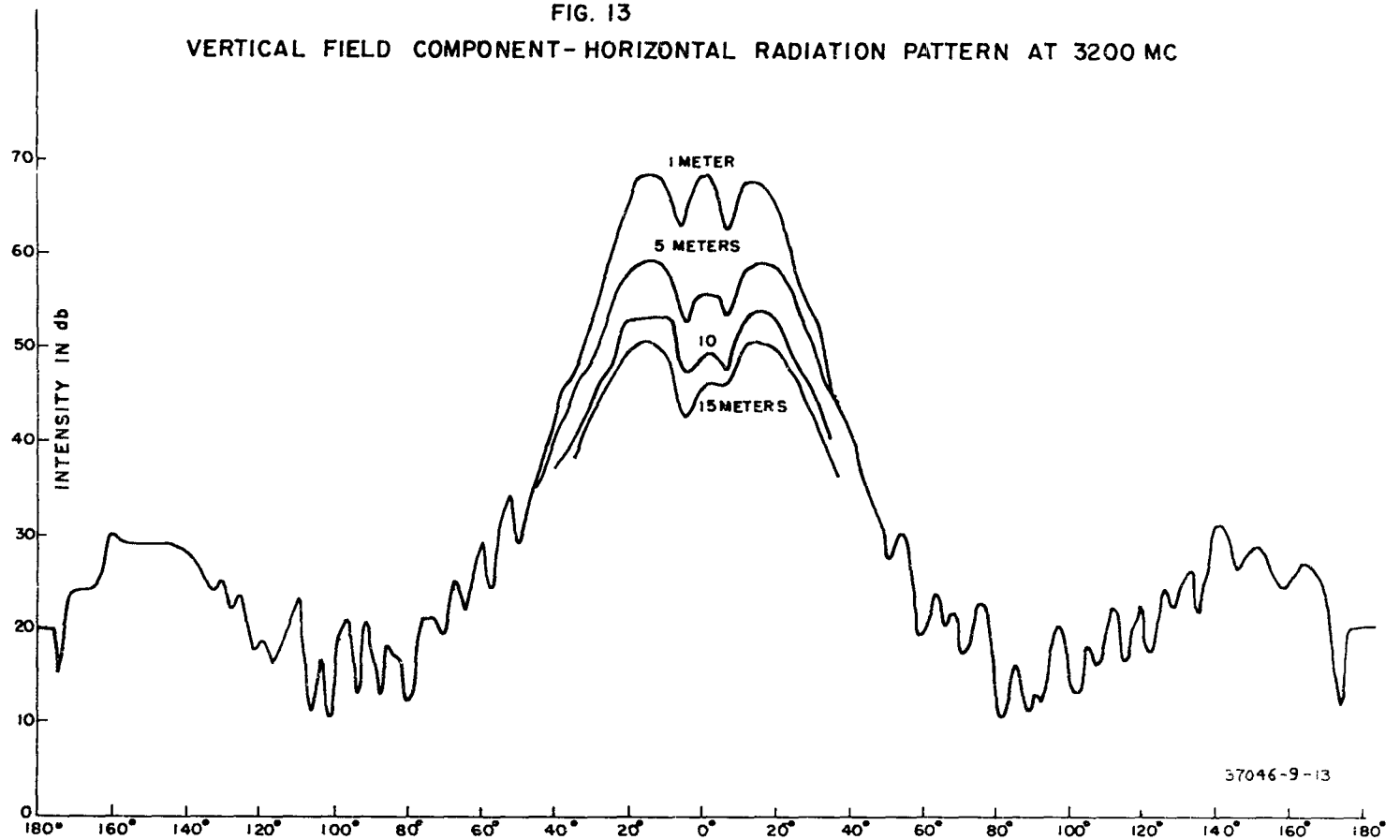



FIG. 15

DECREASE IN FIELD INTENSITY AS A FUNCTION OF DISTANCE FOR THE HORIZONTAL FIELD COMPONENT OF THE HORIZONTAL RADIATION PATTERN MEASURED ON THE HORN AXIS.

FIG. 13

VERTICAL FIELD COMPONENT- HORIZONTAL RADIATION PATTERN AT 3200 MC



# PREDICTION OF THE FAR FIELD OF PARABOLOID REFLECTORS EXCITED BY PLANE APERTURES OF ARBITRARY FIELD DISTRIBUTION

H. Zucker
Armour Research Foundation
of Illinois Institute of Technology
Chicago 16, Illinois

**Abstract.** - A transformation equation between the electric field in a plane feed aperture located in the focal plane and the reflected electric field at a paraboloid reflector is derived. The reflector is assumed to be in the far field of the feed aperture. The equation is obtained by determining the incident electric field at the reflector by means of the aperture field method, and the reflected electric field by assuming that the reflector can be considered locally plane. The far fields of the paraboloid are obtained by projecting the reflected electric field on the paraboloid aperture also by using the aperture field method. Specifically the results are applied to a circular feed aperture by expanding the electric field in the aperture in terms of $TE_{m,n}$ circular waveguide crossectional mode components. It is shown that the prediction of the far field radiation pattern of the paraboloid for each mode reduces to the evaluation of single integrals. For a variety of modes the integrals have been evaluated by means of an 1105 computer.

## I. INTRODUCTION

In the design of paraboloid reflectors the primary objective is to generate an aperture illumination which will produce a desired radiation pattern at a certain frequency. However, the illuminating source usually contains harmonics and unharmonics of the operating frequency. The radiation patterns due to the harmonic and unharmonic frequencies will depend on the radiation pattern of the feed. Of particular interest here is to determine the main lobe radiation patterns due to the harmonics, and if these lobe patterns remain within the radiation pattern of the main beam at the operating frequency. If this is not the case, a severe interference problem may result in directions outside the main beam. The most commonly used reflector feeds are dipoles, or rectangular or circular apertures consisting of waveguides or horns. A literature survey revealed that only the radiation pattern of a paraboloid reflector fed with a short dipole has been analyzed directly.[1]

The analysis to follow is concerned with the radiation pattern produced by the reflector when fed with a plane aperture in the focal plane of the reflector. It is assumed that the reflector is in the far field of the feed and there is neglibible reaction of the reflector on the feed. The incident fields at the reflector are determined from the fields at the feed aperture by means of the aperture field method. The determination of radiation fields of the reflector is performed with the assumption that the surface current density and the fields at each point of the reflector are the same as they would be if the reflector could be considered locally as a plane conductor. From the surface current density, the radiation fields can be determined by integration of the radiation of the individual incremental current

elements. For the paraboloid reflector the fields that would be obtained using the current distribution method may also be obtained with a good approximation by projecting the reflected electric field at the reflector on the aperture of the reflector and using the aperture field method to obtain the radiation fields. The analysis below uses the latter method.

Based on the above, a transformation equation between the electric field in the feed aperture and the reflected electric field at the reflector is derived. Specifically the results are applied to a circular feed aperture and the electric field is expanded in terms of $TE_{m,n}$ circular waveguide mode components. The determination of the resulting radiation pattern due to each mode reduces to the evaluation of single integrals. These integrals have been evaluated for a number of modes with the aid of a computer, Some of the radiation patterns are shown.

## II. ANALYSIS

The far electric field, $\mathbb{E}_f$, of a plane aperture in the coordinates of Figure 1 is given by[2]

$$\mathbb{E}_f = -j \frac{\beta e^{-j\beta r}}{4\pi r} \, 1_r \times \left[(-1_z + \alpha 1_r) \times \mathbb{N}\right] \tag{1}$$

where

$\beta = \frac{2\pi}{\lambda}$ = the free space propagation constant

$\lambda$ = free space wavelength

$\alpha$ = ratio of the magnetic field to the electric field in the aperture plane over the same ratio in free space

and

$$\mathbb{N} = \iint_{\text{Aperture}} \mathbb{E}_a \, e^{j (x' \sin\psi \cos\xi + y' \sin\psi \sin\xi)} \, dx' \, dy' \tag{2}$$

$\mathbb{E}_a$ = electric field in the aperture.

The reflected field at the paraboloid reflector will be obtained from (1) by assuming that the reflector is a perfect conductor and that at every point the incident field is reflected as though a plane wave were incident on an infinite plane.

At a plane perfect conductor the relationships between the incident and reflected electric field at the plane is

$$\mathbb{E}_r = -\mathbb{E}_i + 2 \, 1_n \mathbb{E}_i \cdot 1_n \tag{3}$$

$\mathbb{E}_i$ and $\mathbb{E}_r$ are the incident or the reflected field respectively, $1_n$ is the unit normal to the reflecting surface.

Equation (3) is the boundary condition for the electric field at a plane perfect conductor. It states that total tangential component of the

electric field is zero and that the normal components of the incident and reflected electric field are equal.

From (1) and (3) the surface current at the reflector may also be determined by assuming that the reflector can be considered as plane. The relationship between the surface current density and the incident or reflected electric field is[3]

$$\mathbb{J} = \frac{2}{\eta} \, 1_n \times (1_{\pi_i} \times \mathbb{E}_i) = \frac{2}{\eta} \, 1_n \times (1_{\pi_r} \times \mathbb{E}_r) \tag{4}$$

where

$\eta$ = free space intrinsic impedance

$1_{\pi_i}, 1_{\pi_r}$ = direction of propagation of the incident or reflected wave.

The radiation fields due to the reflector may be determined from the surface current distribution by integration or from the reflected electric field at the aperture of the reflector also by integration.

To determine the reflected field or the surface current it is necessary to determine the unit normal to the paraboloid surface. The equation for a paraboloid surface in spherical coordinates is

$$r = \frac{2f}{1 + \cos\psi} \tag{5}$$

where $f$ = focal length.

To determine the unit normal to (5) let

$$\phi = r - \frac{2f}{1 + \cos\psi} = r - \frac{f}{\cos^2 \frac{\psi}{2}} = 0 \tag{6}$$

The unit normal is obtained using the definition of the gradient and is given by

$$1_n = \frac{\nabla \phi}{|\nabla \phi|} \tag{7}$$

Therefore

$$1_n = \pm \frac{1_r - 1_\psi \tan \frac{\psi}{2}}{\sqrt{1 + \tan^2 \frac{\psi}{2}}} = \pm (1_r \cos \frac{\psi}{2} - 1_\psi \sin \frac{\psi}{2}) \tag{8}$$

The normal of interest is with the minus sign.

Expressing the spherical unit vectors in terms of cylindrical unit vectors gives

$$1_n = -1_\rho \sin\frac{\Psi}{2} + 1_z \cos\frac{\Psi}{2} \tag{9}$$

The reflected field at the reflector will be evaluated using (1), (3), and (9). To perform the evaluation, let

$$K = -\frac{j\beta\, e^{-j\beta r}}{4\pi r} \tag{10}$$

and expanding (1) gives

$$\mathbb{E}_i = \mathbb{E}_f = K\left[1_r \cdot \mathbb{N}\,(-1_z + \alpha 1_r) - \mathbb{N}\,(-1_z \cdot 1_r + \alpha)\right] \tag{11}$$

From (9) and (11)

$$\mathbb{E}_i \cdot 1_n = K\left[1_r \cdot \mathbb{N}\,(-\cos\frac{\Psi}{2} + \alpha 1_z \cdot 1_r \cos\frac{\Psi}{2} - 1_r \cdot 1_\rho \sin\frac{\Psi}{2}\right.$$

$$\left. + \mathbb{N} \cdot 1_\rho \sin\frac{\Psi}{2}\,(-1_z \cdot 1_r + \alpha)\right] \tag{12}$$

with $$1_r = 1_\rho \sin\psi - 1_z \cos\psi \tag{13}$$

Equation (12) simplifies to

$$\mathbb{E}_i \cdot 1_n = K\, 1_\rho \cdot \mathbb{N} \sin\frac{\Psi}{2}\,(1 + \alpha\cos\psi) \tag{14}$$

Substituting (9), (11), (13), and (14) into (3) gives for the reflected field

$$\mathbb{E}_r = -K\left\{1_\rho \cdot \mathbb{N} \sin\psi\left[-1_z + \alpha(1_\rho \sin\psi - 1_z\cos\psi)\right] - \mathbb{N}\,(\cos\psi + \alpha)\right.$$

$$\left. + 2(-1_\rho \sin\frac{\Psi}{2} + 1_z \cos\frac{\Psi}{2})\,(1_\rho \cdot \mathbb{N}) \sin\frac{\Psi}{2}\,(1 + \alpha\cos\psi)\right\} \tag{15}$$

Simplifying (15) gives

$$\mathbb{E}_r = K\,\mathbb{N}\,(\cos\psi + \alpha) - K\, 1_\rho \mathbb{N} \cdot 1_\rho\left[\alpha \sin^2\psi - 2\sin^2\frac{\Psi}{2}(1 + \alpha\cos\psi)\right] \tag{16}$$

Equation (16) simplifies further to

$$\mathbb{E}_r = K\,\mathbb{N}\,(\cos\psi+\alpha) + K\,l_\rho\,\mathbb{N}\cdot l_\rho\,(1-\cos\psi)\,(1-\alpha) \tag{17}$$

where K and $\mathbb{N}$ are given by (10) and (2) respectively.

Equation (17) shows that there are no z components of the reflected field. This is to be expected since the properties of the paraboloid reflector are that when excited from the focal point with a point source the direction of the reflected wave is entirely in the z direction. With the assumption made that the paraboloid reflector is in the far field of the excitation aperture the incident wave is in the radial direction and hence the excitation is equivalent to a point source. Equation (17) also shows that if the electric and magnetic field in the excitation aperture are matched to free space which corresponds to $\alpha = 1$ that no cross polarized component is present since the second term which contains a cross polarized component vanishes.

Equation (17) together with (4) can be used to determine the surface current over the aperture. From the surface current the resulting radiation pattern can be determined by means of the current distribution method. The far reflected electric field is then obtained from the following integral[4]

$$\mathbb{E}_{rf} = -\frac{j\omega\mu}{4\pi R}\,e^{-j\beta R}\iint_{\substack{\text{Surface of}\\ \text{Paraboloid}}} l_R \times (\mathbb{J}\times l_R)\,e^{j\beta_r l_r\cdot l_R}\,ds$$

$$= \frac{-j\beta}{2\pi R}\,e^{-j\beta R}\iint_{\substack{\text{Surface of}\\ \text{Paraboloid}}} l_R \times \left\{\left[l_n \times (l_z \times \mathbb{E}_r)\right]\times l_R\right\} e^{j\beta_r l_r\cdot l_R}\,ds \tag{18}$$

However, it has been shown[5] that nearly the same radiation pattern is obtained for small $\theta$ by projecting the reflected electric field at the reflector on the reflector aperture at $z_o$ and using the aperture field method. The phase of the electric field over the aperture with the above approximations is constant. Equation (17) may therefore be considered as a means of determining the transformation of the electric field over the excitation aperture into a corresponding field over the reflector aperture.

For a circular excitation aperture which may consist of a circular waveguide or horn, the field in the excitation aperture can be expanded in terms of transverse components of TE and TM modes. The far field radiation pattern for each mode is known in closed form. One integration with respect to the angular coordinate of the reflected electric field over the reflector aperture can also be performed in closed form. To obtain the far field radiation pattern of the reflector using either method one more integration is necessary with respect to the radial coordinate.

For the rectangular excitation aperture which may consist of a rectangular waveguide or horn, the electric field in the aperture may also be expanded in terms of the transverse components of rectangular TE and TM waveguide modes. The far fields radiation pattern for each mode is also known in closed form. However, the integration over the reflected field in the reflector aperture cannot be performed in closed form. Therefore, two numerical integrations are necessary to determine the far field radiation pattern. Approximations for the integrals have been attempted but thus far have not been successful.

In Appendix A the radiation pattern due to a circular feed aperture is treated using the aperture field method and the three integrations are performed in closed form. The remaining integration has been performed by means of a computer using the following parameters:

| | |
|---|---|
| Radius of the circular aperture | $a = 0.472$ inches |
| Radius of the paraboloid aperture | $\frac{D}{2} = 12$ inches |
| Focal length | $f = 7.2$ inches |
| Fundamental free space wavelength | $\lambda = 1.31$ inches. |

The integrals have been evaluated for all the TE modes that may propagate in a circular waveguide with the above radius a, at the fundamental and harmonics up to the fourth harmonic, n = 4, in 1/2 degree increment in $\theta$, up to $\theta = 45$ degrees.

Figures 2 through 8 show the far electric fields in the principal planes. For other modes the fields have a similar characteristic. The computed results indicate that the major lobes due to the higher order modes are all contained within the major lobe of the fundamental $TE_{11}$ mode.

## III. CONCLUSIONS

1. An equation for the reflected electric field at the paraboloid reflector has been derived in terms of the electric field at the feed aperture. The assumptions made were:

a) the feed aperture is located in the focal plane

b) the reflector is in the far field of the feed

c) the reflector can be considered as locally plane,

d) no action of the reflection on the feed.

2. For any feed aperture for which the far field is known, the radiation due to the reflector reduces to the evaluation of a double integral. For a circular feed aperture the electric field in the aperture can be expanded in terms of the transverse TE and TM mode component. The radiation pattern due to the reflector reduces to the evaluation of single integrals, since one integration can be performed in closed form.

3. The evaluation of the integrals for a circular feed aperture has been performed by means of a 1105 computer. The radiation pattern obtained up to the fourth harmonics indicate that all the major lobes due to higher order modes are contained within the main lobe for the fundamental frequency.

## ACKNOWLEDGEMENTS

This work was performed under the joint sponsorship of the U. S. Army Signal Research and Development Laboratories and the Electromagnetic Compatibility Analysis Center. The author is pleased to acknowledge Mr. D. G. Iliopoulos who performed the computer programming and Mr. M. Pagones for his assistance in preparing the computer program.

## REFERENCES

1. E. M. T. Jones, "Paraboloid Reflector and Hyperboloid Lens Antennas", IRE Transactions on Antennas and Propagation, Vol. Ap-2, No. 3, July 1954, pp 119-127.

2. S. Silver, "Microwave Antenna Theory and Design", Radiation Laboratory Series, McGraw Hill Book Compnay, 1949, p 162.

3. Ibid, pp 145-146.

4. Ibid., p. 149.

5. Ibid., p. 421.

6. Ibid., p. 337.

## APPENDIX A

According to Equation (17) of the text the main part of the reflected field at the reflector is

$$\mathbf{E}_r = \frac{-j\beta_e - j\beta_r}{4\pi r} \mathbb{N} (\cos\psi + \alpha) \qquad (17)$$

where $\mathbb{N}$ according to (2) is

$$\mathbb{N} = \iint_{\text{Aperture}} \mathbf{E}_a \, e^{j (x' \sin\psi\cos\xi + y' \sin\psi \sin\xi)} \, dx' \, dy' \qquad (2)$$

The electric field for TE modes in a circular waveguide in rectangular coordinates is[6]

$$E_x = \frac{j\omega\mu k_{m,n}}{2} \left[ J_{m-1}(k_{m,n}\rho) \sin(m-1)\eta + J_{m+1}(k_{m,n}\rho) \sin(m+1)\eta \right] \qquad (A-1)$$

$$E_y = \frac{j\omega\mu k_{m,n}}{2} \left[ J_{m-1}(k_{m,n}\rho) \cos(m-1)\eta - J_{m+1}(k_{m,n}\rho) \cos(m+1)\eta \right] \qquad (A-2)$$

where

$J_m$ = a Bessel function of order m and $k_{m,n}$ is obtained from the conditional equation

$$J'_m(k_{m,n}a) = 0 \qquad (A-3)$$

The resulting radiation pattern due to the reflected field using the aperture field method will require the evaluation of terms similar to (2), namely

$$\mathbb{N}_r = \frac{-j\beta_e - j\beta 2f}{4\pi} \int_0^{2\pi} \int_0^{D/2} \mathbb{N} \frac{(\cos\psi + \alpha)}{r} e^{j\beta\rho \sin\theta \cos(\xi - \phi)} \rho \, d\rho \, d\xi \qquad (A-4)$$

where

D = diameter of the reflector and r, $\psi$ are related to $\rho$ by the equation for the reflector as will be shown below.

With $\mathbb{N}$ given by (2) four integrations will be required. Three integrations can be performed in closed form. These integrations after substituting (2) into (A-4) and expressing the rectangular coordinates in terms of circular coordiates are

$$\mathbb{I} = \int_0^a \int_0^{2\pi} \int_0^{2\pi} \mathbb{E}_a \, e^{j\beta[\rho \sin\theta \cos(\xi - \phi) + \rho' \sin\psi \cos(\xi - \eta)]} \rho' d\rho' d\xi \, d\eta \tag{A-5}$$

The x component of (A-5) is obtained by substituting (A-1) and is

$$I_x = \frac{j\omega\mu k_{m,n}}{2} \int_0^a \int_0^{2\pi} \int_0^{2\pi} e^{j\beta[(\rho \sin\theta \cos(\xi - \phi) + \rho' \sin\psi \cos(\xi - \eta)]}$$

$$[J_{m-1}(k_{m,n}\rho') \sin(m-1)\eta + J_{m+1}(k_{m,n}\rho') \sin(m+1)\eta] \rho' \, d\rho' \, d\xi \, d\eta \tag{A-6}$$

To perform the integration with respect to $\eta$ use is made of the expansion

$$e^{j\beta\rho' \sin\psi \cos(\xi - \eta)} = J_o(\beta\rho' \sin\psi) + \sum_{n=1}^{\infty} 2j^n J_n(\beta\rho' \sin\psi) \cos(\xi - \eta) \tag{A-7}$$

Substituting (A-7) into (A-6) and using the orthogonality properties of the trigonometric functions gives

$$I_x = \frac{\pi j\omega\mu k_{m,n}}{2} 2j^{(m+1)} \int_0^a \int_0^{2\pi} e^{j\beta\rho' \sin\theta \cos(\xi - \phi)} [J_{m+1}(k_{m,n}\rho') J_{m+1}(\beta\rho' \sin\psi)$$

$$\sin(m+1)\xi - J_{m-1}(k_{m,n}\rho') J_{m-1}(\beta\rho' \sin\psi) \sin(m-1)\xi] \rho' \, d\rho' \, d\xi \tag{A-8}$$

Integrating (A-8) with respect to $\xi$ using (A-7) gives

$$I_x = 2\pi^2 \omega \mu k_{m,n}^{\ } j^{(2m+3)} \int_0^a \Big[ J_{m+1}(\beta\rho \sin\theta)\, J_{m+1}(\beta\rho' \sin\psi)\, J_{m+1}(k_{m,n}\rho') \sin(m+1)\phi$$

$$+ J_{m-1}(\beta\rho \sin\theta)\, J_{m-1}(\beta\rho' \sin\psi)\, J_{m-1}(k_{m,n}\rho') \sin(m-1)\phi \Big] \rho' d\rho' \qquad \text{(A-9)}$$

Next the integration with respect to $\rho'$ may be performed using the Lommel integral relationship for Bessel functions, namely

$$\int_0^x J_{m+1}(\alpha x)\, J_{m+1}(\beta x)\, x\, dx = \frac{x}{\alpha^2 - \beta^2} \left[ \beta J_{m+1}(\alpha x)\, J_m(\beta x) - \alpha J_m(\alpha x)\, J_{m+1}(\beta x) \right] \qquad \text{(A-10)}$$

$$\int_0^x J_{m-1}(\alpha x)\, J_{m-1}(\beta x)\, x\, dx = \frac{x}{\alpha^2 - \beta^2} \left[ \alpha J_m(\alpha x)\, J_{m-1}(\beta x) - J_{m-1}(\alpha x)\, J_m(\beta x) \right] \qquad \text{(A-11)}$$

Substituting (A-10) and (A-11) into (A-9) and combining terms gives

$$I_x = \frac{2\pi^2 k_{m,n}^{\ } a j^{(2m+3)}}{\beta^2 \sin^2\psi - k_{m,n}^2} \Big\{ k_{m,n} J_m(k_{m,n} a) \Big[ J_{m+1}(\beta a \sin\psi)\, J_{m+1}(\beta\rho \sin\theta) \sin(m+1)\phi$$

$$- J_{m-1}(\beta a \sin\psi)\, J_{m-1}(\beta\rho \sin\theta) \sin(m-1)\phi \Big]$$

$$- \beta \sin\psi J_m(\beta a \sin\psi) \Big[ J_{m+1}(k_{m,n} a)\, J_{m+1}(\beta\rho \sin\theta) \sin(m+1)\phi$$

$$- J_{m-1}(k_{m,n} a)\, J_{m-1}(\beta\rho \sin\theta) \sin(m-1)\phi \Big] \Big\} \qquad \text{(A-12)}$$

Using the recurrence relation for Bessel functions

$$J_n'(x) = -\frac{n}{x} J_n(x) + J_{n-1}(x) = \frac{n}{x} J_n(x) - J_{n+1}(x) = \frac{1}{2}\left(J_{n-1}(x) - J_{n+1}(x)\right) \tag{A-13}$$

together with (A-3) simplifies (A-12) to

$$I_x = -2\pi^2 \omega \mu k_{m,n} a j^{(2m+3)} J_m(k_{m,n} a) \left\{ \frac{m J_m(\beta a \sin\psi)}{\sin\psi k_{m,n} a} \left[ J_{m+1}(\beta\rho \sin\theta) \sin(m+1)\phi \right.\right.$$

$$\left. - J_{m-1}(\beta\rho \sin\theta) \sin(m-1)\phi \right] + \frac{k_{m,n} J_m'(\beta a \sin\psi)}{\beta^2 \sin^2\psi - k_{m,n}^2} \left[ J_{m+1}(\beta\rho \sin\theta) \sin(m+1)\phi \right.$$

$$\left.\left. + J_{m-1}(\beta\rho \sin\theta \sin(m-1)\phi \right] \right\} \tag{A-14}$$

With the recurrence relation (A-12), (A-14) may also be expressed as

$$I_x = 4\pi^2 \omega \mu k_{m,n} a j^{(2m+3)} J_m(k_{m,n} a) \left\{ \left[ \frac{m J_m(\beta a \sin\psi)}{\beta \sin\psi k_{m,n} a} J_m'(\beta\rho \sin\theta) \right.\right.$$

$$\left. - \frac{m k_{m,n}}{\beta\rho \sin\theta} \frac{J_m(\sin\theta)}{(\beta^2 \sin^2\psi - k_{m,n}^2)} J_m'(\beta a \sin\psi) \right] \sin m\phi \cos\phi$$

$$- \left[ \frac{m^2}{\beta^2 \sin\psi k_{m,n} a \sin\theta} J_m(\beta a \sin\psi) J_m(\beta\rho \sin\theta) \right.$$

$$\left.\left. - \frac{k_{m,n} J_m'(\beta a \sin\psi)}{\beta^2 \sin^2\psi - k_{m,n}^2} J_m'(\beta\rho \sin\psi) \right] \cos m\phi \sin\phi \right\} \tag{A-15}$$

$I_y$ can be evaluated by analogy to the evaluation of $I_x$ and the analogous equation to (A-14) is

$$I_y = 2\pi^2 \omega \mu\, k_{m,n} a j^{(2m\pm3)} J_m(k_{m,n}a) \left\{ \frac{m J_m(\beta a \sin\psi)}{\sin\psi k_{m,n} a} \left[ J_{m+1}(\beta\rho \sin\theta) \cos(m+1)\phi \right.\right.$$

$$+ J_{m-1}(\beta\rho \sin\theta) \cos(m-1)\phi \Big] + \frac{k_{m,n} J'_m(\beta a \sin\psi)}{\beta^2 \sin^2\psi - k^2_{m,n}} \Big[ J_{m+1}(\beta\rho \sin\theta) \cos(m+1)\phi$$

$$\left. - J_{m-1}(\beta\rho \sin\theta) \cos(m-1)\phi \Big] \right\} \qquad \text{(A-16)}$$

With the recurrence relation (A-13), (A-16) may be expressed as

$$I_y = 4\pi^2 \omega \mu\, k_{m,n} a j^{(2m\pm3)} J_m(k_{m,n}a) \left\{ \left[ \frac{m^2 J_m(\beta a \sin\psi) J_m(\beta\rho \sin\theta)}{\beta \sin\psi k_{m,n} a \beta\rho \sin\theta} \right.\right.$$

$$\left. - \frac{k_{m,n} J'_m(\beta a \sin\psi) J'_m(\beta\rho \sin\theta)}{\beta^2 \sin^2\psi - k^2_{m,n}} \right] \cos m\phi \cos\phi$$

$$+ \left[ \frac{m J_m(\beta a \sin\psi)}{\beta \sin\psi k_{m,n} a} J'_m(\beta\rho \sin\theta) \right.$$

$$\left.\left. - \frac{k_{m,n} m J'_m(\beta a \sin\psi)}{(\beta^2 \sin^2\psi - k^2_{m,n}) \beta\rho \sin\theta} J_m(\beta\rho \sin\theta) \right] \sin m\phi \sin\phi \right\} \qquad \text{(A-17)}$$

Substituting (A-15) and (A-17) into (A-5) then into (A-4) gives

$$\mathbb{N}_r = -\frac{j\beta_e - j\beta 2f}{4\pi} \int_0^{D/2} \left[ I_x I_x(\rho, \sin\psi) + I_y I_y(\rho, \sin\psi) \frac{(\cos\psi + \alpha)}{r} \right] \rho \, d\rho \tag{A-18}$$

The relationship between $\psi$, $\rho$, and r using (5) is

$$r = \frac{\rho}{\sin\psi} = \frac{2f}{1 + \cos\psi}$$

Solving for $\sin\psi$ in terms of $\rho$ gives

$$\sin\psi = \frac{\rho/f}{1 + (\rho/2f)^2} \tag{A-19}$$

and

$$\cos = \left[ \frac{2}{1 + (\rho/2f)^2} - 1 \right] \tag{A-20}$$

A comparison of (A-15) and (A-17) shows that $I_x$ has similar terms to $I_y$ and therefore only the integrals inside the brackets of (A-15) need to be evaluated. $I_y$ may be obtained by multiplication of the term inside the brackets by the proper trigonometric functions. A simpler form for the far electric field is obtained in terms of spherical coordinates. Using (1) the electric field is:

$$\mathbb{E}_{rf} = \frac{j\beta_e - j\beta R}{4\pi R} (1 + \cos\theta) \left[ I_\theta (N_{rx}\cos\phi + N_{ry}\sin\phi) - I_\phi (N_{rx}\sin\phi - N_{ry}\cos\phi) \right] \tag{A-21}$$

where $N_{rx}$ and $N_{ry}$ are the x and y component of $\mathbb{N}_r$. Due to the similarity of term $N_{rx}$ and $N_{ry}$ (A-21) simplifies to

$$\mathbb{E}_{fr} = K_m (1 + \cos\theta) \left[ I_\theta D_1 \sin m\phi + I_\phi D_2 \cos m\phi \right] \tag{A-22}$$

where

$$D_1 = m \int_0^{D/2} \left[ \frac{J_m(\beta a \sin\psi)}{\beta \sin\psi k_{m,n} a} J'_m(\beta \rho \sin\theta) \right.$$

$$\left. - \frac{k_{m,n}}{\beta \rho \sin\theta} \frac{J_m(\beta \rho \sin\theta)}{(\beta^2 \sin^2\psi - k_{m,n}^2)} J'_m(\beta a \sin\psi) \right] \frac{(\cos\psi + \alpha)}{r} \rho \, d\rho \qquad \text{(A-23)}$$

$$D_2 = \int_0^{D/2} \left[ \frac{m^2 J_m(\beta a \sin\psi) J_m(\beta \rho \sin\theta)}{\beta^2 \sin\psi k_{m,n} a \sin\theta} \right.$$

$$\left. - \frac{k_{m,n} J'_m(\beta a \sin\psi)}{\beta^2 \sin^2\psi - k_{m,n}^2} J'_m(\beta \rho \sin\psi) \right] \frac{(\cos\psi + \alpha)}{r} \rho \, d\rho \qquad \text{(A-24)}$$

and

$$K_m = j \frac{e^{-j\beta(R+2f)}}{(4\pi)^2 R} \beta^3 \eta (-1)^m k_{m,n} a J_m(k_{m,n} a) \qquad \text{(A-25)}$$

Equations (A-23) and (A-24) have been evaluated by means of an 1105 computer for $\alpha = 1$ and the parameters given in the text.

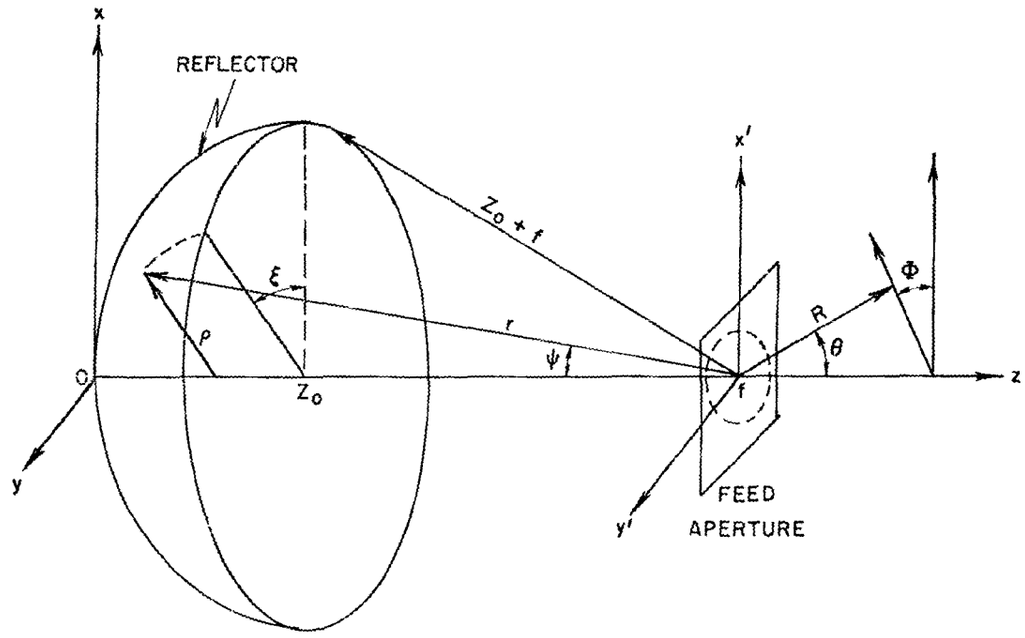



FIG. 1 COORDINATES OF PARABOLOID REFLECTOR AND FEED APERTURE

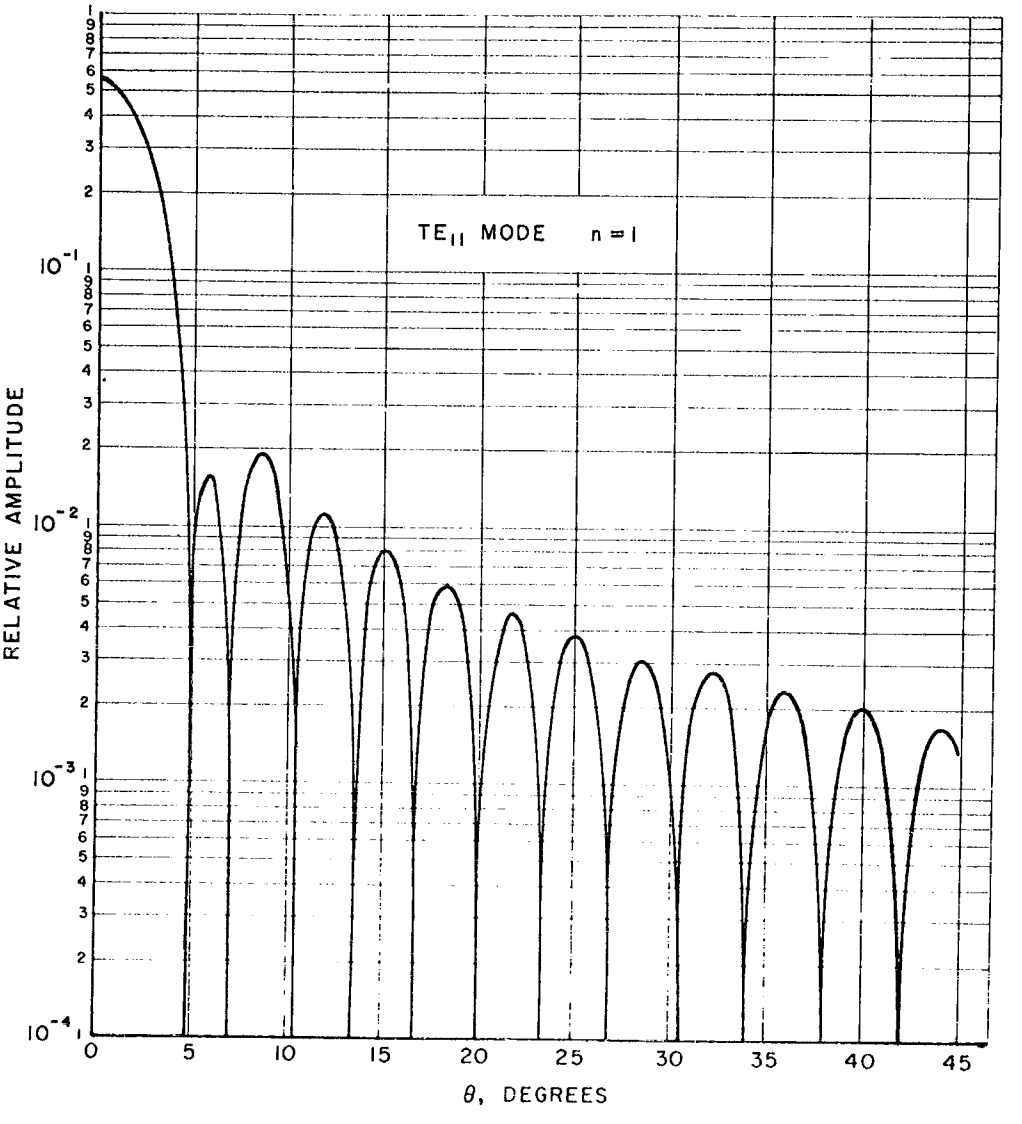



FIG. 2 RELATIVE ABSOLUTE VALUE OF $\frac{E_\Phi}{1+\cos\theta}$ AT $\Phi = 0$

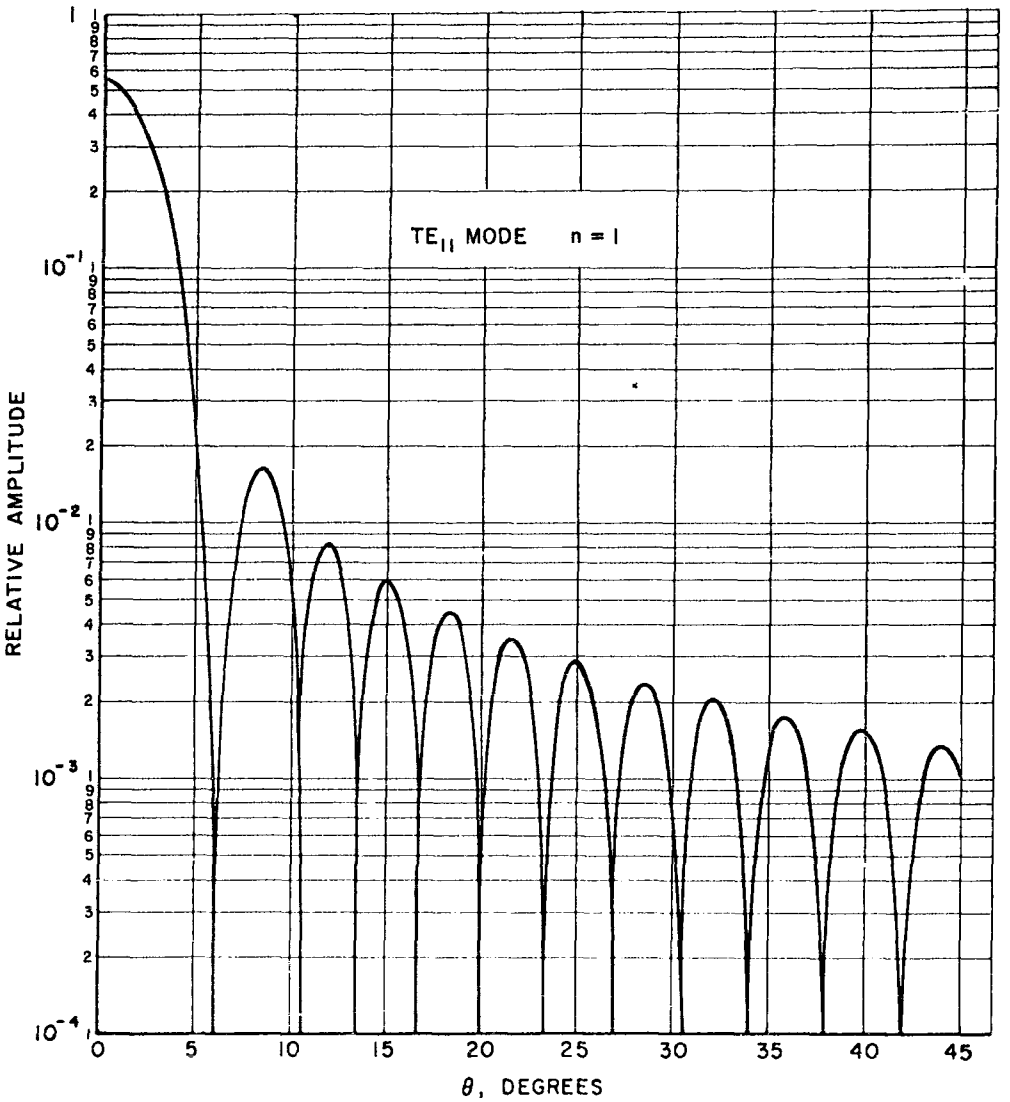



FIG. 3 RELATIVE ABSOLUTE VALUE OF $\frac{E_\theta}{1+\cos\theta}$ AT $\Phi = \frac{\pi}{2}$

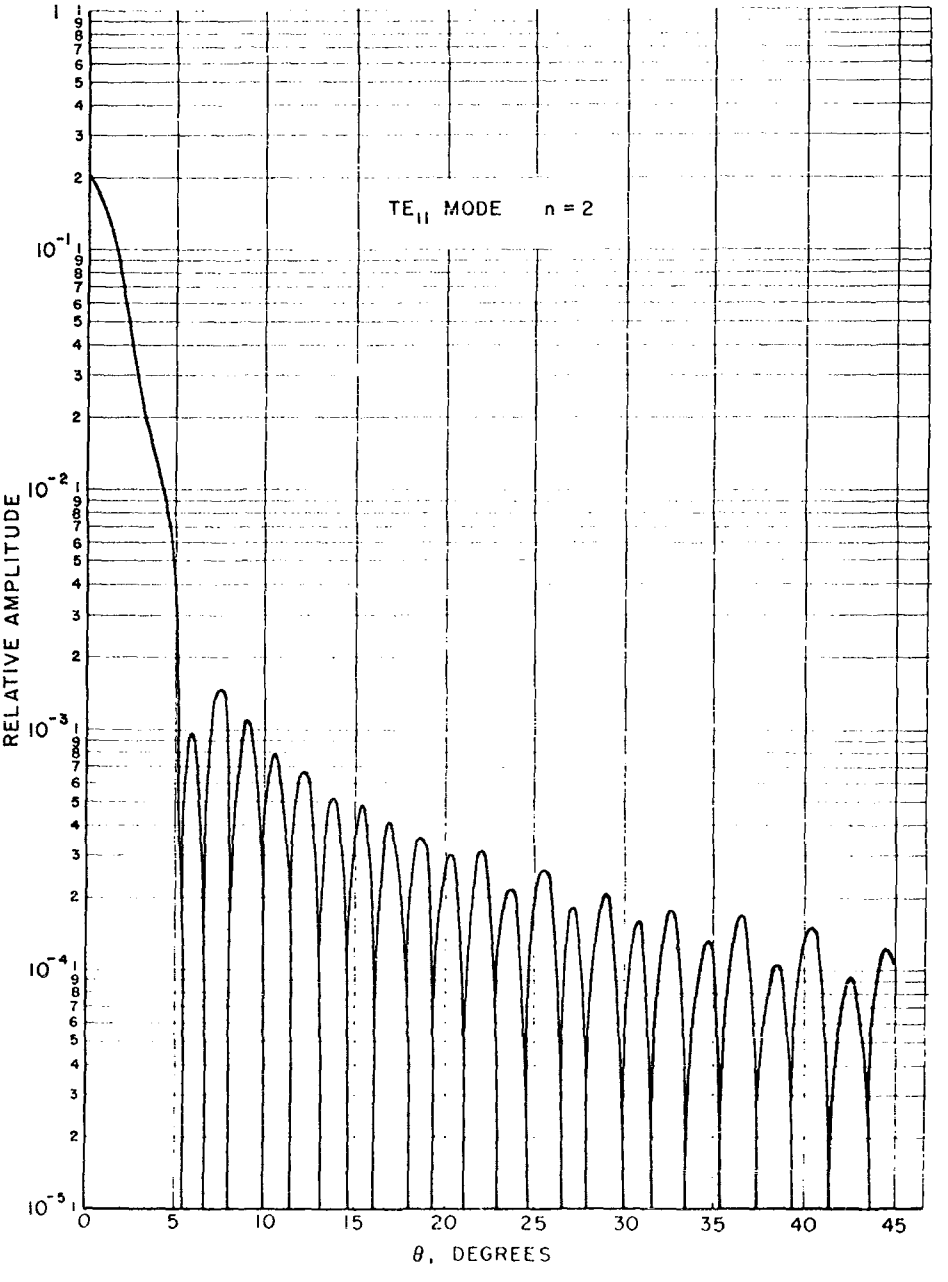



FIG. 4 RELATIVE ABSOLUTE VALUE OF $\frac{E_\Phi}{1+\cos\theta}$ AT $\Phi = 0$

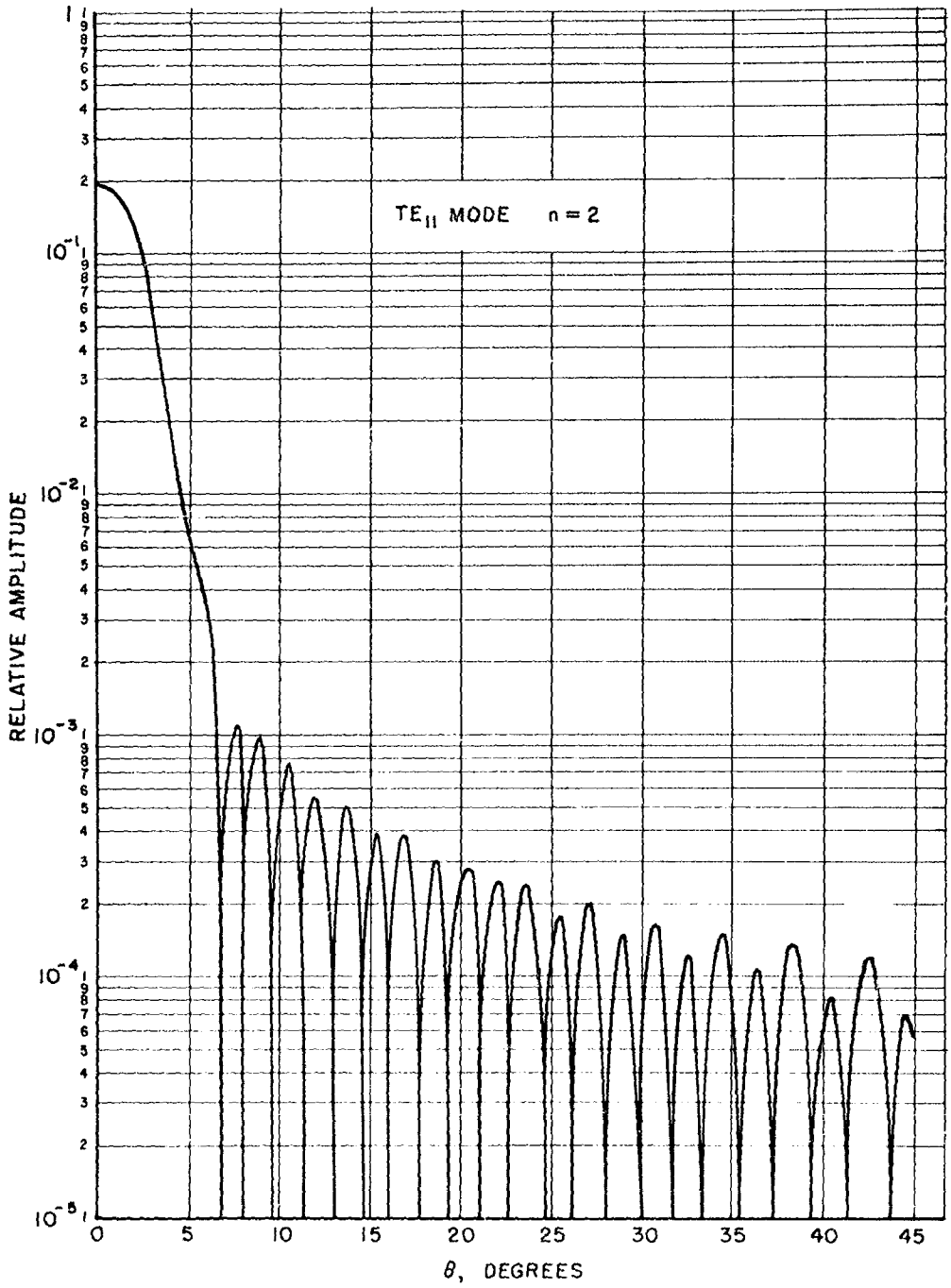



FIG. 5 RELATIVE ABSOLUTE VALUE OF $\frac{E_\theta}{1+\cos\theta}$ AT $\Phi = \frac{\pi}{2}$

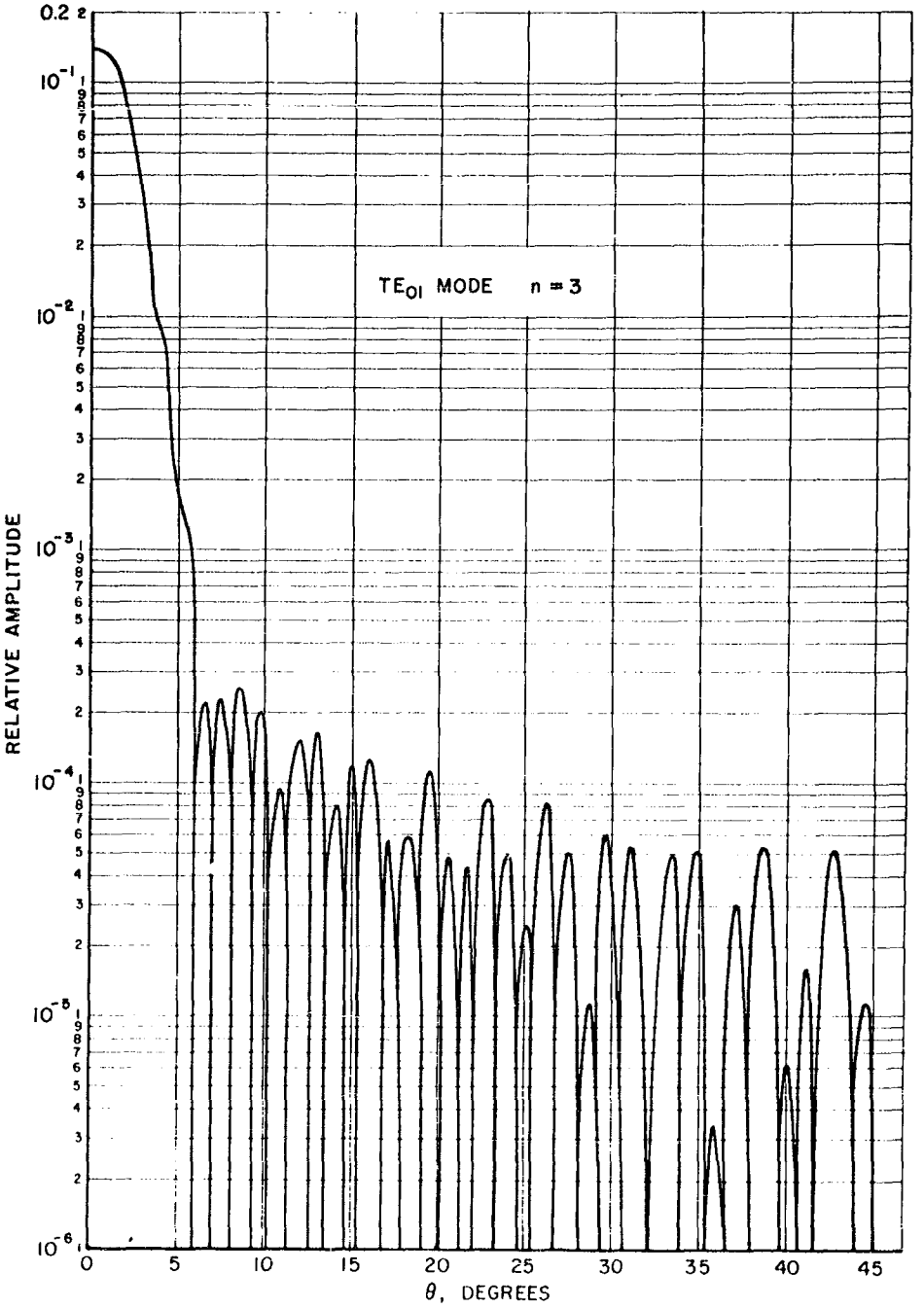



FIG. 6 RELATIVE ABSOLUTE VALUE OF $\frac{E_\Phi}{1+\cos\theta}$

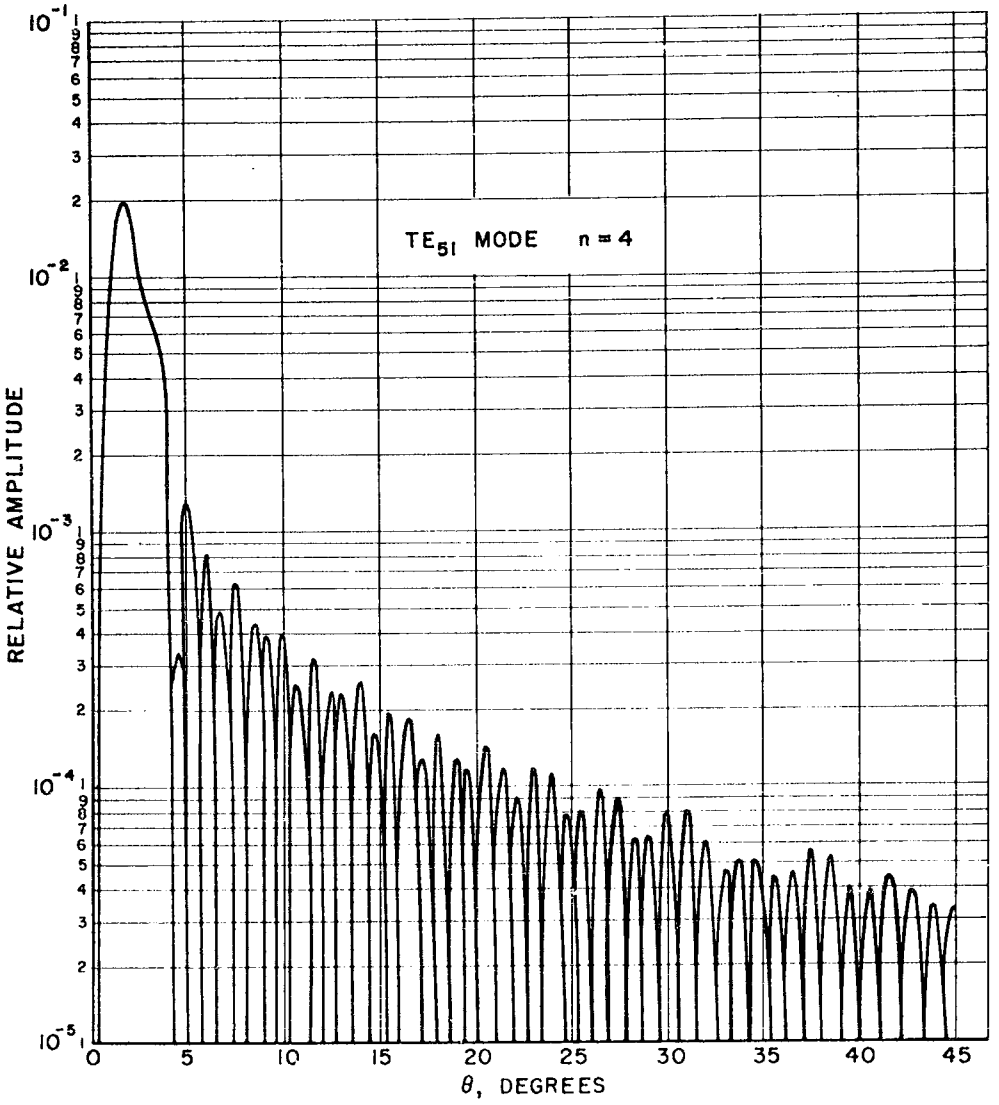



FIG. 7 RELATIVE ABSOLUTE VALUE OF $\frac{E_\Phi}{1+\cos\theta}$ AT $\Phi = 0$

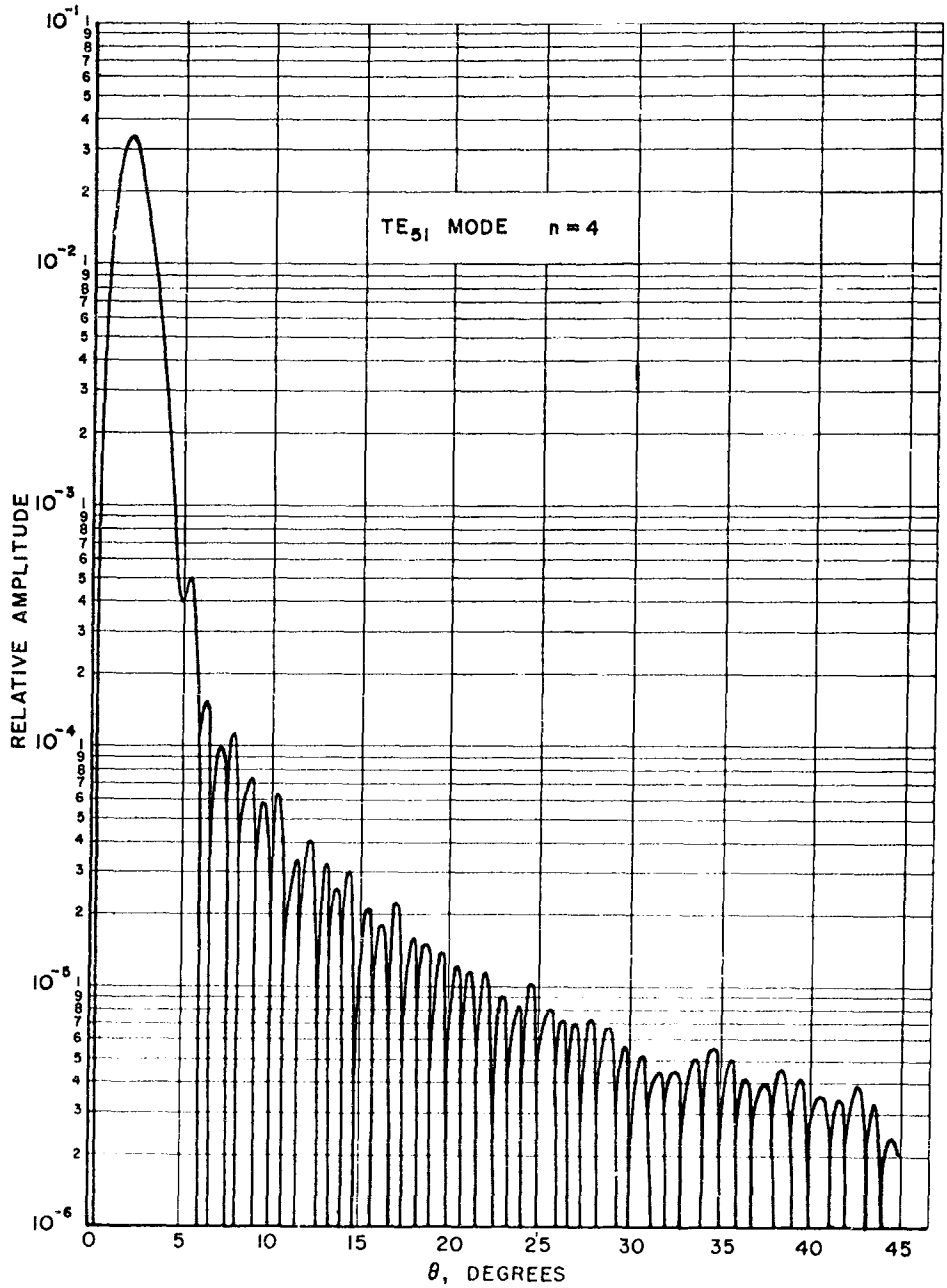



FIG. 8 RELATIVE ABSOLUTE VALUE OF $\frac{E_\theta}{1+\cos\theta}$ AT $\Phi = \frac{\pi}{2}$

# ESTIMATES OF THE RADIATION IN THE SHADOW REGION OF APERTURE ANTENNAS

H. N. Kritikos
The Moore School of Electrical Engineering
University of Pennsylvania
Philadelphia, Pa.

Abstract. - This paper gives estimates of the shadow region radiation of circular aperture antennas. The approach was based on the concepts of microwave optics which is valid for cases where the wavelength is small as compared to the dimensions of the system. This approach directly implies that the shadow region radiation is determined only by the type of primary illumination and by the shape of the boundary of aperture. For the special case of a circular aperture illuminated by Huygens' sources, it was found that, to a first order approximation, the shadow region field depended on the field present immediately next to the aperture. It was also concluded that the minimum back radiation is achieved by a primary illumination which tapers to zero at the boundary with the smoothest possible rate.

## I. INTRODUCTION

With the recent developments in the reduction of the internal noise levels of microwave receivers, the antennas became one of the important factors which limit the sensitivity of receiving systems. An evaluation of the performance of a receiving antenna requires the knowledge of the field pattern not only in the direction of the main beam but in all directions including that of the shadow region.

For the case of aperture antennas, generally the field pattern is well known in the front direction. However, limited information is available for the pattern in the back direction or shadow region. This lack of readily available information motivated the undertaking of this work. For apertures with an axial symmetry, a theoretical study of the field radiation pattern in the shadow region has been made. Because of the special nature of this problem from the many possible approaches available for the solution it was decided to choose the one which offered the greatest possible simplicity and flexibility. This approach is essentially based on Kirchoff's approximation and is valid only for cases where the wavelength is small as compared with the physical dimensions of the system.

By using the asymptotic behavior of the integrals involved in the formulation of the problem it was possible to reduce the results to a simple form and thus avoid the typical lengthy calculations which occur in diffraction problems.

The main conclusions of this work are the following: The field found in the back direction of the axis of revolution of the aperture is always a maximum, and is directly proportional to the field found in the edges of the aperture. The field in the edges is dependent on the type of aperture illumination. For uniform illumination the field at the edges is directly

proportional to the field present in the aperture. For tapered illuminations the field is directly proportional to the rate at which illumination distribution goes to zero at the edges.

It is believed that the obtained results are conservative estimates and that in actual practice other factors such as secondary reflection, etc., will introduce signals which may be larger than those estimated. The value of the above results, however, lies in the fact that they give not only a picture of the mechanism through which the radiation takes place in the shadow region but also, because of their simple form, they provide one with means by which trends can be easily seen and utilized.

## II. METHODS OF CALCULATING THE FIELD PATTERNS OF APERTURE ANTENNAS

The most general approach to the problem of determining the radiation pattern of aperture antennas is that based on the formalism of diffraction theory. [2,4,9] This type of formulation requires the solution of either a partial differential equation with the appropriate boundary value conditions or an integral equation. Unfortunately, the problems which are of interest to us do not belong to the limited class for which exact solutions are available. This implies that either numerical solutions or some approximations have to be used in order to arrive at a final answer. Numerical solutions are always possible but they are cumbersome and usually require the use of a computer. This restricts their usefulness only in cases where one is interested in very accurate solutions and is willing to invest the time needed for programming. In our case the nature of the problem is such that a very detailed determination of the field does not have a practical significance because of the many other factors (such as structural imperfections, reflecting objects, etc.) which in practice can introduce serious deviations from what one might expect from theory. It seems, therefore, that some approximation has to be used in order to bring the final results to a usable form. Before going into the method developed in this work a brief discussion of the work already existing in this area will be given below:

For the case of a feed illuminating a metallic reflector having the shape of a spherical shell, the feed-reflector interaction has been formulated in terms of an integral equation, which was approximately solved by utilizing the properties of integrals with rapidly oscillating kernels. [7] This approach is of considerable theoretical importance because it is based on an exact formulation and it opens the road to the determination of the induced currents on the reflector. A limitation of this method is that it presents the final result as the difference of two quantities, the incident field and the scattered field. The incident field is a quantity which is known, however, the scattered field is only approximately known. Small errors in the scattered field can result in large percentage errors in the total field. This method therefore has to be used with some caution especially in cases where the field in the shadow region is several orders of magnitude below the incident field.

Another series of approximations can be secured by simply assuming a solution in such a way that it is consistent with our intuition and our experience. [1,9,10] The shortcoming of these methods is that they do not allow for higher order corrections in an obvious manner, the great advantage is, however, their great flexibility. In a number of cases the final result can be presented in such a form that theoretical trends can be immediately seen thus having an extremely high practical use. These approximations are valid for cases where the wavelength is small as compared to the physical dimensions of the system and in general have been very successful for calculating the field pattern in the front direction. Following these approximations the most commonly encountered methods for finding field patterns of aperture antennas are:

First, the induced current method, where the current distribution in the reflector is assumed to have a given form and from these induced currents the field pattern is determined.

Second, the aperture method where the field in the aperture is assumed to have a given distribution then using Huygens' principle the field is found for regions lying in front of the aperture. The above two methods given the field only in the front direction. An attempt has been made to extend the induced current method [11] in the back direction. The final result appears, as in the first discussed case, as the difference of two quantities, the incident field and the scattered field. The scattered field is a quantity which was only assumed, therefore, any small error in the assumption can appear as a large percentage error in the difference.

Another possible approach which was investigated was the treatment of the diffraction problem with the aid of the recently developed concepts of diffraction rays. [8] It was found that this approach, although it possesses considerable merit it was not easily adaptable to the problem in hand, especially in cases where the primary illumination of aperture tapers to zero at the edges.

The limitations of the above mentioned techniques and the motivation to arrive at simple, flexible and useful solutions led the author to seek a new solution which is basically an extension of the aperture method. This solution does not present the final result as the difference of two quantities and thus it is free from limitations of the methods available at present. This method is valid only for cases where the wavelength is small as compared to the physical dimensions of the reflector and is based on Kirchoff's approximation. For this reason a brief discussion of Kirchoff's approximation follows.

## III. KOTTLER'S INTEGRALS AND KIRCHOFF'S APPROXIMATION

Kirchoff's approximation is based in Huygens' Fresnel formulation of scalar diffraction problems or Kottler's formulation of electromagnetic diffraction problems. Huygens' Fresnel principle enables

one to determine the field at some point enclosed by arbitrarily chosen surfaces provided one knows the electric and magnetic field in the surface and the sources enclosed by the surface.

For the special case where one has an observation point, a source and an object which obstructs the source, Kirchoff's approximation takes the following form. See Figure I.

A closed surface is constructed around the observation point composed by two open surfaces $S_0$ and $S_1$. Surface $S_0$ is one of the sides of the obstructing object. The contribution of this surface to the field at the observation point is zero.

Surface $S_1$ is an arbitrarily chosen surface. Normally it is chosen in such a way that it is possible to make a good approximation for the field at the surface. The usual approximation being to assume that the field in the surface is the incident field.

This is just a very brief statement of the aspects of the Kirchoff's approximation which are of immediate interest to us. Extensive discussions are available in the literature. [1,2,9,10]

The Kirchoff approximation is only valid for cases where the wavelength is small as compared to the physical dimensions of the system. In the past it has been extremely successful for providing approximate solutions to diffraction problems. The main limitation is the fact that corrections for obtaining more precise results cannot be done in an obvious manner. This leaves its use with some degree of uncertainty, however for a large number of problems it is absolutely the best method to use because other alternatives are so complex and inflexible that their use is not justified by the circumstances.

Having made the Kirchoff approximation one can proceed to determine the field at a point by using the familiar Kottler integrals. [9,10]

One has then,

$$E_s(P)=\frac{1}{4\pi}\int_A \left[-j\omega\mu(\vec{n}\times\vec{H})\varphi + (\vec{n}\times\vec{E})\times\nabla\psi\right] + (n\cdot E)\nabla\psi\, dS - \frac{1}{4\pi i\omega\varepsilon}\oint_{\Gamma_A}\nabla\psi(\vec{\tau}\cdot\vec{H})\, d\ell$$

$$= -\frac{1}{4\pi}\int_A\left[\psi\frac{\partial\vec{E}}{\partial n}-\vec{E}\frac{\partial\psi}{\partial n}\right] dS + \frac{1}{4\pi}\oint_{\Gamma_A}\psi\vec{E}\times\vec{\tau}\cdot d\ell - \frac{1}{4\pi i\omega\varepsilon}\oint_{\Gamma_A}\nabla\psi(\vec{\tau}\cdot\vec{H})\, d\ell \qquad (1)$$

The H component

$$H = -\frac{1}{4\pi}\int_A\left[i\omega\varepsilon(\vec{n}\times\vec{E}_1)\psi + (\vec{n}\times\vec{H})\times\nabla\psi + (\vec{n}\cdot\vec{H})\nabla\psi\right] dS + \frac{1}{4\pi i\omega\mu}\oint_{\Gamma_A}(\nabla\psi)(\vec{\tau}\cdot\vec{E})\, d\ell$$

$$= -\frac{1}{4\pi}\int_A\left[\psi\frac{\partial\vec{H}}{\partial n}-\vec{H}\frac{\partial\psi}{\partial n}\right] dS + \frac{1}{4\pi i\omega\mu}\oint_{\Gamma_A}(\nabla\psi)\vec{E}\cdot d\ell + \frac{1}{4\pi}\oint_{\Gamma_A}\psi\vec{H}\times\vec{\tau}\, d\ell \qquad (2)$$

where $\vec{\tau}$ is the tangent to boundary of the surface and n is the normal

$$\psi = \frac{e^{-ikR}}{R} \qquad k = \frac{2\pi}{\lambda}$$

where $\lambda$ is the wavelength and R is the distance from the observation point to the element of integration.

Letting $U_p$ be any component of E or H field one has for the far field,

$$U_p = \frac{1}{j\pi}\int_A U \frac{e^{-ikR}}{R}\left[(ik + \frac{1}{R})\,\vec{n}\cdot\vec{R} + ik\,\vec{n}\cdot\vec{s}\right] dS \qquad (3)$$

for $ik \gg \frac{1}{R}$ this reduces

$$U_p = \frac{ik}{j\pi}\int_A U \frac{e^{-ikR}}{R}\,(\vec{n}\cdot\vec{R} + \vec{n}\cdot\vec{s})\; dS \qquad (4)$$

where n is the normal to the surface of integration and s is the normal to the wave front.

Another approximation can be constructed by examining the radiation properties of a plane wave element. It can be shown that the radiation field of a plane wave surface element gives the following field.[9,10]

$$E_\theta = \vec{\theta}\,\frac{ike^{-jkR}}{j\pi R}\,(1 + \cos\theta)\,\cos\phi\; E_0 \qquad (5)$$

$$E_\phi = \vec{\theta}\,\frac{ike^{-jkR}}{j\pi R}\,(1 + \cos\theta)\,\sin\phi\; E_0 \qquad (6)$$

where R, $\phi$, $\theta$ are the spherical coordinates and $E_0$ is the amplitude of the element.

These are the formulas on which the subsequent discussion will be based.

## IV. ASYMPTOTIC EVALUATION OF INTEGRALS OF THE FORM

$$\text{a.}\quad Z_1 = \int_a^b e^{ikx}\, g(x)\, dx$$

$$\text{b.}\quad Z_2 = \int_a^b e^{ikf(x)}\, g(x)\, dx$$

In the statement of the Kirchoff approximation the fields were given in an integral form. It is often the case that these integrals cannot be evaluated easily. In a number of cases it is possible by taking into advantage the geometry of the situation to expand the integrand into a series of eigenfunction which can be integrated separately. The difficulty, however, with this approach is that for large values of k this type of series converges very slowly. In this section a series expansion of the above integrals will be given in power of $(\frac{1}{k})$ so that for large k the first term gives a good approximation.

These types of expansion have been already reported in the literature [5,6] with a sufficient degree of generality. In this work only a simple form suited well for our application will be discussed.

Case a. Integrals of the form $Z_1 = \int_a^b e^{ikx}\, g(x)\ dx$

Let us integrate this integral by parts:

$$Z_1 = \frac{e^{ikx}\, g(x)}{ik}\Bigg|_a^b - \int_a^b \frac{e^{ikx}}{ik}\ g'(x)\ dx$$

Again integrating by parts one has,

$$Z_1 = \frac{e^{ikx}}{ik}\ g(x)\Bigg|_a^b - \frac{e^{ikx}\, g'(x)}{(ik)^2}\Bigg|_a^b + \int_a^b \frac{e^{ikx}}{(ik)^3}\ g''(x)\ dx$$

Continuing this process the following series are obtained:

$$Z_1 = \sum_{n=1}^{\infty} \frac{e^{ikx}\, g^{n}(x)}{(ik)^{n+1}} \qquad (7)$$

If the function $g(x)$ is a smoothly varying function then clearly for large k the first few terms are sufficient to give a good estimate of the function $Z_1$.

Case b. Integral of the form $Z_2 = \int_a^b e^{ikf(x)}\, g(x)\, dx$

Method of Stationary Phase.

If the functioning $f(x)$ has a stationary point within the region of integration and if k is large and the function $\frac{g(x)}{f'(x)}$ is of bounded variation then the following approximation is valid. Let $x_o$ the point $f'(x) = 0 \quad x = x_o$. For $f''(x_o) > 0$.

$$Z_2(k) = \frac{g(x_o)}{\sqrt{f''(x_o)}} \sqrt{\frac{2\pi}{k}}\; e^{ikf(x_o) + i\frac{\pi}{4}} + O(\tfrac{1}{k}) \tag{8}$$

For $f''(x_o) < 0$

$$Z(+) = \frac{g(x_o)}{\sqrt{-f''(x_o)}} \sqrt{\frac{2\pi}{k}}\; e^{ikf(x_o) - i\frac{\pi}{4}} + O(\tfrac{1}{k}) \tag{9}$$

More detailed discussion of this expansion can be found in the literature.[5]

## V. THE SHADOW REGION FIELD PATTERN OF A CIRCULAR APERTURE

In the previous section all the background material necessary for the determination of the shadow region field radiation has been presented. In this section this background material will be integrated and estimates of the field pattern and its order of magnitude will be given.

The special case which will be examined is that of circular aperture having a given field distribution in the vicinity of the edges. As it will be seen later in this section the distribution of the field at the edges is all that is necessary for the determination of the shadow region pattern. The field at the edges may arise from either direct radiation of a feed illuminating a parabolic reflector, or, in the case where the primary radiation goes to zero at the edges, from secondary radiation and reflections. As far as this section is concerned the origin of the field at the edges is not important as long as its form is known.

As it was mentioned previously, the problems examined in this study are only limited for cases where the wavelength is small as compared to the dimensions of the system. This allows one to view the situation from a physical optics or more properly from a microwave optics point of view. The immediate conclusions that one can draw is that the diffraction

mechanism has a local character i.e., it is the shape of the boundary separating the illumination from shadow region which determines the diffraction pattern (see Figure II) and not the general shape of the object. One can also predict that for all practical purposes for circular reflectors the field will drop sharply in the sides but then an interference pattern will appear having always a maximum in the vicinity of the axis of revolution of the reflector. The magnitude at the field maximum lying in axis of the order of magnitude of source. This was actually one of the main conclusions of Fresnel when he demonstrated the wave nature of light by placing a point source in front of a sphere and observing that there is a maximum of light intensity in the direction of the line joining the center of the sphere and source.[3]

The specific case which is examined is that where the field in the plane of the aperture has the following general shape:

$$E_z = -\vec{z}\, e^{-ik(r-\rho)} f(r) \cos\phi\, E_0 \quad |H_\phi| = \frac{|E_z|}{\eta} \tag{10}$$

$$E_\phi = \vec{\phi}\, e^{-ik(r-\rho)} f(r) \sin\phi\, E_0 \quad |H_\theta| = \frac{|E_\phi|}{\eta} \tag{11}$$

where z is a cartesian coordinate.

r and $\phi$ are spherical coordinates as shown in Figure II

$$\eta = \sqrt{\frac{\mu}{\varepsilon}}$$

Following an approach based on Kirchoff's approximation the observation point P is enclosed by three surfaces $S_0$, $S_1$, $S_2$. Surface $S_0$ is the back of the reflector, surface $S_1$ is the infinite plane of the aperture minus the area of the aperture, and surface $S_2$ is the infinite semisphere. The contribution of surfaces $S_0$ and $S_2$ is assumed to be zero while the contribution of the surface $S_1$ can be obtained by using Kottler's integrals.

For convenience the expression giving the electric field is rewritten below:

$$E(P) = \frac{ik}{2\pi} \int_A \vec{E}_T \frac{e^{-ikR}}{R} \left[(\vec{n}\cdot\vec{R}) + (\vec{n}\cdot\vec{s})\right] dS$$

$$- \frac{1}{4\pi} \oint_{\Gamma_A} \frac{e^{-ikR}}{R} (\vec{E}_T \times \vec{\tau})\, d\ell + \frac{\vec{R}\, k}{4\pi\omega\varepsilon} \oint_{\Gamma_A} \frac{e^{-ikR}}{R} (\vec{\tau}\cdot\vec{H})\, d\ell$$

Let the first integral be

$$I_1 = \frac{ik}{4\pi} \int_A \vec{E}_T \frac{e^{-ikR}}{R} \left( (\vec{n}\cdot\vec{R}) + (\vec{n}\cdot\vec{s}) \right) dS \tag{12}$$

the second,

$$I_2 = \frac{\vec{R}\ k}{4\pi\omega\varepsilon} \oint_{\Gamma_A} \frac{e^{-ikR}}{R} (\vec{\tau}\cdot\vec{H})\ d\ell \tag{13}$$

and the third,

$$I_3 = -\frac{1}{4\pi} \oint_{\Gamma_A} \frac{e^{-ikR}}{R} (\vec{E} \times \vec{\tau})\ d\ell \tag{14}$$

For the first integral one has

$$\vec{n}\cdot\vec{s} = 0$$

$$\vec{n}\cdot\vec{R} = s\cdot R = \cos\theta$$

It was pointed out previously that most of the contribution to this type of integral comes from points lying close to the boundary. Consequently certain approximations involving the distance R which are valid in the vicinity of the rim of the reflector are made below. Thus one has the typical far field approximation,

$$R = R_0 - r\cos\alpha = R_0 - r\sin\theta\cos(\phi - \phi') \ ; \ \cos\alpha = \sin\theta\cos(\phi - \phi')$$

For the R appearing in the denominator it is sufficient to let $R = R_0$.

Substituting these quantities to the first integral and noticing that $dS = r\,dr\,d\phi$

$$I_1 = \frac{ik}{4\pi} \int_0^{2\pi} \int_\rho^\infty E_T \frac{e^{-ikR_0 + ikr\sin\theta\cos(\phi - \phi')}}{R} \cos\theta\ r\,d\phi\,dr \tag{15}$$

But $\vec{E}_T = \vec{E}_z + \vec{E}_\phi$ therefore from equation 10, one has,

$$I_1 = \frac{ik}{4\pi} \frac{e^{ikR_0}}{R} \cos\theta \int_0^{2\pi} \int_\rho^\infty (-z\cos\phi + \phi \sin\phi)\, E_0\, e^{-ikr}\, e^{-ikr \sin\theta \cos(\phi-\phi')} f(r)\, r\, dr\, d\phi \tag{16}$$

By retaining only the first term of the series given by equation 7 the first integration with respect to the variable r can be performed approximately. In this case only the lower limit contributes to the integral because the field at the upper limit goes to zero. The result is

$$I_1 = \frac{1}{4\pi} \frac{e^{-ikR_0}}{R} f(\rho) \cos\theta \int_0^{2\pi} (-\vec{z}\cos\phi + \vec{\phi}\sin\phi)\, E_0\, \frac{e^{-ikr \sin\theta \cos(\phi-\phi')}}{1 + \sin\theta \cos(\phi-\phi')}\, d\phi + O\left(\frac{1}{k}\right) \tag{17}$$

Notice that the incident field in the surface of integration has the form

$$E_T = -\vec{z}\cos\phi\, f(r) + \vec{\phi}\sin\phi\, f(r) = (-\vec{z}\cos\phi - \vec{x}\sin^2\phi + \vec{y}\sin\phi\cos\phi)\, f(r)$$

$$= (-\vec{z}\cos\phi - \vec{x}\left(\frac{1}{2} - \frac{\cos 2\phi}{2}\right) + \vec{y}\sin\phi\cos\phi\, f(r) \tag{18}$$

Only $E_x$ gives a contribution to the integral, $E_z$ and $E_y$ give zero. Let us now consider small values of the angle $\theta$ therefore the following approximations can be made $\cos\theta \approx 1$, $\sin\theta \approx 0$ in all places except at the expression appearing at the exponent. The integral is then,

$$I_1 = -\frac{1}{8\pi} \frac{e^{-ikr_0 - ik\rho}}{R} \rho f(\rho) \int_0^{2\pi} \vec{x}\, e^{ik \sin\theta \cos(\phi-\phi')} (1 - \cos 2\phi)\, d\phi \tag{19}$$

or

$$I_1 = -\vec{x}\frac{1}{4\pi} \frac{e^{ik(R_0+\rho)}}{R} f(\rho)\rho \left[ J_0(k\rho \sin\theta) - \frac{1}{2\pi} \int_{\phi'}^{2\pi-\phi'} e^{ik\rho \sin\theta \cos\phi} \right.$$

$$\left. (\cos 2\phi \cos 2\phi' - \sin 2\phi \sin 2\phi')\, d\phi \right] \tag{20}$$

Using the expression $J_{\pm n}(x) = \int_0^{2\pi} e^{ik \cos \phi \mp n\phi} \, d\phi$

and also the relation $J_{-n}(x) = (-1)^n J_n(x)$ one obtains

$$I_1 = -\frac{1}{4} \frac{e^{-ik(R_0+\rho)}}{R} \rho f(\rho) \left[ J_0(k\rho \sin \theta) + \cos 2\phi' J_2(k\rho \sin \theta) \right] \qquad (21)$$

where $J_0$ and $J_2$ are Bessel functions of zero and second order. Let us consider the second integral. Notice that

$$\vec{\tau} \cdot \vec{H}_\theta = 0$$

$$\vec{\tau} \cdot \vec{H}_\phi = H_\phi = \sqrt{\frac{\epsilon}{\mu}} |E_z|$$

Also $\omega = \frac{k}{\sqrt{\mu\epsilon}}$

Substituting these in 14 one has

$$I_2 = \frac{R}{4\pi} \int_0^{2\pi} E_z \frac{e^{-ikR}}{R} \, d\phi \qquad (22)$$

Making the same far field approximations as before one has

$$I_2 = \frac{R}{4\pi} \frac{1}{R} E_0 f(\rho) e^{-ik\rho} \int_0^{2\pi} \cos \phi \, e^{-ikR_0 + ik \sin \theta \cos (\phi - \phi')} \rho \, d\phi = 0 \qquad (23)$$

For the third integral one has

$$\vec{E}_\phi \times \vec{\tau} = 0$$

$$\vec{E}_z \times \vec{\tau} = r |E_z|$$

Similarly one can show that,

$$I_3 = \frac{1}{4\pi} \int_0^{2\pi} \vec{r} \left| E_z \right| \frac{e^{-ikR}}{R} \, d\phi = 0 \tag{24}$$

As it was expected the two last integrals vanish leaving no longitudinal components present.

The final result therefore is given by equation 20.

This is a very useful result because it gives the radiation pattern for small angles in the shadow region without having to know exactly the form of the field in the edges of the reflector. Notice that the pattern above has a peak in the axis of the reflector as it was expected from optics.

The field in the axis is

$$E(\text{axis}) = -\frac{\vec{x}}{4} \frac{e^{-ik(R_0+\rho)}}{R} \rho f(\rho) \tag{25}$$

The power flow at any point can be determined with the aid of the Poynting vector which is

$$S = \frac{1}{2} R_e \left( \vec{E} \times \vec{H} \right) \tag{26}$$

Assuming that the far field behaves like a plane wave, one has,

$$E_x = \vec{x} E_0 \qquad\qquad H_y = \vec{y} H_0$$

$$E_0 = \sqrt{\frac{\mu}{\varepsilon}} H_0$$

Then equation 26 becomes

$$S = \frac{1}{32} \vec{R} \frac{\rho^2 f^2(\rho) E_0^2}{R^2} \left( \frac{\varepsilon}{\mu} \right)^{1/2} \tag{27}$$

The power flow per unit stereo angle is

$$P = R^2 S = \frac{1}{32}\ \rho^2 f^2(\rho)\ E_0^2\ \left(\frac{\varepsilon}{\mu}\right)^{1/2} \qquad (28)$$

This is one of the main results of this development because the maximum in the direction of the axis is of great interest. The field arrives at this direction in phase from the edges thus making it the maximum which will stand out from all the maxima of the interference pattern.

## VI. ESTIMATES OF THE SIDE AND SHADOW REGION RADIATION OF A CIRCULAR APERTURE WITH A UNIFORM ILLUMINATION

For cases where the primary illumination is zero to first order in the edges of the reflector a method is required which can give estimates of the field present there from secondary reflections. In order to obtain these estimates the following approximation is made. The field in the plane of the aperture is assumed to be a plane wave, and then using Kirchoff's integration methods the field in the plane of the aperture is determined.

This is a highly idealized method and in actual practice one would expect that deviations from these assumptions will alter the results. However, one might argue that because of the fact that side radiation is some orders of magnitude below the primary pattern and because there are so many other non-controllable factors (such as reflectors from the supporting posts, structural imperfections, reflections from the ground, etc.,) an exact theoretical calculation is of very little practical use.

For this reason this highly idealized situation will be pursued here, with the understanding that it provides estimates which are conservative and that, in actual practice, larger values of field intensity which are predicted here, are likely to be encountered.

From equations 1 and 4, one has

$$E(P) = \frac{1}{4\pi}\int_A E\frac{e^{-ikR}}{R}\ (ik)(\vec{n}\cdot\vec{R}) + in.s)\ dS - \frac{1}{4\pi}\oint_{\Gamma_A}\frac{e^{-ikR}}{R}\ (\vec{E}\times\vec{\tau})\ d\ell +$$

$$+\ \frac{\vec{R}\,k}{4\pi\omega\varepsilon}\oint_{\Gamma_A}\frac{e^{-ikR}}{R}\ (\vec{\tau}\cdot\vec{H})\ d\ell$$

This equation gives the contribution only of the radiation fields; static and induction fields are neglected..because they do not contribute to the far field. For the evaluation of the above integrals one observes that:

$$\vec{n}\cdot\vec{R} = 0$$

$$\vec{n}\cdot\vec{s} = 1$$

$$\vec{E} \times \vec{\tau} = z \cos\phi$$

$$\vec{\tau}\cdot\vec{H} = \cos\phi$$

$$|E_x| = \frac{|H_y|}{\sqrt{\frac{\varepsilon}{\mu}}}$$

This integral will be evaluated for two cases. a - For points lying in the far field and; b - For points lying in the rim of the reflector.

Case a: For the first case, one has, (see Figure II)

$$E(P') = \frac{1}{4\pi}\int_{\psi_1}^{\psi_2}\int_{R_1}^{R_2} E_T\, ik\frac{e^{-ikR}}{R}\, RdRd\psi - \frac{1}{4\pi}\ \vec{z}\oint_{\Gamma_A}\frac{e^{-ikR}}{R}\ \cos\phi\ \rho\ d\phi$$

$$+\ \frac{\vec{R}}{4\pi}\int_{\Gamma_A}\frac{e^{-ikR}}{R}\ \cos\phi\ \rho\ d\phi \qquad (29)$$

or integrating the first integral with respect to the variable R approximately,

$$E(P) = \frac{1}{4\pi}\ x\ E_o\int_{\psi_1}^{\psi_2}(e^{-ikR_1} - e^{-ikR_2})\ d\psi + O(\tfrac{1}{k}) + (\vec{R} - \vec{z})\int_{\Gamma_A}\frac{e^{-ikR}}{R}\cos\phi\ \rho d\phi \qquad (30)$$

These integrals will be evaluated now with the method of the stationary phase. For the first integral let

$$R_{1,2}(\psi) = R_0\cos\psi \mp\sqrt{\rho^2 - R_0^2\sin^2\psi} \qquad (31)$$

The first derivative is

$$R'_{1,2}(\psi) = - R_0 \sin\psi \pm R_0^2 \frac{\sin\psi \cos\psi}{(\rho^2 - R_0^2 \sin^2)} 1/2 \tag{32}$$

The stationary point is at

$$R'_{1,2}(\psi = 0) = 0$$

The second derivative is

$$R''_{1,2}(\psi) = - R_0 \cos\psi \pm R_0^2 \frac{(\cos^2\psi - \sin^2\psi)}{(\rho^2 - R_0^2 \sin^2\psi)^{1/2}}$$

$$- R_0^4 \frac{\sin^2\psi \cos^2\psi}{(\rho^2 - R_0^2 \sin^2\psi)^{3/2}} \tag{33}$$

$$R''_{1,2}(\psi = 0) = - R_0 \pm \frac{R_0^2}{\rho} = \frac{1}{\rho}(- \rho R_0 \pm R_0^2) \tag{34}$$

$$\text{Also } \lim_{R \to \infty} R''_{1,2}(\psi = 0) = \pm \frac{1}{\rho} R_0^2 \tag{35}$$

$$\text{and } R_{1,2}(\psi = 0) = R_0 \pm \rho \tag{36}$$

For the second integral one has

$$R(\phi) = \sqrt{R_0^2 + \rho^2 - 2\rho R_0 \cos(\phi - \phi')} \tag{37}$$

$$R'(\phi) = + \frac{\rho R \sin \phi}{(R_0^2 + \rho^2 - 2\rho R_0 \cos(\phi-\phi'))^{1/2}} \qquad R'(\phi=\phi',\ \phi'+\pi) = 0 \tag{38}$$

$$R''(\phi) = \frac{\rho R \cos \phi}{(R_0^2+\rho^2-2\rho R_0 \cos(\phi-\phi'))^{1/2}} - \frac{\rho^2 R^2 \sin^2 \phi}{(R_0^2+\rho^2-2\rho R_0 \cos \phi)^{3/2}} \tag{39}$$

$$R''(\phi=\phi') = \frac{\rho R}{(R-\rho)} \tag{40}$$

$$R''(\phi=\phi'+\pi) = \frac{\rho R}{R+\rho} \tag{41}$$

$$\text{Also } \lim_{R \to \infty} R''(\phi=\phi',\ \phi'+\pi) = \rho \tag{42}$$

$$\text{and } R(\phi=\phi',\ \phi'+\pi) = R \mp \rho \tag{43}$$

Since in the line integrals there are two stationary points the contribution of both will be taken into account. Using equation 8 the final result as $R \to \infty$ is

$$E(P') = \vec{x} \frac{1}{4\pi} \frac{\rho}{R} \sqrt{\frac{2\pi}{k\rho}} \left(e^{ik(R-\rho)+i\frac{\pi}{4}} - e^{ik(R+\rho)-i\frac{\pi}{4}}\right)$$

$$+ (\vec{R} - \vec{z}) \frac{1}{4\pi} \cos \phi' \frac{\rho}{R} \sqrt{\frac{2\pi}{k\rho}}\ e^{ik(R-\rho)+i\frac{\pi}{4}} - e^{ik(R+\rho) - \frac{\pi}{4}} \tag{44}$$

or

$$E(P') = (\vec{x} + \vec{R} \cos \phi' - \vec{z} \cos \phi') \frac{1}{4\pi} \rho \sqrt{\frac{2\pi}{k\rho}} \frac{e^{ikR}}{R} 2i \sin\left(\frac{\pi}{4} - k\rho\right) \tag{45}$$

$$\text{but } \vec{x} - \vec{R} \cos \phi' = \vec{R} \cos \phi' + \vec{\phi} \sin \phi' - \vec{R} \cos \phi' = \vec{\phi} \sin \phi' \tag{46}$$

Therefore

$$E(P') = (\vec{\phi} \sin \phi' - \vec{z} \cos \phi') \frac{i}{2\pi} \rho \sqrt{\frac{2\pi}{k\rho}} \frac{e^{ikR}}{R} \sin \left(\frac{\pi}{4} - k\rho\right) \qquad (47)$$

Observe that as it was expected no longitudinal components exist in the far field.

Case b: The radiation field in the rim of the reflector and the shadow region field.

For this case a slightly different approach will be used. The field at the edges of the reflector will be taken to be the sum of the individual contributions of each of the surface elements which form the total area of the aperture. Since eventually the results of this development eventually will be used for the determination of the far field in the back direction only the radiation fields of the plane wave area elements will be considered. Using equation 5 where $\theta = \frac{\pi}{2}$ one has for the field at the edges $E_e(P')$,

$$E_e(P') = \frac{E_0}{4\pi} \int_{R_2}^{R_1} \int_{\psi_2}^{\psi_1} (\vec{z} \cos \phi + \vec{\phi} \sin \phi) \frac{e^{-ikR}}{R} ikR \, dR \, d\psi - \frac{\vec{R}}{4\pi} \int_0^{2\pi} \frac{e^{-ikR}}{R} \cos \phi \, \rho d\phi \qquad (48)$$

The second integral because of its radial component does not contribute to the shadow region radiation and for this reason its evaluation will be omitted.

For points lying in the edges $R_2 = 2\rho \cos$ , $R_1 = 0$, $\psi_2 = -\frac{\pi}{2}$, $\psi_1 = \frac{\pi}{2}$, and by integrating with respect to the variable R with the aid of equation 7 one has,

$$E_e(P') = \frac{1}{4\pi} 2 \int_0^{\frac{\pi}{2}} (\vec{z} \cos \phi + \vec{\phi} \sin \phi)(e^{-ikR_2} - 1) \, d\psi + 0 \left(\frac{1}{k}\right) \qquad (49)$$

In this case $R_2 = 2\rho \cos$ and the stationary point occurs, as before, for $\psi = 0$. Also $\phi = f(\psi)$ and for $\psi = 0$; $\phi = \phi_1$, $\phi_1 + \pi$. With equation 8 this reduces to

$$E_e(P') = \frac{1}{4\pi} (z \cos (\phi_1 + \pi) + \phi \sin (\phi_1 + \pi) \, 2 \sqrt{\frac{2\pi}{2k\rho}} e^{ik2\rho - i\frac{\pi}{4}} (z \cos \phi_1 + \phi \sin \phi_1) \pi \qquad (50)$$

or for large kρ

$$E_e(P') = -\frac{1}{4}(\vec{z}\cos\phi_1 + \vec{\phi}\sin\phi_1) \tag{51}$$

This expression gives the field at the edges of the reflector. However, in order to have the results of the previous section apply here one has to show that in the immediate vicinity of the edge of the field behaves as $f(r)e^{-ikr}$.

Let us consider an observation point close to the rim. The field in this point is given by equation 48. Integrating the equation with the aid of equation 7 and omitting the second integral one has

$$E_e(P') = \int_{-\frac{\pi}{2}}^{\frac{\pi}{2}} (\vec{z}\cos\phi + \vec{\phi}\sin\phi)(e^{-ikR_2} - e^{ikR_1})\,d\psi \tag{52}$$

$$\text{In this case } R_2 = R_0\cos\psi + \sqrt{\rho^2 - R_0^2\sin^2} \tag{53}$$

Since the observation point is close to the rim the edge to a first approximation can be taken as an infinite straight line.

Quantity $R_1$ therefore can be approximated

$$R_1 = \frac{d}{\cos\psi} = \frac{R-\rho}{\cos\psi} \tag{54}$$

The first term of the sum of the exponentials can be evaluated as before the second part also can be evaluated by the method of stationary phase by noting that stationary phase occurs for = 0. The final result is:

$$E_e(P') = \frac{1}{4\pi}(\vec{z}\cos\phi + \vec{\phi}\sin\phi)\left(\sqrt{\frac{2\pi}{k\rho}}\,e^{ik(R_0+\rho)-i\frac{\pi}{4}} - \sqrt{\frac{2\pi}{kd}}\,e^{ik(R_0-\rho)+i\frac{\pi}{4}}\right) \tag{55}$$

This is of the form of $(z\cos\phi + \phi\sin\phi)f(R)\,e^{-ik(R-\rho)}$ where the Lim of $(R) = f(\rho)$ from equation 51 can be seen to be $R\to\rho$

$$f(\rho) = \frac{1}{4} \tag{56}$$

For this case it will be instructive to determine the front to back ratio.

The total power going through the aperture is

$$P_T = AS = \pi \rho^2 \frac{1}{2} R_e (\vec{E} \times \vec{H}^*) \tag{57}$$

For a plane wave one has $E_x = \vec{x} E_0$ $\qquad$ $H_y = \vec{y} H_0$

and $\qquad E_0 = \sqrt{\frac{\mu}{\varepsilon}} H_0$

The above expression becomes

$$P_T = \pi \rho^2 \frac{1}{2} E_0^2 \left(\frac{\varepsilon}{\mu}\right)^{1/2} \tag{58}$$

The power flow per unit stereo angle in the axis of the shadow region from equation 56 and 28 is

$$P_b = \frac{1}{128} \rho^2 E_0^2 \tag{59}$$

If one defines the back lobe gain $G_b$ as follows

$$G_b = \frac{4\pi P_b}{P} \tag{60}$$

where P is the total power transmitter by the aperture then,

$$G_b = \frac{4\pi \frac{1}{128} \rho^2 E_0^2}{\pi \rho^2 \frac{1}{2} E_0^2} = \frac{1}{16} \tag{61}$$

The front gain of aperture with uniform illumination is

$$G_f = \frac{4\pi A}{\lambda^2} = \frac{4\pi^2}{\lambda^2} \rho^2 = (k\rho)^2 \tag{62}$$

The front to back ratio is

$$\frac{P_f}{P_b} = \frac{PG_{f/1w}}{PG_{b/1w}} = \frac{G_f}{G_b} = (k\rho)^2\, 16 \tag{63}$$

This is the final result of this section.

## VII. SIDE RADIATION OF APERTURE WITH TAPERED ILLUMINATION

In most cases the aperture is not uniformly illuminated but the illumination tapers to zero in the edges of the reflector.

The side radiation can still be evaluated by using Equation 5. The line integrals are of course equal to zero.

The field for a general distribution $E_0\, g(r)$ at the observation point $P'\ (\rho, \phi_1)$ is

$$E_e(P') = \frac{E_0}{1w} \int_{R_1}^{R_2} \int_0^{\frac{\pi}{2}} 2(\vec{z}\cos\phi - \vec{\phi}\sin\phi) \frac{e^{-ikR}}{R} E_0 ikR\, g(r)\, dR\, d\psi \tag{64}$$

or integrating approximately with respect to R

$$E_e(P') = \frac{E_0}{1w} \int_0^{\frac{\pi}{2}} 2(\vec{z}\cos\phi - \vec{\phi}\sin\phi) e^{-ikR} g(r) \Big|_{R_1}^{R_2} d\psi + \frac{E_0}{1w} \int_0^{\frac{\pi}{2}} (\vec{z}\cos\phi - \vec{\phi}\sin\phi)$$

$$\frac{e^{-ikR}}{k^2} \quad \frac{dg(r)}{dR} \Big|_{R_1}^{R_2} d\psi + O\left(\frac{1}{k}\right) \tag{65}$$

The first term gives zero while the second term can be evaluated as before (see equation 49) to give

$$E_e(P') = \frac{E_0}{1wk}\, i \left[ \left(\vec{z}\cos(\phi_1+\pi) - \vec{\phi}\sin(\phi_1+\pi)\right) 2\sqrt{\frac{2\pi}{2k\rho}}\; e^{-ik2\rho - i\frac{\pi}{4}} \left.\frac{d\,g(r)}{dR}\right|_{\substack{\psi=0 \\ R=2\rho}} \right.$$

$$\left. - (z\cos\phi_1 - \phi\sin\phi_1) \left.\frac{d\,g(r)}{dR}\right|_{\substack{\psi=0 \\ R=0}} \right] \tag{66}$$

For large kρ this gives

$$E_e(P') = -\frac{E_0}{4\pi k}\, i\, \frac{d\,g(r)}{dR}\Bigg|_{R=0} (z\cos\phi_1 - \rho\sin\phi_1) \tag{67}$$

The conclusion is therefore that the field in the edges is directly proportional to the derivative of the illumination distribution function in the edges.

Comparing this with the assumed form of the fields in the edge (eq. 10) it can be shown that

$$f(\rho) = -\frac{i\,E_0}{4\,k}\,\frac{d\,g(r)}{dR}\Bigg|_{R=0} \tag{68}$$

noting that $\dfrac{d\,g(r)}{dR}\Big|_{\substack{R=0\\ \Psi=0}} = \dfrac{d\,g(r)}{dr}\Big|_{r=\rho}$

The power flow in the back is then

$$P_b = \frac{1}{128\,k^2}\,\frac{d\,g(r)}{dr}\,E_0^2\,\rho^2 \tag{69}$$

Notice that this differs from equation 59 by the factor $k^2$. This means that for high frequencies the leakage in back becomes smaller while for a uniform illumination this was a constant.

## VIII. DISCUSSION OF RESULTS

The approach and the final form of the results of this work were such that no involved solutions and computations were necessary. This satisfied one of the main objectives of this study i.e., simplicity and flexibility. As it was discussed previously a number of variables which cannot be properly accounted (such as secondary reflection, etc.) are capable of producing stray signals such that the field pattern, which normally exists there, may be substantially altered. It seem therefore that only an approximate but simple and flexible approach as compared to a precise but involved and lengthy method can be justified by the special circumstances of this problem.

Since, in this study, only cases for which the wavelength is small as compared with the physical dimensions of the system are considered, then the behavior of the field in the shadow region can be better understood, at least qualitatively, from similar problems in optics. For the case where a source illuminates an obstacle one generally expects the following behavior. To a first order approximation, the field in the illumination region is equal to the incident field. In the illuminated to shadow boundary the field normally drops in a manner similar to a Fresnel infinite straight edge diffraction pattern. As one moves deeper into the shadow region contributions from the illuminated shadow boundary of the obstacle come into the picture thus creating an interference pattern. Experience with this type of problem in optics shows that the interference pattern is mainly determined by the shape of the illuminated shadow region boundary of the obstacle. The results of this study, for the special case which was considered, have also shown that the pattern in the shadow region is primarily determined by the field present in the edges of the reflector.

The special case which was examined here was that of a circular aperture with the general type of field present in the edges which one would expect arising from a collection of Huygens' sources located in the plane of the aperture. Because of the fact that the radiation arrives in phase at points lying in the far field in the direction of the axis of the reflector, the field there always has its maximum intensity.

It was found that the power per unit stereo angle radiated in the direction of the axis of the reflector apart from a correction factor is of the order of magnitude of the field present in the edges of the reflector. For small angles from the axis of the reflector the field pattern also was determined. Figure III shows a typical field pattern. The reason why the patterns for $\phi = 0$ and $\phi = \frac{\pi}{2}$ differ is the polarization of the incident radiation.

In determining the shadow region radiation only the general form of the field was necessary to be known in the edges with the only restriction that it was originally generated by some distribution of Huygens' sources. In order to evaluate the effect of the aperture illumination to the shadow region radiation, estimates were made for the radiation found in the edges arising from different types of illumination. For the case of a uniform illumination it was found that the field in the edges apart from a correction factor is of the same order of magnitude, as the field present in the aperture.

For the cases where the illumination tapers to zero in the edges, an already known fact was directly shown here, i.e., that the field in the edges to first order is zero. However, a second order approximation shows that it is directly proportional to the rate at which the illumination goes to zero at the edges and to the wavelength. One of the conclusions therefore is that the minimum shadow region radiation is obtained with a tapered illumination having the smoothest possible transition to zero in the edges.

One of the limitations of the approach which was pursued here i.e., the Kirchoff approximation, is that estimates of its accuracy cannot be made in an obvious and convenient manner. It is well known, however, that careful applications of Kirchoff's approximation have been very successful in a large number of similar problems. For the particular problem examined here the estimates given in this work are believed to be conservative. In actual practice it is expected that other factors (such as secondary reflection, etc.) will tend to create field intensities which will be higher than what is predicted here.

The methods which have been used in this work and particularly the asymptotic evaluation of the integrals form a powerful tool which has potential applications to a number of other problems. For example estimates of the back radiation of apertures with a boundary of other shape than circular can conceivably be given by using these methods. Also for other diffraction problems where it is advantageous to sacrifice extreme precision for considerable saving of effort and time this approach can be of great value.

ACKNOWLEDGEMENTS

The contents of this paper are a result of a contract for "Interference Studies," placed with the University of Pennsylvania by the U.S. Air Force, Rome Air Development Center.

REFERENCES

1. B. Baker and R. Copson, Huygens' Principle, Oxford, The Clarendon Press; 1953.

2. G. J. Bouwkamp, "Diffraction Theory," Reports on Progress in Physics, vol. XVII; 1954.

3. M. Born and R. Wolf, Principles of Optics, Pergamon Press; 1957.

4. T. Chu and R. King, The Scattering and Diffraction of Waves, Harvard, Cambridge; 1959.

5. A. Erdelyi, Asymptotic Expansions, Dover Publication; 1956.

6. D. J. Jones and M. Kline, "Asymptotic Expansion of Multiple Integrals and the Method of Stationary Phase," J. Math. Physics, 37, 1; 1958.

7. H. Kritikos, The Penumbra Region of Aperture Antennas, Dissertation, University of Pennsylvania; 1961.

8. J. B. Keller, "A Geometrical Theory of Diffraction Calculus of Variation and its Applications," Proc. of Symposia in Appl. Math., vol. VII, McGraw-Hill, New York; 1958.

9. J. Stratton, Electromagnetic Theory, McGraw-Hill, New York; 1941.

10. J. Silver, Microwave Antenna Theory and Design, Rad. Lab. Series, McGraw-Hill; 1949.

11. L. B. Tartakovskii, Side Radiation of Ideal Paraboloid With Circular Aperture, Radio Engineering and Electronics, vol. 4, no. 6; June 16, 1960, Trans. from Russian.

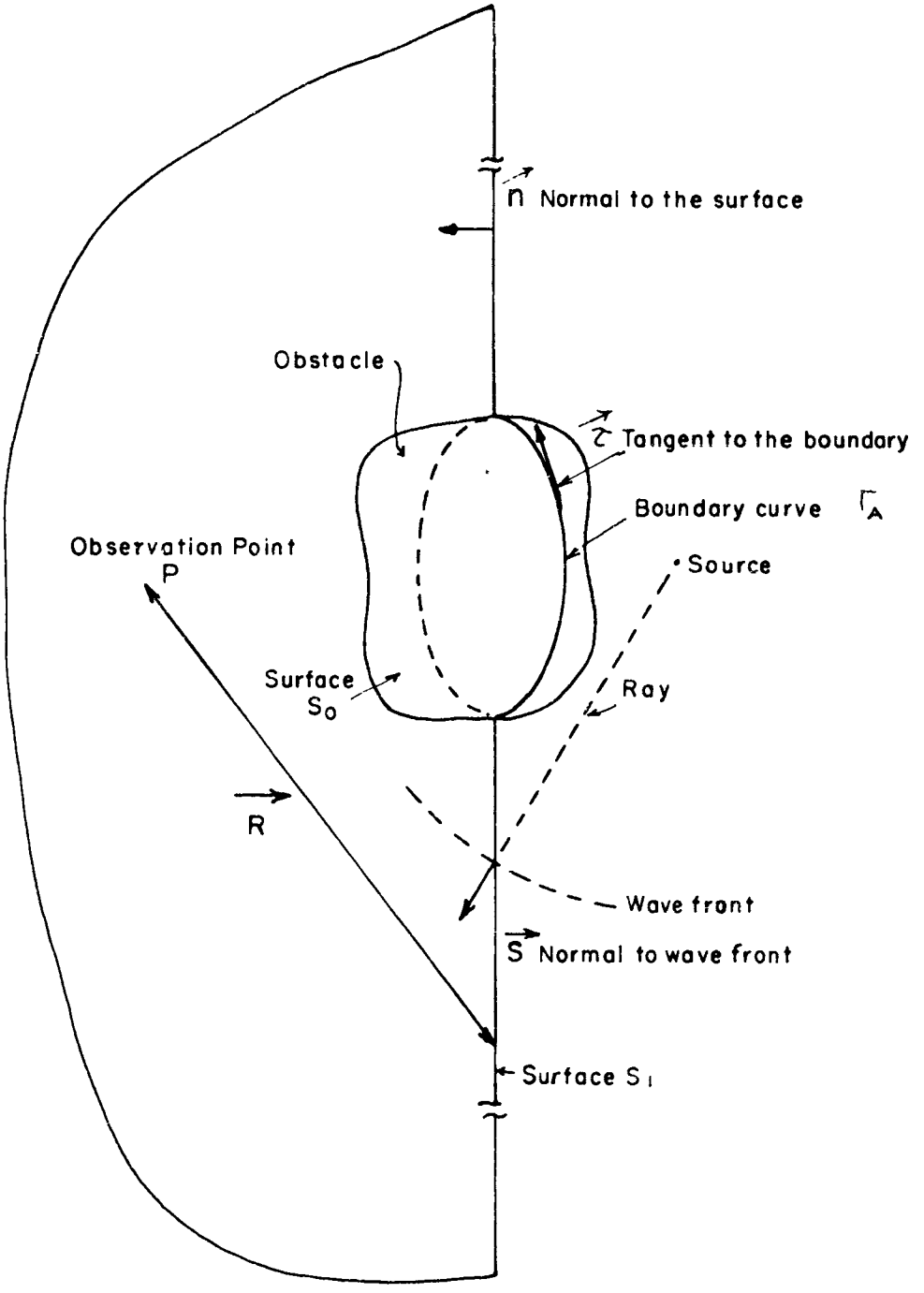



FIGURE I

SURFACES OF INTEGRATION

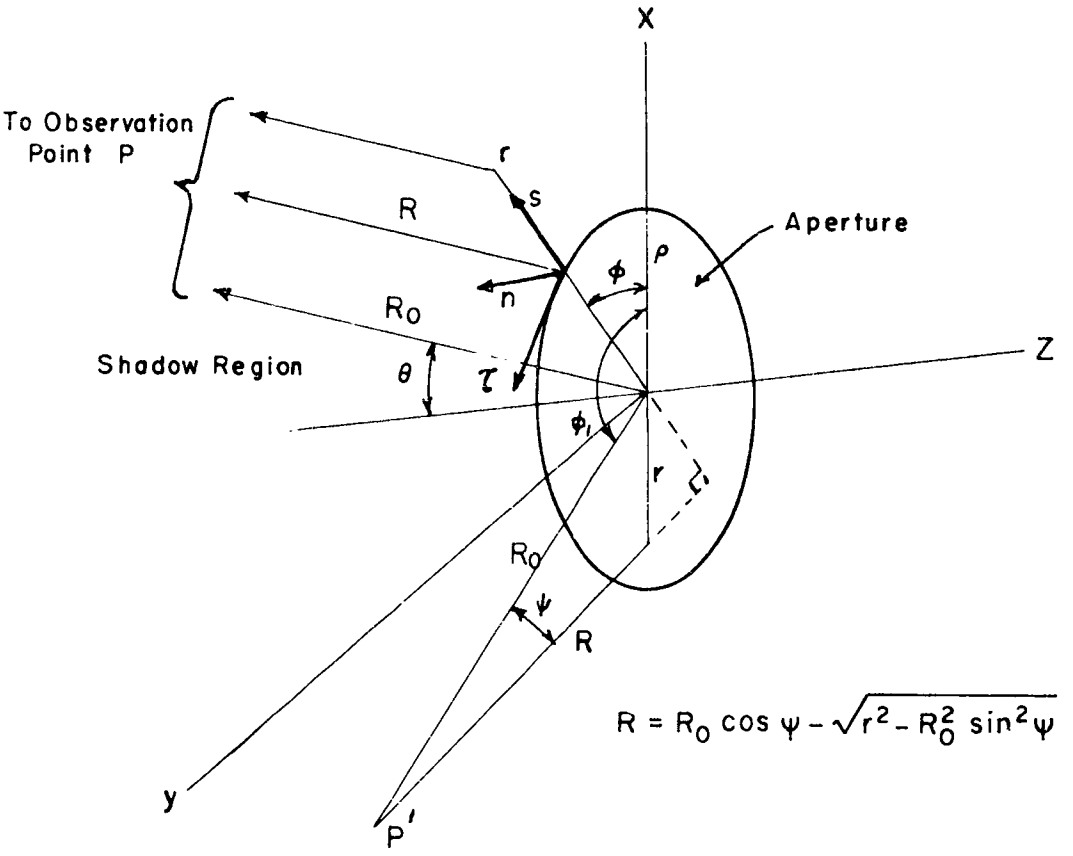
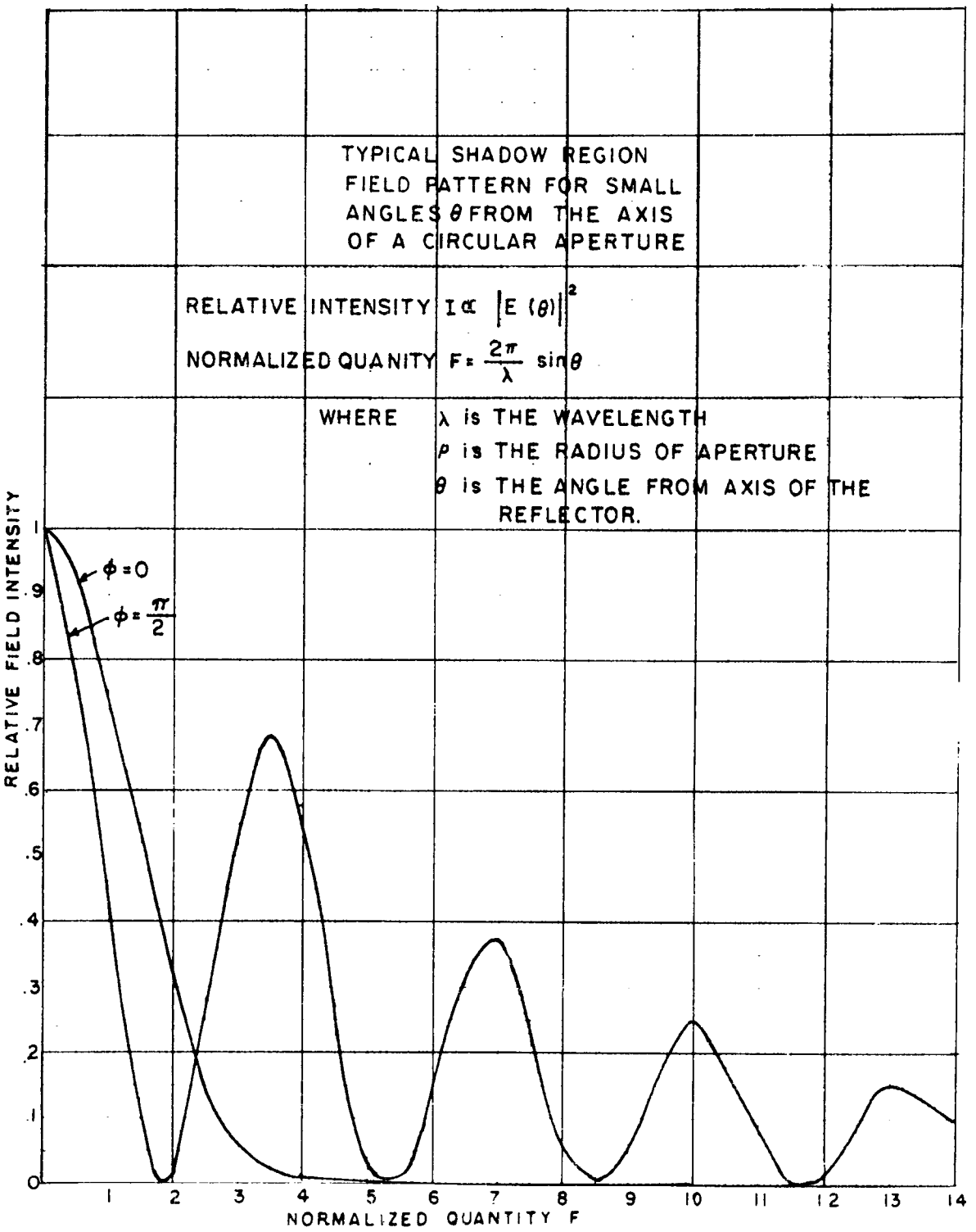



FIGURE II

GEOMETORY OF THE APERTURE


TYPICAL SHADOW REGION FIELD PATTERN FOR SMALL ANGLES θ FROM THE AXIS OF A CIRCULAR APERTURE
RELATIVE INTENSITY I ∝ |E (θ)|²
NORMALIZED QUANITY F = 2π/λ sinθ
WHERE λ is THE WAVELENGTH
ρ is THE RADIUS OF APERTURE
θ is THE ANGLE FROM AXIS OF THE REFLECTOR.
RELATIVE FIELD INTENSITY
φ = 0
φ = π/2
0
.1
.2
.3
.4
.5
.6
.7
.8
.9
1
1 2 3 4 5 6 7 8 9 10 11 12 13 14
NORMALIZED QUANTITY F

# WIDE BAND NOISE INTERFERENCE IN THE HF SPECTRUM

W. H. Gossard, Department of Defense
N. C. Gerson, Vice Chairman, Arctic Committee, USNC for the IGY
C. L. Gandy, Department of Defense

Abstract. - The high frequency radio spectrum is permeated by wide band noise phenomena which goes unnoticed by many radio noise measuring techniques. As a result of exploration into broad band communication systems, the incidence and characteristics of three of the most common wide band interference phenomena were studied and certain measurements of their characteristics have been made. The three noise sources are lightning discharges, automotive ignition and broad band sweepers. The latter type of interference was studied in some detail and the results of a world-wide spectrum sampling effort is reported. Several different display techniques were used. Initial problems of interpretation of these records are of more interest in form than in fact as shown by the interesting wood grain patterns obtained.

The significance of wide band noise on both narrow band and wide band data systems is discussed.

## I. INTRODUCTION

This paper presents for those who are not familiar with wide band spectrum work in the high frequency radio region, some new insight into the phenomena of certain wide band spectrum noises. Investigations of wide band noise are a natural outgrowth of the argument[1] and the necessity for utilizing all of the available spectrum. One side of the argument favors spread spectrum communication techniques. Systems using such technology are being developed and tested experimentally.

## II. BASIC DISCUSSION

Interest in the characteristics of the noise environment in which such systems must operate is a natural follow on. It is not the desire here to discuss S/N relationships in wide band and narrow band

cases, but rather to discuss some of the differences in the noise problems of the two cases.

Noise is considered in this paper as related to the wide band studies to be any energy within the received bandwidth which did not originate as transmitted signal energy. In other words, any distortions of the signal energy spectral components are considered a transmission path or receiver circuit characteristics and are not considered as noise. This leaves basically three sources of noise to consider; Gaussian noise, interfering narrow band noise, and wide band noise.

Wide band h-f communication technology often implies the use of short duration signal elements requiring wide spectra in the order of hundreds of kilocycles for their transmission. The signal energy in any narrow band of frequencies within this spread spectrum is very low - which is true also for the white noise energy in the restricted band. However, the total signal energy in the wide band spectrum is correlatable, whereas the noise energy is not. Since Gaussian noise is the property of the world's statisticians, I can leave that noise in my presentation here. In the narrow band signaling situation wide band impulsive interference provides only a small amount of the total noise energy due to the narrow bandwidths used in narrow band receiving systems.

Although the narrow band signaling noise is not of much concern in the results of our investigations, some discussion of their effect on wide band spread spectrum communication is in order. The narrow band interfering noise spectral energy (QRM) very heavily masks certain energy components of the wide band signal. However, unless the spread spectrum was really clobbered with narrow band, high powered interference sources only a minor number of the total spectral components would be affected.

The main purpose of the investigation of wide band spectral noise on which this paper is based was to determine the extent and characteristics of the third noise source, wide band noise. Many such sources can be easily conjectured, automotive ignition, motor commutator

arcing, welding arcs, industrial processes, sweeping and stepping ionospheric sounders, and many others. In fact, every time a circuit of any kind is energized or de-energized there is a wide band field produced. Certainly most of these circuits have such low energizing and de-energizing levels and such poor coupling characteristics to radiating parts and such poor radiation characteristics that fortunately the greatest part of these fall into a local interference class or below ambient noise and thus do not affect the problem at hand. Those sources which unfortuitously overcome all the hindrances stated are space radiated as wide band noise and must be considered.

If one could imagine every arcing source radiating sufficiently to be detected and with each an independent probability event, then we would have to stop experimenting and also give this problem back to the statisticians.

## III. EXPERIMENTAL RESULTS

The work reported on here was started in 1958 in conjunction with IGY ionospheric studies for wide band extraterrestrial noise sources.[2,3] The initial studies were accomplished by using standard radio receiver equipments characterized by Figure 1.

What was determined from these simple listening tests was that over a very wide range of h-f frequencies there were both simultaneous noise bursts and noise phenomenon with an apparent time delay as a function of frequency. The latter type of noises existed in such a variety of modes that subjective aural identification was considered extremely inaccurate. In some cases, repetitious characteristics were noted which required time storage and strained aural recall. Stop watch measurements were used to convince the experimenters that these noises were of a quasi-repetitious nature.

The next step of the experiment was a modified h-f receiver with a swept VFO sweeping the wide band i-f pass band. The detected i-f envelope was used to intensity modulate a CRO (Figure 2). The sweep rate of the system was 7 sweeps per second and the film advance rate was set at approximately 7 in./min. The r-f band pass of the receiver was

broadened to about 100 kc. The results using this device were startling to say the least as will be shown later in the discussion. At the same time the results (obtained in the Washington, D. C. area) from this device were being studied, a sophisticated h-f sampling equipment[4] was being employed in the San Francisco Bay area and the results were already being studied. Figure 3 is a functional block diagram of the sophisticated system.

The results from the West Coast studies revealed the existence of h-f radiated phenomena which have been nicknamed "h-f sweepers" and "noise trains" by the experimenters. Both of these names are representative of the main characteristics of these phenomena.

Wide band noises were broken down into various classes and sub-classes, which are dependent on the instrumentation and the 500 kc spectrum limitation. For example, the sweepers are called $\alpha$ phenomena and are divided into four sub-classes as described by the form of the time derivative $\frac{\delta f}{\delta t}$.

| | |
|---|---|
| $\alpha_1$ | linear |
| $\alpha_2$ | approximately exponential |
| $\alpha_3$ | apparently varying continuously (e.g., cubic) |
| $\alpha_4$ | discontinuous and other anamolous types |

Figures 4,5,6 and 7 show samples of these phenomena. Figure 8 is a strip of a very disturbed period which almost belongs to the statisticians.

These phenomena evidence repeated patterns of activity, for short periods of time, such that it was possible to tune the wide band system during the repeated conditions in order to track the extent of the frequency excursion. This provided data which indicates that sweepers are extremely wide band phenomena extending well beyond a total excursion of 1.5 mc/s. Figure 9 is a composite of one case investigated. The phenomena which to the observer has an apparent instantaneous wide band $\frac{\delta f}{\delta t}$ characteristic is called a $\beta$ phenomena. Figure 10. It is possible that these phenomena are produced by such sources as ignition systems or in some cases are actually the initial section of sweepers

which was proven to be true when film speed was advanced. Sub-cases for the β phenomena are:

$\beta_1$ isolated event

$\beta_2$ multiple event (over a time interval less than 1 second)

$\beta_3$ repeated or repetitious events

These previous data were from a set of 5 minute samples made 20 Feb 1959 from 18.0 mc/s to 27.25 mc/s. Sweepers were first noted in the 20.5 to 21 mc/s band and thereafter in increasing numbers up to the top of the test spectrum. Such phenomena have been observed at other times down to 3 mc/s and up to 35 mc/s, although the peak of activity has been generally concentrated around 26 mc/s. Results of investigations made on a world-wide basis indicate that the sources of interference are widespread. As many as 4,000 sweepers per hour have been counted. Typical counts and diurnal variations occur as shown in Figure 11. Considering sky wave propagation and the vagaries of the sources, it is almost impossible to draw any positive proof type conclusions about the diurnal variations from these data. Two of the possible explanations are: First, that the variations occur as a result of the vertical lobe pattern of the antenna, which in turn would require the signal to essentially be of solar origin. This has been discounted by other observed phenomena related to the signal structure. Second, that there are many sources spread over the world's industrial centers and that the number observed increase as the F-2 path between the source and the receiving site supports propagation at the observed frequencies.

The higher frequency, i.e., 25 to 26 mc/s predominance of the sweepers indicates that if the second cause is the correct explanation, then the sources in all likelihood have a maximum over-all radiation characteristic, i.e., the combination of r-f source, coupling coefficients and radiation efficiencies favor these higher frequencies. This is not necessarily a valid assumption since the D-layer absorption, path geometry, critical frequency, launch angle and many other factors would

have to be known for a positive assertion on this point. Figure 12 shows a set of data typical of the distribution of sweepers over the 20 to 30 mc/s frequency band.

The most plausible explanation of the source of these sweepers is that they are produced by industrial processes which use large energy r-f inductive or dielectric heating or molding processes which change frequency as the item being processed changes in e.g., shape, dielectric constant, or heat content. This possibility is borne out by the f-m modulation which is found on many, but not all sweeper signals. European data quite naturally gave peaks at 50 cps, U.S. data at 60 cps, and Japanese data a fair amount of both, but mostly 50 cps. A great number of sweepers are f-m modulated with fixed low frequencies (300 cps was limit of observation) other than 50 or 60 cps or with randomly varying low frequencies. D/F bearings from Washington indicated the source to be emanating from about NW; whereas bearings from the San Francisco area indicated the source to be approximately NE. Unfortunately, a co-ordinated D/F program was not made and whether the sweepers were from a common source was not ascertained. Further D/F work is planned using simultaneous recording and D/F bearing data.

The other major characteristic is the sequence of sweepers with almost identical $\frac{\delta f}{\delta t}$. These "sweeper trains" were thoroughly investigated for frequency dispersion. None was found and thus it can be tacitly assumed that each sweeper observed in a train is separately generated. Figure 13 shows the results of the time measurements of a typical sweeper train. Although a deviation of $\pm$ 10% from the mean time was noted for almost all sweeper trains, some trains showed a wider variation, approaching $\pm$ 20%. This was noted mostly where $T_m$ was greater than 10 seconds.

Two major problems arose in the work associated with these studies. One is that wide band noise studies require narrow band ancillaries for a completely instrumented study. The experimental wide band work with its new look at the spectrum was of so much interest in the early phases of this work that the narrow band f-m characteristics

were practically overlooked. The first experiments were narrow band, and f-m modulation was looked for but was not found. Figure 14 is a spectrograph from one of these non-modulated sweepers. It was at the suggestion of Mr. Watts, CRPL, who had observed 60 cps f-m modulation on narrow band spectrograph records, that the further modulation studies and results previously mentioned were made.

The second problem was the discovery of a new signal which appeared to be a multi-valued frequency function with time which showed up in the second system used Figure 2. This signal was nicknamed "wood grain", as you can understand from Figure 15. This phenomena results from wide band $\beta$ type noise sources, however, the peculiar pattern obtains due to the fact that the wide band noise repetition rate is varying at a rate very close to the sweep rate. Due to the wide band characteristic, every time a pulse occurs, a sample is recorded on the output since all frequencies are instantaneously energized. The detected r-f envelope from a narrow band receiver sounds like the typical noises of an automotive ignition system. Calculation of 10 pulses/sweep at a 7 sweep per second rate gives 4,200 pulses per minute. For example, an 8 cylinder car would then be turning a quarter of this rate or 1,050 rpm. It is possible that these signals are of local origin and account for the occasional high density of $\beta$ phenomena, however no positive correlation was found during a limited test period with dense traffic activity. In fact, some of the strongest signals occurred in the early morning hours when the traffic pattern in the vicinity of the Washington test site was at a minimum.

## IV. CONCLUSIONS

There are still a number of unexplained phenomena in the $h_{nf}$ spectrum as seen through the eyes of wide band receiving and display systems. There are still unanswered questions concerning the $\alpha$ type sweepers which are open to further research. Several of these questions follow:

a. What are the actual sources of sweepers, i.e., are they man made or natural phenomena?

b. If natural phenomena, are they terrestrial or extra-terrestrial?

c. If the phenomena is man made, can it be eliminated?

d. What are the error producing effects of sweeper interferences on various types of communications?

e. What error alerting or correcting schemes can be employed? For example, r-f band filters above the desired signal spectrum could be used to develop alerts that interference will occur or to inhibit circuit functions.

REFERENCES

1. Some Notes on Military Communications, J. P. Costas, dated 9/12/60. Not Published.

2. Noise Trains, N. C. Gerson and W. H. Gossard, C.J.P., 37, 1061 (1959).

3. Sweepers, N. C. Gerson and W. H. Gossard, JATP, Vol 17, pgs. 85-88, (1959).

4. Microsecond Sampler Handles 126 Channels, Mark T. Nadir, ELECTRONICS, pgs. 36-39, January 23, 1959.

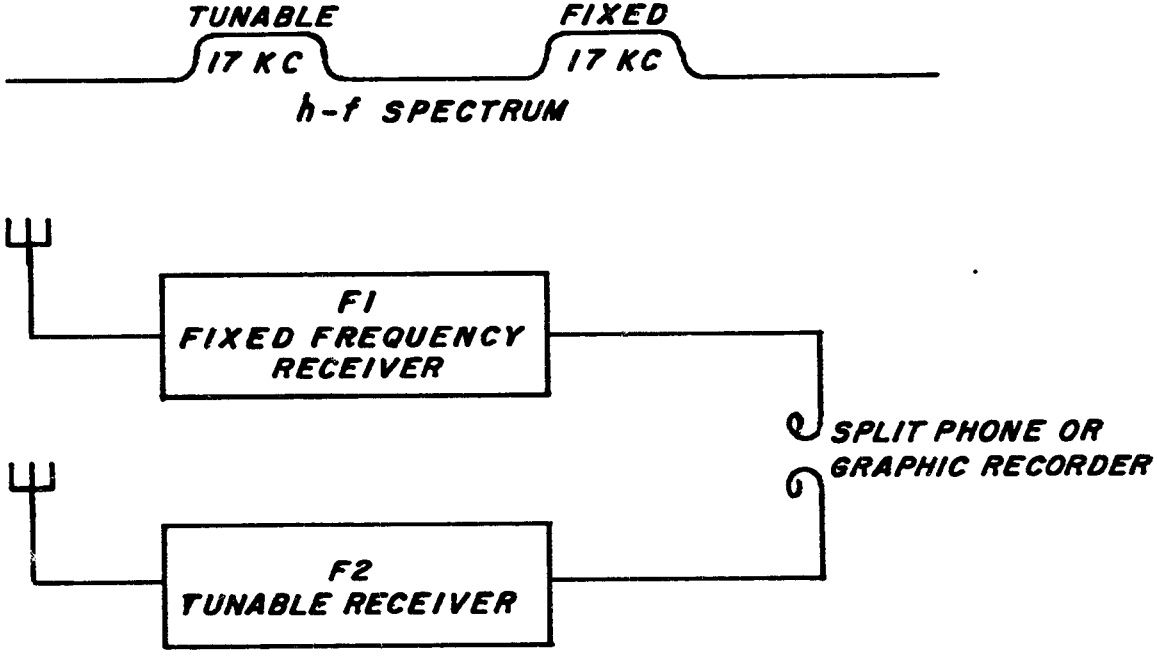



FIGURE 1
SIMPLE WIDEBAND NOISE MONITOR

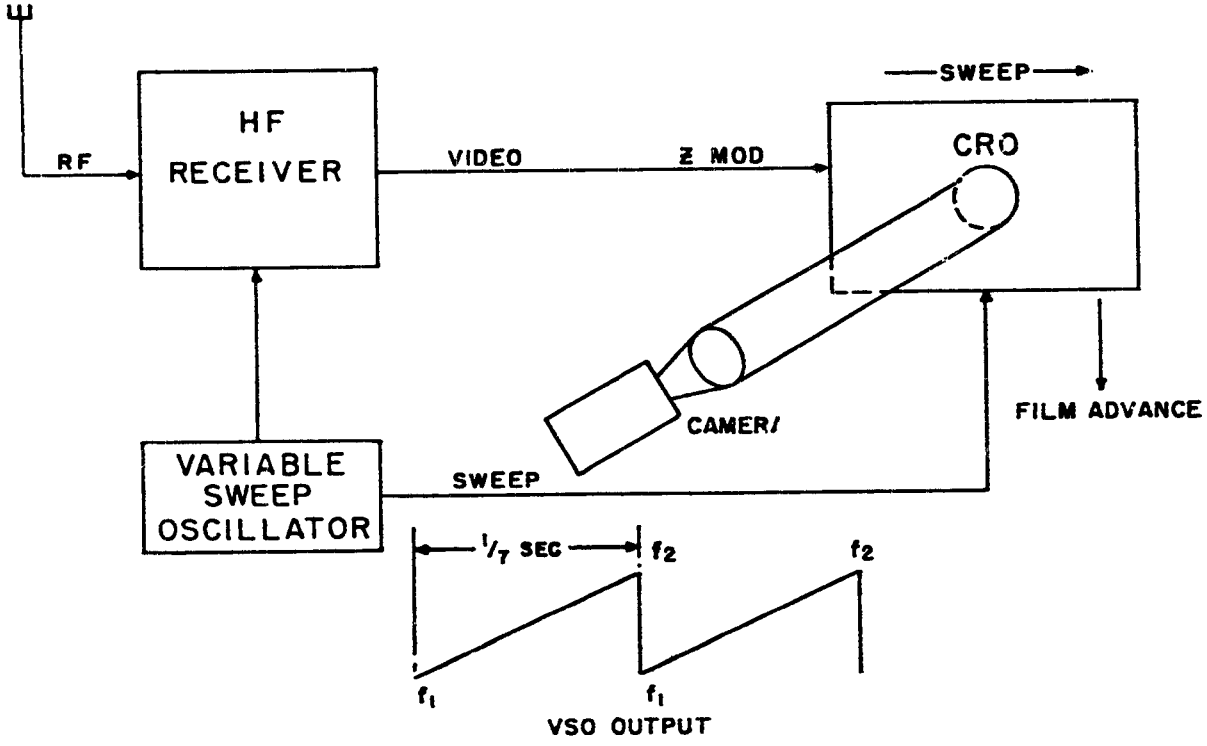



FIGURE 2. SWEPT H.F. RECEIVER FOR SWEEPER STUDIES.

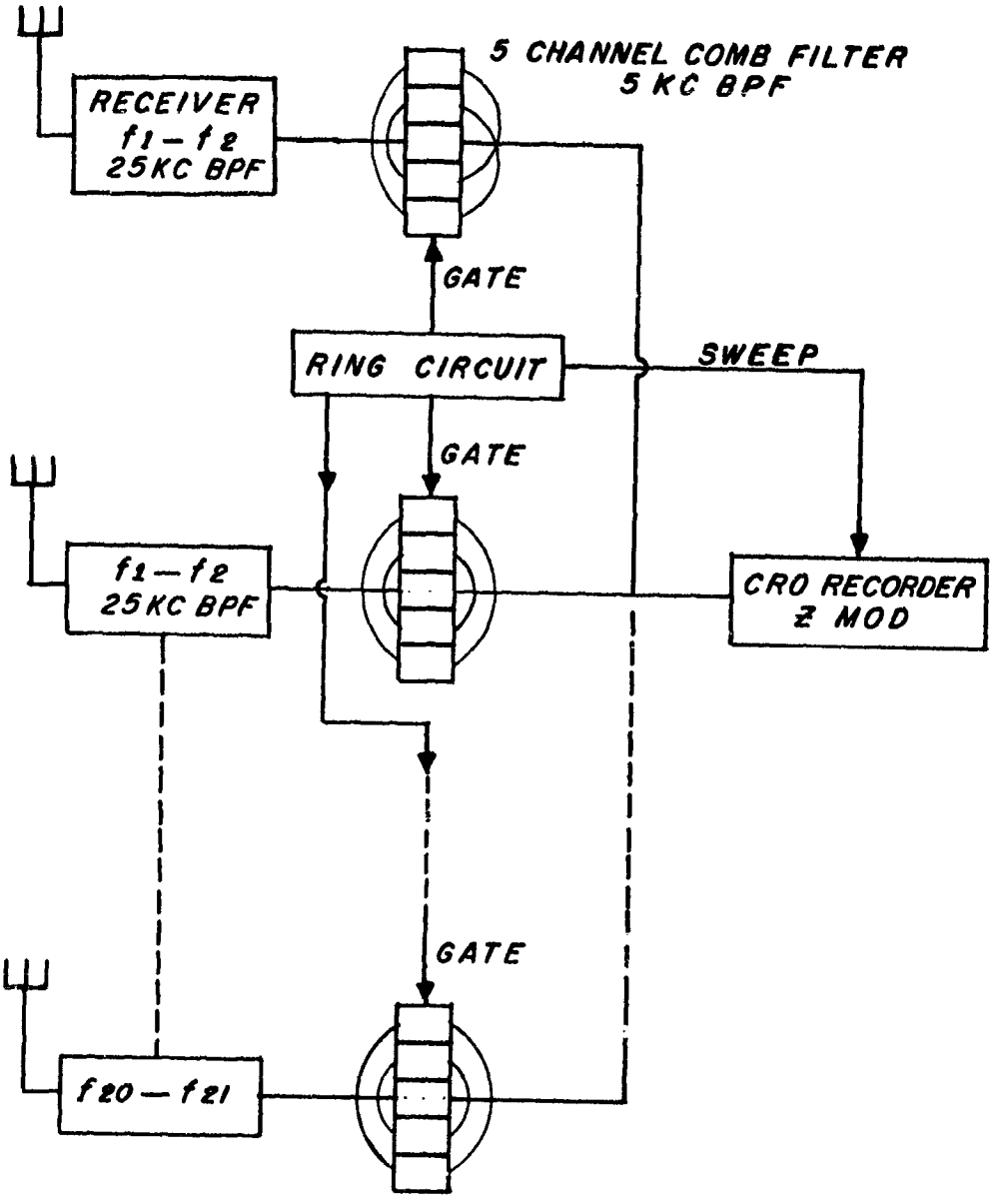
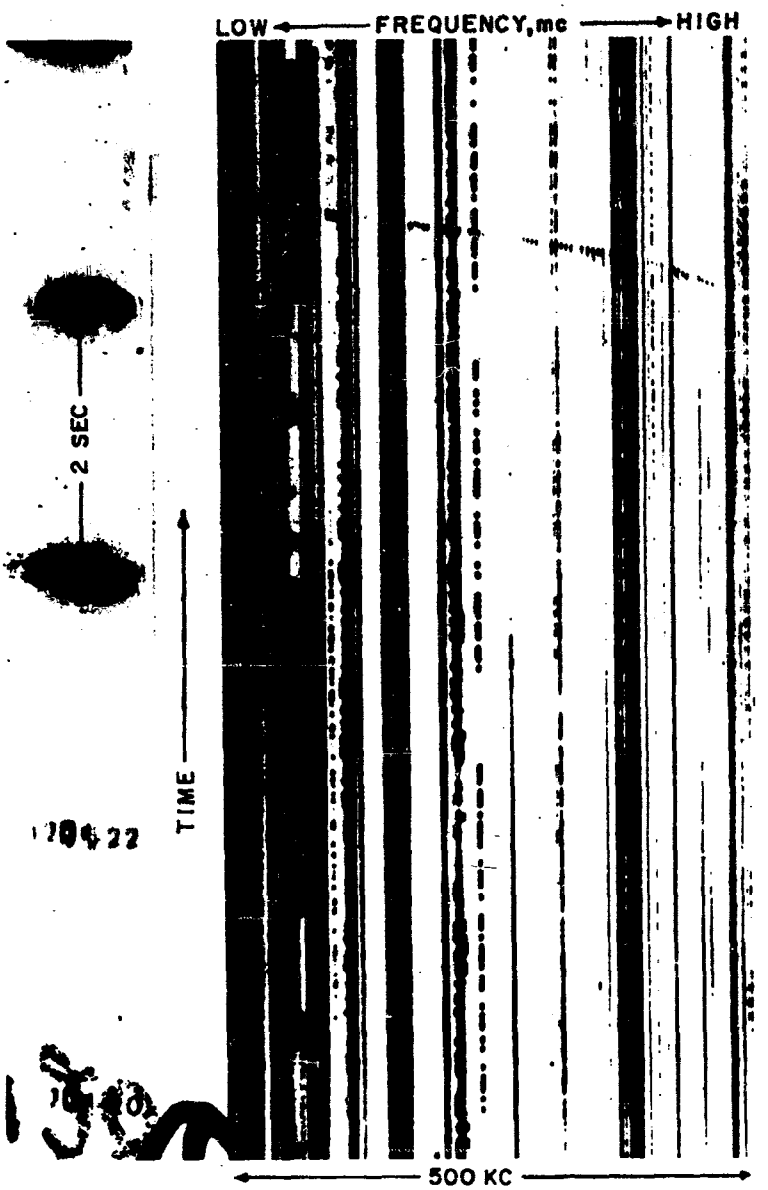
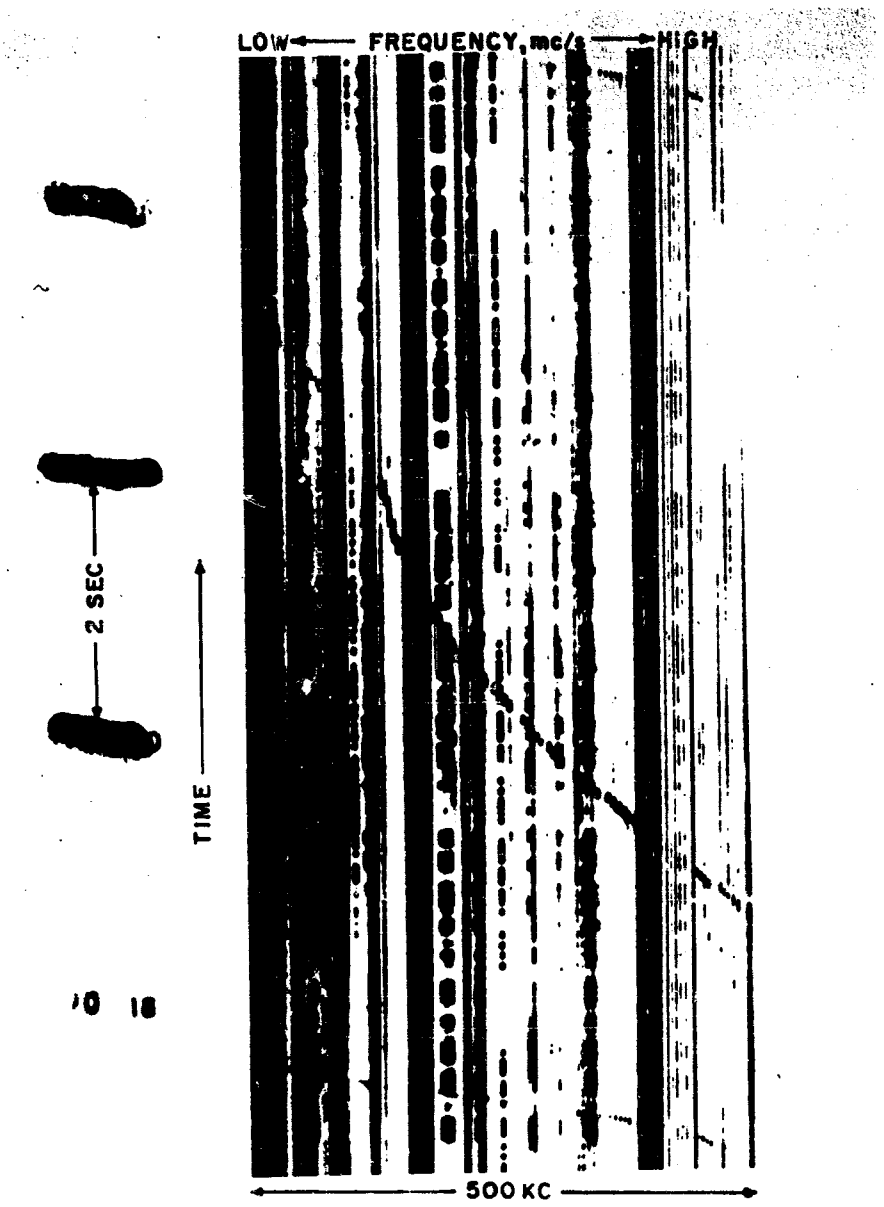



FIGURE 3
500 KC BANDWIDTH RECEIVER-RECORDER SYSTEM

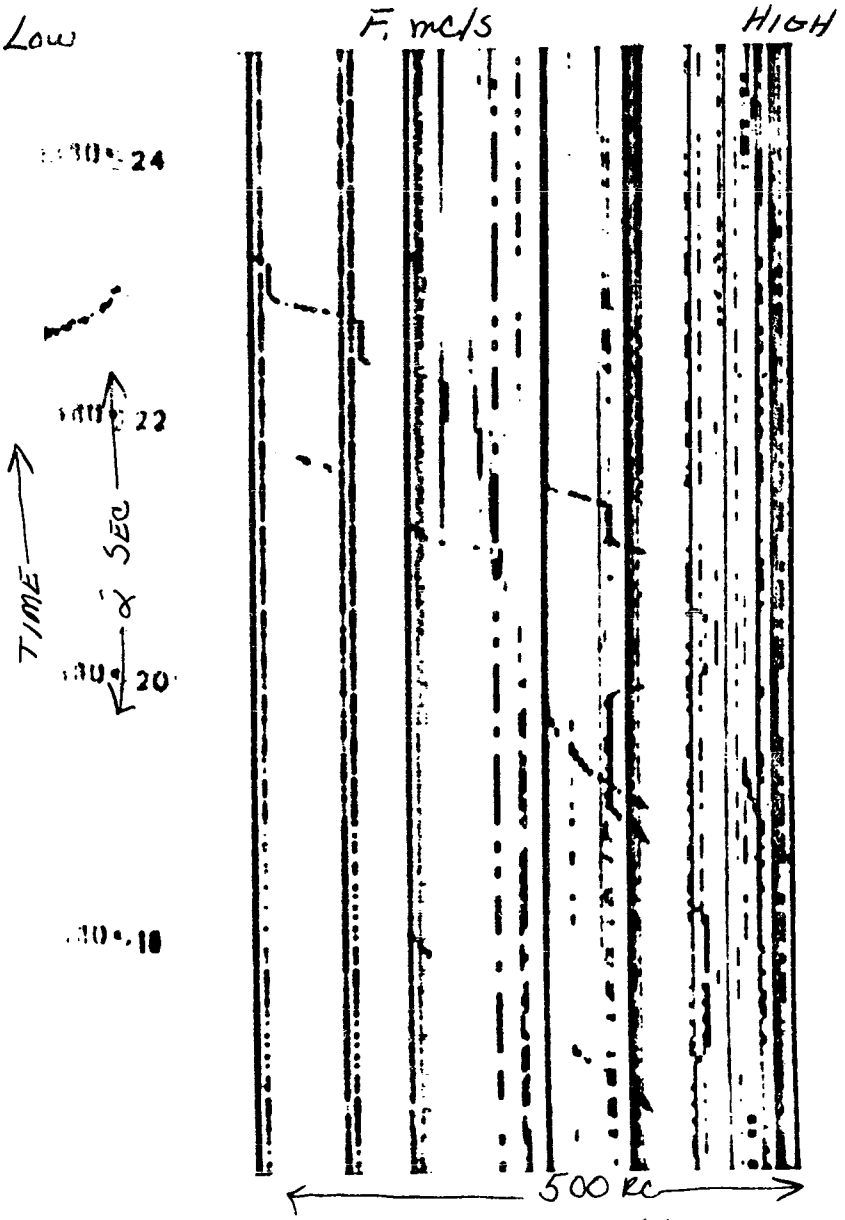



$\alpha / \frac{\delta f}{\delta t}$ SWEEPER – APPROXIMATELY LINEAR

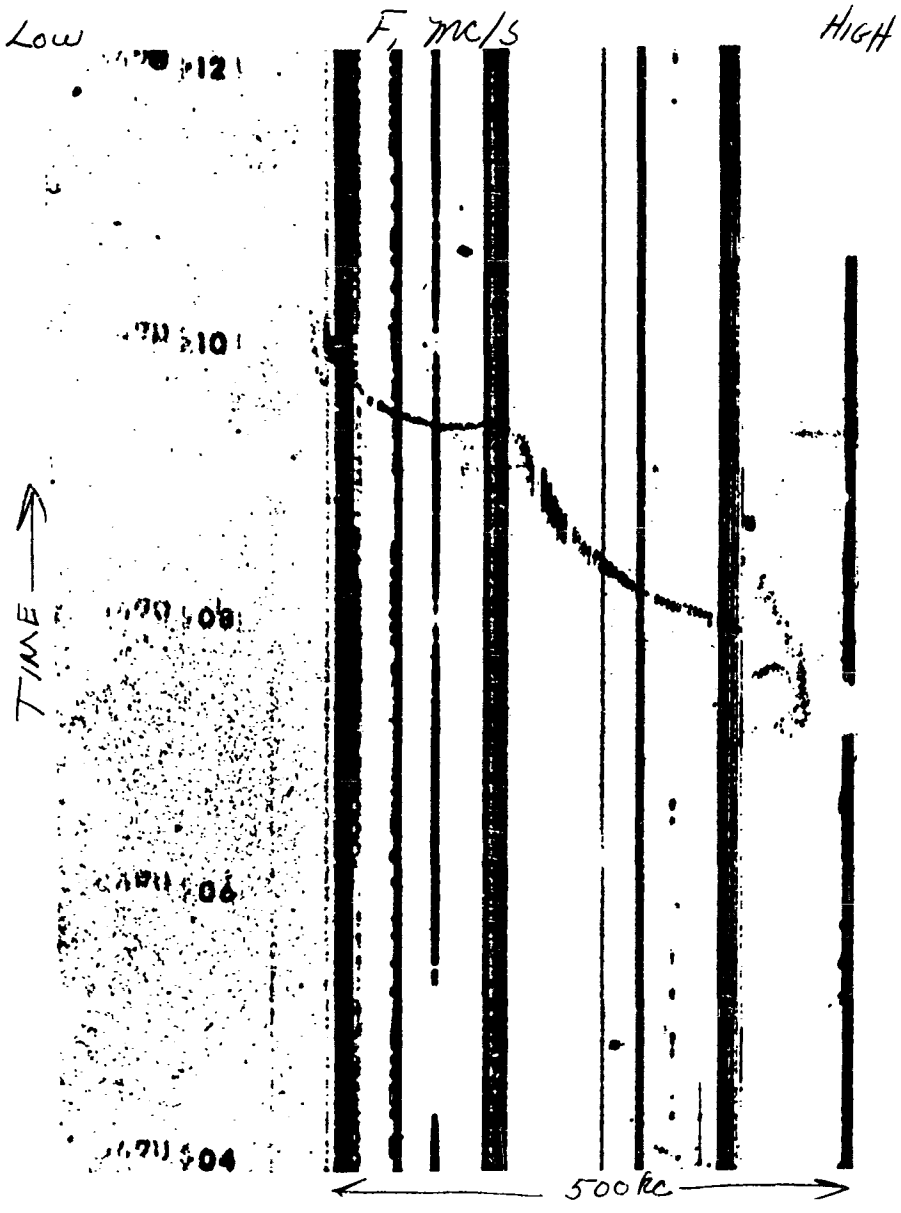
FIGURE 4



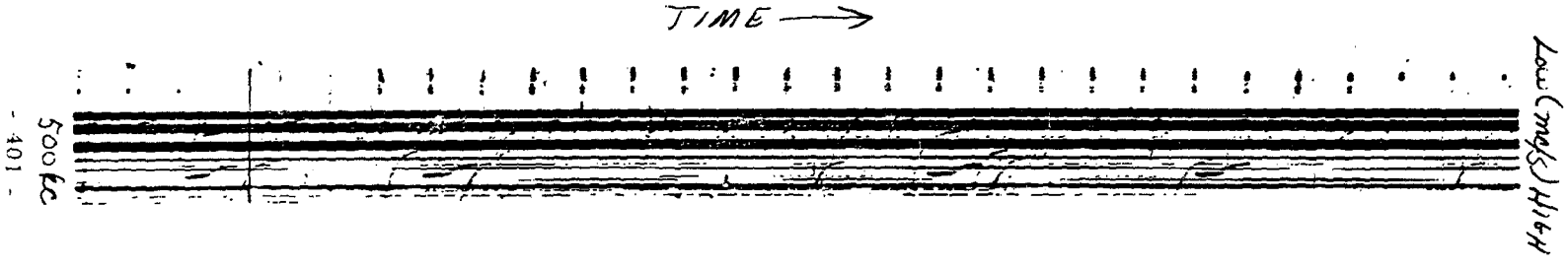

$\mathcal{L}_2$ SWEEPER – APPROXIMATELY EXPONENTIAL
FIGURE 5




$\alpha_5$ APPARENTLY RANDOMLY VARYING $\frac{\delta f}{\delta t}$
FIGURE 6




$\alpha$+ SWEEPER – DISCONTINUOUS $\frac{\delta f}{\delta t}$
FIGURE 7




SWEEPER, DISTURBED CONDITION
FIGURE 8

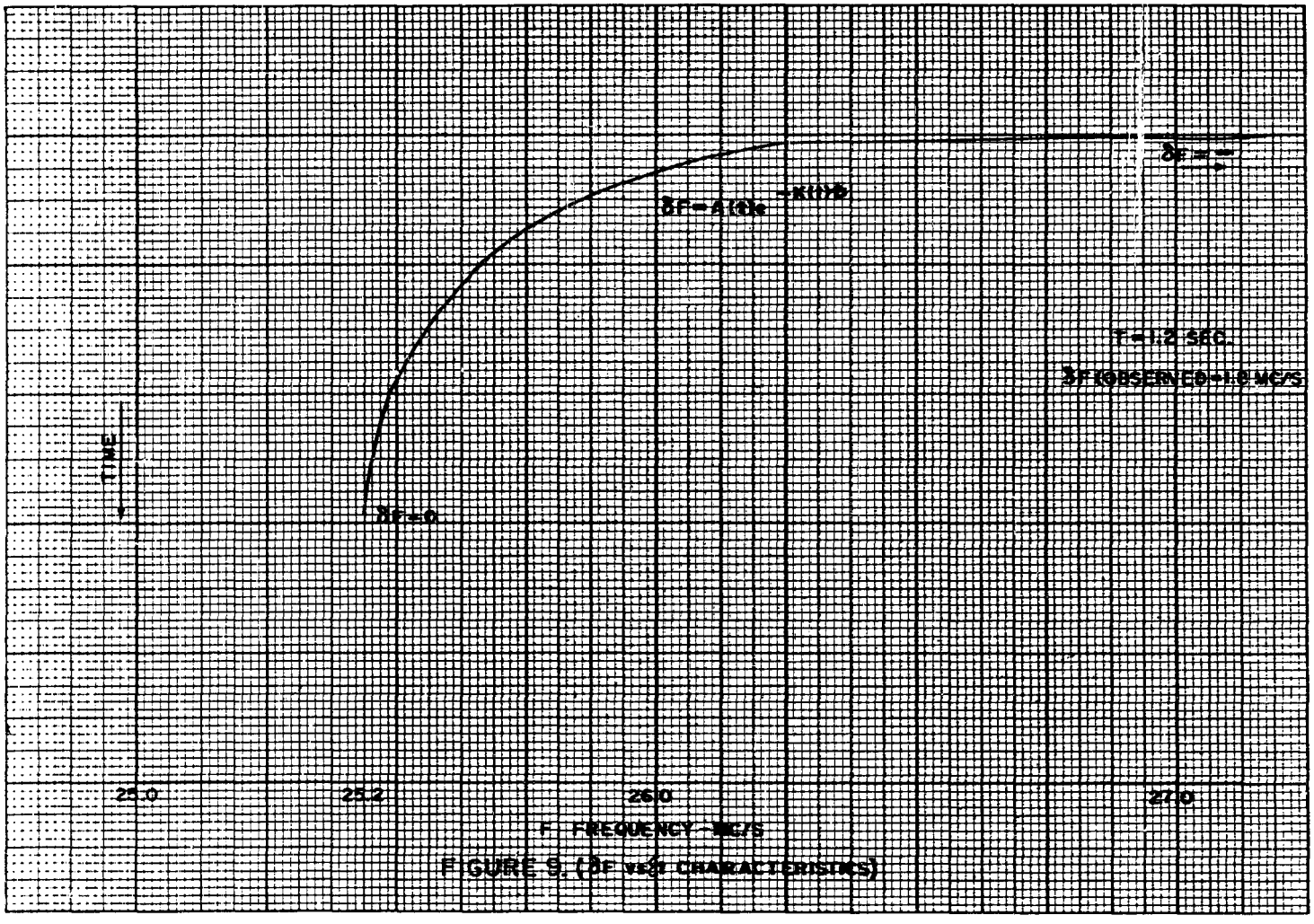
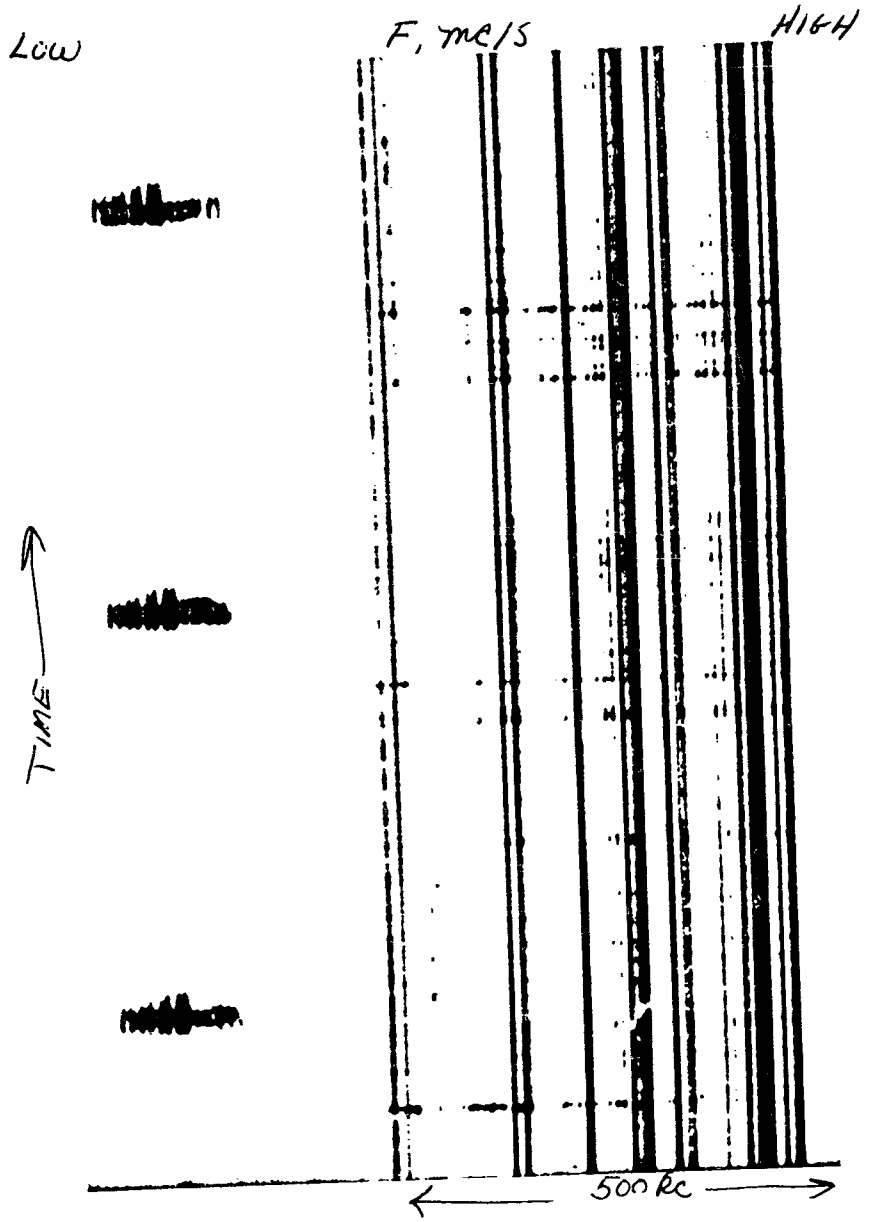
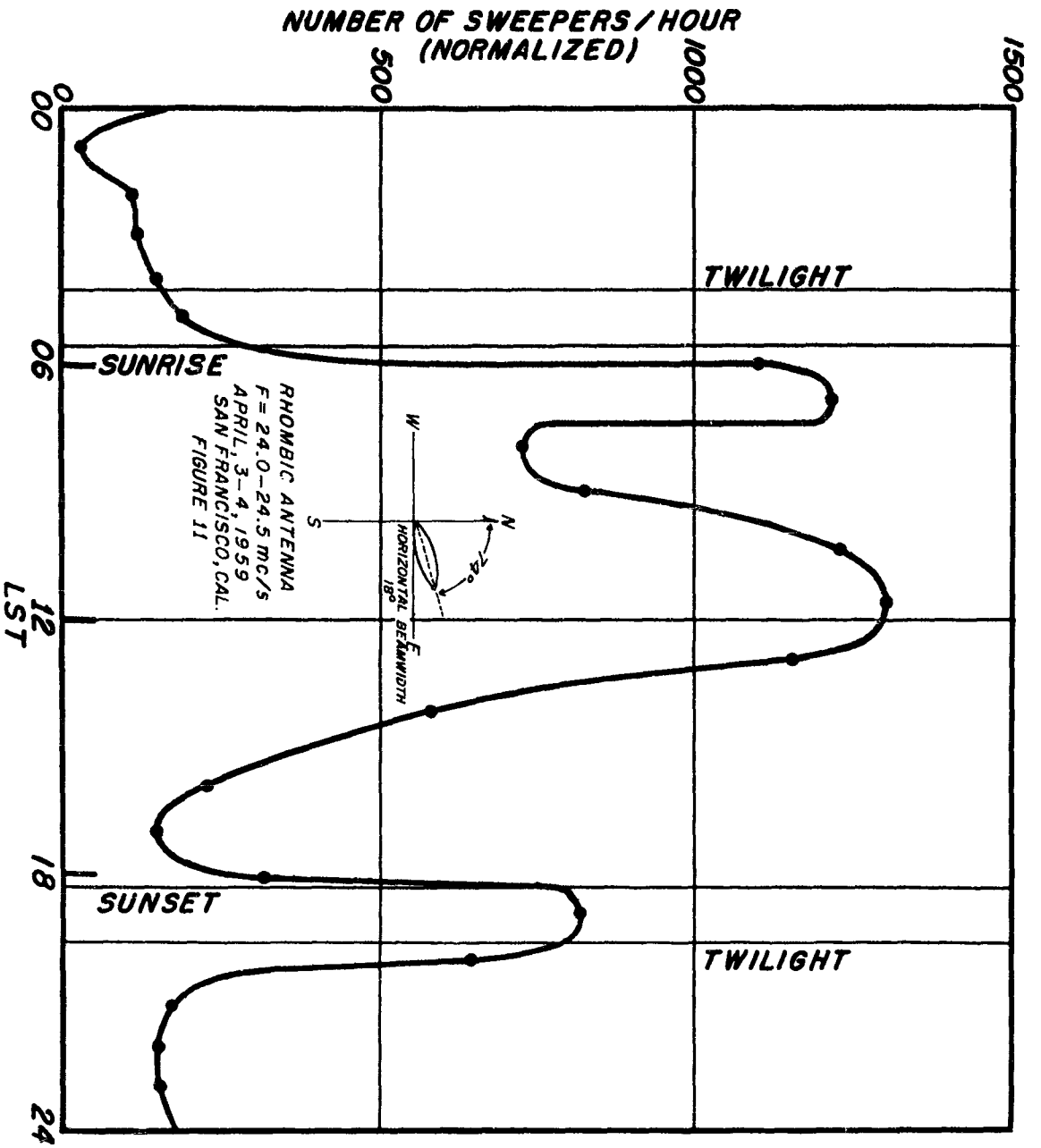
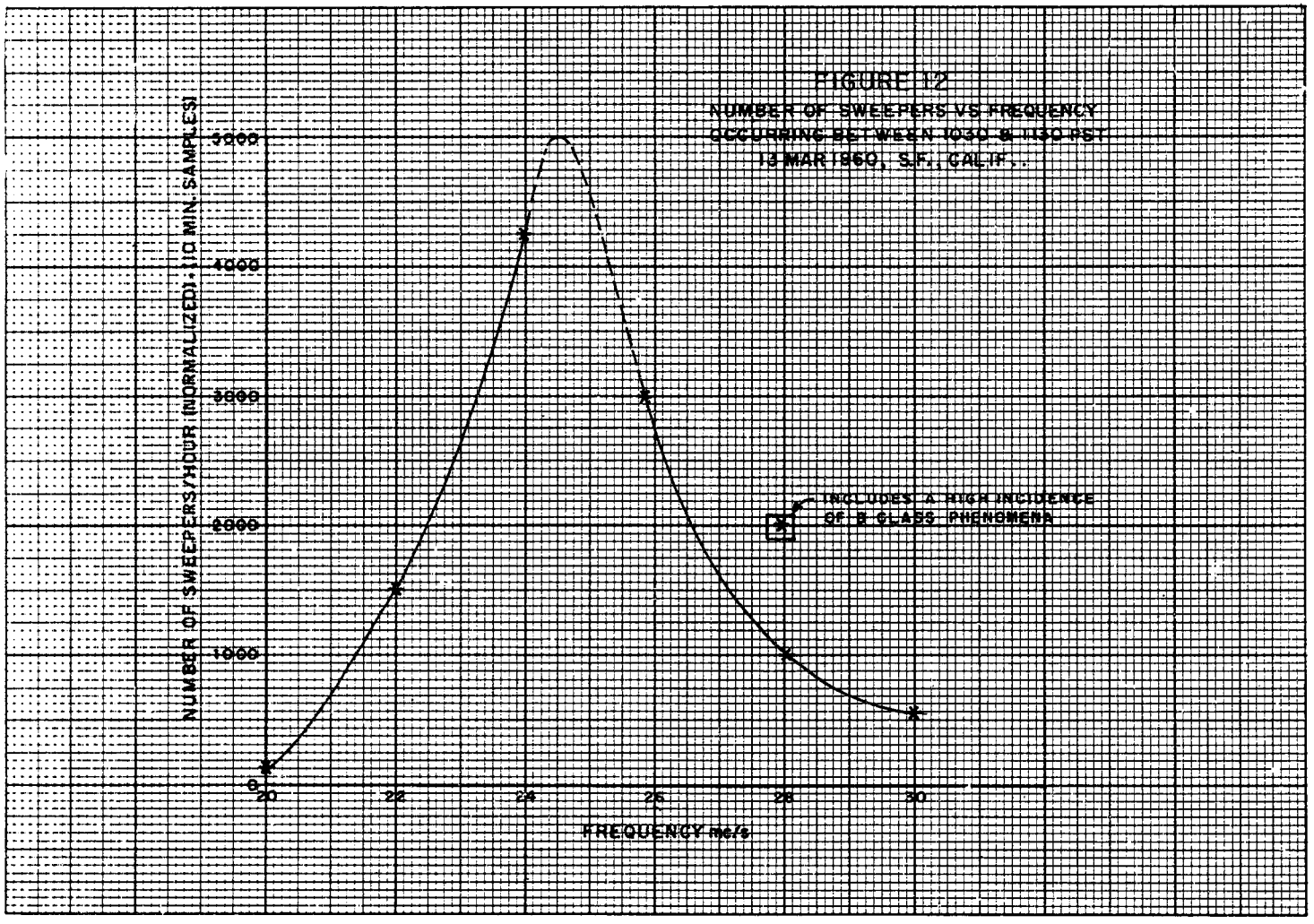



FIGURE 9. (δF vs θ CHARACTERISTICS)




B PHENOMENA
FIGURE 10


NUMBER OF SWEEPERS / HOUR
(NORMALIZED)
0
500
1000
1500
00
06
12
LST
18
24
TWILIGHT
SUNRISE
SUNSET
TWILIGHT
RHOMBIC ANTENNA
F = 24.0 - 24.5 MC/S
APRIL 3 - 4, 1959
SAN FRANCISCO, CAL.
FIGURE 11
W
S
N
HORIZONTAL BEAMWIDTH
18°


FIGURE 12
NUMBER OF SWEEPERS VS FREQUENCY
OCCURRING BETWEEN 1030 & 1150 PST
13 MAR 1960, S.F., CALIF.,
NUMBER OF SWEEPERS/HOUR (NORMALIZED) (10 MIN. SAMPLES)
5000
4000
3000
2000
1000
0
20
22
24
26
28
30
FREQUENCY mc/s
INCLUDES A HIGH INCIDENCE
OF B CLASS PHENOMENA

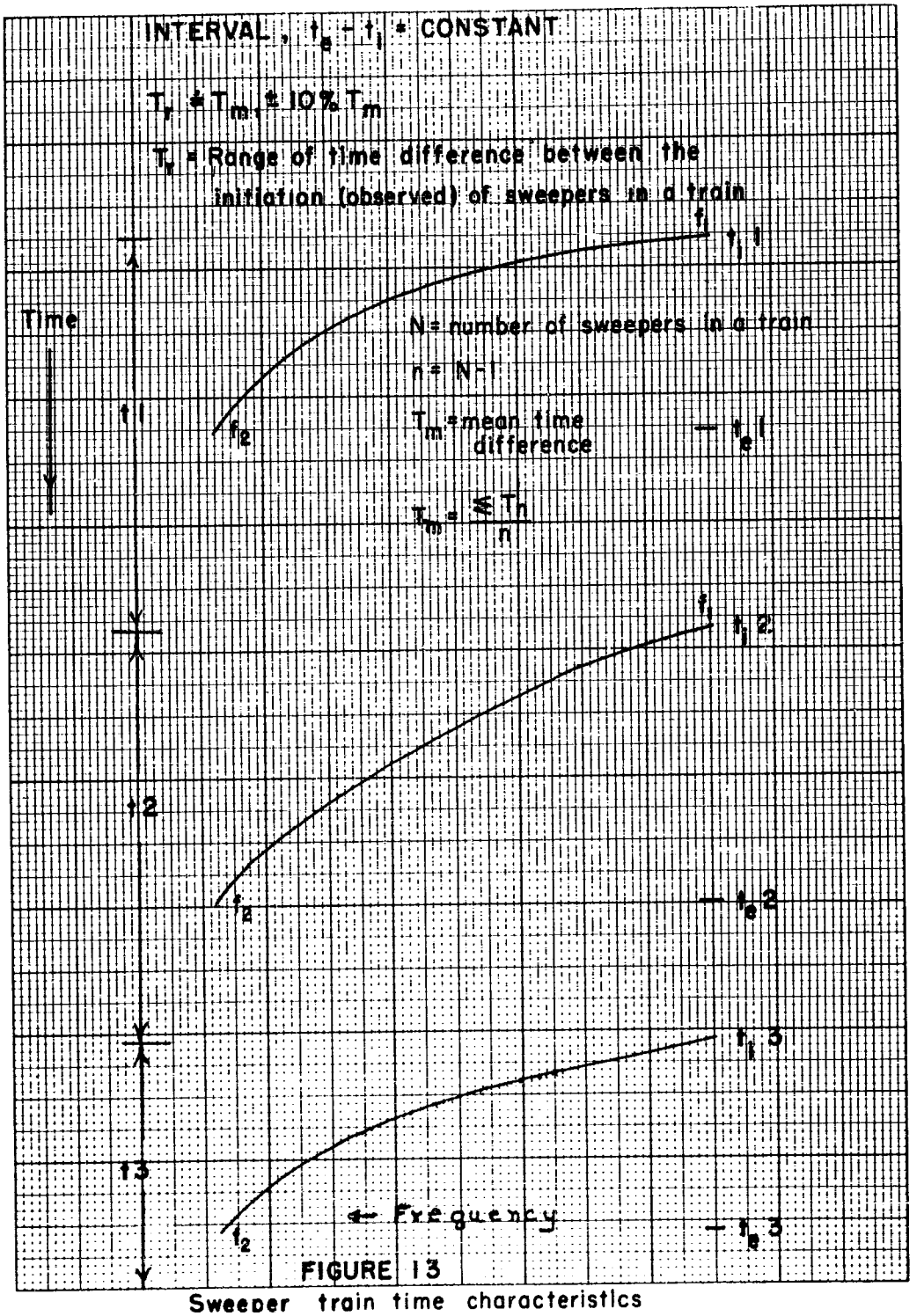



FIGURE 13

Sweeper train time characteristics

1/11/60

26.5 mc/s

2:30 LST., W.DC

narrow

$\delta F \simeq$ 80 kc/sec.

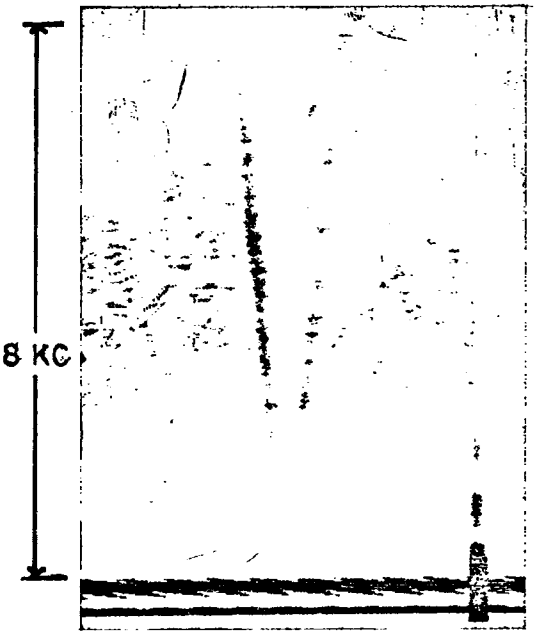



FIGURE 14. UNMODULATED SWEEPER SPECTROGRAPH



SWEEP RATE : 7 SWEEP/SEC
FILM ADVANCE: 22 ipm
BW : 200 kc
CENTER FREQ: 24 mc/s

WOOD GRAIN
FIGURE 15

# NEW METHOD OF INSERTION LOSS MEASUREMENT OF R. F. FILTERS UNDER RATED LOAD CONDITIONS BETWEEN 14 KC TO 1000 MC, AND HIGHER

J. C. Klouda
Elite Electronic Engineering Company
Radio Interference Consultants
Chicago, Illinois

Abstract. - A different approach to measuring the insertion loss of R.F. filters under rated load other than that used in MIL-STD-220A. This method is especially adaptable for use in both the design laboratory and production line testing. Tests on filters can be made with rated D.C. or A.C. current flowing in them. The frequency range through which the insertion loss can be measured is 14 KC to 1000 MC. Frequencies above 1000 MC are being investigated, and from the results of present tests, the range may be extended to 10,000 MC. Results of tests made on various types of filters through different frequency ranges are also included. This includes tests made on ferrites, powdered iron, and moly-perm materials. Comparison test results between MIL-STD-220 are shown, with the possibility of using this procedure as an alternate method of insertion loss measurements under both no load and rated load conditions.

## I. INTRODUCTION

In determining the insertion loss of an R.F. line filter, the effect of rated line current on the insertion loss is normally desired. This rated line current can be D.C. or A.C. at some power frequency such as 60 cycles, or 400 cycles. Depending upon the application of the R.F. filter, it may be desired to know what effect the line current has between the frequency range of 14 KC to 1000 MC, or higher. Considerable deviation of insertion loss from no load to full load may be had if saturation in one form or another occurs in any of the filter elements. Studies and analysis of R.F. filters with varied amounts of line current flowing through them are highly desirable in both designing the filter and from the quality control standpoint. This method used in determining the insertion loss characteristics of the R.F. filter under varying load currents extends the frequency range through which insertion loss measurements may be made. In turn, it gives a much needed tool to both the design engineer and quality control specialist. Several problems encountered in coupling the R.F. energy into the filter circuit over the broad frequency range is discussed. The amount of line current can be continuously varied from zero to 100 amperes or more, depending upon the availability of the power source.

## II. DESIGN OF EQUIPMENT

The basic equipment design consists of provisions for an incoming R.F. signal from the signal generator or transmitter, and an output to be connected to a receiver with a calibrated attenuator. The intermediate portion of the circuit is coupled to both the signal generator and the receiver circuits. Included with the intermediate circuit is provisions for in-

jecting the D.C. or A.C. current at low voltage. A variac regulates a transformer whose secondary is connected into the intermediate circuit. The voltage required on the secondary is normally only that required to overcome the voltage drop of the filter and provide the necessary rated current. The circuit as described in Figure 1 gives good response between the frequency range of 50 MC to 1000 MC. For frequencies between 14 KC and 50 MC, a variation in the coupling networks between the signal generator and the intermediate circuit and the intermediate circuit of the receiver are required. Most of the initial tests with this equipment was done in the current areas of 30 amperes or less. They were also primarily conducted at the power frequency of 60 cycles. Insertion loss readings, with the test setup were made on the basis with and without filter inserted. When a transmitter or high power signal generator was used, extreme caution must be used to shield the transmitter from the receiver. A shielded enclosure or shielded cube provided excellent shielding, and isolated the transmitter effectively from the sensitive calibrated receiver.

## III. MEASUREMENTS ON FERRITES IN 400 MC to 1000 MC FREQUENCY RANGE

To determine the effect of line current on insertion loss measurements of wires covered with ferrite beads and ferrite sleeving, the frequency range of 400 MC to 1000 MC was selected. It is in this range where these ferrite materials are normally used on filament leads, [illegible] leads, and other control leads emanating from a given piece of equipment. The idea of the ferrite beads or sleeves is to eliminate the high frequency interference that may be present on these leads. Some filament leads may carry currents as high as 20 or 30 amperes. One type of ferrite was tested, as an example, over the frequency range of 400 MC to 1000 MC. The ferrite was housed in a completely shielded coaxial device with type N connectors on the input and output. The reason for this was to eliminate, as much as possible, any variations which may be due to the R.F. signal leaking around the ferrite itself. At a frequency of 500 MC, with no load current flowing, it was found that the insertion loss, due to the ferrite material, was 35.6DB. As the current was increased in two ampere steps, the effective insertion loss of the ferrite element decreased. At 14 amperes the insertion loss had dropped to a value of 20.5 DB. At 600 MC the insertion loss at no load was 45 DB. At a 15 ampere load it had dropped to 2[illegible] DB. Similarly at 1000 MC the no load insertion loss figure was 56 DB, while at a current of 15 amperes the insertion loss had again dropped, this time to 40 DB. Figures 2 and 3 show the effective drop in insertion loss in the filter between no load and 15 amperes. Tests were then performed on other types of ferrites with a smaller insertion loss being measured with current flowing.

Results of Insertion Loss Tests on Ferrite Sleeve
with Various Line Current Flowing

| Frequency | No Load | 5 Amp. | 10 Amp. | 15 Amp. |
|---|---|---|---|---|
| 500 MC | 35.6 DB | 30.5 DB | 23.8 DB | 19 DB |
| 600 MC | 45.0 DB | 37.0 DB | 30.0 DB | 26 DB |
| 800 MC | 50.0 DB | 44.0 DB | 37.0 DB | 32 DB |
| 1000 MC | 56.0 DB | 50.0 DB | 44.0 DB | 40 DB |

Results of Insertion Loss vs. Load Current
at a Frequency of 500 MC on Ferrite Sleeve

| 60 cps. Current | Insertion Loss |
|---|---|
| 0 Amperes | 35.6 DB |
| 2 amperes | 34.8 DB |
| 4 amperes | 32.0 DB |
| 6 amperes | 29.0 DB |
| 8 amperes | 26.0 DB |
| 10 amperes | 23.8 DB |
| 12 amperes | 22.0 DB |
| 14 amperes | 20.5 DB |

## IV. EFFECT OF CURRENT FLOWING IN PIE SECTION FILTER WITH FERRITE ROD INDUCTOR

A miniaturized pi-filter with a ferrite rod inductor was checked between the frequency range of 150 KC to 1 MC. Check points were made at 150 KC, 300 KC, and 1 MC. Under no load conditions the insertion loss was 77 DB, 65 DB, and 84 DB respectively. As the current was increased the attenuation dropped until at 5 amperes the insertion loss at 150 KC was 58 DB, at 300 KC, 49 DB, and at 1 MC, 67 DB. Figure 4 shows the curve of this test filter at no load, 1 ampere, 2 amperes, 3 amperes, 4 amperes, and 5 amperes. It can be seen that the insertion loss of the filter network becomes progressively poorer as the current is increased. From the results of these tests it can be seen that if the insertion loss of the filter is required to remain constant over a given current range, this equipment is a very useful tool in making checks on various designs of inductance coils. A small test fixture could be setup and various inductance coils plugged in to determine which one will satisfactorily meet the requirements of the particular suppression requirement. Should other inductances be used to substitute for the original inductance, a check on its saturation characteristics can be readily made to determine its acceptibility. In this manner the final product will not have deteriorated due to a substitution of a supposedly replaceable item.

## V. MEASUREMENTS FROM 14 KC to 250 KC

In determining the insertion loss of filters in the

frequency range of 14 KC to 250 KC, a change in the coupling between the signal generator and intermediate circuits was required. Another change in the coupling network of the intermediate circuit to the receiver was also in order. This change in coupling was necessitated to induce a sufficient amount of R.F. signal into the intermediate filter test circuit. The equipment was setup using powdered iron cores and molybdenum permalloy powder cores to determine the effect of various amounts of A.C. line current. Figure 5 is the curve showing the effect of various amounts of line current on a pi-section filter using powdered iron and molybdenum permalloy cores. It is readily seen that this equipment is a valuable tool in determining the proper design of inductance coils to be used in R.F. line filters at a given current rating.

Results of Insertion Loss Tests
on π Filter Using Powdered Iron Toroid

| Frequency | No Load | 15 Amp. |
|---|---|---|
| 14 KC | 20 DB | 15 DB |
| 40 KC | 32 DB | 27 DB |
| 80 KC | 41 DB | 37 DB |
| 100 KC | 49 DB | 45 DB |
| 150 KC | 60 DB | 56 DB |
| 250 KC | 68 DB | 64 DB |

## VI. CONSIDERATIONS TO BE MADE IN DESIGNING INDUCTOR COILS

Once a given amount of inductance is found to be required for a given filter application, an inductor must now be designed that will meet all of the inductance requirements from no load to full load. Most core manufacturers give B-H curves on the various core material that they have available. By using these curves and the physical dimensions of the core, an approximation can be made of the number of turns for a given inductance at a given current for which the core will not saturate, or have only a small percentage of saturation. A handy formula for this determination is as follows: $H=\frac{.4\pi NI}{L}$ Where H is in oersteds, L is magnetic path in centimeters, N is number of turns, and I is in amperes. Since the formula is an approximation, a certain amount of error is present. To varify your design figures a sample coil can be wound and tested at any given current rating you so desire. A check of the test coil can save many hours in redesigning a filter which does not meet the attenuation requirements of a given job, because of saturation.

## VII. COMPARISON WITH INSERTION LOSS MEASUREMENTS MADE AT NO LOAD IN ACCORDANCE WITH MIL-STD-220

A series of tests were made on a ferrite sleeve filter using the methods put forth by MIL-STD-220 under no load

conditions. This same filter was then tested under no load using the method described in this paper to again determine the insertion loss at no load. The results were found to be very comparable. Some discrepancies were noted. Further investigation is being made at this time to determine the nature of these discrepancies so that this method of measuring insertion loss may become an alternate method to both MIL-STD-220, and MIL-STD-220A. In this way only one test setup would be required for determining the insertion loss of filters under no load or rated load. R.F. line filters could more easily be tested in a practical installation such as a shielded enclosure by using this method of insertion loss measurement. Not only would the filters be checked out for saturation, but also for proper mounting and R.F. isolation. Figure 5 shows the test results comparing the insertion loss of a given filter using the MIL-STD-220 techniques and the proposed techniques as described in this paper.

## VIII. CONCLUSIONS

One of the main advantages of this equipment to measure insertion loss of R.F. line filters at rated current is the wide frequency range through which these measurements can be made. It gives the design engineer an additional tool for both high and low frequency insertion loss tests at rated current which before were impractical. In the area of ferrites it can give much needed information as to the characteristics of different ferrite materials when subjected to high density magnetic fields of low power frequencies. Further investigations are being made at this time to determine how high in frequency insertion loss measurements can be made at various R.F. filters with rated line current flowing through them. It is believed that with certain modifications it can be extended to 10,000 MC.

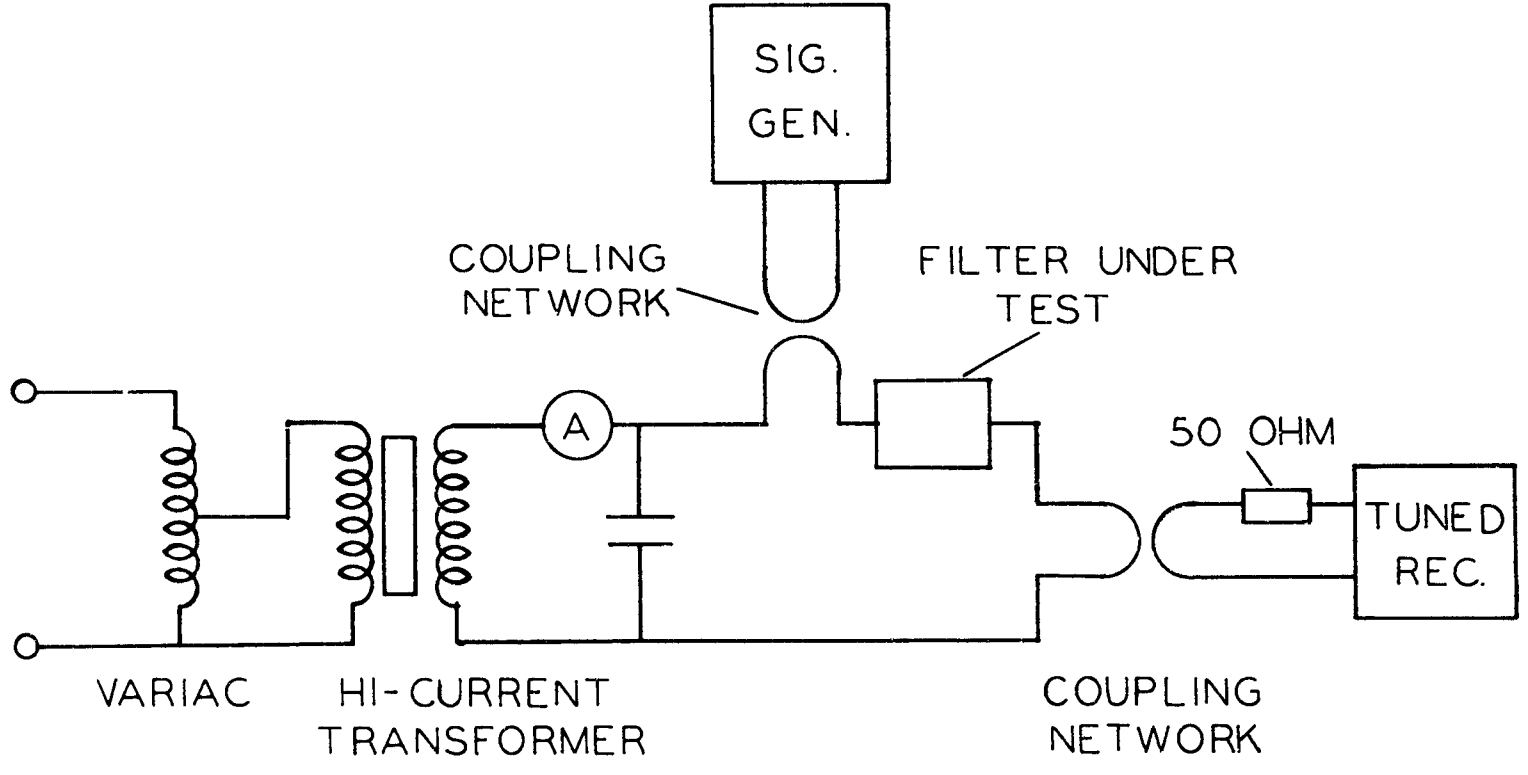



FIG. 1 BASIC CIRCUIT CONFIGURATION FOR INSERTION LOSS TESTS

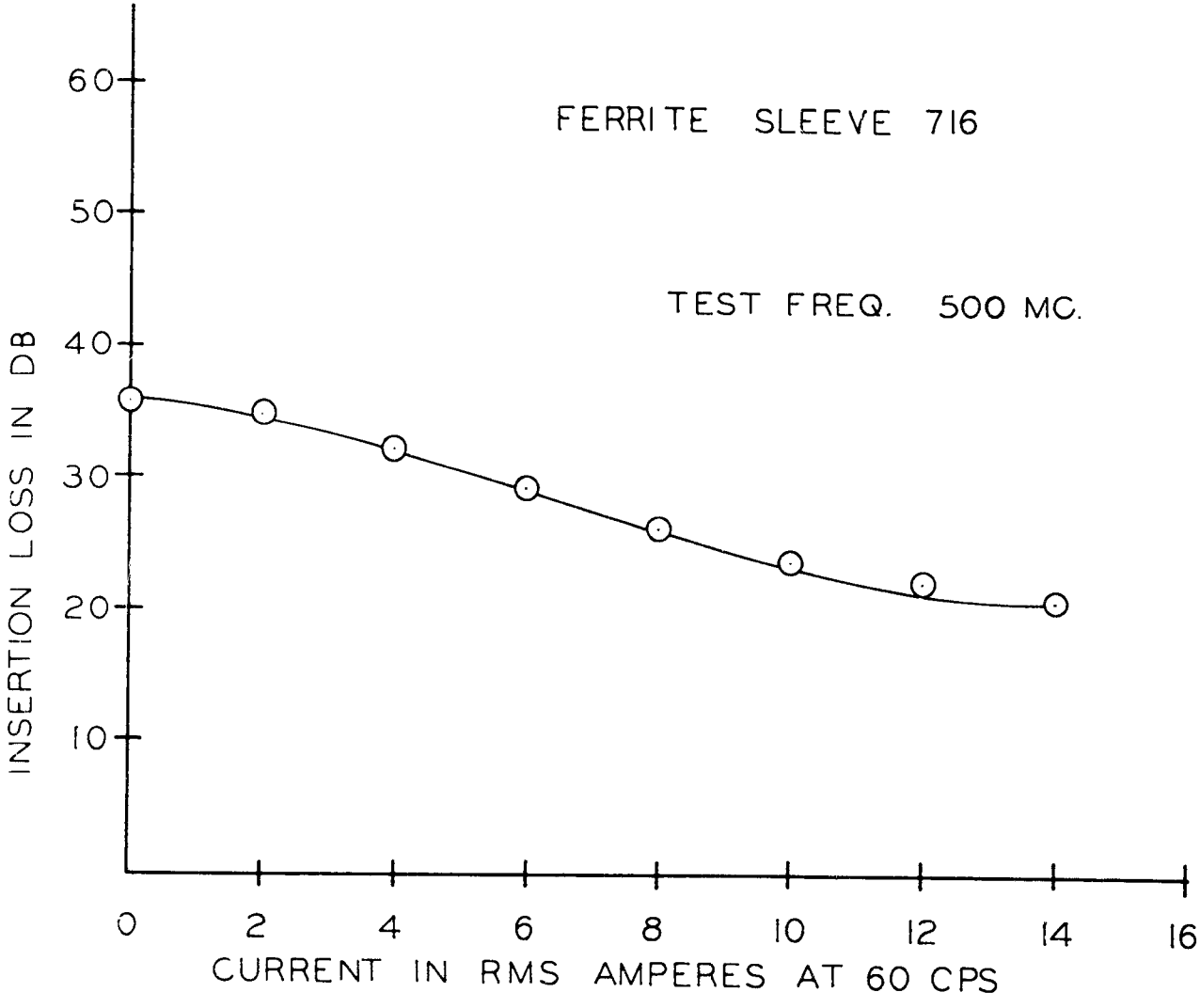



FIG. 2 INSERTION LOSS VS. LOAD CURRENT

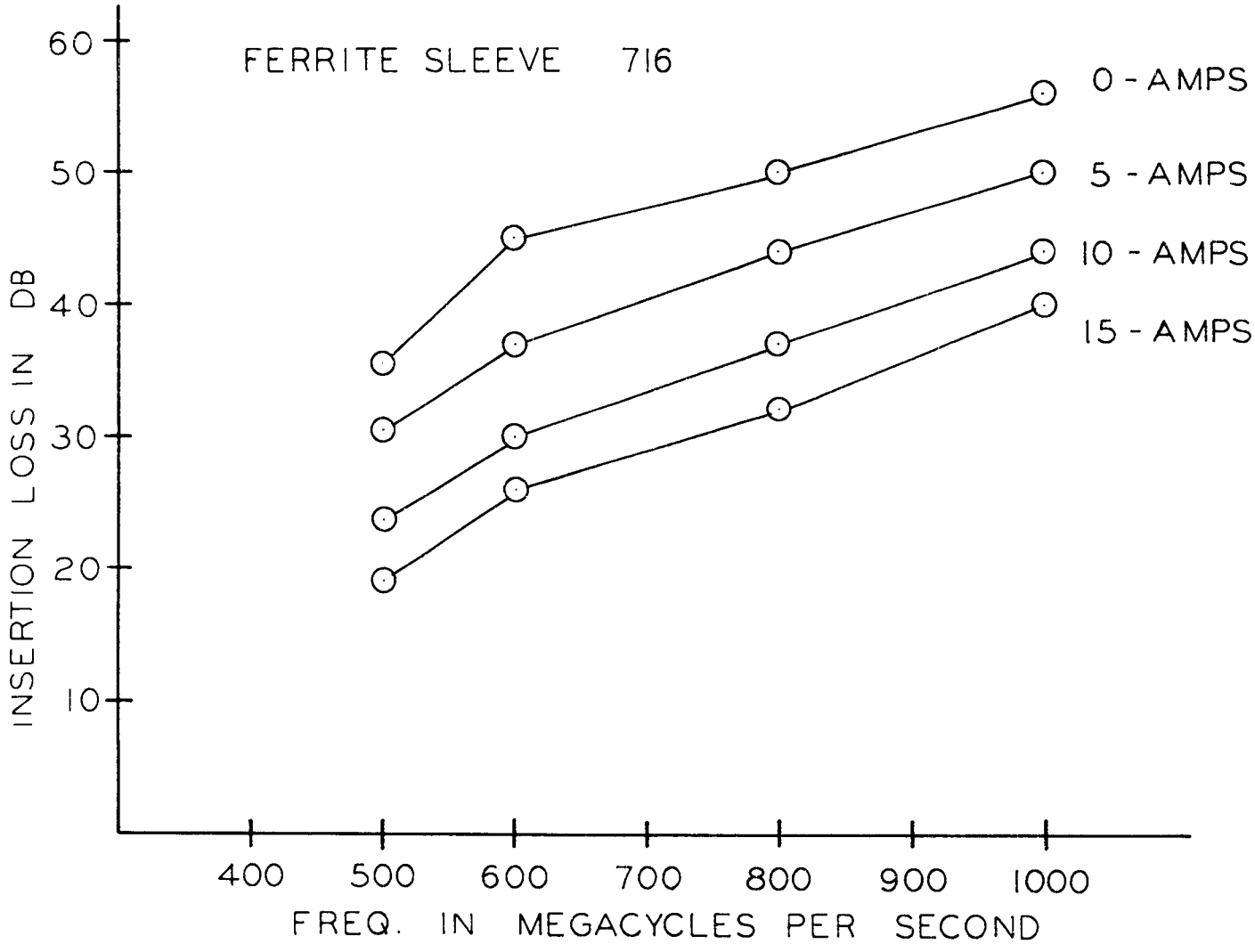



FIG. 3 INSERTION LOSS VS. FREQ. AT VARIOUS LOADS.

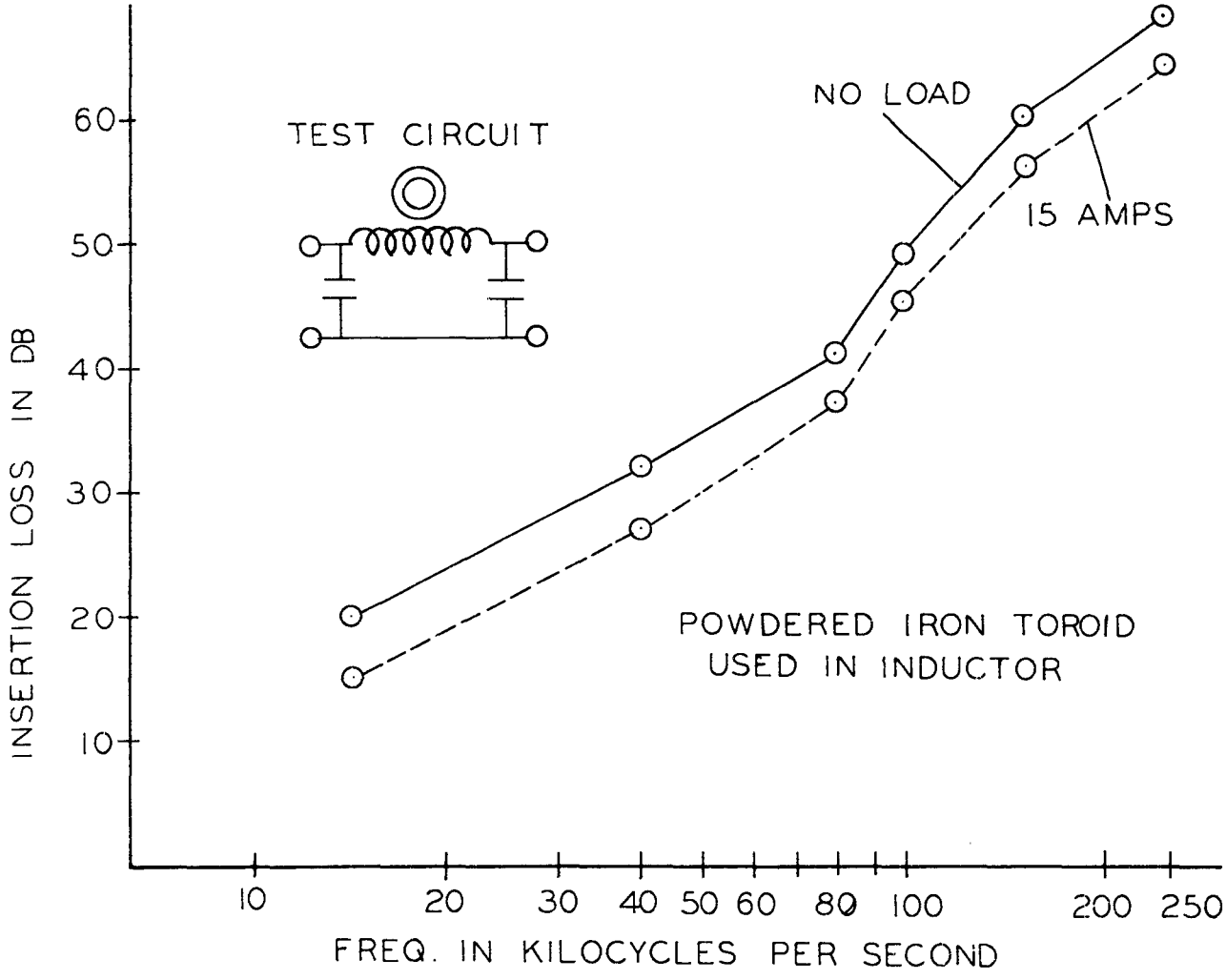



FIG. 4 INSERTION LOSS VS FREQ. FOR TOROID

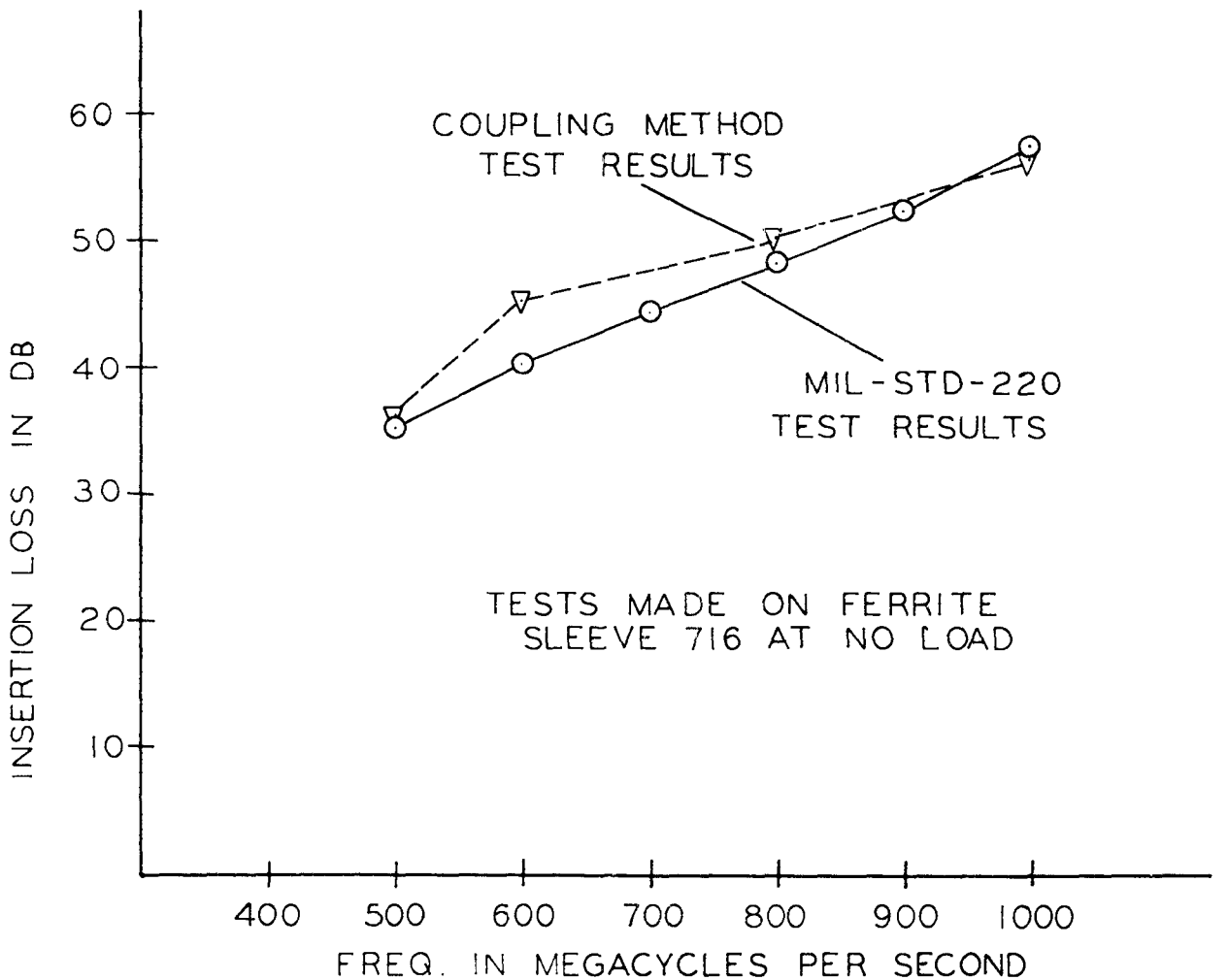



FIG. 5 INSERTION LOSS VS. FREQ. COMPARISON TESTS

# SPURIOUS FREQUENCY MEASUREMENTS IN TRANSMISSION LINES -- A COMPARATIVE REVIEW OF AVAILABLE TECHNIQUES

W. A. Edson and V. G. Price
Electromagnetic Technology Corporation
Palo Alto, California

Abstract. - Several methods for measurement of spurious signal levels in microwave transmission lines have been developed in recent years in response to a growing need for control of radio interference. This paper compares these methods from the standpoint of accuracy, speed, information content and applicability to the present spectrum signature collection plan. To supplement this review, some suggestions are given for application of these methods or improvements thereof to spectrum signature collection, production testing of components and systems, and standards laboratories. It is believed that application of these methods will contribute to the solution of the overall problem of controlling unwanted radiation and reducing radio interference.

## I. INTRODUCTION

This paper is a survey of several methods for transmission line measurement of the signals generated by high power microwave transmitters. For convenience, these signals are classified by type as functional or spurious and by frequency as near-band or far-band. The near-band frequency region is uni-modal and extends from d.c. through the assigned operating band to the cut-off frequency of the first higher-order mode. The far-band is the multi-modal region extending from the upper edge of the near-band to the highest frequency of interest. Measurement of the level and frequency of signals in the near-band is fairly straightforward and is well documented. Measurements in the far-band region are complicated by the multi-modal character of signal propagation; for this reason emphasis in recent years has been placed upon developing techniques for measuring far-band spurious power. Representative of such techniques are the selective mode sampler method described by Lewis;[1] the electric probe analysis method of Forrer and Tomiyasu;[2] a probe method for coaxial lines described by Knop and Cohn;[3] a calorimetric method described by Price;[4] and a Tee-junction waveguide sampling method reported by Sharp and Jones.[5]

Figure 1. illustrates a general measurement technique common to

all these methods. A signal sampling network is installed in a transmission line which conducts signals from a high-power source to a load. The level, frequency and in some instances the relative phases of the sampled signals are the parameters to be determined by measurement. While all of the methods have a common basic approach, they differ considerably in complexity. Furthermore some of the approaches are suitable for production type tests while others are better suited for a standards laboratory. In the following paragraphs these approaches are briefly described and compared.

## II. MEASUREMENT METHODS

### Lewis Method

The signal sampling network used by Lewis is illustrated in Figure 2. His method centers upon the use of a set of mode-selective directional couplers reported by Judy and Angelakos[6] and based on the coupled-wave theory of Miller.[7] Each of the several directional couplers is designed to select by a phase discrimination process one particular mode which may propagate at the measurement frequency. Each bolometer attached to these directional couplers may be equipped with a transmission type wavemeter to select the frequency of measurement. Lewis found that two-hole couplers provide a usable fractional bandwidth of only about 10%; however, there is little doubt that suitably designed multi-hole couplers could both extend the bandwidth and improve the modal selectivity.

Taking into account the associated coupler loss and other calibration factors, the power level indicated by each detector represents the power associated with a given mode. Therefore, the several modal powers at a given frequency must be summed to determine the total power available for radiation. The Lewis method offers a straightforward method for determining with good accuracy the power level of spurious signals in transmission lines. The principal limitation on this method results from difficulties in separating degenerate mode pairs. Thus in practice this method is limited to frequencies below which no more than five or six modes can propagate. Within this range the method is adaptable for use in a standards laboratory as a reference to measure the effectiveness of other measurement schemes.

Forrer and Tomiyasu Method

This technique, illustrated in Figure 3, uses a series of calibrated electric probes located in a prescribed manner on a broad and a narrow wall of a rectangular waveguide to sample the relative power level and the phase angle of the internal fields. Band pass filters are used to separate the particular harmonic signals to be measured from others and from the high power fundamental signal. The mathematical analysis of the raw data to determine the power level of each mode propagating at the measurement frequency is rather involved; therefore a program has been prepared for data processing with a digital computer.[8] In this process the computer performs a numerical Fourier analysis of the input data, which is represented as a set of linear equations. Inversion of the matrices of these equations permits the modal power evaluation to be made. The output of the computer is a table of modal power levels for some particular frequency, at which data was taken. As in the Lewis method, the several modal power levels at a particular frequency must be summed to determine the total power available for radiation.

Because this method can provide an accurate determination of the levels of many spurious signals it is adaptable for use in a standards laboratory. Furthermore, the apparatus may be calibrated to operate over a wide band of frequencies. However, the need for a digital computer for data reduction is a serious disadvantage. Another disadvantage is the lack of sensitivity. To avoid ionization or breakdown, it is necessary that electric probes inserted through the broad wall extend into the waveguide only a very short distance. Such probes operate at coupling losses in the range of 40 to 60 db.

This method may be used up to frequencies for which no more than about 30 modes may propagate. This limitation occurs as a result of the need for matrix inversion. The order of the matrices increases with modal number and when the order of the matrix is high, small inaccuracies in the measured data are exaggerated by the inversion process.

Knop and Cohn Method

This method, illustrated in Figure 4, samples spurious signals in coaxial transmission lines, as contrasted to the rectangular waveguides of

the two previous methods. Except for details associated with the geometry of the probe section it is identical with the method described by Forrer and Tomiyasu. The Knop and Cohn method is attractive because in typical situations a coaxial line propagates fewer modes than does a rectangular waveguide. Therefore, fewer measurements need to be made, and the mathematical analysis is considerably less tedious. Often, through the second and third harmonic only two or three modes propagate. At frequencies where more than two or three modes can propagate it is convenient to use a computer to reduce the data. The foundation for a computer program for the coaxial line case is given in reference[9].

Price Method

This measurement technique utilizes a series of multi-modal absorptive filters to withdraw from the main transmission line all of the power being propagated within certain chosen bands of frequencies. The power abstracted in each band is dissipated in a liquid cooled load in which a temperature rise, relatable to the dissipated power may be observed. The measurement scheme is illustrated in Figure 5. The filter used to separate the spurious frequency power in a particular band must, of course, be effective for each modal signal which propagates within the band. A leaky-wall filter proved to be satisfactory for this function.

This calorimetric method is substantially different from the preceding sampling approaches in that; no modal information need be determined, the sample comprises 100% of the available power in the measurement band, and the method is completely independent of load VSWR at the measurement frequency. The lack of identification of modal power levels is not an important disadvantage in most cases because of the many mode conversions produced in the plumbing systems of typical transmitters. In fact, since total power in a frequency band is measured, one can use a single indicator to read the power level. This method does, however, have several significant limitations: 1. Identification of the frequency of measured signals is not precise, 2. the use of a liquid calorimetric medium is not convenient for integrating the powers absorbed at various locations on the waveguide and 3. the sensitivity of the method is not satisfactory.

With further refinements (for example, controlled Peltier cooling could be used to replace a liquid calorimetric fluid) this method could prove valuable in situations where the load VSWR at the measurement frequency is high. Day-to-day monitoring of the output of an operational transmitter, for example, might be accomplished with this technique.

Sharp and Jones Method

Sharp and Jones reported a waveguide sampling section in which a set of Tee-junctions are used to sample a small portion of the spurious power propagating within the main transmission line. Their method is illustrated in Figure 6. In this figure a set of secondary waveguides incorporating band pass filters are mounted perpendicular to a main waveguide and coupled to the internal fields by means of narrow resonant irises. The number and position of the secondary waveguides depends upon the number of modes propagating at the frequency band under measurement. One group of secondary waveguides is used to measure signals representing the second harmonic frequency. Other groups are used for the third and fourth harmonics. These groups are located so that the highest frequencies (corresponding to the smallest irises) are near the source and the lower frequency waveguides are near the load.

The measurement procedure with this method is to attach a bolometer mount successively to each secondary waveguide and record the power observed. An average is then made of the powers thus sampled to obtain the level of average spurious power at a particular frequency. If the signal is pulsed rather than continuous the peak power may be determined from the PRF and pulse width. Caution is necessary, however, because the spurious frequency pulse envelope is not usually the same as that for the carrier.

Advantages of the Sharp and Jones method which make it attractive are its high sensitivity, its capability of measurement up to the fifth and sixth harmonic region and its insensitivity to load VSWR if enough secondary waveguides are used in each group. The use of calibrated attenuators in the secondary waveguides permit adjustment of the sensitivity of the sampling section to read both very high power spurious signals as well as weak calibration signals. Disadvantages in the method are found in the need for

connecting the power indicating meter successively to each of the several secondary waveguides and in its reported accuracy of ± 3 to ± 5 db. The former limitation could be removed by using an integration device to sum and average the outputs of each bolometer mount in a given group. This would allow a single meter to read the average power level in a particular band. The latter limitation could be removed by the use of tapered transitions to change the dimensions of the measurement section so that no mode is at cut-off in the measurement frequency band.

## III. COMPARISON OF METHODS

The various transmission line measurement methods described in the preceding sections may now be compared on the basis of accuracy, speed, information content and applicability to present and future needs. These characteristics are considered in turn in the following paragraphs.

To make the comparison meaningful it is necessary to assume a uniform set of conditions. It is assumed that the fundamental frequency is 1300 mc, that the measurement frequency range extends to 3000 mc, that the load is well matched to all modes which propagate in this range, and that a 30 db signal-to-noise ratio for the detectors is maintained.

### Accuracy

Exact data on the limiting accuracy of the various measurement methods is still lacking. The values indicated in Table I are those reported in the literature or represent the present authors' estimates of the state of the art. They do not represent the ultimate accuracies attainable by any of the methods.

Table I - PRESENT ACCURACY LIMITS

| Method | Range |
|---|---|
| Lewis | ± 1 db |
| Forrer-Tomiyasu | ± 1 db |
| Knop-Cohn | ± 1 db |
| Price | ± 5 db |
| Sharp-Jones | ± 3 db |

Speed

To compare the speed of the various measurements we have estimated the number of manhours required to make a complete transmission line test from set-up to data reduction. These figures do not include the number of manhours required to operate the transmitter used as source of signal but only those actually used in performing measurements and reducing data. A quantitative comparison of the various measurement methods is given in Table II.

Table II - TIME IN MAN HOURS

| Method | Set-Up | Test | Cali-brate | Reduce Data | Total |
|---|---|---|---|---|---|
| Lewis | 1 | 1/2 | 2 | 1/2 | 4 |
| Forrer-Tomiyasu | 2 | 1 | 3 | 3 * | 9 |
| Knop-Cohn | 1 | 1/2 | 1 | 1 | 3-1/2 |
| Price | 1 | 1/4 | 1 | 1/4 | 2-1/2 |
| Sharp-Jones | 1 | 3/4 | 2 | 3/4 | 4-1/2 |

* Includes computer time on IBM-704 or equivalent.

Information Content

The several measurement methods differ substantially in the amount of information made available about the spurious signals measured. Three types of information are listed in Table III for this comparison. These are power, frequency and type of presentation. Under power the methods are compared as to whether individual or total modal powers are determined at a particular spurious frequency. Under frequency, the methods are compared as to the accuracy of spurious frequency measurement. Under presentation, the methods are compared by the type of read-out device useful for the measurement. A bolometer, for example, would indicate the average power level sampled while an oscilloscope presentation would permit indication of pulse shape as well as peak power.

Table III - INFORMATION CONTENT

| Method | Power | Exact Frequency | Presentation |
|---|---|---|---|
| Lewis | modal | yes | Bolometer or scope |
| Forrer-Tomiyasu | modal | yes | scope |
| Knop-Cohn | modal | yes | scope |
| Price | total | no | calorimeter |
| Sharp-Jones | total | yes | Bolometer or scope |

Applicability

One of the purposes of this comparative review has been to consider the applicability of some transmission line measurement methods to the spectrum signal collection plan now being implemented by the Department of Defense. As the plan now exists, there are no requirements[10] to test transmitters by a transmission line method if multimodal propagation may occur in the line below 12 Gc. Accordingly the plan has no direct requirement for any of the methods presented herein. However, the use of valid transmission line tests either in conjunction with an open field test or in a closed system, may greatly simplify the part of the plan concerned with far-band spurious frequencies.

To illustrate this conjecture consider an open field test associated with a simultaneous transmission line measurement of both near and far-band spurious frequencies. A comparison between the far field data and that derived from the transmission tests will provide a relationship between the two for the particular transmitter involved. Subsequent tests on the same transmitter or on additional transmitters of the same type can then be made with a transmission line technique at considerable savings over that required for the far field tests. Furthermore, a day-to-day monitoring on transmitters in critical areas can be made to insure that a change in spurious frequency generation has not taken place with increase of operational time.

As a separate matter closed system tests, using a dummy load, may be the only practical means for measurement in the far-band of equipment on some ships or in other close-quarter installations.

Open-field tests using a waveguide transmission line sampling device could be accomplished best using the Sharp-Jones method modified to

work properly with the VSWR expected in an operational equipment. The Knop and Cohn method, (also modified by adding additional probes to account for reflected waves) would be satisfactory for coaxial line transmitters.

The needs of laboratory tests to provide reference standards are best fulfilled by the Forrer and Tomiyasu method because of its accuracy and wide frequency coverage. Its sensitivity limitation may be largely overcome in a laboratory test since high power signals would not be involved and deeper probe penetration is possible.

## IV. FUTURE REQUIREMENTS

Requirements for transmission line tests in the future are expected to fall into three classes; 1. open field and closed system tests of operational transmitters, 2. manufacturing production line tests of tubes and filters to insure a specified spurious frequency performance and, 3. standards laboratory reference measurements.

In typical field tests it will be important to be able to measure spurious signals quickly and with a single-meter indicating system. The signal sampling system must respond properly in spite of the existance of substantial reflected waves within the system under test. Adequate directional discrimination will provide a reading indicative of the forward propagating power available for radiation. While an accuracy better than $\pm$ 3 db is desirable, it is not vitally important since the power levels of spurious frequency signals vary more than this amount with transmitter tuning and with aging of the tube. Production tests of tubes should be simple and preferably accomplished with a single-meter indicator. Accuracy should be $\pm$ 2 db or better in this application. It is desirable to provide a multi-modal matched dummy load for this application to simplify the tests. Reference laboratory standard tests will have maximum accuracy and repeatibility as primary objectives at the expense of speed or convenience. In this application it will generally be desirable to identify the modal signals propagating in a line.

## V. CONCLUSIONS

Several transmission line measurement methods for determination of

spurious frequency power levels were reviewed and compared as to accuracy, speed, information content and applicability. With minor improvements several of these methods are directly applicable to the DOD plan for collection of spectrum signatures and to several new areas of measurement which may be expected to develop.

## REFERENCES


1. D. J. Lewis, "Mode Couplers and Multimode Measurement Techniques," IRE-PGMTT, Vol. MTT-7, No. 1, pp. 110-116; Jan. 1959.

2. M. P. Forrer and K. Tomiyasu, "Determination of High Order Propagating Modes in Waveguide Systems," J. App. Phys., Vol. 29, No. 7, pp. 1040-1045, July, 1958.

3. C. M. Knop and S. I. Cohn, "A Multiple Probe Method for the Measurement of Reflected & Transmitted Power in Coaxial Waveguides," Sixth Conference on Radio Interference Reduction & Electronic Compatibility, pp. 525-541, Oct., 1960.

4. V. G. Price, "Harmonic Calorimeter for Power Measurements in a Multimode Waveguide," IRE Nat'l. Conv. Rec., Part 3; 1960.

5. E. D. Sharp and E. M. T. Jones, "A Sampling Technique for the Measurement of Multimode Harmonic Power," Third National Symposium on Radio Frequency Interference, pp. 39-41, June 12, 1961.

6. H. A. Judy and D. J. Angelakos, "Mode Selective Directional Couplers," University of California, Series #60, Issue 119; September 15, 1954.

7. S. E. Miller, "Coupled Wave Theory and Waveguide Applications," Bell System Technical Journal Vol. 33 pp. 661-719, May 1954.

8. V. G. Price, J. P. Rooney and C. Milazzo, "Measurement and Control of Harmonic and Spurious Microwave Energy," Final Report, Phase I, pp. 106-125, ASTIA Document AD-208290, July 8, 1958.

9. V. G. Price, J. P. Rooney, and R. H. Stone, "Measurement and Control of Harmonic and Spurious Microwave Energy"; Final Report, Change A, pp. 44-60, ASTIA Document AD-239-078, March 18, 1960.

10. Military Collection Plan for Spectrum Signatures, Department of Defense, Washington, D.C., paragraph 3.2.3.1, page 22, 1 Sept., 1961.

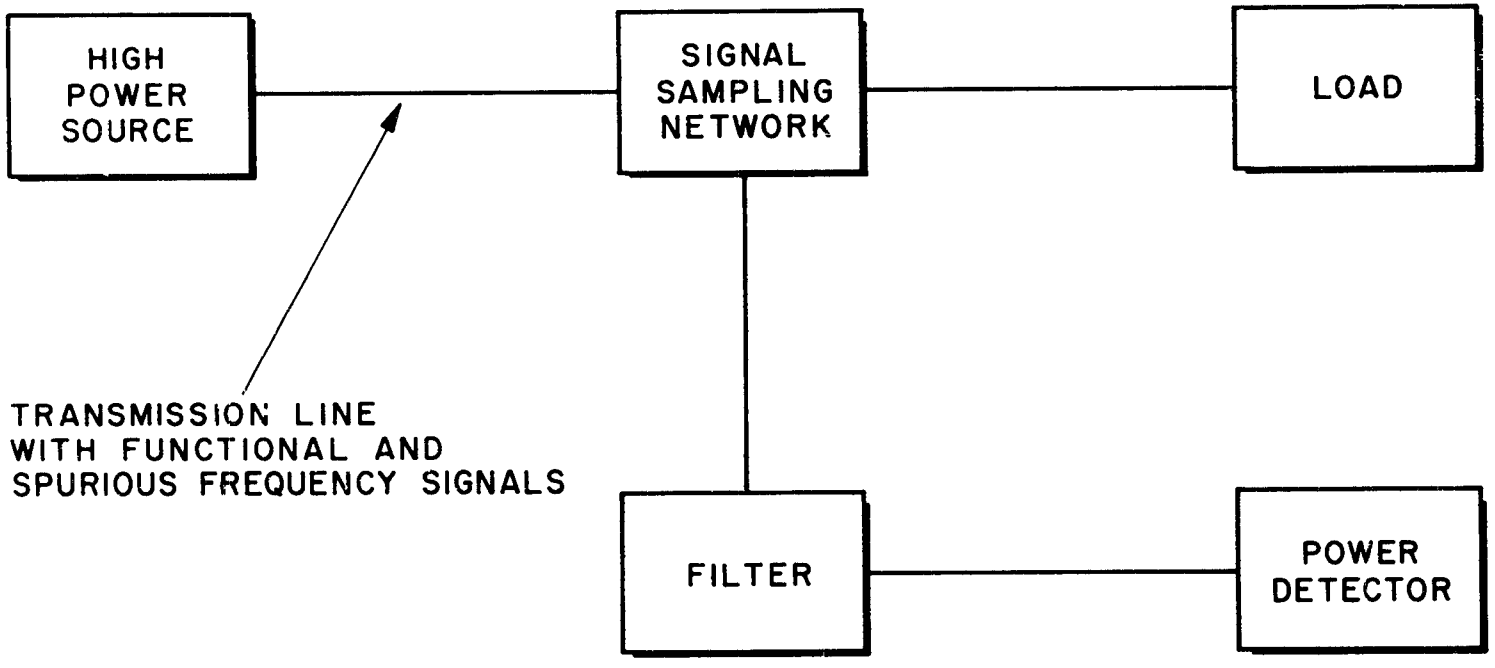



Figure 1. Block Diagram of Transmission Line Spurious Frequency Measurement Apparatus.

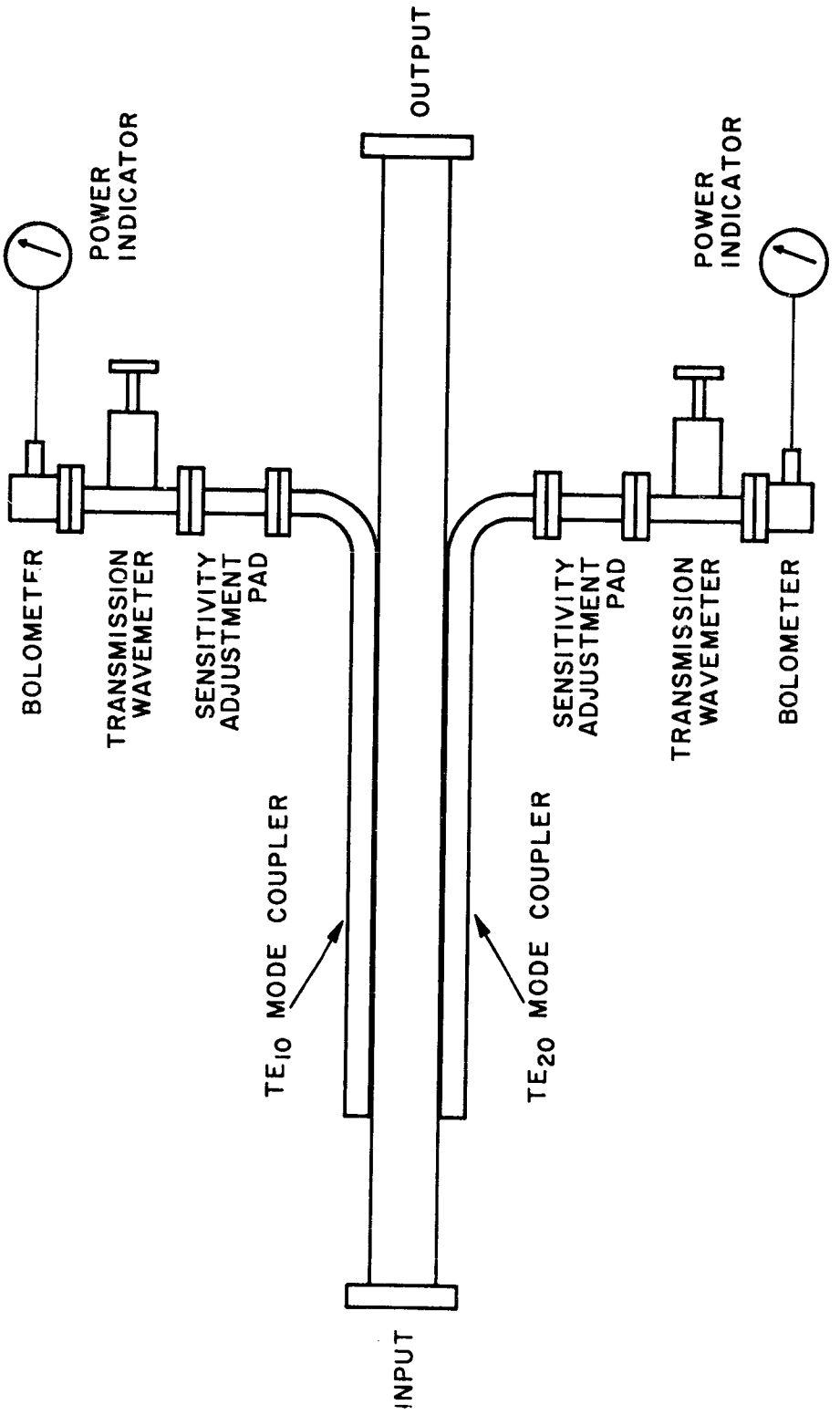



Figure 2. Lewis Type Signal Sampling Network With Two of the Selective Mode Couplers Illustrated.

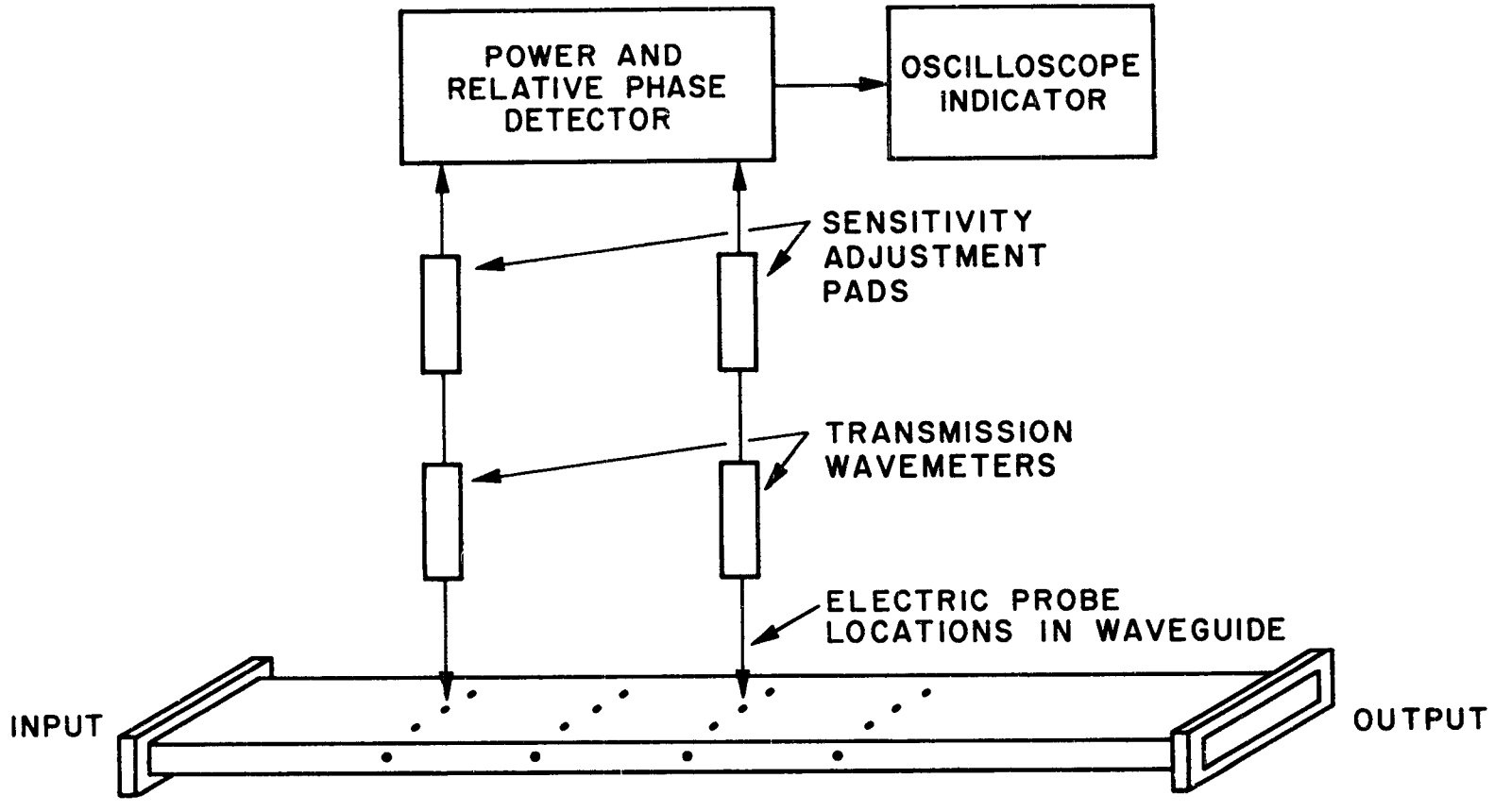



Figure 3. Forrer and Tomiyasu Type Signal Sampling Network and Associated Equipment.

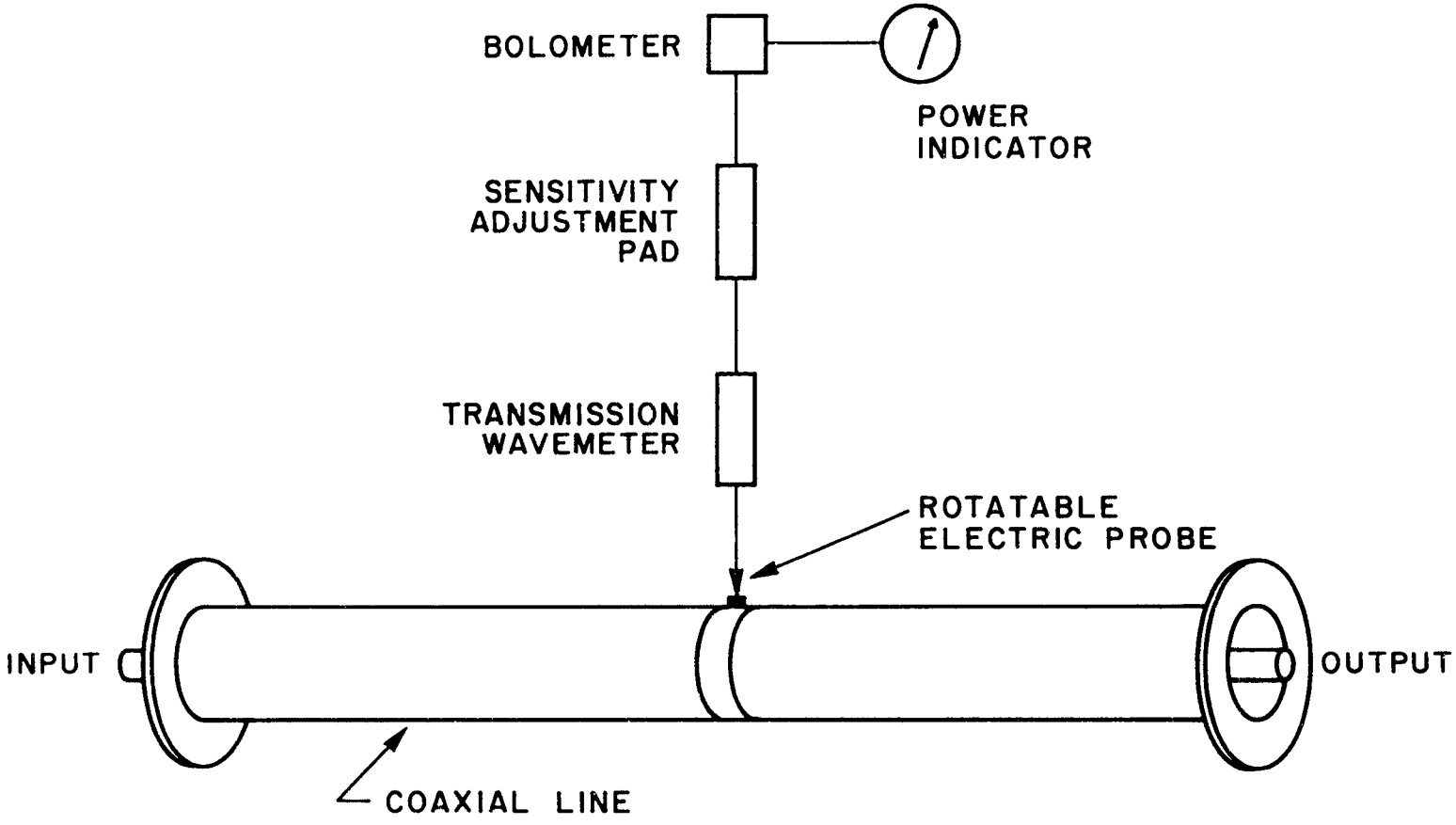



Figure 4. Knop and Cohn Type Signal Sampling Network for Coaxial Lines.

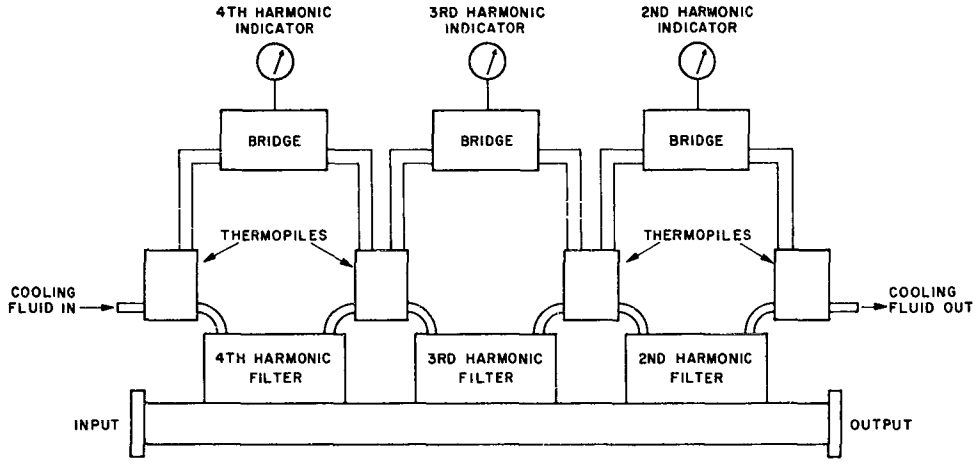



Figure 5. Price Type Signal Sampling Network

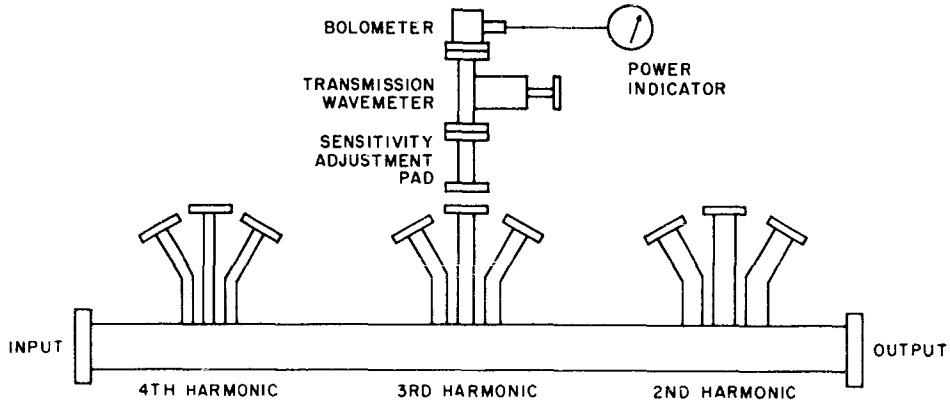



Figure 6. Sharp and Jones Type Signal Sampling Network

# AN INTEGRATED APPROACH TO BONDING, GROUNDING, AND CABLE SELECTION

I. M. Newman and A. L. Albin

Filtron Company, Inc.

Flushing, N. Y.

Abstract. There appears to be considerable confusion over the methods and philosophies of grounding, bonding, and cable treatment which will result in optimum interference reduction. This paper will present means to minimize interference through the proper selection and utilization of various cables, the establishment of a well-bonded ground plane, and the implementation of good bonding techniques, considered from the viewpoint of integrated system requirements.

Bonding and grounding philosophies and the method of inter-connecting equipment racks, cabinets, and instrumentation were investigated. The mechanical and electrical details for establishing a low impedance bond were also studied.

The establishment of a ground plane was required in order to realize the full benefits in reduction of r-f interference coupling and audio crosstalk. The relative advantages of single point and multipoint grounding philosophies will be shown for radio-and audio-frequency applications. The use of a multipoint ground system was recommended in most cases because of its superior advantages for r-f interference control.

The choice of cable, routing, shielding, and grounding techniques that should be implemented to transmit various types of signals was also considered. These recommendations were based on tests performed on shielded, coaxial, and twisted pair cables to measure the interference coupling. The tests covered 60-cycle power frequencies, 15 kc through 29 mc radio frequencies, and pulsed signals. A fundamental issue was the optimum grounding method over the frequency range of interest. The magnitude of shielding isolation that could be achieved under various conditions of shield terminations was also determined.

**Applications will be given to airborne and ground support facilities of a missile installation.**

## I. INTRODUCTION

In recent years radio frequency problems have increased in proportion to the increased complexity of missiles and electronic systems. There appear to be many differences of opinion concerning the methods and philosophies which result in optimum interference reduction. Unfortunately, among many groups of engineers engaged in separate tasks on a large system, such as a missile and its test complex, there is a lack of a concrete or standardized, engineering approach to important considerations such as equipment bonding, shield termination, or a basic ground system philosophy.

This paper will describe problems existing at a government installation, approaches we have taken, and methods and techniques successfully used to minimize interference in the electronic complex. These methods and techniques will include: establishment of a well-bonded ground plane, multipoint and single-point grounding theories, bonding, cable choice, routing, shielding, and grounding techniques. Cable coupling tests will be described to substantiate our grounding philosophy.

## II. DISCUSSION OF PROBLEM

A recent interference reduction program was performed at a large government missile installation. The purpose of this program was to study, measure, analyze and reduce electromagnetic interference in the missile ground electronic checkout complex. The primary function of the electronic complex is to check out space vehicles. Radio frequency interference, often encountered during these checkout procedures, adversely affects the testing operation, which employs both radiated and conducted control and monitoring circuits. Interference has been traced to the building ac and dc power supplies and nearby electrical equipment, as well as rf sources.

Several steps have been taken by the government agency in the past to reduce interference. To this end, portable shielded enclosures in the hangar area have been built at considerable cost. During checkout periods, it has been necessary to perform the checkout operations at night, since the ambient noise level has proven to be somewhat lower during this period. This has resulted in additive cost due to overtime and delays in the vehicle checkout schedule.

Although shielded enclosures of large size were built to protect the missiles from external interference sources during checkout, local interference from electrical and electronic equipment, vehicles, etc., within the enclosures, was a problem. In order to assure a successful missile system checkout, it was necessary to initiate a program for reducing interference in the checkout area.

One of the most important problem areas was the inadequate ground system used for the entire electronic complex. The ground system was found to consist of a single ground stake to which power systems, equipment racks in the various areas, and each missile "track" ground were connected by 2/0 cables. (Figure 1) In some areas this cable, running for a considerable distance, represented a common impedance to a number of equipments and signal returns for numerous circuits. (Figure 2) Particularly at the higher frequencies, major differences in potential can exist between the missile and other points such as the power return and instrumentation racks, the telemetry station and other associated equipments. The absence of an unipotential, or nearly unipotential, ground plane within such a complex contributed greatly to interference problems both in the rf range and at lower frequencies.

Some systems used multipoint grounding and others followed the single-point grounding philosophy. Many of the instrumentation cables examined were noted to have shields floating, which, particularly in long cable runs, increased the radiation from these cables as well as their susceptibility to rf fields in the area. As shown in Figure 3, the shields at the end of the cable were found to be left floating. Note that an insulating braid is used over each shield. In Figure 4 the shields are tied together and bonded at a distant point through a 22 gauge wire. At high frequencies this bond wire has considerable impedance, and the shields are no longer at ground potential. Figures 5 and 6 show additional examples where temporary shield connections were made to ground, and led to radiation of interference.

Another problem encountered was the rf environment within the overall building, which was of sufficient magnitude to prevent or degrade complete checkout of the missile. Many of these interference signals were generated within the building. Inspection of the sources showed that the interference level could be greatly reduced by appropriate interference suppression measures and an rf control program. Interference due to radiation from vehicular ignition systems in fork lifts and trucks represented a major source of interference.

Cases were reported in which instrumentation used for obtaining data during checkout of a missile were inoperative or provided highly unsatisfactory data due to the presence of strong background interference signals and transients. Examination of the equipment enclosures showed that no attempts at shielding had been made. Figure 7 shows open rack construction typical of that employed at the site.

Broadband interference emanating from the dc and 400 cps power sources furnishing power to the missile and laboratory rooms represented another problem. The conducted interference appearing on these lines was coupled into the missile system and also to the ground checkout instrumentation circuitry. The intensity of the conducted signals, especially at the lower frequencies, caused sensitive equipments connected to or coupled to those lines to malfunction.

Finally, objectionable rf coupling was found between cables used to transmit signals from system to system in the ground station complex. As an example, remote indicating equipment connected to the voltage monitoring console located in the instrumentation room, which sequentially samples missile power circuits, was located in the console rooms and in the checkout area. Switching transients from this unit were conducted into many areas due to crosstalk and rf coupling, which was attributed to unsatisfactory cable choice, routing, grounding, and shielding techniques.

## III. APPROACH TO SOLUTION

Due to the severity of the interference, and the problems of attempting to control interference within the existing installation, the systems approach was adopted. That is, common problem areas would be determined, and their possible adverse effects on the system evaluated. The program which was set up established an integrated approach to interference control, necessitated by the dispersion of equipment throughout the site, incompatible interface design, and lack of suitable controls on RFI internal and external to the checkout area.

Analysis of the preliminary study showed that the main interference sources were gasoline engines, power generators, and switching circuits in the checkout equipment. The energy was predominantly conductively coupled on the power lines or radiated from signal and control cables. A program was instituted to:

1. Define techniques for bonding, grounding and shielding structural components and equipments.

2. Analyze signal characteristics and optimize cable selection and treatment.

3. Develop specifications for RFI-free design of equipment and installation, tailored to the system requirements.

4. Reduce interference generation and susceptibility in particular equipments by specific RFI control measures.

### System Ground Plane

The initial step established a well-bonded, low impedance ground plane throughout the complex. After a survey of the ground system was performed

and the architect's ground system specifications reviewed, a revised specification was prepared which established a much improved ground plane. It was impossible to establish a ground grid since the site was completed. The method adopted under these circumstances provided that all metallic structures in the building be well bonded together and act as the ground plane. The RF specification detailed the establishment of a low impedance ground plane by bonding together all metallic structures such as I-beams, cable trays, and the electronic equipment racks. By bonding chassis to racks and racks to cable trays, subsystem grounds were established in each equipment rack or cabinet. By providing good bonding between the chassis and the rack member, between cable shields and the cabinet, and with added shielding, radiation from the equipments and cables was substantially reduced.

Figure 8 shows a view of the cable trays. Note the use of a multi-tray system to separate power and signal cables. The bond straps can be seen in greater detail in Figure 9. Structural members were tack welded, as shown in Figure 10. In areas where improved shielding was required, a sheet-metal cover was fabricated for the tray (Figure 11).

Interference Suppression

In order to reduce the high ambient RF noise level in the building to acceptable limits, measurements were first made to determine the type of interference present in the bay area and trace the interference to its originating source. Among the equipments found to contribute to the general interference background, and in some cases to the specific transients observed, were the following: counters, oscillators, calibrators, tape recorders, print dryers, thermostatically-controlled crystal ovens of receivers, timers, dc motors, digital voltmeters, voltage and frequency monitoring units containing stepping switches, digital recorders, Eput meters, graphic recorders (from which the timing pulse was noted throughout the checkout area) and IBM accounting machines (sorter and reproducing punch).

To minimize radiated interference, shielding kits were installed on all fork lift trucks. Unsuppressed vehicles were restricted to 1,000 foot minimum distance from the area during missile checkout tests.

In an effort to reduce the broadband interference being transmitted from the power generator units to the missile and ground electronic complex, interference tests were performed on these units, to determine filter requirements. The suppression of interference on these lines was very important due to the fact that the power cables extended all over the test area radiating broadband interference.

System Analysis

Existing checkout procedures, particularly compatibility tests and simulated flight tests, were reviewed to minimize the number of accessory cables and equipment units which might contribute to RFI and to provide specific locations and grounding for such equipment, and optimize cable routing.

Characteristics of the signals being transmitted between various ground systems in the missile checkout were analyzed. These signals were categorized to separate high-level, low-level, and power cables. The cable choice, routing, shielding, and grounding techniques used by the installing contractor were studied. Revised cable specifications were prepared to indicate the optimum types of cables to be used to transmit the various signals between systems. This specification also indicated cable routing, and shielding and grounding techniques, to minimize crosstalk and rf coupling between circuits. Studies performed in this area are described below.

## IV. CABLE TESTS

In any missile or electronic installation when various sensitive and low voltage equipments are involved, it becomes extremely important that the optimum cable choice, grounding and shielding techniques are utilized. An extensive laboratory investigation was performed to measure the coupling and crosstalk between various types of cables.

It was necessary to investigate the optimum grounding method to be used on coaxial cables in order to minimize audio frequency crosstalk and rf coupling when coaxial cables are used for signal transmission. As shown in Figure 12, two 17 foot lengths of coaxial cables were placed adjacent to each other and terminated in their approximate characteristic impedance. One cable was excited with a signal generator and the induced voltage developed in the adjacent cable was measured with a field intensity meter or oscilloscope, depending on the frequency band of interest and required sensitivity.

The induced voltage in the receiving cable was measured for four conditions:

a. Sending and receiving cable resistor termination floating at the receiving end.

b. Sending and receiving cable resistor termination grounded at the receiving end.

c. Sending cable resistor termination grounded and receiving cable resistor termination floating at the receiving end.

d. Sending cable resistor termination floating and receiving cable resistor termination grounded at the receiving end.

The shields at the signal generator end of the cables were grounded in all instances.

The following tests were performed on these cables:

a. RF tests
b. AF tests

c. Pulse tests
d. Power frequency tests

Similar tests were run on shielded twisted pair cables.

Radio Frequency Tests

Radio frequency tests were performed on these cables for the frequency interval of 14 kc to 150 kc and from 150 kc to 29 mc. The output voltage of the signal generator was held constant at .1 volt and at 2 volts rms respectively, over each of these frequency ranges.

While performing these tests, it was noted that there was an excessive amount of radiation at both ends of the directly excited cable due to improper shielding at these points. The energy radiated from the directly excited cable coupled directly into the adjacent cable due to shield discontinuities at the terminations. Excellent shielding measures had to be applied at the resistor terminations at the receiving end and also at the connections at the signal generator end of the excited cable in order to eliminate this effect. This is an extremely important requirement which was found to be dominant over the exact method of termination.

Figure 13 shows test results in coupling which can exist between adjacent coaxial cables for the specified shield grounding methods. The results of these tests indicate a relatively high magnitude of coupling when the loads are floating (single-point ground), compared to the multipoint ground circuit. In the case when both terminations are floating the coupling increases rapidly above 3 megacycles. The crosstalk remains close to the receiver background noise level up to 10 megacycles when the sending cable is grounded or floating and the receiving cable is grounded. Resonances at approximately 10 and 20 megacycles are also more pronounced with the loads floating.

A similar version of this test setup was used to measure the isolation between shielded twisted pair cables (see Figure 14). The main difference in the test procedures was that the shields were grounded at the sending and receiving ends of both cables, and the circuit return path was grounded only at the sending end. In other words, the signal current was flowing through the twisted conductors at all times. Figure 15 shows test results over the frequency range of 150 kc to 29 mc. The curves show that shielded twisted pair is superior to the coaxial line when the load must be isolated from ground, particularly in the frequency range above 3 mc. The induced voltage in the twisted pair cable was below the receiver background noise level between 150 kc and 20 mc, and close to the noise level in the range 150 kc to 3 mc for the coaxial lines under both conditions of termination. Results with the grounded coaxial cable compared favorably with those obtained with the twisted pair over most of the range. Under the test conditions, an isolation in excess of 100 db was readily attained with shielded and coaxial cables grounded at both ends.

Video and Power Frequency Tests

Additional tests were made to determine cable coupling parameters in the video and power frequency range. For the pulse tests, the sending cable was energized with a pulse of magnitude 80 volts, a repetition rate of 4 kc, and a pulse width of 2 microseconds. A wideband oscilloscope was used to measure the induced voltage in the receiving cable. This test setup was similar to that shown in Figure 12.

A final test series was performed at 60 cycles per second. These tests were made to determine the magnitude of conducted and induced currents developed in cables when a 60 cycle current was flowing in the ground plane, and to investigate the possible effects that might result from so-called "loops." The shields of signal circuits were grounded at both ends, to investigate if the currents flowing in the shield, due to differences in potential at two points of the structure, would induce currents in the inner conductor and cause malfunctioning or errors in signal circuits. The test setup is shown in Figure 16.

Test results under the conditions of termination previously described -- receiving end grounded or floating -- are shown in Figure 17. They may be compared with the summary also given for the radio frequency tests. It is seen that for the pulse tests, when both terminations of the coaxial cable were grounded, isolation of 78 db was obtained. This case gave only a slight improvement over the ungrounded coaxial termination which provided 72 db isolation. The twisted pair gave 20 db more isolation than the ungrounded coaxial line. The improvement may have been greater, but could not be observed because of the threshold sensitivity of the indicator.

As in the previous tests, the twisted pair provided maximum isolation from ground plane currents at power frequencies. No signal could be detected above the indicator noise level with the twisted pair or the coaxial line ungrounded load. A slight degradation was observed with the coaxial load grounded, but 137 db isolation was still obtained.

## V. CONCLUSIONS

The results of these tests indicate that to minimize rf coupling and crosstalk between coaxial cables, the loads and shields should be bonded to the ground plane at both ends. These results also indicate that a multipoint grounding system is more beneficial to reduce coupling than is a single point grounding system.

However, while multipoint ground circuits are recommended for radio frequency applications, there are some circumstances, primarily in low frequency, low-level applications, such as audio or servo amplifiers, in which single-point grounding is advantageous. When a coaxial cable is grounded at both ends, using the ground plane as the return circuit, 400 cps and 60 cps currents in the ground plane can induce audio frequency interference into extremely

sensitive low-frequency circuits; therefore, single point grounding may be the best approach. However, it must be remembered that by grounding a cable at a single point, a radio frequency interference problem exists.

Thus, there appeared to be a conflict between the optimum choice for radio frequency interference control and the optimum method of grounding for reduction of audio frequency conducted currents. However, use of shielded twisted pair offers a compatible solution.

It was established from these experiments that when sensitive circuits and adjacent high signal levels are transmitted in an electronic system, shielded twisted pair cables offer the maximum isolation, provided the shields are properly grounded at both ends, and the circuit return path grounded at one point. By using the cable in this manner, the ground loop problem, due to heavy currents flowing in the ground plane, and rf coupling due to high signal levels, are both solved. Thus, both radio frequency interference and audio frequency interference can be controlled.

It is important to distinguish the concepts of single and multipoint "grounding" of signal circuits from the establishment of a ground plane. In all cases observed, a good electrical ground plane was essential for consistent performance and maximum interference reduction, and could best be achieved by electrically connecting all metallic surfaces in the system, as described earlier.



FIGURE 1: VIEW OF GROUND WELL

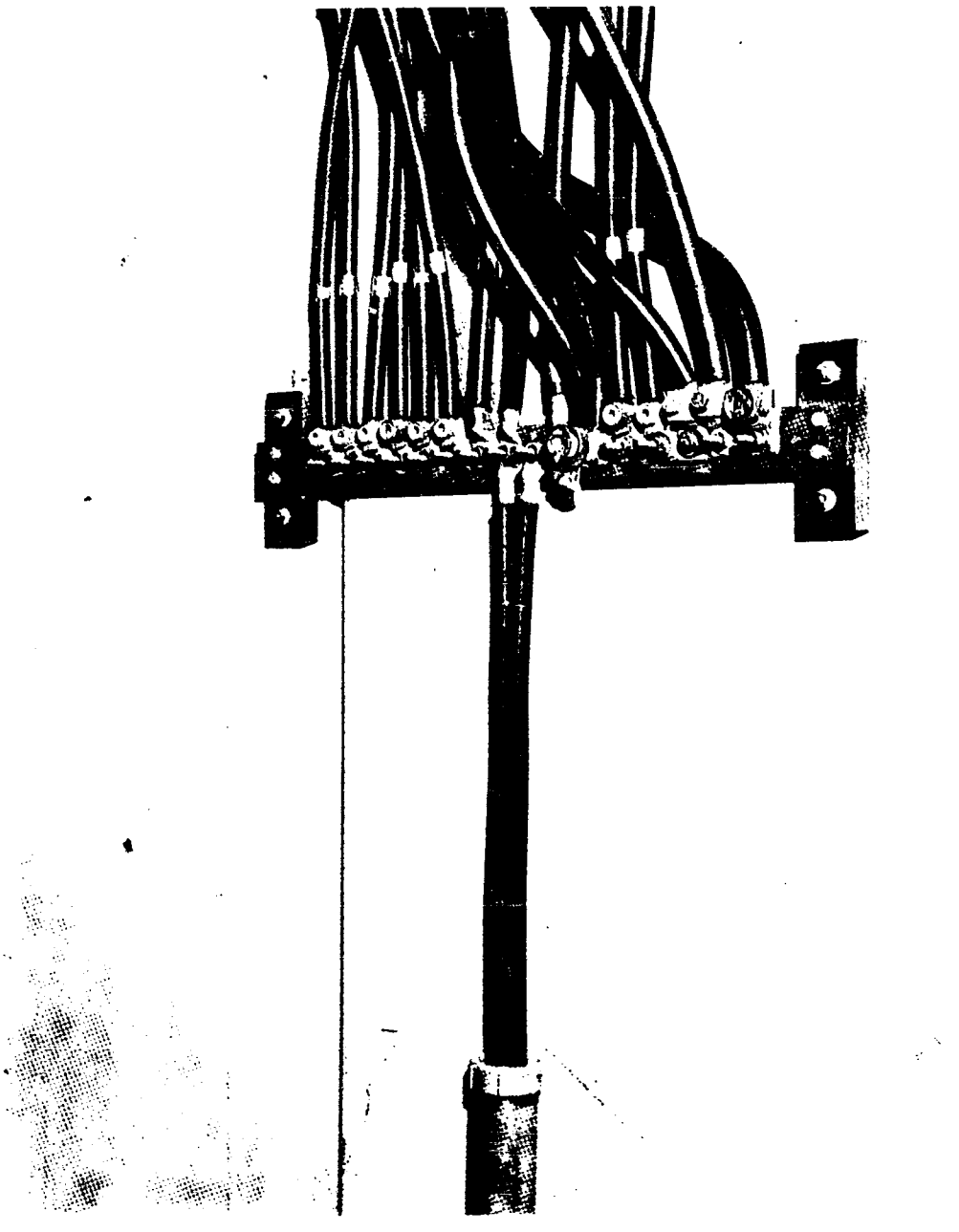


FIGURE 2: GROUND SYSTEM JUNCTION BLOCK

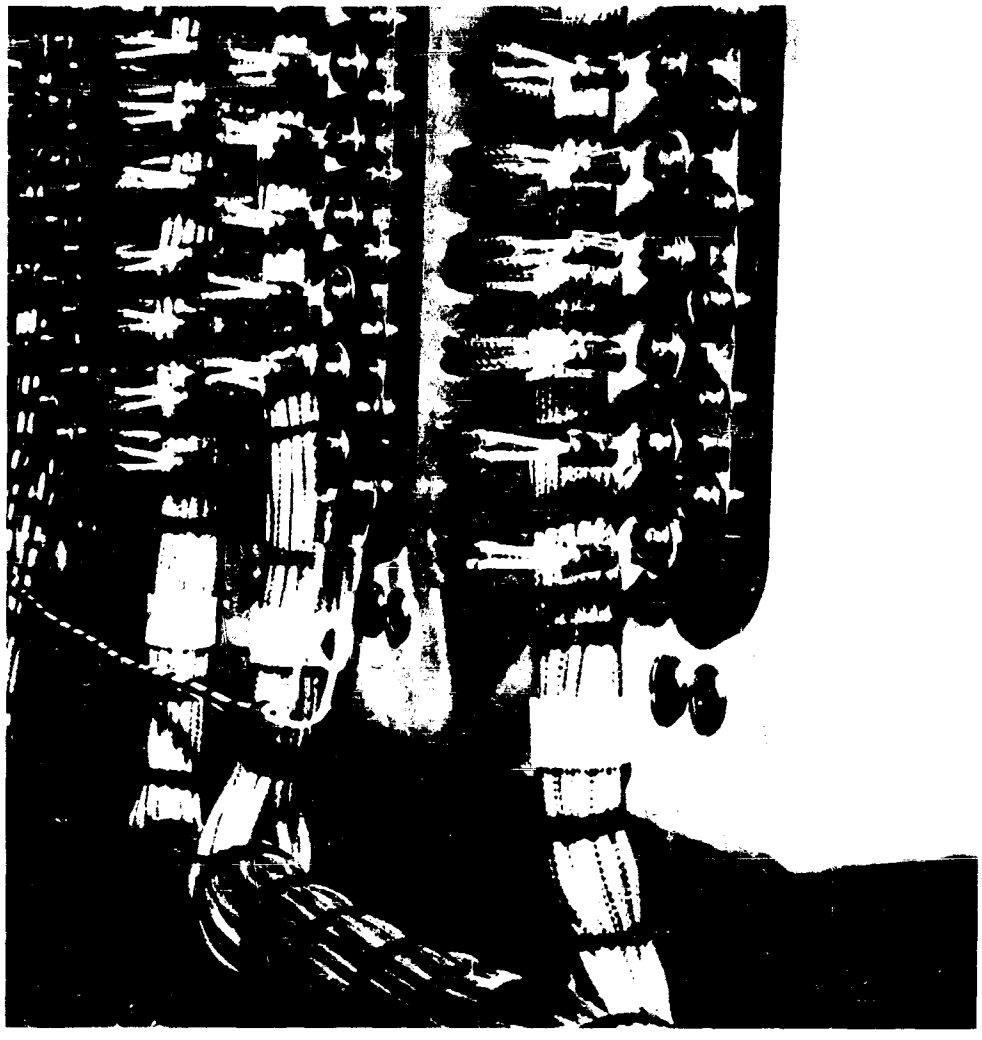


FIGURE 3: TERMINAL PANEL, WITH EXPOSED UNGROUNDED CABLE SHIELDS

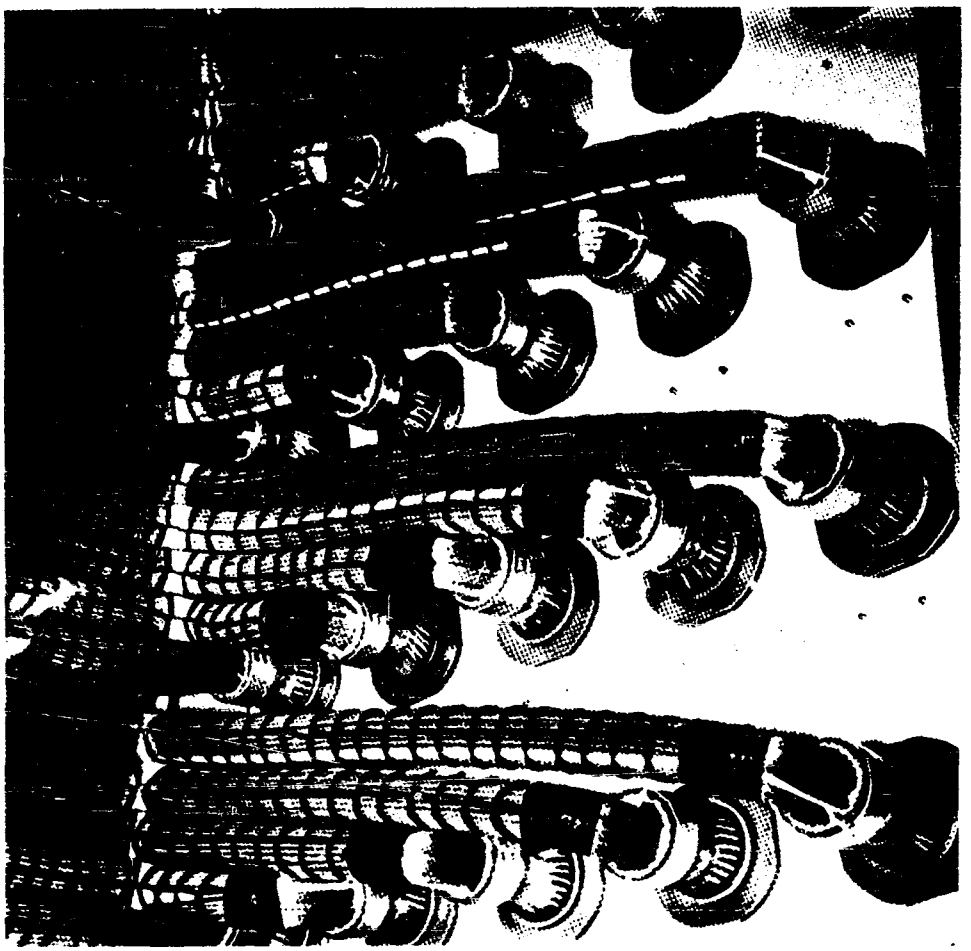


FIGURE 4: CABLE JUNCTION BOX SHOWING GROUND RETURN LEAD (WHITE WIRE) AND SHIELD HALO

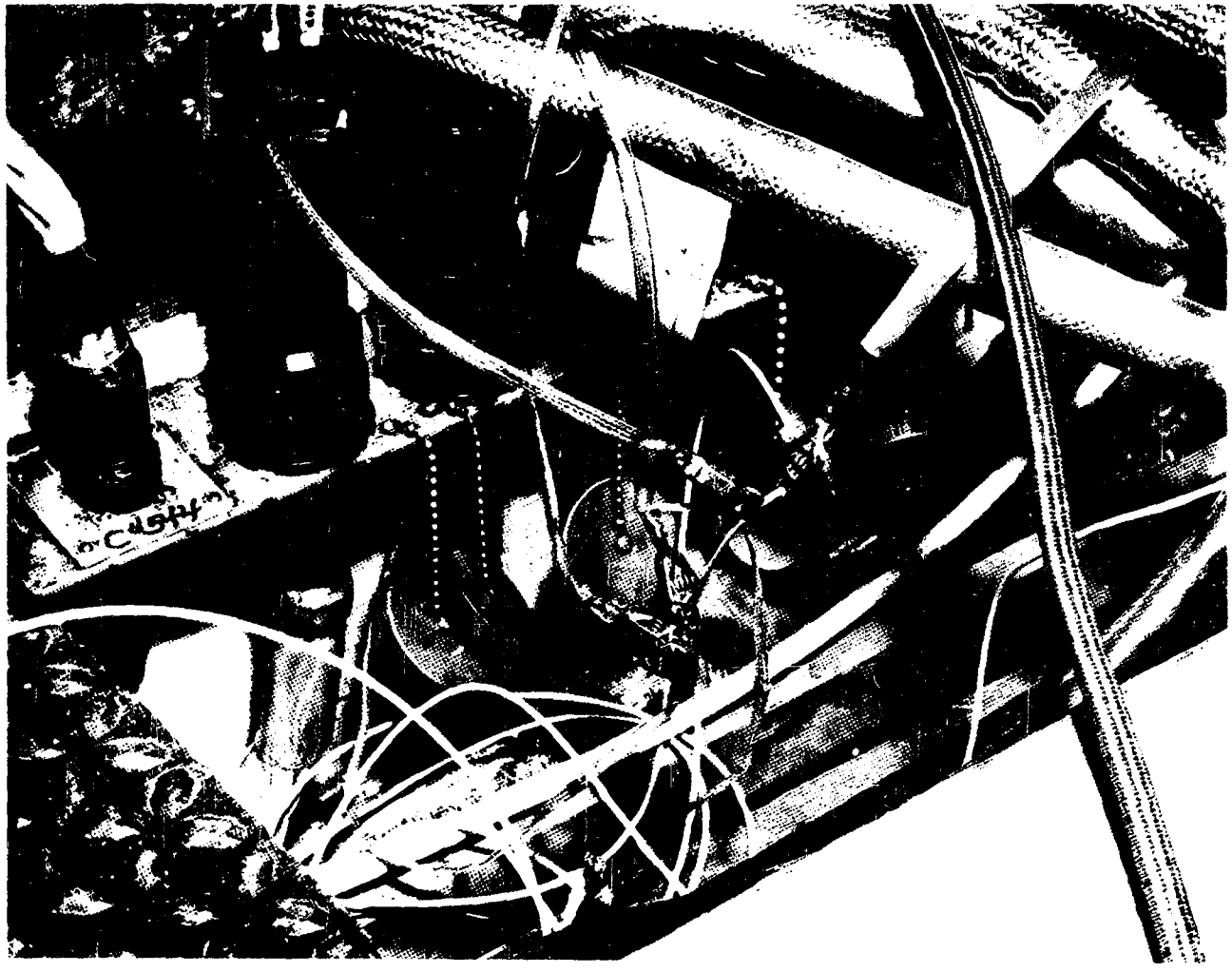


FIGURE 5: VIEW OF CABLE TROUGH WITH POOR SHIELD GROUND RETURNS

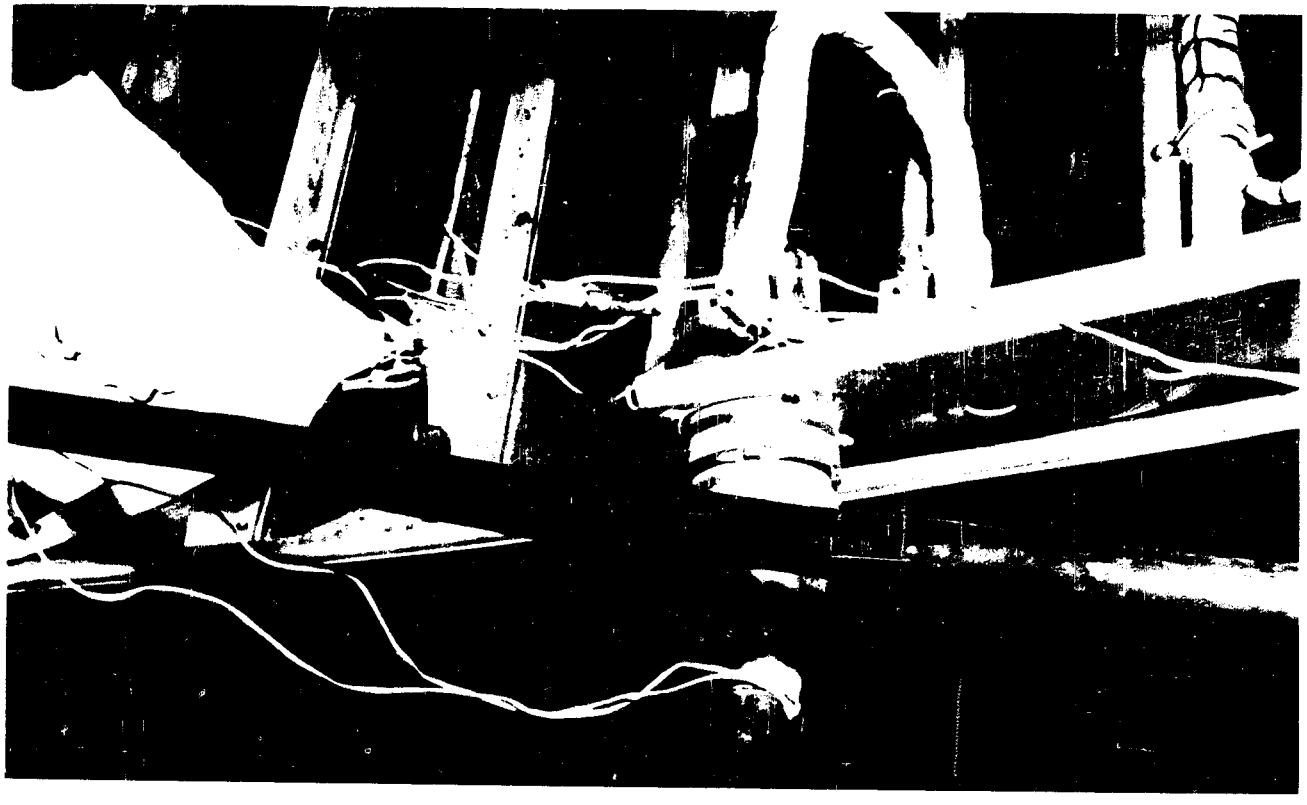


FIGURE 6: CABLE SHIELD TERMINATION WITH EXCESSIVE LEAD LENGTHS

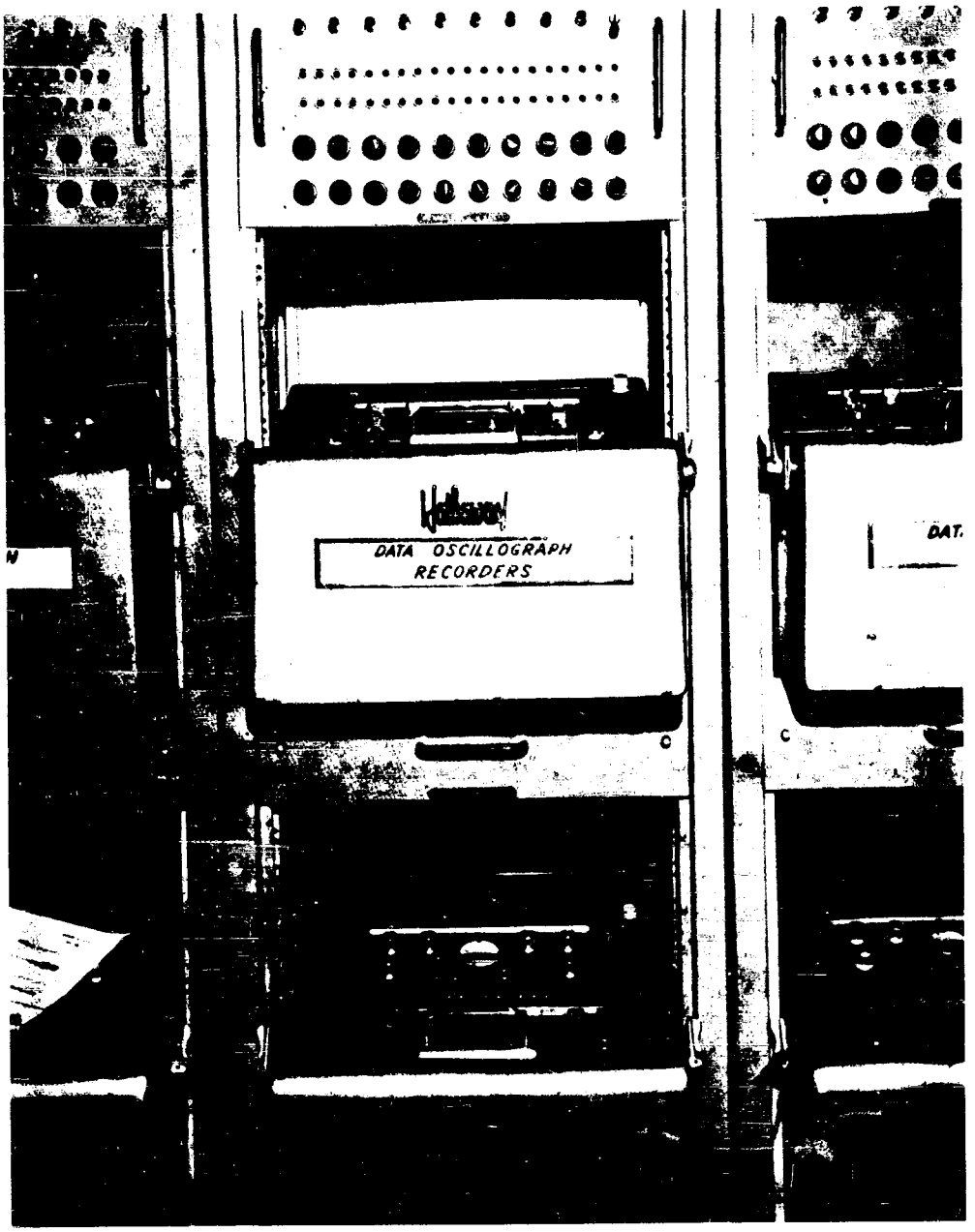



FIGURE 7: OPEN TYPE EQUIPMENT RACKS

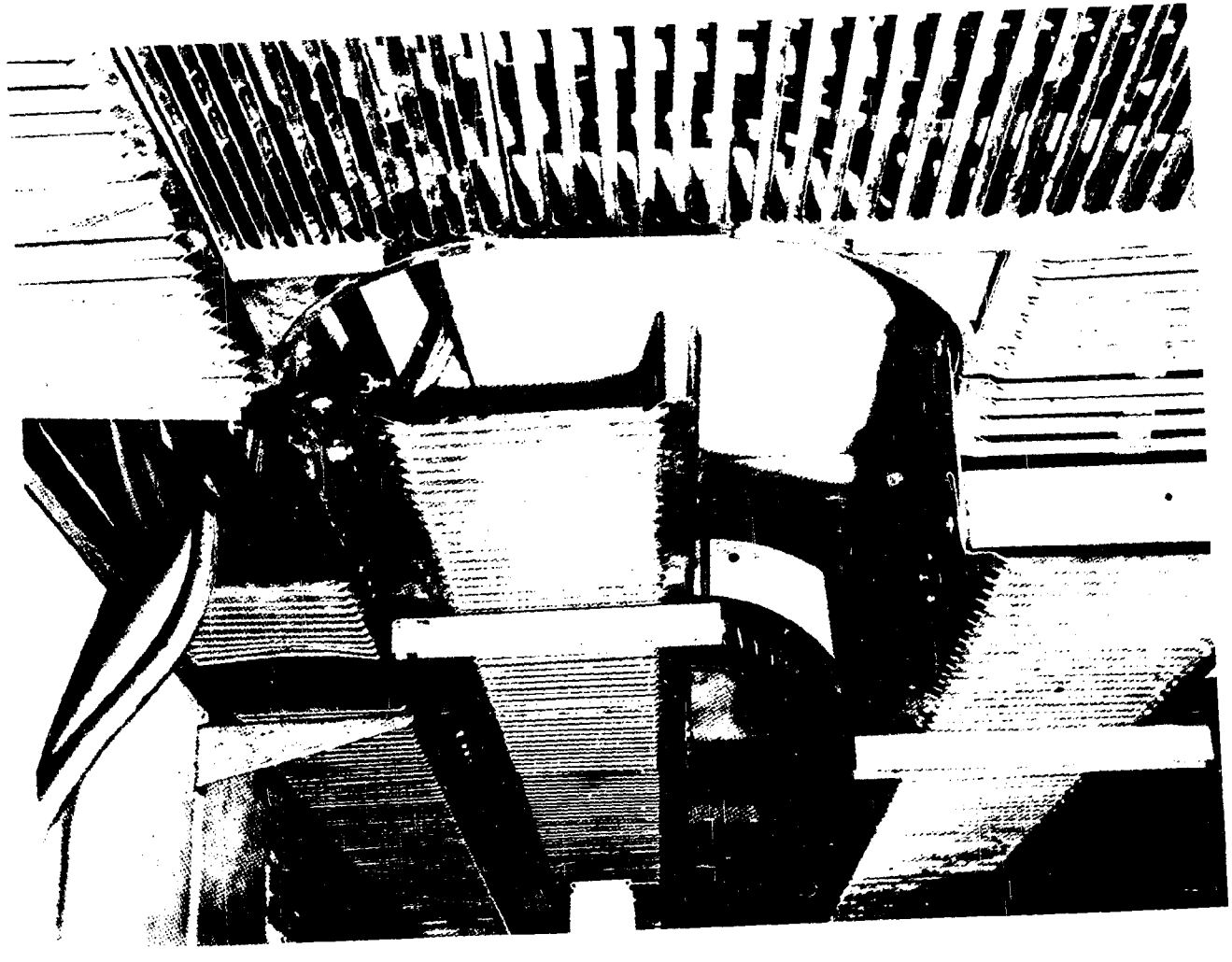


FIGURE 8: OVERHEAD CABLE TROUGHS, SHOWING BONDING STRAPS

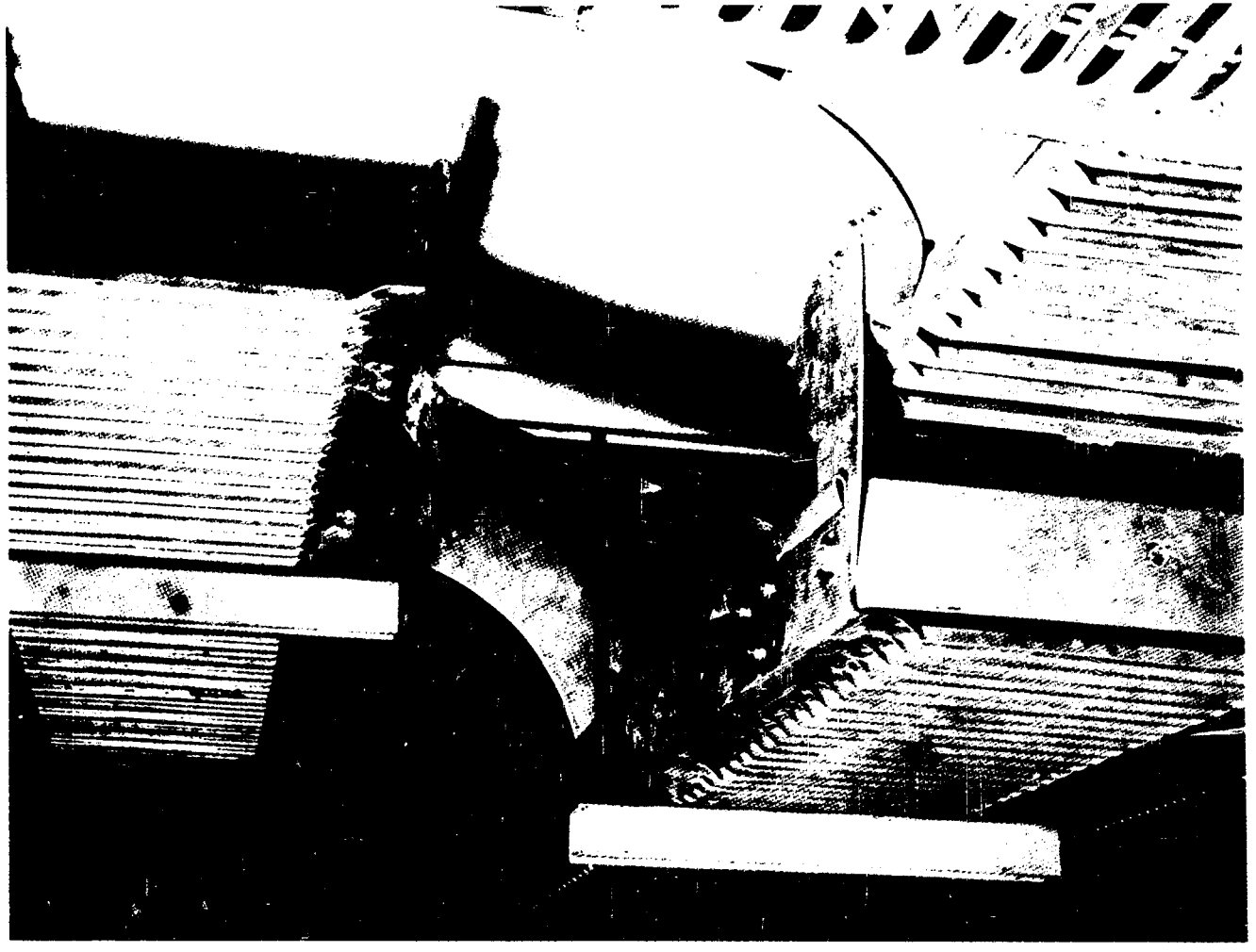


FIGURE 9: DETAIL OF TROUGH BOND STRAP

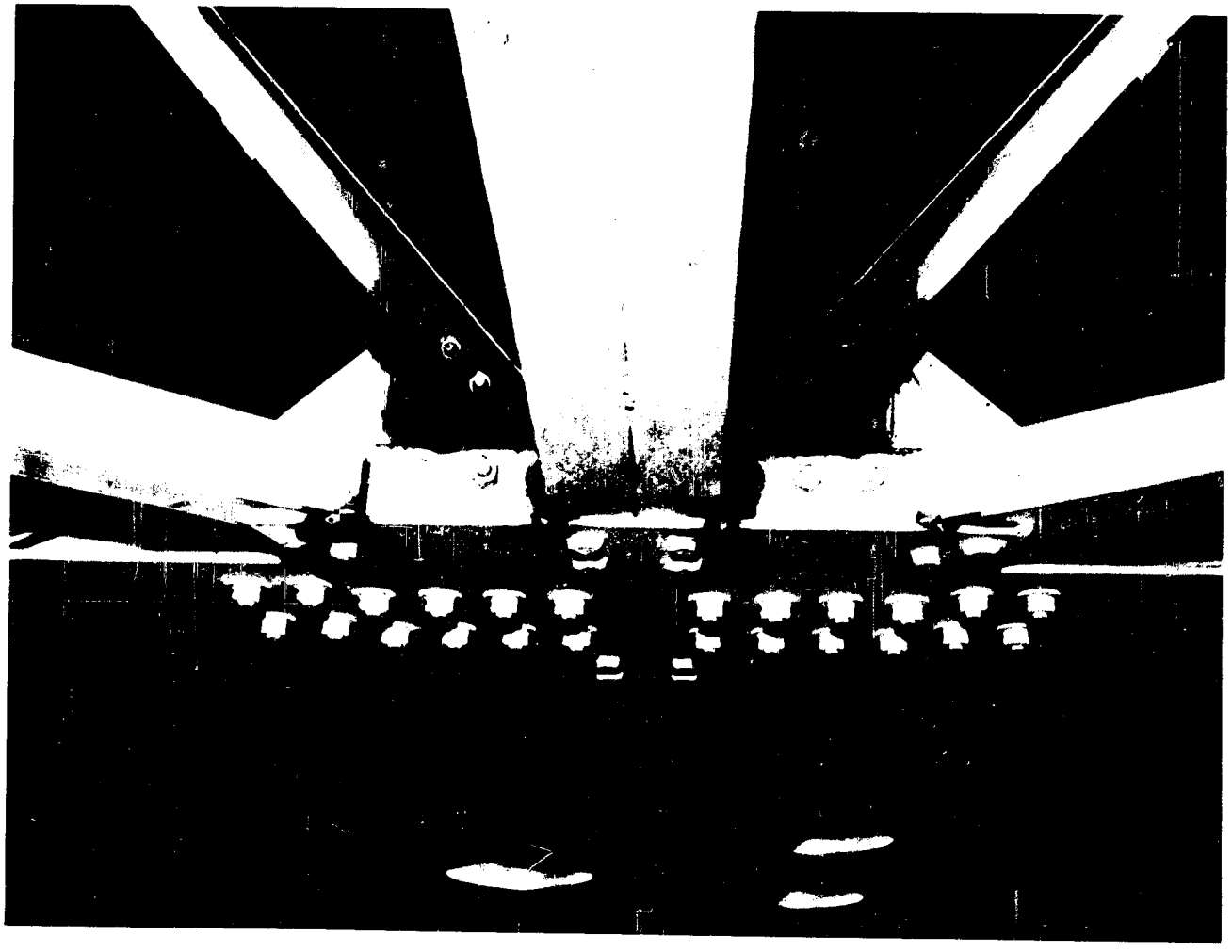


FIGURE 10: TACK WELDED STRUCTURAL MEMBERS FOR IMPROVED BONDING



FIGURE 11: CABLE TROUGH WITH ADDED SHIELD PAN

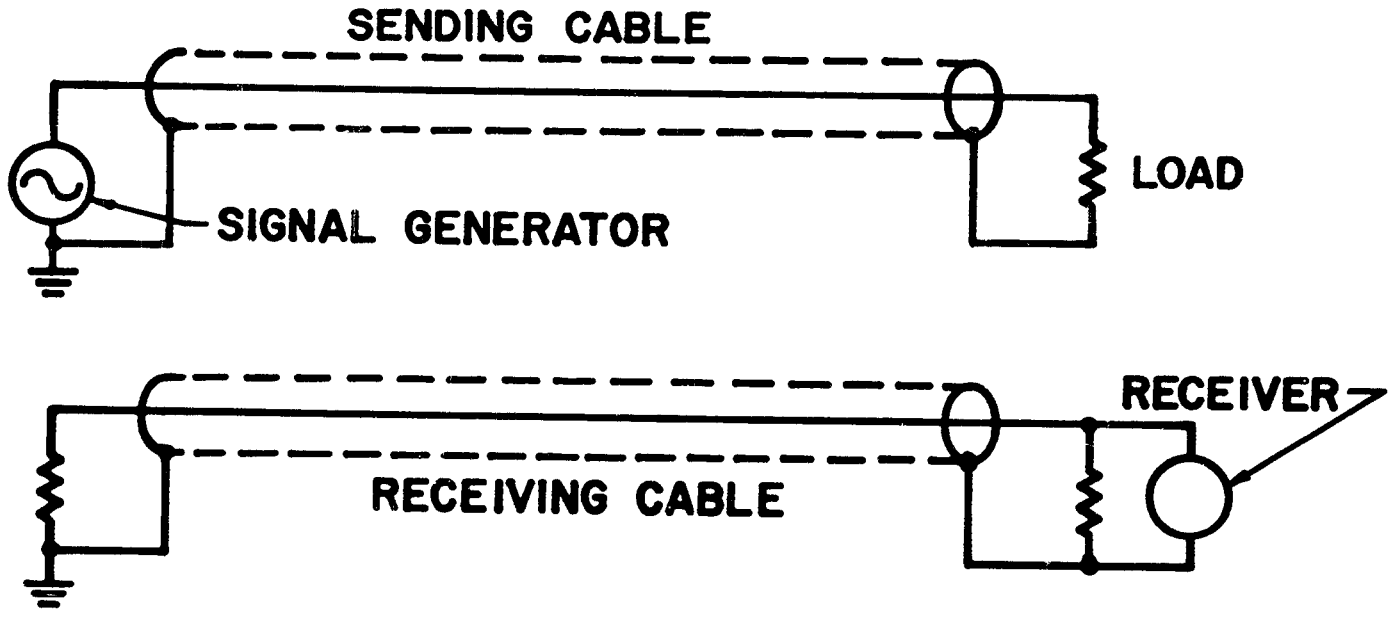



FIGURE 12: TEST SETUP FOR COAXIAL CABLE COUPLING MEASUREMENTS

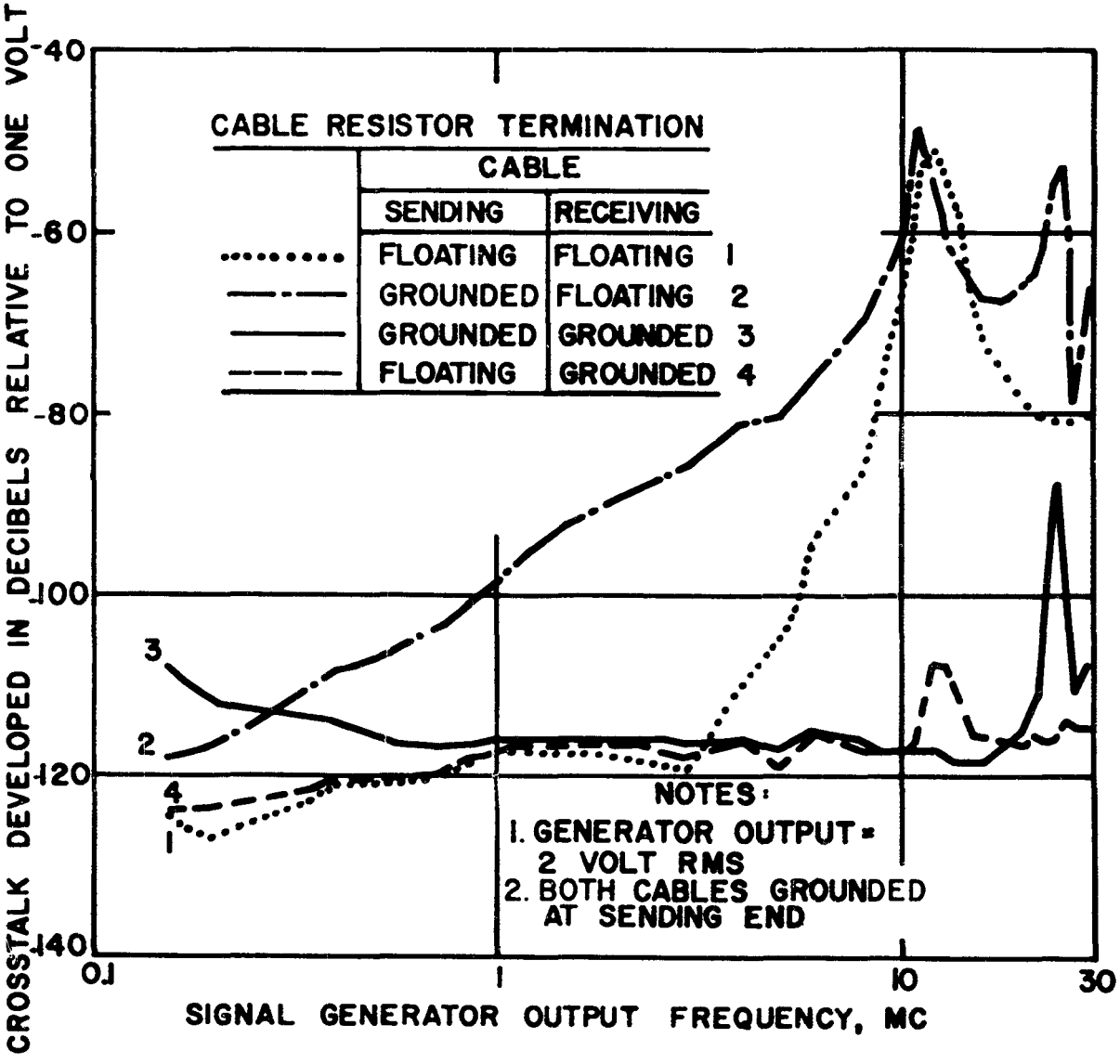



FIGURE 13: MEASURED R-F COUPLING BETWEEN COAXIAL CABLES

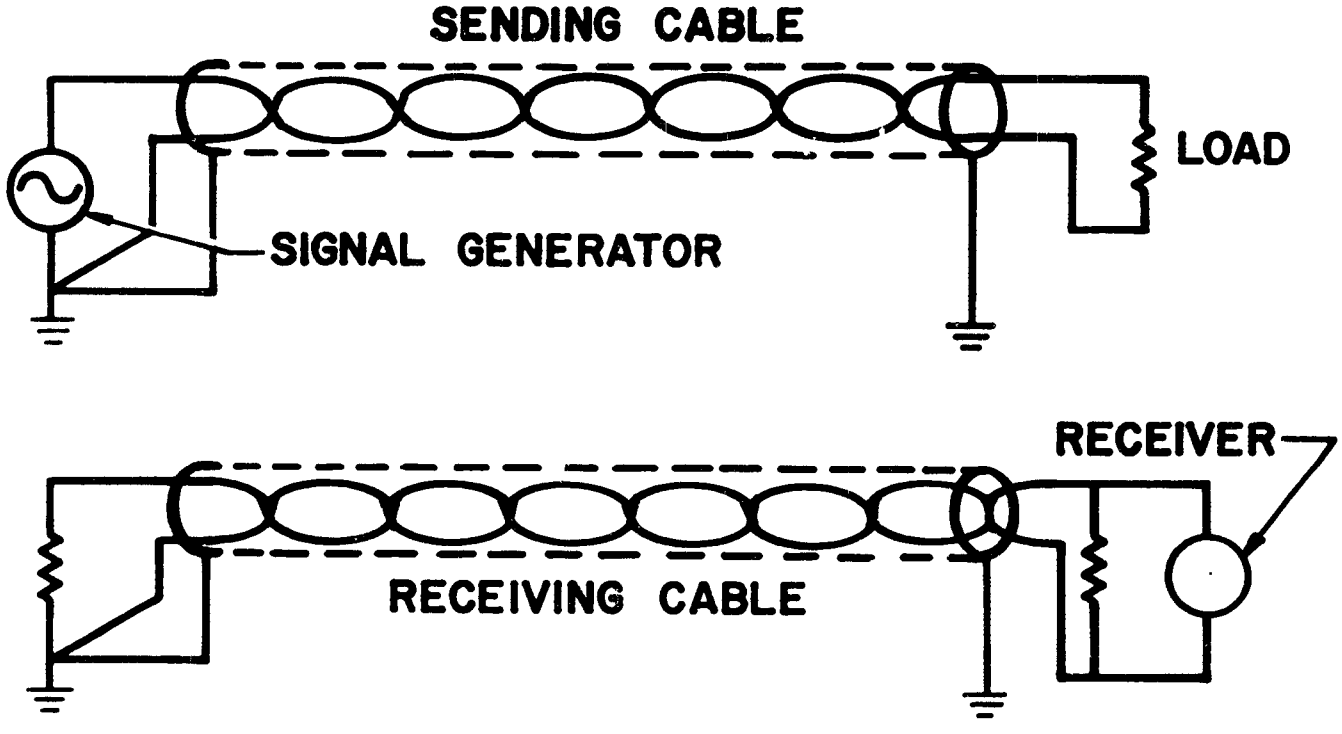



FIGURE 14: TEST SETUP FOR SHIELDED TWISTED PAIR CABLE COUPLING MEASUREMENTS

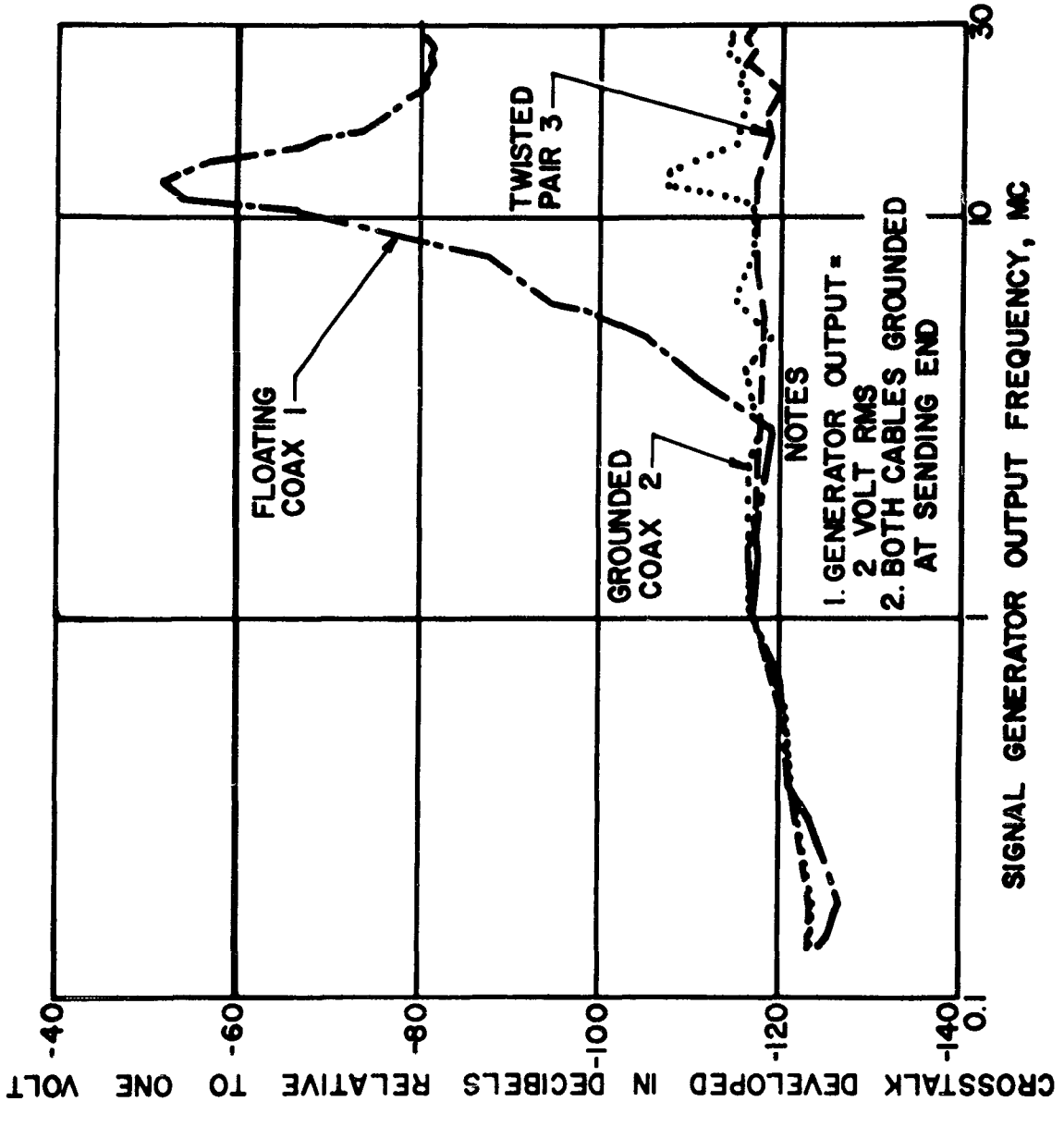



FIGURE 15: MEASURED R-F COUPLING IN SHIELDED CABLES

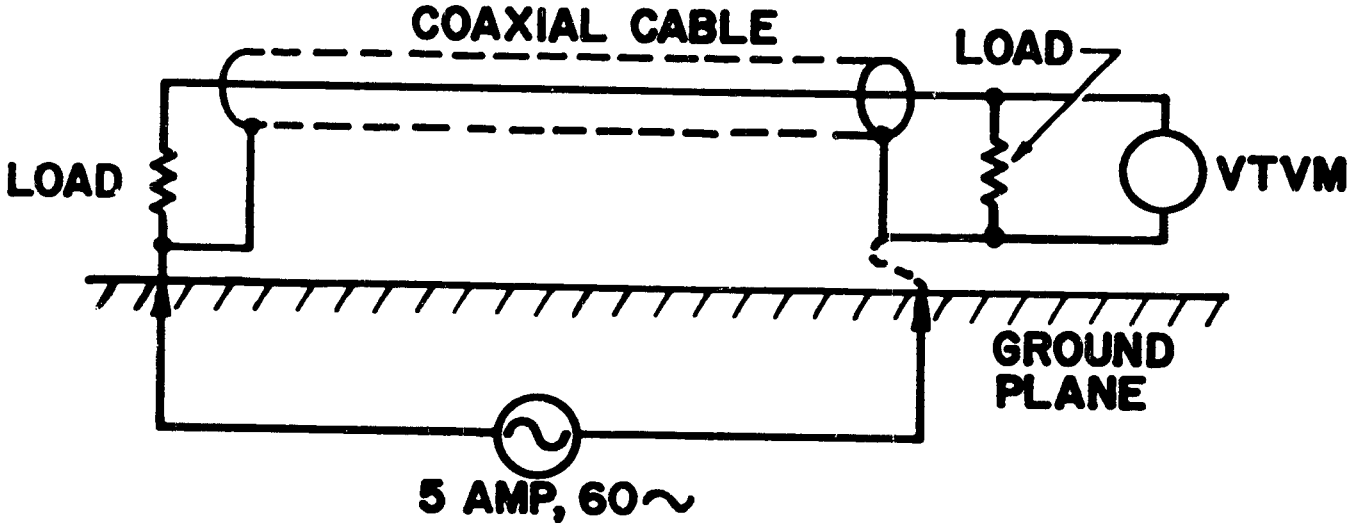



FIGURE 16: TEST SETUP FOR GROUND LOOP COUPLING

| TEST SIGNAL | COAXIAL LINE UNGROUNDED LOAD | COAXIAL LINE GROUNDED LOAD | SHIELDED TWISTED PAIR UNGROUNDED LOAD |
|---|---|---|---|
| RF SINE WAVE<br>2 VOLT RMS<br>0.15 - 29 MC | 117 DB AT 150 KC<br>60 DB AT 10 MC | 108 DB AT 150 KC<br>118 DB AT 10 MC | 123 DB AT 150 KC<br>117 DB AT 10 MC |
| VIDEO PULSE<br>80 VOLT PEAK<br>2 μSEC, 4 KC | 72 DB | 78 DB | 92 DB |
| AC POWER LINE<br>60 CPS, 5 AMP | 148+ DB | 137 DB | 148+ DB |

FIGURE 17: SUMMARY OF ISOLATION FOR CABLE COUPLING AND CROSSTALK

# REQUIREMENTS OF MEASUREMENTS OF SHIELDED INSTALLATIONS

R. G. Klouda
Elite Electronic Engineering Company
Chicago, Illinois

Abstract.- This paper delves into the various practical requirements of shielded installations and how measurements are made under field conditions. Discussions will range from large built-in installations on military sites, to prefabricated types of enclosures. The usefulness of various materials used in shielded installations over a given frequency range will be listed so that a handy reference may be had when a shielding requirement comes up. In the past a compromise between shielding effectiveness and building construction has limited to some extent the usefulness of the shielding. New ideas and techniques will be offered to enhance the shielding effectiveness for these installations.

## I. INTRODUCTION

A demand by the military for building interference free areas which are composite with conventional building practices has increased. This requires the electromagnetic shielded enclosure to be blended in with the architectural design of the building and not be visible to the eye; the overall appearance of the room therefore being basically unaffected by the shielding requirements. This type of construction is typical of AC&W (Aircraft Control and Warning) Sites, which will be discussed here today.

The entire radar site is normally contained in an area of approximately 400 feet by 400 feet. Three to five radar towers are positioned to do their prescribed job of searching, tracking, and height finding. Approximately 200 slant feet away is the Operations Building, a cement block building which houses radar receiving and teletype equipment and the air conditioning facilities. A portion of the Operations Building houses the computors and display equipment. This is the dark room and automatic area that is electromagnetically shielded. The physical size of the room is 80 feet by 40 feet by 14 feet high. The finished wall interior is of conventional dry wall; the ceiling covered with acoustical tile, and the floor of tile covered access panels.

## II. SHIELDING REQUIREMENTS

The functional requirements of the room do not blend easily into the design of an R.F. shielded enclosure. Openings

and protrutions that exist in the room must be R.F. secured. A fair list of them are vent openings, personnel doors, pipes and tubes for heating, pneumatic needs and electrical needs, structual beams, light dimmers, receptacle and luminar boxes, telephone lines, and in the past, interior partitions and windows.

Now, the shielding requirements are obvious since the receiving equipment has certain thresholds of susceptibility, whether they be of the solid state or vacuum tube design. High power radar transmitters, adjacent microwave stations, associated communication equipment and non-technical equipment all place the computors and display equipment in a high R.F. ambient area.

Attenuation requirements have varied in the past and are still in the process of refinement. At the present time a 35 DB attenuation requirement has been specified. The frequency range being covered is 200 KC to 3 KMC. A higher range of frequency and attenuation figures is required at other sites.

Initially there were some conflicts between attenuation requirements and specified methods to be used to obtain this end. One such problem involved the shielding material to be used. Originally 16 by 16 copper screen mesh was specified. This was challanged and laboratory tests had to be conducted to verify this action.

For the laboratory tests a double electrically isolated 24 ounce solid copper cube was designed and constructed. The material under test was applied to the sixth side of the 40 inch cube. Since the five sides of the solid copper cube afforded well over 120 DB of attenuation for the frequencies concerned, the test material could be studied for its shielding effectiveness properties, tolerance to small and random openings, quality of solder seams, and the effects of protrutions through the shielding.

A field intensity, field strength meter was positioned **inside** the cube and the transmitting equipment was operated on the **outside**. Shielding effectiveness tests were then conducted in a general accordance with MIL-E-4957A. Small and random openings were made on the test material and data obtained and evaluated. Protrutions of conducting items were passed through the test material and data obtained and evaluated. From the former tests, the number and size of openings which were previously planned to be used were found to be acceptable when used in conjunction with 24 by 24 copper mesh. The latter tests showed that contemplated openings, due to pipes and small copper tubing would, when properly secured to the enclosure, meet the attenuation requirements. Another facet to this test varified that any protrutions such as a nail or conducting stub, when insulated from the shielded material, re-radiated much more energy into the room then would otherwise occur when its length was a sub-multiple of the test frequency. The value of wave guides which were to be used on protrutions which were constructed of non-conducting material was also investigated with this method. The results of these tests were a definite aid in deciding on the shielding material to be used.

Another conflict in specification was clarified using the 40 inch test cubical. Originally expanded metal lath was to be used from the floor level down. This technique would definitely degradate the attenuation figures since the lath had openings of approximately 1/2 by 3/8 inches. Laboratory shielding effectiveness tests pointed out that the copper screen should be continued down the wall and at least one foot into the floor plane. Still another deficiency lied in the type of R.F. doors to be installed in the shielded area and its vestibules. Common steel tubular doors with bronze weather stripping fastened to the perifery were called for. Past experience had shown that this type was not R.F. effective. The doors were re-designed and fashioned after doors used on prefabricated types of shielded enclosures. Sterrated phosphorous bronze fingers around the perifery of the door, using a three point contact latch proved to be the answer. On certain exit doors, panic hardware was used as the opening mechanism. Upon completion of the shell of the Operations Building in its normal fashion, the first shielding steps were taken. Pockets constructed of copper screen were placed on the ends of the floor beams, the flaps of which were later soldered to the wall shielding material. The wall and ceiling of the shielded area were covered with 24 by 24 copper screen mesh which fastened over the first furring strip. A continuous solder seam was made with the shielding material and around all vent openings, conduit pipes, copper tubes, and receptacles, and luminar boxes. The light dimmers were boxed in with copper screen as well as some steam pipes. As previously decided on the main R.F. wall, covering was brought down the sides of the walls to the cement foundation and overlapped a minimum of one foot into this plane. The remainder of the floor plane was covered with expanded metal lath. Solder seams were continuous on all copper to copper seams and on the floor plane from the wall to a distance inward of ten feet. From the ten foot perifery to the center of the room the expanded metal was spotted every six inches. The screening was brazed completely to the particular ground system in vogue, either a grid or multi-point ground system.

## III. SHIELDING EFFECTIVENESS TESTS

Upon completion of the shielding installation, a complete preliminary shielding effectiveness test took place. Test points required for the R.F. attenuation checks were at 200 KC for both electric and magnetic fields, 1 MC electric field, 18 MC electric field, 400 MC plane wave, 1000 MC plane wave, and 3 KMC microwave. Forty-five watt transmitters were utilized for all test points. Stoddart and Empire Devices field intensity equipment was used for the receiving instrumentation. The tests are conducted with loop, rod and tuned dipole antennae connected to the transmitter and receiver in the required frequency range. Magnetic field tests are performed to determine if seams and bonds were adequate to obtain a good R.F. contact. A good test is to compare readings obtained on two different bonds. If a difference of several DB is

noted, it usually can be attributed to poor soldering or brazing.

For the low frequency tests, 200 KC to 18 MC the receiving equipment was calibrated by placing the receiving antenna four (4) feet from the transmitting antenna. The relative strength of the particular field was recorded in DB. The transmitting equipment and antenna was then placed outside of the shielded enclosure. Except for the fact that the copper screen was now interposed between the two antennae, all other relative aspects and distances remained constant during this test. The difference in readings gave the shielding effectiveness in DB of the shielded enclosure. This test method was continuously repeated along the entire perifery of the room. Both magnetic field and electric field tests were conducted in this manner.

For the plane wave and microwave tests the transmitters were located approximately thirty (30) feet from the enclosure, and the calibration procedure repeated. The entire wall of the shielded enclosure was therefore bathe in a high frequency R.F. field. During these tests an entire section of wall could be probed and attenuation figures obtained.

After the successful preliminary tests, the interior of the Dark Room and Automatic Area are completed. A second furring strip is fastened over the copper screen and onto the first strip. Several methods are fesiable. One method is the use of plastic nails and resin adhesives. Dry wall is then fastened to the second furring strip and acoustic tile to ceiling. During the interim between the preliminary and final shielding effectiveness tests, some additions and modifications that may effect the attenuation figures usually are considered and action taken. The shielding consultant should remain on the scene while these changes are made. The final shielding effectiveness survey will test any of the modifications made.

## IV. CONCLUSIONS

From the experience and information gained from the testing of large military R.F. shielded areas, several conclusions can be drawn. To obtain optimiun attenuation with the shielding material used, the coverage of copper screen must extend at least one foot into the floor plane and not stop at the floor level as was previously specified. The number of personnel doors should be reduced to a minimum and the floor plan of the site should be so arranged as to have a personnel by-pass of the shielded area. This will keep entrance and entry to the automatic area to a minimum. The doors should be of the sterrated phosphorous bronze type with a three point pressure latch. Specifications should be modified to state that the entire vestibule, including the floor, be covered with copper screen. Installation of wave guide cores for vent openings would increase the frequency coverage and attenuation figures for the shielded area. Complete R.F. filtering of all power lines, and other signal lines, phone lines, etc., that enter the room would also enhance the attenuation figures. Re-routing of all unnecessary lines including telephone and power

lines would help to keep R.F. coupling into the shielded area to a minimum.

We hope the techniques used here, and recommendations made, will enhance future shielding effectiveness figures for similar sites.

ACKNOWLEDGMENTS

The author wishes to acknowledge the co-operation and helpful assistance rendered by Mrssrs. Lou Barnard, and John Woodhead of Jelco, Inc., Corp. of Engineers, and Erik A. Lindgren Associates, Inc.

## PART II - PREFABRICATED TYPE SHIELDED ENCLOSURES

### I. INTRODUCTION

We will now consider shielded enclosures of smaller size and of the demountable type. The requirements for a room of this construction will be guided by the following parameters: (1) frequency range through which the tests will be made; (2) ambient levels of interference present and their frequency range; (3) radiated and conducted susceptibility levels of instrumentation operating within the room; (4) military specification limits and requirements; (5) possible future sources of interference with estimates of frequency and intensity; (6) practical materials available for shielded enclosures; (7) power requirements; (8) various signal and metering input circuits; and (9) ventilation and lighting requirements.

### II. R.F. INTERFERENCE SURVEY

To obtain the answers to the afore mentioned parameters, a radio interference survey is conducted at the planned site of the shielded enclosure. Standard tests cover the frequencies from 14 KC to 1000 MC. The major sources of R.F. noise which will be encountered include switching transients of all kinds, ignition noises, electrically functioning production equipment such as welders, dielectric heaters, induction heaters and all other items that generate R.F. energy intentionally or not. If equipment at the site is known to generate R.F. energy above or below the standard test frequency spectrum, consideration should be made in chosing the shielding material to provide adequate R.F. attenuation at these frequencies. Problems will arise if the R.F. susceptibility level of the instrumentation that is to be used in the shielded enclosure is high. Frustrations and errors will be the result of attempts to make accurate measurements under these conditions. To guard against this occurrence extra care must be taken in deciding on the kind of shielding material, and type of room and filters that will be used. The decision is usually made after the R.F. survey. To illustrate by example: From the survey a maximum reading of 1.0 volts per meter at 1MC is recorded. The R.F. radiated susceptibility level for the instruments within the room is 1.0 microvolts per meter. It sufficies to say a 120 DB is required.

Two important requirements are placed on shielded enclosures by certain military specifications. One requirement to facilitate antenna tuning, is the size of the room. A minimum room with dimensions of 20 feet by 10 feet by approximately 12 feet high is called for. The other requirement is that the ambient level present in the shielded room be 6 DB down from the specification limits.

## III. CONSTRUCTION

There are three (3) popular types of room construction now in vogue: (1) single-layer shielding, (2) cell type shielding, and (3) double-layer insulated shielding. The latter is the most sophisticated of the three.

All of the above are constructed in sections so that they are transportable and demountable. (See Figure 1.)

## IV. PRACTICAL MATERIALS

Materials which provide sufficient effectiveness at various frequencies are copper, bronze and galvanized sheet iron. Copper and bronze screening are available, but a mesh less than 18 by 20 should not be used and wire diameter should be a minimum of 0.011 in. The lowest frequencies at which a given shielding effectiveness is required normally determine the type of material to be used. Ferrous materials produce more shielding effectiveness at power frequencies than do non-ferrous materials. Examples of materials having high shielding effectiveness at low frequencies are netic and co-netic materials, while galvanized sheet iron has medium shielding effectiveness at the lower power frequencies. The accompanying table shows shielding effectiveness of a given material at a given frequency.

Non-ferrous materials are used to attenuate magnetic fields at higher frequencies. Here, shielding effectiveness is dependent upon material thickness and must be related to the frequency.[1]

When a given material is decided upon, an increase in shielding effectiveness may be had by increasing the thickness of the material. However, doubling thickness will only increase shielding effectiveness by 6 DB. To increase shielding effectiveness and still not materially increase thickness of the material required, multiple-shielded enclosures are used. If, instead of doubling thickness of the single shield, another shield of the same thickness as the first is placed around the second, with a spacing of approximately 2 in. and isolated electrically from the first, shielding effectiveness of the room should theoretically be increased by the same amount as the shielding effectiveness of the first shield. Distance between the two shields and discontinuities in the shield will decrease total shielding effectiveness slightly. Magnetic field test results of single and double electrically isolated enclosures of copper screening and 3-oz. copper foil are shown in Figure 2. Placing both layers of this material one

on top of the other would have resulted in only a 6 DB increase in shielding effectiveness.

## V. POWER REQUIREMENTS

When bringing AC power into a shielded enclosure, a line filter must be employed which will allow power frequencies to enter but attenuate all other undesirable frequencies. Standard commercial line filters are available with attenuations on the order of 100 DB. These filters are normally placed outside the shielded enclosure. At times, 100 DB attenuation is insufficient to remove the unwanted signals from the power line. To provide higher attenuations, a series of filters has been developed by Elite Electronic Engineering Company. These line filters are divided into two sections. One section is used outside the enclosure and the second section inside. Each filter section has a minimum attenuation of 60 DB through its effective frequency range. Placing both filter sections in series gives an attenuation of 120 DB, or more (Figure 3). Filters made in this manner can be used on single-shield enclosures, double-shield enclosures or cell-type enclosures. When line filters are to be used at frequencies of 400 cps or more, an investigation should be made into the amount of reactive power drawn by the filter. Many filters may draw more current than the 400 cps generator can handle.

## VI. METERING AND INPUT CIRCUITS

Another shielding discontinuity is introduced by insertion of an R.F. feedthrough. An important requirement of the feedthrough connector is that it must allow a specific R.F. current, if required for testing, to enter or leave the shielded enclosure with minimum loss.

The UG-30/U Type N feedthrough adapter exhibits a nominal impedance of 50 ohms and can be used as a feedthrough connector. This feedthrough is ideal for single-shield bulkhead mounting. When multiple shields are used, a special panel must be installed to provide a single shield at the point of R.F. connector entry. In cell-type enclosures, this can decrease enclosure shielding effectiveness at this point. In double electrically insulated enclosures, there may be a decrease in attenuation because of the single layer plus associated multiple connections between inner and outer shields. To alleviate this situation, a special R.F. feedthrough connector was designed by Elite to maintain isolation between both inner and outer shields, and still present a nominal impedance of 50 ohms. The EL-5100-N Uni-Ground Feed-Through enables R.F. connectors to be placed in any location or in any panel in a multi-layer shielded enclosure. Use of a ferrite sleeve over the coaxial conductor also prevents intense external high frequency radiation from entering the shielded enclosure. UHF connectors or BNC connectors are not recommended if a minimum VSWR is desired of the R.F. feedthrough connector.

## VII. VENTILATION

Ventilation openings, if improperly designed, could cause a serious reduction in shielding effectiveness. The amount of air entering or leaving the enclosure is based upon the amount of heat that must be extracted from the room due to electronic equipment in operation, plus the number of operators present during testing. Another ventilation consideration is the amount of R.F. attenuation presented by a particular opening. Screened openings usually have to be extremely large in area to permit sufficient air to flow through the fine mesh required to prevent R.F. leakage. When frequencies above 1000 MC need not be attenuated to a high degree, a multi-layer opening of 1/4 inch copper mesh rapidly decreases in effectiveness. A ventilating opening must then be designed as a waveguide attenuator operating below cutoff at its lowest propagating frequency. In this manner, shielding efficiencies of up to 100 DB can be obtained at frequencies of 10,000 MC. A 1/4 inch diameter tube 1 inch in length would have approximately 102 DB shielding effectiveness at 10,000 MC. A 1/2 inch diameter tube 2-1/4 inch long would give approximately 100 DB effectiveness at 10,000 MC. Openings 1 inch or more in diameter would have little or no attenuation at 7000 MC.[2] To obtain an opening of sufficient size to admit the required volume of ventilating air, these tubes are placed side by side until sufficient air flow is achieved.

## VIII. ILLUMINATION

Lighting requirements can be most easily met by using incandescent sources. This type of lighting normally does not produce any interference. However, in a large enclosure, the heating effect of a sufficient number of lights to produce the required illumination could cause a heat dissipation problem. Fluorescent lamp fixtures are available that are both filtered and shielded. Unfortunately, these fixtures must be considered carefully because the remaining amount of interference present may affect test results obtained in the shielded enclosure.

## IX. TESTING THE ENCLOSURE

After the enclosure has been selected and lighting, ventilation and electrical power inputs considered, a series of tests must be performed to determine if enclosure attenuation requirements are met. These three tests, described below, are made with rod, loop and tuned dipole antennae connected to the transmitter and receiver in the required frequency range.

Magnetic field tests are normally performed in the frequency range of 14 to 200 KC. Tests through this frequency range will determine if the bonds are under sufficient pressure to obtain a good R.F. contact. A good means of comparison for determining whether the seams are making electrical contact is to perform a magnetic field test in the middle of the panel and then

test adjacent seams. If a difference of more than 1 or 2 DB is noted between mid-panel and seam readings, a high R.F. impedance is probably the cause. This can be eliminated by tightening the seams and making another check.

Electric field tests are helpful in determining if there is inadequate bonding of the filters to the shielded enclosure or leakage through the filters themselves. Electric field tests are normally made in the frequency range of 15 to 25 MC.

Plane-wave tests are effective in determining if attenuation in the frequency range of 400 to 1000 MC is sufficient to maintain the shielding effectiveness of the enclosure. The enclosure in subjected to a high intensity field in this frequency range by means of a 45 watt transmitter and tests are made inside the enclosure to determine if there is adequate attenuation. If interference is conducted inside the enclosure, the power line inputs should be throughly investigated. Insufficient decoupling of line filters in multi-layer shielding is usually the problem. When filtering is placed on one side of the enclosure only, as in the conventional line filter, interference may be doupled back in the power line and re-radiated inside the shielded enclosure. With the second section of a two section line filter on the inside shield, any interference induced in the line around the first filter section is further attenuated, permitting more effective use of the shielding effectiveness of the enclosure's inner shield.

With these various aspects of shielded enclosures in mind, the design engineer is better equipped to specify the type of shielded enclosure required for a specific application. [3]

## REFERENCES


1. Total shielding effectiveness of a given material at a given frequency is penetration loss plus reflection loss in DB. For penetration loss (shield effectiveness), see Electronic and Radio Engineering, F. E. Terman, McGraw-Hill Book Company, New York, pp 23, 36; for reflection loss, see Report NADC-EL-54129, U. S. Naval Air Development Center, Johnsville, Pa., p 15.

2. "Designing Noise-Free Enclosure Openings," Arnold L. Albin, Electronics Buyers' Guide, June 1959.

3. Taken in part from "Practical Aspects in Evaluating Shielded Rooms" Electro-Technology, June 1961, James C. Klouda.

TYPES OF SHIELDED ENCLOSURE CONSTRUCTION

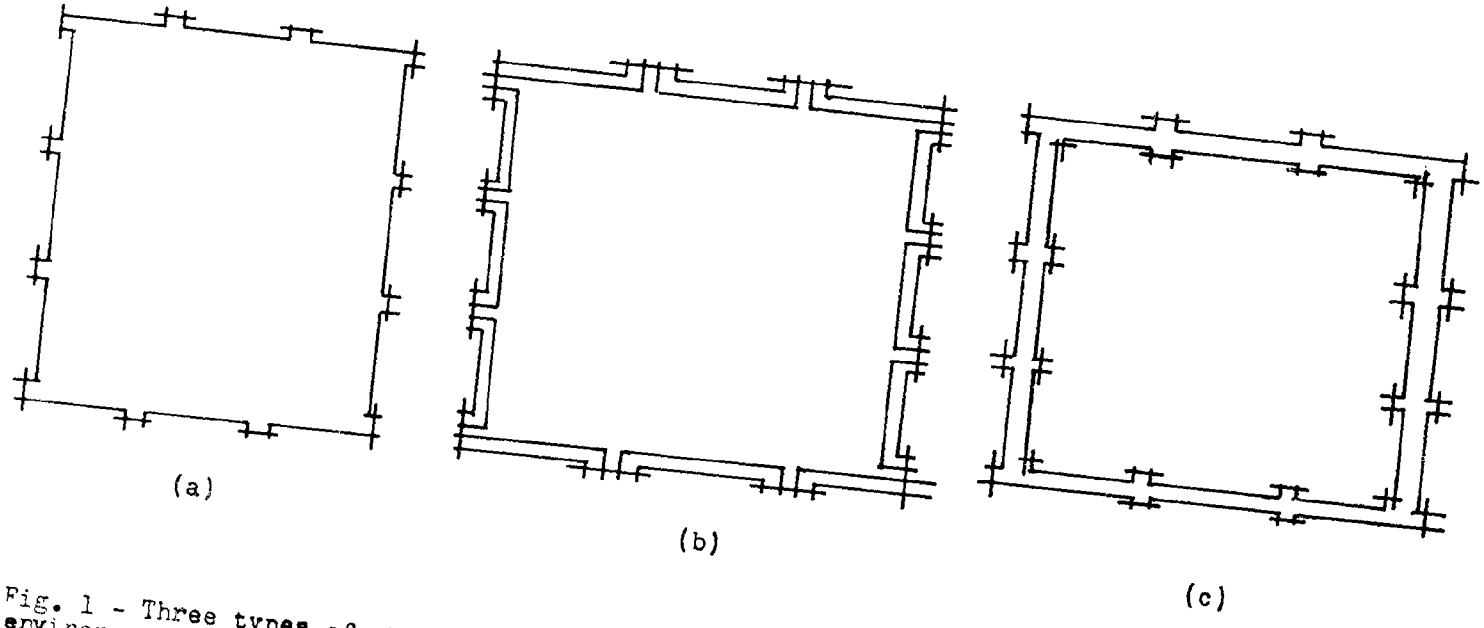



Fig. 1 - Three types of shielded enclosures used to provide an interference-free test environment: (a) single-layer shielding; (b) cell-type shielding; (c) double-layer insulated shielding.

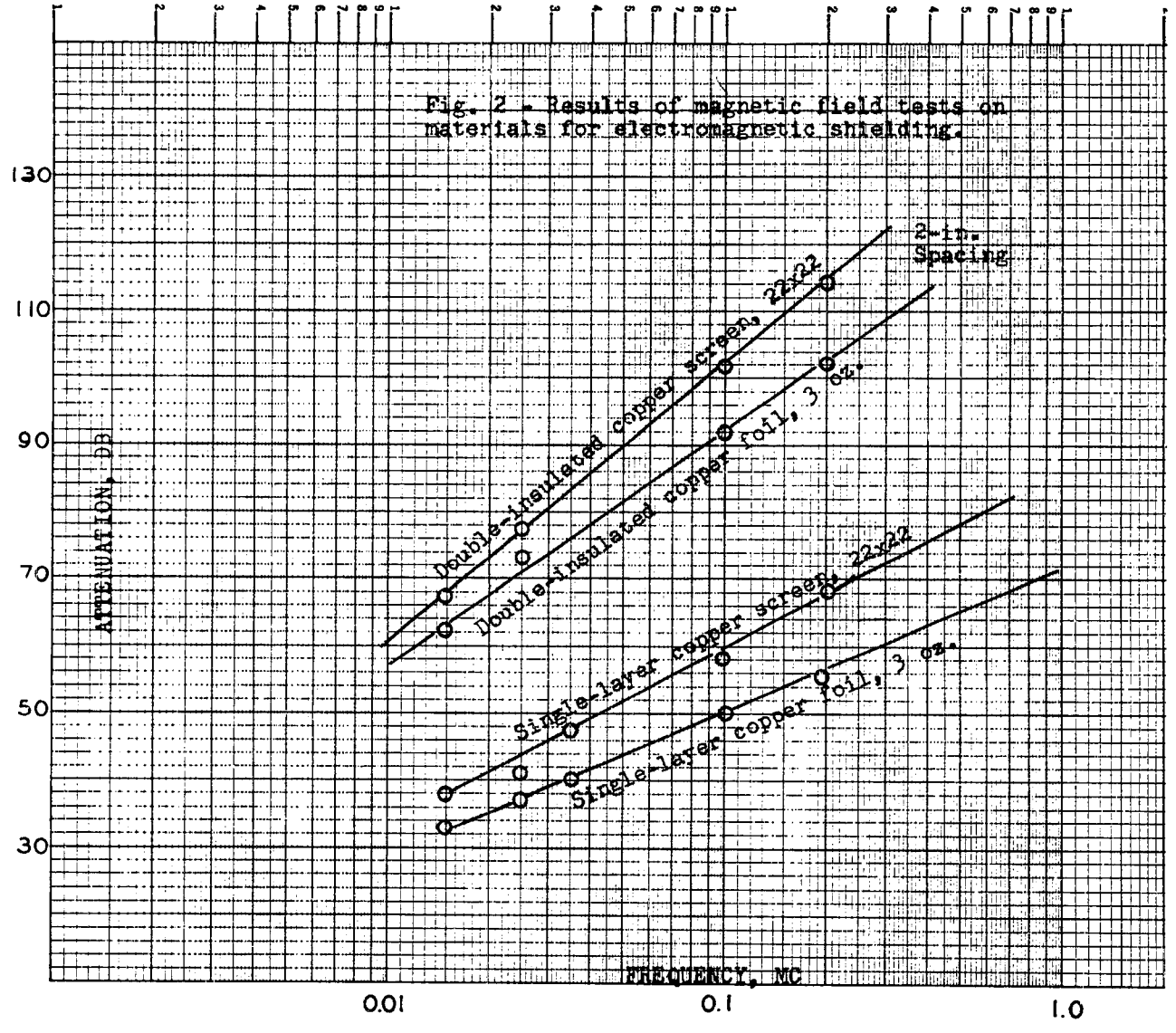



Fig. 2 - Results of magnetic field tests on materials for electromagnetic shielding.

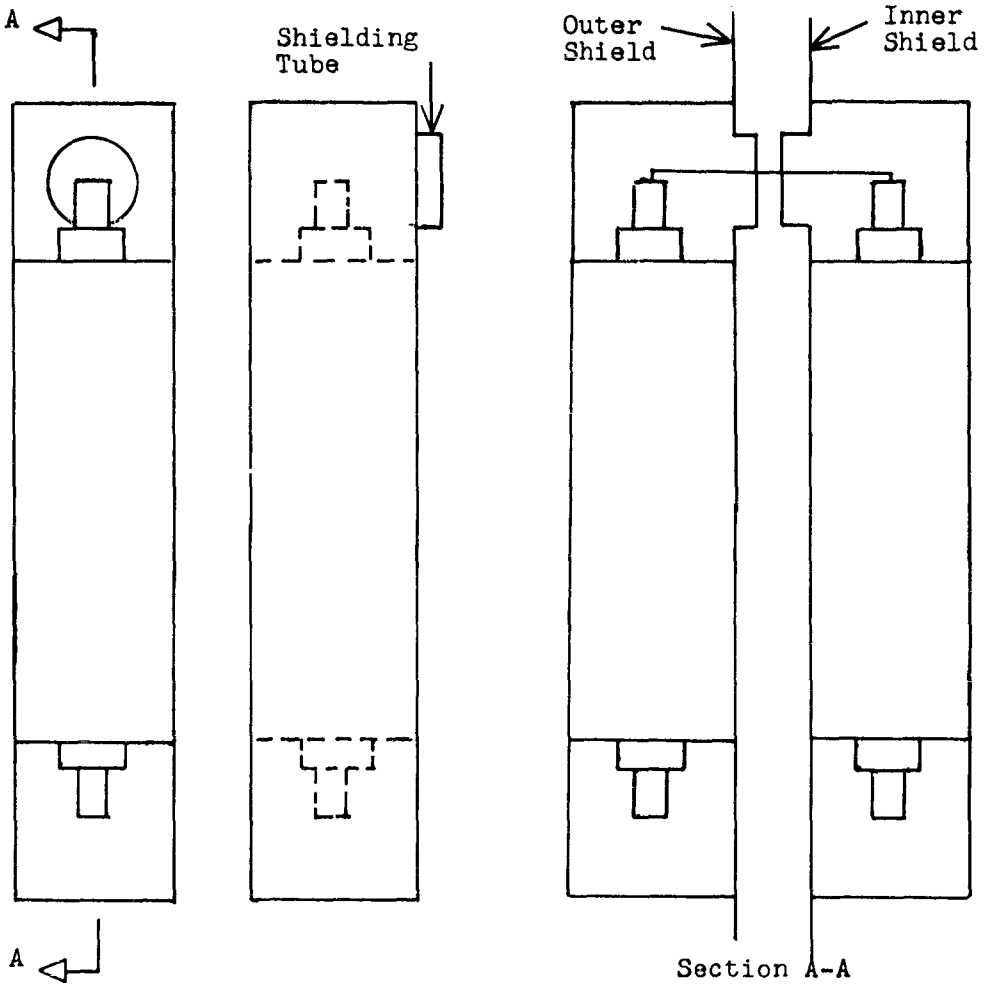



Fig. 3 - Double-section r-f line filter for shielded test enclosure. A small tube is connected to each of the filters, as they enter the shielded enclosure, to prevent radiation from leaking around the filter. In the double electrically insulated enclosure, the tube prevents multiple conducting paths which tend to reduce enclosure shielding effectiveness.

## SHIELDING EFFECTIVENESS OF VARIOUS MATERIALS

| MATERIAL (SINGLE-LAYER) | SHIELDING EFFECTIVENESS DB |
|---|---|
| 0.032-in. COPPER | 55 |
| 0.003-in. COPPER | 29 |
| 22 x 22 MESH COPPER | 35 |
| 18 x 20 MESH BRONZE | 24 |
| 0.032-in. GALVANIZED IRON | 64 |
| 1/4 x 1/4-in. MESH GALVANIZED IRON | 12 |

(COMBINES BOTH PENETRATION LOSS AND RE-FLECTED LOSS. VALUES OBTAINED BY TEST MADE AT 15 KC IN A MAGNETIC FIELD.)

# A POLARIZED DISSIPATIVE RFI SUPPRESSION FILTER

F. N. Hansen
McMillan Industrial Corporation
Ipswich, Mass.

Abstract. - A new filter is described, whereby series inductance and distributed shunt capacitance are combined with electrical loss in a compact device without the use of lumped parameter reactive components and without obtaining the undesirable peaks and valleys which usually characterize the attenuation performance of lumped parameter circuits when plotted in the frequency domain. The addition of a feed-through capacitor on one end acts to polarize this filter, thus obtaining desirable performance for noise suppression at a magnetron.

The filter described in this paper helped solve an unusual RFI-suppression problem. A commercial system designed by a leading electronics manufacturer contained a 2,000 watts magnetron operating at 2,400 mc. Initial design included a metal cage over the magnetron to contain the electromagnetic radiation. The filament leads, fed through the metal housing by means of high voltage ceramic isolators (10,000 WV pulse) supplied the magnetron with about 32 amp. 60 cps filament current and served as negative return for the high voltage. (See Fig. 1.).

It is generally known that these filament-leads incline to transfer RF-energy to the outside of the system. Since this power is radiated, conducted along power lines, also damaging the filament transformer, it is an undesired source of Radio-Interference with communication equipment located at the environment of the magnetron operated apparatus. The usual measures to reduce the RFI by means of applying external chokes and bypass capacitors, shielding of the leads, lead dressing, etc. were not applicable in this case. Finally it was tried to replace the feed-through isolators by feed through capacitors, designed to stand the high voltage. (See Fig. 2)

The RFI-energy conducted along the filaments was reduced to a certain degree. This solution however did not seem practical since, apparently because of reflections, standing waves originated inside the magnetron housing, arcing and sparking on all joints and screws. (Fig. 2)

Therefore, a filter was designed based on the principle of a commercial type of the McMillan Radio - Interference - Suppression filters (B-25). This filter is in its function different from the usual UHF-Microwave filters. (Fig. 3) Series inductance and distributed shunt capacitance are combined with electrical loss in a compact device without the use of

lumped parameter reactive components and without obtaining the undesirable peaks and valleys which usually characterize the attenuation performance of lumped parameter circuits when plotted in the frequency domain.

Before the mechanism of this filter will be discussed further, some results and operational characteristics obtained may be produced.

Fig. 4 shows the attenuation characteristic of a simple filter of this kind. The curve designated "A" shows the attenuation of the filter designed for the above mentioned application. Extremely high voltage requirements combined with rather high current capacity, also elevated temperature on the magnetron housing as such have reduced the electrical length of this filter. The curve designated as "B" offers the attenuation of a regular power line filter for 25 amp., 250 WV, 0-400 cps of about the same geometrical length (about 8 inches).

Fig. 5 (Slide 4) presents a simple sketch of the new lossy filter compared to the generally known lossy line in UHF-techniques. The lossy filter is shown in its simplest form as straight inner conductor for better comparison. The sketch is self-explanatory showing the old lossy line with its resistive inner conductor and shield. The VSWR is well retained; the power transfer is limited. It works like a pad also for the power frequency.

The new filter is designed to transfer power as efficiently as possible, still suppressing undesired superposed high frequencies. Therefore, inner and outer conductors are highly conductive. The losses are produced in the mold between it. The optimum arrangement of its parameter:

$\mu$ = magnetic permeability
$\varepsilon$ = dielectrical constant
$\tan\delta$ = loss tangent
$\ell$ = geometric dimensions

allows the suppression of RFI to an extremely efficient degree.

## SUMMARY

Besides the described application this new principle of designing RFI-suppression filters has found numberless different applications in power installation, electronic instrumentation and aircraft.

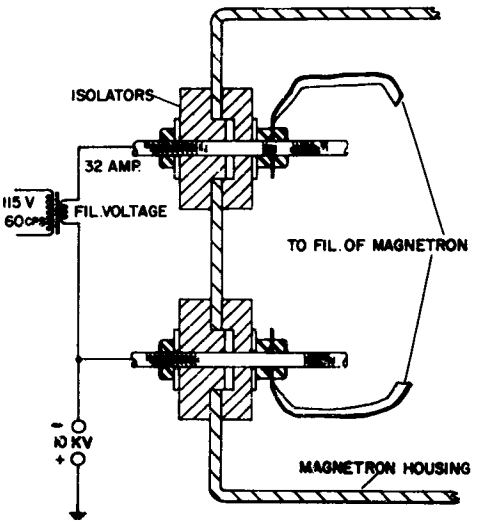

ISOLATORS
32 AMP.
115 V
60 CPS
FIL. VOLTAGE
TO FIL. OF MAGNETRON
10 KV
MAGNETRON HOUSING

FIG. I

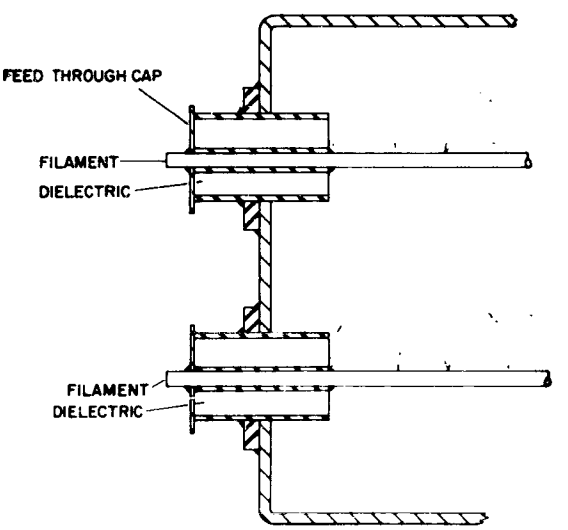

FEED THROUGH CAP
FILAMENT
DIELECTRIC
FILAMENT
DIELECTRIC

FIG. 2

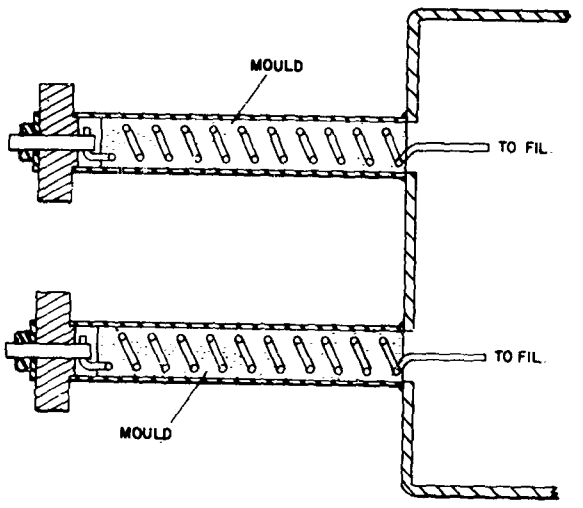



Fig. 3

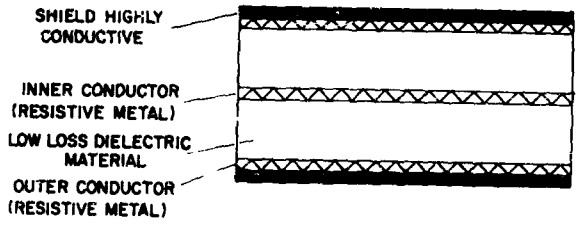



Fig. 4

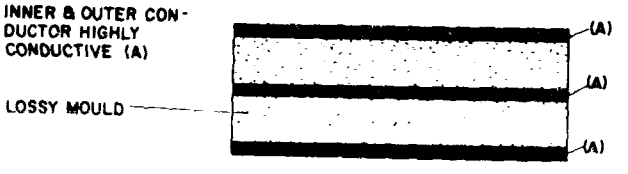
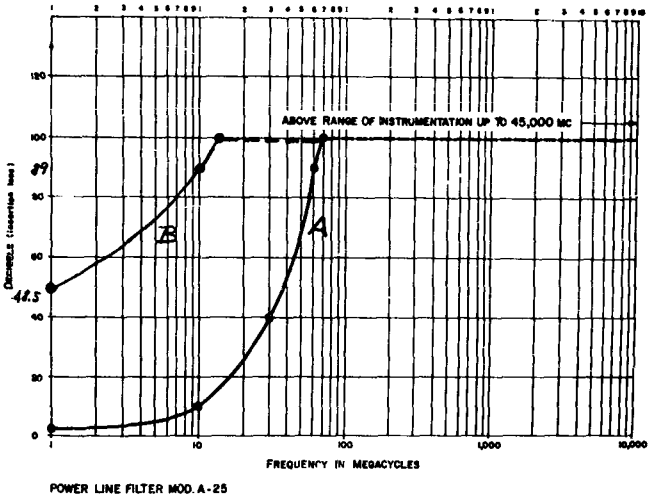



Fig. 5




POWER LINE FILTER MOD. A-25

FIG. 5

# SHIELDING EFFICIENCY CALCULATION METHODS FOR SCREENING, WAVEGUIDE VENTILATION PANELS, AND OTHER PERFORATED ELECTROMAGNETIC SHIELDS

W. Jarva

Filtron Company, Inc.

Flushing, N. Y.

Abstract. - The basic procedures for calculating the shielding efficiency of continuous metallic shields, which were originally developed by S.A. Shelkunoff, have been found to apply equally as well to perforated shields. Methods are developed for calculating the shielding to be expected from discontinuous shields having a wide range of different physical structures, and results are compared with values measured in the laboratory. Theoretical explanations are provided for test results obtained by some investigators, which are essentially independent of frequency, whereas results obtained by others vary radically with frequency. The methods provide means for determining the polarizability of rectangular openings and also permit computation of the difference in shielding measurements obtained with antennas placed close to or far from the shielding barrier.

## I. INTRODUCTION

Many problems arise not only in the field of radio interference but throughout the electronics industry where estimates are required of the percentage of electromagnetic energy that may pass through or be reflected from a perforated metallic surface. The perforations may be part of the equipment design or may be unintentional, and can range from a single opening to many openings per square meter of surface. A few examples are openings in waveguide ventilation panels, radar antenna reflectors, coupling openings between waveguides or resonant cavities, and flaws in shielded enclosures.

In addition to the large number of variables that can exist in the perforated surfaces, other variables due to the environment in which the barrier is to operate must be considered. These variables are functions of such things as distance from the radiating source, type of radiator, type of equipment requiring shielding, and location of the equipment with respect to the barrier.

## II. BASIC SHIELDING EQUATIONS

In accordance with the methods of Schelkunoff,[1] leakage through openings in metal shields has been treated from the viewpoint of transmission line theory. In order to obtain satisfactory estimates of the efficiency of a wide variety of perforated shield designs, it

was found necessary to account for attenuation, reflections, opening area, skin-depth effects, and coupling between closely spaced openings. The shielding efficiency in decibels is expressed in simplified form for ease of engineering application as follows:

$$S_a = A_a + R_a + B_a + K_1 + K_2 + K_3 \quad (1)$$

where

$A_a$ = aperture attenuation = $27.3 \frac{D}{W}$ for rectangular apertures (2)

= $32 \frac{D}{d}$ for circular apertures (3)

D = depth of apertures in inches

W = width of rectangular apertures in inches. For relationship of aperture dimension W to direction of fields, see Figure 1.

d = diameter of circular apertures in inches

$R_a$ = aperture reflection losses

$$= 20 \log_{10} \frac{\left|1 + k\right|^2}{4|k|} \quad (4)$$

$k = \frac{Z_a}{Z_w}$ = ratio of the aperture characteristic impedance to the impedance of the incident wave

= W/3.142r for rectangular apertures and magnetic fields (5)

= d/3.682r for circular apertures and magnetic fields (6)

= jFW $1.7 \times 10^{-4}$ for rectangular apertures and radiated fields (7)

= jFd $1.47 \times 10^{-4}$ for circular apertures and radiated fields (8)

F = frequency in megacycles per second

r = distance from signal source to shield in inches

$j = \sqrt{-1}$

$B_a$ = correction factor for aperture reflections which becomes significant when $A_a$ is less than 10 db

$$= +20 \log_{10} \left| 1 - \frac{(k-1)^2}{(k+1)^2} \; 10^{-\frac{A_a}{10}} \right| \tag{9}$$

$K_1$ = correction factor for the number of openings per unit square when the test antennas are far from the shield in comparison to the distance between holes in the shield. For other distances, see under derivations.

$$= +10 \log_{10} \frac{1}{an} \tag{10}$$

a = area of each hole in square inches

n = number of holes per square inch

$K_2$ = correction factor for penetration of the conductor at low frequencies

$$= -20 \log_{10} \left[ 1 + \frac{35}{p^{2.3}} \right] \tag{11}$$

where p = ratio of the wire diameter to skin depth for screening

= ratio of the skin depth to conductor width between holes for perforated sheets

$$\text{Copper skin depth} = \frac{2.6 \times 10^{-3}}{\sqrt{F}} \text{ inches}$$

$K_3$ = correction factor for coupling between closely spaced shallow holes

$$= +20 \log_{10} \frac{1}{\tanh\left(\frac{A}{8.686}\right)} \tag{12}$$

## III. DERIVATIONS

### Attenuation Calculations ($A_a$)

The first three terms of Equation (1) are equivalent to the equations given by Schelkunoff for continuous metal shields. In Schelkunoff's equations, A represents the attenuation as the wave passes through the metal, whereas in Equation (1), $A_a$ represents the attenuation as the wave passes through the aperture which, for frequencies below cutoff in rectangular guides, is given in reference (1) as:

$$A_a = \frac{\pi D}{W} \sqrt{1 - \left(\frac{f}{fc}\right)^2} \text{ nepers} \tag{13}$$

where f and $f_c$ are the frequency under consideration and the cutoff frequency, respectively. It will be observed from Figure 1 that W is always that hole dimension perpendicular to the E field. Conversion of Equation (13) to decibels for frequencies well below cutoff provides Equation (2) and a similar procedure for circular guides provides Equation (3).

### Reflection Calculations ($R_a$)

Schelkunoff gives reflection losses as being a function of the ratio of the metal intrinsic impedance to the incident wave impedance. Similarly in Equation (4), the reflection losses are calculated as a function of the ratio of the waveguide characteristic impedance below cutoff to the incident wave impedance. The characteristic impedance of a rectangular waveguide well below cutoff is:[1]

$$Z_a = \frac{j\omega\mu W}{\pi} \tag{14}$$

The impedance of the wave emitted by a small loop source at points close to the source compared to a wavelength is:[2]

$$Z_w = j\omega\mu r \tag{15}$$

Taking the ratio of Equation (14) to Equation (15), we have:

$$k = \frac{W}{\pi r}$$

which is the equation for k given by Equation (5) for magnetic fields.

Both Equations (14) and (15) are in MKS units, but in taking the ratio, W and r may be expressed in either inches or meters. Similar procedures provide Equations (6), (7), and (8).

## Corrections to Reflection Calculations ($B_a$)

This factor is given by Schelkunoff for metal shields as:

$$B = 20 \log_{10} \left| 1 - \frac{(k-1)^2}{(k+1)^2} e^{-2\sigma t} \right| \qquad (16)$$

where $\sigma$ and t are, respectively, the complex propagation constant and the thickness of the shield in MKS units. In a waveguide below cutoff, the phase constant approaches zero and the propagation constant becomes equal to the attenuation constant, so that $e^{-2\sigma t}$ becomes equal to the reduction in signal intensity in nepers for twice the depth of the waveguide. The expression $e^{-2\sigma t}$, therefore, may be expressed in decibels and is equal to $10^{-\frac{A_a}{10}}$ which converts Equation (16) to Equation (9).

## Corrections for the Number of Openings that Must Be Considered ($K_1$)

It is obvious that when electromagnetic signals pass through a metal shield by penetration of openings, the amount of power that is transferred from one side of the shield to the other is a function of the number of openings. Not so obvious is the fact that if insertion loss tests are made of the shield, the results will be a function of the distance between the antennas and the surface of the shield, assuming the shield to be centrally located between the antennas. If small antennas of approximately the same size as the openings or smaller are used for test, and they are located on each side and adjacent to one of the openings, the measured shielding efficiency will be that of the opening itself. On the other hand, if the antennas are located at a large distance from the shield in comparison to the distance between holes in the shield, the measured shielding efficiency will be equal to that of a single opening plus the ratio (in decibels) of the total wall area illuminated by the radiator to the total opening area located in the illuminated region. If the openings are evenly distributed, this ratio is a constant, since any change in the wall area illuminated will cause a similar change in hole area. Therefore, the minimum shielding efficiency becomes that of the single opening plus the correction factor of Equation (10). At intermediate points, the shielding efficiency lies between the two values.

Both values are of practical importance. The shielding efficiency near the shield is important for protection of sensitive equipments which may be placed close to the walls (data cables, etc.) and it is specially important in cases where radiation hazards may exist so that personnel are protected who otherwise may unknowingly enter a strong field existing in the vicinity of a poorly designed seam. Calculations of the shielding efficiency in the interior parts of a structure are important since, if advantage is taken of the added shielding efficiency, a considerable reduction in cost of shield construction can be achieved.

## Low Frequency Corrections for Screen-Type Shields ($K_2$)

Numerous tests have shown that the high-frequency shielding efficiency of screening materials can be satisfactorily approximated by assuming that the openings in the screen are equivalent in size to the openings in a flat perforated metal sheet, and the depth of the openings is equal to the wire diameter. At low frequencies when the skin depth becomes comparable to the radius of the wire, a considerable loss in shielding efficiency occurs. This may be considered from the viewpoint that the apertures as waveguides are made wider[3] and shorter by a skin depth. However, this approach runs into difficulty when the skin depth becomes equal to or greater than the wire radius since this is the borderline region where leakage through the metal itself also must be considered. In order to maintain reasonable simplicity for calculation purposes, the test results for a variety of copper screen shields were plotted as a function of skin depth, and an empirical equation was derived for the correction factor as given by Equation (11). It is probable that this correction factor will also be satisfactory for perforated sheet metal, but no test data are available for corroboration.

## Corrections for Closely Spaced Shallow Openings ($K_3$)

When the apertures in a shield are closely spaced and the depth of the openings is small compared to the width, the shielding efficiency has been found to be greater than otherwise would be expected. This is interpreted as being a result of coupling between adjacent holes which becomes important when the attenuation through the openings is small. Considering two such adjacent holes, subjected to an electromagnetic field, it appears that the current induced on the conductor between the holes can flow into one side of a hole and return immediately via the adjacent hole -- in effect merely encircling the conductor. Since the current is the same in closely spaced holes, this is equivalent to placing practically a dead short circuit at the

end of each hole considered as a waveguide. The impedance of the short may be approximated for rectangular holes by the surface impedance presented by the surface of the conductor between the holes,

$$Z_L = \sqrt{\frac{j\omega\mu}{g}} \quad \frac{a}{b} \tag{17}$$

where $\sqrt{\frac{j\omega\mu}{g}}$ is the metal intrinsic impedance (MKS units)

$j = \sqrt{-1}$

$\omega = 2\pi f$

$\mu$ = permeability of the metal = $1.26 \times 10^{-6}$ henries/meter for copper

$g$ = conductivity of the metal = $5.8 \times 10^{7}$ mhos/meter for copper

Direction of the fields and current, and dimensions a and b are shown in Figure 2.

The characteristic aperture impedance given by Equation (14) is $\frac{j\omega\mu W}{\pi}$ at all frequencies being considered. The ratio of $Z_L$ to $Z_a$ is, therefore,

$$\frac{Z_L}{Z_a} = \sqrt{\frac{j\omega\mu}{g}} \quad \frac{a}{b} \quad \frac{\pi}{j\omega\mu W} = \frac{a\pi}{bW}\sqrt{\frac{1}{j\omega\mu g}} \tag{18}$$

At frequencies as low as 10 kc, the expression under the radical is smaller than $10^{-6}$ showing that for all reasonable opening dimensions and any frequency of interest, $Z_L$ is much smaller than $Z_a$.

In accordance with transmission line theory, the input impedance of the guide may be calculated by:

$$Z_i = Z_a \quad \frac{Z_L \cosh\alpha + Z_a \sinh\alpha}{Z_a \cosh\alpha + Z_L \sinh\alpha} \tag{19}$$

where $\alpha$ is the waveguide attenuation in nepers.

Since for the express condition being investigated $\alpha$ is small, and since $Z_L \ll Z_a$, Equation (19) simplifies to:

$$Z_i = Z_a \frac{\sinh \alpha}{\cosh \alpha} = Z_a \tanh \alpha \tag{20}$$

The ratio of the intensities of the reflected wave to the transmitted wave when the attenuation is large is equal to:

$$\frac{(Z_w + Z_a)^2}{4 Z_w Z_a} \tag{21}$$

When the attenuation is small, the ratio becomes:

$$\frac{(Z_w + Z_i)^2}{4 Z_w Z_i} \tag{22}$$

For all practical purposes, the wave impedance $Z_w$ is always much larger than either $Z_a$ or $Z_i$, and the ratio of Equations (22) to (21) reduces to:

$$\frac{Z_a}{Z_i} = \frac{1}{\tanh \alpha} \tag{23}$$

Expressing Equation (23) in decibels provides the correction factor for closely spaced shallow holes as given by Equation (12). It will be observed that since $Z_a$ is always larger than $Z_i$ for $A_a$ equal to 10 db or less, the correction factor is always positive and increases the shielding efficiency.

## IV. COMPARISONS WITH MEASUREMENTS

The results of tests made by many groups who are, or have been, active in shielding work are available for comparison purposes. Many tests have also been made at Filtron on a variety of perforated shields. Unfortunately, standard methods of test have not been devised, which are acceptable to everyone, so that the results obtained must be interpreted in each case in the light of the test methods. In order to clarify the reasons for variations in test results, some discussion is required of test methods.

## Discussion of Test Methods

The methods used for laboratory tests at Filtron consisted entirely of insertion loss tests made with small (3-inch diameter) shielded loops. Primary advantages of the small-loop method are the ability to test small samples, minimizing of environmental reflection effects, and derivation of the shield quality under the most rigorous conditions that could be encountered in actual use. The loops are co-planer and are located with 3.5 inches between loop centers if the thickness of the test sample permits. Co-planer orientation of the loops permits estimates of the wave impedance to be made for calculation of reflection losses. The field emitted in the plane of the loop causes a unidirectional current to flow on the test sample at the point between the loops, and tests that area with a wave having essentially the impedance of a wave from an infinitesimal loop located at the same distance as the center of the test loop.

Some experimenters have used coaxial loops; however, this method of test has a number of disadvantages. The field emitted in the direction of the loop axis causes a circular current to be induced on the test sample. If a straight seam is under test, currents flow in opposite directions over the top and bottom halves of the seam. The wave impedance in the axial direction is zero on the axis and gradually increases with distance from the axis so that the impedance ratios vary from point to point and reflections are difficult, if not impossible, to calculate. In general, tests made with coaxial loops should give lower insertion loss values because of the lower wave impedance and, consequently, lower reflection losses.

Many tests have been reported using antennas housed in metal enclosures. In this case, if the antennas are located deep within the enclosures so that they are far from the test sample in comparison with the dimensions of the enclosures, the test becomes equivalent to an insertion loss test in a waveguide transmission line. The wave impedance becomes equal to the characteristic impedance of the guide for the particular mode being generated. This is particularly significant for tests made with high-impedance antennas. The presence of the metallic enclosure so reduces the wave impedance that the reflection losses become far less than expected with such antennas.

Testing of shielded enclosures for plane waves use the radiation field, and necessitate the use of reasonably efficient antennas separated a considerable distance compared to a wavelength. Use of highly directive antennas, such as helixes or dipoles, with a corner reflector provide highly repeatable and accurate test results. On the other hand, antennas such as the half-wave dipole are so subject to reflections from surrounding objects, observers, etc., that the reliability of the results becomes largely a function of the experience and capability of the testing personnel themselves.

## Metal Screening Tests

Low Impedance Tests. Figures 3 and 4 show the shielding efficiency of 16, 22, 40, and 60 mesh copper screening as measured with co-planer loops. For comparison, four calculations are provided for each curve. Calculations in this case were made with Equations (2), (4), (5), (9), (10), and (11). The agreement between measurements and calculations is within 5 db and in most cases is considerably better. It will be observed that all the curves exhibit a characteristic dip in the region of 200 mc. This is probably due to the loop wave impedance becoming complex, since the current around the loop perimeter is no longer constant.

Figure 5 gives the insertion loss obtained with No. 2 mesh copper screen, again measured with co-planer loops. These tests demonstrate the coupling between shallow closely spaced openings. Calculations were based on Equations (2), (4), (5), (9), (10), (11), and (12), and are in good agreement with the measurements, although the calculations were very nearly equal at 10 mc. The wire diameter was large, so that low-frequency skin depth corrections were small as shown by the flatness of the curves. The somewhat erratic nature of the curves is probably due to the nonhomogenous character of the shields and coupling effects permitted by the low attenuation. Similarity of the curves indicates the presence of some variables in this special case, which are not accounted for in the calculation methods. Since practically all the shielding efficiency is due to reflection losses, the relative changes in the complex guide impedance and complex wave impedance have an accentuated effect at the higher frequencies.

Table 1 shows the shielding efficiency of No. 22 mesh copper screen as given in AFM 100-35.[4] In this case, calculations are slightly high at 1 and 10 mc. The methods of measurement are not known, but comparison with the curve in Figure 3 shows the values are slightly less than those obtained with co-planer loops, and probably the tests were made with the coaxial loop method. The calculation methods were the same as used for Figures 3 and 4.

Plane Wave Tests. Table 1 also lists the measured plane wave shielding efficiency for No. 22 mesh copper screen. Calculations using Equations (2), (4), (7), and (10) give good agreement at the mid frequencies, with a progressively greater disagreement at the lower and higher frequencies. This is expected at the low frequencies because no correction factor was applied for penetration of the conductor. (The factor $K_2$ was derived for loop tests.) Since the details of the methods of test are unknown, no explanation can be offered for the high-frequency discrepancy.

High Impedance Tests. Test results listed in AFM 100-35 as high-impedance measurements are also given in Table 1. The calculations which were made in this case assumed that the actual wave

impedance used in the test setup was equal to that of a 30-inch square waveguide. It is obvious that since the measured values are considerably less than the plane wave results, the wave impedance was substantially less than that of free space (377 ohms). The term high impedance is defined as being greater than that of free space, so that the reported results are actually low-impedance test results, although not as low as obtained with loop tests. It appears that the high-impedance radiator was contained in a metallic enclosure, which substantially reduced its effective wave impedance.

Ventilation Panel Tests. Table 2 lists the results of measurements made on a waveguide-below-cutoff-type ventilation panel. The openings in the panel were 1 7/8 inches square and 2 3/4 inches deep. Tests were made on this sample with both the insertion loss method and with an attenuation method, to demonstrate the inaccuracies inherent in the insertion loss test when the sample is thick compared to the distance between loops.

Calculations were made using Equations (2), (4), and (5). Co-planer loop tests were used. The metal thickness was large compared to skin depth at all frequencies. Since the hole area was much greater than the metal area, none of the correction factors apply. It will be observed that the insertion loss measurement of 25 db is considerably less than the calculated sum of reflection and attenuation losses, which are, respectively, 2.5 and 40 db. For insertion loss, the loops were positioned with their centers 6 inches apart, so the sample could be inserted and a true insertion loss test made. To make the shielding efficiency test, the initial reading (shield out) was made with the loop perimeters touching, everything else remaining the same. This in effect (insofar as the pickup loop could measure the intensity of the incident field without affecting it) would provide two readings which are proportional to the incident field intensity just inside the shield to the transmitted field just outside the shield, conforming to the definition of shielding efficiency.

It is obvious that the difference between the two series of tests must be due to the difference in the initial signal level measured with the shield out. Since the loops were brought closer together from a center separation of 6 inches to that of 3 inches, the ratio of the field intensities is 8 to 1 or 18 db. (At the frequencies and distances under consideration, the field varies inversely as the cube of the distance.)

Therefore, the insertion loss test was too low by about 18 db. Consideration of the physical conditions of the test indicates that when the wave entered the guide, it was confined to the dimensions of the guide, and the inverse cube loss was not permitted for the length of the guide although the usual guide attenuation still applied. In other words, everything else remaining the same, reduction of the test

sample thickness to a small fraction of 6 inches would reduce the "shield-in" insertion loss reading by 18 db because of spreading out of the field. This demonstrates the fact that insertion loss tests are equal to the shielding efficiency only when the test sample is thin compared to the distance between the test antennas.

## Antenna Reflector Calculations

A particular problem that often arises is the question of antenna reflector design, where it is desired to maintain adequate reflection from a surface having maximum opening size. The large openings may be required to minimize wind drag, weight, or for reasons of economy.

A usual design used in the UHF range employs a square mesh of one opening per inch and a conductor diameter of 0.080 inch. Assuming a frequency of 400 mc, Equations (2), (4), (7), (9), and (10) provide a ratio of 8.5 db for the ratio of the incident wave to the transmitted wave. The holes, closely spaced and having an attenuation of only 2.4 db, fall in the category requiring application of the correction factor $K_3$ (Equation 12). This provides an additional reflection of 11.4 db, bringing the total ratio to 19.9 db, which corresponds to a power reflection of about 100 to 1. Comparison with results obtained from a nomograph in the IRE Proceedings of February 1961[5] indicates agreement within about 1 db.

## Polarized Openings

Another problem that is often encountered concerns the ratio of the leakage through an elongated opening when the incident field polarization is parallel to the aperture to that obtained with perpendicular polarization. H. A. Bethe[6] has provided means for calculating the polarization of apertures in infinitely thin walls. As far as is known, no one has approached the problem in a manner which includes the effect of opening depth. An equation for polarizability of rectangular apertures may be obtained by taking the ratio of Equation (1) for the two different directions for each type of field. For instance, the difference in reflection losses for a single opening and low impedance fields would be represented by:

$$R_2 - R_1 = 20 \log \left[ \frac{\frac{\pi r}{2h}\left(1 - 10^{-\frac{A_2}{10}}\right) + 1 + 10^{-\frac{A_2}{10}}}{\frac{\pi r}{2W}\left(1 - 10^{-\frac{A_1}{10}}\right) + 1 + 10^{-\frac{A_1}{10}}} \right] \qquad (24)$$

where h is the longer opening dimension and $A_2$ is the attenuation obtained when the field is polarized parallel to it. $A_1$ is the attenuation with the field polarized parallel to W.

The difference in attenuation would be represented by

$$A_2 - A_1 = 27.3D \left(\frac{1}{W} - \frac{1}{h}\right) \tag{25}$$

Calculations for an aperture 4 inches long and 1/10 inch wide in a metal panel 1/16 inch thick indicate a reflection difference of 24 db and an attenuation difference of 16.5 db, so that the polarizability is equal to 40.5 db. Practical experience has shown that polarizabilities of this magnitude are often encountered in the field.

## V. CONCLUSIONS

The extensive range of variables over which agreement is obtained between calculations and experimental results indicates that the basic concepts introduced by Schelkunoff provide the correct approach to opening leakage. It is concluded that each of the terms of Equation (1) describes, or approximates, with reasonable accuracy, the actual physical events which take place during the shielding process.

Results of general significance indicate that the characteristically flat shielding efficiency curves obtained by many investigators is due to the test method. Variations of reflection losses are eliminated because the source wave impedance and aperture characteristic impedance vary in the same manner with frequency. Use of the shielding materials under actual conditions where the incident wave impedance is either equal to or greater than that of plane waves will provide shielding considerably greater than the measured values. Tests made with loops apply accurately to the minimum shielding to be obtained under any conditions, but tests made with enclosed high-impedance sources require evaluation before they can be applied.

Heretofore, methods for determining the polarizability of unsymmetrical apertures have only been available for infinitely thin metal sheets. The methods described permit calculation of the polarizability of rectangular apertures of any depth. If equations are developed for the characteristic impedance and attenuation constant of apertures of other shapes, then their polarizabilities may also be determined. As a matter of fact, these equations can be developed empirically through a simple series of tests.

Design of antenna reflectors or other reflecting surfaces where minimum weight, cost, or wind drag may be of importance may be performed without the need for previous empirical tests. Present designs can be considerably reduced in metal content if it is known that they will be used only with waves of a particular polarization.

Design of large shielded enclosures for which a particular value of shielding efficiency is known to be required, may be greatly reduced in construction cost if advantage is taken of the added shielding quality provided at the interior regions of the enclosure. The methods described provide means for obtaining the required shielding quality at any desired distance from the shielding barrier.

## REFERENCES


1. S. A. Schelkunoff, "Electromagnetic Waves," D. Van Nostrand Co., Inc., 1943.

2. C. S. Vasaka, "Theory, Design and Engineering Evaluation of Radio-Frequency Shielded Rooms," Bureau of Aeronautics TED Project No. ADC EL-538, 13 August 1956.

3. "Electromagnetic Shielding Principles," Volume 1, RADC TR-56-43A, Rensselaer Polytechnic Institute, Final Report on Contract AF 30(602)-401, An Investigation of Interference From Radar Modulators, March 1, 1956, p. 112.

4. AFM 100-35, USAF Communications-Electronics Doctrine-Mutual Electronic Interference.

5. W. W. Mumford, "Some Technical Aspects of Microwave Radiation Hazards," Proceedings of the IRE, February, 1961.

6. H. A. Bethe, "Lumped Constants for Small Irises," M I T Radiation Laboratory, Report No. 43-22, March 24, 1943.

TABLE I

COMPARISON WITH MEASUREMENTS REPORTED IN AFM 100-35

| Screen Type* | Test Type | Freq (MC) | Meas Values (DB) | Calc Values (DB) |
|---|---|---|---|---|
| No. 22 | Mag | 0.085 | 31 | 28 |
| 15 mil | field | 1.0 | 43 | 45 |
| | | 10.0 | 43 | 49 |
| No. 22 | Plane | 0.2 | 118 | 124 |
| 15 mil | Waves | 1.0 | 106 | 110 |
| | | 5.0 | 100 | 95 |
| | | 100.0 | 80 | 70 |
| No. 22 | Elec | 0.014 | 65 | **65 |
| 15 mil | field | to 60 | | |
| No. 12 | Elec | 0.014 | 50 | **53 |
| 20 mil | field | to 60 | | |

* All screens made of copper.

**These values assume a wave impedance equal to that of a 30-inch square waveguide.

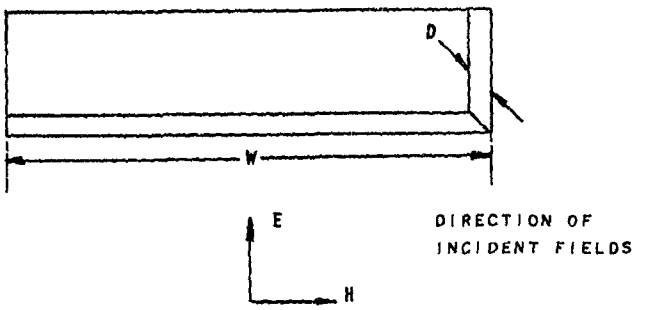
TABLE II

COMPARISONS OF MEASUREMENTS AND CALCULATIONS FOR VENTILATION PANEL WITH 1 7/8 INCH SQUARE OPENINGS 2 3/4 INCHES DEEP

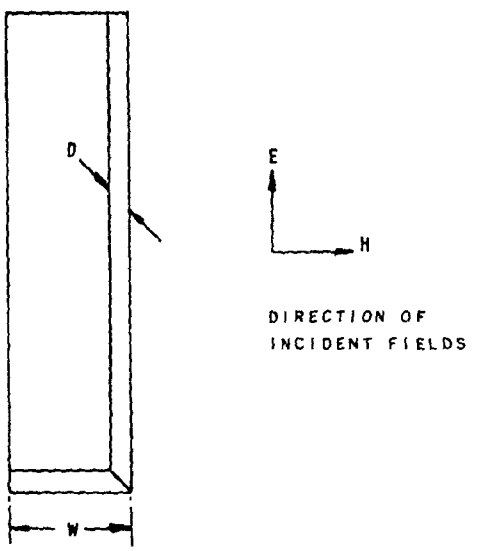
| | Measurements | | Calculations | |
|---|---|---|---|---|
| Freq (MC) | Insertion Loss Test* (DB) | Shielding Efficiency Test* (DB) | Attenuation (DB) | Reflections (DB) |
| 0.15 | **24 | - | 40 | 2.5 |
| 10 | **25.5 | 45 | 40 | 2.5 |
| 25 | **26 | 44.5 | 40 | 2.5 |

* All tests made with co-planer loops.

** Calculated correction for insertion loss tests +18 DB.




(a) FIELD POLARIZED PERPENDICULAR TO LONG DIMENSION




(b) FIELD POLARIZED PARALLEL TO LONG DIMENSION

FIGURE 1. RELATIONSHIP OF RECTANGULAR APERTURE DIMENSION "W" TO DIRECTION OF FIELD COMPONENTS

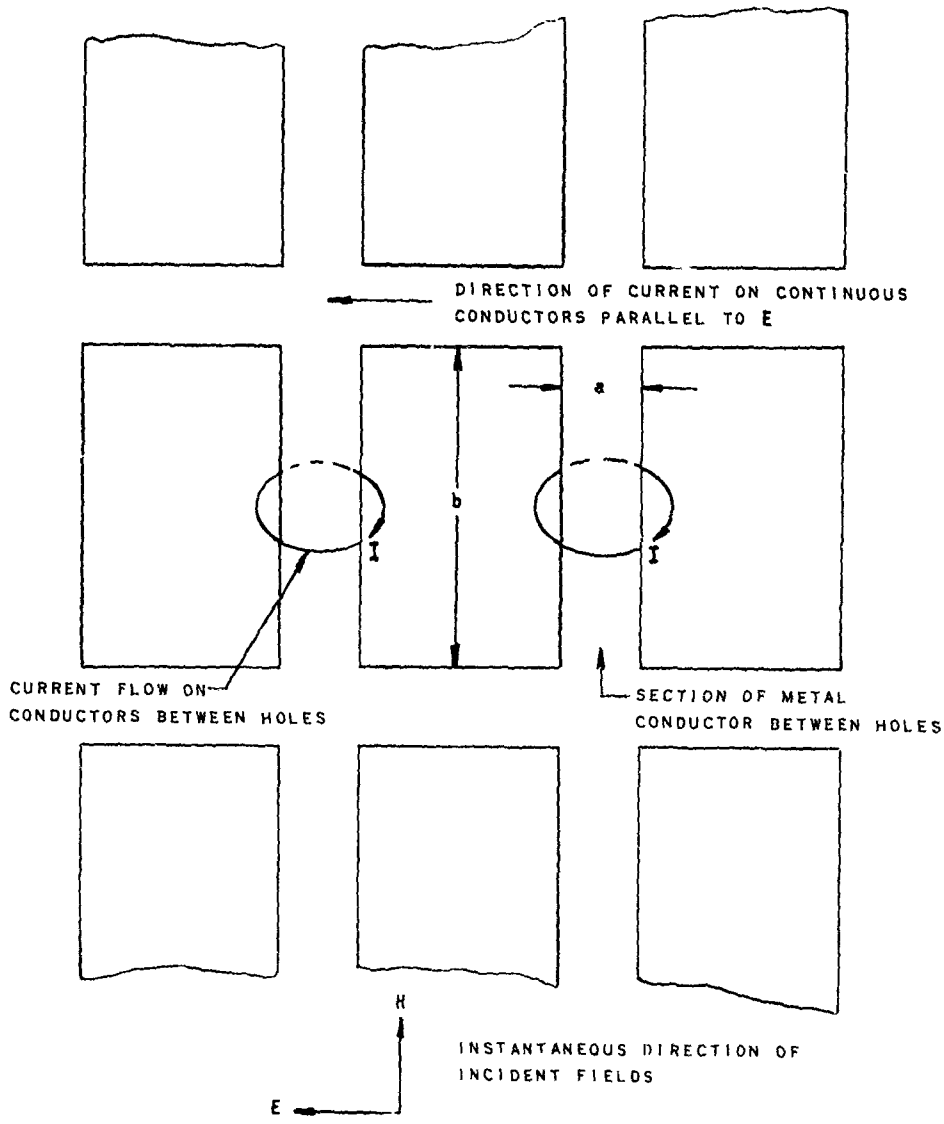



FIGURE 2. CURRENTS INDUCED ON PERFORATED METAL SHEET

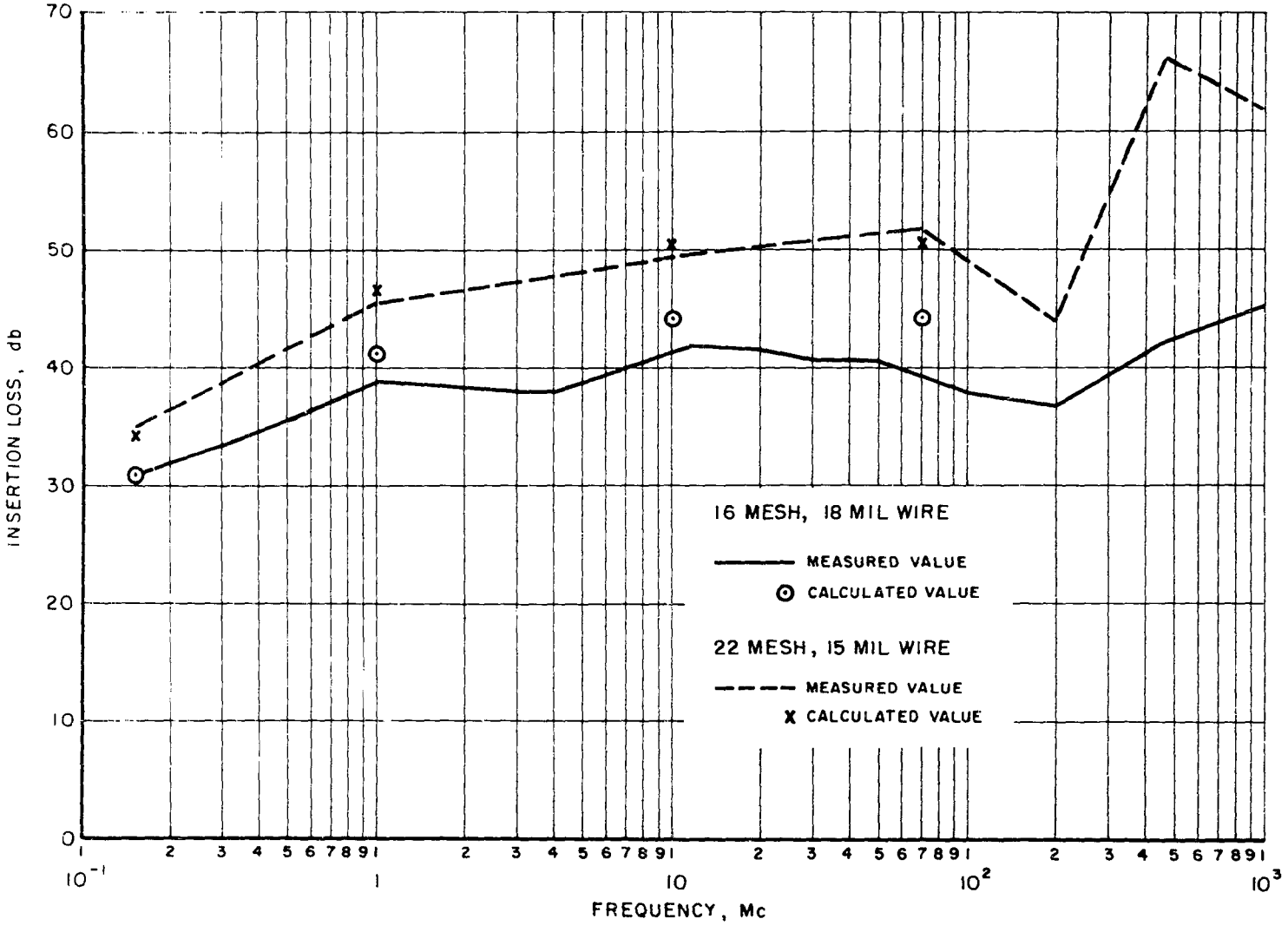



FIG. 3 INSERTION LOSS OF 16 AND 22 MESH COPPER SCREENS

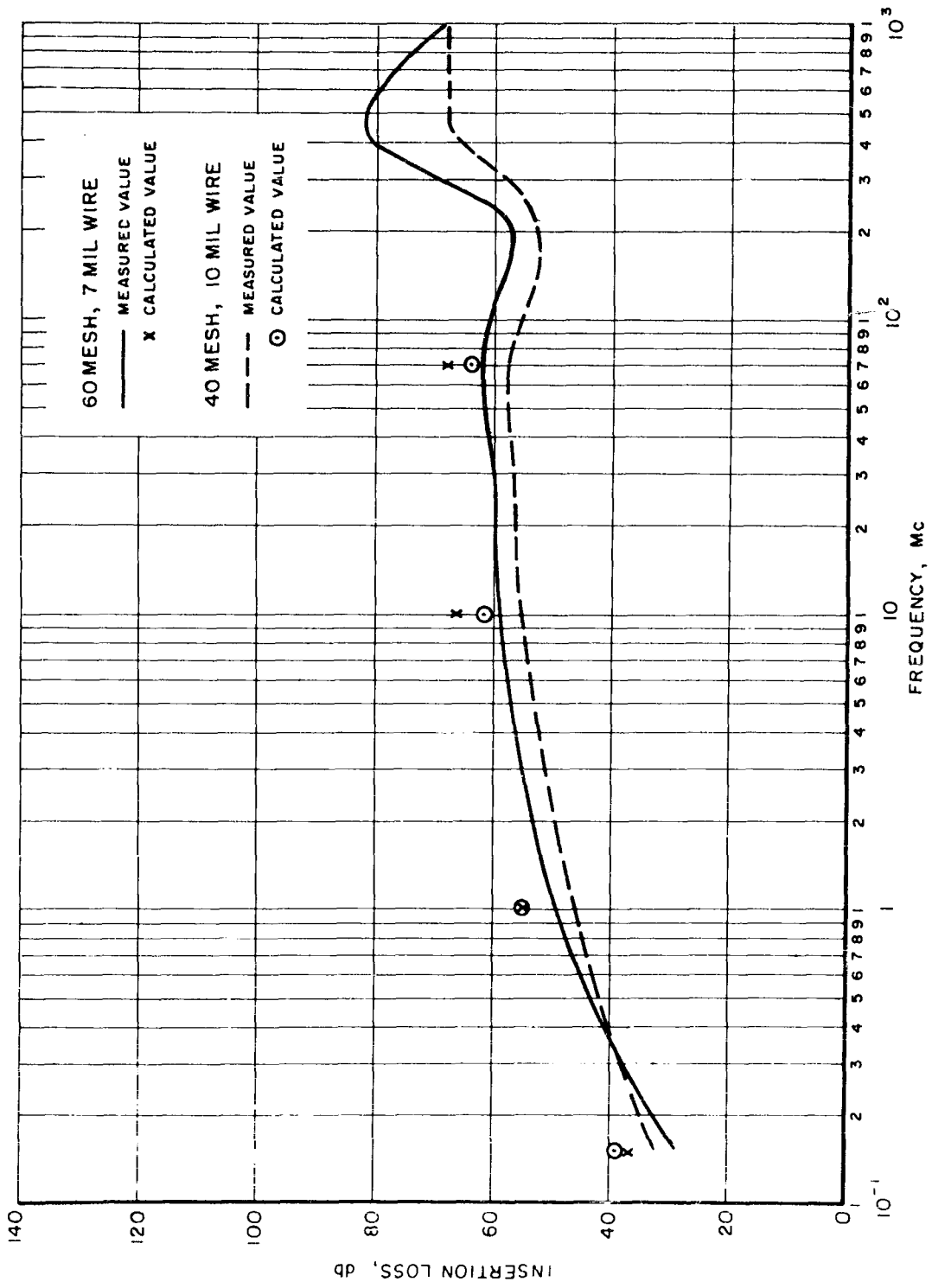



FIG. 4 INSERTION LOSS OF 40 AND 60 MESH COPPER SCREENS

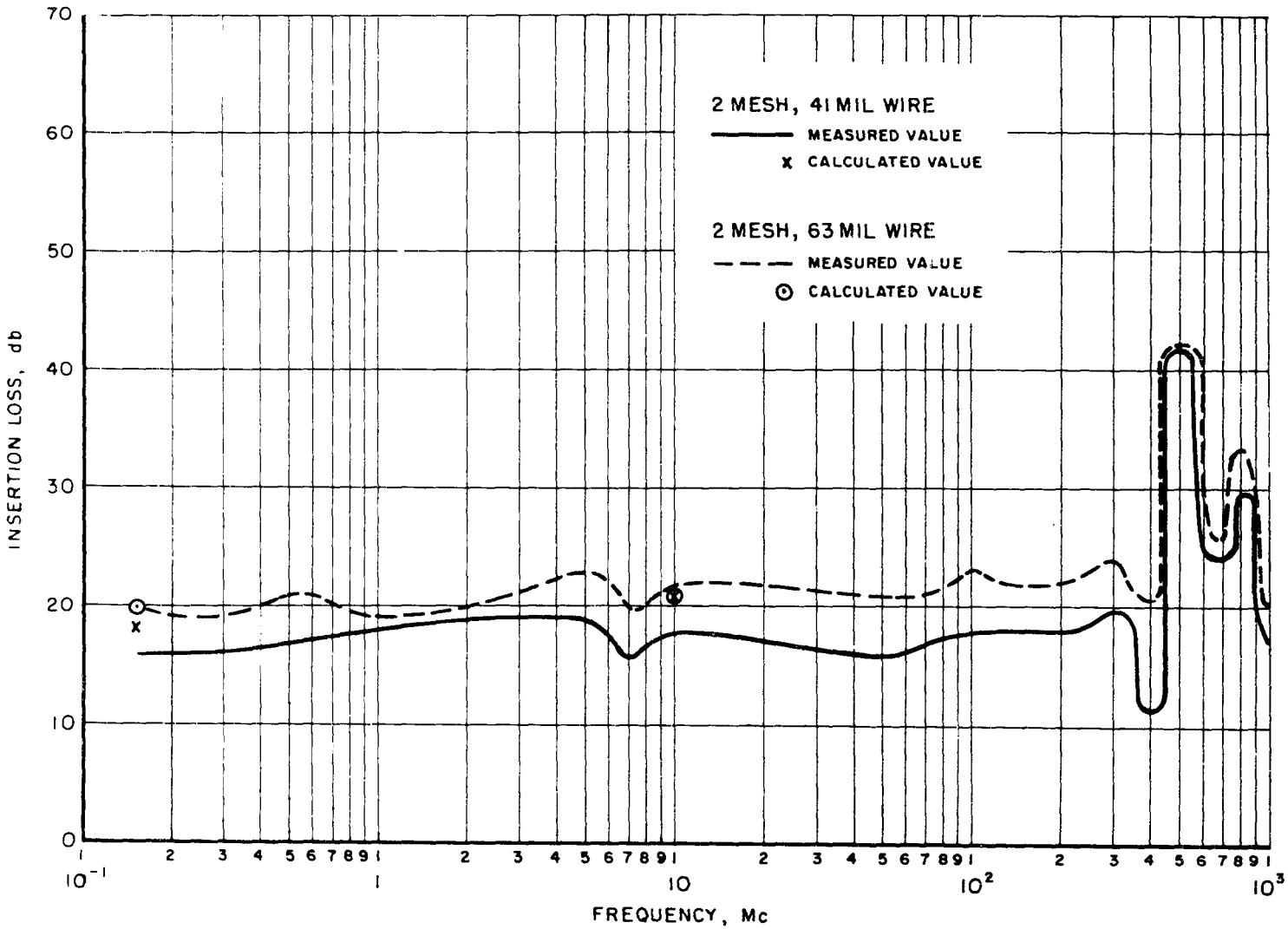



FIG. 5 INSERTION LOSS OF 2 MESH COPPER SCREENS

# RADIO INTERFERENCE AND SUSCEPTABILITY STUDY OF HIGH POWER TRANSMITTER JAMMERS

T. B. Brown and W.S. Schwagart
The Hallicrafters Company
Chicago, Illinois

Abstract. - This paper will be concerned with the study of radio frequency interference suppression on a group of three airborne high power transmitter barrage jammers.

The scope of this presentation will be primarily a historical account of the efforts of three project design groups to qualify the equipments to military radio interference requirements. It is intended that the information contained herein will be of maximum help to those actively engaged in qualifying similar military equipment. For this reason, emphasis is placed on practical approaches rather than theoretical.

Because the equipments are classified, reference will not be made to nomenclature and specific operating frequencies. A brief description of the three transmitter systems is as follows:

1) A microwave, "S" band, system consisting of
   a) Transmitter unit containing a voltage tuned high power carcinotron with suitable high voltage and noise modulation circuitry.
   b) An oil circulating heat exchanger unit.
   c) A control indicator.

2) A UHF system consisting of
   a) A driver unit with a noise source and low level distributed amplifier.
   b) An amplifier unit which features a high power traveling-wave tube.
   c) A control indicator unit.

3) A VHF system consisting of
   a) A power supply unit.
   b) Two transmitter units, one low band and the other high band - both featuring a noise source with low and high level distributed amplifiers.

It is probably safe to say that during the design of an airborne barrage jammer the engineering staff encounters almost every type of RFI suppression problem known. The fact that the barrage jammer design is deliberately aimed at producing high level wide band radio frequency interference to smother radar reception creates a most interesting challenge in channeling this energy to the antenna only. The engineering solutions to suppression of noise conducted in the power lines and noise radiated from the

equipment range from the application of well-known techniques through the examination of the latest most sophisticated methods. One familiar fundamental point loomed large throughout the evolution of these projects. The initial evaluation of RFI problems in the early design stages was an absolute necessity and without it, size and weight would unquestionably have been much higher.

All of the three equipments evolved from previous studies in which prototypes were designed and submitted for Air Force countermeasure tests. Even before this work culminated in contract awards for fully qualified production units, studies had been made on prototypes to determine the problems in designing to meet specification MIL-I-26600. Information from these studies then was used to generate Radio Interference Control Plans for the pre-production prototypes.

The preliminary parallel studies of these three equipments pointed out one salient fact. A maximum effort to suppress radiated and line conducted noise at the circuit level was to be retarded by the presence of certain design requirements. Some of these requirements and their effects are:

1) Plug-in modules which render continuous shielding difficult and in some cases impossible.

2) A high system reliability requirement which, in some instances, was at odds with the quantity of extra components necessary to provide adequate suppression.

3) Space factors of the circuit modules which, in some instances, did not permit room for adequate circuit suppression or shielding.

Because of these factors, it seemed evident that a large share of the noise suppression effort must be relegated to the filtering of conductors leaving the transmitter and the shielding provided by the external case and front panel.

Actually, the entire noise suppression task on each of the three equipments became an effort to combine best practical circuit suppression techniques with rigorous shielding and filtering.

There were several fundamental suppression techniques used in common to all three transmitters, as listed below:

1) Filament and B+ leads were by-passed at each point of entry to or exit from a module.

2) Shielding was used on all signal leads to suppress radiation and to prevent crosstalk.

3) Each module featured a single ground return point.

4) Where possible, all module ground conductors were returned to a single equipment ground point to minimize circulation of ground currents.

5) All conductors leaving transmitter chassis to external cables are heavily filtered. Filter assemblies are bonded to the front panel.

From this basic starting point each equipment design staff branched off into whatever direction appeared most suitable for its particular unit.

Shielding

One of the main problems encountered in the design of the three transmitters was the conflict of radiation suppression with air cooling requirements. There is of course no mystery in the fact that, wherever forced air is used to dissipate heat, the intake and outlet openings also permit the emanation of radio frequency energy. If the level of RF energy present is high and there is little reserve in air flow capacity, an acute problem can arise in attempting to suppress radiation without overheating the equipment. All non-solid shielding materials such as perforated metal, fine mesh copper screening, and metal honeycomb present a pressure drop to airflow. Metal honeycomb is the "cadillac" of these materials, for very high electric field attenuations are obtainable up through the microwave band with negligible air pressure drop. Honeycomb, however, has the disadvantages of occupying far greater volume and costing far more than either screening or perforated metal. As an example, panels of honeycomb vary in thickness from 1/4 to 3/4" depending upon attenuation desired and the production cost of 1/4" material is approximately 50 cents a square inch. Hence, from the product design standpoint in airborne equipment the first choice is low volume inexpensive flat perforated metal or screening with honeycomb called upon for the impossible situations.

In this trio of transmitters, perforated metal, screening, and honeycomb all found various applications. The microwave transmitter showed the least difficulty of the three. Here, an oil circulating heat exchanger dissipates the bulk of the heat. There are some components mounted in air, but a blower of more than adequate capacity is employed to cool them, and the pressure drop in metal screening is of little significance. In the first models, oiled dust filters with three layers of coarse aluminum screen were used in the air intake and two air outlets. The dust filters were found inadequate to handle the high level of low frequency modulation in the transmitter until a single layer of fine mesh screening was added to each filter. Radiation in the microwave region is no problem incidentally, as long as the RF plumbing is tightly sealed, since a carcinotron oscillator is the only source and is inherently almost a perfect shield chamber.

In the VHF transmitter, however, the high level distributed amplifier is rich in RF fields above 100 MC and is also entirely dependent upon forced air for cooling.

The transmitter case is divided into two decks, the upper and the lower, with two compartments in the lower deck and three compartments in the upper deck. One common blower provides air for cooling all of the tubes in the transmitter.

All forms of non-solid shielding in the outer case were tried with poor results in cooling until honeycomb was applied. Some inconvenience was suffered in that the 1/4" thick honeycomb could be placed nowhere except on the external surface of the cover. Attenuations of from 30 to 90 DB above 100 KC are achievable with honeycomb thickness varying from 1/4 to 3/4 inch. Below 100 KC, H-field attenuations of honeycomb become inferior to that obtainable with perforated metal or fine mesh screening.

The UHF transmitter consists of two units, a low level driver and a power amplifier both air cooled. In the driver, no problem was experienced with perforating the cover for air outlet. The power amplifier employing a traveling-wave tube which confines the passband energy quite well, showed uncomfortable levels of intermodulation products in the 50 MC region. Forced air cooling was dangerously inhibited in suppression of the intermodulation products until honeycomb was employed in air inlet and outlet openings.

The foregoing emphasis on the applications for shielding forced air ports is not intended to leave the impression that this was the only shielding problem in the three transmitter jammers. Everywhere throughout the construction of the units will be found the application of woven mesh gasketing between dust covers and panels and module chassis. Where rough cast surfaces bear on smooth panels, aluminum mesh embedded in sheet neoprene was glued to the casting with conductive cement to prevent radiation leaks between panel and casting.

Some of the shielding methods for individual transmitters as now related will illustrate the diversity in solutions.

The top of the VHF transmitter case is removable to allow access to the modules of the upper deck. Shielding in the form of beryllium copper finger stock was riveted to the outside edges of this cover to provide good contact to the case and prevent RFI radiation.

The UHF transmitter consists of two sections, one transmitter unit and one power amplifier unit. The transmitter unit is divided into three modules constructed as drawers which slide into three compartments in the transmitter case. Beryllium copper finger stock was used to ground the drawers to the transmitter case. Connecting cables between modules were placed in metal channels to prevent crosstalk.

The philosophy of the project groups in selecting beryllium copper fingers rather than woven metal mesh gasketing was that finger stock would retain its resiliency better after a large number of engagements and disengagements with the top cover. Since the cover on the VHF transmitter and the drawers of the UHF transmitter must be removed for any maintenance, it was expected that the fingers would have better life characteristics. Experience in the Microwave dust cover has shown, however, that the use of monel in woven metal mesh gaskets for this type of application is quite satisfactory.

In both the microwave and VHF units, active and spare fuses were sources of radiation. Active fuses sometimes act like antennas, radiating the low frequency noise from diode power supplies. Also, the complete lack of shielding in commercial fuseholders permits any internal high frequency noise to pour through the opening in an otherwise well shielded panel. Typical solutions were solid metal shields placed on spare fuseholders in the microwave transmitter, while ceramic capacitors bypassing active fuses proved sufficient. In the VHF transmitter, where all fuseholders were grouped together, a shield comprised of solid metal with wire mesh gasketing was used to surround the fuse cluster on the front panel.

Actually, fuse suppression problems have been plaguing the electronic equipment designer for so long that it is strange no concerted effort to market a shielded fuseholder has been made. It is recommended that enterprising fuse manufacturers review this market potential.

One of the difficult compromises in RFI product designing stems from the eternal conflict between military metal finishing specifications and interference specifications. The task of establishing direction to the mechanical designers activities can be simplified if, at the project inception, the principle is firmly stressed that noise suppression requirements take precedence when incompatible with paint finishing specifications. Corrosion problems because of dissimilar metals in RF gaskets and adjacent surfaces was once a trying problem. Now with such materials as aluminum, monel, copper and silver-plated copper available in commercially available metal mesh gaskets, the task of choosing compatible metals has been greatly simplified.

Filters

In all of the three transmitters, filter assemblies in shielded compartments inclosing the main connectors were employed. The packaging of the filters however, was determined by the space available. In the VHF transmitter, sufficient volume was available to permit the use of hermetically sealed capacitors and coils installed in compartments with removable covers. In both the microwave and UHF equipments, however, filtering volume was at a premium and the employment of completely sealed and potted connector filter assemblies with high density packing of components was mandatory.

Since the designer often faces a choice between these two styles of filter packaging, it is worthwhile to summarize their relative merits. In general, it can be said that the unpotted filter assembly with removable covers offers high ease of maintenance, since any defective component may be replaced. Its disadvantages are poor space economy and in some cases poorer price economy.

The sealed filter connector package permits the greatest density of components and in production volume can often be purchased at less cost. However, the failure of any one component necessitates the replacement of the entire package, which in the instance of one assembly in the microwave comprises twenty-two filter circuits. Hence, the design of the filter must be directed toward the achievement of extremely high reliability.

Inasmuch as sealed multi-circuit filters are becoming more common in airborne equipment applications and the reliability requirements for airborne equipments are continuing to rise, it is worthwhile to review some of the problems the equipment designer faces in specifying and procuring filters. The design procedures in selecting the optimum filter circuit and circuit parameters have been thoroughly discussed in the literature. Essentially, the only electrical design problem in multi-circuit filters not common to single filters is leakage or crosstalk between circuits. This can become a serious problem at frequencies above 1 MC if adequate precautions are not taken. In a well designed multi-circuit filter, one will usually find that good high frequency bypassing techniques have been employed at the filter input; that internal to the enclosure the input is well shielded from the output section; and that magnetic coupling between adjacent coils has been minimized through the use of toroids. Let us say that all this has been done and a filter package prototype is at hand which permits the equipment to comply with the applicable radio noise specification. Let us say further that all electrical components have been selected with the applicable environmental extremes carefully considered. And finally, let us say that a reliability analysis has been made using the most sophisticated mathematical tools and a satisfactory reliability factor has been predicted. There then remains one more task for the equipment designer to perform - completely review the internal construction and workmanship of the preproduction prototype. The following items comprise a list of headaches experienced in the products of some of the top filter manufacturers in this country:

1) Inadequate stripping of formvar wire causing cold solder connections after many hours of use.

2) Too low a gauge on wire from coils to terminals, permitting breakage caused by varying stresses in the potting compound.

3) The use of potting compounds that react chemically with solder causing eventual open circuits and/or holes in the soldered can seams allowing the entrance of moisture.

4) Poorly conceived filter cans that permit excessive stress on solder seams also resulting in eventual leakage holes.

5) Too great a reliance upon potting compound to mechanically support components.

6) Improper insulation between adjacent circuits permitting eventual circuit-to-circuit or circuit-to-ground shorts.

Perhaps it would require unusual clairvoyance for the design engineer with responsibility for purchased parts approval to detect or anticipate all the design weaknesses of the types mentioned. Experience has shown, however, that the following minimum procedure will weed out the majority of defects and is well worth the time and cost:

1) Request the vendor to supply one prototype, unpotted and unsealed. Examine the wired interior thoroughly and write down all possible visible trouble spots using plain common sense as a guide.

2) Using a completely finished sealed and potted sample, cut filter into sections and inspect for air pockets in the potting compound.

3) Perform the following on at least three and preferably more samples:
   a) Temperature cycle (-55 to 100°C) for 100 to 200 cycles with a continuous monitoring of continuity on all circuits.
   b) Humidity and temperature cycle (to applicable specification).
   c) Following humidity a voltage flash test on all terminals at $2\frac{1}{2}$ times rated voltage.

4) Where space permits, insist that capacitors be hermetically sealed even though the filter enclosure is potted and solder sealed.

5) In writing the filter specification, leave absolutely nothing to imagination. There is no substitute for rigorously spelling out all environmental requirements, current and voltages, permissible temperature rise, voltage drop, and minimum insertion losses, and voltage flash ratings.

MIL-F-15733, the only military specification available on filters, is often used as a guide but is suitable only to the extent that detailed environmental and other special requirements are included.

In the transmitter jammer group, the primary power sources are 115 volts, 3-phase, 400 CPS, 4-wire and 28 VDC. With the AC neutral and DC negative combined in one ground conductor, five filters are required for power input. Power circuit filtering was always separated physically from other filtering to avoid heat dissipation and crosstalk problems.

Each jammer system consists of three units. Placement of filtering depended upon the function of the units, which were not uniform. Hence, the distribution of filtering among the three units of each system was unique to the system. In the microwave equipment, filtering was required in the transmitter unit and found unnecessary in either the heat exchanger or control unit.

The VHF equipment, however, comprised of power supply, transmitter, and control units required filtering in all but the latter.

In some instances, rigorous filtering at the module source was necessary in addition to main filtering of unit output cabling. Examples of this are found in the UHF transmitter equipment, which employs traveling-wave tube circuitry.

Noise from the diode rectifiers of the driver power supply was found on the power leads. Bypassing each diode with a disc capacitor minimized the noise on these leads. Noise was also being conducted and radiated from the bias leads of the power amplifier tubes. RF chokes were placed at grids suppressing noise from this source.

A connector on the front panel which provides a means of metering voltage and signal levels of the multiplier module was a high level source of radiating noise. A filter box was constructed with feedthrough capacitors in each lead. The connector was mounted on the box and the assembly mounted to the front panel.

The signal input and the TWT protect circuit were coupled to the tube with a "T" connection allowing signal to be conducted on the control chassis leads. A special filter was designed to connect into the "T" providing isolation between the signal and the protect circuit. Also, with the cathode tied to the filament internal of the tube, the filament leads were conducting a large amount of signal to the power lines. A filter was installed in the power leads at the TWT filament transformer.

The effect of a high equipment reliability goal in some instances prevented the use of simple bypass capacitors when the quantity required to accomplish suppression was considered excessive and the same result could be obtained with a filter.

An example may be found in the VHF transmitter where resonances in plate and grid lines of the final stage caused spurious signals to appear in the transmitter output.

These responses could be suppressed with bypass capacitors at the tubes but this required considerable space in the compartment and restricted air flow. A bandpass filter was designed to eliminate these responses from the transmitter output, conserving space in a crowded compartment and reducing the number of components used by approximately twenty, thus increasing the reliability of the transmitter.

Another example of the effort to minimize in the quantity of components is found in the high voltage rectifier circuits of the microwave transmitter. Over 70 diodes are used in one rectifier circuit. In order to source suppress the high level 100 to 300 KC noise from the diodes, a capacitor bypass across each diode was considered. A higher reliability factor, however, could be achieved by accomplishing the necessary attenuation with large capacitors and chokes in the pi-type line filters.

## Antenna Conducted Spurious Frequency Measurements

The conduct of tests for the measurement of low level spurious frequencies existent in the antenna circuit was a requirement in the frequency range of 150 KC to 1 GC. The basic test method used was to obtain a sample of the transmitter output fed to a higher power 50-ohm dummy load. The sample signal was taken from an appropriate coupler to a suitable calibrated receiver such as the Empire Devices NF-105 and the Polarad FIM units. Considerable difficulty was experienced, however, in obtaining suitable couplers commercially for this work.

It was necessary that couplers provide at least 30 DB of attenuation in the passband of the various transmitters to protect the input circuits of the receivers. The attenuation outside of the passband must be low enough to allow measurement of any spurious present. Commercially available couplers were useable from 30 MC to 10 GC, however, below 30 MC the attenuation increased so rapidly they were not useable. Therefore, an important part of this test program was to become the development of special low pass coupling devices.

Several methods for measuring the 150 KC to 30 MC range were developed. For measurements on UHF transmitters, the simplest method consisted of a lossy coaxial line connected from the transmitter output to the receiver input. The length of the line was calculated to give 30 DB of attenuation at the transmitter output frequency. Below 50 MC the attenuation decreased rapidly, allowing the measurement of any low level spurious present. Absorbing the transmitter power caused a temperature rise that required cooling of the line. The line was coiled on a wooden frame and spaced so the air could circulate around the cable.

A second method was devised using a special coaxial voltage divider which when placed in series between the transmitter output and an insulated high power 50-ohm load, interrupts the ground return circuit of the load with a 0.1 ohm resistor. The voltage developed across the 0.1 ohm resistor is fed to a receiver through a 50-ohm matching resistor. In this measurement system, the transmitter, coaxial voltage divider and receiver are bonded to a copper ground plane. The dummy load is not grounded. The system was found useable to 900 MC.

A third method for measuring low frequency antenna conducted on microwave transmitters was the use of a specially designed coaxial coupler with reactive elements in series with the probe suitably chosen to offer high attenuation of 30 to 40 DB above 1 GC. An excellent lo-pass characteristic was obtained in this coupler with attenuation decreasing to less than 1 DB at all frequencies below 10 MC.

## Susceptability

The topic of susceptability has been relegated to the end of this discussion primarily to end with a cheerful note. Although, at the inception of the project, some fears were expressed over the effects of susceptability on the characteristics of the noise output, no problem of any kind has ever been experienced with audio or RF conducted or RF radiated susceptability tests.

## CONCLUSION

The equipment described has now been delivered to the Air Force in substantial quantities, has been subjected to operational tests, and is a part of Air Force training programs. To date, no evidence of incompatibility within the control of the designer and manufacturer has occurred. The endeaver to improve the system's performance continues, however, not only from an operational standpoint but also from the viewpoint of increasing the effectiveness, economy, and reliability of parts used for radio interference suppression.

# RECEIVER SUSCEPTIBILITY UNDER MULTI-MODE CONDITIONS

Paul C. Yuen and J. J. Krstansky
Armour Research Foundation
Chicago, Illinois

Abstract. - This paper describes a series of experimental tests made on a radar receiver to determine the response of the RF portion of the radar to signals propagated in different modes at various frequencies which correspond to spurious responses of the receiver. The data obtained from these measurements provides an insight into signal propagation in practical radar systems utilizing rectangular waveguide at frequencies removed from the design frequency band.

The test procedure used in the measurement of mode sensitivity is described. The modes which were propagated include the $TE_{10}$, $TM_{11}$, $TE_{01}$, $TE_{20}$, $TE_{30}$, and $TE_{02}$. Mode exciters and converters were used to excite the desired mode.

The date obtained, data evaluation and comments pertaining to measurement problems are also presented. Results of the tests indicate that the spread in sensitivity to the various modes decreases as the frequency of the test signal is increased. The $TM_{11}$ mode is the major cause of the larger spread at the lower frequencies.

## I. INTRODUCTION

In order to obtain data on the behavior of the RF system of a typical radar receiver under multi-mode conditions, a series of tests have been set up to measure the mode sensitivity of a radar system. These measurements have been designed to determine at various points in the RF system the conversion of energy from one propagating mode to other modes. The data obtained from these measurements is intended to provide an insight into signal propagation in a practical waveguide system at frequencies other than the design frequency band, and also should lead to a measurement technique for receiver sensitivity under multi-mode conditions.

## II. TEST PROCEDURE

A block diagram of the radar receiver which was tested is shown in Figure 1. As shown, the antenna consists of a reflector with a "pill box" parabolic-cavity feed system. Two 90° H-bends and a twist connect the feed to a rotary joint which is of coaxial-line construction rather than rectangular waveguide. A special Y-shaped junction section connects the rotary joint to the receiving channel and the transmitting channel. A directional coupler is also included as an integral part of the Y-junction.

From the Y-section the receiving channel consists of a TR tube, a coaxial-cavity-type tunable preselector, a matching iris, and the frequency converter. The iris is used to tune out susceptance introduced into the waveguide by the local oscillator coupling loop.

The RF system of the radar operates over a band of frequencies from 3100 to 3500 mc. All stubs and joints have been designed for minimum mismatch over this bandwidth. However, the introduction of signals into the system at frequencies higher than those in the design band can lead to conversion of energy from one mode to other modes due to severe mismatch conditions. The stubs and cavities in the system are fairly narrow-band

device and will not operate satisfactorily outside the design band.

The measurements which were performed on the radar receiver consisted of exciting selected modes at selected frequencies at different input points in the RF system of the radar. At each test point the mode exciters and mode converters were connected to the input point with all secceeding RF sections also connected. Thus, at test point 3, the system being tested included the preselector, the matching iris and the frequency converter. By selectively adding RF sections, the effects of the added sections can be obtained by comparison with the previous results. This method permitted the use of the IF and video stages of the receiver, and thus an MVs test condition could be used as a standard reference condition throughout the test.

At each of selected test input points, each of the mode exciters and mode converters were connected to the radar system. Signal power at the test frequency was inserted into the system by means of the mode exciter. The input power required to obtain a minimum visible signal was then determined. A measurement of the VSWR in the line connecting the mode exciter to the signal generator permitted the output power reading on the signal generator to be corrected for mismatched load conditions.

## III. MODE EXCITERS AND CONVERTERS

Six readily excited modes were used for the tests. These included the $TE_{10}$, $TE_{01}$, $TM_{11}$, $TE_{20}$, $TE_{30}$ and $TE_{02}$ modes. All modes were for the rectangular S-band waveguide used in the radar system. The first three modes, $TE_{10}$, $TE_{01}$ and $TM_{11}$ were excited directly by the proper mode exciters. The $TE_{20}$ and the $TE_{30}$ modes were obtained by exciting the $TE_{10}$ mode and converting it, using properly-designed mode converters. The $TE_{02}$ mode was obtained by exciting the $TE_{01}$ mode and converting it. Sketches of the six mode exciters and converters are shown in Figure 2.

In order to determine the propagation of each mode through the RF system of the radar, frequencies above the cutoff frequency for each of the six modes, and frequencies below the cutoff frequency for each of the modes except the $TE_{10}$ mode were selected. A diagram containing the cutoff frequencies for various modes propagating in S-band rectangular waveguide is shown in Figure 3.

## IV. DISCUSSION OF TESTS

Figure 4 contains a block diagram of the equipment setup for the mode measurements. The mode exciter was driven by a signal generator whose output was filtered to remove harmanics. An adjustable short on the end of the mode exciter (for $TE_{10}$ and $TE_{01}$ modes,) and a stub tuner were used to match the mode exciter to the signal generator and maximize the signal. A slotted line and VSWR meter were inserted in the line to measure the standing wave ratio. The VSWR reading can then be used to correct the output reading, if necessary, of the signal generator due to mismatched presented by the mode exciter as a load on the generator.

For the $TE_{10}$, $TE_{01}$, and $TM_{11}$ modes, the mode exciter was connected to each selected input point by means of an adapter section. The adapter section was an eighteen inch waveguide section which causes higher-order modes, which may have generated, to be attenuated before reaching the frequency converter section. The adapter section was also constructed so as to permit its connection to the different flanges used at the various input points.

For the $TE_{20}$ and $TE_{30}$ modes the $TE_{10}$ mode exciter was connected to the $TE_{20}$ or $TE_{30}$ mode converter and then to the adapter section. For the $TE_{02}$ mode, the $TE_{01}$ mode exciter was connected to the $TE_{02}$ mode converter and then to the adapter section. The adapter section was connected to the desired input point on the radar system.

The six modes were introduced into the RF system of the radar at three different input planes:

1. $90^{\circ}$ H-bend
2. T-R tube
3. Crystal Mixer

These three input planes correspond to points 7, 4, and 1 respectively, of Figure 1.

The local oscillator and preselector of the radar were tuned to a receiver frequency of 3240 mc and the preselector tuning was disabled so that the preselector attenuation curve remained constant throughout the tests. The radar local oscillator was used for tests at 3240 mc. External signal sources were used to provide local oscillator power at the other test frequencies which were:

| | |
|---|---|
| 3240Mc | 5540Mc |
| 4140Mc | 8190Mc |
| 4896Mc | 9971Mc |

At these selected frequencies some variation in crystal current was encountered. This was due to the lack of sufficient isolation between the mode exciters and converters, and the mixer and was most pronounced at input plane 1, the mixer. It was found that movement of the adjustable short to match the mode exciters to the signal generator caused variations in the crystal current. The local oscillator coupling loop, designed to function as a directional coupler within the design band, did not perform well at out-of-band frequencies. Consequently, some power was radiated towards the input and this was reflected by the short back towards the crystal. Varying the short position varied the relative phase between the local oscillator power coupled directly to the mixer and that reflected from the short. This caused variations in the crystal current which were too large to be handled by means of an attenuator between the signal source and the mixer since the maximum output power from the signal source was not sufficiently high to allow for the added attenuation.

A crystal current of one milliampere was set as the standard and all data taken at other values of crystal current were referred to this standard. In order to correct all data to this reference current a set of calibration curves was obtained. This set is plotted in Figure 5.

The basic data taken was the sensitivity of the radar system for each of the six modes introduced at each of three input planes at each of the six test frequencies. The sensitivity measurement consisted of measuring the minimum visible signal (MVS). This was obtained by introducing a pulse signal of the same width as that used in the radar. The level of the signal was then reduced until it was just visible in the noise.

Each measurement was repeated three times and the average value taken as the test datum. Tests showed that a repeatability of one decibel was obtained. That is, the three readings for one test point did not differ by more than one decibel, and average readings when repeated after several hours agreed to within one decibel.

## V. TEST RESULTS AND DISCUSSION

Table I lists the sensitivity readings of the radar for signals of each of the six modes at each of the six frequencies introduced at each of the three input planes. The data are given in decibels referred to one milliwatt.

These data are plotted in Figures 6, 7, 8 and 9. Figures 6, 7 and 8 contain plots of mode sensitivity vs frequency for inputs at the 90° H-bend, the T-R tube, and the crystal mixer, respectively. Figure 9 contains plots of sensitivity for the $TE_{10}$, $TE_{01}$, and $TM_{11}$ modes vs frequency at each of the three inputs.

Examination of the data in Table I and the curves plotted from these data shows that:

(a) signals introduced at the 90° H-bend (input to the RF system) are attenuated strongly outside of the design band; e.g., the $TE_{10}$ mode sensitivity decreases from -97 dbm to -47 dbm. The attenuation appears to reach a maximum in the 5 to 8 kmc region and then decreases. Thus the $TE_{10}$ mode sensitivity reaches a minimum of -25 dbm and then rises to -43 dbm at 9971 Mc.*

(b) signals introduced at the T-R tube appear to suffer attenuation which fluctuates with frequency. Thus the $TE_{10}$ mode has a sensitivity of -97 dbm at 3240 Mc. The sensitivity decreases to 4896 Mc, increases to 8190 Mc, and then decreases, reaching -55 dbm at 9971Mc.

(c) $TE_{10}$, $TE_{20}$, and $TE_{30}$ signals introduced directly at the mixer suffer generally increased attenuation with frequency; e.g., the $TE_{10}$ mode sensitivity decreases from -99 dbm at 3240 Mc to -64 dbm at 9971 Mc. $TM_{11}$, $TE_{01}$ and $TE_{02}$ signals suffer decreased attenuation from 3240 to 5540 Mc, and then increasing attenuation with increasing frequency.

Probably the most striking point obtained from these figures is that for signalsintroduced at each one of the input planes the spread in sensitivities for the six modes tends to decrease with increasing frequency. That is, the difference in sensitivity between the mode with the highest sensitivity and that with the lowest sensitivity becomes less as the frequency becomes higher. Table II gives the differences in the sensitivity (in decibels) between the $TE_{10}$ and higher order modes. The difference (in decibels) between the highest sensitivity and lowest sensitivity is also listed as the spread. As can be seen, the spread at each of the input planes decreases with increasing frequency.**

---

* These statements are valid only for the limited data obtained in the tests. The actual plot of attenuation vs frequency would probably be a very rapidly fluctuating curve. For examples of the variation of attenuation with frequency of typical preselection cavities see I. Reingold, "Characteristics of Microwave Duplexer Tubes under Spurious Radiation Conditions," Fifth Conference on Radio Interference Reduction and Electronic Compatibility, 1959, pp 578-600.

** except for the spreads at 8190 Mc for input signals at the 90° H-bend and the mixer.

For signals inserted at the 90° H-bend the spread decreases from 37 db at 3240 Mc to 7 db at 9971 Mc. For input signals at the T-R tube the spread decreases from 42 db to 6 db. For input signals at the mixed the spread decreases from 38 db to 6 db.

Also of importance is the relatively sharp decrease in the spread as the signal frequency is increased from 4140 Mc to 4896 Mc. The change is from 47 db to 18 db at the 90° H-bend, from 50 db to 8 db at the T-R tube and from 32 db to 18 db at the mixer. This sharp change is due to the effects of the $TM_{11}$ mode. If the $TM_{11}$ mode is excluded so that only TE modes are considered, then the spreads are

| | 3240 Mc | 4140 Mc |
|---|---|---|
| 90° H-bend | 27 (37) | 16 (47) |
| T-R | 30 (42) | 11 (50) |
| Mixer | 27 (38) | 14 (32) |

The quantities in parentheses are the spreads if the $TM_{11}$ mode is included. In every case the spread is decreased by excluding the $TM_{11}$ mode.

The cutoff frequency for the $TM_{11}$ mode in S-band waveguide is 4.875 Mc so that at 3240 Mc and at 4140 Mc the $TM_{11}$ mode is cut off while at 4896 Mc and higher frequencies the $TM_{11}$ mode can propagate with relatively low losses. Thus in the radar system the division between relatively large and small spreads appears to be linked to the cutoff of the $TM_{11}$ mode, which is the TM mode of lowest order.

Table III contains listings for each mode of the difference in decibels between the sensitivity at the 90° H-bend and the sensitivity at the T-R tube, and between the sensitivity at the 90° H-bend and the sensitivity at the mixer output.

Signals introduced at the 90° H-bend travel through the entire RF receiving channel to the mixer. Signals introduced at the T-R tube travel through the T-R tube, preselectro, matching iris and frequency converter sections. Signals introduced at the mixer unit bypass all the other RF sections and travel directly to the local oscillator coupling loop and the crystal mixer. These two sets of data thus give a measure of the attenuation of each mode caused by the different sections of the RF system.

The data presented in Table III show two interesting trends:

1. The attenuation of the RF system is not a smooth function of frequency but fluctuates with the frequency. As an example, consider the data in the first row of Table III. These listings give the difference (in decibels) between the sensitivity for $TE_{10}$ signals introduced at the 90° H-bend and for $TE_{10}$ signals introduced at the input to the T-R tube. As shown, there is no difference in sensitivity, and hence in attenuation, at 3240 Mc between the 90° H-bend and the T-R tube. At 4140 Mc the sensitivity at the TR tube is 12 db greater than at the 90° H-bend; at 4896 Mc it is 3 db greater; at 5540 Mc, 27 db greater; at 8190 Mc, 41 db greater; and at 9901 Mc it is 12 db greater.

2. There are three cases where the sensitivity is higher for signals introduced at the 90° H-bend than for signals at the T-R tube despite the larger path length, and the added attenuation (due to the rotary joint) of the 90° H-bend input. These cases are at 3240 Mc for the $TE_{01}$, $TE_{02}$ and $TM_{11}$ modes.

The increased sensitivity despite the added path length and attenuation due to the rotary joint is probably due to conversion of part of the higher-order mode to the $TE_{10}$ mode. At 3240 Mc all higher-order modes are cut off so that only the $TE_{10}$ mode can propagate as a wave. The matching posts and rotary joint in the waveguide are designed for operation in the band of 3100 to 3500 Mc. For signals at frequencies outside this design band these units become obstructions and discontinuities in the waveguide, and part of the energy in the higher-order modes can be converted to energy in the $TE_{10}$ mode. This results in a higher sensitivity reading.

Figures 10 and 11 contain plots of the attenuation versus frequency of the six modes:

$TE_{10}$
$TE_{20}$
$TE_{01}$
$TM_{11}$
$TE_{30}$
$TE_{02}$

below their cutoff frequencies, and above their cutoff frequencies, respectively. Figure 10 contains the attenuation for each mode due to the signal frequency being below the cutoff frequency and where losses are neglected. Figure 11 contains the attenuation for each mode for frequencies above cutoff but including wall losses due to copper walls.

As can be seen, the attenuation is high for frequencies below the cutoff frequency and low for frequencies above the cutoff frequency. At 3240 Mc all higher-order modes are cut off and only the $TE_{10}$ mode propagates. Thus conversion of energy in the higher-order modes to the dominant $TE_{10}$ mode can result in a higher sensitivity.

Table IV contains listings of the difference in decibels between the sensitivity at 3240 Mc and the sensitivity at the other test frequencies for each of the input planes and each of the modes. These data are a measure of the selectivity of sections of the radar's RF system using 3240 Mc as a reference.

A final test was performed in which the radar's own local oscillator was used for all mode tests. This test consisted of measuring selected spurious responses of the radar tuned to approximately 3240 Mc, using the six different modes at the input to the 90° H-bend. The results of these tests are shown in Table V. The same general trends noted in data obtained using a substitute l.o. signal are encountered when the actual spurious responses are being measured.

## VI. CONCLUSIONS

The following conclusions can be drawn from the results obtained on the tests to determine mode sensitivity of the radar system:

1. For signals introduced at each of the three input planes the spread in sensitivities for each of the six modes used in the tests in general decreases with increasing frequency. As an example, as shown in Table II, for input signals at the 90° H-bend, the spread narrows from 37 db at 3240 Mc to 7 db at 9971 Mc.

2. The narrowing of the spread of sensitivities with increasing frequency indicates that the measured sensitivity of the radar can be obtained without concern for the mode distribution set up in the waveguide system if

(a) the frequency is sufficiently high that several modes can be propagated; i.e., not cut off,

(b) an excitation mode is used which is not cut off,

(c) some uncertainty in the results is accepted; for the radar tested this uncertainty appears to be within 7 db at 9971 Mc.

3. $TE_{01}$, $TM_{11}$ and $TE_{02}$ signals at 3240 Mc have a higher sensitivity when introduced at the H-bend input than at the T-R tube, despite the longer path length and greater selectivity of the former input. This effect is believed to be due to conversion of the $TE_{01}$, $TM_{11}$ and $TE_{02}$ modes, all of which are cut off at 3240 Mc, to the $TE_{10}$ mode which can propagate at this frequency.

4. No sharp increase in the sensitivity of any of the modes studied was observed as the frequency of the mode was increased. A sharp increase in sensitivity would be expected on the basis of the curves of Figures 10 and 11 as the signal frequency was increased from below cutoff to above cutoff for each mode. However, these curves are approximations and do not include the effects of losses in the waveguide for frequencies below cutoff. Inclusion of these losses changes the shape of the attenuation-versus-frequency curve, smoothing it out so that the attenuation changes more gradually with frequency and no sharp variations are obtained.

5. The $TM_{11}$ mode shows a variation in sensitivity of 59 db between 3240 Mc and 4140 Mc for input at the H-bend. Examination of the data in Table I indicates that much of this large attenuation is being caused by the preselector.

6. Attenuation of the various modes is caused not only by the preselector but also by the rotary joint. The latter unit is of coaxial-line construction and hence its use in the waveguide system requires transitional sections and matching units. These are designed for operation in the 3100 to 3500 Mc frequency band. At frequencies outside this design band severe mismatch conditions can result, leading to both attenuation and mode conversion.

7. The attenuation of the rf system does not increase monotonically with frequency. As shown in Table I, the measured sensitivity fluctuates considerably with frequency. This is of importance since it implies that a selectivity curve for the RF system cannot be specified accurately without taking data at frequency intervals small compared to the fluctuations of the selectivity curve. The selectivity curve is also a sensitive function of the preselector cavity tuning, a fact which means that a different selectivity curve must be obtained for each setting of the preselector.

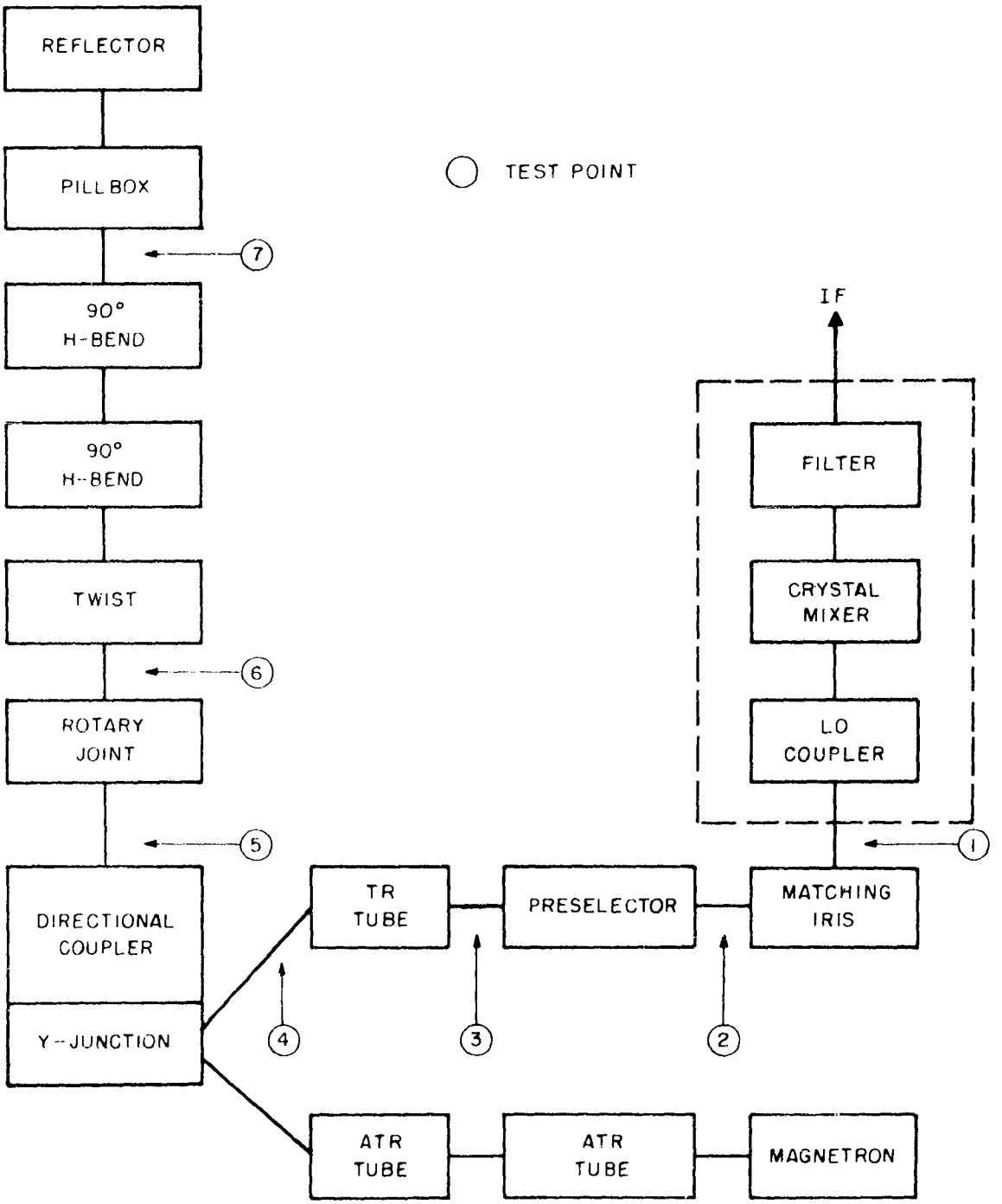
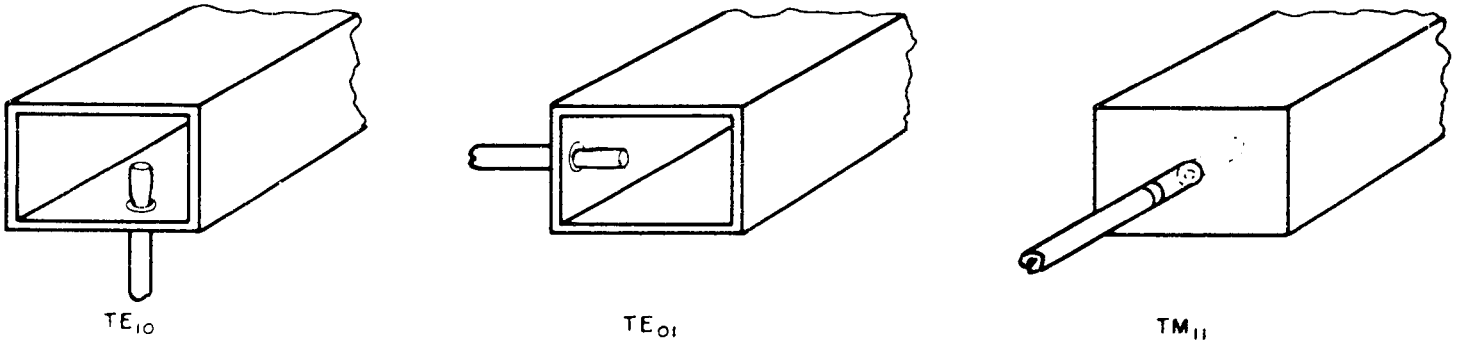
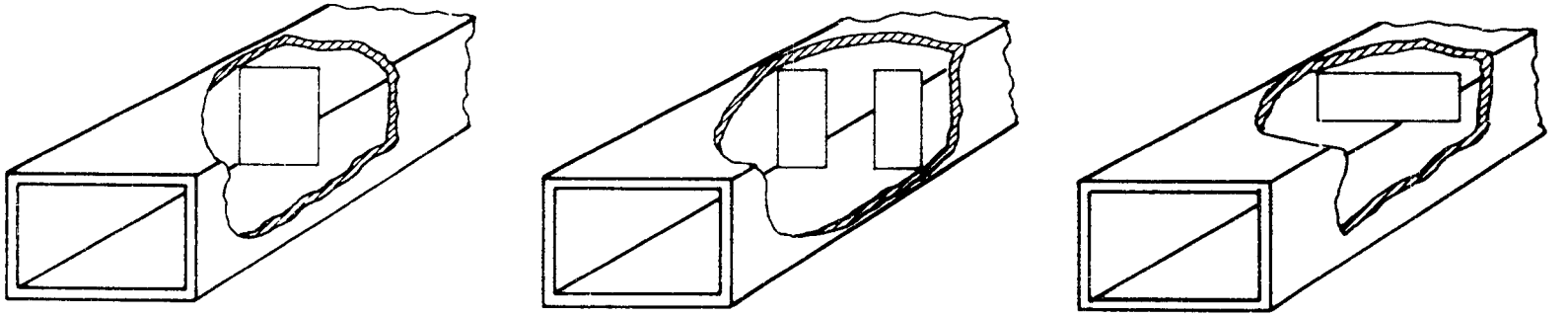



FIG. 1 RF SECTION




(a) MODE EXCITERS




(b) MODE CONVERTERS

FIG. 2 SKETCHES OF MODE EXCITERS AND CONVERTERS

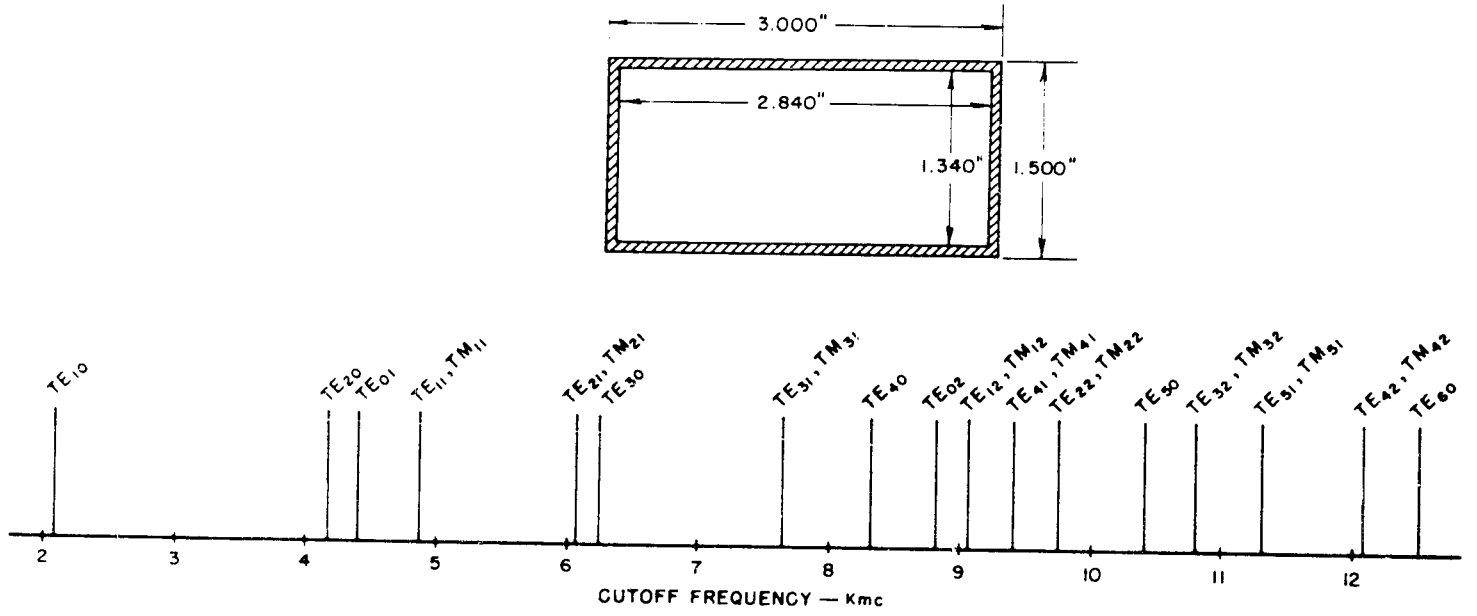



FIG. 3 CUTOFF FREQUENCIES FOR MODES PROPAGATING IN S-BAND RECTANGULAR WAVEGUIDE

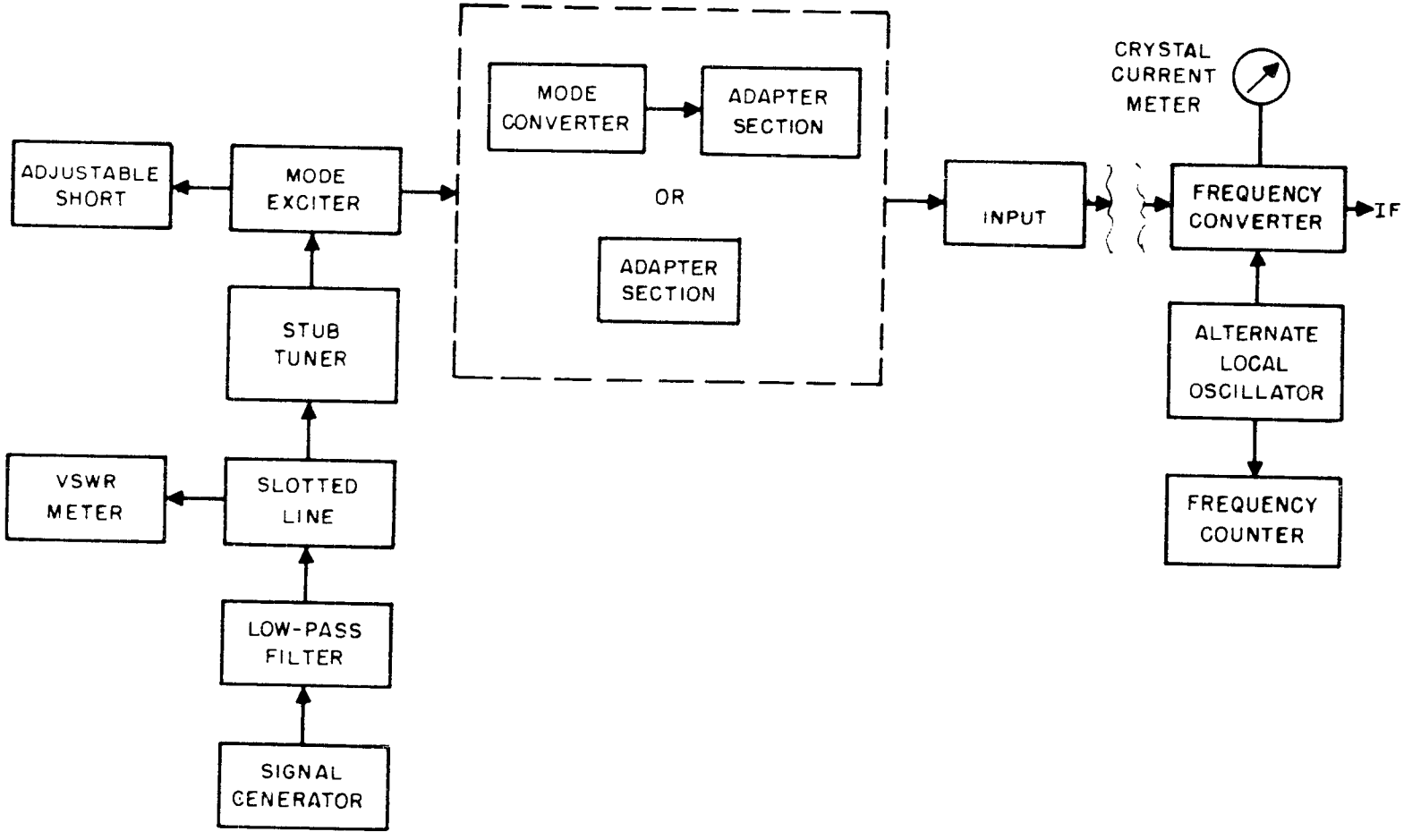



FIG. 4 BLOCK DIAGRAM OF EQUIPMENT TEST SETUP

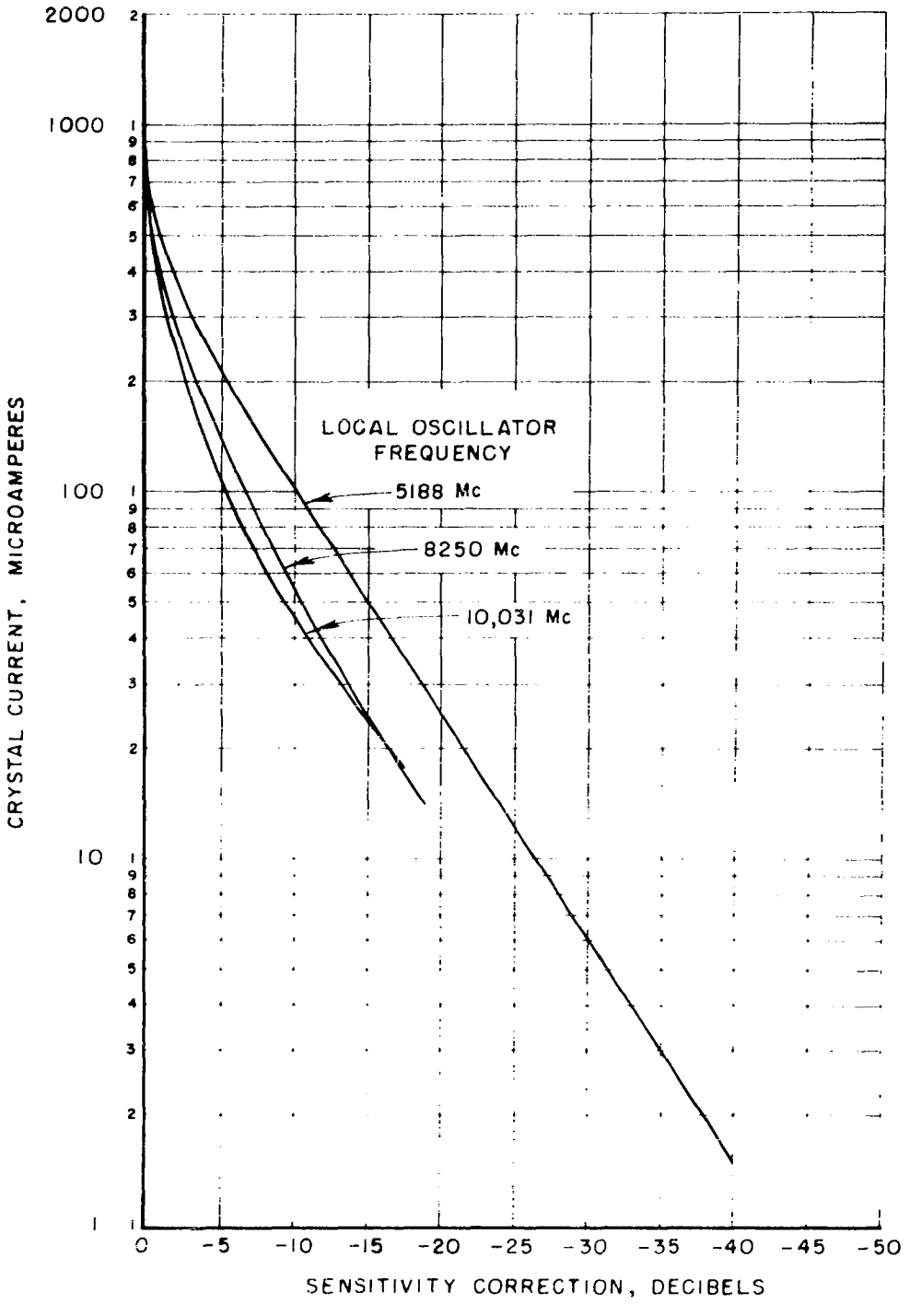



FIG 5 SENSITIVITY CORRECTION CURVES FOR MIXER CRYSTAL

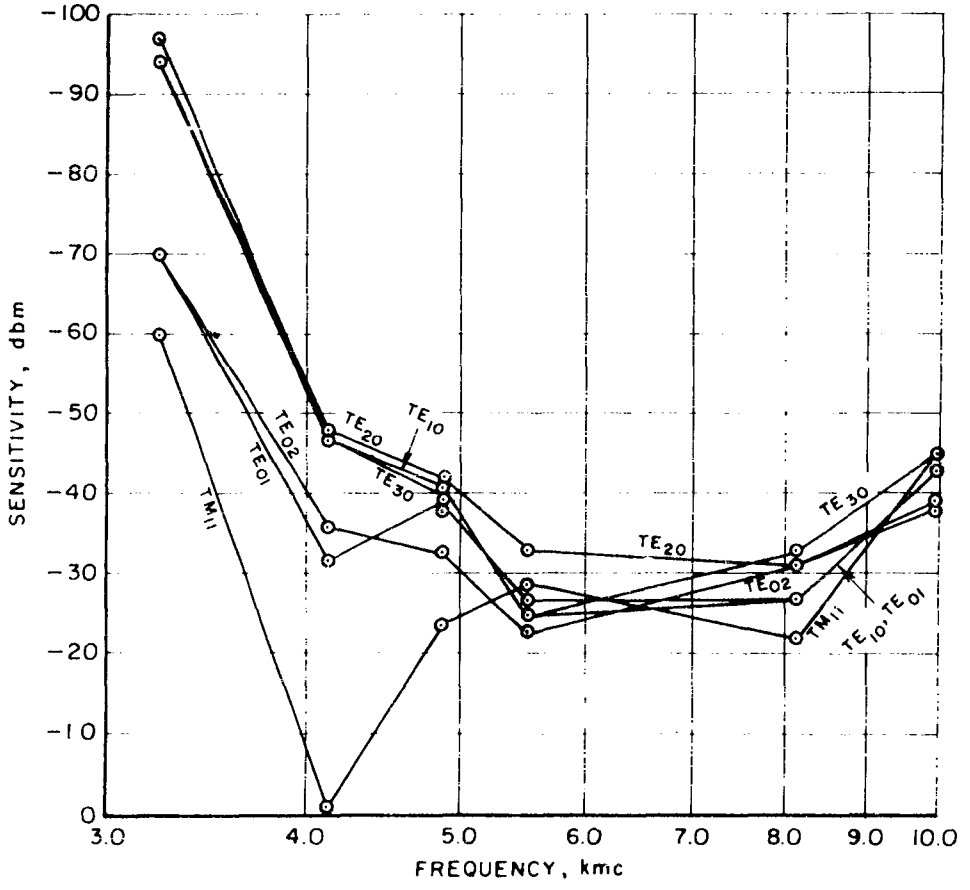



FIG 6 MODE SENSITIVITY VERSUS FREQUENCY FOR INPUT AT 90° H-BEND

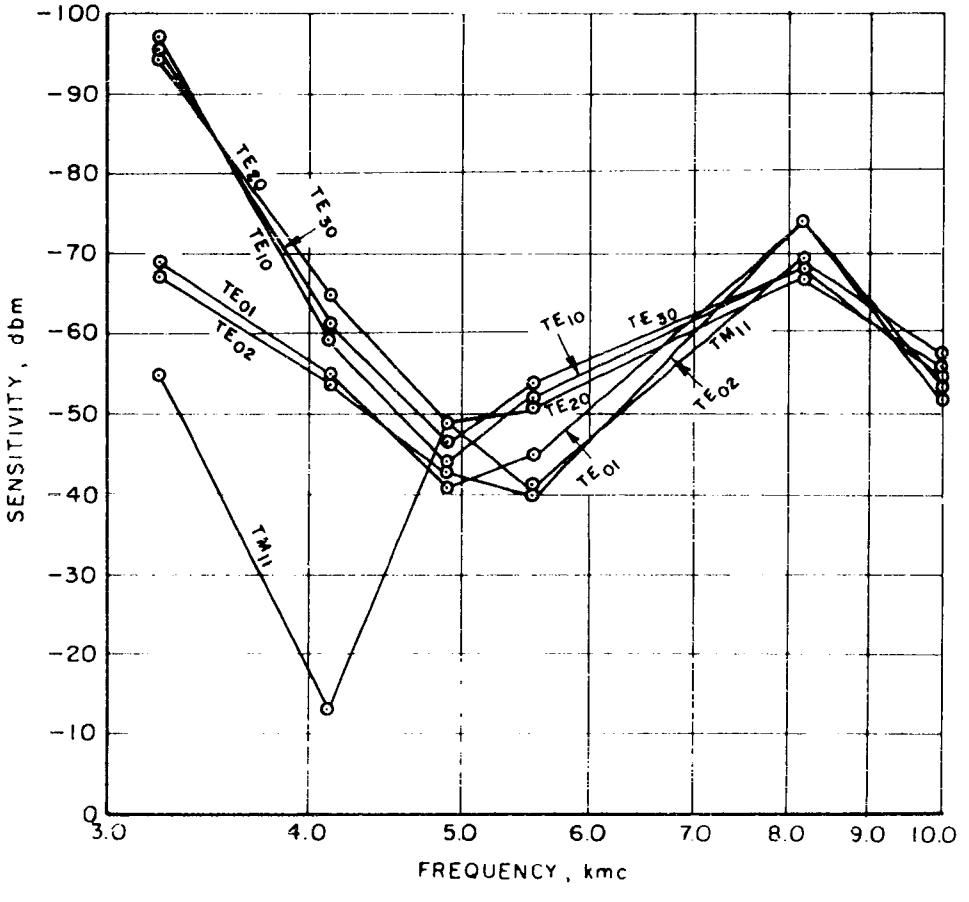



FIG 7 MODE SENSITIVITY VERSUS FREQUENCY FOR INPUT AT T-R TUBE

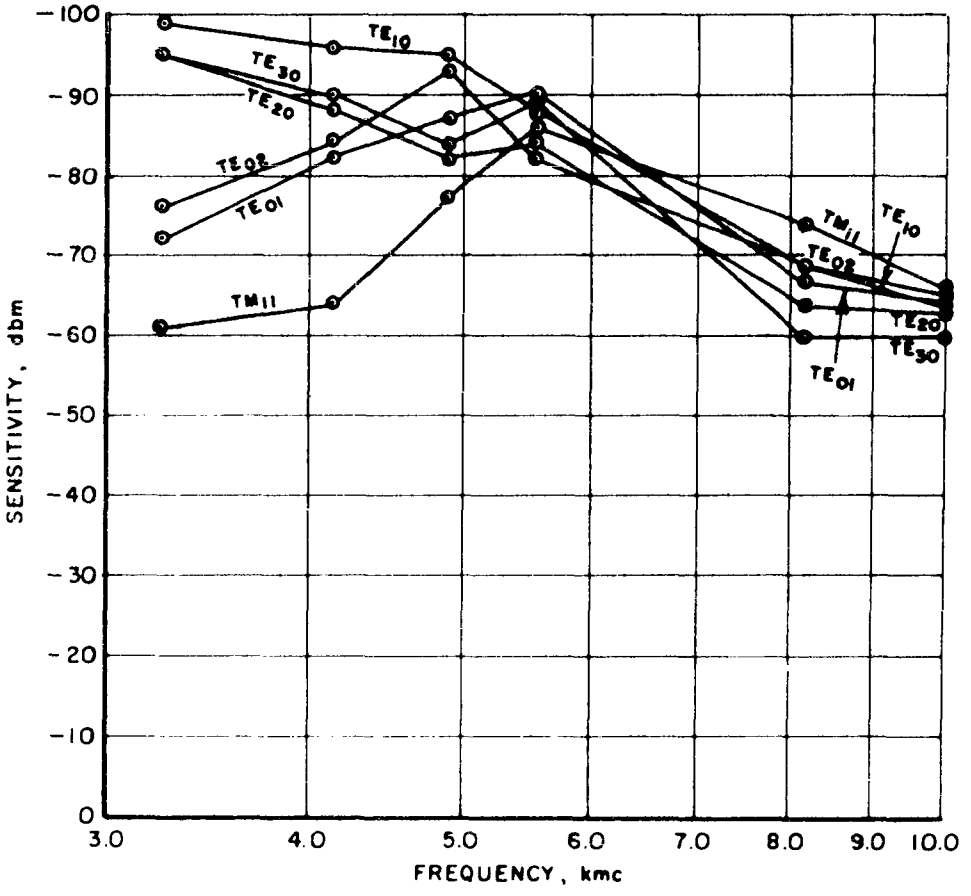



FIG 8 MODE SENSITIVITY VERSUS FREQUENCY FOR INPUT AT CRYSTAL MIXER

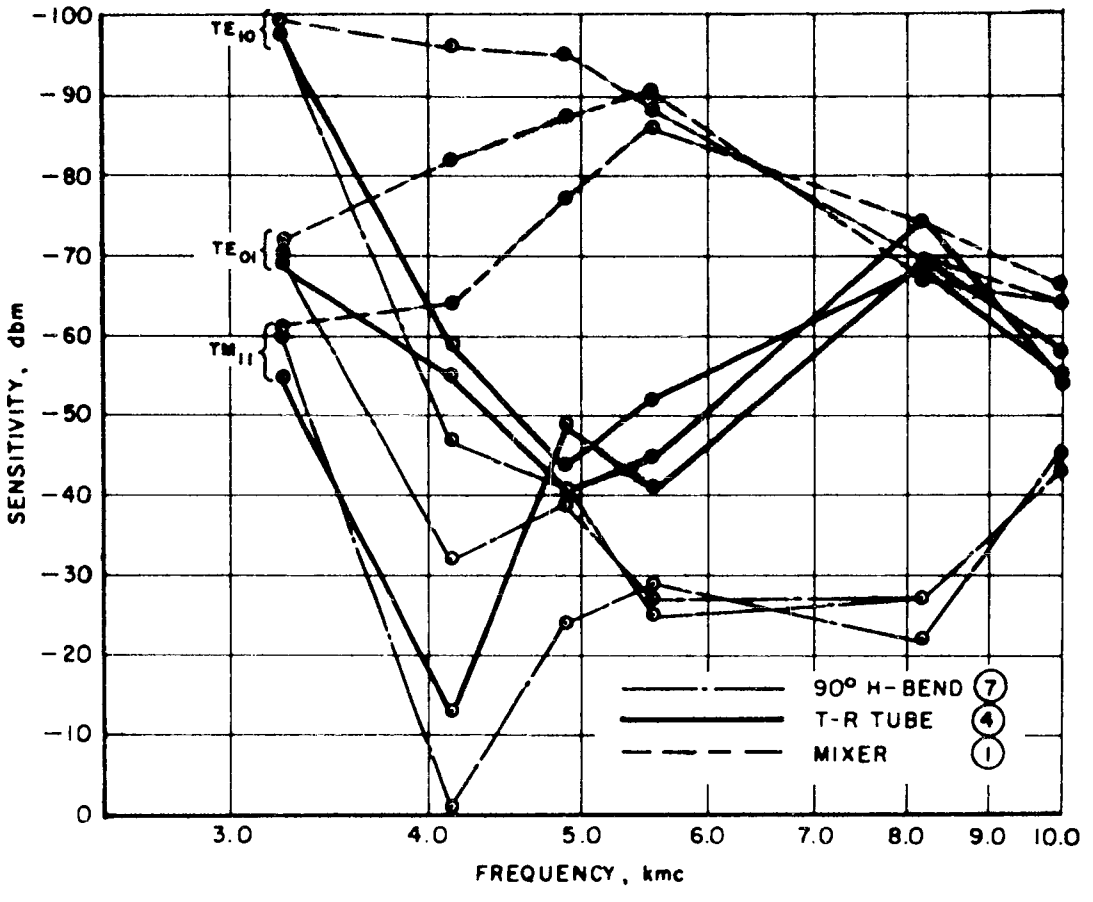



FIG. 9 MODE SENSITIVITY VERSUS FREQUENCY FOR $TE_{10}$, $TM_{11}$ AND $TE_{01}$ MODES AT INPUTS ①, ④ AND ⑦

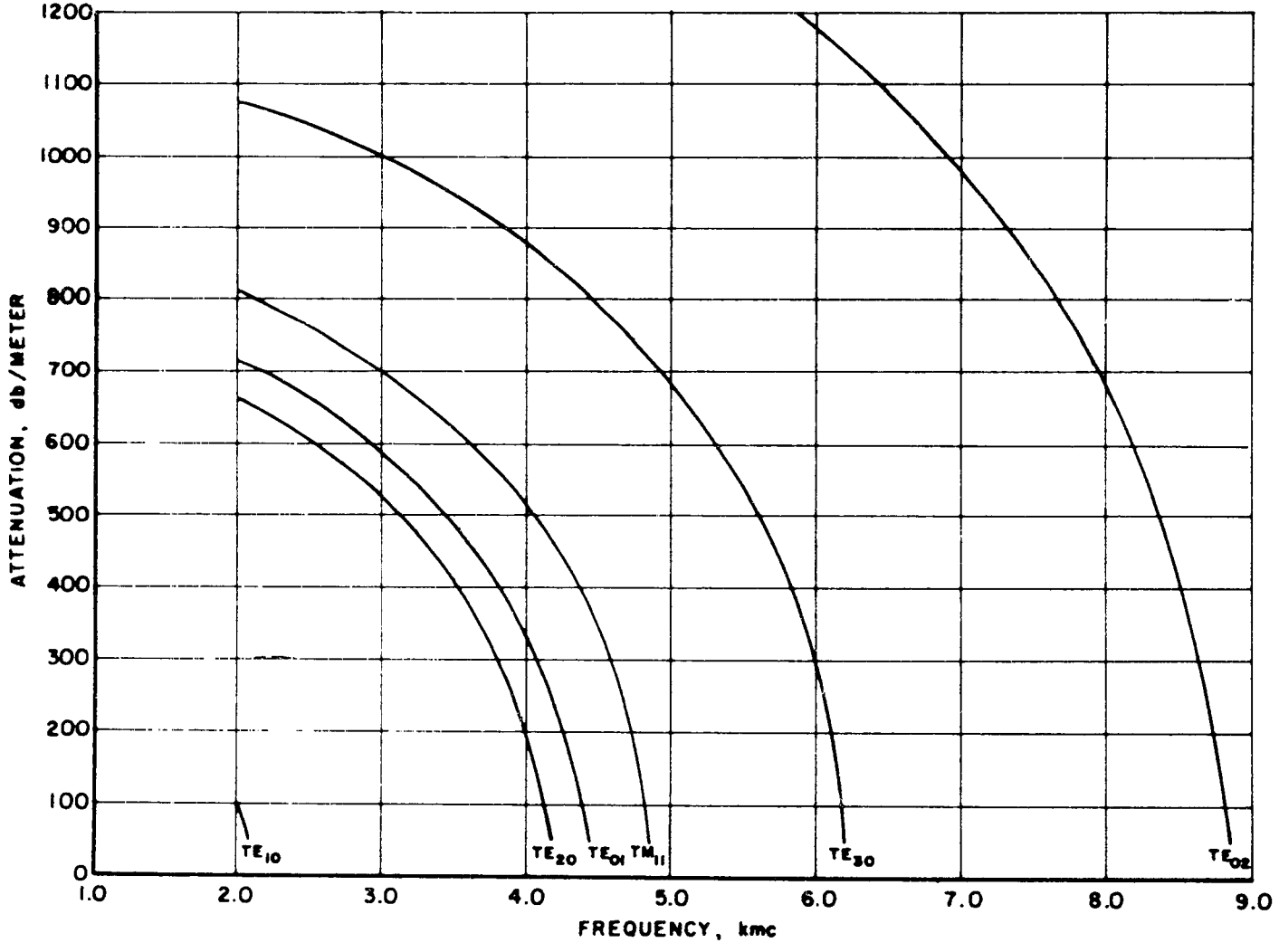



FIG. 10 ATTENUATION OF MODES BELOW THEIR CUTOFF FREQUENCIES

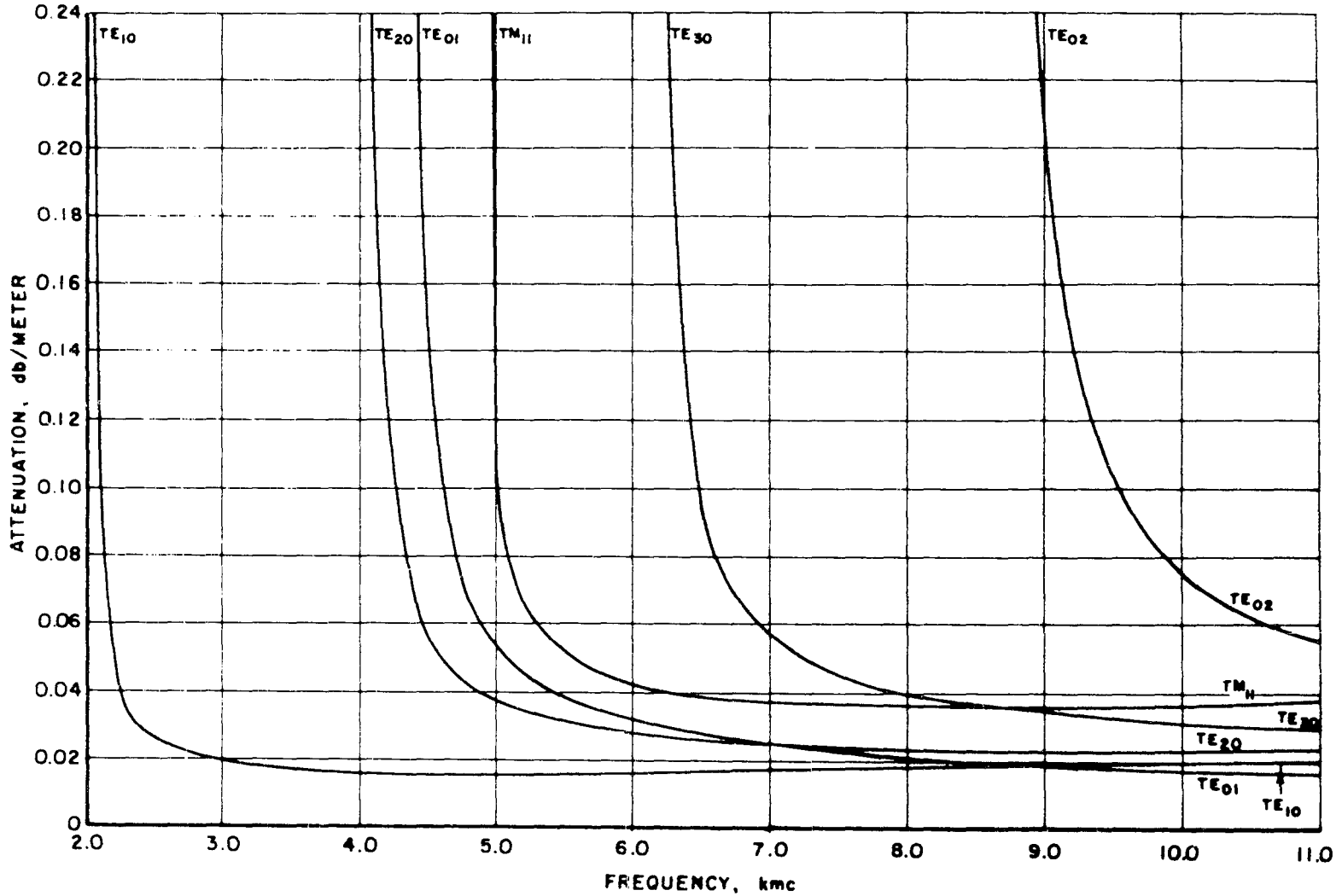



FIG. 11 ATTENUATION OF MODES ABOVE THEIR CUTOFF FREQUENCIES

Table I

Radar Sensitivity* vs Frequency for Six Modes and Three Signal Input Planes

| Input Plane | Mode Exciter and Converter | Frequency - Mc 3240 | 4140 | 4896 | 5540 | 8190 | 9971 |
|---|---|---|---|---|---|---|---|
| 7 90° H-Bend | $TE_{10}$ | -97 | -47 | -41 | -25 | -27 | -43 |
| | $TE_{10}+TE_{20}$ | -94 | -48 | -42 | -33 | -31 | -38 |
| | $TE_{01}$ | -70 | -32 | -39 | -27 | -27 | -43 |
| | $TM_{11}$ | -60 | - 1 | -24 | -29 | -22 | -45 |
| | $TE_{10}+TE_{30}$ | -94 | -47 | -40 | -25 | -33 | -45 |
| | $TE_{01}+TE_{02}$ | -70 | -36 | -33 | -23 | -31 | -39 |
| 4 T-R Tube | $TE_{10}$ | -97 | -59 | -44 | -52 | -68 | -55 |
| | $TE_{10}+TE_{20}$ | -94 | -65 | -49 | -51 | -67 | -56 |
| | $TE_{01}$ | -69 | -55 | -41 | -45 | -74 | -54 |
| | $TE_{11}$ | -55 | -13 | -49 | -41 | -69 | -58 |
| | $TE_{10}+TE_{30}$ | -95 | -61 | -47 | -54 | -68 | -54 |
| | $TE_{01}+TE_{02}$ | -67 | -54 | -43 | -40 | -74 | -52 |
| 1 Mixer | $TE_{10}$ | -99 | -96 | -95 | -88 | -69 | -64 |
| | $TE_{10}+TE_{20}$ | -95 | -88 | -82 | -84 | -64 | -63 |
| | $TE_{01}$ | -72 | -82 | -87 | -90 | -67 | -64 |
| | $TM_{11}$ | -61 | -64 | -77 | -86 | -74 | -66 |
| | $TE_{10}+TE_{30}$ | -95 | -90 | -84 | -89 | -60 | -60 |
| | $TE_{01}+TE_{02}$ | -76 | -84 | -93 | -82 | -69 | -65 |

*Sensitivities are listed in decibels referred to one milliwatt (dbm)

TABLE II

Difference in Sensitivity in db Between $TE_{10}$ and Higher-Order Modes

| Input Plane | Mode Exciter and Converter | Frequency - Mc 3240 | 4140 | 4896 | 5540 | 8190 | 9971 |
|---|---|---|---|---|---|---|---|
| 7 $90^{o}$ H-Bend | $TE_{10}+TE_{20}$ | -3 | +1 | +1 | +8 | +4 | -5 |
| | $TE_{01}$ | -27 | +15 | -2 | +2 | 0 | 0 |
| | $TM_{11}$ | -37 | -46 | -17 | +4 | -5 | +2 |
| | $TE_{10}+TE_{30}$ | -3 | 0 | -1 | 0 | +6 | +2 |
| | $TE_{01}+TE_{02}$ | -27 | -11 | -8 | -2 | +4 | -4 |
| | Spread | 37 | 47 | 18 | 10 | 11 | 7 |
| 4 T-R Tube | $TE_{10}+TE_{20}$ | -3 | +6 | +5 | -1 | -1 | +1 |
| | $TE_{01}$ | -28 | -4 | -3 | -7 | +6 | -1 |
| | $TM_{11}$ | -42 | -46 | +5 | -11 | +1 | +3 |
| | $TE_{10}+TE_{30}$ | -2 | +2 | +3 | +2 | 0 | -1 |
| | $TE_{01}+TE_{02}$ | -30 | -5 | -1 | -12 | +6 | -3 |
| | Spread | 42 | 50 | 8 | 14 | 7 | 6 |
| 1 Mixer | $TE_{10}+TE_{20}$ | -4 | -8 | -13 | -4 | -5 | -1 |
| | $TE_{01}$ | -27 | -14 | -8 | +2 | -2 | 0 |
| | $TM_{11}$ | -38 | -32 | -18 | -2 | +5 | +2 |
| | $TE_{10}+TE_{30}$ | -4 | -6 | -11 | +1 | -9 | -4 |
| | $TE_{01}+TE_{02}$ | -23 | -12 | -2 | -6 | 0 | +1 |
| | Spread | 38 | 32 | 18 | 8 | 14 | 6 |

TABLE III

Difference in db Between Sensitivity at 90° H-Bend* (Input Plane 7) and Sensitivity at T-R Tube (Input Plane 4), and Mixer (Input Plane 1)

| Mode Exciter and Converter | Input Plane | Frequency - Mc 3240 | 4140 | 4896 | 5540 | 8190 | 9971 |
|---|---|---|---|---|---|---|---|
| $TE_{10}$ | 4 | 0 | +12 | +3 | +27 | +41 | +12 |
| | 1 | +2 | +49 | +54 | +63 | +42 | +21 |
| $TE_{10}+TE_{20}$ | 4 | 0 | +17 | +7 | +18 | +36 | +18 |
| | 1 | +1 | +40 | +40 | +51 | +33 | +25 |
| $TE_{01}$ | 4 | -1 | +23 | +2 | +18 | +47 | +11 |
| | 1 | +2 | +50 | +48 | +63 | +40 | +21 |
| $TM_{11}$ | 4 | -5 | +12 | +25 | +12 | +47 | +13 |
| | 1 | +1 | +63 | +53 | +57 | +52 | +21 |
| $TE_{10}+TE_{30}$ | 4 | +1 | +14 | +7 | +29 | +35 | +9 |
| | | +1 | +43 | ∓44 | +64 | +27 | +15 |
| $TE_{01}+TE_{02}$ | 4 | -3 | +18 | +10 | +17 | +43 | +13 |
| | 1 | +6 | +48 | +60 | +59 | +38 | +26 |
| Average for | 4 | =1 | +16 | +9 | +20 | +42 | +13 |
| All 6 Modes | 1 | +2 | +49 | +50 | +60 | +39 | +22 |
| Maximum deviation from Average | 4 | 4 | 9 | 16 | 9 | 7 | 5 |
| | 1 | 4 | 14 | 10 | 9 | 13 | 7 |

*90° H Bend used as a reference

Table IV

Difference in db Between Sensitivity at 3240 dbc and Sensitivity at Other Test Frequencies

| Input Plane | Mode Exciter and Converter | Frequency - Mc 4140 | 4896 | 5540 | 8190 | 9971 |
|---|---|---|---|---|---|---|
| 7 90° H-Bend | $TE_{10}$ | -50 | -56 | -72 | -70 | -54 |
| | $TE_{10}+TE_{20}$ | -46 | -52 | -61 | -63 | -56 |
| | $TE_{01}$ | -38 | -31 | -43 | -43 | -27 |
| | $TM_{11}$ | -59 | -36 | -31 | -38 | -15 |
| | $TE_{10}+TE_{30}$ | -47 | -54 | -69 | -61 | -49 |
| | $TE_{01}+TE_{02}$ | -34 | -37 | -47 | -39 | -31 |
| 4 T-R Tube | $TE_{10}$ | -38 | -53 | -45 | -29 | -42 |
| | $TE_{10}+TE_{20}$ | -29 | -45 | -43 | -27 | -38 |
| | $TE_{01}$ | -14 | -28 | -24 | + 5 | -15 |
| | $TM_{11}$ | -42 | - 6 | -14 | -14 | + 3 |
| | $TE_{10}+TE_{30}$ | -34 | -48 | -41 | -27 | -41 |
| | $TE_{01}+TE_{02}$ | -13 | -24 | -27 | + 7 | -15 |
| 1 Mixer | $TE_{10}$ | - 3 | - 4 | -11 | -30 | -35 |
| | $TE_{10}+TE_{20}$ | - 7 | -13 | -11 | -31 | -32 |
| | $TE_{01}$ | +10 | +15 | +18 | - 5 | - 8 |
| | $TM_{11}$ | + 3 | +16 | +25 | +13 | + 5 |
| | $TE_{10}+TE_{30}$ | - 5 | -11 | - 6 | -35 | -35 |
| | $TE_{01}+TE_{02}$ | + 8 | +17 | + 6 | - 7 | -11 |

| Dial Freq. | Meas. Freq. | P Q S | $TE_{10}$ | Recheck RCK $TE_{10}$ | $TE_{20}$ | $TE_{30}$ | $TM_{11}$ | $TE_{01}$ | $TE_{02}$ | $f_o$ 3240 MC |
|---|---|---|---|---|---|---|---|---|---|---|
| 3158 | | | 2 | | | | | | | |
| 3245 | 3238 | 1 1 - | 96 | 95 | 93 | 93 | 60 | 66 | 65 | $TE_{10}$ |
| 3275 | 3267 | 2 2 - | 28 | 30 | 26 | 23 | N.R. | N.R. | N.R. | |
| 3285 | 3277 | 3 3 - | 10 | 9 | 2 | 7 | N.R. | N.R. | N.R. | |
| 3335 | 3327 | 2 2 + | 14 | 13 | 11 | 10 | N.R. | N.R. | N.R. | |
| 3360 | 3356 | 1 1 + | 48 | 47 | 44 | 45 | 3 | 18 | 16 | |
| 5000 | 4978 | | 7 | 6 | 6 | 6 | N.R. | 0 | 3 | $TE_{20}$, $TE_{01}$, $TM_{1}$ |
| 6075 | | | -- | 4 | 7 | 6 | 4 | 5 | 1 | $TE_{30}$ |
| 6200 | | | -- | 2 | 2 | 0 | 2 | >0 | >0 | |
| 6580 | 6540 | 2 1 - | 36 | 41 | 41 | 44 | 28 | 45 | 41 | |
| 6695 | 6660 | 2 1 + | 32 | 36 | 36 | 37 | 11 | 37 | 38 | |
| 9840 | 9839 | 3 1 - | 3 | 15 | 14 | 15 | 19 | 20 | 14 | $TE_{02}$ |
| 9955 | 9960 | 3 1 + | 16 | 15 | 15 | 16 | 10 | 17 | 15 | |

TABLE V. LIST OF SPURIOUS RESPONSE SENSITIVITIES OF RADAR TUNED TO 3240 MC AS A FUNCTION OF MODE AT 90° H BEND

# A SURVEY OF FM RECEIVER TECHNIQUES FOR REDUCING COCHANNEL AND ADJACENT-CHANNEL INTERFERENCE

Elie J. Baghdady,* Harold G. Fritz, Ahmad F. Ghais, and Joseph M. Gutwein
ADCOM, Inc.
Cambridge, Mass.

ABSTRACT

The characteristics of CW-type and impulsive disturbances in FM are briefly described in order to bring out their differences from message modulation. Fundamental aspects of receiver design to ensure proper functional performance in various parts of the receiver are then pointed out. This is followed by a survey of various receiver signal-processing operations that lead to important reductions and often virtual elimination of the interference or its consequent disturbances.

Among the techniques described are those for enabling a desired signal to be received in the presence of other undesired signals that may be stronger or weaker than the desired signal -- including feedforward and feedback around the limiter, dynamic and static trapping, phase-locked loops and frequency compressive feedback. Practical design considerations are pointed out in every case.

---

* Also of the Department of Electrical Engineering and Research Laboratory of Electronics, Mass. Inst. of Tech., Cambridge, Mass.

Note: This paper will be published in the "Proceedings of the Eighth Conference on Radio Interference and Electronic Compatibility."

# CAPTURE EFFECTS OF DIODE ENVELOPE DETECTORS -- A DETERMINANT OF RECEIVER SELECTIVITY

J. E. Bridges
Armour Research Foundation
Chicago, Illinois

Abstract. - The diode-envelope detector plays a significant role in determining the true selectivity characteristics of a receiver. A review of the basic equations relating to envelope detection shows that the carrier to interference ratio is a significant parameter in the determination of adjacent channel interference effects. It is shown that when the carrier-to-interference ratio is large, additional selectivity is obtained by the capture effect. Under impulse-noise or other interference conditions, where the carrier-to-interference ratio is less than one, the diode detector process is captured by the noise or interference and the desired signal is significantly degraded, well beyond the effects indicated by the usual RF and IF selectivity response.

A method of recapturing the weaker of two adjacent channel signals impressed on a diode detector without greatly modifying the IF response will be briefly discussed. In this case, the "Q" of one of the L-C circuits of the IF amplifier is increased so as to enhance the desired carrier amplitude. Appropriate post-detection filtering is designed to restore the desired waveshape and to give added effective selectivity.

## I. INTRODUCTION

The second detector is often regarded as just another circuit element, -- not much different than other components found in any communications or radar receiver. It is, perhaps, regarded as slightly more complex than resistors or condensers, but far simpler than any of the other components. This may be true, but the same cannot be said about the operation and performance of the diode detection process.

Many college texts present only a cursory treatment of the detection process -- in spite of its important influence on the operation of communication receivers and, other certain conditions, radar receivers. A number of excellent papers, however, have been published on this subject.[1-8]

To thoroughly understand the basic operation of a second detector we must ask ourselves this question, just what does the second detector do? All it does, if properly designed, is to follow the envelope of the IF signals impressed upon it. So the clue to understanding the diode detection process lies not within the thermionic or crystal diode in itself, but in the peculiar way in which the various signals presented to the detector combine to form an envelope. I should emphasize that I am referring to the so-called linear diode detectors.

To see how the various signals combine to form an envelope consider the following simple example, which many of you are familiar with. Assume two sinusoidal waveforms which have very nearly the same frequency. These waveforms are described in Equation 1. 1 which shows the sum of these two frequencies.

$$e(t) = a\cos\omega t + b\cos\nu t \qquad (1.1)$$

$$e(t) = [a^2+b^2+2ab\cos(u-v)t]^{1/2}\cos[ut - \Phi(a, b, (v-u)t)]$$

If Equation (1. 1) is suitably manipulated, Equation (1. 2) can be derived. This shows an envelope function which amplitude modulates a phase modulated carrier. It is this envelope function in which we are most interested.

Figure 1. 1 illustrates this a little bit more vividly. Figure 1. 1(a) illustrates the type of envelope encountered when both signals are of the same amplitude. We note that we have a distorted sine-wave type modulation and also a rather pronounced phase modulation at the time when the envelope is very nearly zero. This phase modulation is of importance in FM receivers, but is of little concern in the diode envelope detection process. Figure 1. 1(b) illustrates the case where one of the amplitudes is approximately twice the other amplitude. We note that the envelope is approaching an undistorted sine wave and that the envelope looks very similar to usual AM modulated envelope. Figure 1. 1(c) illustrates the case where one signal is considerably larger than the other; and, in this case, the envelope is very similar to the envelope of an amplitude modulated sine-wave carrier.

Now assume a more complex example; that of the envelope developed by two amplitude modulated carriers, where u is the angular frequency for the desired carrier, and v and w are the angular frequencies of its sidebands, where x is the angular frequency of the undesired carrier, and y and z are the angular frequencies of the undesired carrier's sideband; also, where a is the amplitude of the desired carrier, and b and c are the amplitudes of the desired carrier sidebands, where d is the amplitude of the interfering carrier and e and g are the amplitudes of the interfering carrier's two sidebands. These are graphically illustrated in Figure 1. 2. In addition, we must also assume that the difference between the two carrier frequencies is small compared to the average frequency of the two carriers. Equation 1. 3 defines the instantaneous waveform.

$$e(t) = a\cos ut + b\cos vt + c\cos wt + d\cos xt + e\cos yt + g\cos zt \qquad (1.3)$$

As has been derived previously,[9] the envelope function of Eq. 1. 3 can be expressed as follows by Eq. 1. 4.

$$\begin{aligned}\text{envelope} = \{&a^2+b^2+c^2+d^2+e^2+g^2 + 2ab\cos(v-u)t + 2ac\cos(w-u)t \\ &+ 2ae\cos(y-u)t + 2ag\cos(z-u)t + 2bc\cos(w-v)t \\ &+ 2bd\cos(x-v)t + 2be\cos(y-v)t + 2bg\cos(z-v)t \\ &+ 2cd\cos(x-w)t + 2ce\cos(y-w)t + 2cg\cos(z-w)t \\ &+ 2de\cos(y-x)t + 2dg\cos(z-x)t + 2eg\cos(z-y)t\}^{1/2}\end{aligned} \qquad (1.4)$$

To simplify Equation 1.4 so as to permit a fairly simple explanation, assume each carrier to be modulated 30% or less and that the desired carrier to the interfering carrier has a ratio of two or more. Equation 1.4 then reduces to the following for an error of approximately 10% or less in the signal-plus-noise to noise amplitude ratio.

$$\text{envelope} = \left\{ a^2 + d^2 + 2abcos(v-u)t + 2accos(w-u)t + 2adcos(x-u)t + 2decos(y-x)t + 2dgcos(z-x)t \right\}^{1/2} \quad (1.5)$$

Defining predetection carrier to interference ratio as, $s = a/d$ and noting that $b = \frac{1}{2} m_a a$ where "$m_a$" is the % modulation of the desired carrier Equation 1.5 reduces to that indicated in Equation 1.6.

$$\text{envelope} = \left\{ a^2 + a^2/s^2 + 2a^2 m_a cos\omega_a t + \frac{2a^2}{s} cos(x-u)t + \frac{2a^2 m_i}{s^2} cos\omega_i t \right. \quad (1.6)$$

where $\omega_a$ is the desired moduation and $\omega_i$ the interfering modulation and $m_i$ % modulation of interfering carrier.

Equation 1.6 is now in a form that can be expanded by the binomial theorem which then gives us the approximate detector output as indicated by Equation 1.7.

$$\text{envelope} = a + a/2s^2 + am_a cos\omega_a t + a/s cos(x-u)t + m_i a/s^2 cos\omega_i t \quad (1.7)$$

Equation 1.7 illustrates the basic capture effect. Note that for every db reduction of the interfering carrier, the modulation of the interfering carrier is reduced at twice that rate. If the interfering carrier is reduced in amplitude by 1 db, its modulation will be reduced by 2 db. This effect is often known as modulation suppression[10] It should be emphasized that this capture effect applies only to the modulation of the interfering carrier. We note also the 4th term in Equation 1.7 exists and this is the beat note between the desired carrier and the interfering carrier. The amplitude of this beat note is directly proportional to the amplitude of the interfering carrier. If the frequency difference between the interfering carrier and the desired carrier lies in the audio or video bandwidth following the detector, no capture effect exists for this beat note. If, however, the difference between the interfering and desired carrier frequencies is outside the audio or video bandwidths, then this term can be neglected provided that it does not desensitize the video or audio sections of the receiver.

The modulation suppression effect may perhaps be intuitively explained in a different manner. The diode detector may be considered as a sort of mixer or converter stage. Perhaps it can be imagined to be something like a switch. This switch is opened and closed at some frequency. If one sinusoidal signal is considerably larger than another sinusoidal signal, this switch is opened and closed at the rate determined by the larger signal frequency. In this case, the information contained in the frequency

and phase relationships of the larger carrier and its sidebands is preserved, since all that has been done is to simply transfer the signals at IF frequency to dc, so that the carrier is at 0 frequency. But in the case of the weaker signal and its sidebands, the informational relationships contained between its sidebands is now virtually destroyed. These weaker signals exist as beats only between the larger carrier. Thus the modulation of the weaker carrier is suppressed by the capture effect, and the amplitude of the weaker signal's modulation is a function of the ratio of a larger carrier to the smaller carrier.

It is also necessary to discriminate between two types of interfering conditions, that of co-channel interference and adjacent channel interference. In the case of co-channel interference where two carriers occupy the same channel, the modulation suppression effect does exist but is considerably masked because the audio or video bandwidth will pass the beat note between the desired carrier and the interfering carrier. In the case of adjacent channel interference, the beat note between the two carriers is suppressed by the filtering action of the video or audio circuits, but the modulation of the interfering carrier remains. Under these circumstances the modulaltion suppression effect is of importance and as will be developed in a later section can be shown to effectively increase the selectivity of a communications type receiver.

## II. AN EXAMPLE OF THE IMPORTANCE OF THE CAPTURE EFFECT

The following example will illustrate the importance of the capture effect. Consider the situation indicated in Figure 2. 1. Illustrated is a typical field interference condition. Perhaps the object of this configuration is to predict the interference effects. There is a desired transmitter and an interfering transmitter of which both signals are received by the front end of a communications receiver. These are subsequently amplified by the IF amplifier and are rectified by the linear-envelope diode detector. The output of the diode detector then passes through an audio amplifier and thence to a loud speaker. At the output of the loud speaker or the terminals of the loud speaker we have a distortion analyzer or some other type of root-mean-square amplitude indication. Figure 2. 2(a) illustrates the IF response of this type of receiver and Figure 2. 2(b) illustrates the acoustical output as a function of the modulating frequency.

Now suppose that frequency of the interfering transmitter can be varied at constant radiated power output. In addition, let assume that the desired transmitter may have a 400 cycle modulation and that the interfering transmitter would have perhaps a 1000 cycle modulation. At the start of the test the frequency of the interfering transmitter is adjusted to that of the desired transmitter, thus giving a co-channel interference situation. The ratio of the carrier of the desired transmitter to the undesired carrier is made equal to two. By means of a distortion analyzer, signal plus noise-to-noise ratio can be determined. In this case the signal is the 400 cycle note. The automatic gain control of the receiver is disabled and fixed by means of a battery. Then the frequency of the interfering transmitter is varied at constant output and the signal-plus-noise to noise ratio is noted as well as the components of the various frequencies at the second detector and at the acoustical output.

The approximate theoretical results of such a procedure by the use of Equation 1. 7 is indicated in Figure 2. 3. Curve A is the usual amplitude response of the intermediate frequency amplifier. Curve B

represents the desired modulation as a function of the difference frequency between the desired and undesired carriers. Curve C is the amplitude of the carrier-to-carrier beat note at the second detector. Curve D is representative of the amplitude of the interfering modulation if the capture effect is not taken into account. Curve E is representative of the interfering carriers modulation when the capture effect is taken into account. Curve F shows the actual output from the loud speaker of the carrier-to-carrier beat note. In Figure 2.3, the heavy lines are representative of actual outputs whereas the dotted lines are present only for purposes of illustration and comparison.

We note that the carrier-to-carrier beat note is relatively uneffected by the capture effect and exists in full magnitude until the carrier difference ($f_i - f_o$) is greater than the audio bandwidth. The interfering carriers modulation, however, within the audio bandwidth is suppressed by approximately 6 db. Where the IF amplifier's response begins to severely attenuate the interfering carriers amplitude and where the carrier-to-carrier beat note is reduced by the audio circuits the capture effect becomes more important and the undesired carrier's modulation falls off at a much greater rate than that indicated by the usual IF selectivity response.

Another example may more clearly illustrate the capture effects is as follows:

Assume that the interfering carrier for the co-channel interference condition is twice as large as the desired carrier. With these amplitude conditions, the frequency of the interfering carrier at constant output is slowly varied to the adjacent channel conditions. Figure 2.4 illustrates this condition. As before, Curve A represents the usual amplitude response to the IF amplifier. Curve B represents the amplitude of the 400 cycle desired modulation. Curve C represents the carrier-to-carrier beat note at the detector. Curve E represents the actual acoustical output of the undesired 1000 cycle modulation and Curve F represents the carrier-to-carrier acoustical output. In this case we note that Curve B, the desired modulation is suppressed about 6 db for the co-channel interference case by the capture effect. As the frequency of the interfering carrier is varied to the adjacent channel conditions, the carrier-to-interference ratio gradually approaches two or more, in which case the diode is recaptured by the desired carrier. During the time that the diode detector is captured by the undesired carrier, the modulation of the interfering carrier follows that of the IF response. However, when the desired carrier captures the diode detector, the interfering carrier's modulation again falls off at a much greater rate than that indicated by the usual IF amplitude response.

In short, by a very simple example, several of the basic factors which effect the performance of the diode envelope detector have been shown. The most important factor is of course the carrier-to-interference ratio. A second important factor of interest is the response of the IF amplifiers prior to the detector and the response of the video or audio amplifiers subsequent to the detector. Other important factors are obvious, such as the location of the desired carrier within the IF response and the location of the undesired carrier within the IF response. Also not taken into account but important was the frequency of the modulating signals and the degree of modulation.

The effect of impulse noise on the diode detector is very similar to that of a continuous wave carrier which is larger than the desired signal.

If the amplitude of the impulse noise ringing components in the IF becomes larger than the amplitude of the desired carrier, the diode detector is captured by the impulse noise. Under these conditions, the frequency and phase relationships between the desired carrier and its modulation are suppressed. This may be important in various A-M multiplex systems. It is also worthwhile to mention that this is another reason for suppressing the impulse noise prior to the IF and second detector.

A knowledge of the operation of the second detector is important in the measurements of noise figure of the receiver. To measure the ENSI of the receiver, the inserted carrier should be many times larger than the noise. This is spelled out in tests by Terman and Petit in Receiver Measurements, pages 408 to 410.

If thermal noise is applied to the diode detector, the precise analysis is too complex to be innumerated here. An approximate solution is illustrated in[9] and a more precise solution to some of the effects is given by Rice[5] and Goldman.[6] Figure 2.5 illustrates some of these effects. In this illustration the rms amplitude of the noise is normalized at unity and the rms amplitude of a larger sine wave is normalized at 2.8 times the amplitude of the noise. Of interest is the amplitude of the AC signals following the detector when a carrier is present and when the carrier is not present. We note that more than twice the noise power exists following the second detector when a large carrier is present than when it is absent. This occurs because the detection efficiency is reduced and the noise has to supply a type of quasi-carrier. The data illustrated in Figure 2.5 is approximate and a more thorough discussion is given in the listed references, and applies where the audio bandwidth following the detector is equal or greater than the 1/2 power IF bandwidth.

## III. REMEDIES

There are a number of techniques that can be employed to improve the capture effect. Only the simplest will be discussed here. The detection system described in the following paragraphs is capable of improving only adjacent channel interference problems, where the interfering signal at the second detector is larger than the desired signal for the conventional IF design, and where the difference in frequency between the two carriers is larger than the audio or video bandwidth.

Figure 3.1 shows a simple superheterodyne receiver except that two other elements have been added. Prior to the detector, the "Q" of one of the tuned circuits is allowed to increase by a factor of four for this example. In the case of tube circuits, this increases the IF gain while at the same time narrows the IF bandwidth. In the case of double-side-band A-M, this increased "Q" circuit should be located in the center of the I-F response. As large an increase in "Q" is desirable which is consistent with other design factors, such as local oscillator stability. Now if the desired A-M carrier is tuned at the peak of this new response, its higher frequency sidebands will be significantly attenuated, ; To reconstitute the appropriate amplitude relationships, a low-frequency deemphasis circuit can be added to the post-detection filtering. In the case of audio, pre-emphasis of the higher audio frequencies could also be considered.

Figure 3.2(a) shows the relative amplitude response of the peaked I-F response. Note that this response is simlar to that of Figure 2.2(a), except that the gain has been considerably increased in the center

portion of the IF response. Figure 3.2(b) shows Curve A, the low-frequency de-emphasis to equalize the low-frequency emphasis introduced by the IF peaking. For comparison, Curve B shows the post-detection filter response for the remaining audio portion.

If the concept shown in Figure 3.2 is used to enhance the reception of the weaker of two adjacent channel signals, the weaker signal is tuned to the peak of the IF response shown in Figure 3.2(a). Thus the carrier amplitude of the weaker signal, in this illustration is increased by a factor of four over that found in the usual IF response. If this action increases the desired carrier to interfering-carrier ratio sufficiently, say to 2 or greater, the detection process is captured by the smaller but desired signal and the modulation of the undesired carrier is then suppressed.

Assume that the interfering carrier for the co-channel interference condition is twice as large as the desired carrier as defined by the usual IF response. Figure 2.4 illustrates this condition. If the peaking de-emphasis techniques shown in Figure 3.2 are now substituted for the usual IF design as shown in Figure 2.4 and 2.2 the desired carrier will now become larger than the interfering carrier for all adjacent channel interfering conditions. Figure 3.3 illustrates this condition. As before, Curve A represents the usual amplitude response of the IF amplifier. Curve B represents the amplitude of the 400 cycle desired modulation. Curve C represents the carrier-to-carrier beat note at the detector. Curve E represents the acoustical output of the undesired 1000 cycle modulation and Curve F represents the carrier-to-carrier acoustical output.

As the frequency of the interfering carrier is varied form a co-channel interference condition to an adjacent channel interference condition, note that this scheme offers little benefit in the co-channel interference case, since the carrier-to-carrier beat note Curve F, predomonates at somewhere greater than a carrier difference of 7 kc, the benefits of the IF peaking now become apparent. The modulation of the desired carrier, Curve B, is suppressed for a much smaller range of tuning for the interfering carrier. In addition, the modulation of the undesired carrier, Curve E, is rapidly suppressed, once the interfering carrier is tuned out of the peak response. The following table illustrates the benefits of the IF peaking and post-detection de-emphasis scheme over the conventional approach.

Relative Audio Output Amplitudes

| $f_i - f_o$ | Conventional | | | Peaked | | |
|---|---|---|---|---|---|---|
| | Desired c's Modulation | S/N | Interfering c's Modulation | Desired c's Modulation | S/N | Interfering c's Modulation |
| 8 kc | .2 | .5 | .4 | .3 | 1.5 | .2 |
| 15 kc | .3 | 30 | .01 | .3 | 120 | .002 |

From Figures 2.4 and 3.3

The foregoing example was chosen to illustrate the principles involved and may not be the best practical solution. As mentioned previously, circuit and frequency stability pose challenging design problems. If transistors are employed, additional gain in the audio and video sections may have to be used, since gain is not always exchangeable for bandwidth in the case of transistors.

## IV. EXPERIMENTAL EXAMPLE

It is always interesting to obtain some experimental data to further illustrate analytical results. A collection of equipment to do this is illustrated in Figure 4.1, and is self-explanatory. Great care was taken so as not to overload any portion of the IF or detector circuits. The HP 608C output frequency was tuned to the center of the IF response, and could, if desired, be modulated about 30% by a 400 cycle tone. It represents the desired carrier and its modulation. The undesired carrier was generated, but inherently without modulation, by the Kay Verisweep. We can, however, consider its dc output as its modulation. The Verisweep's operation was adjusted so that its frequency varied from about 29 mc to 31 mc at a 60 cycle rate. The horizontal deflection of the 'scope was synchronized to the Verisweep's sweep rate. The bandpass filter is utilized to eliminate the carrier-to-carrier beat note except at the peak IF response. By means of the dual trace sampling plug-in unit, the output at the second detector and at the filter could be photographed sequentially for comparison.

Figure 4.2 A, B, and C shows the 'scope trace for various carrier to interference ratios without modulation. Note that in C, the dc output of the interfering carrier is suppressed, but that the beat note between the carriers was increased. D, E, and F of Figure 4.2 shows similar results except that the desired carrier was modulated 30%. D and E illustrate very dramatically the modulation suppression of the desired carrier when the interfering carrier is larger or of comparable amplitude. Note that at the outer edges of the trace, where the interfering carrier is blanked by the Verisweep circuit design, the detector behaves normally and detects the desired modulation.

## V. CONCLUSIONS AND RECOMMENDATIONS

The so-called linear diode detection process is by no means linear and it plays a major role in determining the receiver's true selectivity. The most important factor is the ratio of the desired carrier to interfering carriers. This ratio is, of course, a function of the predetection IF response. Also playing a major role is the post-detection frequency response. This behavior of the second detector complicates the measurement of interference and noise. Although simple approximate equations may be employed to overcome this measurement drawback, measurement of the RMS signal prior to the second detector seems to be the most straightforward.

One hesitates to make any broad and generalized recommendations in view of the wide variety of equipments and field situations. Nevertheless, if one must put his head on the block, it would seem desirable to considerably modify the current AM receiver design practices, within practical limits, so that the IF response is as narrow as possible, and then, after detection, de-emphasizing the lower frequencies. An alternate approach to post-detection de-emphasis would be to pre-emphasize the higher audio frequencies at the transmitter. It should be emphasized that this IF peaking

improves only the conventional DSB or vestigial SB AM transmission and reception systems with reasonable degrees of modulation. There is no indication that the basic comparisons previously made between SSB, DSB FM and the like have been changed.

BIBLIOGRAPHY


(1) W. R. Bennett, "Response of a linear rectifier to signal and noise," JOUR. ACOUS. SOC. AMER., vol. 15, p. 164; January, 1944.

(2) E. G. Fubini, D. C. Johnson, "Signal-to-noise ratios in AM receivers." PROC. I.R.E., vol. 36, p. 1461; December, 1948.

(3) D. E. Middleton, "Rectification of a sinusoidally modulated carrier in the presence of noise," PROC. I.R.E., vol. 36, p. 1467; December, 1948.

(4) S. R. Ragazzini, "The effect of fluctuation voltages on a linear detector," PROC. I.R.E., vol. 30, p. 277; June, 1942.

(5) S. O. Rice, "Mathematical analysis of random noise," BELL SYS. TECH. JOUR., vol. 23, pp. 282-332; July, 1944; vol. 24, pp. 46-156; January, 1945.

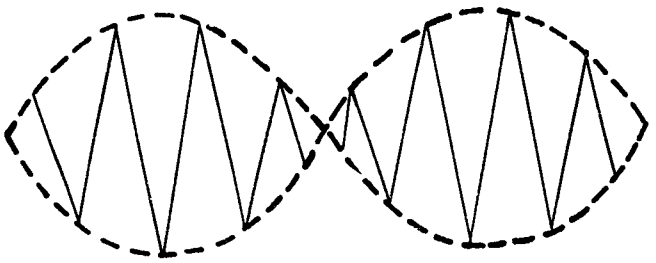
(6) S. Goldman, "Frequency Analysis, Modulation and Noise," McGraw-Hill, New York, N. Y., p. 246; 1948.

(7) A. H. Schooley, S. F. George, "Input vs output signal-to-noise characteristics of linear, parabolic, and semi-cubical detectors," NEC PROC., vol. 17, p. 151; 1951.

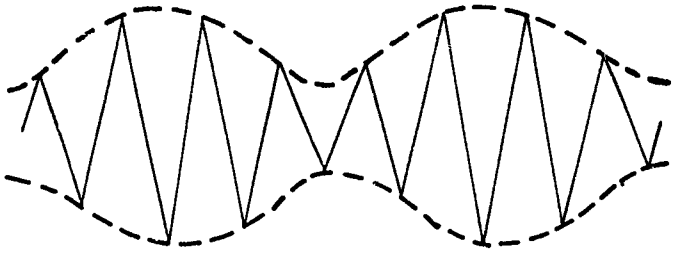
(8) D. G. Tucker, "Linear rectifier and limiters," WIRELESS ENG., vol. 29, p. 128; May, 1952.

(9) J. E. Bridges, "Detection of Television Signals in Noise," PROC. I.R.E., vol. 42, p. 1396; September, 1954.

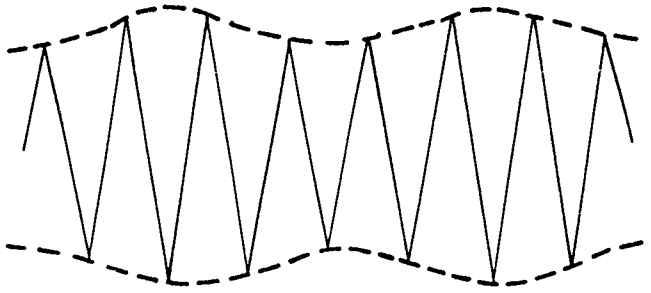
(10) F. E. Terman, "Radio Engineers Handbook," McGraw-Hill, New York, N. Y., p. 577; 1943.



a = b FIG. I.I(a)



a = 2b FIG. I.I(b)



a >> b FIG. I.I(c)

FIG. I.I

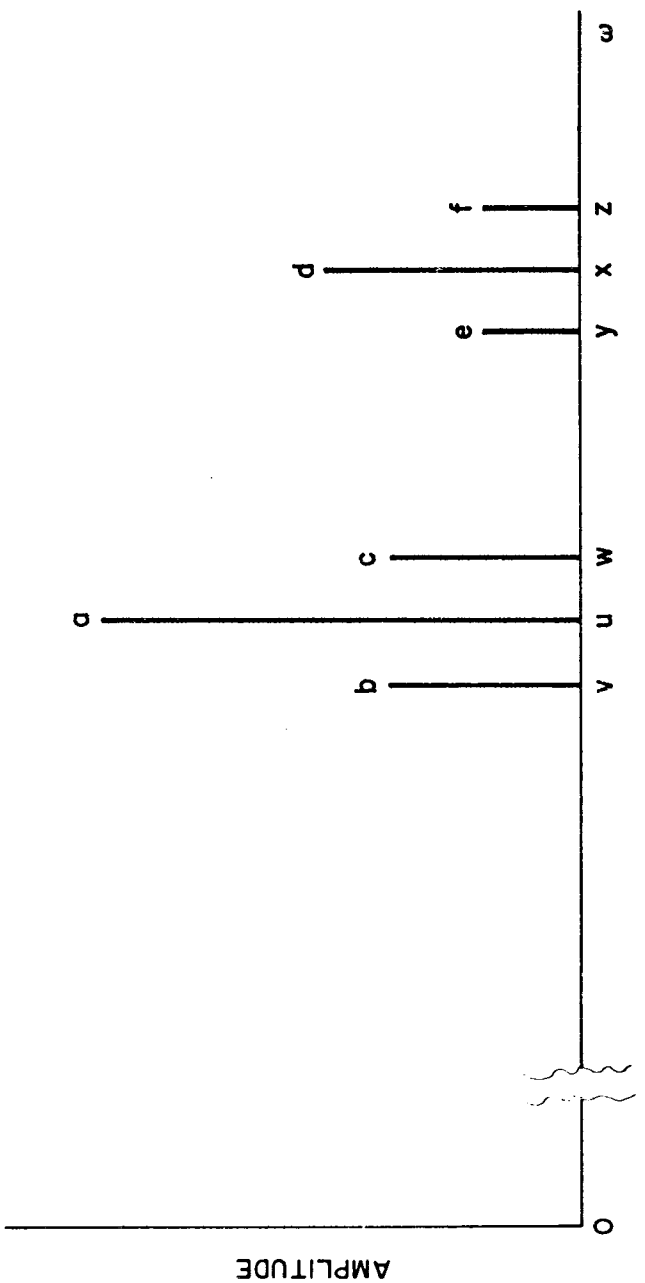



FIG. I.2

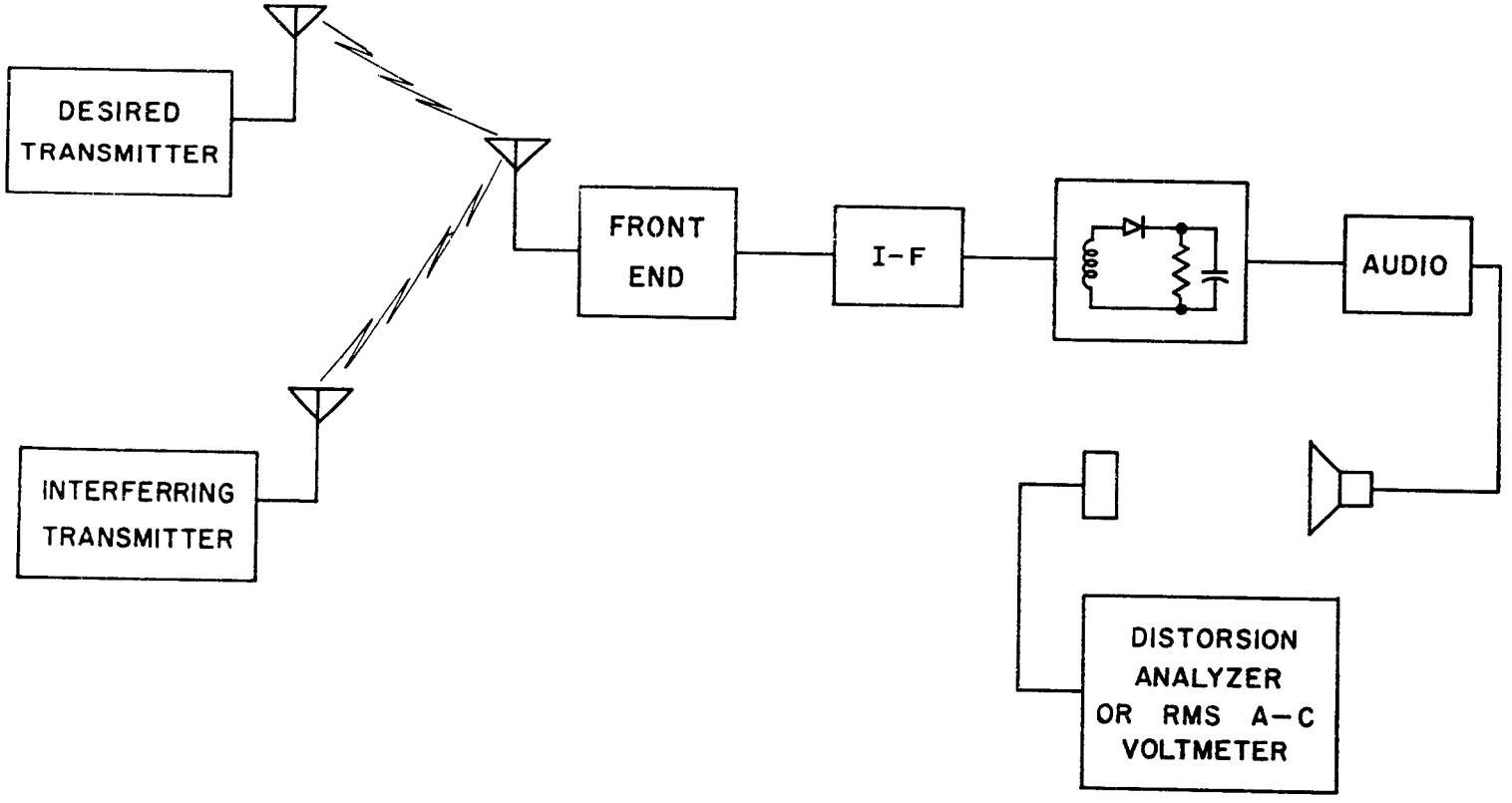

DESIRED
TRANSMITTER
INTERFERRING
TRANSMITTER
FRONT
END
I-F
AUDIO
DISTORSION
ANALYZER
OR RMS A-C
VOLTMETER

FIG. 2.1

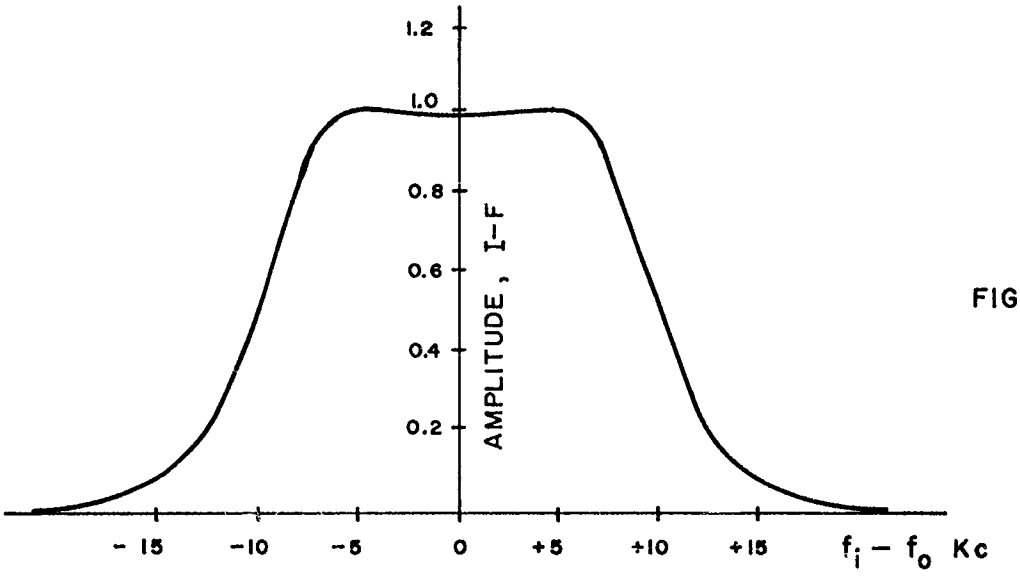



FIG. 2.2 (a)

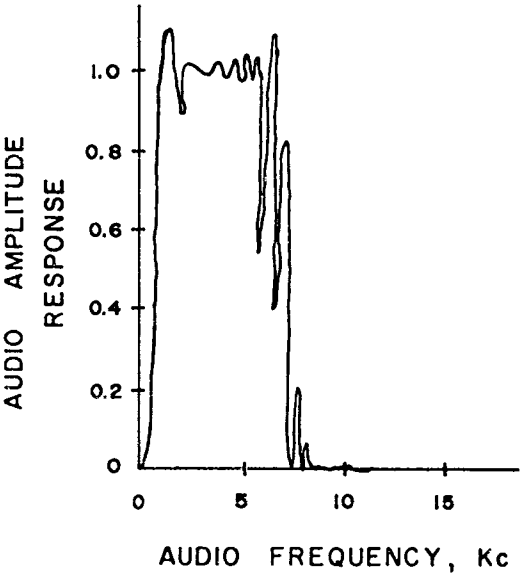



FIG. 2.2 (b)

FIG. 2.2

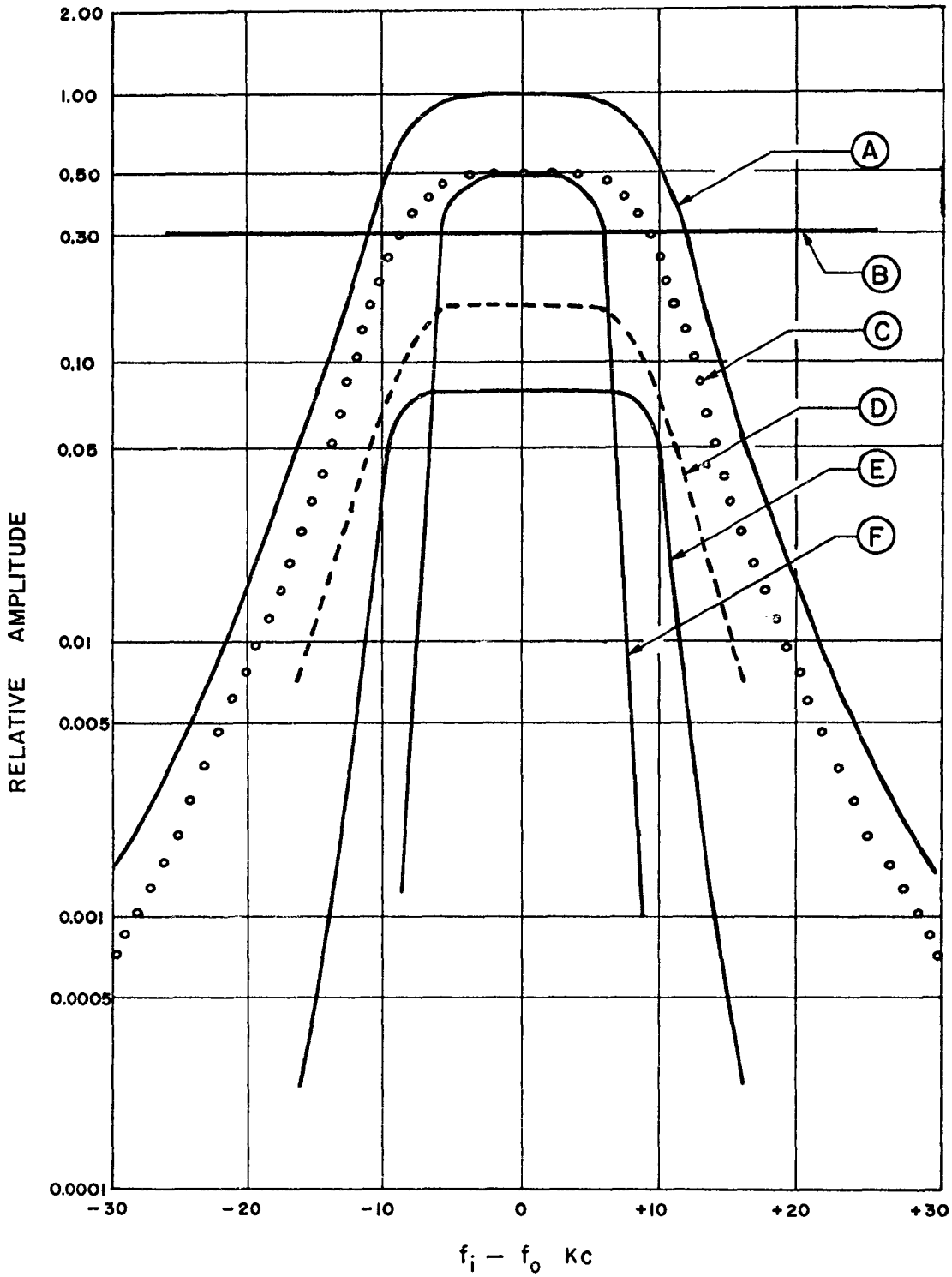

2.00
1.00
0.50
0.30
0.10
0.05
0.01
0.005
0.001
0.0005
0.0001
RELATIVE AMPLITUDE
-30
-20
-10
0
+10
+20
+30
$f_i - f_o$ Kc
A
B
C
D
E
F

FIG. 2.3

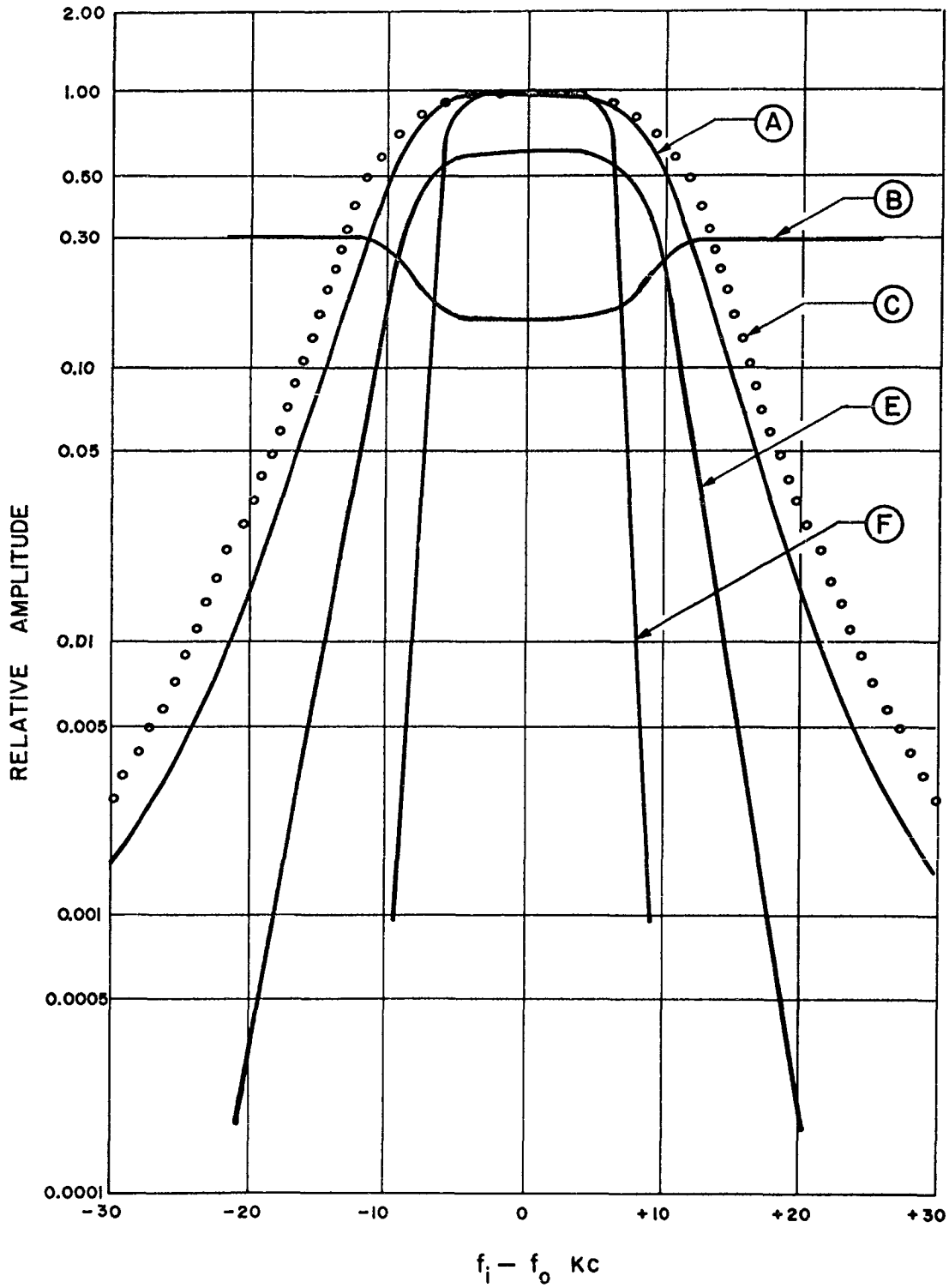
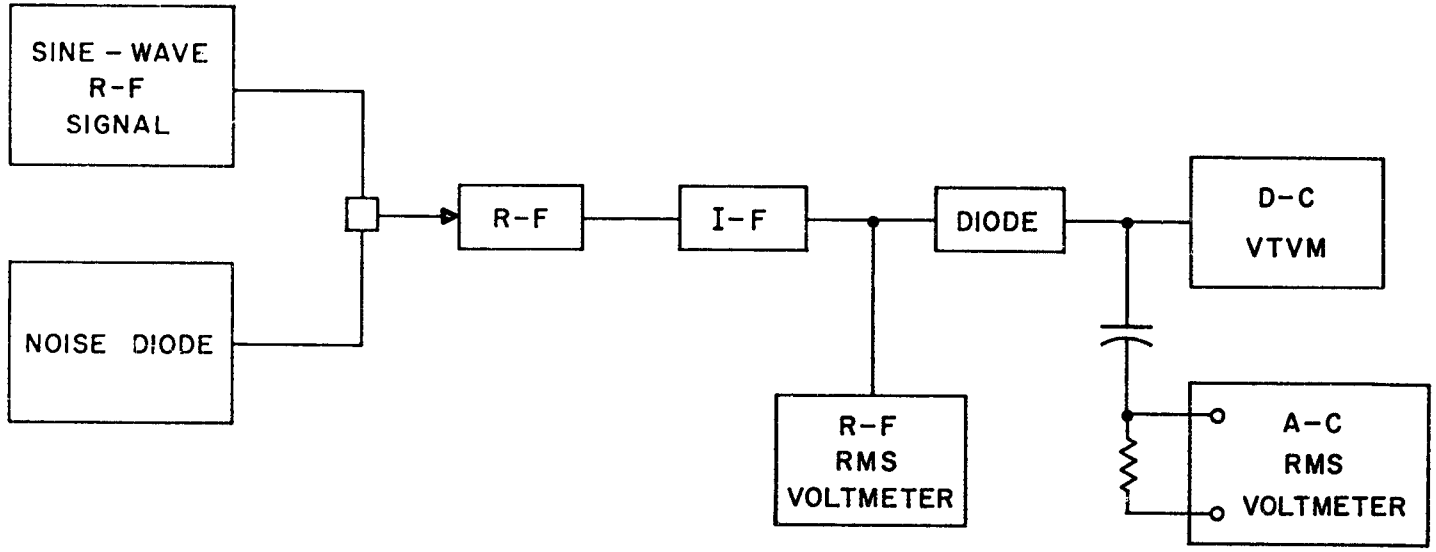

2.00
1.00
0.50
0.30
0.10
0.05
0.01
0.005
0.001
0.0005
0.0001
RELATIVE AMPLITUDE
-30
-20
-10
0
+10
+20
+30
$f_i - f_o$ Kc
A
B
C
E
F

FIG. 2.4




| | R-F RMS VOLTMETER | D-C VTVM | A-C RMS VOLTMETER |
|---|---|---|---|
| NOISE ALONE | $\sqrt{1}$ | $0.9\,K_1$ | $0.67\,K_2$ |
| NOISE + LARGER SINE-WAVE | $\sqrt{9}$ | $3.0\,K_1$ | $1.00\,K_2$ |
| SMALLER SINE-WAVE ALONE | $\sqrt{1}$ | $1.0\,K_1$ | 0.00 |

FIG. 2.5

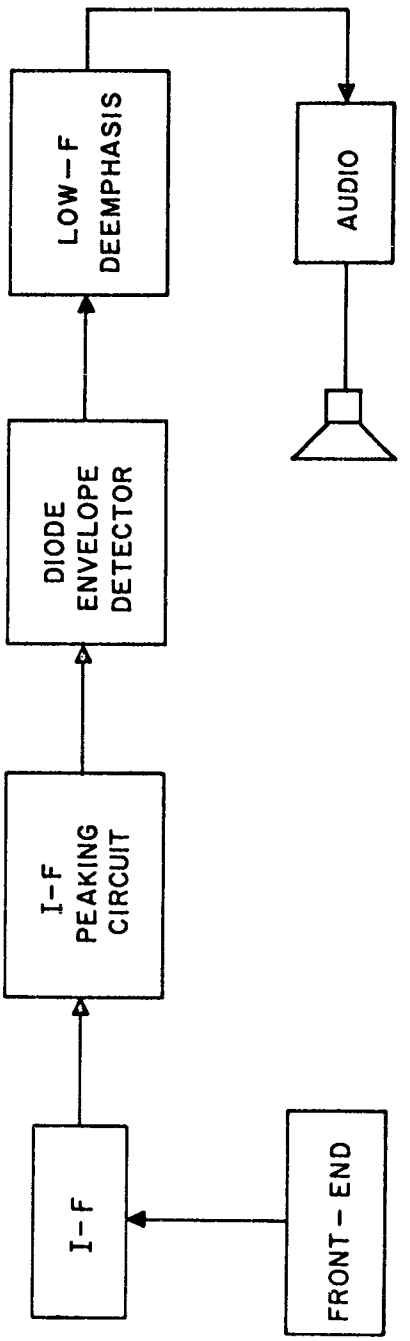

FRONT – END
I – F
I – F PEAKING CIRCUIT
DIODE ENVELOPE DETECTOR
LOW – F DEEMPHASIS
AUDIO

FIG. 3.1

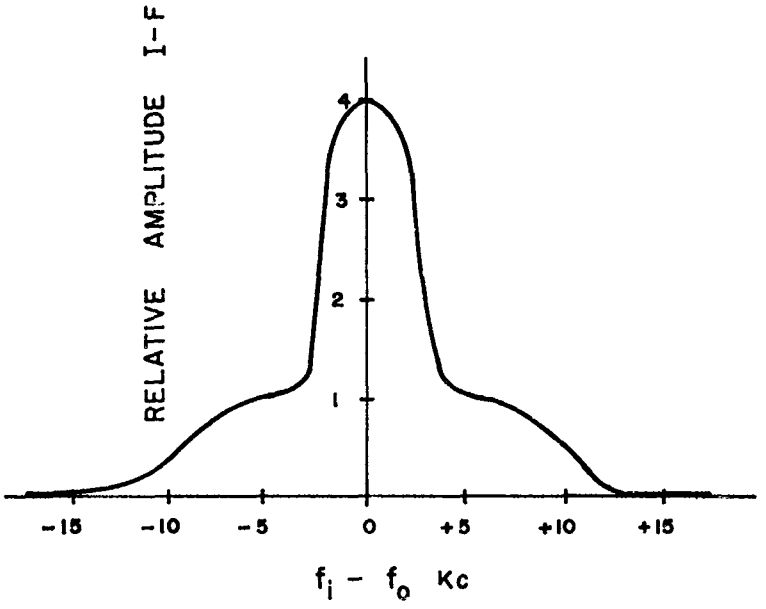



FIG. 3.2 (a)

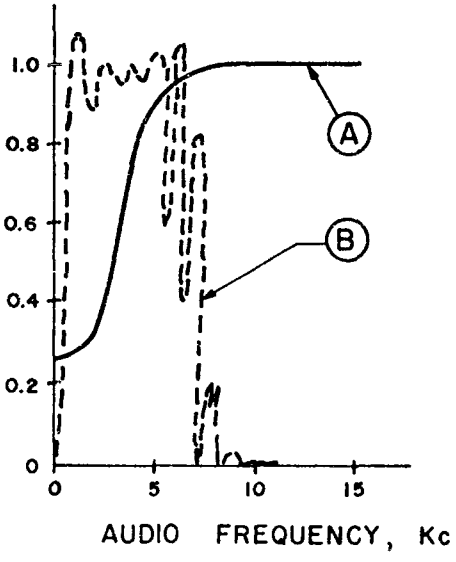



FIG. 3.2 (b)

FIG. 3.2

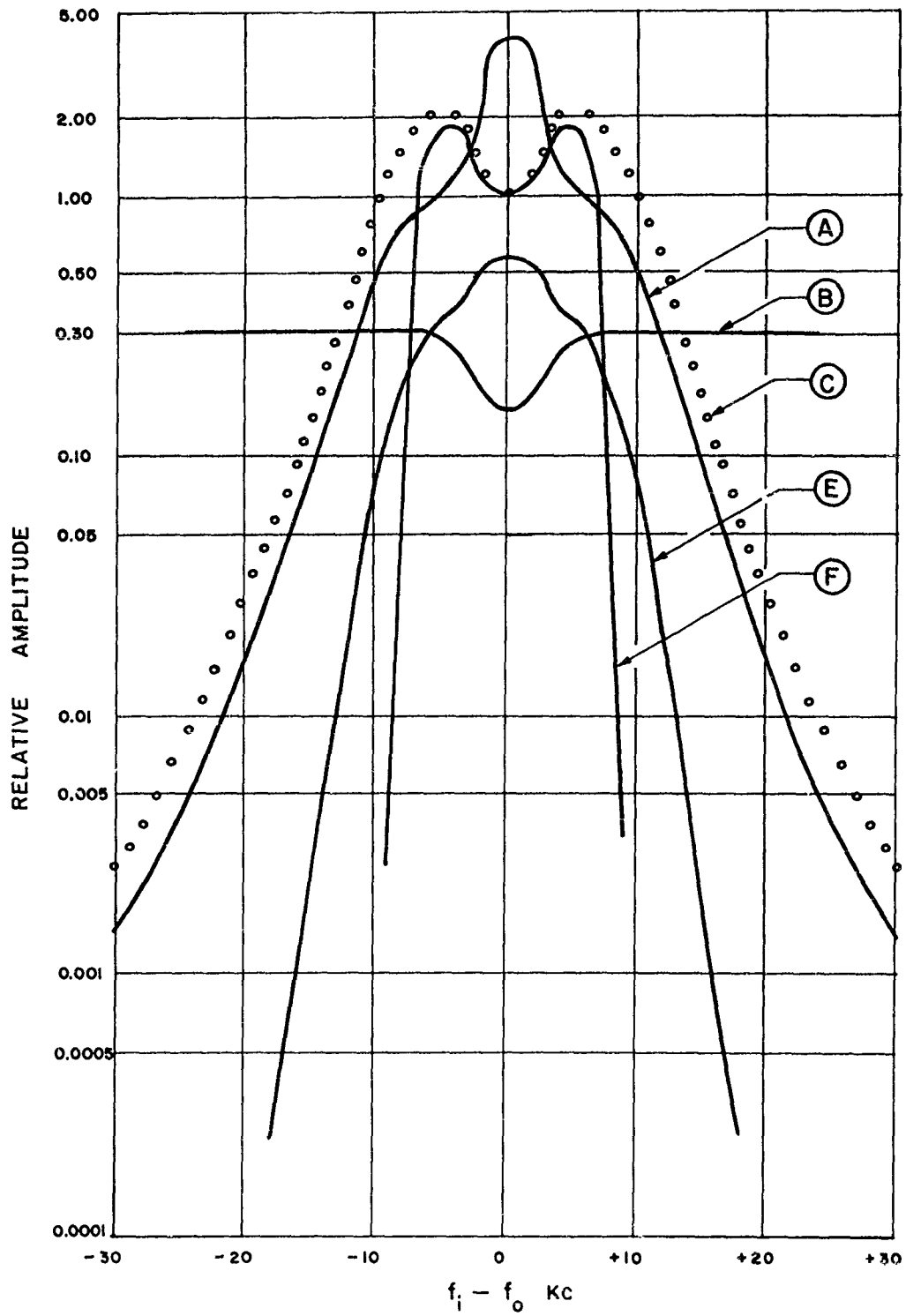

5.00
2.00
1.00
0.50
0.30
0.10
0.05
0.01
0.005
0.001
0.0005
0.0001
RELATIVE AMPLITUDE
-30
-20
-10
0
+10
+20
+30
$f_i - f_o$ Kc
A
B
C
E
F

FIG. 3.3

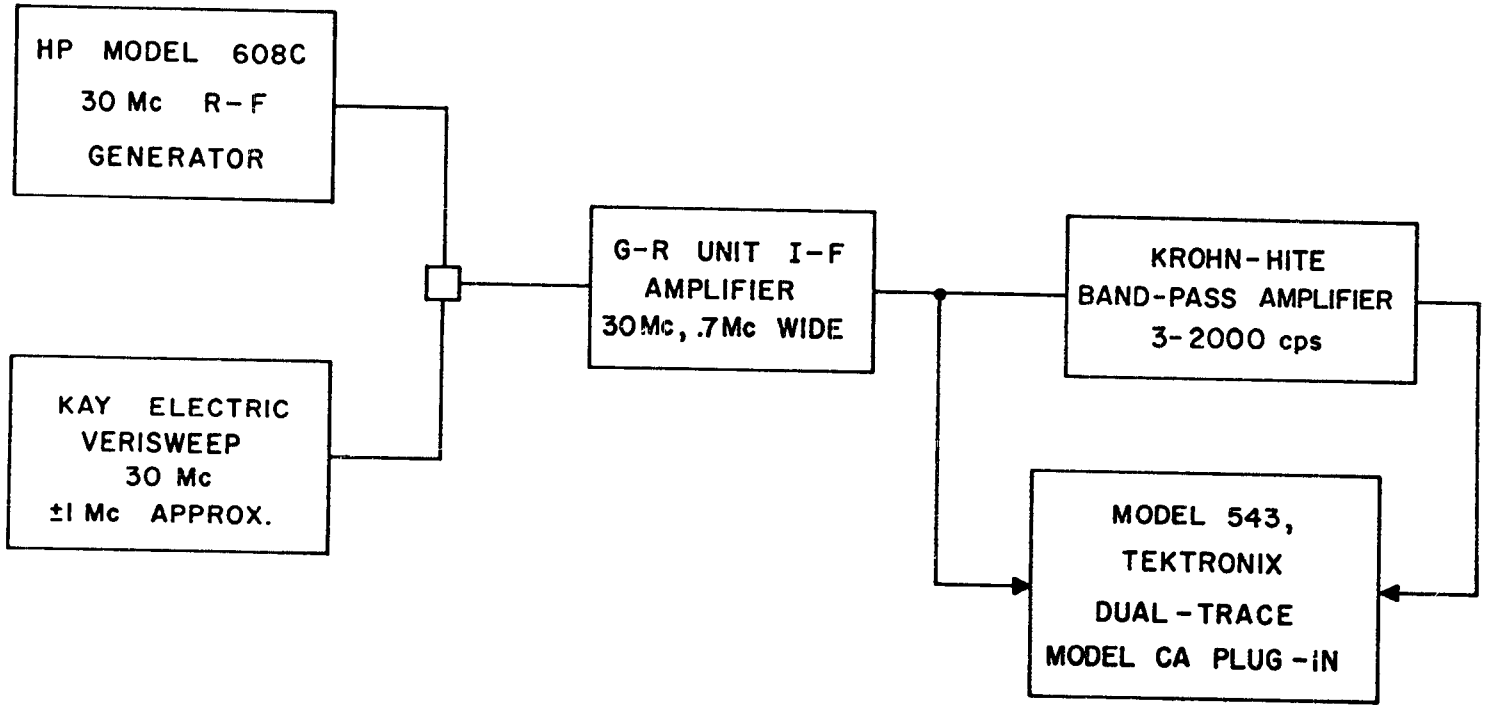
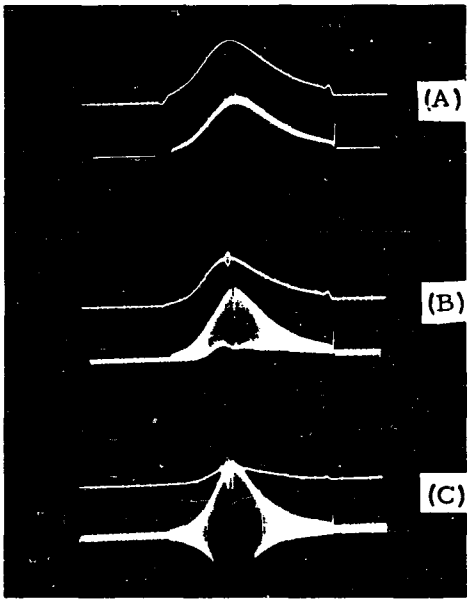

HP MODEL 608C
30 Mc R-F
GENERATOR
KAY ELECTRIC
VERISWEEP
30 Mc
±1 Mc APPROX.
G-R UNIT I-F
AMPLIFIER
30Mc, .7Mc WIDE
KROHN-HITE
BAND-PASS AMPLIFIER
3-2000 cps
MODEL 543,
TEKTRONIX
DUAL-TRACE
MODEL CA PLUG-IN

FIG. 4.1



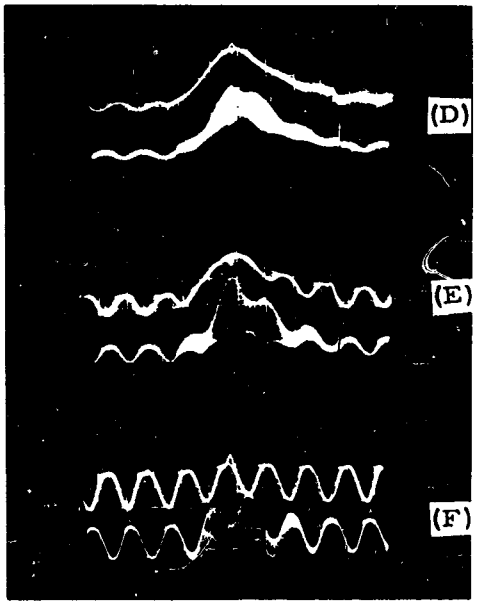

(A) Top -- Low-pass filter output for sweep only
Bottom -- Output at second detector for sweep only s = 0
Scale 1 cm vert. = .5 volts

(B) Top -- Low-pass filter output to sweep + carrier
Bottom -- Output at second detector to sweep + carrier s = 1
Scale 1 cm vert. = .5 volts

(C) Top -- Low-pass filter output to sweep + carrier
Bottom -- Output at second detector to sweep + carrier s = 3
Scale 1 cm vert. = .5 volts

1 cm horizontal about 1/3 mc
center frequency 30 mc

Fig. 4.2




(D) Top -- Low-pass filter output to sweep + carrier 30/ mod.
Bottom -- Output at second detector to sweep + carrier 30% mod. s = .5
Vert., 1 cm = .5 volts

(E) Top -- Low-pass filter output to sweep + carrier 30% mod.
Bottom -- Output at second detector to sweep + carrier 30% mod. s = 1
Vert., 1 cm = .5 volts

(F) Top -- Low-pass filter output to sweep + carrier 30% mod.
Bottom -- Output at second detector to sweep + carrier 30% mod. s = 3
Vert., 1 cm = 1 volt

1 cm horizontal about 1/3 mc
center frequency about 30 mc

Fig. 4.2

# A 1-TO 10-KMC PANORAMIC RECEIVING SYSTEM FOR RFI MONITORING

R. Powers
Rome Air Development Center
Rome, N.Y.

R. H. Sugarman and K. E. Walker
American Electronic Laboratories, Inc.
Philadelphia, Penna.

Abstract. - A voltage-swept Panoramic Superheterodyne Receiving System covering the range from 1 kmc to 10 kmc has been developed for the rapid intercept and monitoring of radio frequency interference. Known as the AN/GRR-9, the equipment is contained in a standard 6-foot relay rack except for the indicators, which are in a separate bench-mounted case, and the antennas, which may be mounted on a tripod or a rotatable mast.

The entire frequency range of 1 to 10 kmc is covered continuously and simultaneously in four bands (1 to 2 kmc, 2 to 4 kmc, 4 to 7.2 kmc and 7.2 to 10.3 kmc) at sweep rates of either 15 cps or 60 cps with receiver sensitivities as high as -95 dbm. Each band is provided with a cathode-ray tube indicator which displays signal amplitude vs. frequency.

Discussed in detail are the antennas, the RF input filtering and mixing stage, the carcinotron-type local oscillators with special leveling and sweep linearity correction circuits, the linear and logarithmic IF amplifiers, the indicator and control unit, and the power supply system.

## I. INTRODUCTION

The AN/GRR-9 is a wide-range Panoramic Superheterodyne Receiving System covering the frequency range of 1 kmc to 10.3 kmc and intended for rapid indication of frequency and amplitude of radiated signals within its band. The entire frequency range is swept and displayed continuously and simultaneously in four bands at sweep rates of either 15 cps or 60 cps. The receiver has been designed particularly for monitoring radio frequency interference in the above range and may be adapted to recording such signals over long periods of time. It can be utilized to monitor potential equipment installation sites or test ranges to determine rapidly the presence of objectionable interfering signals with a high probability of intercept. Where precise readings of frequency and field intensity are required, it is a useful, time-saving instrument for indicating signal areas within the entire 1-to 10-kmc range, which may be analyzed in more detail with a manually tuned field intensity meter. The AN/GRR-9 Receiver should find application in coarse presentations of transmitter spectral signatures and in analyzing emission characteristics of wide-band jamming systems. The system is designed for installation at either a fixed ground site or in a van for mobile operation.

## II. GENERAL DESCRIPTION

Figure 1 is a photograph of the complete AN/GRR-9 Receiving System, with the exception of the associated antennas. When installed in a mobile van,

the antennas may be externally mounted on a tripod or on a rotatable mast.

As illustrated, the equipment consists of six cases, five of which may be contained in a standard 6-foot relay rack. The sixth unit is the indicator-control chassis, which may be located at distances up to 25 feet from the remainder of the equipment. The five rack-mounted units consist of, from top to bottom, the 7.2-to 10.3-kmc RF-IF drawer, the 4-to 7.2-kmc RF-IF drawer, the 2-to 4-kmc RF-IF drawer, the 1-to 2-kmc RF-IF drawer, and the power supply system.

A simplified block diagram of the system is illustrated in Figure 2. Linear horn antennas covering the frequency ranges of 1 to 2, 2 to 4, 4 to 7, and 7 to 10 kmc respectively feed the signals through a coaxial cable to a corresponding RF-IF chassis. Each chassis contains an RF section (heavy outline) consisting of a bandpass filter, a balanced mixer, a voltage-tuned local oscillator and a local oscillator output attenuator. Each RF component is designed for operation over its corresponding frequency band. Identical to all of the RF-IF chassis are the local oscillator sweep circuit, the power-leveling circuit and the 30-mc IF preamplifiers and IF amplifiers.

Detected video signals from each of the receivers are displayed on corresponding "plug-in" cathode-ray tube indicators having illuminated scales and located on the indicator-control chassis. This chassis also contains the sweep generator which provides the common sweep voltages for the cathode-ray tubes and the local oscillators. As will be discussed later, no provisions have been made for image rejection; the resultant presentation of two signals separated by 60 mc providing an aid to recognition of the presence of weak signals. The system power supply, which is the final unit, provides D.C. voltages of -1600V, -150V, +150V and +300V to all other chassis.

## III. EQUIPMENT DETAILS

### Antennas

Each band of the receiver is provided with a separate linearly polarized horn antenna which is of an AEL standard design. These antennas are shown in Figure 3. Each horn includes a broadband transformer waveguide-to-coaxial adaptor for connection to a coaxial line. The horns have equal E-and H-plane beamwidths and may be oriented for maximum output to determine signal polarization. The minimum beamwidth of any antenna is not less than 15 degrees. The gain varies from 12 db (over a dipole) at 1 kmc to 17 db at 10 kmc. The VSWR is 1.7 or less at frequencies below 7.2 kmc and 2.8 or less at 10.3 kmc.

### RF Components

Figure 4 is a top-view photograph of a typical RF-IF drawer. The receiver input stage consists of a bandpass, preselector filter. The bandpass filters have a nominal insertion loss of 1.5 db with signal attenuation 40 db or greater within 10% of the band edges. These preselectors combine their characteristics with the pass band characteristics of the balanced mixer to preclude essentially all spurious reception outside of the intended band.

Special broadband, balanced coaxial hybrid mixers covering the full

width of each band are utilized to achieve improved performance. Increased receiver sensitivities are obtained through partial cancellation of the noise generated in the local oscillator. This is accomplished by outphasing of the noise at the IF preamplifier input while the desired signal is made to phase additively. This type of mixer also provides higher isolation between the local oscillator and the antenna terminal, thereby reducing oscillator radiation.

Local Oscillators

The broadband, rapid scanning operation of the panoramic receiving system is made possible by use of electronically tuned backward wave oscillators (BWO) to provide local oscillator signals to the mixer. The carcinotron or permanent magnet type of backward wave oscillator is used. Tubes which have been employed in the systems developed are listed as follows:

| Frequency Band (kmc) | Tube Type | Improved Tube Type |
|---|---|---|
| 1-2 | QK546 (CO315) | QKB931 |
| 2-4 | QK691 --- | QKB816A |
| 4-7 | QK528 (CO94) | QKB760A |
| 7-10 | QK610 (CO43) | QKB831 |

An attenuator is provided between the local oscillator and the balanced mixer to fix the level at which the local oscillator is maintained with respect to required crystal current. Also, the attenuator isolates the output of the local oscillator from any undesirable standing waves caused by mismatch in the mixer.

Curvature and Leveler Circuits

Although the backward wave oscillators provide the basic local oscillator signal power required, they suffer from two properties which must be corrected in order to utilize them in a receiving system of this nature. As shown by typical tube characteristics in Figure 5, backward wave oscillator output frequency is a non-linear function of the input sweep voltage. This would result in a non-linear calibration of the horizontal "frequency" scale of the cathode-ray tube indicators. In addition, tube power output varies quite irregularly over the tuning range and can have a ratio as high as 40 to 1. Non-limited power outputs could result in excessive receiver sensitivity variations, higher noise levels, and possibly, burnout of the mixer crystal.

To correct these deficiencies of the backward wave oscillators, sweep curvature and power-limiting circuits have been employed in the AN/GRR-9. Figure 6 is a simplified diagram showing operating principles of these two circuits.

The curvature circuit contains an amplifier tube whose plate load includes seven diodes. Each diode is biased at a different reference voltage, the value of which is adjusted by means of corresponding separate potentiometers arranged in a ladder-voltage divider network. As the linear sawtooth sweep voltage is applied to the amplifier, its output becomes curved through plate load shunting action as each diode becomes conductive. Each reference voltage is variable to allow for changing of the curvature to accommodate backward wave oscillator tubes having different characteristics.

The curved sweep voltage is applied through a differential amplifier and a series push-pull output amplifier to the backward wave oscillator. The differential amplifier serves as a high impedance feedback point, feedback being used to present a low impedance source to the backward wave oscillator and to stabilize amplifier operation with temperature, power supply and tube or circuit component changes.

In the power-leveling method employed, as shown in Figure 6, mixer crystal current produced by the backward wave oscillator is compared with a reference signal in a differential amplifier. The resultant error signal, through the D.C. isolator circuits, corrects the grid bias of the backward wave oscillator to maintain essentially constant crystal current in the RF mixer.

IF Components

The output of the balanced mixer is connected to a push-pull 30-mc IF preamplifier, which is built on a separate chassis in order to achieve maximum circuit stability. The unbalanced output of this amplifier is connected through a short coaxial cable to the main 30-mc IF amplifier. The IF strips are shown in Figure 4. The over-all IF bandwidth is 8 mc, which provides for reception of pulse signals of 1/2 microsecond duration or greater. A continuous IF gain control is provided for each channel on the front of the indicator-control panel. The IF amplifiers may also be switched to logarithmic operation. A 60-db dynamic range is provided in this mode of operation for both visual observation of signals widely varying in amplitude and also to facilitate recording of signals over long periods of time.

Indicators and Control

All indicators and controls of the entire system are arranged on a 19-inch rack panel on the front of the indicator cabinet, as shown in Figure 7. The indicators are 3-inch, rectangular cathode-ray tubes lined up in order of RF frequency. Thus, looking at the front of the indicator panel, one sees four tubes with 1.0 kmc marked on the left side of the left tube and 10.2 kmc marked on the right side of the extreme right tube. Each tube has an illuminated graticule with a frequency-calibrated scale engraved thereon. Video indicators are on sub-chassis which slide in and out of the main video indicator panel. Each indicator is provided with controls for beam focusing and positioning, and a VIDEO GAIN control. IF GAIN controls for each channel are located just below the indicator for that channel. A SWEEP RATE switch selects backward wave oscillator and indicator sweep rates of 15 cps or 60 cps. The only other controls provided and required for the operation of the receiving system are the power supply switches and a metering switch. These switches are located along the bottom of the indicator panel. There is also an audio output provided for each channel and a combined output for all channels. Sawtooth sweep signals are available at these outputs for operation of other remote indicators or recorders.

Figure 8 is a photograph of the 4- to 7.2-kmc indicator with two CW signals present. Because of the lack of image rejection, as previously mentioned, the signals appear as two pips side-by-side (actually 60-mc separation), thus serving to identify true signals, particularly in the presence of baseline noise at maximum IF gain settings. The spike at the start of the sweep has occurred

with several backward wave oscillator tubes. The CW signal on the left at 4.3 kmc is approximately -80 dbm, while the CW signal on the right at 6.6 kmc is -85 dbm. The linear IF gain setting was at three-quarter maximum value. With low noise backward wave oscillator tubes, receiver sensitivities run on the order of -95 dbm. Frequency calibration is limited to 2 percent of the indicated frequency.

Pulse-modulated signals are displayed as a pair of pips whose height varies rhythmically, depending on PRF. The brightness of the pips are less than those from a CW signal. Pulse stretching is used to increase the visibility of short pulse signals.

Power Supplies

The power supply drawer contains the principal supply voltages for the entire equipment. A top view photograph of this unit is given in Figure 9. This chassis consists of two subassemblies. Looking at the front panel, one sees that the transistorized power supply section is to the right. The voltages from this unit are +300, +150 and -150 volts.

The other section contains the vacuum tube-regulated -1600 volt supply. The rated drain for the -1600, +300 and -150 volt supplies is 200 milliamps. The rated current for the +150 volts is 500 milliamps.

The transistorized power supplies have been provided to conserve space and to minimize heat generation and power requirements. Measures to protect the transistors from burnout caused by short circuits on the supply output have been included. The power supplies are designed to work on 104 to 126 volts, 50 to 70 cycles.

## IV. CONCLUSIONS

The 1-to 10-kmc panoramic receiving system described can serve as a highly useful instrument in signal environment evaluations. Leveling and curvature techniques which overcome detrimental backward wave oscillator characteristics have been incorporated. The indicator cabinet, which can be remotely located from the rest of the equipment, serves as a convenient master control unit and provides a readily discernible display of intercepted signals over the entire 1-to 10-kmc frequency range.

## ACKNOWLEDGEMENTS

The consultation and guidance of Messrs. B. Lindeman and L. R. Moses of Rome Air Development Center, and R. S. Markowitz and C. J. Fowler of American Electronic Laboratories, Inc., is acknowledged. The AN/GRR-9 Receiver was developed under Air Force Contract No. AF30(602)-1894.

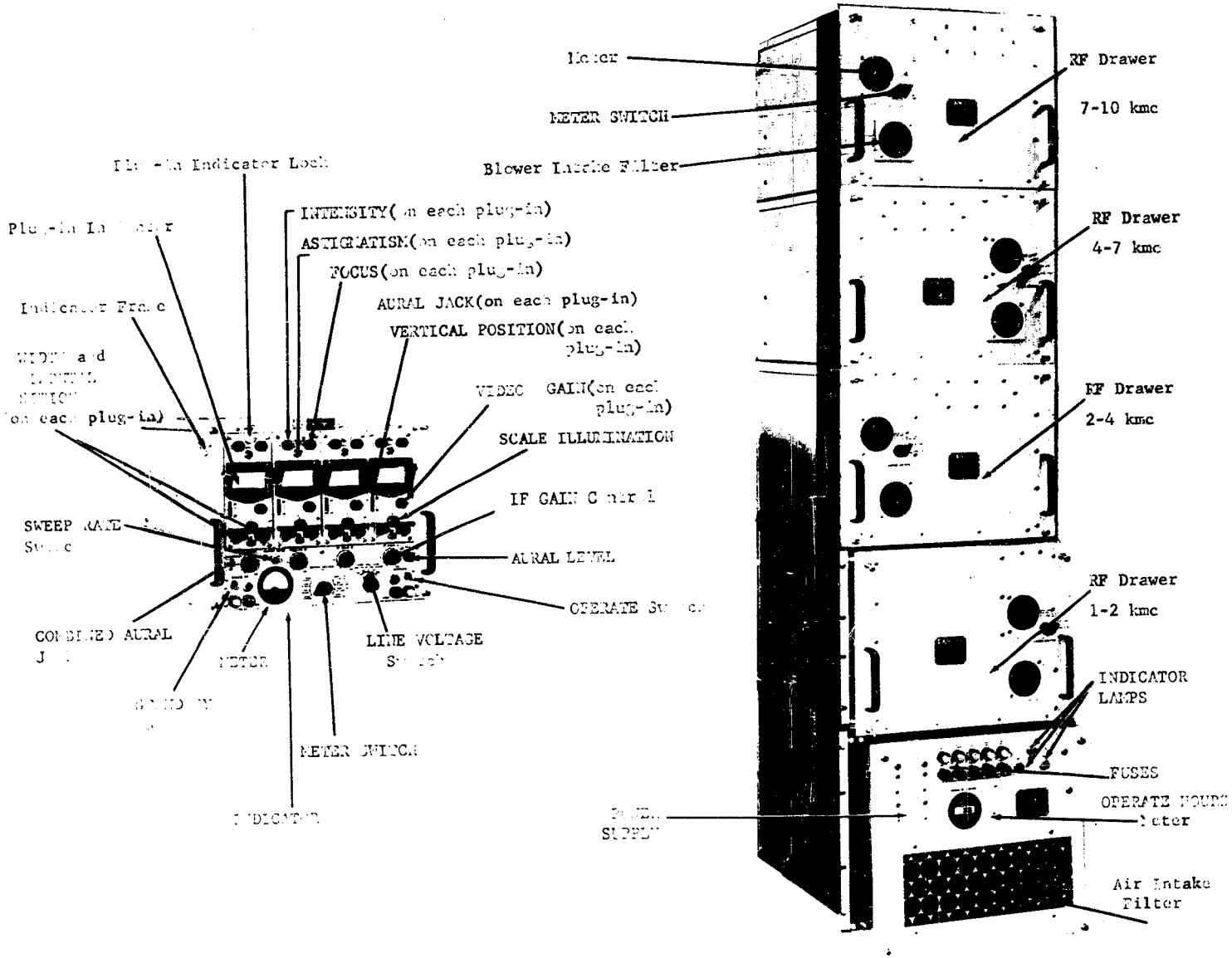



Figure 1. Receiving Set, Panoramic [illegible] AN/CRR-9(XM-1)

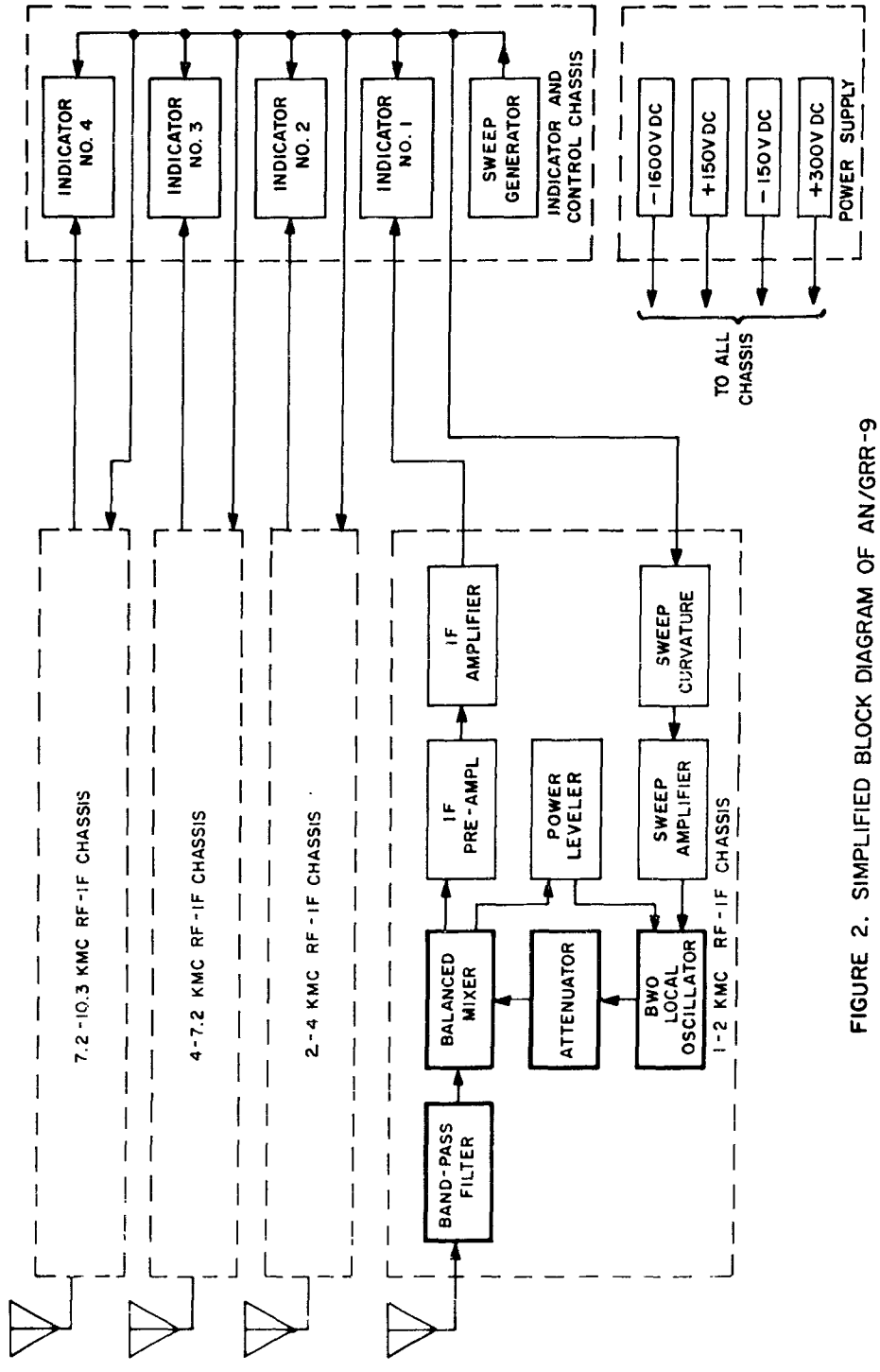



FIGURE 2. SIMPLIFIED BLOCK DIAGRAM OF AN/GRR-9

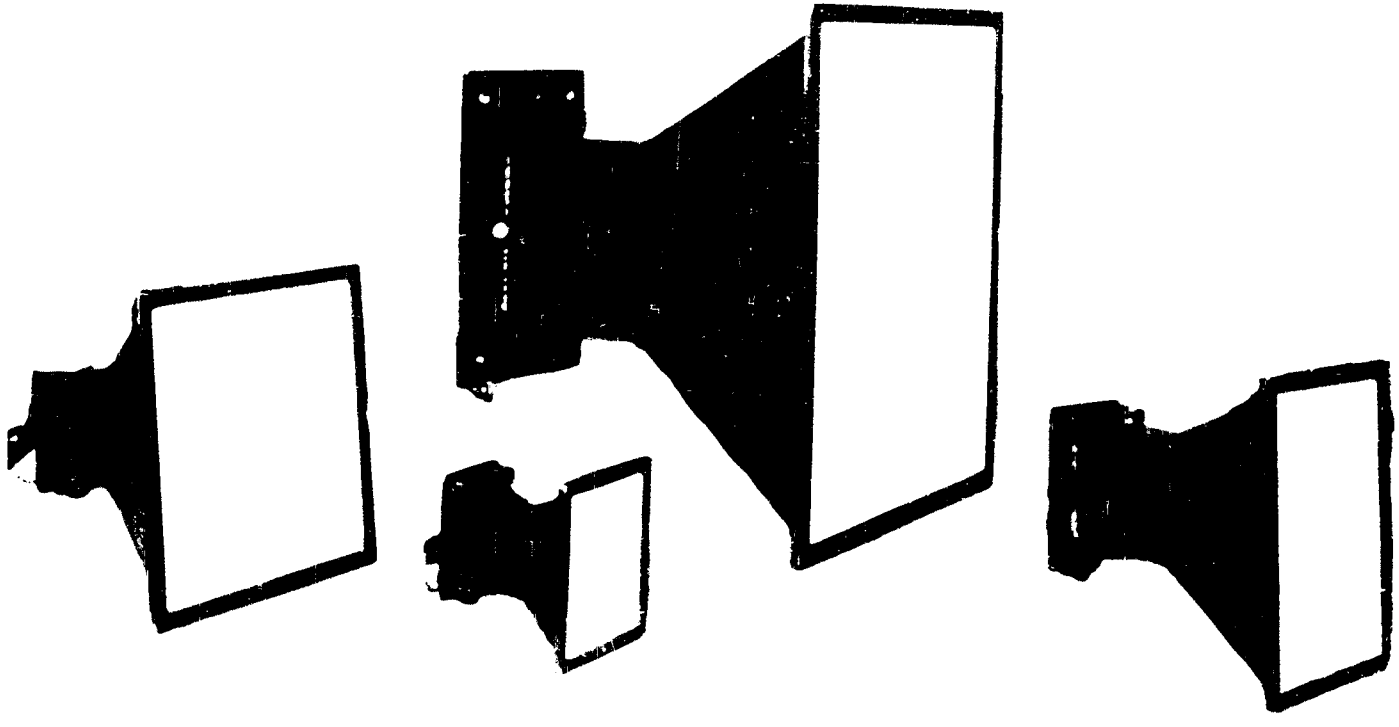


Figure 3 . Antennas For AN/GRR-9.

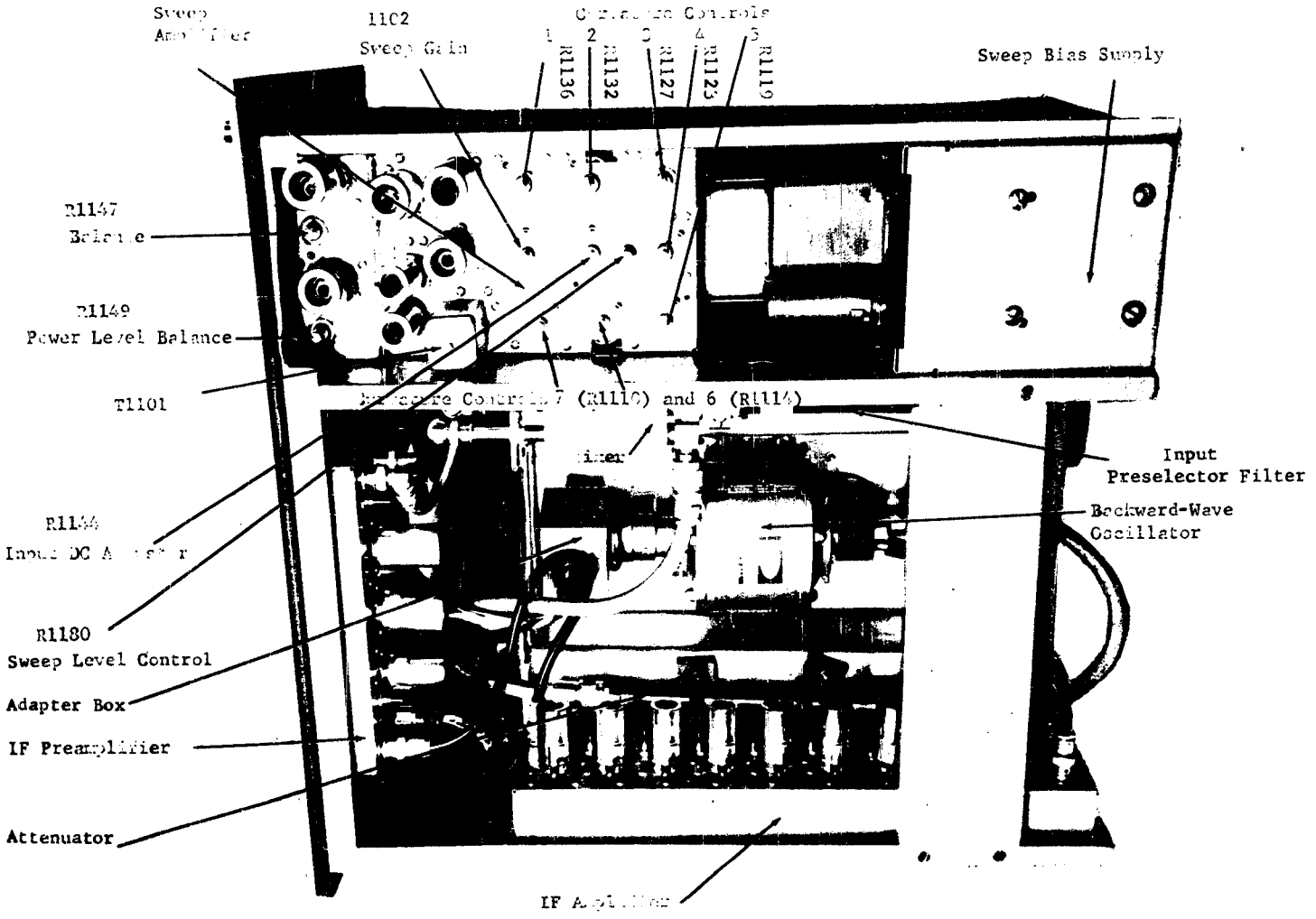



Figure 4 . Typical IF Drawer, Top View.

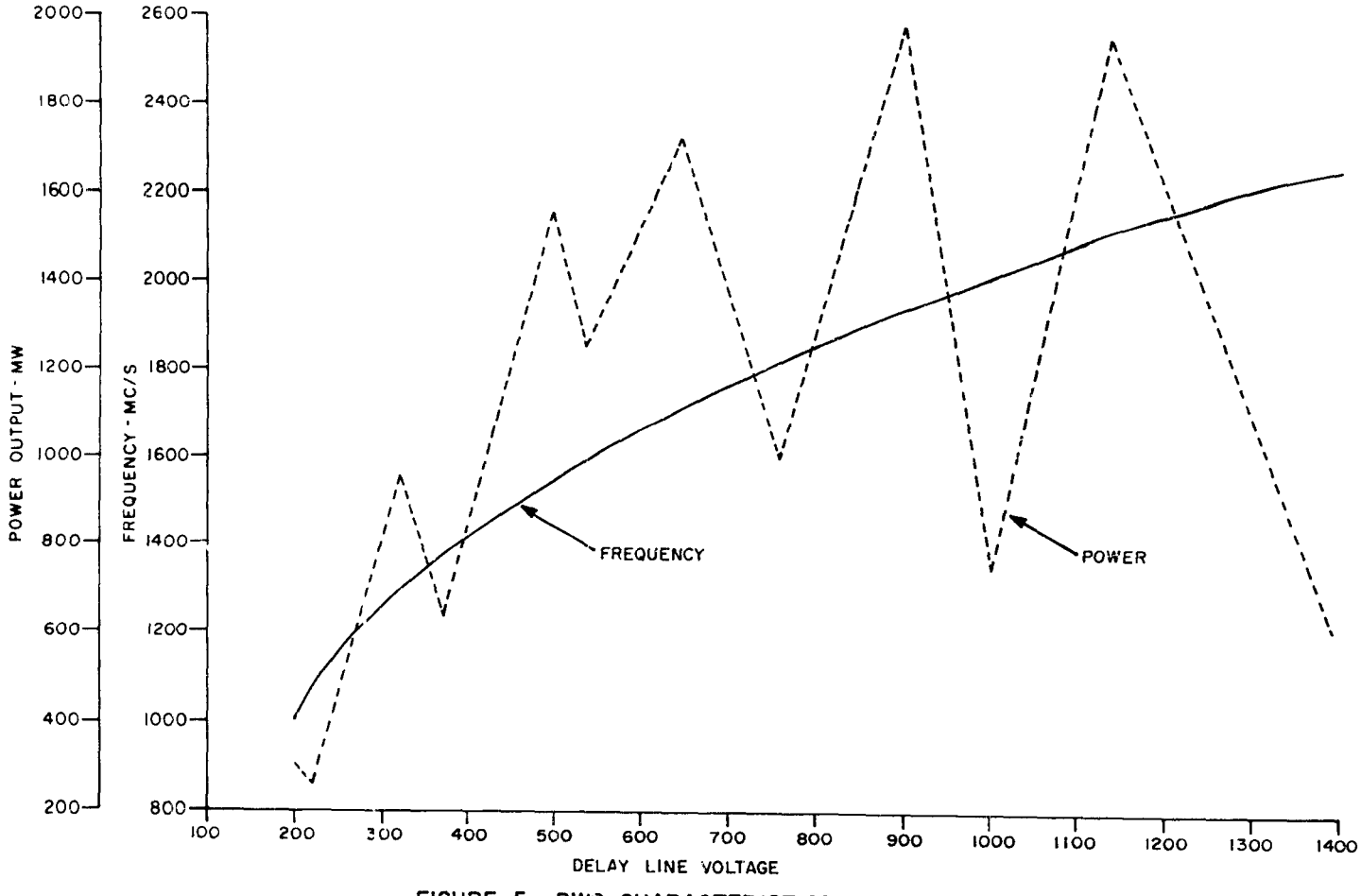



FIGURE 5. BWO CHARACTERISTICS TYPE QK546

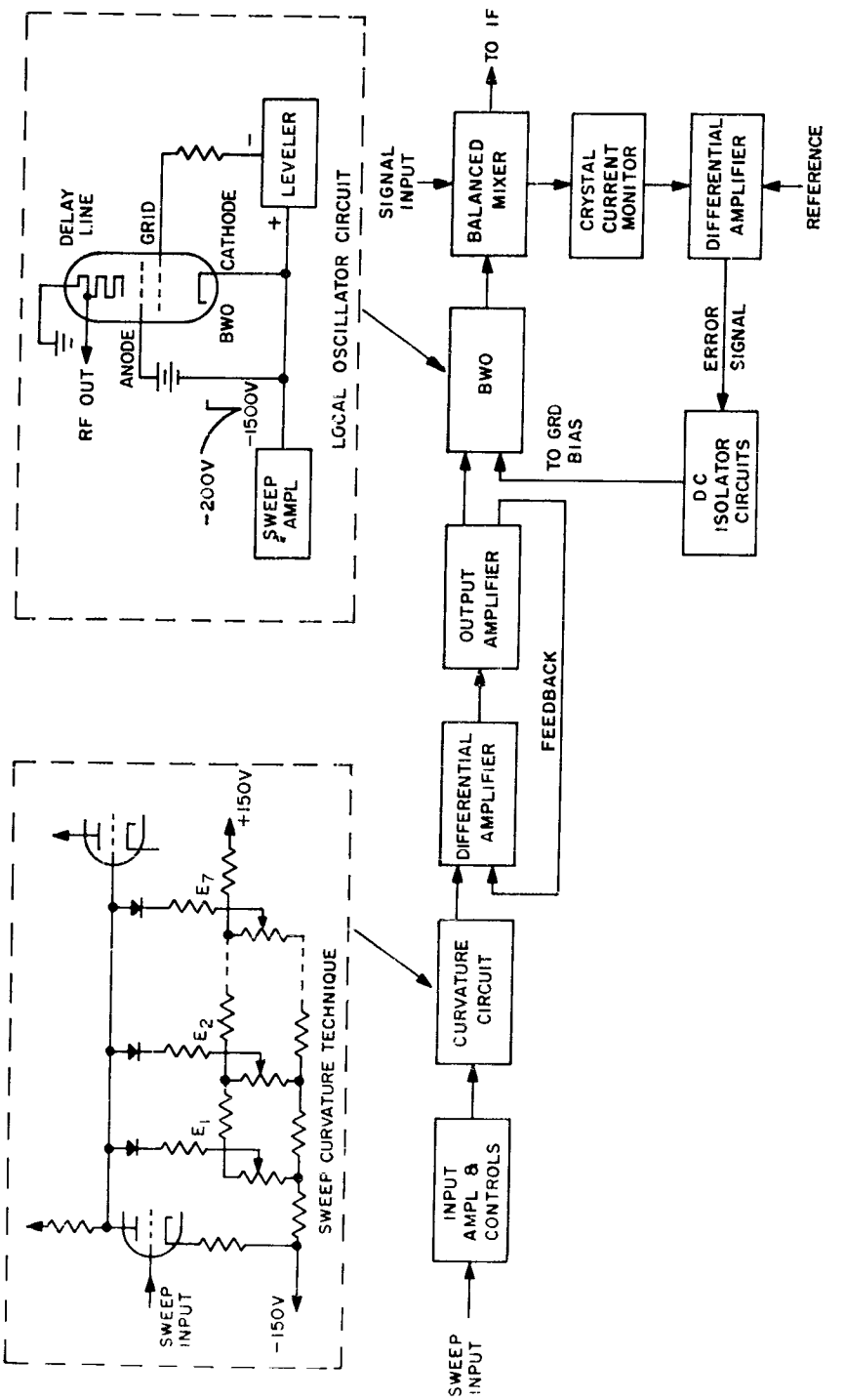



FIGURE 6. CURVATURE AND LEVELER TECHNIQUES

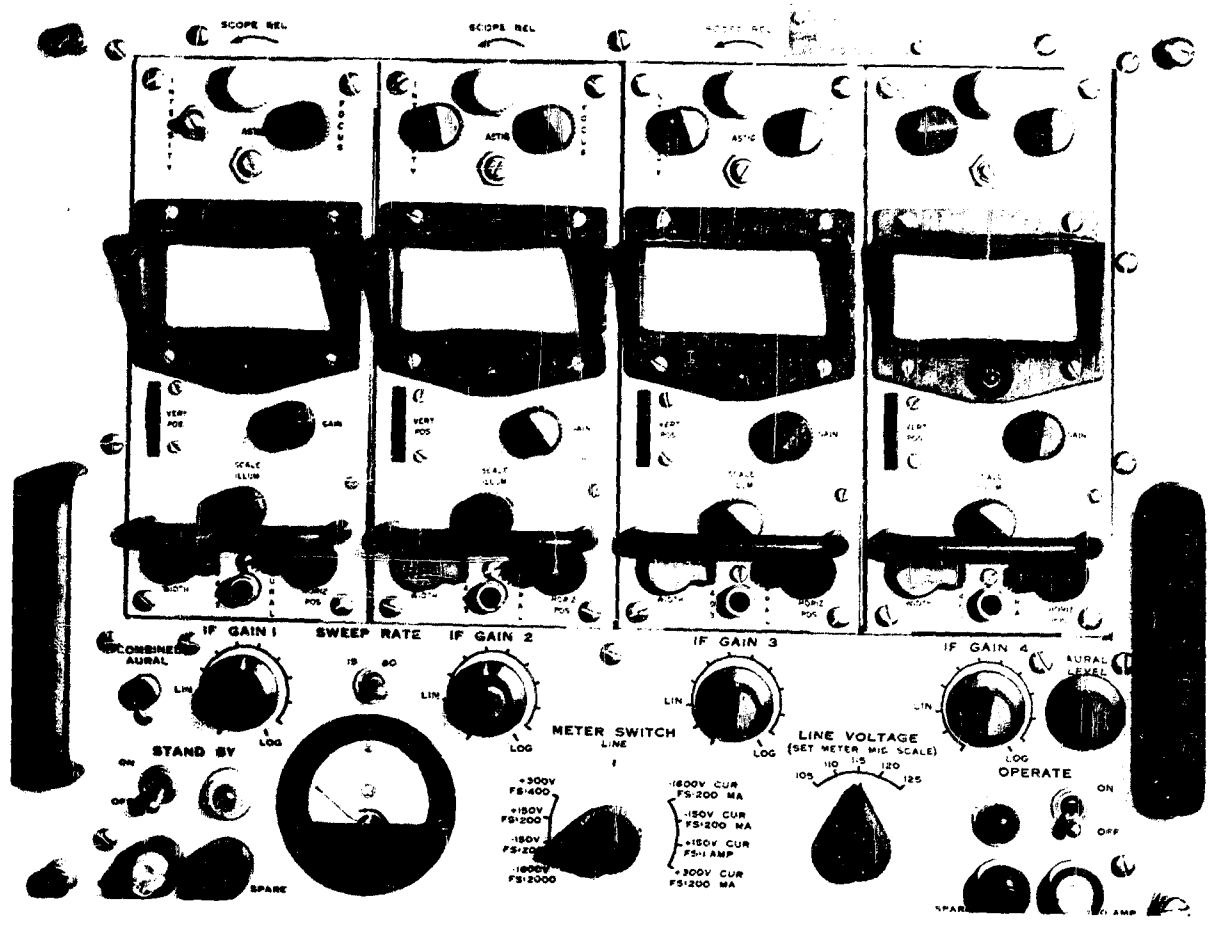



Figure 7 . Indicator-Control Unit.

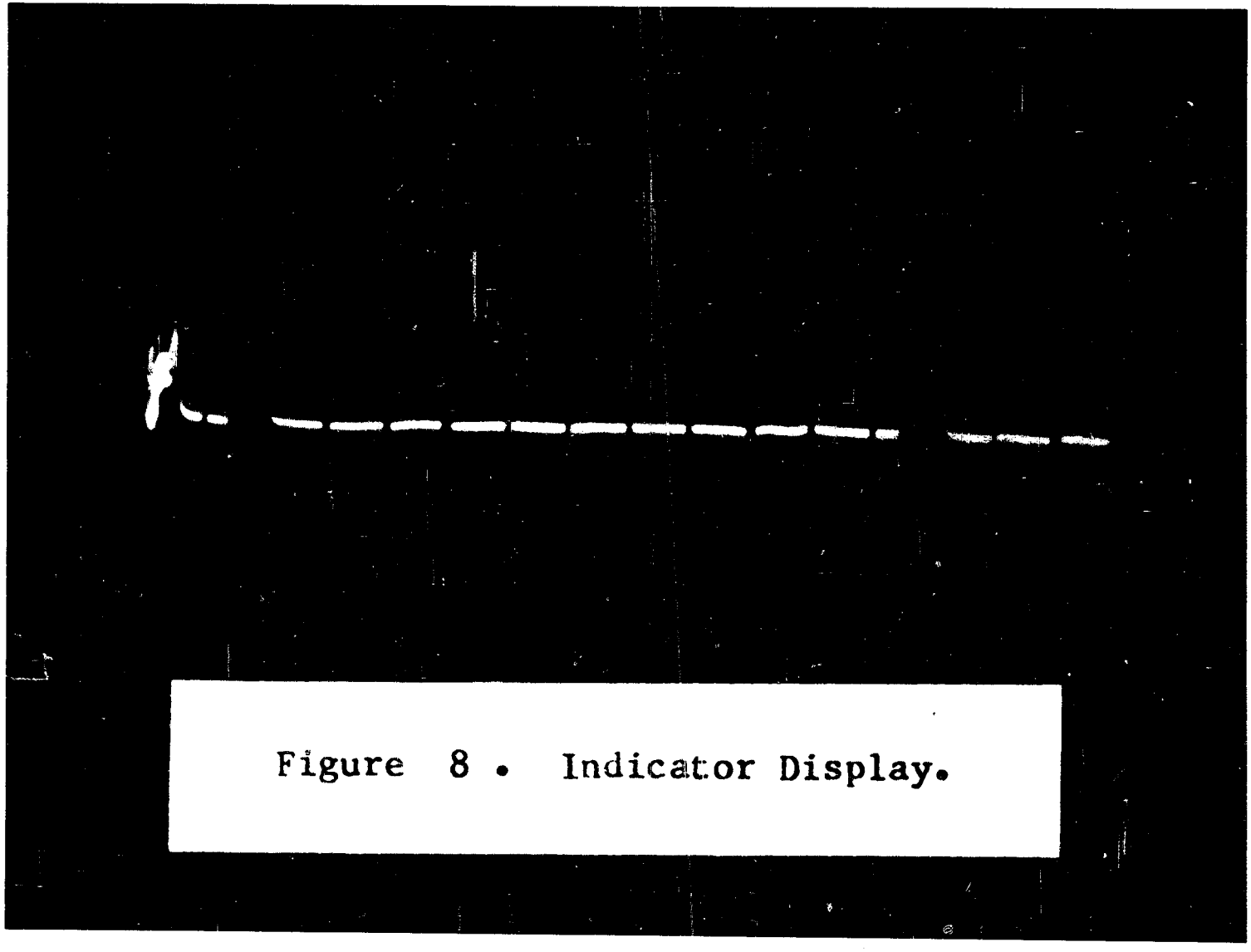


Figure 8 . Indicator Display.

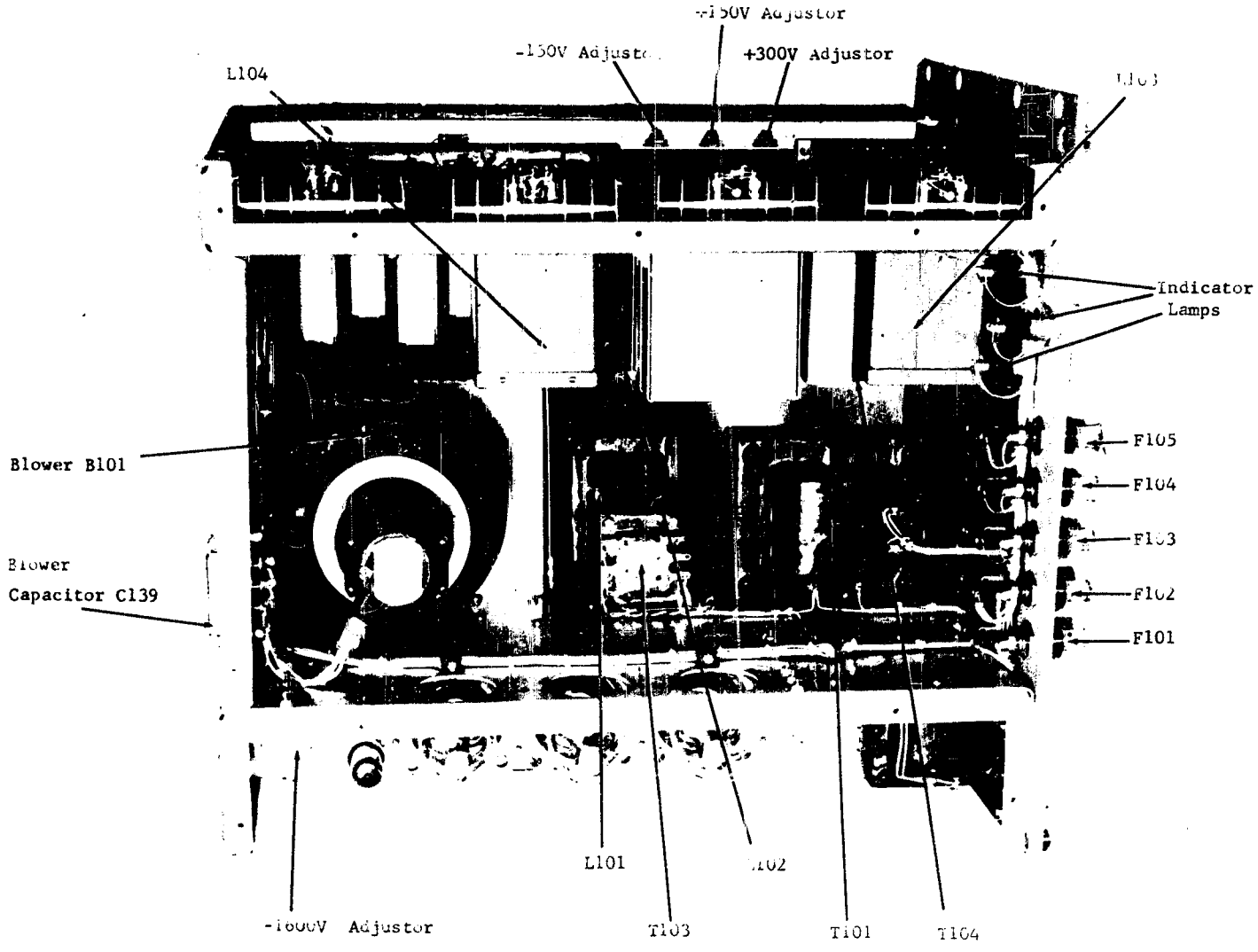



Figure 9 . Power Supply, Top View.

# NEW INSTRUMENTATION FOR ACCURATE MEASUREMENT OF BROADBAND INTERFERENCE IN THE 1 TO 10 KMC FREQUENCY RANGE

by
G. LOPEZ and M. ENGELSON
Polarad Electronics Corp.
Long Island City,N.Y.

Abstract. - This paper describes a multi-bandwidth receiver for measurement of broadband interference in the 1 - 10 Kmc frequency range. The effect of impulse bandwidth on receiver response to pulsed signals of unknown energy distribution is considered. The pulse width - impulse bandwidth relationship is determined experimentally and approximations of the sin x/x equation are used to substantiate these results.

Subsequent discussion details the development of instrumentation to fulfill the required objectives. Special attention is given to the use of wide band, fast response circuitry utilizing solid state components.

## I. INTRODUCTION

There are, at the present time, available several radio noise and interference meters covering the frequency range of 1-10 G C/sec. The instrument to be described (Polarad C. F. I.) is the most recent addition in this frequency range. The goal was to improve on the operating characteristics of existing instruments in the following respect:

1. Weight and size.
2. Accuracy and range of phenomena to be measured. Particular emphasis was placed on the low frequency response of the direct peak reading V.T.V.M., the bandwidth arrangement for the measurement of broadband phenomena, dynamic range and measurement accuracy.

The weight and size requirement was achieved by extensive transistorization. The equipment under discussion contains only five tubes - a klystron microwave oscillator, a high input impedance peak, V.T.V.M. and a low noise signal preamplifier.

The impulse generator calibrator is calibrated against a cw standard on a point by point basis in order not to sacrifice accuracy for cw measurements. High broadband measurement accuracy can be achieved by using the substitution rather than full scale calibration method of measurement. The general emphasis, in the field of accuracy, was placed on broadband measurement techniques. To this end the instrument has three carefully controlled bandwidths. The bandwidths are controlled by passive switchable filters and are independent of I.F. aging and detuning since the overall I.F. amplifier bandwidth is wider than the filters. One of the filters is adjusted to have an impulse bandwidth of 1 mc/sec, and a meter scale has been calibrated directly in uv/mc and db above 1 uv/mc for direct broadband measurements without conversion factors.

The front end noise voltage indicated by the peak V.T.V.M. is proportional to the impulse bandwidth used. With an impulse bandwidth change of 1 to 10 there is a noise voltage increase of 20db. If we assume that the

internal noise is about 10 db above 1 uv (3 uv) for the low bandwidth case, the sensitivity in the wide bandwidth case would be 30 db above 1 uv. A conventional display of 40 db above 1 uv full scale would, therefore, mean a total indicator range of only 10 db under wide bandwidth conditions. The requirement for a 70 db dynamic range was therefore established.

## II. THE BROADBAND MEASUREMENT PROBLEM

One of the prime requirements of any new measuring instrument is that its results be compatible with those obtained with instruments already in existence. This problem of agreement between measurements taken with different instruments is particularly troublesome for the case of the field intensity meter measuring broadband interference. Broadband interference is measured in terms of spectral intensity namely, db above a microvolt per mc/sec (D.B.M.C.). Measurement in terms of D.B.M.C. is presumably independent of receiver bandwidth, thus making measurements obtained with different instruments comparable so long as their impulse bandwidths are known. Getting the spectral intensity by dividing the peak meter indication by the receiver bandwidth is however, accurate only when the interference is impulsive in nature over the frequency range of the receiver bandwidth. This is usually not the case when the interference is caused by pulsed R.F. The spectrum of a rectangular pulse has the well known sinx/x configuration which, if the pulse is sufficiently wide, cannot be treated as an impulse.

[1,2,3,4,5,6]

Several recent papers have dealt with various aspects of the broadband measurement problem.

The effect of the pulse width bandwidth product on the recorded spectral intensity can be calculated ( see appendix). The following experimental and calculated data was obtained:

Error in Spectral Intensity as a function of the Pulse Width Bandwidth Product

| Pulse Width Bandwidth Product. BT | 0 | .1 | .2 | .5 | .8 | 1.0 |
|---|---|---|---|---|---|---|
| Computed error(db) | 0 | .1 | .3 | .8 | .3 | 4.6 |
| Error taken from ref. 3(db) | 0 | 0 | 1 | 2 | 3 | 5 |
| Error determined by experimentation (db) | 0 | 0 | 2 | 3 | 4 | 5 |

The reason for the difference between the calculated and observed errors at low pulse width bandwidth products is probably due to the rounded shape of the actual pulse and the non ideal (square) I.F. response curve. The less square the pulse the less is its sidelobe content, and the greater is the difference from a theoretically square pulse at low pulse widths. It is observed that the pulsed R.F. interference measurement problem is peculiar in that the interference, depending on the pulse width receiver bandwidth product, is neither broadband nor narrowband. The interference can with reasonable accuracy be treated as broadband if the pulse width bandwidth product is less than 0.1 and as narrow band (cw) if the pulse width bandwidth product is more than one. The uncertain area of pulse width bandwidth products between 0.1-1.0 can be eliminated by providing for bandwidth changes. In this connection it is desirable to have a third bandwidth in order to easily determine which of the other two bandwidths, broad or narrow band, to use of the measurement. The interference would be treated as broadband if $TB \leq .1$ and as narrow band if $TB \geq 1.0$. An example will illustrate the above statement. Given a wide pulse, such that TB=2 then for a bandwidth 1/2 the maximum or TB=1, it is observed that the peak V.T.V.M. indication hardly changes at all. It can then be surmised that the pulse is wide enough

to be treated on a cw basis when using the wide receiver bandwidth. If on the other hand the interference is caused by a very narrow pulse, say TB =0.05, for a bandwidth increase of five times the minimum bandwidth or TB = 0.25, the meter reading will change by a factor of approximately five. This interference can obviously be treated on an impulsive basis. Thus by switching between the two bandwidths, it is possible to determine the most accurate manner of treating the interference, namely narrow or broadband. For the unlikely case of interference caused by a pulse width such that $TB_{min} = 0.1$ and $TB_{max} = 1.0$, the interference could equally well be treated as narrow or broadband, depending on the bandwidth used.

## III.DESCRIPTION OF SYSTEM (FIG.1)

The receiver under discussion (Polarad CFI) is a triple conversion superheterodyne receiver covering the frequency range from 1-10 KMC. (fig. 2). Calibration is obtained by an impulse generator with flat output over the entire frequency range.

The following specifications apply:

| | |
|---|---|
| Frequency Range | 1000mc to 10,000mc |
| Method of calibration | Impulse Generator |
| Input impedance | 50 ohms |
| Sensitivity (1 mc BW @ S=N) | -90 dbm (min) |
| Impulse Bandwidths | 1 mc,5mc,8mc |
| Image and spurious response rejection | 60db down |
| Video bandwidth | 12mc |
| Weighting circuits | Avg, quasi-peak, peak, slideback-peak |

The frequency range of the receiver is covered in four bands (typical tuning head band shown in fig.3).

| | |
|---|---|
| Band I | .950-2040 Mc |
| Band II | 1900-4340 Mc |
| Band III | 4200-7740 Mc |
| Band IV | 7300-10,000Mc |

Preselection is employed in each band to reduce the image response, located at twice the first IF from the desired signal, to greater than 60db down. Because of the relatively high 1st IF frequency of 260 MC, a two cavity preselector design provides the necessary off-band attenuation. The preselector 3 db bandwidth varies from 8-10 Mc at the low bands to 18-25 Mc at the high bands. The preselector is cam driven along the band simultaneously with a klystron cavity oscillator which delivers fundamental L.O. power to the 1st mixer.

Alignment of the preselector and cavity oscillator is facilitated with use of anti-back lash gears and rigid tuning mechanisms. With this mechanical arrangement, frequency accuracy is held to 1%.Digital frequency readout is obtained by the use of a decade counter.

Further frequency stability is obtained by AFC. A D.C. feedback voltage, which is opposite in polarity to signal or oscillator drift, is applied to the klystron repeller. Capture and hold-in capability is largely determined by the IF discriminator bandwidth and the repeller mode width.

The 1st conversion results in a 260 Mc IF. Amplification at this frequency is obtained with two broadband grounded grid amplifiers. Ceramic planar triodes are employed to achieve an IF noise figure of 5 db. The gain of the 260 Mc IF is 18 db with a bandwidth of 20 Mc. Vacuum tubes were selected over transistors in this application.

At the time of development comparative noise figures and gain, with solid state devices, were obtainable only with experimental units of moderately high price. Transistors are however, presently available with performance somewhat equivalent to the planar triode. However, it has been shown[7] that the non-linearities inherent in transistors are such, that noise figure measurements are meaningful only in the absence of signal. Tests have shown that because of cross modulation effects, improvement of S/N ratio as a function of input signal does not follow the expected increase.

Obviously, one of the requirements of a receiver used for RFI is that its susceptibility to cross modulation be negligible. Methods are outlined to reduce the high cross-modulation effect prevalent in RF Transistor amplifiers. However, they entail compromises which ultimately increase the noise figure of the amplifier. By employing vacuum tubes at the front end, this problem is not encountered. Sufficient gain is obtained by the grounded grid amplifiers, so that noise contribution by succeeding mixer and amplifying stages is negligible.

Conversion to 140 Mc IF takes place immediately following the two stages of 260 MC triode amplifiers. L.O. power is supplied by a frequency doubler driven by a crystal controlled 60 Mc transistor oscillator. This oscillator also drives a tripler to generate 180 Mc L.O. power for the final conversion to 40 Mc. The amplifier chain at 140 Mc consists of five synchronously tuned transistor stages, three of which are AGC controlled. Overall gain is 20db with 25 Mc BW. The stages used for AGC are biased for reduced gain to obtain optimum operating conditions for the wide dynamic range required. Interstage coupling is simplified with the use of toroidal ferrite cores. Efficient coupling is obtained and interstage feedback is minimum because of its self-contained field. The tuned inductance of the primary is purposely made small so that collector capacity can be adequately loaded externally.

A third and final conversion results in a 40 Mc IF. A transistor stage is used as a mixer with 180 Mc L.O. emitter injection. Six stages of 40 Mc IF amplifications follow, the last stage being a 5639 pentode. High power output requirements (20 db dynamic range), with 14 Mc overall IBW, made it necessary to employ a tube. A 3K ohm detector load is required to obtain the bandwidth. RF detection efficiency with a 3K load is slightly greater than 50%. The output tube must therefore, swing at least 50 VRMS to produce the required output at the detector. To transistorize this stage requires a transistor of approximately 5 watt collector dissipation and at least a 100V collector-base voltage rating. Such a transistor is costly and adds additional difficulties in the driver stages. The tube used is rated at 4w plate dissipation and is driven by a low-power transistor of the drift-field type, 2N384. Overall IF 3 db bandwidth is 10 Mc, and the video BW following RF detection is 12 Mc. The multiple impulse bandwidth provision takes the form of a filter chassis which is inserted in the 40 Mc IF amplifiers chain.

The filter chassis contains two filter networks with impulse bandwidths of 1 mc and 5 mc selectable by a front panel switch. A third

position on the switch marked 8 mc does not contain a filter, but feeds through the signal with only the normal IF and video bandwidth restrictions. The filters used are double tuned, critically coupled networks. Insertion loss of the narrow band filter is approximately 4 db, and the 5 Mc filter is 1 db. A 40MC IF amplifier is used in conjunction with the filter networks to compensate for the unequal transmission loss. A change in d.c. operating point of the transistor amplifier results in a change of gain when the system is switched to the 5 and 8 Mc positions. Two adjustment pots are used to precisely set the gain in the mid and wide band condition so that there is no visible change in output meter indication as a function of bandwidth. This is only true for high level signals. Signals close to noise will be modified by virtue of noise changes. The overall IF bandwidth of 10Mc plays a negligible part in determining receiver impulse bandwidth in the narrow and intermediate positions. Changes in the 10Mc wide IF bandwidth, due to different transistor parameters and temperature effects, has no effect on the 1 and 5Mc IBW of the receiver. Furthermore, critical alignment of an IF amplifier to a specified bandwidth is not necessary. Stability in the wide-band condition is obtained by controlling the video bandwidth. Impulse bandwidth is determined by the combined bandwidth of RF, IF and Video stages. It was mentioned earlier that the video BW is 12Mc, therefore in the narrow and intermediary bandwidth conditions the impulse BW is strictly a function of the narrow IF filters. However, in the wide band position, the combined responses of video and IF amplifiers result in an impulse BW of 11 Mc. Bandwidth reduction of the video stages is accomplished by a capacitivie adjustment which reduces the video bandwidth to obtain a system IBW of 8mc.

The wide bandwidth of this receiver could create a problem on the output peak reading voltmeter. Under the wideband conditions the receiver is capable of passing a .06 micro sec pulse unattenuated. At high duty cycles the charge current requirements for a simple RC detector circuit are satisfied by conventional circuits of proper bandwidth. But as the duty cycle is lowered the problem becomes one of supplying extremely high charging current pulses of short duration.[8] The large charge current requirements make it desirable to have a low source impedance. The combination of emitter follower and junction diode make an almost ideal driving source with no complexity.

The output impedance of an emitter follower is approximately

$$R_o = \frac{R_g}{B + 1}$$

$R_o$ = output impedance
$R_g$ = source impedance
$B = \frac{\Delta IC}{\Delta IB}$ = Current gain

The detector output load impedance is approximately 3K. A 2N1143 transistor is used as an output video stage, with a typical beta of 30. Substituting these values results in an $R_o$ of approximately 100.

The diode that is used as a peak detector should meet the two following requirements:

1. It must have high conduction capability.
2. Back resistance must be sufficiently high so that loading on the VTVM stage is negligible.

A search through the multitude of junction diodes available shows that where high conduction is available a low back resistance usually is present.

Certain computer silicon diode types, however, are an exception. They combine high conduction capability with extremely high back resistance. Measurements of unselected units with a milli$\mu$ammeter indicated leakage currents of no greater than 3 milli$\mu$amperes. This is equivalent to a back resistance of greater than 200 Megohms. The conduction characteristics are such that with a forward current equal to 1 ampere the voltage drop across the diode is typically 1 volt. The effective diode resistance in the forward region is typically 1 ohm. Thus the transistor and diode combination represent a source impedance of approximately 100 ohms. This low source impedance characteristic coupled with high speed recovery time, make the transistor diode circuit ideal for this application.

The circuit shown in fig. 4 represents the peak reading VTVM. Because of the low source impedance of the transistor-diode combination, a load capacitance of .01 uf is acceptable and yet maintain the charge time requirements. This circuit does not require the use of electrometers or special vacuum tubes to obtain a proper discharge time. The low duty cycle response of this VTVM is shown in fig. 4. Vacuum tubes were chosen over transistors to properly realize a high d.c. impedance. A dual triode stage serves as a VTVM in a cathode coupled configuration that provides a high degree of linearity.

There are many methods of AGC used to obtain wide dynamic range in transistor superheterodyne receivers. If the transistor is used as a gain control element, then it can be connected to utilize its forward or reverse bias characteristic, to obtain gain control. Each system has its pros and cons. As a rule more dynamic range can be obtained with reverse AGC, but forward AGC has superior signal overload properties.

Still other methods are available to the designer in the form of diode networks which control interstage signal transfer. In these methods forward diodes or reverse diodes (eg. Varicap) are employed in shunt signal circuits. With conventional receivers, these methods can be used with a degree of success, dependent on the type of signal received and its presentation at the output. Reverse AGC was chosen over the other AGC schemes because of its uniform gain characteristics. With this technique the output gain characteristics is reproducable within $\frac{1}{2}$ db.

The impulse generator employed, produces a flat spectrum over the entire operating frequency range. A 150V impulse of .02 nano sec. duration is keyed at 1000 cycles to generate this spectrum. Peak output of the impulse generator is set at 60 db over 1 uv/mc (-47dbm) for receiver of 1 MC IBW and is variable over a 20 db range. Periodic reversal of charging voltage on the shorting contacts significantly decrease the effect of single contact corrosive build up. All video circuitry employed to drive the generator is transistorized; because of this, power needed to drive the generator is below 30 watts.

The entire receiver is constructed in a manner to facilitate manufacturing and provide ease of maintenance, the circuits shown in fig. 1 are housed in individual sub-chassis. All the sub-chassis are easily secured and removed from the main frame. Transistorized power supplies included. Tuning head chassis are interchanged quickly and no internal or external hand connections are necessary to prepare the receiver for operation. This modular type of construction adds versatility

to the receiver. Since receiver elements can be readily integrated, the form factor of the receiver can be easily adjusted to fit specific requirements, both from a mechanical and electrical viewpoint.

## IV. CONCLUSIONS

The conclusions that can be drawn from this project are many and varied. The major points are that: - Transistors, if properly utilized, can contribute markedly to RIFI receiver design. The compatibility problem, getting the same results with different instruments, can be successfully solved. For the case of the present receiver, the solution takes the form of three switchable bandwidths. This is the first of a new generation of solid state Field Intensity Receivers.

## APPENDIX
## EFFECT OF PULSE WIDTH BANDWIDTH PRODUCT ON MEASURED SPECTRAL INTENSITY

Assuming a rectangular R.F. pulse (figure 6) we find that the frequency spectrum of the envelope has the well known sin x/x distribution (figure 7.) The spectral intensity at the carrier frequency (frequency that is being pulsed) is $F(fo) = \frac{ET}{2} \times$

$\left[1 + \frac{\sin 2 \quad foT}{2 \quad foT} \quad \exp(-J2\pi \quad foT)\right]$ which reduces to $\frac{ET}{2}$ for $foT > 2$. The lowest I.F. of the C.F.I. is 40 mc/sec. F (fo) can therefore be taken as ET/2 down to a pulse width of $T = \frac{2}{40 \times 106} = .05$ usec.

The peak meter indication will be determined by the portion of the frequency distribution that falls within the video amplifier passband after detection, as shown in figure 8.

The deviation of the peak meter reading follows: The integrated impulse bandwidth , for the case of many stages in cascade is:

$$B = \frac{1}{Go} \int_0^\infty \left|G(f)\right| \, df$$

Also

$$Vp = S \, Go \, B = \int_0^\infty S \left|G(f)\right| \, df$$

S is the spectral intensity, which is $C \, \frac{\sin \pi fT}{\pi fT}$

thus

$$Vp = C \int_0^\infty \frac{\sin \pi fT}{\pi fT} \left|G(f)\right| \, df$$

Assuming a rectangular passband characteristic normalized to 1 (fig? ) we get

$$Vp = C \int_{fo}^{fo + B/2} \frac{\sin \pi fT}{\pi fT} \, df$$

Thus the peak pulse level reaching the V.T.V.M. is

$$Vp = C \int_{fo}^{fo + B/a} \frac{\sin \pi fT}{\pi fT} \, df =$$

$$= \frac{C}{\pi T} \int_{fo}^{fo + B/2} \frac{\sin x}{x} \, dx = K \int_{fi}^{f_1 + B/2} \frac{\sin x}{x} \, dx$$

T = Pulse width
B = Band width
f = Deviation from center frequency (fo)

The spectral intensity computed from the above peak voltage reading is

$$F'(f) = \frac{K}{TB} \int_{fo}^{fo+B/2} \frac{\sin x}{x}\, dx$$

The true spectral intensity is of course, K, which we can normalize to K=1.

$$F'(f) = \frac{1}{TB} \int_{fo}^{fo+B/2} \frac{\sin x}{x}\, dx$$

$\int_0^x \frac{\sin x}{x} dx$ is the so-called sine integral Si x, values of this integral can be found in any mathematical table of functions. It is now possible to determine the effect of the bandwidth pulse width product on the spectral intensity measured by the receiver. For example:

Let $\frac{1}{T} \times B = 1$ at this point x = ft

f= deviation from center frequency which is equal to the video bandwidth (B)

f = B and x = T

$$F'(f) = \frac{1}{x} \frac{\sin x}{x} dx = \frac{1.86}{} = .593$$

at B T = 0.8

$$F'(f) = \frac{1}{X} \int_{.o}^{.8} \frac{\sin x}{X} dx = \frac{1.778}{.8} = .706$$

at B T = .5

$$F'(f) = \frac{1}{x} \int_{.o}^{.5} \frac{\sin x}{x} dx = \frac{1.36}{.5} = .867$$

at B T = .2

$$F'(f) = \frac{1}{X} \int_{o}^{.2} \frac{\sin x}{x} dx = \frac{.607}{.2} = .965$$

at B T = 0.1

$$F'(f) = \frac{1}{x} \int_{o}^{.1} \frac{\sin x}{x} dx = \frac{.31}{.314} = .985$$

The computed error is:

| BXT Pulse width bandwidth product | 0 | .1 | .2 | .5 | .8 | 1.0 |
|---|---|---|---|---|---|---|
| F (f) | 1.0 | .985 | .965 | .867 | .706 | .593 |
| Error d.b. $20\log_{10} \frac{1}{F(f)}$ | 0 | 0.1 | .3 | .8 | 3 | 4.6 |

## BIBLIOGRAPHY


1. Response of Ideal Radio Noise Meter to Continuous Sine Wave, Recurrent Impulses and Random Noise. D.B. Geselowitz, I.R.E. Trans. PGRFI Vol. 3 no.1 May 1961.

2. Suppression of Spurious Outputs from Pulsed Transmitters. P. Varlashkin, S.L. Brown, F.J. Morris 3rd Conference on Radio Interference Reduction 1957.

3. The relationship between Broad-Band Interference Measurements (B.B.M.C.) and Pulsed - C.W. signals. L. R. Pangborn I.R.E. Convention March 1961.

4. Significance of I.F. Bandwidth in R.F. Interference Measurements, R. B. Schulz, 3rd National Symposium on R.F.I. June 1961.

5. Instrumentation for Radio Interference Measurements. F. Haber, R. M. Showers, Electronic Industries March 1961.

6. Detection of Impulse Signals in Random Noise. A. H. Gottfried, K. Ikrath, 3rd Conference on Radio Interference Reduction 1957.

7. Noise Modulation effects in Transistor Receivers. W.A. Rheinfelder, Solid State Journal, July 1961, Vol. 2 No.7.

8. Technical Memo No.M-1801 "A New Peak VTVM for low duty cycle pulses" July 5,1956 - Signal Corps Task No. 2224A.

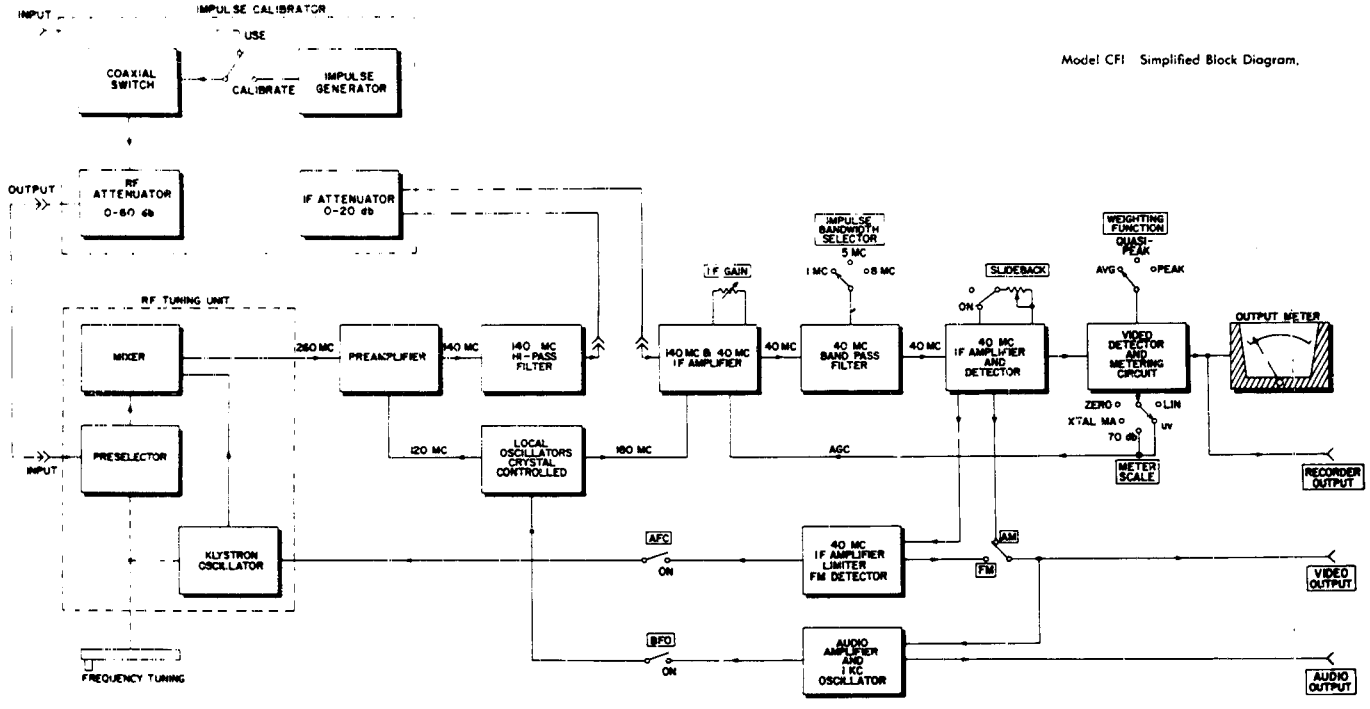



Figure 1
System Block Diagram

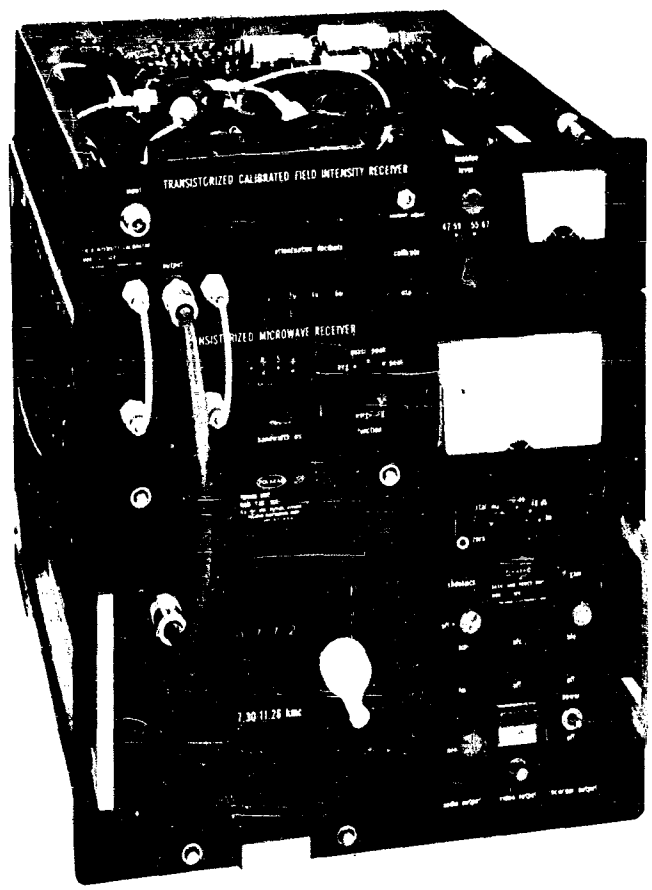



Figure 2
Calibrated Field Intensity Receiver

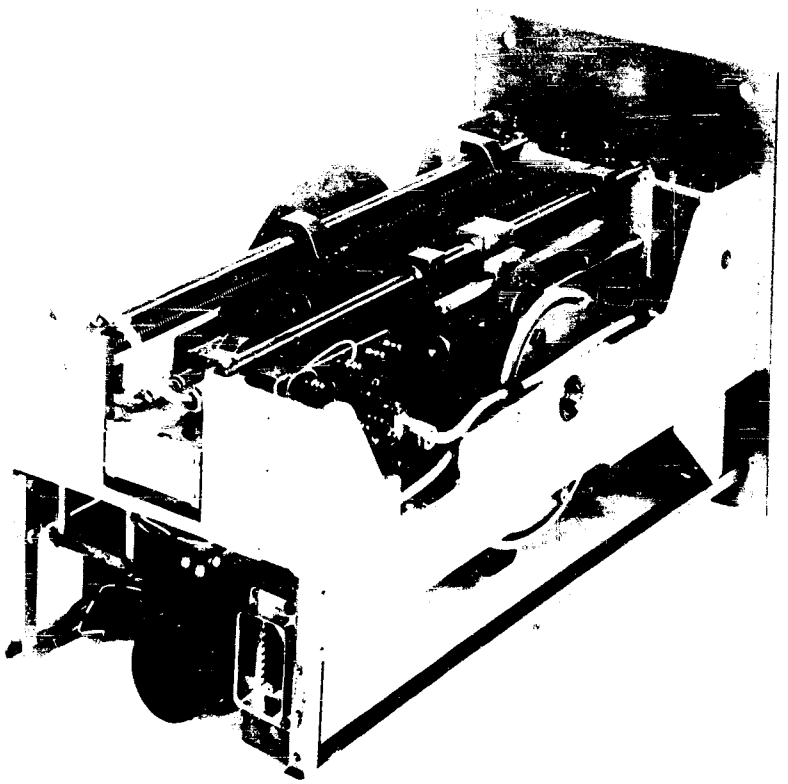


Figure 3
Tuning Head Chassis

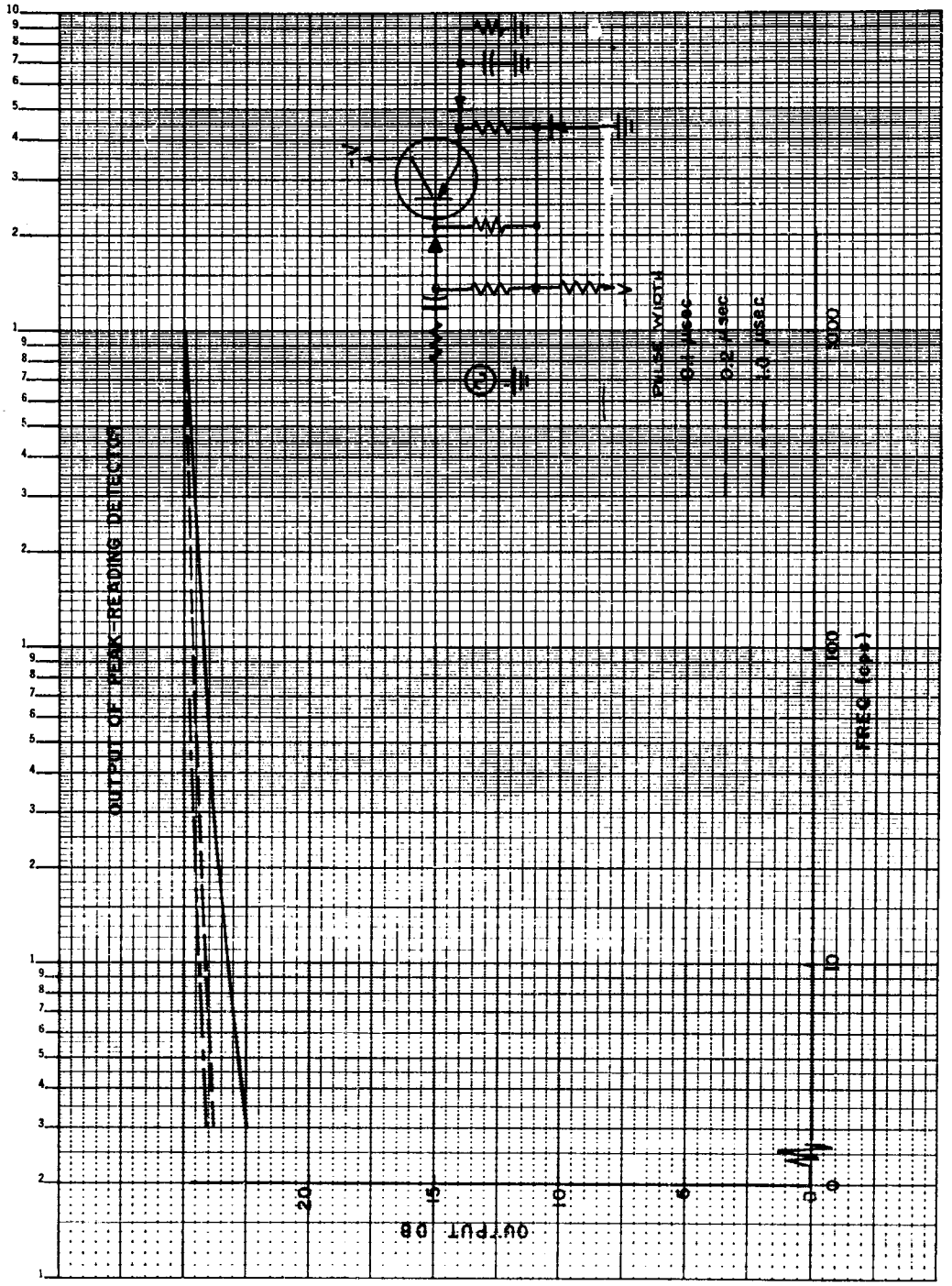



Figure 4
Low Frequency Response of Peak VTVM

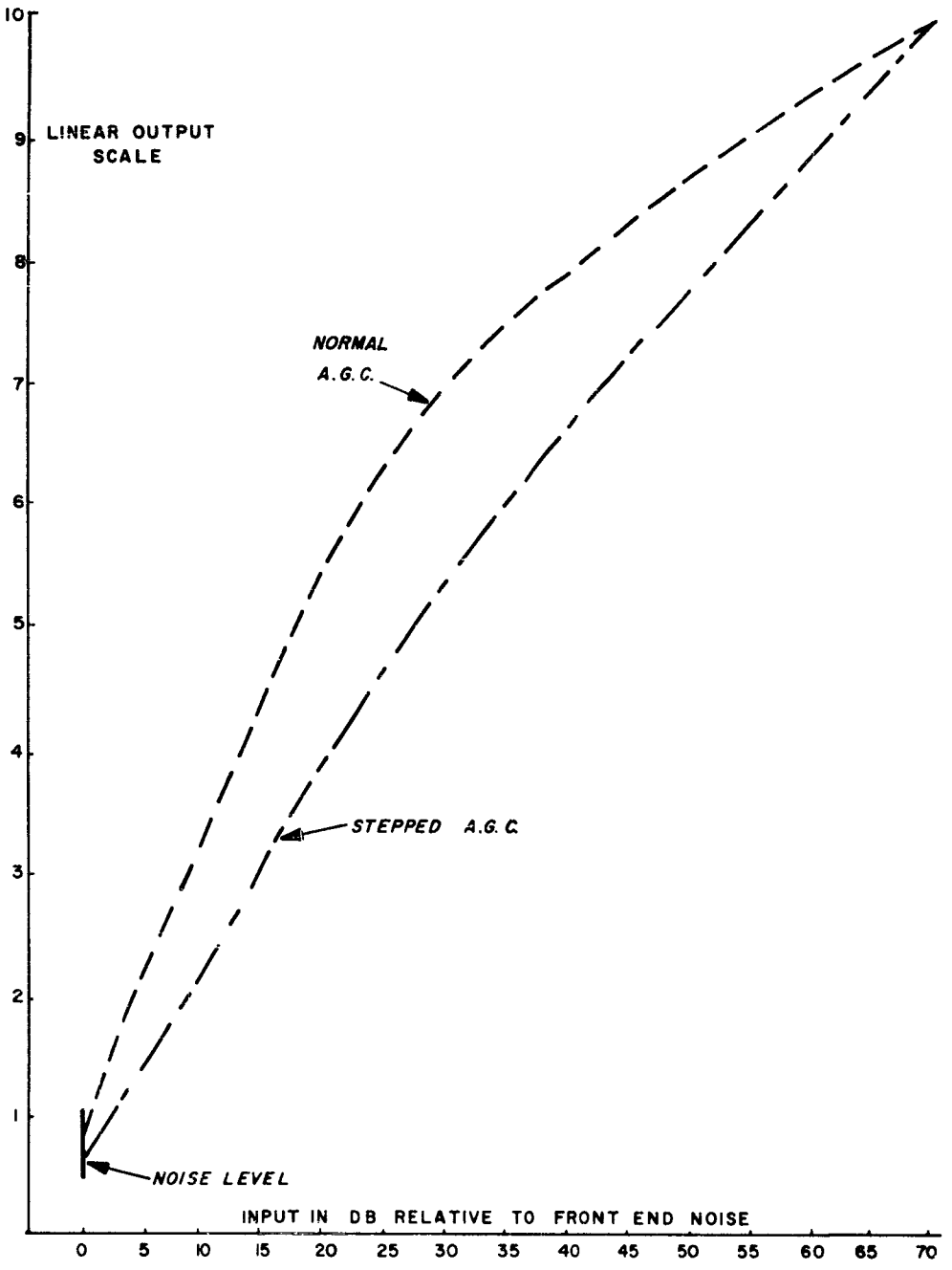
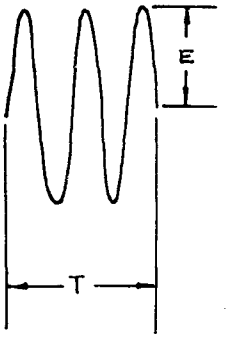
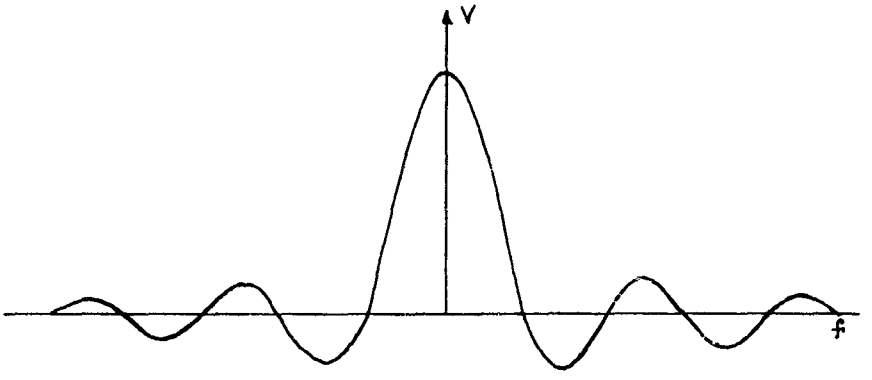



Figure 5
A.G.C. Characteristic



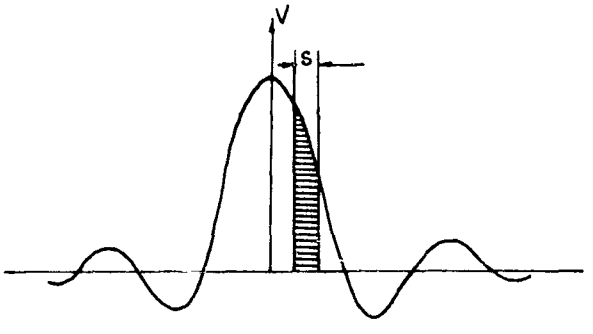

RF PULSE

fig 6



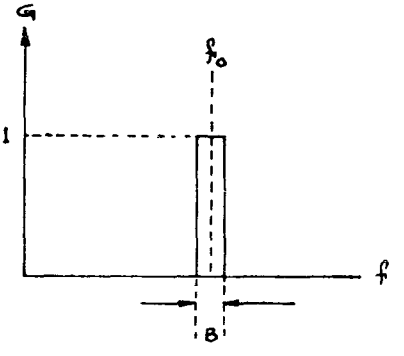

$\frac{\sin x}{x}$ SPECTRAL DISTRIBUTION

fig 7




BANDPASS CHARACTERISTIC DETERMINES PORTION OF ENERGY PASSED

fig 8




NORMALIZED IDEAL PASS BAND

fig 9

# A SENSITIVE RECORDING SYSTEM FOR HARMONIC PATTERN MEASUREMENTS AT MICROWAVE FREQUENCIES

R. J. Doviak and D. J. Lewis
The Moore School of Electrical Engineering
University of Pennsylvania
Philadelphia, Pennsylvania

**Abstract.** - A recording system having a high sensitivity and a broad dynamic range was developed and tested. A high sensitivity is obtained through the use of a microwave receiver as the detector. To obtain the necessary range and freedom from nonlinearities, a servo feedback system in conjunction with a calibrated attenuator is used to maintain the detected signal at a constant level. At L band frequencies the system has a total dynamic range of over 100 db. The setup is adaptable to standard microwave generators and detectors.

## I. INTRODUCTION

The measurement of antenna patterns at frequencies beyond the normal design band of the antenna is an exacting task because of the need to observe complex field distributions. The need for an antenna pattern recording system, having a large dynamic range and a strictly linear relation between the recorded results and actual power levels, is apparent. The use of a system which combines simplicity and versatility with a large dynamic range is therefore desirable. Such a recording system has been developed. Conventional pattern recorders are dependent upon the linear and non-linear characteristics of crystal detectors and mixers and are limited in dynamic range due to deviation from these characteristics when input power levels exceed certain bounds. Extremely sensitive low noise receiving systems, such as those employing parametric amplifiers or masers, are limited in their input power range because of changes in their characteristics at relatively low power levels and hence full advantage of the increased sensitivity cannot be achieved.

In the proposed system the crystal detector, mixer, parametric or maser element, will always be operated at a constant level of input signal thereby eliminating the dependence of system linearity on volt-ampere characteristics.

## II. PRINCIPLE OF OPERATION

The prime component in the recording system is a precision variable attenuator which controls the level of the input signal. A "waveguide below cut-off" type attenuator, which is characterized by its stability and accuracy, has been used successfully. This attenuator has the advantage of having a linear dependence between insertion loss (in db) and coupling distance. Other types of precision attenuators having a minimum insertion loss of zero db are available and may easily be utilized in the system.

The basic components used in this system are shown in block diagram form in Fig. 1. The transmitter output level, which is modulated by an audio signal frequency, $f_m$, equal to the carrier frequency of the servo system, is controlled by the variable attenuator and fed to the transmitting antenna. The transmitted signal can be detected by using a simple microwave crystal detector and tuned amplifier or a more complex superheterodyne receiver. The detected signal at frequency $f_m$ is fed to a difference amplifier where an "error" voltage proportional to the difference between a reference voltage and the signal is amplified and sent to the field winding of a servo motor which controls the setting of the attenuator. The reference voltage is chosen to have the same frequency as the modulation voltage of the microwave transmitter. When the received signal level exceeds the reference voltage level, the servo motor drives the attenuator to increasing levels of attenuation until a received signal is attained having the same amplitude as the reference voltage level. When the transmission loss between the two antennas is increased due to antenna rotation, resulting in a decrease of received signal level at the difference amplifier, the "error" voltage "returns" the attenuator setting to lower levels of attenuation until the received signal equals the reference voltage level. In this manner, a continuous record of the varying transmission loss between transmitter and receiver can be obtained.

The normally closed switch is used to cut off the reference voltage at the zero db setting of the attenuator dial in order to prevent the servo motor from driving the attenuator beyond its mechanical limits.

The position of the attenuator dial is recorded by coupling a potentiometer to its shaft. A dc voltage, proportional to the angular position of the shaft, is conveyed from the variable arm of the potentiometer to a high impedance dc recorder. The indicator records the angular position which for a "waveguide below cut-off" type attenuator is linearly proportional to the attenuation in db of transmitted power. The antenna's angular position is relayed to the recorder in the conventional manner as shown in Fig. 1.

## III. GENERAL CONSIDERATIONS

The system maintains a constant level of receiver input signal determined by the level of the reference voltage, $V_r$, and the gain of the receiver $G_r$. The accuracy and linearity that can be achieved is primarily limited by the characteristics of the variable attenuator employed. The difference voltage $(V_s - V_r)$ is related to the servo-motor control voltage $V_c$ by the relationship

$$\left|V_s - V_r\right| G_d = V_c \qquad (1)$$

where $G_d$ is the gain of the difference amplifier and $V_s$ the signal voltage. $V_c$ is determined primarily by the load torque characteristics of the servo-motor. In order that the servo motor responds to an input control voltage, $V_c$ must be greater than or equal to $V_{min}$, where $V_{min}$ is the minimum voltage

needed to activate the servo motor.

It is convenient to define a system accuracy parameter, p, by the relation

$$p = 10 \log \frac{V_s}{V_r} \tag{2}$$

A factor of 10 is used in equation (2) because we are considering a video receiver in which the output voltage is proportional to the input power. Substituting equation (1) into (2), we obtain

$$|p| \geq 10 \log \left[ 1 + \frac{V_{min}}{V_r} \frac{1}{G_d} \right] \tag{3}$$

Equation (3) is plotted in Fig. 2 for values of $V_{min} = 30$, and $G_d = 100$, which are the characteristics of the system used. The figure indicates close agreement between the experimental points obtained and equation (3).

The dynamic range of the system is limited on the high end by the maximum power level of the transmitter. The low end limitation is determined by the noise level of the system and the required system performance.

In obtaining qualitative information, it is found that dynamic range must be sacrificed for increased system performance and accuracy. Consider the servo motor to have the ideal characteristics as shown in Fig. 3. Also to simplify the analysis we shall only consider the steady state operating conditions of the motor.

A given load-torque level determines the minimum control voltage $V_{min}$ below which the servo motor is not activated. Maximum sensitivity is obtained when the system gain $G_d G_r$ is set to a value such that the noise voltage level $V_n$ is equal to $V_{min}$. With the above considerations it is possible to obtain a quantitative value for the dynamic range as a function of system accuracy. Assuming that noise voltage ($V_n$) originates only in the crystal detector, the $(S/N)_c$ voltage ratio at the control windings is defined by

$$\left(\frac{S}{N}\right)_c = \frac{|V_s - V_r|}{V_n} \tag{4}$$

or rewriting

$$\left(\frac{S}{N}\right)_c = \left| \frac{V_s}{V_r} - 1 \right| \left(\frac{V_s}{V_n}\right)\left(\frac{V_r}{V_s}\right) \tag{5}$$

Substituting from equation (2) and solving for p we obtain

$$|p| = 10 \log \left[ \frac{\left(\frac{S}{N}\right)_i}{\left(\frac{S}{N}\right)_i - \left(\frac{S}{N}\right)_c} \right] \tag{6}$$

where $\left(\frac{S}{N}\right)_i = \frac{V_s}{V_n}$.

The dynamic range of the system is given by

$$R_{db} = 10 \log \frac{P_t}{P_o} \tag{7}$$

where $P_t$ is the available transmitter power and $P_o$ the power level at which video crystal is operated. The demodulated signal power output, $P_s$, is related to the input rf power $P_o$ and crystal diode conversion loss C(db) by[1]

$$P_s = \frac{P_o}{\log^{-1}\left(\frac{C}{10}\right)} \tag{8}$$

The signal to noise voltage ratio at the input to the audio receiver is

$$\left(\frac{S}{N}\right)_i = \sqrt{\frac{P_s}{P_n}} \tag{9}$$

where $P_n$ is the crystal noise power at the modulation frequency $f_m$. $P_o$ and the noise power level, $P_n$, are related to $(S/N)_i$ and crystal diode conversion loss by

$$\left(\frac{S}{N}\right)_i = \sqrt{\frac{1}{\log^{-1}\frac{C}{10}} \frac{P_c}{P_n}} \tag{10}$$

where C = conversion loss in db.

Solving for $P_o$ we obtain

$$P_o = P_n \left(\frac{S}{N}\right)_i^2 \log^{-1} \frac{C}{10} \tag{11}$$

and substituting (9) into (7) R becomes

$$R_{db} = 10 \log \left[\frac{P_t}{P_n} \frac{1}{\left(\frac{S}{N}\right)_i^2}\right] - C \tag{12}$$

Substituting for $(S/N)_i$ from equation (6) we obtain the relation between dynamic range and accuracy.

$$R_{db} = 10 \log \left[\frac{P_t}{P_n} \frac{\left(1 - \frac{1}{\log^{-1}\frac{p}{10}}\right)}{\left(\frac{S}{N}\right)_c^2}\right] - C \tag{13}$$

Measured values of noise power at a servo carrier frequency of 60 cps were about -65 dbm. The conversion loss of video crystals average about 5 db.[2] The limits on values of $(S/N)_c$ are not easily defined, but appear to be dependent on the servo motor and noise characteristics. However, a value of about 0.2 has been experimentally found for the system described below. Substituting the above values in equation (13) and simplifying it results that

$$R_{db} \simeq 100 - C + 10 \log 8 P_t + 10 \log \left[ \frac{\log^{-1} \frac{|p|}{10} - 1}{\log^{-1} \frac{|p|}{10}} \right] \qquad (14)$$

Equation (12) is plotted in Fig. 4 as a function of system accuracy for a transmitted power level of 1 milliwatt. Also plotted in the figure are experimental points obtained for a crystal detector having a noise power of -62 dbm. Hence, with this system, a crystal video detector offers a 59 db dynamic range with an accuracy of less than ± 0.3 db. Other sources of error such as gear back-lash, friction, etc. were not considered in the above analysis. The use of a 60 cps carrier frequency caused an excess of noise due to cable pick-up and may account for the differences between experimental points and the theoretical curve.

Crystal diode noise power at audio frequencies obey an inverse frequency law[3] and one may expect an improvement in the sensitivity and consequently an increase in dynamic range if the carrier frequency is somewhat higher than 60 cps. For instance, at a frequency of 1000 cps the noise power may be decreased by as much as 10 db. However, at still higher frequencies the noise power is independent of frequency and no advantage would be gained by increasing the carrier frequency of the servo system indefinitely.

The use of a more sensitive receiving system will extend the range of operation considerably with increased accuracy and dynamic range. For instance the use of a superheterodyne receiving system, as described below, having a sensitivity of about 105 dbm resulted in a system having a dynamic range of about 100 db with an accuracy better than ± 0.3 db.

## IV. DESCRIPTION OF SYSTEM

The physical layout of a typical feedback measurement system, which was developed and constructed for a series of antenna pattern measurements at harmonic frequencies, is shown in Figs. 5 to 7. In this setup a double conversion superheterodyne receiver is used as a detector to obtain the maximum possible range. A series of Hewlett-Packard signal generators provide the signal power. A typical pattern record obtained with this system is shown in Fig. 8. The important system characteristics (response speed, range and accuracy) are tabulated in Table 1.

The feedback servo assemply is mounted on an adjustable bracket which can be attached to the panel grips of several different signal generators. The attenuator dial knob on the signal generator is replaced with a small gear which meshes with the drive gear on the servo motor. With this arrangement, the internal attenuator of the signal generator forms part of the feedback loop. A total frequency range of from 1 kmc to 10 kmc was possible with the signal generators used with this unit. The potentiometer used in the voltage divider circuit activating the recorder pen is mounted on the same panel and is geared to the attenuator shaft to provide a dc output signal which is linearly related to db of attenuation.

The servo amplifier and its associated power supply is mounted in a six foot relay rack together with the recorder. The same rack also supports the servo amplifier and power supply for the recorder roll servo. A control panel at the top of the relay rack contains the biasing circuits used to adjust the zero level and scale factor for the recorder pen.

The modulation and reference voltages are taken directly from the 60 cycle power line. This permitted us to drive a small 60 cycle two phase servo motor directly from the output of the servo amplifier. However, as would be anticipated, stray pickup is a serious problem when this frequency is used.

The basic servo system was also used for obtaining continuous records of insertion loss as a function of frequency. The arrangement was basically the same as for the antenna pattern measurements, except that the signal generator frequency dial was linked through a second servo system to the recorder roll drive. A broadband crystal mount with a tuned audio amplifier was used in place of the superheterodyne receiver to avoid the problem of keeping the detector tuned to the same frequency as the signal generator. The results of these tests were extremely promising. It was possible to obtain plots of insertion loss as a function of frequency with a great deal more precision and accuracy than can be obtained from point by point techniques.

## V. REFERENCES


1. Torrey and Whitmer, "Crystal Rectifiers," Vol. 15, Radiation Laboratory Series, p. 25.

2. Ibid, p. 193

3. Ibid, p. 32

| RESPONSE SPEED DB/SEC | RANGE DB | ACCURACY DB |
|---|---|---|
| 35 db/sec | 100 db | ± 0.3 |

TABLE I

FIGURE 1
BLOCK DIAGRAM OF RECORDING SYSTEM

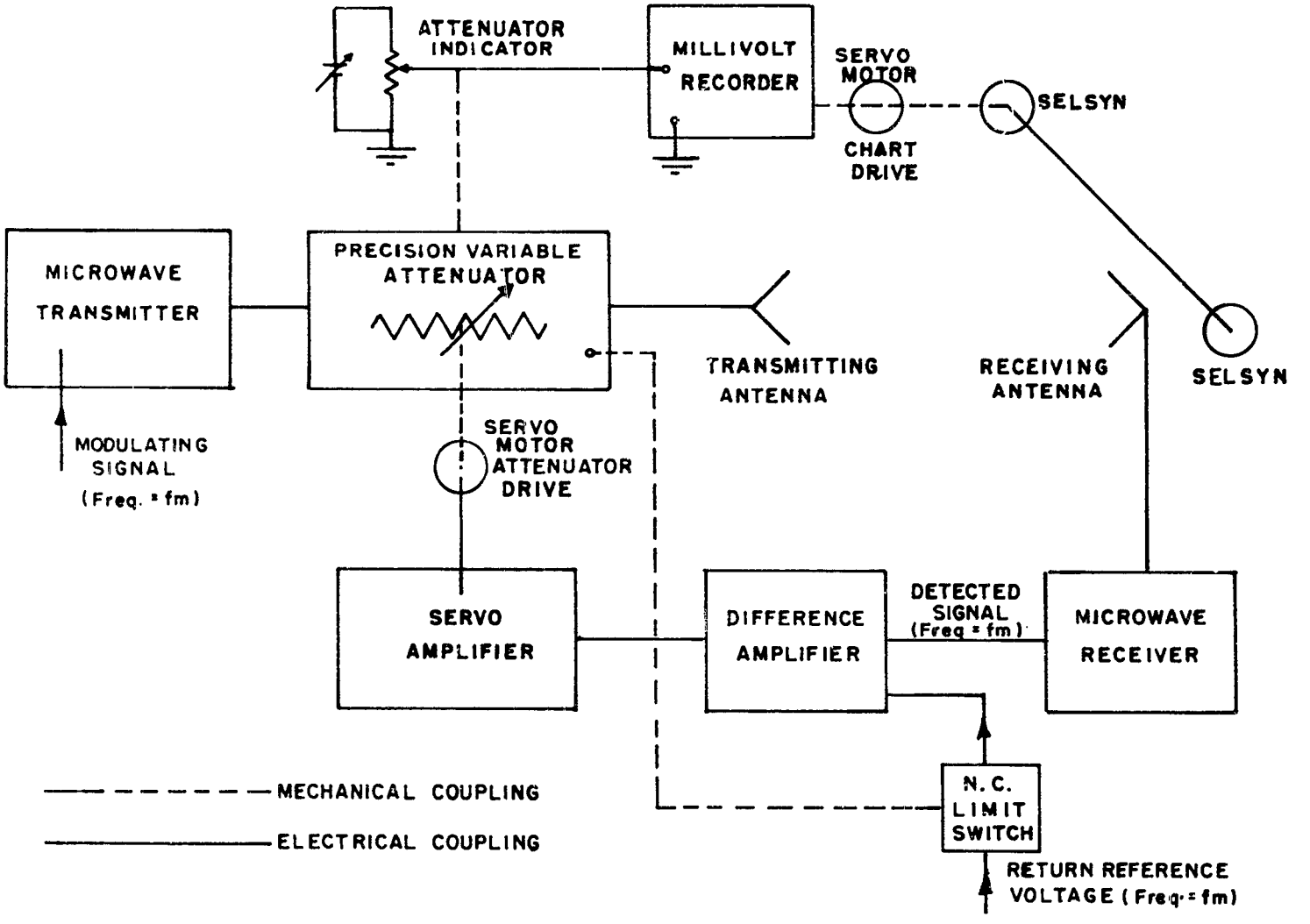


FIGURE 2

SYSTEM ACCURACY p VERSES
RETURN REFERENCE VOLTAGE $V_R$

Gd = ≅ 100
Vmin ≙ 30

⊕ Experimental points

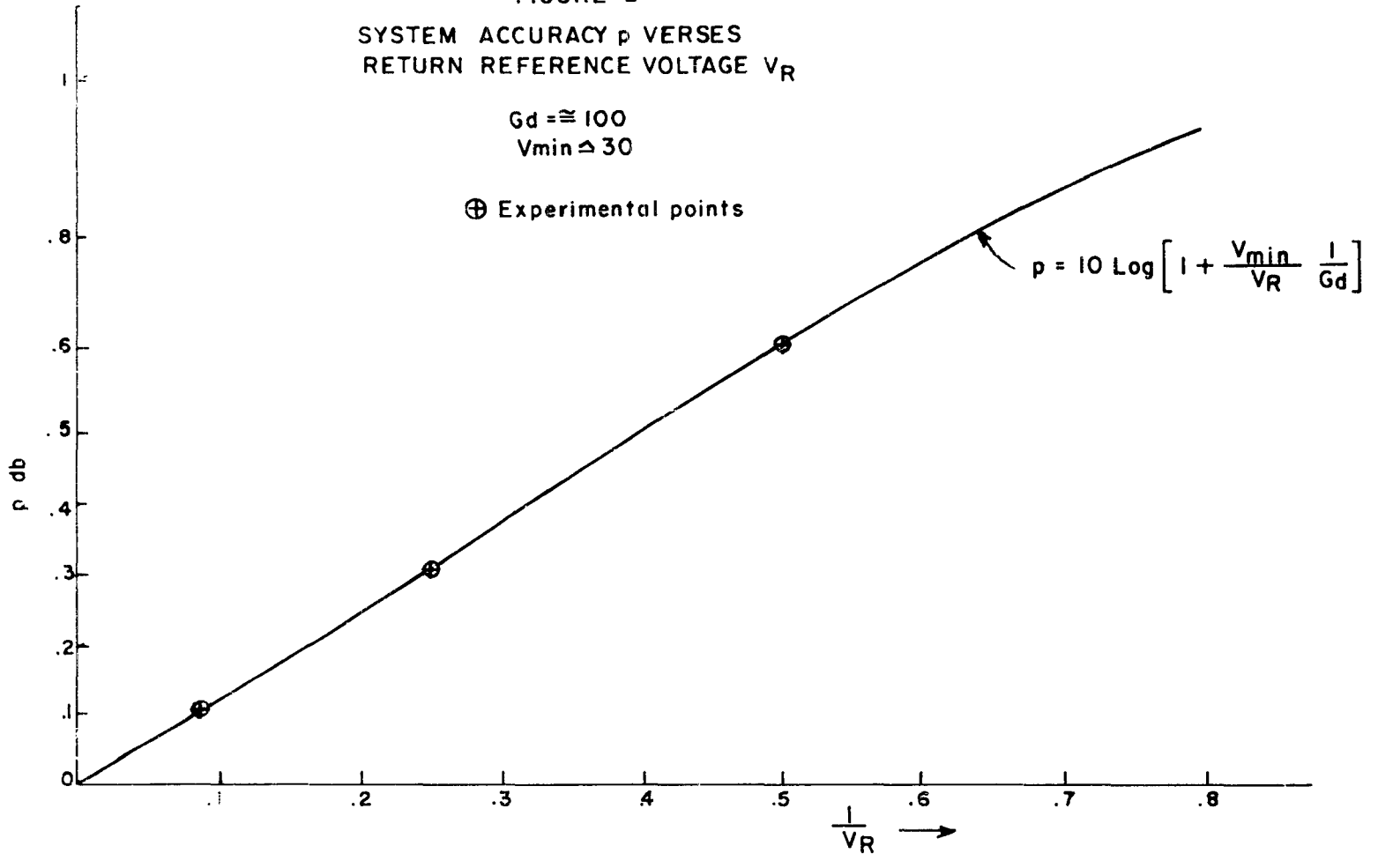


FIGURE 3

TORQUE-SPEED CHARACTERISTICS OF IDEAL SERVO-MOTOR CONTROL VOLTAGE $V_c$ AS PARAMETER

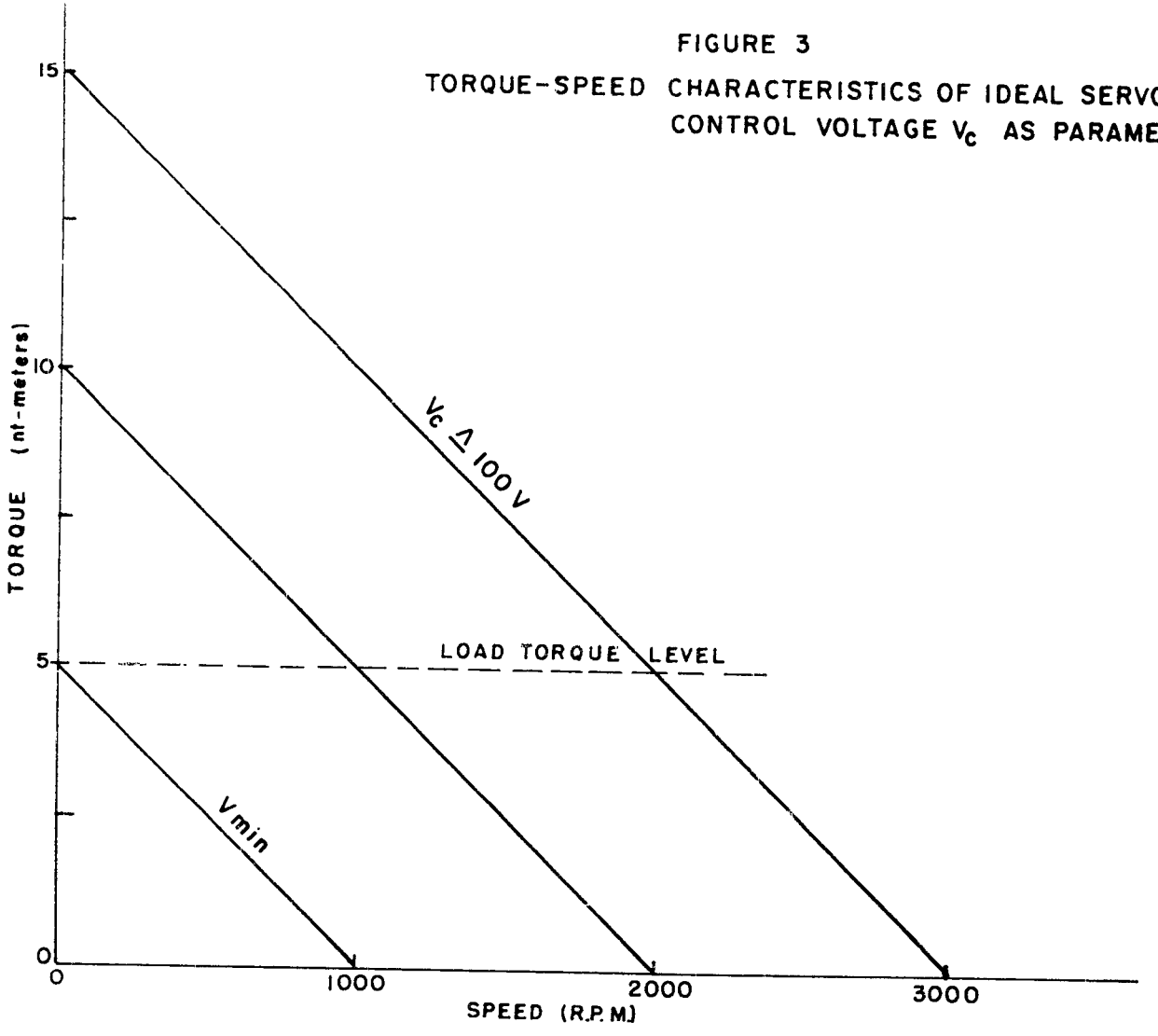


FIGURE 4

DYNAMIC POWER RANGE R VERSES SYSTEM ACCURACY PARAMETER P

for $P_t = 10^{-3}$ WATTS

C = 5 db

+ EXPERIMENTAL POINTS

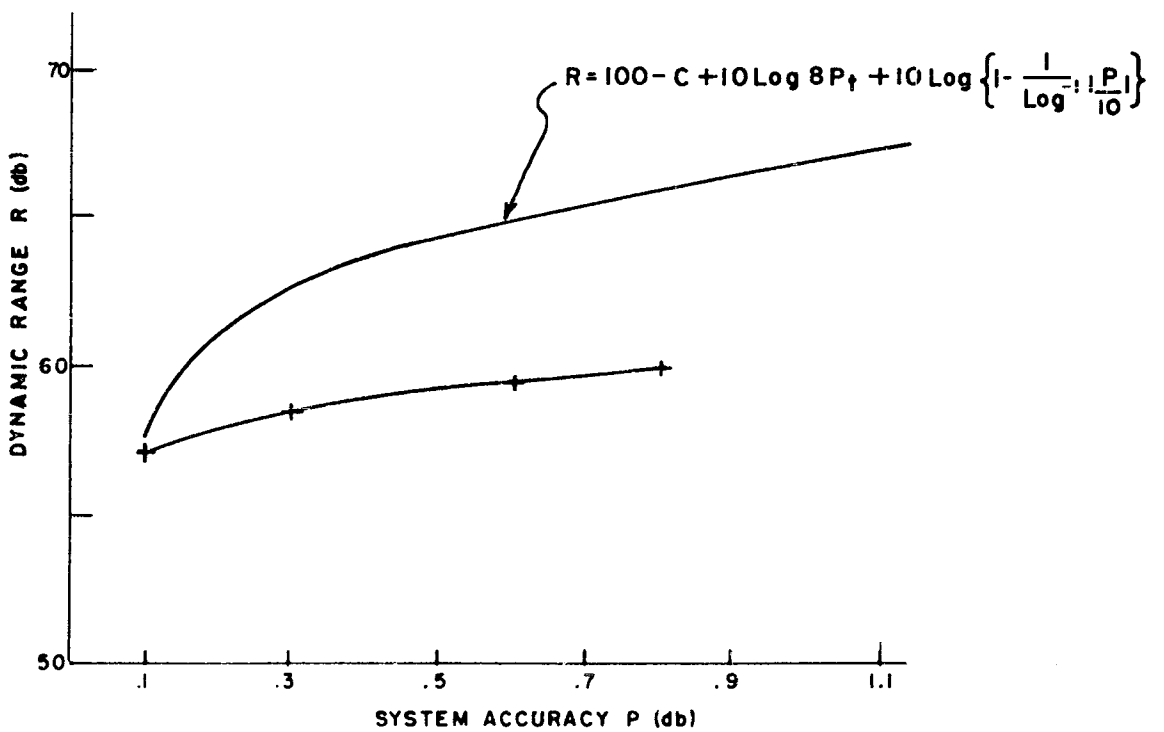




FIG. 5

Transmiter and Attenuator Servo - motor

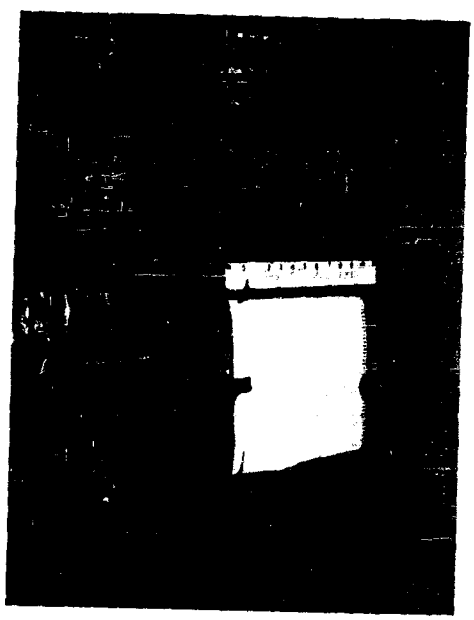


FIG. 6

Millivolt Recorder and Biasing Circuits.

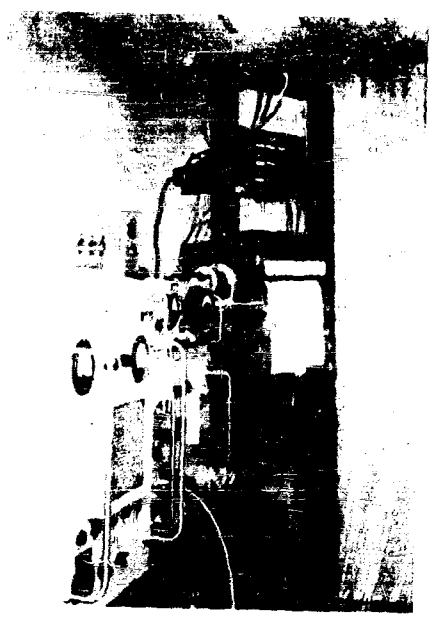
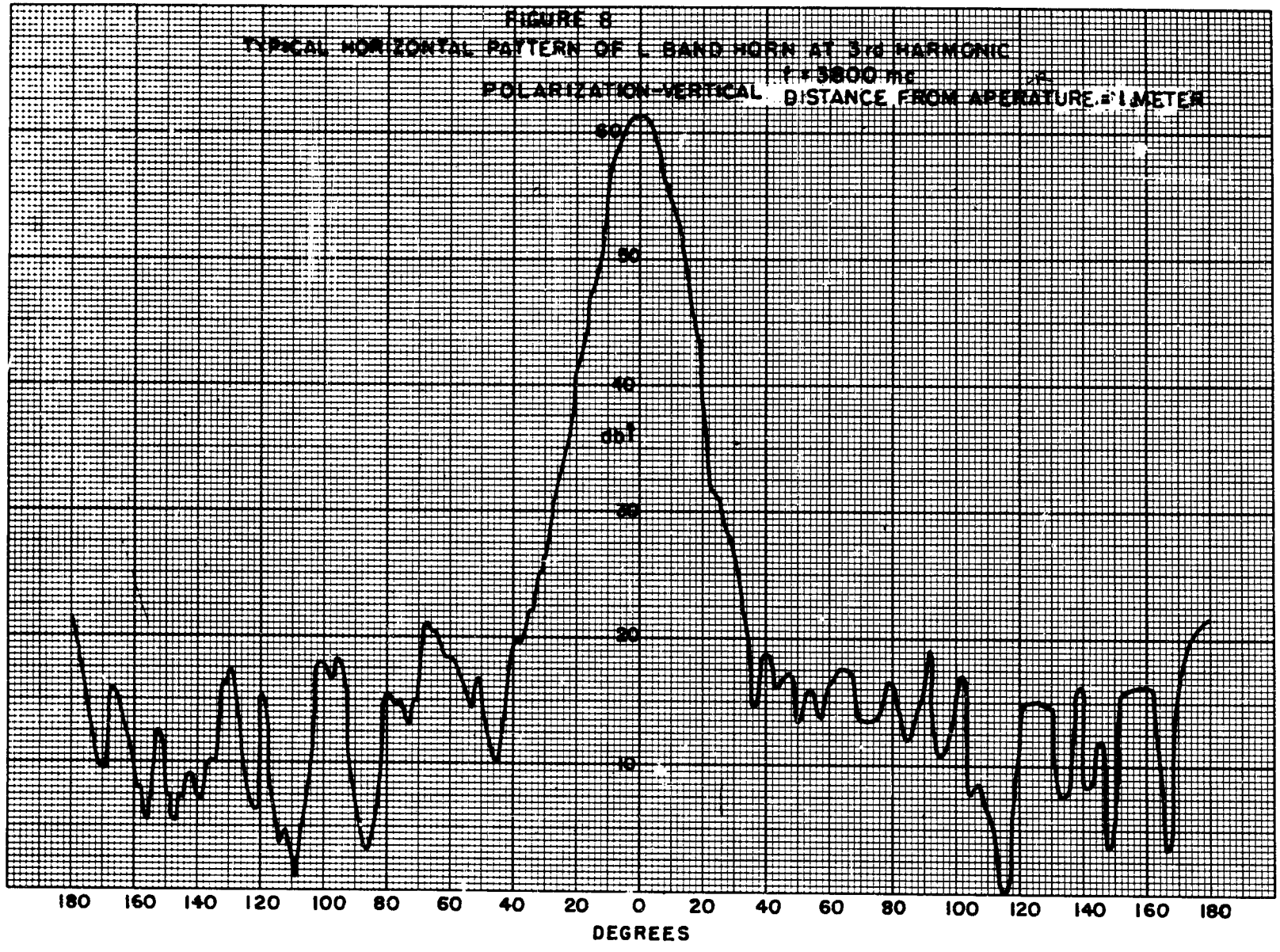


FIG. 7

Super Heterodyne Receiving System and Antenna Pattern Recorder.

FIGURE 8
TYPICAL HORIZONTAL PATTERN OF L BAND HORN AT 3rd HARMONIC
f = 3800 mc
POLARIZATION-VERTICAL DISTANCE FROM APERATURE = 1 METER



# THE VOICE INTERFERENCE ANALYSIS SET, AN INSTRUMENT FOR EVALUATING THE PERFORMANCE OF A VOICE COMMUNICATION CHANNEL

W. M. Grim, Jr.
General Electronic Laboratories, Inc.
Cambridge, Massachusetts

Abstract. - The Voice Interference Analysis Set rapidly and accurately analyzes the performance of a voice communication channel in the presence of interference. The analysis is computed on the basis of a 14-band Articulation Index calculation as developed by French and Steinberg. A modulated pilot tone, which replaces the usual speech signal, is transmitted over the link under test. At the receiver, the tone is used to normalize the interference so that noise-to-signal ratio measurements can be made in each of the bands. The individual channel outputs are then properly combined to produce the final output.

Analog and coded digital outputs are provided in addition to a front panel indication.

In addition to simple cases of white and shaped noise, the system can evaluate, individually and in combination, complicated cases involving reduced transmission-path bandwidth, peak clipping at the transmitter, narrow band interference, and interrupted interference.

Self check features and malfunction alarms are included for monitoring the performance of the system.

## I. INTRODUCTION

The Voice Interference Analysis Set is a system designed to analyze rapidly the performance of a voice communication channel in the presence of external and system noise. The analysis is made on the output of the channel and the results are presented in terms which can be readily interpreted in terms of word score.

A system type test is desirable because it is a complete voice communication system which is under test. All components should be tested under conditions simulating, as closely as possible, the normal operating conditions of the system. Because the talker and the listener are also parts of the system, their characteristics must be considered in any test of the complete system in order to obtain valid results. Tests measuring the detailed electrical characteristics of a receiver alone are desirable, but in themselves do not indicate how the system will perform for speech transmission under actual conditions.

A simple method of evaluating system performance is to measure signal-to-noise ratio at the output of the receiver. However, when an attempt is made to convert this measurement to Articulation Index (AI), a standard

system-performance parameter, gross errors can arise in the conversion. Fig. 1 shows the range of AI possible for different forms of interfering signal as a function of output signal-to-noise ratio.

The standard method of measuring system performance is the listener test in which a number of people listen through the system to a list of words read by a talker. Systems are then scored by the percentage of words correctly understood. Such tests usually require a trained crew of at least ten people and approximately 15 minutes is required for each test. Thus, the listener test is not satisfactory where large amounts of data must be gathered in short periods of time.

A relatively recent theory of speech intelligibility indicates that the information lies in the syllable envelope pattern rather than in the fine details of the speech waveform. This theory was based on the fact that trained operators can "read" speech spectrograms, and "write" words which, when played back properly, can be understood. Practical machines[1] operating on this Pattern Correspondence principle have been designed and built at General Electronic Laboratories. Unfortunately, such a machine requires a "clean-line" sample of the speech waveform in close time correspondence with the sample used to modulate the transmitter.

The Voice Interference Analysis Set (VIAS) described in this paper was designed to provide a method for system testing which had none of the disadvantages of either the listener test, the Pattern Correspondence machine, or the signal-to-noise ratio measurement method. The system is capable of making a complete measurement in 30 seconds. It was designed by General Electronic Laboratories, Inc. specifically for use in the Electromagnetic Environmental Test Facility being developed for the U. S. Army Signal Corps by Pan American World Airways, Inc. and Bell Aerosystems Corp.

Although developed for the specific purpose mentioned above, the equipment is sufficiently versatile to be used directly, or with minor modification, in any situation where system degradation due to interference must be rapidly and accurately evaluated in accordance with psychoacoustic principles.

## II. BASIC OPERATING PRINCIPLES

The VIAS is essentially an analog computer, designed to instrument the AI method of performance calculation originated by French and Steinberg[2] and modified by Beranek[3]. In this method of computation, the speech frequencies between 200 and 6100 cycles are divided into a number of equally contributing bands, usually 20. The signal-to-noise (S/N) ratio in each band is determined and expressed logarithmically on a scale where unity or fully contributing corresponds to a S/N ratio of plus 18 db and zero or non-contributing corresponds to an S/N ratio of minus 12 db. Ratios above or below these values are rated as unity or zero respectively. These individual channel contributions are summed and divided by the number of channels used. The result is the AI for the system. Curves for converting the calculated AI to word score for different vocabularies appear in the literature.[4]

No speech is actually transmitted in this machine. A modulated pilot tone, located near the peak of the normal speech spectrum, is used to provide a reference level. Because the speech spectrum shape is known, the levels of speech can be directly inferred from the reference tone for the machine calculation of S/N ratio.

As originally developed, the AI calculation was valid for only steady-state wide-band noise. Subsequent modifications by Kryter[5] extend the calculation for cases where peak clipping exists at the transmitter, for narrow band interference, and for interrupted types of interference.

## III. PHYSICAL DESCRIPTION

The complete VIAS consists of three major components: the Analyzer, the Test Signal Generator, and the Self Check Signal Generator. The Analyzer is housed in a standard 77" high cabinet. The remaining units occupy 24-1/4" and 15-3/4" of panel space in a standard 19" relay rack.

The entire set contains 127 vacuum tubes exclusive of power supplies and requires approximately 2 kilowatts from a 115-volt, 60 cps, single-phase line, for operation.

Pictures of the units are shown in Fig. 2.

## IV. SYSTEM OPERATION

A block diagram of the VIAS is shown in Fig. 3 together with the transmitter and receiver portions of the voice communication channel under test. Subsequent sections of this paper refer to this figure.

In operation, a tone generator supplies a 950-cycle tone triangularly modulated at a 5-cps rate for modulation of the transmitter. The average output level corresponds to the average power of speech. The modulation simulates the time-varying power characteristics of the speech waveform.

The output voltage of the receiver under test includes the components near 950 cycles representing the speech output and, in general, noise components related to the interference. The transducer response network shown in Fig. 3 passes for further processing only those components which correspond to the acoustic output of the transducer used with the system.

A filter separates the 950 cycle tone components from the noise components. The tone is detected to provide a slowly varying direct current for controlling the gain of the log amplifier. The log amplifier is a high-gain operational amplifier with a logarithmic diode in the feedback path so that its closed-loop gain for the noise components fed to it is inversely proportional to the magnitude of this direct current. Thus, the output of the log amplifier is a noise whose amplitude is proportional to the input noise-to-signal ratio.

For convenience in the instrumentation, two shaping networks are included in this portion of the system to weight the frequency distribution of the noise in a manner inversely proportional to the normal speech spectrum. Thus, the noise spectrum level at any frequency at this point in the system is made to be proportional to the noise-to-speech ratio at the same frequency at the input to the system.

As required by the French and Steinberg computation method, the noise is separated into bands for analysis. Fourteen are used in this machine. The bandwidth for each filter is selected to provide equal contribution to AI for each band. The gain through the filter and its associated amplifier is adjusted so that the noise output is proportional to the noise-to-speech ratio in the band with the same proportionality constant for each channel.

Because the machine actually measures noise voltages corresponding to noise-to-speech ratio, it is convenient for the remainder of this discussion to think of the machine as measuring degradation of AI, (1 - AI), rather than AI directly.

The output of each channel is detected to provide a direct voltage proportional to the noise. A limiter at the detector output limits the voltage to the 30-db range with limits corresponding to zero and fully contributing channels. Such limiting is necessary to prevent an extremely noisy channel from producing more than its permissible amount of degradation and to prevent an extremely quiet channel from cancelling out the degrading effects of noise in other channels. Such limiting is required by the AI calculation technique.

The limited output of each channel is logarithmically weighted and combined in a summing network. The output of the summing network is integrated for approximately seventeen seconds to provide an analog output indication. This particular output is in terms of degradation, "0" representing a quiet system. A simple stepping-switch analog-to-digital converter provides a 12-wire, 20-state output code for driving punch card or other data recording machines as well as a 10-state front-panel indication.

In addition to performing an AI calculation on broadband noise, the machine will evaluate narrow-band and interrupted interference and the beneficial and detrimental effects of peak clipping at the transmitter end, as well as combinations of these effects. The methods by which a machine evaluates these conditions is outlined in the subsequent paragraphs.

A modification of the AI calculation to account for the effects of narrow band interference, the so-called spread-of-masking correction, states that interference in any band actually affects all other bands to a degree dependent on both the separation between the analysis band in question and the frequency of the interference and on the frequency of the interference itself.

The machine evaluates this effect, in the case of the upward spread of masking, by connecting the input of each channel detector to all of the lower frequency channels through a network with the proper attenuation value. There is no correction for a less well-established effect, downward spread-of-masking, in this machine. This correction, although minor, could be included by a similar network.

It is well known that peak clipping of a voice signal at the transmitter will result in improved performance in the presence of interference, primarily because the average side-band power can be increased.[6] This equipment reproduces this effect. As mentioned previously the modulated signal for the transmitter is a modulated tone designed to simulate the

average level of speech. If peak clipping is incorporated in the transmitter, a normal adjustment of the tone input will result in an increased transmitter output at 950 cycles. Because this will now result in an enhanced receiver tone output, the gain for noise as determined by the log amplifier will be reduced. Thus, detected output voltages and the corresponding degradation will be reduced. AI as indicated by the digital output will be correspondingly increased. In contrast to the enhancement in the presence of noise, peak clipping causes a reduction in intelligibility when no interference is present. The machine is designed to make an appropriate correction for this effect.

A study of the Kryter[5] procedure for calculating the effects of interrupted noise on AI indicates that for higher interruption rates the results are dependent only on the duty cycle of the noise. Corrections in this region are obtained by taking advantage of the fact that the channel filters essentially average the noise of higher rates. By selecting a detector form whose response is proportional to the average output, the correction is arrived at without further circuitry.

Correction at low interruption rates is obtained by designing the detectors to follow the envelope of the interrupted interference. However, because of the statistical nature of the noise, considerable filtering is demanded in the detector and so this design goal has been somewhat compromised.

The basic AI concept implies that channels which have no information (speech) have no contribution to index. The machine is thus provided with contribution switches for ten of the end channels. These switches have three positions: full, half, and zero contributing. The system is arranged so that when a channel is zero contributing, the AI is reduced by an amount equivalent to full error in the channel and the channel is prevented from producing further reduction even if noise is present. When the switch is in the half-contributing position, the AI is reduced by half of the maximum single channel reduction and the reduction due to noise is limited to an additional half channel. Information for determining the setting of these switches must be obtained by a normal frequency response check on the complete system including the input and output transducers.

The logic and timing circuit consists of accurate timer to set the integration period as well as the relay logic necessary to accept input control pulses, $T_0$, $T_1$, and $T_2$, and perform all the internal switching necessary for a measurement. Examples of internal switching functions are: reset commands for the timer, stepping switch, and integrator; removal of response corrections during a check cycle; alarm indication; and timer initiate pulses.

## V. MONITORING PROVISIONS

Self Check provisions for periodic calibration are provided in order to provide a quick check of the performance of the machine. A Self Check Signal Generator consisting of a source of 950 cycle tone and a source of noise shaped to have the spectral distribution similar to that of speech is

provided as a piece of auxiliary equipment. By means of internal feedback and built-in attenuators, signals of various, accurately known, signal-to-noise ratios are conveniently available. In normal system operation, a Self Check Signal Generator is permanently wired to the analyzer but not electrically connected.

When a check cycle is initiated by means of a button on the Analyzer, the input is automatically transferred from the system being tested to the output of the Self Check Signal Generator, and all corrections for system frequency response are removed. The Analyzer then performs a normal analysis on the test signal. If the error in output is more than 5%, an alarm indication is provided.

For greater reliability, the output of the Test Signal Generator is continuously monitored.

The input line to the Analyzer is continuously monitored to provide an alarm in the event of a receiver or transmission line failure resulting in no pilot tone and no noise input.

## VI. SYSTEM PERFORMANCE

When analyzing interference consisting of white noise or speech-shaped noise, a properly adjusted system will provide answers within 2% of the theoretical results under laboratory conditions. Variations of up to 5% may be expected under field conditions. A typical curve for white noise is shown in Fig. 4.

The result for cases in which peak clipping exists at the transmitter show up to 7% error in the laboratory; deviations of up to 10% may be expected in the field. A typical curve showing performance in the presence of peak clipping is shown in Fig. 5.

The results for cases of broadband interrupted interference are not as accurate as those mentioned above; errors up to 30% have been recorded for low duty cycle (20%) medium rate (100 IPS) interruptions. For all other curves tested (all combinations of 10, 100, 1000 interruptions per second and 20%, 40%, 70% duty cycle) the deviations from published data[7] were typically less than 15% of AI.

## VII. CONCLUSIONS

The Analysis Set described in this paper should be a great aid in making interference measurements when the results are desired in psychoacoustic terms. Although designed specifically for use in the Electromagnetic Environmental Test Facility, the equipment is capable of operating in any situation where rapid and accurate determination of the effects of noise on the performance of a voice communication link is desired.

## ACKNOWLEDGEMENTS

This equipment was designed and built under Bell Aerosystems Corp. Sub-contract No. 4102.

The author wishes to thank L. S. Billig, P. C. Hayden and E. L. Maddox of General Electronic Laboratories, Inc., whose advice, encouragement, and hard work contributed materially to the success of this project.

## REFERENCES

1. H. Schwarzlander, "Intelligibility Evaluation of Voice Communications," Electronics, vol. 32, p. 88-91; May 1959.

2. N. R. French and J. C. Steinberg, "Factors Governing the Intelligibility of Speech Sounds," Journal of the Acoustical Society of America, vol. 19, p. 90-119; 1949. Bell Telephone System Technical Publication, Monograph B-1436, 1947.

3. L. L. Beranek, "The Design of Speech Communication Systems," Proceedings of the Institute of Radio Engineers, vol. 35, p. 880-890; 1947.

4. K. D. Kryter, "The Effects of Noise on Man," The Journal of Speech and Hearing Disorders, Monograph Supplement #1, p. 57-89; September 1950.

5. "Proposed American Standard Method for the Calculation of the Articulation Index," American Standards Association Sub-committee S3-W36, K. D. Kryter, Chairman; first draft July 1960, second draft October 1961. Second draft published as "Technical Report 61-28," Air Force Electronic Systems Division, Operational Applications Office, L. G. Hanscom Field, Bedford, Mass.

6. W. Wathen-Dunn and D. W. Lipke, "On the Power Gained by Clipping Speech," Journal of the Acoustical Society of America, vol. 30, p. 36-40; 1958.

7. G. A. Miller and J. C. R. Licklider, "The Intelligibility of Interrupted Speech," Journal of the Acoustical Society of America, vol. 22, p. 167-173; 1950.

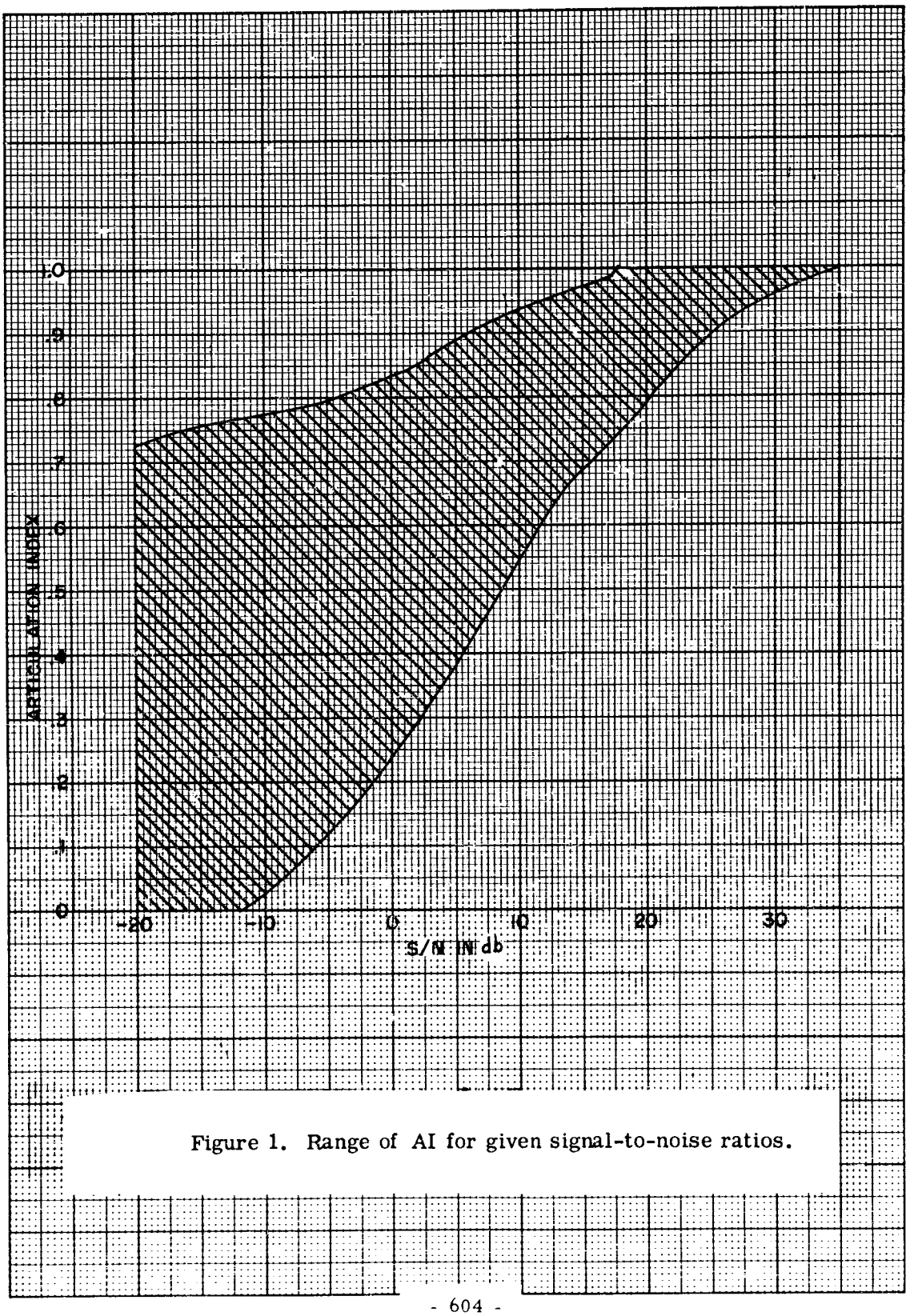



Figure 1. Range of AI for given signal-to-noise ratios.

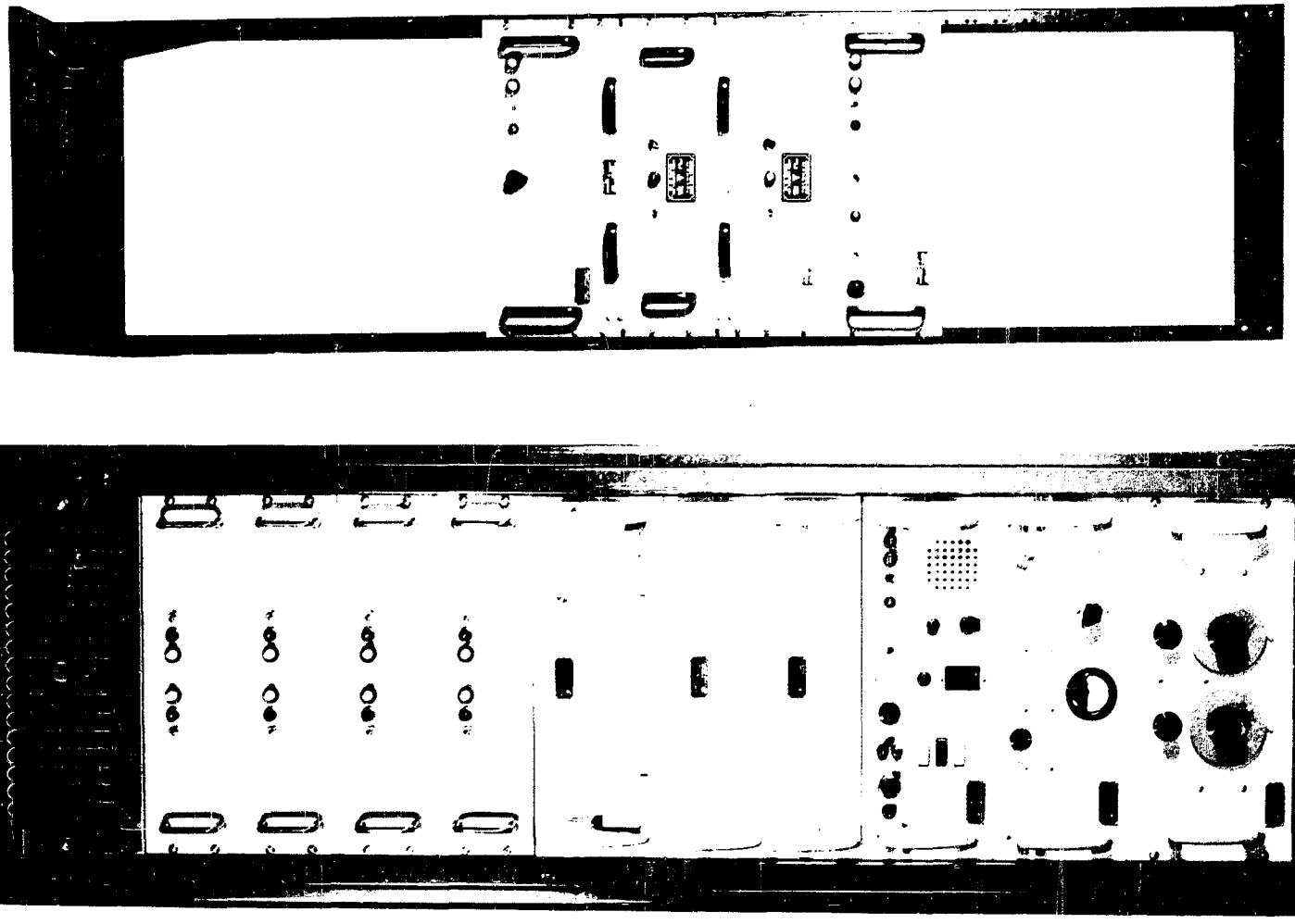


Fig. 2 Units of the Voice Interference Analysis Set.

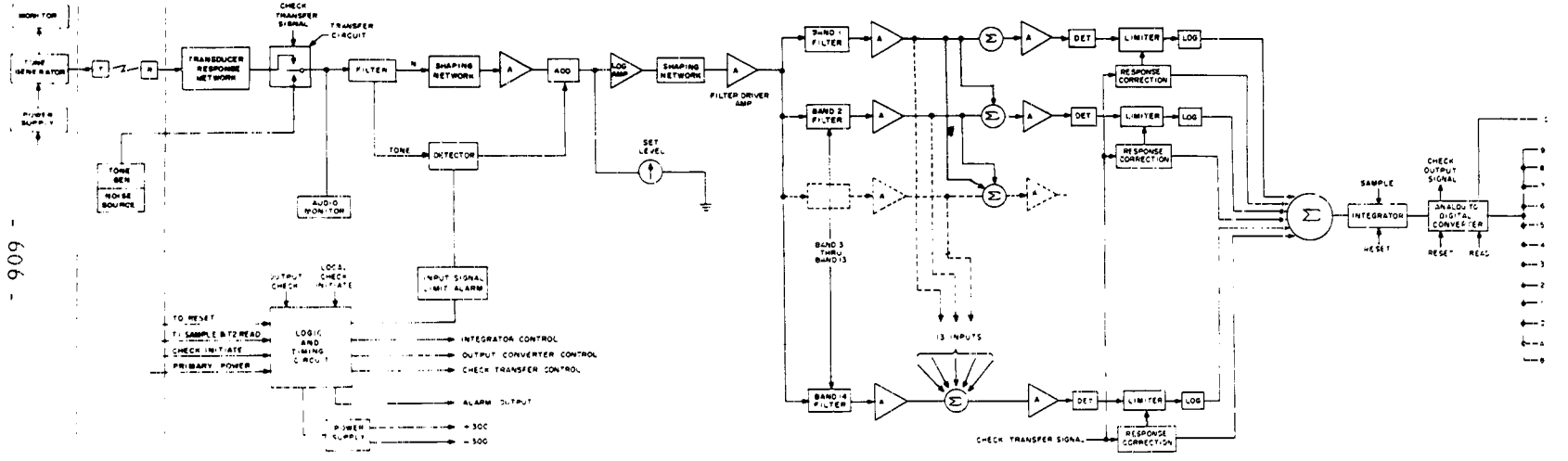



Fig. 3 Block diagram of the VIAS.

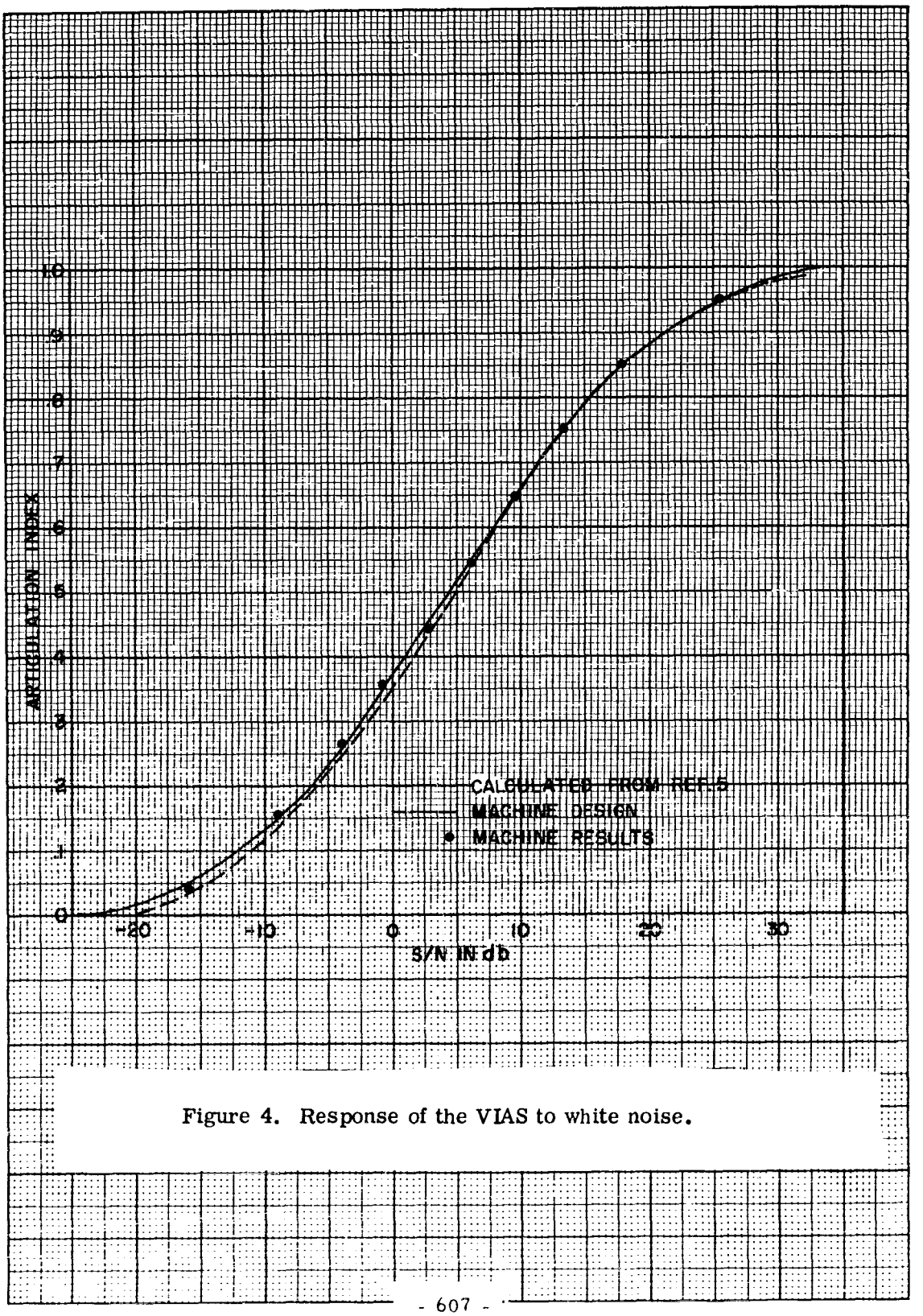



Figure 4. Response of the VIAS to white noise.

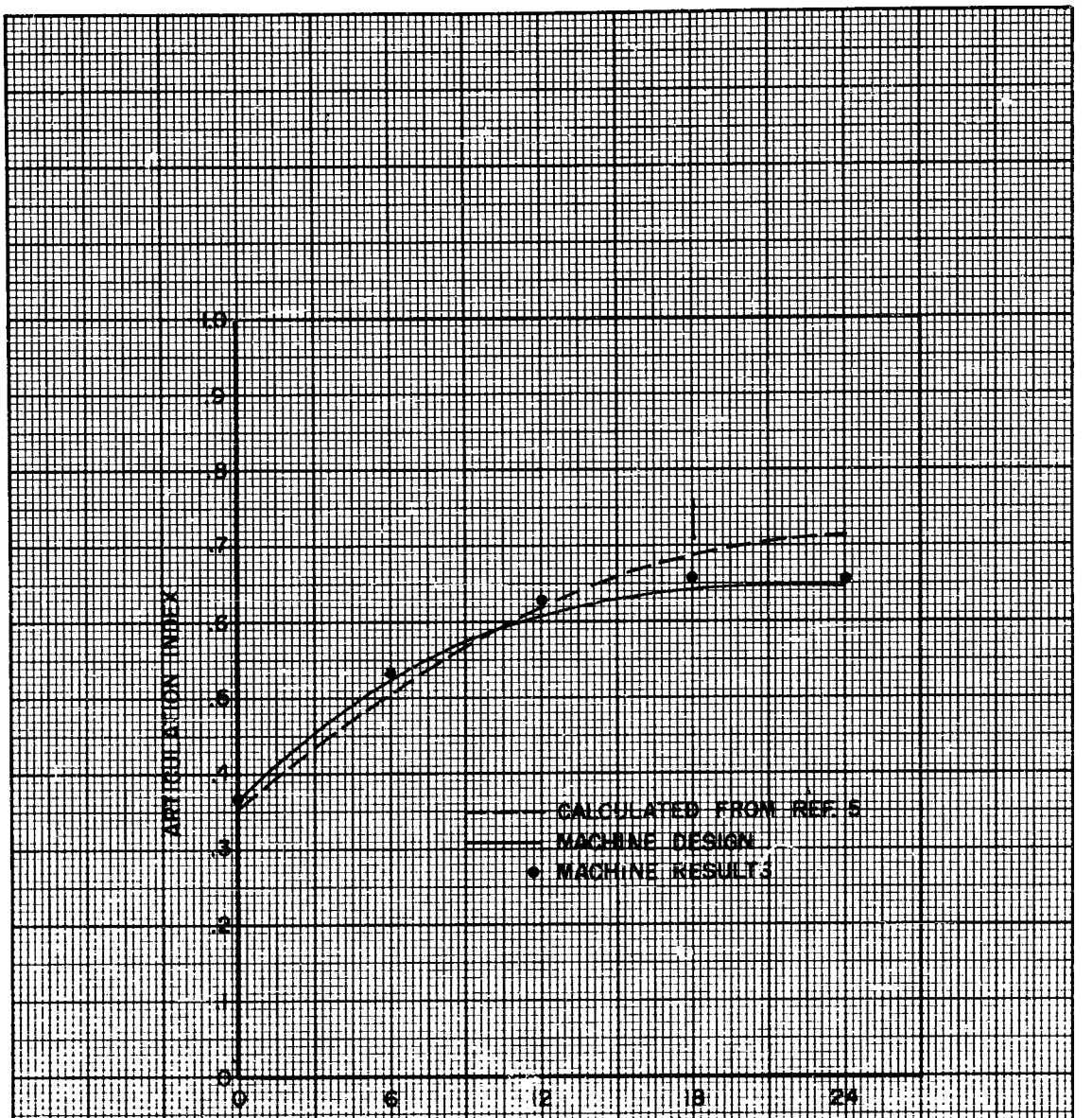



Figure 5. Response of the VIAS for peak-clipped signals.

# ELECTROMAGNETIC COMPATIBILITY IN MICROMINIATURIZATION

J. W. Hohmann and J. D. Meindl
U. S. Army Signal Research and Development Laboratory
Fort Monmouth, N. J.

Abstract. - This paper discusses the present trends in microelectronics and the anticipated rf interference problems. The various miniaturization techniques and the state of the art are outlined.

## I. INTRODUCTION

Today much money and effort are being expended in the general field of microelectronics. Virtually every large electronics firm has committed itself to at least an exploratory program in this area. There is no reason to think that this effort will decrease in the near future; however, there is a wide range of opinions as to how far and how fast miniaturization will be carried. Rather fantastic packing densities have been forecast which at present are completely unrealistic because of power dissipation limitations. The levels of miniaturization discussed in this paper are those which are presently feasible and which are just beginning to appear on the market.

Except for a few limited cases, little has been done to determine the electromagnetic compatibility of these miniature circuits. This is the case for a variety of reasons, one being that the small size inherently reduces many coupling problems. Perhaps even more important, very few subsystems, let alone systems, have actually been constructed from miniaturized circuits; therefore, it has not been necessary to consider the radio-frequency interference problems very thoroughly. This situation, however, is rapidly changing and within one to two years, many electronic equipments will be thoroughly studied to determine the feasibility of complete or partial miniaturization. At that time a substantial electromagnetic compatibility study will be required.

Basically, there are two interference problems: One concerns the undesired coupling between the microcircuits, and the other the interference that originates external to them. Customarily, the interference radiated from an equipment itself must be considered, but microminiaturized equipment will operate at such low power levels that the radiated energy will be negligible in practically all cases. The most typical problem will be the situation in which only part of a system is miniaturized. The engineer responsible for radio-frequency interference will have to determine if the remaining unminiaturized components will adversely affect the operation of the miniaturized section. This would be difficult without an understanding of the general miniaturization techniques. A detailed knowledge of fabrication techniques is unnecessary; however, the engineer should be familiar with the different types of miniature resistors and capacitors available.

## II. BASIC COMPONENTS

There are three typical resistors, two of which are shown in Fig. 1. In solid silicon circuits the bulk resistor is simply a bar of semiconductor

with ohmic contacts on both ends. This type of resistor is limited to relatively low values for various reasons. For example, if the bar is too thin or too narrow, its lack of physical strength makes it difficult to handle. The second silicon type, the diffused-layer resistor, is shown in (B) and (C) of Fig. 1. A thin layer of p-type material is formed in the n-type bar. When reversed biased, the p-n junction isolates the diffused layer from the rest of the bar. Since the diffused region can be very narrow and thin, the value of this resistor can be much higher than the bulk resistor. In reference to Fig. 1, (C) is a modified version of (B). The third type of miniature resistor is the thin-film-deposited resistor. In this method a resistive material is deposited on an insulating substrate. The resistive material may be chosen from a wide range of materials varying from common nichrome to little-known alloys. Here again the deposited layer may be quite small in cross section, thereby facilitating the production of high resistances.

There are two basic types of capacitors: thin film and p-n junction. The thin-film capacitor is composed of two conducting layers with a film of dielectric in-between. One common configuration is successive layers of silicon, silicon oxide, and a deposited metal. Another type of thin-film capacitor consists of successive layers of deposited metal, insulator, and another layer of deposited metal. Ordinarily the upper limit on these capacitors will be in the 0.005 microfarad range. The other typical capacitor is a p-n junction type. Basically the p-n junction operates as a diode; however, if the junction is reverse biased, it can be utilized as a capacitive element. The maximum capacitance that can be produced in this manner is several thousand picofarads.

One very promising aspect of the above circuit elements is the ease with which they may be combined to form distributed RC networks, as shown in Fig. 2. In this case the diffused layer has a relatively high conductivity. The p-n junction supplies the capacitance, and the bulk material functions as the resistance. There are numerous contact arrangements for this simple configuration that can be used to obtain a variety of electrical characteristics from the structure. For instance, there could have been only one contact on the bottom instead of two. This one contact could have been in the middle, at either end, or anywhere in-between. There could have been three contacts on the bottom instead of two. These variations are almost unlimited and each one has different characteristics.

There have been several attempts to produce miniature inductors, the best of which has been only moderately successful. Since no one has introduced a really satisfactory means of producing miniature inductors, a circuit to be miniaturized ordinarily should be completely redesigned to avoid the use of inductances. This, of course, is not always possible, but a significant reduction in the number of inductors used in typical circuits may be expected.

In many instances, the relative ratios of active to passive components can be expected to change sharply when the circuits are miniaturized. In the past, economics has demanded that the number of active components be held to a minimum because of the low relative cost of high-grade resistors and capacitors. Particularly in a miniaturized solid silicon circuit, a diode or transistor will often be cheaper to make than a resistor or capacitor. Therefore, the percentage of active components can be expected to increase by

a factor of two or three.

Actually there are three basic approaches used to form miniature circuits: the discrete component, the multilayer thin-film, and the semiconductor solid-circuit approaches. These are in the development phase, and some hardware representing each of them is in pilot-line production.

## III. DISCRETE COMPONENT CIRCUIT

In the discrete component approach, each component is produced separately and miniaturized individually. One program of this type that has received considerable attention is the micromodule system proposed by the Signal Corps. In this concept each component is placed on an individual ceramic wafer and then several wafers are stacked to form a module, as shown in Fig. 3. On each wafer which is standard size 0.31 X 0.31 X 0.01 inches, the connections are brought out to the notches. Twelve riser wires placed in the notches are used to connect the components to form the desired circuit. After the proper connections are made by soldering, the whole unit is encapsulated in epoxy for protection. The finished module may be plugged into a printed circuit board in the same way as for a transistor. The height of a module depends upon the number and type of components needed.

At present, two pieces of equipment--the Helmet Radio and the Micropac Computer--are being fabricated from micromodules. The Helmet Radio, designed for use at the infantry squad level, is in the prototype stage. The Micropac Computer (Fig. 4) is completely compatible with the Army Field Data System and can replace a much bulkier computer having the same capacity. It has a volume of 3 cu. ft. and weighs 100 lbs. Its memory of magnetic cores has a capacity of 2000 words and it can be increased to 4000 or 6000 words. The whole unit has a power requirement of 1500 w. A prototype model will be completed by September 1962. At this stage of development, the radio-frequency interference problems in the Helmet Radio have not received very much attention. It appeared that the i.f. stages in the radio might cause some difficulty; therefore, a metal can was placed around each i.f. module as a shield. In the prototype models, this arrangement has been perfectly satisfactory. The computer has not been subjected to externally produced rf interference tests such as those described by Harder and Powers of IBM,[1] and there are no plans to conduct these tests. Individual subsystems, however, have been examined analytically, and no difficulties were foreseen under normal operating conditions.

To present a more precise idea of the interference problem, let us consider a module containing one digital circuit. If the module is 4/10-inch high, the largest loop that could be coupled to outside magnetic interference is 0.124 sq. in. To produce an erroneous signal, the induced voltage would have to be at least 100 mv. This means that to cause an error, the external interference would have to exceed a dB/dt of 0.12 gauss/sec. These figures are based on causing an error in a digital circuit completely contained in one module. Of course the loops formed on the printed circuit board that holds the modules could be several times larger. Good design dictates that these loops should be less susceptible to interference than the ones contained completely within a module.

Another discrete component approach, which is receiving attention, involves placing a complete circuit inside conventional transistor cans such as

the TO-5 or TO-18. Very-small components are individually bonded to a single substrate or header. Fine gold wires are used to interconnect the components, and then the can is sealed by welding. The finished package is very similar to the standard transistor can, except that it has eight to twelve leads instead of three. This type of unit is now for sale by several firms and may soon be appearing in equipment.

Placing the circuit in such a small volume makes it unlikely that an erroneous signal could be induced in one of the internal loops in the circuit. It is doubtful that the largest loop in this can has an area exceeding 0.002 sq. in. These circuits, however, must be interconnected by printed circuit boards or by some similar technique, thereby producing somewhat larger loops for flux linkage.

## IV. THIN-FILM CIRCUIT

There has been a very substantial effort involved in fabricating all types of components by thin-film techniques. This technique has met with varying degrees of success depending upon the component involved. Resistors and capacitors can be produced accurately and reliably, but inductors, transistors, and diodes have not been successfully produced. Fabrication of multilayer passive structures is very promising. Numerous thin-film resistors and capacitors can be deposited on top of one another to form a complex multilayer structure and insulating layers deposited between the components provide isolation.

Figure 5 represents the 16 layers formed coincident with each other to produce a typical digital circuit. All the necessary interconnections are also supplied by the depositions. The completed structure is only a few mils thick. This particular device was developed under a Signal Corps program. The multilayer structure can be made small enough to be effectively used as a single component in the discrete component circuits described previously. In these multilayer structures, magnetic coupling is not much of a problem but capacitive coupling obviously is. The coupling within a single structure is sufficiently large to require that it be taken into consideration in the initial design. The coupling between adjacent structures can be substantial; therefore, care must be used in the physical layout of the system.

## V. SOLID-STATE INTEGRATED CIRCUIT

The third, and by far the most publicized, microcircuit technique is the semiconductor solid-state integrated circuit. The customary definition of a solid-state integrated circuit requires that all the components of the circuit be located in or on one block of silicon. By a series of diffusions and depositions, the desired components are formed and interconnected. This type of construction is inherently smaller and potentially quite reliable. The increase in reliability is expected due partly to fewer and simpler interconnections. At present, integrated circuits have two serious drawbacks: The circuit elements have loose tolerances because of fabrication limitations, and the production-line yield is low with a corresponding high cost. Fabrication processes, however, are certain to improve and will provide integrated circuits with tremendous potential.

Before any particular integrated circuit is described, a brief explanation of the diffusion process would be helpful. At the present time a large percentage of the available diodes and transistors are made by diffusion--the basic process used to produce integrated circuits. The process begins with a

silicon wafer. First, a layer of silicon oxide is formed by passing steam over the wafer. After the oxide is formed, the surface is coated with photoresist. With a small accurate mask, the appropriate areas are exposed and developed. Afterwards the wafer is rinsed in hydrofluoric acid. The acid does not attack the photoresist but it does remove the oxide where it is exposed. Once the oxide is removed, the wafer can be placed in the diffusion apparatus. The material to be diffused into the silicon wafers is placed in a diffusant boat. As the boat is heated, a vapor is formed that has the proper materials, and the wafer is surrounded by this vapor. The vapor slowly diffuses into the parts of the silicon wafer laid bare by the photoetch and acid bath. This is a relatively slow process usually measured in hours. A diode can be formed by a single diffusion while a transistor requires two separate diffusions--some types of transistors even require three. In general, two or three diffusions are sufficient to produce typical integrated circuits.

Figure 6 is a detailed picture of a typical NOR circuit in integrated form. At the top is the standard circuit drawing. The circuit in the middle, (B), is exactly the same as (A); it is rearranged to simplify the explanation of the bottom circuit. There is one small difference--the individual resistor and capacitor of (A) have been changed to a distributed network in (B). The actual silicon integrated circuit is represented by (C). The large bars are composed of solid silicon and used as bulk resistors. The four round dots to the left are the input diodes, which are formed on the bar by diffusion. A fine gold wire connects each diode to the appropriate input lead. Just to the right of the diodes, the distributed RC network can be seen. The large rectangular raised area is a silicon-oxide layer with a metal electrode on its surface so that the result approximates the distributed network shown in (B). Just to the right of the distributed network, there is a small rectangle. This is an ohmic contact, which means that a small area of conductor is alloyed to the silicon bar to provide a good lead bond at that point. A gold wire runs from this contact to the base of the transistor, as shown in (B). The resistor $R_B$ is the bulk resistance between the ohmic contact and the tab at the bottom labeled (-V). The transistor is located on the shorter bar. It is formed on this bar, and the remaining component, $R_C$, is the bulk resistance between the collector of the transistor and the tab labeled (+V).

Figure 7, another example of an integrated circuit, illustrates the versatility of the technique. The standard circuit diagram is shown in the upper left, and the same circuit redrawn is shown in the lower left. Again the individual resistor and capacitor have been replaced by a distributed network. The model on the upper right shows only the bulk resistors. Below it is the completed circuit, including two transistors, gold wires, and the deposited layers forming the distributed RC network. This circuit is enclosed in a package, 0.250 X 0.125 inches in outside dimensions. As far as interference is concerned, the most critical loop would be the one containing the emitter and base of a transistor. In this circuit, the area of this loop is estimated to be 0.0003 sq. in. Therefore, to induce a signal of 25 mv in this loop would require a dB/dt of 12.9 gauss/sec. As in any other system, these circuits must be interconnected, thus larger, more critical loops almost certainly will be formed. This is unfortunate, but not too serious. The overall size reduction will be such that these unavoidable loops in an integrated circuit system will have perhaps only 1 % of the area of a similar loop in a piece of conventional equipment.

## VI. SPECIAL HIGH-SPEED PROBLEMS

Some very complex radio-frequency interference problems are found in Project "Lightening," a 1000-Mc tunnel diode computer using discrete miniature component circuitry. This extremely high-speed operation with semiconductor devices, plus the reduced size of the equipment, has made the design very difficult. The three main problem areas are due to high-speed operation. Delays due to wire length are significant and require optimum location of components. Signal-waveform distortion is greatly increased. Signal crosstalk becomes sufficiently large to require shielding a large part of the wiring. One type of shielding is accomplished by using a channel wiring assembly whereby the wires already covered by insulation are placed in slots (Fig. 8). Because the surfaces of these slots are metal-plated, the resulting configuration is virtually a coaxial transmission line. The circuits are placed on wafers and then the wafers are placed in the holder as shown. Since this computer is a tunnel-diode device, all components must be held to a tight tolerance, usually 1 %. This requires that the transmission lines and their terminations be laid out very carefully. It is found that a large part of the interference problem is due to common ground return paths. By designing to isolate the ground return paths as completely as possible, the electromagnetic coupling was reduced to an acceptable level, and the desired operating speed was obtained.

## VII. CONCLUSIONS

There are several types of miniaturization not mentioned in this paper, one being the molecular circuit. Its omission is not intended to imply that it is not a promising method, but the ones described are much nearer to the hardware stage. Also, each of the three types of circuits: discrete component, thin-film, and solid circuit, is not exclusive, i.e., these types may be used separately or combined to produce equipment.

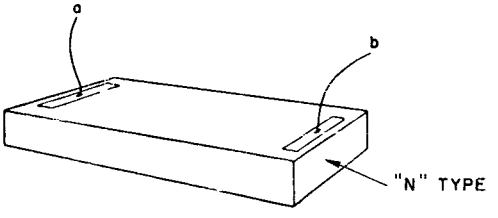
In conclusion, considering interference effects, it can be stated that most miniaturized equipments appear to be less susceptible to external radio-frequency interference than their full-size equivalents. This is basically due to the smaller areas and volumes available for coupling and the relative ease with which smaller volumes can be shielded. Miniaturized circuits, however, will operate at lower power levels and thereby forfeit part of the advantage gained by their small size.

## REFERENCES

1. J. A. Harder and R. L. Powers, "Radio Interference and Susceptibility Study of a Solid-State Digital Computer," Sixth Annual RF Interference Conference.

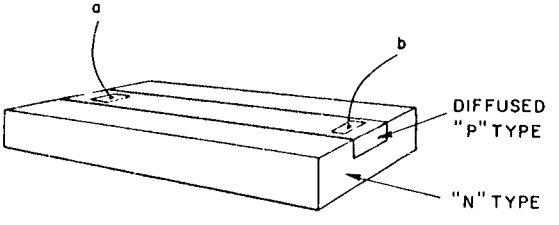
2. J. W. Lathrop, R. E. Lee, and H. Phipps, "Semiconductor Networks for Microelectronics," Electronics; May 1960.

3. E. Luedicke and A. H. Medwin, "Microsystem Computer Techniques," Radio Corporation of America.



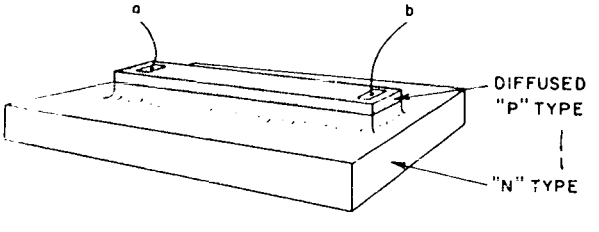

Bulk Semiconductor Resistor

(A)



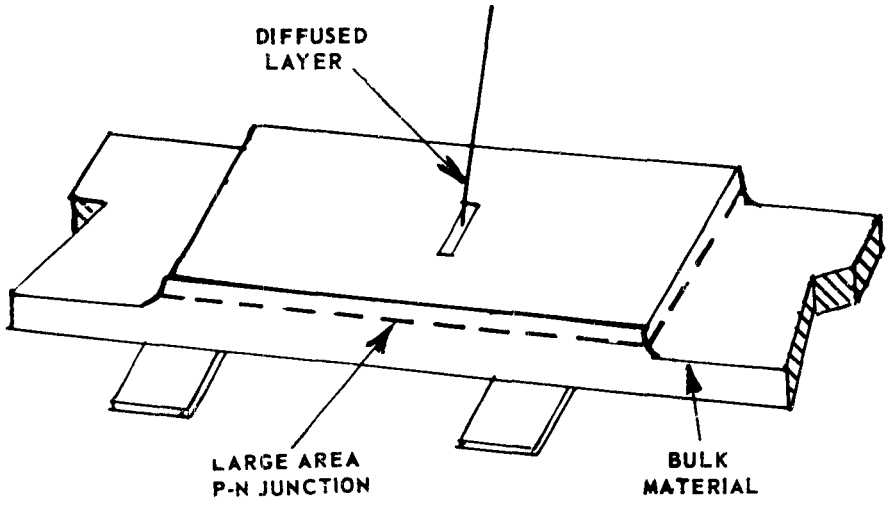

Diffused-Layer Resistor

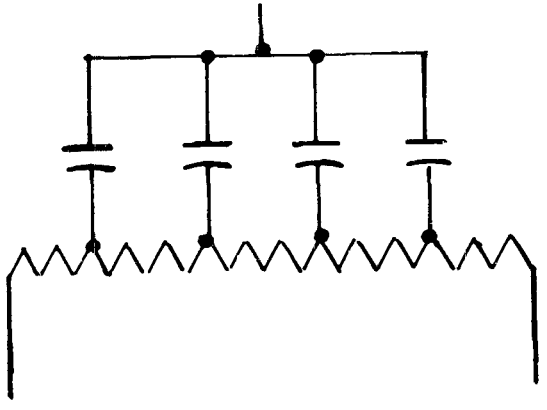
(B)



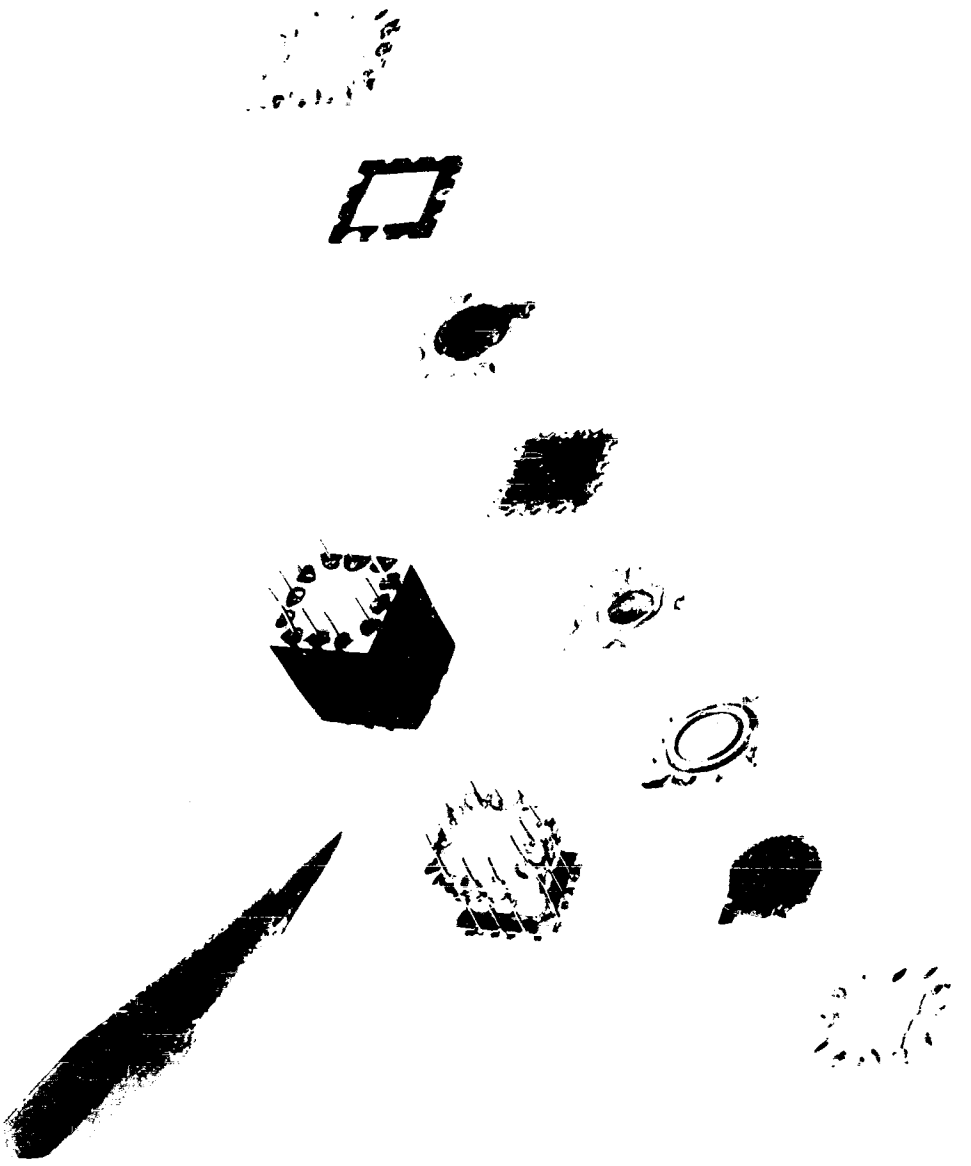

Mesa-Etched Diffused Resistor

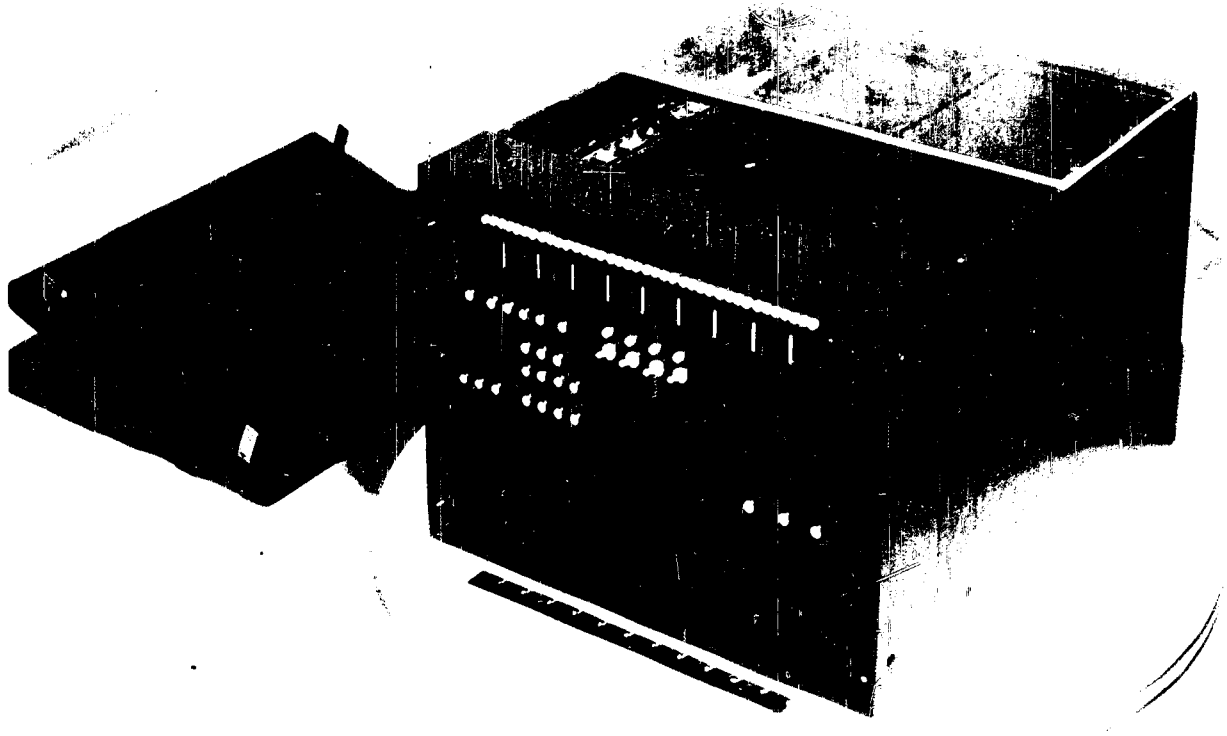
(C)



SEMICONDUCTOR DISTRIBUTED-CONSTANT
R-C NETWORK WITH ITS EQUIVALENT CIRCUIT

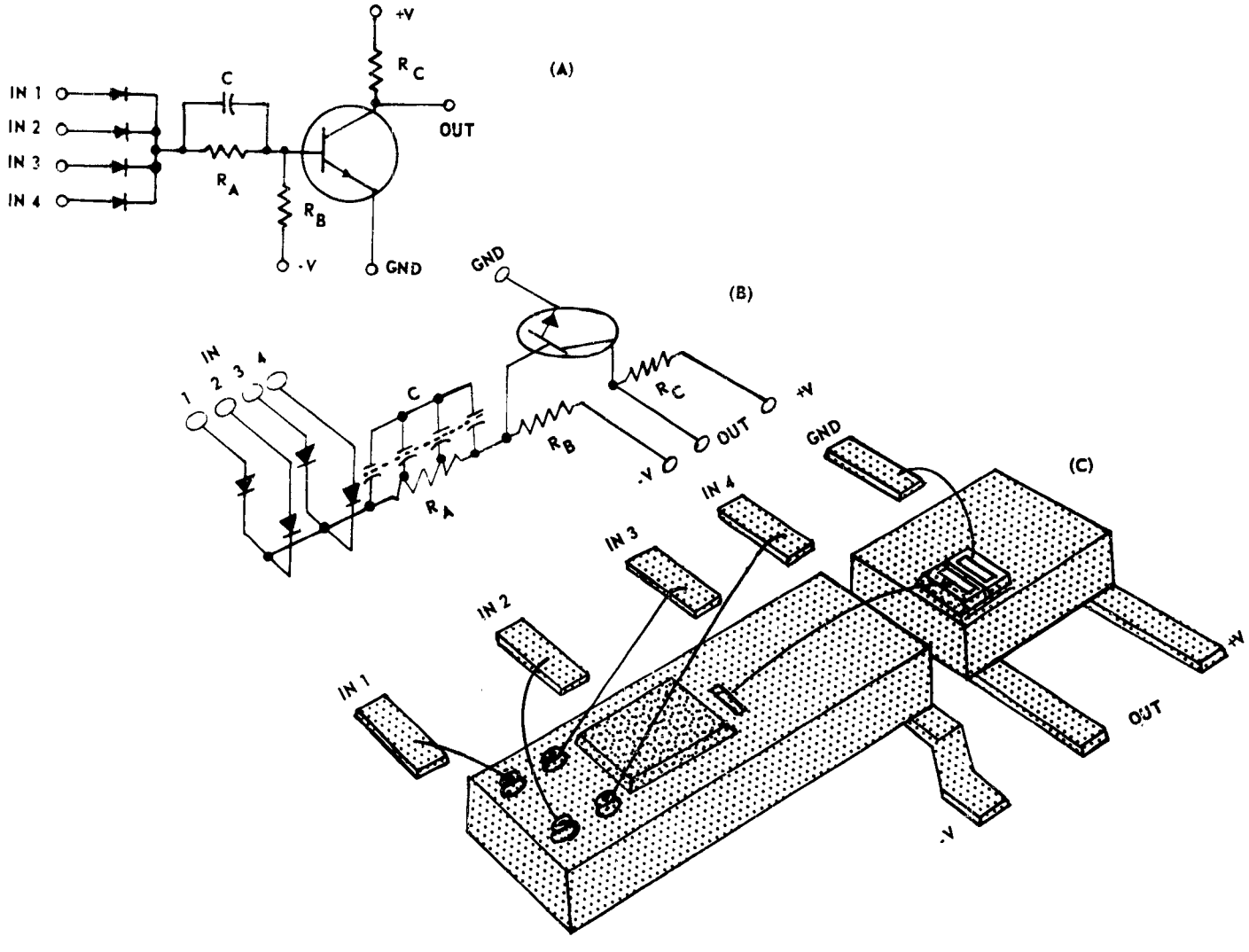


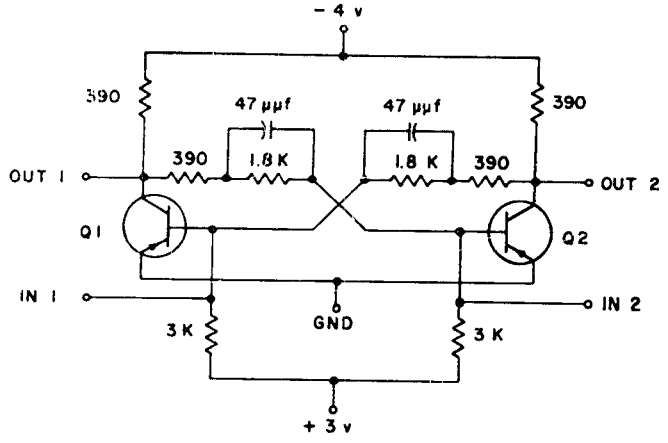


MM MICROPAC COMPUTER

M-60-1306

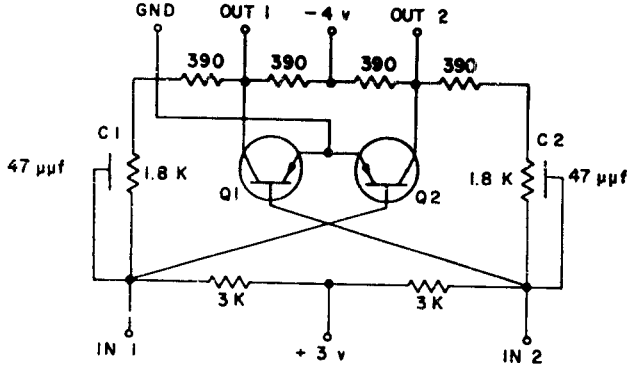
IBM


(A)
+V
$R_C$
C
IN 1
IN 2
IN 3
IN 4
OUT
$R_A$
$R_B$
-V
GND
(B)
GND
IN
1
2
3
4
C
$R_C$
+V
OUT
$R_B$
-V
$R_A$
(C)
GND
IN 4
IN 3
IN 2
IN 1
+V
OUT
-V

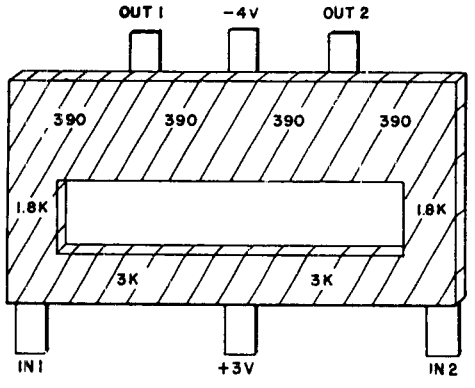



(A)

Bistable Multivibrator

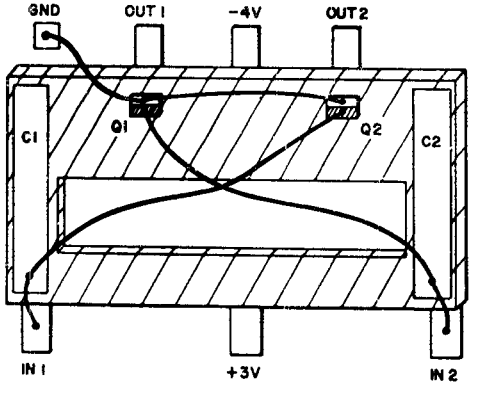



(B)



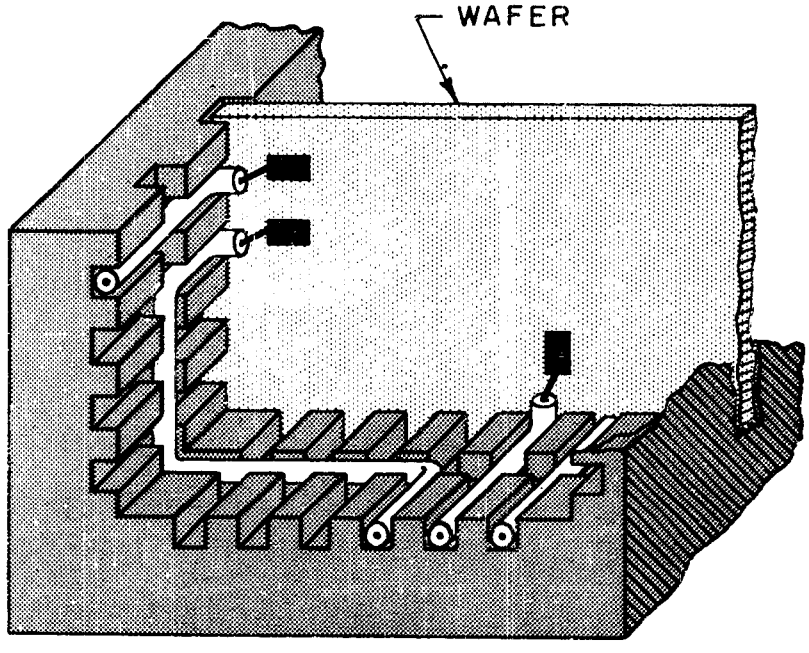

Solid Circuit Resistors of Figure 7B

(A)




Solid Circuit Bistable Multivibrator

(B)




WAFER INTERCONNECTION WITH TRANSMISSION LINES

# INTERFERENCE EFFECTS IN PARAMETRIC AMPLIFIERS

M. L. Wright
Airborne Instruments Laboratory
Melville, L.I., N.Y.

Abstract. - This paper presents an interference analysis for the one-port difference-frequency parametric amplifier and the results of interference measurements on both a microwave and an audio frequency one-port amplifier. Saturation, intermodulation, cross modulation, desensitization and problems peculiar to parametric amplifiers are analyzed and discussed.

## I. INTRODUCTION

During the past few years, increasing numbers of parametric amplifiers of many types have been used as low noise amplifiers in receivers. Their use has brought increased system sensitivity to weak signals and has generally reduced noise levels to a point where external-device losses are significant.

The advantage of increased signal sensitivity provided by these amplifiers could be negated by a vastly increased susceptibility to interference. Although weaker signals could be received they may be masked by a high level of interference generated in the amplifier. Previous interference investigations have been limited to saturation effects [1] in parametric amplifiers. It is the purpose of this paper to present the results of an analysis and measurements of additional nonlinear interference effects such as cross modulation, intermodulation and desensitization. The analysis and measurements are for a one-port difference-frequency configuration, but the methods used here can be applied to other types as well.

It should be emphasized that the measurements made here are on amplifiers in current use and do not represent optimum conditions for interference suppression.

## II. PARAMETRIC AMPLIFIER ANALYSIS

### Parametric Amplifier Operation

At present many different types of parametric amplifiers exist but only a few are in general use. The electron beam [2] and multiple diode types [3] have specific advantages and applications; however, the single diode parametric amplifier seems most popular. In single diode configurations [4] the one-port difference-frequency mode appears to be the most widely used and is the mode of operation discussed in this paper. Sum frequency and two-port

difference-frequency modes are used, but appear to have no advantages except for some specialized applications.

The one-port difference-frequency amplifier [5] has identical input and output frequencies and exhibits gain due to a negative resistance effect. Because the amplifier has only one port a circulator is normally used to provide separate input and output terminals. For this paper such devices are considered as being external to the amplifier although they are normally included in the amplifier package.

The amplifier port of the circulator can be considered as being terminated in a load $-Z_L$ and the voltage gain is then given by the reflection coefficient,

$$K = \frac{(-Z_L) - Z_0}{(-Z_L) + Z_0} = \frac{Z_L + Z_0}{Z_L - Z_0} \qquad (1)$$

which is greater than one. As shown below, the negative resistance effect occurs as a result of positive resistance loading at a frequency higher than the signal.

Small Signal Theory

The usual small signal theory [4] considers the varactor as a time-varying capacitance at the pump frequency. In order for this to hold, the pump must be the only large signal present. In this analysis all frequencies are applied to a nonlinear Q vs. v curve, and each voltage may take on any amplitude. This method is less accurate for small signal conditions but the use of large signals is more easily handled.

A voltage variable capacitance diode or varactor can be assumed to have a charge vs. voltage characteristic represented by a power series such as

$$Q = q_0 + av + bv^2 + cv^3 + \ldots . \qquad (2)$$

The voltage v is the sum of the voltages that exist at the diode terminals. (Only three frequencies are considered here but to be consistent with later sections, which include more frequencies, the subscripts 2, 7 and 9 are used.) For this analysis a signal frequency $w_2$, an idler frequency $w_7$ and a pump $w_9$ are of interest and

$$v = v_2 e^{jw_2 t} + v_2^* e^{-jw_2 t} + v_7 e^{jw_7 t} + v_7^* e^{-jw_7 t} + v_9 e^{jw_9 t} + v_9^* e^{-jw_9 t} \qquad (3)$$

where $v_n = \frac{|V_n|}{2} e^{j\phi n}$ and $v_n^* = \frac{|V_n|}{2} e^{-j\phi n}$

Substituting (3) into (2) and equating the result to a sum of charge variations at the frequencies of interest

$$Q = q_2 e^{jw_2 t} + q_2^* e^{-jw_2 t} + \ldots + q_9^* e^{-jw_9 t} \qquad (4)$$

gives equations for sinusoidal charge variations at these frequencies. Differentiating these equations with respect to time and neglecting products of small signals gives equations for signal currents in terms of voltages.

$$I_2 = jw_2(av_2 + bv_9 v_7^*) = Y_{22} v_2 + Y_{27} v_7^* \qquad (5)$$

$$I_7^* = -jw_7(av_7^* + bv_9^* v_2) = Y_{77}^* v_7^* + Y_{72}^* v_2 \qquad (6)$$

These equations suggest a shunt representation of the varactor with various Y equivalents as shown above.

Equations (5) and (6) can be used to determine the normal operation of the amplifier. The signal current may be found by substituting (6) into (5),

$$I_2 = Y_{22} v_2 - \frac{Y_{27} Y_{72}^* v_2}{Y_{77}^* + Y_{X7}} = I_{02} - Y_{X2} v_2 \qquad (7)$$

where $I_{On}$ = input current generator at $w_n$

$I_n = I_{On} - Y_{Xn} v_n$

$Y_{Xn}$ = external admittance at $w_n$

The midband voltage gain is:

$$K_v = \frac{v_2}{v_{02}} = \frac{1}{1 - \frac{G_{neg}}{G_{x2}}} \qquad \text{where } G_{neg} = \frac{w_2 w_7 b^2 v_9^2}{G_{x7}} \qquad (8)$$

The $G_{neg}$ term, describing the negative conductance of the amplifier, depends on a frequency conversion factor $w_2 w_7 b^2 v_9^2$ and the external idler loading $G_{x7}$. Unless otherwise noted, all calculations and measurements were made at 20 db power gain

where $G_{neg}/G_{x2} = 0.9$.

Gain Change Effects

From Equation (8) it is apparent that the gain is determined by the difference between unity and $G_{neg}\ G_{x2}$ which, under high gain conditions, is almost one. Under these conditions small changes in $G_{neg}$ or $G_{x2}$ will cause large changes in gain. Differentiating (8) with respect to $G_{x2}$ we obtain the incremental change in gain

$$\frac{\Delta K_v}{K_v} = K_v \frac{\Delta G_{x2}}{G_{x2}} \qquad (9)$$

This change in gain is assumed to be caused by changes in the real part only of $Y_{x2}$ although a similar expression can be obtained for complex changes.

The gain can be changed also by changes in $G_{neg}$ as well as the external loading. This term can be changed in several ways, all of which involve higher order terms than are present in equations (5) and (6) which were used to derive the small signal gain. In order to examine these terms and their effect on the amplifier, additional frequencies must be assumed to exist at the varactor.

Nonlinear Amplifier Operation

In order to predict the amplifier behavior with many frequencies present, the interactions between all signals must be calculated. This can be done by assuming that more frequencies exist at the diode and then computing the effect of these additional frequencies on the amplifier behavior.

Nine frequencies will be assumed to exist at the varactor and their spectrum is shown in Figure 1. Frequencies $w_1$ through $w_4$ are assumed to be within the signal passband of the amplifier and $w_5$ through $w_8$ are the corresponding idlers where $w_{idler} = w_{pump} - w_{signal}$. The pump frequency is again $w_9$. Within the signal passband $w_2$ and $w_3$ are considered as input or applied signals and $w_1$ and $w_4$ are products generated in part by the mixing of $w_2$ and $w_3$. These frequencies $w_1$ and $w_4$ will be needed in a later section and are included here for convenience. The voltage v in equation (2) is now the sum of the nine frequencies $w_1$ through $w_9$.

$$v = v_1 e^{jw_1 t} + v_1^* e^{-jw_1 t} + \ldots . v_9^* e^{-jw_9 t} \qquad (10)$$

Substituting (10) into (2) only up to the cube term, collecting terms and differentiating as before gives us equations as follows.

$$I_1 = jw_1\left[(a + cv_t^2)\ v_1 + bv_9v_8^* + c(v_2^*v_3^* + v_6v_7)\ v_2\right] \quad (11)$$

$$= Y_{11}v_1 + Y_{18}v_8^* + Y_{12}v_2$$

$$I_2 = jw_2\left[(a + cv_t^2)\ v_2 + (bv_9 + cv_3v_6)\ v_7^*\right] \quad (12)$$

$$= Y_{22}v_2 + Y_{27}v_7^*$$

$$I_7^* = -jw_7\left[(a + cv_t^2)\ v_7^* + (bv_9^* + cv_3^*v_6^*)\ v_2\right] \quad (13)$$

$$= Y_{77}^*v_7^* + Y_{72}^*v_2$$

$$I_8^* = -jw_8\left[(a + cv_t^2)\ v_8^* + bv_9v_1 + c(v_2v_3^* + v_6v_7^*)\ v_7^*\right] \quad (14)$$

$$= Y_{88}^*v_8^* + Y_{81}^*v_1 + Y_{87}^*v_7^*$$

$$\text{where } v_t^2 = v_1^2 + v_2^2 + v_3^2 + \ldots + v_9^2$$

Equations (12) and (13) now include higher order terms neglected in (5) and (6). With these equations we can calculate the change in $G_{neg}$ due to the applied signals.

It is of interest to note that (12) and (13) reduce to (5) and (6) when all voltages are small compared to the pump voltage. It is only when the signal or idler voltages become comparable to the pump voltage $v_9$ that they change the operation of the device. Under this condition, the Y's should not be considered as admittances but only as convenient substitutions for which the true nonlinear expression must finally be used.

If a "desired" signal $v_2$ is assumed small and $v_3$, an "interfering" signal, is assumed comparable to $v_9$, $G_{neg}$ becomes

$$G_{neg} = w_2w_7(b^2v_9^2 + 2bcv_3v_6v_9 + c^2v_3^2v_6^2) \quad (15)$$

$$= w_2w_7b^2v_9^2\left[1 + \frac{2cPv_3^2}{bv_9} + \frac{c^2P^2v_3^4}{b^2v_9^2}\right] \quad (16)$$

$$\approx w_2 w_7 b^2 v_9^2 \left[1 + \frac{2cPv_3^2}{bv_9}\right] = G_{neg} + \Delta G_{neg} \qquad (17)$$

$$\text{where } P = \frac{v_{idler}}{v_{signal}} = \frac{v_{9-n}}{v_n}$$

Differentiating (8) with respect to $G_{neg}$ gives the following incremental change in gain.

$$\frac{\Delta K_v}{K_v} = K_v \frac{\Delta G_{neg}}{G_{x2}} \qquad (18)$$

Under high gain conditions $|G_{x2}| \simeq |G_{neg}|$ and

$$\frac{\Delta K_v}{K_v} \approx K_v \frac{\Delta G_{neg}}{G_{neg}} = K_v \frac{2cPv_3^2}{bv_9} = Fv_3^2 K_v \qquad (19)$$

This change in voltage gain depends on the operating gain $K_v$ and $v_3^2$ which is a measure of the interfering power at $w_3$. This change in gain is normally called desensitization. It is the change in gain at one frequency due to the presence of a large signal at another frequency. If $w_2$ and $w_3$ are CW signals equation (19) is consistent with this definition.

Assume for the moment that $w_3$ is a 100% square wave modulated signal and that the amplifier bandwidth is sufficient to pass the modulation frequency sidebands. Under these conditions the output signal at $w_2$ will be decreased by an amount $\Delta K_v/K_v$ whenever $v_3$ is applied. Since $v_3$ is a modulated signal, this modulation will depend on the magnitude of $\Delta K_v/K_v$. This modulation of a desired signal by a modulated interfering signal is called cross modulation and it is useful to think of this cross modulation as a time-varying desensitization. In this manner, a single device characteristic can be applied to two interference phenomena.

Modulated signals are normally described by an average amplitude and a modulation index rather than by a peak amplitude and a change from that peak. Alternatively, if the interfering signal has an average value of $v_3'$ and a modulation index of m, the normalized average value of $v_2$ is

$$v_2' = 1 - F(V_3')^2 (1 + m^2) \qquad (20)$$

and the modulation index of M of $v_2'$ is

$$M = 2Fm\ (v_3')^2 \qquad (21)$$

By the use of (20) and (21), it is possible to convert from peak values to quantities commonly used to describe modulated signals. In either case, the quantity F is important in determining the amount of interference that will be produced under a given set of conditions.

If in equation (12) and (13) all voltages are assumed small except for $v_2$, $v_7$, and $v_9$ the amplifier behavior for large input signals can be derived by replacing $v_t^2$ by its parts. Substituting as above and collecting terms, equations (12) and (13) become

$$I_2 = jw_2\ (a + cv_2^2)\ v_2 + jw_2\ (bv_9 + cv_2v_7)\ v_7^* \qquad (22)$$

$$= Y_{22}v_2 + Y_{27}v_7^*$$

$$I_7^* = -jw_7\ (a + cv_7^2)\ v_7^* - jw_7\ (bv_9 + cv_2^*v_7)\ v_2 \qquad (23)$$

$$= Y_{77}^*v_7^* + Y_{72}^*v_2$$

Under midband conditions and neglecting detuning effects the gain expression is identical to the small signal gain, equation (8), derived previously. In this case,

$$G_{neg} = w_2w_7b^2v_9^2\left[1 + \frac{2cPv_2^2}{bv_9} + \frac{c^2P^2v_2^4}{b^2v_9^2}\right] \qquad (24)$$

$$= w_2w_7b^2v_9^2\left[1 + Fv_2^2 + \left(\frac{F}{2}\right)^2 v_2^4\right] \qquad (25)$$

where $F = \frac{2cP}{bv_9}$ as in equation (19)

Note that the same factor F occurs in (25) as well as (19) and that equation (19) also describes the onset of a loss in gain due to large signals. This loss in gain is called saturation.

The factor F is seen to enter into expressions for desensitization, cross-modulation and saturation, and it is convenient to use the basic quantity F as a figure of merit for interference effects involving changes in gain. In this case a small number F is desireable and represents a greater tolerance to interference.

Parametric Amplifier Intermodulation

From equation (11), the intermodulation (IM) is:

$$I_1 = Y_{11}v_1 + Y_{18}v_8^* + Y_{12}v_2 = -v_1Y_{x1} \qquad (26)$$

Substituting for the necessary idler terms and rearranging, equation (26) becomes:

$$v_1 = \frac{v_2\left(Y_{12} + \frac{Y_{18}Y_{87}^*Y_{72}}{(Y_{t7}^*)(Y_{t8}^*)}\right)}{Y_{x1} + Y_{11} - \frac{Y_{18}Y_{81}^*}{Y_{t8}^*}} \qquad (27)$$

where $Y_{t8}^* = Y_{88}^* + Y_{x8}^*$

$Y_{t7}^* = Y_{77}^* + Y_{x7}^*$

Note that an equivalent amount of IM would be produced at the output if an effective IM generator of

$$I_{01} = v_2\left(Y_{12} + \frac{Y_{18}Y_{87}^*Y_{72}}{Y_{t7}^*\,Y_{t8}^*}\right) \qquad (28)$$

were connected to the input. Because this source is approximately independent of the amplifier gain and frequency response, it will be used as a measure of the intermodulation performance of the amplifier.

Assuming all frequencies are subject to midband conditions,

$$I_{01} = jv_2\left(w_1c\left[v_2^*v_3^* + v_6v_7\right] - \frac{w_1w_8w_7bb^*v_9\left[c(v_2v_3 + v_6v_7^*)\right]}{Y_{t7}^*\,Y_{t8}^*}\right)$$

$$= jv_2w_1c\,(v_2v_3 + v_6v_7)\left(1 - \frac{w_7w_8b^2v_9^2}{Y_{t7}\,Y_{t8}}\right) \qquad (29)$$

$$= jv_2^2v_3w_1c\,(1 + p^2)^2$$

Note that this expression is of the form $IM = Kv_1v_2^2$ and that the effect of intermodulation at idler frequencies can be included by the factor $(1 + p^2)^2$.

The intermodulation expression (20) assumes that all signals are under midband conditions. In most normal interference situations, the midband conditions do not apply and the above expression should be considered as specifying the maximum intermodulation that a particular amplifier may generate. The actual value of intermodulation will generally be lower than the calculated value.

## III. INTERFERENCE MEASUREMENTS

The results of measurements on two one-port parametric amplifiers will be presented here. One is a microwave amplifier operating at 1400 mc with an X-band pump. The other is a low frequency prototype of the microwave amplifier and has the same equivalent circuit as is assumed for the microwave amplifier, except for component values. This amplifier was constructed to facilitate some of the measurements required for interference prediction. This low frequency amplifier operates at 1400 cps with a pump and idler of 18.2 and 16.8 kc respectively. For the more important types of interference both amplifiers were measured but for some effects only the more appropriate one was used.

### Load Sensitivity

A measurement was made of the sensitivity of the low frequency prototype amplifier to changes in external load and the results are shown in Figure 2. This figure shows the expected behavior as predicted by equation (9), with the load sensitivity becoming greater with increasing gain.

### Cross Modulation and Desensitization

Although cross modulation and desensitization arise from the same source, the measurement of each effect will generally be different. The microwave amplifier, with a bandwidth of 15 mc, is capable of passing all necessary sidebands of some commonly used modulation frequency. (1000 cps used here.) For this amplifier a measurement of cross modulation is more sensitive and accurate than desensitization and will be shown here.

Figure 3 shows, as a function of frequency, the amount of 100% square wave modulated interfering power required to produce a level of either 1% or 10% modulation on the desired signal. The groups of lines for 1% and 10% modulation represent different desired signal input levels and the cross modulation is seen to be relatively unaffected by the desired signal level. The cross modulation does depend on the interfering signal level and, as can be observed from Figure 3, the interfering signal power required for 10% modulation is 10 times that required to produce 1% modulation. This is the behavior that is predicted by equation (19). The cross modulation as a function of interfering signal power was measured at a single frequency for values of CM from .1% to 50% and the relation indicated by equation (19) holds quite well over this range. The variation of CM with frequency shown in Figure 3 is caused by the varying attenuation, with frequency,

The low-frequency amplifier, with only a 12 cps bandwidth, would require the use of very low modulation frequencies in measuring cross modulation. For this reason, and also because the short term amplitude stability of this amplifier is quite good, the CW desensitization was measured instead of the cross modulation. The amplifier stability was such that changes in gain of 1% could be measured. The variation of gain with interfering signal power is shown in Figure 4. The "2 for 1" behavior holds well for changes in gain up to about 8 db.

Saturation Measurements

The saturation characteristic of the low-frequency amplifier is shown in Figure 5. This amplifier saturates about 20 db lower than most microwave amplifiers due to the small pump voltage required to produce gain. However, the behavior of this amplifier is representative of that obtained with other amplifiers which saturate at higher levels.

Intermodulation Measurements

Intermodulation measurements were made on both the microwave and the low-frequency amplifiers. In both cases, the generated intermodulation product power levels are measured as functions of the two interfering signal power levels. In all IM measurements, the functional behavior of the IM output power is as predicted by equation (29). This equation can be expressed in terms of power inputs and outputs as

$$P_{IM} = P_1 + 2P_2 + C_{IM} \qquad (30)$$

The P's are in DBM and are to be added munerically (not as powers), with $P_2$ the interfering signal closest to the intermodulation product in frequency and $P_1$ the other interfering signal. If the intermodulation constant $C_{IM}$ is in DBM also, the IM power output $P_{IM}$ will be in DBM. An example of this behavior is shown in Figure 6 for the low frequency amplifier. The constant $C_{IM}$ is +80 DBM in this case and equation (30) can be used to predict the IM power output for any non-saturated region. For example, if $P_1$ = -50 DBM at fa and $P_2$ = -50 DBM at fb, $P_{IM}$ = -50 + 2 (-50) + 80 = -70 DBM. This is the value shown in Figure 6. The calculated value of $C_{IM}$ is 85 DBM and is higher than the measured value, as expected.

The results of IM measurements on the microwave amplifier are shown in Figures 7 and 8. In both measurements, the IM product is at the center of the passband and one input signal is outside the band. In Figure 7, the other input signal is in the amplifier passband and $C_{IM}$ is 40 DBM. When the second interfering

signal is placed outside the band the intermodulation constant drops to 33 DBM. This is indicative of the increased attenuation of this interfering signal as it moves further from the amplifier passband. A series of measurements were made in which allowances were made for amplification and/or attenuation of all signals present, and the results of these measurements show that under these conditions $C_{IM}$ is a constant. The use of a fictitious IM input generator in the analysis is thus justified by the measurements.

Interference Peculiar to Parametric Amplifiers

Perhaps the most serious interference problem generated by a parametric amplifier is pump power leakage from the signal port. Typical measured pump power outputs range from approximately +5 DBM to -30 DBM depending on frequency and the specific configuration used. In many cases this can cause considerable interference to nearby equipment if this source of RF power is unknown to the user. Devices to suppress this interference have been built into circulators specifically developed by A.I.L. for use with parametric amplifiers and a pump leakage reduction of 20 db has been obtained over wide frequency ranges.

A potential interference problem within the amplifier is the generation of false signal frequency outputs due to mixing of the pump with inputs near the idler or sum frequencies. This effect is similar to intermodulation but is caused by input frequencies well above the signal frequency. The microwave amplifier design used here has an inherent rejection of input signals in this frequency range and the measured interfering signal output was small ($< -80$ DBM) even with high level (0 DBM) inputs. The interference reducing circulator described above also attenuates interference of this type by attenuating the interfering signals before they reach the amplifier.

## IV. CONCULSIONS

The interference characteristics of one-port parametric amplifiers can be summarized by restating their calculated behavior as described in equations (8), (9), (19), (25), and (29). Each equation predicts a certain interference behavior with varying inputs and contains constants which determine the absolute level of the generated interference. The experimental evidence agrees quite well with the predicted variation; however, the absolute interference amplitudes agree only approximately with the calculated values. In many cases, the calculated value is adequate for practical use in determining interference although it is only approximate ($\pm$ 5 db). For intermodulation the calculated value is the maximum which should be encountered and the actual interference should be less severe. The reason for the difficulty in calculating the interference constants lies partly in the original Q vs. v approximation. The power series in equation (2) does not converge as rapidly as is desireable, and higher order

terms may contribute a significant error.

A practical difficulty encountered in microwave amplifier interference measurements is the uncertainty of the relation between diode voltage and input power at the frequencies of interest. The interference is determined by the interfering voltages at the diode but only the available input power is known. The methods used to determine the diode voltages from the input power are usually indirect and are sometimes subject to considerable error.

The interference problems in parametric amplifiers, and also in many other devices, can be roughly divided into two types:

1. gain change effects.

2. generation of additional frequencies.

It has been shown that the same amplifier parameters are involved in all gain change effects discussed and a different set of parameters can be used to describe the generation of one particular additional frequency. It would be convenient if these or similar parameters could be used as figures of merit for interference effects. This would facilitate the comparison of different amplifiers and enable comparison with similar types of devices such as traveling wave tubes. Eventually, such figures of merit could become part of the specification of the device along with gain, bandwidth and other parameters.

## ACKNOWLEDGEMENTS

The contents of this paper are a result of work undertaken on U. S. Air Force Contract Number AF 30(602)-2384.

## REFERENCES

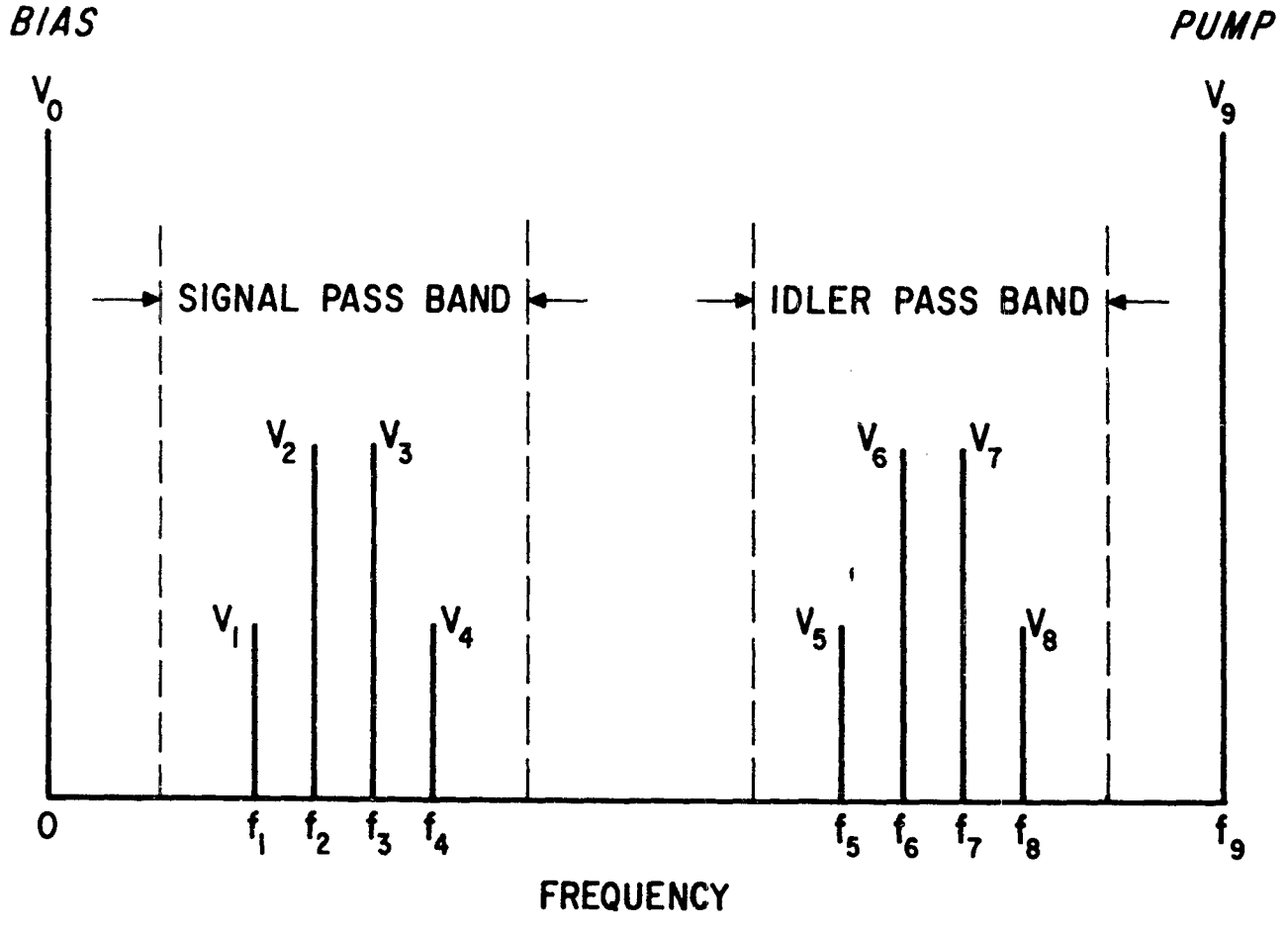
1. F. A. Olson, "Large-Signal Properties of Microwave Cavity-Type Parametric Circuits," Stanford Technical Report No. 315-1, February 8, 1960.

2. R. Adler, et al, "A Low-Noise Electron-Beam Parametric Amplifier," Proceedings of the I.R.E., vol. 46, pp. 1756-1757, October 1958.

3. D. I. Breitzer and E. W. Sard, "Low Frequency Prototype Backward-Wave Reactance Amplifier," Proceedings of the I.R.E., vol. 47, No. 5, pp. 995-996, May 1959.

4. H. E. Rowe, "Some General Properties of Nonlinear Elements," Part II, Small Signal Theory, Proceedings of the I.R.E., vol. 46, No. 5, p. 850, May 1958.

5. J. C. Greene and E. W. Sard, "Optimum Noise and Gain-Bandwidth Performance for a Practical One-Port Parametric Amplifier," Proceedings of the I.R.E., vol. 48, No. 9, p. 1583, September 1960.




FREQUENCY SPECTRUM AT VARACTOR TERMINAL

Fig. I

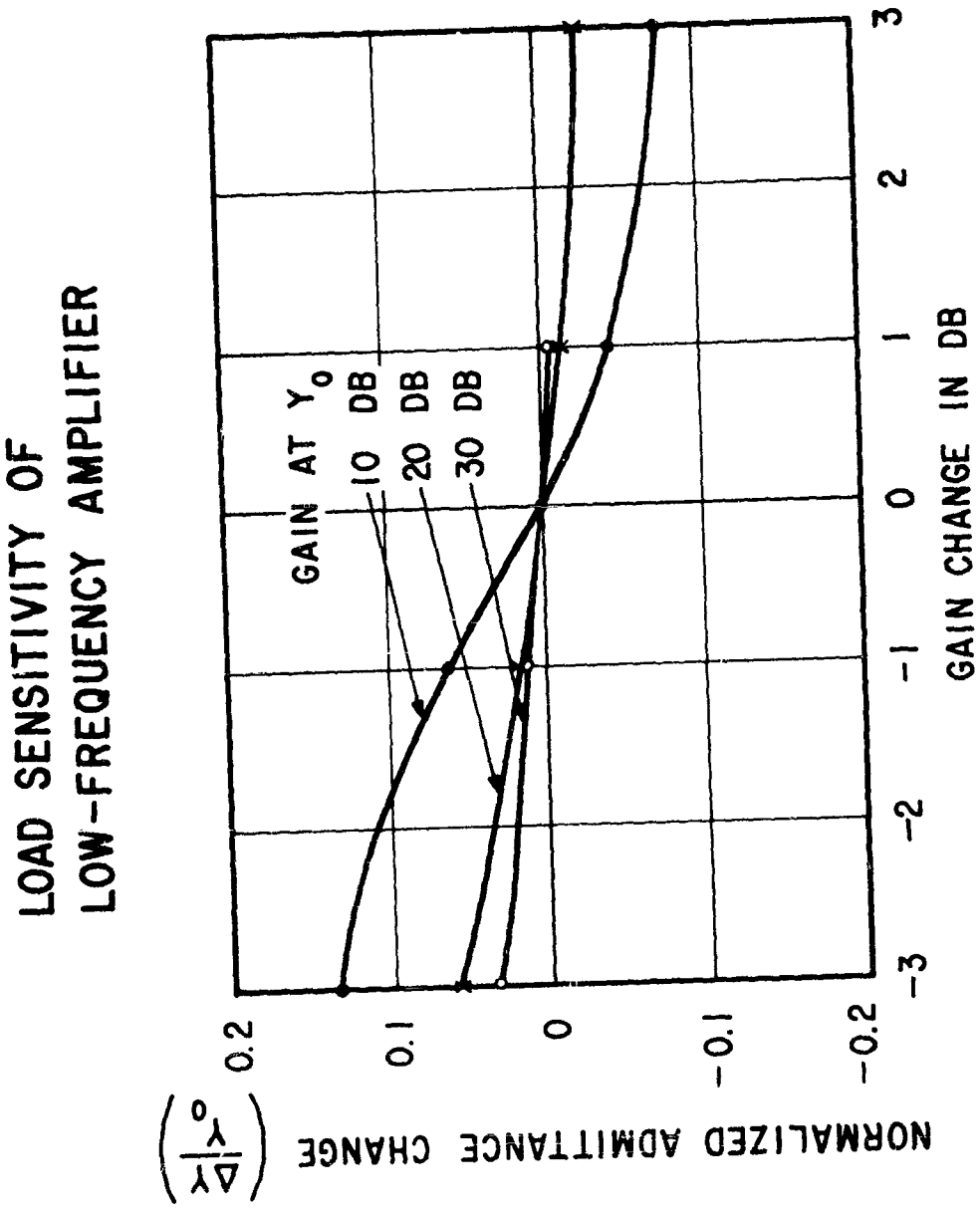

LOAD SENSITIVITY OF
LOW-FREQUENCY AMPLIFIER
GAIN AT $Y_0$
10 DB
20 DB
30 DB
GAIN CHANGE IN DB
3
2
1
0
−1
−2
−3
NORMALIZED ADMITTANCE CHANGE $\left(\frac{\Delta Y}{Y_0}\right)$
0.2
0.1
0
−0.1
−0.2

Fig. 2

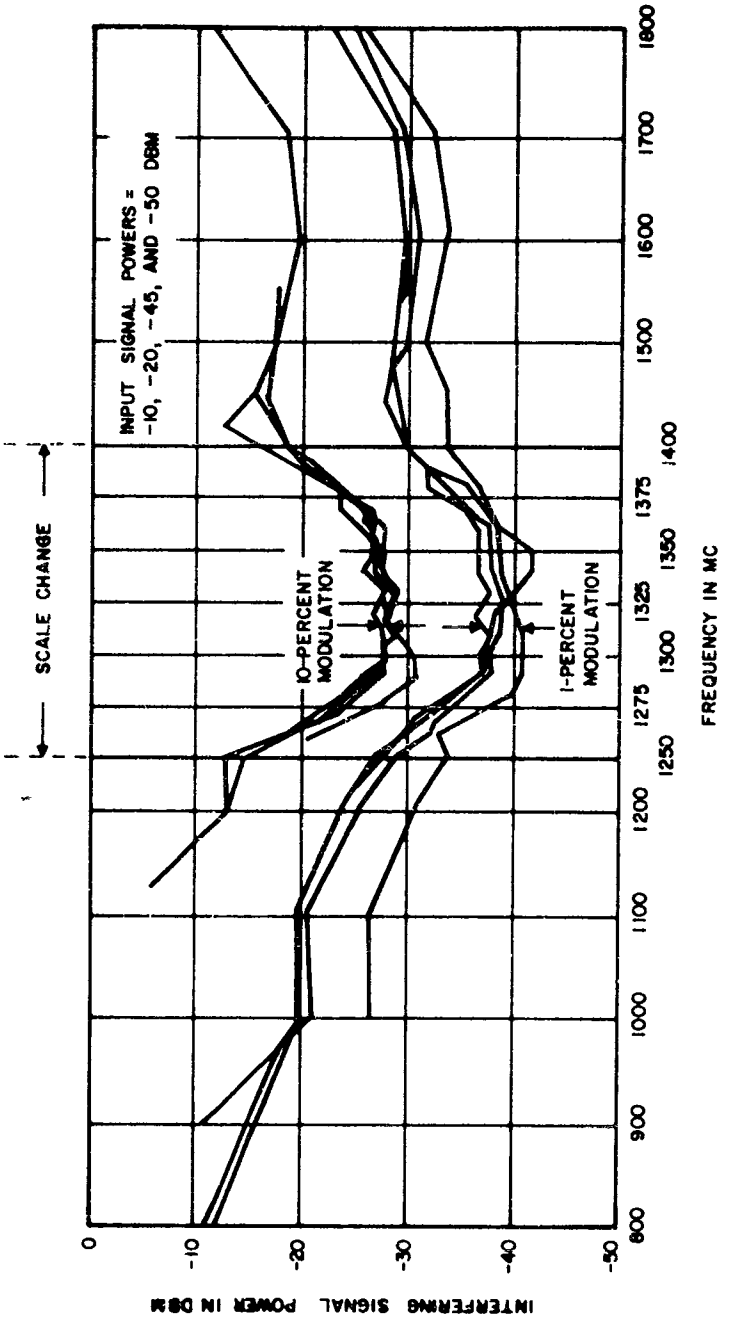
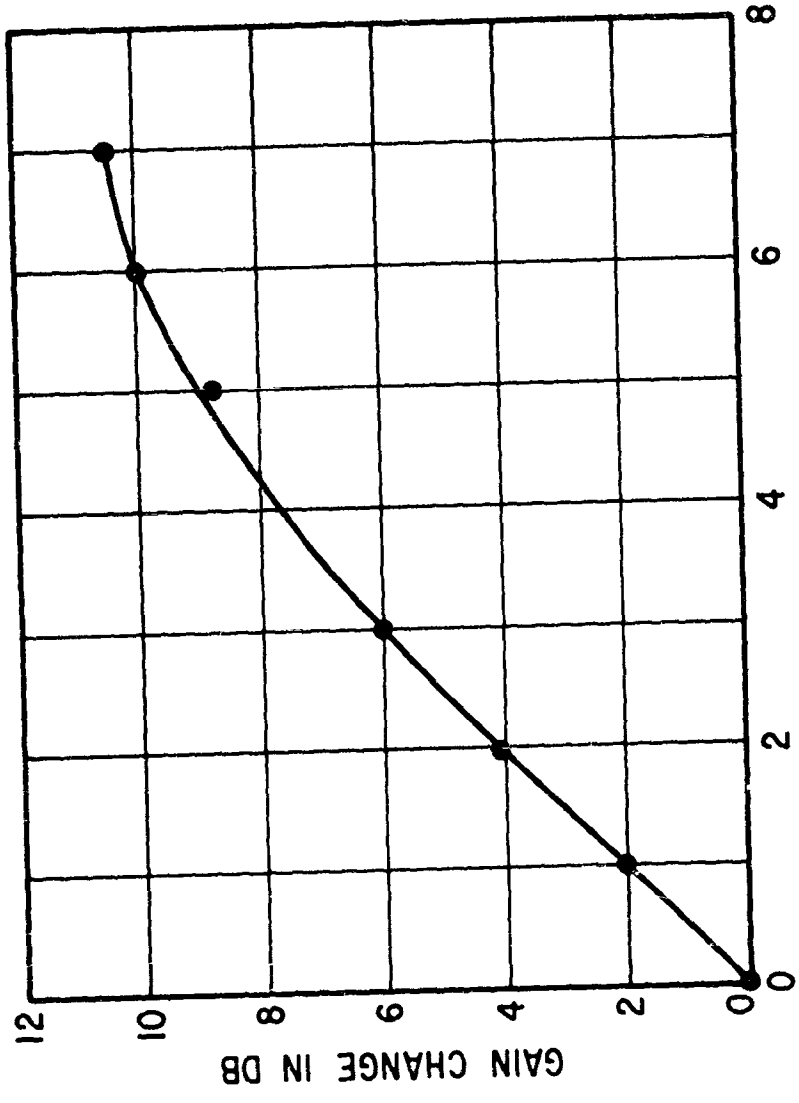
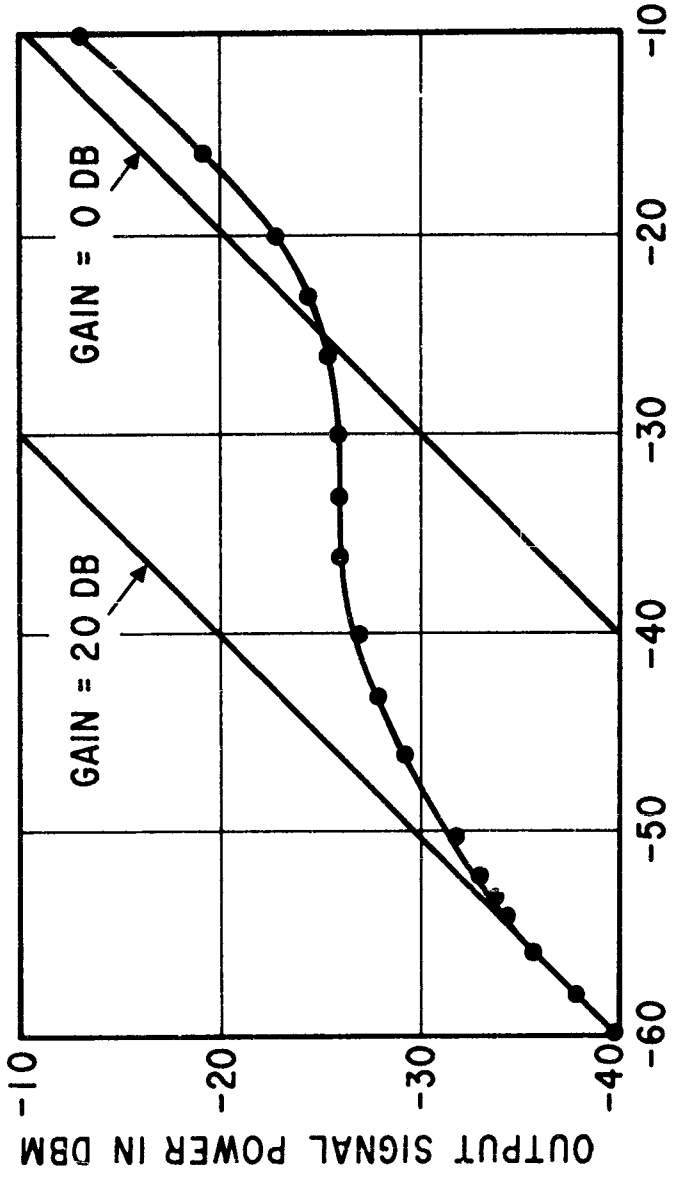



FIGURE 3 CROSS-MODULATION MEASUREMENTS




CENTER FREQUENCY GAIN CHANGE VS
INTERFERING SIGNAL LEVEL

Fig. 4




LOW-FREQUENCY PARAMETRIC-AMPLIFIER TRANSFER CHARACTERISTIC

Fig. 5

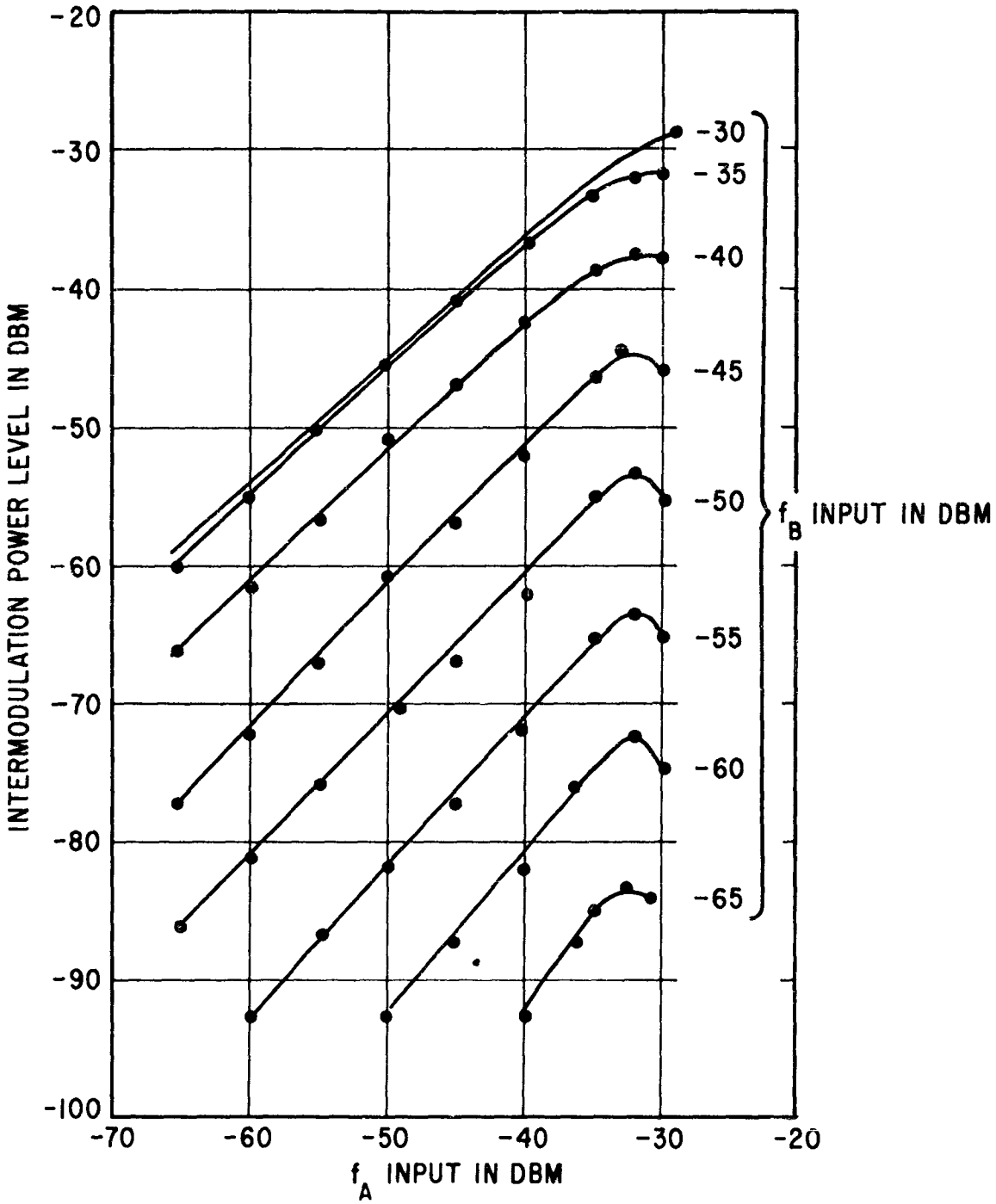
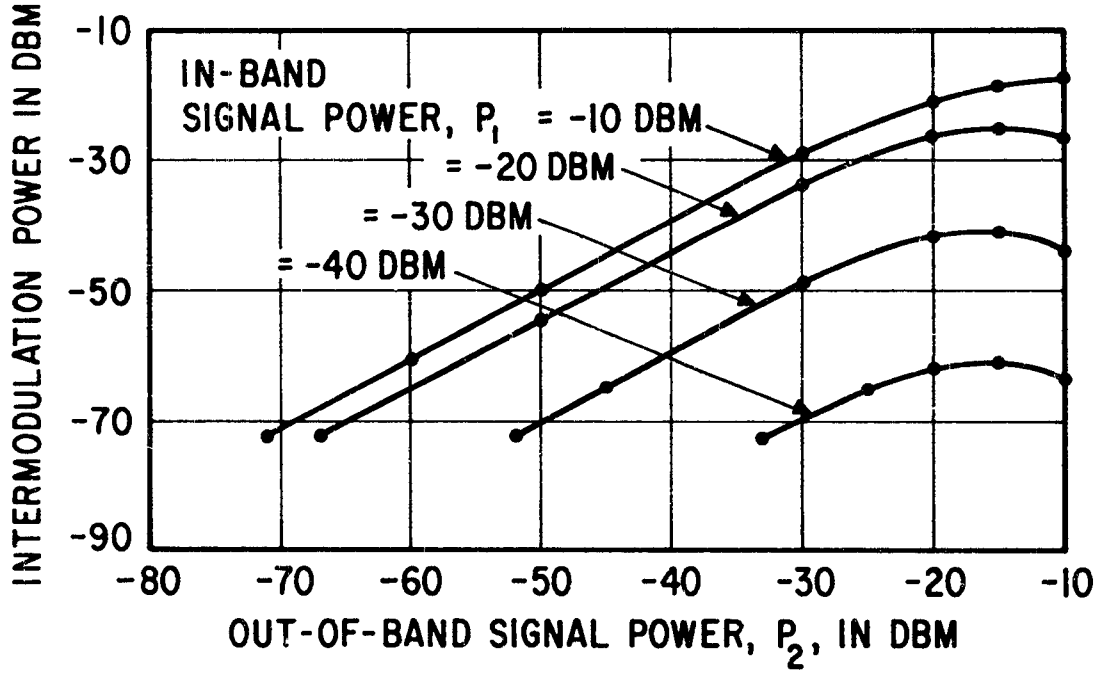
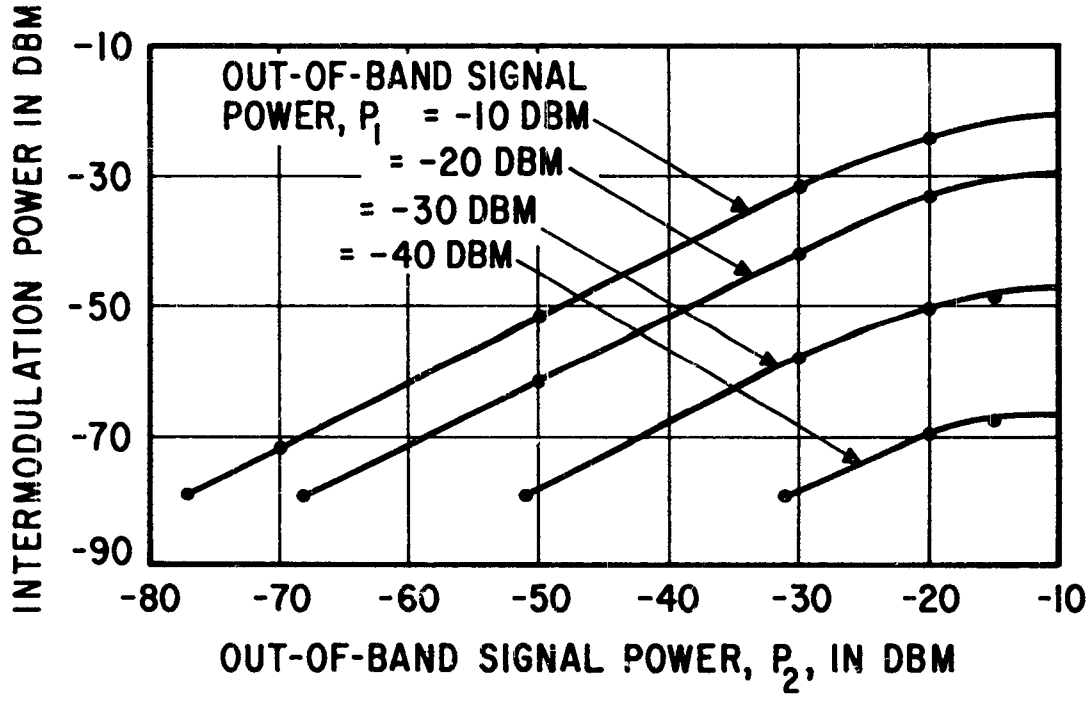



Fig. 6 **INTERMODULATION RESPONSE FOR LOW-FREQUENCY AMPLIFIER**




INTERMODULATION RESPONSE DUE TO ONE SIGNAL IN BAND AND ONE SIGNAL OUT OF BAND

Fig. 7




## INTERMODULATION RESPONSE DUE TO BOTH SIGNALS OUT OF BAND

Fig. 8

# INTERFERENCE IN MASERS

J. F. Lyons

Airborne Instruments Laboratory
Melville, New York

Abstract. - Maser amplifiers exhibit unusual interference characteristics. On a study program currently in progress these characteristics are being investigated analytically and, within the limits of available maser equipments, experimentally. To date some interesting results have been obtained. Among those discussed in this paper are (1) saturation and dynamic range characteristics which are a function of the duty-cycle of the input signal, (2) inherently long maser gain recovery time after saturation, (3) cross-modulation characteristics which are predictable, (4) the absence of intermodulation, and (5) predictable gain stability. Extensive experimental interference data obtained on an S-band maser shows close correlation with the analytical results.

## I. INTRODUCTION

The extremely low-noise character of the maser r-f preamplifier leads systems men and receiver engineers to consider using this device in new receiving systems. In todays electromagnetic environment this choice may or may not be wise depending upon the specific maser properties included in the generic classification, interference characteristics. Generally speaking this classification includes any maser property (for example, gain stability, saturation level and intermodulation) which is a potential source of interference in an adverse electromagnetic environment. This paper discusses the interference characteristics of the traveling-wave type of maser (TWM). The earlier maser type, the cavity maser, has been succeeded by the TW-type which exhibits far superior electrical performance. There is nothing lost by the emission of the cavity maser.

An adequate preliminary discussion of maser theory would be far too lengthy for inclusion in this paper. As a compromise, the author refers the readers to several excellent references[1,2,3,4,5]. In addition, all analytical effort is a simple nature.

## II. ANALYSIS

### Pass Band

It is possible to calculate the instantaneous amplification bandwidth of the TWM. DeGrasse, Schulz-DuBois and Scovil[5] express the electronic gain of a TWM as

$$G_b = -27.3\, X''_+ F_+ \frac{f\ell}{V_g}, \qquad (1)$$

where

$X_+$ = imaginary component of the magnetic susceptibility for magnetic fields with positive circular polarization,

$F_+$ = filling factor for magnetic fields with positive circular polarization.

$$X''_+ = \frac{\pi}{2\mu_0 h}(g\beta)^2(\rho_{\bar{m}} - \rho_{\bar{m}'})\, g(f-f_0)\left|\langle \bar{m}' | \delta_+ | \bar{m} \rangle\right|^2$$

and consequently

$$X_+''(f) = Kg(f - f_o)$$

where

$g(f - f_o)$ = function that describes the frequency variation of $X_+''$.

We are mainly concerned with $g(f - f_o)$, which describes the line shape of the maser material and determines the shape of the instantaneous amplification bandwidth of the TWM. (This assumes that no artificial means, such as stagger tuning, have been used to increase this bandwidth.) If one makes the usual assumption that the line shape of the maser material is Lorentzian, then DeGrasse et.al. show that

$$g(f-f_o) = \frac{2}{\pi B_m} \frac{1}{1+\left(2\frac{f-f_o}{B_m}\right)^2},$$

where

$B_m$ = bandwidth of the maser material

It should be recalled that the net maser gain, $G_{(db)}$, is equal to the electronic gain of the maser material, $G_{e(db)}$, minus the losses, $L_{o(db)}$, in the slow-wave structure. Introducing the frequency-variable term into the gain expression, we find

$$G_{e(db)} \frac{1}{1+\left(2\frac{f-f_o}{B_m}\right)^2} - L_{o(db)} = G_{(db)} \qquad (2)$$

when $f - f_o$,

$$G_{o(db)} = G_{e(db)} - L_{o(db)}$$

We can solve for the 3-db bandwidth as a function of $B_m$ and $G_e$ by letting $G_{db} = G_{o(db)} - 3$.

$$G_{e(db)}\left[\frac{1}{1+\left(\frac{BW_{3db}}{B_m}\right)^2}\right] - L_{o(db)} = G_{e(db)} - L_{o(db)} - 3$$

$$BW_{3db} = B_m\sqrt{\frac{3}{G_{e(db)}-3}} \qquad (3)$$

This relation is the same as that obtained in reference 5.

Saturation Level Transfer Characteristic and Desensitization

The character of maser saturation is evident in the expression[4]

$$\frac{T_{SIG}}{T_o} = \frac{\left[1+\left(\frac{\tau_{IDL}}{\tau_{SIG}}\right)^{-1}\right]\left[1 + W_{SIG}\,\frac{\tau_{SIG}\,\tau_{IDL}}{\tau_{SIG}+\tau_{IDL}}\right]}{1 - \frac{\tau_{SIG}\,f_{IDL}}{\tau_{IDL}\,f_{SIG}}} \qquad (4)$$

where

$T_{sig}$ = signal temperature in degrees K

$T_o$ = maser bath temperature in degrees K

$\tau_{sig}$ = signal relaxation time

$\tau_{idl}$ = idler relaxation time

$W_{sig}$ = signal transition probability

$f$ = frequency

Gain saturation in a TWM occurs when

$$W_{sig}\,\frac{\tau_{sig}\,\tau_{idl}}{\tau_{sig}+\tau_{idl}}$$

becomes significant compared to unity. We know that the signal transition probability, $W_{sig}$, is a linear function of the squared magnetic field at the signal frequency[4]. Thus saturation is a direct function of average power and duty-cycle.

Dr. Butcher[2] has calculated the absolute input power level in a TWM which produces a prescribed degree of saturation or a specific reduction in gain. In terms appropriate to a TWM and its slow-wave structure Dr. Butcher finds

$$P_{IN} = b_{TWM}\,\frac{(G_t'/G_t)^{-1} - \exp\left[-(|Q_m|/|Q_c|)\log(G_t'/G_t)\right]}{(|Q_c|/|Q_m|)-1} \qquad (5)$$

where

$G_t$ = small signal gain

$G_t'$ = large signal gain

$\frac{1}{Q_c} = \frac{1}{Q_o} - \frac{1}{Q_m}$ = the net quality factor of the periodic resonators in the presence of the active maser material

$Q_o$ = quality factor of the periodic resonators in the absence of the active material

$Q_m$ = the magnetic quality factor of the active maser material

and in the MKS system of units,

$$b_{TWM} = (v_g\,v_c)/32\pi(\beta/h')^2\eta\,T_{1s}\,T_{2s}\,(1-r_p r_s)\,D\,G_t\,\mu_o \qquad (6)$$

where

$v_g$ = group velocity in slow-wave structure

$v_c$ = volume of active maser material

B = Bohr magneton

h' = Planck's constant, h, divided by 2

N = filling factor of maser

$T_{1s}$ = spin-lattice relaxation time for signal transition

$T_{2s} = \tau_{sig}$ = spin-spin relaxation time for signal transition

$r_p$ = Overhauser parameter for the pump transition

$r_s$ = Overhauser parameter for the signal transition

D = period of the slow-wave structure

$G_t$ = small-signal gain

$u_o$ = permeability of free-space

Thus using Dr. Butchers expressions for gain saturation in a TWM, one can accurately predict the absolute input power level which produces any prescribed degree of gain saturation.

Intermodulation and Cross-Modulation

An interesting property of maser amplifiers is the absence of intermodulation. The absence of intermodulation does not imply the absence of cross-modulation; in fact, maser amplifiers do exhibit predictable cross-modulation. The apparent contradiction is attributed to a basic principle of maser operation--that saturation is based on average power, $f(v^2)$, rather than peak voltage.

Suppose we consider the cause of saturation in RF amplifiers and mixers; in every case, active elements are involved--that is, vacuum tubes, transistors, crystals, klystrons, and tunnel diodes--and saturation occurs when the input signal voltage exceeds the linear portion of the element's E-I characteristic. This nonlinearity in the transfer characteristic is the source of intermodulation and cross-modulation, as well as saturation.

The maser amplifier cannot be described by an E-I characteristic; instead, a power transfer characteristic (power output versus power input) is basic in describing its behavior. The net effect of this characteristic is that, even at saturation levels, the transfer impedance of a maser is constant; thus, the equivalent E-I characteristic is linear. The gain of the maser amplifier to input signals depends on the average power contained in the signal.

For analysis purposes, one can assume that the maser amplifier has a perfectly linear E-I characteristic and a gain that is a function of the average input power. When two or more input signals are present, we expect the input impedance for each to be constant (nonlinearity is required for intermodulation) and the amplifier gain for each to be a function of the total average input power.

In summary, the maser amplifier gain is a function of the total average power contained in the input signals (whose frequencies are within the maser passband). Intermodulation as conventionally defined is nonexistent.

Gain Stability

In a practical TWM, gain instability is caused almost exclusively by fluctuations in the externally applied d-c magnetic field. We can calculate the instability from this source by considering the magnetic linewidth function of the maser material and the current stability in the electromagnet. The magnetic and frequency linewidths are related by the gyromagnetic ratio of the electron which is = 2.8 Mc per oersted. In a practical maser the primary d-c magnetic field is usually derived from a permanent magnet. In tunable masers, tickler coils wound on the permanent magnet vary the net applied d-c magnet field sufficiently to tune the maser amplification band as required. Fluctuations in this applied field relate directly to the known regulation of the current flowing through the tickler coils. For example, if an applied magnetic field is derived from a permanent magnet of 2000 gauss and an electromagnet of 100 gauss with 0.1% stability, then the net applied field of 2100 gauss has an instability of $\pm$ 0.1 gauss. As in the case of the frequency linewidth, the magnetic linewidth of the maser material is assumed Lorentzian. The gain of a TWM as a function of the magnetic field fluctuation can then be determined from

$$G_{(db)} = G_{e(db)}\ \chi''(H_{dc} - H_{dc_{(o)}}) - L_{o(db)} \qquad (7)$$

where

$$\chi'' = \chi_o''\ \frac{1}{1 + 4\left[\frac{H_{dc} - H_{dc_{(o)}}}{B_{mag.}}\right]^2}$$

Gain Recovery Time

The gain of a TWM in decibels can be expressed as

$$G_{(db)} = K_{(db)}\ X'',$$

and at $f_o$,

$$G_{o(db)} = K_{(db)}\ X_o''$$

where K is some constant. Becker[6] et.al. have shown that, during recovery from a saturating signal,

$$X'' = X_o''\ (1 - e^{-t/T}),$$

where T is the spin-lattice relaxation time of the maser material. Using these relations we note that

$$G_{(db)}\ \left(\frac{t}{T}\right) = G_{o(db)}\ (1 - e^{-t/T})$$

The time for gain recovery to within 3 db of full gain, $G_o$, can be found from

$$e^{-t/T} = 1 - \frac{G_{o(db)} - 3}{G_{o(db)}} \qquad (8)$$

## III. EXPERIMENTAL CORRELATION

Test TWM Description

Airborne Instruments Laboratory recently completed the development and testing of an S-band traveling-wave maser (TWM). Table I summarizes the characteristics of this maser. Figure 1

shows the peak maser gain versus frequency as the instantaneous amplification band is tuned through the bandwidth of the slow-wave structure. Figure 2 shows a typical instantaneous amplification band.

Passband

The Airborne Instruments Laboratory TWM uses pink ruby with about 0.05 percent chromium concentration. Assuming that the bandwidth of this material is about 60 Mc[4], we can compare the prior analytical prediction with the experimental bandwidth of 21 Mc shown in Figure 2. From equation 3 and with $G_0$ = 40 db, we find that $BW_{3db}$ = 17 Mc; this compares favorably with the 21 Mc, which included a stagger-tuned effect. Even more significant is a comparison of the entire experimental passband of the TWM with the corresponding analytical result. This can be accomplished using equation 2; the close correlation obtained is shown in figure 3.

Saturation Level, Transfer Characteristic and Desensitization

Previously we noted that the gain saturation level in a TWM is a direct function of duty-cycle. This effect is clearly indicated in the experimental gain saturation data presented in Figure 4. Another interesting observation in this figure is the input signal level which reduces the TWM gain 3 db from the nominal small signal gain. For c-w input signals this level is -48 dbm. Using Dr. Butcher's results, equations 5 and 6, and the detailed S-band TWM design data we can obtain a comparison between this experimental saturation level and the corresponding analytical results. In the S-band TWM the unloaded quality factor, $Q_c$, of the periodic resonators is about 1000 and the absolute value of the magnetic quality factor, $Q_m$, is about 150. Thus $Q_m / Q_c$ is approximately 0.85 and, from equation 5, the input power level which produces a 3 db reduction in gain is approximately equal to $b_{TWM}$. A calculation of $b_{TWM}$ is more involved and is performed below. Applying equation 6 to the S-band TWM with;

| | |
|---|---|
| $u_o = 1.257 \times 10^{-6}$ | (henry-meter$^{-1}$) |
| $v_g = 3 \times 10^8/70$ | (meters - sec$^{-1}$) |
| $v_c = 6.47 \times 10^{-6}$ | (meter$^3$) |
| $B = 9.27 \times 10^{-24}$ | (joule/weber-meter$^2$) |
| $h' = 6.623 \times 10^{-34}/2$ | (joule-sec) |
| $\eta = 0.5$ | dimension less |
| $T_{1s} = 0.2$ | (sec) |
| $T_{2s} = 0.55 \times 10^{-8}$ | (sec) |
| $rp = r_s = 0.5$ | dimension less |
| $D = 2 \times 10^{-3}$ | (meter) |
| $G_t = 1000$ | dimension less |

yields

$$b_{TWM} = \frac{3\times10^8\times6.47\times10^{-6}\times(6.623)^2\times10^{-68}\times 1/1.257\times10^{-6}}{70\times32\pi\times4\pi^2\times(9.27)^2\times10^{-48}\times0.5\times0.2\times0.55\times10^{-8}\times0.75\times0.2\times10^{-2}\times10^3}$$

$$\cong 3\times10^{-8} \text{ watts}$$

Thus the S-band TWM gain is reduced by 3 db for signal inputs at a level of -45 dbm. This closely correlates with the experimental value of -48 dbm.

Intermodulation and Cross-Modulation

In addition to the simple qualitative previously presented, the prediction that intermodulation is nonexistent in maser amplifiers can be justified by quantitative experimental data. To this end a simple experiment was performed. The basic premise was that the existence of intermoduation in a device implies nonlinearity in its transfer impedance. For a single input signal, a nonlinear transfer impedance would result in the generation of harmonics. This permits simple measurements of harmonic outputs to be substituted for the more elaborate measurements of intermodulation products. The circuit used (figure 6) permitted observation f second- and third-harmonic output power levels down to 60 db below the fundamental output power level. The absence of harmonic output power above this level is considered verification of the practical nonexistence of intermodulation in maser amplifiers.

The experiment was performed by exciting the maser with an input signal 40 db above the saturation level, and observing the second- and third-harmonic output power. Within the 60 db measurement range of the test circuits, no output power was detected at either the second- or third-harmonic frequencies.

The performance of the test circuit can easily be examined to determine possible misinterpretation of observation.

1. Sensitivity of second-stage receiver:

| | |
|---|---|
| Bandwidth | 2 Mc |
| Noise Figure | 15 db |
| Filter loss | 10 db |

Thus the sensitivity is -86 dbm for unity signal-to-noise ratio; -95 dbm would be an observable change in output level (greater than 0.5 db change).

2. Harmonic content of input signal:
The relative attenuation of the second harmonic power (4460 Mc) when the triple-tuned input filter is tuned to the signal frequency (2230 Mc) is calculated as follows:

$$\frac{BW_{4460}}{BW_{3db}} = \frac{4460-2230}{7.5} = 295 = 2^n$$

where n = 8.2. Rejection of filter is 18 db per octave times the number of octaves, n, and equals 147 db. Thus the second-harmonic input to the TWM is below the noise level of the TWM (about -127 dbm for a 2 Mc post-receiver bandwidth).

3. Signal levels

| | |
|---|---|
| Signal generation output | +16 dbm |
| TWM input at $f_o$ | +10 dbm |
| Signal level at TWM output | 0 dbm (10 db structure loss in TWM) |
| Structure loss in TWM at $2f_o$ | 35 db |

Thus, the second-harmonic output power could be observed, if present, to levels 60 db below the level of the fundamental output power.

Gain Stability

The measured gain stability for the S-band TWM was (1) long-term stability = $\pm$ 0.2 db and (2) short-term stability = $\pm$ 0.05 db. These figures include appreciable contributions from the post-receiver and the measurement apparatus. Figure 7 presents equation 7 in graphical form for the parameters of the S-band TWM; namely, $B_{magnetic}$ = 20 oersteds, $G_{e(db)}$ = 40 db and $L_{o\ (db)}$ = 10 db. This TWM used a permanent magnet with a magnetic field of 2280 oersteds combined with tickler coils that permitted tuning the total field from 2380 to 2480 oersteds. The latter range tunes the TWM passband from 2120 to 2370 Mc. The current required in the tickler coils was between 1 and 2 amperes; the regulation was 0.1 percent. This yields a magnetic-field stability of $\pm$ 0.2 oersted; from figure 7, the observed gain stability should be $\pm$ 0.016 db. The discrepancy between the predicted and the experimental stability is due to contributions from the post-receiver and the measurement apparatus.

Gain Recovery Time

Figure 8 shows the details of the measurement set-up employed to measure the gain recovery time of the S-band, TWM. The functional operation of this circuit is self-explanatory. Figure 9 presents a gain recovery photograph obtained with this circuit. Figure 10 is a graphical analysis of the TWM gain recovery characteristic. This data was obtained from the photograph of Figure 9 and some associated calibration data. Note, that using equation 8, the overall gain recovery time for the S-band TWM with $G_o$ = 30 db corresponds to $e^{-t/T}$ = 0.1 which occurs, from figure 10, at t = 50 milliseconds. The detailed analysis of figure 10 dramatizes the presence of three distinct recovery time constants. One must conclude that cross-relaxation processes are occuring in addition to the normal spin-lattice relaxation process. The accounts for the large discrepancy between this experimental recovery time and the much longer recovery time that would be predicted using the spin-lattice relaxation time of ruby (in the hundreds of milliseconds) and the prediction method described in a report by Becker et.al[6].

## IV. CONCLUSIONS

In this paper we have attempted to develop simple methods for predicting the interference characteristics of the TWM. The judgement of our success is left to the reader. Present effort by many laboratories towards improving the performance characteristics of the TWM is primarily in the areas of new maser materials, impurity doping techniques and the utilization of cross-relaxation mechanisms. In anticipation of these maser advances, further effort of a nature similar to that reported in this paper is certainly desirable.

## ACKNOWLEDGEMENTS

The work reported in this paper is part of a more general study program, "Interference Analysis of New Components and Circuit Techniques" being conducted by Airborne Instruments Laboratory under Rome Air Development Center Contract AF30(602)-2384. The guidance of S. Becker, Project Engineer at AIL, and

R. Miller, RADC Program Manager and the technical consultation of S. Okwit and Dr. F. Arams of AIL is gratefully acknowledged.

REFERENCES

1. P. N. Butcher, "An Introduction to the Theory of Solid-State Masers," Proc. of I.E.E., Paper No. 3220E, February 1960.

2. P. N. Butcher, "Theory of Three-Level Paramagnetic Masers," Proc. of I.E.E., Parts 1-4, Paper nos. 2641-44, May 1958.

3. H. E. D. Scovil, "The Three-Level Solid-State Maser," Proc. of I.R.E., Trans. of PGMTT, vol. MTT-6, No. 1, p 29, January 1958.

4. E. O. Schulz-DuBois, H.E.D. Scovil, and R.W. DeGrasse, "Use of Active Material in Three-Level Solid State Masers," BSTJ, vol 38, p 335-352, March 1959.

5. R. W. DeGrasse, E. O. Schulz-DuBois, and H.E.D. Scovil, "The Three-Level Solid State Traveling-Wave Maser," BSTJ, Vol. 38, p 305-334, March 1959.

6. S. Becker, F. G. Haneman, P. Kalisiak, J. Lyons, G. W. Thomson, and M. L. Wright, "Interference Analysis of New Components and Circuit Techniques," Second Quarterly Progress Report under RADC Contract AF30(602)-2384, AIL Report No. 8899-I-2, June 1961.

TABLE I

SUMMARY OF S-BAND TWM CHARACTERISTICS

| | |
|---|---|
| **ELECTRICAL** | |
| Frequency range (tunable) | 2120 to 2370 Mc |
| Amplification bandwidth (typical) | 21 Mc |
| Net Forward gain | 30 db |
| Net reverse isolation | 100 db |
| Noise Temperature | 10 $\pm$ 2°K |
| Saturated output power | -27.5 dbm |
| Recovery time | 50 milliseconds |
| Gain stability: | |
| Long-term | $\pm$ 0.2 db |
| Short-term | $\pm$ 0.05 db |
| **DESIGN** | |
| Active maser material | Pink ruby (0.065 percent chromium concentration) |
| Slow-wave structure | Comb |
| Internal isolators | YIG* disks |
| DC magnetic field | 2.38 to 2.48 kilo-oersteds |
| Pump frequency | 12,420 to 12,730 Mc |
| Pump power (approximate) | 100 mw |
| Bath temperature | 1.8°K |
| Cooling | Open cycle with helium |
| **MECHANICAL** | |
| Length of slow-wave structure | 6 1/2 inches |
| Weight of TWM assembly | 180 pounds (includes magnet weight of 110 pounds) |
| **OTHER** | |
| Helium capacity in dewar | 5.5 liters |
| Operating time between helium recharges | 6 to 8 hours |

*Yttrium-iron garnet.

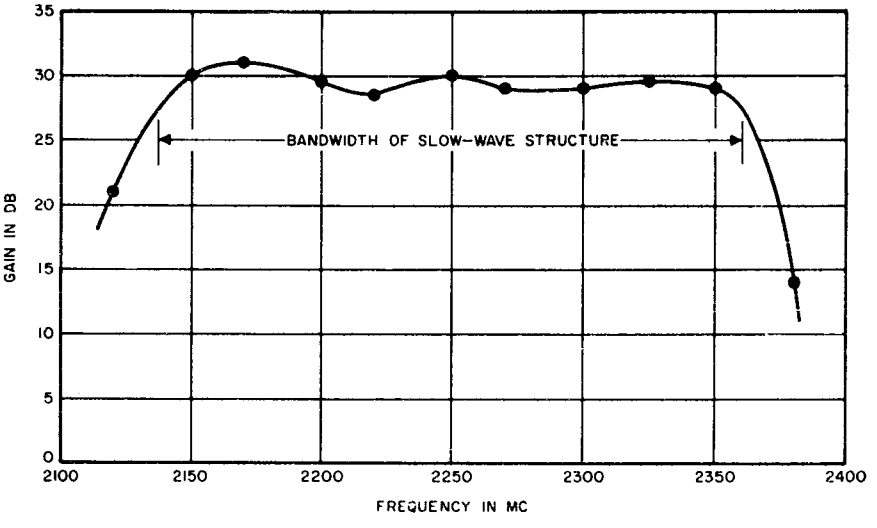



FIGURE 1. NET MASER GAIN VS OPERATING FREQUENCY

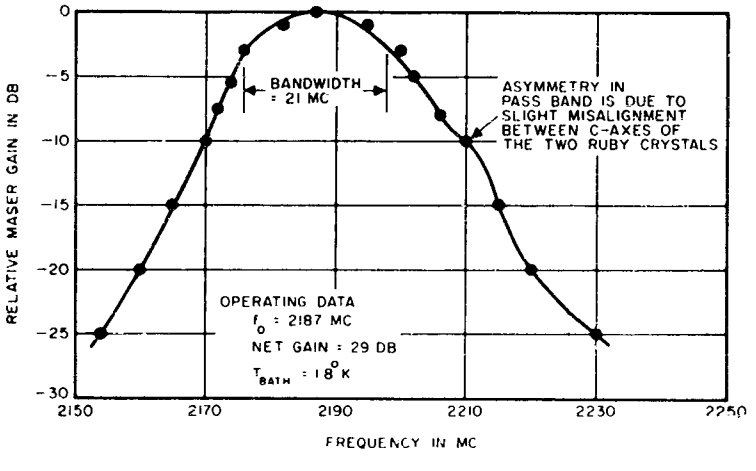



FIGURE 2. TYPICAL MASER PASS BAND

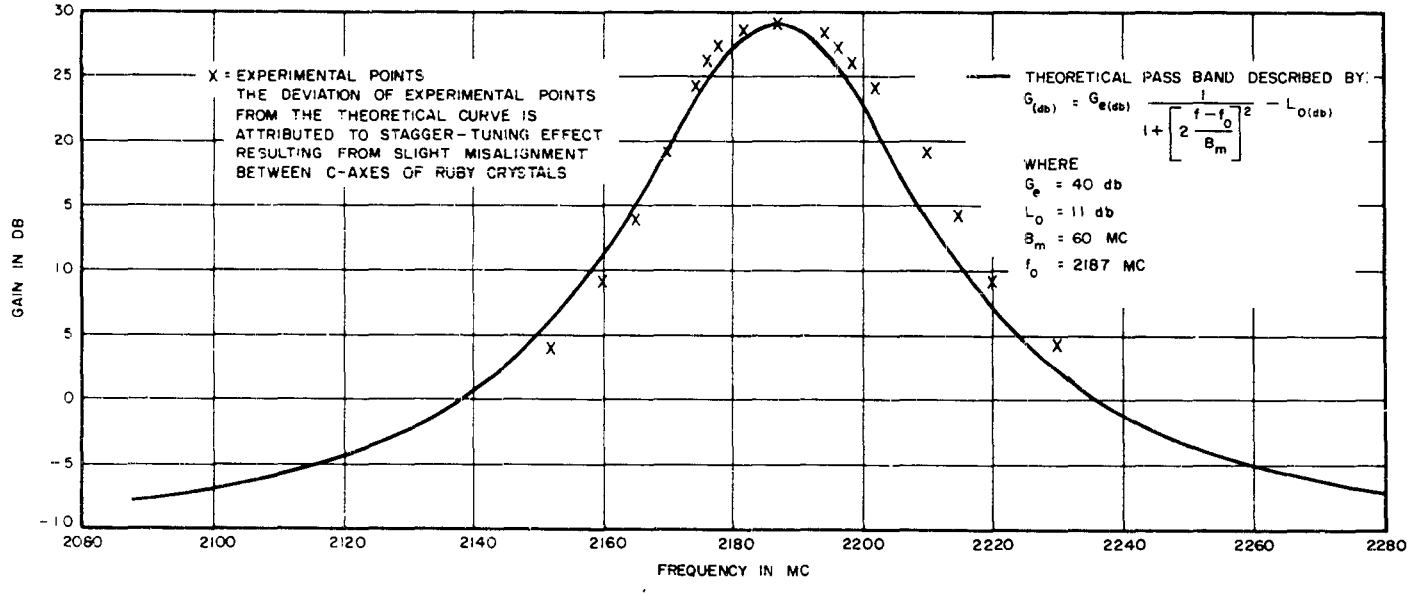



FIGURE 3 COMPARISON OF THEORETICAL AND EXPERIMENTAL TWM PASS BANDS

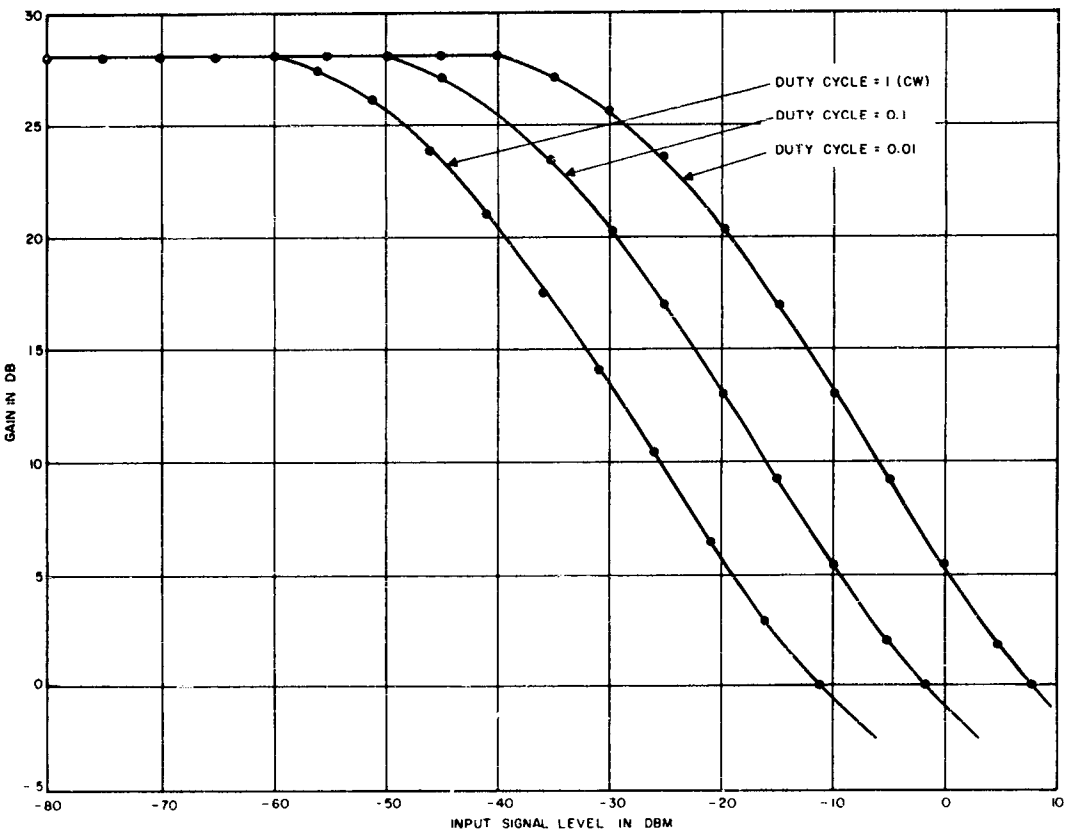



FIGURE 4. GAIN SATURATION AS A FUNCTION OF DUTY CYCLE

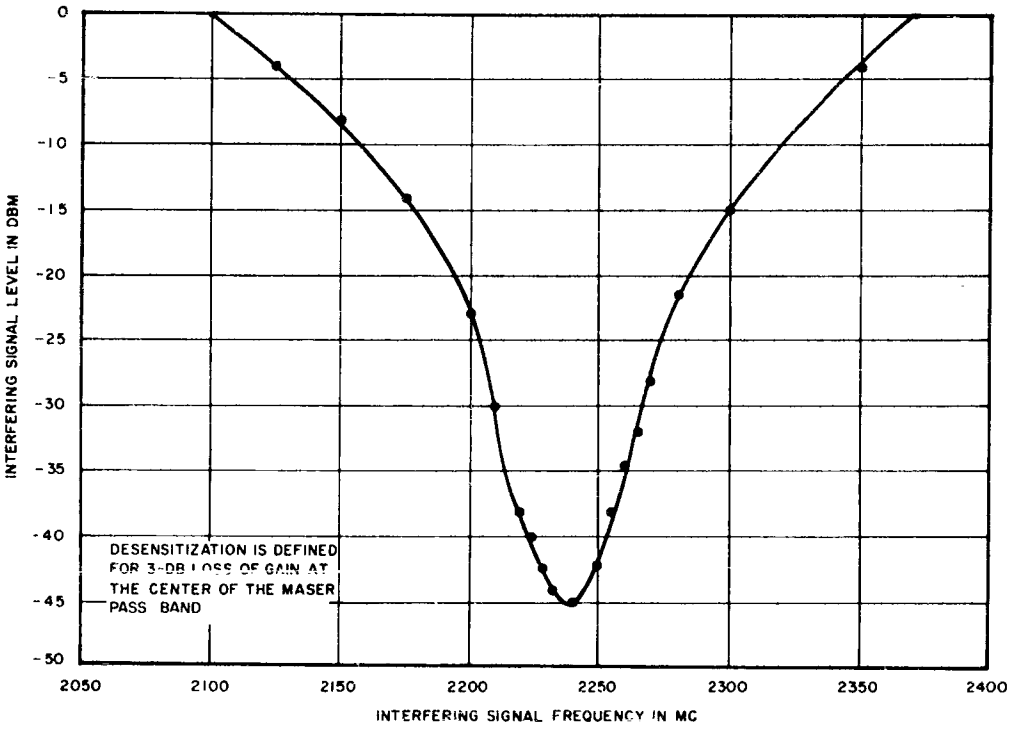
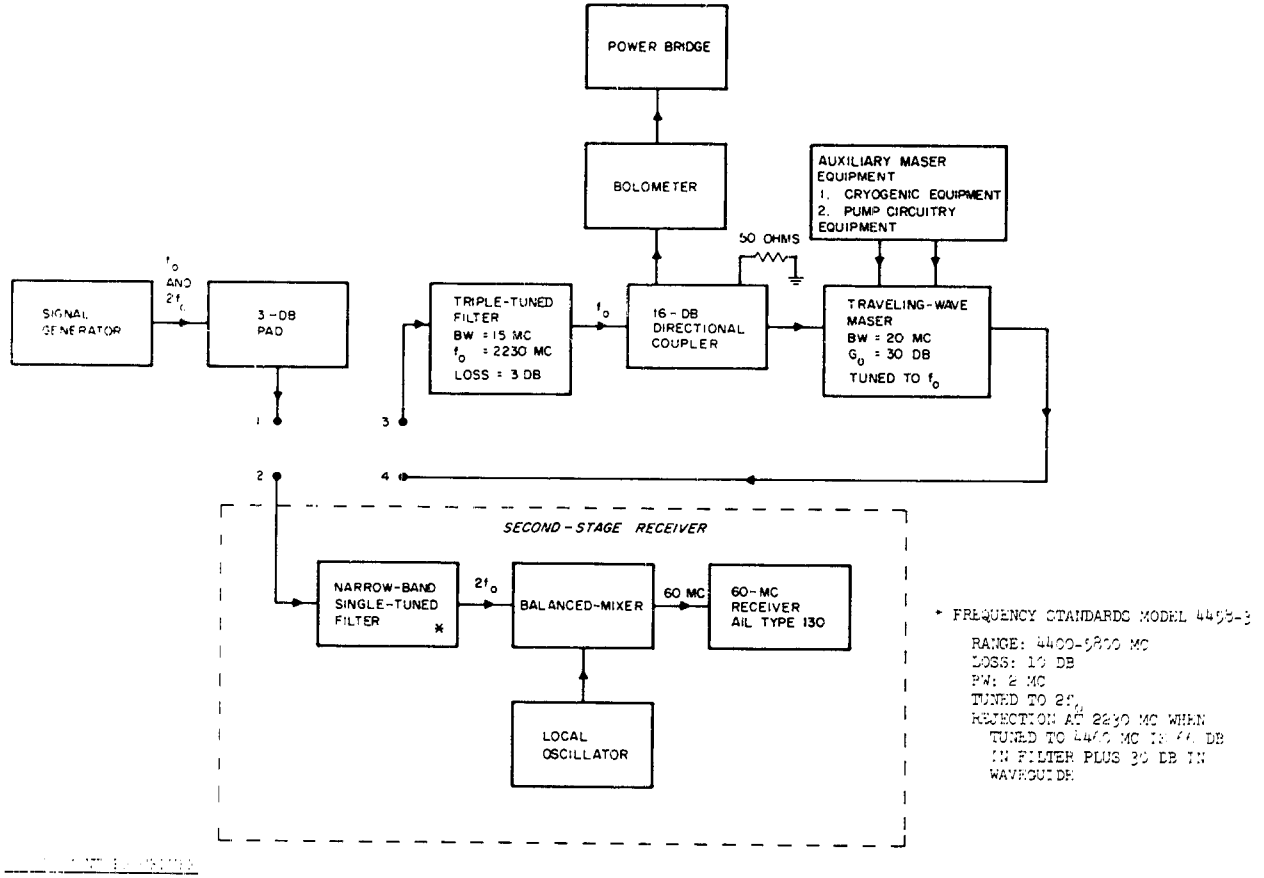



FIGURE 5 DESENSITIZATION CHARACTERISTIC




* FREQUENCY STANDARDS MODEL 4405-3
RANGE: 4400-5800 MC
LOSS: 10 DB
PW: 2 MC
TUNED TO $2f_o$
REJECTION AT 2230 MC WHEN TUNED TO 4460 MC IS 44 DB IN FILTER PLUS 30 DB IN WAVEGUIDE

NOTES:

1. SWITCHES 1 AND 2 ARE CLOSED AND THE SECOND-STAGE RECEIVER IS TUNED TO THE SECOND-HARMONIC FREQUENCY OF THE SIGNAL GENERATOR.
2. SWITCHES 1, 2, AND 3 ARE CLOSED AND THE TRIPLE-TUNED FILTER IS ADJUSTED TO MAXIMIZE THE POWER AT THE FUNDAMENTAL FREQUENCY.
3. THE SECOND-HARMONIC POWER GENERATED IN THE TWM IS INDICATED BY THE SECOND-STAGE RECEIVER.

FIGURE 6 CIRCUIT ARRANGEMENT AND PROCEDURE FOR MEASURING SECOND-HARMONIC POWER GENERATED IN TWM

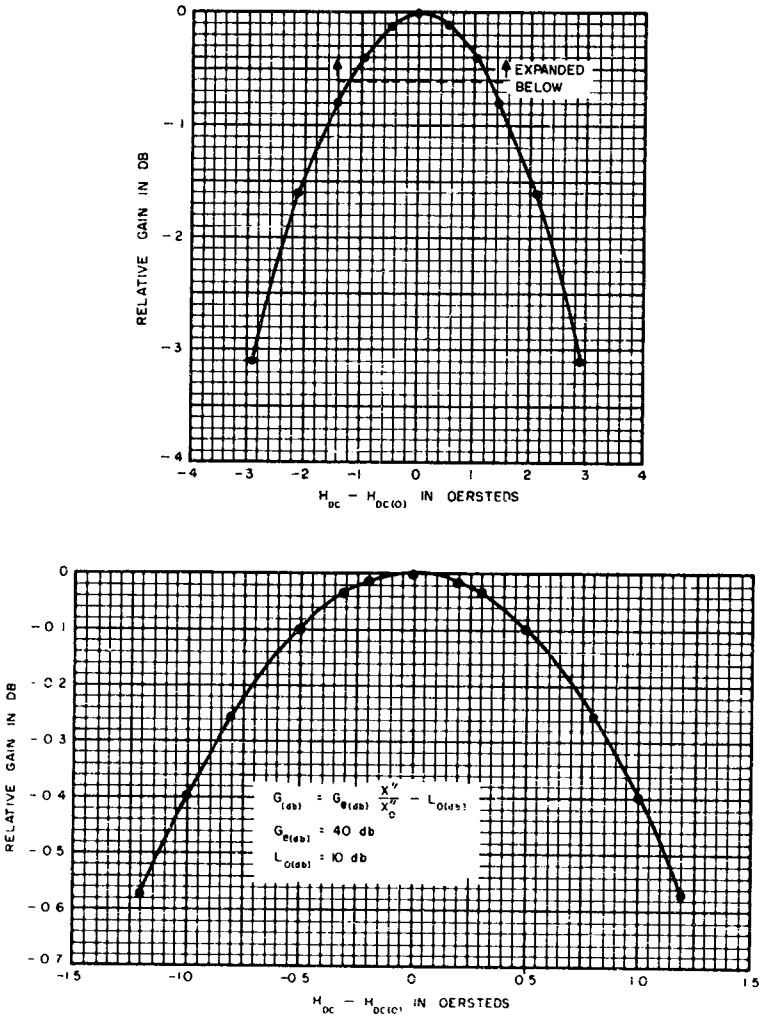



FIGURE 7 RELATIVE GAIN OF S-BAND TWM AS A FUNCTION OF DC MAGNETIC FIELD FOR MAGNETIC LINE WIDTH OF 20 OERSTEDS

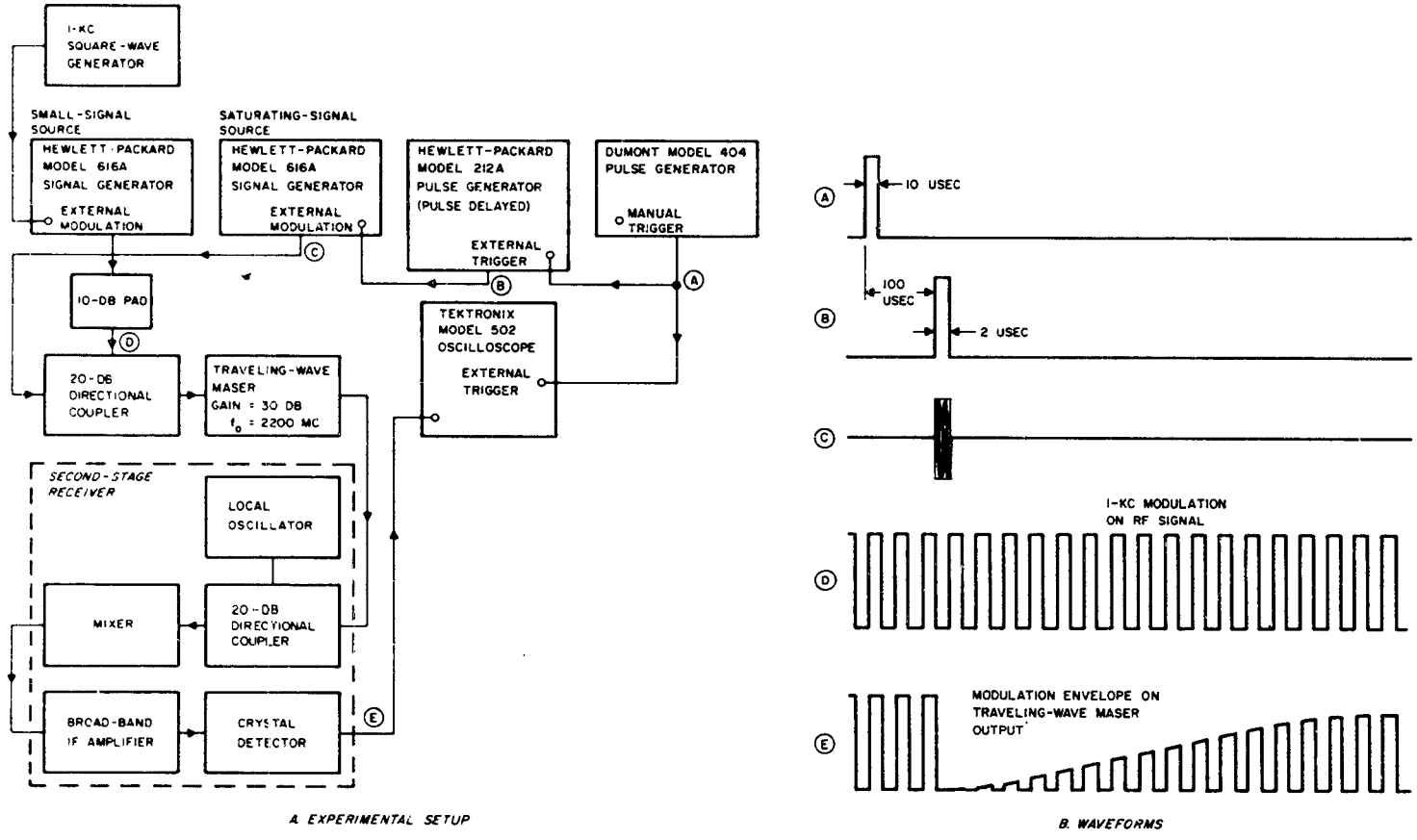



FIGURE 8 . MEASURING TWM GAIN RECOVERY TIME

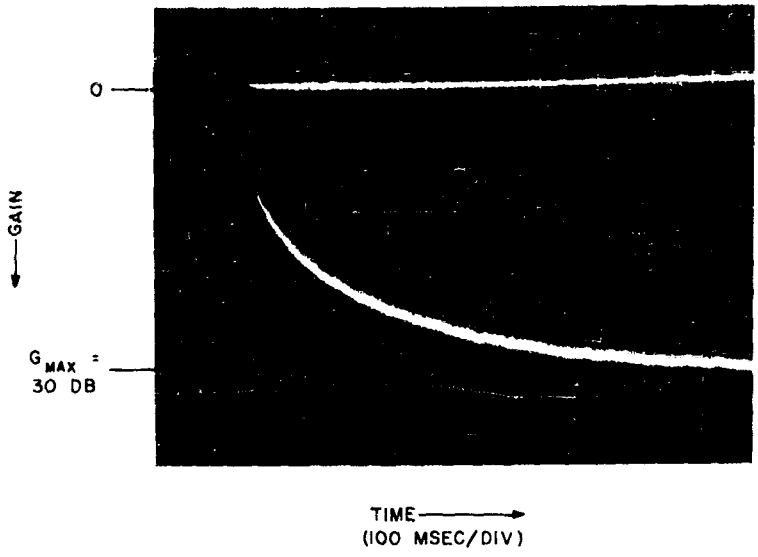



FIGURE 9 GAIN-RECOVERY CHARACTERISTIC

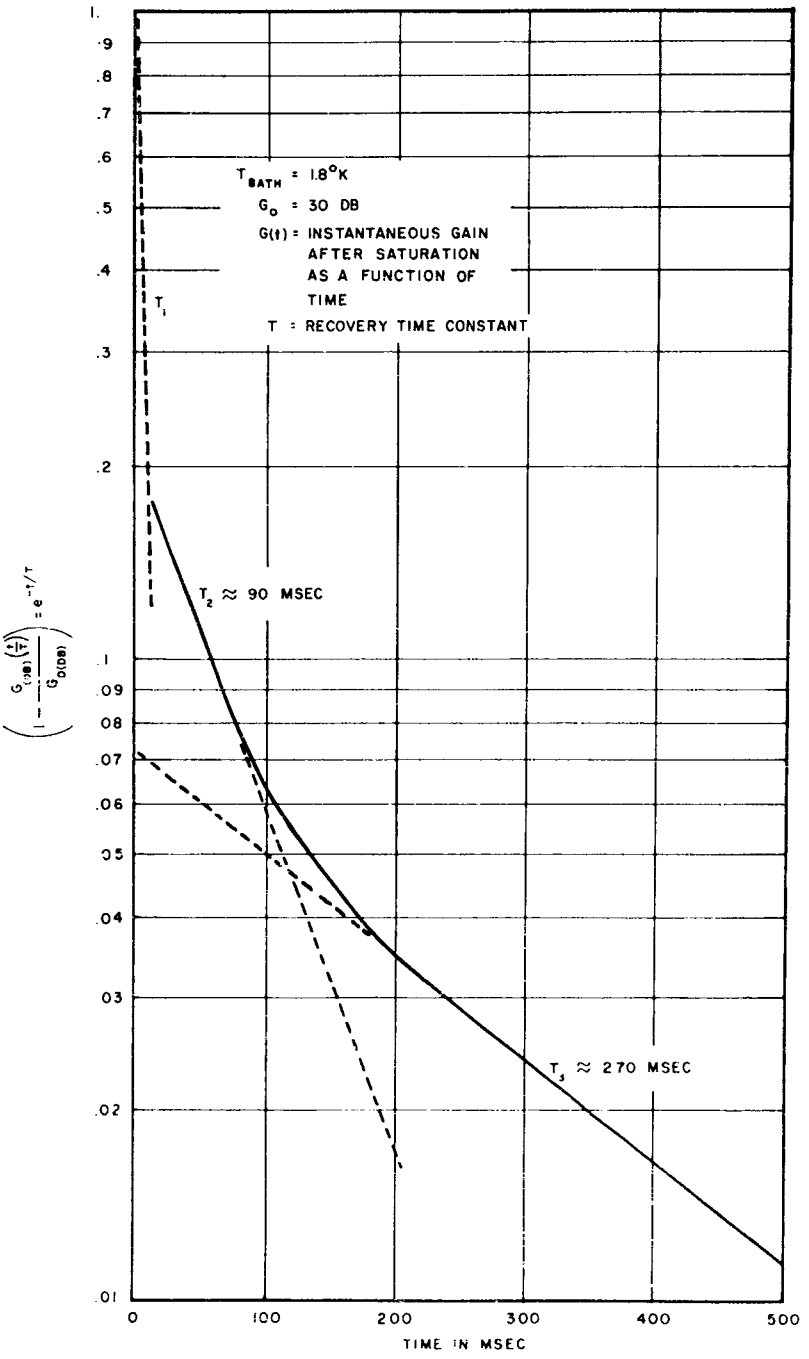



FIGURE 10 RECOVERY CHARACTERISTIC OF TWT

# FIELD EVALUATION OF THE NCEL INTERFERENCE-ATTENUATING POWER CONDUCTOR

D. B. Clark and J. L. Brooks
U. S. Naval Civil Engineering Laboratory
Port Hueneme, California

Abstract. - The field evaluation of a 4.0-mile installation of 13.2 KV, 3-phase, power distribution wires replaced with special interference-attenuating conductor developed at the U. S. Naval Civil Engineering Laboratory was completed in January 1961. The power line, wrapped with high-permeability tape was tested at the U. S. Army Electronic Proving Ground, Fort Huachuca, Arizona. NCEL engineers and technicians made survey measurements of the broad-spectrum electromagnetic interference (30 cycles per second to 1,000 megacycles) induced at the end of the line with large-impulse noise generators. The special line, with large magnitudes of interference at its beginning, is shown to attenuate effectively over the broad frequency spectrum to bring the noise level of the line down to the level of the natural ambient in about half the length of the line. A 30-kw load placed on the power line did not make any measurable change in its attenuating properties.

Impedance measurements of the power line as a transmission line showed it to be independent of line terminations, and that considerable attenuation was present.

Field intensity measurements made to determine the electrical-field profile with respect to distance from the line, showed that the intensity decreased rapidly in greater than inverse square with distance, indicating a field propagated along the line, with no measurable radiation away from the line.

Saturation effects on attenuation from large a-c and d-c power currents to the high-permeability metal tape wrapped on the test conductor, as measured in the laboratory are shown. The effect on attenuation of saturation currents with variation of the wrapped gap are described.

The effect of the high-permeability tape thickness on attenuation is considered theoretically and experimentally, and it shows that attenuation is proportional to tape thickness until the thickness is of the order of one "skin depth." The potential applications and limitations of the new interference suppressing line are presented.

Background. - At all points in space there exists an electromagnetic environment. Some of the parameters which can describe this environment include electric and magnetic field intensities, frequency, polarization, phase, and impedance. Our electronic communications and control systems are required to function properly in the presence of this environment, and the undesirable interaction of this with our systems is termed electromagnetic interference. Some of the means which are employed to protect vulnerable systems against potential interference include shielding and isolation, filtering, polarization, and circuit design.

Areas which are separated by considerable distance from any population centers, or industrial activities, generally have low-intensity electromagnetic environments. Such areas are usually chosen for the location of very sensitive electronic systems such as radio telescopes, and satellite and missile tracking systems because they are extremely vulnerable to electromagnetic interference. It is always necessary to supply and distribute electrical power for these installations, and this usually requires the use of power generated at some distance from the area.

Power transmission lines and other current-carrying conductors are utilized to deliberately conduct electromagnetic energy at power or signal frequencies from the point of generation to the desired area of their utilization. Unfortunately, when these conductors are in place, they are available to absorb electromagnetic interference energies and convey them with low attenuation into areas where they can become a critical problem in interference.

Current-carrying conductors can violate the integrity of electromagnetic-sensitive areas by complex combinations of three basic modes of propagation; radiation from the conductors as antennas, conduction of electrical currents by the conductors, and induction by magnetic and electrical fields associated with the conductors.

The first, radiation is probably the least of the offenders for extended lengths of transmission lines.[1] When a conductor antenna is many wavelengths long in one direction, the pattern of the radiated energy is that for a "long wave" or Beverage antenna and has its narrow, maximum lobe in the direction of the conductor. Interference can be avoided from this source by assuring that sensitive areas are not in line with long stretches of transmission lines.

For short sections of power lines where the length of line continuous in any particular direction is of the order of a wavelength or less, the radiation is broad beam and its effect is much harder to control.

Conducted interference from power lines is a serious offender. The line connects interference sources to sensitive loads by means of a direct low-attenuation connection. The fraction of available noise power delivered to a load at any particular frequency depends on the relationship of the load impedance to the impedance of the line, and the amount of noise power induced by the source depends on a similar relationship of the noise source impedance to the line impedance.

Mutual induction can couple noise energy from a line to other wiring and circuits such as a transformer couples from primary to secondary for the magnetic fields. The electric field gradients which exist around current-carrying lines can induce voltages in any conductors which intersect a portion of this electrical gradient.

Any noise currents on the power lines carry with them their associated magnetic and electric induction fields, components of which diminish, approximately, as the reciprocal square of the distance from the line. At low frequencies, penetration of these induction fields can be significant into the earth, into metal buildings, or other supposed shielding which has been effective at higher frequencies. Physical separation of about 600 feet from long lines is usually sufficient to obtain the natural ambient, at broadcast frequencies and higher.

Electromagnetic energies which use power line conductors as a propagating mechanism have a choice of several modes. For a long line where discontinuities are neglected, the propagation is considered as Principal Wave (TEM wave). For this mode the conductors act in pairs, with one as a go and the other as a return. With a multiwire line, numerous combinations are possible, including all of the wires as a go and the earth as a return. The preferred combination, or the one which propagates the greatest energy at any particular frequency, is the one with lowest impedance.

With one conductor as a current go and another as a return, the external field at a remote point, a great distance away compared to the distance between conductors, is essentially zero. This is because the two currents, 180 degrees out of phase are nearly superimposed, and their field components cancel at a distance. Where the conductors are far apart compared to their distance from a point in question, the induced field can be of much greater intensity. Relating this to the case of a power line, induced fields of the modes which have the earth as a return conductor can have greater intensities near the line than fields from closely spaced pairs.

The natural attenuation which interference experiences on power conductors is due to the loss resistance, a combination of the d-c and a-c resistance of the conductor. For good conductors, such as copper and aluminum, the d-c resistance is very small, determined by the resistivity and size of the wire. The a-c resistance is proportional to the square root of the frequency, permeability, and resistivity, but for a good conductor does not become an appreciable factor until very high frequencies are reached.

The increase of a-c resistance with frequency is due to a crowding of the a-c current towards the skin of the conductor which is known commonly as skin effect. By providing a high permeability coating for the conductor, this skin effect can be greatly enhanced, to increase the value of the a-c resistance significantly. This effect is derived in detail in Appendix A.

A large loss resistance for the power line conductor effects the reduction of interference due to the power line in several ways. Conducted interference is burned up as a heat loss, and the amount of noise energy delivered to the sensitive loads, thus greatly reduced.

The radiated and absorbed energy is reduced, because of greater antenna losses due to this increase in a-c resistance, and due to the increase in impedance of the line compared to the load and radiation impedances. This effect can be examined in detail in Appendix B.

## I. INTRODUCTION

Field tests were conducted at the U. S. Army Electronic Proving Ground, Fort Huachuca, Arizona, by personnel from the U. S. Naval Civil Engineering Laboratory. To determine the radio frequency attenuation and propagation characteristics of a special interference-attenuating conductor developed at NCEL, the conductor was installed on an actual power line. Laboratory test results and a theoretical treatment of this special conductor were previously reported.[2] Fort Huachuca, Arizona was chosen as the test site because personnel at the proving ground were currently involved with interference problems presented by noisy power lines and were very interested in NCEL's efforts to control it. They supported the test by providing one of their existing power line installations for test, by providing men and equipment to install the experimental power line conductors, and by giving logistic support in the tests.

USAEPG personnel independently made extensive field intensity measurements on and near the untreated power line 21 October to 7 November 1960 and later, 14 November to 22 November 1960 with the conductors taken down and removed. A third set of measurements was made 19-28 December 1960 after the conductors wrapped with high permeability tape were installed. Peak noise measurements were made during these three test periods. The results of these tests will be reported separately by the U. S. Army Electronic Proving Ground, Fort Huachuca, Arizona.

The transmission line made available for use at Fort Huachuca was an isolated 13.2 KV 3-conductor 3-phase power line approximately 5 miles long. The conductors were #6AWG annealed copper strung on wooden poles and crossarms. The pin type insulators installed were of the radio freed variety which have a conductive glaze fired on portions of the inner and outer surface. The line delivered power to a bunker in the USAEPG east range artillery impact area. The power line runs parallel to the southern edge of the range for 4-$\frac{1}{2}$ miles, makes a 100-degree turn, extends for 2100 feet then goes through step-down transformers into an underground cable which runs beneath the impact area to the bunker. The poles were spaced about 300 feet apart and were given consecutive identification numbers from 0-76 beginning with the transformers at the end of the overhead line.

Fort Huachuca is in a high-altitude desert area, dry except for part of the summer months. The area is subject to severe lightning storms during the year, particularly during the summer. As protection against lightning, the power line has a fourth wire which runs along the tops of the poles and is grounded at each pole. The ground conductor extends approximately six feet into the ground at each pole and is wound helically around the pole base. The presence of this fourth ground wire complicated analysis and affected some of the test results.

## II. IMPEDANCE MEASUREMENTS

Tests at NCEL

The characteristic impedance and attenuation of a transmission line may be determined by first measuring the impedance at the sending end with the receiving end short-circuited, then measuring the impedance with the far end open-circuited.

The following equations are then used to calculate the characteristic impedance, attenuation, and phase shift of the line using the two measured impedance values.[3]

$$Z_o = \sqrt{Z_s(s)\, Z_s(o)} \qquad (1)$$

$$\alpha + j\,B = \frac{1}{2L} \ln \left[ \frac{1 + \sqrt{\frac{Z_s(s)}{Z_s(o)}}}{1 - \sqrt{\frac{Z_s(s)}{Z_s(o)}}} \right] \qquad (2)$$

where
- $Z_o$ = characteristic impedance
- $\alpha$ = attenuation in nepers
- B = phase shift in radians
- L = length of line in miles
- $Z_s(s)$ = short-circuit sending end impedance
- $Z_s(o)$ = open-circuit sending end impedance

With the transmission line measurement approach in mind, a laboratory test setup was constructed in the 100-foot steel-shielded building at NCEL. A diagram of the test apparatus is shown below. A 94-foot length of the wrapped conductor to be tested was strung between the two end walls of the building near the center. The shell of the building itself comprised a coaxial return for the signal path.

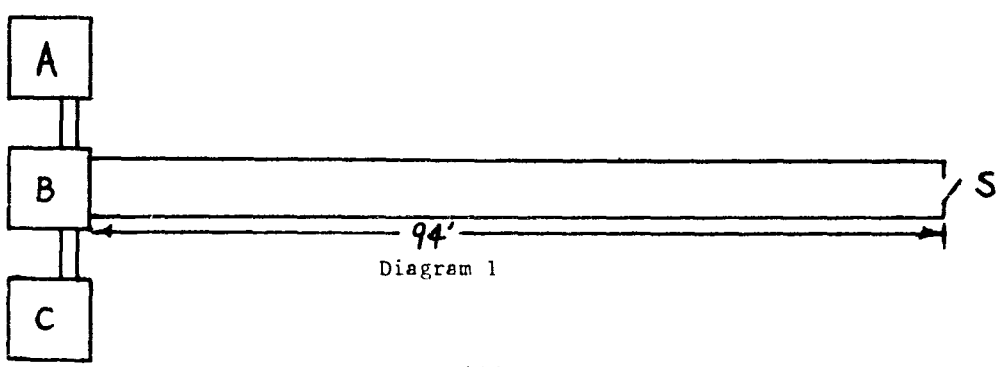


Diagram 1

A = radio frequency signal generator
B = radio frequency impedance bridge
C = sensitive null detector
S = shorting switch

The Laboratory computer was programmed using the equations described previously to reduce the complex measurement data to values of attenuation, phase shift, and characteristic impedance.

The approach taken to determine the power current effects on radio frequency characteristics is similar to the previously mentioned method, with the exception that large power currents (both a-c and d-c), were passed through the wrapped conductor to determine their saturation effects. This required a modification of the test setup as shown below.

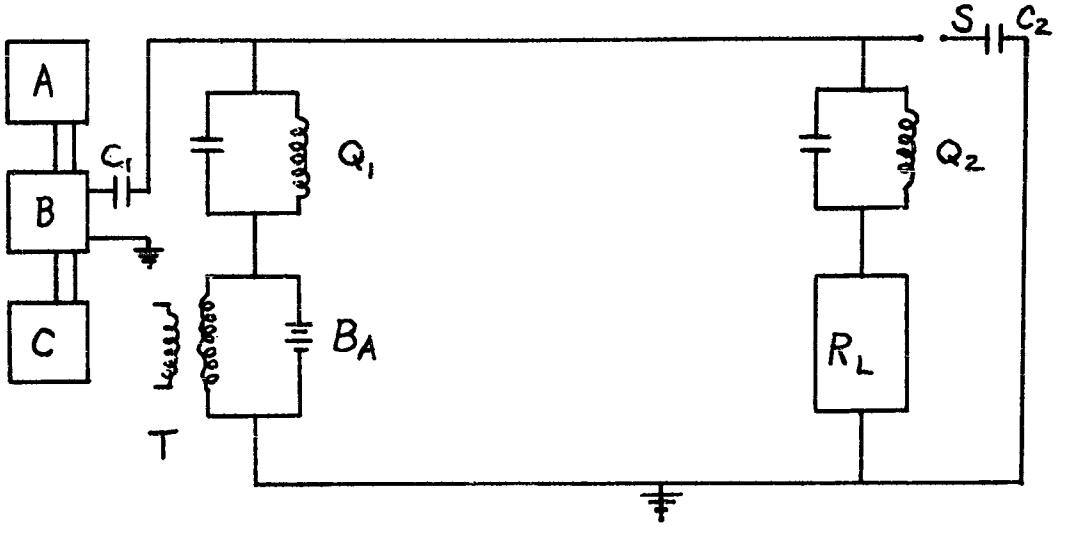



Diagram 2

A = radio frequency signal generator
B = radio frequency impedance bridge
C = sensitive null detector
$C_1$ and $C_2$ = power-current-blocking capacitors
$Q_1$ and $Q_2$ = radio-frequency-blocking impedances
T = 60-cycle power transformer
$B_a$ = d-c power supply
$R_L$ = power current load

With this arrangement, it was possible to run power current and r.f. current simultaneously in the wrapped conductor without damaging the sensitive r.f. bridge. Since these large power currents had to pass through the tuned circuit coils, it was necessary that they be constructed of large diameter wire.

The tuned circuits presented a loading effect to the r.f. circuit which had to be compensated for in the data analysis.

Results of measurements of attenuation and impedance made on a 94-foot test piece of the line to be used at Fort Huachuca, are shown in Figure 1. Construction of this special conductor is shown in Figure 2. It has a 7 mil thick, silicon-iron, high permeability tape wrapped with a nominal 10 mil gap on #6AWG copper conductor. The results of the power current effects on the r.f. characteristics are shown in the curves in Figure 3 and 4. The conductor described in Figure 3 was that shown in Figure 2. The conductors described in Figure 4 were made of $\frac{1}{4}$-inch copper tubing wrapped with $\frac{1}{4}$-inch wide high permeability metal tape having a thickness of .004 inch.

These curves show very little difference between a-c and d-c power current saturation effects. However, there is a definite saturation effect due to the flow of power current, and the smaller the gap the higher the attenuation and the more susceptible to saturation the line becomes. Conversely, the wider the gap, the lower the attenuation becomes, and the less susceptible is the line to saturation effects. It should be noted that even though the smaller gap is more affected by saturation, its attenuation curve at 1 mc remains higher than those of the wider gaps, throughout the range of currents applied.

The next point of importance to be derived from these curves is the range of currents at which the major loss in attenuation is suffered. this seems to be between 5 and 20 amperes a-c or d-c.

## Tests at Fort Huachuca, Arizona

The tests at Fort Huachuca were performed on an actual high-voltage 3-phase line. It was intended that measurements on the line be made in the same manner as performed in the Laboratory at NCEL. The problem, however, was considerably more complicated, because there were now three conductors and a static ground wire and the earth as a return.

To make impedance measurements, the power to the line was cut and air switches were inserted (one in each phase) at approximately 4-$\frac{1}{2}$ miles from the transformer bank on pole 76. Then, by attaching a 4-foot-wide phosphor bronze screen to the three overhead power conductors a connection to the impedance bridges was made by means of a low-impedance lead. A reference ground was established by laying about 60 feet of the 4-foot-wide screen on the ground perpendicular to the line. The far end was terminated by disconnecting from the transformers and connecting to ground for short-circuit measurements, and by leaving the wires disconnected for open-circuit measurements.

## Procedure for Bare Line Impedance Measurements, June 1960

The impedance measurements were divided into three main groups, each group having three parts.

Test 1. This test was made in order to learn the effect of the transformer bank on the line impedance; consequently, the transformers were left connected for this test. The following three conditions (the same for all 3 tests) were tested:

Phase (a) 3 wires as go, earth return, ground wire floating
Phase (b) 3 wires as go, ground wire and earth return
Phase (c) 4 wires as go, earth return

Tests 2 and 3. These tests comprise the open-circuit, short-circuit tests. The transformer bank was disconnected, and the lines were all shorted to ground for Test 2. The lines were tied together but left hanging free for Test 3.

Results of Bare Line Impedance Measurements.

The results of Test 1 are plotted in Figure 5; these curves show that with the transformer bank connected the difference between the three phases is almost negligible. The results of Tests 2 and 3 gave the characteristic impedance and attenuation. These were computed and are plotted in Figures 6 and 7, for each of the three phases.

A comparison of the curves for the three different conditions shows little difference between phase (a) and phase (b). However, there was a noticeable change when the ground wire was connected to the other three as a go, phase (c). This difference is caused in part by the fact that the ground wire was grounded at each pole. The attenuation values shown in Figure 10 were obtained by using the measured impedance data in equation (2). Equation (2) was derived from the following relation:

$$\tanh[(\alpha + j\beta)L] = \sqrt{\frac{Z_s(s)}{Z_s(o)}} \qquad (3)$$

Procedure for Wrapped Line Impedance Measurements, January 1961

The special wrapped line was installed on the east range power line at Fort Huachuca prior to the arrival of NCEL personnel on January 9. The three current-carrying conductors of the three-phase line were replaced by the special wrapped line from pole 0 to 69, approximately 4 miles. The overhead ground wire was left in its original state.

An inspection of the installation showed that the outside, vinyl, weather-protective wrapping had been severed in numerous places along the line during installation. The wind had unraveled some of this covering, leaving streamers hanging from the line. These were repaired before testing began. Since no significant results other than attenuation data were obtained in the June 1960 tests with impedance measurements, very little time was allotted to them on the January 1961 test.

Therefore, with the wrapped line, only the open-circuit and short-circuit impedance measurements in phases (a) and (b) were repeated to obtain attenuation data. The hookup and test procedure were exactly the same as those for Tests 2 and 3 described earlier. Measurements were made from the same location, pole 76, as previously, since the line could be disconnected conveniently at this point. This meant that 2100 feet of untreated line preceded the 4 miles of wrapped line.

Results of Wrapped Line Impedance Measurements.

The results of these tests are shown in Figures 8 and 9. It is worthwhile noting that the wrapped line shows very little difference between the open-circuited and short-circuited configurations. This is an indication of large losses in signal strength in the wires, resulting in weak reflections at the sending end, and a more effectively infinite line.

## III. FIELD INTENSITY MEASUREMENTS

### Measurements on Bare Power Line, June 1960

Procedure for Interference Survey of Bare Line. A survey was made, in June 1960, of the electromagnetic noise field in the vicinity of the original untreated 13.2 KV power line. Measurements of noise intensities, in the frequency range 14 kc to 400 mc, were made, using standard-specification EMI meters;[4] these meters are listed in Table 1.

The receivers were mounted and transported in an Army 3/4-ton truck and trailer. An interference-suppressed AN/GSA-14 gasoline-powered generator provided filtered power at 120 volts a-c 60 cycles. Measurements were made at pre-selected locations under and near the power line. Field intensity levels at selected frequencies in the spectrum of interest

Table 1. EMI Meters Used in Field Intensity Measurements

| | Serial No. | Frequency Range |
|---|---|---|
| AN/URM-41 | 301-21 | 20 c - 15 kc |
| AN/URM-6 | 159-7 | 14 kc - 150 kc |
| AN/PRM-1 | 140-6 | 150 kc - 25 mc |
| AN/URM-47 | 208-36 | 25 mc - 400 mc |
| AN/URM-17 | 155-26 | 400 mc - 1,000 mc |

were recorded for receiver detector settings of Peak, Quasi-peak, and F.I. (average). All other frequencies in the range were monitored, and the intensity levels from unidentifiable noise sources were recorded in addition to the pre-selected frequencies.

Three power-line insertion filters, developed for the Laboratory by a manufacturer, to pass the power currents but to attenuate higher frequencies, were inserted in the power line for evaluation.

The field measurement survey included locations on either side of this filter installation. The Quasi-peak intensity measurements, taken in this survey (corrected by various factors of the particular receivers and antennas) and levels of instrument internal noise are plotted in Figures 10 and 11.

Results of Interference Survey of Bare Line.

The interference survey shown in Figures 10 and 11 indicates that the noise level of the line increases slightly as the power source end is approached (pole 76-77). The noise measured was determined as random noise. At pole 76 and beyond, the test line approaches (within 100 feet) and runs parallel to a 13 KV feeder line from the Sulphur Springs Valley Electric Company which furnishes power to Fort Huachuca. Figures 10 and 11 show that noise measurements made near this feeder line have the same general distribution in frequency as those on the east range 13.2 KV line, and that noise appears to be from the same sources. The power isolation filters located at pole 7 gave about 20 db of attenuation below 1 mc. Above 1 mc their attenuation decreased with increase in frequency. These filters were left in the line, and were subsequently struck by lightning. No provision had been made to provide an arc-over gap for lightning protection. One filter was destroyed by the lightning, another badly burned in the fire that resulted, and the third was unharmed (see Figure 12).

Wrapped-Line Field Strength Measurements, January 1961.

Procedure for Interference Survey of Wrapped Line. Upon arrival of the NCEL test personnel, a preliminary investigation for possible noise sources along the newly installed experimental line was made, using the battery-operated AN/PRM-1. The noise levels encountered were very low. A survey was then made (in the frequency range 14 kc to 1,000 mc) of the electrical component of the field intensity vector at several locations using the EMI meters shown in Table 1, mounted in an Army 3/4 truck and trailer. These locations were 2100 feet from the beginning of the experimental line (pole 76) under the untreated portion of the distribution link, at the point where the new line began (pole 69), two miles down the new experimental line (pole 33), 3-1/3 miles down the new line where it changes direction 100 degrees (pole 7), and at a point 2100 feet out perpendicular to the line at pole 7. (This latter location was chosen to establish the natural ambient away from the line.) Readings were taken along the line at mid-span, directly underneath the conductors, at an approximate ground plane height of 3 feet.

Results of Survey of Wrapped Line. Processed electrical field intensity readings for the preliminary survey in units of microvolts per meter per kilocycle bandwidth, Quasi-peak, are shown in Figure 13. They are compared to the internal noise of the meter converted to similar units with the exception of the antenna factor, and a power-line-interference reference line which has been presented in a recently suggested revision to MIL-I-16910(A) BUSHIPS Interference Limits and Specifications.

The levels shown were essentially those of the internal meter noise above 400 kc. They were considerably less than the levels of noise intensity for this frequency range measured in June 1960, and showed the need for a strong noise source if the effect of the wrapped line was to be assessed adequately.

Wrapped-Line Field Intensity Measurements, January 1961 Using Noise Generators. The accurate measurement of attenuation (on a line where the attenuation rate with distance is significant) requires the availability of sufficient initial signal field strength to make readings at several locations along the line. Since it was desirable to determine attenuation properties over a wide band of frequencies, from 60 cycles through 1,000 megacycles, and the available noise levels found on the line were very low, it was necessary to provide a strong signal source which could generate this range of frequencies. Another requirement, for accurate measurements of signal along the line, was a means of coupling a signal source over this wide band of frequencies into the line while it was hot, without generating erroneous signal components from the coupling itself.

All of these requirements were satisfied by the use of three impulse generators which were powered by the high electric gradient existing around the energized power conductors (see Figure 14). The generator consists of an adjustable gap in a short length of electrical conductor which intersects the electrical voltage gradient around the power conductor. The large copper sphere is added to provide more capacity (and thus more energy) to the impulses generated. The increase in capacity also provides a control on the arcing at the gaps, such that a single discharge, a few miscroseconds in duration, is generated on each half-cycle of the power voltage, rather than numerous arcs during each half-cycle. The generators were installed with the power line energized, and the gaps adjusted for continuous arcing.

The interference level from the generators was monitored several times each day directly under the generators with the AN/PRM-1 receiver at 1.05 mc, in the Peak, Quasi-peak, and field intensity positions, and recorded levels were essentially constant.

Electrical field intensity measurements were made using the EMI meters shown in Table 1. An operator was provided for each meter, and an attempt was made to take readings at each successive location in exactly the same way and with the same physical arrangement. Two vehicles carried the two AN/GSA-14 suppressed generators which were located 200 feet away from the line at each location, on opposite sides of the line. Meters were set up directly under the center of the span in two sets, approximately 20 feet apart, and powered by separate generators.

After a set of intensity measurements was made under the line (which was under no load except for the reactive charging currents), a 30-kw resistive load was added at the line end. A repeat of measurements at several locations was made.

At several locations, measurements were repeated with the EMI receivers, located 25 feet outboard at center span of the outermost line conductor. This was done to compare line noise to the limits suggested in a new revision of MIL-I-16910(A) Interference Specifications. In addition, measurements were made at larger distances from the line in an investigation of the profile of electrical field intensity as a function of distance from the line.

Results of Field Intensity Measurements Using Noise Generators. Smoothed curves of the electrical field intensity measurements as a function of frequency at the various locations are shown in Figures 15 and 16. The frequency distribution of the noise provided by the impulse generators is shown and is similar in the lower portion of the spectrum to the noise on the bare line measured in June 1960 (see Figure 10).

The measurements of electrical intensity as a function of distance away from the line, shown in Figures 17, 18, and 19 demonstrates a very rapid diminution of intensity, with no further decrease beyond 300 feet from the line.

To determine values of attenuation by the wrapped line from field intensity readings of the broad noise generated on the line, measurements over the frequency spectrum were made at 11 separate locations under the line. The physical setup of instruments and measurement procedures were duplicated at each location. Each point on the attenuation curve, for the wrapped power line was obtained from intensity measurements, and represents a slope, determined by a least squares fitting from readings at these 11 locations (Figures 20 and 21). Two sets of readings were taken, at some locations, to include data from loading the line with a 30-kw resistive load, but no measurable difference was detected in the intensity readings. These attention curves, Figures 20 and 21, show considerable attenuation in frequencies above the audio range, with increase in attenuation proportional to the square root of frequency, and some attenuation at audio frequencies, starting with the second harmonic of 60 cycles. The dispersion of readings at the audio frequencies was much greater as a result of the effects of standing waves at frequencies where the attenuation was lower and the point sampling which resulted from the limited number of measurement locations. The attenuation curve for the wrapped line is compared to values obtained for attenuation on the bare line from field intensity and impedance measurements and the means of determining the particular values indicated in Figure 21. The dispersion and inherent error in the bare-line attenuation measurements, determined from intensity measurements, was greater than for the wrapped line as a result of reflections and standing waves.

## IV. EARTH-RESISTIVITY MEASUREMENTS

### Procedure

As described by Sunde[5], the earth resistivity may be measured from four conducting rods driven into the earth, as shown in Figure 22.

The equation for the earth resistivity $\rho$ as derived from this configuration is:

$$\rho = 2\pi a \left(\frac{V}{I}\right) \qquad (4)$$

where $\rho$ = earth resistivity in meter-ohms
a = distance between ground rods in meters
V = potential between center rods in volts
I = current entering rod 1 and leaving rod 2

An instrument was constructed at NCEL which would accurately make the measurements indicated above. It contained a potentiometer to measure the voltage, which in practice was quite small, ranging from .001 volt to .015 volt.

Dry-cell batteries were used for the power supply, and a switching network was included to provide reverse polarity readings to overcome the effect of stray ground currents and polarization at the rods.

Results

During the first test at Fort Huachuca (June 1960), an attempt was made to measure earth resistivity by using a milliammeter and a vacuum tube voltmeter. The readings obtained were unusable due to ground currents, polarization of the ground rods, and inaccuracy in reading voltages.

For the next test (January 1961), preparations had been made for better instrumentation, and the measurement activity proceeded smoothly. Extensive resistivity tests were made on the ground beneath the line, and along its entire length. These tests gave an average value of $86.56 \pm \sigma_1$ meter-ohms for a depth of 30 meters and an average value of $68.87 \pm \sigma_2$ meter-ohms for a depth of 10 meters, where $\sigma_1 = 24.715$ and $\sigma_2 = 22.712$.

## V. CONSIDERATIONS CONCERNING HIGH-PERMEABILITY TAPE THICKNESS

Procedure

A theoretical treatment was made to determine the optimum tape thickness for a given permeability. The following equation, derived by Ramo and Whinnery[6] to describe the surface impedance of a coated conducting material, can be applied to the condition of a coated conductor where the thickness of the coating is small compared to the conductor diameter:

(5)

$$Z = \frac{R_{S_1}(1+j)}{2\pi r}\left[\frac{\sinh(T_1 d) + K_2/K_1 \cosh(T_1 d)}{\cosh(T_1 d) + K_2/K_1 \sinh(T_1 d)}\right]$$

where $\bar{Z}$ = complex impedance of coated conductor
$R_{s1}$ = resistance per square of coating material
$R_{s2}$ = resistance per square of conductor material
d = thickness of coating material
$\tau_1 = \frac{(1+j)}{\delta}$ $\qquad \delta = \frac{1}{\sqrt{\pi f \mu_1 \sigma_1}}$ = skin depth
$\sigma_1$ = conductivity
$\mu_1$ = permeability

It can be shown that the attenuation of a transmission line is directly proportional to the a-c resistance of its conductors.[3] For this reason, the real part of the complex line impedance - the a-c resistance - is plotted in Figure 23, against tape thickness for various frequencies at a fixed permeability.

Results

It is apparent from the curves in Figure 23 that the higher the operating frequency the less the tape thickness required to obtain the maximum attenuation for a given permeability. However, below the knee of the curve, the thicker the tape the more the attenuation. And the higher the permeability the more rapidly the maximum attenuation is reached.

The inference from these curves is that the attenuation is proportional to the thickness of the tape up to the point where the skin depth is approximately equal to the tape thickness, after which the attenuation is essentially independent of the tape thickness.

A 100-foot, $\frac{1}{4}$-inch, copper conductor was wrapped with a single and then double layer of the 4-mil tape used for attenuation measurements in previous tests, and its attenuation was measured at 1 mc as a function of saturation current. The results of this test are shown in Figure 24. It shows that doubling the thickness of the tape essentially doubled the attenuation.

## VI. SIGNIFICANT FINDINGS AND DISCUSSION

Impedance Measurements

The transmission line type impedance measurements made on the power line under test at Fort Huachuca were intended to provide additional information on the attenuation of the line. Where line losses were low, as were those on the original bare power line made in June 1960, the resulting values of attenuation (derived for the frequency range 70 kc to about 30 mc) followed a logical trend and were very close to values of attenuation, for the bare line, derived from a measure of relative field intensities of the noise on the line. These are plotted in Figure 21 and are derived from an average of values obtained for phases (a) and (b) shown in Figure 7.

The wrapped-line impedance measurements, made in January 1961, resulted in values which varied so slightly with changes in the line terminations, that the ideal transmission line equation did not yield results, except at the extreme low end of the frequency range in which impedance measurements were made (Figure 21).

Of the several combinations used in connecting the static ground wire at the measuring end, the smoothest impedance phase and attenuation curves were obtained, in phase (b), by leaving the static wire untouched, and measuring from the connection of the three power conductors to the earthed ground plane. This corresponded to the mode which was driven by the noise generators.

Field Intensity Measurements

The noise measured on the power line chosen for test at Fort Huachuca was greatest on the end of the line which was closest to other power lines, and residential sources. The spectrum distribution and level of intensity of noise on the commercial Sulphur Springs Valley Electric Company line, which comes within 50 to 60 feet of one end of the tested line, was similar to that measured on the test line at the point of closest approach (pole 76); this implies that they were energized by common noise sources or by coupling noise from one to the other. This line noise was considerably higher in June 1960 than it was in January 1961 (compare Figures 10 and 13). This is probably due to static from thunder storms prevalent during summer months but lacking during the winters. This was very beneficial to the wrapped-line tests, as it allowed measurements of attenuated noise intensity to lower ambient levels.

The significant intensity measurements, which show clearly the effect of the wrapped line, can be seen in Figures 15 and 16 where the intensity under the line near the impulse generators is compared to 1800 feet down the bare line, 1800 feet down the wrapped line, 1/2 mile and 3 miles down the wrapped line. The level from the noise generators, after 3 miles of the wrapped line, is down to the natural ambient over the range of frequencies shown, 10 kc - 1,000 mc. The ambient level is shown in Figure 13 for 2,000 feet south of the line at pole 8.

Also significant is the low level of noise intensity measured 400 feet perpendicular to the long line near the noise generators (Figure 15). It shows that a few hundred feet of space from a very noisy, long, power line is very effective in providing isolation for equipment from the large intensity levels found under and very near the line.

Attenuation Measurements

The full capabilities of the attenuating effects of this new line were not realized in the Fort Huachuca installation, since the overhead static ground was left unwrapped.

But, it demonstrates what the developed line will do in the presence of an untreated conductor.

The attenuation curve, obtained from field intensity measurements shown in Figure 21 for the wrapped line, represents a least-squares fit to a set of points. Each of these points in turn represents a least-squares fit which determined a slope for the relative electrical intensity readings taken at the 11 locations along the wrapped line, at each of the designated frequencies. The slope of the attenuation curve (.458) is very nearly the square root of frequency; this was suggested by an earlier study[2] of attenuation by a long, wrapped conductor isolated in space, part of which is reproduced in Appendix A. The attenuation of this line is significantly greater, with the new, wrapped conductor in place, than with the original untreated line.

The dispersion of the readings in the audio frequency range (Figure 20), where the attenuation is much less for the wrapped line, is considered to result from standing waves and from taking measurements at a limited number of locations. However, even in this low range of frequencies, the attenuation by the lossy line is equivalent to that of the bare line at frequencies 10,000 times higher. Although measurements were made at 30 and 60 cycles per second, the dispersion was large, and the resulting attenuation slopes were too low to be shown on this graph.

## VII. CONCLUSIONS

This newly developed line should be very useful, in reducing power line noise to ambient level, where two or three miles or more of line are available for installation of an isolating section of this wrapped conductor.

Although the Fort Huachuca test was conducted with #6AWG conductor wrapped with a 7-mils-thick tape, and installed on a 13.2 KV line there is no indication that other conductor sizes and tape thicknesses could not be used, and installed on lines of different voltage. The cost of this particular developmental line was approximately $1,000 per mile of conductor, and was fabricated for the Laboratory by Genistron, Incorporated, Los Angeles, California. Future purchases of this line will specify an extruded (rather than wrapped) insulation coating at an expected reduction in price, with an anticipated improvement in mechanical strength, and with improved wear and corrosion resistance.

## VIII. RECOMMENDATIONS

It is recommended that, during the preliminary design stages of new power installations for electromagnetically sensitive areas, an ambient noise survey be conducted in the area. The survey should cover the broad frequency spectrum and include any specific frequencies to be used at the site. To be most effective, it should monitor over 24-hour periods, and should represent sample measurements throughout the year.

This will establish the minimum noise level for later interference control measures. Further, in designing these new installations, power distribution lines should be considered as antennas and be arranged so that sensitive equipment layouts will not lie in the path of the main lobes of these antennas. Where noisy electrical equipment must be included in the area, provisions should be made for containing it in an isolated shielded enclosure with filtered power connections, or with blocking filters in the line.

It is also recommended that any overhead, high-voltage, distribution lines be constructed with radio-freed insulators and non-metallic crossarm braces, and be strung with special lossy conductors such as described in this report.

## ACKNOWLEDGEMENT

The authors wish to express appreciation for the excellent support given to their tests by military and civilian personnel at the U. S. Army Electronic Proving Ground, Fort Huachuca, Arizona, and in particular to Mr. W. R. Foley, Frequency Coordinator, for his advice and help with the arrangements. In addition, the help in January 1961 tests of Mr. Edill Rivera provided by Genistron, Incorporated, Los Angeles, manufacturers of the wrapped line, is acknowledged.

## REFERENCES

1. Jenssen, M. "On Radiation from Overhead Transmission Systems." Proceedings, The Institute of Electrical Engineering, Part III, Vol. 97 (1950), Pp. 166-78.
2. U. S. Naval Civil Engineering Laboratory. TR-062, Contiguous Wrapping of Transmission Line Conductors with High-Mu Tape for Large Radio-Interference Attenuation, by D. B. Clark and R. D. Hitchcock. Port Hueneme, California, 7 March 1960.
3. Johnson, W. C. Transmission Lines and Networks. McGraw-Hill Book Company, Inc., New York, 1950. Pp. 115-116, 144.
4. Bureau of Ships, Specification MIL-I-16910(A), Interference Measurement, Radio, Methods and Limits. 30 August 1954.
5. Sunde, E. D. Earth Conduction Effects in Transmission Systems, 1st Ed. D. Van Nostrand Company, Inc., New York, 1949. Pp. 44-46.
6. Ramo, S., and Whinnery, J. R. Fields and Waves in Modern Radio. Wiley & Sons, New York, 1953. Pp. 249-250.
7. U. S. Army Electronic Proving Ground. Technical Memorandum, Measurement of Electrical Noise at the U. S. Army Proving Grounds, by W. R. Foley. Fort Huachuca, Arizona, February 1961.

## BIBLIOGRAPHY

1. Hinchman Corporation. Field Study of Electromagnetic Interference from High-Voltage Transmission Lines. Detroit, Michigan, 1957.
2. Hund, A. Short Wave Radiation Phenomena Vol. I and II. McGraw-Hill Book Company, Inc., New York, 1950.
3. NCEL. TR-033, Some Theoretical Considerations Concerning Radiation from Overhead Transmission Lines, by A. M. Intrator. Port Hueneme, California, 28 June 1953.

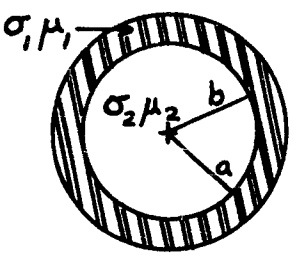
4. Skilling, H. H. Electric Transmission Lines. McGraw-Hill Book Co., Inc., New York, 1951.
5. Smythe, W. R. Static and Dynamic Electricity. McGraw-Hill Book Co., Inc., New York, 1950.
6. Zinn, M. K. "Wave Propagation Over Continuously Loaded Wires." Bell System Technical Journal, Vol. 9, 1930.

Appendix A

DERIVATION OF INTERNAL IMPEDANCE FOR CYLINDRICAL COPPER CONDUCTOR COATED WITH HIGH-MU MATERIAL

*Reprinted, with additions, from NCEL TR-062

The internal impedance per unit length for a cylindrical conductor is defined as the ratio of the tangential component of the electric field at the outer surface to the total current in the conductor; thus,




$$Z_s = \frac{[E_z]_{r=b}}{I} \qquad (6)$$

$\mu_1$ = permeability of coating

$\mu_2$ = permeability of conductor

$\sigma_1$ = conductivity of coating

$\sigma_2$ = conductivity of conductor

where b is the outer radius of the high-$\mu$ coating as shown in the schematic above. Field and current components are expressed in cylindrical coordinates, r, $\phi$, z; the z axis is parallel to the axis of the conductor.

Expressions for $E_z$ and I are found by solving the second-order partial differential equation for the current in the conductor. This differential equation is:

$$\nabla^2 \vec{i} = j\omega\mu\sigma\vec{i} \qquad (7)$$

Where $\mu$ and $\sigma$ are the permeability and conductivity of the conductor and $\vec{i} = \vec{i}_0 e^{j\omega t}$ = current density (amperes per unit area). In solving Equation 7 it is assumed that

$$\partial/\partial z = 0$$

$$\partial/\partial\phi = 0$$

$$i_r = 0$$

$$i_\phi = 0$$

Therefore, in cylindrical coordinates,

$$\nabla^2 \vec{i} = \vec{a}_z \left( \frac{d^2 i_z}{dr^2} + \frac{1}{r} \frac{di_z}{dr} \right) = \vec{a}_z j\omega\mu\sigma i_z$$

(8)

$$\frac{d^2 i_z}{dr^2} + \frac{1}{r} \frac{di_z}{dr} + \tau^2 i_z = 0 \qquad \tau = (-j\omega\mu\sigma)^{1/2}$$

A general solution of this differential equation is

$$i_z = A J_0(\tau r) + B H_0^{(1)}(\tau r) \tag{9}$$

where $J_0(\tau r)$ and $H_0^{(1)}(\tau r)$ are the zero-order Bessel and Hankel functions of the first kind respectively.

In the copper (region 2), the constant, B, must vanish since $H_0^{(1)}(\tau r)$ is infinite at r = o, so that

$$\begin{aligned} i_{z_2} &= A_2 J_0(\tau_2 r) \\ i_{z_1} &= A_1 J_0(\tau_1 r) + B_1 H_0^{(1)}(\tau_1 r) \end{aligned} \tag{10}$$

where $\tau_2 = (-j\omega\mu_2\sigma_2)^{1/2}$ ; $\tau_1 = (-j\omega\mu_1\sigma_1)^{1/2}$

It is necessary to compute only the ratio, $\frac{B_1}{A_1}$ in order to find $Z_s$.

This ratio is found from the conditions at the boundary between regions 1 and 2. Since the tangential components of E and H must be continuous at this boundary, we can write

$$\left[E_{z_2}\right]_{r=a} = \left[E_{z_1}\right]_{r=a}$$

(11)

$$\left[H_{\phi_2}\right]_{r=a} = \left[H_{\phi_1}\right]_{r=a}$$

Then, since $E_z = i_z/\sigma$

and $\partial E_z/\partial r = \mu\, \partial H\phi/\partial t = j\omega\mu H\phi$

we have

$$\frac{A_z}{\sigma_2} J_0(\tau_2 a) = \frac{1}{\sigma_1}\left[A_1 J_0(\tau_1 a) + B_1 H_0^{(1)}(\tau_1 a)\right]$$

(12)

$$\frac{\tau_2 A_2}{j\omega\mu_2\sigma_2} J_0'(\tau_2 a) = \frac{\tau_1}{j\omega\mu_1\sigma_1}\left[A_1 J_0'(\tau_1 a) + B H_0^{(1)'}(\tau_1 a)\right]$$

where $J_0'(\tau r) = \dfrac{d\, J_0(\tau r)}{d(\tau r)}$

Hence, dividing and rearranging, we get the following:

$$\frac{B_1}{A_1} = \frac{\sqrt{\frac{\mu_1}{\mu_2}}\, J_0'(\tau_1 a) J_0(\tau_2 a) - \frac{\mu_1}{\mu_2}\sqrt{\frac{\sigma_2}{\sigma_1}}\, J_0'(\tau_2 a) J_0(\tau_1 a)}{\frac{\mu_1}{\mu_2}\sqrt{\frac{\sigma_2}{\sigma_1}}\, J_0'(\tau_2 a) H_0^{(1)}(\tau_1 a) - \sqrt{\frac{\mu_1}{\mu_2}}\, J_0(\tau_2 a) H_0^{(1)'}(\tau_1 a)} \quad (13)$$

Now, $I = 2\pi b \left[H\phi_1\right]^{at}_{r=b}$

Therefore,

$$Z_s = \frac{\left[E_z\right]_{r=b}}{I} = \frac{(-j)^{\frac{1}{2}}\sqrt{\omega\mu_1}}{2\pi b\sqrt{\sigma_1}}\left[\frac{J_0(\tau_1 b) + B_1/A_1 H_0^{(1)}(\tau_1 b)}{J_0'(\tau_1 b) + B_1/A_1 H_0^{(1)'}(\tau_1 b)}\right] \quad (14)$$

For large values of the argument, $\tau_1 b$, the expression in brackets reduces to j. Hence,

$$\left[Z_s\right]_{\tau_1 b \to \infty} = \frac{(-j)^{\frac{1}{2}}\sqrt{\omega\mu_1}}{2\pi b\sqrt{\sigma_1}}\, j = \frac{(j+1)\sqrt{\omega\mu_1}}{2\sqrt{2}\,\pi b\sqrt{\sigma_1}} \quad (15)$$

Zs may also be expressed as

$$Z_s = R_{ac} + j\,\omega\,L_i \tag{16}$$

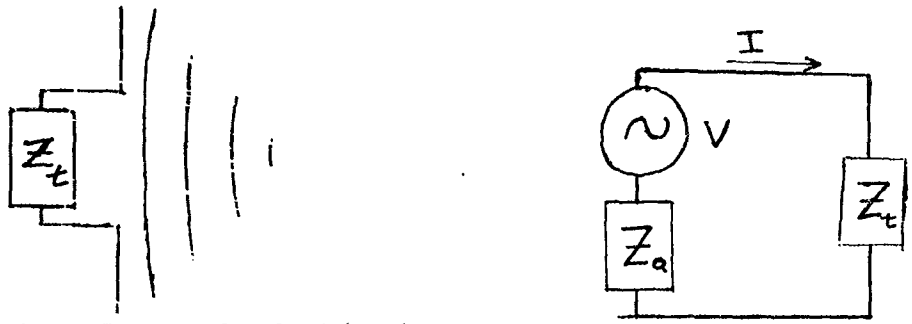
where Rac the surface resistivity is skin-effect resistance and $L_i$ is the internal reactance.
Thus, for larger values of frequency and permeability

$$R_{ac} = \frac{\sqrt{\omega \mu_1}}{2\sqrt{2}\,\pi b \sqrt{\sigma_1}} \tag{17}$$

Appendix B

DERIVATION OF ANTENNA POWER DELIVERED TO LOAD

Any electromagnetic wave collector or antenna, such as a power line, can be considered a collecting device that delivers energy from the incident wave to a terminating impedance. This is suggested in the following diagram, with its accompanying equivalent circuit:




where $Z_t$ = complex load impedance
$Z_a$ = complex antenna impedance
V = voltage induced by the field of the passing electromagnetic wave

This will produce a current I through the terminating impedance $Z_t$ according to $I = \frac{V}{Z_t + Z_a}$ where I and V are effective or rms values. (18)

The antenna and terminating impedances considered in this fashion are usually complex:

$$Z_a = R_a + jX_a \tag{19}$$

$$Z_t = R_t + jX_t \tag{20}$$

The antenna resistance $R_a$ may be further divided into two parts

$$R_a = R_r + R_L \tag{21}$$

Here $R_r$ will be considered a radiation resistance which is useful in determining the real power radiated or scattered by the antenna, and $R_L$ is the loss resistance from which the real power or heat loss in the antenna can be calculated. This particular loss resistance is the significant factor which increases considerably when the conductor is wrapped with a high-permeability tape to attenuate interference.

If we consider W as the real power delivered by the antenna to the terminating load impedance, then

$$W = I^2 R_t \tag{22}$$

and, from Equations 8 to 11, becomes

$$W = \frac{V^2 R_t}{(R_p + R_L + R_t)^2 + (X_a + X_t)^2} \tag{23}$$

Thus, an increase in loss resistance $R_t$ and antenna reactance $X_a$, both of which are increased similarly by adding the tape wrapping to the line conductor, causes a decrease proportional as their square of the real power delivered by the line which acts as an antenna to a load. It causes a similar reduction in the re-radiated power, scattered by the antenna, and a reduction in the total power collected and accepted by the line as an antenna.

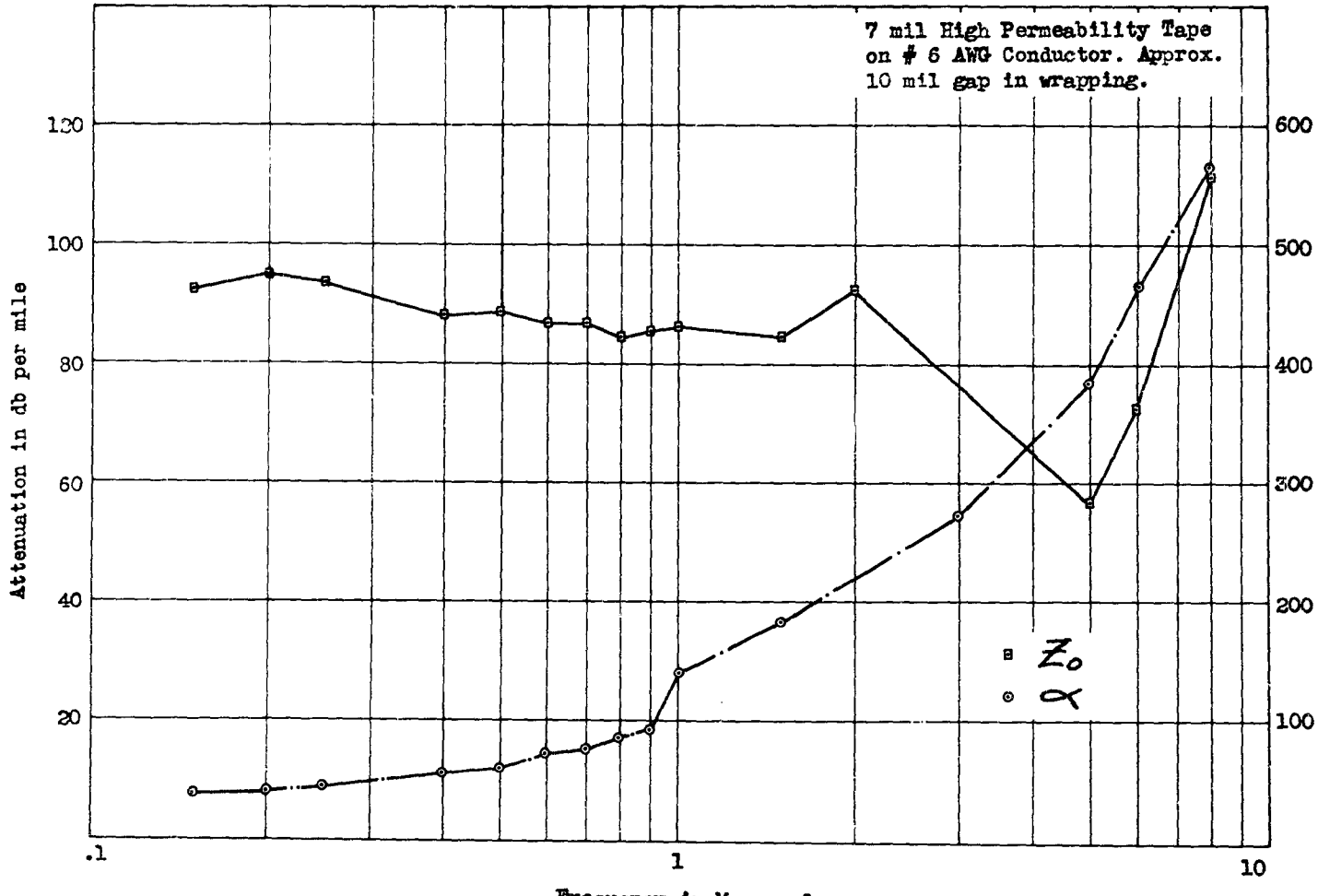
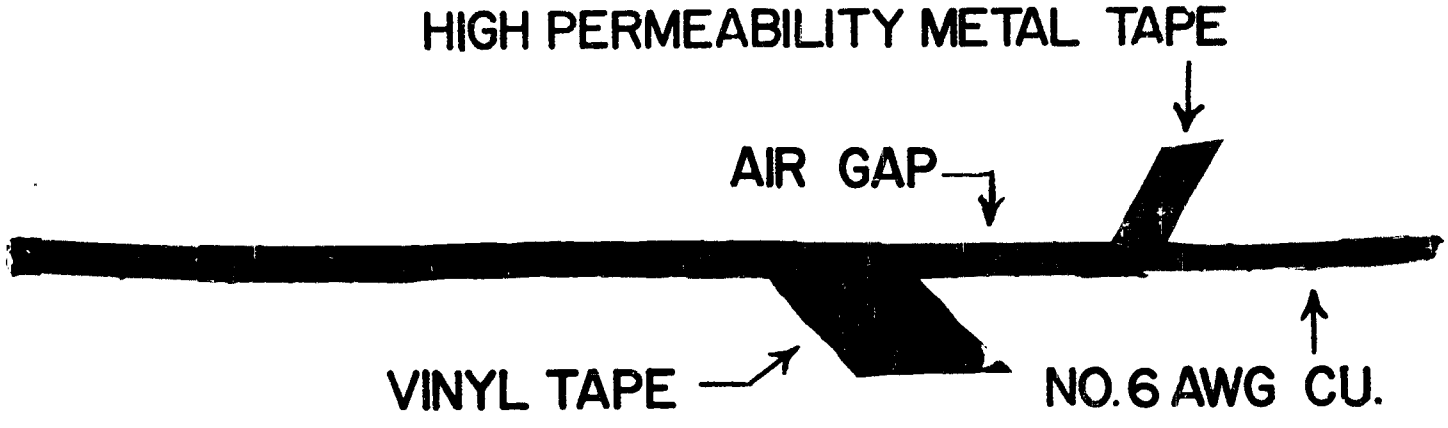



Figure 1. Attenuation and Impedance For Test Piece, Fort Huachuca Line Installation.




INTERFERENCE SUPPRESSED POWER LINE-SECTION

Fig. 2 Interference Suppressed Power Line-Section.

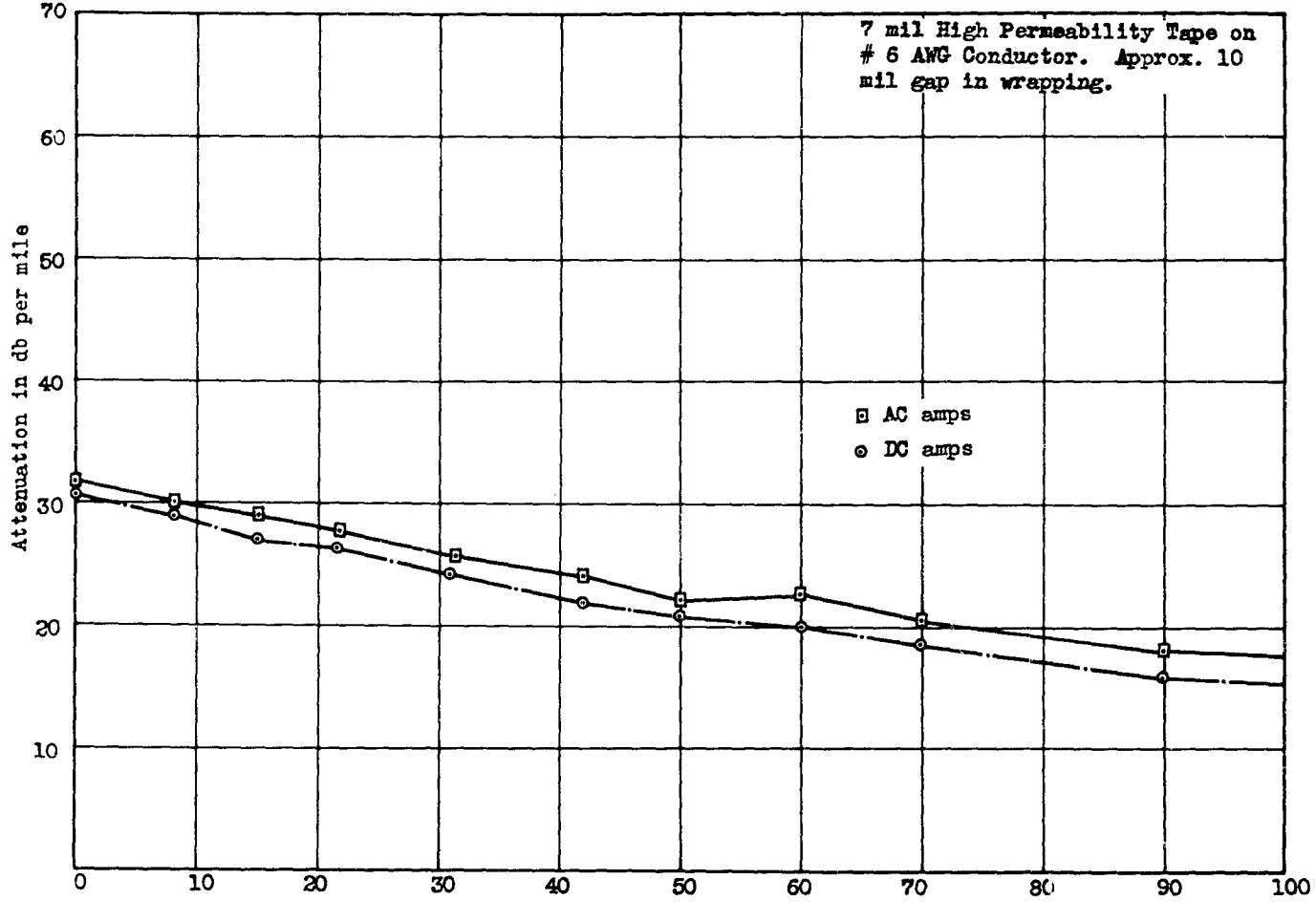



Figure 3. Current Effects on Attenuation For Test Piece, Fort Huachuca Line Installation.

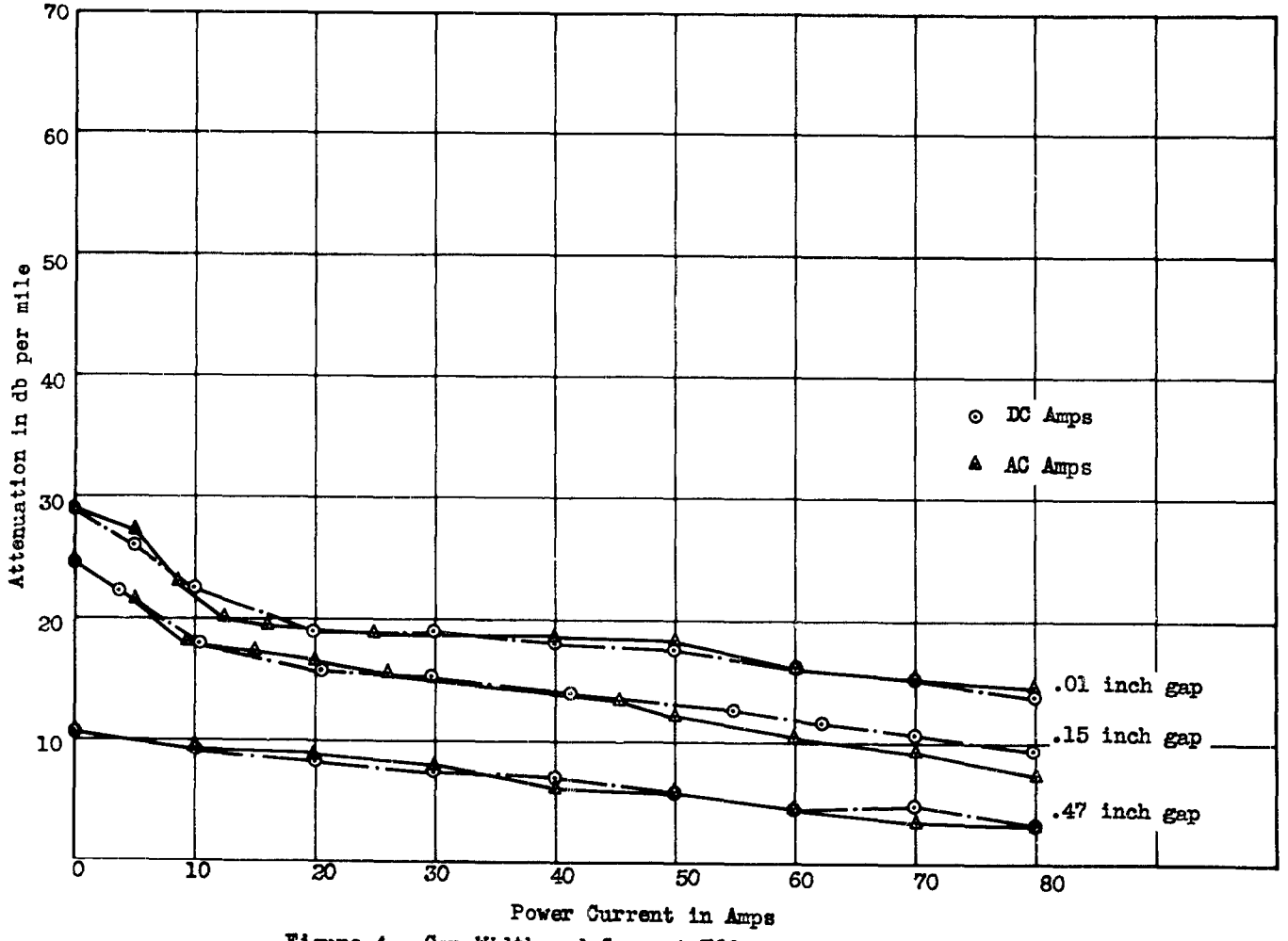



Figure 4. Gap Width and Current Effects on Attemuation.

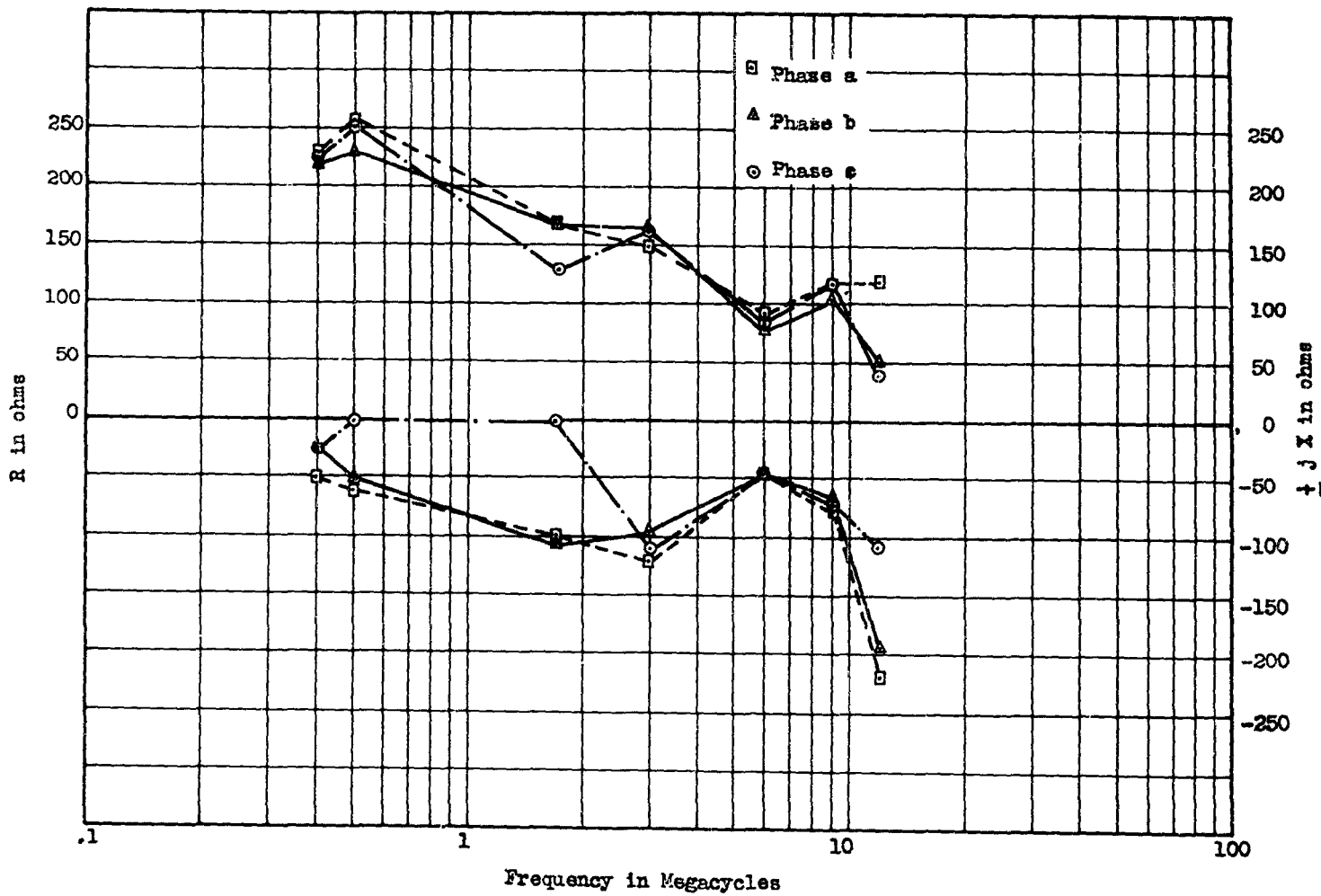



Figure 5. Line Characteristics With Transformers as Load.

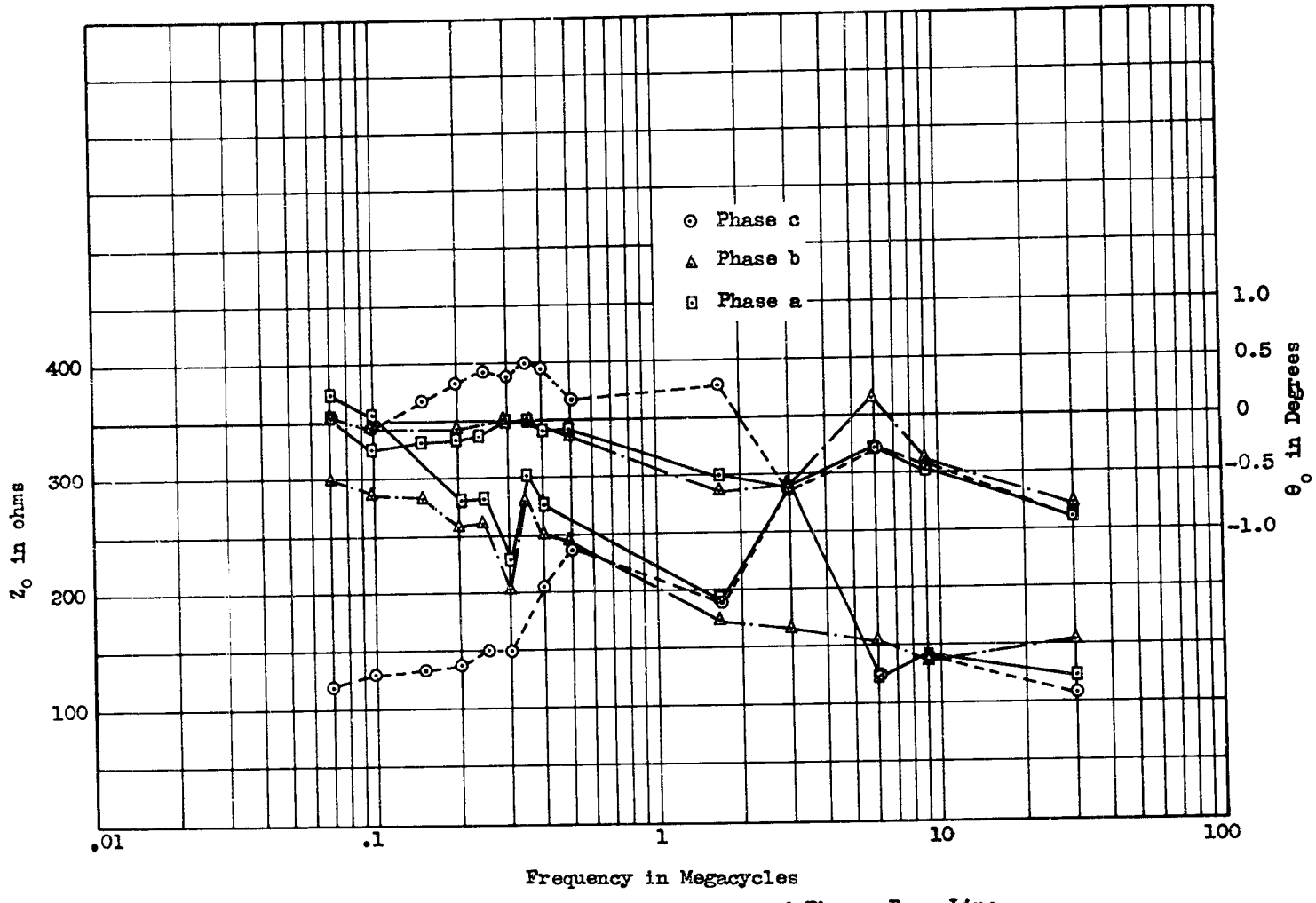



Figure 6. Characteristic Impedance and Phase, Bare Line.

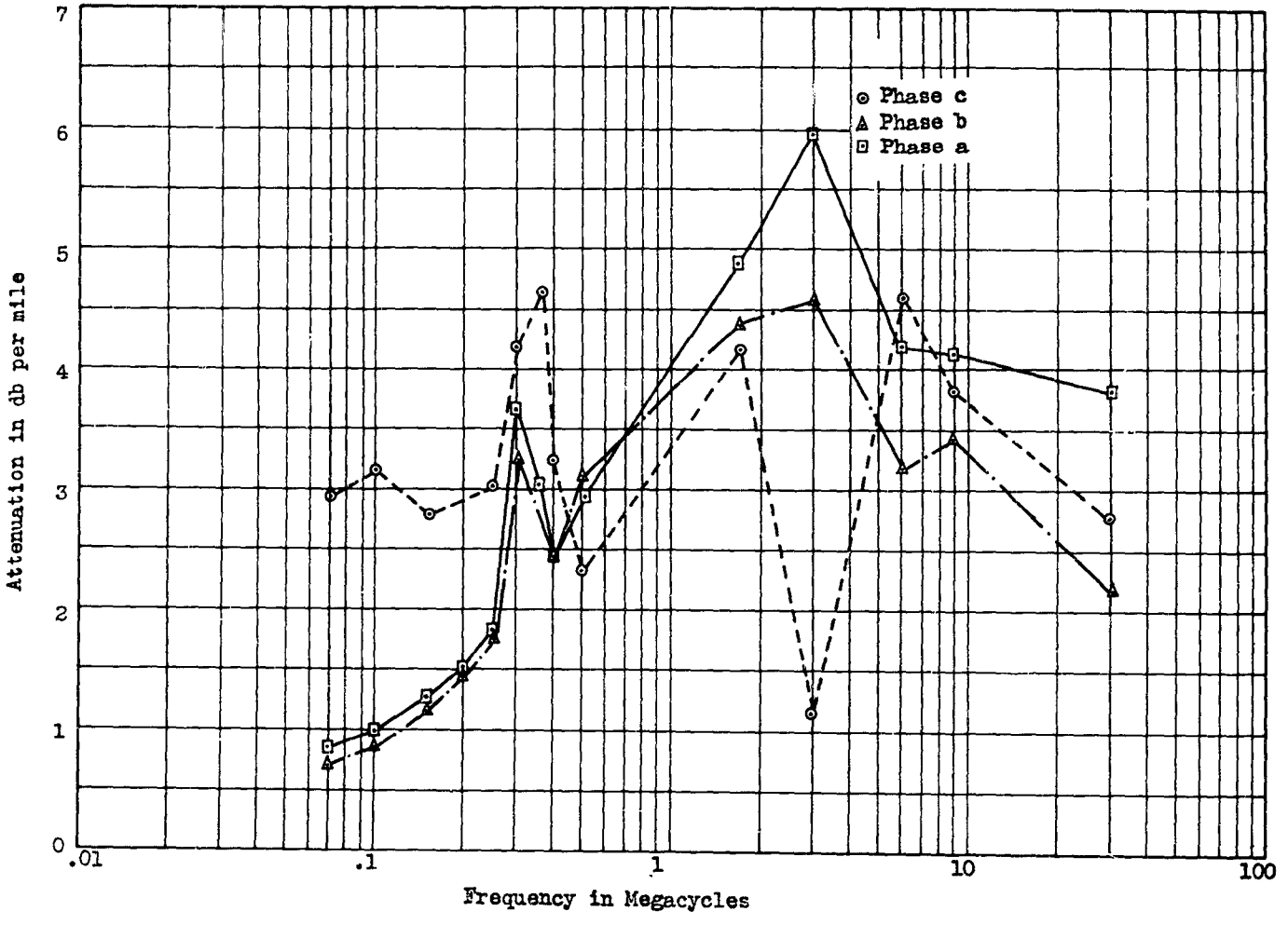



Figure 7. Bare Line Attenuation From Impedance Measurements

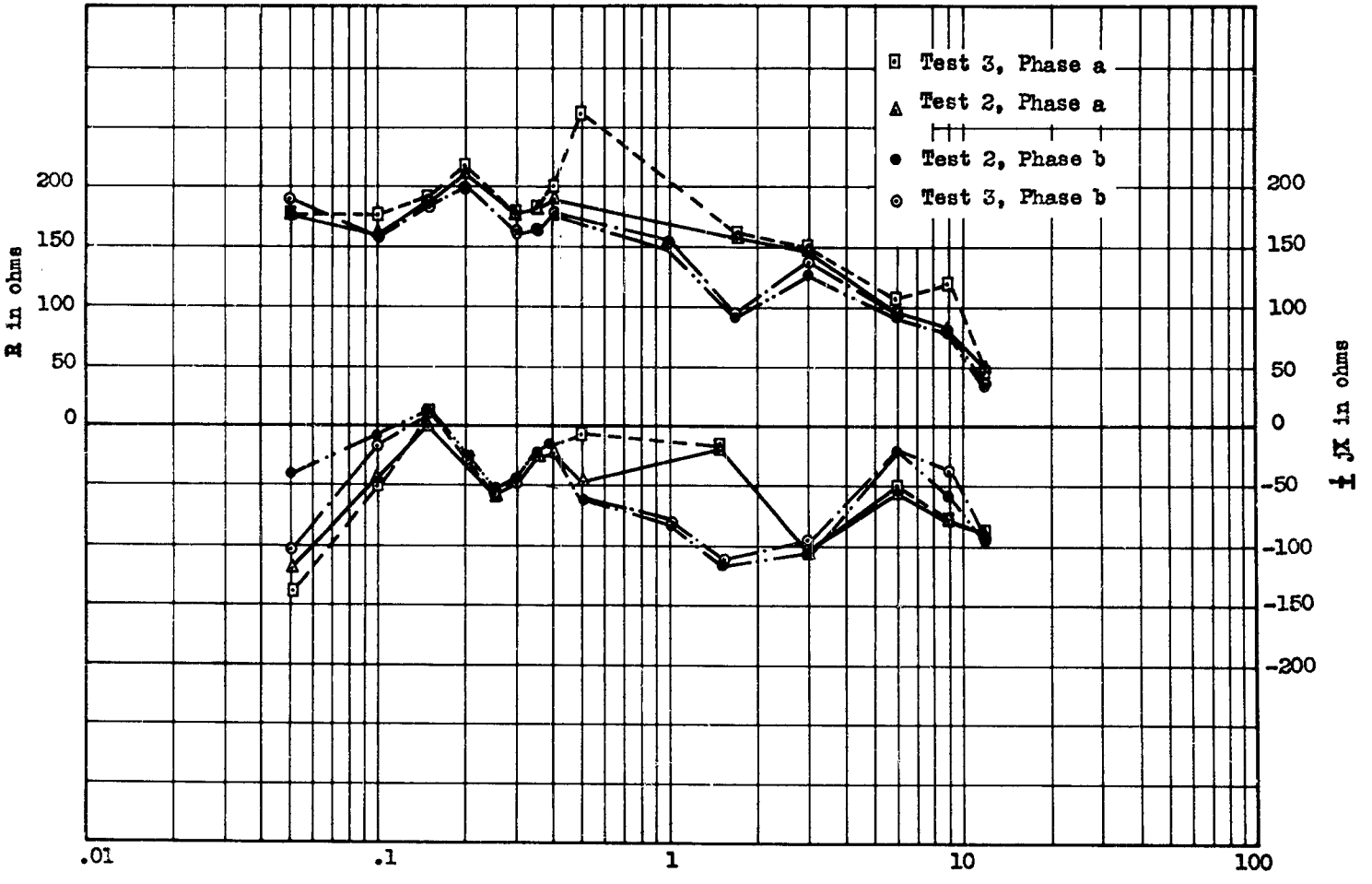



Figure 8. Impedance Measurements, Wrapped Line, Phase a and b.

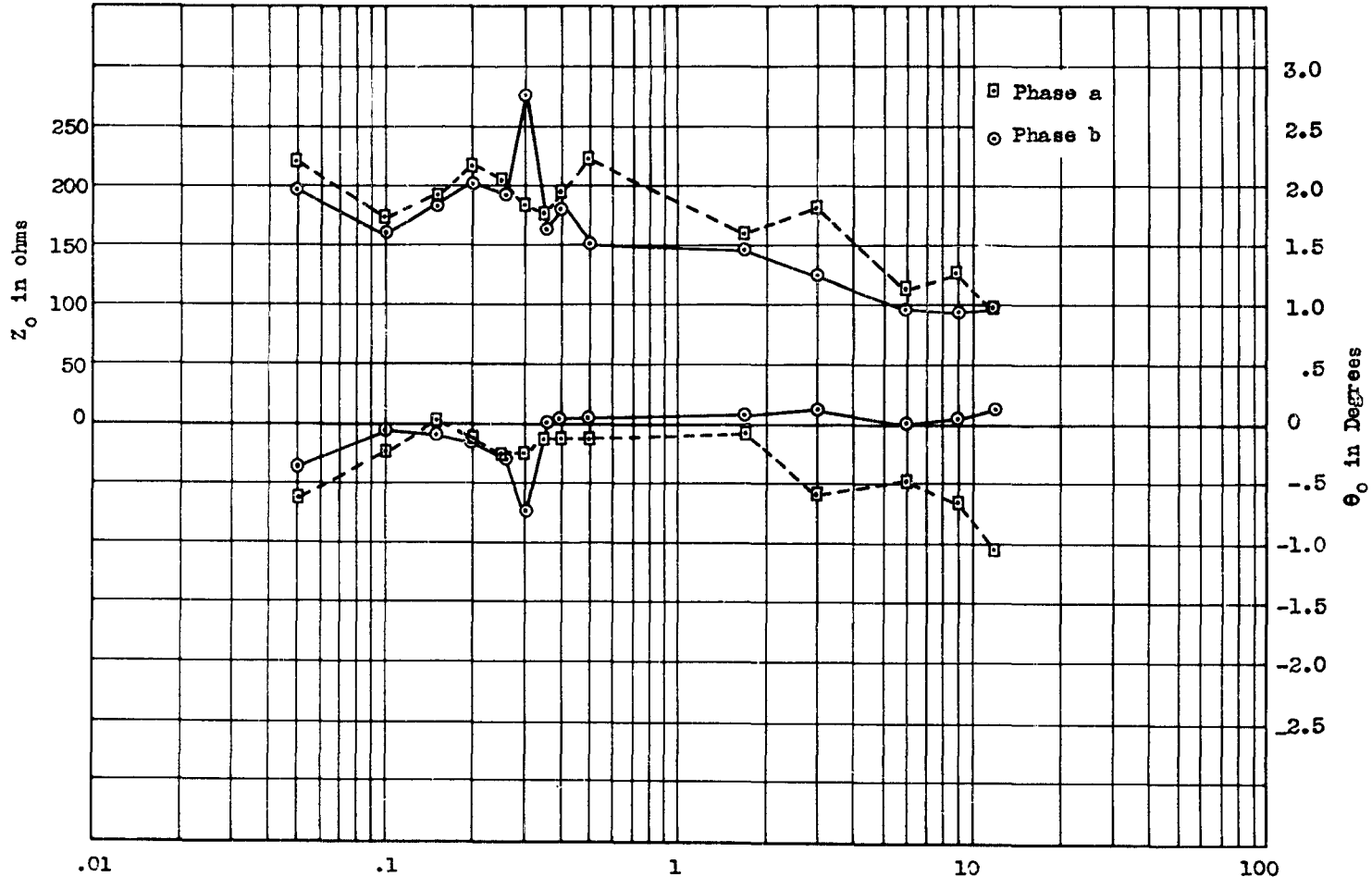



Figure 9. Characteristic Impedance and Phase, Wrapped Line

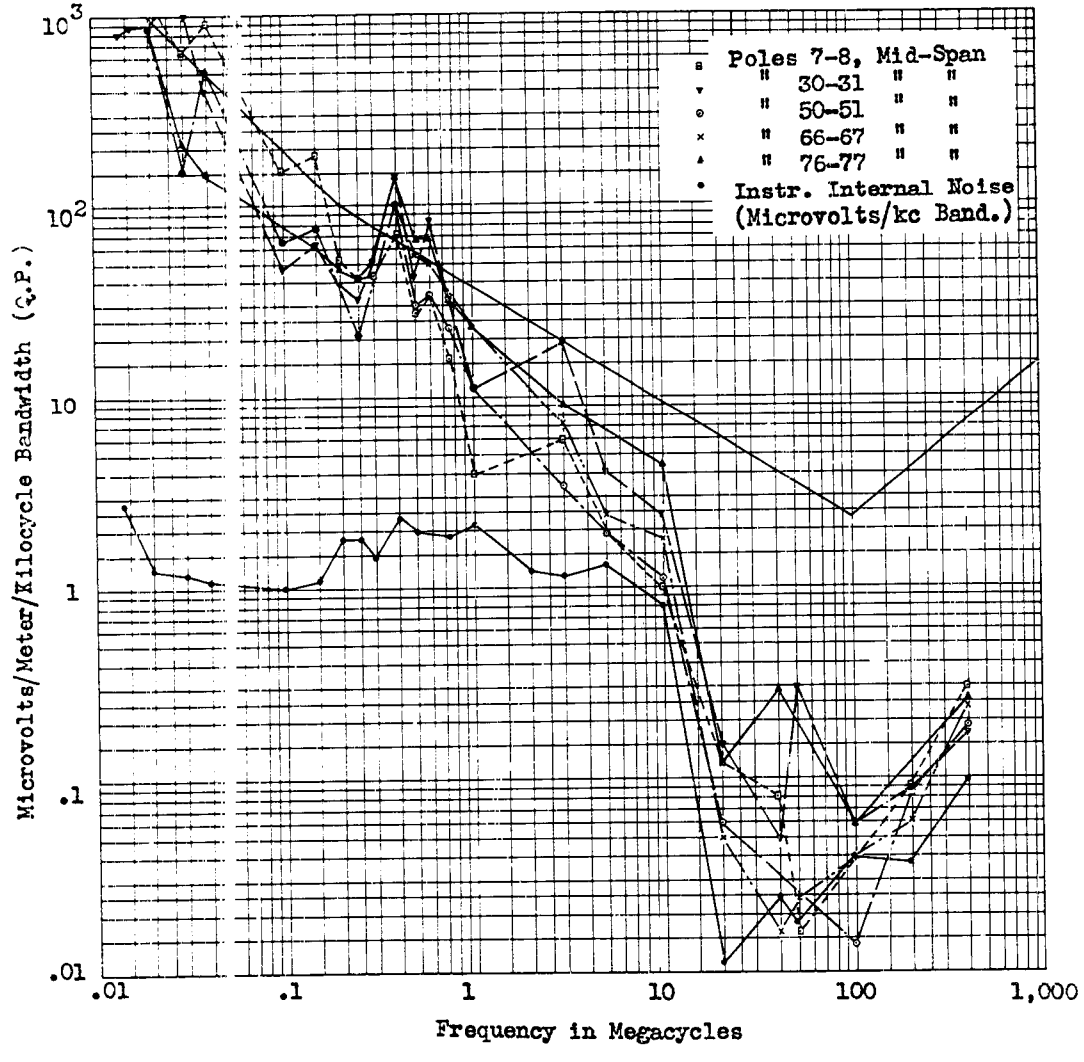



Figure 10. Power Line Noise Survey, June 1960, Part I.

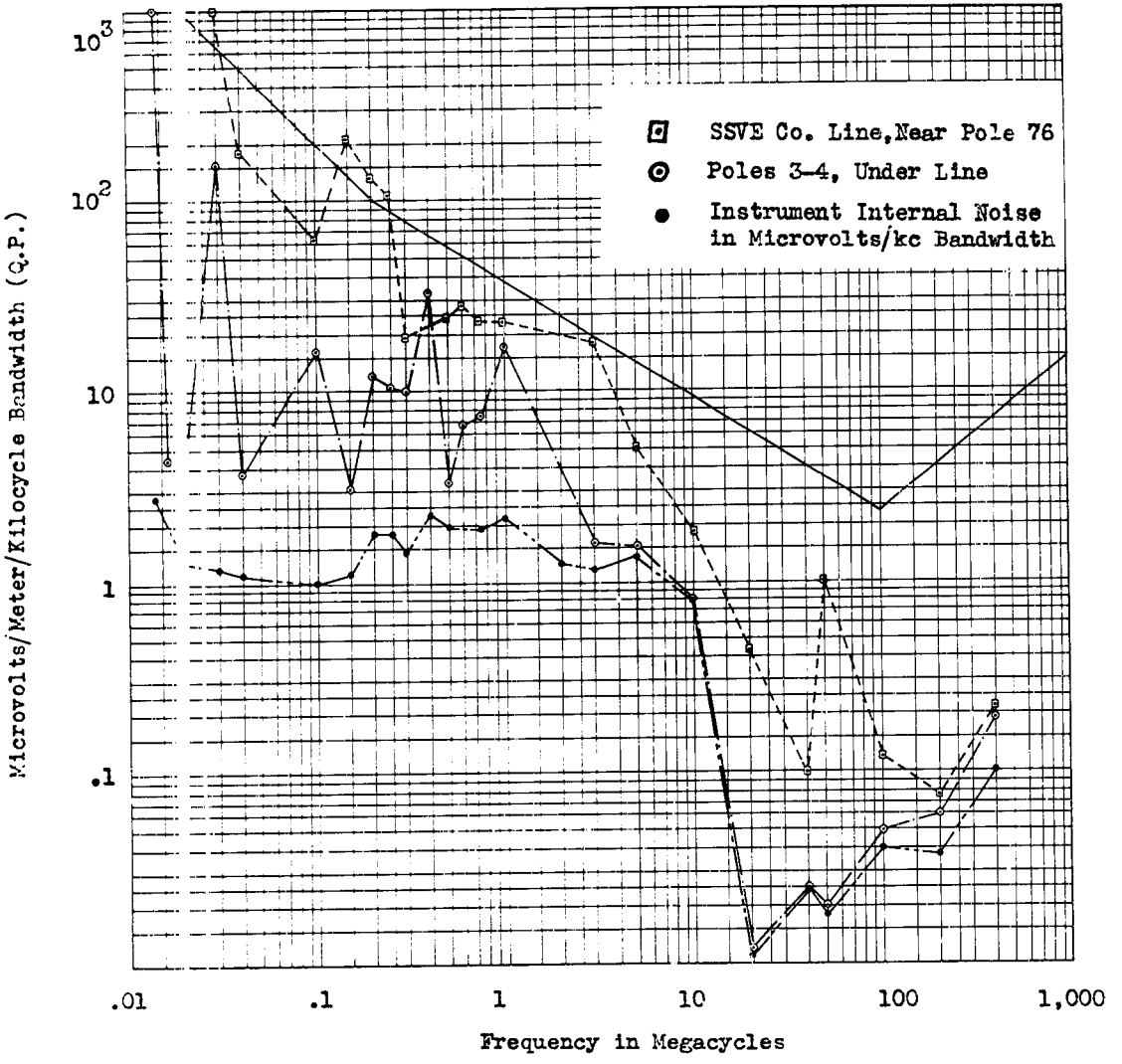



Figure 11. Power Line Noise Survey, June 1960, Part II.



Figure 12. Power Line Insertion Filter Damage.

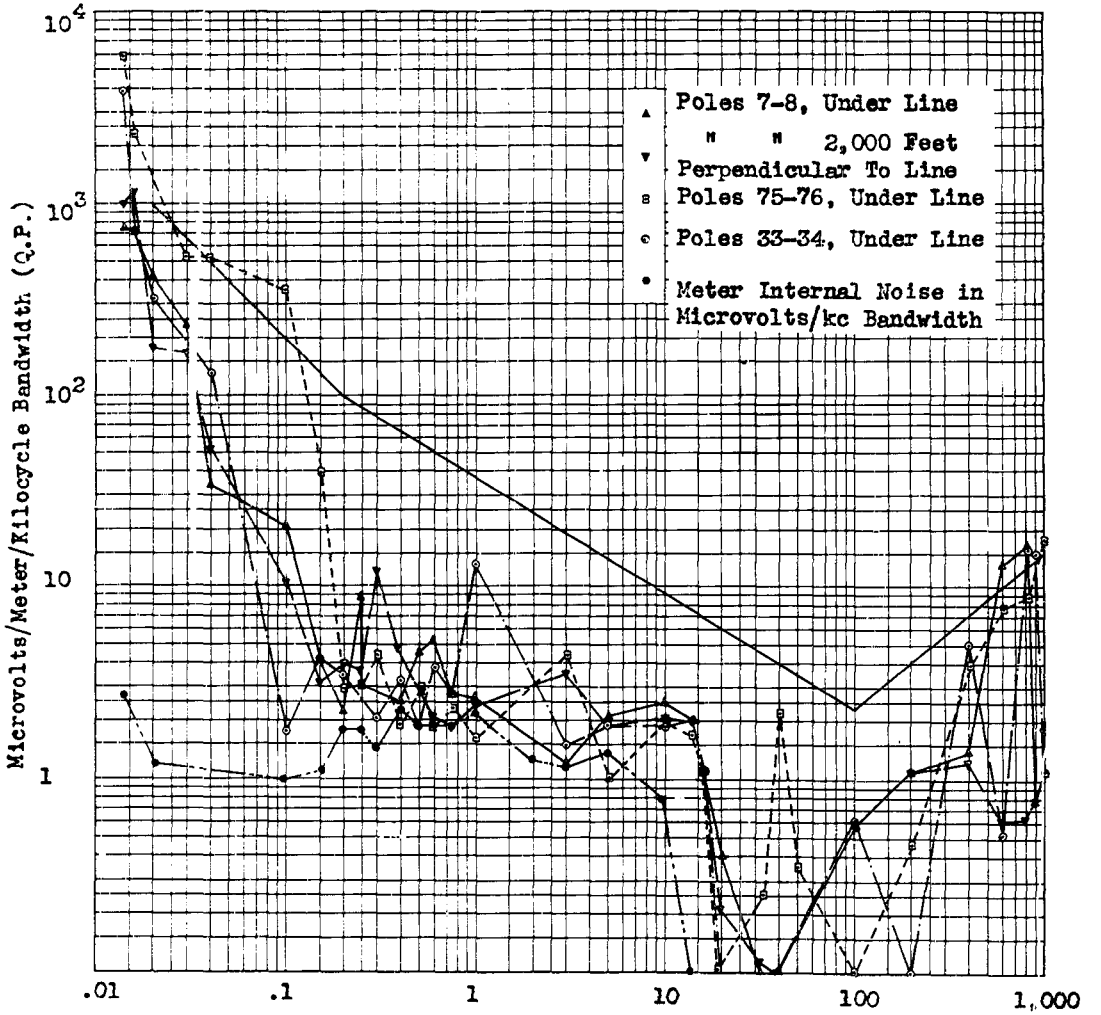



Figure 13. Power Line Noise Survey, January 1961.

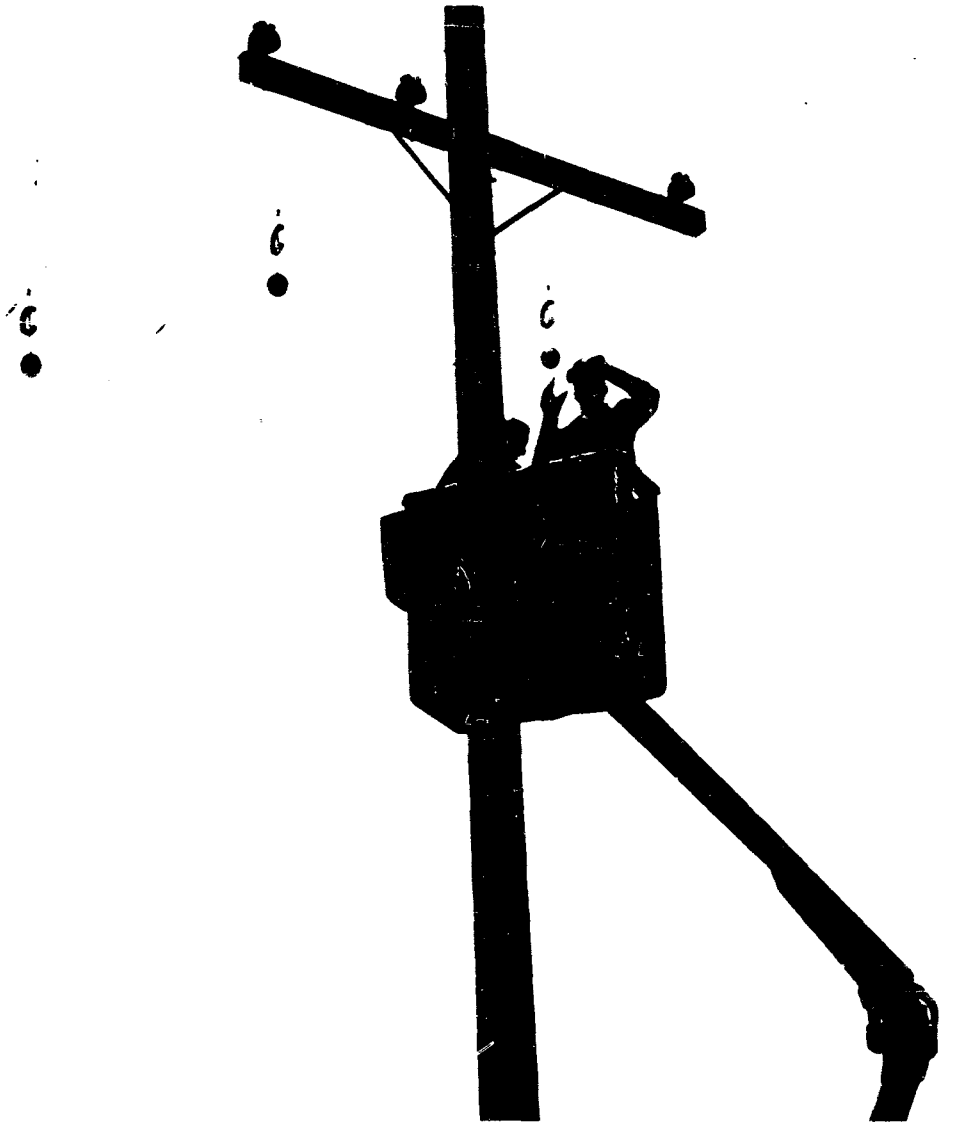


Fig. 14 Impulse Noise Generator Installation

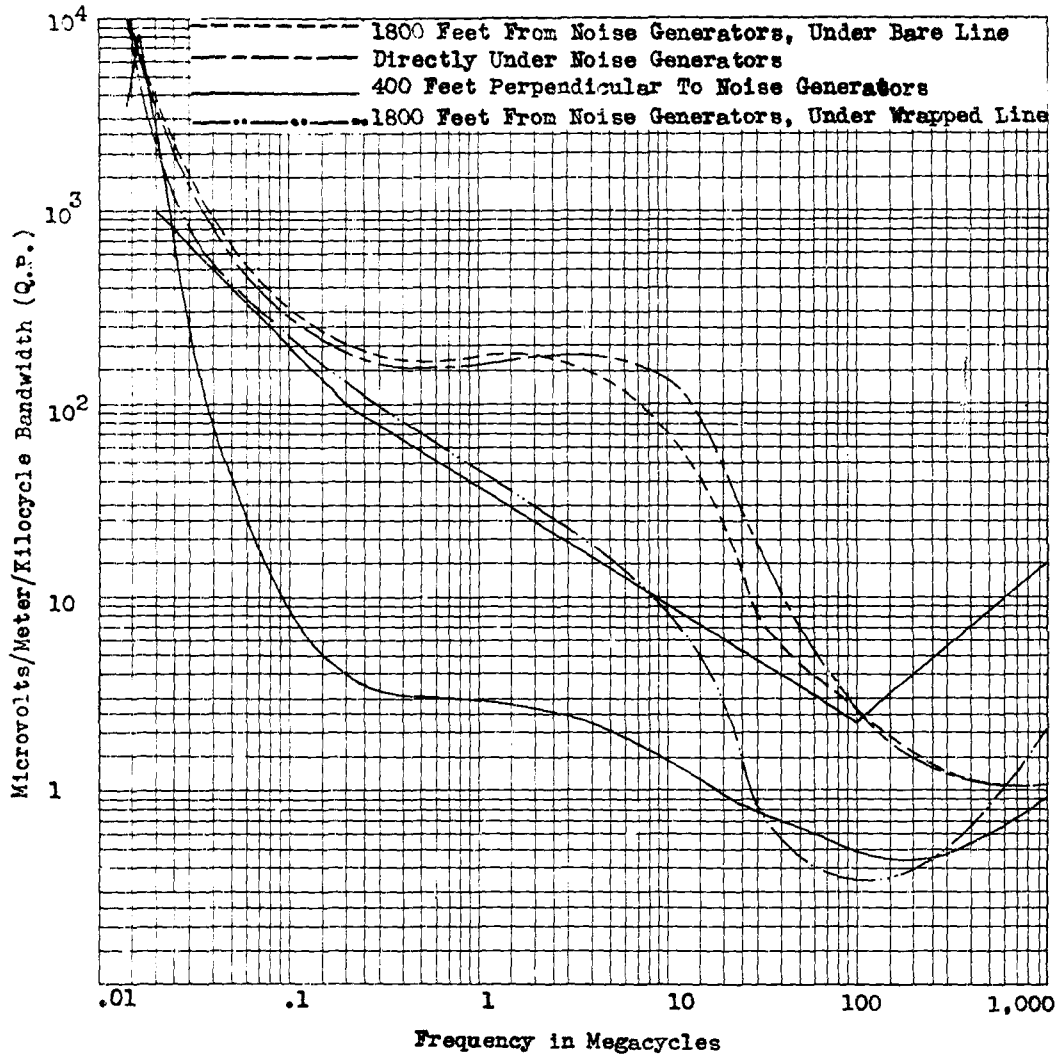



Figure 15. Electrical Field Intensity Measurements With Noise Generators, I.

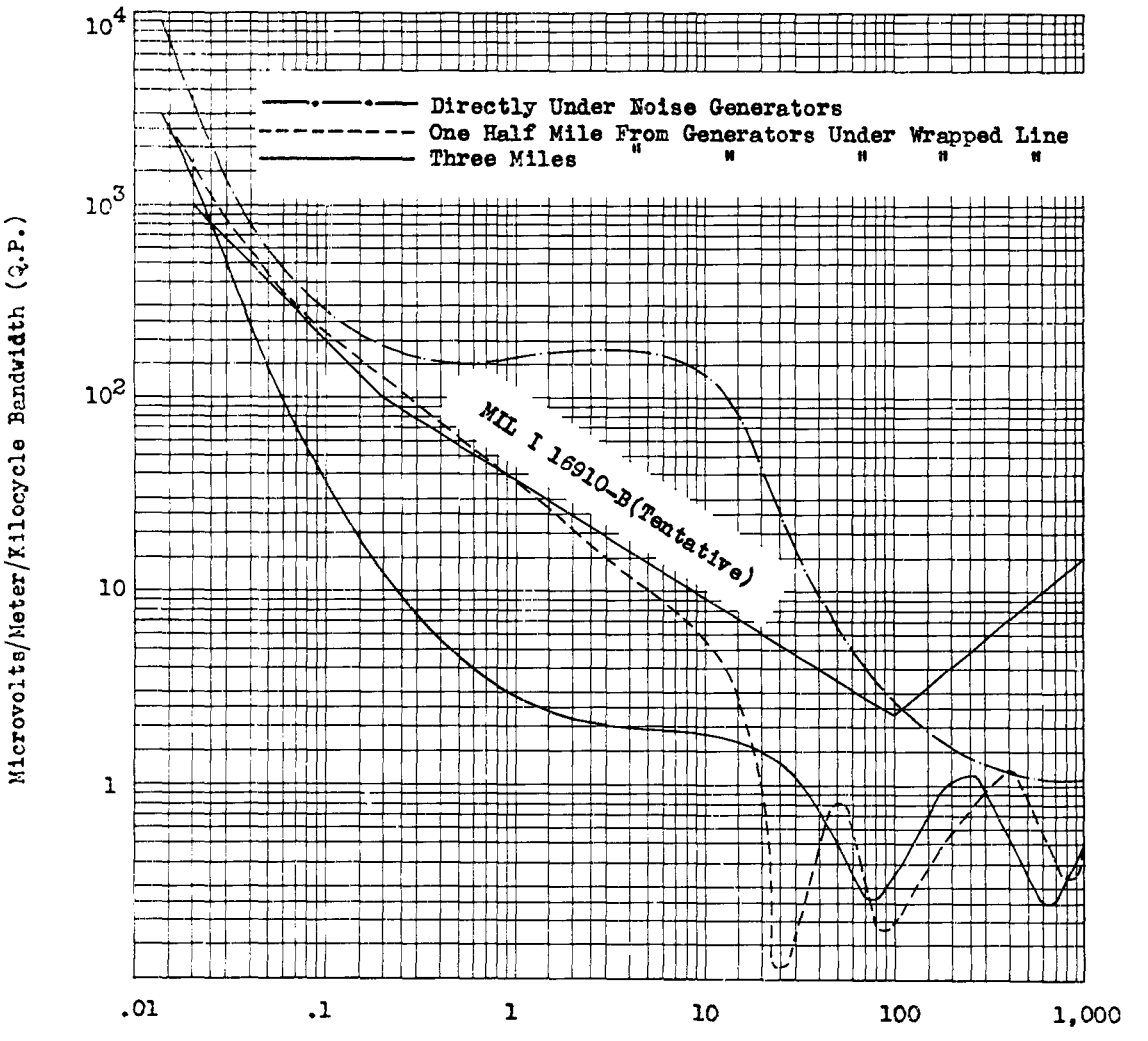



Figure 16. Electrical Field Intensity Measurements With Noise Generators, II.

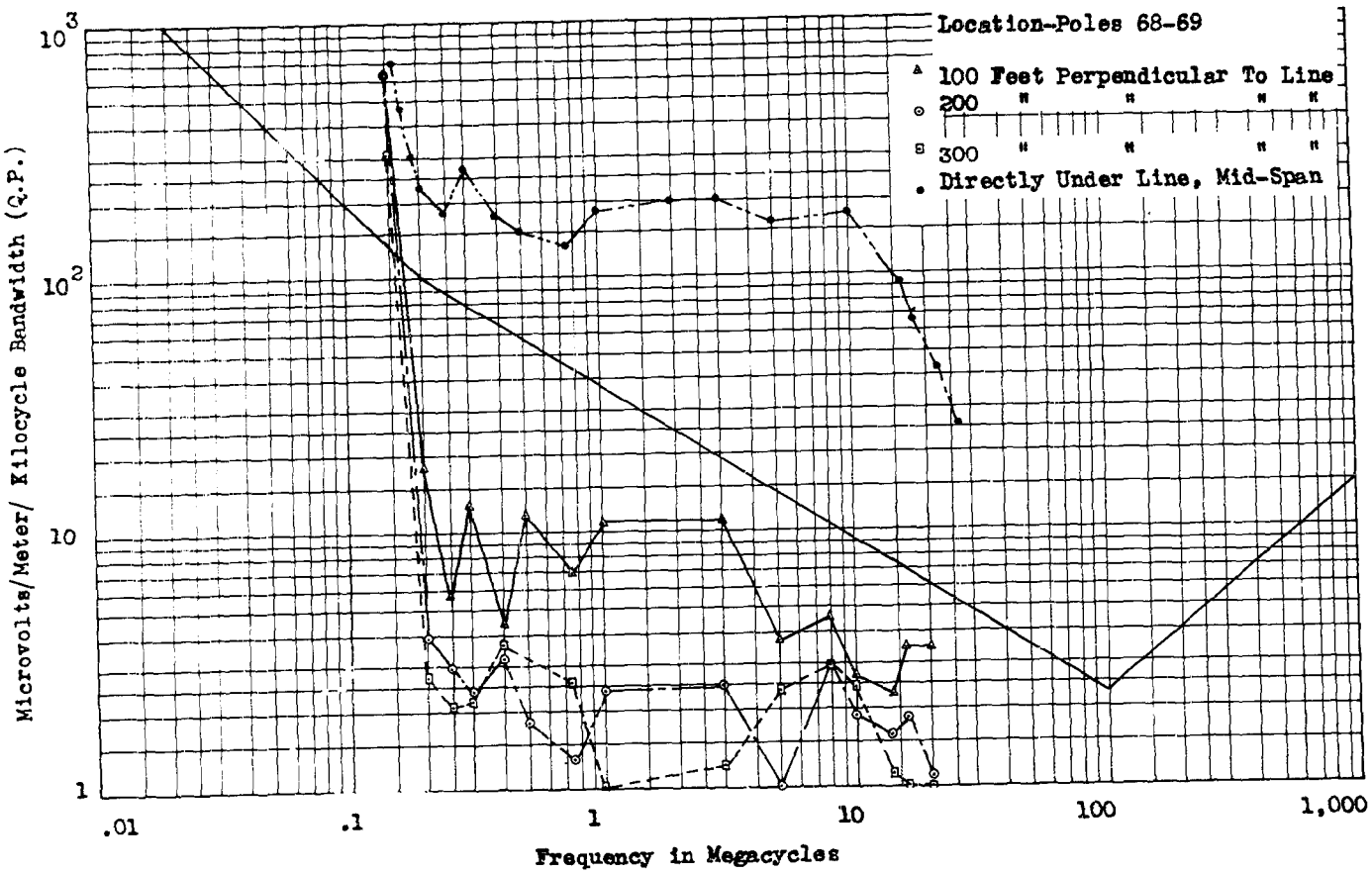



Figure 17. Electrical Field Intensity, Profile With Distance I.

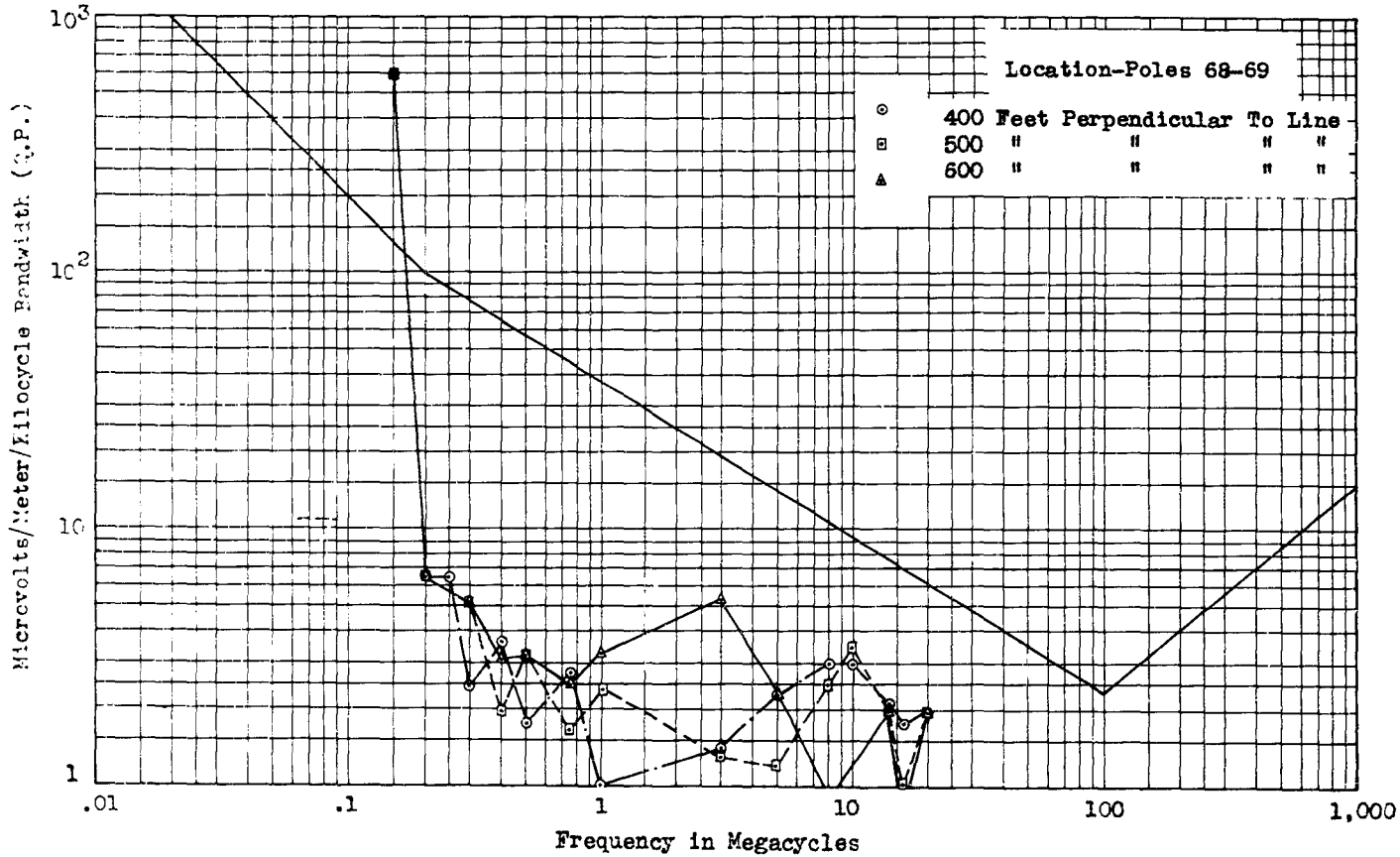



Figure 18. Electrical Field Intensity, Profile With Distance From Line II.

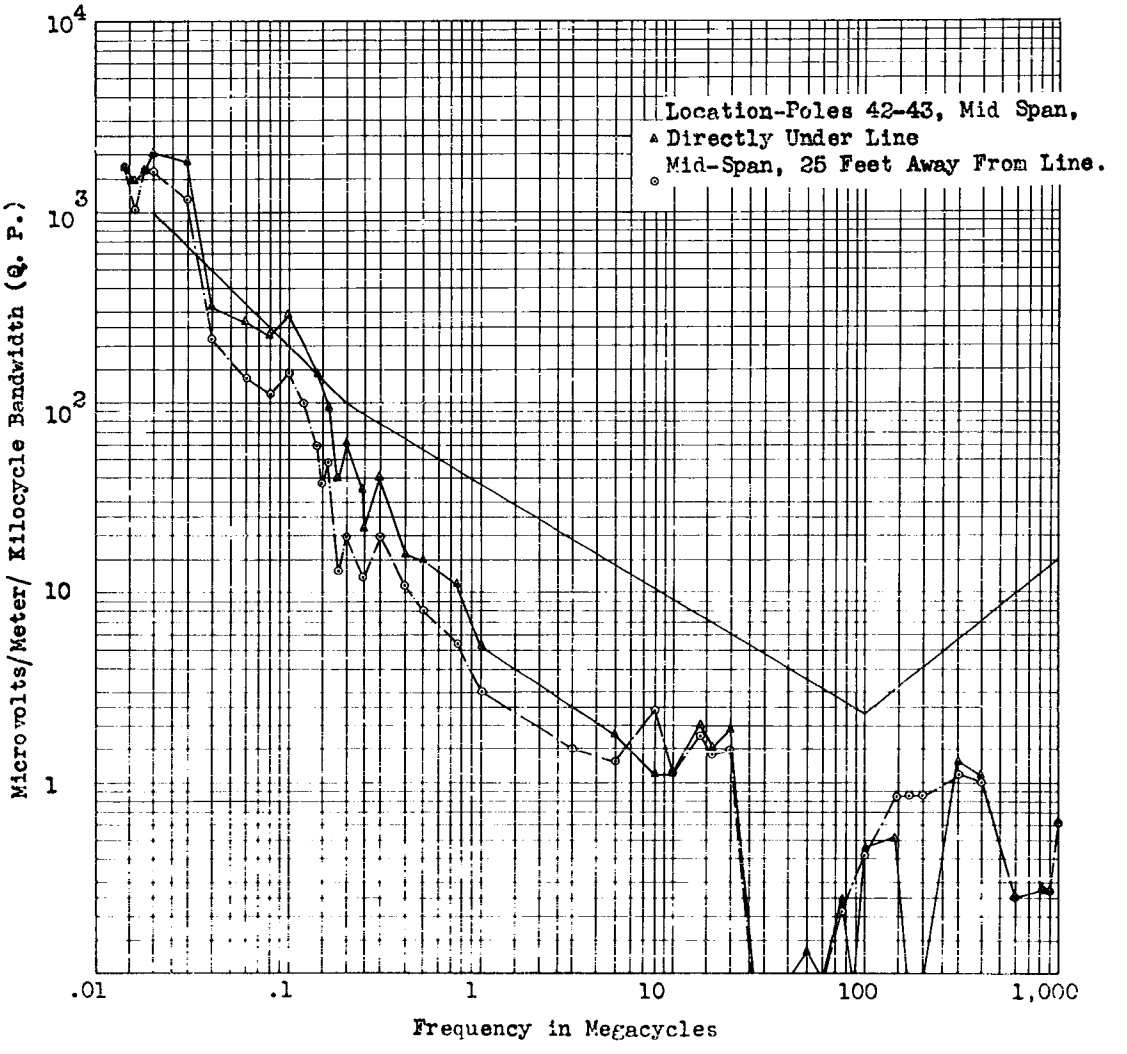



Figure 19. Electrical Field Intensity, Profile With Distance From Line, III.

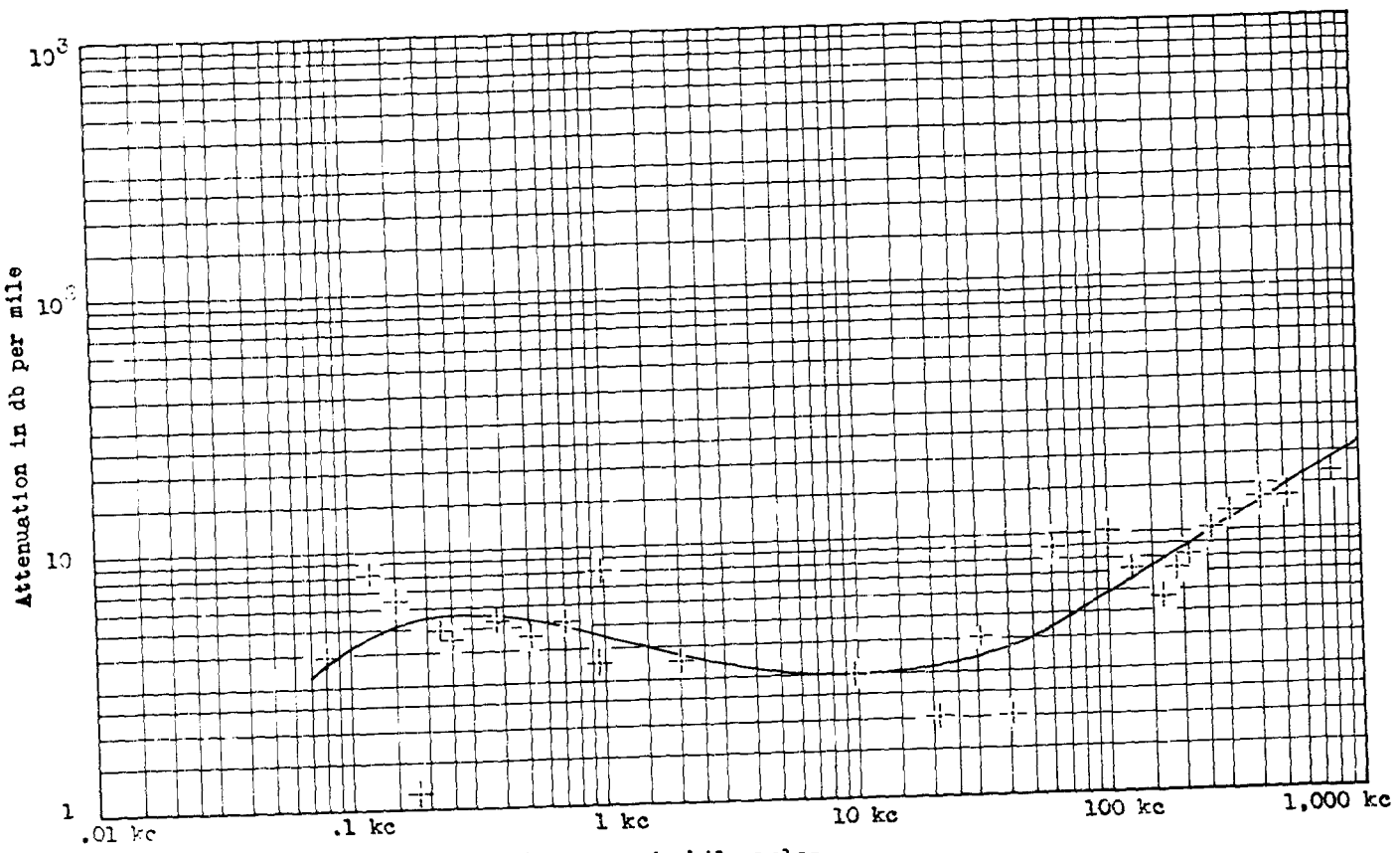



Figure 20. Wrapped Line Attenuation Curve, Lower Frequency Range.

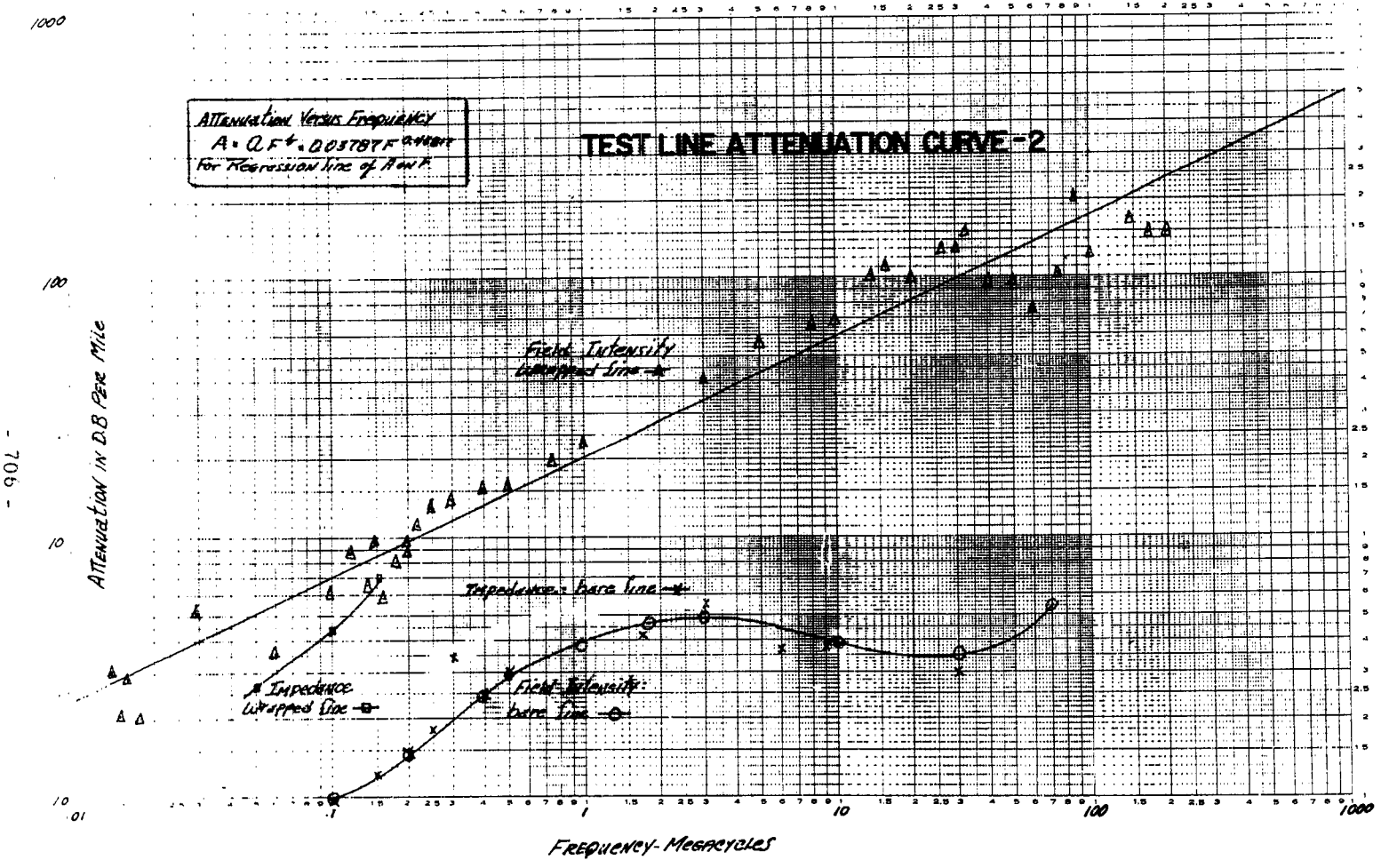



Figure 21. Wrapped Line and Bare Line Attenuation Curves

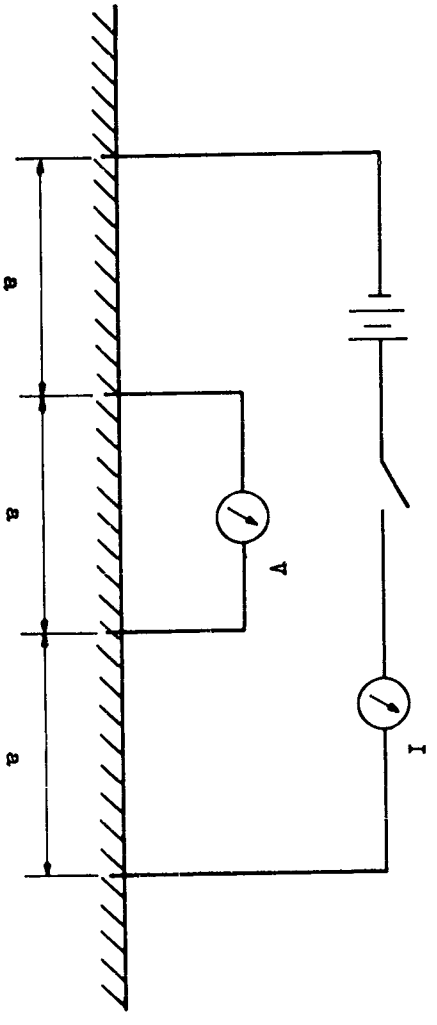



Fig. 22 Earth Resistivity Measurement Diagram

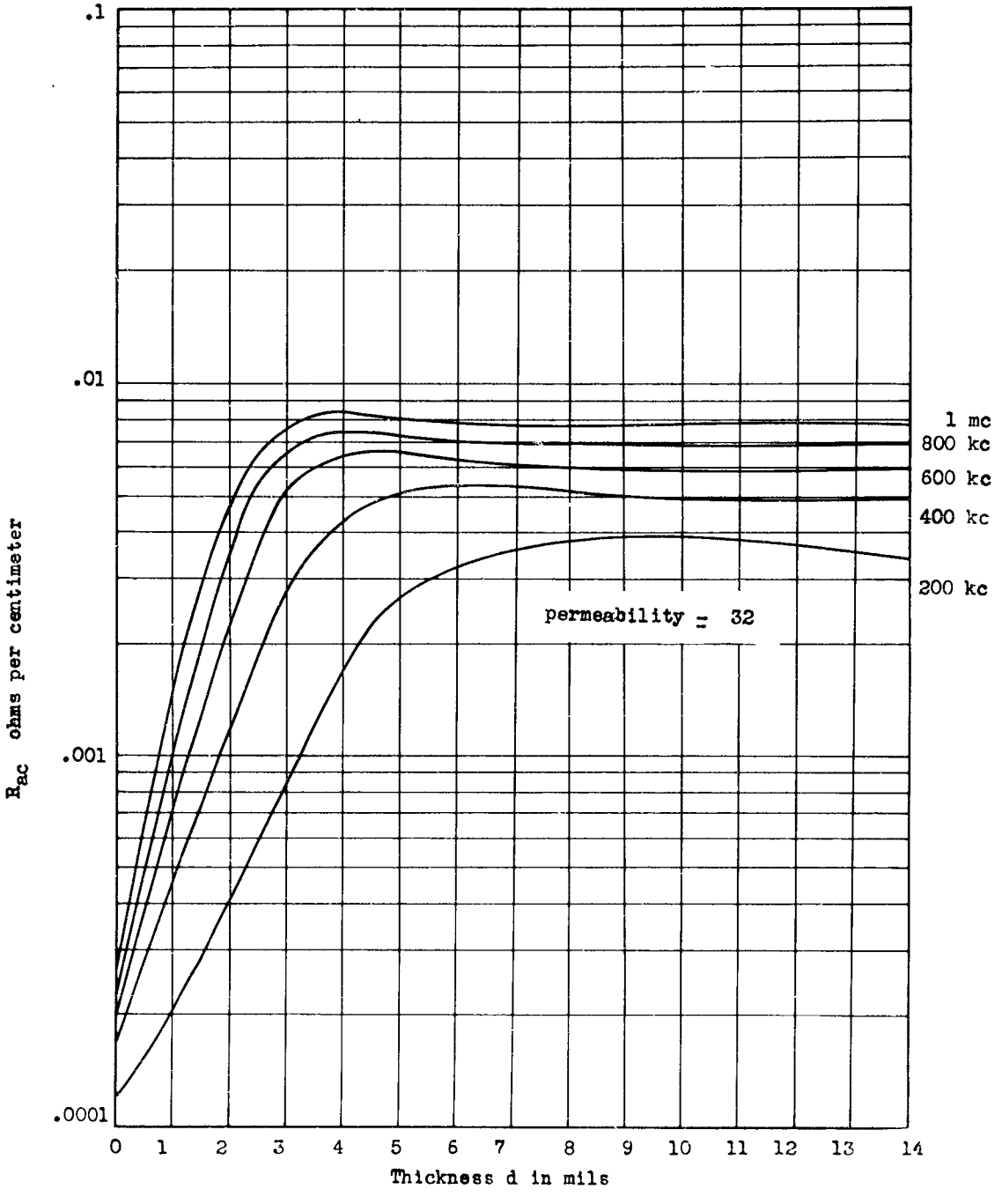



Figure 23. Calculated Curves, Tape Thickness versus A C Resistance.

# SKIN CURRENT PROBES

J. F. Fischer, Jr.
Genistron, Incorporated
Los Angeles, California

Abstract. - In order to map dc and low frequency currents flowing on metallic surfaces the development of probes from dc to 15 kc was carried out. The investigations were laid out to determine the distortions created by the probes as well as their sensitivities. The relative directivity of the ac probe was determined. The dc probe utilizes a Hall Effect sensor, and the flux collector parameters were investigated to give an optimum design. A technique for determining the exact magnitude of current flowing in a skin is described, and a series of measurements indicate that less than a 10% error is incurred.

## I. INTRODUCTION

Due to the increasing need for a device capable of measuring skin currents for interference control purposes, a program for developing such a probe was initiated.

For the purposes of this report, a skin current probe will be defined as a device capable of producing an output signal when subjected to a current flowing on a metallic surface. The output signal will be proportional to this current flow.

Investigation of earlier skin current probes indicate that devices of this type, (principally small loop probes), have been used mainly to determine relative values of skin currents at different positions on a surface, or to compare the relative output of various methods of feeding energy to a surface. Mapping of current distributions on the surface of aircraft and missiles and comparison of these current maps for various types of antennas causing the currents was the primary concern of these previous investigations.

The techniques utilized in these measurements indicate that uncertainty of the influence of the presence of the probe and its method of insertion create the primary problems associated with the techniques.

D.C. currents and alternating currents up to 15 kc will be considered in this development.

## II. KNOWN FIELD

In order to develop skin current measuring devices, it was considered necessary to have a known distribution of current. Then the distorting effects, created by the probe on the field could be analyzed.

The following is not considered to be proof, but merely a restatement of facts that have been proven in many texts on electromagnetic fields, and are

restated to indicate the theory utilized to establish a known field. In a uniform dielectric or magnetic medium, the electrostatic and magnetic potentials satisfy Laplace's equation. There is thus a close analogy between the field and boundry equations in electrostatics, magnetostatics, and steady current flow. Therefore, the solution of any problem in one of these three will give the solution of the corresponding problem in either of the remaining two.

In setting up a known field, the case of two electrodes of excellent conductivities immersed in a uniform conducting medium will be considered. Taking advantage of the previous paragraph, the solution of this case may be obtained from that of an analogous electrostatic problem, of two point charges, of equal magnitude and opposite sign. The family of equipotential lines close to the charges are almost spheres, then become pear shaped with the pointed section outward. The plane perpendicular to and bisecting the center line is also an equipotential surface. The field lines of the electrostatic problem will be equivalent to the current lines in a conducting material.

The magnetic field associated with this current flow must be considered since the pickup devices used will be sensitive to the magnetic field or field density. This presents no serious problem since the magnetic intensity at any point due to a current flowing in a linear conductor is proportional to the intensity of the current.

Maxwell's equations for an alternating current show that the magnetic field will decrease with increasing depth from the surface. If the magnetic field is static, the magnetostatic field will be the same in the conductor as it would be in a non-conductor of the same permeability. As the frequency increases, external a.c. magnetic flux lines approaching a perfect conductor will not penetrate its surface, but will bend away and pass tangentially. Therefore, two electrodes (one a source and one a sink) passing a steady current through a uniform conductor, will produce a current distribution, having constant magnitudes, of circular arcs between the electrodes. The electric potential lines are orthogonal to those of the current lines. The flow of currents in a conducting media when the electromagnetic fields are variable will also be considered, but they will be such that the displacement current is negligible. This condition will be satisfied as long as the electromagnetic fields are varying relatively slowly. The error in neglecting displacement current for the frequency range considered in this development is negligible, since the highest frequency considered was 15 kc.

Two electrodes with equal and opposite charges separated by air is equivalent to the two electrodes in a conducting medium. The field lines of the electrostatic problem are equivalent to the current lines in the conducting material.

The field lines are defined by:

a) $Q_1 \cos \Phi_1 + Q_2 \cos \Phi_2 = K$

Thus using this equation, the theoretical magnitudes at any point from the electrodes can be determined. Figure #1 indicates the coordinate system and an example demonstrates the method used.

The arc drawn that cuts $Q_1$, P, $Q_2$ will exhibit at any point on its locus the same relative magnitude compared to the referenced straight line between the $Q_1$ and $Q_2$. Setting up a series of arcs terminating on the electrodes will enable the determination of the theoretical values at many places on the conducting skin.

## III. A.C. PROBE DEVELOPMENT

Initial measurements in the 30 cps to 15 kc region were started with a small loop feeding an NM-40 receiver. The method of generating the skin currents is shown in Figure #2. A copper skin 12" x 20" with electrodes 6 inches from each edge was utilized. However, measurements with this loop were discontinued because of insensitivity below 200 cps. Measurements were resumed utilizing an air core winding with as many turns as practicable on a 1/4" cube bobbin. Approximately 10,000 turns of number 50 wire was placed on the bobbin and measurements were again resumed. These measurements were unsatisfactory because the magnetic fields associated with the leads that made up the electrodes were of such magnitude as to produce a considerable probe output and obscure the contribution produced by the skin currents. These effects manifested themselves in the form of asymmetrical pickup by the probe. That is, 180° orientation of the winding from its position of maximum pickup did not result in the same readings. Maximum reduction of these effects was achieved by increasing the size of the metallic surface to a 3' x 6' sheet of aluminum on which the electrodes were placed on the short dimension 2 feet apart. In addition, the electrode leads were encased in iron conduit which had a wall thickness of 1/8". To further reduce any anomalies the 10,000 turn winding was encased in a mu-metal shield that was open in the direction of the skin under test. This shield also provided isolation from fields set up by currents in devices other than the skin under observation. To further reduce anomalies in any measurements due to electrostatic effects, the opening in the mu-metal shield was covered with copper 0.005 inches thick.

Alteration of the fields from their true value due to the proximity of the loop and its shield were considered, and a disk of Teflon 1/2" thick was made part of the probe to separate it from the skin. This also enabled the measurements to be made with some uniformity by providing a known separation between the loop and skin. An outline of the entire probe and its components are shown in Figure #3.

Mapping of one-half of the 3' x 6' skin with the 10,000 turn probe was done at 70 cps, 1 kc, and 15 kc. All these measurements indicated the relative current distribution to be approximately the same. The measurements are shown in Figures 4, 5, and 6. The area inside the dotted curves (on Figures 4, 5, and 6) which roughly correspond to the maximum distance from

the electrodes and the edges of the metal surfaces, exhibit magnitudes which differ from the theoretically predicted by one db or less. In fact, at approximately the geometric center of the half sheet, the current magnitudes were as theorectically predicted. This further indicated that deviations from the theoretical were due to the fields from the electrode leads, and the concentration of currents on the edges.

The mapping indicated that current magnitudes were approximately as expected. The heaviest concentration being along each edge of the skin. This concentration most likely occurs because the lines of current are forced to flow along the edge until they regain their natural path. Theoretically, if this edge did not exist (infinite sheet) no bunching would occur.

In order to further substantiate the accuracy of the measurements, a small winding was fixed in one place above the skin. Its output was monitored before and after the test probe was placed in the near vicinity. The output of the fixed winding varied less than 0.5 db even when the test probe was moved to within 1/8" of the fixed probe. These measurements were made at 70 cps, 1 kc, and 15 kc. Therefore, it is concluded that any field distortions created by this probe are negligible over this frequency range, and that the current distributions mapped are truly representative of the actual distribution.

Measurements were then conducted to determine the relative directivity of the probe. This measurement was carried out in order to determine the directional characteristics of the probe and the degree of shielding from magnetic fields generated away from the skin.

The measurements were conducted utilizing as a source, the magnetic field generated by a current in a winding of small dimensions. The skin current probe was then set up as a receiver. The size of the source and the distance separating the source from the receiver were of such magnitude that the magnetic field could be considered emanating from a point source, which provided a uniform field across the aperture of the skin current probe.

The probe was set up on a mount that could be rotated horizontally about one point through 360°. The coordinates of this system are such that the zero degree position occurs when the probe, oriented about a vertical axis, has the aperture of the mu-metal shield pointing directly at the source. The 180° position occurs when the mu-metal aperture is pointing directly away from the source. The 90° and 270° positions are then perpendicular to each side of the probe.

With the source emergized and the probe in the 0 degree position, the probe was then rotated about a horizontal axis to obtain maximum pickup or proper polarization. Then the relative output of the probe was recorded for every 15° of rotation about the vertical axis. These measurements were performed at 100 cps, 1 kc, and 15 kc and are shown in Figures 7, 8, and 9.

The measurements indicate that over the low frequency portion of the spectrum, diffraction around the mu-metal shield occurred, so that only about 10 db of shielding was achieved from the 120 to the 240 degree positions. This would correspond to 10 db of shielding for any fields coming from 30 to 90 degrees above the skin under test. The pickup was definitely from diffraction because placement of a magnetic shield over, but not touching, the copper aperture dropped the signal intensity to the ambient of the NM-40 receiver. The deepest nulls that occurred were near the 90 and 270 degree positions, and were the result of attenuation provided by the shield. These positions would normally correspond to a winding orientation such that the greatest number of turns would be cut by the magnetic field. Thus, without this shield the greatest output would result at the 90 and 270 degree positions.

At 15 kc, the pattern shows a decrease in the diffraction effect due to an increase amount of shielding from 90 to 270 degrees. Also, the increased output at 45° from the 0° position indicates that at these higher frequencies the shield does not alter the primary directivity of the winding, until a greater amount of the shield is physically interposed between the source and winding.

Due to the directivity and close proximity of this probe to any skin under test, any measurement made of skin currents should be fairly accurate.

An effort was made to increase the degree of shielding from external fields by placing the winding deeper within the mu-metal can. Unfortunately, the degree of attenuation in the desired pickup directions was increased also.

A larger diameter shield may have reduced this effect; however, the increased distortion of the field because of the greater surface area was considered to be more detrimental than the possibility of anomalies created by external fields.

## IV. D.C. PROBE DEVELOPMENT

The characteristics of a Hall Effect generator appeared to have promise as a d.c. skin current probe. The first measurements were hampered by the lack of a sufficiently sensitive detector. However, a Hewlett-Packard type 425AR d.c. microvoltmeter provided the ability to carry out the measurements when the Hall sensor output was at least one microvolt.

Measurements were started with an Ohio Semi-Conductor HS-51 Indiun Antimonide sensor. However, upon application of a d.c. control current, an output of approximately 0.3 mv was obtained without any skin current flowing. This output was determined to be due to the resistive zero component (units of $r_o$ = volts/amps) and not due to an external magnetic field. The output, which exists without an external magnetic field, is caused by the physical configuration of the Hall generator (the bias current develops a voltage

gradient between the Hall output terminals). The magnitude of this unwanted output may be reduced by careful manufacturing techniques. Other sensors were investigated and a Siemens FA-24 sensor indicated the lowest resistive zero component, which had a magnitude of 23 microvolts.

Siemens literature also indicated a method of compensating for the resistive zero component by external circuitry. However, the Hewlett-Packard 425AR has a meter which is set at zero in its center position. Therefore, the resistive zero component was zeroed out with the meter's control circuit rather than the external circuitry indicated by Siemens. In all measurements with the FA-24, a d.c. control current of 230 milliamperes was used. This was a compromise between sensitivity and the amount of resistive zero output.

Sensitivity of the FA-24 was such that one microvolt of Hall output corresponds to approximately 0.05 gauss. Mapping of the d.c. field created by two electrodes mounted 2 feet apart on a 3' x 6' sheet of aluminum was carried out first. This was done with an FA-24 sensor alone. No flux collectors were used to increase the sensitivity. However, in order to provide field magnitudes somewhat in excess of the minimum measurable, a total of 320 amperes flowing in the skin was required. The results of these measurements are shown in Figure #10. Here again, as in the a.c. measurements, the fields from the electrode leads and bunching of currents along the edges of the sheet create anomalies such that the measured magnitudes did not always correspond to those theoretically predicted. However, inside the dotted areas of Figure #10, the measured relative magnitudes are within one db of the theoretical.

Some effort was exerted to improve the sensitivity by utilizing flux collectors. The materials used were Hy-Mu 800, and General Ceramic's Q-1 Ferrite. Carpenter Steel Company manufactures Hy-Mu 800. It is a vacuum melted material consisting of nickel and molybdenum balanced iron. The FA-24 sensor has a length of 3/4" and a width of 3/8", and the Hy-Mu 800 in the form of 0.004" laminations were stacked to the sensor's dimensions. The length of the collectors were then varied from 4.5" to 9". The gains vary from 27 db to 35 db. These gain values were determined by utilizing the field created by 2 large permanent magnets set 3 feet apart. The method of determining the gain was to place the Hall sensor by itself exactly half-way between the poles and measure the Hall output. Next, the flux collectors were added, and with the Hall sensor at its original position the Hall output was again measured. The ratio of these two readings yielding the gain.

The laminations making up the flux collector were held in place by a rectangular fiberglass tube. The sensor was placed in the center and each half of the flux collector was butted up against it as tightly as possible. No attempt was made to make the collector of larger cross sectional area and taper down to the dimensions of the sensor.

In order to determine some of the factors involving flux collector gain an investigation of various collector parameters was carried out. The

General Ceramic Q-1 Ferrite material used as a collector was in the form of 1/4" O.D. rods. The gain versus length was studied and was found to vary from 22 db, for a length of one inch each side of the sensor, to 38 db for a length of 12-1/2" each side of the sensor.

The outer diameter of the flux collector was varied while holding the length constant. However, no change in gain was noted. Thus, it appears that no significant improvement in gain will result once the active portion of the Hall sensor is covered with the collector material.

Another conclusion reached is that the Hy-Mu 800 material, having a higher permeability than Q-1, yields a higher flux collector gain for the same length of material. A comparison of the Hy-Mu 800 flux collector gains and the Q-1 gains are shown in Figure #11.

Mapping with a Hy-Mu 800 collector having a total length of 6" and a gain of 30 db could then theoretically be accomplished with 10 amperes of d.c. current flowing in the 3' x 6' sheet of aluminum. This would correspond to sensing magnetic fields as low as about $1.5 \times 10^{-3}$ gauss.

Measurements using the Hy-Mu 800 6" collector were carried out with 47 amperes of total current flowing in the skin. These measurements are shown in Figure #12, and exhibit about the same characteristics as those taken with the sensor alone. Again, inside the dotted area, agreement between relative measured magnitudes and those theoretically predicted were within one db of each other.

Distortion of the magnetic field with the Hall sensor alone should have been at the very minimum possible. All mapping was carried out with the sensor 0.75" above the skin. Since the mapping carried out with the flux collector had the same general characteristics, it is considered that the distortion of the field was not significant at this height above the skin.

Further investigation of the distorting effects of the collector were carried out. This consisted of placing a Hall sensor flat against the skin and monitoring its output while the collector was moved to various positions adjacent to the sensor. The maximum alteration of the sensor output occurred with the middle of the sensor 0.75" directly above the sensor. This deviation in output was about 8.5%, which corresponds roughly to a 0.75 db change. Therefore, the current distributions do not appear to be severely altered, and accurate mapping of d.c. fields can be carried out with this probe.

It appears that any increase in sensitivity will have to come from an increased output of the Hall device or increased sensitivity of the detector. Increase in flux collector size is not desirable because of the increased distortion caused by the probe and because mapping of small increments of area will not be possible. Also, increased sensitivity will also lead to inaccuracies caused by the earth's magnetic field.

## V. MAPPING OF HIGHER PERMEABILITY SKINS

An investigation was carried out to determine whether the skin current probes (both d.c. and a.c.) developed would have a change in sensitivity and/or capability of accurately mapping a metallic skin having a permeability greater than aluminum or copper. A soft iron skin having dimensions 1/16" x 3' x 6' was energized with current flow between two electrodes.

Mapping at both d.c. and a.c. was again carried out with the probes that had previously been described.

A total of 50 amperes of direct current was passed through the skin, and the mapping with the d.c. probe is shown in Figure #13.

The anomalies created by the edges of the skin and the electrode fields were still present; however, the data inside the dotted curve agrees to within 1 db, or less, with that theoretically predicted. No decrease in sensitivity was noted. The capability of measuring d.c. magnetic fields as low as $1.5 \times 10^{-3}$ gauss appears to be possible no matter what permeability the skin has.

Mapping with the a.c. probe was carried out at 100 cps, 1 kc, and 15 kc. These measurements are shown in Figures 14, 15, and 16. The mapped areas inside the dotted curves yield approximately the same results as with the aluminum skin. No degradation of sensitivity was noted.

## VI. DETERMINATION OF ABSOLUTE CURRENT FLOW

In order to measure the absolute magnitude of a.c. current in a skin, the transfer impedance of the 10,000 turn probe was determined by placing a known current through a strip of copper which had the same width as the probe aperture. The probe was oriented for maximum pickup and then its Teflon spacer was placed directly against the copper strip. The values of transfer impedance in db above 1 ohm are shown in Figure #17.

The sensitivity of the 10,000 turn probe was determined from the measured values of transfer impedance and voltage output. At 100 cps, 1 kc, and 15 kc, the sensitivity of the probe is respectively $1.25 \times 10^{-3}$, $1.25 \times 10^{-4}$, and $1.25 \times 10^{-5}$ gauss.

Theoretically, it is possible to determine the total current flow by summing the absolute readings taken of each skin segment. Stoddart Aircraft Company, in their final report for the U. S. Navy (Contract NB8-3189) carried out an investigation of this kind in the R.F. region.

The method here is to simply move the probe from one side of the skin to the other in jumps equivalent to the probe's aperture, and perpendicular to the general direction of current flow. This particular investigation

required 75 readings since the probe aperture covered slightly less than one inch segment of the skin under test, which had a total of 6 feet. A total current of one ampere was calculated to have been flowing in the skin. The summation of these readings indicated a measured value of 0.91 amperes. Some of this error occurred because of the difficulty in positioning the probe without over-lapping or skipping part of a skin segment. However, a 9% error is not considered objectionable, and the probability of increased accuracy when mapping a smaller skin is plausible.

The frequency of these measurements was 1 kc. The method of carrying of these measurements is shown in Figure #18. The ability to determine the absolute value of current flowing in any segment of skin will be of considerable benefit, especially where certain magnitudes are considered detrimental.

## VII. CONCLUSION

Within the sensitivities specified accurate mapping of skin currents between d.c. and 15 kc may be carried out. Furthermore, these probes are even more useful since they have the ability to determine absolute values of current, which might be harmful or detrimental.

## ACKNOWLEDGEMENTS

The work described above was carried out at General Dynamics/ Astronautics as a portion of U. S. Air Force Contract AF 33(616)-7393, (Development of Improved Techniques for Current Probes), which was under the cognizance of Communications Laboratory, Wright Air Development Division, now Aeronautical Systems Division.

Acknowledgement is gratefully made to Messrs. L. Chase, D. Grisel, and S. Babcock for their assistance, and to C. Hatchett and L. Clough for continuing the development of Current Probes.

Field Equation Is: $Q_1 \cos \theta_1 + Q_2 \cos \theta_2 = K$

Let $Q_1 = -Q_2$ $Q_1 = +1$ $Q_2 = -1$

Then: $\cos \theta_1 - \cos \theta_2 = K$

Solving For K At Points Such As P (below) Yields:

$\theta_1 = 32°$ $\theta_2 = 103°$

$\cos 32° - \cos 103° = K$

$0.85 - (-0.23) = 1.08 = K$

Relative Magnitudes Are Referenced To Straight Line Between Electrodes.

K For That Line Is:

$\theta_1 = 0°$ $\theta_2 = 180°$

$\cos 0° - \cos 180° = 1 \quad -(-1)=2=K$

Signal At P Is Down By 20 log 2 / 1.08 = -5.3 db.

Choosing A Point On An Arc Between The Electrodes Will Yield The Relative Signal Level That Should Be Present.

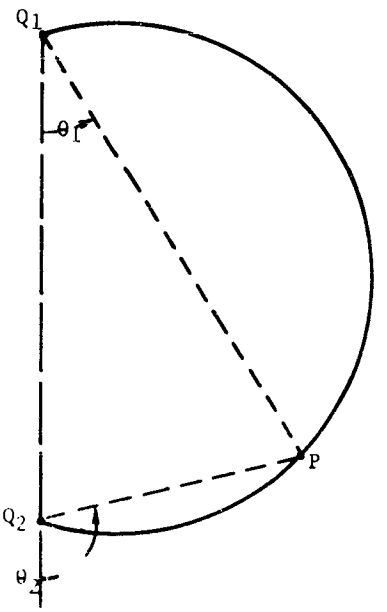



Figure 1. Sample Calculations For Theoretical Current Distribution

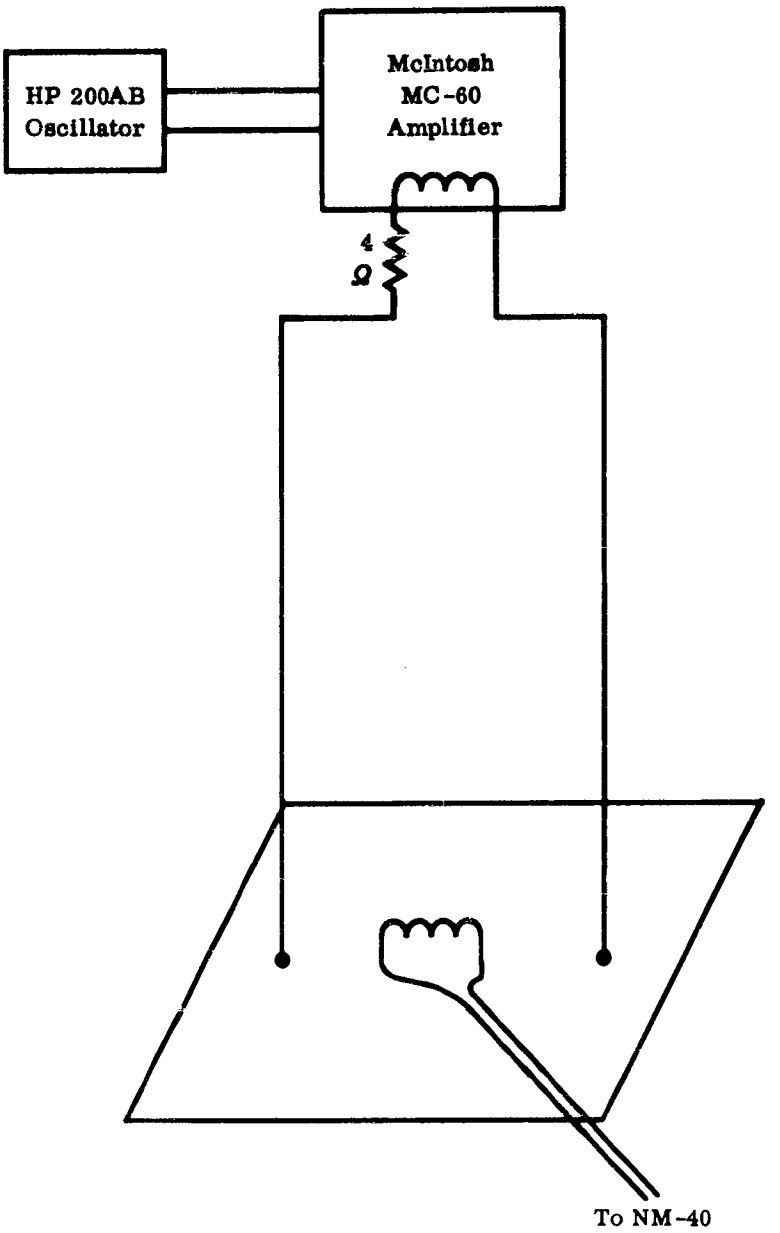
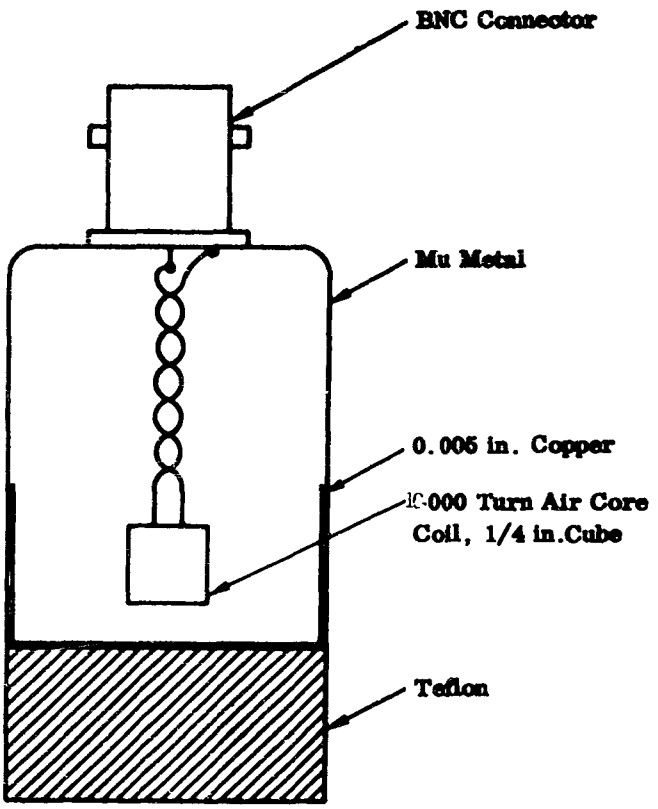



Figure 2. Set Up For Generating Skin Currents




Shown 2 X Actual Size

Figure 3. Skin Current Probe

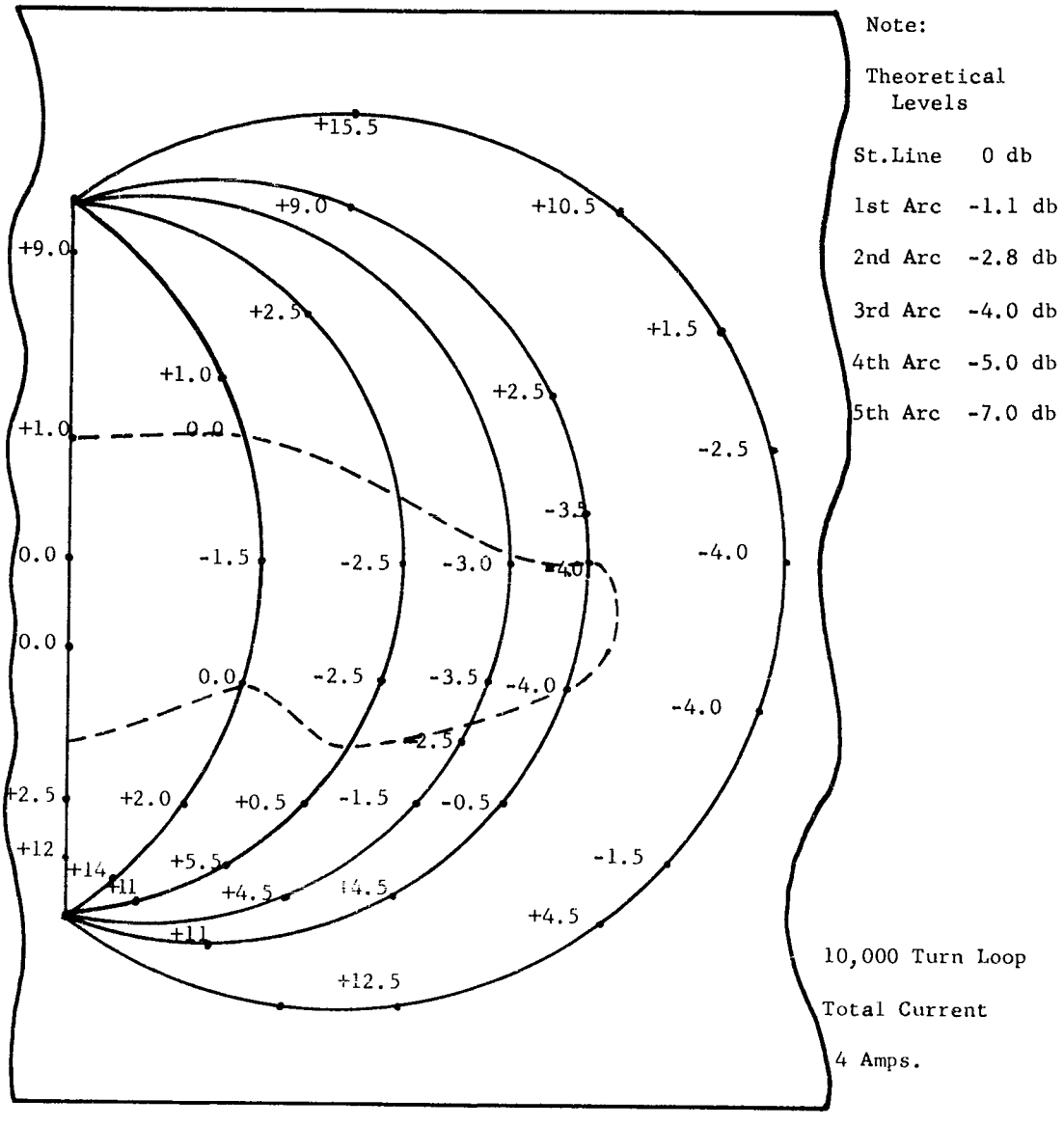



Figure 4. Relative Current Amplitude Measured At 70 cps

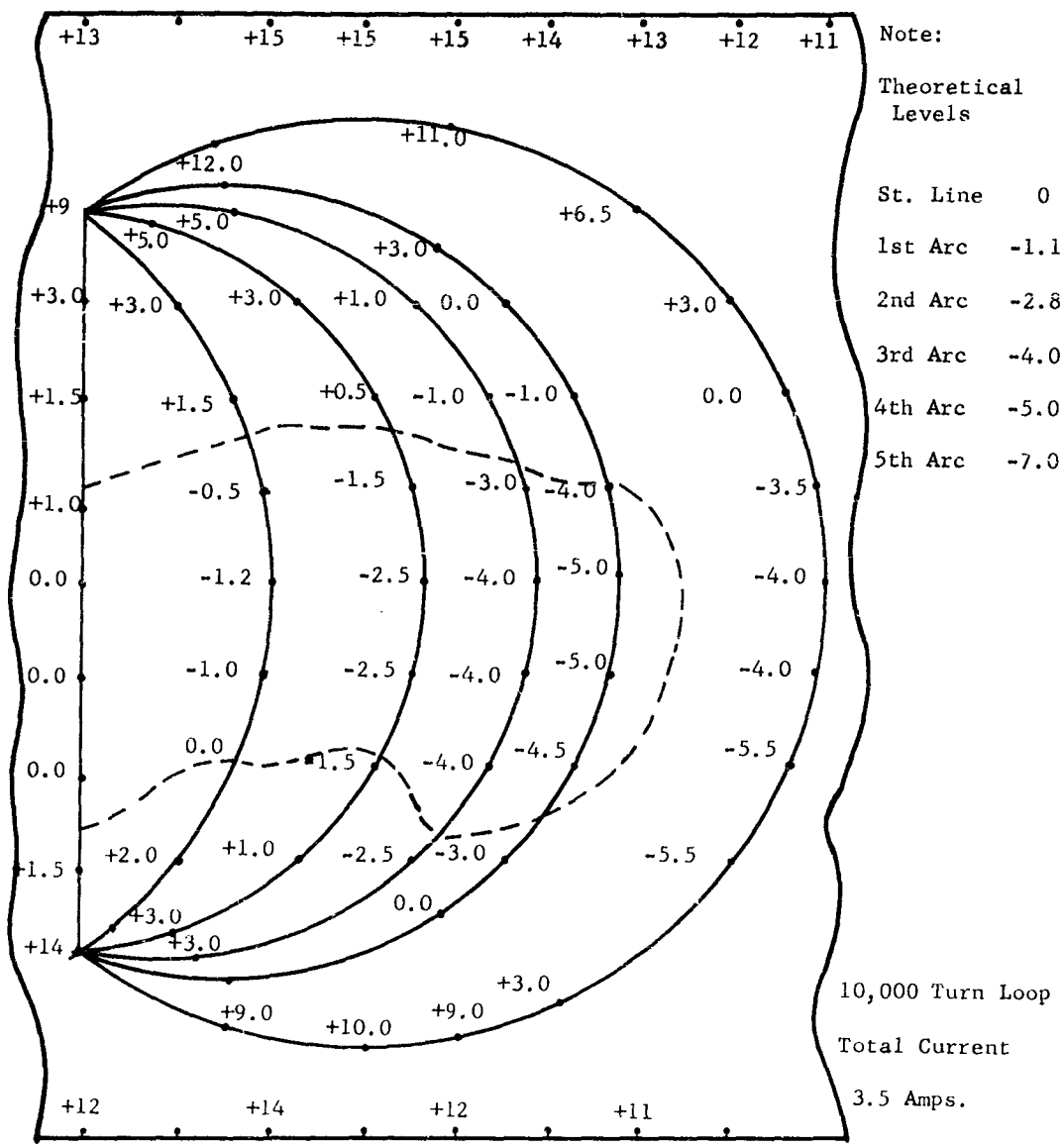
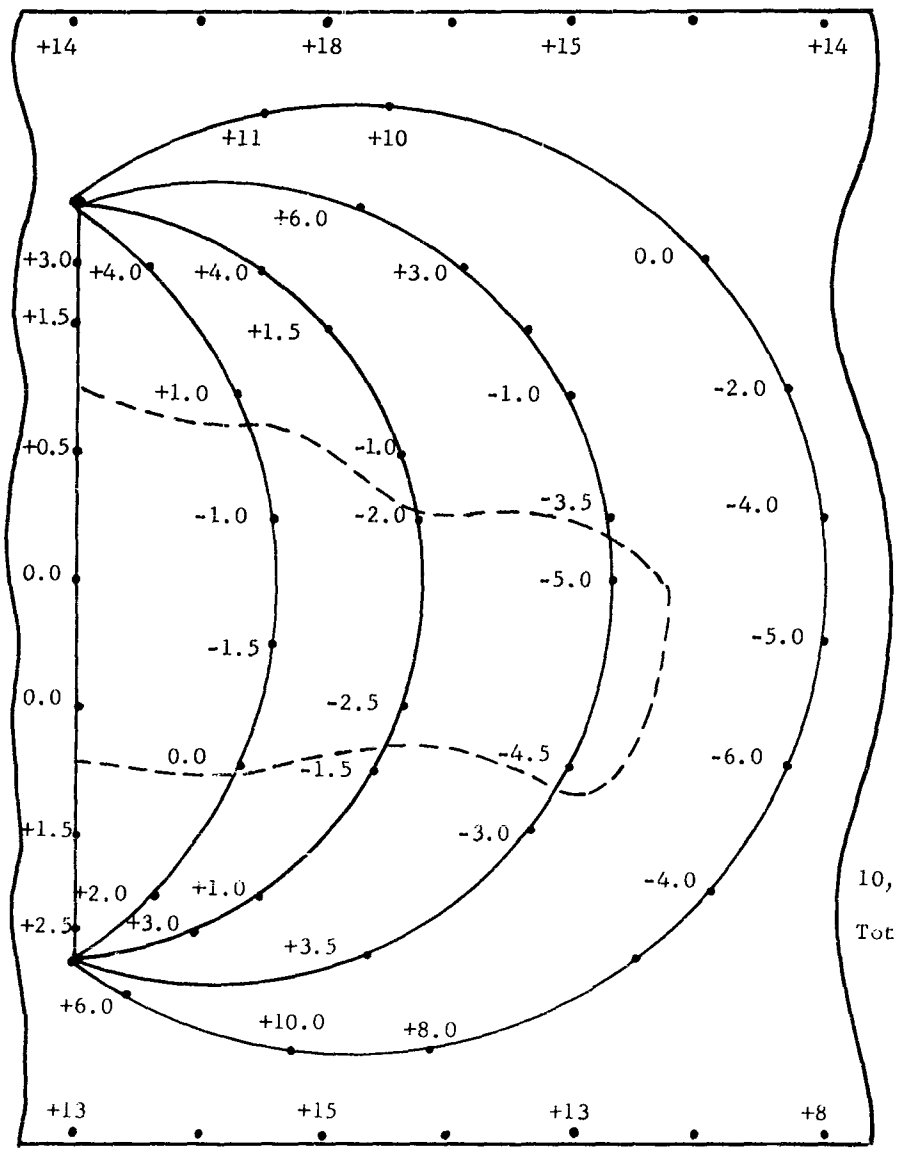



Figure 5. Relative Current Amplitudes Measured At 1 kc




Note:

Theoretical Levels

St. Line 0 db

1st Arc -1.1 db

2nd Arc -2.8 db

3rd Arc -4.0 db

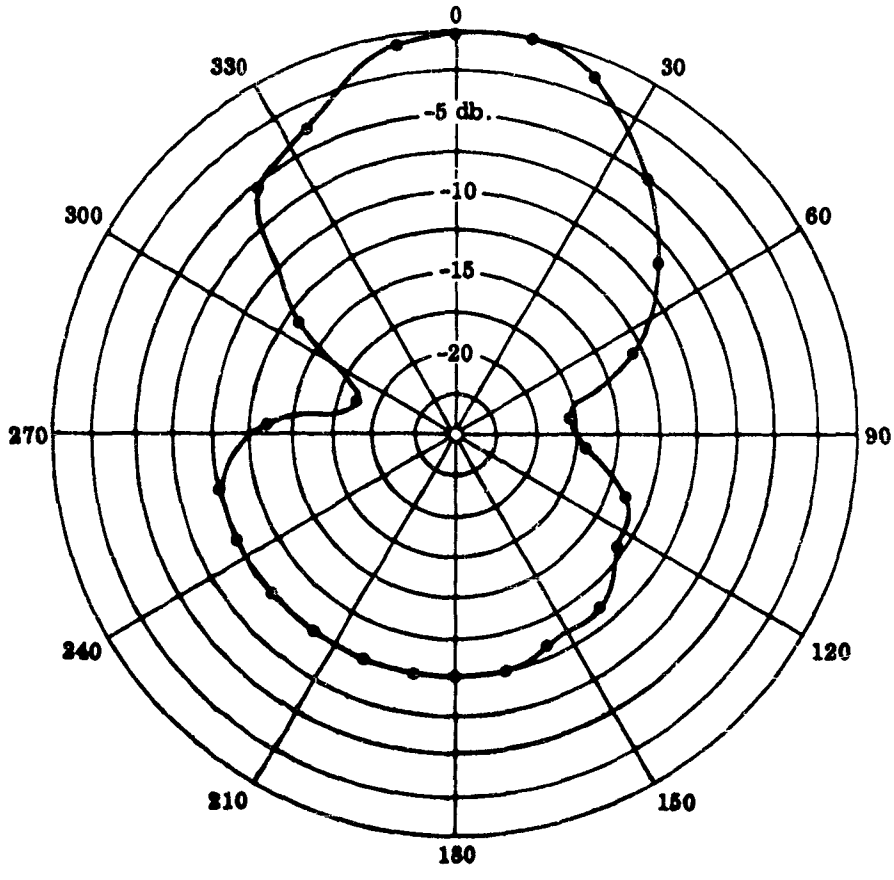
4th Arc -5.0 db

5th Arc -7.0 db

10,000 Turn Loop

Total Current 1 Amp.

Figure 6. Relative Current Amplitudes Measured At 15 kc

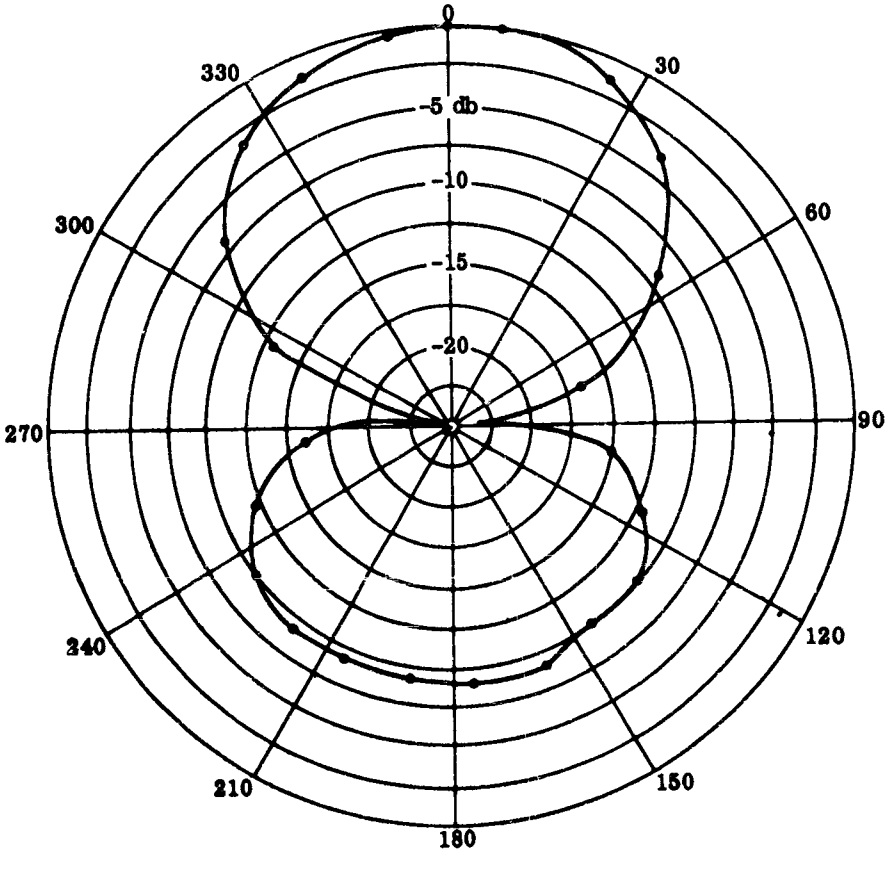



• Depth of Winding Inside Shield - 1/8 in.

Directivity of Skin Current Probe at 100 cps

Frequency = 100 cps

Figure 7. Directivity of Skin Current Probe At 100 cps

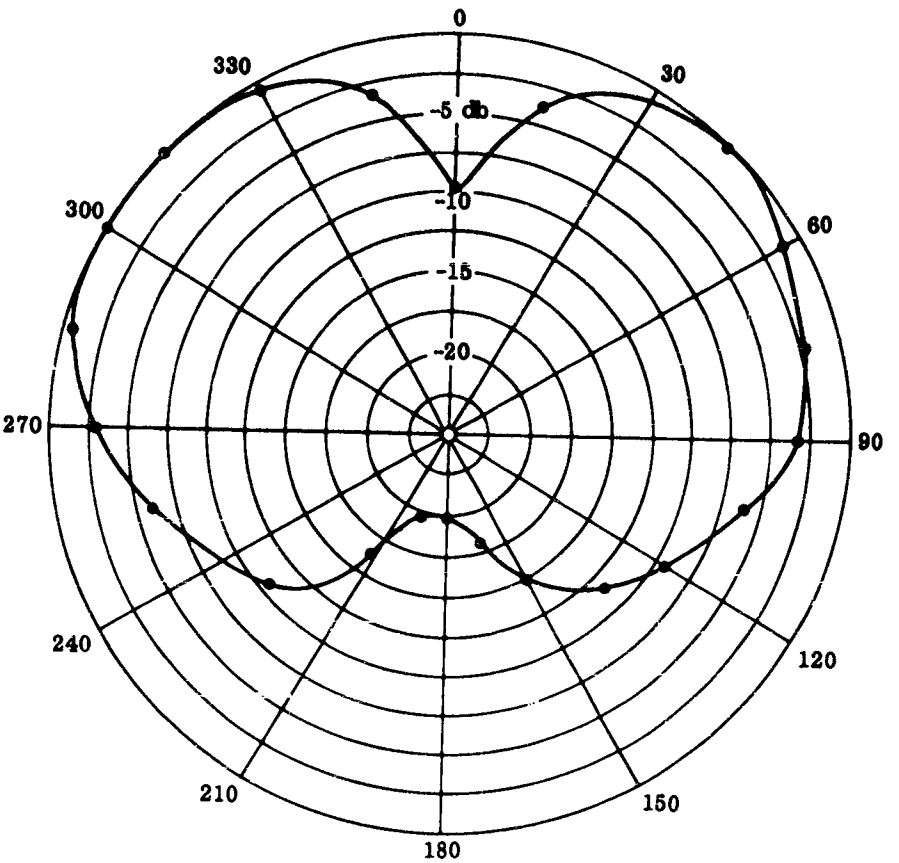



Frequency = 1 kc

Depth of Winding Inside Shield = 1/8 in.

Directivity of Skin Current at 1 kc

Figure 8. Directivity of Skin Current At 1 kc




Directivity of skin current probe at 15 kc
Frequency = 15 kc

Depth of Winding Inside Shield 1/8 in.

Figure 9. Directivity of Skin Current At 15 kc

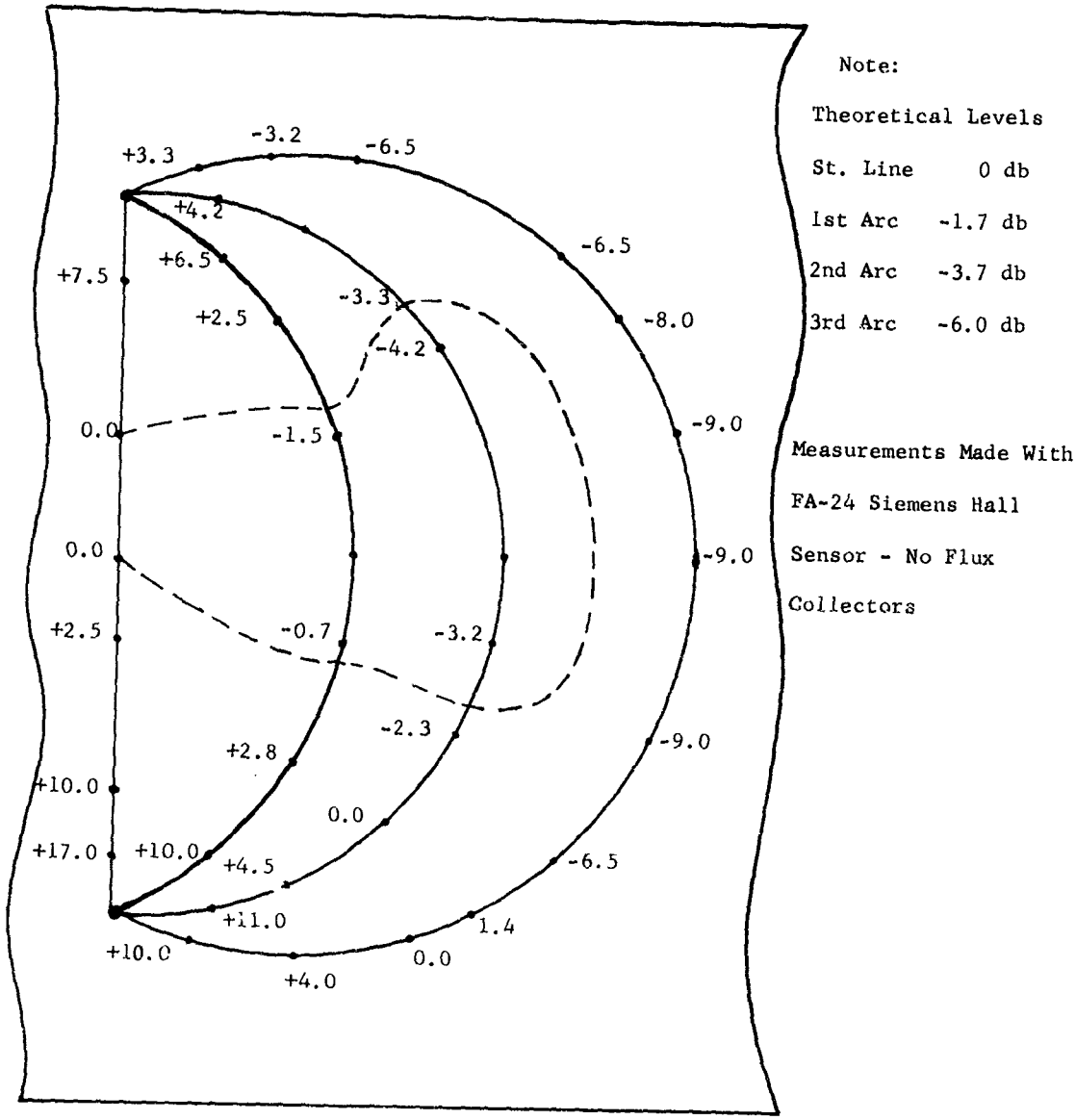



Figure 10. D-C Measurements of Relative Current Amplitudes At 320 Amperes

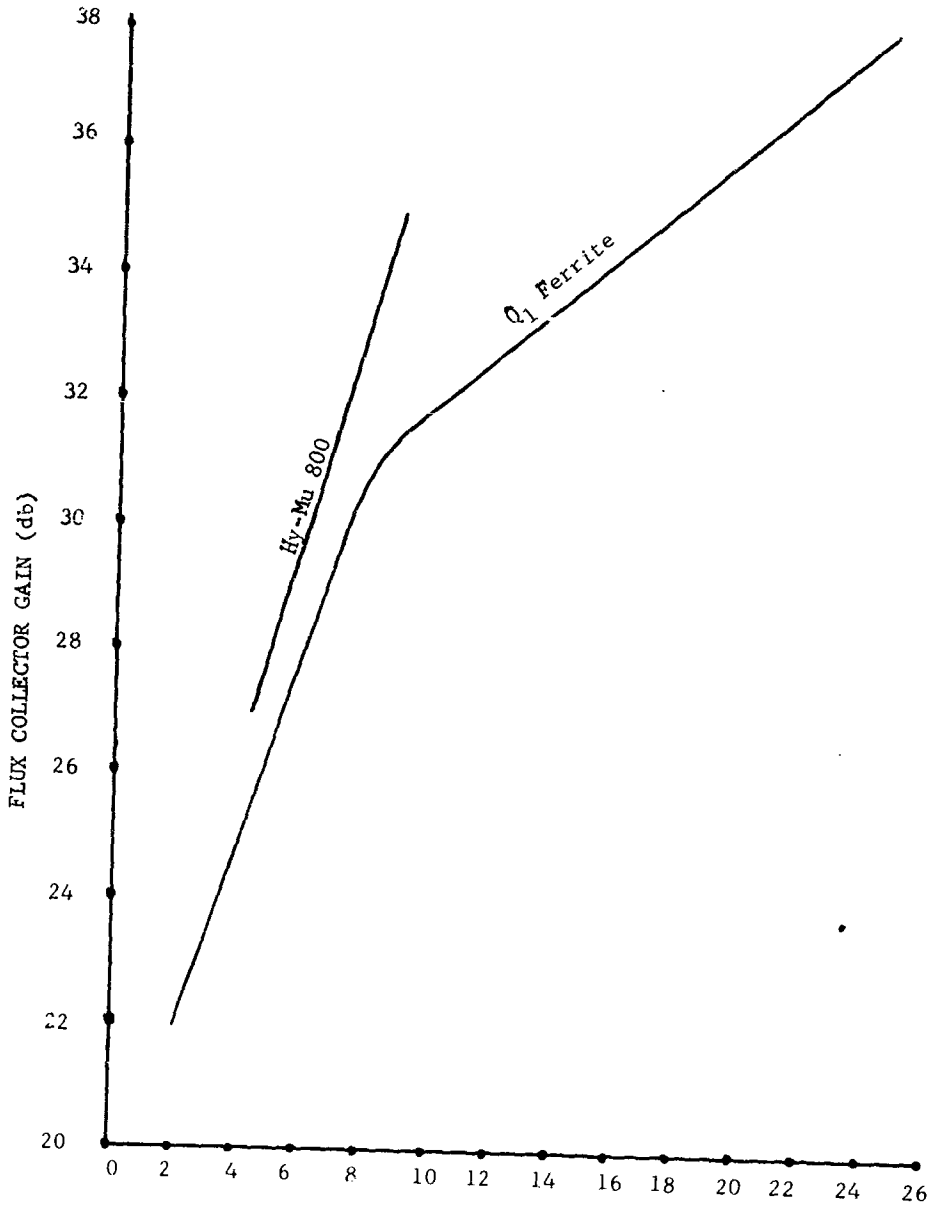
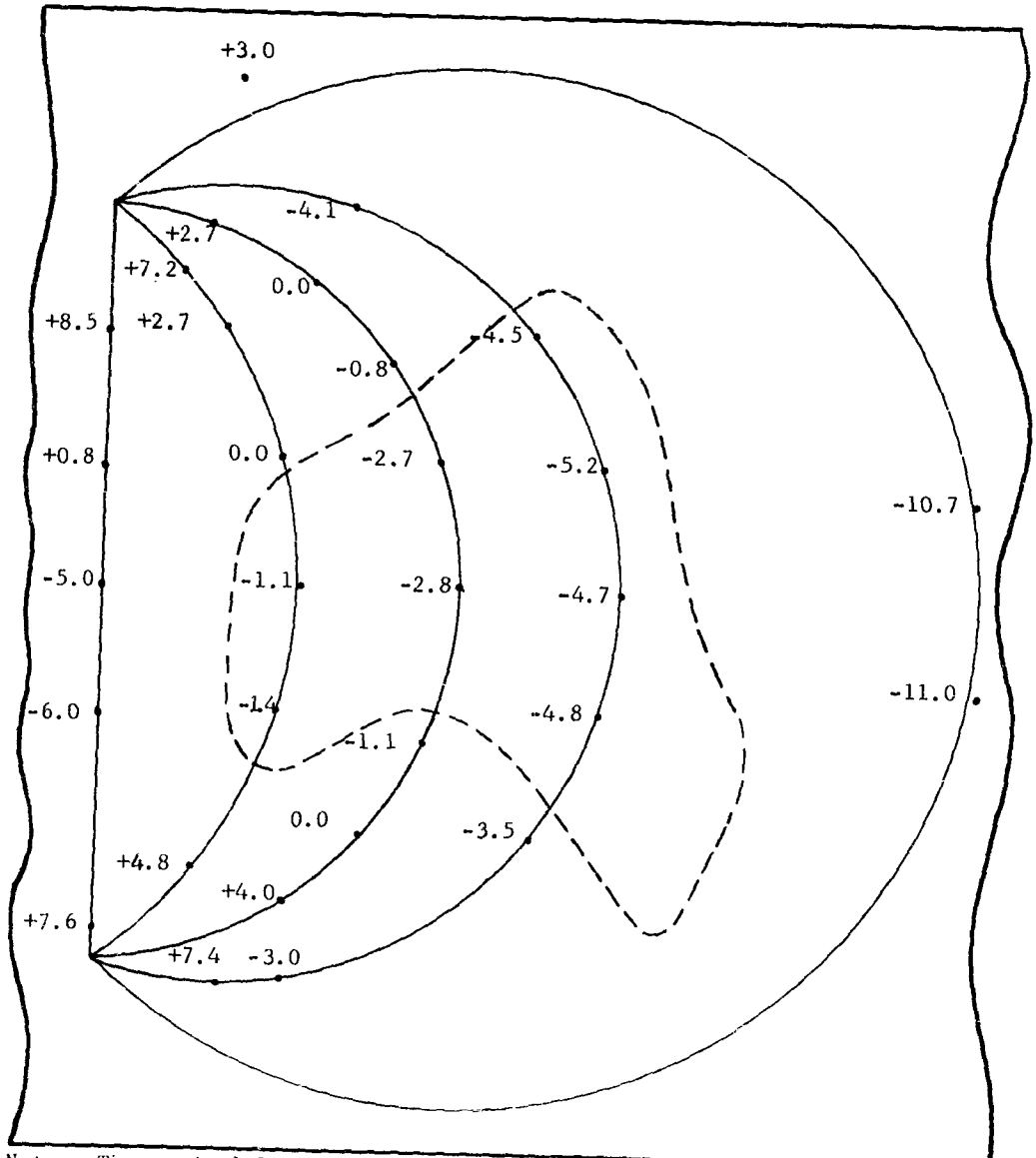


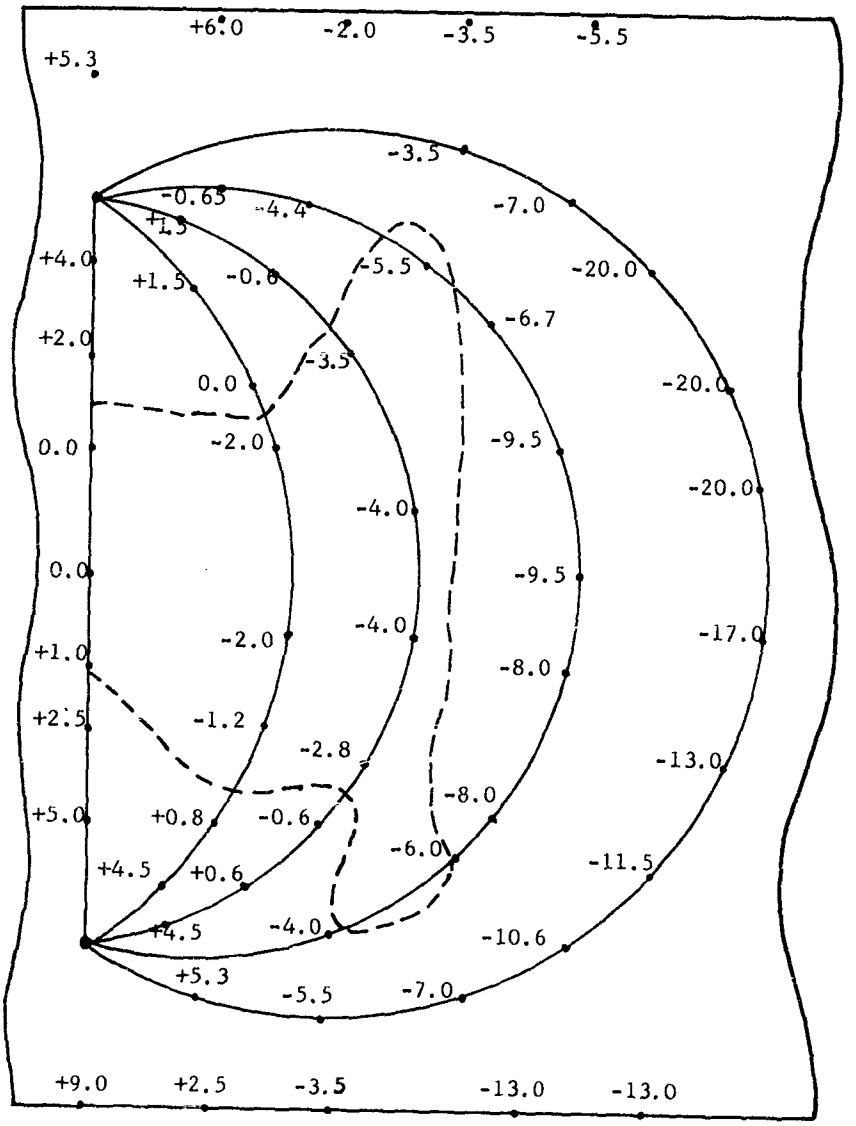

Figure 11. Flux Collector Gain Versus Flux Collector Length




Note: Theoretical Levels
St. Line 0 db
1st Arc -1.1 db
2nd Arc -2.8 db
3rd Arc -4.8 db
4th Arc -8.5 db

Flux Collector
Hy-Mu 800
Gain 30 db
FA-24 Siemens Hall Sensor

Figure 12. D-C Measurements of Relative Current At 47 Amperes

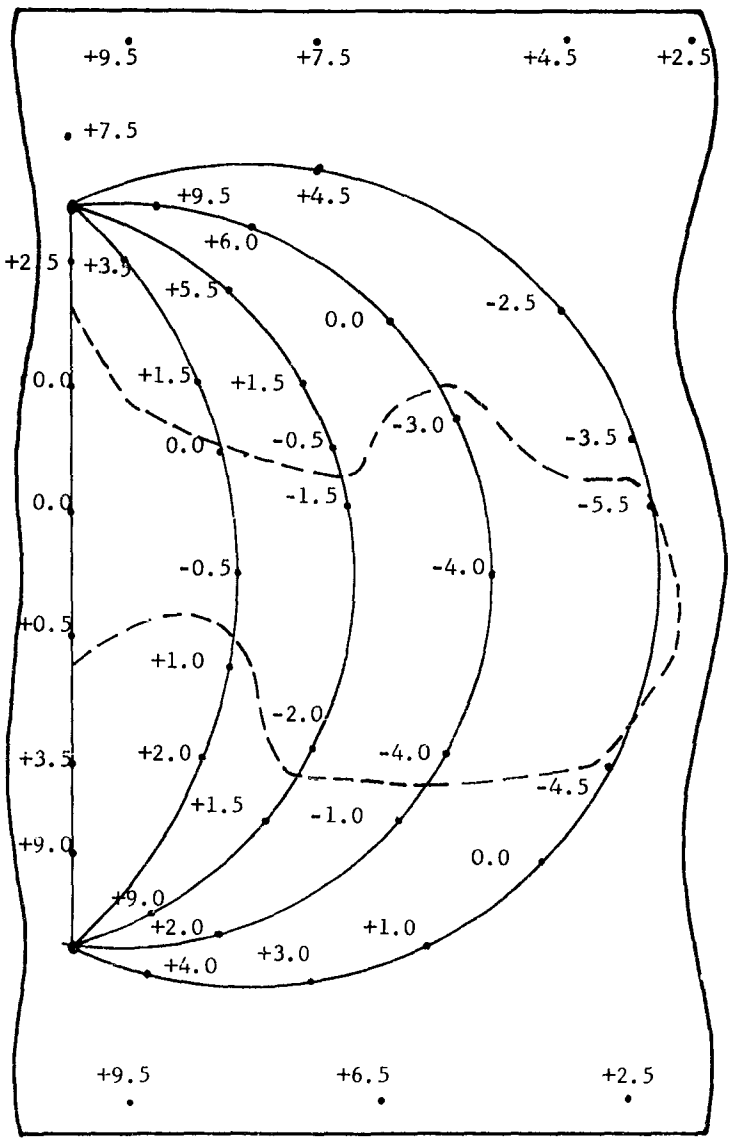



Note: Theoretical Levels

| | |
|---|---|
| St. Line | 0 db |
| 1st Arc | -1.3 db |
| 2nd Arc | -3.0 db |
| 3rd Arc | -5.0 db |
| 4th Arc | -7.0 db |

Measurements Made With FA-24 Siemens Hall Sensor And Flux Collector Having A Gain of 30 db.

Figure 13. D-C Measurements of Relative Current Amplitudes At 50 Amperes




Note:

Theoretical Levels

| | |
|---|---|
| St. Line | 0 db |
| 1st Arc | -1.0 db |
| 2nd Arc | -2.0 db |
| 3rd Arc | -3.5 db |
| 4th Arc | -5.3 db |

10,000 Turn Loop

Total Current 2.5 Amps.

Figure 14. Relative Current Amplitudes Measured At 100 cps

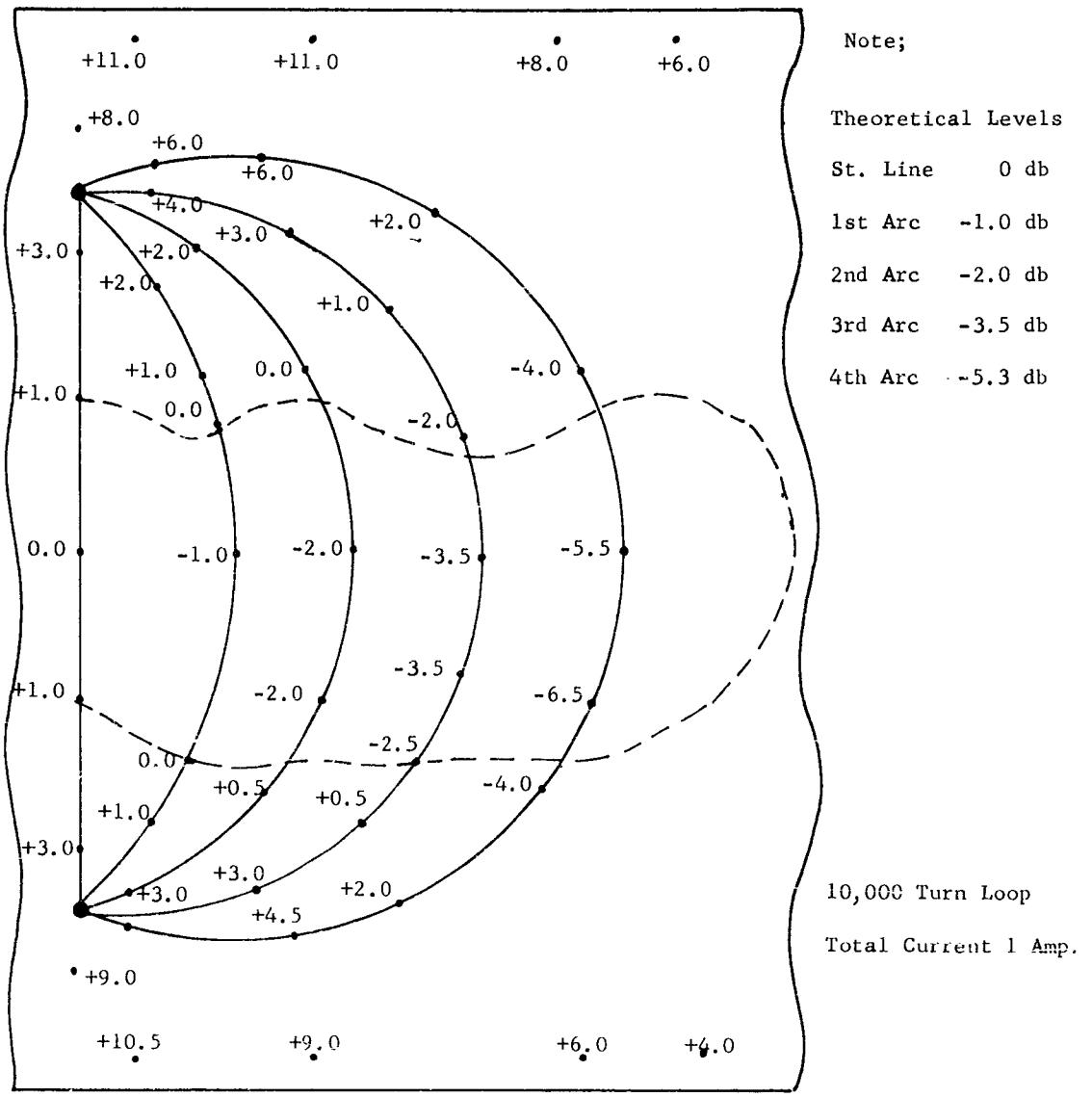



Figure 15. Relative Current Amplitudes
Measured At 1000 cps

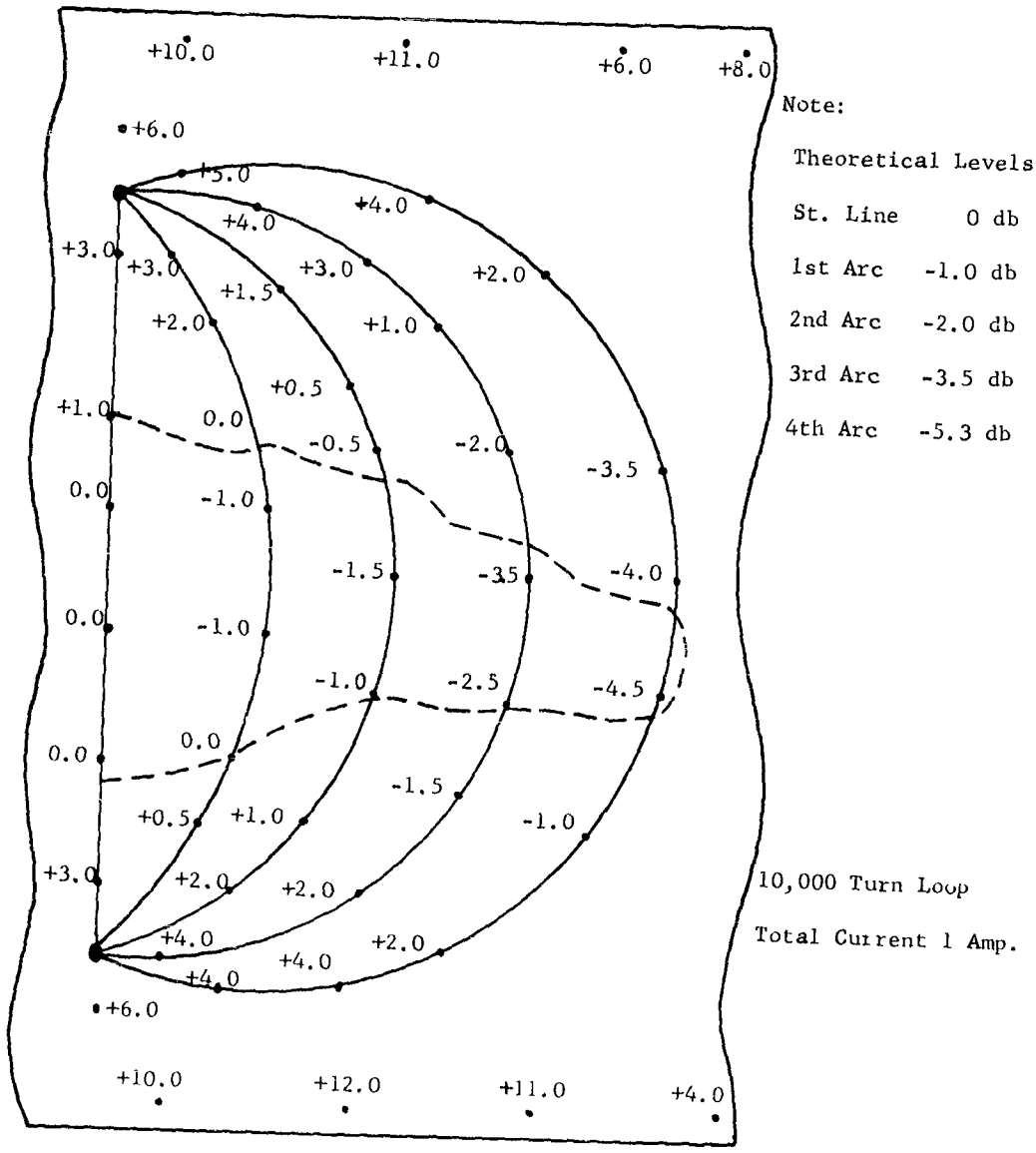



Figure 16. Relative Current Amplitudes Measured At 15 kc

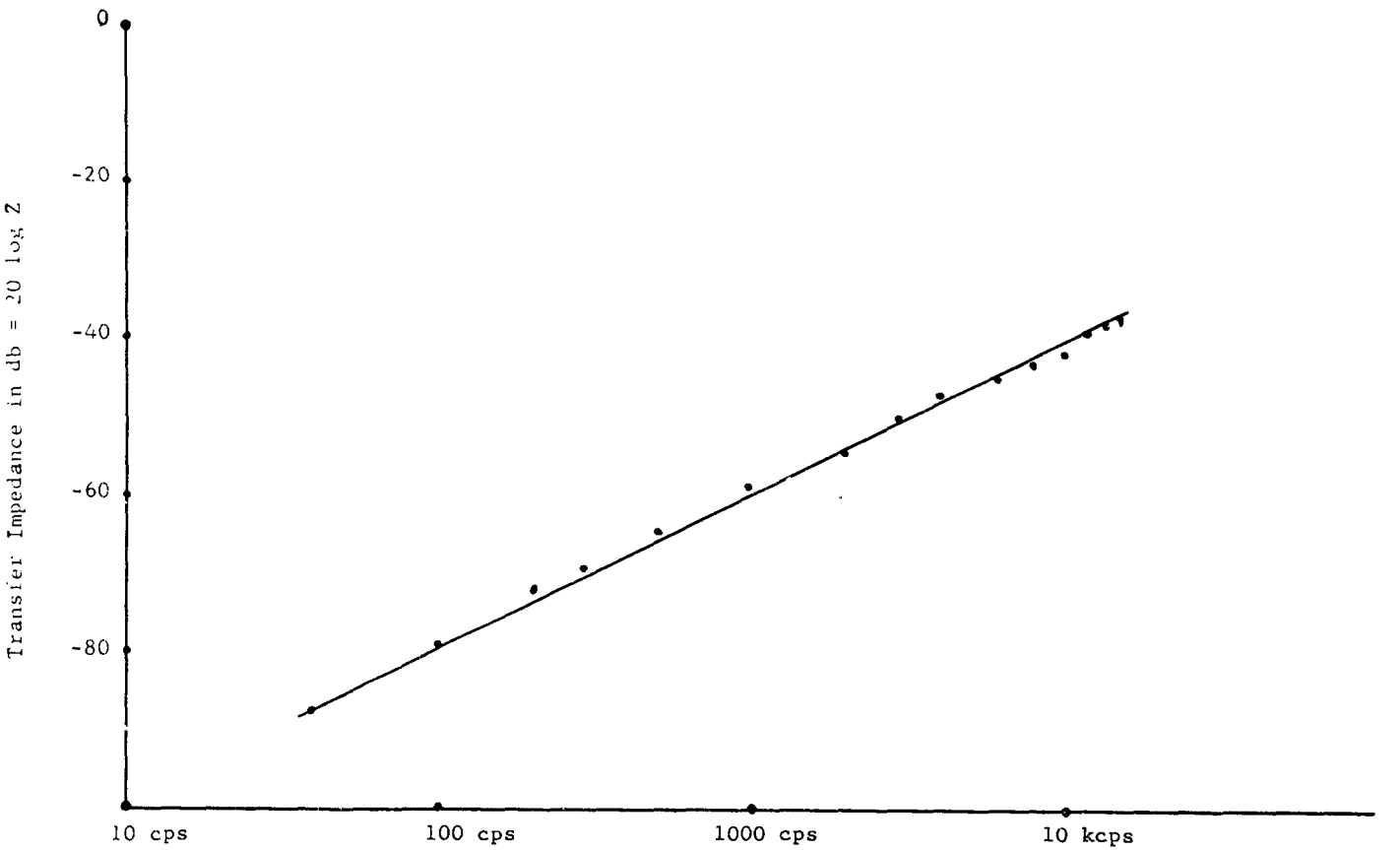
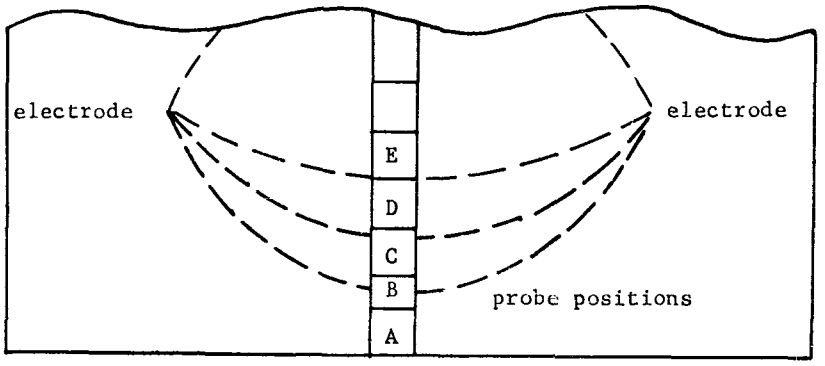



Figure 17. Transfer Impedance Versus Frequency (10,000 Turn Loop)




Total Current Flow Is Equal To The Summation The Readings Yield.

If The Probe Has To Be Positioned At An Angle To Get An Integral Number Of Skin Segments, Multiply The Reading By (1 / cos θ) To Obtain The True Value Of Maximum Current.

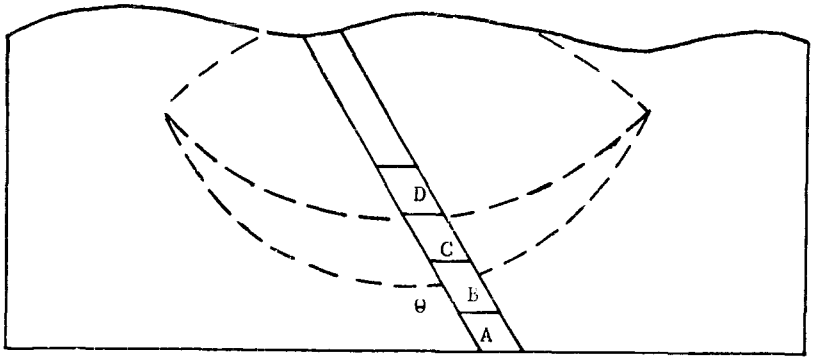



Figure 18. Determination of Absolute Current Magnitudes

# THE INTERFERENCE PROBLEM ASSOCIATED WITH POWER SYSTEMS AND COMMUNICATION LINES

By

R. F. Ficcki

RCA Service Company

Abstract: The history of the problem is first outlined in which it is shown for a considerable time up to the recent present, the interference problem was readily handled by inductive coordination committees. In the U. S. this included even the joint use of poles in rural areas. But the communication systems that were involved were normally unessential telephone services which as long as the noise did not render voice transmission unintelligible and as long as acoustical shock was avoided, presented no overall serious problem. With large extended military systems using digital communication techniques, the problem emerges into an entirely different light. The signal to noise ratio becomes more critical and pulses generated by unwanted signals can completely alter the character of the transmitted message so that erroneous information may be transmitted. This problem comes into sharp focus because of the fact that large ground communication systems are being installed in isolated areas in which oftentimes, the communication line has to traverse an area, which, because of its site advantages, has already been used by a power transmission line. An example of this is the use of a ravine to eliminate the need of crossing over a high hill or mountain. A further consideration is the fact that on many of the newer systems, the communication line is buried in the earth.

The theory necessary to determine the effect of the power system on a communication line has been worked out many years ago. But like most theoretical treatments, it is necessary to do considerable improvising to come up with practical working tools to determine the effects of power systems. Empirical formulas are developed and their use is explained. Specific examples of the effect of a power system on a communication line is worked out. Finally, general rules are developed which will give guide lines as to how this particular interference problem can be minimized.

## I. Introduction

The developing needs of the various missile programs in the U.S. have imposed the need for extensive space requirements so these missile systems may be properly installed. Obviously such extensive space requirements can only be met by the emplacement of the Missile systems in areas of low population density. In this way, hardened underground sites can be readily obtained and no great limitation will be imposed on the normal conduct of business in the affected area. In at least one of these systems, the Minuteman, these hardened underground sites are interconnected by means of buried communication cables. These cables generally connect from site to site using the most direct route, with adequate attention being given to the fact that unusual physical problems should be avoided if possible. If, for example, to traverse from point A to point B it were necessary to cross over an elevated section of ground, and an alternate route that was less direct, but alongside a road that skirted this elevation, then the choice would be made to follow the road and avoid the elevation. Generally all these topographical situations should be used to advantage: roads, valley, ravines, railroad right-of-way, etc. will be followed. It would appear that this approach would facilitate the installation problem and, generally speaking, this is quite true. Installation of a buried cable system is facilitated when every natural advantage of a site is

utilized. But there is another side of the coin that must be considered; someone has been there before. For years, the U. S. has prided itself on the fact that electric power and telephone communications has been brought to the most inaccessible regions. And it is a record to be justly proud of; we do have rural electrification and rural telephone systems. But these services when brought to remote areas have also used natural site advantages. It comes as no great shock that, when a buried communication cable is installed connecting two hardened sites, it must traverse an area whose natural advantages have already been utilized by a power company. It is true that the cable link can be installed along a road and thereby avoid an arduous cross-country path, but when such an installation is made, the communication cable path parallels a high voltage transmission line.

When a high voltage transmission line and a communication cable are operated in close proximity, certain undesirable effects may be produced in the communication cable which may interfere with its intended operation. These electrical interference effects can result in the malfunctioning or non-functioning of the communication cable, physical damage to the communication cable that will degrade its reliability or intermittent damage which will develop a requirement for more frequent maintenance. Obviously, the most directly damaging effect would be the rendering of the communication system inoperative or, at least, to cause the communication system to operate at level below that which is considered satisfactory performance. Such electrical interference effects which appear as a result of extraneous voltages and currents in a communication system may be minimized by measures that are applicable to either system above or to both systems. In the situation under discussion, the measure that can be applied to the communication systems will be elaborated.

## 2. General Background

Historically, the interaction of the electrical effects between power and communication systems has been known as the inductive coordination problem. The Bell System and the Edison Electric Institute have published much of the important work in this field. These publications represent the most important respository of such information and are of great use to the communication and power industry. This inductive coordination may be defined as the location, design, construction, operation and maintenance of power and communication systems in conformity with harmoniously adjusted methods which will prevent interference. This coordination problem becomes more severe as the power systems grow larger and as the communications systems become more sensitive and their use more critical. And this problem is very broad: it includes power transmission circuits, d-c and a-c railway signal circuits, the effect of high voltage transmission circuits on low voltage supply circuits, currents on underground pipe lines, etc. For the purposes of this paper, the effect of a power transmission line on a communication system will be the case under consideration.

## 3. Statement of the Problem

In the installation of one of the large extended missile systems it was found in connecting two sites that the communication cable had to traverse, so that the installation problems would be minimized, an area that would require this communication cable to roughly parallel a 100 KV power line for approximately 2.7 miles. The exposure was not exactly parallel but varied as the contour of the ground varied. The 100 KV power system was an aerial line supported on transmission towers as shown in Figure I and was a 3 wire grounded system with additional characteristics that it transmitted this raw power with the usual harmonics and variable loading. The communication cable is direct buried multiconductor, triple jacketed polyethylene cable used for the transmission of digital messages with 10 mil copper shield and

2-10 mil steel tapes. A cross section of this communication cable is shown in Figure 2. The exposure of this communication cable system to the power system is shown in Figure 3.

4. Solution to the Problem

For any practical application of the results that can be calculated for such an exposure, limiting values for induced voltage, current, etc. must be known. One would expect the limiting values to be determined by technical considerations only, but because of the relatively complex mathematics involved to describe adequately the physical phenomena under consideration and because of the necessity of making a great number of empirical approximations to eliminate the difficulties imposed by the mathematics, limits that can be imposed are primarily a matter of judgement by experts. The limits that are used are those recommended by the Directives of the C. C. I. F. (Commite Consultatif International Telephonique). The C. C. I. F. has specified that the maximum tolerable interference level to be 2 Miltivolts r. m. s. for telephone circuits. It was decided that this would be a satisfactory criteria for the communication system.

Since this communication cable is buried in the earth, a matter of prime consideration is the determination of how the current will travel in the surrounding soil and how these currents will affect the communication cable. The distribution of an a. c. current in soil, which determines the mutual, inductance between the communication systems and a power system with a ground return may be deduced from Maxwell's equations. However, to simplify these deductions, it is generally assumed that the relative magnetic permiability of the soil is unity and the displacement currents are negligible compared with conduction currents.

To calculate the inductive interference produced in the communication cable, it is sufficient to find the average force along the axis of the communication cable induced by the current flowing in the power system with a ground return.

The first calculation will be made to find the voltage per unit length induced in the communication cable.

The relationship between the various electrical parameters are given in the following formulae:

$$M = -j \frac{i}{\omega \sigma I} \quad (1)$$

$$\omega \sigma IM = -ji \quad (2)$$

where: $\omega = 2\pi f$

$\sigma$ = conductivity of the soil - .01 mho/meter

I = inducing current in amps from the power system

M = Mutual inductance in H/m

i = current density in the ground

The following symbols are used in the ensuing test and they are best defined at this point. (cf. Figure 1)

a = horizontal distance between power line and communication line in meters.

b = Height of the power line above the surface of the ground in meters.

c = Height of the communication line above the surface of the ground in Meters or for buried cable as in this case, depth below the surface of the ground.

d = Actual distance between power line and communication line in meters.

D = Distance between communication conductor and image of the power conductor on the surface of the ground in Meters.

$\sigma$ = conductivity of the soil in mhos per meter

$\omega = 2\pi f$

$\mu_o = 4\pi \times 10^{-1}$

$\alpha = \sqrt{\mu_o \sigma \omega} \qquad \alpha' = \sqrt{\sigma f}$

$\rho = \alpha' a \qquad P_d = \alpha' d \qquad P_D = \alpha' D$

J.R. Carson* in his classical paper has presented formulas for calculating inductive disturbances from power line in neighboring communication lines. He points out that at the time of writing this paper that the problem of wave propagation along a communication transmission line composed of an overhead wire parallel to the surface of the ground does not appear to have been satisfactorily solved. The solution that was presented emerged in the following general equation:

$$M = j \cdot \frac{\mu_o}{\pi} \int_0^\infty \left[ \sqrt{\mu^2 + j} - \mu \right] e^{-b\alpha\mu} \; e^{c\alpha\sqrt{\mu^2+j}} \cos(\alpha a \mu) \quad (3)$$

The evaluation of the integral in equation (3) is an involved task and requires certain assumptions to be made. Most authorities in the field agree that approximate solutions can be used that will give results that can be verified by field measurements. In all of these approximate formulas $\alpha = 2.8 \times 10^{-3}$ and it is the combination of this with other constants that determines which approximation may be used. As long as the expression p 180 is always satisfied, this approximation of Carson's formula may be used:

$$M = \frac{\mu_o}{4\pi} \left\{ \begin{array}{l} 12.981 - 2\ln\rho d + 2.649 \times 10^{-3} \alpha'(b+c) \\ -j\left[\frac{\pi}{2} - 2.649 \times 10^{-3} \alpha'(b+c)\right] \end{array} \right\} \frac{H}{m} \quad (4)$$

* "Wave Propagation in Overhead Wires with Ground Return," BTL Monograph, B219, November 1926.

Authorities agree that all (b+c) terms can be neglected, therefore equation (4) reduces to:

$$M = \frac{\mu_o}{4\pi} \left\{ 12.981 - 2 \ln p_d - j \frac{\pi}{2} \right\} \frac{H}{m} \qquad (5)$$

This equation (5) is also valid for b and/or c $<$ o i.e. for communication cables buried in the coil at the usual depths which is the case under discussion. M depends now, apart for $\alpha'$ (which is a function of frequency and soil conductivity) only upon the actual distance d between conductors. Since the phase is irrelevant, the j term can be dropped and equation (5) reduces to:

$$M = \frac{\mu_o}{4\pi} \left\{ 12.981 - 2 \ln p_d \right\} \frac{H}{m} \qquad (6)$$

By utilizing equation (6), numerical values for M may be calculated. The next step is to develop the means to utilize this value of M to obtain a value of voltage that will be induced around the communication line given a current flowing in the power system. If a current I is flowing in a power circuit, it will induce in a neighboring communication circuit, a voltage proportional to the rate of change of I and to the quantity M, which is the coefficient of mutual inductance between both of the circuits as defined by the equation:

$$e_{comm} = - M \frac{dI}{dt} \qquad (7)$$

If I is a sinusoidal a.c. current with an angular frequency $\omega$, then $e_{comm}$ is also sinusoidal and

$$e_{comm} = - j\omega M I \qquad (8)$$

By solving equation (8) the value of the voltage induced around the buried communication cable may be obtained. To solve this equation, it is necessary to know

values for M and I . It has already been shown how values can be developed for M [see Equation (6)] and it will now be shown as to what are the necessary factors that are to be considered in determining a value for I .

The power system that is under consideration is a three phase, four wire system with a solidly ground neutral. In such a system there are three kinds of currents that can flow in the system that are of interest:

(1) A line to ground fault current that occurs when a line is unintentionally grounded.

(2) A line current in normal operation.

(3) A residual current that flows in normal operation due to an unbalance in loading of the system.

In the three cases described, current only flows in the grounded neutral in case (1) and case (3). However, since the experience of the power industry indicates that line to fault ground currents are twenty times as large as line currents and line currents are usually ten times as large as residuals, it would appear that that area of primary interest is concerned with fault currents because if they do not cause excessive voltages to be induced certainly the line currents and residual currents will not cause any problem.

A site survey was made on a particular missile system and it was found that the power system had a calculated three phase fault current of 920 amperes and a line to ground fault current of 1500 amperes. The line current averaged around 50 amperes and the average residual current was about 5 amperes. These are rather typical values for 100 KV systems. It was also found that these particular fault currents occurred on the average of about 19 faults per year in the particular locals. These large fault currents will induce rather large voltages around the communication cable and are very important when occurring, but this must be

traded off by a statistical analysis predicting the probability of large values of induced voltages. The normal line current will be flowing all the time but unless an unbalance exists no currents will be flowing in the neutral. Consequently, the important values of I to be used are:

Fault Current = 1500 amps

Residual Current = 5 amps

5. Numerical Calculations

To facilitate calculation, the exposure will be treated as separate sections with average figures employed where practical. These sections are tabulated in Table No. 1.

Using equation (6) values for Mau obtained as follows:

(a) For section a,

$$M = \frac{4\pi \times 10^{-7}}{4\pi} \left\{ 12.981 - 2\ln 37.6 - j\frac{\pi}{2} \right\} \frac{H}{m}$$

$$M \sim 5.7 \times 10^{-7}$$

(b) For section $a_2$

$$M = \frac{4\pi \times 10^{-7}}{4\pi} \left\{ 12.981 - 2\ln 52.8 - j\frac{\pi}{2} \right\} \frac{H}{m}$$

$$M \sim 5.0 \times 10^{-7}$$

(c) For section $a_3$

$$M = \frac{4\pi \times 10^{-7}}{4\pi} \left\{ 12.981 - 2\ln 78.0 - j\frac{\pi}{2} \right\} \frac{H}{m}$$

$$M \sim 4.3 \times 10^{-7}$$

(d) For section $a_4$

$$M = \frac{4\pi \times 10^{-7}}{4\pi} \left\{ 12.981 - 2\ln 102 - j\frac{\pi}{2} \right\} \frac{H}{m}$$

$$M \sim 3.7 \times 10^{-7}$$

(e) For section $a_5$

$$M = \frac{4\pi \times 10^{-7}}{4\pi} \left\{ 12.981 - 2 \ln 142 - j\frac{\pi}{2} \right\} \frac{H}{m}$$

$$M \sim 3.1 \times 10^{-7}$$

(f) For section $a_6$

$$M = \frac{4\pi \times 10^{-7}}{4\pi} \left\{ 12.981 - 2 \ln 176 - j\frac{\pi}{2} \right\} \frac{H}{m}$$

$$M \sim 2.6 \times 10^{-7}$$

(g) For section (b)

$$M = \frac{4\pi \times 10^{-7}}{4\pi} \left\{ 12.981 - 2 \ln 30.8 - j\frac{\pi}{2} \right\} \frac{H}{m}$$

$$M \sim 6.1 \times 10^{-7}$$

(h) For section (c)

$$M = \frac{4\pi \times 10^{-7}}{4\pi} \left\{ 12.981 - 2 \ln 34.7 - j\frac{\pi}{2} \right\} \frac{H}{m}$$

$$M \sim 5.9 \times 10^{-7}$$

(i) For section (d)

$$M = \frac{4\pi \times 10^{-7}}{4\pi} \left\{ 12.981 - 2 \ln 44.0 - j\frac{\pi}{2} \right\} \frac{H}{m}$$

$$M \sim 5.4 \times 10^{-7}$$

(j) For section (e)

$$M = \frac{4\pi \times 10^{-7}}{4\pi} \left\{ 12.981 - 2 \ln 54.5 - j\frac{\pi}{2} \right\} \frac{H}{m}$$

$$M \sim 5.0 \times 10^{-7}$$

These values of M are summarized in Table No. 2.

If values of M as shown in Table 2 are substituted in equation (8) for currents that are representative of fault currents at 1500 amps and residual currents at 5 amps, the results for the induced voltage around the communication cable are summarized in Table No. 3. This summary lists all the voltages which are presented to the communication cable and, lacking other considerations, would be the interfering voltages

that would be induced into the cable. But there are other important considerations that have been designed into the cable and which effectively reduce the magnitude of these inducing voltages.

6. Shielding Effectiveness of Cable

The cross section of the cable as shown in Figure 2 shows that the copper shield and steel tapes are a protection against these induced voltages. All values shown in Table No. 3 are subject to the shielding factor of the communication cable sheath. The sheath of this cable can be a most efficient screening conductor because of its small separation form, and its particular position with respect to the inducing or induced line, even though it does not provide a perfect screen against magnetic induction. The mutual inductance between sheath and inductor is practically equal to the self-inductance of the sheath, with both circuits having a ground return. Induced voltage between inducing conductor and sheath of the induced cable equals the resistance drop of the sheath current. Experience has indicated that $e_{comm}$, the induced voltage around the conductor, as calculated, is somewhat less than the voltage $e_{comm}$ because of a number of factors that have to be considered:

(1) The shielding effectiveness of the sheath, which empirical measurements have shown to be in the order of - 6db.

(2) The attenuation caused by the fact that for practical purposes the communication cable is made up of perfectly balanced pairs. This has been estimated to be on the order of - 80db, although a more conservative figure, and one which shall be used because it has wider acceptance is - 60db.

The addition of, these two figures - 6db and - 60db or - 66db ($e'_{comm} \approx e_{comm} \times 5 \times 10^{-4}$ or - 66db) is the effective attenuation of the induced voltage by the cable shielding. These figures are tabulated in Table No. 4.

7. Effect on Each Section of Exposure

Now that the values for $e'_{comm}$ have been obtained, it now is necessary to determine the total induced voltage for each section of exposure subjected to different dimensional parameters. These are shown in Table No. 5.

8. Conclusions - Effect of Exposure

It can be readily seen that from Table No. 5, if $e'_{comm}$ is taken for the whole line and the length of exposure is 2.7 miles or 4,370 meters, that the voltage induced by fault currents will be 635 mv., the voltage induced by residual currents will be 2.218 mv. Comparing these voltages to the original criteria established of 2 mv., it is clear that exposure to the power line will be serious in the case of fault currents. In the case of residual currents in the power system, the magnitude of 2.218 mv. is so close to the acceptable value of 2 mv. that it is considered to be acceptable. Since the three phase power system is three wire grounded neutral, current will not normally flow in the neutral and when the system is unbalance residual current will flow; this has already been discussed.

Although it is not exactly a cable system parameter, it must be pointed out that in the existing installed systems, the cable terminating equipment for this cable will contain band pass filters to effectively reduce all 60 cycle components by approximately - 50db. This, however, must be considered as insurance and will not be considered as part of the shielding effectiveness of the cable.

All the induced voltages which has been considered up to now have been at the fundamental frequency of the power line - 60 cycles per second. Obviously there are some harmonic frequencies which will be detremental. In telephone communication, frequencies around 1000 cycles are the most detrimental, because they have the greatest impact on voice communication. From the experience on this particular system, it was found that the most important frequency would be the eleventh harmonic or 660 cycles.

From Equation (6), it can be seen that M is a function of $p_d$ and $p_d \cdot \alpha$'a . Since $d = \sqrt{\sigma f}$ , then

$$M = \frac{\mu_o}{4\pi} \left\{ 12.981 - 2 \ln\left[(\sqrt{\sigma f}) \times d\right] - j\frac{\pi}{2} \right\} \qquad (9)$$

As f increases, the value of M becomes smaller as the value of $2 \ln\left[(\sqrt{\sigma f}) \times d\right]$ approaches 12.981 .

But this is not a linear relationship and the effect of the square root and the logarithum must be covered. Also as the value of M becomes smaller with the increased frequency, the value of I will become smaller because this will be based on the energy contained in the harmonics. If it can be assumed that the I of the eleventh harmonic is 10% of the fundamental frequency, then all the values of $e_{comm}$ will be divided by a factor of 10. By making such an assumption, it can be readily seen that analyzing this exposure for 60 cycles is the worst case and if it is no problem at 60 cycles, it will be no problem at higher frequencies. Actually the effect of harmonics will have to be considered in more detail but are beyond the scope of this paper.

## 8. Conclusions

The preceding analysis shows that with a few simple facts that are generally available, one can determine what effect a power line would have on a nearby communication system. The technique that was demonstrated makes possible a quick approximation so that design criteria may be developed while the communication system is being installed. There is much additional work that can be done along these lines; it would be very advantageous to develop a nomograph to be used by installation engineers so that they can have a quick guide to the permissible minimum separation.

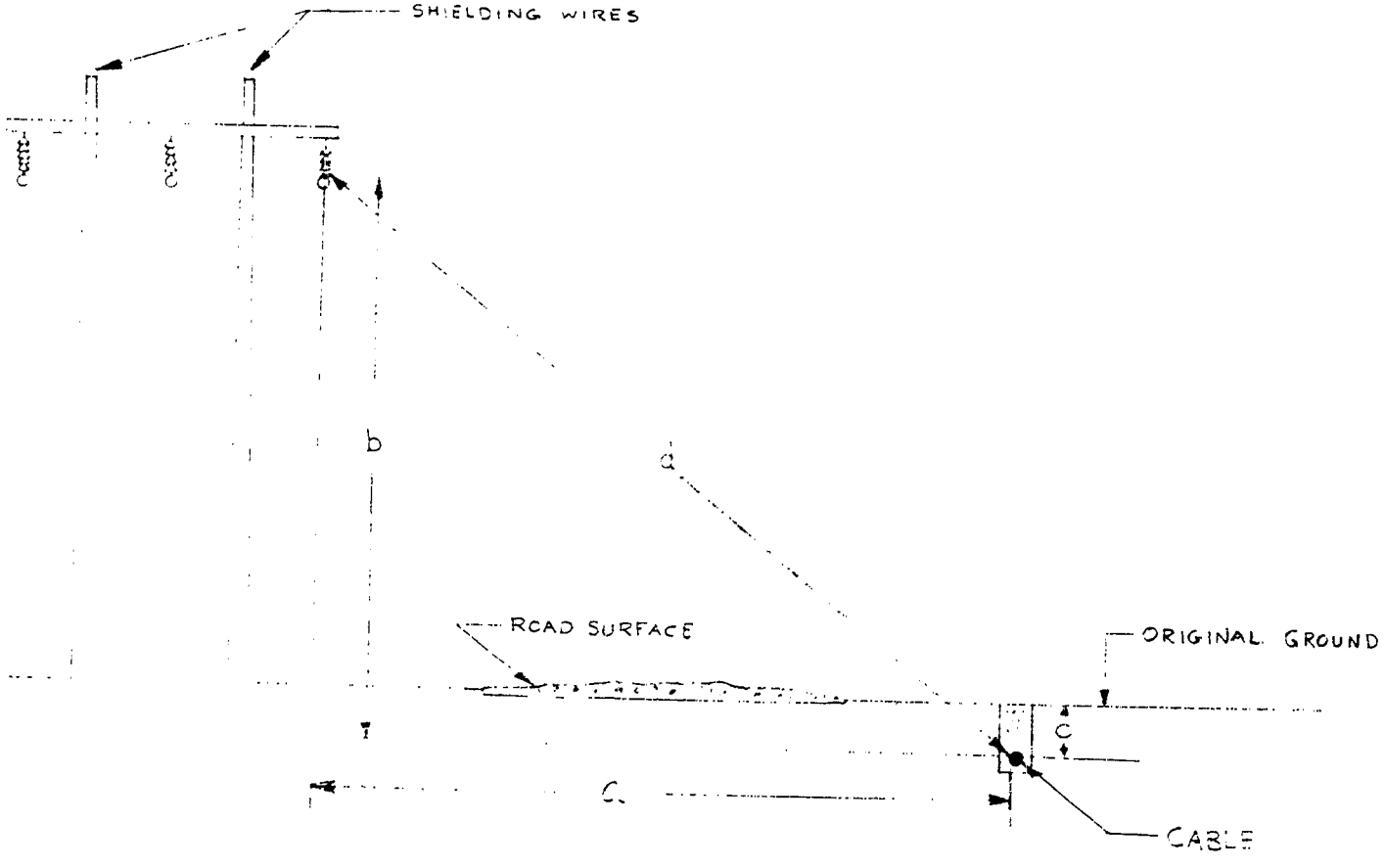



Fig. 1

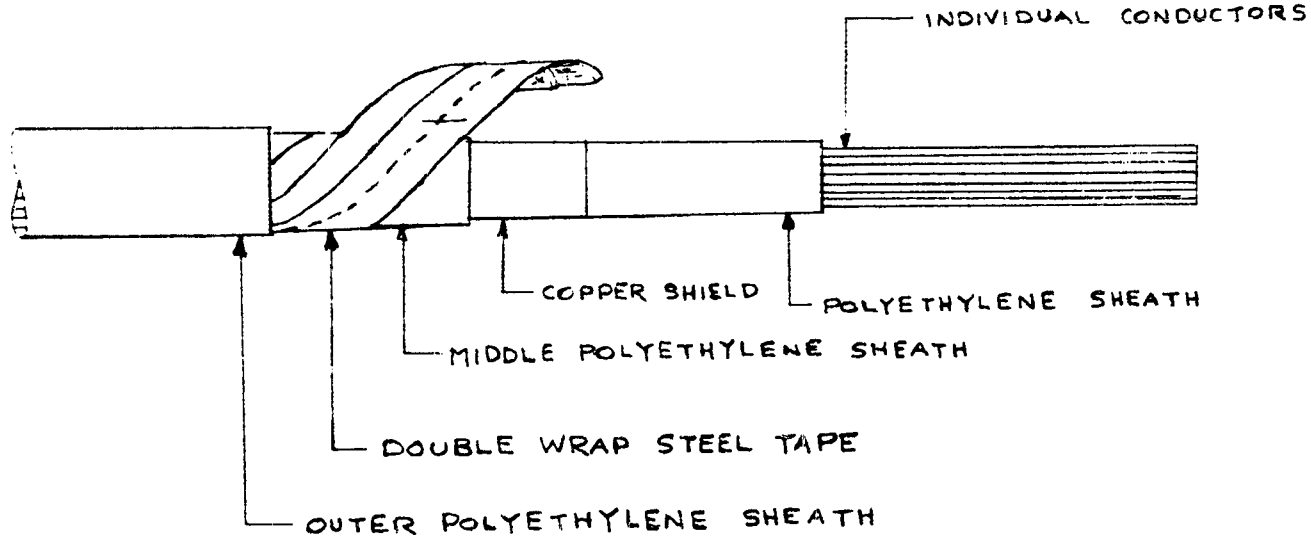

INDIVIDUAL CONDUCTORS
COPPER SHIELD
POLYETHYLENE SHEATH
MIDDLE POLYETHYLENE SHEATH
DOUBLE WRAP STEEL TAPE
OUTER POLYETHYLENE SHEATH

Fig. 2

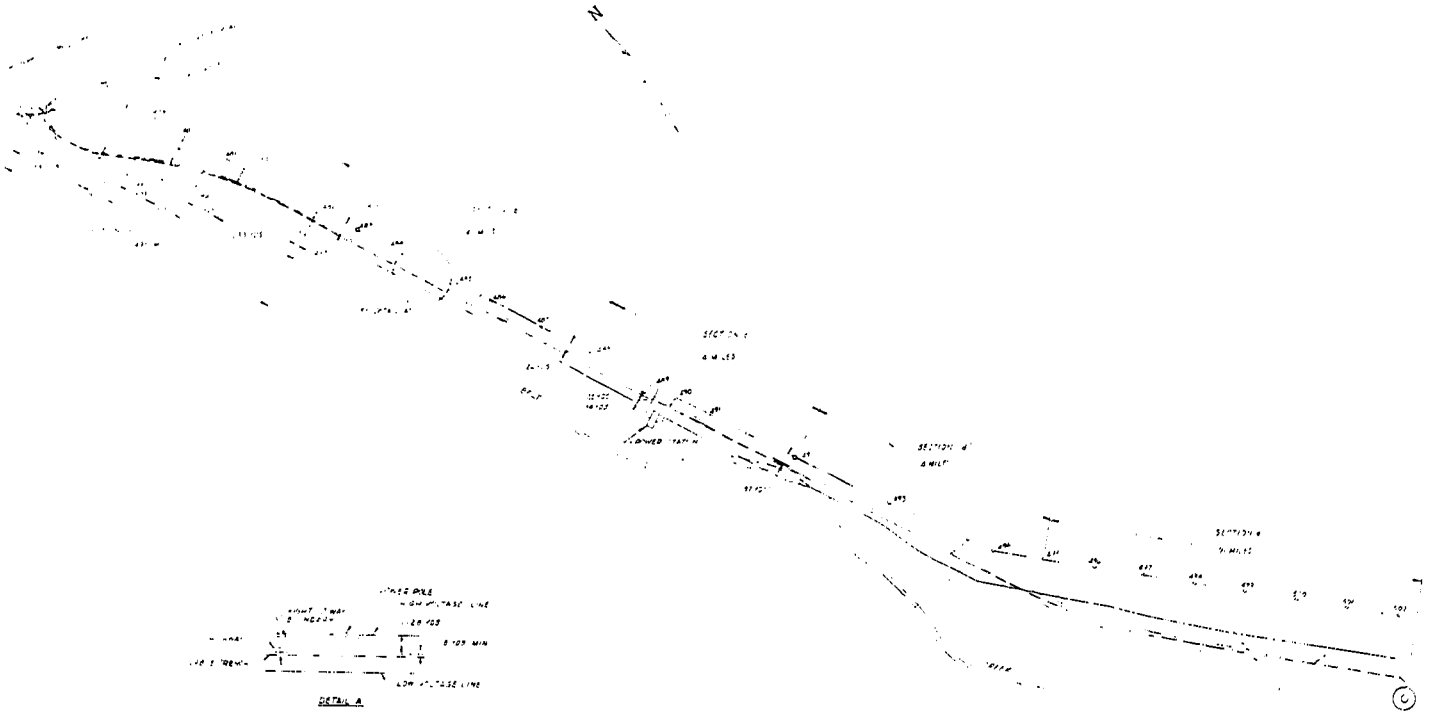



Fig. 3

TABLE 1

PARAMETERS OF VARIOUS EXPOSED SECTIONS

| SYMBOL | SECTION a | | | | | | SEC. b | SEC. c | SEC. d | SEC. e |
|---|---|---|---|---|---|---|---|---|---|---|
| | $a_1$ | $a_2$ | $a_3$ | $a_4$ | $a_5$ | $a_6$ | | | | |
| a (in meters) | 42 | 53 | 75 | 110 | 150 | 183 | 28.5 | 42 | 51 | 64 |
| b (in meters average) | 25 | 40 | 66 | 70 | 80 | 100 | 12 | 13 | 22 | 30 |
| c (in meters) | 1 | 1 | 1 | 1 | 1 | 1 | 1 | 1 | 1 | 1 |
| d (in meters) | 48.2 | 67.2 | 100 | 130 | 182 | 225 | 39.5 | 44.4 | 56.2 | 70.8 |
| $\sigma$ (in mhos per meter) | .01 | .01 | .01 | .01 | .01 | .01 | .01 | .01 | .01 | .01 |
| f ( in cps) | 60 | 60 | 60 | 60 | 60 | 60 | 60 | 60 | 60 | 60 |
| $\mu_o = 4\pi \times 10^{-7}$ | K | K | K | K | K | K | K | K | K | K |
| $\alpha = 2.8 \times 10^{-3}$ (K') | K' | K' | K' | K' | K' | K' | K' | K' | K' | K' |
| $\rho = \alpha' a$ | 32.8 | 41.4 | 58.5 | 85.8 | 117.0 | 156.0 | 30 | 32.8 | 39.8 | 50 |
| $P_d = \alpha' d$ | 37.6 | 52.8 | 78.0 | 102.0 | 142.0 | 176.0 | 30.8 | 34.7 | 44.0 | 54.5 |
| Length of Exposure (in meters) | 270 | 110 | 110 | 110 | 110 | 260 | 658 | 640 | 640 | 1460 |
| Note $\alpha' = .78$ (K'') | K'' | K'' | K'' | K'' | K'' | K'' | K'' | K'' | K'' | K'' |

TABLE 2

| Exposure | M(H/m) |
|---|---|
| Section $a_1$ | $5.7 \times 10^{-7}$ |
| Section $a_2$ | $5.0 \times 10^{-7}$ |
| Section $a_3$ | $4.3 \times 10^{-7}$ |
| Section $a_4$ | $3.7 \times 10^{-7}$ |
| Section $a_5$ | $3.1 \times 10^{-7}$ |
| Section $a_6$ | $2.6 \times 10^{-7}$ |
| Section b | $6.1 \times 10^{-7}$ |
| Section c | $5.9 \times 10^{-7}$ |
| Section d | $5.4 \times 10^{-7}$ |
| Section e | $5.0 \times 10^{-7}$ |

TABLE 3

Values of $e_{COMM}$ in Volts/Meter

| Section | Fault Current I = 1500 a | Residual Current I = 5a |
|---|---|---|
| $a_1$ | $321 \times 10^{-3}$ | $1.07 \times 10^{-3}$ |
| $a_2$ | $282 \times 10^{-3}$ | $.94 \times 10^{-3}$ |
| $a_3$ | $243 \times 10^{-3}$ | $.81 \times 10^{-3}$ |
| $a_4$ | $209 \times 10^{-3}$ | $.69 \times 10^{-3}$ |
| $a_5$ | $175 \times 10^{-3}$ | $.58 \times 10^{-3}$ |
| $a_6$ | $147 \times 10^{-3}$ | $.49 \times 10^{-3}$ |
| b | $345 \times 10^{-3}$ | $1.15 \times 10^{-3}$ |
| c | $333 \times 10^{-3}$ | $1.11 \times 10^{-3}$ |
| d | $306 \times 10^{-3}$ | $1.02 \times 10^{-3}$ |
| e | $282 \times 10^{-3}$ | $.94 \times 10^{-3}$ |

TABLE 4

Values of $e_{COMM}$ in Volts/Meter

| SECTION | Fault Current 1500 a | | Residual Current 5a | |
|---|---|---|---|---|
| | $e_{COMM}$ X $10^{-3}$ | $e_{COMM}$ X $10^{-3}$ | $e_{COMM}$ X $10^{-3}$ | $e_{COMM}$ X $10^{-3}$ |
| $a_1$ | 321 | .16 | 1.07 | .0005 |
| $a_2$ | 282 | .14 | .94 | .0005 |
| $a_3$ | 243 | .12 | .81 | .0004 |
| $a_4$ | 209 | .10 | .697 | .0003 |
| $a_5$ | 175 | .087 | .584 | .0003 |
| $a_6$ | 147 | .073 | .49 | .0003 |
| b | 345 | .17 | 1.15 | .0006 |
| c | 333 | .167 | 1.11 | .0006 |
| d | 306 | .15 | 1.02 | .0005 |
| e | 282 | .14 | .94 | .0005 |

$e_{COMM} - e_{COMM} \times 5 \times 10^{-4}$

or -66 db

TABLE 5

Induced Voltage/Section of Exposure

| SECTION | Fault Current 1500a | | | Residual Current 5a | | |
|---|---|---|---|---|---|---|
| | $(e'_{COMM} \times 10^{-3})$ V/M | Exposure in meters | Volts x $10^{-3}$ | $(e_{COMM} \times 10^{-3}$ V/M | Exposure in meters | Volts x $10^{-3}$ |
| a | .12 | 970 | 116 | .0004 | 970 | .388 |
| b | .17 | 660 | 112 | .0006 | 660 | .396 |
| c | .17 | 640 | 107 | .0006 | 640 | .384 |
| d | .15 | 640 | 96 | .0005 | 640 | .320 |
| e | .14 | 1460 | 204 | .0005 | 1460 | .73 |
| TOTALS | | | 635 | | | 2.218 |

# A DIGITAL REPRESENTATION OF INTERFERENCE WITHIN A COMMUNICATION RECEIVER INCLUDING THE DEMODULATION PROCESS

N. Wilde*, A. J. Hoehn, and L. A. Follett
Bell Aerosystems Company
Division of Bell Aerospace Corporation
Tucson, Arizona

Abstract.--This paper discusses a representation of the response of both am. and fm. communication receivers to a desired signal and one or more interfering signals. The representation is suitable for the analysis of interference prediction problems by means of digital computation techniques. The final form of this representation is a program for the IBM 709 digital computer.

An expression is written for the resultant of a number of steady-state voltages in terms of an envelope function and phase function associated with the if. carrier. The effect of linear and square-law am. detectors is simulated, as well as the angular modulation detection process. The resultant demodulated wave is then subjected to trigonometric analysis to determine its spectral content.

## I. INTRODUCTION

Communications receivers are usually evaluated on the amount of desired information available at the output of the receiver. Many methods have been devised to compare various receivers (or the same receiver under varying circumstances), but most methods center around spectrum analysis. It is therefore desirable to obtain a discrete frequency analysis of the output of the detector as a function of its input.

An IBM 709 computer program has been developed which presents a printed statement of the various frequencies and associated amplitudes in the detector output. As input, the program requires that steady-state unmodulated sinusoidal voltages be presented to the input to the detector. Therefore, input to the computer program can be limited to the amplitudes and associated frequencies of the output signals of the if. amplifier. As originally written, the program assigned random phase angles to each of the signals. The program has been modified, however, to permit addition of signals with coherently-related spectral components to the resultant of the random-phased signals. Thus, with the expenditure of but little more time, the effect of modulation, on some of the signals at least, may be included in the computation.

The input signals are added linearly to obtain the total function (of time) presented to the detector. The program operates on the amplitude of this resulting function in the case of am. detection. The time rate of change of the phase angle of the total function is processed in the angular modulated case. As indicated in the mathematics which follow, generalized representations for any number of signals can be written in compact mathematical form for either case.

* Mr. N. Wilde is now associated with Phillips Petroleum Company, Idaho Falls, Idaho.

Thus the program actually begins with the frequency or amplitude function without a need to derive the total function as presented to the detector.

At the user's option, either linear or square-law am. detection may be evaluated. In the case of square-law am. detection, the mathematics lead directly to the desired spectrum information. For the linear am. or the fm. case, it is necessary to subject the appropriate time function to a numerical trigonometric series evaluation to obtain the desired information. The mathematical and general computer techniques follow.

## II. LINEAR COMBINATION OF IF. SIGNALS

As indicated above, the output signal from the if. amplifier is considered to be the resultant of a number of steady-state unmodulated sinusoidal voltages. If a receiver has been properly tuned, the desired carrier signal will be centered in the if.-bandwidth. Let the desired signal be given by the expression

$$A_o \cos (\omega_o t + \phi_o)$$

and let each one of $n$ interfering signals be given by the expression

$$A_i \cos \left[(\omega_o + \delta_i)t + \phi_i\right]$$

The term $\delta_i$ is the angular frequency difference between the desired signal and the $i^{th}$ interfering signal. The term will be negative if the interfering signal has a lower frequency than the desired signal and positive if it has a higher frequency.

Associated with the desired signal and each of the interfering signals is a random-phase angle represented by the symbol $\phi_i$. If the random-phase angles of the interfering signals are referred to the phase angle of the desired signal, then the desired signal-phase angle can have any arbitrary value. This value has been chosen as zero (that is, $\phi_o = 0$).

The total steady-state signal presented to the detector is

$$f(t) = A_o \cos \omega_o t + \sum_{i=1}^{n} A_i \cos \left[(\omega_o + \delta_i)t + \phi_i\right] \qquad (1)$$

Expanding the summation terms into the product of two angles and recombining the trigonometric functions yields

$$f(t) = R \cos (\omega_o t + \theta) \qquad (2)$$

where

$$R^2 = \left[A_o + \sum_{i=1}^{n} A_i \cos(\delta_i t + \phi_i)\right]^2 + \left[\sum_{i=1}^{n} A_i \sin(\delta_i t + \phi_i)\right]^2 \quad (3)$$

and

$$\tan\theta = \frac{\sum_{i=1}^{n} A_i \sin(\delta_i t + \phi_i)}{A_o + \sum_{i=1}^{n} A_i \cos(\delta_i t + \phi_i)} \quad (4)$$

The function R is the voltage envelope of the desired carrier frequency. It is an undesired effect produced by the interfering signals. The expression for $R^2$, equation (3), can be written in a more useful form by squaring and collecting terms. The resulting expression is

$$R^2 = b_o + \sum_{i=o}^{n} \sum_{j=i+1}^{n} b_{ij} \cos(\rho_{ij} t + \psi_{ij}) \quad (5)$$

where

$$b_o = A_o^2 + \sum_{i=1}^{n} A_i^2$$

$$b_{ij} = 2 A_i A_j$$

$$\rho_{ij} = \delta_i - \delta_j$$

$$\psi_{ij} = \phi - \phi_j$$

Note that $\delta_o = 0$ and $\phi_o = 0$

The general form of equation (5) is

$$R^2 = \beta_o + \beta_1 \cos X_1 + \beta_2 \cos X_2 \cdots + \beta_m \cos X_m \quad (6)$$

The series in equations (5) and (6) will give m cosine terms where

$$m = \frac{n(n+1)}{2} \quad (7)$$

The function $\theta$ is a time varying phase angle associated with the carrier frequency. It also is an undesired effect caused by the interfering signals. The time rate of change (that is, the first derivative with respect to time) of $\theta$ is of interest in connection with receivers for angular-modulated waves and therefore will be developed.

With reference to equation (4), let

$$S = \sum_{i=1}^{n} A_i \sin (\delta_i t + \phi_i) \tag{8}$$

$$S' = \frac{dS}{dt} = \sum_{i=1}^{n} A_i \delta_i \cos (\delta_i t + \phi_i) \tag{9}$$

$$C = A_o + \sum_{i=1}^{n} A_i \cos (\delta_i t + \phi_i) \tag{10}$$

$$C' = \frac{dC}{dt} = \sum_{i=1}^{n} A_i \delta_i \sin (\delta_i t + \phi_i) \tag{11}$$

Equation (4) can now be written as

$$\theta = \tan^{-1} \frac{S}{C}$$

whence

$$\frac{d\theta}{dt} = \frac{CS' - SC'}{R^2} \tag{12}$$

where $R^2 = C^2 + S^2$ according to equations (3), (8), and (10).

The expression for $(d\theta/dt)$ can be written in a more useful form by substituting equations (8), (9), (10), and (11) into equation (12), expanding and collecting terms. The result is

$$\frac{d\theta}{dt} = \frac{a_o + \sum_{i=0}^{n} \sum_{j=i+1}^{n} a_{ij} \cos (\rho_{ij} t + \psi_{ij})}{R^2} \tag{13}$$

where

$$a_o = \sum_{i=1}^{n} A_i^2 \delta_i$$

$$a_{ij} = A_i A_j (\delta_i + \delta_j)$$

and the variables $\rho_{ij}$ and $\psi_{ij}$ have been defined in equation (5). The general form of equation (13) is

$$\frac{d\theta}{dt} = \frac{\alpha_o + \alpha_1 \cos X_1 + \alpha_2 \cos X_2 \cdot \cdot \cdot + \alpha_m \cos X_m}{\beta_o + \beta_1 \cos X_1 + \beta_2 \cos X_2 \cdot \cdot \cdot + \beta_m \cos X_m} \tag{14}$$

As an example consider the case of a desired carrier, $A_o$, and three interfering carriers $A_1$, $A_2$, and $A_3$. In this case $R^2$ is given, in the notation of equation (6), as follows:

$$\beta_o = b_o = A_o^2 + A_1^2 + A_2^2 + A_3^2 \tag{15a}$$

$$\beta_1 \cos X_1 = 2A_oA_1 \cos (\delta_1 t + \phi_1) \tag{15b}$$

$$\beta_2 \cos X_2 = 2A_oA_2 \cos (\delta_2 t + \phi_2) \tag{15c}$$

$$\beta_3 \cos X_3 = 2A_oA_3 \cos (\delta_3 t + \phi_3) \tag{15d}$$

$$\beta_4 \cos X_4 = 2A_1A_2 \cos (\delta_1 - \delta_2)t + (\phi_1 - \phi_2) \tag{15e}$$

$$\beta_5 \cos X_5 = 2A_1A_3 \cos (\delta_1 - \delta_3)t + (\phi_1 - \phi_3) \tag{15f}$$

$$\beta_6 \cos X_6 = 2A_2A_3 \cos (\delta_2 - \delta_3)t + (\phi_2 - \phi_3) \tag{15g}$$

The numerator of the expression for the differentiated phase angle, $(d\theta/dt)$, is expressed in the notation of equation (14) as:

$$\alpha_o = a_o = A_1^2\delta_1 + A_2^2\delta_2 + A_3^2\delta_3 \tag{16a}$$

$$\alpha_1 \cos X_1 = A_oA_1\delta_1 \cos (\delta_1 t + \phi_1) \tag{16b}$$

$$\alpha_2 \cos X_2 = A_oA_2\delta_2 \cos (\delta_2 t + \phi_2) \tag{16c}$$

$$\alpha_3 \cos X_3 = A_oA_3\delta_3 \cos (\delta_3 t + \phi_3) \tag{16d}$$

$$\alpha_4 \cos X_4 = A_1A_2(\delta_1 + \delta_2) \cos \left[(\delta_1 - \delta_2)t + (\phi_1 - \phi_2)\right] \tag{16e}$$

$$\alpha_5 \cos X_5 = A_1A_3(\delta_1 + \delta_3) \cos \left[(\delta_1 - \delta_3)t + (\phi_1 - \phi_3)\right] \tag{16f}$$

$$\alpha_6 \cos X_6 = A_2A_3(\delta_2 + \delta_3) \cos \left[(\delta_2 - \delta_3)t + (\phi_2 - \phi_3)\right] \tag{16g}$$

The denominator of (14) is identical with (6) and (15). It is further noted that the number of terms in (6) and in the numerator of (14) is in agreement with equation (7).

## III. DETECTION OF RESULTANT WAVE FORM

The expression desired above describes the result of a linear combination of many signals in the if. amplifier. Neither amplitude nor phase of any of these signals is restricted in the analysis. The next step is to examine the effect of demodulator on the resultant wave. Linear and square-law envelope detectors are considered in this analysis as well as the so-called fm. detector, which actually detects the rate of change of phase with time; that is, $(d\theta/dt)$.

## IV. DETECTORS FOR AMPLITUDE MODULATION

The work of Rice[1] and others has shown that the output current I of many important nonlinear devices is related to the input voltage V by the integral over a contour C; that is,

$$I = \frac{1}{2\pi} \int_C F(ju)\, e^{jV}\, du \tag{17}$$

where F(ju) is a given function such that I and V are related by the above expression. If the frequency spectrum of V is restricted to a relatively narrow band such as the if. bandwidth in communication type receivers, the frequency spectrum of I is restricted to narrow bands located around the harmonics of the midband frequency of V. The narrow spectrum located about the nth harmonic is

$$G_n(R) = \frac{1}{\pi} \int_C F(ju)\, J_n(uR)\, du \qquad n > 0 \tag{18}$$

where R is the envelope of V and $J_n(uR)$ is a Bessel function of the nth order. In a communication type receiver, the low frequency spectrum about the zero harmonic (dc) is the audio spectrum of interest. Since only the positive frequencies have physical significance, only this half of the spectrum is considered. The low-frequency spectrum, including the dc term, is

$$G_o(R) = \frac{1}{2\pi} \int_C F(ju)\, J_o(uR)\, du \tag{19}$$

The linear detector with cutoff at V = 0 is of major consideration. The output is

$$I = \begin{cases} 0 & V < 0 \\ V & 0 > V \end{cases} \tag{20}$$

Using the function

$$F(ju) = \frac{\alpha}{(ju)^2} = -\frac{\alpha}{u^2} \tag{21}$$

and integrating equation (19) gives the result

$$G_o(R) = \frac{\alpha}{\pi} R \tag{22}$$

The square-law detector is also of interest. It is a special case of the nth law detector where n, an integer, equals two. The output is

$$I = \alpha V^n \tag{23}$$

and

$$F(ju) = \frac{\alpha n!}{(ju)^{n+1}} \tag{24}$$

For n = 2, the integral yields

$$G_o(R) = \frac{\alpha}{2} R^2 \tag{25}$$

In both cases, $\alpha$ is a constant associated with a given detector. If, as is the case in interference analysis, interest is confined to the relative magnitude of certain values in the low-frequency spectrum (for example, the interference) in comparison with some other standardizing value obtained from the same detector (for example, the desired signal) the detector constant divides out. Thus the relative spectrum, $G_r$, is

$$G_r(R) = R \tag{26}$$

and for the square-law detector

$$G_r(R) = R^2 \tag{27}$$

## V. DETECTOR FOR ANGLE-MODULATED WAVES

Consider a communication-type fm. receiver utilizing a balanced detector having a linear response over the frequency range of interest and preceded by an ideal limiter. If the rate of change of phase ($d\theta/dt$) about the carrier phase is relatively slow, then the output of the detector is a low-frequency spectrum concentrated about and including a dc term. This low-frequency spectrum, which is analogous to the low-frequency spectrum from an

am. detector, is the audio spectrum of interest. It is represented by

$$G_o(\theta) = \alpha \frac{d\theta}{dt} \tag{28}$$

The rate of change of the phase angle is a function of the if. bandpass. The parameter $\alpha$ is a constant associated with a given detector. If only relative values are of interest, then

$$G_r(\theta) = \frac{d\theta}{dt} \tag{29}$$

## VI. AUDIO SPECTRUM ANALYSIS

Equations (17) through (29), based on the work of Rice, are included to establish the fact that equations (6) and (14), for $R^2$ and $(d\theta/dt)$, are indeed the mathematical expressions for the detected wave.

Now that an expression for detected output has been established in the time domain, the next step is to express this in the frequency domain as a relative energy spectrum.

In the case of an am. square-law detector, as given by equations (6) and (27), the desired information is obtained simply by squaring the coefficient of each to produce the energy spectrum.

Unfortunately, for the purposes of this analysis, the linear detector is most frequently found in actual receivers, and its output is given by the square root of a finite trigonometric series.

The fm. detector output is given by equations (14) and (29). A spectral analysis of the ratio of two finite trigonometric series must be performed in this case.

## VII. COMPUTATION

The following is a discussion of a spectral analysis method for the preceding two cases, which is particularly suited for machine computation.

The desire to obtain a frequency spectrum immediately suggests a Fourier series analysis. However, a Fourier series is an infinite series, whereas a finite series is required. The usual method of obtaining a finite series is simply to terminate the Fourier series at a point where the coefficients tend to become negligible. This approach is somewhat indefinite since the cutoff point cannot be known prior to the start of computation.

A different approach to a trigonometric series, based on the highest

harmonic of interest is available.[2] Let $G_r(R)$ and $G_r(\theta)$ be represented by $G_o(Y)$, which will be called the generalized audio signal. In both cases $G_o(Y)$ is an even function containing cosines only. Hence, the odd coefficients are all equal to zero and only the even coefficients need be determined.

The procedure is as follows: Set the function $G_o(Y)$ equal to a finite trigonometric series.

$$G_o(Y) = (1/2)a_o + a_1 \cos Y + a_2 \cos 2Y \cdots + a_{(p-1)} \cos (p-1)Y \quad (30)$$

A set of p equations can now be written by evaluating equation (30) at a number of points equal to p. See figure 1 and equation (31).

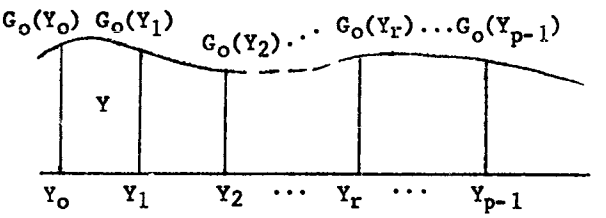



Figure 1

$$G_o(Y_o) = (1/2)a_o + a_1 \cos Y_0 + a_2 \cos 2Y_0 + \cdots + a_{p-1} \cos (p-1)Y_o$$

$$G_o(Y_1) = (1/2)a_o + a_1 \cos Y_1 + a_2 \cos 2Y_1 + \cdots + a_{p-1} \cos (p-1)Y_1$$

$$G_o(Y_2) = (1/2)a_o + a_1 \cos Y_2 + a_2 \cos 2Y_2 + \cdots + a_{p-1} \cos (p-1)Y_2$$

$$\text{etc.} \quad (31)$$

The number of terms and the number of equations equal the number of harmonics of interest. The simultaneous solution of these equations will yield values for the various coefficients. Fortunately, the orthogonal properties of these equations permit a simple general expression for the coefficients, which is

$$a_r = (2/p) \sum_{k=1}^{p} G_o(Y_k) \cos \left[(2k - 1)r\pi/2p\right] \quad (32)$$

where the generalized subscript r has the values $0 \leq r \leq (p - 1)$.

The coefficients thus determined do not have the same exact numerical values as the corresponding coefficients in an infinite Fourier series because of the discrete method of evaluating them. But, these coefficients, when substituted into equation (31) do give an exact solution for $G_o(Y_r)$ at r. Between

these points (r = 1, r = 2, etc.), the solution for $G_o(Y)$ is approximated by a straight line between the two adjacent points. If a sufficiently high maximum harmonic is chosen (p is large), then $G_o(Y)$ is very closely approximated by the resulting small straight line segments.

It is of interest to note that the same result could have been obtained by expressing as a finite summation over discrete increments the Fourier coefficient integral

$$a_r = \frac{1}{\pi} \int_{-\pi}^{+\pi} G_o(Y) \cos pY \, dY \tag{33}$$

Such a procedure gives a result identical with equation (32).

Selecting Y sufficiently small and p sufficiently large will produce a fine-frequency analysis of $G_o(Y)$. Only the audio portion of this spectrum is of interest. If all interfering signals were removed, the entire audio spectrum would disappear leaving only a dc term due to the desired carrier. Consequently, this spectrum can be considered an interference or noise spectrum due to interfering carriers. The gain of the receiver, and hence this spectrum, can be normalized to a standard audio output, $a_s$. In general, the standard output, $a_s$, would be taken as the detected signal from a tone-modulated am. wave modulated 100 per cent, or the full voltage output over the linear portion of the discriminator in an fm. receiver. The resulting expression is

$$\frac{G_o(Y)}{a_s} = \frac{a_o}{2a_s} + \frac{a_1}{a_s} \cos Y + \frac{a_2}{a_s} \cos 2Y \cdots + \frac{a_{p-1}}{a_s} \cos (p - 1)Y \tag{34}$$

The desired relative energy spectrum information is obtained by squaring the normalized coefficient of each term.

## VIII. COMPUTER PROGRAM

Flow diagrams illustrating the steps involved in programing the above process are presented in figures 2 and 3.

## ACKNOWLEDGMENT

The work described in this paper was sponsored by the Field Test Directorate, U. S. Army Electronic Proving Ground, Fort Huachuca, Arizona, under contract Nr. DA-36-039-SC-80424.

## REFERENCES


1. Rice, S. O., "Mathematical Analysis of Random Noise," Reprinted from Bell System Technical Journal, Vols. 23 and 24 in "Noise and Stochastic Processes" edited by Nelson Wax, New York: Dover Publications, Inc., 1954, pp 133-294.

2. Guillemin, E. A., "The Mathematics of Circuit Analysis," pp 501-506, New York: John Wiley and Sons, Inc., 1949.

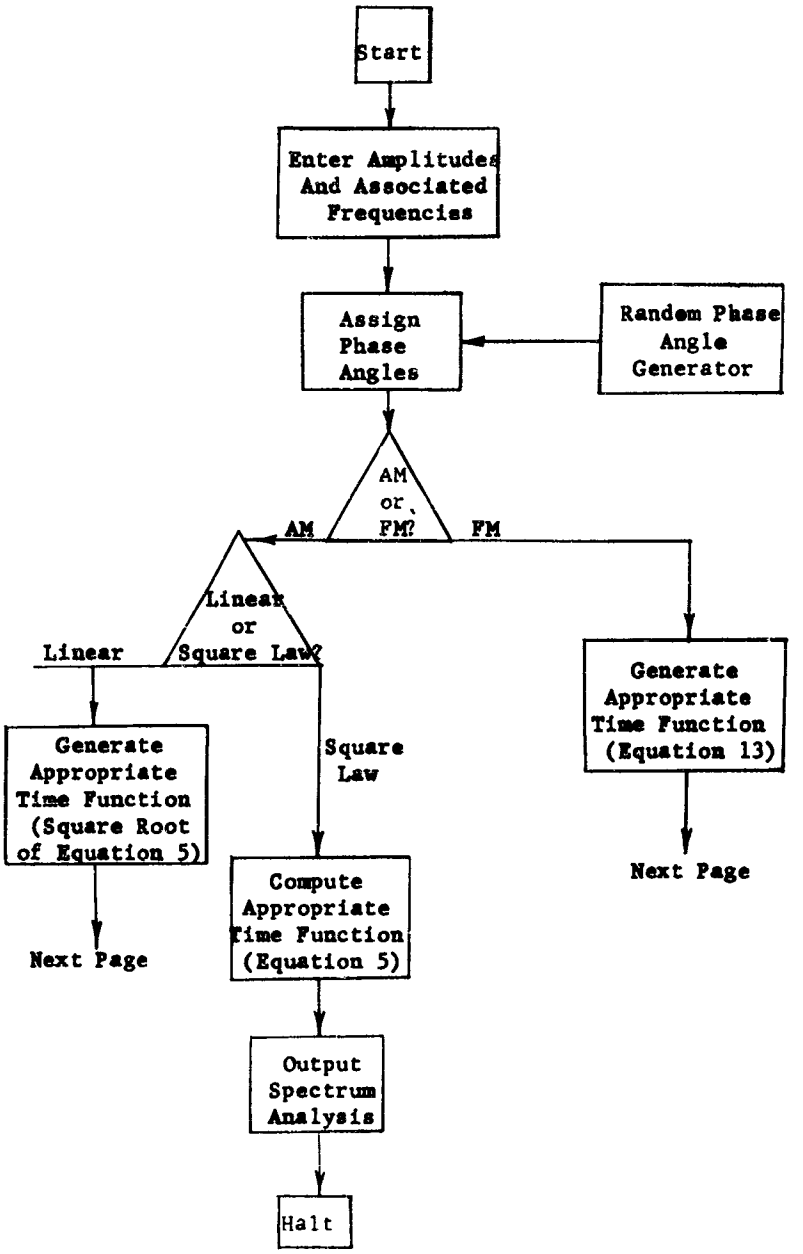
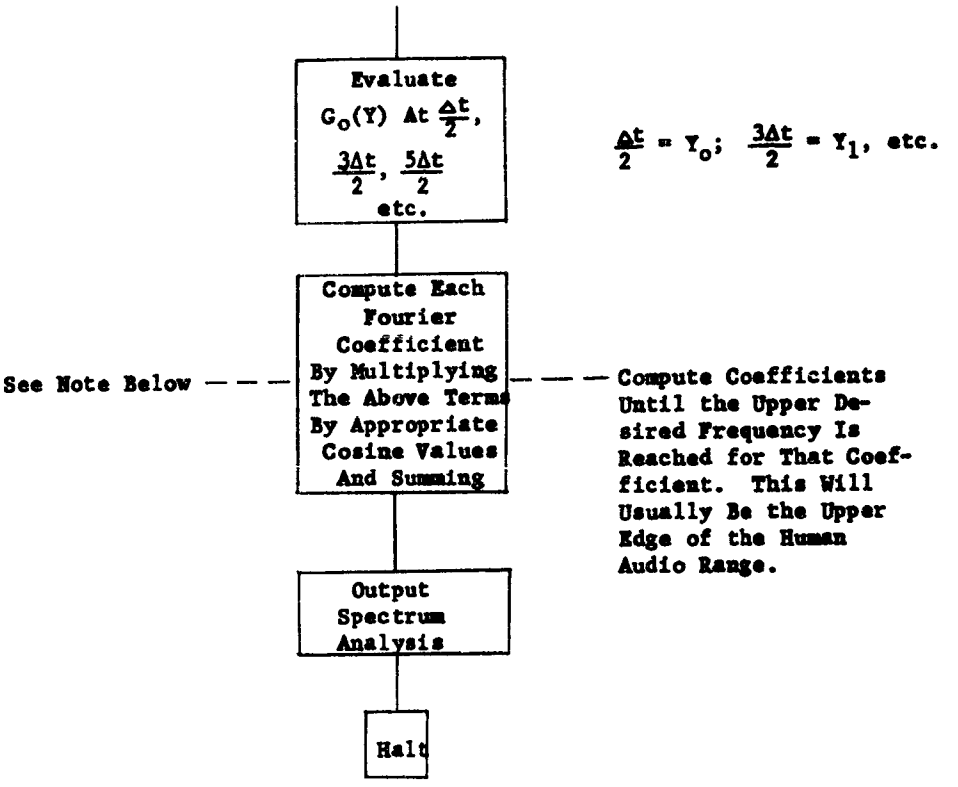



Figure 2. General Program Flow Diagram
Data Entry and Function Generation Section




Note: The formula used here is actually:

$$a_k = \sum_{j=1}^{2p-1}{}' \frac{4G_o(Y_j)}{p} \cos \frac{\pi kj}{p} \qquad \text{for } j \text{ odd only}$$

This allows an area summation as indicated:

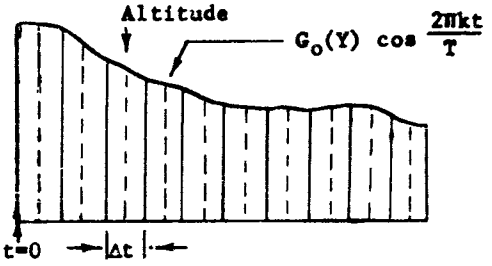



Figure 3. General Program Flow Diagram
Function Evaluation and Coefficient Computation Section

# ENGINEERING ASPECTS OF THE EMETF INTERFERENCE-PREDICTION MODEL

A. J. Hoehn
Bell Aerosystems Company
Division of Bell Aerospace Corporation
Tucson, Arizona

Abstract.--This paper contains the basic equations and simulation methods used in the interference-prediction model developed as a part of the Electromagnetic Environmental Test Facility. The model is designed for use on the IBM-709 computer at Fort Huachuca. Its purpose is to extend and amplify the usefulness of the field facility installation in southern Arizona. The model, therefore, is capable of interference-prediction calculations for much larger and more complex electronic configurations than actually installed in the field facility. Availability of the actual emitters, however, will make it possible to validate the model against actual field measurements. Lack of such validation has severely hampered design of prediction models in the past.

Methods are discussed for the establishment of mathematical functions representing the transmitter, antennas, propagation path, receiver, and scoring method. Each function is considered in the light of past efforts as well as from information currently available and expected in the future (from the Spectrum Signature program, for example). Reasons for the choice of simulation methods for each of the functions are given in detail on the basis of engineering needs of the expected users.

## I. INTRODUCTION

The Field Facility of the Electromagnetic Environmental Test Facility (EMETF) is designed as a proving ground for equipments operated in a typical military deployment situation. Results obtained from it will be of an over-all operational nature. For example, it will be possible to determine that a given receiver experiences interference in a specific, measured amount, and that this interference occurs when certain transmitters operate. It also will be possible to isolate the offending transmitters as units. But measurements from the facility will not necessarily identify specific characteristics of a given equipment as contributing to the interference, although the measurements may provide clues to these deficiencies. The environmental facility is, in other words, a system test facility capable of pointing up troubles which would not be obvious from laboratory measurements of individual equipments.

The system involved is complex. It involves technical characteristics of the equipments, tactical deployments, and factors such as terrain and climate which pertain to the location. Included also are human factors resulting from varied capabilities of those operating and maintaining the equipment. Installation of sufficient equipment in the environmental test facility to isolate and evaluate all these factors would be a costly and inefficient process.

Fortunately this is not necessary. A computer-mechanized prediction model of the system can be constructed which will include data from laboratory measurements of equipment, experimental determinations of terrain and meteoro-

logical factors, and laboratory studies of human factors. Because of the complexity of the system, a basic tenet of the approach has been the necessity of validation of the model. Validation can be accomplished only by comparison of results predicted by the model with those measured in the field.

Ideally the model should be constructed so that the influence of each major factor could be isolated and varied independently of all others. Thus the influence of each factor on the entire system could be determined by computation. Once the model has been shown to agree with measured results from the facility, computations may be made with confidence on larger situations, different terrain conditions, and new locations.

It may readily be seen that the interference prediction model and the controlled-test facility of the electromagnetic environment at the U. S. Army Electronic Proving Ground (USAEPG) complement one another. Indeed, the one is necessary to the other.

## II. GENERAL DESCRIPTION OF MODEL

The basic concept of the model is shown in figure 1. It is seen to be a completely straightforward, engineering approach. The underlying philosophy in development of this model has been to put together one which could be tested and validated by physical measurement on a piece-by-piece, as well as on an overall basis.

The general form of the model will be a set of mathematical expressions or equations separated into a number of mutually independent, multiplicative factors. Each factor will represent a physical entity affecting the problem. Each factor in the model will be in the form of an expression which, when evaluated, will reflect the effect of that particular factor on the entire interference problem. Each factor in the equation(s) will have an independent input and will produce a separate output, so that a factor-by-factor analysis of the model may be made. Consideration of all factors in the model will simulate an actual situation, and will permit a prediction of radio-frequency interference to be expected in a given tactical situation.

The requirement for a close link with the field facility also influenced the form of the model. Each calculation is presented in the form most suitable for field verification.

Some advantages in computing time are claimed for the so-called "stochastic model," which would involve assignment of values to each block of figure 1 by random sampling from a probability distribution function (pdf) representing the physical quantity in the block. (This process is often mistermed the Monte Carlo approach.) It was decided, however, to defer consideration of a stochastic model until the engineering model had been validated. The reasons for this were:

a. There is insufficient knowledge at present of the true probability distribution functions of many of the factors in the model.

b. It has not been completely demonstrated at this time that for comparable accuracies the stochastic model would have a significant advantage over

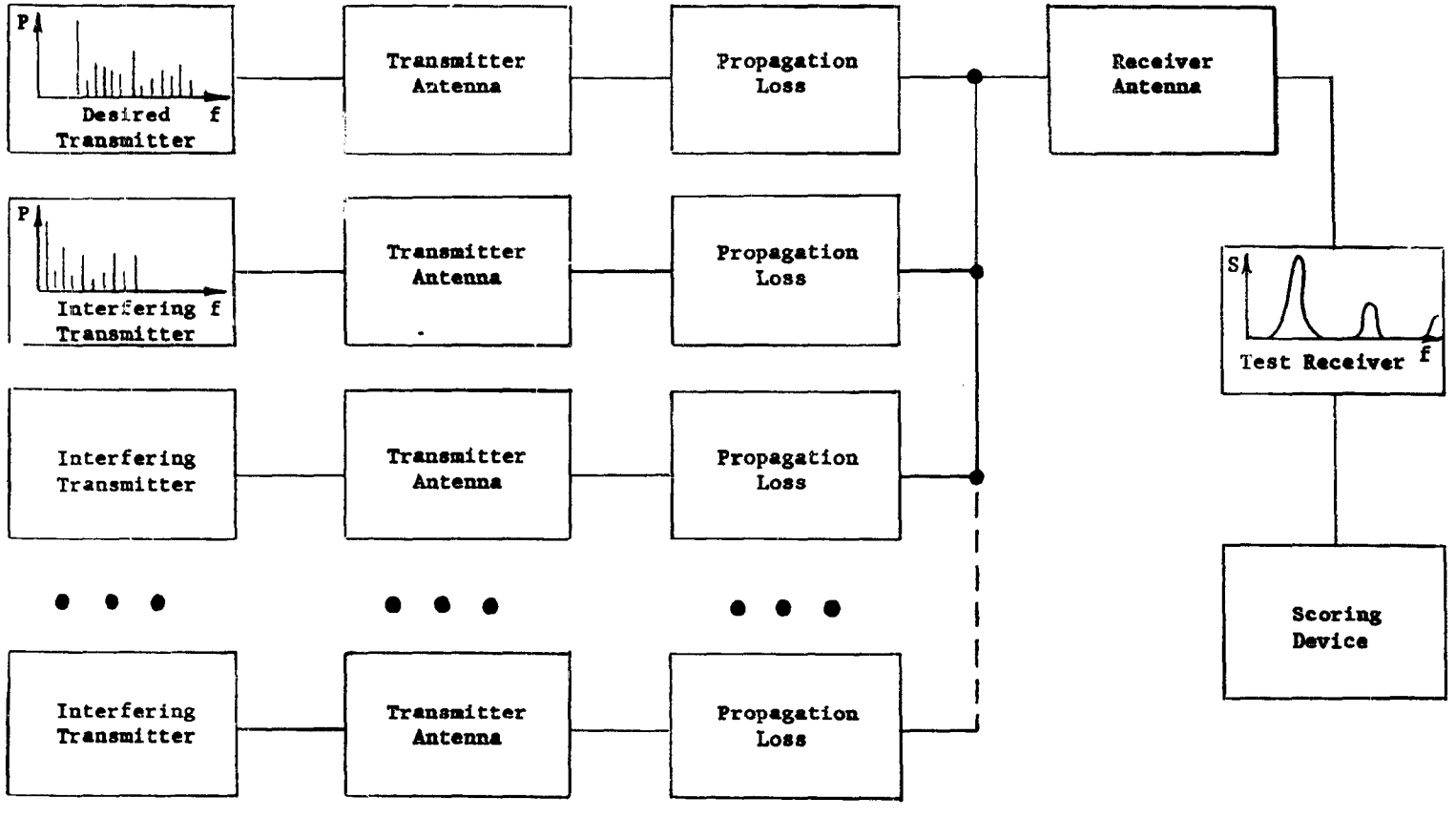



Figure 1. Basic Concept of Prediction Model

the engineering model in terms of computing time.

c. It is believed that the first step is to develop a model which faithfully depicts the physical facility. Once such a model has been developed and validated, it then becomes the standard of excellence, and many other time-saving schemes can be compared against it. The scale of effort of these comparisons will then have been reduced in effort to a computer exercise, and the painful process of validation from field measurements will no longer be necessary.

## III. PHYSICAL BASIS FOR THE PREDICTION EQUATIONS

As indicated above, it was decided early in the program that emphasis must be placed on development of a strong theoretical backbone for the model. This could then be modified or improved by field experiment to attain the desired accuracy.

The over-all problem has been broken down into four general classifications for the purpose of investigation. These are:

a. Transmitter radiated power.

b. Propagation path loss.

c. Receiver response to environment.

d. Scoring methods.

## IV. TRANSMITTER RADIATED POWER

One of the basic requirements of any prediction modeling program is the availability of a complete set of reliable spectrum signature data. These data will be required both in the development of the prediction model and in the validation of the final product. Accurate comparisons between field measurement and calculated results cannot be expected if the data upon which the calculations are based are not reliable.

The need for standard measuring and reporting methods has been recognized by the Department of Defense, and measurements are now being made to a preliminary set of specifications. As a result of these measurements, and of previous programs sponsored by the Signal Corps, data are available which give output power as a function of frequency for a number of transmitters used in the EMETF. These power spectra measurements, exemplified in the transmitter boxes of figure 1, essentially comprise the transmitter functions.

It is assumed that knowledge of the transmitter signatures is available from previously performed laboratory experiments. From the Tri-Service specifications, however, it will be noted that many of the transmitter measurements are made on resistive loads, and that receiver measurements are made from signal generators through standard dummy antennas. This is desirable, in that it makes for uniformity of measurement, regardless of where performed. It also requires

that additional measurements be performed to relate these laboratory measurements to the actual effective radiated power. In particular, there are installed in the EMETF Field Facility many vehicular transmitters and receivers. On vehicles, one antenna is generally used for both the transmission and reception modes. Vehicular antennas are generally whips which are inductively "loaded" to improve radiation characteristics at the fundamental frequency. No attempt was, or could be made, by the designer to control impedance or antenna pattern at the various frequencies at which spurious transmissions or responses have been observed. Even in the fundamental frequency range, the vehicle dimensions usually are appreciable in terms of a wavelength and contribute to the over-all antenna radiation pattern. Measurements on the unmounted vehicular antenna are meaningless.

It thus became necessary to measure the following quantities and to include them as part of the antenna function in the model:

a. Antenna Pattern. This is a measure of the radiated field strength as a function of azimuthal angle, elevation angle, and frequency.

b. Effective Radiated Power (ERP). This gives a measure relating the transmitter signature to the gain and impedance characteristics of the vehicular antenna.

Antenna field tests were performed with these objectives in mind to obtain data for an antenna function.

In the model, therefore, the transmitter power output at each harmonic frequency is modified both by a function proportional to the antenna pattern and by a second function which relates transmitter power output to effective radiated power from an omnidirectional antenna. This second function is different from the ordinary gain specification in that the impedance mismatch between transmitter and antenna is included in the relation between transmitter power into a resistive load and effective radiated power.

Measurements also were made with the vehicular radio in the receiving mode. For this measurement, standard signal generators were mounted in the field intensity (FI) vehicle and driven around the circle while transmitting to the vehicular-mounted receiver under test. Receiver output was measured and recorded in a manner similar to that used for the laboratory spectrum signature measurement. Measurements were made at the fundamental and all significant spurious frequencies.

It is of interest to note that many of the spurious responses noted in the resistive measurements were undetectable under actual radiation conditions.

## V. COMPUTATION OF PROPAGATION PATH LOSS

Computation of propagation path loss for the EMETF prediction model will be based essentially on the free-space equation modified to account for the effect of the earth and its atmosphere. Provision will be made in the computer program to account for the effects of terrain, vegetation, meteorology, and other factors. This permits the easy introduction of factors found at a later date to be important, and the equally facile elimination of factors found from experience

not to contribute to the path loss. Symbolically, the path loss, L, might be expressed as

$$L = \begin{bmatrix}\text{Free-space}\\ \text{equation}\\ \text{(decibels)}\end{bmatrix} + \begin{bmatrix}\text{Spherical earth}\\ \text{correction}\\ \text{(decibels)}\end{bmatrix} + \begin{bmatrix}\text{Terrain}\\ \text{factor}\\ \text{(decibels)}\end{bmatrix} + \begin{bmatrix}\text{Vegetation}\\ \text{factor}\\ \text{(decibels)}\end{bmatrix} + \cdots + \begin{bmatrix}\text{Additional factors}\\ \text{found from experience}\\ \text{(decibels)}\end{bmatrix} \quad (1)$$

All propagation path loss computations begin with the well-known expression for free space, then modify it in various ways. Normally one of the first decisions required of the individual making the computation is a choice between the so-called plane-earth and spherical-earth formulas. If such a decision has been made here, it has been made in favor of a spherical earth. Actually, the equations and machine judgments are set up so that such choices are made without the necessity of artificial determinations as to the relative flatness or roundness of the earth.

Basic path loss is computed as between omnidirectional antennas, since the transmitter and receiver antenna functions will account for all antenna effects in the model. The effect of long-term meteorological variations has not been introduced at this time, but may be included easily as a factor in equation (1) if found desirable in the future.

Scatter-propagation effects have not yet been included, pending a more thorough study of the effects of these phenomena on a field army. These long-time and long-distance effects are not considered to be of as much immediate importance to a field army situation as those for which equations are written in this paper. They are important, of course, and will be added to the program later.

Three regions are normally defined for computation of path loss over a smooth spherical earth. As illustrated in figure 2, these three regions are:

a. The optical-interference region.

b. The diffraction region.

c. The transition region, located between the interference and diffraction regions.

Decision as to the region in which a receiving antenna is located is made according to whether it is:

a. Well within line-of-sight of the transmitter (optical-interference region).

b. Well beyond line-of-sight of the transmitter and into the shadows (diffraction region).

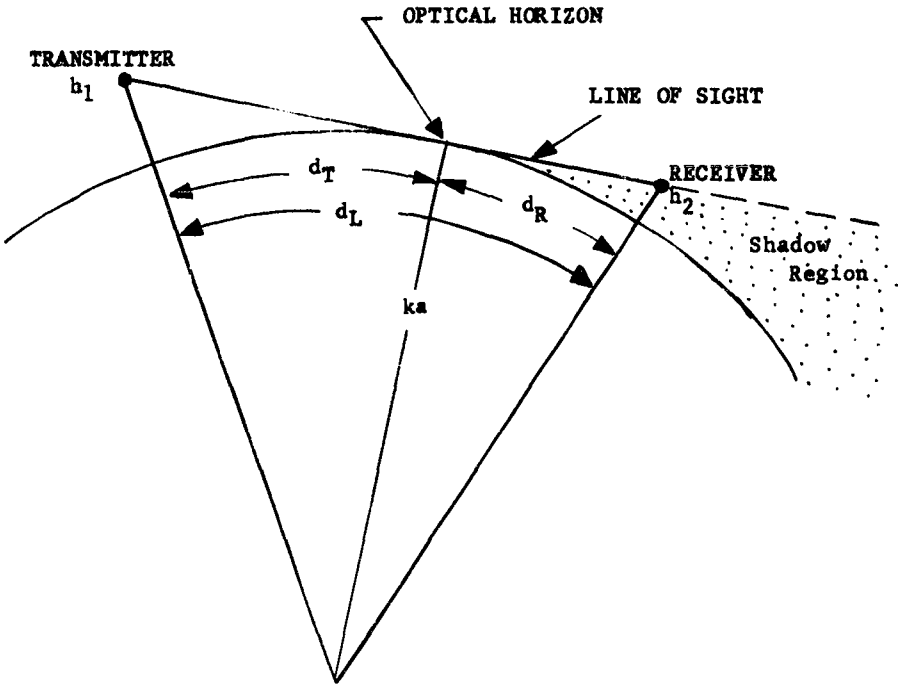



Figure 2. Geometry for Radio Propagation Over Earth

c. In the vicinity of the optical horizon, extending slightly into both of the other two (transition region).

The optical formulas become inaccurate, and actually approach infinite path loss as the horizon is approached. On the other hand, the diffraction formulas, in the form normally used, give path-loss values which are too small in the transition region. This situation is illustrated in figure 3. The usual procedure in the past has been to compute a few values at points well inside both the optical and diffraction regions, and to sketch a free-hand curve connecting the two sets of points. This procedure is not suitable for machine computation and other alternatives were sought.

In general, the optical-interference equations are satisfactory up to the first quadrature point. Location of this point is indicated on figure 3 and derived in the appendix. Study of the van der Pol-Bremmer equations, which form the basis for the diffraction computations, indicated that most of the error in the neighborhood of the optical horizon was contained in the height factor. Therefore a new equation for the height factor was fitted to available data so that the procedure now followed is:

a. At the first quadrature point and all points nearer the transmitter, the optical-interference equations are used.

b. At the points beyond the quadrature point, the modified diffraction formulas are used.

## VI. BASIC EQUATIONS

The basic equations used in the computation are derived in an appendix to this paper. They are also presented in a companion paper[1] in connection with the computer-programing aspects of the model and will not be presented here.

An important factor to note, however, is that the maximum field strength which may ever occur is equal to twice that predicted from the free-space equation. This situation occurs when the reflected ray encounters a perfect reflector and, in addition, arrives at the receiver exactly in phase with the direct ray. Stated in another way, the minimum path loss which may ever be encountered is equal to the path loss predicted by the free-space equation decreased by six decibels.

This figure of free-space path loss less six db is used in a rapid culling process designed to eliminate all radiations which are too weak to affect the computation at the receiver being tested. If, after application of an attenuation factor given by the above criterion, the signal at the receiver is below threshold, that signal may be safely disregarded in all further calculations.

Considerable effort and study has been expended on the terrain factor, which, in general, adds to the path loss between transmitter and receiver. In order to attack this problem, however, it was necessary to establish a firm definition of the so-called "effective antenna height." Just a cursory glance of the literature proves that this quantity has not been well defined in the past, and often has been made a matter of judgment on the part of the individual performing the computation. In order that a firm basis for machine computation may be established, the following convention has been adopted.

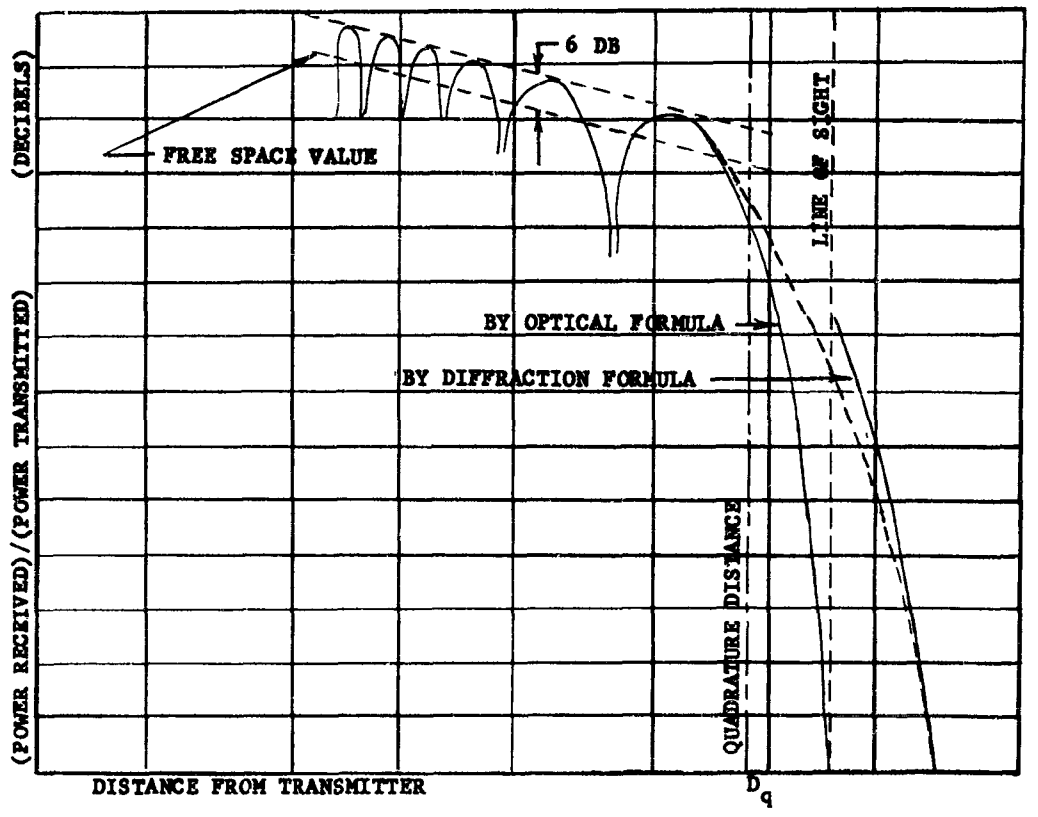



Figure 3. Comparison Between Optical-Interference and Diffraction Formulas in Computation of Path Loss

"The datum plane (or great circle) shall be the ground elevation of either transmitting or receiving antenna, whichever is lower. Effective height of the lower antenna shall be its structural height above ground; effective height of the higher antenna shall be its structural height above ground plus the difference between its ground elevation and that of the datum."

Within the last three decades scores of theoretical papers have been published which treat the calculation of path losses over mountain obstacles and irregular terrain. Many of the published papers are highly theoretical and impose boundary conditions which are not generally realizable in nature. Others have been based on empirical or statistical determinations, but to the present time have not appeared in a form suitable for machine computation.

Some of the most significant and most useful work has been done by the National Bureau of Standards (NBS). A recently published NBS memorandum report[2] gives an extensive review, which covers all the aspects of telecommunication performance, including propagation with all known factors involved. Computational methods presented, however, require considerable calculation and frequent reference to graphical data before answers in terms of path loss between given points can be obtained.

An earlier paper by Egli[3] summarizes the work of many investigators in the field, and leads to a statistical description of the correction factor. The median path loss at a given frequency is found by adding the statistically-derived median deviation to the path loss as calculated from smooth-earth theory. This median deviation from the theoretical smooth-earth value is called the "terrain factor." According to Egli it varies inversely with frequency and is independent of distance. It also appeared that the distribution of received path loss over irregular terrain expressed in decibels above the median value is normally distributed.

The most obvious limitation of Egli's analysis is the aggregation of all types of terrain into a single statistical picture. According to theory an ideal smooth earth with uniform electrical characteristics would have a standard deviation of zero in the signal-strength distribution. Mountainous terrain, on the other hand, would be expected to have a very large deviation. These observations have also been borne out by experiment. Although it may be difficult to specify criteria defining different types of terrain, at least gross differences in terrain must be recognized on a quantitative basis.

In a recent study for the Television Allocations Study Organization (TASO), A. H. LaGrone[4] has proposed an empirical method for terrain correction which seems to provide a more accurate assessment of the influence of rough terrain on the received signal.

The method requires a knowledge of the terrain profile between the transmitter and receiver. The resulting correction is of the form

$$db = c\left[\pm\frac{\sqrt{h_1 - h_2}}{\exp(d_{1r})} \pm \frac{\sqrt{h_2 - h_3}}{\exp(d_{2r})} \pm \frac{\sqrt{h_3 - h_r}}{\exp(d_{3r})}\right] \qquad (2)$$

Signs of the factors in the correction term are the same as the slope between the two points involved. The factor, c, is a function of frequency.

Meaning of the various height and distance elements of the equation is illustrated in figure 4. It is readily apparent that terrain obstacles nearest the receiver have the greatest effect on the correction. One factor still under study is the number of obstacles which must be taken into account in order to obtain a satisfactory correction.

Consistently throughout LaGrone'e work it is pointed out that additional validation is necessary. Also, since the interest of the TASO committee was primarily in television frequency allocation, most of their studies were limited to the vhf and uhf bands. The range of frequencies in the EMETF Field Facility is considerably greater.

For this reason an experiment was designed to extend and validate the proposed method of computing terrain correction factors. A location was chosen in the Gila Bend, Arizona, area so that a smooth path and a rough path could be illuminated easily from the same transmitter. The locations of the two profile lines selected for the experiment are shown in figure 5. The paths begin at the point "A" and extend approximately 24 miles to the point "J" and include 9 test points. A manual profile of the rough terrain path is shown on figure 6 and of the smooth profile on figure 7. The test points on the rough and smooth paths are equally spaced from the source location; that is, test point $C_S$ on the smooth path is exactly the same distance from the transmitter as test point $C_R$ on the rough path. The rough-path test points were selected to give a sample of high elevations, G and H; low elevations, B, E, F, and I; and medium elevations, D and J.

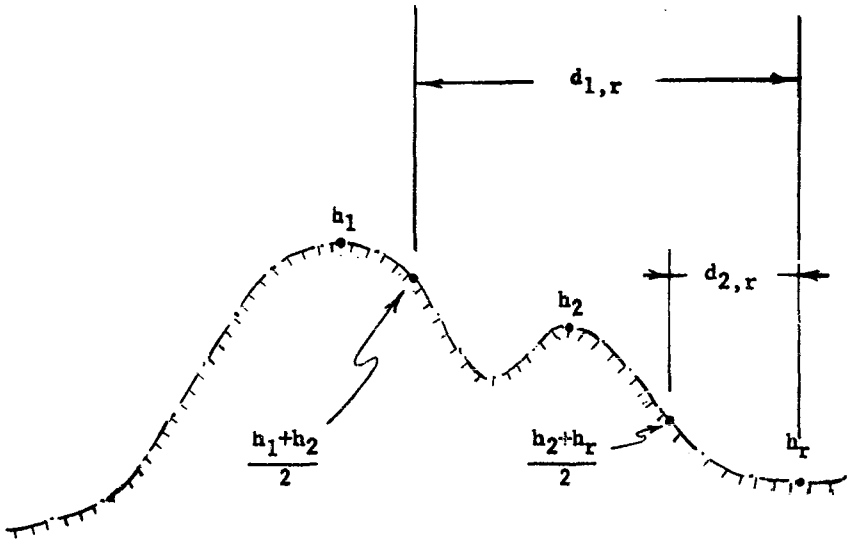
The measurement technique is as shown in figure 8. Source transmitters are located at the common point A. Two monitors, one on the rough path and one on the smooth path, are used to make simultaneous measurements with the test vehicles along the contour. A corner reflector is used to increase the effective radiated power of the higher frequency transmitters. The corner reflector has been designed so that a center pivot makes rapid rotation from smooth path to rough path possible.

The technique minimizes the effect of local meteorological conditions normally expected from day to day, week to week, and month to month. It also makes possible a rapid calculation of the path loss between the monitor position and any test point. Initially an antenna height of 7 feet has been used at both transmitter and receiver sites. Later the transmitter height may be raised to 30 feet to study the effect of antenna height on the path loss.

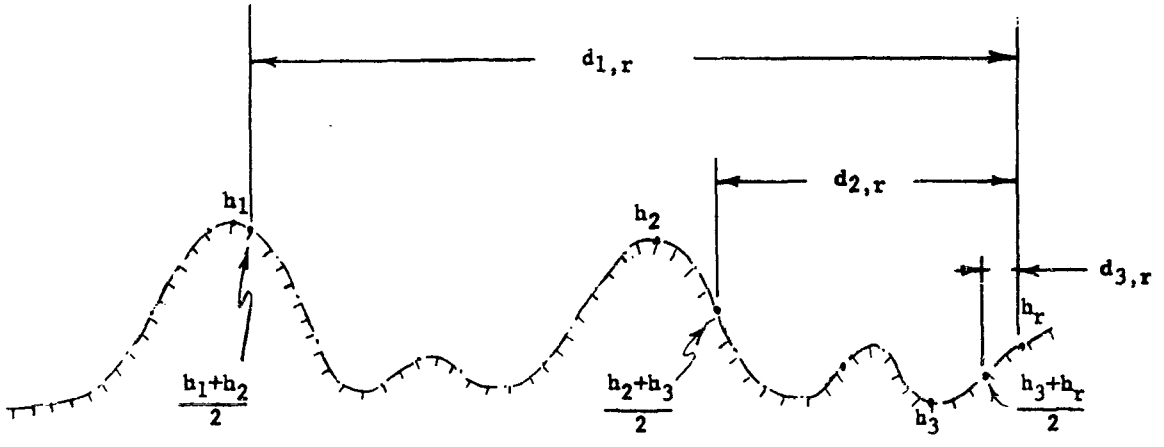
The frequencies covered in the tests are approximately 2.5, 4.0, 16.1, 53.9, 220.8, and 512.3 megacycles per second.

The same data also will be used to isolate meteorological variations. Therefore, a measurement program of approximately 12 months' duration is in progress in order to get a complete picture for all seasons of the year. The meteorological measurements are being made by members of the U. S. Weather Bureau working in cooperation with the Meteorology Department, USAEPG.

Since the tests are not yet complete, a report on their results is not possible at this time. Preliminary results have been sufficiently encouraging that the decision has been made to include a LaGrone-type calculation in the program.




$$db = c\left[-\left|h_1 - h_2\right|^{\frac{1}{2}} e^{-d_{1,r}} - \left|h_2 - h_r\right|^{\frac{1}{2}} e^{-d_{2,r}}\right]$$




$$db = c\left[-\left|h_1 - h_2\right|^{\frac{1}{2}} e^{-d_{1,r}} - \left|h_2 - h_3\right|^{\frac{1}{2}} e^{-d_{2,r}} + \left|h_3 - h_r\right|^{\frac{1}{2}} e^{-d_{3,r}}\right]$$

Figure 4. Examples of the Application of db Equation to Terrain Types 3 and 4

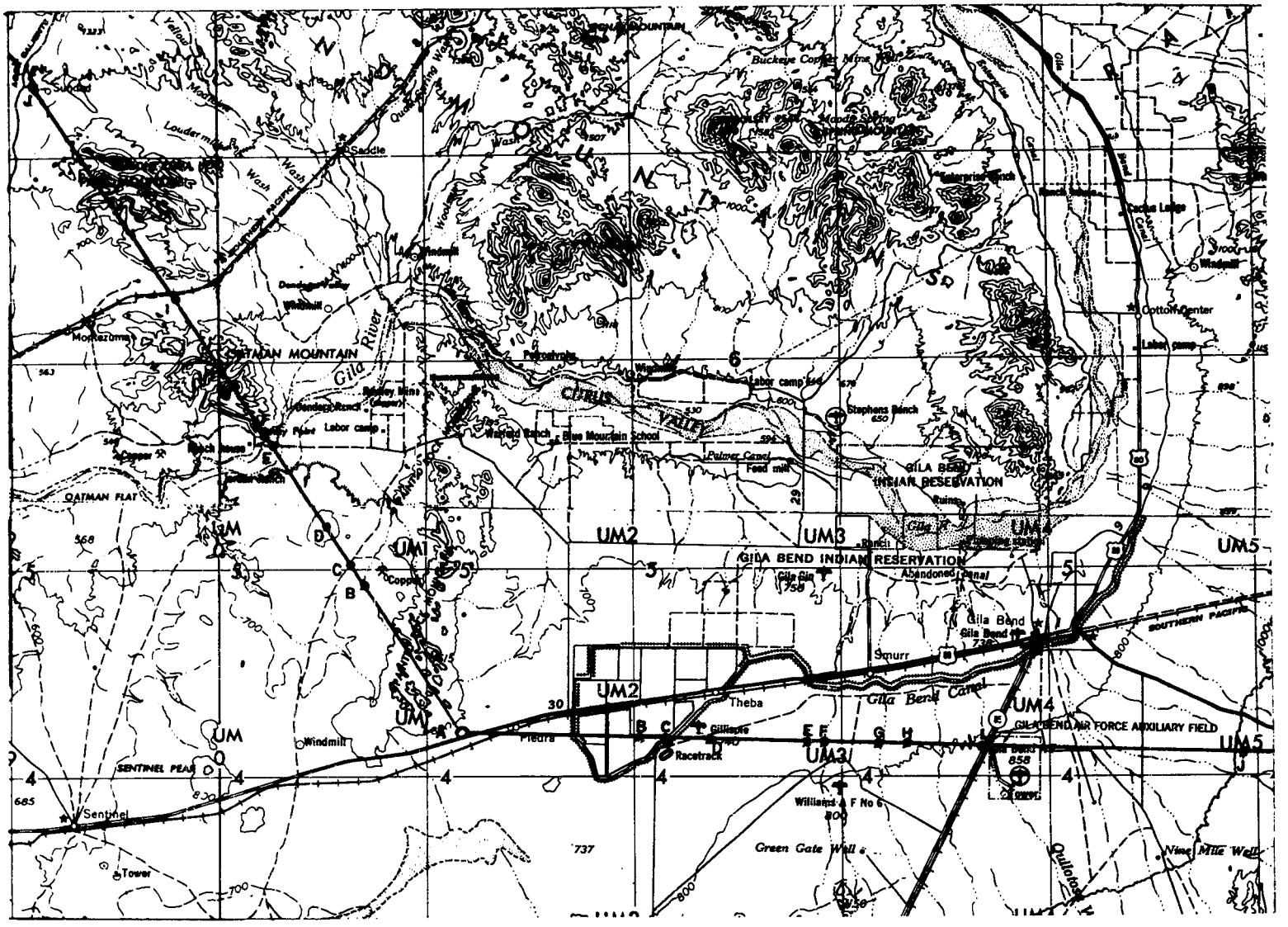



Figure 5. Map Showing Rough and Smooth Profile

Manual profile of rough terrain along Base Line showing locations of test points.

SCALE: 1 cm = 1 mile

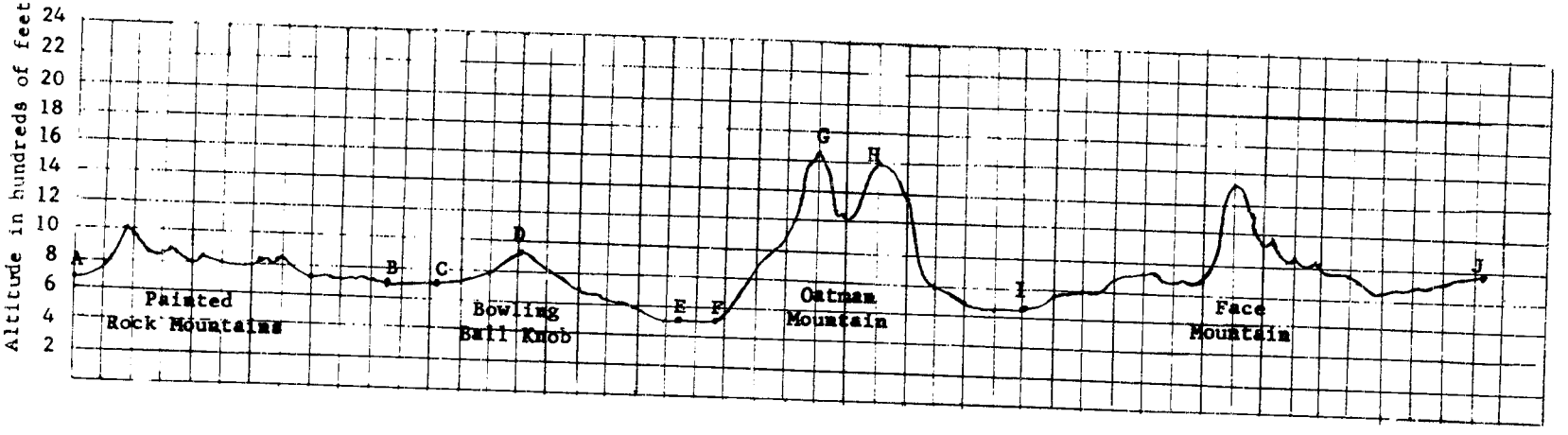



Figure 6. Manual Profile of Rough Terrain

Manual profile of smooth terrain along Base Line showing locations of test points.

SCALE: 1 cm = 1 mile

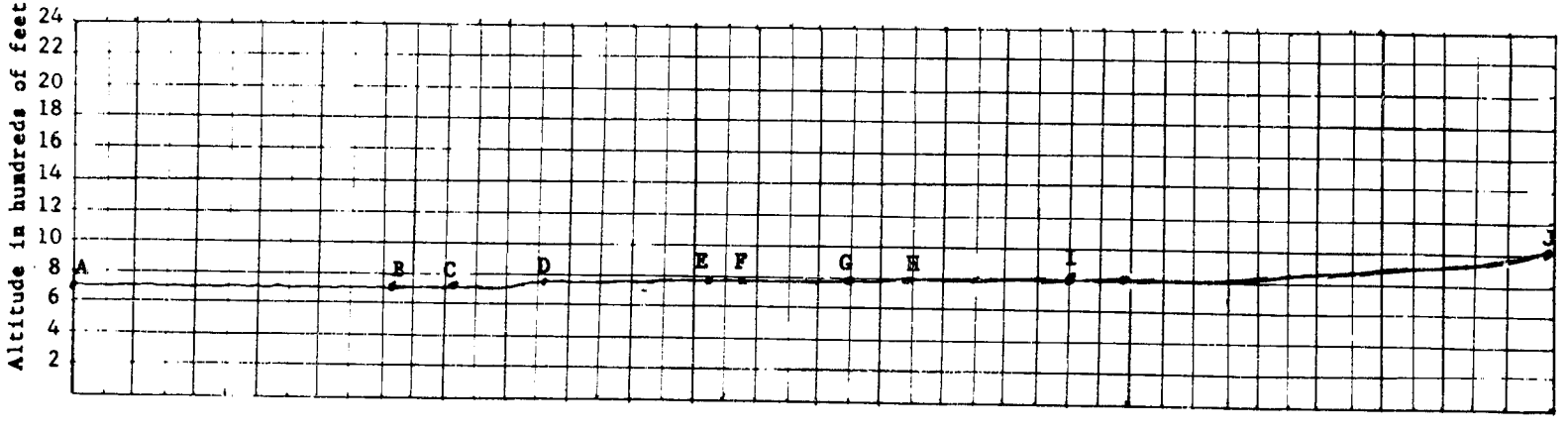



Figure 7. Manual Profile of Smooth Terrain

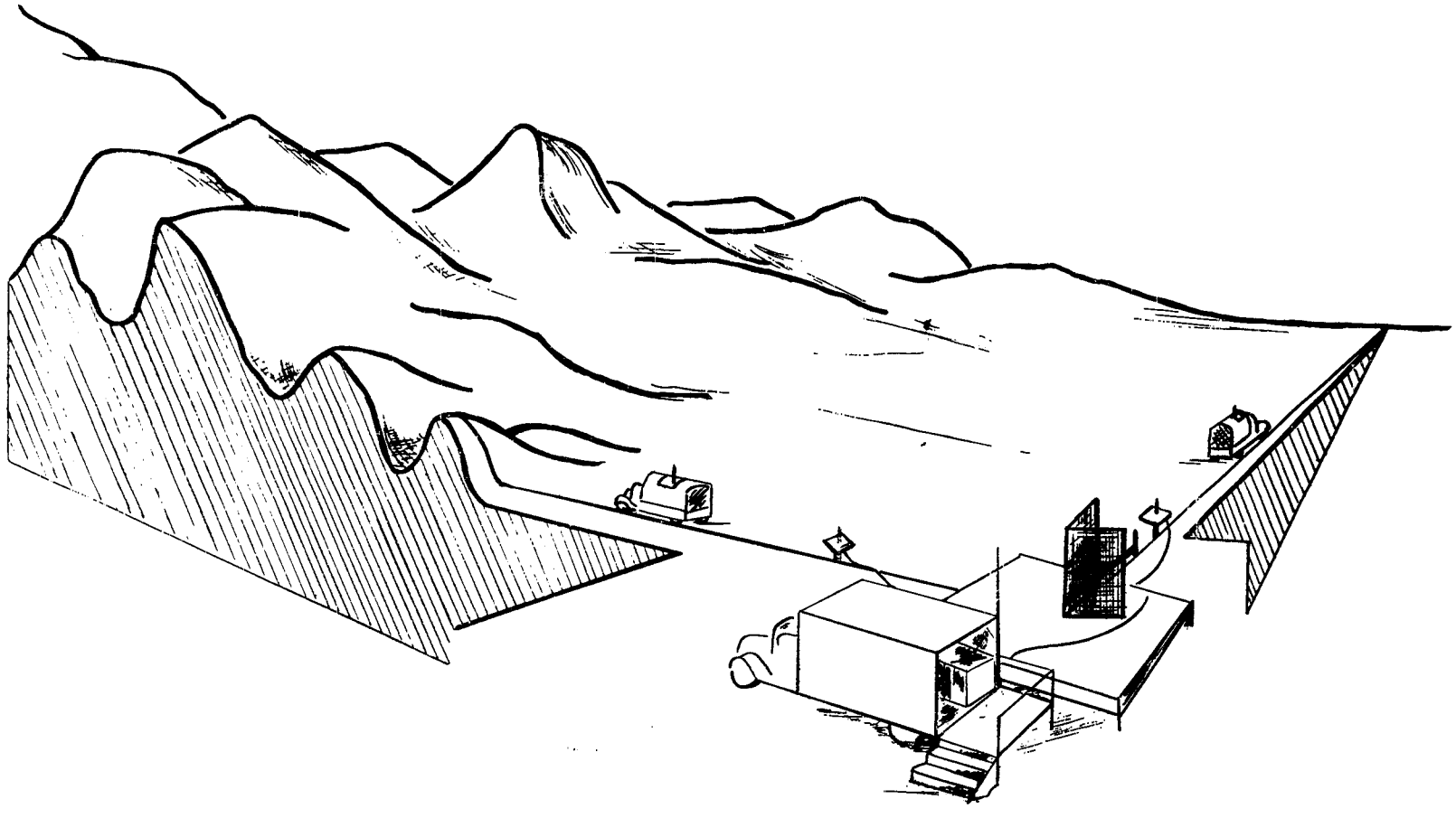


Figure 8. Profile Measurement Concept

In addition to the above profile measurements, studies leading to determination of an average terrain correction factor have been in progress. The goal here is to obtain a correction factor for terrain which may be somewhat less accurate than the profile factor, but which can be computed much more easily. Studies of data previously reported in the literature indicate average path loss to increase with frequency, and also to increase as the terrain becomes more rugged. The computer programs are being written to take into account both the variation with frequency and the variation with ruggedness. Ruggedness is measured in units of $\Delta h$, where $\Delta h$ is the difference in height between the peaks and valleys of a region. This is believed to give considerably more quantitative information to the computation than the expedient occasionally suggested of assigning mean values to something rather loosely defined as "mountainous terrain," "rolling hills," or "flat" earth.

A correction for vegetation will be made in a manner similar to the average terrain correction. Path loss is known to increase with frequency and with increasing thickness of vegetation. These will be stored in the computer as a matrix of values. The rows of this matrix will account for increasing thickness of vegetation and its columns will account for increasing frequency.

An additional advantage of this type of programing is its flexibility. As better data become available on average terrain or vegetation conditions, it will be a simple matter to improve the calculation without changing the program.

## VII. RECEIVER RESPONSE TO ENVIRONMENT

The process involved in determining the strength of signals received at the receiver under test is quite simple in concept. It consists essentially of transferring each transmitter signature across the intervening distance to the receiver, taking into account the appropriate propagation loss.

The net result of such a computation is a large amount of knowledge describing power spectra, but no information on phase relationships among the received signals. It may safely be assumed, however, that these rf voltages have random phase. There are two reasons for this:

a. The on-off cycling of transmissions by the various radiators at the rf level can occur only in a random fashion.

b. Changes in phase due to the propagation path may be considered to be random because of the geographical dispersion of the transmitters.

It is practical to compute the resulting power spectrum at the receiver input terminals, particularly after insignificant emissions have been culled out early in the computational process. Receiver selectivity is the main factor in reducing the number of signals to be considered. Many of the signals will be rejected by the selective circuits of the receiver. Of those which do pass, a certain discrete number may be expected to have a significantly greater strength than any of the others. The remainder which pass will have a random amplitude as well as phase. Reasons for this are:

a. There exists a wide variation in output power among the various transmitters in any deployment.

b. The transmitters are located at different distances from the receiver; hence, the signals experience different transmission losses.

Calculations necessary to consider these signals individually would be prohibitively long and time consuming. Furthermore, no information is presently available on their collective contribution to interference in the receiver. Existing information as recorded in technical literature is restricted to the mathematical analysis of the response of receivers to a desired signal plus one or possibly two interfering signals. Random noise may or may not be present. Such simple situations are susceptible to mathematical description, but are not descriptive of a tactical situation in which many interfering signals may be present. Preliminary studies indicate that any straightforward, brute-force attempt to extend previous mathematical works to include many interfering signals will lead to prohibitive mathematical complexities.

At the other extreme, the performance of receivers responding to random noise has been analyzed in countless different ways. Between these two extremes exists a great void which includes the practical case of many interfering signals.

In the past acceptance ratios have been used as a method of evaluating the interference situation. An acceptance ratio for a communication receiver is defined as the ratio, in decibels, of a desired signal to an interfering signal which will define the tolerable limit of satisfactory information reception. Thus, a step function is postulated, wherein a receiver experiences zero interference if the ratio of desired-to-interfering signal is greater than the acceptance ratio, but is considered completely jammed if the signal-to-interference ratio declines below this value.

Acceptance ratios, in general, are highly subjective and must be closely related to a particular receiver. They are restricted to one-at-a-time consideration of interfering transmitters, and are not considered completely satisfactory, even by those who developed them. To date, however, very little else has been developed to describe interference to communication receivers. Other methods for handling this problem were therefore sought.

The information required to perform a receiver calculation is available from several sources. The first source of information is the measurements being made according to the Military Collection Plan for Equipment Spectrum Signatures. This plan will provide information on the following receiver characteristics:

a. Sensitivity

b. Spurious response

c. Intermodulation

d. Dynamic range

e. Adjacent-channel interference

f. Selectivity

Information on inherent noise of the receiver will also be available.

Based on the above types of information, the receiver function for the EMETF interference prediction model has been developed as follows:

a. The frequency and amplitude of all signals which may be present in the if. amplifier of the receiver are determined from application of the above characteristics to signals presented at the receiver input terminals. As discussed above, the selection and elimination process takes place at several points in the computation as various attenuation and selectivity factors are applied to the signals radiated in the area. As a result of this process the thousands of frequencies actually radiated are reduced to something on the order of a hundred or less in the if. amplifier.

b. Of these hundred signals, a relatively small number, say 5 to 10, may be expected to have amplitudes significantly greater than their neighbors. These few are called "discrete interfering signals."

c. The power content of the remainder, be it 100 or 1,000 is summed. This procedure is valid since there is, in general, no coherence between the signals. Also studies, both experimental and theoretical, by Bell Aerosystems Company in Tucson, have indicated that signals of random phase and amplitude, in numbers greater than about 10, approach a normal distribution for all practical purposes. Figure 9 illustrates the resulting probability distribution function of 10 such signals.

d. To the power content of the random interferers is added other random noise present in the if. amplifier. This includes thermal agitation noise in the input circuits, shot noise, cosmic disturbances in the atmosphere, and so forth. The sum total of the result is an expression for total noise power, normally distributed. To this remains to be added the desired signal and the discrete interfering signals.

It will be recalled that the frequency spectrum of a normal distribution consists of lines of uniform height at all frequencies in the band. Accordingly the normally distributed function is translated into such a spectrum, with the height of the lines adjusted to represent the total power contained in the function. To this is added the power at each of the frequencies of the discrete interfering signals plus the desired signal. (See figure 10.) This composite signal is then operated on by the computer detection program which:

a. Converts the power spectrum into voltages, assigning random phases to the voltages in the process.

b. Sums the voltages in a linear fashion, then simulates the detection process on the resultant wave. As required, the simulated detection process may be that of an fm. detector or that performed by either a linear or square-law am. detector.

c. Performs a Fourier analysis on the resultant audio (or video) power spectrum, which is then ready for scoring.

The above is discussed in greater detail in a companion paper.[5]

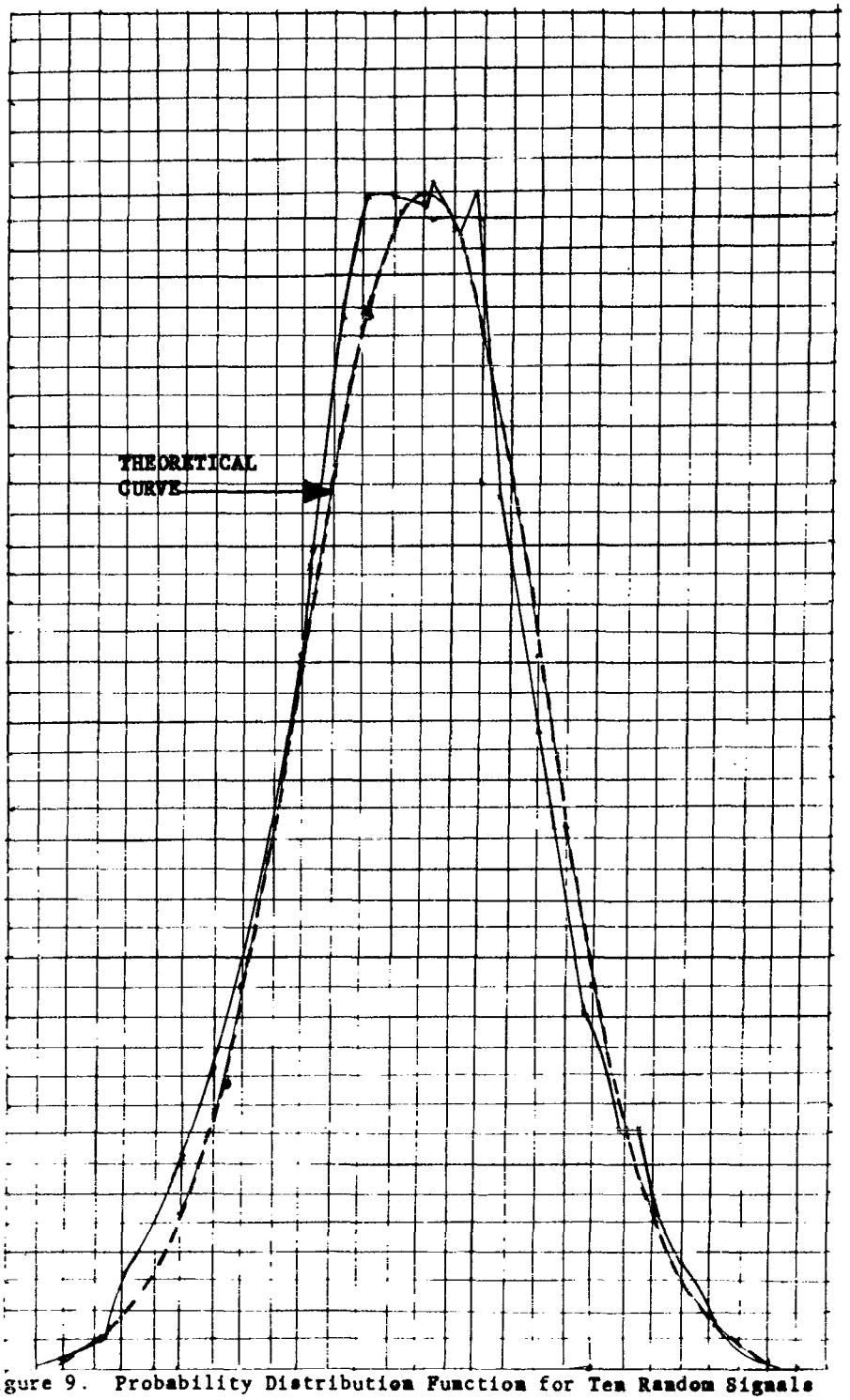



Figure 9. Probability Distribution Function for Ten Random Signals

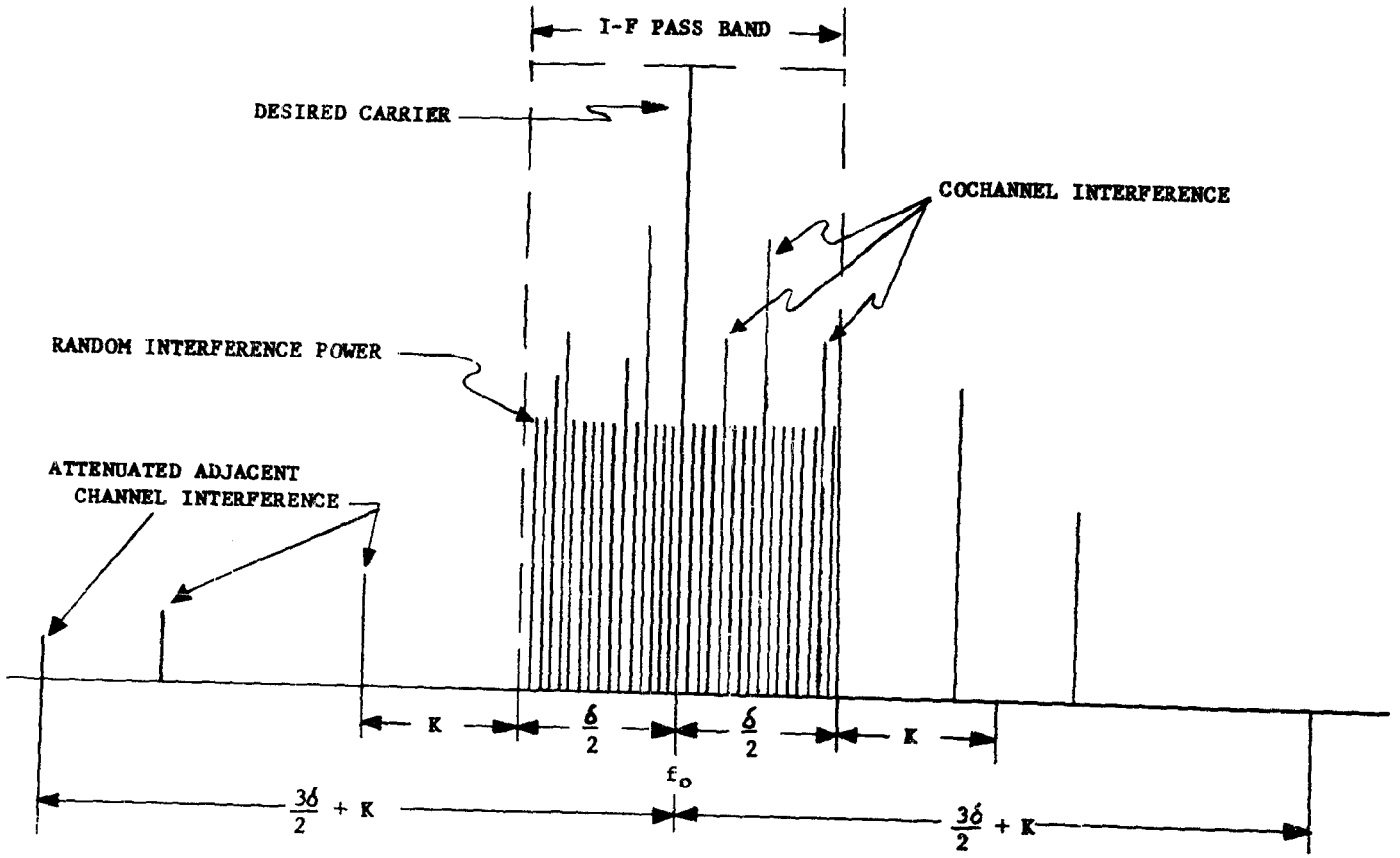



Figure 10. Spectrum of Signals Presented to Demodulator

## VIII. SCORING METHODS

Scoring in the EMETF model is accomplished by a computation which actually simulates the interference detection equipment (IDE) installed in the field. Since an audio noise plus signal-power spectrum is available from the previous computation, it is relatively simple to divide the audio spectrum into the prescribed 14 bands. These bands are of unequal width in frequency, but each contributes equally to the intelligibility according to the French and Steinberg theory. Signal-to-noise ratios in each of the bands can be computed and the articulation index determined, just as in the field equipment. In addition, it will also be possible to obtain a signal-to-noise ratio of the complete audio spectrum. This number will be useful for comparisons with other field tests where IDE equipment may not be used.

## ACKNOWLEDGMENT

The work described in this paper was sponsored by the Field Test Directorate, U. S. Army Electronic Proving Ground, Fort Huachuca, Arizona, under contract Nr. DA-36-039-SC-80424.

## REFERENCES

1. Scott, John B., "The Computer Approach to the Interference-Prediction Model of the Electromagnetic Environmental Test Facility," Proceedings of the 7th Conference on Radio Interference Reduction and Electronic Compatibility, Armour Research Foundation, Illinois Institute of Technology, November, 1961.

2. National Bureau of Standards, Memorandum Report, Telecommunications Performance Standards, Tropospheric Systems, Volume 5 of 6.

3. Egli, John, "The Radio Propagation Above 40 Mc Over Irregular Terrain," PROC. IRE, 45, pp 1383-1391 (1957).

4. LaGrone, A. H., "Forecasting Television Service Fields," PROC. IRE, 48, pp 1009-1015 (June, 1960).

5. Wilde, N., Hoehn, A. J., and Follett, L. A., "A Digital Representation of Interference Within a Communication Receiver Including the Demodulation Process," Proceedings of the 7th Conference on Radio Interference Reduction and Electronic Compatibility, Armour Research Foundation, Illinois Institute of Technology, November, 1961.

## APPENDIX

## PROPAGATION OF RADIO WAVES OVER A FINITELY CONDUCTING SMOOTH SPHERICAL EARTH

1. Distance Formulas--General. Different methods of computation are expedient for the three regions considered in the present report. The three regions are:

a. The optical-interference region.

b. The diffraction region.

c. The transition region, located between the interference and diffraction regions.

2. Cross Reference. In order to facilitate cross reference between this paper and the reports of the National Bureau of Standards, Central Radio Propagation Laboratory,[1] the following relation must be observed:

$$\phi = \pi - c \tag{1}$$

where $\phi$ is the angle used in these reports (and by Burrows and Attwood[2]) and c is the angle used and tabulated in the NBS publications.

3. Assumptions:

Uniform Gradient. The usual assumption is made that the index of refraction of the atmosphere has a uniform negative gradient with increasing altitude. The effect of this on radio propagation may be taken into account by considering the atmosphere to be homogeneous over an earth whose radius has been increased from $a$ to $ka$. The factor $k$ is a function of the earth's radius and the refractive gradient (dn/dh) and is given by

$$k = \frac{1}{1 + a(dn/dh)} \tag{2}$$

For standard atmosphere, the gradient is given approximately by

$$(dn/dh) = -(1/4a) \tag{3}$$

so that, for standard atmosphere

$$k = 4/3 \tag{4}$$

To this approximation, the radius of the equivalent earth equals $8.49 \times 10^6$ meters (5,280 miles). Exact values of refractive gradient may be substituted in equation (2) if local conditions are to be taken more carefully into account. Methods of making these computations may be found in the references. The National Bureau of Standards, in particular, has done much work in this area.

Smooth Earth. In all calculations it is assumed that the earth is smooth. Terrain effects will be handled by means of a separate factor.

4. Distance Formulas--Computations. Quantitative measures of the distances from transmitter and receiver to the optical horizon may be made from consideration of figure A-1. From the figure it may be seen that

$$ka/(ka + h_1) = \cos (d_T/ka) \tag{5}$$

For distances, $d_T$, of 3,500 miles or less the first two terms of the series expansion for the cosine may be used within an accuracy of one per cent; thus

$$\cos (d_T/ka) = 1 - (1/2)(d_T/ka)^2 \tag{6}$$

Expanding to the left side of equation (5) by the binomial theorem and equating to the right side of equation (6)

$$1 - (h_1/ka) = 1 - (1/2)(d_T/ka)^2 \tag{7}$$

from which

$$d_T = (2\ ka\ h_1)^{1/2} \tag{8}$$

By a similar procedure

$$d_R = (2\ ka\ h_2)^{1/2} \tag{9}$$

so that

$$d_L = d_T + d_R = \sqrt{2\ ka}(\sqrt{h_1} + \sqrt{h_2}) \tag{10}$$

Thus the criteria which determine whether a receiver at a distance d from a transmitter is in its interference or diffraction region are:

(a) Optical-Interference Region:

$$d < \sqrt{2\ ka}\ (\sqrt{h_1} + \sqrt{h_2}) \tag{11}$$

(b) Diffraction Region:

$$d > \sqrt{2\ ka}\ (\sqrt{h_1} + \sqrt{h_2}) \tag{12}$$

Actually, the optical formulas become inaccurate as the horizon is approached. The diffraction formulas, in the simplified form presented in this report, have the same failing. After study of the van der Pol-Bremmer equations upon which the diffraction formulas are based, it was found that most of the error in the diffraction equations occurred in the antenna height term. A height correction term has been fitted to experimental and calculated results and is presented in equation (88). Optical formulas are used up to the quadrature point (72) and the modified diffraction formulas beyond.

5. Geometric Distance Formulas. The key to all geometric distance formulas is determination of tan $\Psi$, shown in figure A-2. It should be noted that antenna heights and angles are greatly exaggerated in the figure.

It is readily seen that

$$\theta_1 = d_1/ka \tag{13}$$

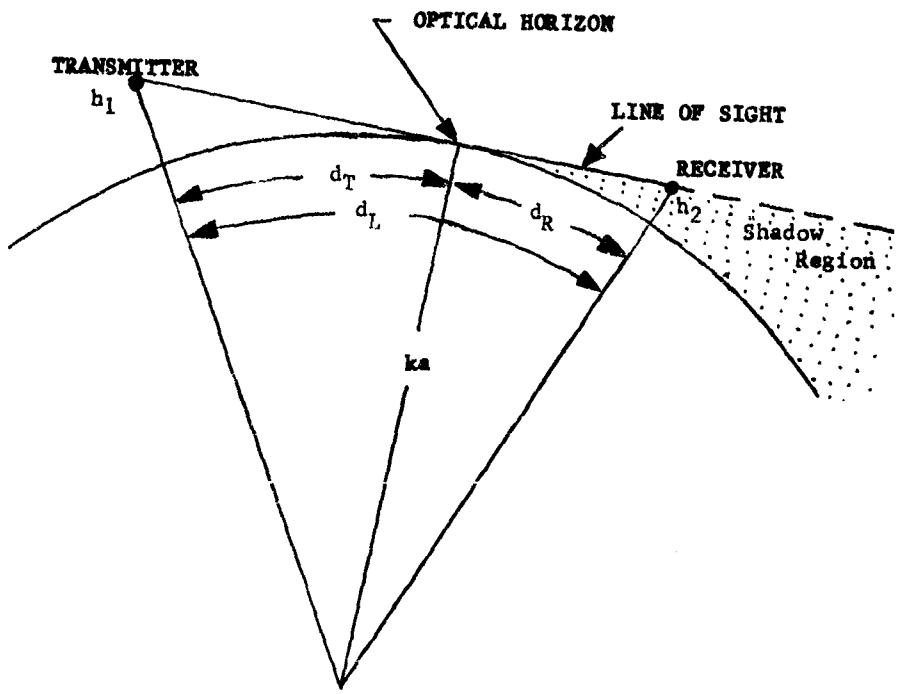



Figure A-1. Geometry for Radio Propagation Over Earth

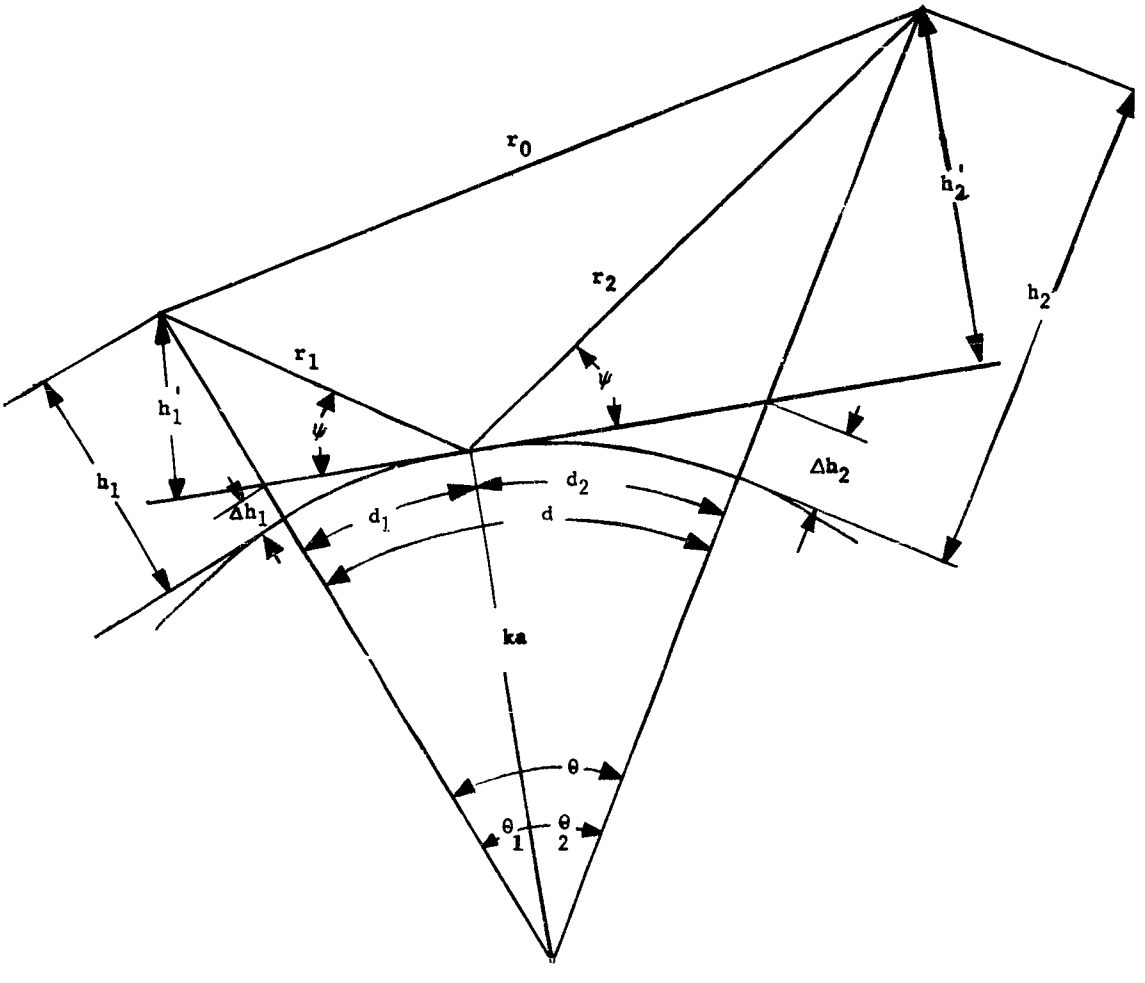



Figure A-2. Geometry for Interference Region

$$\theta_2 = d_2/ka \tag{14}$$

$$\theta = d/ka = (d_1 + d_2)/ka \tag{15}$$

$$h_1' = (h_1 - \Delta h_1) \cos \theta_1 \tag{16}$$

$$\tan \psi = \frac{h_1'}{(ka + \Delta h_1) \sin \theta_1 + (h_1 - \Delta h_1) \sin \theta_1}$$

$$= \frac{(h_1 - \Delta h_1) \cos \theta_1}{(ka + h_1 \sin \theta_1} \tag{17}$$

If $d_1 < 1{,}250$ miles, an error of less than one per cent is introduced by letting

$$\sin \theta_1 = \theta_1 \tag{18}$$

$$\cos \theta_1 = 1 \tag{19}$$

Under these conditions

$$\tan \psi = \frac{(h_1 - \Delta h_1)/d_1}{1 + h_1/ka} \tag{20}$$

Now $h_1$ is of the order, at most, of a few miles while ka is approximately 5,280 miles. Little is lost, therefore, in writing

$$\tan \psi = (h_1 - \Delta h_1)/d_1 \tag{21}$$

From equations (15), (16), and (21) a more useful form for $\tan \psi$ may be obtained:

$$\tan \psi = (h_1' + h_2')/d \tag{22}$$

It is necessary to evaluate $\Delta h_1$ and $\Delta h_2$ in order to make use of the equations. By referring to figure A-2 it may be seen that an antenna of height $\Delta h_1$ would be located a distance $d_1$ from its optical horizon. Thus, from equation (8)

$$\Delta h_1 = d_1^2/2ka \tag{23}$$

so that

$$h_1' = h_1 - (d_1^2/2ka \tag{24}$$

$$h_2' = h_2 - (d_2^2/2ka) \tag{25}$$

Making use of equations (24) and (25), equation (22) may now be written in the form

$$\tan \psi = \frac{h_1 + h_2}{d} - \frac{d_1^2 + d_2^2}{2kad} \tag{26}$$

Consider the quantity $(d_1^2 + d_2^2)/2kad$. Following Burrows and Attwood[1] (p. 387) let

$$d_1 = (d/2)(1 + b) \tag{27}$$

and

$$d_2 = (d/2)(1 - b) \tag{28}$$

so that the sum of $d_1$ and $d_2$ is still d. Squaring equations (27) and (28) and adding

$$d_1^2 + d_2^2 = (d^2/2)(1 + b^2) \tag{29}$$

The general expression for $\tan\psi$ in terms of b is then

$$\tan\psi = \frac{h_1 + h_2}{d} - \frac{d(1 + b^2)}{4ka} \tag{30}$$

The fact that the sum of $d_1$ and $d_2$ is always d establishes a condition on b; namely

$$0 < |b| < 1 \tag{31}$$

The greatest correction would result as

$$|b| \to 1 \tag{32}$$

so that the expression for $\tan\psi$ with maximum correction subtracted is

$$\tan\psi = \frac{h_1 + h_2}{d} - \frac{d}{2ka} \tag{33}$$

If it is desired that the d/2ka term have an effect on the result which is less than p per cent, a criterion which will always assure this is given by

$$\frac{h_1 + h_2}{d} \geq \left[\frac{d}{2ka}\right]\left[\frac{100}{p}\right] \tag{34}$$

If the criterion is met, $\Delta h$ may be neglected in all equations to follow. This means that $h_1$ may be interpreted as $h_1$, and $h_2$ as $h_2$.

If the criterion is not met, $d_1$ must be computed. It was previously written that

$$d_1 = (d/2)(1 + b) \tag{27}$$

and

$$d_2 = (d/2)(1 - b) \tag{28}$$

Let

$$h_1 = (h_1 + h_2)(1 + c)/2 \tag{35}$$

and

$$h_2 = (h_1 + h_2)(1 - c)/2 \tag{36}$$

where b is to be computed. Its physical significance is indicated by

$$b = (d_1 - d_2)/(d_1 + d_2) \tag{37}$$

and

$$c = \frac{h_1 - h_2}{h_1 + h_2} \tag{38}$$

It is assumed that $h_1 > h_2$ and $d_1 > d_2$ so that b and c will always be positive. This is always possible because of the principle of reciprocity. It previously has been shown in equation (21) that

$$h_1'/d_1 = h_2'/d_2 \tag{39}$$

or

$$(h_1/d_1) - (d_1/2ka) = (h_2/d_2) - (d_2/2ka) \tag{40}$$

Substituting for $d_1$ and $d_2$ from equations (27) and (28)

$$\frac{h_1 + h_2}{d}\left[\frac{1 + c}{1 + b}\right] - \frac{d(1 + b)}{4ka} = \frac{h_1 + h_2}{d}\left[\frac{1 - c}{1 - b}\right] - \frac{d(1 - b)}{4ka} \tag{41}$$

which simplifies to

$$\left[\frac{h_1 + h_2}{d}\right] \cdot \frac{2(c - b)}{1 - b^2} = \frac{bd}{2ka} \tag{42}$$

Solving for c

$$c = b + bm(1 - b^2) \tag{43}$$

where

$$m = d^2/4\ ka(h_1 + h_2) \tag{44}$$

Solution of equation (43) for b then permits $d_1$ and $d_2$ to be obtained from equations (27) and (28).

With $d_1$ and $d_2$ known it is then possible to compute $h_1'$ and $h_2'$ from equations (24) and (25).

6. Path Difference. All quantities will be written in terms of the equivalent heights $h_1'$ and $h_2'$ with the understanding that $h_1$ and $h_2$ may be written instead if the tan $\psi$ criterion is met.

$$r_o = \left[d^2 + (h_1' - h_2')^2\right]^{1/2}$$

$$= d\left[1 + (1/2)(h_1' - h_2')^2/d^2 - (1/8)(h_1' - h_2')^4/d^4 + \ldots\right] \quad (45)$$

$$r_1 + r_2 = \left[d^2 + (h_1' + h_2')^2\right]^{1/2}$$
$$= d\left[1 + (1/2)(h_1' + h_2')^2/d^2 - (1/8)(h_1' + h_2')^4/d^4 + \ldots\right] \quad (46)$$

$$r_1 + r_2 - r_o = d\left[2h_1'h_2'/d^2 - h_1'h_2'(h_1'^2 + h_2'^2)/d^4 + \ldots\right]$$
$$= (2h_1'h_2'/d)\left[1 - (h_1'^2 + h_2'^2)/2d^2\right] \quad (47)$$

7. Path Ratio. The path ratio is easily shown from the above to be

$$r_o/(r_1 + r_2) = 1 - 2h_1'h_2'/d^2 + h_1'h_2'(h_1'^2 + h_2'^2)/d^4 - \ldots \quad (48)$$

8. Calculations Involving Electrical Quantities. In the following paragraphs, equations are presented which will be used in calculation of path loss over a smooth spherical earth. Many of the equations are presented without derivation, since these are readily available in the references. References 2 and 3 are particularly recommended for these derivations. Equations developed independently of the referenees have been presented in full. In addition, the development of some equations contained in the references is presented here so that evaluation may be made of the effect of terms neglected in the original derivation.

a. Basic free space equation (between omnidirectional radiators)

$$\frac{P_r}{P_t} = \left[\frac{\lambda}{4\pi d}\right]^2 \quad (49)$$

It is required only that $\lambda$ and d be in the same units.

b. Spherical earth effect in the optical interference region

Multiply free-space equation by the factor $A^2$

$$A^2 = (1 - K)^2 + 4K \sin^2 (\Delta/2) \quad (50)$$

where

$$K = (F_2/F_1)\, \rho D \quad (51)$$

and

$$\Delta = \delta + \phi - \pi \quad (52)$$

$F_1^2$ is the fraction of the maximum antenna power gain in the direction of the direct ray.

$F_2^2$ is the fraction of the maximum antenna power gain in the direction of the reflected ray.

$\rho$ and $\phi$ are the modulus and angle of the reflection coefficient; that is

$$R = \rho \exp(j\phi) \tag{53}$$

D is the divergence factor introduced to account for the decreased gain produced by the spreading of a wave reflected from a spherical surface.

$\delta$ is the phase retardation caused by the fact that the path length $r_1 + r_2 > r_o$.

c. Calculation of reflection coefficient (see Equation 92, ff.)

For vertical polarization:

$$R_v = \rho_v \exp(j\phi_v) = \frac{\epsilon_c \sin\psi - \sqrt{\epsilon_c - \cos^2\psi}}{\epsilon_c \sin\psi + \sqrt{\epsilon_c - \cos^2\psi}} \tag{54}$$

For horizontal polarization:

$$R_h = \rho_h \exp(j\phi_h) = \frac{\sin\psi - \sqrt{\epsilon_c - \cos^2\psi}}{\sin\psi + \sqrt{\epsilon_c - \cos^2\psi}} \tag{55}$$

In both cases

$$\epsilon_c = \epsilon_r + j60\lambda\sigma \tag{56}$$

$\epsilon_r$ is the dielectric constant of the earth (dimensionless).

$\lambda$ is the wave length (meters).

$\sigma$ is the ground conductivity (mho/meter).

$\psi$ is shown in figure A-2.

d. Calculation of phase retardation angle, $\delta$

$$\delta = \frac{2\pi}{\lambda}(r_1 + r_2 - r_o) \tag{57}$$

e. Calculation of divergence factor, D

From Kerr[3] (equation 365, p. 99) the exact expression for the divergence factor, D, is

$$D = \left[1 + \frac{4}{ka} \cdot \frac{d_1 d_2}{d} \cdot \frac{1}{\sin 2\psi}\right]^{-1/2} \tag{58}$$

but

$$\sin 2\psi = 2 \sin\psi \cos\psi \tag{59}$$

$$= \frac{2 h_1' d_1}{h_1'^2 + d_1^2}$$

whence

$$D = \left[1 + \frac{4}{ka} \cdot \frac{d_1 d_2}{d} \cdot \frac{h_1'^2 + d_1^2}{2h_1' d_1}\right]^{-1/2} \tag{60}$$

$$= \left[1 + \frac{2d_2 h_1'}{ka\ d} + \frac{2d_2 d_1^2}{ka\ dh_1'}\right]^{-1/2}$$

Now $d_2$ is always less than d and $h_1'$ will always be much less than ka; hence, the second term in the above expression may be neglected. Thus the expression becomes

$$D = \left[1 + \frac{2d_2 d_1^2}{ka\ dh_1'}\right]^{-1/2} \quad \text{or} \quad D = \left[1 + \frac{2d_1 d_2^2}{ka\ dh_2'}\right]^{-1/2} \tag{61}$$

Recalling that

$$(h_1'/d_1) = (h_2'/d_2) = \tan\psi$$

equation (61) may be put in a form such that the relative heights of $h_1$ and $h_2$ are immaterial. Thus the formula for computation is

$$D = \left[1 + \frac{2d_1 d_2}{ka\ d\ \tan\psi}\right]^{-1/2} \tag{62}$$

Care must be taken in the evaluation of formulas for D, since in general neither term in equation (62) may be neglected with respect to the other.

f. Calculation of distance to first quadrature, $d_q$. In order to determine the regions of validity for path losses computed from the optical-interference equations and those computed from the diffraction equations, it is necessary to know the distance from the transmitter to the most remote quadrature point in the interference region. Such determinations are usually made by assuming that K in equation (50) is equal to unity so that the first quadrature occurs when

$$\Delta = \pi/2 \tag{63}$$

It may readily be seen from equations (52) and (57) that $\Delta$ is smallest when d is largest, so that the first quadrature is the one most remote from the transmitter.

$$\Delta = \delta = (2\pi/\lambda)(r_1 + r_2 - r_o) = \pi/2 \tag{64}$$

The path difference $(r_1 + r_2 - r_o)$ is approximated as

$$r_1 + r_2 - r_o = 2h_1' h_2'/d \tag{65}$$

The problem is to determine the distance, d, from the equations without knowledge of $d_1$ and $d_2$. Burrows and Attwood give an approximation for the path difference (their equation 82) which requires that $h >> h_1$.

This is

$$r_1 + r_2 - r_o = \frac{2h_1h_2}{d} - \frac{dh_1}{ka} \tag{66}$$

An approximation which gives very satisfactory results regardless of the relative heights of $h_1$ and $h_2$ is achieved by replacing the subtractive term in equation (66) by

$$\frac{h_1h_2\sqrt{h_1^2 + h_2^2}}{(h_1 + h_2)^2} \cdot \frac{d}{ka} \tag{67}$$

Making use of this approximation, equation (64) may be written in the form

$$\frac{2h_1h_2}{d} - \frac{h_1h_2}{(h_1 + h_2)} \cdot \frac{\sqrt{h_1^2 + h_2^2}}{(h_1 + h_2)} \cdot \frac{d_q}{ka} = \frac{\lambda}{4} \tag{68}$$

$$\frac{h_1h_2\sqrt{h_1^2 + h_2^2}}{ka\,(h_1 + h_2)^2}\, d_q^2 + \frac{\lambda}{4}\, d_q - 2h_1h_2 = 0 \tag{69}$$

Let

$$\alpha = \frac{(h_1 + h_2)^2\, ka}{2h_1h_2\sqrt{h_1^2 + h_2^2}} \tag{70}$$

Then

$$\frac{1}{2\alpha}\, d_q^2 + (\lambda/4)d_q - 2h_1h_2 = 0 \tag{71}$$

and

$$d_q = \alpha\left[\sqrt{\left(\frac{\lambda}{4}\right)^2 + \frac{4h_1h_2}{\alpha}} - \frac{\lambda}{4}\right] \tag{72}$$

g. Spherical earth effect in the diffraction region. The correction for the presence of the earth in the diffraction region involves the calculation of a single mode of the van der Pol-Bremmer expression for propagation over a finite, spherical earth. The correction requires multiplication of the free space equation by a factor $A^2$ where

$$A = 2A_1\, F_s\, H_T\, H_R \tag{73}$$

The fundamental equations are established so that, if the earth were plane and perfectly conducting, the value of A would be 2. Imperfect conductivity of the earth requires introduction of the factor $A_1$. The spherical shape of the earth

Table I
Summary of Geometric Distance Formulas

Examine to see if the following criterion is satisfied for a predetermined allowable percentage error, p.

$$(h_1 + h_2)/d \geq (d/2\ ka)\ (100/p)$$

Criterion Satisfied

$$\tan \Psi = (h_1 + h_2)/d$$

$$h_1' = h_1$$

$$h_2' = h_2$$

$$d_1 = h_1/\tan \Psi$$

$$r_1 + r_2 - r_o = (2h_1\ h_2/d)\left[1 - (h_1^2 + h_2^2)/2d^2\right]$$

$$r_o/(r_1 + r_2) = 1 - 2h_1\ h_2/d^2 + h_1\ h_2(h_1^2 + h_2^2)\ d^4$$

Criterion Not Satisfied

$$c = (h_1 - h_2)/(h_1 + h_2)$$

$$m = d^2/4ka(h_1 + h_2)$$

Compute b from cubic equation

$$c = b + bm(1-b^2)$$

$$d_1 = (d/2)(1 + b)$$

$$d_2 = (d/2)(1 - b)$$

$$h_1' = h_1 - (d_1^2/2ka)$$

$$h_2' = h_2 - (d_2^2/2ka)$$

$$\tan \Psi = h_1'/d_1 = h_2'/d_2 = (h_1' + h_2')/d$$

$$r_1 + r_2 - r_o = (2h_1'\ h_2'/d)\left[1 - (h_1'^2 + h_2'^2)/2d^2\right]$$

$$r_o/(r_1 + r_2) = 1 - 2h_1'\ h_2'/d^2 + h_1'h_2'(h_1'^2 + h_2'^2)/d^4$$

causes introduction of the screening, or shadow factor $F_s$ which also is less than one. $H_T$ and $H_R$ are the height factors, respectively, of the transmitter and receiver. The basic equations are written in terms of antennas located at ground level. The factors $H_T$ and $H_R$, in general greater than unity, are introduced to account for a rise in field strength in the diffraction region as antenna height is raised.

(1) Plane earth factor, $A_1$

To an approximation sufficient for present purposes, the plane earth factor is given by

$$A_1 = 1/p' \, d \tag{74}$$

where, for vertical polarization

$$p_v' = \frac{2\pi}{\lambda} \frac{\left[(\epsilon_r - 1)^2 + (60\sigma\lambda)^2\right]^{1/2}}{\epsilon_r^2 + (60\sigma\lambda)^2} \tag{75}$$

and for horizontal polarization

$$p_h' = (2\pi/\lambda) \left[(\epsilon_r - 1)^2 + (60\sigma\lambda)^2\right]^{1/2} \tag{76}$$

It will be noted that

$$p_v' = p_h' \Big/ \left[\epsilon_r^2 + (60\sigma\lambda)^2\right] \tag{77}$$

The above expressions are satisfactory except for the case of vertical polarization over sea water at distances less than $50/p'$ and wave lengths greater than one meter ($f < 300$ Mc). This special case will not be considered at present, but will be added to the program at a later date.

(2) Shadow factor, $F_s$

Well within the diffraction region the shadow effect produces an exponential drop in field strength. Except for the case noted above in connection with the factor $A_1$, the shadow factor is

$$F_s = \left[2.507(sd)^{3/2} \exp(-1.607\, sd)\right] + 0.8 \exp\left[-(sd)^{3/2}\right] \tag{78}$$

where

$$s = (2\pi/\lambda)^{1/3}/(ka)^{2/3} \tag{79}$$

Equation (78) is quite accurate provided

$$sd \geq 1.5 \tag{80}$$

It introduces very little error, even up to values given by

$$sd = 0.2 \tag{81}$$

(3) Height-gain factors, $H_T$ and $H_R$

In computing the height-gain factors it is convenient to distinguish between low and high antennas. Low antennas are those lower than a critical height, $h_c$, and high antennas are those higher than $h_c$. The critical height is determined from

$$h_c = 30\lambda^{2/3} \tag{82}$$

For low antennas the gain is a function of Q and $\ell h$, where

$$Q = \epsilon_r/60\sigma\lambda \tag{83}$$

and

$$\ell = \left[2\pi p'/\lambda\right]^{1/2} \tag{84}$$

The magnitude of H for a low antenna is given by

$$H_L = \left[1 + \frac{2\ell h}{4Q^2 + 1} + \ell^2 h^2\right]^{1/2} \tag{85}$$

For a height larger than $4/\ell$, the above simplifies to

$$H_L = \ell h \tag{86}$$

Thus the radio gain when both antennas are low would be expressed as

$$A = 2A_1 F_s \, (H_L)_T \, (H_L)_R \tag{87}$$

If the antennas are higher than $h_c$, the height-gain function increases exponentially. The increase in gain over $\ell h$ is represented by g, where

$$g = \frac{0.377 \exp\left(2.275 \sqrt{m'h}\right)}{(m'h)^{1/4}(2.77m'h + 0.86)} \tag{88}$$

The above expression for g was obtained by fitting curves to obtain values which agree with calculation and experiment. In the expression

$$m' = (4\pi^2/\lambda^2 ka)^{1/3} \tag{89}$$

Thus the height-gain factor for a very high receiving antenna would be

$$(H_H)_R = g\ell h \tag{90}$$

h. Reflection coefficient (vertical polarization). The reflection coefficient for vertical polarization is given exactly by

$$\rho \exp(j\phi) = \frac{\epsilon_c \sin\psi - \sqrt{\epsilon_c - \cos^2\psi}}{\epsilon_c \sin\psi + \sqrt{\epsilon_c - \cos^2\psi}} \tag{54}$$

where

$$\epsilon_c = \epsilon_r + j60\sigma\lambda \tag{56}$$

Consider

$$\epsilon_c - \cos^2\psi = (\epsilon_r - \cos^2\psi) + j60\sigma\lambda \tag{91}$$

and let

$$\epsilon' = \epsilon_r - \cos^2\psi \tag{92}$$

$$Q' = (\epsilon_r - \cos^2\psi)/60\sigma\lambda = \epsilon'/60\sigma\lambda \tag{93}$$

$$Q = \epsilon_r/60\sigma\lambda \tag{83}$$

and

$$\psi' = \sin\psi \tag{94}$$

Then

$$\epsilon_c \sin\psi = \psi' \epsilon_r \left[1 + j(1/Q)\right] \tag{95}$$

and

$$\left[\epsilon_c - \cos^2\psi\right]^{1/2} = \sqrt{\epsilon'}\left[1 + j(1/Q')\right]^{1/2} \tag{96}$$

$$\exp(j\phi) = \frac{\psi'\epsilon_r\left[1 + j(1/Q)\right] - \sqrt{\epsilon'}\left[1 + j(1/Q')\right]^{1/2}}{\psi'\epsilon_r\left[1 + j(1/Q)\right] + \sqrt{\epsilon'}\left[1 + j(1/Q')\right]^{1/2}} \tag{97}$$

The above may be put into the form

$$\rho e^{-j\phi} = \frac{(a - b) - j(c - d)}{(a + b) + j(c + d)} \tag{98}$$

where

$$a = \psi'\epsilon_r \tag{99}$$

$$b = \sqrt{\epsilon'/2Q'}\left[\sqrt{Q'^2 + 1} + Q'\right]^{1/2} = \sqrt{\epsilon_r Q'/2Q}\left[\sqrt{1 + (1/Q')^2} + 1\right]^{1/2} \tag{100}$$

$$c = \sqrt{\epsilon_r(Q'/2Q)}\left[\sqrt{1 + (1/Q')^2} - 1\right]^{1/2} \tag{101}$$

$$d = \psi'\epsilon_r/Q \tag{102}$$

Therefore

$$\rho = \left[\frac{a^2 + b^2 + c^2 + d^2 - 2(ab + cd)}{a^2 + b^2 + c^2 + d^2 + 2(ab + cd)}\right]^{1/2} \tag{103}$$

thus

$$\rho^2 = \frac{1 - \dfrac{\psi'\sqrt{2\epsilon_r(Q'/Q)}\left(\left[\sqrt{1 + (1/Q')^2} + 1\right]^{1/2} + (1/Q)\left[\sqrt{1 + (1/Q)^2} - 1\right]^{1/2}\right)}{\psi'^2\epsilon_r\left[1 + (1/Q)^2\right] + (Q'/Q)\sqrt{1 + (1/Q')^2}}}{1 + \dfrac{\psi'\sqrt{2\epsilon_r(Q'/Q)}\left[\sqrt{1 + (1/Q')^2} + 1\right]^{1/2} + (1/Q)\left[\sqrt{1 + (1/Q)^2} - 1\right]^{1/2}}{\psi'^2\epsilon_r\left[1 + (1/Q)^2\right] + (Q'/Q)\sqrt{1 + (1/Q)^2}}} \tag{104}$$

since

$$b^2 + c^2 = \epsilon_r(Q'/Q)\sqrt{1 + (Q'/Q)^2} \tag{105}$$

$$a^2 + d^2 = \psi'\epsilon_r^2\left[1 + (1/Q)^2\right] \tag{106}$$

and

$$(\epsilon_r/Q) = (\epsilon'/Q') \tag{107}$$

To obtain the phase angle, write

$$e^{j\phi} = \frac{(a^2 - b^2) - (c^2 - d^2)}{(a + b)^2 + (c + d)^2} - j\,\frac{2(ac - bd)}{(a + b)^2 + (c + d)^2} \tag{108}$$

$$\tan(\phi) = \frac{2(ac - bd)}{(a^2 + d^2) - (b^2 + c^2)} \tag{109}$$

$$\tan(\phi) = \frac{\psi'\sqrt{2\epsilon_r(Q'/Q)}\left(\left[\sqrt{1 + (1/Q')^2} - 1\right]^{1/2} - (1/Q)\left[\sqrt{1 + (1/Q')^2} + 1\right]^{1/2}\right)}{\psi'^2\epsilon_r\left[1 + (1/Q)^2\right] - (Q'/Q)\sqrt{1 + (1/Q')^2}} \tag{110}$$

Both the expression for $\rho$ and that for tan ($\phi$) are exact.

i. Brewster angle (vertical polarization). The pseudo-Brewster angle occurs when

$$\rho = 0 \tag{111}$$

and

$$\tan\phi = \infty \tag{112}$$

Applying these conditions to the expressions for $\rho$ and tan $\phi$

$$2(ab + cd) = a^2 + b^2 + c^2 + d^2 \tag{113}$$

and

$$a^2 + d^2 = b^2 + c^2 \tag{114}$$

whence

$$2(ab + cd) = 2(a^2 + d^2) \tag{115}$$

Now

$$ab = \psi' \epsilon_r \sqrt{\epsilon_r Q'/2Q} \left( \left[ \sqrt{1 + (1/Q')^2} + 1 \right]^{1/2} \right) \tag{116}$$

$$cd = \psi' \epsilon_r \sqrt{\epsilon_r Q'/2Q} \left( \left[ \sqrt{1 + (1/Q')^2} - 1 \right]^{1/2} \right) \tag{117}$$

$$a^2 + d^2 = \psi'^2 \epsilon_r^2 \left[ 1 + (1/Q)^2 \right] \tag{118}$$

$$\sqrt{\epsilon_r/2} \sqrt{Q'/Q} \left( \left[ \sqrt{1 + (1/Q')^2} + 1 \right]^{1/2} + \left[ \sqrt{1 + (1/Q')^2} - 1 \right]^{1/2} \right)$$

$$= \psi' \epsilon_r \left[ 1 + (1/Q) \right] \tag{119}$$

$$\sin \psi_b = \frac{\sqrt{Q'/Q} \left( \left[ \sqrt{1 + (1/Q')^2} + 1 \right]^{1/2} + \left[ \sqrt{1 + (1/Q')^2} - 1 \right]^{1/2} \right)}{\sqrt{2\epsilon_r} \left[ 1 + (1/Q)^2 \right]} \tag{120}$$

where $\psi_b$ is the pseudo-Brewster angle.

Horizontal polarization

$$\rho e^{j\phi} = \frac{\sqrt{\epsilon_c - \cos^2\psi} - \sin\psi}{\sqrt{\epsilon_c - \cos^2\psi} + \sin\psi} \tag{55}$$

$$\rho_e^{j\phi} = \frac{\sqrt{\epsilon'} \left[ 1 + j(1/Q') \right]^{1/2} - \psi'}{\sqrt{\epsilon'} \left[ 1 + j(1/Q') \right]^{1/2} + \psi'} \tag{122}$$

$$= \frac{\sqrt{\epsilon'} \sqrt{\frac{\epsilon'}{2Q'}} \left[ \sqrt{Q'^2 + 1} + Q' \right]^{1/2} + j \left[ \sqrt{Q'^2 + 1} - Q' \right]^{1/2} - \psi'}{\sqrt{\epsilon'} \sqrt{\frac{\epsilon'}{2Q'}} \left[ \sqrt{Q'^2 + 1} + Q' \right]^{1/2} + j \left[ \sqrt{Q'^2 + 1} - Q' \right]^{1/2} + \psi'}$$

$$= \frac{\frac{1}{\sqrt{2}} \epsilon' \left[ \sqrt{1 + (1/Q')^2} + 1 \right]^{1/2} - \psi' + j \frac{\epsilon'}{\sqrt{2}} \left[ \sqrt{1 + (1/Q')^2} - 1 \right]^{1/2}}{\frac{\epsilon'}{\sqrt{2}} \left[ \sqrt{1 + (1/Q')^2} + 1 \right]^{1/2} + \psi' + j \frac{\epsilon'}{\sqrt{2}} \left[ \sqrt{1 + (1/Q)^2} - 1 \right]^{1/2}}$$

which is of the form

$$\rho e^{j\phi} = \frac{(x - y) + jw}{(x + y) + jw} \tag{123}$$

which may be written

$$\rho e^{j\phi} = \frac{(x^2 - y^2 + w^2) + j2wy}{(x + y)^2 + w^2} \tag{124}$$

$$\tan(+\phi) = \frac{2wy}{x^2 - y^2 + w^2} \tag{125}$$

$$= \frac{2\psi' \frac{\epsilon'}{\sqrt{2}}\left[\sqrt{1 + (1/Q')^2} - 1\right]^{1/2}}{\frac{\epsilon'^2}{2}\left[\sqrt{1 + (1/Q')^2} + 1\right] - \psi'^2 + \frac{\epsilon'^2}{2}\left[\sqrt{1 + (1/Q')^2} - 1\right]}$$

$$\tan(\phi) = \frac{\sqrt{2}\psi'\left[\sqrt{1 + (1/Q')^2} - 1\right]^{1/2}}{\epsilon'\sqrt{1 + (1/Q')^2} - \psi'^2} \tag{126}$$

$$\rho^2 = \frac{x^2 + y^2 + w^2 - 2xy}{x^2 + y^2 + w^2 + 2xy} \tag{127}$$

$$\rho^2 = \frac{\epsilon'^2\sqrt{1 + (1/Q')^2} + \psi'^2 - \sqrt{2}\,\psi'\epsilon'\left[\sqrt{1 + (1/Q')^2} + 1\right]^{1/2}}{\epsilon'^2\sqrt{1 + (1/Q')^2} + \psi'^2 + \sqrt{2}\,\psi'\epsilon'\left[\sqrt{1 + (1/Q')^2} + 1\right]^{1/2}} \tag{128}$$

## REFERENCES


1. National Bureau of Standards, Memorandum Report, Telecommunications Performance Standards, Tropospheric Systems, Volume 5 of 6.

2. Burrows, Charles R., and Attwood, Stephen S., "Radio Wave Propagation," Academic Press, Inc., New York, 1949.

3. Kerr, Donald E., "Propagation of Short Radio Waves," McGraw-Hill Book Company, Inc., New York, 1951.

# A FACILITY FOR THE INVESTIGATION OF RADIO-INTERFERENCE PROBLEMS

L. F. Babcock
Bell Aerosystems Company
Division of Bell Aerospace Corporation
Tucson, Arizona

Abstract.--The ever-increasing problem of electromagnetic interference and the consequent deterioration of communication channels has led to the design and development of a field facility in southern Arizona to determine methods of alleviating the problem. Bell Aerosystems Company has been given the responsibility by the United States Army Electronic Proving Ground to create a facility for the investigation of the electromagnetic interference problems which an army corps would encounter during combat.

At the present time, approximately 12,000 electromagnetic radiating devices, all located within a geographical area of 40 by 60 miles, are used by an army corps. To represent the electromagnetic environment created by these devices, military equipment is being used to provide a realistic representation of actual conditions.

Representative quantities of equipment, placed in such a manner as to produce an accurate representation of full-scale deployments, are positioned around a test site to permit a few equipments to represent many. Various items of electronic equipment will be placed into this environment and the amount of degradation in performance created by or affecting these equipments will be measured.

Automatic environment control, interference measurement, and data recording will permit the accomplishment of up to 1,000 tests per day. An IBM 709 computer will be used to program the environment and to analyze the interference data.

The facility in concept is sufficiently versatile to generate almost any conceivable configuration of electromagnetic environment and can be expanded or modernized as may be required for future utilization.

## I. INTRODUCTION

As long ago as World War II, the United States Army recognized the existence of an interference problem caused by the use of a large amount of communication and electronic equipment in a relatively confined area. Exercise Feeler was conducted prior to the invasion of Normandy in June, 1944, to obtain a measure of the severity of the problem and to determine corrective action which would minimize its effects. In spite of the improvements thus accomplished, considerable difficulties were experienced during the actual invasion. Since that date, the amount of electronic equipment in use by the Army has increased by a factor of about 4 or 5. There are now about 12,000 transmitters assigned within an army corps which normally occupies an area about 40 miles wide and 60 miles long. Furthermore, there is every reason to expect that the number of transmitters in use will continue to increase in the future.

Consequently, in 1955 the Army initiated a special study known as

Project Monmouth to ascertain the extent of the interference problem which would exist in the future. This study concluded that considerable interference could be anticipated and recommended that theoretical and experimental investigations be initiated to determine more precisely the parameters causing interference in radio equipment. It was further recommended that an electronic test sector simulating the combat environment be created. As a result of this effort, the Army established a technical requirement for the Electromagnetic Environmental Test Facility (EMETF). Subsequently a contract was awarded to Pan American World Airways with the Bell Aerosystems Company being a major subcontractor with the responsibility of establishing the interference test facility.

## II. ELECTROMAGNETIC ENVIRONMENTAL TEST FACILITY

The present contract covers a period of two years, ending in March of 1962. During this period the contractor will complete a facility capable of testing all communication equipment currently assigned to a division in the electromagnetic environment created by the communication equipment assigned to a corps.

It was determined that only by use of a field facility in conjunction with a RFI Prediction Model could the Army obtain the data that are required to establish the causes of interference. Such a facility would be designed to recreate the electromagnetic environment which would actually be expected to occur under combat conditions. It would then be possible to place various items of electronic equipment into this environment and to observe whether any degradation in performance occurred. A realistic field facility is required since it assures valid results. Meteorological and terrain effects, for example, cannot be duplicated in the laboratory. This is to be a proving-ground type of facility for final evaluation of equipment suitability. The required size of the facility is determined by the range of the equipment involved, and by the size of the area over which a realistic electromagnetic environment is required. Figure 1 shows the size of the facility which is being built during the present two-year contract. It is the size of an army corps area, extends approximately 6[illegible] miles east from Gila Bend, and is approximately 40 miles wide. This site was chosen for the facility because it is sparsely populated and is subjected to comparatively little electromagnetic radiation. It is also near Fort Huachuca from which the Army directs the program. The inner rectangle marked by a double X indicates the land occupied by the center division. All tests for interference are being conducted within this area. The remainder of the facility is used only to generate the necessary electromagnetic environment.

Obviously the most realistic method for establishing such an environment would be actually to disperse troops into the field and to have all electronic equipment operated in the normal manner. Such a scheme, however, is impracticable since an army corps contains approximately 12,000 radiating devices; even if only radio operators were deployed in the field, the cost of the program on a long-term basis would be prohibitive. Furthermore, many human errors would be encountered in such an approach and automatic operation is thus much more desirable.

A realistic environment requires the use of actual military equipment to create the environment. Simulators used for this purpose would not generate all transmitter harmonics, spurious radiations, and other out-of-band signals in addition to the normal signals. Out-of-band signals which a transmitter radi-

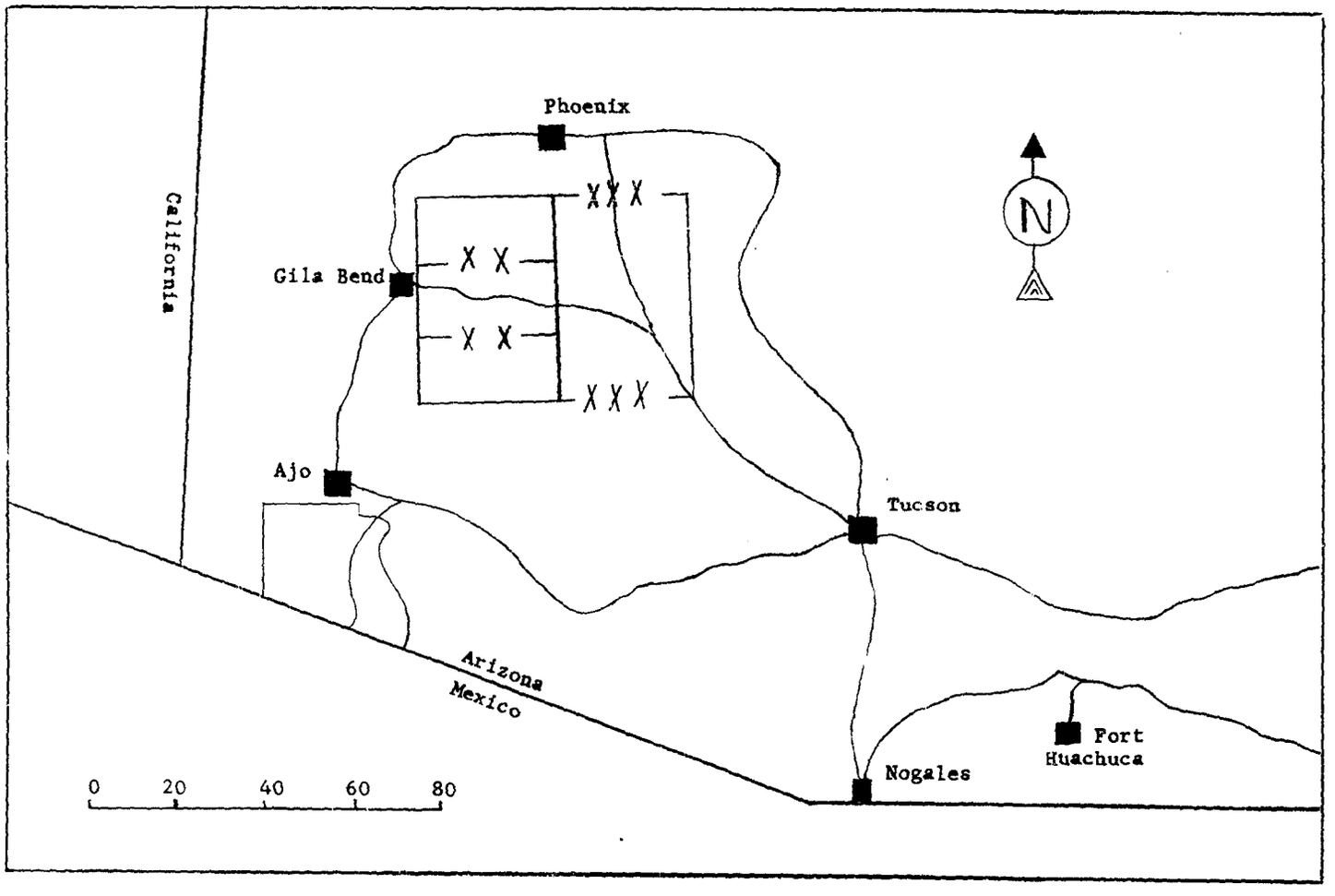



Fig. 1 Electromagntic environmental Test Facility.

ates are expected to be one of the major sources of interference. There are a number of advantages obtained by the use of actual Army hardware. First is the assurance that the electromagnetic environment thus created is realistic. Second is the ability to modify the equipment in accordance with modification work orders which the Army releases from time to time to improve the performance of existing equipment. Thus it is possible to keep the environment up to date. Third is the fact that the Army equipment is in production and available. Consequently, the facility can be built in a shorter period of time and at less expense than if it were first necessary to design and then fabricate some sort of electronic device to be used instead of Army equipment.

## III. EQUIPMENT REDUCTION PRINCIPLES

There are several factors which were used to justify the reduction in the number of transmitters required to create a complete and realistic environment.

The first factor is that most of the Army communication equipment is operated in groups or nets with 5 or 10 units assigned a single frequency. Only one transmitter in a net is ever operated at a time. Consequently, it is generally possible to replace all sets in a net by a single transmitter and to increase the duty cycle of this transmitter so that it represents the signal from any radio set in the net. There are certain exceptions to this rule, such as when a net contains more than one type of transmitter or when various transmitters of the net are close to several test sites. Since there are about 1,800 nets within an army corps, this factor allows an equipment reduction of about 6:1.

The second factor is to eliminate all transmitters which do not contribute to the electromagnetic environment at the test sites because of their low-power or directional type antennas. In considering the elimination of such sets, it is first necessary to establish the points at which interference testing will be accomplished. Since it is desired to test all types of communication equipment in an army division under any likely condition of environment, it would first be thought that the facility must be capable of testing for interference at any point within the division area and that it would therefore be necessary to create an accurate environment over the entire division area. Further study indicates that this is not so, as shown in figure 2.

Each symbol or mark on the figure represents an active Army transmitter. Only the area occupied by the center division is shown. The flank divisions contain similar deployments of equipment. It can be noted from this figure that there is little change in the type of equipment deployed along any vertical line; for example, AN/PRC-6 and AN/PRC-10 "walkie talkies" are almost always deployed near the front, and the equipment used by the artillery is further to the rear.

Consequently, equipment deployed along any line parallel to the forward edge of the battle area will contain few changes in types deployed, whereas along a line extending from the front of the battle area towards the rear, the types and the configuration of equipment deployed are continuously variable. As a result of this situation, it has been established that similar types of interference will be encountered along any line parallel to the forward edge of the battle area; therefore, it is necessary to test for interference only along

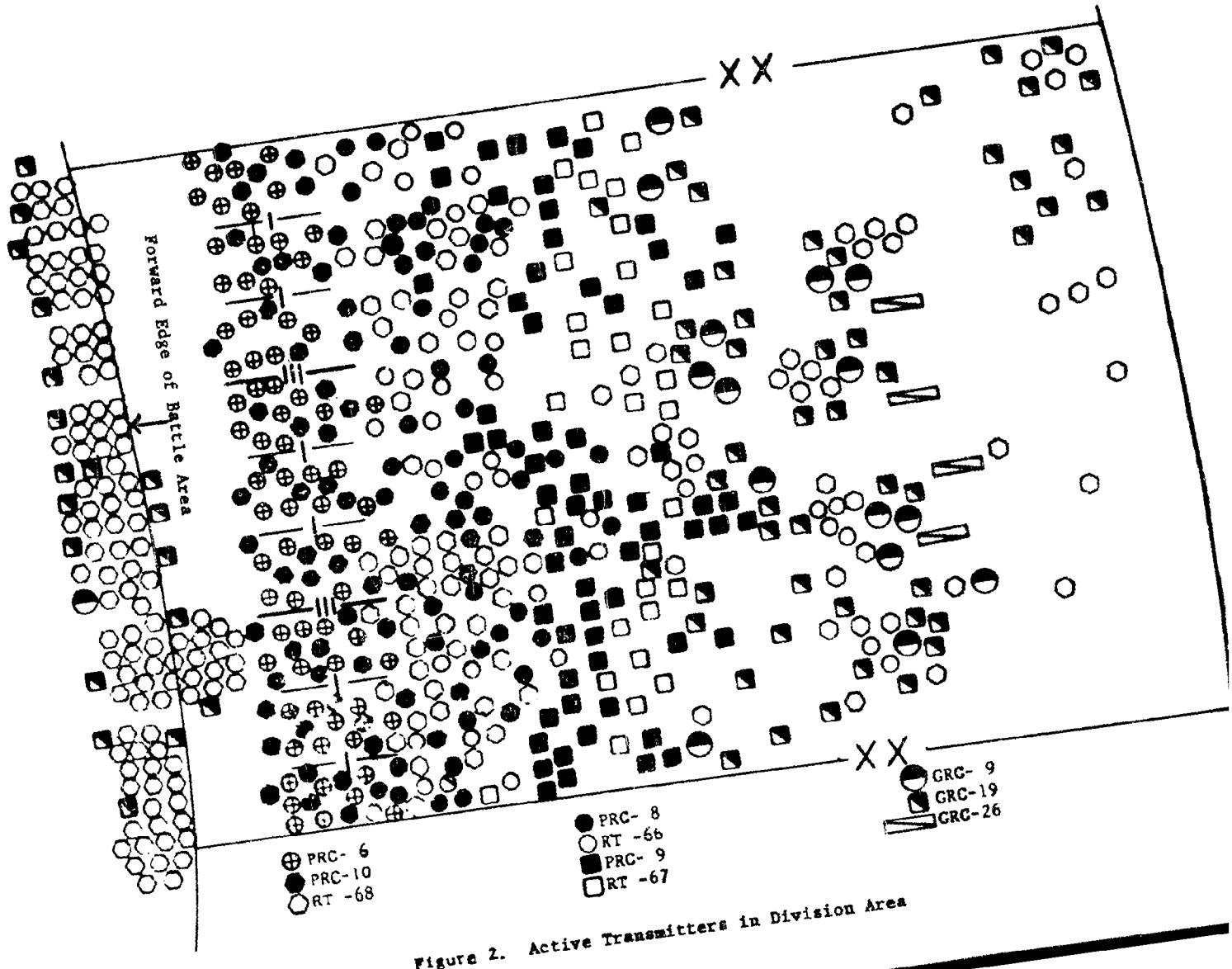



Figure 2. Active Transmitters in Division Area

a single line perpendicular to the forward edge of the battle area. Minor changes of electromagnetic environment which would exist at other points can be duplicated on this line by slight changes in the location of certain transmitters. Two sites have been established along this line at which to test for interference. Each test site is located at a point of high equipment density since maximum interference is expected at such locations. Additional test sites will be installed as required when the facility is expanded.

When the test site positions, which are permanent, have been established, it is possible to determine which of the 12,000 radio sets operating in the corps area would never be able to radiate a significant signal into either test site. Many low-powered radio sets can thus be eliminated from the facility because their range from the test site is so great that they do not contribute to the environment at that point. Certain higher-powered equipments with directional antennas, such as the AN/TRC-24 radio relay, can be eliminated from the facility for the same reason.

The third factor is that certain of the 12,000 radio sets within the corps area are assigned to troops being held in reserve. Such equipment is only rarely operated and, in fact, is usually ordered to maintain radio silence. Therefore, most of this equipment was eliminated from the field facility.

After all three of these factors have been applied to reduce the number of transmitters which must be retained, it turns out that about 412 sets are actually required to generate a realistic electromagnetic environment within the two sites at which tests will be made for interference. This is a much more workable number than 12,000 and begins to indicate that it is practicable to use actual military equipment to generate the necessary signals.

The next item to be considered is the manner in which the 412 required radio sets will be positioned in the field. First the battlefield situation which is to be duplicated within the test facility must be established. This is accomplished by the preparation of a tactical scenario which describes in detail for a given instant during a battle the positions of all troops and equipment in the field. Next the three factors which were discussed earlier are applied to establish which items of equipment can be eliminated. There are about 412 sets retained with each located at a different position in the facility. They would then be assigned the frequency and rf power level with which they would be expected to operate in a tactical situation. They would also be provided with the proper type of antenna and modulation signal.

Since a costly and complex facility would be required to control, modulate, and power this number of sets, it was established that they should be grouped in some manner to simplify the problem. The only objection to such a scheme is that when the location of a piece of equipment is changed, the amplitude of the signal which it would radiate into the test sites might also change.

To minimize this effect, no item of equipment is moved by an amount which would change the level of the signal radiated into the test site by more than a few db. This means that no set will be moved in range with respect to the test sites by an amount greater than about 25 per cent. Application of

this rule allows the equipment deployed over a large area to be grouped about a single point in cases where the range to the test sites is great. At shorter ranges, smaller groupings are required. In the immediate vicinity of the test sites, equipment will be individually deployed in the location specified by the tactical scenario. The entire field facility will contain a total of 26 groups of equipment deployed as shown in figure 3.

## IV. ENVIRONMENT GENERATOR SITES

An air-conditioned van (figure 4) will be installed at each of the 24 environment generator van sites. These vans will house the necessary control devices to allow all equipment within the group to be operated automatically. Up to 40 transmitters can be controlled at each site. These sites will: (1) provide modulation for all types of radio communication equipment; (2) supply station identification for all transmitters within the group; (3) record any malfunctions which occur; (4) provide both primary and emergency communication as required for the conduct of tests and for safety; (5) control any transmitter in the group to either on or standby; and (6) provide personnel comfort for the two persons assigned to operate and maintain the complex of equipment in and around each van.

A separate, portable, gasoline-driven motor generator will supply the electrical power required by each van. These vans are called environment generator or EG vans since their primary purpose is to house the electrical distribution systems and control equipment for the environment generators at the EG sites.

A Spiral-4 cable will be run from the Forward Test Site to each EG van. It will carry control signals from the master control station to each site. It will also allow telephone communication with all other sites in the facility. Wire was chosen for the control medium since it allows the facility to be operated without the addition of any nontactical radio signals.

A typical van interior is shown in figure 5. Each van contains an IBM Model 523 Gang Summary Punch which is used as a card reader to control all transmitters, which are called environment generators or EG's, to on or standby. Each column on the IBM card controls a single environment generator. Each card controls all environment generators associated with a single van to a preplanned condition of on or standby. Thus, a specific condition of environment is set up. Each time that the card reader is advanced to the next card, a new condition of environment is achieved. During actual field tests, a common tone signal from the master control station is used to advance all card readers in all EG vans to the subsequent card, simultaneously. In this manner, all transmitters in all sites can be controlled to any predetermined configuration of on or standby.

To assure that the proper card is being read by each card reader, a special card check circuit was devised to read the serial number of the active card in each van. The numbers from all vans are coded into a group of tones and are sent over the wire lines to the Forward Test Site. Here the tones are decoded and checked to assure that cards with the same serial number are being read in each van. If a card in one van should jam or be out of sequence, it would be detected immediately and the test stopped automatically before data were collected.

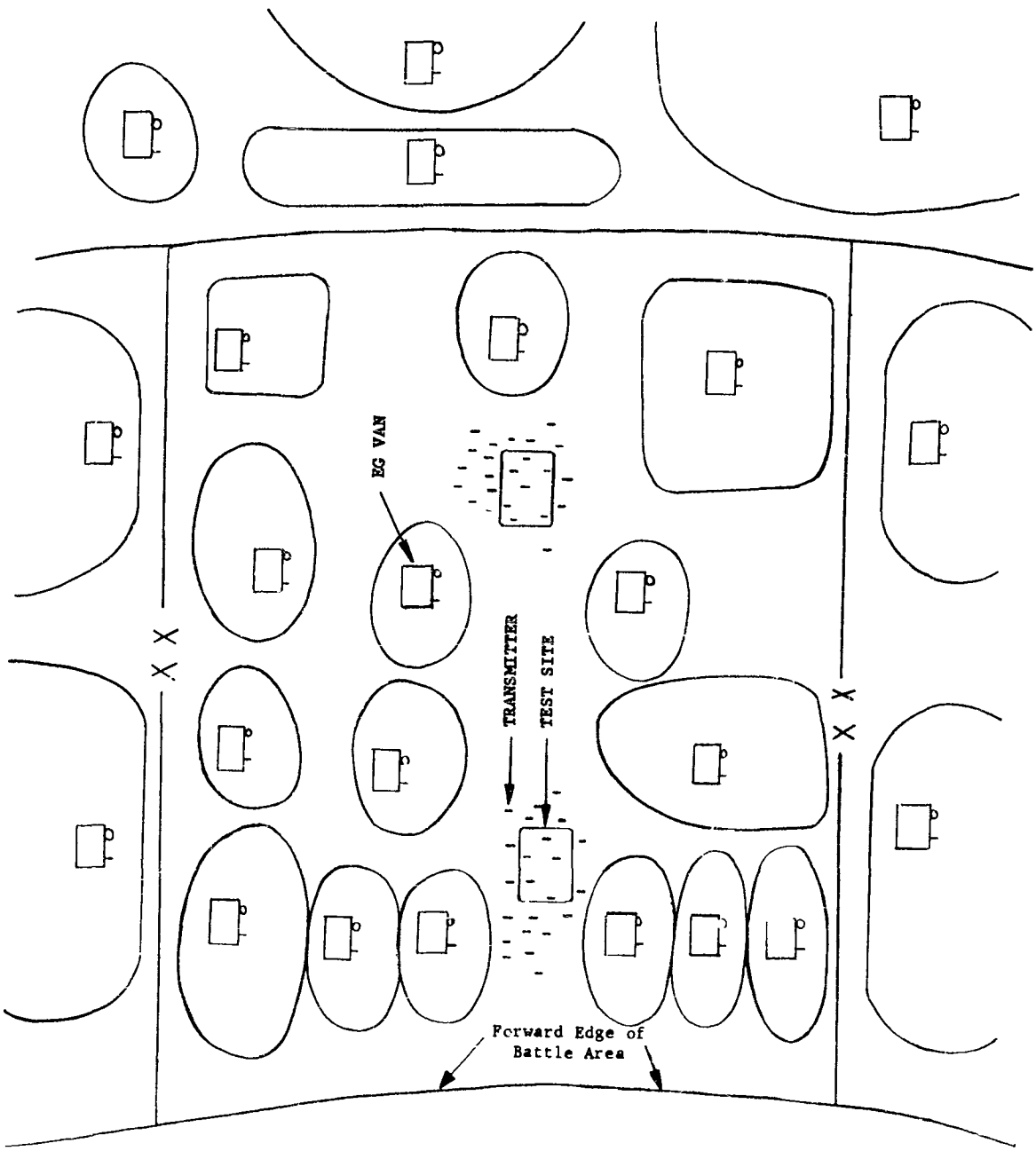



Figure 3. Transmitter Grouping Around Vans

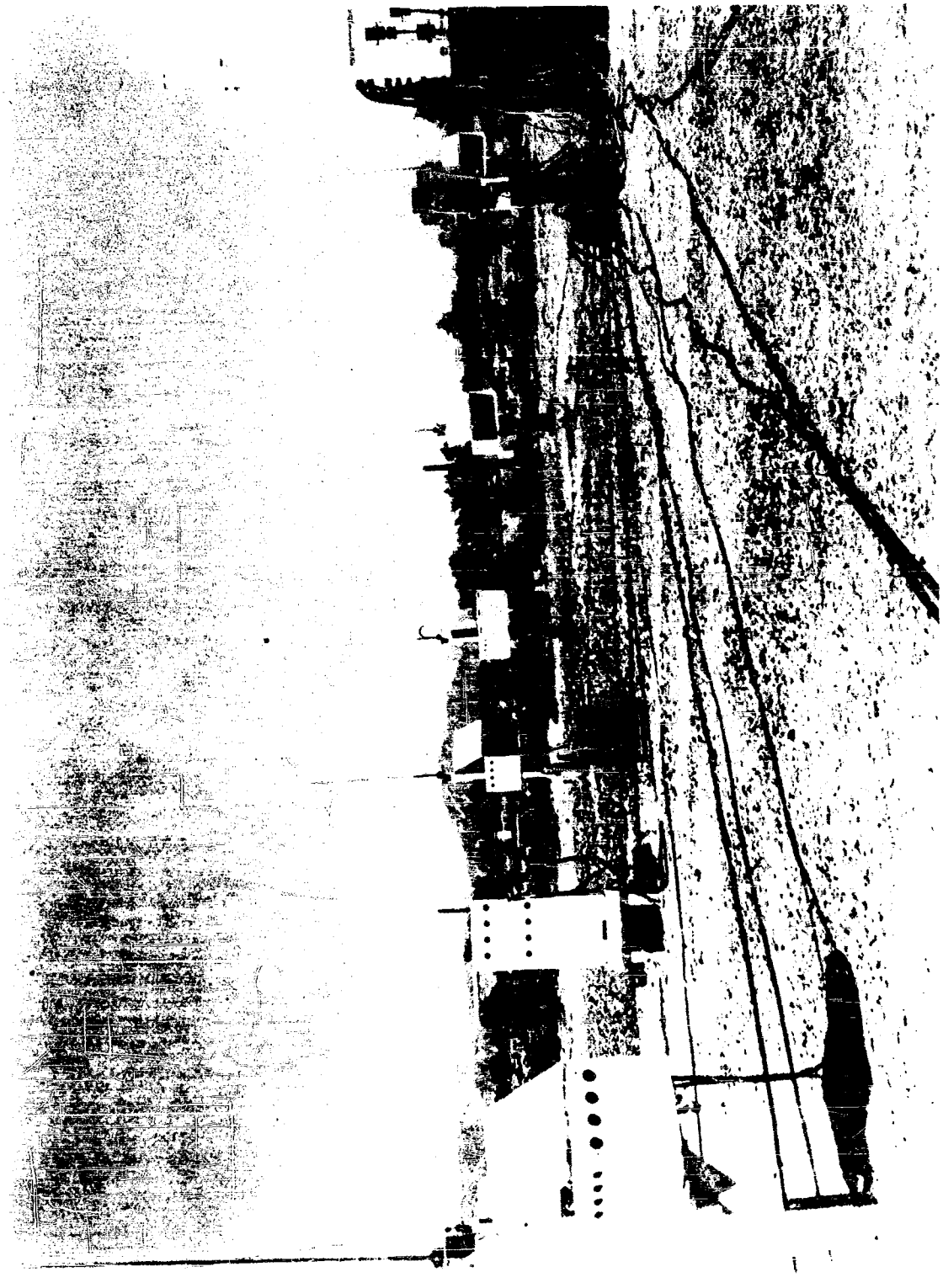


Figure 4. EG Van with Externally Deployed Environment Generators

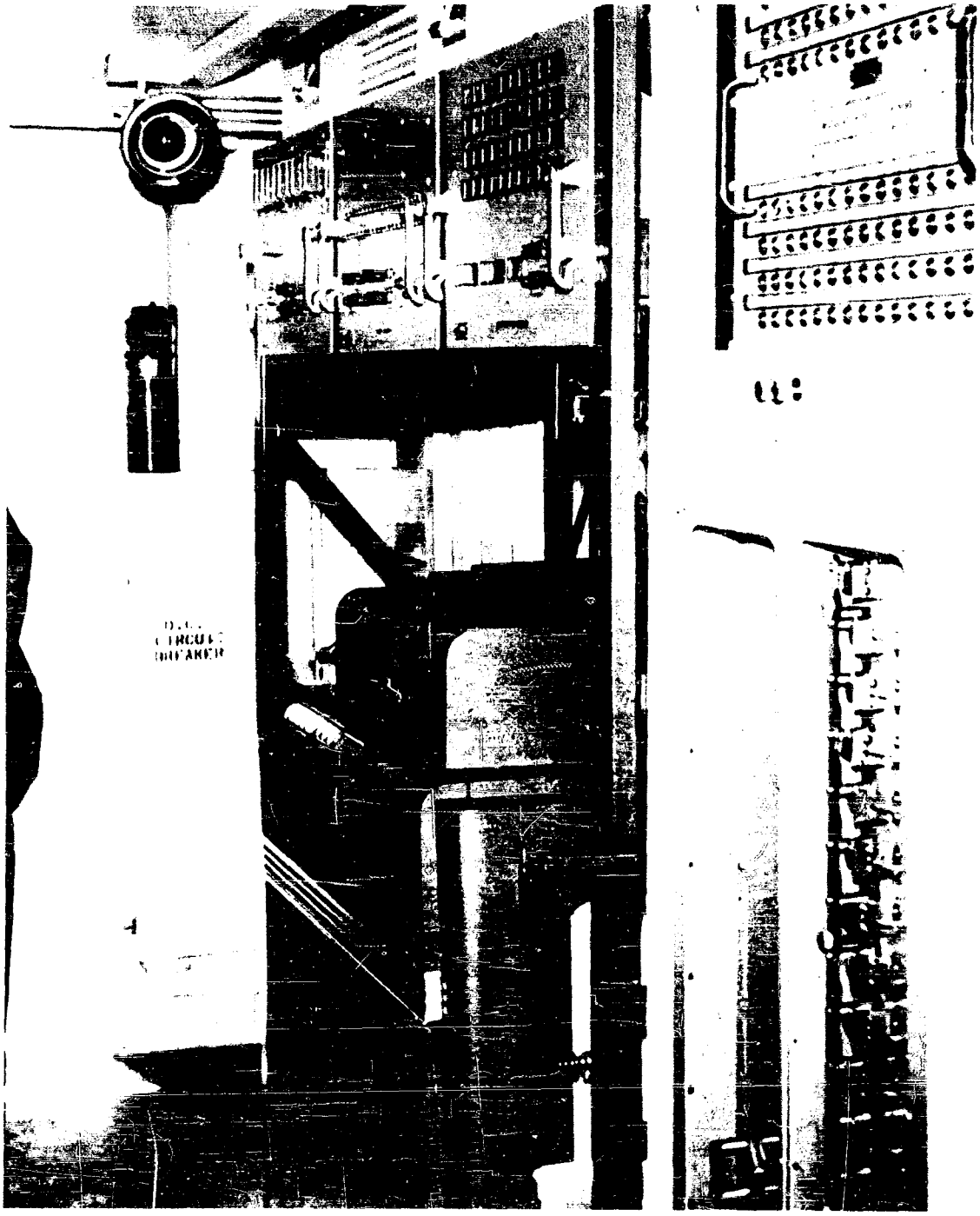


Figure 5. Typical Van Interior

It is possible to set up a single condition of environment and to test for interference in this environment at a maximum rate of about one measurement each 30 seconds. The entire process is automatic.

When a large number of transmitters are grouped into a small area about a van, it is necessary to assure that no interactions occur between the various equipments and that the antenna patterns are not distorted by other antennas in proximity. Consequently, a study has been performed to determine to what extent transmitting antennas can be mounted on the EG van and what minimum spacing is allowable between the various antennas. As a result, it has been determined that all equipment can be located within a few-hundred-foot radius of the van. The van contains three or four transmitters with their associated antennas mounted on the roof. All other transmitters will be mounted on posts external to the van. These sets will be controlled, modulated, and powered by a cable which connects them to the van.

A unit called a control box has been designed and built by the Bell Aerosystems Company to incorporate the necessary features of control and of automatic performance monitoring in each military transmitter. By using a separate unit, it is necessary to make only a slight modification to the transmitter itself and this modification can readily be removed. One control box is required for each transmitter deployed in the field. The control box accepts signals decoded from the IBM card reader and uses them to key its associated transmitter on or off. Cables from the van connect to the control box as shown in figure 6.

The control box also monitors the rf power output and modulation levels of the transmitter and compares them with the allowable limits which are preset into the box. If either the modulation or the power level is found to be outside of the acceptable limit, the transmitter is automatically turned off and an alarm sounded to notify the operator of the malfunction.

The malfunction information is also automatically recorded on the IBM card by the gang summary punch at each van. In this way a record is maintained of the transmitters which were actually on during each test, as well as of those which were programed to come on. It is not intended to stop the test because of the malfunction of one or more environment generators. Rather, it is planned to analyze the results based on the environment which was actually created for each test.

Each control box is installed in a secure wooden shelter adjacent to the transmitter with which it operates. This shelter will: (1) provide protection from the weather, (2) prevent unauthorized persons from tampering with the device, and (3) act as a shipping carton whenever it is necessary to move the equipment to a new location. Each shelter is fastened to a pole which is firmly embedded in the ground as shown in figure 6.

At the beginning of each day of test, each shelter door will be unlocked and opened to allow free circulation of air for cooling. Next, each transmitter will be set to the frequency desired for the first series of tests and will be checked for proper performance. Many of these sets are designed for use at either of two power levels or with any of several types of antennas. The EG van operator will set up each transmitter to the desired configuration. He will also provide the necessary ground plane to simulate either vehicular or personnel mounting of the equipment. The entire facility will then be set

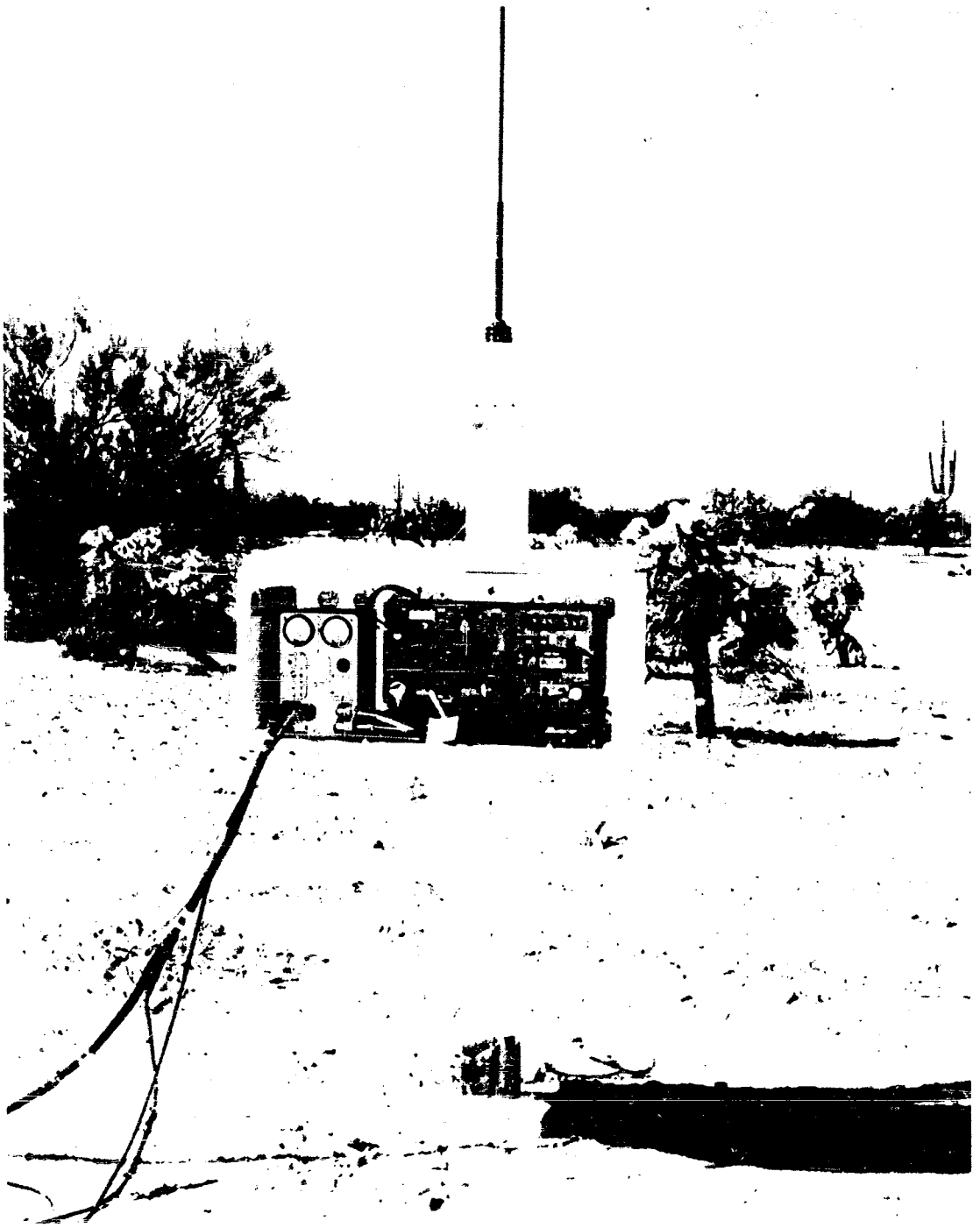


Figure 6. Control Box with Cables Attached

up to represent a single instant of a battle. A series of preplanned automatic tests will then be conducted to establish the severity of interference for this configuration of equipment with various combinations of transmitters on and off. The IBM 709 computer at the United States Army Electronic Proving Ground, Fort Huachuca, Arizona, will be used to analyze data collected during these tests. Results will indicate which transmitter or combination of transmitters contributed to the interference at each receiver under test. After these tests have been completed, additional tests would probably be performed with all transmitters deployed in the same locations but with different frequency assignments or other variables inserted. Finally, the desirable tests for this instant of the battle would have been completed.

Next, it would be necessary to redeploy the equipment to represent a new battlefield situation and then to run additional tests. Generally, it will be possible to do this by moving the individual environment generators to new positions in the field or by adding and deleting certain types of equipment. Occasionally it also will be necessary to move entire environment generator vans to new locations. The facility has been designed with this in mind so that both the vans and the environment generators can be moved, as required, with a minimum amount of lost time.

It is not intended to test for interference in real time but rather to do so in a series of static steps or snapshots. Such a scheme is much more workable because it is thereby much more simple and less costly to record the exact conditions under which the data were collected.

As an example, assume that tests are to be conducted to determine the interference effects caused by a battalion of tanks advancing through an organization of infantry troops. These tests could be accomplished by taking all of the electronic equipment assigned to the tanks and placing it at one of the vans toward the rear of the corps area. After the desired interference tests were completed, the equipment would be moved into other vans progressively nearer to the front and additional tests made for each deployment. Ultimately, complete information would thus be obtained to determine the interference effects caused by the battalion of tanks at any point during its advance.

To maintain complete realism of the environment, it is necessary that each piece of equipment radiate the same signals that it would in combat. This requires that all communication sets be modulated in the usual manner. It was also established that for maximum realism it would be preferable not to modulate several radio sets from a common signal source. A multichannel tape-loop recorder (figure 7) was chosen as being the best solution to the problem. It allows excellent versatility since the radio sets can be modulated by voice, noise, tones, babble of voices, or any other signal which may be desired in the future. For the present, all transmitters will be modulated in the normal manner. The tape unit is capable of supplying a maximum of 50 modulation signals simultaneously. Some of these signals are obtained by staggering heads at different points along the tape loop. Consequently, one track on the tape can be used to generate several messages. Obviously all such messages generated from a single track on the tape are identical but each is delayed several seconds with respect to the other and can thus be considered as independent. The tape message contains station identification information and each transmitter is thereby operated in accordance with military and Federal Communications Commission regulations.

Each EG van contains both a primary and an emergency communication

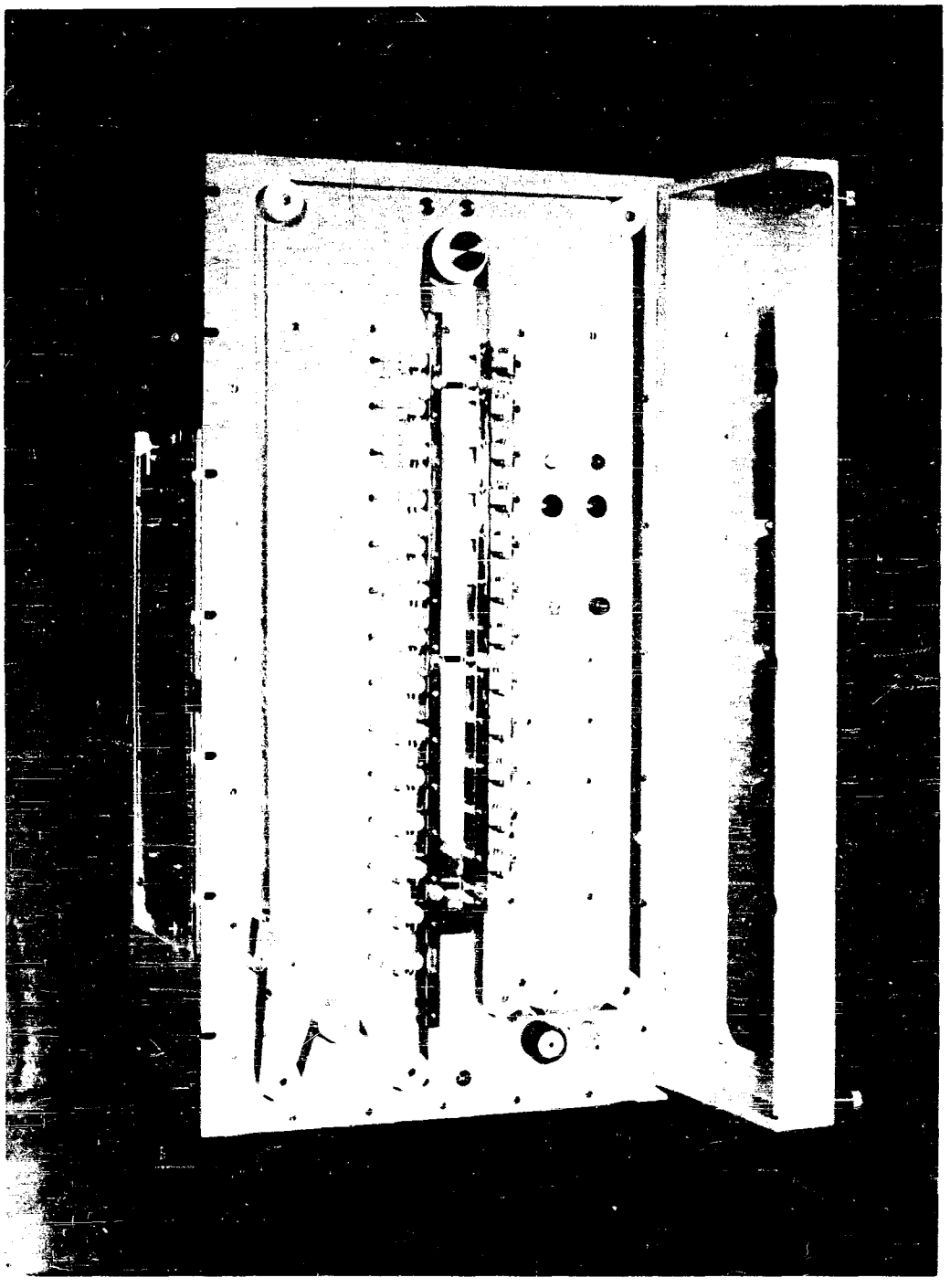


Figure 7. Tape Loop Reproduce Unit

system. The primary device is a field telephone connected by a wire to the Forward Test Site. The secondary system, intended for emergency use only, consists of a monitor receiver tuned to the emergency channel frequency and of a separate military transceiver which can be operated in the conventional manner. This transceiver is also used as an environment generator and cannot therefore be used as a monitor receiver. It is for this reason that a separate monitor receiver is installed in each EG van.

After the initial setup, the operation of each environment generator van is completely automatic. Two men are assigned to each of the 24 EG vans. Stated differently, less than 100 men are required to operate a facility which simulates the simultaneous operation of up to 12,000 transmitting devices. Furthermore, this is done by automatic methods so that there is much less chance of human errors affecting the test results.

## V. TEST SITES

Two test sites are provided in the division area. (See figures 8 and 9.) All tests for interference will be made in one of these areas. It is, therefore, at these two sites that it is intended to maintain an accurate electromagnetic environment. In the future it is planned to add two additional test sites in the corps area to test for interference in equipment normally assigned at the corps level.

The entire environment will be controlled over wire lines from the Forward Test Site. Special control circuitry has been devised so that it is possible to turn off all transmitters in all vans by use of two switches located at the Forward Test Site. This feature allows the entire facility to be silenced if required for special tests or if there is ever any reason to believe that it may be causing interference in any civil equipment located near the test facility. Such a feature permits the guilt or innocence of the facility to be determined rapidly.

Each test site also contains a group of environment generators or transmitters located at distances of up to about 6,000 feet from the test building. These units are operated in a manner identical to those at an EG van except that it is necessary at the test site to deploy the sets at greater range. This is true since at the test site these sets must be deployed in about the same position as in combat to assure that the proper signal levels are maintained at the test point.

Each test site contains at least one of every common type of communication receiver currently in use by the Army. To test for interference a test link is set up. This test link consists of a test transmitter which can be positioned at any EG van or at either test site and is used to radiate the test signal to the receiver under test. Thus, a test link is set up for evaluation. Any environment generator can be used as a test transmitter by applying a special test signal to it for modulation.

## VI. INTERFERENCE ANALYSIS

Next, let us consider how to determine and record the amount of interference encountered by these test links. Since the prime consideration in the



Figure 8. Forward Test Site Shelter

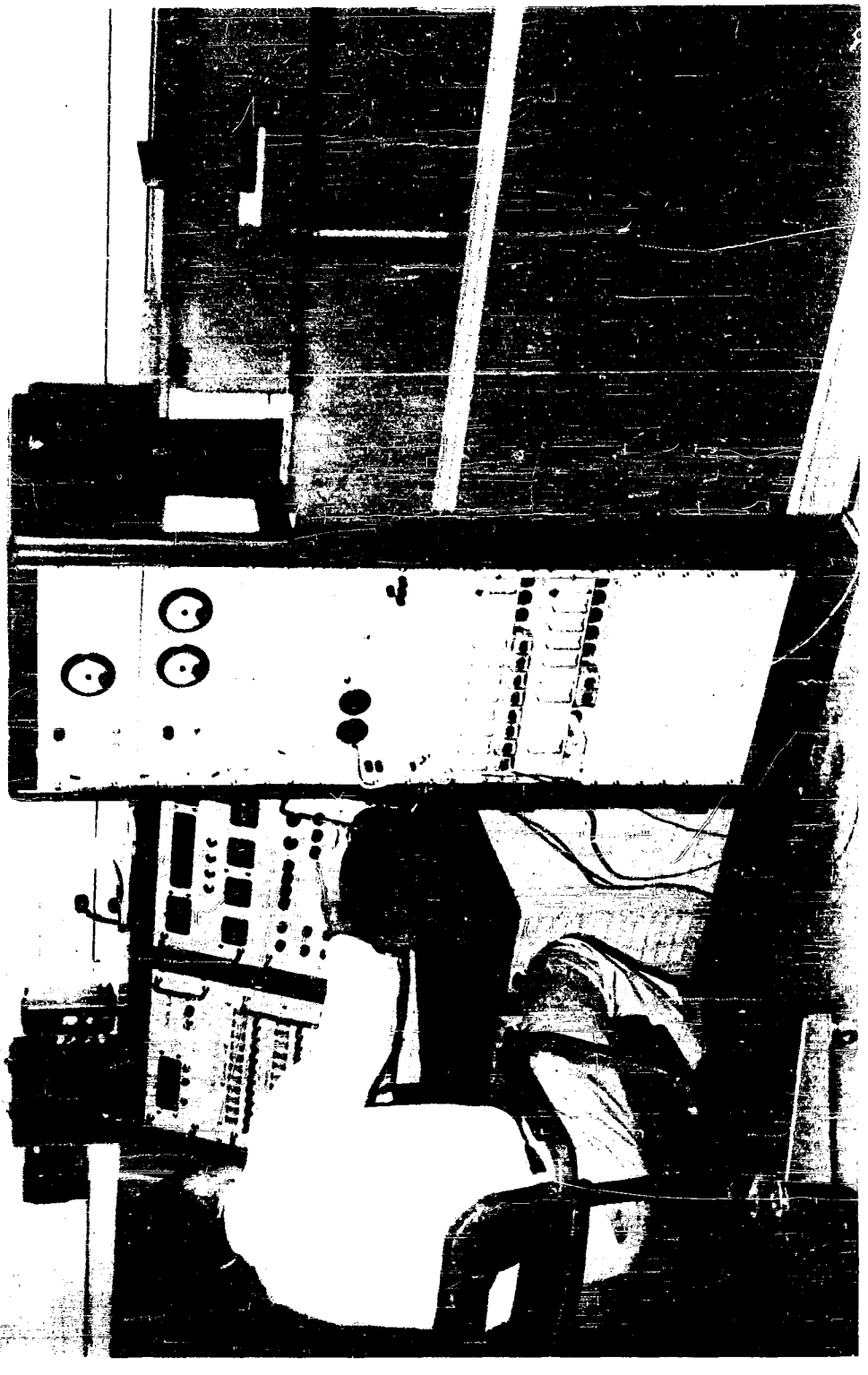


Figure 9. Control Equipment Installed in Forward Test Site Shelter

transmission of any message is intelligibility, it is this parameter which will be measured.

The desirability of making such an intelligibility measurement was recognized several years ago by the United States Army Signal Research and Development Laboratory and, as a result, several study and development programs were initiated. One of these programs was the development by the General Electronic Laboratories (GEL), under Signal Corps contract, of an instrument known as the Speech Systems Test Set, or Licklider Machine. Its purpose is to measure the loss of information through a speech communication system caused by interference, noise, insufficient bandwidth, or any other characteristic which may serve to degrade the intelligibility of the desired message. In essence, the Speech Systems Test Set is a standard listener, providing an objective and repeatable analysis of the voice message, so difficult to obtain with a subjective human listener.

The Speech Systems Test Set is a relatively sophisticated system and provides somewhat more capability than is required for a field device. After a discussion with engineers at General Electronic Laboratories, it was concluded that a simplified version of this equipment would be suitable for our purpose and would provide rapid and accurate assessment of speech communication systems in the field. This assessment is made at the output of each receiver under test by utilizing a standard test message of such duration that the interference effects of any given environment can be completely determined within a 30-second interval. In this way the interference effects of roughly 1,000 different conditions of environment can be determined in an 8-hour day.

Ten of these devices are being built for the facility.

For proper operation of this device, a special test message consisting of a single tone is transmitted to the test receiver. At the output of the test receiver, this tone is used by the interference analysis equipment to adjust the gain of the signal to a standard level.

Psychoacoustic theory states that the ability of a system to transmit speech intelligence can be estimated by measuring the signal-to-noise power in each of several equally contributing audiofrequency bands. In the system being discussed, the normalized signal is divided into 14 audio bands in accordance with French and Steinberg's theory. The db value of the signal-to-noise ratio in each band is then summed to provide an analog voltage proportional to articulation index. This index can be converted to word score by means of a standard curve. To complete the process, the output signal is converted into digital form suitable to be recorded by being punched on an IBM card.

For cw and radio-teletypewriter applications, where the information is basically digital, the interference detection process is greatly simplified and consists of the direct comparison of the received message with the standard message. The output from the device in this case is the per cent of characters correctly received. These data are also punched on an IBM card for permanent storage. A single IBM card at each test site is used to record the interference results for all test receivers at that site. One card is required for each 30-second test.

It is possible to test up to 13 test links for interference at one time since there are 13 independent interference detection systems being pro-

vided. This allows a large increase in the rate at which data can be collected. Ten of these devices will be for the testing of voice-modulated systems, and three for radio teletypewriter or cw equipment. The 13 units can be divided between the Forward and Rear Test Sites in any desired combination. It is thus possible to determine the effects of the environment on as many as 13 types of military receivers during a single set of tests.

Both of the interference detection schemes described are versatile in that they can operate with any communication system which uses the same type of transmission. Consequently, their use is not limited to a few presently existing types of receivers but rather they can be readily adjusted to function with any new communication set which the Army may want to test. As a result, it is a simple matter to test any new developmental communication device and to determine its ability to operate under the electromagnetic conditions of combat.

## VII. PROGRAMING AND DATA ANALYSIS

Next let us consider the programing and data analysis aspects of the facility. To review, you will recall that it was stated earlier that IBM punched cards are used to control the environment, and that any configuration of transmitters can be turned on for any test. The only requirement is that the programing scheme must be preplanned and all cards punched in advance of the test.

Therefore, it is possible to establish the traffic density under which each set would be operated during combat conditions, and from such information to generate a series of typical configurations of activated transmitters. It may be found desirable to use such a plan for certain tests, but presently it is believed that interference data can be obtained much more rapidly by the use of a systematic, rather than a realistic, program plan.

With the systematic approach, all environment generators could first be turned off and the intelligibility of each test link measured. For the next test, all environment generators could be turned on and the reduction in intelligibility noted for each test link. If no loss occurred, it would have been established that no interference was encountered and that no transmitter or combination of transmitters for that particular frequency assignment and deployment would cause interference. The test would therefore be completed.

If, on the other hand, interference were discovered during the initial test, the next step would be to schedule the environment producing transmitters in such a manner as to allow the transmitter or group of transmitters causing trouble to be isolated.

To accomplish this the environment generators are turned on successively in accordance with one or more of the following:

(1) Tables of balanced lattice squares. These have the characteristics that all pairs are produced, but each pair appears in only one test.

(2) Tables with redundancies to create all pairs and/or triples. These have the characteristic that the unique pairs in the lattice

square will appear in at least two tests.

(3) Schedules to test the effect of each transmitter separately. Although this is not efficient in terms of test time, it will nevertheless be used in some cases due to the straight-forward nature of the data obtained by this means.

It is quite possible that a combination of transmitters may be required to create an interference condition; for example, where certain of their harmonics beat together and form intermodulation products which are within the passband of the test receiver. It is doubtful if multiples greater than triples will be of any consequence. The lattice square and redundant tables together with the data reduction logic should allow isolation of the EG's causing the condition.

It is planned to use the IBM 709 computer available at the United States Army Electronic Proving Ground, at Fort Huachuca, Arizona, both to generate the Environmental Generators "On-Off" schedule used to program the environment and also to analyze the data obtained during field tests. After the combinations of equipment which cause interference have thus been isolated, they can be brought into the laboratory, if desired, to be analyzed for the purpose of determining why they caused interference, and, perhaps to recommend a solution to the problem.

The facility will be useful in studying and evaluating: (1) suggested changes to the present method for assigning frequencies; (2) recommended modifications to present day hardware; (3) proposed change to the conditions under which specific equipment can be best utilized; and (4) new equipments now under development from the interference standpoint.

## VIII. ELECTROMAGNETIC MONITORING

There are two primary requirements in this facility for electromagnetic monitoring. The first is to assure that no unauthorized signals are radiated from the facility. The second is the need to collect information on signals which are generated outside the facility and which cause interference in our test links.

For these purposes, five frequency monitoring vans are being built. Four of these vans will be stationed about the perimeter of the test facility (figure 10). The fifth van will be available for use at any point within the facility for detailed analysis of the rf spectrum or for special tests.

## IX. INTERFERENCE PREDICTION MODEL

In parallel with the field test facility, Bell Aerosystems Company is also developing an interference prediction model which consists of a series of equations to describe the complex electromagnetic environment and its effect upon the device under test. In other words, if all of the factors causing interference such as transmitter characteristics, meteorological and terrain conditions, and receiver characteristics can be expressed mathematically with sufficient accuracy, it should then be possible to calculate the amount and type of interference which would be expected.



Figure 10. Periphery Frequency Monitoring Van

Interference results taken from the field facility are being used to validate the prediction model. Later the model will be used to modify the field test results so that they express what the situation would have been if the tests had been made, for example, in the tropics or Alaska, or under other different conditions such as changes in weather. Thus it is seen that the mathematical and the field test approaches are intended to complement each other and that neither can accomplish the entire task without the other.

## 7. PLANS FOR EXPANSION

It is not intended to imply that all of the Army's interference problems can be solved within the present facility. Many types of expansion are possible and studies and tests being made at present will assist in determining which are needed most. For example, noncommunication equipment such as radars might be added to the environment. Equipment from other branches of the military used in support of the Army might also be added. This would include Air Force and Navy devices. To go further one might add units used by our allies or even the enemy to get a more complete re-creation of the tactical situation. Another possibility is that of expanding to an army-size environment consisting of three complete corps plus the rear army area.

It may also be desirable to add the effects of the human operator during future tests. Tests with the present facility are aimed toward the investigation of equipment problems only. It is realized that human effects also contribute to the problem. It may be determined also that it would be desirable to establish an airborne test site for the investigation of drone and aircraft interference problems in more detail.

It will further, of course, be necessary to modernize the range to incorporate new items of equipment as they are made available. This will be a continual process.

It is not intended to infer that the present facility without the previously mentioned features of expansion is of little value. On the contrary, it will be capable of investigating and solving a vast number of interference problems.

The present program is essentially on schedule. The facility has been designed with the need for expansion in mind. It is therefore possible to modify or expand it, as is later found to be desirable, with little duplication of time or money.

## ACKNOWLEDGMENT

The work described in this paper was sponsored by the Field Test Directorate, U. S. Army Electronic Proving Ground, Fort Huachuca, Arizona, under contract Nr. DA-36-039-SC-80424.

# THE COMPUTER APPROACH TO THE INTERFERENCE-PREDICTION MODEL OF THE ELECTROMAGNETIC ENVIRONMENTAL TEST FACILITY

J. B. Scott
Bell Aerosystems Company
Division of Bell Aerospace Corporation
Tucson, Arizona

Abstract.--This paper describes the computer program as related to the interference-prediction model of the Electromagnetic Environmental Test Facility. The required data, the flow of data through the computer, and the underlying electrical and mathematical concepts of the mathematical model are discussed.

## I. INTRODUCTION

An Army corps contains approximately 15,000 devices that radiate electromagnetic energy. These radiators are deployed in an area approximately 40 miles wide and 60 miles long. Investigation of the electromagnetic environment produced by these radiators requires that each radiator be individually examined for its effect upon the environment. Examination of 15,000 or more items by manual techniques for even a simple yes-no answer would be a tremendous chore. An interference-prediction model capable of considering the effects of many emitters must therefore be computer mechanized.

## II. THE COMPUTER PROGRAM

The IBM 709 data processing system at Fort Huachuca is ideally suited to simulate a complex electromagnetic environment. The speed of the system, with its flexible input-output devices and magnetic tape storage, imposes no practical limitation on the simulation program. The modular concept of the factors influencing an electromagnetic environment readily lends itself to computer simulation techniques. Various physical factors are isolated, described mathematically, and simulated. The program, following the modular concept, is written as a series of subroutines controlled by a master program which calls for each subroutine in the proper sequence. There is necessarily some interaction between subroutines. Each subroutine, however, is designed to simulate a particular portion of the environment that, insofar as possible, can be isolated from other portions. As equations are developed which more accurately represent various physical phenomena, it is necessary to modify or rewrite only those subroutines that are affected and thus leave the major portion of the program undisturbed.

The computer program is designed to use the "snapshot" concept. A particular environmental situation defined by a given set of parameters is called a snapshot. One pass through the program will provide a numerical environment evaluation based on one given set of parameters. The program can be run on a snapshot-by-snapshot basis or can be run continuously to provide a sequence of environment snapshots. When run continuously, a dynamic situation can be represented if the snapshots are considered to be separated by an increment of time, and if one or more of the parameters are varied from one snapshot to the next. Figure 1 is a block diagram showing the sequence of events that occur during the

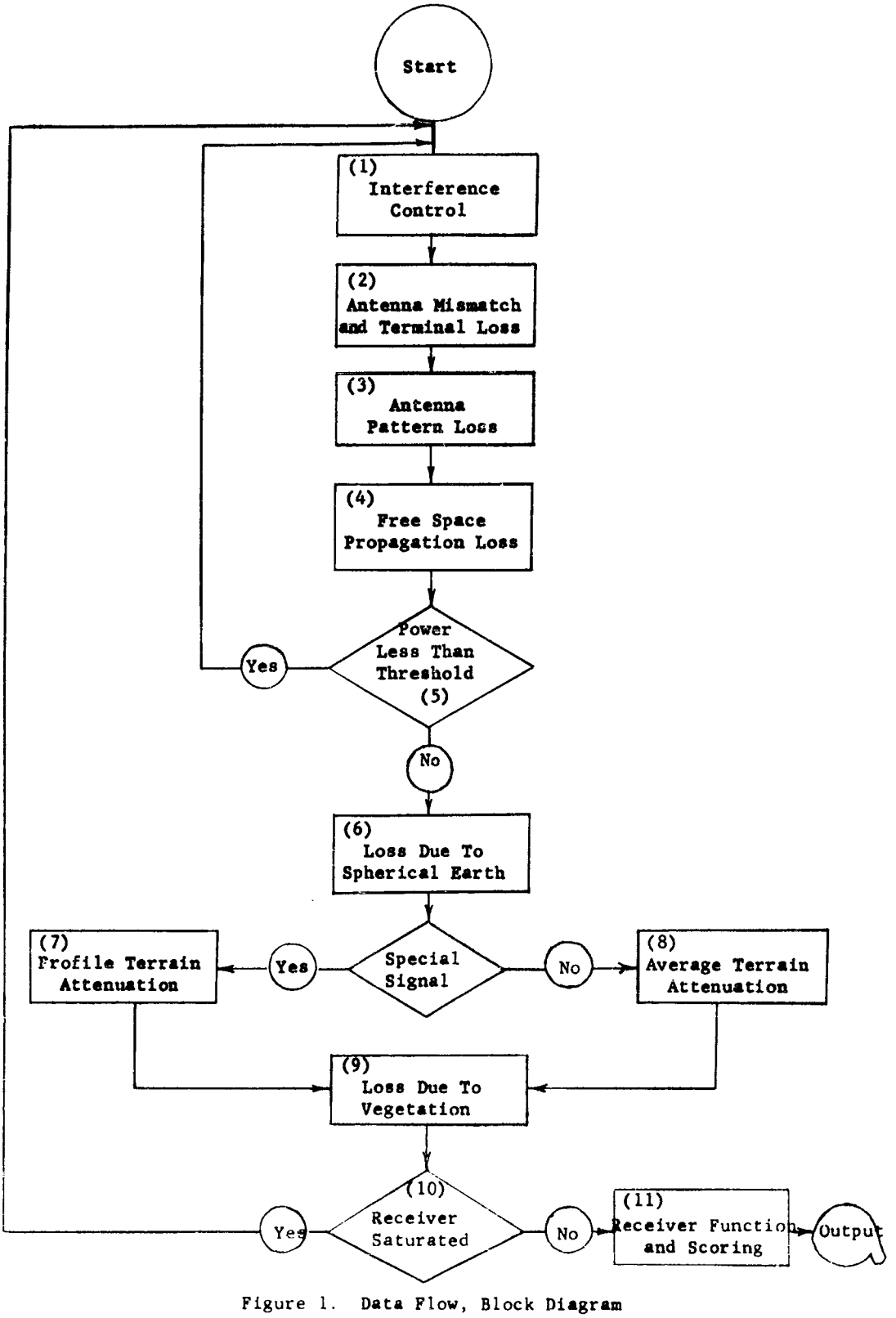



Figure 1. Data Flow, Block Diagram

running of the program. A description of the function of each block in the diagram follows:

Interference Control (Block 1)

The interference control block represents the housekeeping necessary to operate the system and the comparisons necessary to eliminate most of the transmitters that do not contribute to the interfering environment. The operations and decisions in the order in which they occur are as follows:

1. A receiver is chosen from the environment and data concerning its location, assigned frequency, antenna type, and antenna orientation are stored in the computer memory.

2. A search is conducted on a file of permanent receiver spectrum signature data pertaining to that particular type of receiver. When found, this information is stored in the memory of the computer. It consists of measured receiver characteristics such as frequencies acceptable to the receiver, selectivity, and sensitivity. Frequencies acceptable to the receiver and sensitivity levels of these frequencies are represented in the computer in the form of a table of acceptable frequencies and corresponding relative sensitivity values. This table will be called the F table. Frequencies in the F table are those representing spurious responses and intermodulation characteristics of the receiver. They have been obtained from actual measurements made on the various receivers of interest. Predictions of spurious response frequencies and intermodulation frequencies are calculated from the following expressions. Relative sensitivity values are those that have been measured.

Spurious response

$$f_a = \frac{pf_{lo} \pm f_{if}}{q}$$

Intermodulation

$$f_t = f_1 - f_2$$

$$f_t = 2f_1 - f_2$$

$$f_t = 3f_1 - 2f_2$$

where

$f_a$ is a spurious response acceptable to the receiver,

$f_{lo}$ is the local oscillator frequency,

$f_{if}$ is the if. frequency,

p is a positive integer or zero denoting the harmonic order of the local oscillator,

q is a non-zero integer denoting the harmonic order of the input signal,

$f_t$ is the tuned frequency,

and

$f_1$ and $f_2$ are interfering signal frequencies.

The existence of cochannel and adjacent channel interference is determined from information contained in the file of permanent receiver data. Assuming a rectangular if. pass band, the band width, $\delta$, is given and the corresponding adjacent channel attenuation is given. Signals whose frequencies, f, are such that:

$$f_t - \frac{\delta}{2} \leq f \leq f_t + \frac{\delta}{2}$$

present the possibility of cochannel interference and signals whose frequencies are such that:

$$k + f_t + \frac{3}{2}\delta > f > f_t + \frac{\delta}{2} + k$$

or

$$-k + f_t - \frac{3}{2}\delta < f < f_t - \frac{\delta}{2} - k$$

where $k \geq 0$ takes into account guard bands between channels, present the possibility of adjacent channel interference. These frequency ranges and corresponding sensitivity values are stored in the F table to be used later in the program to determine signal power level required to interfere with the receiver at that frequency.

3. A transmitter is chosen from the environment and data concerning its location, assigned frequency, antenna type, and antenna orientation are stored in the computer memory.

4. A search is conducted on a permanent transmitter spectrum signature file to locate the data corresponding to that particular type of transmitter. Each frequency with associated power level can now be considered as a monofrequency transmitter. And, for simulation purposes, an actual transmitter is represented by its spectrum signature data as a composite of many monofrequency transmitters.

5. When the desired transmitter spectrum signature has been located in the file, the frequency of each monofrequency transmitter is compared against each $f_a$ (that is, spurious response) element in the F table. If no F table elements match the transmitted frequencies, the transmitter is discarded and another transmitter is chosen from the environment and steps 3, 4, and 5 of this section are repeated until all transmitters have been examined. If an F table element matches the transmitted frequency, there exists the possibility of an

interfering signal and a further investigation must be made. This investigation is described by blocks 2 through 11 of figure 1. When all transmitters in the environment have been investigated, another receiver is chosen from the environment and steps 1 through 5 are repeated until all receivers have been investigated.

Antenna Mismatch and Terminal Loss (Block 2)

At this point in the program a match has been found between an element in the F table and a transmitter frequency. It is now necessary to examine the power output of the transmitter at this frequency and to modify it by appropriate loss factors before assessing its contribution to the electromagnetic environment at the receiver site.

The first modification to the transmitter power output is called "antenna mismatch and terminal loss," since it results from antenna cable loss and impedance mismatch. This modification to the output power is necessary since many spectrum signature measurements are made into a resistive load. If the antenna and transmitter are matched at the fundamental frequency, then measurement of the fundamental into a resistive load is quite realistic. However, a mismatch occurs at other frequencies, namely harmonics of the fundamental, so that if measurements of power at those frequencies are made into a resistive load, an unrealistic power output is reported.

A search is conducted on a file of antenna information to determine the terminal power loss. This information is stored in the form of a four-dimensional matrix of which the dimensions represent type of equipment, type of antenna, harmonic, and measured power loss. When the power loss has been located for both transmitter and receiver antennas, these numbers are subtracted from the transmitter power output to provide a more realistic power input to the antenna terminals.

Antenna Pattern Loss (Block 3)

This portion of the program accounts for the loss of power due to the transmitter and receiver antennas. The term "loss" will be used in most cases throughout this paper to represent a change in the transmitter power output, it being understood that the quantity may be negative, thus representing a gain in power.

A search is conducted on an antenna pattern file to find the antenna pattern information associated with both the transmitter and receiver antenna. This information has been compiled as the result of field measurements and appears in the form of a three-dimensional array of elements whose dimensions are azimuth angle, elevation angle, and loss. When the correct antenna pattern loss information has been extracted from the file, the angles that determine the orientation of the transmitter and receiver antennas are calculated and the antenna pattern loss factor is extracted from the array of elements and subtracted from the transmitter power output.

Free Space Propagation Loss and Comparison with Receiver Sensitivity (Blocks 4 and 5)

Computation of propagation path loss for the EMETF prediction model is

based on the free-space equation modified to account for the effect of the earth and its atmosphere. Provision is also made to account for the effects of terrain, vegetation, meteorology, and other factors. Symbolically, the ratio of power received, $P_r$, to power transmitted, $P_t$, can be expressed as:

$$\frac{P_r}{P_t} = \left[\begin{matrix}\text{Free-space} \\ \text{factor}\end{matrix}\right]^2 \times \left[\begin{matrix}\text{Spherical earth} \\ \text{correction factor}\end{matrix}\right]^2 \times \left[\begin{matrix}\text{Terrain} \\ \text{factor}\end{matrix}\right]^2 \times \cdots \times \left[\begin{matrix}\text{Additional} \\ \text{factors}\end{matrix}\right]^2$$

The free-space factor is given by:

$$\frac{\lambda}{4\pi d}$$

where $\lambda$ is the wave length of the transmitted signal and d is the distance between transmitter and receiver. Neglecting, for the moment, such phenomena as tropospheric scatter, the maximum theoretical power, $P_m$, that could be expected to be received at a receiver site from any given transmitter would be

$$P_m = P_t\left[\frac{2\lambda}{4\pi d}\right]^2$$

which occurs under line-of-sight conditions when the wave reflected from the earth's surface reinforces the direct wave. $P_m$ thus serves as a criterion for eliminating many potentially interfering signals from further analysis. A description of this process follows:

At this point in the computer program a signal has been found that is a possible source of interference to the receiver under consideration. The power level of the signal has been modified by the antenna terminal loss and the antenna pattern loss. In the process of finding the signal, many transmitted signals have been discarded by the F table comparison process. Elimination of the signals from further analysis greatly reduces the time required to process a problem. A further reduction of the number of transmitted signals of no interest is accomplished by calculating $P_m$ and comparing this value with the sensitivity of the receiver to the power level of the signal under consideration. This comparison is accomplished by searching the F table for the frequency corresponding to the frequency of the signal under consideration and comparing the associated measured sensitivity level with $P_m$. If $P_m$ is greater than this sensitivity level, the transmitted signal must be further analyzed. If $P_m$ is less than the measured sensitivity of this receiver to the frequency under consideration, the signal is discarded as being of no interest and another signal is chosen for analysis.

Loss Due to Spherical Earth (Block 6)

The calculations involved in the spherical-earth correction factor to the free-space path loss factor are quite lengthy and a detailed development will not be presented in this paper. The reader is referred to Burrows and Attwood,[1] the National Bureau of Standards,[2] Kerr,[3] or Hoehn[4] for the development of this theory.

Two interference regions are presumed: an optical interference region and a diffraction region. The optical interference region is characterized by line-of-sight calculations. The spherical-earth correction factor to the free-space path loss factor is given by:

$$A^2 = (1 - K)^2 + 4K \sin^2 \left(\frac{\Omega}{2}\right)$$

where

$A^2$ is the spherical earth correction factor,

$K = \rho D$,

$\Omega = \delta + \phi - \pi$,

$\rho$ and $\phi$ are the modulus and angle of the reflection coefficient, $R = \rho \exp(j\phi)$,

D is the divergence factor introduced to account for the decreased gain produced by the spreading of a wave reflected from a spherical surface,

and

$\delta$ is the phase retardation caused by the fact that the path length of the reflected wave is longer than the path length of the direct wave.

It will be noted from the theory that these parameters are functions of basic electrical quantities such as the dielectric constant of the earth, the wave length of the propagated wave, the ground conductivity, and the refractive gradient of the earth's atmosphere.

The diffraction region is characterized by beyond line-of-sight calculations. The correction for the presence of the earth in the diffraction region involves the calculation of a modified single mode of the van der Pol-Bremmer expression for propagation over a finite, spherical earth.

This spherical-earth correction factor can be expressed as:

$$A^2 = \left[2A_1 \, F_S \, H_T \, H_R\right]^2$$

where $A_1$ accounts for imperfect conductivity of the earth, $F_S$ accounts for the screening effect caused by the spherical shape of the earth, and $H_T$ and $H_R$ account for height effects associated with the transmitter and receiver antenna, respectively. $A^2$ in this case, as with the previous $A^2$, is a function of the same basic electrical quantities.

At this point in the program, the strength of the signals that have not been eliminated by the F table comparison tests or the $P_m$ receiver sensitivity test are further modified by the spherical-earth correction factor. This

requires that a test be conducted to determine if the receiver lies in the optical interference region or in the diffraction region. If the receiver lies in the optical interference region, the optical spherical earth correction factor is evaluated and applied to the transmitted signal strength. If the receiver lies in the diffraction region, the diffraction spherical-earth correction factor is evaluated and applied to the transmitted signal strength.

The existence of a test implies that a criterion has been established to determine the outcome. Comparisons of field test results with calculated data indicate that a high correlation results when optical interference region calculations are used up to the first quadrature point and when diffraction region calculations are used beyond the first quadrature point. Consequently, the first quadrature point, $D_q$, has been chosen as the dividing line between the optical and diffraction regions. Mathematically, the expression for the distance to the first quadrature point is given by:[4]

$$D_q = \alpha\left[\sqrt{\left(\frac{\lambda}{4}\right)^2 + \frac{4h_1h_2}{\alpha}} = \frac{\lambda}{4}\right]$$

where

$$\alpha = \frac{(h_1 + h_2)^2\, ka}{2h_1h_2\sqrt{h_1^2 + h_2^2}} \quad \text{and}$$

$h_1$ is the transmitter antenna height, $h_2$ is the receiver antenna height, $\lambda$ is the wave length of the transmitted signal, and a is the radius of the earth. The factor k, when multiplied by a, provides an effective earth's radius to account for the effect of the earth's atmosphere on the radio wave. It is a function of the gradient of the index of refraction of the atmosphere and is given by:

$$k = \frac{1}{1 + a(dn/dh)}$$

where dn/dh is the gradient of the index of refraction. For standard atmosphere, the gradient is given by:

$$dn/dh = -(1/4a)$$

so that $k = 4/3$.

The physical significance of $D_q$ can be seen from figure 2. The curve represents path loss as a function of the distance, d, from the transmitter as calculated by the optical interference equations. The points of relative maximum signal strength, $P_1$, $P_2$, and $P_3$, occur when the reflected wave is in phase with the direct wave. The points of least relative signal strength, $M_1$, $M_2$, and $M_3$, occur when the reflected wave is 180 degrees out of phase with the direct wave. In a manner of speaking, it may be said that a period of the function plotted in figure 2 occurs between $P_1$ and $P_2$, between $P_2$ and $P_3$, and between $P_3$ and line of sight. $D_q$, then, is the point 90 degrees beyond the beginning

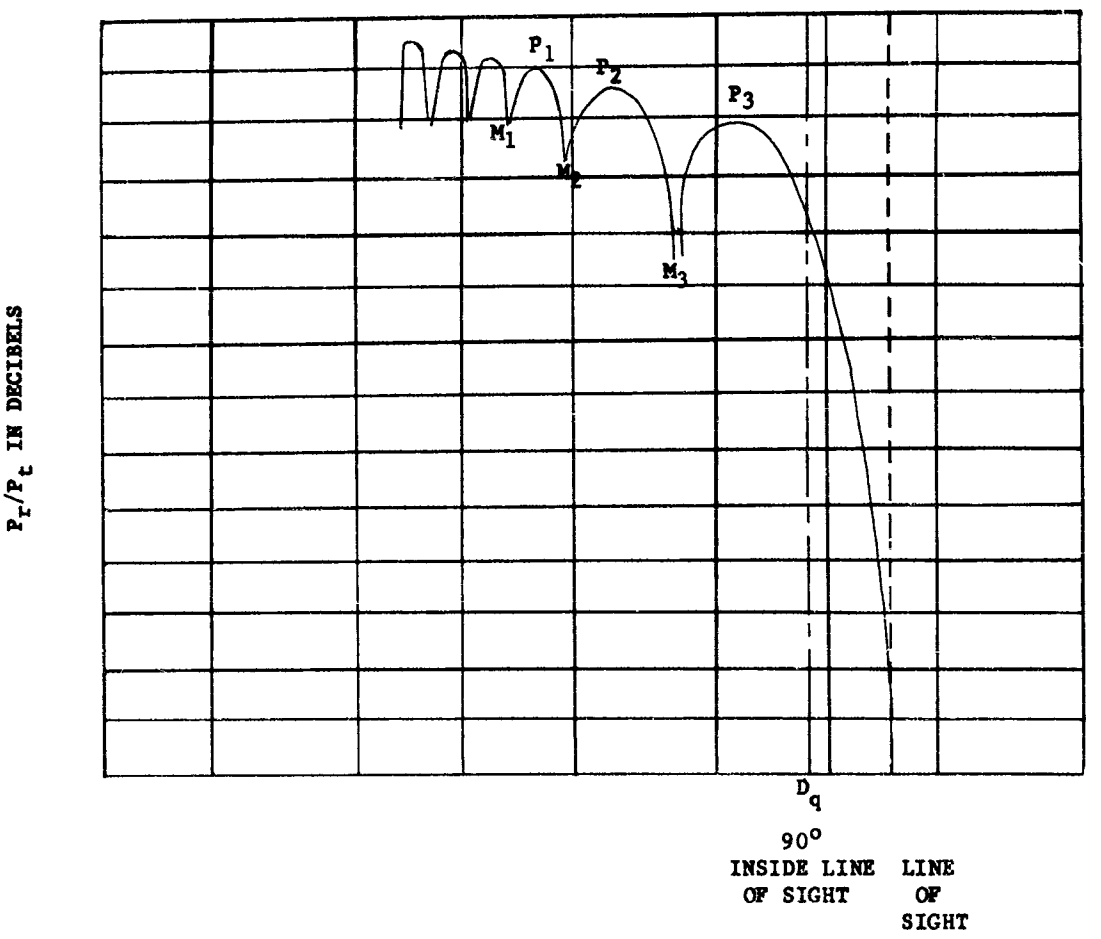



Figure 2. Determination of Quadrature Point

of the last period before the line-of-sight distance.

Loss Due to Terrain and Vegetation (Blocks 7, 8, and 9)

Data are being compiled and field tests are being conducted to determine methods of predicting the effects of terrain and vegetation on path loss. Evidence at this time seems to indicate that the best method for handling this problem with the computer will be to store data on magnetic tape in matrix form. The stored data will represent path loss factors, in the one case as a function of frequency and terrain type, and in the other case as function of frequency and vegetation. Transmitted signals will then be modified by information contained on the magnetic tape.

In some cases, it will be desirable to perform a more thorough analysis on path loss as a function of terrain. Special signals, such as the fundamental of the desired transmitter, will be subjected to this analysis. Preliminary test results indicate that calculations based on the equations for path loss as a function of profile, as developed by A. H. LaGrone[5] in 1960, provide good correlation with experimental field tests. This equation is of the form:

$$db = c\left[\pm\frac{\sqrt{|h_n - h_{n-1}|}}{\exp(d_n,o)} \pm \cdots \pm \frac{\sqrt{|h_3 - h_2|}}{\exp(d_3,o)} \pm \frac{\sqrt{|h_2 - h_1|}}{\exp(d_2,o)} \pm \frac{\sqrt{|h_1 - h_o|}}{\exp(d_1,o)}\right]$$

where

c is an experimentally-determined constant,

$h_n$ are the altitudes at all relative maximums along the terrain profile between the transmitters and the receiver with the exception of $h_1$ which is the altitude of the relative minimum nearest the receiver,

and

the $d_{n,o}$'s are the distances from the receiver to points on the profile where the altitude is given by:

$$\frac{h_n + h_{n-1}}{2}$$

These parameters are illustrated in figure 3.

A computer subroutine was written to evaluate this equation using, as input, a matrix of stored terrain information. The matrix, called an altitude matrix, consists of an array of numbers representing altitudes of the terrain at predetermined uniform intervals in the environment being studied. Using the coordinates of the transmitter and receiver, and the altitude matrix, the subroutine determines the terrain profile, provides all maximums and minimums necessary to evaluate LaGrone's equation, and calculates the db deviation in power due to terrain characteristics.

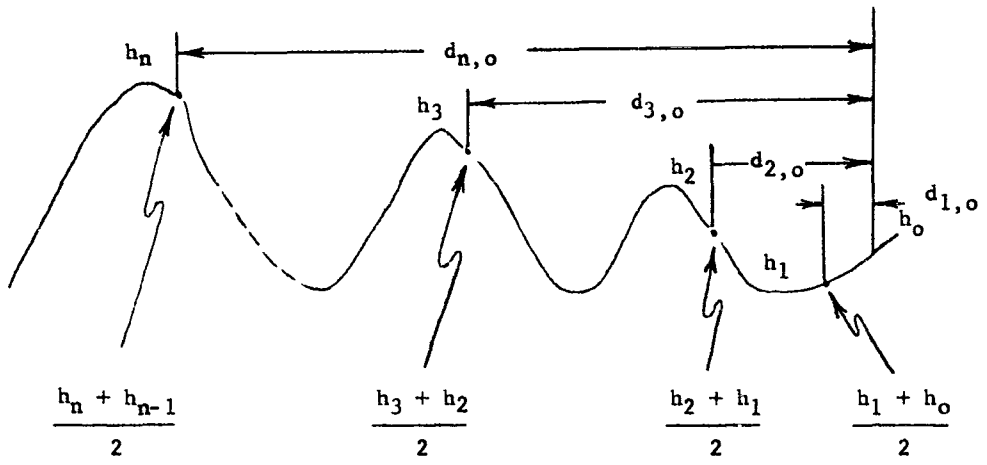



Figure 3. Terrain Profile Determination

Corrections of the LaGrone type may be expected to give a fairly high degree of accuracy, but require considerable computation. To make thousands of computations in this manner would require excessive computer time and even worse, excessive preparation of data for the computer. Use of these formulas in the EMETF prediction model will therefore be limited to important transmissions such as those within the test link and those from high-powered interfering transmitters.

Receiver Function, Scoring Function, and Output (Blocks 10 and 11)

Transmitted signals which reach this portion of the program have been modified by many factors such as antenna factors, free space factor, spherical-earth correction factors, terrain, and vegetation factors. At this point a test is conducted to determine if the signal strength is sufficiently strong to interfere with the receiver. The power level of the signal is again compared with the corresponding receiver threshold-sensitivity value from the F table. If the signal strength is less than the receiver sensitivity, the signal is discarded, a new transmitter frequency is chosen, and the complete process is repeated. If the signal strength is greater than the receiver sensitivity, two things occur: signal strength and transmitter-receiver identifying information is printed out for human analysis and the frequency and power level of the signal are stored in the computer memory to be used in an interference scoring process[4] when all signals interfering with a particular receiver have been determined.

When all signals affecting a particular receiver have been determined, one more test is required before presenting these signals to the portion of the computer program which simulates the demodulator and performs the scoring function. This test is necessary to determine if the receiver has been saturated due to the presence of the desired and undesired signals. The saturation level is determined from measured data called "dynamic range" which is recorded to give an indication of receiver behavior between the standard response level and the limiting response level. The upper limit of the dynamic range is considered to be the saturation point. If the sum of the power input to the receiver exceeds the saturation point, a condition of complete interference is assumed, the demodulator and scoring portion of the program is omitted, and a new receiver is chosen from the environment for analysis.

If the saturation point has not been exceeded, the signals now present in the if. stage of the receiver are presented to the demodulator. The signals are represented as a sequence of functions of the form:

$$A_o \cos (\omega_o t + \phi_o)$$

$$A_1 \cos (\omega_1 t + \phi_1)$$

$$\vdots$$

$$A_n \cos (\omega_n t + \phi_n)$$

and can be added to give the signal as received by the demodulator. The signal is represented by a function of the form:

$$\sum_{i=0}^{n} A_i \cos (\omega_i t + \phi_i)$$

This expression can be put in the following form:[6]

$$R \cos (\omega_o t + \theta)$$

where $R^2$ is a transcendental function composed of trigonometric terms which are functions of time and $\theta$ is the arc tangent of the ratio of two trigonometric functions of time.

In the case of an am. receiver, we are interested in R for linear detectors and $R^2$ for square-law detectors. In the fm. case, we are interested in $d\theta/dt$, which is the ratio of two trigonometric functions of time. In all three cases, we want the output of the detector to be of the form:

$$f(t) = a_o + a_1 \cos p_1 t + a_2 \cos p_2 t + \ldots + a_p \cos p_p t$$

(where p is the audio angular frequency) so that spectral information can be obtained for scoring purposes. $R^2$ is of this form. R and $d\theta/dt$ can be put in this form by numerical evaluation of the Fourier coefficients, $a_o$, $a_1$, ... $a_p$.

The scoring process is accomplished by dividing the audio spectrum

into increments of unequal width in frequency, but each of which contributes equally to the intelligibility according to the French and Steinberg theory. Signal-to-noise ratio in each band is computed and an articulation index determined.[6]

## III. COMMENTS ON THE COMPUTER PROGRAM

If 15,000 transmitters were operating in the vicinity of a receiver and if each transmitter were emitting a minimum of 10 signals, in essence the effects of at least 150,000 monofrequency transmitters would have to be investigated. If each investigation required but one minute of computer time, the needed 2,500 hours of computer time would, I'm afraid, tax even the resources of IBM's facilities, to say nothing of the taxpayers' pocketbook. For this reason, decision-making procedures have been incorporated into the design of the computer program such that noninterfering signals are detected as soon as possible and immediately discarded. Only signals of importance are subjected to the complete analysis. It would be premature at this time to publish running times of the program since enough cases have not been tested to provide the required figures.

It is readily admitted that this program will not provide the solution to all radio frequency interference problems. As more knowledge about the subject becomes available, and as methods are found to describe the knowledge mathematically, changes in the program will have to be made. More and more people are beginning to realize that making changes in a computer program of this complexity can be a tremendous task. For this reason, extreme care has been taken to write the program anticipating the need for change. Every step in the prediction process which can be distinguished from others has been written as a closed subroutine such that deletion of that step or insertion of another step requires changing only a few instructions in a control program which calls for each subroutine as it is needed. Another advantage to this system is that the subroutines can be separated from the main program and used as separate programs when it is desired to independently test various portions of the prediction model.

Worthy of mention, perhaps, is the fact that construction of the prediction model has been based, whenever possible, on measured test results. Transmitter and receiver spectrum signatures are used to simulate transmitters and to determine frequencies acceptable to receivers, antenna pattern measurements and terminal loss measurements provide the basis for simulation of the antenna function, and field tests to determine loss due to terrain and vegetation provide data for predicting loss due to these factors. Construction of a model based on physical reality should provide the much desired accuracy required of such a program. On the other hand, results of the program, being dependent on measured results of physical parameters, can be no more accurate than those physical measurements.

## ACKNOWLEDGMENT

The work described in this paper was sponsored by the Field Test Directorate, U. S. Army Electronic Proving Ground, Fort Huachuca, Arizona, under contract Nr. DA-36-039-SC-80424.

## REFERENCES


1. Burrows, Charles R., and Attwood, Stephen S., Radio Wave Propagation, Academic Press, Inc., New York, 1949.

2. National Bureau of Standards, Memorandum Report, Telecommunications Performance Standards, Tropospheric Systems, Volume 5 of 6.

3. Kerr, Donald E., Propagation of Short Radio Waves, McGraw-Hill Book Company, Inc., New York, 1951.

4. Hoehn, A. J., "Engineering Aspects of the EMETF Interference-Prediction Model," Proceedings of the 7th Conference on Radio Interference Reduction and Electronic Compatibility, Armour Research Foundation, Illinois Institute of Technology, November, 1961.

5. LaGrone, Alfred H., "Forecasting Television Service Fields," Proceedings of the IRE, June, 1960.

6. The theoretical aspects of this section can be found in: Wilde, N., et al., "A Digital Representation of Interference Within a Communications Receiver Including the Demodulation Process," Proceedings of the 7th Conference on Radio Interference Reduction and Electronic Compatibility, Armour Research Foundation, Illinois Institute of Technology, November, 1961.

## RECENTLY ISSUED REPORTS

As a contribution towards the exchange of information in the field of radio interference, the following pages contain information regarding recently issued RI technical reports. The referenced reports have been issued since January 1, 1960.

## SEVENTH CONFERENCE ON RADIO INTERFERENCE REDUCTION AND ELECTRONIC COMPATIBILITY

## RECENTLY ISSUED REPORTS

| ORGANIZATION | CONTRACT NUMBER | SECURITY CLASSIFICATION | TITLE OF REPORT | DATE | COPIES OBTAINABLE FROM |
|---|---|---|---|---|---|
| American Bosch Arma Corporation; Garden City, N.Y. | | None | EMC ORGANIZATION (G. Yabroudy) | 7/61 | Arma Engineering (House Organization) |
| | | None | WEAPON SYSTEMS AND EMC (D. Wildfeuer) | 7/61 | Arma Engineering (House Organization) |
| | | None | EMC- PREDICTION TECHNIQUES (D. Wildfeuer) | 7/61 | Arma Engineering (House Organization) |
| | | None | DESIGN PRECAUTIONS FOR EMC Part I (W. Goodhue) | 10/61 | Development Services Department |
| | | None | DESIGN PRECAUTIONS FOR EMC Part II (A. Mastaudrea) | 10/61 | Development Services Department |
| | | None | RF MEASUREMENTS (W. Sennello) | 10/61 | Development Services Department |
| | | None | EMC - FOREWORD (J. Regazzi) | 7/61 | Arma Engineering (House Organization) |
| | | None | EMC - SURVEY (J. Sexton) | 7/61 | Arma Engineering (House Organization) |

| | | | | | |
|---|---|---|---|---|---|
| Armour Research Foundation of Illinois Institute of Technology; Chicago, Ill. | DA-36-039 SC-87176 | Conf. | DIRECTORY OF ELECTRONIC EQUIPMENT CHARACTERISTICS - RADAR TYPES (First through Third Quarterly Reports and Final Report) | 9/60 11/61 | USASRDL; Fort Monmouth, New Jersey |
| | AF 30(602)-2375 | Unclass. | APPLICATION OF OPERATIONS RESEARCH TO INTERFERENCE (First through Third Quarterly Reports) | 12/61 | RADC |
| | | Secret | Supplement to Second Quarterly | | |
| | AF 33(616)-7337 | Unclass. | ELECTROMAGNETIC COMPATIBILITY CONTROL TECHNIQUES | 11/60 | Communication Laboratories Aeronautical Systems Division |
| Federal Communications Commission | | Unclass. | CONTROL OF RFI FROM NONLICENSED APPARATUS | 9/61 | FCC Washington 25, D.C. |
| Filtron Company, Inc. | AF 33(600)-37829 | Unclass. | FUNDAMENTAL ASPECTS OF CABLE SELECTION AND USE | 8/60 | Air Force |
| | AF 33(600)-40845 | Unclass. | GROUNDING AND BONDING PRACTICES | 12/60 | Air Force |
| | DA-30-069-ORD-3111 | Secret | SURVEY OF RADIO INTERFERENCE ENVIRONMENT at NASA Missile Test Facilities, Redstone Arsenal, Alabama | 7/60 | NASA |

| ORGANIZATION | CONTRACT NUMBER | SECURITY CLASSIFICATION | TITLE OF REPORT | DATE | COPIES OBTAINABLE FROM |
|---|---|---|---|---|---|
| Frederick Research Corporation | | | WHY RF GROUNDS? A. H. Sullivan, Jr. | 9/60 | Frederick Research Corporation |
| | | | Notes on SPECTRUM SIGNATURE MEASUREMENT PROBLEMS J.J. Dozier and A. H. Sullivan, Jr. | 10/61 | Frederick Research Corporation |
| General Dynamics/ Electronics, Rochester, N.Y. | AF 30(602)-1719 | Unclass. | ELECTROMAGNETIC COMPATIBILITY (RFI) Summary Report on AN/GLR-1 | 6/61 | T. E. Ganias |
| | " | " | SHIELDING EFFECTIVENESS OF SHIELD-AIR AND PAULLIN HONEYCOMB Report 136 | 12/60 | T. E. Ganias |
| | " | " | FLEXOWRITER, PUNCH AND READER INTERFERENCE TESTS Report No. 117 | 9/60 | T. E. Ganias |
| | " | " | CONDUCTED AND RADIATED r-f INTERFERENCE OF A CHARACTRON TUBE Report No. 87 | 6/60 | T. E. Ganias |
| | " | " | RADIATED RFI OF A BREADBOARD MODEL OF ELEXOWRITER RELAY DRIVER Report No. 44 | 3/60 | T. E. Ganias |

| | | | | | |
|---|---|---|---|---|---|
| General Dynamics/ Electronics, Rochester, N.Y. | NOw-60-0319 | Unclass. | INTERFERENCE TESTS OF A SONOBUOY SYSTEM TEST GENERATOR AN/ARM-54 | 6/61 | T. E. Ganias |
| Georgia Institute of Technology | DA-36-039-sc-74855 | Conf. | ELECTRONIC EQUIPMENT INTERFERENCE CHARA. - COMMUNICATION TYPE Receiver Spectrum Signatures, Volumes 107 through 111 and Volumes 207 through 210 | 5/60 to 4/61 | USASRDL |
| | " | " | ELECTRONIC EQUIPMENT INTERFENCE CHARA. - COMMUNICATION TYPE Transmitter Spectrum Signatures, Volumes 314 through 321 | 8/60 to 1/61 | USASRDL |
| | DA-36-039-sc-87183 | Secret | ELECTRONIC EQUIPMENT INTERFERENCE CHARA. - COMMUNICATION TYPE Transmitter Spectrum Signatures, Volumes 322 through 324 | 4/61 to 5/61 | USASRDL |
| | DA-36-039-sc-74855 | Conf. | ELECTRONIC EQUIPMENT INTERFERENCE CHARA. - COMMUNICATION TYPE, (Quarterly Rpt. No. 11) | 1/60 to 3/60 | USASRDL |

| ORGANIZATION | CONTRACT NUMBER | SECURITY CLASSIFICATION | TITLE OF REPORT | DATE | COPIES OBTAINABLE FROM |
|---|---|---|---|---|---|
| Georgia Institute of Technology | DA-36-039-sc-74855 | Conf. | ELECTRONIC EQUIPMENT INTERFERENCE CHARA. - COMMUNICATION TYPE, (Quarterly Rpt. No. 12) | 4/60 to 6/60 | USASRDL |
| | DA-36-039-sc-74855 | Unclass. | RADIO FREQUENCY INTERFERENCE BIBLIOGRAPHY, WITH ABSTRACTS, (Appendix to Quarterly Rpt. No. 12, above) | 6/60 | USASRDL |
| | DA-36-039-sc-74855 | Conf. | ELECTRONIC EQUIPMENT INTERFERENCE CHARA. - COMMUNICATION TYPE (Quarterly Rpt. No. 13) | 7/60 to 9/60 | ASTIA |
| | DA-36-039-sc-74855 | Unclass. | ELECTRONIC EQUIPMENT INTERFERENCE CHARA. - COMMUNICATION TYPE (Final Technical Rpt,) | 12/60 | ASTIA |
| | DA-36-039-sc-74855 | Unclass. | SPECTRUM SIGNATURE AND SYNTHESIS OF INTERFERENCE FREE COMMUNICATIONS SYSTEMS (Interim Status Rpt. No. 1) | 5/60 | ASTIA |
| | DA-36-039-sc-87183 (Cont. of Contract DA-36-039-sc-74855) | Unclass. | ELECTRONIC EQUIPMENT INTERFERENCE CHARA. - COMMUNICATIONS TYPE (First Quarterly Rpt. No. 15) | 11/60 to 2/61 | ASTIA |

| | | | | | |
|---|---|---|---|---|---|
| Georgia Institute of Technology | DA-36-039-sc-87183 (Cont. of Contract DA-36-039-sc-74855 | Conf. | ELECTRONIC EQUIPMENT INTERFERENCE CHARA. - COMMUNICATION TYPE (Second Quarterly Rpt. No. 16) | 3/61 to 2/61 | ASTIA |
| | DA-36-039-sc-87183 (Cont. of Contract DA-36-039-sc-74855 | Unclass. | ELECTRONIC EQUIPMENT INTERFERENCE CHARA. - COMMUNICATION TYPE Volume 3 | 5/61 | ASTIA |
| Office of the Area Frequency Coordinator, U.S. Army Signal Missile Support Agency, White Sands Missile Range, New Mexico | AFC Proj. # FC-05 (51-537A) | Unclass. | SPECTRUM UTILIZATION CHARA. /Telemetry Transmitter, Vector Mfg. Co. Inc., TUFT-50 | 9/60 | USASMSA |
| | AFC Proj. # FC-05- (51-537A) | Unclass. | SPECTRUM UTILIZATION CHARA. /Telemetry Transmitter, Parsons 7501 w/filter 7504 | 9/60 | " |
| | AFC Proj. # FC-05- (51-533) | Unclass. | SPECTRUM UTILIZATION CHARA. /Telemetry Transmitter, Radiation Inc. 3115-3B w/RF filter ARK Electronics TM-2S | 8/60 | " |

| ORGANIZATION | CONTRACT NUMBER | SECURITY CLASSIFICATION | TITLE OF REPORT | DATE | COPIES OBTAINABLE FROM |
|---|---|---|---|---|---|
| Office of the Area Frequency Coordinator, U.S. Army Signal Missile Support Agency, White Sands Missile Range, New Mexico | AFC Proj. # FC-05- (51-532) & (51-529) | Unclass. | SPECTRUM UTILIZATION CHARA./Radio Plane Transmitter Assy; c/o Telemetry Transmitter, Bendix TXV-17 RF filter Assy #1046142, RF Amplifier, Rheem REL 09-9, and RF filter, Bendix TNL-14 | 8/60 | USASMSA |
| | AFC Proj. # FC-05- (51-520) | Unclass. | SPECTRUM UTILIZATION CHARA./Telemetry Transmitter, Bendix TXV-13 | 7/60 | " |
| | AFC Proj. # FC-05- (51-519) | Unclass. | SPECTRUM UTILIZATION CHARA./Telemetry Transmitter, Radiation Inc. 3115-3B | 8/60 | |
| | AFC Proj. # FC-05- (51-518) | Unclass. | SPECTRUM UTILIZATION CHARA./Telemetry Transmitter, Electro-Mechanical Research Inc. 121B-28 | 9/60 | " |
| | AFC Proj. # FC-05- (51-512) & (51-506) | Unclass. | SPECTRUM UTILIZATION CHARA./Telemetry Transmitter, Radiation Inc. 3115-3B w/and w/o ARK Electronics filter TM-2S | 7/60 | " |
| | AFC Proj. # FC-05- 51-511) | Unclass. | SPECTRUM UTILIZATION CHARA./Transmitter, General Electric VO36NR | 7/60 | " |

| | | | | | |
|---|---|---|---|---|---|
| Office of the Area Frequency Coordinator, U.S. Army Signal Missile Support Agency, White Sands Missile Range, New Mexico | AFC Proj. # FC-05- (51-501) | Unclass. | SPECTRUM UTILIZATION CHARA./Telemetry Transmitter, Lockheed Part #1308423, c/o Telechrome 1472 w/1632-A filter | 5/60 | USASMSA |
| | AFC Proj. # FC-05- (51-500) | Unclass. | SPECTRUM UTILIZATION CHARA./Receiver, Nems Clarke Inc. 1502A w/pre amp PR-203 | 5/60 | " |
| | AFC Proj. # FC-05- (51-497) | Unclass. | SPECTRUM UTILIZATION CHARA./Telemetry Transmitter, Lockheed Part #1308423-501 | 5/60 | " |
| | AFC Proj. # FC-05- (51-493) | Unclass. | SPECTRUM UTILIZATION CHARA./Telemetry Transmitter, Radiation Inc. 3021-26 | 5/60 | " |
| | AFC Proj. # FC-05- (51-491) | Unclass. | SPECTRUM UTILIZATION CHARA./Receiver, Nems Clarke Inc. 1400, w/pre amp PR-203 | 5/60 | " |
| | AFC Proj. # FC-05- (51-460) Part I | Unclass. | SPECTRUM UTILIZATION CHARA./Radar Set, AN/MPQ-12 and AN/MPQ-18 | 1/60 | " |

| ORGANIZATION | CONTRACT NUMBER | SECURITY CLASSIFICATION | TITLE OF REPORT | DATE | COPIES OBTAINABLE FROM |
|---|---|---|---|---|---|
| Office of the Area Frequency Coordinator, U.S. Army Signal Missile Support Agency, White Sands Missile Range, New Mexico | AFC Proj. # FC-05- (51-616) | Unclass. | SPECTRUM UTILIZATION CHARA. /Transmitter, General Electric VO19WR | 6/61 | USASMSA |
| | AFC Proj. # FC-05- (51-592) | Unclass. | SPECTRUM UTILIZATION CHARA. /Telemetry Transmitter, United Electro Dynamics, TR-10 | 5/61 | " |
| | AFC Proj.# FC-05- (51-588) | Unclass. | SPECTRUM UTILIZATION CHARA. /Radar Set, HAWK High Power CW Illuminator | 4/61 | " |
| | AFC Proj.# FC-05- (51-587) | Unclass. | SPECTRUM UTILIZATION CHARA. /Telemetry Transmitter, Gilfillan 88660-2 | 4/61 | " |
| | AFC Proj. # FC-05- (51-609) | Unclass. | SPECTRUM UTILIZATION CHARA. /Telemetry Transmitter, Gilfillan 88660-2 and 86600 | 6/61 | " |
| | AFC Proj.# FC-05- (51-569) | Unclass. | SPECTRUM UTILIZATION CHARA. /Telemetry Transmitter, Bendix TXV-13 w/ filter TNL-14 | 2/61 | " |

| | | | | | |
|---|---|---|---|---|---|
| Office of the Area Frequency Coordinator, U.S. Army Signal Missile Support Agency, White Sands Missile Range, New Mexico | AFC Proj. # FC-05- (51-574) | Unclass. | SPECTRUM UTILIZATION CHARA. /Telemetry Transmitter, Telechrome 1483A1 and 1483A3 | 3/61 | USASMSA |
| | AFC Proj. # FC-05- (51-562) | Unclass. | SPECTRUM UTILIZATION CHARA. /Receiver, Babcock BCR-42 | 2/61 | " |
| | AFC Proj. # FC-05- (51-561) | Unclass. | SPECTRUM UTILIZATION CHARA. /Telemetry Transmitter, North American 273-720400 | 2/61 | " |
| | AFC Proj. # FC-05- (51-556) | Unclass. | SPECTRUM UTILIZATION CHARA./Radar Beacons, AN/DPN-42 and AN/DPN-32 | 1/61 | " |
| | AFC Proj. # FC-05- (51-541) | Unclass. | SPECTRUM UTILIZATION CHARA. /Receiver, AN/DRW-11 | 3/61 | " |
| | AFC Proj. # FC-05- (51-524) | Unclass. | SPECTRUM UTILIZATION CHARA. /Leach Corp., Model A1W1-4C Command Receiver | 3/61 | " |

| ORGANIZATION | CONTRACT NUMBER | SECURITY CLASSIFICATION | TITLE OF REPORT | DATE | COPIES OBTAINABLE FROM |
|---|---|---|---|---|---|
| Office of the Area Frequency Coordinator, U.S. Army Signal Missile Support Agency, White Sands Missile Range, New Mexico | AFC Proj. # FC-05- (51-427) | Unclass. | SPECTRUM UTILIZATION CHARA. /Radar Beacon, AN/APN-91(XA-1) | 2/61 | USASMSA |
| | AFC Proj. # FC-05- (5162011) | Unclass. | SPECTRUM UTILIZATION CHARA. /United Electro Cynamics Inc. Model TR-10 (Modified) Telemetry Transmitter | 9/61 | " |
| | AFC Proj. # FC-05- (5162002) | Unclass. | SPECTRUM UTILIZATION CHARA. /Telemetry Transmitter, United Electro Dynamics TR-10 | 7/61 | " |
| | AFC Proj. # FC-05- (5162001) | Unclass. | SPECTRUM UTILIZATION CHARA. /Advanced Electronics Corporation Model T2A-26, Telemetry Transmitter | 8/61 | " |
| | AFC Proj. # FC-05- (52-499) | Unclass. | SPECTRUM UTILIZATION CHARA./Receiver, AN/ ARC-44 | 4/60 | " |
| | AFC Proj. # FC-05- (52-485) | Unclass. | SPECTRUM UTILIZATION CHARA. /Receivers, AN/ TRC-1 and AN/ARC-27 | 6/60 | " |

| | | | | | |
|---|---|---|---|---|---|
| Office of the Area Frequency Coordinator, U.S. Army Signal Missile Support Agency, White Sands Missile Range, New Mexico | AFC Proj. # FC-05- (5362029) | Unclass. | ANTENNA CHARA./AS-799 | 9/61 | USASMSA |
| | AFC Proj. # FC-05- (5362028) | Unclass. | ANTENNA CHARA. /6' & 10' Parabolic w/helical feed (2250 MCS) | 9/61 | " |
| | AFC Proj. # FC-05- (5362027) | Unclass. | ANTENNA CHARA. / Helical, Andrew H-19110A-13 | 9/61 | " |
| | AFC Proj. # FC-05- (5362024) & (5362004) | Unclass. | FIELD INTENSITY/Radar, AN/MPQ-12 | 7/61 | " |
| | AFC Proj. # FC-05- (5362018) | Unclass. | SPECTRUM UTILIZATION CHARA. /Transmitter, Motorola U-41G31 | 8/61 | " |
| | AFC Proj. # FC-05- (5362012) | Unclass. | RADIATION HAZARDS/ Radar, Nike Hercules (HIPAR) | 8/61 | " |
| | AFC Proj. # FC-05- (5362009) | Unclass. | SPECTRUM UTILIZATION CHARA. /Transmitter, G. E. UA6B | 8/61 | " |

| ORGANIZATION | CONTRACT NUMBER | SECURITY CLASSIFICATION | TITLE OF REPORT | DATE | COPIES OBTAINABLE FROM |
|---|---|---|---|---|---|
| Office of the Area Frequency Coordinator, U.S. Army Signal Missile Support Agency, White Sands Missile Range, New Mexico | AFC Proj. # FC-05- (5362005) | Unclass. | RADIATION HAZARDS/ Radar, Nike Zeus Acquisition | 8/61 | USASMSA |
| | AFC Proj. # FC-05- (53-613) | Unclass. | ANTENNA CHARA. /15' Parabola Andrew D15M | 7/61 | " |
| | AFC Proj. # FC-05- (53-612) | Unclass. | ANTENNA CHARA. / Boeing 49-4442 | 8/61 | " |
| | AFC Proj. # FC-05- (53-611) | Unclass. | SPECTRUM UTILIZATION CHARA. /Radar, AN/FPS-16 | 7/61 | " |
| | AFC Proj. # FC-05- (53-598) | Unclass. | RADIATION HAZARDS/ Radars, AN/FPS-33 and AN/FPS-6A | 7/61 | " |
| | AFC Proj. # FC-05- (53-590) | Unclass. | ANTENNA CHARA. /AT-785, 786, 787, 788, 789, & 790/ UPM-88 | 7/61 | " |
| | AFC Proj. # FC-05- (53-542) | Unclass. | ANTENNA CHARA. /UHF Turnstile | 7/61 | " |

| | | | | | |
|---|---|---|---|---|---|
| Office of the Area Frequency Coordinator, U.S. Army Signal Missile Support Agency, White Sands Missile Range, New Mexico | AFC Proj. # FC-05- (53-448) | Unclass. | RADIATION HAZARDS/ Radar, AN/FPS-16 | 8/61 | USASMSA |
| | AFC Proj. # FC-05- (53-586) | Unclass. | ANTENNA CHARA. / Corner Reflector, Andrew 3605 (Modified) | 5/61 | " |
| | (53-528) | | Andrew 3605A | 8/60 | " |
| | AFC Proj. # FC-05- (53-582) | Unclass. | RADIATION HAZARDS/ Radars, AN/MPQ-12 and AN/MPQ-18 | 5/61 | " |
| | AFC Proj. # FC-05- (53-581) | Unclass. | RADIATION HAZARDS/ Radars, M-33 (S-Band), MSQ-1, MSQ-1A, M-33 (X-Band) | | |
| | AFC Proj. # FC-05- (53-564) | Unclass. | ANTENNA CHARA. /ARCAS Missile | 1/61 | " |
| | AFC Proj. # FC-05- (53-599) | Unclass. | SPECTRUM UTILIZATION CHARA. /Radar, AN/FPS-33 | 3/61 | " |

| ORGANIZATION | CONTRACT NUMBER | SECURITY CLASSIFICATION | TITLE OF REPORT | DATE | COPIES OBTAINABLE FROM |
|---|---|---|---|---|---|
| Office of the Area Frequency Coordinator, U.S. Army Signal Missile Support Agency, White Sands Missile Range, New Mexico | AFC Proj. # FC-05- (53-554) (53-551) | Unclass. | SPECTRUM UTILIZATION CHARA. /Radar, AN/FPS-6A | 1/61 7/60 | " |
| | AFC Proj. # FC-05- (53-553) | Unclass. | ANTENNA CHARA. /Tri-helical, Machine Products Inc. MPB-7-3-0 | 2/61 | " |
| | AFC Proj. # FC-05- (53-548) | Unclass. | SPECTRUM UTILIZATION CHARA. /Teletype 28ASR, w/Subscriber Set A131 | 10/61 | " |
| | AFC Proj. # FC-05- (53-536) | Unclass. | ANTENNA CHARA. /Yagi, Jasic Labs 259 | 8/61 | " |
| | AFC Proj. # FC-05- (53-530) | Unclass. | RADIO INTERFERENCE SURVEY of Nike Zeus Power Plant at White Sands Missile Range, New Mexico, AFC Report # PP-3-11-60-RIS | 11/60 | " |
| | AFC Proj. # FC-05- (53-513) | Unclass. | ANTENNA CHARA. /Quadra Loop, p/o Aerobee Missile | 9/60 | " |

| | | | | | |
|---|---|---|---|---|---|
| Office of the Area Frequency Coordinator, U.S. Army Signal Missile Support Agency, White Sands Missile Range, New Mexico | AFC Proj. # FC-05- (53-408) | Unclass. | SPECTRUM UTILIZATION CHARA. /Radar, AN/FPS-16 | 2/60 | USASMSA |
| | AFC Proj. # FC-05- (53-505) | Unclass. | ANTENNA CHARA. /Radiosonde, T-435/AMT-57 | 5/60 | " |
| | AFC Proj. # FC-05- (53-498) | Unclass. | ANTENNA CHARA. /Band Stubs, Installed on HIGH-BALL III Missile | 5/60 | " |
| | AFC Proj. # FC-05- (53-496) | Unclass. | SPECTRUM UTILIZATION CHARA. /Honest John Engine Generator Set, M-25 | 5/61 | " |
| | AFC Proj. # FC-05- (53-482) | Unclass. | ANTENNA CHARA. /Helical, Andrew H19110A-4 | 3/60 | " |
| | AFC Proj. # FC-05- (53-478) | Unclass. | SPECTRUM UTILIZATION CHARA. /Radar, TPS-23 | 3/60 | " |
| | AFC Proj. # FC-05- (51-566) | Conf. | SPECTRUM UTILIZATION CHARA. of PROJECT MERCURY Command Receiver (U) | 2/61 | " |

| ORGANIZATION | CONTRACT NUMBER | SECURITY CLASSIFICATION | TITLE OF REPORT | DATE | COPIES OBTAINABLE FROM |
|---|---|---|---|---|---|
| Office of the Area Frequency Coordinator, U.S. Army Signal Missile Support Agency, White Sands Missile Range, New Mexico | AFC Proj. # FC-05- (51-481) | Conf. | SPECTRUM UTILIZATION CHARA. /Radio Set, AN/MPQ-7 | 3/60 | USASMSA |
| | AFC Proj. # FC-05 (51-469A) | Conf. | SPECTRUM UTILIZATION CHARA. /Transmitter, AN/ ALT-6B and Antennas, AT-581 & 589/ALT | 6/60 | " |
| | AFC Proj. # FC-05- (53-610) | Conf. | SPECTRUM UTILIZATION CHARA. /Radar, Nike Hercules (HIPAR) | 6/61 | " |
| | AFC Proj. # FC-05- (53-601) | Conf. | ANTENNA CHARA. /AT962 (XE-1) | 6/61 | " |
| | AFC Proj. # FC-05- (53-600) | Conf. | ANTENNA CHARA. /Slotted Waveguide Antenna, W.L. Maxson 1238 | 6/61 | " |
| | AFC Proj. # FC-05- (53-507) | SRD | ELECTROMAGNETIC ENVIRONMENT EXISTING IN LOS ANGELES ARADCOM AREA (LA-14 & LA-55) | 7/60 | " |
| | AFC Proj. # FC-05- (53-552) | Conf. | FIELD INTENSITY SURVEY of SWAMI & RADAR-EYE at Dyess Air Force Base, Abiline, Texas(U) | 12/60 | " |

| | | | | |
|---|---|---|---|---|
| Office of the Area Frequency Coordinator, U.S. Army Signal Missile Support Agency, White Sands Missile Range, New Mexico | Unclass. | SPECTRUM UTILIZATION/ Receiver AN/DRW-11 (XE-1) | 4/60 | USASMSA |
| | Unclass. | SPECTRUM UTILIZATION/ Telemetry Transmitter ASCOP TK-M7 | 4/60 | " |
| | Secret | ELECTROMAGNETIC RADIATION HAZARDS TO PYROTECHNIC DEVICES at White Sands Missile Range (U) (Phase I) | 12/60 | " |
| | Unclass. | SPECTRUM UTILIZATION/ Corsett TM-4-31 Telemetry Transmitter | 4/61 | " |
| | Unclass. | SPECTRUM UTILIZATION/ ASCOP FCT-1 Telemetry Transmitter | 4/61 | " |
| | Unclass. | SPECTRUM UTILIZATION/ Dorsett TR-30 Telemetry Transmitter | 5/61 | " |
| | Unclass. | SPECTRUM UTILIZATION/ Gilfillan Model 88660-2 Telemetry Transmitter | 5/61 | " |

| ORGANIZATION | CONTRACT NUMBER | SECURITY CLASSIFICATION | TITLE OF REPORT | DATE | COPIES OBTAINABLE FROM |
|---|---|---|---|---|---|
| Office of the Area Frequency Coordinator, U.S. Army Signal Missile Support Agency, White Sands Missile Range, New Mexico | | Conf. | SPECTRUM UTILIZATION/ and/or Interference Chara. of Drone Control Receiver BCR-25 (U) | 5/61 | USASMSA |
| | | Conf. | SPECTRUM UTILIZATION/ AVCO Model AD-319600 Radio Receiver (U) | 5/61 | " |
| | | Unclass. | SPECTRUM UTILIZATION/ Tele-Dynamics 1004A Telemetry Transmitter | 6/61 | " |
| | | Unclass. | SPECTRUM UTILIZATION CHARA. /Babcock, BCR-39 Command Destruct Receiver | 6/61 | " |
| | | Unclass. | SPECTRUM UTILIZATION CHARA. /R. S. Electronics Corporation Model 2621 UHF FM Receiver | 6/61 | " |
| | | Unclass. | SPECTRUM UTILIZATION CHARA. /Telechrome Model 1483A1 (Modified) VHF Telemetry Transmitter | 8/61 | " |

| | | | | | |
|---|---|---|---|---|---|
| Office of the Area Frequency Coordinator, U.S. Army Signal Missile Support Agency, White Sands Missile Range, New Mexico | | Unclass. | SPECTRUM UTILIZATION CHARA. /Leach Corporation Veri Min Command Receiver Model A1W125C | 7/61 | USASMSA |
| | | Unclass. | SPECTRUM UTILIZATION/ Bendix Dropsonde Type 2 AMQ-15 Transmitter | 9/61 | " |
| Polarad Electronics Corporation Long Island City, New York | AF 30(602) 2117 | Conf. | RADIATION AND INTERFERENCE EVALUATION OF AN/ FPS-26 FREQUENCY DIVERSITY RADAR IN OPERATION AT THE 609TH ACWRON, WUFAULA, ALA. | 10/60 | RADC |
| | AF 30(602) 2117 | Conf. | RADIATION AND INTERFERENCE EVALUATION OF AN/ FPS-7 FREQUENCY DIVERSITY RADAR IN OPERATION AT THE 693RD ACWRON, DAUPHIN ISLAND, ALA. | 2/61 | RADC |
| | AF 30(602) 2117 | Conf. | RADIATION AND INTERFERENCE EVALUATION OF AN/ FPS-27 FREQUENCY DIVERSITY RADAR IN OPERATION AT THE 627TH ACWRON, CRYSTAL SPRINGS, MISS. | 6/61 | RADC |

| ORGANIZATION | CONTRACT NUMBER | SECURITY CLASSIFICATION | TITLE OF REPORT | DATE | COPIES OBTAINABLE FROM |
|---|---|---|---|---|---|
| Polarad Electronics Corporation Long Island City, New York | | Unclass. | NOTES ON MICROWAVE MEASUREMENTS 3RD EDITION | 9/61 | Polarad |
| | | Unclass. | SPECTRUM ANALYZER TECHNIQUES | 9/61 | Polarad |
| | | Unclass. | DESIGNING RFI-FREE COMMUNICATION SYSTEMS | 5/61 | Polarad |
| | | Unclass. | THE EFFECT OF CLIMATIC ENVIRONMENTS ON RADIO FREQUENCY INTERFERENCE | 9/59 | R. E. Shewmaker |

UNCLASSIFIED

UNCLASSIFIED